近畿大学医学部消化器内科学教室

平成 25 年度　年報

Kinki University School of Medicine

Department of Gastroenterology and Hepatology

Annual Report-2013-

近畿大学医学部　消化器内科学
近畿大学医学部附属病院　光学治療センター
近畿大学医学部附属病院　中央超音波診断・治療室
近畿大学医学部堺病院　消化器内科
近畿大学医学部奈良病院　消化器・内分泌内科

年報 Annual Report 2013

近畿大学医学部消化器内科学教室

医局員集合写真

第8回 Kinki GUT Club 平成26年1月19日

目　　次

2013 年 Annual Report の発刊にあたって

近畿大学消化器内科学教室主任教授　工藤正俊

1.はじめに

2013 年の教育、研究、診療の実績をお届けします。近畿大学医学部に消化器内科学教室が新設されたのは平成 11 年 4 月であります。従って平成 26 年 3 月で区切りの 15 年が経過したことになります。開設当初は医局のスペースも 2 部屋のみでスタッフ 8 名、研修医 6 名、計 14 名での出発でありました。現在では狭山の本院に籍を置くスタッフは約 40 名、また堺病院や奈良病院もそれなりに人材・設備共に整いつつあります。

しかしながら、私立医大の宿命かもしれませんが、2004 年より始まった新臨床研修医制度の余波をまともに受けて消化器内科も毎年 5～6 人から 12～13 人入局していた入局者数が最近では激減し、また次第に開業あるいは結婚退職、郷里への U ターンなどの退職者も増え、現在なお厳しい状況に置かれているというのが現状です。ただし、ここ数年は 2-4 人の入局がコンスタントに続いており、良い傾向が見え始めました。今後の更なる消化器内科学教室の発展のために医局員一同が一致団結して診療、研究、教育活動に専念していかなければならない重要な時期であると考えております。

2.診療活動

別添えの資料をご覧頂ければ一目瞭然でありますが、消化器内科の年間の入院及び外来収入、及びそれを合計した総収入は平成 11 年の開設初年度は約 8 億程度でありましたが、平成 25 年には 32 億円を超える収入となっており、病院経営にも多大の貢献をしております。平成 25 年度は病院全体も約 13.5 億の黒字決算となりました。消化器内科の貢献も大きいと考えております。また一日平均入院患者数も年間を通して 80 人前後、平均在院日数も 8 日を切っており極めて多忙な診療活動を行っていることがおわかり頂けると思います。腹部超音波検査の件数も確実に右肩上がりであり、内視鏡の件数も総件数が平成 25 年度は 24,763 例と着実に上昇を示しております。また、肝癌に対するラジオ波治療（RFA）の総件数も多く、日経新聞や朝日新聞、読売新聞、週刊朝日等にも度々取り上げられ、総件数としては連続 8 年以上、日本国内の 2 位もしくは 3 位（内科と外科の件数、及び転移性肝癌を含めて）に位置づけられるという実績を残しております。ラジオ波は平成 11 年 6 月より開始し、平成 24 年 12 月末の時点で総件数 4,000 例に達しており、5 年生存率は 70%強と、手術とほぼ同等の治療成績が得られております。現在、C 型肝炎治療を積極的に行っており、大阪南部から C 型肝炎・肝癌を根絶したいと願っています。平成 26 年からはいよいよ IFN free の経口剤（DAA）のみによる治療が開始される予定となっており、難治性の Ib 型高ウイルス検査の SRV 率も 90%以上となることが見込まれています。B 型肝炎も核酸アナログで制御されるようになっている現在益々、肝癌の治療が重要になってくるものと思われます。

平成 15 年度に導入した早期胃癌に対する内視鏡的粘膜下層切開剥離術（ESD）も確実に症例数が増え、今後も益々増え続けていくものと考えております。もちろん、ESD 関連の研究論文も少しずつ増えていっております。また、高度先進医療としての大腸 ESD も平成 22 年より開始され、症例も増加しています。また従来より行っていた胆膵グループによる超音波内視鏡検査の件数も増加しています。平成23年度には内視鏡室が光学治療センターに格上げとなり、スペースも拡充されました。平成 23 年 11 月 27 日に第 1 回目を行った関西消化器内視鏡ライブコースも第 2 回目を平成 24 年 11 月 25 日に行われ、第 3 回目は平成 26 年 2 月 9 日に行い、約 300 人の参加者を得て成功裏に終わりました。

御承知のように大和川以南は一般に「南大阪」と呼ばれておりますが、その南大阪の人口は約 260 万にも達しております。その 240 万人の医療圏の中で特定機能病院大学医学部は近畿大学のみであります。その意味でこの 240 万人の方々の健康を守るのが我々に課せられた使命であります。さらには、平成 35 年には医学部・病院が泉ヶ丘の駅の隣接した地に新築移転する計画が発表されました。消化器内科も含めた近畿大学医学部の発展がさらに期待されます。

3.教育活動

教育は当然のことながら大学医学部の役割の極めて根幹を占める重要な部分であります。消化器内科学は消化器コースの内の肝臓の責任科であり、肝臓のユニットを 1 週間担当している他、上部消化管、下部消化管、胆膵のユニットや臨床腫瘍コースならびに画像診断のコースでも講義を担当しております。更には病因・病態のコースの 3 週間のうち 1 週間の責任科として大変多忙な教育活動を行っております。5 年生 6 年生のクリニカルクラークシップも例年 6 年生を常時 6 人程度受け入れており、講義や総括など充実した bed side 教育となるよう全力を尽くしております。国家試験の成績も是非とも向上させなければなりません。

平成 20 年 10 月から病院長に任ぜられ、今期で 3 期目となりましたのでその公務のために教育活動の多くの部分を北野准教授、松井講師はじめ多くの講師の先生方にご負担をおかけすることになってしまい、申し訳なく思っております。消化器コース及び病因・病態コースあるいは日々のクリニカルクラークシップ等の教育活動では決して手を抜かず積極的に行っていくつもりですので何卒ご容赦下さい。この紙面をお借りして感謝とお詫びを申し上げたいと思います。

3. 研究活動

（1）論文業績

英文論文の発表は 1999 年消化器内科の設立当初は一桁台でありましたが、年と共に確実に増加し、3 年目からは平均 20 編以上の英文論文がコンスタントに出るようになりました。2010 年の英文論文数は 51 編に達しました。残念ながら 2011 年は 48 編、2012 年は 44 編にとどまりました。しかし、2013 年には再び 55 編と 50 編の大台に回復しました。また 15 年間の総インパクトファクターは 1403.761 点であり英文総論文数は 438 編ですので、近畿大学消化器

内科のような小さな所帯の教室としてはまずまずの結果を残せているのではないかと思っております。来年以降は最低、英文原著論文は 60 編以上を目標に頑張っていきたいと考えておりますので教室員の皆様の自覚と更なる奮闘を期待致しております。

（2）厚生労働省科学研究費補助金事業研究班の活動

平成 22 年度に採択された厚労科研（がん臨床部門）**「進行・再発肝細胞癌に対する動注化学療法と分子標的薬併用による新規治療法の確立を目指した臨床試験（Phase III）ならびに効果を予測する biomarker の探索研究」**（工藤班）の主任研究者として日本発のエビデンスを創出すべく、努力していまいりました（平成 22－24 年)。また平成 23 年度には厚労科研（難病･がん等の疾患分野の医療の実用化部門）**「慢性ウイルス性肝疾患の非侵襲的線化評価法の開発と臨床的有用性の確立」**（工藤班）の主任研究者としても採択され、多くの大学との協同研究を行いました（平成 23－25 年)。平成 26 年度には厚生労働科学研究委託費（肝炎等克服実用化研究事業（肝炎等克服緊急対策研究事業))「慢性ウイルス性肝炎の病態把握（重症度・治療介入時期・治療効果判定・予後予測）のための非侵襲的病態診断アルゴリズムの確立」という課題が採択となり、更に 3 年間新しいエビデンスを創出すべく頑張りたいと思っております。またその他にも下記の厚労科研の分担研究者として教室の先生方に実務を担当して頂いております。この場をお借りして感謝申し上げます。

① 「抗悪性腫瘍薬による肝炎ウイルス再活性化の調査とその対応に関する研究」（池田班）（国立がん研究センターがん研究補助金）
② 「初発肝細胞癌に対する肝切除とラジオ波焼灼両方の有効性に関する多施設共同研究」（國土班）（厚労科研）
③ 「進行肝胆膵がんの治療法の開発に関する研究」（奥坂班）（国立がん研究センターがん研究補助金）

（3）今後の研究の方向性

今年の消化器内科の論文も一覧するとやはりまだまだ Impact factor の高い雑誌に掲載されているのは少ないようです。やはり Impact factor 15 点以上の雑誌を目指すには prospective な比較試験など中･長期的な視野に立った研究計画を組んで質の高い臨床研究を進めて行くことが現時点での我々に課せられた最も大きな課題と考えております。臨床試験については 2008 年 9 月 11 日に大阪府より認証を受けた NPO 法人「日本肝がん臨床研究機構（JLOG)」を中心に現在 7 つの prospective study が走っております。なかでも SELECTED study は H24 年 10 月に終了し、ポジティブな結果が得られたため平成 25 年の AASLD で oral 発表すると共に、NEJM にも投稿予定です。来年中には SILIUS 試験の結果も出る予定です。これからも世界へ向けて発信できるような成果を出して行くつもりでおります。もちろん、retrospective な解析研究で新しいデータを publish していくという努力も今後も続けていかなければなりません。

また基礎研究の分野でも西田直生志准教授、櫻井俊治講師、萩原智講師

を中心に積極的に研究を進めて頂いており、今後の publication を期待しております。

もう一つの重要な点は私が常日頃申し上げておりますように症例観察の重要性であります。臨床においては一例一例がたとえ同じ病名であったとしても一例として同じ症例はありません。同じ病気でも一つとして全く同一であるということはなく、何か異なるメッセージを発信しているのです。そのことを的確にキャッチすることにこそ意味があるという目で一例一例の患者さんを注意深く診療し観察していくことこそが最も大事であると考えています。そのような注意深い観察から新しい臨床的な発見も生まれてきますし、また逆にそのような観察眼が生まれる素地としては臨床家として真面目に臨床と向き合って最高の level に到達している必要があります。そのような点で日々の臨床の現場には”clinical pearl”とでも言うべきものがあちこちに転がっている、まさに宝の山であります。そのような理由で症例観察に基づいたケースレポートを書くということも極めて、その本人の勉強になることはもちろんのこと、今後の新しい疾患概念の確立、新しい治療法の着想などに結びつき得る重要な姿勢であると思われます。残念ながら、ケースレポートは最近の Impact factor 重視主義の多くの Journal から採用されない傾向にはありますが、それでも short report や Letter to the Editor などとしては採用されますので業績をあげるという目的ではなく、症例をキチンと観察・整理して document していくという姿勢に立つことは重要であります。すなわち症例の観察研究を報告することは我々、アカデミアに籍を置く者に課せられた使命であると自覚すべきと考えております。

大規模な前向きな比較試験を行うべきということと症例の観察研究とでは全く正反対の次元の違うことを述べているように思われるかもしれません。しかしこの 2 つは臨床を知り尽くし、かつ、臨床をじっくり真面目にやっている医師にしかできないことであるという点で共通していることであります。基礎研究あるいは臨床に結びつくかもしれない基礎研究までは MD ではなくとも PhD でも実行可能なことであり、その field ではしばしば PhD の方が quality の高い研究成果を上げ得るかも知れません。しかしながら、臨床の疑問点にもとづいた基礎研究もしくは本当に臨床に直結するような基礎研究や症例の観察研究、および大規模臨床試験などはその価値を知り得る MD にしかできないことであることは間違いありませんし、それらを遂行し得るのは患者さんと日々正面から向き合っている最高水準の医師にしかできない研究であります。そのような点でこの二つは決して矛盾するものではありませんし、両方ともに臨床家こそがやるべき研究であります。

以上、述べた 2 つの異なったアプローチは、我々の教室の研究の方向性として今後も積極的に実行して行きたいと思っております。繰り返しになりますが、臨床的な発想に基づく、あるいは臨床に本当に必要な基礎的データを抑えるという研究は、大変重要ですのでそれらは引き続き継続していかなくてはなりません。

2009 年に私が立ち上げた日本肝がん分子標的治療研究会（第 1 回研究会: 2010 年 1 月 16 日、参加者 450 人）は年 2 回開かれております。これからは C 型肝炎も B 型肝炎も、ほとんどが経口剤だけで容易に治癒して行く時代になり

ますので、相対的に肝癌治療の重要性が増してゆきます。また肝癌はこれからは分子標的治療が大変重要な治療のひとつとなる時代ですのでゲノム生物学教室（西尾和人教授）との共同研究は今後も継続していきたいと思っています。特許も出願することが出来ましたし、Impact Factor が 7 以上の雑誌にもこの分野で 2-3 編通りました。臨床的ニーズに基づいた基礎研究で成果を上げることほどエキサイティングなことはありません。是非とも近畿大学から肝癌に関して臨床に貢献できる基礎的エビデンスを次々と発信して行きたいと心から願っています。

(3) Research Conference

現在消化器内科では定期の各グループの臨床カンファレンスに加え、毎週火曜日の早朝の 1 時間みっちりと Research Conference を行っております。このカンファレンスでは全て英語で Presentation から Discussion までを行っております。ほとんど 1 年を通じて海外からの留学生がおりますし、特筆すべき点としてこれまではアジアの留学生が中心でしたが平成 22 年はイタリア人の Dr. Lorenzo が apply してできたことです。これも日本における肝細胞癌研究の leading center としてヨーロッパの国からも認知され始めている証拠であると思いますので大変喜ばしいと思っております。平成 23 年には世界で最も古い歴史のあるイタリアボローニャ大学の Prof. Bolondi の教室から Dr. Alberto がやってきて 3 か月の研修を終えて帰りました。そのような留学生にも配慮して Research Conference は英語で行っておりますが、やはりこの English Research Conference というのが消化器内科が行っているカンファレンスの中でも最も重要であると考えております。もちろん、このカンファレンスへの出席は本人の自発的意欲に基づくものではありますが、毎週多くの教室員に参加して頂いております。以下にこの数年の出席率を示しますが、出席率の高い医局員ほどやはり研究に対する activity が高い傾向にあると感じておりますので今後も引き続き積極的に参加して頂きたいと思っております。

副次的な効果としてこのカンファレンスを通じて海外で英語で Discussion できる英語力や自信も自然と磨かれるものと確信しております。

English Research Conference 出席状況

教室員	2008		2009		2010		2011		2012		2013	
	出席回数	出席率	出席回数	出席率	出席回数	出席率	出席回数	出席率	出席回数	出席率	出席回数	出席率
工藤	27/27	100%	20/20	100%	29/29	100%	23/23	100%	32/32	100%	25/25	100%
樫田	−	−	−	−	12/19	63%	20/23	87%	27/32	84%	19/25	76%
西田							5/5	100%	24/32	75%	10/25	40%
北野	25/27	93%	16/20	80%	21/29	72%	21/23	91%	25/32	78%	21/25	84%
松井	22/27	81%	18/20	90%	23/29	79%	23/23	100%	30/32	94%	23/25	92%
上嶋	6/27	22%	3/20	15%	12/29	41%	7/23	30%	9/32	28%	6/25	24%
櫻井	−	−	−	−	17/19	89%	20/23	87%	25/32	78%	15/25	60%

南	19/24	79%	1/2	50%	−	−	13/14	93%	31/32	97%	22/25	88%
萩原	11/24	46%	5/20	25%	9/29	31%	11/23	48%	10/32	31%	9/25	36%
井上	17/25	68%	16/20	80%	25/29	86%	21/23	91%	23/32	72%	17/25	68%
矢田	7/11	64%	14/19	74%	26/29	90%	14/23	61%	9/32	28%	15/25	60%
坂本	19/27	70%	1/2	50%	12/19	63%	11/23	48%	20/32	63%	15/25	60%
北井	15/27	56%	8/20	40%	15/29	52%	13/23	57%	20/32	63%	16/25	64%
朝隈	16/27	59%	12/20	60%	11/29	38%	15/23	65%	15/32	47%	15/25	60%
永井	18/19	95%	17/20	85%	14/29	48%	12.5/23	54%	23/32	72%	14/25	56%
川崎	23/27	85%	6/20	30%	4/29	14%	6/23	26%	4/32	13%	2/25	8%
田北	1/2	50%	13/20	65%	15/29	52%	7/23	30%	9/23	39%	12/25	48%
早石	10/19	53%	9/19	47%	5/29	17%	8/23	35%	9/23	39%	−	−
田中	−	−	−	−	−	−	−	−	24/27	89%	18/25	72%
山田	−	−	−	−	−	−	−	−	23/25	92%	15/25	60%
山雄	−	−	−	−	−	−	−	−	−	−	14/25	56%
永田	−	−	13/15	87%	16/29	55%	12/23	52%	11/32	34%	2/25	8%
今井	−	−	9/15	60%	18/29	62%	10/23	43%	13/32	41%	7/25	28%
有住	−	−	7/15	47%	15/29	52%	17/23	74%	26/32	81%	18/25	72%
鎌田	−	−	11/15	73%	15/29	52%	10/23	43%	16/32	50%	9/25	36%
高山	−	−	4/7	57%	−	−	13/14	93%	16/32	50%	16/25	64%
宮田	−	−	9/15	60%	16/29	55%	14.5/23	63%	22/32	69%	15/25	60%
岡元	−	−	−	−	−	−	−	−	−	−	12/25	48%
峯	−	−	9/15	60%	17/29	59%	17/23	74%	19/32	59%	19/25	76%
足立	−	−	−	−	−	−	8/14	57%	22/32	69%	17/25	68%
大本	−	−	−	−	−	−	12/14	86%	29/32	91%	19/25	76%
門阪	−	−	−	−	−	−	12/14	86%	22/32	69%	16/25	64%
千品	−	−	−	−	−	−	−	−	29/32	91%	22/25	88%
南(知)	−	−	−	−	−	−	−	−	−	−	21/25	84%

4.学会活動および海外における活動

2013 年における国内の学会発表については 69 演題、国際学会の発表については 35 演題、海外特別講演は 22、国内特別講演は 56 でありました。私自身の海外出張は 2013 年は 25 回とこれは例年よりやや多い回数となりました。

2013 年

1. 1 月 22 日-25 日　GIDEON steering committee meeting に出席 (San Francisco)

2. 2 月 1 日－6 日　世界超音波医学会(WFUMB)理事会に理事長として出席(Ha Noi)

3. 3 月 15 日-19 日　世界超音波医学会(WFUMB)エラストグラフィーコンセンサス会議へ出席　(Washington DC)

4. 4 月 7 日-11 日　肝臓病医学専門家会議に参加 (New York)

5. 4 月 12 日-14 日　肝癌アジア太平洋インベスティゲーターミーティングへ出席(Singapore)

6. 4 月 25 日-29 日　ヨーロッパ肝臓学会(EASL)へ出席
オプティミススタディーステアリングコミッティーへ出席(Amsterdam)

7. 4 月 30 日-5 月 5 日　世界超音波医学会(WFUMB)で講演
世界超音波医学会(WFUMB)理事会へ理事長および学会長として出席(Sao Paulo)

8. 5 月 9 日-11 日　E7080 アジア太平洋インベスティゲーターミーティングへ出席(Singapore)

9. 5 月 14 日-17 日　Laennec Liver Society Meeting へ出席 (Singapore)

10. 5 月 17 日-20 日　第 3 回世界超音波医学会(WFUMB)Center of Exellence にて講演(Jakarta)

11. 5 月 22 日-24 日　アジア超音波医学会(AFSUMB)教育講演会へ出席・講演
アジア超音波医学会(AFUSMB)理事会へ理事として出席(Seoul)

12. 6 月 8 日-9 日　TRACER スタディーのデータモニタリング委員会へ出席(Hong Kong)

13. 6 月 9 日　GIDEON Investigator Meeting へ出席 (Singapore)

14. 7 月 4 日-8 日　アジア太平洋肝癌専門家会議(APPLE)にて講演４つ・司会３つ(Pusan)

15. 7 月 25 日-27 日　世界超音波医学会(WFUMB)Center of Excellence 設置記念ワークショップにて講演 (Ulaanbaatar)

16. 8 月 4 日-9 日　世界超音波医学会(WFUMB)理事会へ出席 (Copenhagen)

17. 8 月 22 日-23 日　CAMIT 腹部超音波シンポジウムにて講演 (Beijing)

18. 9 月 11 日-17 日　国際肝癌学会(ILCA)理事会へ出席
国際肝癌学会(ILCA)にて口頭発表 4 題
(Washington DC)

19. 9 月 28 日-10 月 1 日　シンガポール超音波医学会にて講演
アジア超音波医学会ワークショップにて 2 講演
クアラルンプール会場視察(2014 年アジア超音波医学会会場) (Singapore)

20. 10 月 4 日-5 日　台湾消化器病学会にて講演(Taipei)

21. 10 月 18 日-20 日　アジア造影超音波会議にて講演(Taipei)

22. 10 月 24 日-26 日　第 7 回国際肝癌 MRI フォーラムにて発表 (Shanghai)

23. 10 月 31 日-11 月 7 日　米国肝臓学会(AASLD)にて発表
(Washington DC)

24. 11 月 20 日-24 日　第3回アジア太平洋肝臓学会(APASL)主催肝癌シングルトピックカンファレンスにて発表
(Cebu City)

25. 12 月 20 日-21 日　ソナゾイドによる肝癌スクリーニングについての臨床試験ワークショップにて講演(Seoul)

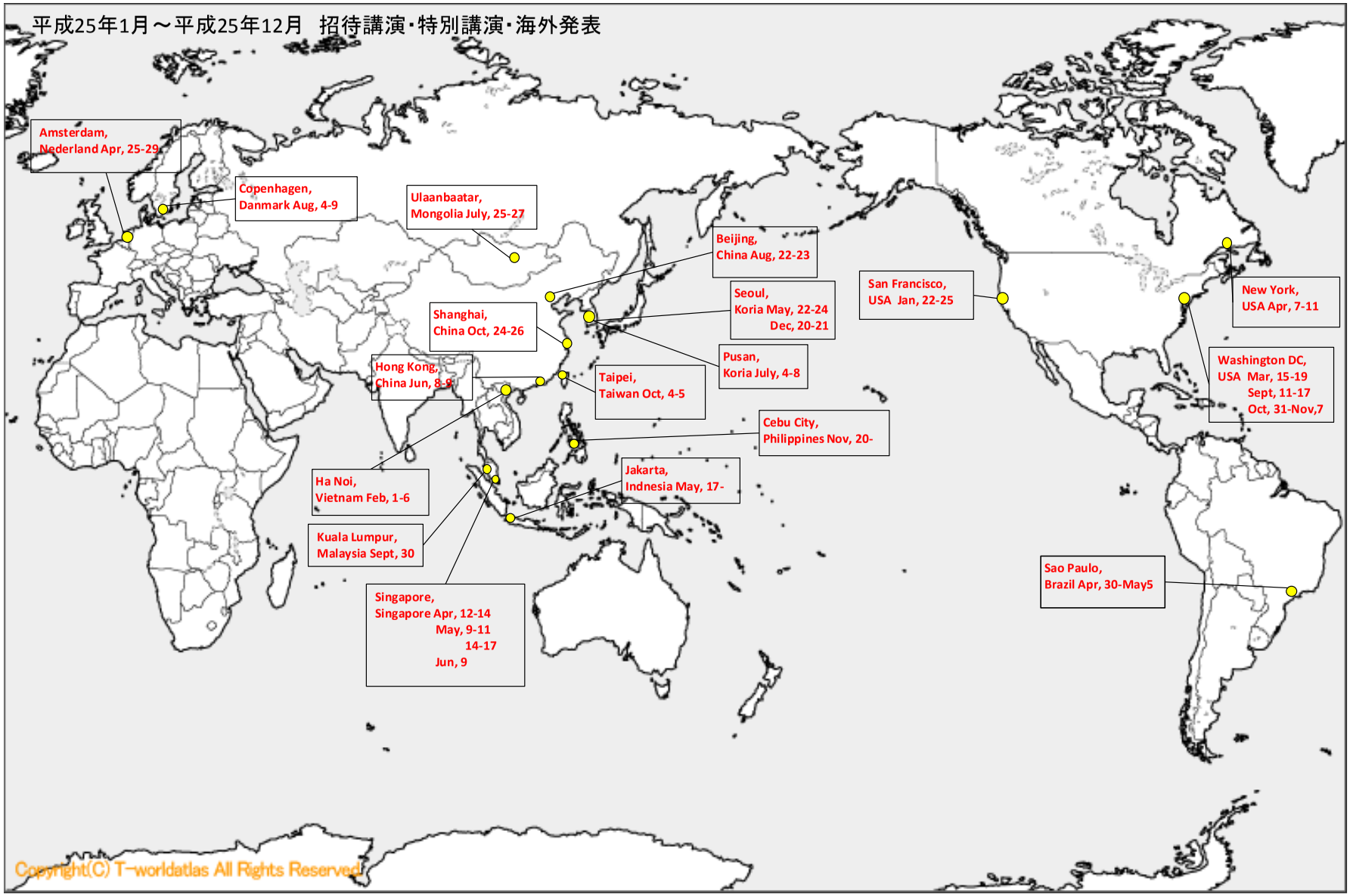
平成25年1月～平成25年12月　招待講演・特別講演・海外発表
Amsterdam,
Nederland Apr, 25-29
Copenhagen,
Danmark Aug, 4-9
Ulaanbaatar,
Mongolia July, 25-27
Beijing,
China Aug, 22-23
Seoul,
Koria May, 22-24
Dec, 20-21
Shanghai,
China Oct, 24-26
Hong Kong,
China Jun, 8-9
Pusan,
Koria July, 4-8
Taipei,
Taiwan Oct, 4-5
San Francisco,
USA Jan, 22-25
New York,
USA Apr, 7-11
Washington DC,
USA Mar, 15-19
Sept, 11-17
Oct, 31-Nov,7
Cebu City,
Philippines Nov, 20-
Jakarta,
Indnesia May, 17-
Ha Noi,
Vietnam Feb, 1-6
Kuala Lumpur,
Malaysia Sept, 30
Singapore,
Singapore Apr, 12-14
May, 9-11
14-17
Jun, 9
Sao Paulo,
Brazil Apr, 30-May5
Copyright(C) T-worldatlas All Rights Reserved

平成25年1月～平成25年12月　招待講演・特別講演

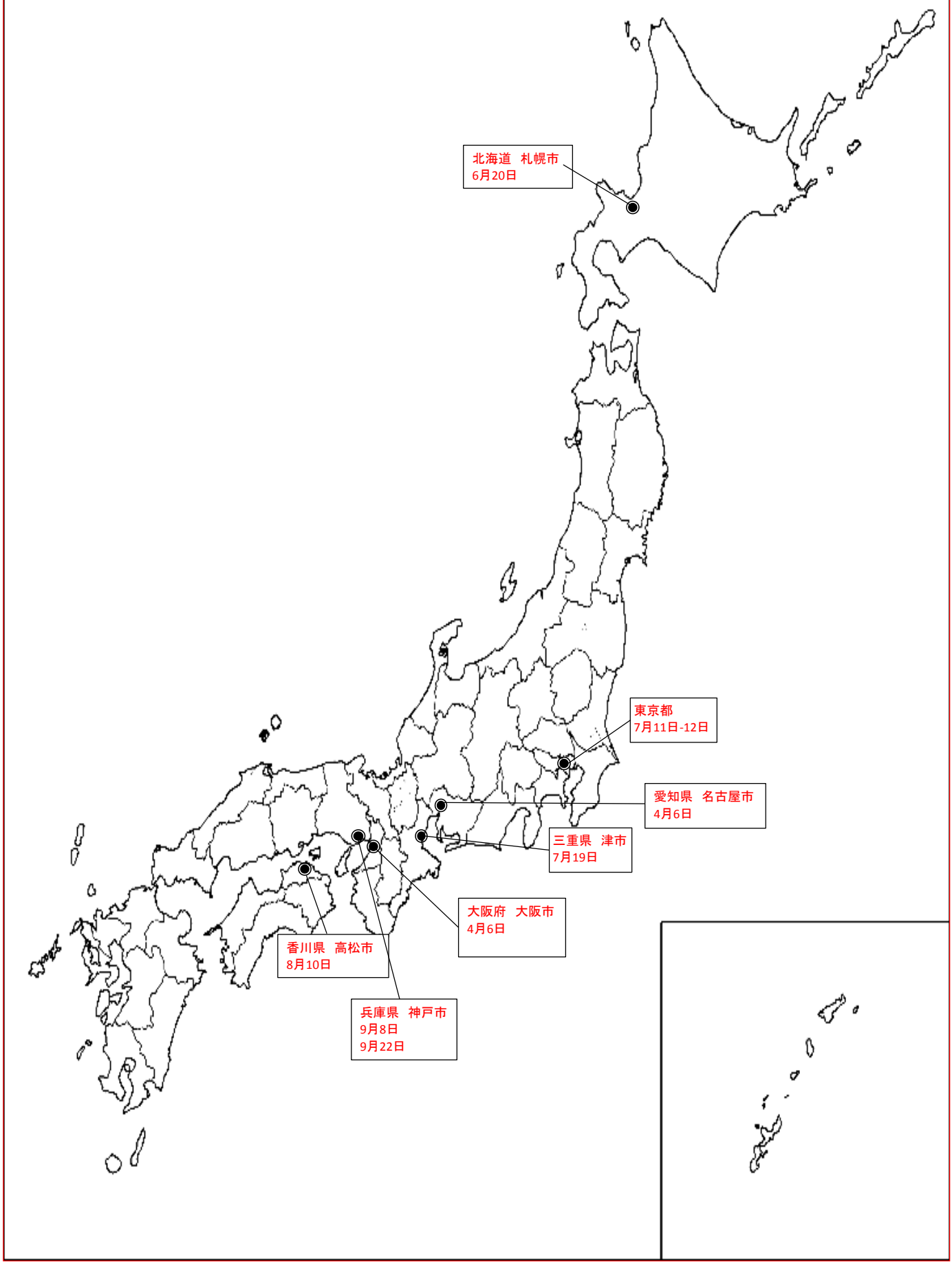

5. 留学生受け入れ

留学生の受け入れですが、1999 年から 2000 年にかけて中国上海から Ding Hong 先生（丁　紅）（上海医科大学)、2001 年には中国広州から Wen YL 先生（文　艶玲）（中山医科大学)、2002 年には中国広州から Zheng RQ 先生（鄭栄琴）（中山医科大学)、2003 年には中国重慶より Zhou Pei（周　佩）（人民解放軍重慶病院)、2004 年にはカンボジアより Ly Sokhey 先生、2005 年にはタイから Worawan Chinamnan 先生、同じく 2005 年に若干時期を違えてインドから Kaushal Madan 先生（All India Institute of Medical Science: AIIMS)、2007 年 Kunal Das 先生を受け入れました。2008 年 Yu Xia（北京、中国)、2009 年 Md. Nadiruzzaman（バングラディシュ)、2010 年 Lorenzo Andreana（イタリア）が来ていました。またエジプトから Alshimaa 先生も来られました。2011 年にはマレーシアから Hadzri 先生が来られましたし、またイタリア　ボローニャ大学からも Alberto 先生が来られました。2012 年 7 月 - 9 月には中国から Dr.Zhang Shuo も受け入れました。2013 年 10 月にはマレーシアから Chai Soon Ngiu 先生が来られました。このように毎年、留学生が日中友好協会、笹川財団や日本消化器病学会、日本超音波医学会のフェローシップ留学生あるいは自国での fund をもって私どもの教室を希望して頂き、受け入れてきました。また来年度以降も先生方にはご迷惑をお掛けするかと思いますが、これも国際交流、アジアや世界への日本の貢献、各々の英語力に磨きをかけるという意味で有益と思いますので何卒御理解・御協力のほどお願い申し上げます。

6. 人事について

冒頭でも述べましたが、2003 年までの入局者は毎年 5、6 名～12、13 名と大学内でも最も多くの入局者がおりましたが、2004 年に新臨床研修医制度が開始されてからの入局者、すなわち 2006 年の入局者は 2 名に留まり、2007 年の入局者も 1 名に留まりました。2008 年には 8 名もの入局者が入って来られました。2011 年は 3 名の研修医が入局し、2012 年にも 3 名が入局しました。反面、2-3 人の方が医局を離れました。従いまして依然、医局としての体制は大変厳しい状況にあります。このような状況の中で南大阪では大阪大学や大阪市大、和医大、奈良医大などがそれぞれの大学に人を引き上げているという状況のため、消化器内科医が激減し、南大阪の多くの公的病院では消化器内科医がほとんどゼロの状態が続いております。そのあおりで近医からの紹介患者や外来患者数は激増し、消化器内科の診療にも大きな負担がかかっております。しばらくはこのような状況が続くものと思われるますので、本学ならびに分院の奈良病院、堺病院ともに結束して一人でも多くの人に入局して頂き、教育・研究・診療を円滑に行っていきたいと考えております。

7. NPO 法人「日本肝がん臨床研究機構（Japan Liver Oncology Group)」の活動

1. **JLOG 0801 trial**「肝癌早期診断のための多施設共同無作為化比較試験（Sonazoid-Enhanced LivEr Cancer Trial　for　Early Detection

（SELECTED Study））」
→2012 年 10 月終了、現在データ解析中、学会および論文発表予定

2. **JLOG 0901 trial** 「進行・再発肝細胞癌に対する動注化学療法と分子標的薬併用による新規治療法の確立を目指した臨床試験（Phase III）ならびに効果を予測する biomarker の探索研究（Randomized Controlled Trial Comparing Efficacy of Sorafenib versus Sorafenib In combination with Low dose cisplatin/fluorouracil hepatic arterial InfUSion chemotherapy in Patients with Advanced Hepatocellular Carcinoma And Explolatory Study of Biomarker Predicting Its Efficacy (SILIUS Phase III trial)）」

→**2010 年より厚労科研に移行**（厚生労働省科学研究費補助金　厚生労働省科学研究費補助金事業研究班（がん臨床部門）平成 23 年度「進行・再発肝細胞癌に対する動注化学療法と分子標的薬併用による新規治療法の確立を目指した臨床試験（Phase III）ならびに効果を予測する biomarker の探索研究」（工藤班））→2013 年で終了

3. **JLOG 0902 trial**「早期肝癌診断における EOB-MRI の有用性に関する多施設共同研究（Diagnosis of Early LIver Cancer Through EOB-MRI(DELICATE Study)）」

4. **JLOG 1001 trial** 「切除不能肝細胞癌に対する肝動脈化学塞栓療法（TACE）とソラフェニブの併用療法第 II 相臨床試験（Phase II study: Transcatheter Arterial Chemoembolization Therapy In Combination with Sorafenib (TACTICS Study)）」

5. **JLOG 1002 trial**「慢性肝疾患における非侵襲的弾性検査法を用いた肝線維化評価予測に関する研究(Assessment of Liver FIBROsis by Real-time Tissue ELASTography in Chronic Liver Disease (FIBROELAST Study))」

→**2011 年より厚労科研に移行**（厚生労働省科学研究費補助金事業研究班（難病・がん等の疾患分野の医療の実用化部門）平成 23 年度「慢性ウイルス性肝疾患の非侵襲的線化評価法の開発と臨床的有用性の確立」（工藤班））

6. **JLOG 1003 trial**「非侵襲的弾性検査法を用いた肝線維化度評価によるウイルス性肝炎患者における肝発癌・門脈圧亢進症の発現予測（Prediction of Incidence of Liver Cancer or porTal Hypertension in Patients with Viral Hepatitis by Use of Real-time Tissue Elastography (PICTURE Study)）」

→**2011 年より厚労科研に移行**（厚生労働省科学研究費補助金事業研究班（難病・がん等の疾患分野の医療の実用化部門）平成 23 年度「慢性ウイルス性肝疾患の非侵襲的線化評価法の開発と臨床的有用性の確立」（工藤班））

7. **JLOG 1004 trial**「インスリン抵抗性を合併する C 型代償性肝硬変患者を対象とした BCAA 顆粒製剤の肝細胞癌抑制効果に関する第 III 相臨床試験（BCAA Granule for patients with Hepatitis C-related Liver Cirrhosis and Insulin Resistance On the Effect of Reduction of Carcinogenic RisK in the Liver(Phase III study)(BLOCK Study)）」

8. おわりに

この年報を作成にあたりましては例年の如く、教授秘書、医局秘書の秘書連合軍の 13 名の皆様に全面的に編集をして頂き大変感謝を致しております。また、医局員の皆様にも大変この一年お世話になりました。この一年間も大変なハードワークではありましたが、無事皆様の頑張りにより乗り切ることができました。この場をお借りして深く感謝申し上げます。2010 年には念願の一病棟まるまる消化器内科が占めるという状態が実現しましたし、腹部超音波室も拡充されました。2013 年 12 月には救急災害棟も完成いたしました。光学治療センターの拡充も終了しましたので何卒昨年以上にモチベーションを上げて頂いて日本一、あるいは世界一の消化器内科学教室へ育つようにご尽力頂きたいと思います。2014 年も教育・診療・研究において、特に英文論文、新しい研究の立ち上げということについては 2013 年以上に積極的に取り組んでいきたいと考えておりますので医局員全員が共通の価値観と消化器内科の将来の方向性に対するベクトルを共有し、心を一つにして邁進して頂きたいと祈念・期待しております。

2014 年 9 月　大阪狭山にて

2013 年度表彰式一覧

- Highest Impact Factor Award 2013(最高インパクトファクター賞)

1 位　櫻井俊治　　8.650（Cancer Res）
2 位　北野雅之　　7.553（Am J Gastroenterol）

※　3 位　西田直生志　3.730（Plos One）
※　工藤正俊　2.725（Digest Dis）

- Most Numbers of Paper Award 2013（最多英文論文発表賞）

1 位　西田直生志　6 本（Plos One, Oncology-Basel×2, Digest Dis×3）
2 位　南　康範　3 本（Digest Dis, Oncology-Basel, Gut Liver）
2 位　櫻井俊治　3 本（Cancer Res, Digest Dis, Liver Cancer）

※　工藤正俊　7 本

- Total Highest Impact Factor Award 2013（累積最高インパクトファクター賞）

1 位　西田直生志　16.235（6 本）
2 位　櫻井俊治　　11.375（3 本）

※　3 位　北野雅之　7.553（1 本）
※　工藤正俊　10.415（7 本）

- 最多入院受持患者賞

1 位　宮田　剛　217 人
2 位　矢田典久　203 人

※　3 位　足立哲平　184 人

- 最多緊急内視鏡賞

1 位　門阪薫平　72 件
2 位　大本俊介　64 件

※　3 位　田中梨絵　58 件

- 最多外来患者診療賞

1 位　北野雅之　2,190 人
2 位　松井繁長　2,171 人

※ 3 位　上嶋一臣　1,946 人
※ 工藤正俊　1,837 人

工藤正俊（くどうまさとし）

（平成 26 年 9 月 18 日更新）



昭和 29 年	愛媛県西条市生まれ
昭和 53 年	京都大学医学部 卒業
同	京都大学医学部附属病院 勤務（研修医）
昭和 54 年	神戸市立中央市民病院内科　勤務（研修医）
昭和 55 年	同　消化器内科　医員
昭和 60 年	同　消化器内科　副医長
昭和 62 年	カリフォルニア大学留学（デービスメデイカルセンター）
平成元年	神戸市立中央市民病院消化器内科　副医長　復職
平成　4 年	同　消化器内科　医長
平成　9 年	近畿大学医学部第２内科学　助教授
平成 11 年	近畿大学医学部消化器内科学 教授　現在に至る
（現在の併任）	近畿大学医学部附属病院病院長（平成 20 年 10 月～現在）
	近畿大学医学部中央臨床検査部長（平成 20 年 10 月～現在）
	近畿大学医学部光学治療センター長（平成 20 年 10 月～現在）
	近畿大学医学部高度先端医療センター長（平成 20 年 10 月～現在）
	近畿大学医学部 NICU 部長（平成 22 年 10 月～現在）
	近畿大学医学部附属病院救急災害センター長（平成 25 年 9 月 1 日～現在）
	近畿大学医学部奈良病院消化器・内分泌内科 教授（兼務）
	近畿大学医学部堺病院消化器科 教授（兼務）
	神戸市立中央市民病院消化器内科 顧問（兼務）

主な所属学会

日本消化器病学会（財団評議員・指導医・専門医）、日本肝臓学会（理事・指導医・専門医・国際委員会委員長）、日本消化器内視鏡学会（社団評議員・指導医・専門医・ネットワーク委員会委員）、日本超音波医学会（理事長・指導医・専門医・国際交流委員会委員長）、日本内科学会（評議員・認定内科医）、日本高齢消化器病学会（理事）, 日本核医学会（評議員・専門医）、日本肝癌研究会（常任幹事・追跡調査委員長・取扱規約委員・肝癌治療効果判定基準作成委員会委員長・事務局代表）、日本肝移植研究会（世話人）、肝血流動態イメージ研究会（幹事）、日本腹部造影エコー・ドプラ診断研究会（事務局・代表世話人）、肝癌治療シミュレーション研究会（副代表幹事・企画委員）、超音波治療研究会（常任世話人）、日本肝がん分子標的治療研究会（代表世話人・事務局代表）、日本消化器内視鏡財団（評議員）、日本臨床腫瘍学会（評議員・保険委員会委員（2013 年 4 月－現在））、日本癌学会（評議員）、米国肝臓学会（AASLD）（肝癌部門企画運営委員：Steering Committee of hepatobiliary malignancy）、米国消化器病学会（AGA）、世界肝臓学会 （IASL）、欧州肝臓学会（EASL）、米国消化器内視鏡学会（ASGE）など。

委員・資格など

- 世界超音波医学会（WFUMB）, Immediate Past President（前理事長）
- アジア超音波医学会（AFSUMB）Secretary（庶務担当理事）
- 国際肝癌学会（ILCA）理事（Founding Board Member, Governing Board Council Member）
- 米国肝臓学会（AASLD）肝癌部門運営委員会委員（Steering Committee Member）
- 日本肝がん臨床研究機構（JLOG）（理事長）
- 世界保健機構（WHO）Blue Book「Classification of the Tumor」改訂委員（平成 21 年 5 月 1 日）
- ウイルス肝炎研究財団　日米医学協力研究会肝炎専門部会研究員
- International Liver Thought Leadership Study (ILCS), Council member
- アジア太平洋肝癌専門家会議（APPLE）理事長（President）

- Editor-in-Chief: Liver Cancer (Karger, Basel)

受賞

- 米国核医学会 Berson-Yalow Award 受賞（平成元年 6 月）
- 日本対がん協会がん研究助成奨励賞 受賞（平成 4 年 3 月）
- 日本消化器病学会奨励賞 受賞（平成 4 年 4 月）
- 日本核医学会賞 受賞（平成 5 年 10 月）
- 米国超音波医学会（AIUM）学会賞受賞（平成 15 年 6 月 4 日）
- ボローニャ大学医学部医学会名誉会員賞（平成 18 年 9 月 15 日）
- フィリピン超音波医学会名誉会員（Honorary Member of PSUCMI）（平成 20 年 3 月 19 日）
- アジア太平洋消化器病学会（APDW）OKUDA Award 受賞（平成 20 年 9 月 13 日）
- 北米放射線学会 Certificate of Merit 受賞（平成 20 年）
- インド肝臓学会 Madangopalan Award 受賞（平成 21 年 3 月 28 日）
- 北米放射線学会 Cum Laude 賞受賞（平成 21 年 12 月）（7000 編の論文中上位 10 編に採択）
- 日本肝臓学会「日本肝臓学会機関誌 Highest Citation 賞」受賞（平成 22 年 6 月）
- JISAN Lecture Award Presented by Korean Society of Ultrasound in Medicine（平成 22 年 5 月）
- 米国超音波医学会名誉会員賞（AIUM Honorary Member Award）受賞（平成 23 年 4 月）
- 韓国超音波医学会名誉会員賞（KSUM honorary Award）受賞（平成 23 年 5 月）
- 日本肝臓学会「日本肝臓学会機関誌 Highest Citation 賞」受賞（平成 23 年 6 月）（2 回目）
- Romanian Society of Ultrasound in Medicine and Biology（SRUMB）Honorary Award 受賞（平成 23 年 6 月）
- 北米放射線学会 Certificate of Merit 受賞（平成 23 年 11 月）（2 回目）
- USE 論文賞（応用物理学会論文賞）」受賞（平成 24 年 11 月）

著書（単著）

- Contrast Harmonic Imaging in the Diagnosis and Treatment of Liver Tumors （Springer-Verlag 2003）
- 肝腫瘍における造影ハーモニックイメージング（医学書院 2001）

編集

- 松井 修, **工藤正俊**,編集: 消化器疾患の造影エコーUp Date. 南江堂, 東京, 2003.
- **工藤正俊**, 編集: 肝細胞癌治療の最近の進歩, 消化器病セミナー97, へるす出版, 東京, 2004.
- 河田純男, 白鳥康史, **工藤正俊**, 榎本信幸, 編集, 小俣政男, 監修: 肝疾患 Review 2004, 日本メディカルセンター, 東京, 2004.
- 河田純男, 白鳥康史, **工藤正俊**, 榎本信幸, 編集, 小俣政男, 監修: 肝疾患 Review 2006-2007,日本メディカルセンター, 東京, 2006.
- 河田純男, 横須賀收, **工藤正俊**, 榎本信幸, 編集, 小俣政男, 監修: 肝疾患 Review 2008-2009, 日本メディカルセンター, 東京, 2008.
- 河田純男, 横須賀收, **工藤正俊**, 榎本信幸, 編集, 小俣政男, 監修: 肝疾患 Review 2010-2011, 日本メディカルセンター, 東京, 2010.
- 幕内雅敏, 菅野健太郎, **工藤正俊**, 編集: 今日の消化器疾患治療指針 第 3 版, 医学書院, 東京, 2010.
- **工藤正俊**, 泉 並木, 編集: 症例から学ぶ ウイルス肝炎の治療戦略. （株）診断と治療社, 東京, 2010.
- **工藤正俊**, 編集: 肝細胞癌の分子標的治療, アークメディア, 東京, 2010.
- 山雄健次, **工藤正俊**, 編集: 見逃し、誤りを防ぐ!肝・胆・膵癌画像診断アトラス, 羊土社, 東京, 2010.
- **工藤正俊**, 編集: 医学のあゆみ「肝癌の分子標的治療」, 医歯薬出版株式会社, 東京, 2011.
- **工藤正俊**, 編集:「肝細胞がん診療の進歩: Up-To-Data」,最新医学社, 大阪, 2011.
- **工藤正俊**, 編集: 朝倉内科学, 矢崎義雄,「総編集」, 朝倉書店, 東京, 2013.
- **工藤正俊**,國分茂博,編集：EOB-MRI/ソナゾイド造影超音波による肝癌の診断と治療,医学書院,東京,2013

EDITER-IN－CHIEF: Liver Cancer (Basel), World J Hepatology (China)

Associate Editor: Journal of Oncology (Germany),肝胆膵（アークメディア））

EDITORIAL BOARD:

国際学術雑誌: International Journal of Clinical Oncology (Tokyo) Ultrasound in Medicine and Biology (ELSEVIER, New York) Hepatology International (Springer, New York) Liver International (Blackwell, UK) World Journal of Gastroneterology Liver Cancer Review Letters

国内学術雑誌: 肝胆膵、肝胆膵の臨床、その他の学会誌 (3)

論文査読委員

J Clin Oncol(18.832), Lancet Oncol (22.589), Gastroenterology(11.675), Hepatology(11.665), J

Hepatol(9.264), Oncologist(3.910), Am J Gastroenterol(7.282), Endoscopy(5.210), Clin Exp Metastas(4.113), Cancer Sci(3.846) , Expert Rev Mol Diagn(4.652) , Eur Radiol(3.594) , Liver Int(3.840), J Gastroenterol(4.160) , Eur J Clin Invest(2.736), J Nucl Med(6.381), J Gastroen Hepatol(2.410), Oncology-Basel (International Journal of Cancer Research and Treatment)(2.538), Ultrasound Med Biol(2.493) , Acta Paediatr(1.955), Hepatol Int(2.963) , Eur J Gastroen Hepat (1.598) , J Hepato-Bil-Pan Scu (1.963), Hepatol Res(1.857), Int J Clin Oncol(1.437), Jpn J Clin Oncol(1.856), Internal Med(1.037), J Clin Ultrasound(0.808), Biomark Med(1.247), Hepato-Gastroenterol(0.677), Ann Nucl Med(1.386), Expert Review of Anticancer Treatment(0), J Cancer Res Ther (0.825), CSR National Registry(0), J Gastrointest Liver (1.434), Cancer Informatics(0), Expert Review of Proteomics and Future Oncology(0)

SIENTIFIC PAPER PUBLICATION:

学術論文	英文論文: 526 (IF: 1829.628)	
	和文論文: 806	
教科書 (単著)	英文: 2	和文: 6
分担執筆	英文: 21	和文: 246

特別講演・招待講演・教育講演:

国際学会: 310
国内学会: 624

科学研究費等外部資金の獲得状況

- 文部科学省科学研究費補助金　基盤研究(A)　2 件（総額 1,100 万円）
  基盤研究(B)　6 件（総額 2,311 万円）
  基盤研究(C)　12 件（総額 1,240 万円）
  挑戦的萌芽研究　3 件（総額　310 万円）
  （主任研究者）　（　260 万円）
  「肝細胞癌の発癌・進展の分子機序: 造影超音波クッパー相と遺伝子発現を用いた融合解析」
  （分担研究者）　（　50 万円）
  「肝細胞癌のソラフェニブ著効例における感受性規定遺伝子変異の探索」（主任研究者　西尾和人）
- 知的クラスター創生事業（がんペプチドワクチン）　1 件（総額　10 万円）
- 車両財団がん研究助成金　1 件（総額　100 万円）
- 学会奨励研究補助金　6 件（総額　530 万円）
- 医師会・民間医学振興財団等研究補助金　32 件（総額 2,089 万 5 千円）
- 国立がん研究センターがん研究開発費（分担研究者）　（　245 万円）
  「抗悪性腫瘍薬による肝炎ウイルス再活性化の調査とその対応に関する研究」（班長　池田公史）
- 国立がん研究センターがん研究開発費（分担研究者）　（　12 万円）
  「進行肝胆膵がんの治療法の開発に関する研究」（班長　奥坂拓志）
- 厚生労働省科学研究費　**主任研究者**　5 件（総額 2 億 2,375 万円）
  1. （がん臨床研究事業）
  「進行・再発肝細胞癌に対する動注化学療法と分子標的薬併用による新規治療法の確立を目指した臨床試験（Phase III）ならびに効果を予測する biomarker の探索研究」
  2. （難病・がん等の疾患分野の医療の実用化研究事業）
  「慢性ウイルス性肝疾患の非侵襲的線化評価法の開発と臨床的有用性の確立」
- 厚生労働省科学研究費　**分担研究者**　29 件（総額 3,325 万円）
  1. （肝炎等克服緊急対策研究事業）
  「血小板低値例へのインターフェロン治療法の確立を目指した基礎および臨床的研究」（班長　西口修平）
  2. （がん臨床研究事業）
  「初発肝細胞癌に対する肝切除とラジオ波焼灼両方の有効性に関する多施設共同研究」（班長　國土典宏）
  3. （肝炎等克服緊急対策研究事業）
  「肝がんの新規治療法に関する研究」（班長　本多政夫）
  4. （難治性疾患克服研究事業）
  「多発肝のう胞症に対する治療ガイドライン作成と試料バンクの構築」（班長　大河内信弘）
  5. （難病・がん等の疾患分野の医療の実用化研究事業）
  「慢性ウイルス性肝疾患患者の情報収集の在り方等に関する研究」（班長　相崎英樹）

ガイドライン策定委員会委員

- 「科学的根拠に基づく肝癌診療ガイドライン」（日本肝臓学会編），金原出版
- 「慢性肝炎の治療ガイドライン」（日本肝臓学会編），文光堂
- 「肝癌診療マニュアル」（日本肝臓学会編），医学書院
- 「肝癌治療効果判定基準」（日本肝癌研究会取扱い規約委員会編），肝臓
- 臨床病理「肝癌取り扱い規約」（日本肝癌研究会編）
- Clinical Practice Guidelines for Hepatocellular Carcinoma, Japan Society of Hepatology, Hepatology Research
- General Rules for the Clinical and Pathological Study of Primary Liver Cancer, 3rd English Version, Liver Cancer Study Group of Japan, Kanehara, Tokyo, 2010
- Response Evaluation criteria in the Cancer of the Liver (RECICL), Liver Cancer Study Group of Japan, Hepatology Research
- 「多発肝のう胞症に対する治療ガイドライン」

特許取得

発明の名称：　ソラフェニブの効果予測方法
出願番号：　特願 2011-104275
出願日：　2011 年 5 月 9 日
発明者：　荒尾徳三、松本和子、西尾和人、工藤正俊
出願人：　学校法人近畿大学

発明の名称：　N 型糖鎖を利用した膵臓癌の診断方法
公開番号：　特許公開 2009-270996
公開日：　2009 年 11 月 19 日
発明者：　荒尾徳三、松本和子、西尾和人、坂本洋城、北野雅之、工藤正俊
出願人：　住友ベークライト株式会社

全国規模の学会・研究会事務局

- 日本肝癌研究会（**事務局・追跡調査委員長・常任幹事**）
- 日本腹部造影エコー・ドプラ診断研究会（**代表世話人・事務局**）
- NPO 法人日本肝がん臨床研究機構（**理事長・事務局**）
- 日本肝がん分子標的治療研究会（**代表世話人・事務局**）

全国規模の研究会世話人・役員

平成 6 年 4 月–8 年 3 月	日本超音波医学会腹部造影エコー研究部会幹事
平成 7 年 11 月–現在	肝血流動態イメージ研究会世話人
平成 8 年 4 月–現在	日本腹部造影エコー・ドプラ造影研究会世話人（事務局兼務）（平成 25 年より代表世話人）
平成 9 年 7 月–現在	肝動脈塞栓療法研究会世話人
平成 10 年–現在	国際造影超音波研究会（現、Asia Contrast Ultrasound Imaging Society）世話人
平成 11 年 10 月–現在	臨床消化器病研究会世話人
平成 11 年 7 月–現在	西日本肝臓研究会世話人
平成 13 年 5 月–現在	肝疾患フォーラム世話人
平成 14 年 4 月—現在	犬山シンポジウム会員
平成 14 年 9 月–現在	日本消化器画像診断研究会世話人
平成 16 年–現在	Liver Forum in Kyoto 世話人
平成 18 年–現在	肝癌治療シミュレーション研究会副代表幹事
平成 19 年 11 月–現在	日本超音波治療研究会常任世話人
平成 20 年–現在	日本肝がん分子標的治療研究会（代表世話人）

関西地区研究会代表世話人

・平成 11 年–平成 19 年	関西造影超音波研究会（代表世話人）
・平成 13 年–現在	関西 B 型肝炎研究会（代表世話人）
・平成 14 年–現在	肝癌局所治療研究会（代表世話人）
・平成 14 年–現在	大阪消化器化学療法懇話会（代表世話人）
・平成 15 年–現在	臨床消化器病フォーラム（代表世話人）
・平成 18 年–平成 22 年	Bay Area Gut Club（代表世話人）
・平成 18 年–平成 22 年	South Osaka Liver Club（代表世話人）
・平成 19 年–現在	関西肝血流動態イメージ研究会（代表世話人）

・平成 20 年-現在　　Kinki Liver Club（**代表世話人**）
・平成 21 年-現在　　南大阪肝疾患研究会（**代表世話人**）
・平成 21 年-現在　　南大阪肝胆膵疾患研究会（**代表世話人**）

関西地区研究会世話人

・平成 2 年-現在　　大阪肝穿刺生検治療研究会世話人
・平成 6 年-現在　　兵庫インターベンショナルラディオロジー研究会世話人
・平成 8 年-現在　　肝胆膵治療フォーラム・神戸世話人
・平成 9 年-現在　　京都肝疾患懇話会世話人
・平成 9 年-現在　　肝臓分子生物学研究会
・平成 11 年-平成 18 年　肝代謝コロキウム世話人
・平成 11 年-現在　　大阪肝胆膵懇話会世話人
・平成 11 年-現在　　南大阪肝胆膵疾患研究会世話人
・平成 11 年-現在　　南大阪消化器病懇話会世話人
・平成 11 年-現在　　南大阪肝疾患研究会世話人
・平成 11 年-平成 24 年　消化器ラウンドテーブルディスカッション世話人
・平成 11 年-平成 18 年　泉州肝臓病研究会世話人
・平成 11 年-平成 18 年　大阪肝炎ミーティング世話人
・平成 12 年-現在　　大阪肝臓病談話会世話人
・平成 12 年-現在　　関西経皮内視鏡的胃瘻造設術研究会世話人
・平成 12 年-現在　　肝疾患座談会 in Kyoto 世話人
・平成 12 年-現在　　近畿肝癌談話会常任幹事
・平成 13 年-現在　　関西肝血流動態イメージ研究会世話人
・平成 16 年-平成 23 年　あおい肝臓研究会世話人
・平成 18 年-現在　　大阪肝臓ミーティング世話人
・平成 19 年-現在　　近畿・超音波内視鏡研究会顧問

全国規模の国内研究会主催（会長）

・1997 年 2 月　　第 3 回肝血流動態イメージ研究会（神戸）
・1996 年 10 月　　第 1 回日本造影エコードプラ診断研究会（神戸）
・2005 年 2 月　　第 11 回肝血流動態イメージ研究会（横浜）
・2007 年 9 月　　第 2 回肝癌治療シミュレーション研究会（大阪）
・2008 年 9 月　　第 49 回日本消化器画像診断研究会（大阪）
・2010 年 1 月　　第 1 回日本肝癌分子標的治療研究会（神戸）
・2014 年 2 月　　第 20 回肝血流動態・機能イメージ研究会（大阪）（予定）

国内学会主催（会長）

・第 45 回日本肝臓学会総会（2009 年 6 月）,神戸
・第 83 回日本超音波医学会学術集会（2010 年 5 月）,京都
・第 50 回日本肝癌研究会（2014 年 6 月）,京都
・第 89 回日本超音波医学会学術集会（2016 年 5 月）,京都（予定）

近畿地区学会主催（会長）

・第 82 回日本消化器内視鏡学会近畿支部例会（2009 年 8 月）
・第 95 回日本消化器病学会近畿支部例会（2011 年 8 月）

国際学会主催（会長）

・JSH Single Topic Conference on HCC (2005年), Awaji-shima
・The 3rd International Kobe Liver Cancer Symposium on HCC (IKLS) (2009年6月), Kobe
・The 2nd Asia Pacific Primary Liver Cancer Expert Meeting (APPLE)(2011年7月), Osaka
・The 14th WFUMB 2013(世界超音波医学会)(2013年5月), Sao Paulo(Co-President with Leandro Fernandez and Giovanni Guido Cerri)
・The 4th International Kyoto Liver Cancer Symposium(IKLS) (2014年6月6-7日),Kyoto
・the 8th International Liver Cancer Association (ILCA) (国際肝癌学会) (2014年9月5日-7日),Kyoto (Co-President with Peter Galle)
・The 6th Asia Pacific Primary Liver Cancer Expert Meeting (APPLE)(2015年7月),Osaka(予定)
・AFSUMB 2016 (アジア超音波医学会)　(2016年5月),Kyoto (予定)

消化器内科学教室業績抜粋

参考までに

	1999	2000	2001	2002	2003	2004	2005	2006	2007	2008		2009	2010	2011	2012	2013	2014	計
英文論文 （著書・分担執筆を含む） （Impact Factor）	8 44.626	12 38.663	27 62.069	13 19.776	22 53.353	21 73.701	25 63.245	15 39.819	31 96.273	45 146.061	英文論文 （著書・分担執筆を含む） （Impact Factor）	26 98.7	51 124.732	48 146.139	46 170.726	55 211.257	76 314.275	521 1389. 14
英文論文 （著書・分担執筆）	1	1	4	0	1	1	0	0	0	2	英文論文 （著書・分担執筆）	0	1	0	2	0		13
和文論文 （著書・分担執筆を含む）	37	41	43	34	31	54	45	39	46	73	和文論文 （著書・分担執筆を含む）	81	130	65	54	24		443
海外学会発表	2	9	4	6	24	23	14	14	17	26	海外学会発表	20	35	66	52	36		139
国内学会発表	46	59	71	114	107	81	70	52	77	89	国内学会発表	64	96	102	62	120		766
海外特別講演	0	11	4	11	8	18	16	25	18	36	海外特別講演	34	43	35	35	49		147
国内特別講演	37	40	40	52	37	38	39	27	38	40	国内特別講演	64	93	75	60	56		388
単著教科書			1		1 （英文）						単著教科書							2

近畿大学医学部消化器内科　英文論文総数（497編）

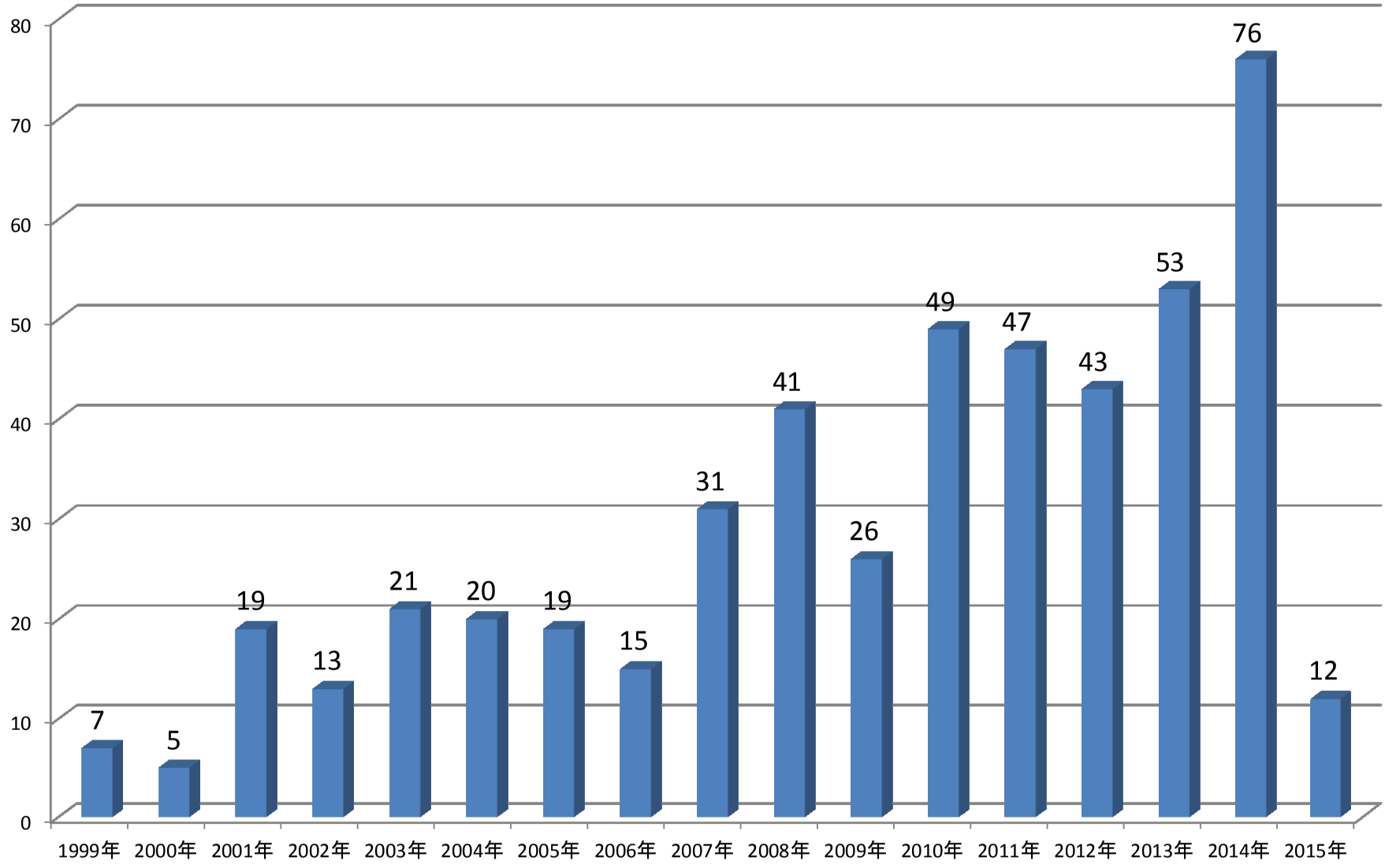

近畿大学医学部消化器内科　英文論文　Impact Factor総数
（IF=1677.163）

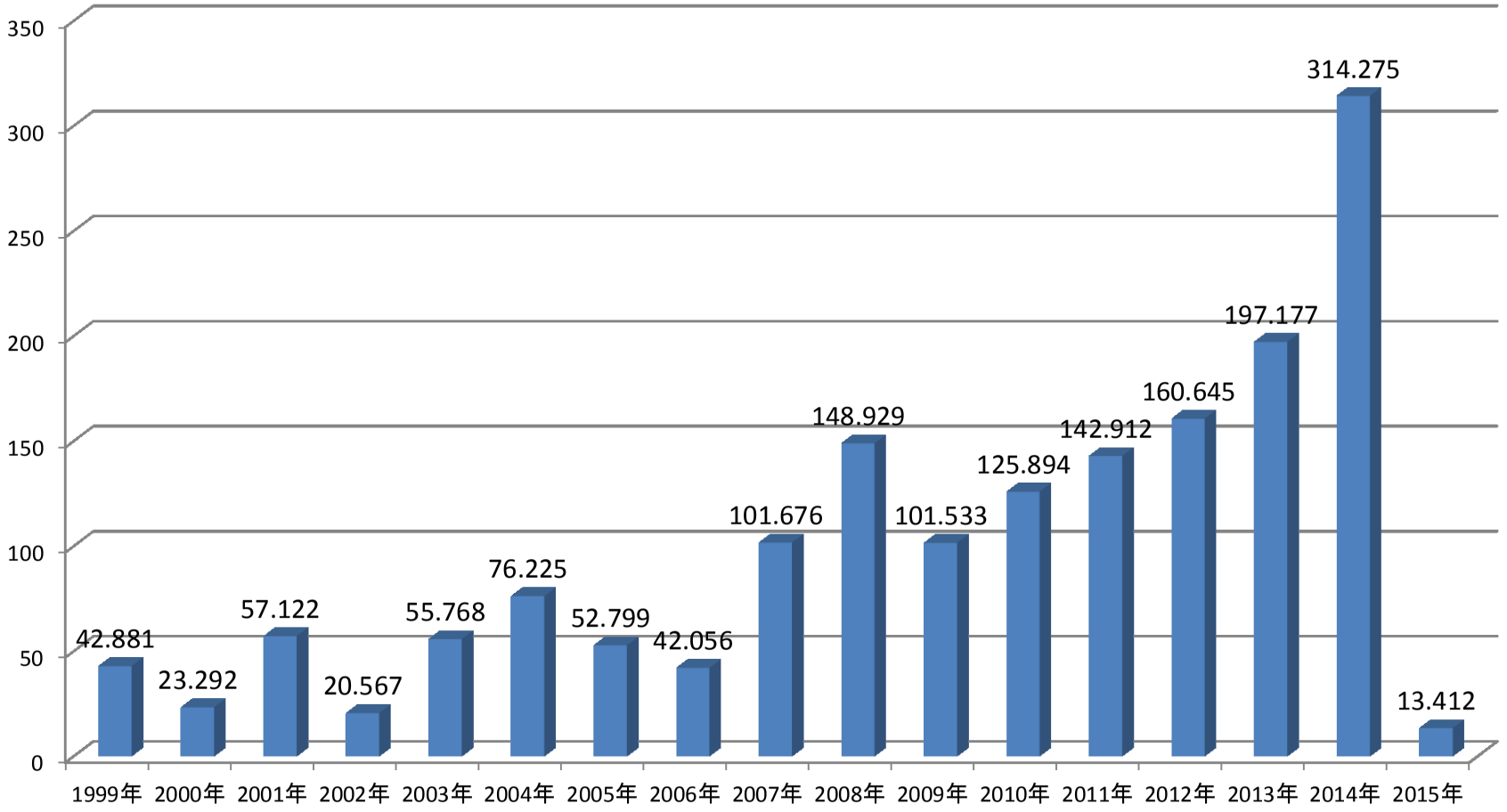

消化器内科年度別診療実績

	H11	H12	H13	H14	H15	H16	H17	H18	H19	H20	H21	H22	H23	H24	H25
稼働床	40	44	44	44	60	78	78	77	76	73	85	84	84	84	80
稼働率	107.2%	98.5%	126.7%	148.2%	121.0%	89.5%	95.3%	89.2%	94.7%	96.3%	91.8%	89.9%	85.8%	89.0%	93.0%
日平均入院患者数	40.0	43.3	55.8	65.2	72.6	69.8	74.4	68.7	72.0	70.3	70.3	76.1	72.0	74.7	77.7
平均在院日数	31.1	25.6	21.4	18.6	15.4	14.7	12.8	10.7	10.5	9.6	9	8.6	7.9	7.2	7.2
年間入院収入	501,570,188	570,616,464	801,199,124	923,171,333	1,065,481,449	1,023,271,279	1,152,778,111	1,106,484,453	1,224,122,968	1,244,806,271	1,312,812,506	1,516,925,835	1,417,104,402	1,535,069,456	1,587,632,536
年間外来収入	314,641,639	334,517,979	386,084,329	530,035,297	635,562,806	649,876,475	818,049,485	966,247,389	1,013,910,559	1,257,804,553	1,432,350,698	1,464,645,183	1,529,385,181	1,610,826,432	1,626,442,898
消化器内科年間収入	816,211,827	905,134,443	1,187,283,453	1,453,206,630	1,701,044,255	1,673,147,754	1,970,827,596	2,072,731,842	2,238,033,527	2,502,610,824	2,745,163,204	2,981,571,018	2,946,489,583	3,145,895,888	3,214,075,434

消化器内科年間入院収入

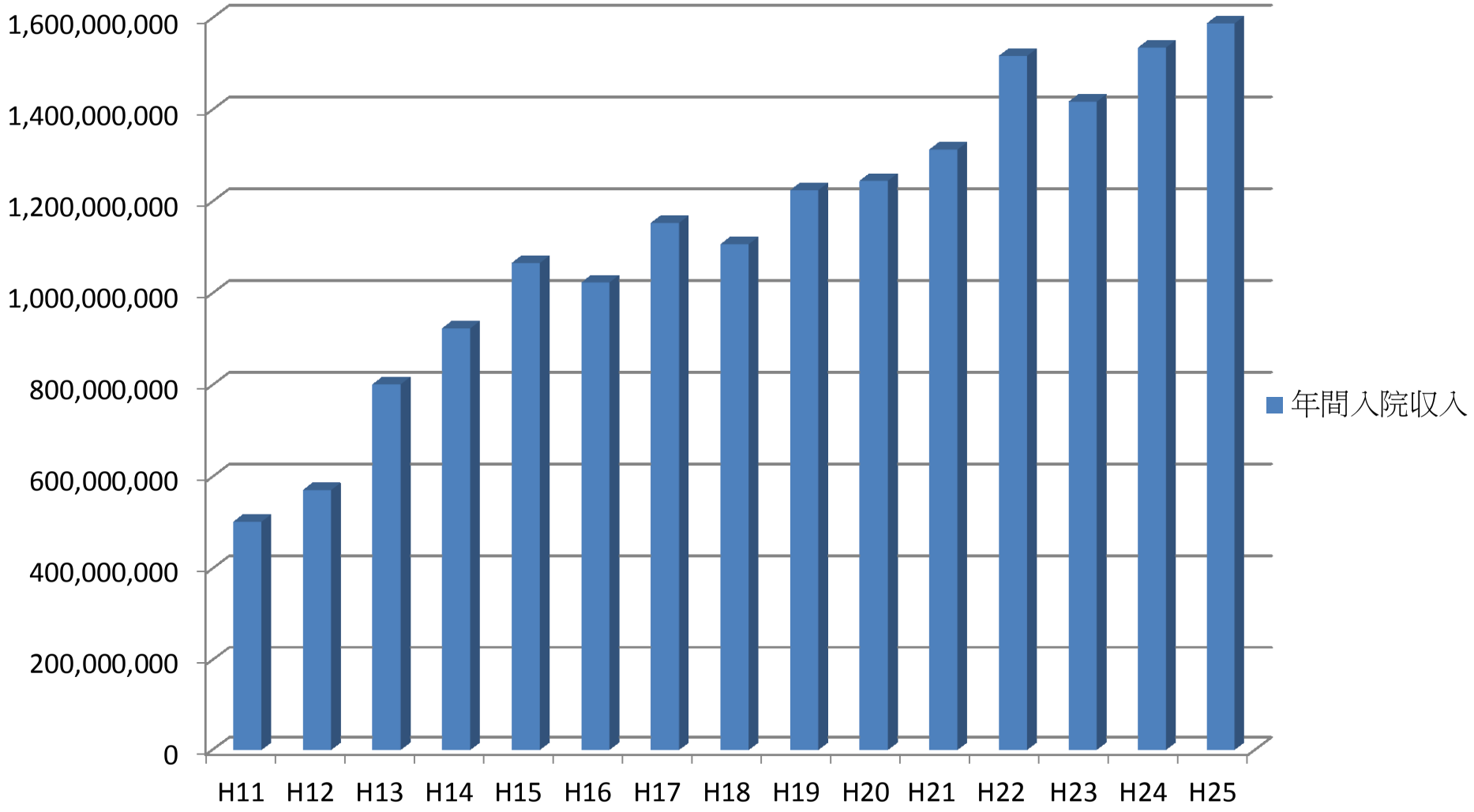

消化器内科入院診療実績

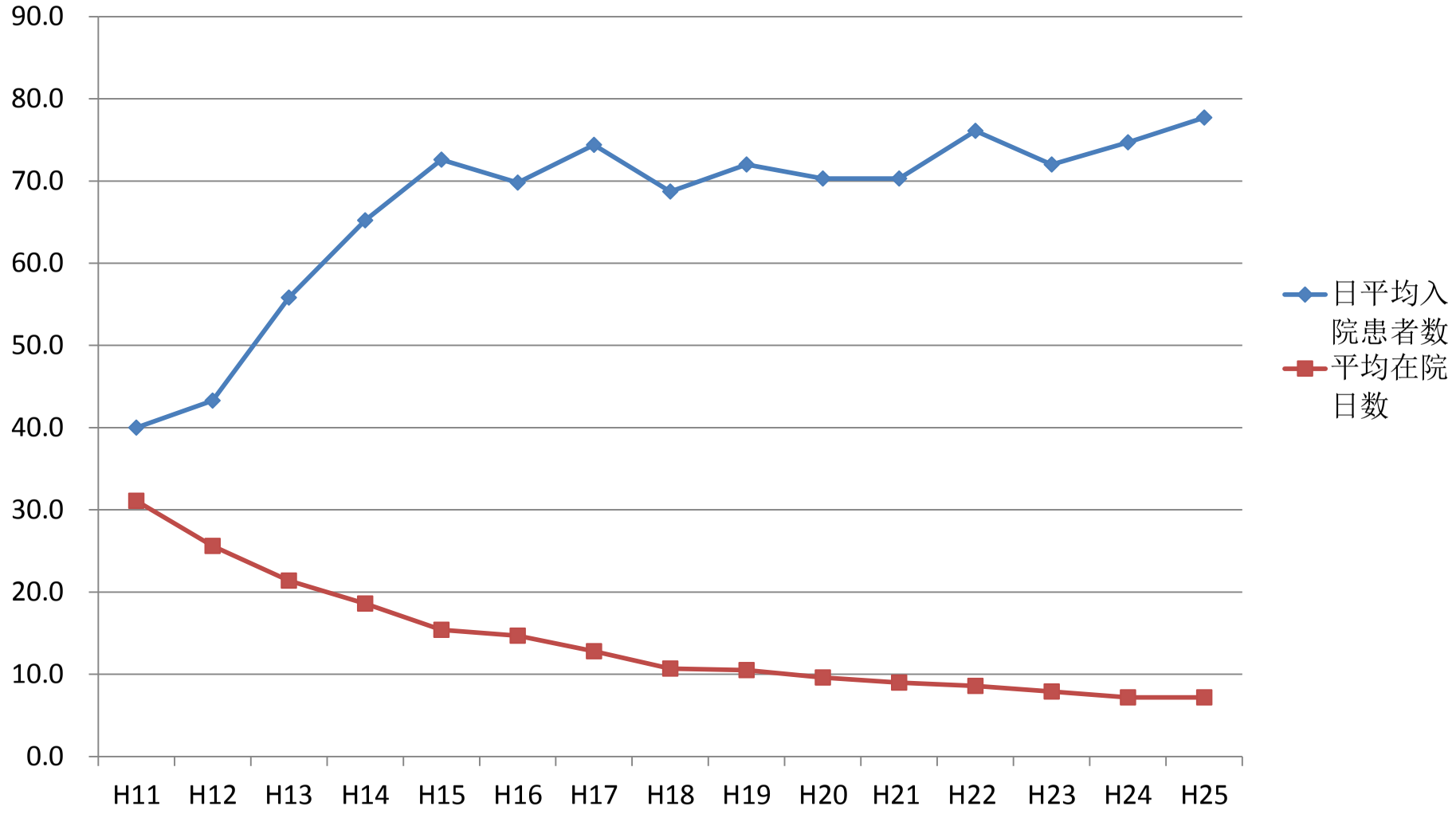

消化器内科年間外来収入

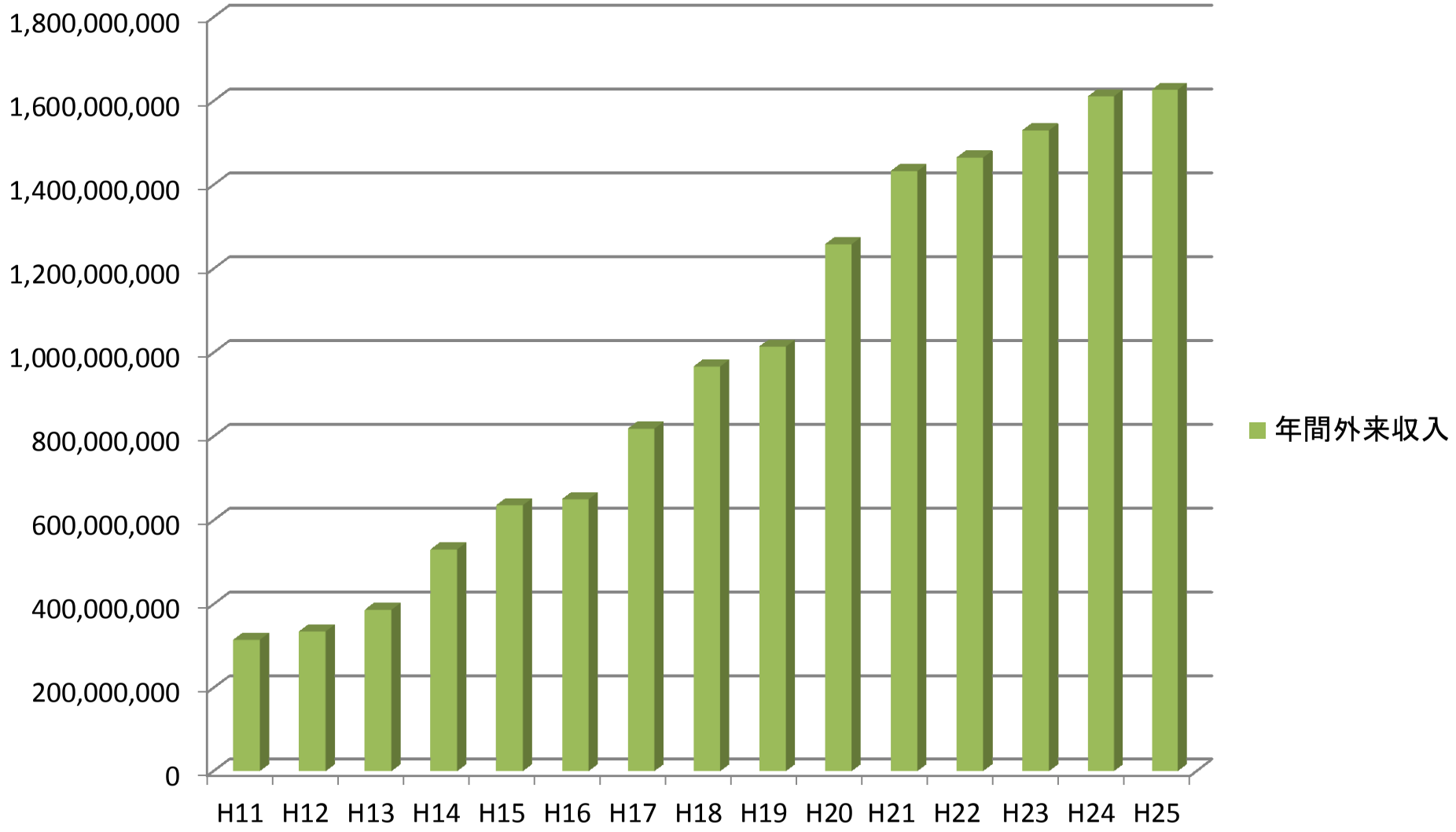

消化器内科年間総収入

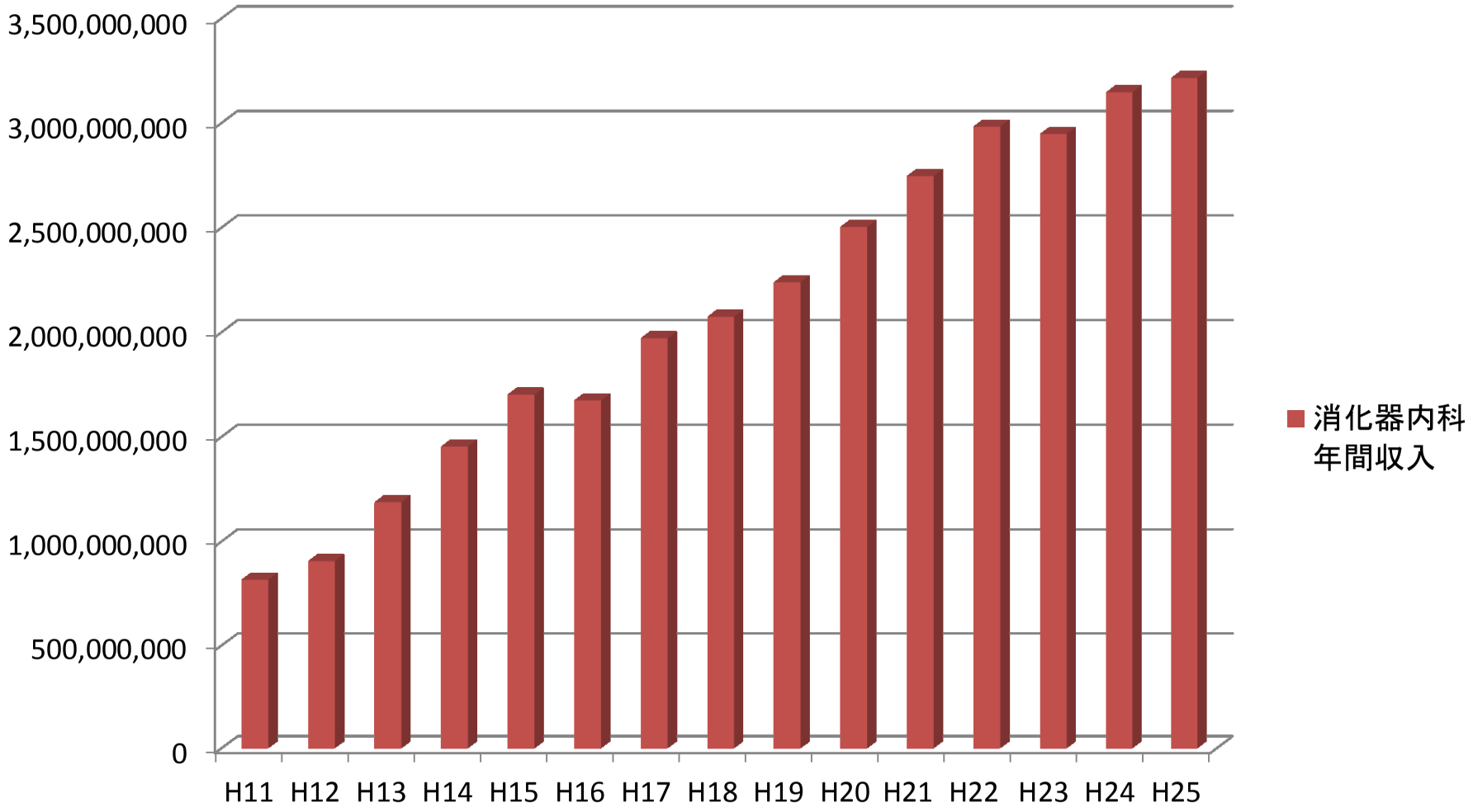
3,500,000,000
3,000,000,000
2,500,000,000
2,000,000,000
1,500,000,000
1,000,000,000
500,000,000
0
H11
H12
H13
H14
H15
H16
H17
H18
H19
H20
H21
H22
H23
H24
H25
消化器内科
年間収入

経皮的局所治療･肝生検総件数

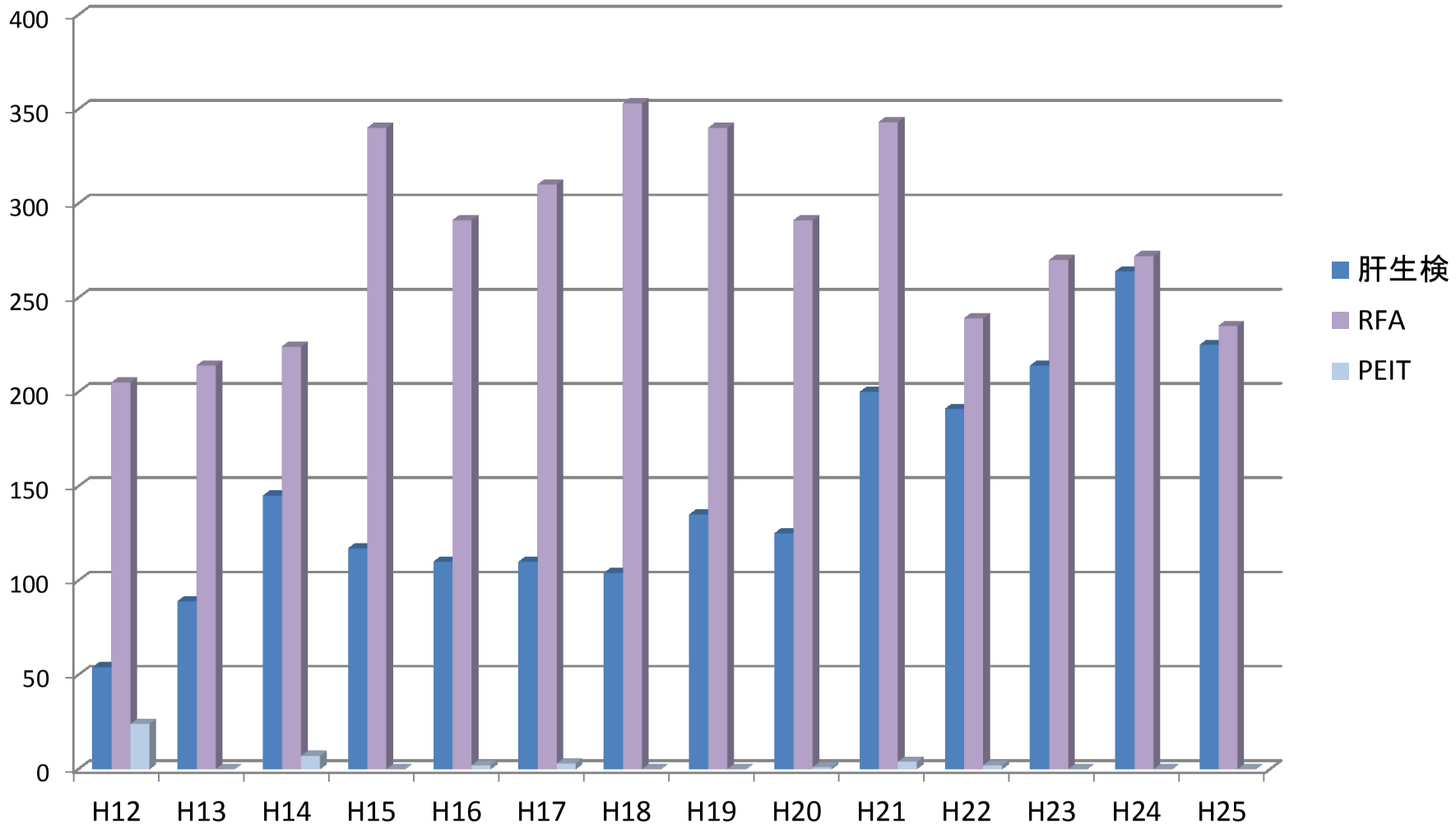

腹部造影エコー検査

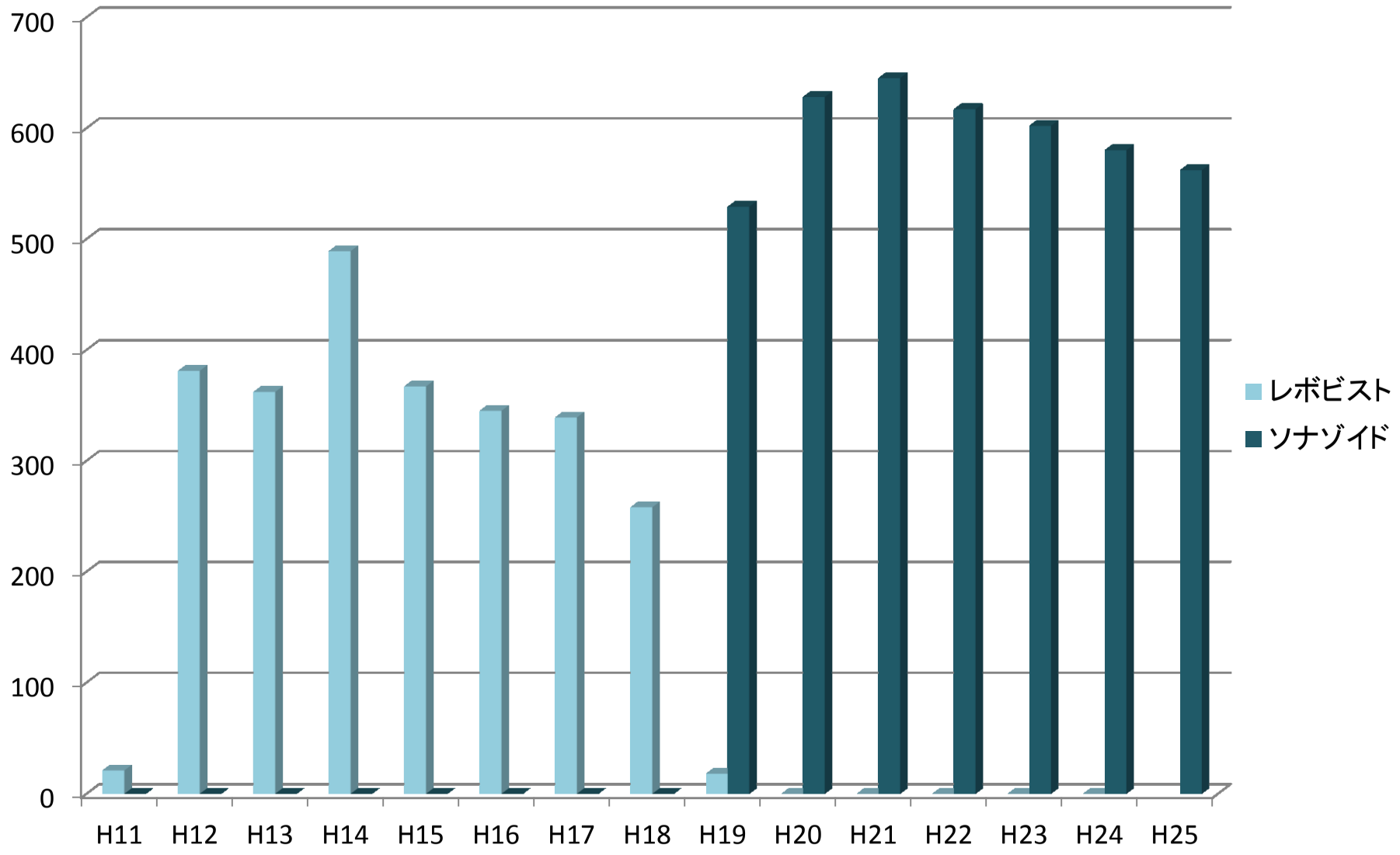
700
600
500
400
300
200
100
0
H11
H12
H13
H14
H15
H16
H17
H18
H19
H20
H21
H22
H23
H24
H25
レボビスト
ソナゾイド

内視鏡部年報

検査	H11	H12	H13	H14	H15	H16	H17	H18	H19	H20	H21	H22	H23	H24	H25
胃・十二指腸ファイバー球部	4032	4318	4434	4780	4926	5208	5453	5934	6534	6588	6742	7215	7640	8205	8831
乳頭部・肛側	165	160	187	181	263	254	327	316	373	365	482	520	441	462	533
大腸ファイバースコピー	1537	1479	1433	1648	1883	1947	2175	2548	2796	2904	2754	2934	3047	3320	3699
気管支ファイバースコピー	420	412	376	429	428	434	445	417	426	450	475	558	561	537	430
小腸ファイバースコピー	1	0	3	3	0	0	4	0	37	75	62	63	81	110	87
計（スクリーニング）	6155	6369	6433	7041	7500	7843	8404	9215	10166	10382	10515	11290	11770	12634	13580
胃生検	1509	1650	1851	1908	2005	2101	2473	2533	2412	2261	2175	2134	2095	2066	2195
大腸生検	1028	970	831	829	861	869	952	1143	1088	987	932	1001	946	1027	1107
気管支生検	245	222	227	265	260	296	281	314	302	314	345	393	371	338	304
小腸生検	1	0	0	2	0	0	1	0	11	8	12	18	17	27	35
計	2783	2842	2909	3004	3126	3266	3707	3990	3813	3570	3464	3546	3429	3458	3641
胆道ドレナージ	43	43	60	66	121	96	151	122	141	142	234	225	169	167	250
乳頭切開	15	19	14	11	44	44	46	44	48	46	74	132	102	102	112
乳頭バルーン拡張術	0	6	8	2	1	0	9	11	13	5	5	9	4	0	0
結石除去	16	24	15	17	38	49	55	51	62	65	86	130	87	95	96
食道静脈瘤結紮術	72	79	51	62	97	100	75	58	81	83	62	69	78	68	51
硬化療法	2	9	13	13	23	12	7	4	5	12	11	7	14	11	3
EISL	-	22	52	56	47	54	40	27	22	11	26	31	36	21	32
食道ブジー	116	137	124	152	210	308	252	246	234	308	284	269	256	213	186
APC	6	8	22	23	25	32	24	52	72	65	68	32	33	31	-
異物除去	6	2	3	11	14	17	14	11	18	21	14	20	22	21	33
胃ポリペクトミー	12	18	18	16	7	12	9	1	2	0	1	2	4	2	1
大腸ポリペクトミー	257	300	296	344	397	111	89	66	41	20	22	42	37	74	46
EMR（胃・食道）	27	24	64	73	70	73	90	100	52	127	52	39	143	208	200
ESD(胃・食道)	-	-	-	-	36	32	52	51	71	82	98	109	110	167	143
ＥＭＲ（大腸）	-	-	-	-	-	290	373	470	443	458	467	484	476	556	680
緊急内視鏡検査	84	114	135	291	425	485	487	337	265	192	272	308	330	232	1007
凝固止血バイポーラ	35	48	50	91	91	68	89	52	51	32	63	63	81	117	209
色素撒布法	216	291	459	724	1194	1470	1582	1909	1753	1731	1891	1937	2013	2171	2797
トロンビン被覆療法	81	88	113	193	198	236	294	369	387	319	326	282	332	335	312
アルト被覆療法	41	41	52	97	91	96	180	161	190	144	182	130	133	178	-
経皮内視鏡的胃瘻造設術	-	14	18	10	15	23	33	28	54	33	69	74	87	74	59
超音波内視鏡（胃）	48	77	181	170	205	249	293	379	505	523	622	895	989	1346	1460
超音波内視鏡（大腸）	-	17	28	6	8	5	5	0	1	0	1	0	4	9	8
計	1077	1381	1776	2428	3357	3836	4203	4498	4511	4419	4930	5289	5430	6031	7542

消化管内視鏡検査件数年次推移

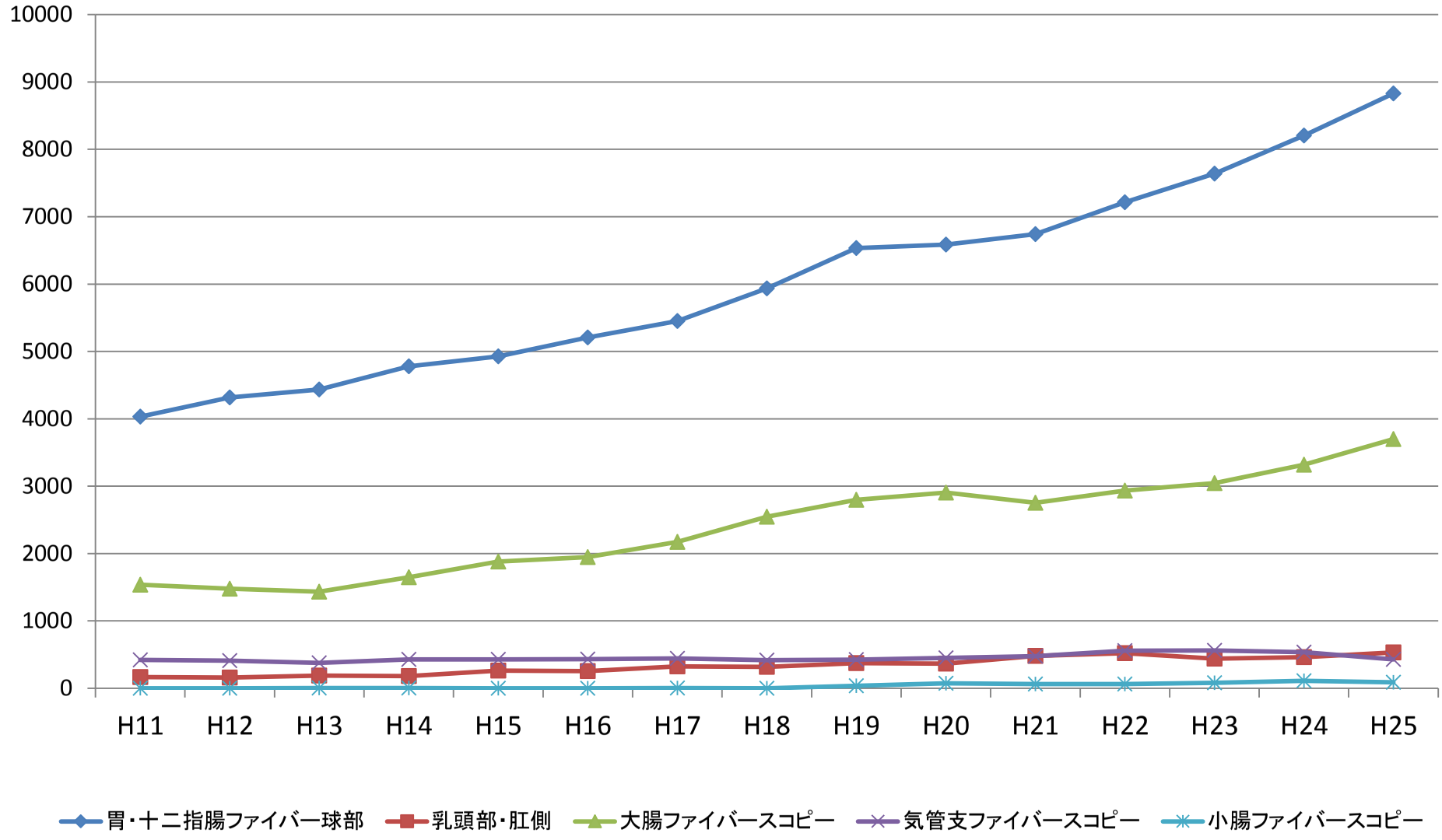

緊急内視鏡検査

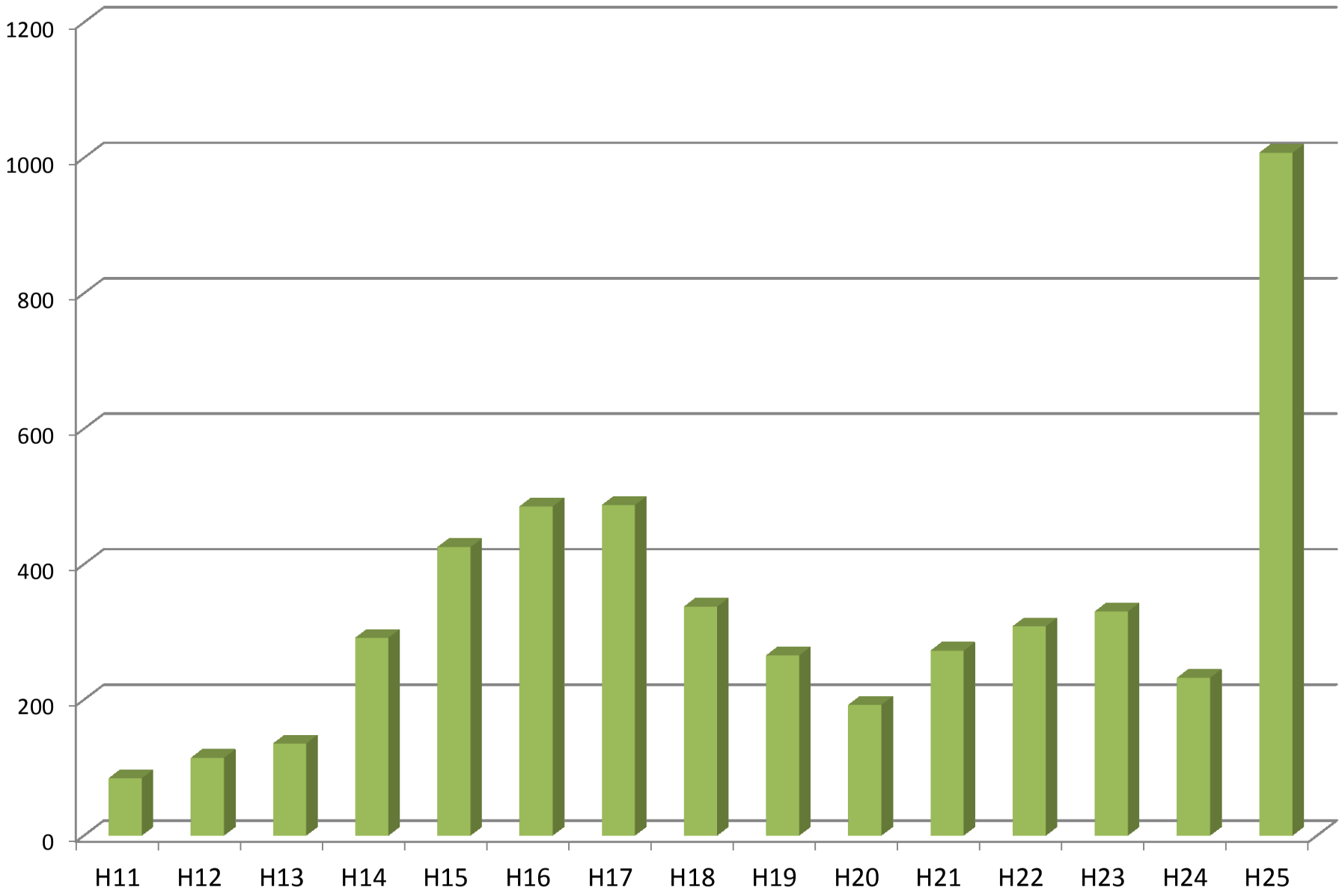
1200
1000
800
600
400
200
0
H11
H12
H13
H14
H15
H16
H17
H18
H19
H20
H21
H22
H23
H24
H25

内視鏡下生検総件数

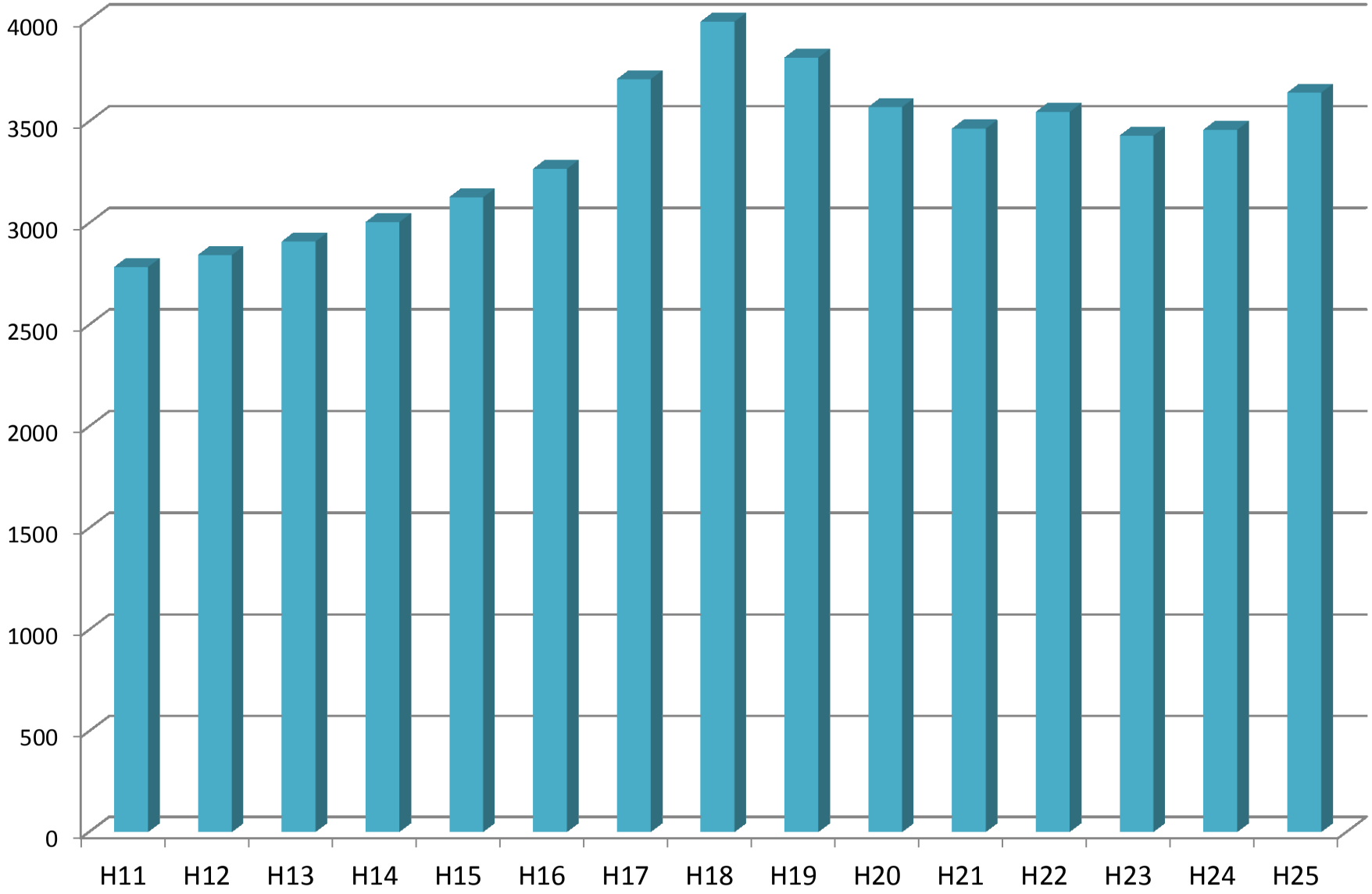
4000
3500
3000
2500
2000
1500
1000
500
0
H11
H12
H13
H14
H15
H16
H17
H18
H19
H20
H21
H22
H23
H24
H25

早期癌に対する内視鏡的粘膜下層切開剥離術
ESD(胃・食道）

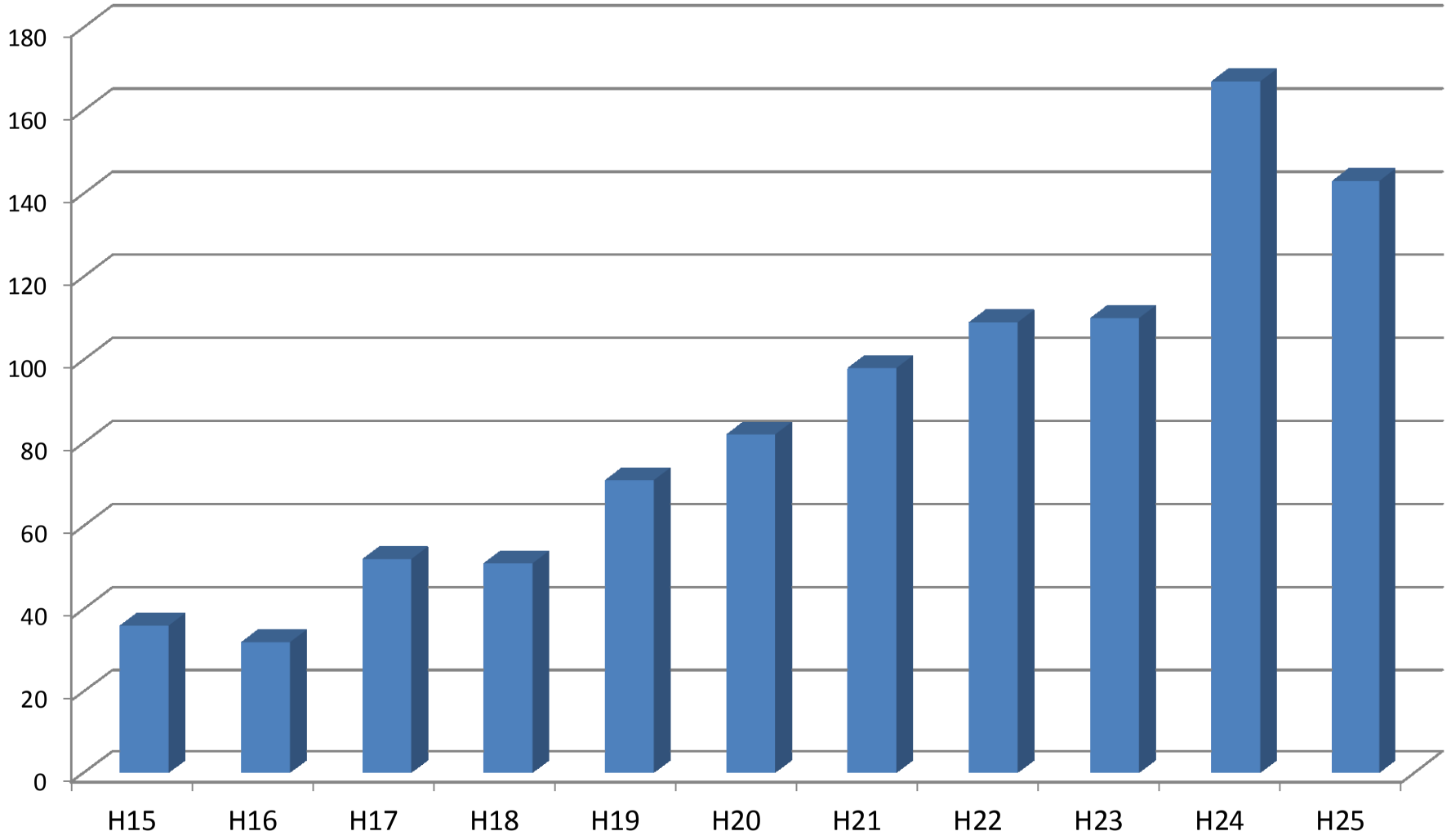

内視鏡検査（スクリーニング）数

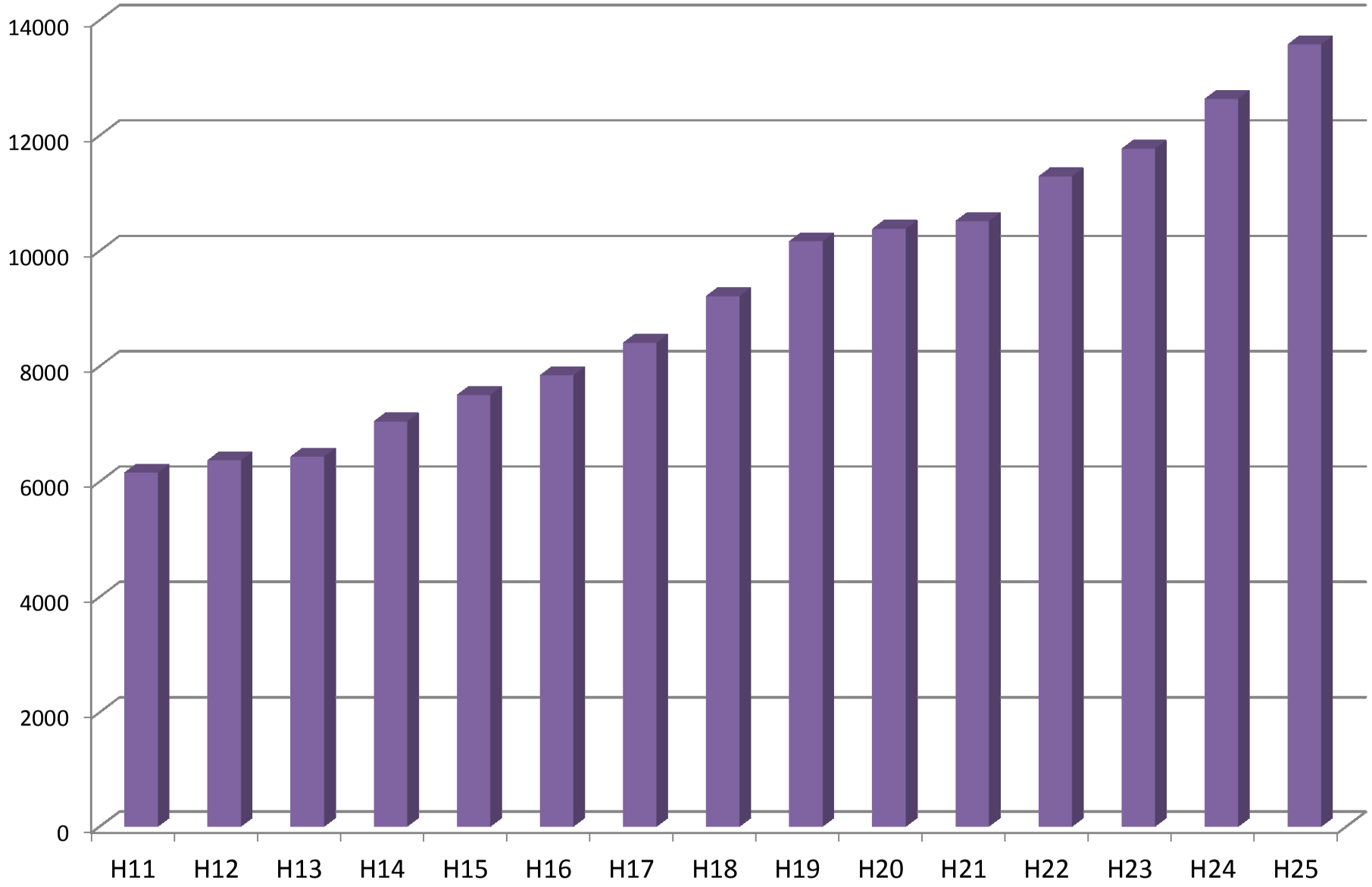

近畿大学　消化器内科学教室医局員

（平成 26 年 6 月現在）

主任教授	工藤正俊	S53	肝臓・消化器・肝癌の診断と治療
教授（内視鏡部）	樫田博史	S58	下部消化管
准教授	汐見幹夫	S55	上部・胆膵内視鏡（関空クリニック所長・教授兼務）
	西田直生志	S60	肝臓病学・肝癌の分子生物学
	北野雅之	H2	消化管全般・胆膵疾患
講師	松井繁長 (医局長)	H3	食道静脈瘤止血・上部消化管
医学部講師	上嶋一臣 (病棟医長)	H7	慢性肝炎・肝癌の治療
	櫻井俊治 (外来医長)	H7	上部消化管・分子生物学
	南　康範	H9	肝疾患・消化器一般
	萩原　智	H10	肝疾患・消化器一般
	井上達夫	H11	肝疾患・消化器一般
	矢田典久	H11	肝疾患・消化器一般
	坂本洋城	H12	胆膵疾患・消化器一般
	朝隈　豊	H14	上部消化管・消化器一般
	北井　聡	H14	肝疾患・消化器一般
助教			
	米田　頼晃	H13	消化器一般
	岡崎　能久	H13	消化器一般
	田北雅弘	H15	肝疾患・消化器一般
	今井　元	H17	胆膵疾患・消化器一般
	山雄健太郎	H18	胆膵疾患・消化器一般
	山田光成	H18	消化器一般
	有住忠晃	H19	肝疾患・消化器一般
	鎌田　研	H19	胆膵疾患・消化器一般
	峯　宏昌	H19	消化器一般
	宮田　剛	H19	胆膵疾患・消化器一般
	高山政樹	H19	消化器一般
	足立哲平	H20	肝疾患・消化器一般
	大本俊介	H20	消化器一般
	門阪薫平	H20	胆膵疾患・消化器一般
	田中梨絵	H22	消化器一般
	千品寛和	H22	消化器一般
	河野匡志	H22	消化器一般
	南　知宏	H23	消化器一般
	岡元寿樹	H23	消化器一般

非常勤	仲谷達也	H3	仲谷クリニック
	中岡良介	H8	山本病院内科
	福田信宏	H10	朝日大学附属村上病院　消化器内科
	市川　勉	H13	内海町いちかわ診療所
	黒木恵美	H12	肝疾患・消化器一般
	柴田千栄	H15	肝疾患・消化器一般
	上田泰輔	H15	肝疾患・消化器一般
大学院 4 年	足立哲平	H20	肝疾患・消化器一般
	大本俊介	H20	消化器一般
	門阪薫平	H20	胆膵疾患・消化器一般
大学院 2 年	南　知宏	H23	消化器一般
	千品寛和	H22	消化器一般
大学院 1 年	山雄健太郎	H18	胆膵疾患・消化器一般
	河野　匡志	H22	消化器一般

実験助手　鏡　郁子
垣井麻莉

データマネージャー（CRC 業務）
児玉美由紀

臨床研究補助　弓削公子

教授秘書　田中真紀
村橋亜季
本廣佳香

日本肝癌研究会　田村利恵
前原なつみ

医局秘書　胡桃由佳
朝隈　智
山本有紀

分院勤務

堺病院	辻　直子	S60	近畿大学堺病院	准教授・科長
	谷池聡子	H7	近畿大学堺病院	診療講師
	川崎正憲	H15	近畿大学堺病院	診療講師
	奥村直巳	H21	近畿大学堺病院	臨床助教
	高場雄久		近畿大学堺病院	臨床助教
	松本　望		近畿大学堺病院	臨床助教
	丸山康典		近畿大学堺病院	臨床助教
	尾崎　信人		近畿大学堺病院	臨床助教

奈良病院	川崎俊彦	S58	近畿大学奈良病院消化器内分泌内科	准教授
	岸谷　譲	S62	近畿大学奈良病院消化器内分泌内科	講師
	宮部欽生	H14	近畿大学奈良病院消化器内分泌内科	診療講師
	清水昌子	H12	近畿大学奈良病院消化器内分泌内科	診療助教
	茂山朋広	H17	近畿大学奈良病院消化器内分泌内科	診療助教
	奥田英之	H19	近畿大学奈良病院消化器内分泌内科	診療助教
	木下大輔	H20	近畿大学奈良病院消化器内分泌内科	臨床助教
	秦　康倫	H21	近畿大学奈良病院消化器内分泌内科	臨床助教
	永田嘉昭	H16	近畿大学奈良病院消化器内分泌内科	臨床助教
	永井知行	H16	近畿大学奈良病院消化器内分泌内科	臨床助教

他病院勤務	山本健二		岡本クリニック	
	林　道友		医療法人恵和会　林内科クリニック	院長
	中里　勝		上ヶ原病院	
	南野達夫	S55	なんの医院	
	水野成人	S61	神戸薬科大学　医療薬学研究室	
			近畿大学奈良病院消化器内分泌内科	非常勤医師
	鍋島紀滋	S61	三菱京都病院消化器内科	
	由谷逸朗	S62	高石藤井病院	
	川端一史	H 元年	川端内科クリニック	
	米田　円	H 元年	米田内科胃腸科	
	渡邉和彦	H3	結核予防会大阪府支部相談診療所	
	森村正嗣	H3	森村医院	
	仲谷達也	H3	仲谷クリニック	

福永豊和	H4	北野病院消化器内科
遠田弘一	H7	慈温堂遠田医院　院長
遠田由紀		
亀山千晴	H7	しあわせクリニック
小牧孝充	H7	富田林病院消化器内科
鄭　浩柄	H8	神戸市医療センター中央市民病院
中岡良介	H8	山本病院内科
末冨洋一郎	H8	末冨放射線科医院
福田信宏	H10	朝日大学歯学部附属村上記念病院　消化器内科
小川　力	H11	高松赤十字病院　消化器内科
坂口康浩	H11	河崎内科病院
梅原　泰	H11	辻　腎太郎クリニック
加藤玲明	H11	宝塚市立病院消化器内科
		近畿大学奈良病院消化器内分泌内科　非常勤医師
宮本容子	H12	近畿大学奈良病院消化器内分泌内科　非常勤医師
梅原康湖	H12	JR 大阪鉄道病院　非常勤医師
永島美樹	H12	桃坂クリニック
工藤可苗	H12	乾医院
市川　勉	H13	内海町いちかわ診療所
冨田崇文	H14	冨田病院
齊藤佳寿	H14	介護老人保健施設　徳田山
高橋俊介	H14	市立堺病院
西尾　健	H14	南堺病院
坂本康明	H15	（医）坂本クリニック
早石宗右	H18	医療法人早石会　早石病院
山本典雄	H19	医療法人山紀会　内科

医局員の略歴
および近況

汐見　幹夫

2013 年の反省

１月の内視鏡学会近畿セミナー座長、３月の消化器病学会総会、５月の内視鏡学会総会の座長は無事終了できました。

また、12 月の内視鏡学会近畿セミナーを会長として無事開催させていただきました。ご協力いただいた諸先生方にはこの場をお借りして御礼申し上げます。当初参加者は学会からの指示で 250 名の予定でしたが、実際には 410 名のご参加をいただきました。喜ぶべきことなのですが、予約していた会場が手狭になってしまい机が使用できなくなり、参加者の皆様にはご不便をおかけすることになってしまいました。見通しの甘さを反省しております。

2014 年の抱負

対外的な活動を継続したいと思っています。

５月の内視鏡学会総会では口演の座長を務めさせていただきます。

座長だけでなく、６月には以前工藤教授も代表世話人をされた「関西 PEG・栄養研究会」という胃瘻の研究会を当番世話人としてお世話させていただく予定です。昨年のように参加者にご不便をおかけしないよう、しっかり準備したいと思っています。

工藤教授だけでなく、汐見も還暦でした。結婚 30 周年でもあったので、ちょうど開園 30 周年のディズニーランドで子供たちに祝ってもらいました。

まつい　しげなが
松井　　繁長
平成 3 年　　近畿大学医学部卒業
平成 3 年　　近畿大学第二内科入局
平成 11 年　近畿大学消化器内科助手
平成 14 年　近畿大学消化器内科講師
平成 18 年　近畿大学消化器内科医局長


専門領域
消化器病、消化器内視鏡、門脈圧亢進症、食道、胃静脈瘤
早期胃癌の内視鏡診断・治療

所属学会
日本内科学会、日本消化器病学会、日本消化器内視鏡学会
日本門脈圧亢進症学会、日本消化管学会
資格
日本内科学会認定医
日本消化器病学会（専門医、学会評議員）
日本消化器内視鏡学会（指導医、学術評議員）
日本門脈圧亢進症学会評議員
日本消化管学会胃腸科認定医
近畿大学医学博士

今年も近畿大学消化器内科のブランド化に向けて、消化管グループとして、
グループの活性化を図りながら、臨床、研究、学外活動に頑張っていきます。

櫻井　俊治

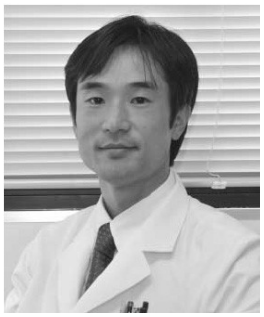

1995 年 3 月　京都大学　医学部　卒業
1995 年 5 月　神戸市立中央市民病院　医師
1997 年 4 月　天理よろづ病院　医師
2004 年 3 月　京都大学大学院　博士課程修了
2004 年 9 月　京都大学　医学部　助手
2008 年 4 月　カリフォルニア大学サンディエゴ校　客員研究員
2010 年 4 月　近畿大学　医学部　講師
現在に至る

診療内容：消化管早期癌、炎症性腸疾患の治療
研究内容：炎症から発癌の分子機序の解明と新規治療・診断法の開発

2013 年を振り返ると、内視鏡治療と炎症性腸疾患の診断と治療において幾許かの進捗があったと感じています。早期消化管癌や潰瘍性大腸炎・クローン病の多くの患者さんの治療を明らかな合併症なくさせていただきました。昨年秋に劇症の潰瘍性大腸炎の患者さんが立て続けに二名入院され、そのうち一人は高齢であり、感染症などの合併症のないように細心の注意を払いながら治療を行いました。最終的には兵庫医大の内野基先生に手術していただき、現在元気に外来に通院されております。もう一人は若い方でありましたが、あらゆる内科治療に抵抗性で、外科的加療を選択していただきましたが、同じく元気に外来に通院されております。学術的には、工藤教授より昨年の“論文最多賞”をいただきました。また学会シンポでの発表、国際学会の座長、研究会の幹事および世話人などを務めさせていただきました。

20014 年は、近大に赴任して 5 年目の区切りの年であります。工藤正俊教授、樫田博史教授のご指導のもと臨床と研究においてますます精進し、“近大まぐろ”のような、日本一、世界一の“近大〇〇“を目指して、労苦を惜しまず邁進していきたいと思います。ご指導、ご鞭撻よろしくお願いいたします。

サクランボ追伸

南　康範

昨年の年報ではサクランボ好きが講じてサクランボの木を購入し、咲いた花に受粉作業をしたことを記しました。その後についてご報告します。

10 輪程度の花が咲き、毎朝 6 時に起床しての受粉作業をしたところ 2 つの花の根元（子房）が膨らみ始めました。残念ながら 1 つは不受精果だったのか成長が途中で止まり落果しましたが、一粒のサクランボ（佐藤錦）は緑色の子房が徐々に大きくなって行きました。そして少しづつ赤く色づき始めたのですが、春は虫の季節です。果樹でも特にサクランボは病気や害虫が付き易いですので注意が必要です。食するため薬品は使えないので、色の悪い葉（病気が疑わしい）は早めに摘除したり、アブラムシなどには割り箸で駆除するなどの手間は惜しみませんでした。また、野鳥も大敵です。近くに林や公園があることから庭に野鳥が時々来ているので、サクランボが食べられやしないかと気が気ではありませんでした。実を付けたサクランボの鉢を庭木の下に隠れるよう置くと言うお粗末な対策だけだったので心配でなりません。私が帰宅してまずしたことはサクランボが大丈夫かを確認することでした。苦労と愛情の甲斐あって幸い野鳥や虫に気付かれることなく実も更に大きく赤くなったのですが、5 月のある日のことです。しばらく雨もなく暑い日でもあったので少し多めに夕方の水やりをした次の日ですが、大事な大事なサクランボの実に傷が…。鳥に啄まれたのか⁉とかなり落胆しましたが、妻に「裂果じゃないの？」と指摘されました。「裂果」とは実が水分を摂り過ぎて弾けることを言いますが、今回は前日の水やりが悪かった結果でした。例えば林檎や蜜柑と言った果樹は数ヵ月かけてゆっくり成熟しますが、サクランボは開花から約 1 ヵ月と言う短期間で成熟することから 5 月の水やりは少なめが大事となります。しかし、少なすぎれば萎れるのでバランスが必要です。五月雨に当たり過ぎれば容易に裂果することは知っていましたが、1 回の水やりでも失敗するとの教訓を得ました。

この実は裂果したまま成熟させ、見た目は悪いものの普通に甘く美味しいサクランボでした。さて、今年は昨年と比べて花芽が多いことから沢山花が咲きそうです。目標は家族でサクランボ 1 粒づつ以上と言うことから 3 個以上の収穫を目指します。

略歴：

平成 9 年 3 月　近畿大学医学部卒業

平成 9 年 4 月　近畿大学医学部旧第 1 外科入局

平成 10 年 7 月　八尾徳洲会病院外科

平成 11 年 4 月　近畿大学医学部大学院（外科学）入学

平成 12 年 7 月　旧第 1 外科から消化器内科へ出向

平成 15 年 3 月　近畿大学医学部大学院（外科学）卒業

平成 15 年 4 月　近畿大学医学部消化器内科 助手

平成 18 年 5 月　近畿大学医学部消化器内科 医学部講師

平成 20 年 12 月～平成 21 年 3 月　University California, San Diego (UCSD) の Department of Radiology に Visiting fellow として短期留学

平成 21 年 4 月　近畿大学医学部堺病院

平成 23 年 4 月　近畿大学医学部消化器内科

資格：外科専門医、肝臓専門医、消化器病専門医、消化器内視鏡専門医
超音波専門医・指導医

役職：　*World Journal of Radiology,* an Editorial Board Member
日本超音波医学会 査読委員

今後の目標

消化器内科　永井　知行

まずは私事ですが、13 年 10 月 7 日に入籍、14 年 2 月 1 日に披露宴を挙げさせて頂きました。その際に消化器内科医局・病院関係者などから多くの祝福を頂き、この場をかりて御礼申し上げます。

私の妻は同じ消化器内科の医師であり、学会や外勤先（青葉丘病院当直や富田林病院の外来・検査）の代診をお願いすることがあり（すでにお願いしていますが…）、皆様も会われるかもしれません。その時は温かく接して頂ければ幸いです。

去年と今年の年始は披露宴の準備に追われ、本当に一瞬で時間が過ぎていきました。最近は少し落ち着きつつあり、今後は臨床と研究において邁進していきたいと思います。

今年は研修医からの入局がなく厳しい 1 年になりそうですが、力を合わせて頑張っていきましょう！

略歴）

04 年　　近畿大学医学部　卒業

04 年～ 06 年　　神戸労災病院　臨床研修医

06 年～ 08 年　　市立岸和田市民病院　消化器内科

08 年～現在　　近畿大学医学部附属病院　消化器内科

所属学会）

日本内科学会、日本消化器病学会、日本消化器内視鏡学会、日本肝臓学会

日本癌学会、日本臨床腫瘍学会、日本分子標的学会、米国癌学会

専門医・学位）

日本内科学会認定医、日本消化器病学会専門医、日本内視鏡学会専門医

医学博士（平成２３年度）

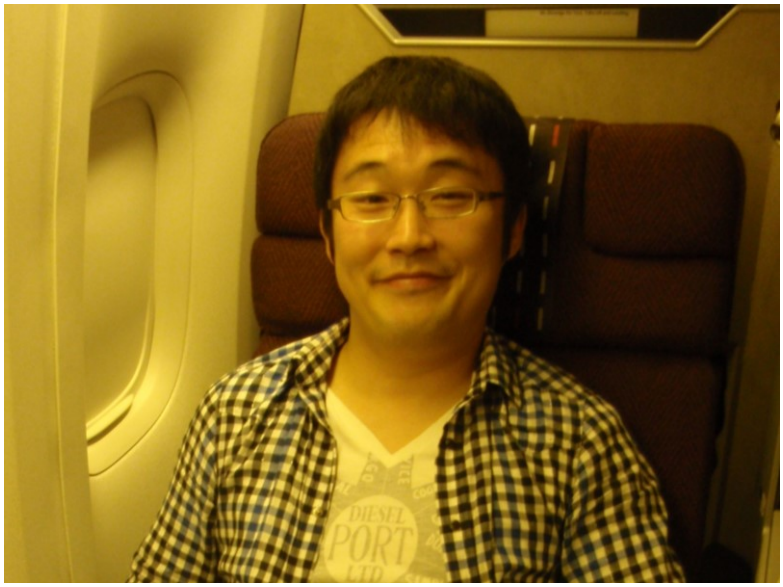

有住忠晃　徳島出身

略歴
昭和 57 年 2 月 6 日：出生
昭和 60 年 4 月：鳴門聖母幼稚園入園
昭和 63 年 4 月：北島町立北島北小学校入学
平成 6 年 4 月：北島町立北島中学校入学
平成 9 年 4 月：徳島県立徳島北高校入学
平成 12 年 4 月：代々木ゼミナール原宿校入学
平成 13 年 4 月：近畿大学医学部医学科入学
平成 19 年 4 月：近畿大学医学部付属病院研修医
平成 21 年 4 月：近畿大学医学部付属病院　消化器内科　入局
平成 21 年 4 月：近畿大学医学部大学院内科学系　入学
平成 25 年 10 月：くしもと町立病院
平成 26 年 1 月：近畿大学医学部付属病院　消化器内科
現在に至る

2013 年の反省と 2014 年の目標
2013 年は串本病院に出向させていただき地域医療について学ばせていただきました。3 カ月と短い期間でしたが非常に充実した貴重な体験となりました。しかし学会発表や論文に関しては自分自身や皆さんが納得することができる程の業績を残せていません。そこで 2014 年は 2013 年以上に日常診療・研究・学会発表・論文を頑張ります。また私生活でも何か一つ大きなことをやり遂げたいと考えております。具体的な内容はまだ何も考えていません・・・。

峯　宏昌

平成 19 年 3 月：近畿大学医学部卒業
平成 19 年 4 月：近畿大学医学部付属病院　研修医
平成 21 年 4 月：近畿大学医学部消化器内科　助教
平成 22 年 4 月：近畿大学医学部大学院内科学系　入学
平成 26 年 3 月：近畿大学医学部大学院内科学系　卒業

2014 年 3 月にお陰さまをもちまして、無事に大学院を卒業することとなりました。
もう二度と受けたくないと思うほどの緊張感で終わった公聴会でしたが、卒業まで至ったのは櫻井先生、樫田教授、工藤教授をはじめ、多くの方々にご指導ご鞭撻いただいた御陰と思っています。
また NST でなかなか参加できない内視鏡治療においても､樫田教授や松井先生のご配慮で、時間を調整いただき、研鑽を積ましていただいています。
2014 年で医師免許を取得し 8 年目、入局して 6 年目となりました。気づけば自分より上の先生方が少なくなり、自分より下の先生方が増えつつあり、世間で言う中間管理職的な位置になってきたように感じます。
自分が入局した時におられた先生方のような、頼りになる先輩医師として後輩に感じてもらえるようにまだまだ研鑽を積む必要がありそうです。

近畿大学医学部奈良病院　消化器・内分泌内科　2013 年年報（1～12 月）

１．スタッフ

准教授	川崎俊彦（昭和 58 年卒）
講師	岸谷　譲（昭和 62 年卒）
診療講師	清水昌子（平成 12 年卒）（12 月退職）
診療講師	宮部欽生（平成 14 年卒）（6 月退職）
助教 B	永田嘉明（平成 16 年卒）（6 月赴任）
診療助教	茂山朋広（平成 17 年卒）（4 月より非常勤に）
診療助教	奥田英之（平成 19 年卒）
診療助教	木下大輔（平成 20 年卒）
診療助教	秦　康倫（平成 21 年卒）
非常勤医師	水野成人

２．臨床業績

1 日平均外来患者	79.5 人
1 日平均在院患者	23.4 人
平均在院日数	9.4 日
上部内視鏡検査	3223 件（含 ESD 75 件）
下部内視鏡検査	1668 件（含 EMR 293 件+ESD3 件）
ERCP	169 件
超音波内視鏡	34 件（含 EUS-FNA 5 件）
腹部超音波	2527 件
腹部血管造影	106 件
ラジオ波治療	34 件

3．学会業績

（１）第 90 回日本消化器内視鏡学会近畿支部例会
「EUS-FNA で術前診断が可能であった神経性腫瘍の 1 例」

（２）第 28 回日本糖尿病合併症学会「右鎖骨の溶血性変化のため前胸部悪性腫瘍を疑われた二次性糖尿病の一例」

（３）第 91 回日本消化器内視鏡学会近畿支部例会
「食欲不振を契機に発見された巨大脾腫瘍の１例」

4．学会業績（研究会）
（１）生駒消化器癌カンファレンス 2013
「難治性食道カンジダ症を合併した食道疣状癌の 1 症例」
（２）第 4 回奈良病診連携を考える会
「早期胃癌の診断と内視鏡治療」

川崎俊彦

略歴

昭和 58 年	京都大学医学部医学科専門課程卒業
昭和 58 年	京都大学医学部附属病院（研修医）
昭和 59 年	大阪府済生会野江病院（内科医員）
昭和 61 年	京都大学医学部附属病院（第一内科医員）
平成２年	京都桂病院（内科医員）
平成５年	Diagnostic Radiology, Yale University School of Medicine, (Visiting Scientist)
平成６年	神戸中央市民病院（内科副医長）
平成６年	西神戸医療センター（内科副医長）
平成９年	西神戸医療センター（内科医長）に昇進
平成 12 年	近畿大学医学部附属病院（講師）
平成 16 年	大阪北逓信病院第１内科（部長）
平成 22 年	近畿大学医学部奈良病院消化器・内分泌内科（准教授）
平成 25 年	近畿大学医学部奈良病院消化器・内分泌内科（教授）

2013 年の反省と 2014 年の抱負。

2013 年は 4 月に茂山医師が開業のため非常勤となり，5 月末には長らく内視鏡診療を支えてくれた宮部医師が実家近くの病院へと転勤されました。6 月よりは近大本学より永田医師が宮部医師の代わりに赴任されましたが，一人欠員状態が続き苦しい状態でした。更に，清水医師が御懐妊され，9 月より長期休業に入り 11 月より一時復帰されましたが，12 月に正式に退職され，二人欠員となり更に苦しい状態が続いています。

このため，学会活動は、総会１題，地方会 2 題，研究会 2 題とほぼ休眠状態だったのは，臨床優先のため仕方がなかったと思います。

その中で，EUS-FNA5 例を含む，超音波内視鏡を 34 例実施でき，ようやく超音波内視鏡が普通の検査の仲間入りができたのは大きいのではないかと思います。

2014 年は 5 月末に永田医師が開業の為に退職することが決定しているので，何とか近大本学からの補充をお願いしたいところです。

消化器内科学業績一覧(2013 年)

Ⅰ. 英文論文

1. 2013 **Kudo M**: Advances in Liver Fibrosis Imaging and Hepatocellular Carcinoma: Update in 2013. **Oncology** 84:1-2, 2013.(IF: 2.613)

2. 2013 Fujimoto K, Kato M, **Kudo M**, Yada N, Shiina T, Ueshima K, Yamada Y, Ishida T, Azuma M, Ymasaki M,Yamamoto K, Hayashi N, Takehara T: Novel image analysis method using ultrasound elastography for non-invasive evaluation of hepatic fibrosis in patients with chronic hepatitis C. **Oncology** 84:3-12, 2013. (IF: 2.613)

3. 2013 Yada N, Morikawa H, Fujimoto K, Kato M, Kawada N, **Kudo M**: Assessment of liver fibrosis with real-time tissue elastography in chronic viral hepatitis. **Oncology** 84:13-20, 2013. (IF: 2.613)

4. 2013 **Kudo M**, Matsui O, Sakamoto M, Kitao A, Kim T, Ariizumi S, Ichikawa T, Kobayashi S, Imai Y, Izumi N, Fujinaga Y, Arii S: Role of gadolinium-ethoxybenzyl-diethylenetriamine pentaacetic acid-enhanced magnetic resonance imaging (Gd-EOB-DTPA MRI) in the management of hepatocellular carcinoma: Consensus at the Symposium of the 48th Annual Meeting of the Liver Cancer Study Group of Japan. **Oncology** 84:21-27, 2013. (IF: 2.613)

5. 2013 Inoue T, **Kudo M**, Hatanaka K, Arizumi T, Takita M, Kitai S, Yada N, Hagiwara S, Minami Y, Sakurai T, Ueshima k, Nishida N: Usefulness of contrast-enhanced ultrasonography to evaluate the post treatment responses of radiofrequency ablation for hepatocellular carcinoma; comparison with dynamic CT. **Oncology** 84:51-57, 2013. (IF: 2.613)

6. 2013 Minami Y, **Kudo M**: Therapeutic response assessment of transcatheter arterial chemoembolization for hepatocellular carcinoma: US, CT and MRI. **Oncology** 84:58-63, 2013. (IF: 2.613)

7. 2013 Minata M, Harada K, **Kudo M**, Ikai I, Nishida N: The prognostic value of vascular endothelial growth factor in hepatocellular carcinoma for predicting metastasis after curative resection. **Oncology** 84:75-81, 2013. (IF: 2.613)

8. 2013 Nishida N, Arizumi T, Takita M, Nagai T, Kitai S, Yada N, Hagiwara S, Inoue T, Minami Y, Ueshima K, Sakurai T, Ida H, **Kudo M**: Quantification of tumor DNA in serum and vascular invasion of human hepatocellular carcinoma. **Oncology** 84:82-87, 2013. (IF: 2.613)

9. 2013 Minata M, **Kudo M**, Harada K, Ikai I, Nishida N: Expression of E-cadherin

and vascular endothelial growth factor in non-cancerous liver is associated with recurrence of HCC after curative resection. **Oncology** 84:88-92, 2013. (IF: 2.613)

10. 2013 Nishida N, **Kudo M**: Recent advancementsincomprehensive genetic analyses for human hepatocellular carcinoma. **Oncology** 84:93-97, 2013. (IF: 2.613)

11. 2013 Claudon M, Dietrich CF, Choi BI, Cosgrove DO, **Kudo M**, Nolsoe CP, Piscaglia F, Wilson SR, Barr RG, Chammas MC, Chaubal NG, Chen MH, Clevert DA, Correas JM, Ding H, Forsberg F, Fowlkes JB, Gibson RN, Goldberg BB, Lassau N, Leen EL, Mattrey RF, Moriyasu F, Solbiati L, Weskott HP, Xu HX: Guidelines and good clinical practice recommendations for contrast enhanced ultrasound (CEUS) in the liver-update 2012: a WFUMB-EFSUMB initiative in cooperation with representatives of AFSUMB, AIUM, ASUM, FLAUS and ICUS. **Ultrasound Med Biol** 39:187-210, 2013. (IF: 2.099)

12. 2013 Hasegawa K, Kokudo N, Makuuchi M, Izumi N, Ichida T, **Kudo M**, Ku Y, Sakamoto M, Nakashima O, Matsui O, Matsuyama Y, for the Liver Cancer Study Group of Japan.: Comparison of resection and ablation for hepatocellular carcinoma: a cohort study based on a Japanese nationwide survey. **J Hapatol** 58:724-729, 2013. (IF: 10.401)

13. 2013 Sakurai T, **Kudo M**, Umemura A, He G, Elsharkawy AM, Seki E, Karin M: p38 α inhibits liver fibrogenesis and consequent hepatocarcinogenesis by curtailing accumulation of reactive oxygen species. **Cancer Res** 73:215-224, 2013. (IF: 9.284)

14. 2013 Claudon M, Dietrich CF, Choi BI, Cosgrove DO, **Kudo M**, Nolsoe CP, Piscaglia F, Wilson SR, Barr RG, Chammas MC, Chaubal NG, Chen MH, Clevert DA, Correas JM, Ding H, Forsberg F, Fowlkes JB, Gibson RN, Goldberg BB, Lassau N, Leen EL, Mattrey RF, Moriyasu F, Solbiati L, Weskott HP, Xu HX: Guidelines and good clinical practice recommendations for contrast enhanced ultrasound (CEUS) in the liver-update 2012: a WFUMB-EFSUMB initiative in cooperation with representatives of AFSUMB, AIUM, ASUM, FLAUS and ICUS. **Ultraschall Med** 34:11-29, 2013. (IF: 4.645)

15. 2013 Watanabe T, Yamashita K, Sakurai T, **Kudo M**, Shiokawa M, Uza N, Kadoma Y, Uchida K, Okazaki K, Chiba T: Toll-like receptor activation in basophils contributes to the development of IgG4-related disease. **J Gastroenterol** 48:247-253, 2013. (IF: 4.020)

16. 2013 Nagata Y, **Kudo M**, Nagai T, Watanabe T, Kawasaki M, Asakuma Y, Hagiwara S, Nishida N, Matsui S, Kashida H, Sakurai T: Heat shock protein 27 expression is inversely correlated with atrophic gastritis and intraepithelial neoplasia. **Digest Dis Sci** 58:381-388, 2013. (IF: 2.550)

17. 2013 Park JW, Amarapurkar D, Chao Y, Chen PJ, Geschwind JF, Goh KL, Han KH, **Kudo M**, Lee HC, Lee RC, Lesmana LA, Lim HY, Paik SW, Poon RT, Tan CK, Tanwandee T, Teng G, Ceng AL: Consensus recommendations and review by

an International Expert Panel on Interventions in Hepatocellular Carcinoma (EPOIHCC). **Liver Int** 33:327-337, 2013. (IF: 4.412)

18. 2013 Minami Y, **Kudo M**: Radiofrequency ablation of liver metastases from colorectal cancer: a literature review. **Gut Liver** 7:1-6, 2013. (IF: 1.494)

19. 2013 Arao T, Ueshima K, Matsumoto K, Nagai T, Kimura H, Hagiwara S, Sakurai T, Haji S, Kanazawa K, Hidaka H, Iso Y, Kubota K, Shimada M, Utsunomiya T, Hirooka M, Hiasa Y, Toyoki Y, Hakamada K, Yasui K, Kumada T, Hidenori Toyoda, Sato S, Hisai H, Kuzuya T, Tsuchiya K, Izumi N, Arii S, Nishio K, **Kudo M**: FGF3/FGF4 Amplification and Multiple lung Matastases in responders to sorafenib in hepatocellular carcinoma. **Hepatology** 57:1407-1415, 2013. (IF: 11.190)

20. 2013 Izumi N, Asahina Y, Kurosaki M, Yamada G, Kawai T, Kajiwara E, Okamura Y, Takeuchi T, Yokosuka O, Kariyama K, Toyoda J, Inao M, Tanaka E, Moriwaki H, Adachi K, Katsushima S, **Kudo M**, Takaguchi K, Hiasa Y, Chayama K, Yatsuhashi H, Oketani M, Kumada H: Inhibition of hepatocellular carcinoma by PegIFNα-2a in patients with chronic hepatitis C: a nationwide multicenter cooperative study. **J Gastroenterol** 48:382-390, 2013. (IF: 4.020)

21. 2013 Takayasu K, Arii S, Sakamoto M, Matsuyama Y, **Kudo M**, Ichida T, Nakashima O, Matsui O, Izumi N, Ku Y, Kokudo N, Makuuchi M, Liver Cancer Study Group of Japan: Clinical implication of hypovascular hepatocellular carcinoma studied in 4,474 patients with solitary tumour equal or less than 3 cm. **Liver Int** 33:762-770, 2013. (IF: 4.412)

22. 2013 Hyodo T, Murakami T, Imai Y, Okada M, Hori M, Kagawa Y, Kogita S, Kumano S, **Kudo M**, Mochizuki T: Hypovascular nodules in patients with chronic liver disease: risk factors for development of hypervascular hepatocellular carcinoma. **Radiology** 266:480-490, 2013. (IF: 6.214)

23. 2013 Hagiwara S, **Kudo M**, Osaki Y, Matsuo H, Inuzuka T, Matsumoto A, Tanaka E, Sakurai T, Ueshima K, Inoue T, Yada Y, Nishida N: Impact of peginterferon Alpha-2b and entecavir hydrate combination therapy on persistent viral suppression in patients with chronic hepatitis B. **J Med Virol** 85:987-95, 2013. (IF: 2.217)

24. 2013 **Kudo M***: Early Hepatocellular Carcinoma: Definition and Diagnosis. **Liver Cancer** 2(2):69-72, 2013. (IF: 0.000)

25. 2013 Matsui S, Kashida H, **Kudo M**: Senile systemic amyloidosis localized to the stomach. **Digest Endosc** 25:468-469, 2013. (IF: 1.989)

26. 2013 Mine H, Sakurai T, Kashida H, Matsui S, Nishida N, Nagai T, Hagiwara S, Watanabe T, **Kudo M**: Association of gankyrin and stemness factor

expression in human colorectal cancer. **Digest Dis Sci** 58:2337-2344, 2013. (IF: 2.550)

27. 2013 Inaba Y, Kanai F, Aramaki T, Yamamoto T, Tanaka T, Yamakado K, Kaneko S, **Kudo M**, Imanaka K, Kora S, Nishida N, Kawai N, Seki H, Matsui O, Arioka H, Arai Y: A randomized phase II study of TSU-68 in patients with hepatocellular carcinoma treated by transarterial chemoembolization. **Eur J Cancer** 49:2832-2840, 2013. (IF: 4.819)

28. 2013 Takayama M, Matsui S, Kawasaki M, Asakuma Y, Sakurai T, Kashida H, **Kudo M**: Efficacy of treatment with rebamipide for endoscopic submucosal dissection-induced ulcers. **World J Gastroenterol** 19:5706-5712, 2013. (IF: 2.433)

29. 2013 **Kudo M***: Chronic liver diseases and hepatocellular carcinoma: an update for 2013. **Digest Dis** 31:405-407, 2013. (IF: 1.832)

30. 2013 Nishida N, Iwamura S, Ida H, Hagiwara S, Kagioka Y, Minami Y, Maetani Y, Itoh K, **Kudo M**: Clinical and histological features of different types of Budd-Chiari syndrome: a Comparison of 4 cases. **Digest Dis** 31:408-414, 2013. (IF: 1.832)

31. 2013 Yada N, **Kudo M***, Chung H, Watanabe T: Autoimmune hepatitis and immunoglobulin G4-associated autoimmune hepatitis. **Digest Dis** 31:415-420, 2013. (IF: 1.832)

32. 2013 Sugimoto K, Kim SR, Shamy AE, Imoto S, Ando K, Kim KI, Tanaka Y, Yano Y, Kim SK, Hasegawa Y, Fujinami A, Ohta M, Takashi H, Hotta H, Hayashi Y, **Kudo M**: Factors of response to pegylated interferon/ribavirin combination therapy and mechanism of viral clearance. **Digest Dis** 31:421-425, 2013. (IF: 1.832)

33. 2013 Kim SR, Shamy AE, Imoto S, Kim KI, Sugimoto K, Kim SK, Tanaka Y, Hatae T, Hasegawa Y, Fujinami A, Ohta M, Hotta H, **Kudo M**: Prediction of response to pegylated interferon/ribavirin combination therapy for chronic hepatitis C genotypes 2a and 2b and high viral load. **Digest Dis** 31:426-433, 2013. (IF: 1.832)

34. 2013 Sugimoto K, Kim SR, Shamy AE, Imoto S, Fujioka H, Kim KI, Tanaka Y, Yano Y, Kim SK, Hasegawa Y, Fujinami A, Ohta M, Hatae T, Hotta H, Hayashi Y, **Kudo M**: Outcome of double-filtration plasmapheresis plus interferon treatment in nonresponders to pegylated interferon plus ribavirin combination therapy. **Digest Dis** 31:434-439, 2013. (IF: 1.832)

35. 2013 Sakurai T, **Kudo M**, Watanabe T, Itoh K, Higashitsuji H, Arizumi T, Inoue T, Hagiwara S, Ueshima K, Nishida N, Fukumoto M, Fujita J: Hypothermia protects against fulminant hepatitis in mice by reducing reactive oxygen species production. **Digest Dis** 31:440-446, 2013. (IF: 1.832)

36. 2013 Nishida N, **Kudo M**: Oxidative stress and epigenetic instability in human hepatocarcinogenesis. **Digest Dis** 31:447-453, 2013. (IF: 1.832)

37. 2013 Kim SK, Marusawa H, Eso Y, Chiba T, **Kudo M**: Novel mouse models of hepatocarcinogenesis with stepwise accumulation of genetic alterations. **Digest Dis** 31:454-458, 2013. (IF: 1.832)

38. 2013 Nishida N, Arizumi T, Takita M, Kitai S, Yada N, Hagiwara S, Inoue T, Minami Y, Ueshima K, Sakurai T, **Kudo M**: Reactive oxygen species induce epigenetic instability through the formation of 8-hydroxydeoxyguanosine in human hepatocarcinogenesis. **Digest Dis** 31:459-466, 2013. (IF: 1.832)

39. 2013 Tsuji N, Ishiguro S, Sasaki Y, **Kudo M***: CD-34 expression in noncancerous liver tissue predicts multicentric recurrence of hepatocellular carcinoma. **Digest Dis** 31:467-471, 2013. (IF: 1.832)

40. 2013 Inoue T, Hyodo T, Murakami T, Takayama Y, Nishie A, Higaki A, Korenaga K, Sakamoto A, Osaki Y, Aikata H, Chayama K, Suda T, Takano T, Miyoshi K, Koda M, Numata K, Tanaka H, Iijima H, Ochi H, Hirooka M, Imai Y, **Kudo M**: Hypovascular hepatic nodules showing hypointense on the hepatobiliary-phase image of Gd-EOB-DTPA-enhanced MRI to develop a hypervascular hepatocellular carcinoma: a nationwide retrospective study on their natural course and risk factors. **Digest Dis** 31:472-479, 2013. (IF: 1.832)

41. 2013 Minami Y, Hayaishi S, **Kudo M***: Radiofrequency ablation for hepatic malignancies: is needle tract cauterization necessary for preventing iatrogenic bleeding? **Digest Dis** 31:480-484, 2013. (IF: 1.832)

42. 2013 Makino Y, Imai Y, Igura T, Kogita S, Sawai Y, Fukuda K, Hori M, **Kudo M**, Murakami T: Usefulness of the extracted-overlay function in CT/MR-ultrasonography fusion imaging for radiofrequency ablation of hepatocellular carcinoma. **Digest Dis** 31:485-489, 2013. (IF: 1.832)

43. 2013 **Kudo M***, Osaki Y, Matsunaga T, Kasugai H, Oka H, Seki T, the Osaka Liver Cancer Study Group: Hepatocellular carcinoma in Child-Pugh C cirrhosis: prognostic factors and survival benefit of nontransplant treatments. **Digest Dis** 31:490-498, 2013. (IF: 1.832)

44. 2013 **Kudo M***: Alpha-fetoprotein-L3: Useful or Useless for Hepatocellular Carcinoma? **Liver Cancer** 2(3-4):151-152, 2013. (IF: 0.000)

45. 2013 Sakurai T, **Kudo M***: Molecular link between liver fibrosis and hepatocellular carcinoma. **Liver Cancer** 2(3-4):365-366, 2013. (IF: 0.000)

46. 2013 Das K, **Kudo M***, Kitano M, Sakamoto H, Komaki T, Takagi T, Yamao K: Diagnostic value of endoscopic ultrasound-guided directional eFLOW in

solid pancreatic lesions. **J Med Ultrason**, 40:211-218, 2013. (IF: 0.740)

47. 2013 **Kudo M***, Shiina T, Moriyasu F, Iijima H, Tateishi R, Yada N, Fujimoto K, Morikawa H, Hirooka M, Sumino Y, Kumada T: JSUM ultrasound elastography practice guidelines: liver. **J Med Ultrason** 40:325-357, 2013. (IF: 0.740)

48. 2013 Kagawa Y, Okada M, Yagyu Y, Kumano S, Kanemitsu M, **Kudo M**, Murakami T: Optimal scan timing of hepatic arterial-phase imaging of hypervascular hepatocellular carcinoma determined by multiphasic fast CT imaging technique. **Acta Radiol** 54:843-850, 2013. (IF: 1.350)

49. 2013 Nouso K, Miyahara K, Uchida D, Kuwaki K, Izumi N, Omata M, Ichida T, **Kudo M**, Ku Y, Kokudo N, Sakamoto M, Nakashima O, Takayama T, Matsui O, Matsuyama Y, Yamamoto K, the Liver Cancer Study Group of Japan: Effect of hepatic arterial infusion chemotherapy of 5-fluorouracil and cisplatin for advanced hepatocellular carcinoma in the Nationwide Survey of Primary Liver Cancer in Japan. **Brit J Cancer** 109:1904-1907, 2013. (IF: 4.817)

50. 2013 Cheng AL, Kang YK, Lin DY, Park JW, **Kudo M**, Qin S, Chung HC, Song X, Xu J, Poggi G, Omata M, Lowenthal SP, Lanzalone S, Yang L, Lechuga MJ, Raymond E, for the SUN1170 HCC Study Group: Sunitinib versus sorafenib in advanced hepatocellular cancer: results of a randomized phase III trial. **J Clin Oncol** 10;31:4067-4075, 2013. (IF: 17.879)

51. 2013 Johnson PJ, Qin S, Park JW, Poon RT, Raoul JL, Philip PA, Hsu CH, Hu TH, Heo J, Xu J, Lu L, Chao Y, Boucher E, Han KH, Paik SW, Avina JR, **Kudo M**, Yan L, Sobhonslidsuk A, Komov D, Decaens T, Tak WY, Jeng LB, Liu D, Ezzeddine R, Walters I, Cheng AL: Brivanib versus Sorafenib as first-line therapy in patients with unresectable, advanced hepatocellular carcinoma: results from the randomized Phase 3 BRISK-FL study. **J Clin Oncol** 31:3517-3524, 2013. (IF: 17.879)

52. 2013 Llovet JM, Decaens T, Raoul JL, Boucher E, **Kudo M**, Chang C, Kang YK, Assenat E, Lim HY, Boige V, Mathurin P, Fartoux L, Lin DY, Bruix J, Poon RT, Sherman M, Blanc, JF, Finn RS, Tak WY, Chao Y, Ezzeddine R, Liu D, Walters I, Park JW: Brivanib in patients with advanced hepatocellular carcinoma who failed or were intolerant to sorafenib: or for whom sorafenib faied results from the randomized phase 3 BRISK-PS study. **J Clin Oncol** 31:3509-3516, 2013. (IF: 17.879)

53. 2013 Nishida N, **Kudo M**, Nishimura T, Arizumi T, Takita M, Kitai S, Yada N, Hagiwara S, Inoue T, Minami Y, Ueshima K, Sakurai T, Yokomichi N, Nagasaka T, Goel A: Unique association between global DNA ypomethylation and hromosomal alterations in human hepatocellular carcinoma. **Plos One** 8(9):e72312, 2013. (IF: 3.534)

54. 2013 Kitano M, Yamashita Y, Tanaka K, Konishi H, Yazumi S, Nakai Y, Nishiyama O, Uehara H, Mitoro A, Sanuki T, Takaoka M, Koshitani T, Arisaka Y, Shiba M, Hoki N, Sato H, Sasaki Y, Sato M, Hasegawa K, Kawabata H, Okabe Y,

Mukai H: Covered self-expandable metal stents with an anti-migration system improve patency duration without increased complications compared with uncovered stents for distal biliary obstruction caused by pancreatic carcinoma: a randomized multicenter trial. **Am J Gastroenterol** 108: 1713-1722, 2013. (IF: 9.213)

55. 2013 Yasuda I, Nakashima M, Iwai T, Isayama H, Itoi T, Hisai H, Inoue H, Kato H, Kanno A, Kubota K, Irisawa A, Igarashi H, Okabe Y, Kitano M, Kawakami H, Hayashi T, Mukai T, Sata N, Kida M, Shimosegawa T: Japanese multicenter experience of endoscopic necrosectomy for infected walled-off pancreatic necrosis: The JENIPaN study. **Endoscopy** 45: 627-634, 2013. (IF: 5.196)

Ⅱ. 和文論文（著書・分担執筆）

1. 2013 北野雅之, 坂本洋城, 工藤正俊: コンベックス走査式 EUS による描出法. 消化器内視鏡プロフェッショナルの技-上級者へのステップアップのために-, 第 83 回日本消化器内視鏡学会総会記念出版, 監修 小原勝敏, 編集 入澤篤志, 日本メディカルセンター, 東京, p100-104, 2013. (分担執筆)

2. 2013 井上達夫, 工藤正俊: 肝癌のエコー検査の進め方と判読時のポイント. 「生理検査領域」, 検査診断学への展望―臨床検査指針: 測定データ判読のポイント―, 監修 第 62 回日本医学検査学会記念誌編集委員会, 編集 野村　努, 正田孝明, 横田浩充, 香川県臨床検査技師会編集委員会, 南江堂, 東京, p420-427, 2013. (分担執筆)

3. 2013 井上達夫, 工藤正俊: 肝細胞癌[診断]. 専門医のための消化器病学(第 2 版), 監修 小俣政男, 千葉　勉, 編集 下瀬川徹, 渡辺　守, 金子周一, 樫田博史, 医学書院, 東京, p418-424, 2013. (分担執筆)

4. 2013 上嶋一臣, 工藤正俊: 進行肝癌治療： Q67 ソラフェニブの効果が期待できる肝細胞癌を事前に把握できますか？ 肝癌診療 Q&A, 編著 池田健次, 中外医学社, 東京, p271-273, 2013. (分担執筆)

Ⅲ. 和文論文

1. 2013 坂本洋城, 北野雅之, 今井　元, 鎌田　研, 宮田　剛, 門阪薫平, 大本俊介 千品寛和, 工藤正俊: 癌性疼痛に対する超音波内視鏡下腹腔神経叢ブロック. 特集「胆膵内視鏡新潮流」, 肝胆膵 66: 59-64, 2013.

2. 2013 大本俊介, 北野雅之, 工藤正俊: 典型的露出腫瘤型十二指腸乳頭部癌. “とことん知りたい ERCP の手技のコツ, もう迷わない！後方斜視鏡の挿入から, 乳頭の観察, 深部挿管まで”, 消化器内視鏡レクチャー 1: 587-590, 2013.

3. 2013 大本俊介, 北野雅之, 前川　清, 工藤正俊: 膵腫瘍における体外式超音波検査の進歩. 特集「胆膵癌の早期診断フロントライン」, 肝胆膵 66: 307-314, 2013.

4. 2013 上嶋一臣, 工藤正俊: 肝癌の治療 分子標的薬治療. 特集「肝炎から肝硬変・肝癌まで」, 臨牀と研究 90: 216-221, 2013.

5. 2013 北野雅之, 工藤正俊: EUS ガイド下胆道ドレナージ術の新展開. 今月のテーマ「胆膵疾患に対する Interventional EUS の新展開」, 日本消化器病学会雑誌, 110:557-567, 2013.

6. 2013 松井繁長, 工藤正俊: 胃炎～H. pylori 除菌によるアプローチ～. Medicament News 第 2129 号: 4-6, 2013.

7. 2013 工藤正俊, 土谷 薫, 角谷眞澄, 池田公史: 座談会「肝細胞癌の治療効果判定-RECIST, mRECIST, RECICL-」. The Liver Cancer Journal 5: 13-21, 2013.

8. 2013 上嶋一臣, 工藤正俊: 最近の臨床試験とその解釈①SILIUS 第Ⅰ相試験とその解釈. The Liver Cancer Journal 5: 24-31, 2013.

9. 2013 萩原 智, 櫻井俊治, 上嶋一臣, 永井知行, 西田直生志, 工藤正俊: ソラフェニブ治療における JNK 活性の重要性-CD133 との関連も含めて. The Liver Cancer Journal 5: 58-59, 2013.

10. 2013 今井 元, 北野雅之, 大本俊介, 門阪薫平, 宮田 剛, 鎌田 研, 山雄健太郎, 坂本洋城, 工藤正俊: 急性胆嚢炎に対する EUS ガイド下ドレナージ術. 特集「ドレナージ大全」, 胆と膵 34: 925-928, 2013.

11. 2013 鎌田 研, 北野雅之, 工藤正俊: 造影超音波. 特集「Diagnostic and Interventional EUS-現状と将来展望」, 臨床 消化器内科 28: 1689-1696, 2013.

12. 2013 工藤正俊: 肝癌診療の East/West での相違とグローバルに於けるコンセンサスの方向性. 特集「肝癌診療のこれまでと今後-アジアをリードする日本の役割」, クリニシアン 613 号, 2013 (印刷中)

13. 2013 上嶋一臣, 工藤正俊: 再発肝臓癌. 特集「治せる再発がん・治せない再発がん」, 癌と化学療法, 2013 (締切 平成 25 年 4 月 19 日)

14. 2013 井上達夫, 工藤正俊: 解剖がわかれば走査がわかる 決定版 超音波検査テクニックマスター～腹部・下肢編～. Vascular Lab, 2013 (締切 平成 25 年 6 月 10 日)

15. 2013 矢田典久, 工藤正俊: 2.AIH と IgG4 関連病態. Ⅱ.既知の肝胆膵疾患との関連性, 特集「IgG4 と肝胆膵」, 肝胆膵, 2013 (締切 平成 25 年 7 月 23 日)

16. 2013 上嶋一臣, 工藤正俊: 肝細胞がん. 特集「最新がん薬物療法学-がん薬物療法の最新知見-」, 日本臨床, 2013 (締切 平成 25 年 8 月 1 日)

17. 2013 工藤正俊: Meeting Report. ILCA2013, The Liver Cancer Journal, 2013 (締切 平成 25 年 10 月 20 日)

18. 2013 工藤正俊: エッセイ (仮). 炉辺閑話 2014, 2014 (締切 平成 25 年 11 月 29 日)

19. 2013 北野雅之, 中井陽介, 山雄健次: 座談会: 消化器疾患に対する超音波内視鏡

検査－欧米と日本－. 特集「消化器疾患に対する超音波内視鏡検査－現況と将来展望」, 最新医学 68: 1677-1693, 2013.

20. 2013 北野雅之: 膵管非癒合. 専門医のための消化器病学（第 2 版）, 監修 小俣政男, 千葉 勉, 編集 下瀬川徹, 渡辺 守, 金子周一, 樫田博史, 医学書院, 東京, p658-661, 2013.

Ⅳ. 招待講演・特別講演（海外）

（2012 年記載漏れ分）

1. **Kudo M**: Invited Lecture “Interventional US for liver tumors.” The 10th Congress of Asian Federation of Societies for Ultrasound in Medicine and Biology (AFSUMB), Bali, Indonesia, November 7-10, 2012.

2. **Kudo M**: Invited Lecture “Double contrast US for surveillance of HCC.” The 10th Congress of Asian Federation of Societies for Ultrasound in Medicine and Biology (AFSUMB), Bali, Indonesia, November 7-10, 2012.

3. **Kudo M**: Invited Lecture “Sonazoid-enhanced US in the management of HCC.” The 10th Congress of Asian Federation of Societies for Ultrasound in Medicine and Biology (AFSUMB), Bali, Indonesia, November 7-10, 2012.

4. **Kudo M**: Invited Lecture “Interventional and contrast EUS for pancreatobiliary tumors.” The 10th Congress of Asian Federation of Societies for Ultrasound in Medicine and Biology (AFSUMB), Bali, Indonesia, November 7-10, 2012.

---

1. **Kudo M**: Special Lecture “Surveillance of hepatocellular carcinoma with CEUS using a unique contrast agent-Sonazoid.” “CEUS of liver lesions”, 14th World Congress of the world federation for ultrasound in medicine and biology (WFUMB) 2013, Sao Paulo, Brazil, May 2-5, 2013.

2. **Kudo M**: Special Lecture “a) Liver (Strain)” “Elastography”, 14th World Congress of the world federation for ultrasound in medicine and biology (WFUMB) 2013, Sao Paulo, Brazil, May 2-5, 2013.

3. **Kudo M**: Invited Lecture “Contras enhanced ultrasound (CEUS) in diagnostic imaging”. 3rd World Federation of Ultrasound in Medicine and Biology (WFUMB) Center of Excellence Seminar, 8th Annual Meeting of the Indonesian Society of Oncology Imaging (ISOI), 20th Annual Meeting of the Indonesian Society of Ultrasound in Medicine (ISUM), Jakarta, Indonesia, May 18-19, 2013.

4. **Kudo M**: Invited Lecture “Modern imaging approach to pancreatic tumours”. 3rd World Federation of Ultrasound in Medicine and Biology (WFUMB) Center of Excellence Seminar, 8th Annual Meeting of the Indonesian Society of Oncology Imaging (ISOI), 20th Annual Meeting of the Indonesian Society of Ultrasound in Medicine (ISUM), Jakarta,

Indonesia, May 18-19, 2013.

5. **Kudo M**: Invited Lecture “Liver elastography in the evaluation of liver fibrosis”. 3rd World Federation of Ultrasound in Medicine and Biology (WFUMB) Center of Excellence Seminar, 8th Annual Meeting of the Indonesian Society of Oncology Imaging (ISOI), 20th Annual Meeting of the Indonesian Society of Ultrasound in Medicine (ISUM), Jakarta, Indonesia, May 18-19, 2013.

6. **Kudo M**: Invited Lecture “Recent advances in ultrasound techniques for treatment guidance for liver tumours”. 3rd World Federation of Ultrasound in Medicine and Biology (WFUMB) Center of Excellence Seminar, 8th Annual Meeting of the Indonesian Society of Oncology Imaging (ISOI), 20th Annual Meeting of the Indonesian Society of Ultrasound in Medicine (ISUM), Jakarta, Indonesia, May 18-19, 2013.

7. **Kudo M**: Invited Lecture “How to evaluate treatment response in HCC: a mRESIST criterion enough?” “Unresolved Issues for Advanced HCC ”, The 4th Asia-Pacific Primary Liver Cancer Expert Meeting (APPLE),Busan, Korea, July 5-7, 2013.

8. **Kudo M**: Invited Lecture “Sorafenib in patients with liver dysfunction:Final analysis of GIDEON.” “Unresolved Issues for Advanced HCC ”, The 4th Asia-Pacific Primary Liver Cancer Expert Meeting (APPLE),Busan, Korea, July 5-7, 2013.

9. **Kudo M**: Invited Lecture “Treatment strategy for early stage of HCC.” “APPLE Consensus Workshop”, The 4th Asia-Pacific Primary Liver Cancer Expert Meeting (APPLE), Busan, Korea, July 5-7, 2013.

10. **Kudo M**: Invited Lecture “New druggable targets in HCC.” “Early Morning Work Shop 1 II. Hepatocellular Carcinoma: Genomics, Pathways & Targets”, The 4th Asia-Pacific Primary Liver Cancer Expert Meeting (APPLE), Busan, Korea, July 5-7, 2013.

11. **Kudo M**: Invited Lecture “What is TACE failure/refractory? Literature update and arriving at consensus.” “EPOIHCC”, The 4th Asia-Pacific Primary Liver Cancer Expert Meeting (APPLE), Busan, Korea, July 5-7, 2013.

12. **Kudo M**: Invited Lecture “Imaging assessment of tumor response.” “Controversial issues in early HCC”, The 4th Asia-Pacific Primary Liver Cancer Expert Meeting (APPLE), Busan, Korea, July 5-7, 2013.

13. **Kudo M**: Invited Lecture “Ultrasound elastography for non-invasive diagnosis of liver fibrosis”. Program of WFUMB COE Launching Workshop, Ulaanbaatar, Mongolia, July 25-27, 2013.

14. **Kudo M**: Invited Lecture “Interventional and contrast-enhanced EUS for pancreatobiliary diseases.” Program of WFUMB COE Launching Workshop, Ulaanbaatar, Mongolia, July 25-27, 2013.

15. **Kudo M**: Invited Lecture “Resection vs. ablation in very early HCC” Seventh Annual

Conference International Liver Cancer Association (ILCA), Washington D.C., USA, September 13-15, 2013.

16. **Kudo M**: Lecture "Diagnosis of diffuse liver diseases." Medical ultrasound society, Singapore 11th Annual Seminar in conjunction with AFSUMB Workshop 2013, Singapore, September 28-29, 2013.

17. **Kudo M**: Special Lecture "Management of Hepatocellular Carcinoma: Recent Progress." "Special Lecture (Ⅱ)", Taiwan Digestive Disease Week 2013 (TDDW), Taipei, Taiwan, October 5-6, 2013.

18. **Kudo M**: Invited Lecture "Contrast-enhanced EUS of GI disorders", The 5th Asian Conference of Ultrasound Contrast Imaging (ACUCI 2013), Taipei, Taiwan, October 19-20, 2013.

19. **Kudo M**: Invited Lecture "Diagnosis of Gross Pathological Classification of HCC by Kupffer phase CEUS", The 5th Asian Conference of Ultrasound Contrast Imaging (ACUCI 2013), Taipei, Taiwan, October 19-20, 2013.

20. **Kudo M**: Invited Lecture "APASL Guidelines." "Clinical practice guidelines: paradigms in management of HCC venue", 3rd APASL Single Topic Conference HCC IN 3D, Cebu, Philippines, November 21-23, 2013.

21. **Kudo M**: Invited Lecture "Management of intermediate stage HCC." "Current treatment strategies for HCC venue", 3rd APASL Single Topic Conference HCC IN 3D, Cebu, Philippines, November 21-23, 2013.

22. **Kudo M**: Invited Lecture "Ongoing trial with Sonazoid in Japan", Workshop for a Clinical Trial of HCC Screening with Sonazoid, Seoul, Korea, December 20, 2013.

23. Kitano M: Invited Lecture "Pancreatic EUS: Imaging distinguishes benign from neoplastic lesions". 10th Annual Rocky Mountain interventional Endoscopy Course, February 14-15, 2013, Colorado, USA.

24. Kitano M: Invited Lecture "FCMS for BPS; When? How?". "Recent update pancreatic stenting", Bonastent Summit 2013 in Busan, April 5-7, 2013, Paradise Hotel, Busan, Korea.

25. Kitano M: Invited Lecture "EUS in gastric cancer-Does it alter clinical management?" "Upper GI EUS", 3rd Practical Workshop in Diagnostic and Therapeutic Endoscopic Ultrasound, May 23-24, 2013, Hong Kong, China.

26. Kitano M: Invited Lecture "Contrast enhanced and elastography in EUS", 3rd Practical Workshop in Diagnostic and Therapeutic Endoscopic Ultrasound, May 23-24, 2013, Hong Kong, China.

27. Matsui S: Invited Lecture "Endoscopic submucosal dissection (ESD) procedure and management of complications associated with ESD for esophagogastric cancer.", 第一会天津市消化器早期がん・がん前病変国際フォーラム, June 2, 2013,

Tianjin, China.

28. Kitano M: Invited Lecture “Contrast-enhanced EUS: Can this replace EUS-FNA or just fancy?” Sessin Ⅲ “Technical advances on EUS-guided tissue acquisition for pancreatic lesions”, International Digestive Endoscopy Network 2013 with the 12th Korea-Japan Joint Symposium on Gastrointestinal Endoscopy, June 8-9, 2013, Grand Hilton Seoul, Korea.

29. Kitano M: Invited Lecture “ERCP: Beyond enteroscopy and cap”. Video lecture Ⅱ “Tips for successful ERCP in surgically altered anatomy”, International Digestive Endoscopy Network 2013 with the 12th Korea-Japan Joint Symposium on Gastrointestinal Endoscopy, June 8-9, 2013, Grand Hilton Seoul, Korea.

30. Kitano M: Invited Lecture “Contrast harmonic echo in EUS: the principles” 1st European CH-EUS Workshop, September 19-20, 2013, Hospital Prive Jean Mermoz, Lyon, France.

31. Kitano M: Invited Lecture “Other indication” 1st European CH-EUS Workshop, September 19-20, 2013, Hospital Prive Jean Mermoz, Lyon, France.

32. Kitano M: Invited Lecture “EUS-guided celiac neurolysis and block: ending the pain” 18th Annual Endoscopic Ultrasonography Live 2013, November 8-10, 2013, the University of Chicago Medicine Center for Care and Discovery, Cicago, USA.

33. Kitano M: Invited Lecture “Contrast agents and elastography: enhancing EUS” 18th Annual Endoscopic Ultrasonography Live 2013, November 8-10, 2013, the University of Chicago Medicine Center for Care and Discovery, Cicago, USA.

34. Nishimura N, Mori M, Nishida N: Landscape of DNA methylation status of human hepatocellular carcinoma revealed by the human methylation BeadChip 450K. AACR 104th Annual Meeting 2013, Washington, D.C., USA, April 6-10, 2013.

35. Yasuda I, Nakashima M, Iwai T, Isayama H, Itoi T, Hisai H, Inoue H, Kato H, Kanno A, Kubota K, Irisawa A, Igarashi H, Okabe Y, Kitano M, Kawakami H, Hayashi T, Mukai T, Kida M, Shimosegawa T: Japanese muliticenter experience of endscopic necrosectomy for infected walled-off pancreatic necrosis: JENIPaN study. Digestive Disease Week (DDW) 2013, May 19-21, 2013, Orlando, FL, USA.

36. Yoshida K, Nagasaka T, Umeda Y, Yokomichi N, Mori Y, Kubota N, Morikawa T, Takehara Y, Takehara K, Shigeyasu K, Nyuya A, Shiwaku R, Suno M, Nishida N, Fujiwara T, Goel A: Accumulation of epigenetic alteration could predict malignant formation in intraductal papillary mucinous neoplasm (IPMN). Digestive Disease Week (DDW) 2013, May 19-21, 2013, Orlando, FL, USA.

37. Yokomichi N, Nagasaka T, Nishida N, Umeda Y, Mori Y, Morikawa T, Kubota N, Yoshida K, Takehara Y, Takehara K, Shigeyasu K, Nyuya A, Shiwaku R, Suno M, Fujiwara T, Goel A: Cytokeratin 19 staining is a novel, predictive biomarker for extra-hepatic metastasis in hepatocellular carcinoma. Digestive Disease Week (DDW) 2013, May 19-21, 2013, Orlando, FL, USA.

38. Morikawa T, Nagasaka T, Yoshida K, Mori Y, Kubota N, Takehara Y, Yokomichi N, Nishida N, Takehara K, Shigeyasu K, Nyuya A, Shiwaku R, Suno M, Fujiwara T, Goel A: Fecal DNA methylation assay for the identification of a multiple gastrointestinal cancers including pancreatic cancer. Digestive Disease Week (DDW) 2013, May 19-21, 2013, Orlando, FL, USA.

39. Kubota N, Nagasaka T, Toda K, Mori Y, Morikawa T, Umeda Y, Yokomichi N, Yoshida K, Takehara Y, Takehara K, Nyuya A, Shiwaku R, Shigeyasu K, Suno M, Nishida N, Fujiwara T, Goel A: Genetic and epigenetic alteration in the netrin-1 receptors, unc5c and DCC, constitutes a previously unrecognized pathway in gastric cancer progression. Digestive Disease Week (DDW) 2013, May 19-21, 2013, Orlando, FL, USA.

40. Mori Y, Nagasaka T, Tazawa H, Umeda Y, Morikawa T, Kubota N, Yoshida K, Takehara Y, Yokomichi N, Takehara K, Shigeyasu K, Nyuya A, Shiwaku R, Suno M, Nishida N, Fujiwara T, Goel A: MGMT methylation as a novel biomarker for the identification of stage Ⅲ colorectal cancers at high-risk of disease recurrence following curative surgery. Digestive Disease Week (DDW) 2013, May 19-21, 2013, Orlando, FL, USA.

41. Nishimura T, Mori Y, Uemoto S, Nishida N: Loss at long arm of chromosome 4 as predictive factor for recurrence of human hepatocellular carcinoma after orthotopic living-donor liver transplantation. 2013 ASCO Annual Meeting, **Chicago**, USA, May 31-June 4, 2013.

42. Nishimura N, Mori M, Nishida N: Landscape of DNA methylation status of human hepatocellular carcinoma revealed by the human methylation BeadChip 450K. AACR 104th Annual Meeting 2013, Washington, D.C., USA, April 6-10, 2013.

43. Yasuda I, Nakashima M, Iwai T, Isayama H, Itoi T, Hisai H, Inoue H, Kato H, Kanno A, Kubota K, Irisawa A, Igarashi H, Okabe Y, Kitano M, Kawakami H, Hayashi T, Mukai T, Kida M, Shimosegawa T: Japanese muliticenter experience of endscopic necrosectomy for infected walled-off pancreatic necrosis: JENIPaN study. Digestive Disease Week (DDW) 2013, May 19-21, 2013, Orlando, FL, USA.

44. Yoshida K, Nagasaka T, Umeda Y, Yokomichi N, Mori Y, Kubota N, Morikawa T, Takehara Y, Takehara K, Shigeyasu K, Nyuya A, Shiwaku R, Suno M, Nishida N, Fujiwara T, Goel A: Accumulation of epigenetic alteration could predict malignant formation in intraductal papillary mucinous neoplasm (IPMN). Digestive Disease Week (DDW) 2013, May 19-21, 2013, Orlando, FL, USA.

45. Yokomichi N, Nagasaka T, Nishida N, Umeda Y, Mori Y, Morikawa T, Kubota N, Yoshida K, Takehara Y, Takehara K, Shigeyasu K, Nyuya A, Shiwaku R, Suno M, Fujiwara T, Goel A: Cytokeratin 19 staining is a novel, predictive biomarker for extra-hepatic metastasis in hepatocellular carcinoma. Digestive Disease Week (DDW) 2013, May 19-21, 2013, Orlando, FL, USA.

46. Morikawa T, Nagasaka T, Yoshida K, Mori Y, Kubota N, Takehara Y, Yokomichi N, Nishida N, Takehara K, Shigeyasu K, Nyuya A, Shiwaku R, Suno M, Fujiwara T, Goel A: Fecal DNA methylation assay for the identification of a multiple gastrointestinal cancers

including pancreatic cancer. Digestive Disease Week (DDW) 2013, May 19-21, 2013, Orlando, FL, USA.

47. Kubota N, Nagasaka T, Toda K, Mori Y, Morikawa T, Umeda Y, Yokomichi N, Yoshida K, Takehara Y, Takehara K, Nyuya A, Shiwaku R, Shigeyasu K, Suno M, Nishida N, Fujiwara T, Goel A: Genetic and epigenetic alteration in the netrin-1 receptors, unc5c and DCC, constitutes a previously unrecognized pathway in gastric cancer progression. Digestive Disease Week (DDW) 2013, May 19-21, 2013, Orlando, FL, USA.

48. Mori Y, Nagasaka T, Tazawa H, Umeda Y, Morikawa T, Kubota N, Yoshida K, Takehara Y, Yokomichi N, Takehara K, Shigeyasu K, Nyuya A, Shiwaku R, Suno M, Nishida N, Fujiwara T, Goel A: MGMT methylation as a novel biomarker for the identification of stage Ⅲ colorectal cancers at high-risk of disease recurrence following curative surgery. Digestive Disease Week (DDW) 2013, May 19-21, 2013, Orlando, FL, USA.

49. Nishimura T, Mori Y, Uemoto S, Nishida N: Loss at long arm of chromosome 4 as predictive factor for recurrence of human hepatocellular carcinoma after orthotopic living-donor liver transplantation. 2013 ASCO Annual Meeting, **Chicago**, USA, May 31-June 4, 2013.

Ⅴ. 招待講演・特別講演（国内）

1. 工藤正俊: 特別講演「肝胆膵領域の造影エコーの現況と展望」, 第 26 回日本腹部造影エコー・ドプラ診断研究会, 平成 25 年 4 月 6 日, ホテルグランヴィア大阪, 大阪.

2. 工藤正俊: 特別講演「肝細胞癌診療の新しいパラダイム」, 第 10 回臨床消化器病フォーラム, 平成 25 年 4 月 6 日, ウインクあいち, 愛知.

3. 工藤正俊: 特別講演「肝細胞癌治療の現状」, 第 3 回札幌肝疾患フォーラム, 平成 25 年 6 月 20 日,ニューオータニイン札幌, 北海道.

4. 工藤正俊: TACE と動注化学療法: 分子標的薬との併用. ワークショップ 3「肝細胞癌に対する TACE・肝動注化学療法・放射線療法の適応と治療成績」, 第 49 回日本肝癌研究会, 平成 25 年 7 月 11 日-12 日, 京王プラザホテル, 東京.

5. 工藤正俊: 特別講演「肝発癌の予測と分子標的治療」, 固形がんの基礎と臨床-インフォメーションからコミュニケーションへ-, 第 2 回三重先端がんフォーラム, 平成 25 年 7 月 19 日, 三重大学医学部, 三重.

6. 工藤正俊: 特別講演「肝炎, 肝癌治療の最近の話題」, 東四国ベアネットカンファレンス, 平成 25 年 8 月 10 日, JR ホテルクレメント高松, 香川.

7. 工藤正俊: 特別講演 肝臓領域「ソノグラファーへの望む！肝臓エコー」, JSS 関西第 20 回地方会学術集会, 平成 25 年 9 月 8 日, 神戸国際会議場, 兵庫.

8. 工藤正俊: 特別講演「超音波診断の最新動向: 腹部領域を中心に」, 第 31 回日本乳腺甲状腺超音波医学会学術集会, 平成 25 年 9 月 22 日, 神戸国際会議場, 兵庫.

9. 工藤正俊: 特別講演「超音波診断の最新動向: 腹部領域を中心に」, 日本超音波医学会第 40 回関西地方会学術集会, 平成 25 年 11 月 9 日, 大阪国際会議場, 大阪.

10. 北野雅之: 講演「EUS を用いた消化器内視鏡診断と治療」. 第 26 回日本消化器内視鏡学会近畿セミナー, 平成 25 年 1 月 6 日, 京都テルサ, テルサホール, 京都.

11. 松井繁長: 特別講演「低用量アスピリンによる消化管粘膜障害の現状と治療」. 南和医療学術講演会, 平成 25 年 1 月 12 日, 橿原ロイヤルホテル, 奈良.

12. 北野雅之: 特別講演「EUS-FNA の基礎から治療への応用まで」. 第 21 回日本消化器内視鏡学会北陸セミナー, 平成 25 年 1 月 20 日, 石川県政記念しいのき迎賓館, 石川.

13. 松井繁長: 講演「低用量アスピリンによる消化管粘膜傷害のリスクマネジメント」. 消化器フォーラム, 平成 25 年 1 月 26 日, シェラトン都ホテル大阪, 大阪.

14. 松井繁長: 講演「H.pylori 除菌治療の現状と留意点」. タケプロン発売 20 周年記念講演会, 平成 25 年 1 月 31 日, ホテル・アゴーラリージェンシー堺, 大阪.

15. 坂本洋城: 特別講演「胆膵疾患に対する Interventional EUS-Up to date-」. 第 18 回播磨消化器内視鏡懇話会, 平成 25 年 3 月 9 日, 姫路商工会議所, 兵庫.

16. 松井繁長: 特別講演「H.pylori 除菌治療の現状と課題」. 学術講演会, 平成 25 年 3 月 14 日, 耳原総合病院, 大阪.

17. 坂本洋城: デモンストレーション「ERCP・EUS デモンストレーション」. 大阪胆膵内視鏡研究会第 2 回大阪胆膵内視鏡ライブ, 平成 25 年 3 月 16 日, 公益財団法人田附興会医学研究所北野病院, 大阪.

18. 北野雅之: ミニセミナー「超音波内視鏡による診断と治療」. 第 13 回西宮消化器病フォーラム, 平成 25 年 4 月 4 日, ノボテル甲子園, 兵庫.

19. 北野雅之: 特別講演「超音波内視鏡の基礎から最先端治療まで」. 第 10 回臨床消化器病フォーラム, 平成 25 年 4 月 20 日, ホテルグランヴィア大阪, 大阪.

20. 北野雅之: 講師, 第 2 回 EUS-FNA トレーニングコース, 平成 25 年 4 月 21 日, オリンパスメディカルシステムズ技術開発センター石川, 東京.

21. 北野雅之: 次世代超音波観測装置. 特別企画「最新の機器開発報告」, 1. 超音波内視鏡の取組み, 2) 臨床報告, 消化器内視鏡促進連絡会第 30 回総会, 平成 25 年 5 月 9 日, ホテルグランヴィア京都, 京都.

22. 坂本洋城: オブサーバー「Meet the professor＝ How do we treat this case?」. 平成

25 年 5 月 11 日，グランドプリンスホテル京都，京都.

23. 北野雅之：私はこう考える～Covered WallFlex™の有用性 当院の使用経験と成績から～. エキスパートセミナー27「エキスパートに学ぶ WallFlex™ Biliary RX Stent の選択基準～Covered? or Uncovered? エビデンスから導き出される最善の治療を目指して～」，第 85 回日本消化器内視鏡学会総会，平成 25 年 5 月 12 日，国立京都国際会館，京都.

24. 坂本洋城：手技の実際「EUS ガイド下治療に標準化を目指して-胆道ドレナージ-」. 第 4 回超音波内視鏡下治療研究会，平成 25 年 5 月 12 日，国立京都国際会館，京都.

25. 松井繁長：症例提示「バレッド食道癌」. 第 418 回大阪胃研究会，平成 25 年 5 月 15 日，ホテルグランヴィア大阪，大阪.

26. 松井繁長：特別講演「H.pylori 除菌治療の新しい展開」. 第 10 回泉州 Closed Meeting，平成 25 年 5 月 30 日，スターゲイトホテル 関西エアポート，大阪.

27. 北野雅之：特別講演「膵疾患診療の最近の Topics」. 第 23 回りんくう消化器病研究会，平成 25 年 6 月 15 日，りんくう総合医療センター，大阪.

28. 汐見幹夫：特別企画：PEG に関するアンケート調査報告.「PEG の現況に関するアンケート-集計結果報告-」，第 19 回関西 PEG・栄養研究会，平成 25 年 6 月 15 日，ホテル大阪ベイタワー4 階 ベイタワーホール，大阪.

29. 上嶋一臣：ランチョンセミナー「肝癌の集学的治療～経カテーテル療法から分子標的薬まで～」. 第 8 回日本肝がん分子標的治療研究会，平成 25 年 6 月 22 日，和倉温泉「加賀屋」，石川.

30. 松井繁長：講演「お腹の痛みと胃の病気」. 第 49 回日本消化器病学会近畿支部市民公開講座，平成 25 年 6 月 22 日，ビッグ・アイ多目的ホール，大阪.

31. Sakamoto H: Invited Lecture “EUS-guided gallbladder drainage”. Tokyo Conference of Asian Pancreato-biliary International Endoscopist 2013 (T-CAP 2013), June 22-23, 2013, Ito International Research Center, Japan.

32. 松井繁長：講演「低用量アスピリンによる消化管粘膜障害の現状と対策」. 生駒市医師会講演会，平成 25 年 6 月 28 日，生駒メディカルセンター，奈良.

33. 南　康範：講演「Defect Re-perfusion image による診断」. 腹部造影超音波フォーラム 2013，平成 25 年 6 月 29 日，TKP ガーデンシティ品川，東京.

34. 松井繁長：特別講演「門脈圧亢進症について」. GSK 社内勉強会，平成 25 年 7 月 19 日，GSK 近畿リージョナルオフィス，大阪.

35. 北野雅之：講演「最新の EUS 事情-診断から治療まで- Interventional EUS」. 第 12 回新別府病院内視鏡ライブセミナー，平成 25 年 7 月 20 日，国家公務員共済組合連合会新別府病院，大分.

36. 松井繁長：講演「上部消化管における治療について」．社外講師勉強会，平成 25 年 7 月 26 日，日本製薬株式会社，大阪.

37. 松井繁長：講演「ESD 後潰瘍に対するムコスタの有用性」．Mucosal Conference，平成 25 年 9 月 5 日，ホテルモントレグラスミア大阪，大阪.

38. 樫田博史：講演「大腸腫瘍診断における NBI 拡大内視鏡」．日本消化器病学会近畿支部第 43 回教育講演会，平成 25 年 9 月 28 日，大阪国際交流センター，大阪.

39. 北野雅之：特別講演「胆膵疾患の EUS 診断-Update-」．第 15 回新都心胆膵カンファレンス，平成 25 年 10 月 1 日，東京医科大学病院，東京.

40. 久保正二，上嶋一臣：特別企画「肝癌診療 国内外の Up to date」，第 21 回日本消化器関連学会週間 JDDW2013（第 17 回日本肝臓学会大会・第 55 回日本消化器病学会大会・第 86 回日本消化器内視鏡学会総会・第 11 回日本消化器外科学会大会・第 51 回日本消化器がん検診学会大会・第 44 回日本消化器吸収学会総会合同），平成 25 年 10 月 9 日-12 日，グランドプリンスホテル高輪，東京.

41. 松井繁長：特別講演「NSAIDｓ、LDA による消化管粘膜傷害のリスクマネジメント」，第 348 回診療懇話会，平成 25 年 10 月 16 日，伊都医師会，和歌山.

42. 松井繁長：特別講演「食道疾患の現状と診断、治療-GERD/好酸球性食道炎も含めて-」．第 7 回南河内消化器カンファレンス，平成 25 年 10 月 19 日，SAYAKA ホール，大阪.

43. 北野雅之：特別講演「非切除胆膵癌により胆道・十二指腸狭窄に対するステンディングの現状と展望」．第 11 回甲信越胆・膵内視鏡フォーラム，平成 25 年 11 月 22 日，ベルクラシック甲府，山梨.

44. 萩原　智：PEG-IFNα2a 少量長期療法における発癌リスクの検討-IL28B 遺伝子多型との関連も含めて-．第 34 回南大阪肝胆膵研究会，平成 25 年 1 月 26 日，ホテルアゴーラリージェンシー堺，大阪.

45. 萩原　智：HBs 抗原消失を目指したエンテカビルと PEG-IFN48 週併用療法の高価について．第 10 回 Osaka Liver Collaboration Meeting，平成 25 年 2 月 7 日，ホテル日航大阪，大阪.

46. 坂本洋城：膵頭部分枝型膵 IPMN の経過観察中に出現した膵体部膵癌の 1 切除例．第 58 回日本消化器画像診断研究会，平成 25 年 3 月 1 日-2 日，ロワジールホテル那覇，沖縄.

47. 山雄健太郎，花田敬士，福田敏勝：外科的治療を行った慢性膵炎症例の長期成績．パネルディスカッション 2「慢性膵炎に対する内視鏡治療の現状」，第 85 回日本消化器内視鏡学会総会，平成 25 年 5 月 10 日-12 日，国立京都国際会館，京都.

48. 峯　宏昌，高山政樹：当院における薬剤性消化管障害による緊急上部内視鏡検査の検討．シンポジウム 1「薬剤性消化管傷害の現況と対策」，日本消化器内視鏡学会近畿支部第 90 回支部例会，平成 25 年 6 月 22 日，大阪国際交流センター，大阪.

49. 足立哲平，松井繁長，樫田博史：下部消化管出血に対する緊急内視鏡検査の検討．シンポジウム 2「下部消化管出血性疾患の現況とその対応」，日本消化器内視鏡学会近畿支部第 90 回支部例会，平成 25 年 6 月 22 日，大阪国際交流センター，大阪.

50. 上嶋一臣：TACE 不応の定義と後治療（ソラフェニブ）の立場から．Debates Session「TACE はどこまで続けるか？」，第 13 回関西肝血流動態イメージ研究会，平成 25 年 7 月 27 日，オーバルホール，大阪.

51. 山田光成，樫田博史，松井繁長，櫻井俊治，朝隈　豊，永田嘉昭，川崎正憲，峯　宏昌，永井知行，高山政樹，足立哲平，肥田仁一，武本昌子，仁科慎一，賴　晋也，　前西　修，佐藤隆夫：腹痛を契機に発見された服腔内原発 Ewing 肉腫の 1 例．日本消化器病学会近畿支部第 99 回例会，平成 25 年 9 月 28 日，大阪国際交流センター，大阪.

52. Adachi T, Matsui S, Kashida H: Usefulness of single-balloon endscopy for the small bowel lesions. Japan Digestive Disease Week 2013 (JDDW). Tokyo, Japan, October 9-12, 2013.

53. 川崎正憲，松井繁長，樫田博史：高齢者に対する胃癌 ESD の検討．シンポジウム 2「高齢者における内視鏡診療の問題点と対策（消化管）」，日本消化器内視鏡学会近畿支部第 91 回支部例会，平成 25 年 11 月 16 日，大阪国際交流センター，大阪.

54. 足立哲平，朝隈　豊，樫田博史：大腸腫瘍性病変の形態と内視鏡治療成績の検討．ビデオシンポジウム「大腸腫瘍性病変の内視鏡診断と治療」，日本消化器内視鏡学会近畿支部第 91 回支部例会，平成 25 年 11 月 16 日，大阪国際交流センター，大阪.

55. 岡元寿樹，松井繁長，樫田博史：興味ある経過を示した胃アミロイドーシスの一例．日本消化器内視鏡学会近畿支部第 91 回支部例会，平成 25 年 11 月 16 日，大阪国際交流センター，大阪.

56. 櫻井俊治：講演：ランチョンセミナー2「潰瘍性大腸炎の直腸病変に対する新しい治療選択ペンタサ®坐剤 1g の評価と可能性-私はこう使う-」．日本消化器内視鏡学会近畿支部第 91 回支部例会，平成 25 年 11 月 16 日，大阪国際交流センター，大阪.

VI. 学会発表（海外シンポジウム）

1. Kitano M, Kadosaka K, Sakamoto H, Imai H, Kamata K, Miyata T, Omoto S, Yamao K, **Kudo M**: Estimation of EUS features of choronic pancreatitis in comparison with clinical symptoms. International Pancreatic Research Forum 2013 (IPRF), Sendai, Japan, July 27, 2013.

2. **Kudo M**, Lencioni R, Ye SL, Bronowicki JP, Chen XP, Dagher L, Furuse J, Geschwind JF, Guevara LL, Papandreou C, Sanyal AJ, Takayama T, Yoon SK, Venook A, Nakajima K, Marrero J: Regional differences in treatment history, practices and outcomes: final

analysis of GIDEON (Global Investigation of therapeutic DEcisions in hepatocellular carcinoma and Of its treatment with sorafeNib). Oral Communications, Seventh Annual Conference International Liver Cancer Association (ILCA), Washington D.C., USA, September 13-15, 2013.

3. **Kudo M**, Finn R, Poon RT, Blanc JF, Han G, Yan L, Yang J, Lu L, Tak WY, Yu X, Lee JH, Lin SM, Wu C, Tanwandee T, Shao G, Walters I, Dela Cruz C, Poulart V, Wang JH: A randomized, double-blind, multicenter phase 3 study of Brivanib versus placebo as adjuvant therapy to trans-arterial chemoembolization (TACE)in patients with unresectable hepatocellular carcinoma (HCC): Initial results. Oral Communications, Seventh Annual Conference International Liver Cancer Association (ILCA), Washington D.C., USA, September 13-15, 2013.

4. Okita K, Kumada H, **Kudo M**: Effects on survival prognosis by peretinoin, an acyclic retinoid: five-year follow-up of phase 2/3 randomized placebo-controlled trial. Oral Communications, Seventh Annual Conference International Liver Cancer Association (ILCA), Washington D.C., USA, September 13-15, 2013.

5. **Kudo M**, Kumada H, Ikeda K, Kawazoe S, Osaki Y, Ikeda M, Okusaka T, Tamai T, Suzuki T, Kadowaki T, Funahashi Y, O'Brien JP, Okita K: Updated results from phase1/2 trial of lenvatinib (E7080), a multi-targeted tyrosine kinase inhibitor, and biomarker correlative analyses in patients (Pts) with advanced hepatocellular carcinoma (HCC). Seventh Annual Conference International Liver Cancer Association (ILCA), Washington D.C., USA, September 13-15, 2013.

6. Omoto S, Kitano M, **Kudo M**: The role of EUS in diagnosis and treatment of autoimmune pancreatitis. Japan Digestive Disease Week 2013 (JDDW). Tokyo, Japan, October 9-12, 2013.

7. Kitano M, Imai H, **Kudo M**: EUS-guided hepaticogastrostomy for treatment of obstructive jaundice in patients with malignant hilar biliary stricture after transpillary drainage is ineffective or unsuccessful. Japan Digestive Disease Week 2013 (JDDW). Tokyo, Japan, October 9-12, 2013.

8. Sakamoto H, Kitano M, **Kudo M**: Predictive factors for pain relief after endscopicultrasound-guided plexus neurolysis. Japan Digestive Disease Week 2013 (JDDW). Tokyo, Japan, October 9-12, 2013.

Ⅶ. 学会発表（海外一般演題）

1. Cainap C, Qin S, Huang HW, Chung I, Pan H, Cheng Y, **Kudo M**, Kang Y, Chen P, Toh H-C, Gorbunova V, Eskens F, Qian J, McKee MD, Ricker JL, Carlson DM, El-Nowiem S: Phase III Trial of Linifanib Versus Sorafenib In Patients With Advanced Hepatocellular Carcinoma (HCC). 2013 Gastrointeritinal Cancers Symposium (ASCO-GI 2013), San Francisco, USA, January 24-26, 2013.

2. Yada N, Hagiwara S, Arizumi T, Takita M, Kitai S, Inoue T, Minami Y, Ueshima K, Nishida N, **Kudo M**: Noninvasive assessment of liver fibrosis by measurement of LF index in patients with chronic viral hepatitis. Digestive Disease Week (DDW) 2013, Orlando, USA, May 19-21, 2013.

3. Nagata Y, Sakurai T, Takayama M, Nagai T, Kawasaki M, Asakuma Y, Hagiwara S, Nishida N, Matsui S, Kashida H, **Kudo M**: Heat shock protein 27 expression is inversely correlated with intraepithelial neoplasia and positively correlated with poor differentiation of gastris cancer. Digestive Disease Week (DDW) 2013, Orlando, USA, May 19-21, 2013.

4. Matsui S, **Kudo M**, Kashida H, Asakuma Y, Kawasaki M, Sakurai T: The clinical characteristics and endoscopic treatment of hemorrhagic duodenal varices. Digestive Disease Week (DDW) 2013, Orlando, USA, May 19-21, 2013.

5. Kitano M, Takeyama Y, Miyata T, Kamata K, Sakamoto H, Imai H, Kadosaka K, Omoto S, **Kudo M**: EUS-guided drainage for treatment of postoperative complications after pancreatic surgery. Digestive Disease Week (DDW) 2013, Orlando, USA, May 19-21, 2013.

6. Miyata T, Kitano M, Sakamoto H, Imai H, Kamata K, Kadosaka K, Omoto S, **Kudo M**: Role of contrast-enhanced harmonic EUS in differentiating malignant from benign lymphadenopathy. Digestive Disease Week (DDW) 2013, Orlando, USA, May 19-21, 2013.

7. Tsuji N, Okumura N, Taniike S, Takaba T, Matsumoto N, Kono M, Maruyama Y, **Kudo M**: Verrucous antral gastritis is not related to H. pylori-positive chronic gastritis, but is related to a high BMI and barrett's esophagus. Digestive Disease Week (DDW) 2013, Orlando, USA, May 19-21, 2013.

8. Tsuji N, Okumura N, Taniike S, Takaba T, Matsumoto N, Kono M, Maruyama Y, **Kudo M**: Time trends for helicobactor pylori eradication rate of the first-line and second-line Japanese regimens and clarithromycin resistance. Digestive Disease Week (DDW) 2013, Orlando, USA, May 19-21, 2013.

9. Yada N, **Kudo M**: Diagnostic performance of liver fibrosis with real-time tissue elastography in chronic viral hepatitis C. International Symposium "Elastography of the liver in Asia", The 86th Annual Scientific Meeting of the Japan Society of Ultrasonics in Medicine, Osaka, May 14-26, 2013.

10. Marrero J, Lencioni R, Ye SL, **Kudo M**, Bronowicki JP, Chen XP, Dagher L, Furuse J, Geschwind JF, Guevara LLd, Papandreou C, Sanyal AJ, Takayama T, Yoon SK, Nakajima K, Venook a: Final analysis of GIDEON (Global Investigation of therapeutic DEcisions in hepatocellular carcinoma [HCC] and Of its treatment with sorafeNib [Sor]) in >3000 Sor-treated patients (pts): clinical findings in pts with liver dysfunction. American Society of Clinical Oncology (ASCO) 49th Annual Meeting, **Chicago**, USA, May 31-June 4, 2013.

11. Cheng AL, Finn R, **Kudo M**, Llovet JM, Qin S, Berre ML, Krissel H, Bruix J: Regoranib in patients with hepatocellular carcinoma (HCC) progressing following Sorafenib: an ongoing randomized, double-blind, phase Ⅲ trial. American Society of Clinical Oncology (ASCO) 49th Annual Meeting, **Chicago**, USA, May 31-June 4, 2013.

12. Cheng AL, Qin S, Park JW, Poon R, Raoul JL, Philip PA, Hsu CH, Hu TH, Heo J, Xu J, Lu L, Chao Y, Boucher E, Han KH, Paik SW, Avina JR, **Kudo M**, Liu D, Ezzeddine R, Walters I, Johnson P: First-line Brivanib (BRIV) Versus Sorafenib (SOR) in Unresectable, Advanced Hepatocellular Carcinoma (HCC): Asia/Non-Asia Survival Results in Phase 3 BRISK-FL Study. Asian Pacific Association for the Study of the Liver (APASL) 2013, Singapore, June 6-10, 2013.

13. Omoto S, Kitano M, **Kudo M**: The role of EUS in diagnosis and treatment of autoimmune pancreatitis. Tokyo Conference of Asian Pancreato-biliary International Endoscopist 2013 (T-CAP 2013), June 22-23, 2013, Ito International Research Center, Japan.

14. Miyata T, Kitano M, **Kudo M**: Role of contrast-enhanced harmonic EUS in differentiating malignant from benign lymphadenopathy. Tokyo Conference of Asian Pancreato-biliary International Endoscopist 2013 (T-CAP 2013), June 22-23, 2013, Ito International Research Center, Japan.

15. Nishida N, **Kudo M**, Chishina H, Arizumi T, Takita M, Kitai S, Yada N, Hagiwara S, Inoue T, Minami Y, Ueshima K, Sakurai T, Yokomichi N, Nagasaka T, Goel A: Unique association between global DNA hypomethylation and chromosomal alterations in human hepatocellular carcinoma. 7th Annual Conference International Liver Cancer Association (ILCA), Washington D.C., USA, September 13-15, 2013.

16. Kitai S, **Kudo M**, Izumi N, Sakamoto M, Matsuyama Y, Ichida T, Nakashima O, Matsui

O, Ku Y, Kokudo N, Matsunaga T, Makuuchi M: Validation of staging systems for hepatocellular carcinoma: a comparison of the Bm-JIS score, the JIS score and the BCLC staging. 7th Annual Conference International Liver Cancer Association (ILCA), Washington D.C., USA, September 13-15, 2013.

17. Inoue T, Arizumi T, Ueshima K, Nishida N, **Kudo M**: The factors related to the vascularization of border line lesions detected as low intensity on hepatobiliary phase image of GD-EOB-DTPA MRI. 7th Annual Conference International Liver Cancer Association (ILCA), Washington D.C., USA, September 13-15, 2013.

18. Arizumi T, Ueshima K, Takita M, Kitai S, Yada N, Hagiwara S, Minami Y, Sakurai T, Nishida N, **Kudo M**: Sorafenib treatment for non-hypervascular hepatocellular carcinoma. 7th Annual Conference International Liver Cancer Association (ILCA), Washington D.C., USA, September 13-15, 2013.

19. Lencioni R, **Kudo M**, Marrero J, Venook A, Ye SL, Bronowicki JP, Chen XP, Dagher L, Furuse J, Guevara LLd, Papandreou C, Sanyal AJ, Takayama T, Yoon SK, Nakajima K, Geschwind JF: Final analysis of GIDEON (Global Investigation of therapeutic DEcisions in hepatocellular carcinoma [HCC] and Of its treatment with sorafeNib): safety and outcomes by prior transarterial chemoembolization (TACE) use. CIRSE 2013, Barcelona, Spain, September 14-18, 2013.

20. Bronowicki JP, Lencioni R, Ye SL, **Kudo M**, Papandreou C, Nakajima K, Venook A, Marrero J: Final analysis of GIDEON (Global Investigation of therapeutic DEcisions in hepatocellular carcinoma and Of its treatment with sorafeNib) in>3000 sorafenib-treated patients: prognostic value of baseline characteristics and staging systems. Poster presented at the European Cancer Congress 2013 (ECCO-ESMO-ESTRO), Amsterdam, Netherlands, September 27-October 1, 2013.

21. Sakamoto H, Kitano M, **Kudo M**: Differential diagnosis of SMT and evaluation of malignant potential GISTS by contrast enhanced harmonic EUS. 21th United European Gastroenterology Week (UEGW), Berlin, Germany, October 12-16, 2013.

22. Sakamoto H, Kitano M, **Kudo M**: Predictive factors for pain relief after endoscopic ultrasound-guided upper plexus neurolysis. 21th United European Gastroenterology Week (UEGW), Berlin, Germany, October 12-16, 2013.

23. Kashida H, Adachi T, Sakurai T, Asakuma Y, Kawasaki M, Nagai T, Mine H, Takayama

M, Matsui S, **Kudo M**: The learning curve of endoscopic submucosal dissection in the colorectum. 21th United European Gastroenterology Week (UEGW), Berlin, Germany, October 12-16, 2013.

24. Ogawa C, **Kudo M**, Arasawa S, Shibatouge M: The usefulness of the epoch method "Defect re-perfusion imaging" to diagnose HCC using new agent sonazoid. The 5th Asian Conference of Ultrasound Contrast Imaging (ACUCI 2013), Taipei, Taiwan, October 19-20, 2013.

25. **Kudo M**, Ueshima K, Osaki Y, Hirooka M, Imai Y, Aso K, Numata K, Ichinose M, Kumada T, Izumi N, Sumino Y, Akazawa K: B-mode ultrasonography versus contrast-enhanced ultrasonography for surveillance of hepatocellular carcinoma: a prospective multicenter randomized controlled trial. The 64th Annual Meeting of the American Association for the Study of Liver Disease (AASLD), Washington D.C., USA, November 1-5, 2013.

26. Nishida N, **Kudo M**, Arizumi T, Takita M, Kitai S, Yada N, Inoue T, Hagiwara S, Minami Y, Sakurai T, Ueshima K, Nagasaka T, Goel A: Role of oxidative stress and epigenetic alteration on chronic hepatitis C-related human hepatocarcinogenesis. The 64th Annual Meeting of the American Association for the Study of Liver Disease (AASLD), Washington D.C., USA, November 1-5, 2013.

27. Sanyal AJ, Lencioni R, Ye SL, **Kudo M**, Venook A, Bronowicki JP, Chen XP, Dagher L, Furuse J, Geschwind JF, Guevara LL, Papandreou C, Takayama T, Yoon SK, Nakajima K, Marrero J: Safety and outcomes by disease etiology in sorafenib-treated uHCC patients in clinical practice: final analysis of GIDEON (Global Investigation of therapeutic DEcisions in hepatocellular carcinoma and Of its treatment with sorafeNib). The 64th Annual Meeting of the American Association for the Study of Liver Disease (AASLD), Washington D.C., USA, November 1-5, 2013.

28. Geschwind JF, **Kudo M**, Marrero J, Venook A, Ye SL, Bronowicki JP, Chen XP, Dagher L, Furuse J, Guevara LL, Papandreou C, Sanyal AJ, Takayama T, Yoon SK, Nakajima K, Lencioni R: Final analysis of GIDEON (Global Investigation of therapeutic DEcisions in hepatocellular carcinoma and Of its treatment with sorafeNib): regional trends, safety, and outcomes in patients receiving concomitant transarterial chemoembolization. 99th Scientific Assembly and Annual Meeting (RSNA 2013), Chicago, USA, December 1-6, 2013.

Ⅷ. 学会発表

（国内シンポジウム・パネルディスカッション・ワークショップ）

1. 上嶋一臣，有住忠晃，工藤正俊：ソラフェニブ治療後の後治療についての検討．シンポジウム「進行肝細胞癌に対してネクサバールを含んだ治療を、どう生命予後改善につなげるか？」， 第 7 回日本肝がん分子標的治療研究会，平成 25 年 1 月 19 日，じゅうろくプラザ，岐阜．

2. 小川　力，森岡弓子，野田晃世，上田祐也，宮本由貴子，野上明子，吉岡正博，石川哲朗，松中寿浩，玉置敬之，柴峠光成，河合直之，山岡竜也，石川順英，廣瀬哲朗，西平友彦，嶋田俊秀，荻野哲朗，工藤正俊：CTHA と比較したソナゾイド US による nodule in nodule の HCC の診断とその問題点．シンポジム 2「肝血流・機能イメージのバイオマーカー的意義を探る」，第 19 回肝血流動態イメージ研究会，平成 25 年 1 月 26 日～27 日，東京ビッグサイト「国際会議場」，東京．

3. 大本俊介，北野雅之，工藤正俊：膵腫瘍に対する造影ハーモニック EUS（CH-EUS）の有用性について．シンポジウム 1「消化器診療におけるイノベーション」，日本消化器病学会近畿支部第 98 回例会，平成 25 年 2 月 16 日，神戸ポートピアホテル，兵庫．

4. 松井繁長，樫田博史，工藤正俊：十二指腸静脈瘤の病態と治療．ワークショップ 7「異所性静脈瘤・胃静脈瘤の病態と治療」，第 49 回日本腹部救急医学会総会，平成 25 年 3 月 13 日-14 日，福岡国際会議場，福岡．

5. 南　康範，工藤正俊，村上卓道：Interventional radiology における支援画像「FlightPlan」の有用性．シンポジウム 2「肝画像診断の最前線」，第 99 回日本消化器病学会総会，平成 25 年 3 月 21 日-23 日，城山観光ホテル，かごしま県民交流センター，鹿児島．

6. 今井　元，北野雅之，工藤正俊：EUS 下胆道ドレナージ術の有用性．シンポジウム 9「非切除胆膵癌に対する内視鏡的 intervention の進歩」，第 99 回日本消化器病学会総会，平成 25 年 3 月 21 日-23 日，城山観光ホテル，かごしま県民交流センター，鹿児島．

7. 坂本洋城，北野雅之，工藤正俊：EUS 下腹腔内神経叢融解術の成績とその適応．ワークショップ 12 胆膵疾患に対する interventional EUS の現状」，第 99 回日本消化器病学会総会，平成 25 年 3 月 21 日-23 日，城山観光ホテル，かごしま県民交流センター，鹿児島．

8. 大本俊介，工藤正俊，北野雅之：当院における膵仮性嚢胞に対する TherapeuticEUS の工夫と成績．パネルディスカッション 2「慢性膵炎に対する内視鏡治療の現状」，第 85 回日本消化器内視鏡学会総会，平成 25 年 5 月 10 日-12 日，国立京都国際会館，京都．

9. 門阪薫平，北野雅之，工藤正俊：早期慢性膵炎と糖尿病の関連について．パネルディスカッション 3「生活習慣病と内視鏡」，第 85 回日本消化器内視鏡学会総会，平成 25 年 5 月 10 日-12 日，国立京都国際会館，京都．

10. 坂本洋城，北野雅之，工藤正俊：胃粘膜下腫瘍の EUS-FNA の成績と造影ハーモニック EUS による鑑別診断の試み．ワークショップ 2「胃粘膜下腫瘍の臨床的取り扱い」，第 85 回日本消化器内視鏡学会総会，平成 25 年 5 月 10 日-12 日，国立京都国際会館，京都．

11. 宮田　剛，北野雅之，工藤正俊：EUS 下膵管・胆道ドレナージ術の方法と成績．VTR シンポジウム 2「Interventional EUS の進歩」，第 85 回日本消化器内視鏡学会総会，平成 25 年 5 月 10 日-12 日，国立京都国際会館，京都.

12. 坂本洋城，北野雅之，工藤正俊：超音波内視鏡（EUS）による膵疾患の診断と治療．シンポジウム 17「体腔内超音波の現状と展望」,日本超音波医学会第 86 回学術集会，平成 25 年 5 月 24 日-26 日，大阪国際会議場，大阪.

13. 工藤正俊：消化器診断の立場から．パネルディスカッション 24「Real-time Tissue Elasstography～10 年の歩み～」，日本超音波医学会第 86 回学術集会，平成 25 年 5 月 24 日-26 日，大阪国際会議場，大阪.

14. 坂本洋城，北野雅之，工藤正俊：EUS-FNA と造影ハーモニック EUS によるステージⅠ膵癌の検討．パネルディスカッション 17「小膵癌：超音波検査を用いたステージⅠへのアプローチ」，日本超音波医学会第 86 回学術集会，平成 25 年 5 月 24 日-26 日，大阪国際会議場，大阪.

15. 北野雅之，坂本洋城，工藤正俊：膵疾患診断における造影ハーモニック EUS 検査の有用性．パネルディスカッション 26「消化器疾患診断に造影超音波は必要か？」，日本超音波医学会第 86 回学術集会，平成 25 年 5 月 24 日-26 日，大阪国際会議場，大阪.

16. 今井　元，北野雅之，大本俊介，門阪薫平，宮田　剛，鎌田　研，坂本洋城，工藤正俊：膵疾患に対する造影超音波検査．パネルディスカッション 27「膵腫瘍の診断に最も有用な画像診断法は？：画像診断の現状とピットフォール」日本超音波医学会第 86 回学術集会，平成 25 年 5 月 24 日-26 日，大阪国際会議場，大阪.

17. 有住忠晃，上嶋一臣，田北雅弘，北井　聡，　井上達夫，　矢田典久，萩原　智，南　康範，櫻井俊治，西田直生志，工藤正俊：進行肝細胞癌のソラフェニブ治療における腫瘍血流と治療効果との関連．ワークショップ 1「分子標的薬の効果予後予測因子から治療法対象を考える」，第 8 回日本肝がん分子標的治療研究会，平成 25 年 6 月 22 日，和倉温泉「加賀屋」，石川.

18. 門阪薫平，北野雅之，工藤正俊：経乳頭的治療不能悪性胆道狭窄に対する EUS 下胆道ドレナージ術の有用性．ワークショップ「超音波内視鏡を用いた胆膵疾患の診断と治療の現況」，日本消化器内視鏡学会近畿支部第 90 回支部例会，平成 25 年 6 月 22 日，大阪国際交流センター，大阪.

19. 上嶋一臣，有住忠晃，工藤正俊：肝がん化学療法からみた肝動注リザーバーの生き残る道～SILIUS Phase Ⅲ trial の重要性～．シンポジウム 1「肝細胞癌に対する肝動注療法の生き残る道」，第 38 回リザーバー研究会，平成 25 年 6 月 28 日-29 日，かがわ国際会議場，香川.

20. 上嶋一臣，有住忠晃，工藤正俊：TACE または肝動注化学療法とソラフェニブの併用療法の重要性．シンポジウム 1「肝癌における分子標的治療の最前線」，第 49 回日本肝癌研究会，平成 25 年 7 月 11 日-12 日，京王プラザホテル，東京.

21. 南　康範，工藤正俊，中居卓也：近畿大学病院における大腸癌肝転移の治療ストラテ

ジー．パネルディスカッション 2「転移性肝癌治療のアルゴリズム」，第 49 回日本肝癌研究会，平成 25 年 7 月 11 日-12 日，京王プラザホテル，東京.

22. 有住忠晃，大﨑往夫，工藤正俊：ソラフェニブ治療例の生存期間からみた画像診断法による効果判定規準の問題点と再評価．シンポジウム 2「肝細胞癌における画像診断法の最前線」，第 49 回日本肝癌研究会，平成 25 年 7 月 11 日-12 日，京王プラザホテル，東京.

23. 井上達夫，村上卓道，工藤正俊：EOB-MRI の肝細胞相で低信号に描出される乏血性結節の多血化因子の検討～多施設共同 retrospective study～．パネルディスカッション 3「肝乏血性腫瘤の診断と治療戦略」，第 49 回日本肝癌研究会，平成 25 年 7 月 11 日-12 日，京王プラザホテル，東京.

24. 鎌田　研，北野雅之，工藤正俊，大本俊介，門阪薫平，今井　元，坂本洋城，竹山宜典：IPMN 経過観察における EUS の有用性～造影 EUS による診断も含めて～．特別企画 1 ディベート「分枝型 IPMN の診療：内科 vs 外科 vs 病理」，第 44 回日本膵臓学会大会，平成 25 年 7 月 25 日-26 日，仙台国際センター，宮城.

25. 宮田　剛，北野雅之，工藤正俊：急性・慢性膵炎の治療における Interventional EUS の有用性．特別企画 2 ビデオシンポジウム「急性膵炎・慢性膵炎に対する内視鏡・腹腔鏡治療の最前線」，第 44 回日本膵臓学会大会，平成 25 年 7 月 25 日-26 日，仙台国際センター，宮城.

26. 門阪薫平，北野雅之，工藤正俊：早期慢性膵炎 EUS 画像所見と糖尿病の関連について．パネルディスカッション 2「膵内外分泌相関の新しい展開」，第 44 回日本膵臓学会大会，平成 25 年 7 月 25 日-26 日，仙台国際センター，宮城.

27. 櫻井俊治，峯　宏昌，樫田博史，工藤正俊：大腸発癌における幹細胞の制御機能．シンポジウム 2「発がんとがん予防の科学と実践」，第 24 回日本消化器癌発生学会総会，平成 25 年 9 月 5 日-6 日，石川県立音楽堂，石川.

28. 松井繁長，樫田博史，朝隈　豊，川崎正憲，工藤正俊：十二指腸静脈瘤の病態と治療方針．要望演題 11「異所性静脈瘤の病態と治療 1」，第 20 回日本民脈圧亢進症学会総会，平成 25 年 9 月 19 日，名古屋国際会議場，愛知.

29. 今井　元，北野雅之，工藤正俊：EUS 下胆道ドレナージ術の可能性．シンポジウム 1「胆道ドレナージの現状と新たな展開」，第 49 回日本胆道学会学術集会，平成 25 年 9 月 19-20 日，ヒルトン東京ベイ，千葉.

30. 萩原　智，工藤正俊，大﨑往夫：HBs 抗原消失を目指したエンテカビルと PEG-IFNα2b 48 週併用療法の効果について．シンポジウム「ウイルス性肝炎治療の最前線」，日本消化器病学会近畿支部第 99 回例会，平成 25 年 9 月 28 日，大阪国際交流センター，大阪.

31. 井上達夫，工藤正俊，村上卓道：肝細胞癌の早期発見における EOB-MRI と造影超音波検査の有用性．パネルディスカッション 1「肝・胆・膵腫瘍性病変早期発見に向けた取り組み」，日本消化器病学会近畿支部第 99 回例会，平成 25 年 9 月 28 日，大阪国際交流センター，大阪.

32. 有住忠晃，上嶋一臣，工藤正俊：TACE 不応の進行肝細胞癌患者に対するソラフェニブ開始時期の検討．パネルディスカッション 2「根治治療不能進行消化器癌に対する治療選択」，日本消化器病学会近畿支部第 99 回例会，平成 25 年 9 月 28 日，大阪国際交流センター，大阪．

33. 大本俊介，北野雅之，工藤正俊：進行膵癌に対する Gemcitabine（GEM）/Erlotinib 併用療法の二次化学療法の治療成績．パネルディスカッション 2「根治治療不能進行消化器癌に対する治療選択」，日本消化器病学会近畿支部第 99 回例会，平成 25 年 9 月 28 日，大阪国際交流センター，大阪．

34. 高山政樹，松井繁長，樫田博史，工藤正俊：当院における OGIB 症例の検討．シンポジウム 2「原因不明消化管出血の診断と治療の最前線」，日本消化器病学会近畿支部第 99 回例会，平成 25 年 9 月 28 日，大阪国際交流センター，大阪．

35. 工藤正俊：肝臓がんの集学的治療．腫瘍別シンポジウム「消化器がん研究の進歩と今後の展望」，Multimodal treatment of hepatocellular carcinoma. Symposia on specific tumors 〝Cancer research on digestive organs: yesterday, today, and tomorrow〞，第 72 回日本癌学会学術集会，平成 25 年 10 月 3-5 日，パシフィコ横浜，神奈川．

36. 矢田典久，萩原　智，工藤正俊：各種超音波エラストグラフィによる肝線維化診断．パネルディスカッション 5「非侵襲的肝病態評価法の適応と限界」，第 21 回日本消化器関連学会週間 JDDW2013（第 17 回日本肝臓学会大会・第 55 回日本消化器病学会大会・第 86 回日本消化器内視鏡学会総会・第 11 回日本消化器外科学会大会・第 51 回日本消化器がん検診学会大会・第 44 回日本消化器吸収学会総会合同），平成 25 年 10 月 9 日-12 日，品川プリンスホテル，東京．

37. 鎌田　研，北野雅之，工藤正俊：IPMN 国際診療ガイドライン 2012 年度版の検証～EUS の位置づけはどこにあるか？～．パネルディスカッション 7「IPMN 新コンセンサス診療ガイドラインの検証」，第 21 回日本消化器関連学会週間 JDDW2013（第 17 回日本肝臓学会大会・第 55 回日本消化器病学会大会・第 86 回日本消化器内視鏡学会総会・第 11 回日本消化器外科学会大会・第 51 回日本消化器がん検診学会大会・第 44 回日本消化器吸収学会総会合同），平成 25 年 10 月 9 日-12 日，グランドプリンスホテル新高輪国際パミール，東京．

38. 鎌田　研，北野雅之，工藤正俊：造影ハーモニック EUS のよる胆嚢病変の鑑別診断．ワークショップ 6「胆道疾患の診断・治療に有用な画像診断-内視鏡診断から三次元画像診断」，第 21 回日本消化器関連学会週間 JDDW2013（第 17 回日本肝臓学会大会・第 55 回日本消化器病学会大会・第 86 回日本消化器内視鏡学会総会・第 11 回日本消化器外科学会大会・第 51 回日本消化器がん検診学会大会・第 44 回日本消化器吸収学会総会合同），平成 25 年 10 月 9 日-12 日，グランドプリンスホテル新高輪国際パミール，東京．

39. 坂本洋城，北野雅之，工藤正俊：乳頭括約筋切除術を行わない Trans-catheter biliary endoscopy の有用性の検討．ワークショップ 6「胆道疾患の診断・治療に有用な画像診断-内視鏡診断から三次元画像診断」，第 21 回日本消化器関連学会週間 JDDW2013（第 17 回日本肝臓学会大会・第 55 回日本消化器病学会大会・第 86 回日本消化器内視鏡学会総会・第 11 回日本消化器外科学会大会・第 51 回日本消化器がん検診学会大会・第 44 回日本消化器吸収学会総会合同），平成 25 年 10 月 9 日-12 日，グランドプリンスホテル新高輪国際パミール，東京．

40. 門阪薫平，北野雅之，工藤正俊：機能性ディスペプシアの早期慢性膵炎が存在する可能性について．ワークショップ 12「機能性ディスペプシア-診断と治療の現況を巡って-」．第 21 回日本消化器関連学会週間 JDDW2013（第 17 回日本肝臓学会大会・第 55 回日本消化器病学会大会・第 86 回日本消化器内視鏡学会総会・第 11 回日本消化器外科学会大会・第 51 回日本消化器がん検診学会大会・第 44 回日本消化器吸収学会総会合同），平成 25 年 10 月 9 日-12 日，グランドプリンスホテル新高輪国際パミール，東京．

41. 今井　元，北野雅之，工藤正俊：切除不能胆道狭窄での EUS 下胆道ドレナージの位置づけ．ワークショップ 14「胆道癌の胆管ドレナージの標準化-手術症例と非手術症例」，第 21 回日本消化器関連学会週間 JDDW2013（第 17 回日本肝臓学会大会・第 55 回日本消化器病学会大会・第 86 回日本消化器内視鏡学会総会・第 11 回日本消化器外科学会大会・第 51 回日本消化器がん検診学会大会・第 44 回日本消化器吸収学会総会合同），平成 25 年 10 月 9 日-12 日，グランドプリンスホテル新高輪国際パミール，東京．

42. 櫻井俊治，樫田博史，工藤正俊：肝発癌および治療抵抗性獲得における幹細胞の役割．ワークショップ 16「消化器癌に対する幹細胞研究の現状と展望」，第 21 回日本消化器関連学会週間 JDDW2013（第 17 回日本肝臓学会大会・第 55 回日本消化器病学会大会・第 86 回日本消化器内視鏡学会総会・第 11 回日本消化器外科学会大会・第 51 回日本消化器がん検診学会大会・第 44 回日本消化器吸収学会総会合同），平成 25 年 10 月 9 日-12 日，品川プリンスホテル，東京．

43. 今井　元，北野雅之，工藤正俊：EUS ガイド下胆管ドレナージ術における工夫とトラブルシューティング．ワークショップ 23「胆膵内視鏡のトラブルシューティング《ビデオ》」，第 21 回日本消化器関連学会週間 JDDW2013（第 17 回日本肝臓学会大会・第 55 回日本消化器病学会大会・第 86 回日本消化器内視鏡学会総会・第 11 回日本消化器外科学会大会・第 51 回日本消化器がん検診学会大会・第 44 回日本消化器吸収学会総会合同），平成 25 年 10 月 9 日-12 日，品川プリンスホテル，東京．

44. 梅原康湖，辻　直子，工藤正俊：プロポフォールを用いた外来内視鏡検査の安全性・有用性と患者満足度の検討．ワークショップ 25「プロフォールを活用する」，第 21 回日本消化器関連学会週間 JDDW2013（第 17 回日本肝臓学会大会・第 55 回日本消化器病学会大会・第 86 回日本消化器内視鏡学会総会・第 11 回日本消化器外科学会大会・第 51 回日本消化器がん検診学会大会・第 44 回日本消化器吸収学会総会合同），平成 25 年 10 月 9 日-12 日，品川プリンスホテル，東京．

45. 宮田　剛，北野雅之，工藤正俊：EUS におけるミタゾラムとプロポフォールによる鎮静に対する BIS モニター（Bispectral index monitoring）の有用性の検討．ワークショップ 25「プロフォールを活用する」，第 21 回日本消化器関連学会週間 JDDW2013（第 17 回日本肝臓学会大会・第 55 回日本消化器病学会大会・第 86 回日本消化器内視鏡学会総会・第 11 回日本消化器外科学会大会・第 51 回日本消化器がん検診学会大会・第 44 回日本消化器吸収学会総会合同），平成 25 年 10 月 9 日-12 日，品川プリンスホテル，東京．

46. 工藤正俊，上嶋一臣：肝細胞癌に対する分子標的治療：現状と問題点．シンポジウム 15「消化器癌に対する分子標的薬-最近の動向」，第 21 回日本消化器関連学会週間 JDDW2013（第 17 回日本肝臓学会大会・第 55 回日本消化器病学会大会・第 86 回日本消化器内視鏡学会総会・第 11 回日本消化器外科学会大会・第 51 回日本消化器がん検診学会大会・第 44 回日本消化器吸収学会総会合同），平成 25 年 10 月 9 日-12 日，グランドプリンスホテル新高輪国際パミール，東京．

47. 大本俊介，北野雅之，工藤正俊:当院における EUS 下胆道および膵管ドレナージの工夫と成績．シンポジウム 1「消化器領域超音波の最前線-診断からインターベンションまで」，日本超音波医学会第 40 回関西地方会学術集会，平成 25 年 11 月 9 日，大阪国際会議場，大阪.

48. 門阪薫平，北野雅之，工藤正俊：高齢者または ADL 不良の急性胆嚢炎および胆管炎例に対する EUS 下胆嚢ドレナージ術．シンポジウム 1「高齢者における内視鏡診療の問題点と対策（胆膵)」,日本消化器内視鏡学会近畿支部第 91 回支部例会，平成 25 年 11 月 16 日，大阪国際交流センター，大阪.

49. 高場雄久，辻　直子，工藤正俊：高齢者における大腸ポリペクトミーの安全性と予後．シンポジウム 2「高齢者における内視鏡診療の問題点と対策（消化管)」，日本消化器内視鏡学会近畿支部第 91 回支部例会，平成 25 年 11 月 16 日，大阪国際交流センター，大阪.

50. 永井知行，樫田博史，工藤正俊：(追加発言 3）当院における高齢患者の EMR 治療成績と問題点．シンポジウム 2「高齢者における内視鏡診療の問題点と対策（消化管)」，日本消化器内視鏡学会近畿支部第 91 回支部例会，平成 25 年 11 月 16 日，大阪国際交流センター，大阪.

51. 山雄健太郎，北野雅之，工藤正俊：当院における EUS 下ドレナージ術の成績．ワークショップ 1「内視鏡ステント治療の現状と問題点（胆膵)」，日本消化器内視鏡学会近畿支部第 91 回支部例会，平成 25 年 11 月 16 日，大阪国際交流センター，大阪.

IX. 学会発表（国内一般演題）

1. 萩原　智，櫻井俊治，工藤正俊：ソラフェニブ治療における JNK 活性の重要性-CD133 との関連も含めて-．第 7 回日本肝がん分子標的治療研究会，平成 25 年 1 月 19 日，じゅうろくプラザ，岐阜.

2. 千品寛和，井上達夫，田中梨絵，山田光成，有住忠晃，田北雅弘，北井　聡，矢田典久，萩原　智，南　康範，上嶋一臣，西田直生志，工藤正俊，隈部　力，中島　収：腫瘍内出血を認めた肉腫様肝癌の 1 例．第 19 回肝血流動態イメージ研究会，平成 25 年 1 月 26 日～27 日，東京ビッグサイト「国際会議場」，東京.

3. 足立哲平，松井繁長，樫田博史，工藤正俊：当院におけるヘリコバクターピロリ除菌治療成績の検討．第 9 回日本消化管学会総会学術集会，平成 25 年 1 月 25 日-26 日，京王プラザホテル，東京.

4. 千品寛和，井上達夫，田中梨絵，山田光成，有住忠晃，田北雅弘，北井　聡，矢田典久，萩原　智，南　康範，上嶋一臣，西田直生志，工藤正俊：腫瘍内出血を呈した肉腫様肝癌の 1 例．日本消化器病学会近畿支部第 98 回例会，平成 25 年 2 月 16 日，神戸ポートピアホテル，兵庫.

5. 茂山朋広，秦　康倫，木下大輔，奥田英之，宮部欽生，清水昌子，岸谷　譲，川崎俊彦，佐藤克明，辻江正徳，井上雅智，太田善夫，工藤正俊：肝細胞癌に合併した膵 solid-pseudopapillary neoplasm の 1 例．日本消化器病学会近畿支部第 98 回例会，平

成 25 年 2 月 16 日，神戸ポートピアホテル，兵庫.

6. 木下大輔，川崎俊彦，岸谷　譲，清水昌子，宮部欽生，茂山朋広，奥田英之，秦　康倫，工藤正俊，太田善夫：胃粘膜下腫瘍様形態を呈した膵扁平上皮癌の 1 例．日本消化器病学会近畿支部第 98 回例会，平成 25 年 2 月 16 日，神戸ポートピアホテル，兵庫.

7. 南　知宏，朝隈　豊，足立哲平，高山政樹，峯　宏昌，永田嘉昭，永井知行，川崎正憲，櫻井俊治，松井繁長，樫田博史，工藤正俊：同時多発早期胃癌 11 病変に対し内視鏡治療を施行した 1 例．日本消化器病学会近畿支部第 98 回例会，平成 25 年 2 月 16 日，神戸ポートピアホテル，兵庫.

8. 八木澤朋弘，足立哲平，高山政樹，峯　宏昌，永田嘉昭，永井知行，川崎正憲，朝隈豊，櫻井俊治，松井繁長，樫田博史，工藤正俊，大東弘治，吉岡康多，上田和毅，筑後孝章：腸重積を契機に発見された回腸癌の 1 例．日本消化器病学会近畿支部第 98 回例会，平成 25 年 2 月 16 日，神戸ポートピアホテル，兵庫.

9. 河野匡志，丸山康典，松本　望，高場雄久，奥村直己，山本典雄，冨田崇文，梅原康湖，谷池聡子，森村正嗣，米田　円，山田　哲，辻　直子，船井貞住，落合　健，前倉俊治，南　康範，工藤正俊：閉塞黄疸を合併した黄色肉芽腫性胆嚢炎の一例．日本消化器病学会近畿支部第 98 回例会，平成 25 年 2 月 16 日，神戸ポートピアホテル，兵庫.

10. 足立哲平，高山政樹，峯　宏昌，永井知行，永田嘉昭，川崎正憲，朝隈　豊，櫻井俊治，松井繁長，樫田博史，工藤正俊：当院のヘリコバクターピロリ除菌治療における PPI 別検討．第 99 回日本消化器病学会総会，平成 25 年 3 月 21 日-23 日，城山観光ホテル，かごしま県民交流センター，鹿児島.

11. 櫻井俊治，樫田博史，工藤正俊：慢性膵炎における p38MAPK，HSP27 の役割．第 99 回日本消化器病学会総会，平成 25 年 3 月 21 日-23 日，城山観光ホテル，かごしま県民交流センター，鹿児島.

12. 永田嘉昭，櫻井俊治，足立哲平，高山政樹，峯　宏昌，永井知行，川崎正憲，朝隈豊，松井繁長，樫田博史，工藤正俊：胃粘膜上皮の HSP27 発現は上皮内癌の発生リスクと負の相関を示す．第 99 回日本消化器病学会総会，平成 25 年 3 月 21 日-23 日，城山観光ホテル，かごしま県民交流センター，鹿児島.

13. 今井　元，北野雅之，工藤正俊，門阪薫平，大本俊介，鎌田　研，宮田　剛，坂本洋城：超音波内視鏡下胆嚢ドレナージ術の有用性．第 99 回日本消化器病学会総会，平成 25 年 3 月 21 日-23 日，城山観光ホテル，かごしま県民交流センター，鹿児島.

14. 大本俊介，北野雅之，山田光成，門阪薫平，宮田　剛，鎌田　研，今井　元，坂本洋城，工藤正俊：膵仮性嚢胞に対する Interventional EUS．第 99 回日本消化器病学会総会，平成 25 年 3 月 21 日-23 日，城山観光ホテル，かごしま県民交流センター，鹿児島.

15. 田中梨絵，上嶋一臣，千品寛和，有住忠晃，田北雅弘，北井　聡，井上達夫，　矢田典久，萩原　智，南　康範，西田直生志，工藤正俊：肝血管筋脂肪腫の 3 例．第 99 回日本消化器病学会総会，平成 25 年 3 月 21 日-23 日，城山観光ホテル，かごしま県民交流センター，鹿児島.

16. 櫻井俊治，樫田博史，工藤正俊：慢性膵炎における p38MAPK，HSP27 の役割．第 99 回日本消化器病学会総会，平成 25 年 3 月 21 日-23 日，城山観光ホテル，かごしま県民交流センター，鹿児島．

17. 永田嘉昭，櫻井俊治，足立哲平，高山政樹，峯　宏昌，　永井知行，川崎正憲，朝隈豊，松井繁長，樫田博史，工藤正俊：胃粘膜上皮の HSP27 発現は上皮内癌の発生リスクと負の相関を示す．第 99 回日本消化器病学会総会，平成 25 年 3 月 21 日-23 日，城山観光ホテル，かごしま県民交流センター，鹿児島．

18. 田中梨絵，井上達夫，有住忠晃，田北雅弘，北井　聡，矢田典久，萩原　智，南　康範，　上嶋一臣，西田直生志，樫田博史，工藤正俊：肝原発神経内分泌腫瘍の 1 例．第 26 回日本腹部造影エコー一・ドプラ診断研究会，平成 25 年 4 月 6 日，ウインクあいち，愛知．

19. 横川美加，辻裕美子，前野知子，塩見香織，前川　清，樫田博史，工藤正俊：造影を行なった小腸良性腫瘍の 1 例．第 26 回日本腹部造影エコー一・ドプラ診断研究会，平成 25 年 4 月 6 日，ウインクあいち，愛知．

20. 大本俊介，北野雅之，工藤正俊：造影ハーモニック EUS(CH-EUS)における膵腫瘍血流評価の検討．第 26 回日本腹部造影エコー一・ドプラ診断研究会，平成 25 年 4 月 6 日，ウインクあいち，愛知．

21. 矢田典久，萩原　智，工藤正俊：Real-time tissue quantification (VTTQ)による自己免疫性肝炎の治療評価．日本超音波医学会第 86 回学術集会，平成 25 年 5 月 24 日-26 日，大阪国際会議場，大阪．

22. 野田晃世，小川　力，森岡弓子，柴峠光成，村川佳子，河合直之，木太秀行，嶋田俊秀，工藤正俊：VINCENT を用いた超音波検査指導の有用性．日本超音波医学会第 86 回学術集会，平成 25 年 5 月 24 日-26 日，大阪国際会議場，大阪．

23. 小川　力，工藤正俊，野田晃世，柴峠光成，村川佳子，河合直之，木太秀行，嶋田俊秀，廣瀬哲朗，西平友彦：Defect re-purfusion imaging による新しい HCC の診断方法とその教育システム．日本超音波医学会第 86 回学術集会，平成 25 年 5 月 24 日-26 日，大阪国際会議場，大阪．

24. 前野知子，横川美加，辻　裕美子，塩見香織，前川　清，井上達夫，南　康範，西田直生志，八木　誠，工藤正俊：超音波を施行した 0 歳児の嘔吐症例の検討．日本超音波医学会第 86 回学術集会，平成 25 年 5 月 24 日-26 日，大阪国際会議場，大阪．

25. 田中梨絵，南　康範 田北雅弘，北井　聡，井上達夫，矢田典久，萩原　智，上嶋一臣，西田直生志，工藤正俊：肝血管筋脂肪腫の 3 例．日本超音波医学会第 86 回学術集会，平成 25 年 5 月 24 日-26 日，大阪国際会議場，大阪．

26. 門阪薫平，北野雅之，　大本俊介，鎌田　研，宮田　剛，今井　元，坂本洋城，工藤正俊：早期慢性膵炎 EUS 画像所見と糖尿病との関連．日本消化器内視鏡学会近畿支部第 90 回支部例会，平成 25 年 6 月 22 日，大阪国際交流センター，大阪．

27. 南　康範，早石宗右，有住忠晃，田北雅弘，北井　聡，矢田典久，井上達夫，萩原智，上嶋一臣，西田直生志，工藤正俊，鄭　浩柄：経皮的ラジオ波焼灼術後の穿刺経路焼灼は必要か？：後出血予防の検討．第 49 回日本肝癌研究会，平成 25 年 7 月 11 日-12 日，京王プラザホテル，東京．

28. 西田直生志，工藤正俊：エピゲノム変異からみたヒト肝発癌における喫煙の影響と GST 遺伝子多型に関する研究．第 28 回喫煙科学研究財団助成研究発表会，平成 25 年 7 月 22 日-23 日，京王プラザホテル，東京．

29. 今井　元，北野雅之，工藤正俊：経乳頭的治療不能悪性胆道狭窄に対する Antegrade drainage 併用治療の有用性．第 44 回日本膵臓学会大会，平成 25 年 7 月 25 日-26 日，仙台国際センター，宮城．

30. 田中梨絵，井上達夫，千品寛和，有住忠晃，田北雅弘，北井　聡，矢田典久，萩原智，南　康範，上嶋一臣，西田直生志，工藤正俊，兵頭朋子，村上卓道：肝原発神経内分泌腫瘍の 1 例．第 13 回関西肝血流動態イメージ研究会，平成 25 年 7 月 27 日，オーバルホール，大阪．

31. 山雄健太郎，坂本洋城，北野雅之，工藤正俊：非 EST 症例に対する経カテーテル胆道内視鏡（Trans-catheter endoscopy；TCE）のコツとピットフォール．第 49 回日本胆道学会学術集会，平成 25 年 9 月 19-20 日，ヒルトン東京ベイ，千葉．

32. 門阪薫平，北野雅之，工藤正俊：ERCP 不能な悪性胆道狭窄における急性胆嚢炎および胆管炎例に対する EUS 下ドレナージ術の有用性について．第 49 回日本胆道学会学術集会，平成 25 年 9 月 19-20 日，ヒルトン東京ベイ，千葉．

33. 宮田　剛，北野雅之，工藤正俊：切除不能胆道癌に対する集学的治療における胆道マネジメントの重要性．第 49 回日本胆道学会学術集会，平成 25 年 9 月 19-20 日，ヒルトン東京ベイ，千葉．

34. 大本俊介，北野雅之，工藤正俊，中居卓也，竹山宜典：胆管癌として切除された良性胆管病変の 4 例．第 49 回日本胆道学会学術集会，平成 25 年 9 月 19-20 日，ヒルトン東京ベイ，千葉．

35. 谷池聡子，尾崎信人，丸山康典，河野匡志，松本　望，高場雄久，奥村直己，山本典雄，冨田崇文，梅原康湖，森村正嗣，米田　円，山田　哲，辻　直子，船井貞往，落合　健，前倉俊治，工藤正俊：転移性腫瘍との鑑別を要した肝腫瘤を合併した十二指腸乳頭部癌の 1 例．日本消化器病学会近畿支部第 99 回例会，平成 25 年 9 月 28 日，大阪国際交流センター，大阪．

36. 岩西美奈，萩原　智，鍵岡賛典，南　知宏，有住忠晃，田北雅弘，北井　聡，井上達夫，矢田典久，南　康範，　上嶋一臣，櫻井俊治，西田直生志，工藤正俊：急性発症型自己免疫性肝炎の一例．日本消化器病学会近畿支部第 99 回例会，平成 25 年 9 月 28 日，大阪国際交流センター，大阪．

37. 鍵岡賛典，萩原　智，岩西美奈，南　知宏，　有住忠晃，田北雅弘，北井　聡，矢田典久，井上達夫，南　康範，　上嶋一臣，櫻井俊治，工藤正俊：急激な肝機能低下をきた

した Budd-Chiari 症候群の 1 例. 日本消化器病学会近畿支部第 99 回例会, 平成 25 年 9 月 28 日, 大阪国際交流センター, 大阪.

38. 古川健太郎, 北野雅之, 田中梨絵, 大本俊介, 門阪薫平, 鎌田　研, 宮田　剛, 今井元, 坂本洋城, 工藤正俊: Walled off necrosis に対して EUS 下内外瘻術を施行後に再発を認めた一例. 日本消化器病学会近畿支部第 99 回例会, 平成 25 年 9 月 28 日, 大阪国際交流センター, 大阪.

39. 千品寛和, 井上達夫, 南　知宏, 岡元寿樹, 山田光成, 田中梨絵, 有住忠晃, 田北雅弘, 北井　聡, 矢田典久, 萩原　智, 南　康範, 上嶋一臣, 西田直生志, 工藤正俊: 慢性C型肝炎に対するテラプレビル3剤併用療法中に結核性リンパ節炎を発症した1例. 日本消化器病学会近畿支部第 99 回例会, 平成 25 年 9 月 28 日, 大阪国際交流センター, 大阪.

40. 井上達夫, 工藤正俊: Gd-EOB-DTPA MRI 肝細胞相で低信号に描出される結節の多血化因子の検討多施設共同 retrospective study. 第 21 回日本消化器関連学会週間 JDDW2013（第 17 回日本肝臓学会大会・第 55 回日本消化器病学会大会・第 86 回日本消化器内視鏡学会総会・第 11 回日本消化器外科学会大会・第 51 回日本消化器がん検診学会大会・第 44 回日本消化器吸収学会総会合同）, 平成 25 年 10 月 9 日-12 日, 品川プリンスホテル, 東京.

41. 南　康範, 工藤正俊, 中居卓也: 当院における大腸癌肝転移の治療ストラテジー. 第 21 回日本消化器関連学会週間 JDDW2013（第 17 回日本肝臓学会大会・第 55 回日本消化器病学会大会・第 86 回日本消化器内視鏡学会総会・第 11 回日本消化器外科学会大会・第 51 回日本消化器がん検診学会大会・第 44 回日本消化器吸収学会総会合同）, 平成 25 年 10 月 9 日-12 日, 品川プリンスホテル, 東京.

42. 峯　宏昌, 櫻井俊治, 工藤正俊: 大腸発癌における幹細胞の制御機構. 第 21 回日本消化器関連学会週間 JDDW2013（第 17 回日本肝臓学会大会・第 55 回日本消化器病学会大会・第 86 回日本消化器内視鏡学会総会・第 11 回日本消化器外科学会大会・第 51 回日本消化器がん検診学会大会・第 44 回日本消化器吸収学会総会合同）, 平成 25 年 10 月 9 日-12 日, 品川プリンスホテル, 東京.

43. 田北雅弘, 有住忠晃, 北井　聡, 井上達夫, 矢田典久, 萩原　智, 南　康範, 上嶋一臣, 西田直生志, 工藤正俊: 肝のう胞に対するオレイン酸モノエタノールアミン注入療法の検討. 第 21 回日本消化器関連学会週間 JDDW2013（第 17 回日本肝臓学会大会・第 55 回日本消化器病学会大会・第 86 回日本消化器内視鏡学会総会・第 11 回日本消化器外科学会大会・第 51 回日本消化器がん検診学会大会・第 44 回日本消化器吸収学会総会合同）, 平成 25 年 10 月 9 日-12 日, グランドプリンスホテル新高輪, 東京.

44. 田北雅弘, 萩原　智, 工藤正俊: C 型肝炎に対する 3 剤併用療法の高齢者における認容性の検討. 第 21 回日本消化器関連学会週間 JDDW2013（第 17 回日本肝臓学会大会・第 55 回日本消化器病学会大会・第 86 回日本消化器内視鏡学会総会・第 11 回日本消化器外科学会大会・第 51 回日本消化器がん検診学会大会・第 44 回日本消化器吸収学会総会合同）, 平成 25 年 10 月 9 日-12 日, グランドプリンスホテル新高輪, 東京.

45. 辻　直子, 丸山康典, 河野匡志, 松本　望, 高場雄久, 奥村直己, 山本典雄, 冨田崇文, 梅原康湖, 谷池聡子, 森村正嗣, 米田　円, 山田　哲, 落合　健, 前倉俊治, 本庶　元, 工藤正俊: 慢性胃炎性変化の乏しい C-0 症例のたこいぼびらんに見られる腸上

皮化生についての検討. 第 21 回日本消化器関連学会週間 JDDW2013（第 17 回日本肝臓学会大会・第 55 回日本消化器病学会大会・第 86 回日本消化器内視鏡学会総会・第 11 回日本消化器外科学会大会・第 51 回日本消化器がん検診学会大会・第 44 回日本消化器吸収学会総会合同）, 平成 25 年 10 月 9 日-12 日, グランドプリンスホテル新高輪, 東京.

46. 谷池聡子, 河野匡志, 丸山康典, 松本　望, 高場雄久, 奥村直己, 冨田崇文, 梅原康湖, 森村正嗣, 米田　円, 山田　哲, 辻　直子, 工藤正俊: 上部消化管内視鏡検査前スクリーニングとして実施した胸部 X-ray および心電図より得られた所見についての検討. 第 21 回日本消化器関連学会週間 JDDW2013（第 17 回日本肝臓学会大会・第 55 回日本消化器病学会大会・第 86 回日本消化器内視鏡学会総会・第 11 回日本消化器外科学会大会・第 51 回日本消化器がん検診学会大会・第 44 回日本消化器吸収学会総会合同）, 平成 25 年 10 月 9 日-12 日, グランドプリンスホテル新高輪, 東京.

47. 梅原康湖, 河野匡志, 丸山康典, 松本　望, 高場雄久, 奥村直己, 谷池聡子, 冨田崇文, 森村正嗣, 山田　哲, 米田　円, 辻　直子, 工藤正俊: プロポフォール投与下内視鏡検査で生じる不随意運動の検討. 第 21 回日本消化器関連学会週間 JDDW2013（第 17 回日本肝臓学会大会・第 55 回日本消化器病学会大会・第 86 回日本消化器内視鏡学会総会・第 11 回日本消化器外科学会大会・第 51 回日本消化器がん検診学会大会・第 44 回日本消化器吸収学会総会合同）, 平成 25 年 10 月 9 日-12 日, グランドプリンスホテル新高輪, 東京.

48. 梅原康湖, 河野匡志, 丸山康典, 松本　望, 高場雄久, 奥村直己, 谷池聡子, 冨田崇文, 森村正嗣, 山田　哲, 米田　円, 辻　直子, 工藤正俊: プロポフォール投与下内視鏡検査における飲酒患者, 睡眠薬・精神安定剤内服患者への注意点. 第 21 回日本消化器関連学会週間 JDDW2013（第 17 回日本肝臓学会大会・第 55 回日本消化器病学会大会・第 86 回日本消化器内視鏡学会総会・第 11 回日本消化器外科学会大会・第 51 回日本消化器がん検診学会大会・第 44 回日本消化器吸収学会総会合同）, 平成 25 年 10 月 9 日-12 日, グランドプリンスホテル新高輪, 東京.

49. 高山政樹, 足立哲平, 峯　宏昌, 永田嘉昭, 永井知行, 川崎正憲, 朝隈　豊, 櫻井俊治, 松井繁長, 樫田博史, 工藤正俊: 当院において OGIB と診断されシングルバルーン小腸内視鏡検査を施行した高齢者症例の臨床的検討. 第 21 回日本消化器関連学会週間 JDDW2013（第 17 回日本肝臓学会大会・第 55 回日本消化器病学会大会・第 86 回日本消化器内視鏡学会総会・第 11 回日本消化器外科学会大会・第 51 回日本消化器がん検診学会大会・第 44 回日本消化器吸収学会総会合同）, 平成 25 年 10 月 9 日-12 日, グランドプリンスホテル新高輪, 東京.

50. 奥村直己, 工藤正俊, 辻　直子, 高場雄久, 松本　望, 谷池聡子, 河野匡志, 丸山康典, 山田　哲, 森村正嗣, 米田　円, 梅原康湖, 富田崇文: Clostridium difficile 感染症例の検討. 第 21 回日本消化器関連学会週間 JDDW2013（第 17 回日本肝臓学会大会・第 55 回日本消化器病学会大会・第 86 回日本消化器内視鏡学会総会・第 11 回日本消化器外科学会大会・第 51 回日本消化器がん検診学会大会・第 44 回日本消化器吸収学会総会合同）, 平成 25 年 10 月 9 日-12 日, 品川プリンスホテル, 東京.

51. 千品寛和, 門阪薫平, 田中梨絵, 大本俊介, 宮田　剛, 鎌田　研, 今井　元, 坂本洋城, 北野雅之, 工藤正俊: 膵癌による閉塞性黄疸に対する乳頭括約筋切開術未施行のカバー付金属ステント留置術の成績. 第 21 回日本消化器関連学会週間 JDDW2013（第 17 回日本肝臓学会大会・第 55 回日本消化器病学会大会・第 86 回日本消化器内視鏡学会総会・第 11 回日本消化器外科学会大会・第 51 回日本消化器がん検診学会大会・第 44 回日本消化器吸収学会総会合同）, 平成 25 年 10 月 9 日-12 日, 品川プリンスホテル, 東

京.

52. 萩原　智，西田直生志，工藤正俊：HBs 抗原消失を目指したエンテカビルと PEG-IFN48 週併用療法の効果について．第 15 回葵肝臓研究会，平成 25 年 11 月 9 日，メルパルク京都，京都.

53. 大本俊介，田中梨絵，門阪薫平，鎌田　研，宮田　剛，山雄健太郎，今井　元，坂本洋城，北野雅之，工藤正俊：造影ハーモニック EUS（CH-EUS）における膵腫瘍の血流評価の有用性について．日本超音波医学会第 40 回関西地方会学術集会，平成 25 年 11 月 9 日，大阪国際会議場，大阪.

54. 前川　清，横川美加，辻　裕美子，前野知子，市島真由美，塩見香織，矢野雅彦，井上達夫，南　康範，工藤正俊：Acoustic structure quantification による focal spared area の描出の試み．日本超音波医学会第 40 回関西地方会学術集会，平成 25 年 11 月 9 日，大阪国際会議場，大阪.

55. 前川　清，横川美加，辻　裕美子，前野知子，市島真由美，塩見香織，井上達夫，南康範，工藤正俊：Fly thru による PV Shunt の描出．日本超音波医学会第 40 回関西地方会学術集会，平成 25 年 11 月 9 日，大阪国際会議場，大阪.

56. 横川美加，辻　裕美子，前野知子，市島真由美，塩見香織，前川　清,南　康範，樫田博史，工藤正俊：ソナゾイド造影を施行した小腸腫瘍の 1 例．日本超音波医学会第 40 回関西地方会学術集会，平成 25 年 11 月 9 日，大阪国際会議場，大阪.

57. 大本俊介，北野雅之，工藤正俊：造影ハーモニック EUS における消化器系疾患の鑑別および悪性度診断．日本超音波医学会第 40 回関西地方会学術集会，平成 25 年 11 月 9 日，大阪国際会議場，大阪

58. 辻　裕美子，横川美加，前野知子，市島真由美，塩見香織，前川　清,井上達夫，南康範，工藤正俊：Fly thru による胆嚢（胆石・ポリープ）の描出について．日本超音波医学会第 40 回関西地方会学術集会，平成 25 年 11 月 9 日，大阪国際会議場，大阪.

59. 前野知子，横川美加，辻　裕美子，市島真由美，塩見香織，前川　清,樫田博史，工藤正俊：急速な増大を認めた後腹膜嚢胞性腫瘤の一例．日本超音波医学会第 40 回関西地方会学術集会，平成 25 年 11 月 9 日，大阪国際会議場，大阪.

60. 沼本勲男，朝隈　豊，　岡元寿樹，山田光成，千品寛和，足立哲平，高山政樹，峯　宏昌，永井知行，川崎正憲，櫻井俊治，松井繁長，樫田博史，工藤正俊：血便を契機に発見された上行結腸非上皮性巨大腫瘤の 2 例．日本消化器内視鏡学会近畿支部第 91 回支部例会，平成 25 年 11 月 16 日，大阪国際交流センター，大阪.

61. 東　千尋，山雄健太郎，田中梨絵，大本俊介，門阪薫平，鎌田　研，宮田　剛，　今井元，坂本洋城，北野雅之，工藤正俊：潰瘍性大腸炎に膵胆管合流異常症を合併した 1 例．日本消化器内視鏡学会近畿支部第 91 回支部例会，平成 25 年 11 月 16 日，大阪国際交流センター，大阪.

62. 中田有紀，北野雅之，大本俊介，門阪薫平，宮田　剛，鎌田　研，山雄健太郎，今井

元，坂本洋城，工藤正俊：walled-off necrosis の術前の管理においてメタリックステントによるドレナージが有用であった．日本消化器内視鏡学会近畿支部第 91 回支部例会，平成 25 年 11 月 16 日，大阪国際交流センター，大阪.

63. 吉川恵輔，奥田英之，秦　康倫，木下大輔，清水昌子，岸谷　譲，永田嘉昭，川崎俊彦，太田善夫，工藤正俊：食欲不振を契機に発見された巨大脾腫瘍の一例．日本消化器内視鏡学会近畿支部第 91 回支部例会，平成 25 年 11 月 16 日，大阪国際交流センター，大阪.

64. 尾崎信人，河野匡志，丸山康典，松本　望，高場雄久，奥村直己，山本典雄，冨田崇文，梅原康湖，谷池聡子，森村正嗣，米田　円，山田　哲，辻　直子，落合　健，前倉俊治，工藤正俊：胃 Inverted hamartomatous polyp の一例．日本消化器内視鏡学会近畿支部第 91 回支部例会，平成 25 年 11 月 16 日，大阪国際交流センター，大阪.

65. 田中梨絵，永井知行，千品寛和，山田光成，足立哲平，高山政樹，峯　宏昌，川崎正憲，朝隈　豊，松井繁長，樫田博史，工藤正俊：コーラ溶解法と結石粉砕術で内視鏡的摘出した胃十二指腸動脈瘤の一例．日本消化器内視鏡学会近畿支部第 91 回支部例会，平成 25 年 11 月 16 日，大阪国際交流センター，大阪.

66. 千品寛和，朝隈　豊，南　知宏，　岡元寿樹，山田光成，田中梨絵，足立哲平，峯　宏昌，高山政樹，永井知行，川崎正憲，櫻井俊治，松井繁長，樫田博史，工藤正俊：陥凹を伴った Sessile serrated adenoma/polyp（SSA/P）の 1 例．日本消化器内視鏡学会近畿支部第 91 回支部例会，平成 25 年 11 月 16 日，大阪国際交流センター，大阪.

67. 松本　望，尾崎信人，河野匡志，丸山康典，高場雄久，奥村直己，山本典雄，冨田崇文，梅原康湖，谷池聡子，森村正嗣，米田　円，山田　哲，辻　直子，遠藤英樹，落合　健，前倉俊治，工藤正俊：潰瘍性大腸炎の加療中に壊疽性膿皮症および下肢深部静脈血栓症を合併した 1 例．日本消化器内視鏡学会近畿支部第 91 回支部例会，平成 25 年 11 月 16 日，大阪国際交流センター，大阪.

68. 南　知宏，松井繁長，岡元寿樹，足立哲平，高山政樹，峯　宏昌，永井知行，川崎正憲，朝隈　豊，櫻井俊治，樫田博史，工藤正俊：消化管病変を合併した Henoch-Schonlein 紫斑病（HSP）の一例．日本消化器内視鏡学会近畿支部第 91 回支部例会，平成 25 年 11 月 16 日，大阪国際交流センター，大阪.

69. 大本俊介，北野雅之，門阪薫平，宮田　剛，鎌田　研，山雄健太郎，今井　元，坂本洋城，工藤正俊：造影ハーモニック EUS（CH-EUS）による膵腫瘤性病変の血流の定量化の試み．日本消化器内視鏡学会近畿支部第 91 回支部例会，平成 25 年 11 月 16 日，大阪国際交流センター，大阪.

写真で綴る消化器内科
2013年

肝左葉外側辺縁は見落としに注意！！

1月8日　消化器内科新年会

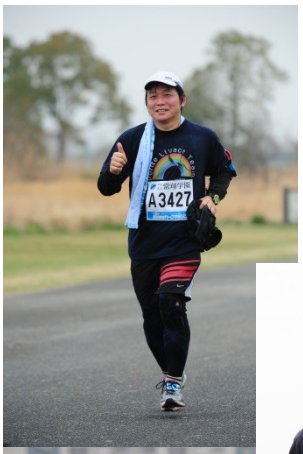

3.20
第3回淀川国際
ハーフマラソン

5.12
丹波三ツ塚マラソン

医局説明会




入局説明会




4.17
3学年講義
（肝臓コース）

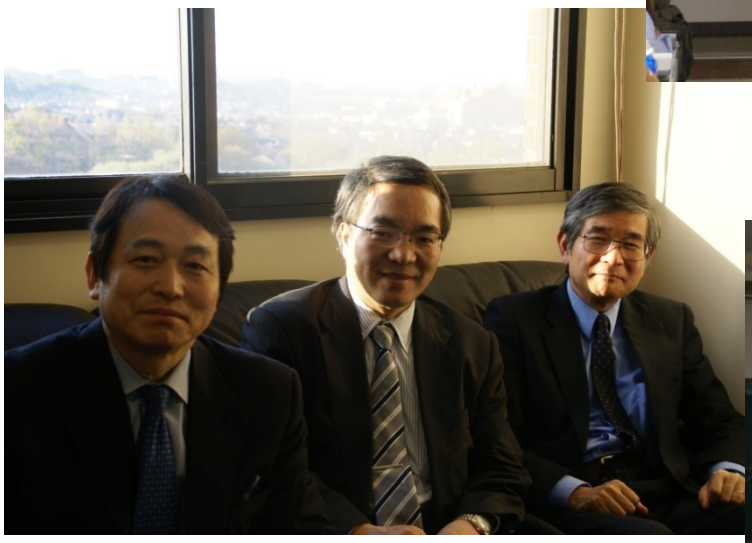

クリクラ学生特別講義

4.12
(芦田・深澤・藤原・永田・土谷・磯野)

4.23
(奥根・嶋原・比留間・青木・東迎・原口)

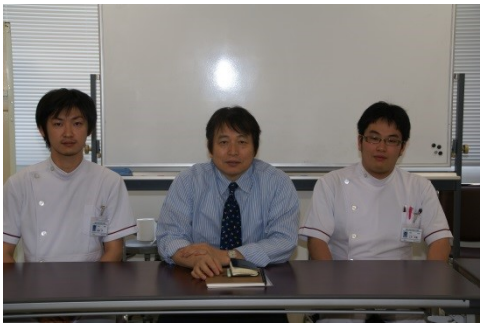

4.23
(船橋・上村)

5.14
(野田・三木・池田・半田・福本)

5.30
(榎園・髙島・三木・杉本・田下)

6.4
(楠本・西村・大澤)

6.13
(白山・秦・山下・大久保・沼田・山口)

6.27
(小澤・玉岡・中村・石橋・大和)

7.9
(舩内・片岡・森山・梶浦)

7.23
(浜田・中・田中・青山・大山)

9.9
(荻野・松野・藤下・田中・風呂谷)

9.26
(宮内・大原・副島・黄・波江野)

10.7
(薮内・村山・北山・吉川・大島)

10.21
(西野・安田・市川・本宮)

10.28
(大西・世良・村谷・河野・小森・倘川)

11.18
（本田・松永・髙島・岩倉・髙）

12.2
（堅田・三ツ石・森 明日香・岩津・空地・森 圭市郎）

12.16
（大原・櫻井・赤澤・田中・藤本・吉田）

1.15
（市川・岡・廣田・正覚・横田）

1.28
（小野・吉内・河野・岡・平川）

5.23
アジア超音波医学界
理事会（ソウル）

5.25
北大 西田先生と（ソウル）

ヨンセイ大学で講演
（ソウル）

シンガポール（NVH）で講演

9.15
国際肝癌学会
(ILCA)理事会

国際肝癌学会（ILCA)にて講演

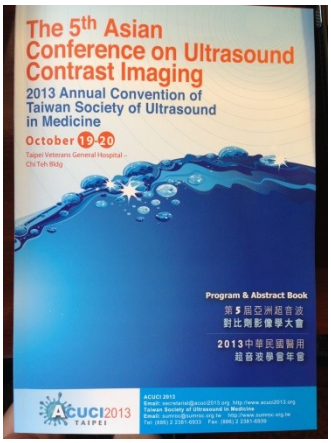

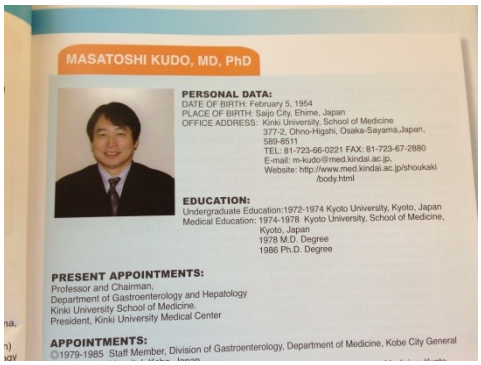

ILCA（ワシントンD.C.)

ACUCI2013

7.5-7
APPLE2013（プサン）

世界超音波医学界理事会
（コペンハーゲン）

国際肝癌研究会
（ワシントンD.C.）

国際移植学会で講演

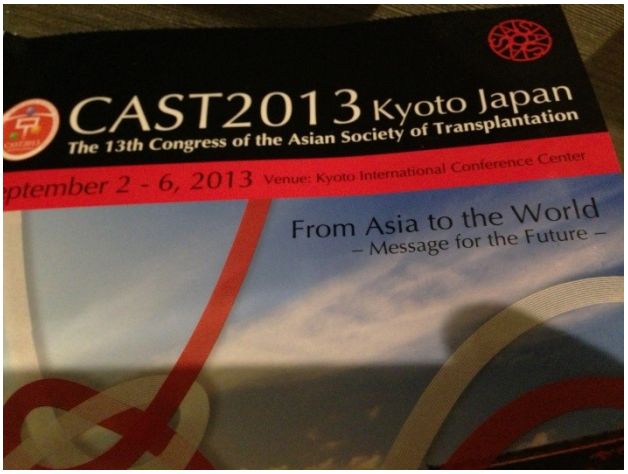

国立シンガポール大学で講演

世界超音波医学会の理事長を終了したことを記念

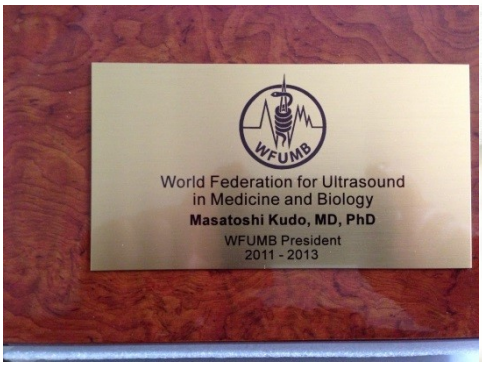

世界超音波医学会長として主催（サンパウロ）

アジア超音波医学会 ワークショップ （ジャカルタ）

Steering Committee Meeting （香港）

Philip Johnson教授

Laennec Meeting （有名なBrunt教授と）

Ian Wanless教授、Niel Thiese教授

AASLD Oral発表

7.26
アジア超音波医学会にて講演（モンゴル）

アジア太平洋肝臓学会（セブ島）

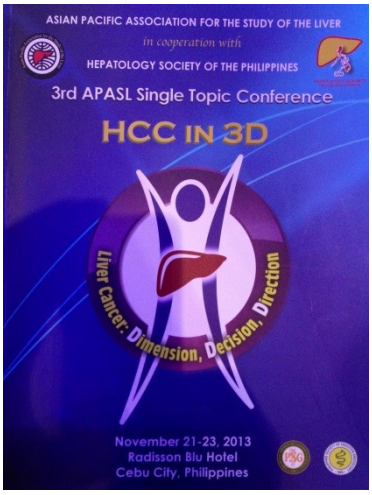

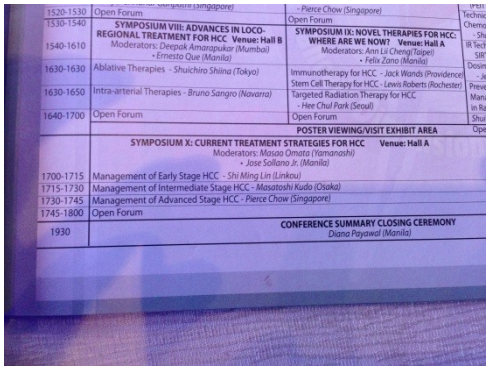

1520-1530	Open Forum	- Pierce Chow (Singapore)
1530-1540	SYMPOSIUM VIII: ADVANCES IN LOCO-REGIONAL TREATMENT FOR HCC Venue: Hall B Moderators: Deepak Amarapukar (Mumbai) • Ernesto Que (Manila)	Open Forum SYMPOSIUM IX: NOVEL THERAPIES FOR HCC: WHERE ARE WE NOW? Venue: Hall A Moderators: Ann Lii Cheng (Taipei) • Felix Zano (Manila)
1540-1610		
1630-1630	Ablative Therapies - Shuichiro Shiina (Tokyo)	Immunotherapy for HCC - Jack Wands (Providence)
1630-1650	Intra-arterial Therapies - Bruno Sangro (Navarra)	Stem Cell Therapy for HCC - Lewis Roberts (Rochester) Targeted Radiation Therapy for HCC - Hee Chul Park (Seoul)
1640-1700	Open Forum	Open Forum
	POSTER VIEWING/VISIT EXHIBIT AREA	
	SYMPOSIUM X: CURRENT TREATMENT STRATEGIES FOR HCC Venue: Hall A Moderators: Masao Omata (Yamanashi) • Jose Sollano Jr. (Manila)	
1700-1715	Management of Early Stage HCC - Shi Ming Lin (Linkou)	
1715-1730	Management of Intermediate Stage HCC - Masatoshi Kudo (Osaka)	
1730-1745	Management of Advanced Stage HCC - Pierce Chow (Singapore)	
1745-1800	Open Forum	
1930	CONFERENCE SUMMARY CLOSING CEREMONY Diana Payawal (Manila)	

医局旅行（鳴門）

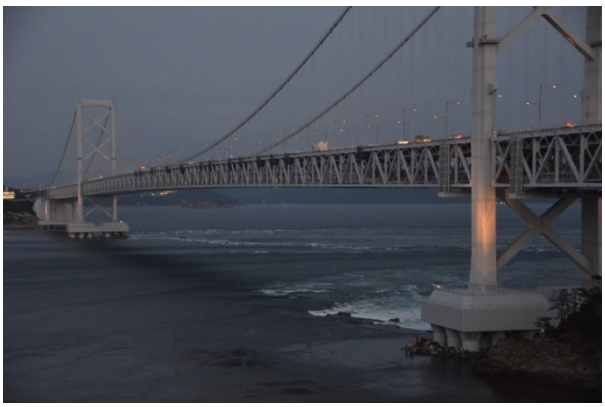

日本肝癌分子標的治療研究会

第8回日本肝がん分子標的治療研究会　　於　和倉温泉加賀屋　　2013年6月21日

（代表世話人：工藤正俊、当番世話人：金子周一教授）

久留米大学で共同研究

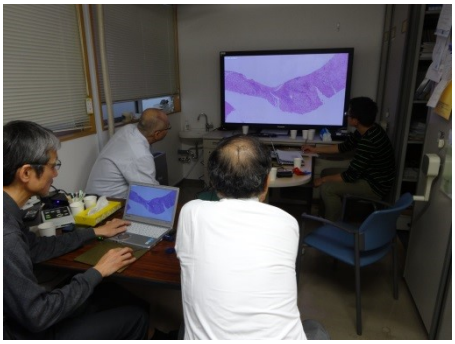
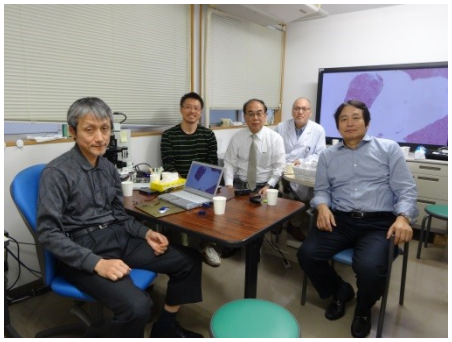
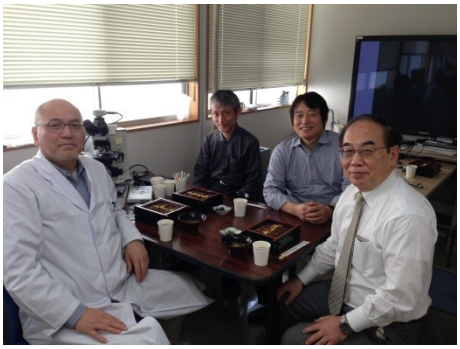

日本臨床腫瘍学会で司会

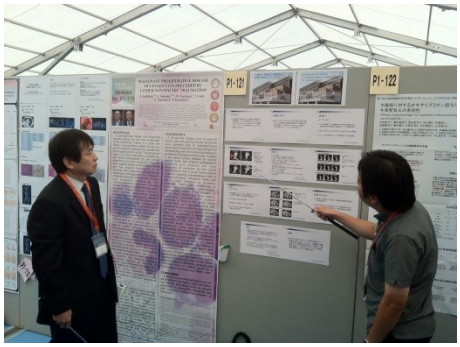

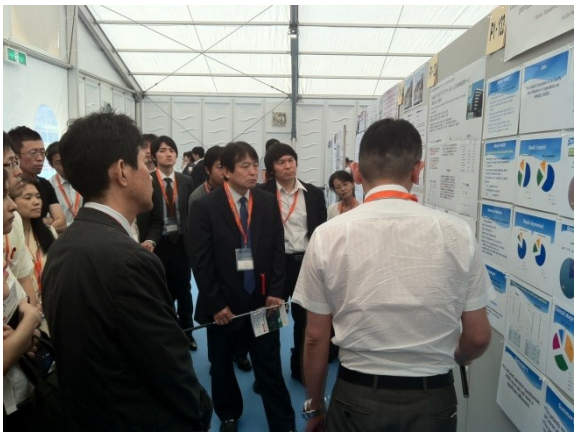

12.8　肝癌撲滅運動　　狭山市民会館

第3回 関西消化器内視鏡ライブコース
2月9日　近畿大学円形講堂および光学治療センター

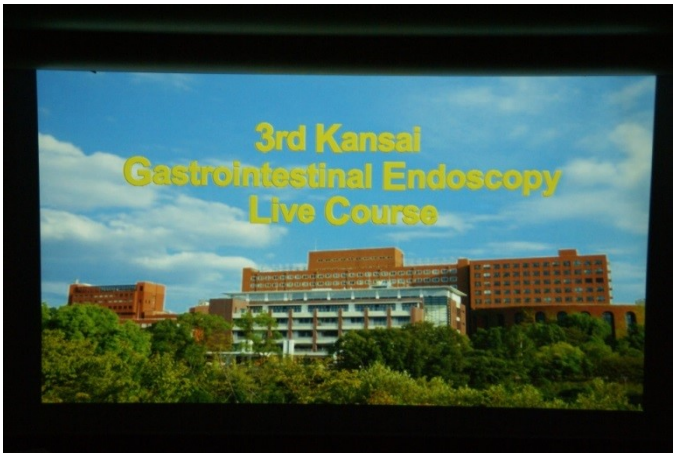

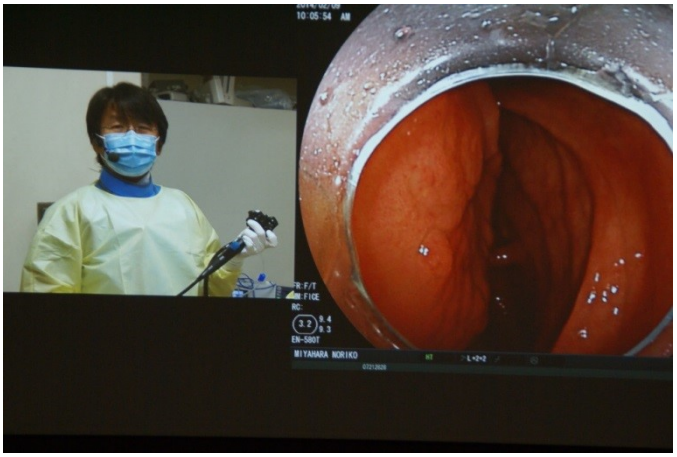

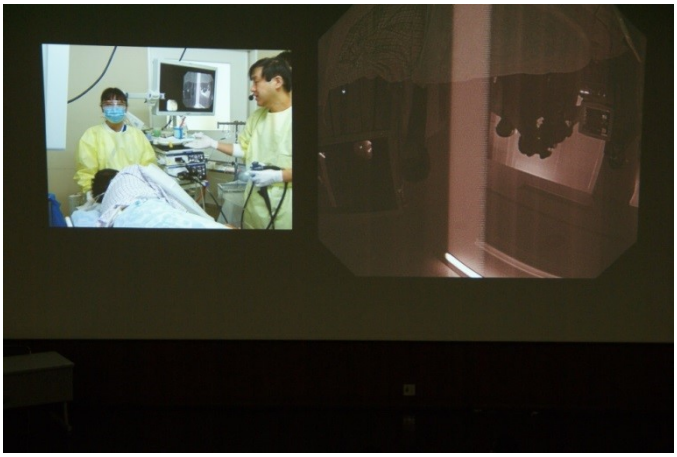

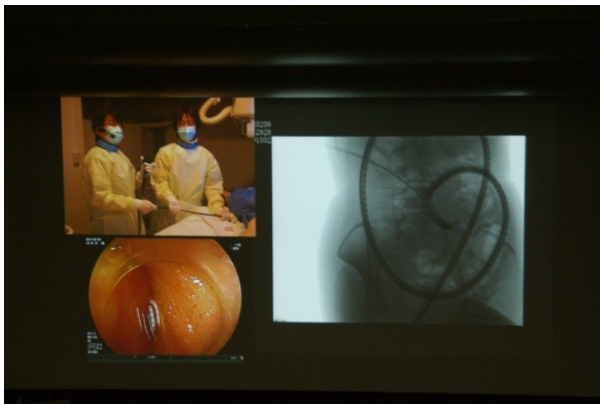

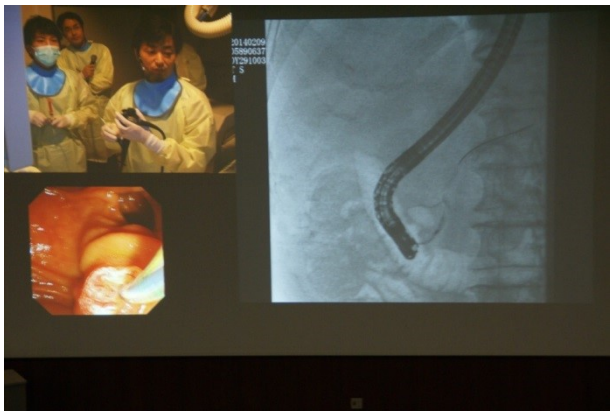

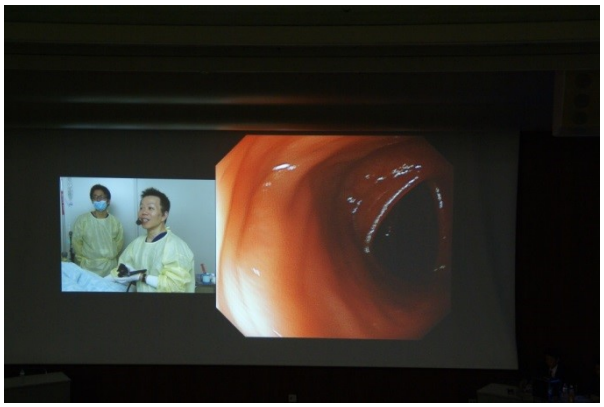

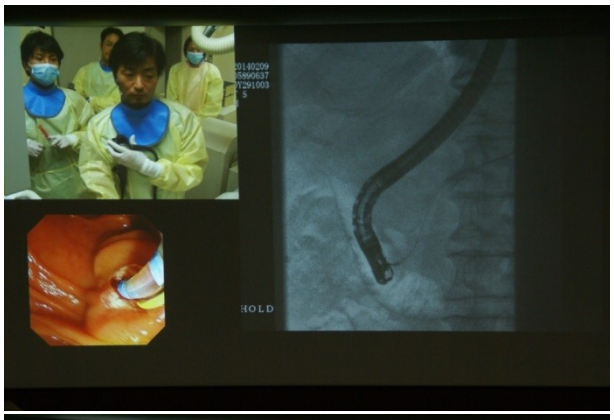
HOLD

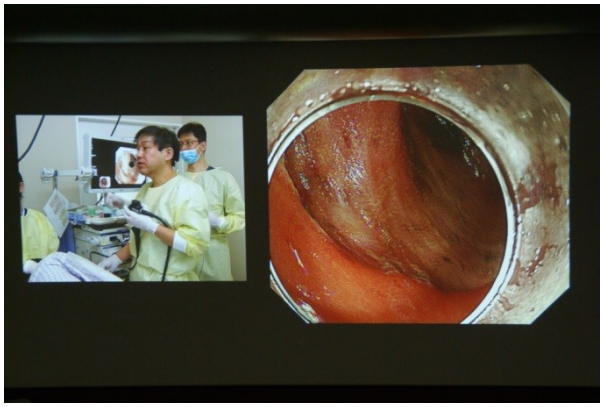

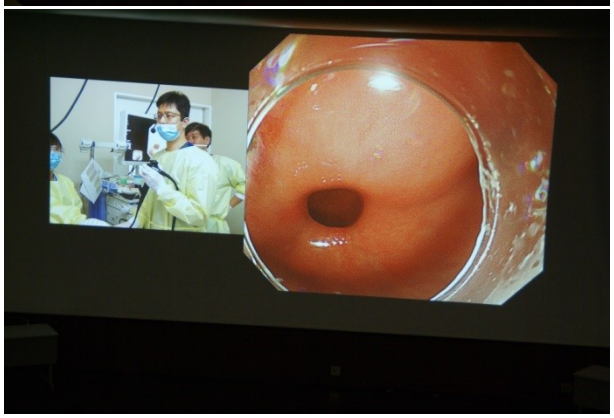

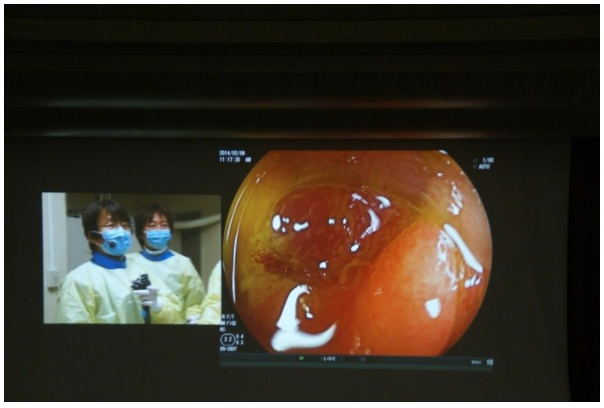

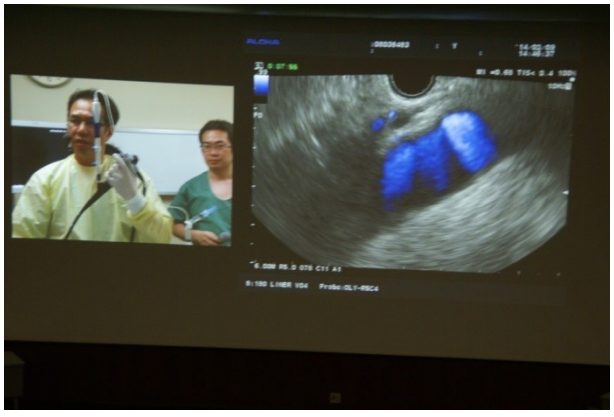

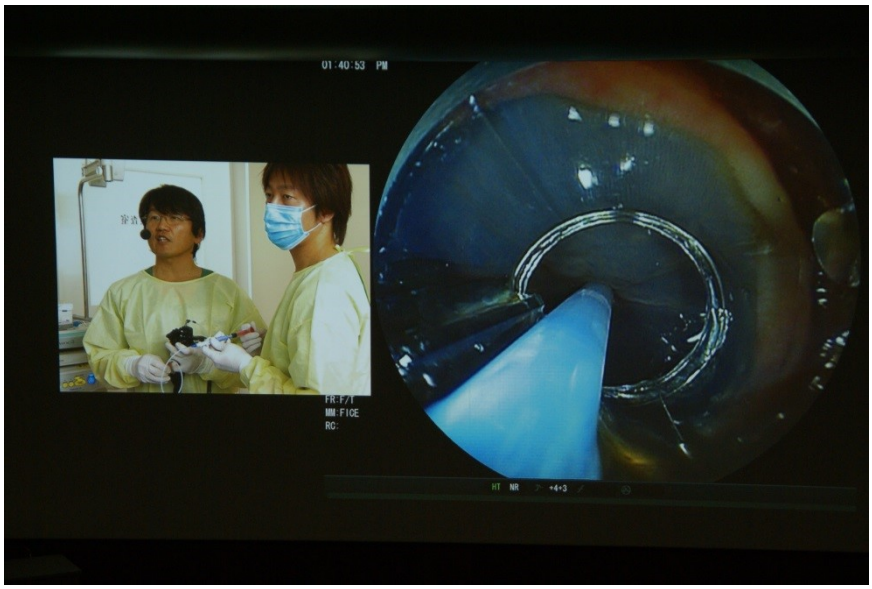
01:40:53 PM
FR:F/I
MM:FICE
RC:

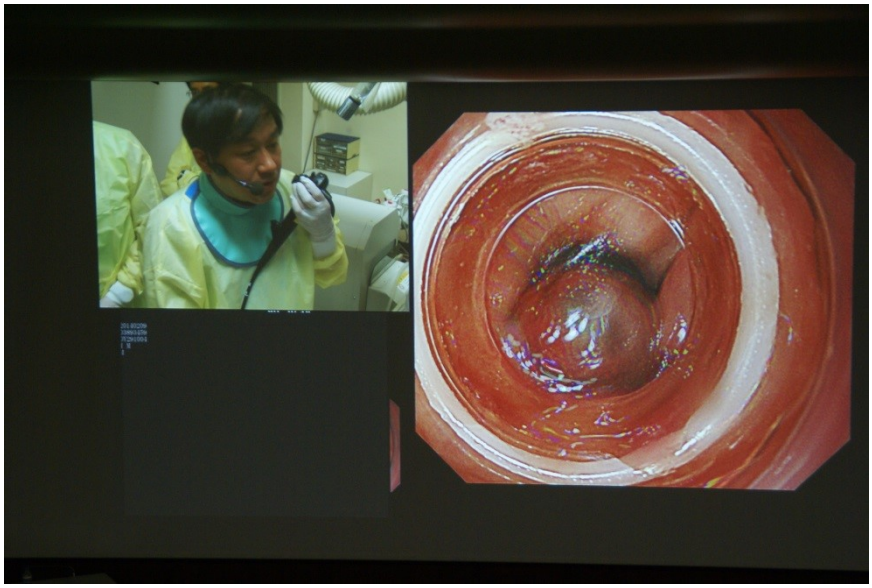

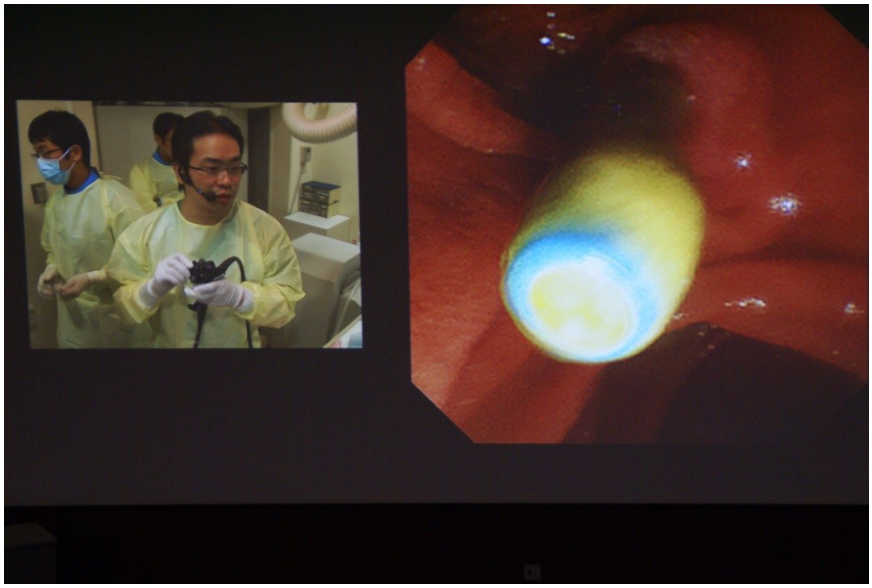

救急災害センター
オープン記念式典

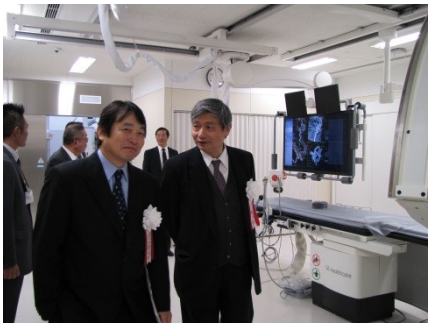

肝臓グループ
忘年会（堺東）

消化器内科忘年(堺東)

2.5　教授室にて
サプライズHappy Birthdayケーキ

同門会にて

病院長室にて

留学生受け入れ
Dr. Chai Soon Ngiu
（マレーシア）

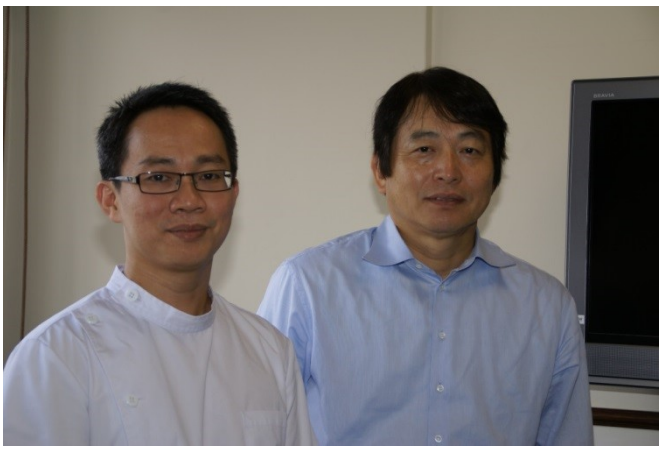

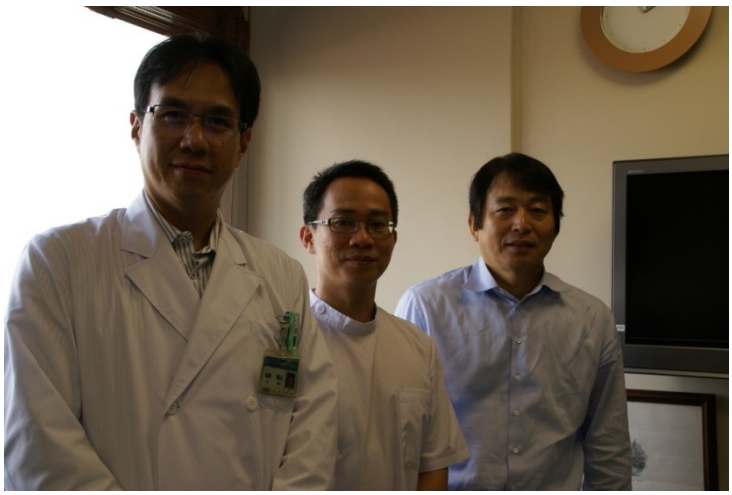

別刷
新聞・雑誌・報道等

Preface

Oncology

Oncology 2013;84(suppl 1):1–2
DOI: 10.1159/000345882

Published online: February 20, 2013

Advances in Liver Fibrosis Imaging and Hepatocellular Carcinoma: Update in 2013

Masatoshi Kudo

Kinki University School of Medicine, Osakasayama, Japan

The 3rd Asia-Pacific Primary Liver Cancer Expert Meeting (APPLE) was held on July 6–8, 2012, in Shanghai, China. In this meeting more than 50 invited international speakers and more than 500 participants from Asian countries participated. Highly scientific lectures followed by active discussion made this meeting an invaluable one.

The 48th Annual Meeting of the Liver Cancer Study Group of Japan was held on July 20–21, 2012, in Kanazawa, Japan. This meeting was also active and outstanding. This supplement issue contains selected articles with a high scientific value from these 2 meetings.

Fujimoto et al. [1] and Yada et al. [2] describe the usefulness of noninvasive techniques in evaluating liver fibrosis using real-time tissue elastography (RTE). RTE is a strain elastography in contrast to shear wave elastography in the diagnosis of liver stiffness. According to these 2 articles, RTE seems to be a promising method in evaluating liver fibrosis stage.

Kudo et al. [3] describe the role of gadolinum-ethoxybenzyl-diethylenetriamine imaging (Gd-EOB-DTPA MRI) in the management of hepatocellular carcinoma (HCC). This is a report based on the votes cast by 144 HCC experts at the 48th Annual Meeting of the Liver Cancer Study Group of Japan. The voting results which achieved more than 67% agreement are summarized as 'consensus statements'. Furthermore, issues which obtained more than 50% agreement are summarized as 'informative statements'. This report presents very interesting results and reflects daily clinical practice on use of EOB-MRI in Japan.

Takayasu [4] contributes a state-of-the-art article on transcatheter arterial chemoembolization (TACE) for unresectable HCC. The author concluded that conventional TACE as well as drug-eluting beads loaded with doxorubicin and yttrium-90 (^{90}Y) microspheres demonstrated a similar median survival.

Kim and Kim [5] report that ^{90}Y radioembolization has a potent anticancer effect with negligible adverse events if appropriate pretreatment evaluations, including dosimetry, calculation of lung shunt fraction and assessment of vascular anatomy, are performed. They concluded that selected populations, for whom TACE would not be effective, are candidates for ^{90}Y radioembolization.

Peng and Chen [6] report that combination therapy of TACE with radiofrequency ablation (RFA) showed better survival and recurrence-free survival than an RFA alone group. Thus, they expect the combination therapy of TACE with RFA to become a standard of care for HCC, which is treatable with RFA, in the future.

Makino et al. [7] discuss how RFA can be performed for HCCs, which have poor conspicuity on grayscale ultrasonography (US), by introducing US fusion imaging with CT/MRI.

Inoue et al. [8] show that contrast-enhanced US (CEUS) can be used to assess the efficacy of RFA for HCC, with the potential of reducing the number of CT scans required for evaluating treatment response.

Minami and Kudo [9] examine therapeutic response assessment of TACE for HCC by US, CT and MRI. The authors conclude that CT is commonly used as the standard imaging technique, but Lipiodol makes it difficult to detect

KARGER

Fax +41 61 306 12 34
E-Mail karger@karger.com
www.karger.com

0030–2414/13/0847–0001$38.00/0

Accessible online at:
www.karger.com/ocl

Masatoshi Kudo, MD, PhD
Division of Gastroenterology and Hepatology, Department of Internal Medicine
Kinki University Faculty of Medicine
377-2 Ohno-Higashi, Osakasayama, Osaka 589-8511 (Japan)
E-Mail m-kudo@med.kindai.ac.jp

the residual tumor on CT. CEUS is a useful tool for assessing the vascularity of the viable tumor in comparison with CT. Dynamic MRI is also useful in demonstrating viable tumor with high sensitivity, but low specificity. We should keep in mind that these 3 techniques have both advantages and disadvantages in response evaluation after TACE.

Tsai et al. [10] report that serum/plasma markers, functional MRI and FDG-PET have been selectively used to predict disease outcome after radiotherapy to HCC.

Wei and Zeng [11] propose that external beam radiotherapy (EBRT) be included in the National Comprehensive Cancer Network since EBRT was more effective than sorafenib for improving patient survival when tested on tumors of comparable metastatic size.

Minata et al. [12] report that evaluating vascular endothelial growth factor in HCC tissue after surgical resection has predictive value for metastatic HCC recurrence. The ability to risk stratify should improve treatment strategies after hepatectomy.

Nishida et al. [13] discuss how methylation status of *APC* sequences could be a promising marker for improving HCC management when considering the strong association between the ratio of the methylated to unmethylated *APC* sequences in serum and the presence of portal vein thrombosis.

Minata et al. [14] show that expression levels of E-cadherin in adjacent noncancerous liver after surgical resection is associated with later metastatic HCC recurrence. Analysis of E-cadherin expression should provide important information for predicting recurrence after curative resection of HCC.

Nishida and Kudo [15] report that recent whole-genome analyses and exome sequencing of tumor DNA have revealed numerous novel alterations to cancer-related genes and pathways critical for HCC development. In addition, various risk factors for HCC, such as the presence or absence of hepatitis B and hepatitis C virus, may affect the mutation profile of the corresponding cancer genome. On the other hand, genome-wide association studies have also identified important single-nucleotide polymorphisms involved in HCC development, which may allow detection of a group at high risk of HCC emergence. Such analyses will clarify how this malignancy can be treated, diagnosed and prevented more effectively.

I believe this supplement issue contains articles with high scientific value and thus will prove to be beneficial for readers of *Oncology*.

Disclosure Statement

The author declares that no conflict of interests exist.

References

1 Fujimoto K, Kato M, Kudo M, Yada N, Shiina T, Ueshima K, et al: Novel image analysis method using ultrasound elastography for noninvasive evaluation of hepatic fibrosis in patients with chronic hepatitis C. Oncology 2013;84(suppl 1):3–13.

2 Yada N, Morikawa H, Fujimoto K, Kato M, Kawada N, Kudo M: Assessment of liver fibrosis with real-time tissue elastography in chronic viral hepatitis. Oncology 2013;84 (suppl 1):14–20.

3 Kudo M, Matsui O, Sakamoto M, Kitao A, Kim T, Ariizumi S, et al: Role of gadolinium-ethoxybenzyl-diethylenetriamine pentaacetic acid-enhanced magnetic resonance imaging in the management of hepatocellular carcinoma: consensus at the symposium of the 48th Annual Meeting of the Liver Cancer Study Group of Japan. Oncology 2013;84 (suppl 1):21–27.

4 Takayasu K: Transcatheter arterial chemoembolization for unresectable hepatocellular carcinoma: recent progression and perspective. Oncology 2013;84(suppl 1):28–33.

5 Kim YH, Kim DY: Yttrium-90 radioembolization for hepatocellular carcinoma: what we know and what we need to know. Oncology 2013;84(suppl 1):34–39.

6 Peng ZW, Chen MS: Transcatheter arterial chemoembolization combined with radiofrequency ablation for the treatment of hepatocellular carcinoma. Oncology 2013;84 (suppl 1):40–43.

7 Makino Y, Imai Y, Ohama H, Igura T, Kogita S, Sawai Y, et al: Ultrasonography fusion imaging system increases the chance of radiofrequency ablation for hepatocellular carcinoma with poor conspicuity on conventional ultrasonography. Oncology 2013;84(suppl 1):44–50.

8 Inoue T, Kudo M, Hatanaka K, Arizumi T, Takita M, Kitai S, et al: Usefulness of contrast-enhanced ultrasonography to evaluate the post-treatment responses of radiofrequency ablation for hepatocellular carcinoma: comparison with dynamic CT. Oncology 2013;84(suppl 1):51–57.

9 Minami Y, Kudo M: Therapeutic response assessment of transcatheter arterial chemoembolization for hepatocellular carcinoma: ultrasonography, CT and MR imaging. Oncology 2013;84(suppl 1):58–63.

10 Tsai CL, Koong AC, Hsu FM, Graber M, Chen IS, Cheng JCH: Biomarker studies on radiotherapy to hepatocellular carcinoma. Oncology 2013;84(suppl 1):64–68.

11 Wei J, Zeng ZC: Is it time to adopt external beam radiotherapy in the NCCN guidelines as a therapeutic strategy for intermediate/advanced hepatocellular carcinoma? Oncology 2013;84(suppl 1):69–74.

12 Minata M, Harada KH, Kudo M, Ikai I, Nishida N: The prognostic value of vascular endothelial growth factor in hepatocellular carcinoma for predicting metastasis after curative resection. Oncology 2013;84(suppl 1):75–81.

13 Nishida N, Arizumi T, Takita M, Nagai T, Kitai S, Yada N, et al: Quantification of tumor DNA in serum and vascular invasion of human hepatocellular carcinoma. Oncology 2013;84(suppl 1):82–87.

14 Minata M, Kudo M, Harada KH, Ikai I, Nishida N: Expression of E-cadherin and vascular endothelial growth factor in noncancerous liver is associated with recurrence of hepatocellular carcinoma after curative resection. Oncology 2013;84(suppl 1):86–90.

15 Nishida N, Kudo M: Recent advancements in comprehensive genetic analyses for human hepatocellular carcinoma. Oncology 2013; 84(suppl 1):91–95.

Oncology

Oncology 2013;84(suppl 1):3–12
DOI: 10.1159/000345883

Published online: February 20, 2013

Novel Image Analysis Method Using Ultrasound Elastography for Noninvasive Evaluation of Hepatic Fibrosis in Patients with Chronic Hepatitis C

Kenji Fujimoto[a, b] Michio Kato[b] Masatoshi Kudo[c] Norihisa Yada[c] Tsuyoshi Shiina[d] Kazuomi Ueshima[c] Yukinori Yamada[e] Tetsushi Ishida[f] Masayoshi Azuma[f] Masaru Yamasaki[g] Keiji Yamamoto[b] Norio Hayashi[h] Tetsuo Takehara[i]

[a]Division of Clinical Research and [b]Department of Internal Medicine, National Hospital Organization Minamiwakayama Medical Center, Tanabe, [c]Department of Gastroenterology and Hepatology, Kinki University School of Medicine, Osakasayama, [d]Human Health Sciences, Graduate School of Medicine, Kyoto University, Kyoto, Departments of [e]Gastroenterology and Hepatology, [f]Internal Medicine and [g]Clinical Laboratory, Kaizuka City Hospital, Kaizuka, [h]Department of Gastroenterology and Hepatology, Japan Labour Health and Welfare Organization, Kansai Rousai Hospital, Amagasaki, and [i]Department of Gastroenterology and Hepatology, Osaka University Graduate School of Medicine, Suita, Japan

Key Words
Real-time tissue elastography · Chronic hepatitis · Ultrasound elastography · Liver fibrosis

Abstract
It has been established that the long-term infection of chronic hepatitis C leads to the increased risk of hepatic fibrosis and hepatocellular carcinoma. Currently, histological diagnosis by invasive and painful liver biopsy is the gold standard for evaluating the hepatic fibrosis stage. Because of a side effect or patient inability to cope with the pain, it is difficult to assess the fibrosis stage frequently using liver biopsy. Recently, instead of liver biopsy, many articles have been published showing the usefulness of ultrasound elastography to evaluate the stage of hepatic fibrosis. We also reported the usefulness of real-time tissue elastography (RTE) for liver fibrosis staging in 2007. However, in our previous report, fibrosis classification was performed manually and the number of patients involved was also small. In the current study, the fibrosis staging is performed automatically using software by characterizing the elastography images. We have also increased the number of patients from 64 to 310. Thus, the aim of this study is to increase objectivity by using a newly developed automatic analysis method. We obtain the Liver Fibrosis Index (LFI), which is calculated from image features of RTE images, using multiple regression analysis performed on clinical data of 310 cases as the training data set. The correlation coefficient obtained between the LFI and the stage of hepatic fibrosis was $r = 0.68$, and significant differences exist between all stages of fibrosis ($p < 0.001$). Our new method seems promising since it has the ability to diagnose fibrosis even in the presence of inflammation.

Introduction

Approximately 700,000 people worldwide are estimated to die annually of hepatocellular carcinoma (HCC), which is the third highest cause of cancer death [1, 2]. HCC often develops in the presence of hepatic fibrosis from long-term infection of chronic hepatitis B and C. It has been reported that the risk of HCC increases as the stage of liver fibrosis progresses [3]. It has been shown that fibrosis treatment using interferon reduces hepatic

KARGER

Fax +41 61 306 12 34
E-Mail karger@karger.com
www.karger.com

0030–2414/13/0847–0003$38.00/0

Accessible online at:
www.karger.com/ocl

Masatoshi Kudo, MD, PhD
Division of Gastroenterology and Hepatology, Department of Internal Medicine
Kinki University Faculty of Medicine
377-2 Ohno-Higashi, Osakasayama, Osaka 589-8511 (Japan)
E-Mail m-kudo@med.kindai.ac.jp

Abbreviations used in this paper

MEAN	Mean of relative strain value within the ROI
SD	Standard deviation of relative strain value within the ROI
%AREA	Area of low strain (blue) within the ROI
COMP	Complexity of low strain (blue) area within the ROI = (perimeter)^2/area
SKEW	Skewness – asymmetry of the histogram
KURT	Kurtosis – peakedness of the histogram
ENT	Entropy – textural complexity
IDM	Inverse Difference Moment – textual local homogeneity
ASM	Angular Second Moment – textual homogeneity

fibrosis and also dramatically reduces the incidence of HCC [4]. Thus, it is important to evaluate the stage of hepatic fibrosis both for establishing treatment and also for monitoring its effectiveness.

Histological diagnosis using liver biopsy is very important for the evaluation of hepatic fibrosis [5–10]. However, because of its invasiveness, liver biopsy cannot be performed frequently. In addition, there is a limitation in the accuracy of liver biopsy due to sampling error [11–13]. Thus, the development of noninvasive tests that are reliable, cost-effective and easy to use is required for evaluating the stage of hepatic fibrosis. Previously, measurement of platelet counts [14] and liver fibrosis marker [15–18] were used as noninvasive tests to evaluate hepatic fibrosis, but generally the basic procedure for evaluating the stage of hepatic fibrosis is to combine the use of these tests with diagnostic imaging techniques, such as ultrasonography.

Ultrasound imaging is the most useful imaging diagnostic technique used for evaluating chronic hepatitis and/or cirrhosis. The image characteristics for evaluating hepatic fibrosis/cirrhosis are the nodular liver parenchyma, heterogeneous internal echo texture, decrease in the volume of right hepatic lobe and increase in the volume of caudate and left hepatic lobe, and the narrowing of the hepatic vein [19, 20]. However, staging of the liver fibrosis using these characteristics is less reliable since the appearance of images can be changed due to differences in ultrasonic power and/or the image settings of the equipment used. Ultrasound tissue characterization has been attempted in the literature for objective evaluation of tissue by analyzing the signals obtained from the ultrasound system, for example intensity of RF signals, extent of scattering [21, 22] and velocity of shear wave generated by a probe in the liver [23].

New methods are emerging to estimate the liver stiffness or the fibrosis, using ultrasound elastography or MRI [24]. There are many forms of elastography that are popular, namely transient elastography (Fibroscan®) [25–28], acoustic radiation forces impulse imaging (ARFI) and our own real-time tissue elastography (RTE) [29–32]. Fibroscan and ARFI measure the velocity of shear waves propagating in the tissue to measure liver stiffness, which is then correlated to fibrosis. However, in the case of Fibroscan, measured liver stiffness is correlated not only with the stage of hepatic fibrosis, but also with grade of inflammation. Therefore, the involvement of many dynamic factors independent of hepatic fibrosis affect the measurement value, such as inflammation or cholestasis. The stage of hepatic fibrosis, which is the goal of the imaging technique, should be defined as the parameter dependent only on the fibrosis of the liver, which is the true pathology to be indicated and should not include other dynamic factors.

Our RTE is different from Fibroscan and ARFI and it measures relative stiffness of the tissue in the region of interest (ROI) and displays the stiffness with color overlaid over the B-mode image in real time. Apart from liver imaging, it has many other clinical applications that have been reported in the literature, such as breast, thyroid, prostate and pancreas [33–36]. RTE image is constructed using tissue strains which are calculated from 2 consecutive frames. The phase difference of RF signals from 2 consecutive frames are calculated to obtain tissue strain and transferred to color codes. The colors in the ROI range from blue to red to show the relative hardness and softness of area inside the ROI [30, 31]. The harder areas are displayed in blue and the softer areas in red.

In our previous work using RTE for liver imaging, we established the usefulness of RTE for the evaluation of hepatic fibrosis of chronic hepatitis C patients. The reported liver elasticity scores, which were scored visually, showed significant correlation with hepatic fibrosis [37]. Our RTE, available as a native mode in an ultrasound system, can be used for evaluating patients even with ascites and severe hepatic atrophy.

Even though our previous paper showed the feasibility of using RTE, the main limitation was that the evaluation of the RTE images was performed visually. While evaluating visually, two radiologists used the increase in a blue area in the RTE image as a criteria for staging hepatic fibrosis. Blue areas of RTE images increased and became patchy as the stage of hepatic fibrosis increased. It was difficult for the radiologists to visually estimate hepatic fibrosis with RTE images since the scoring of fibrosis also depended on the individual examiner's image perspective. In addition, in our previous report, we did not perform any investigation about the relationship between the grade of inflammation and the RTE image. Thus, the aims of this study are: (1) to present a newly developed

image analysis software method to obtain Liver Fibrosis Index (LFI) automatically from image features of RTE images using multiple regression analysis [38–40], (2) to show the effectiveness of this software tool and (3) to establish the relationship between LFI, the stage of fibrosis and the grade of inflammation.

Patients and Methods

Patients

The protocol was created following the Declaration of Helsinki and approved by an independent ethics committee of 3 institutions. For this study, we chose 295 patients with chronic hepatitis C or cirrhosis. Fifty-five patients were excluded from the study (table 1). All these patients were anti-hepatitis C virus and hepatitis C virus RNA positive, and were diagnosed by liver biopsy between May 2005 and December 2009. The patient population included 130 males and 165 females aged between 26 and 76 years old (mean age 56 years; table 1). Fifteen healthy volunteers were also enrolled as a normal control group. We obtained written informed consent from all participants at the National Hospital Organization Minamiwakayama Medical Center, Kaizuka City Hospital and Kinki University Hospital.

Liver Histology

Liver biopsy was performed twice using 18G automatic cutting biopsy needles (Adjustable Temno Biopsy System; Cardinal Health, Waukegan, Ill., USA) under local anesthesia for all study patients. Regardless of benign or malignant tumor, patients who had tumor located in the imaging plane from the right intercostal were excluded from the study. The specimen lengths were 20 mm (range 10–25 mm) and the sections were stained with hematoxylin and eosin and Masson trichrome staining. These sections were examined by 3 pathologists to stage the fibrosis and also to grade the activities. All 3 pathologists were blinded to any clinical data including the results of RTE. Hepatic fibrosis were staged from F0 to F4 according to the following scale: F0 – no fibrosis, F1 – portal fibrosis without septa, F2 – portal fibrosis with septa, F3 – numerous septa without cirrhosis and F4 – cirrhosis. Inflammatory activities were graded from A0 to A3 with the following scale: A0 – no activity, A1 – mild activity, A2 – moderate activity and A3 – severe activity.

The fifteen healthy volunteers were all male, aged between 22 and 52 years (average 31.5), BMI between 17.9 and 24.7 (average 21.0) and their blood tests, such as aspartate aminotransaminase, alanine transaminase, gamma-GTP, total cholesterol and triglyceride, were all within normal limits. All volunteers had no sign of fatty liver in ultrasonography findings, thus no liver biopsy was performed and they were staged F0.

Real-Time Tissue Elastography

HI VISION 900 (Hitachi Medical Corp., Tokyo, Japan) was used for ultrasonography and the probes used were EUP-L52 linear probes (7–3 MHz). We used linear array probes for this study over convex array probes because linear probes have many advantages when internal compression and relaxation induced by the cardiac motion is utilized for obtaining RTE images of the liver. We utilized internal compression and relaxation induced by the cardiac motion instead of manual compression because this is more consistent and reliable. Even though the field of view of a linear array probe is small, the direction of displacement induced by cardiac movement can be set to the surface of the probe, thus making it suitable for RTE analysis. Also, at smaller depth the field of view of a linear probe is much larger than that of convex probes, thus making it more suitable for an RTE image.

After obtaining B-mode images, the ultrasound mode was switched to RTE and scanned from the right intercostal space to observe the right hepatic lobe. RTE images were obtained by holding the probe still at the position where displacement by the cardiac motion in B-mode was in the axial direction. The optimum intercostal space was the position where liver parenchyma was imaged in the deepest area. When the liver was not contracted, RTE images were easily obtained by scanning through the intercostal space of anterior to middle axillary lines. Because the RTE image is formed from the strain values computed from the axial displacement, the position where liver parenchyma moves in a lateral direction due to cardiac motion was not suitable for this study.

The ROI for RTE was set inside liver parenchyma. Regions with large vessels or regions having shadows from ribs were avoided to reduce the artifacts arising from the anechoic region. The tops of the ROI were positioned at a depth of more than 1 cm from the surface of the liver to avoid multiple reflections arising from the surface of the liver.

RTE was performed using a freehand technique, with the linear probe placed at the appropriate position with the patient holding their breath. As mentioned in the previous paragraph, no manual compression/relaxation was applied. The compression/

Table 1. Background of patients and excluded cases

Patients (n = 295)	
Male/female	130/165
Age, years	56 ± 18
Range	26 – 76
ALT, IU/l	59.4 ± 41.1
Total bilirubin, mg/dl	0.9 ± 0.5
Albumin, g/dl	4.0 ± 1.1
Choline esterase, IU/l	270.4 ± 78.4
Total cholesterol, mg/dl	187.4 ± 33.4
Prothrombin time, %	94.2 ± 12.9
Platelet count ($\times 10^4/\mu l$)	16.2 ± 7.7
Fibrosis stage, F0/F1/F2/F3/F4	84/97/65/48
Histological activity, A0/A1/A2/A3	29/90/146/30
Excluded cases (n = 55)	
Poor penetration (n = 20)	
Fatty layer ≥5 mm and muscular layer ≥10 mm	9
Fatty layer ≥5 mm and muscular layer <10 mm	3
Fatty layer <5 mm and muscular layer ≥10 mm	5
Fatty layer <5 mm and muscular layer <10 mm	3
Unstable technique (n = 35)	
Slipping section by body movement	10
Slipping horizontally by cardiac movement	13
Poor cardiac movement	3
Artifact by multiple reflection	9

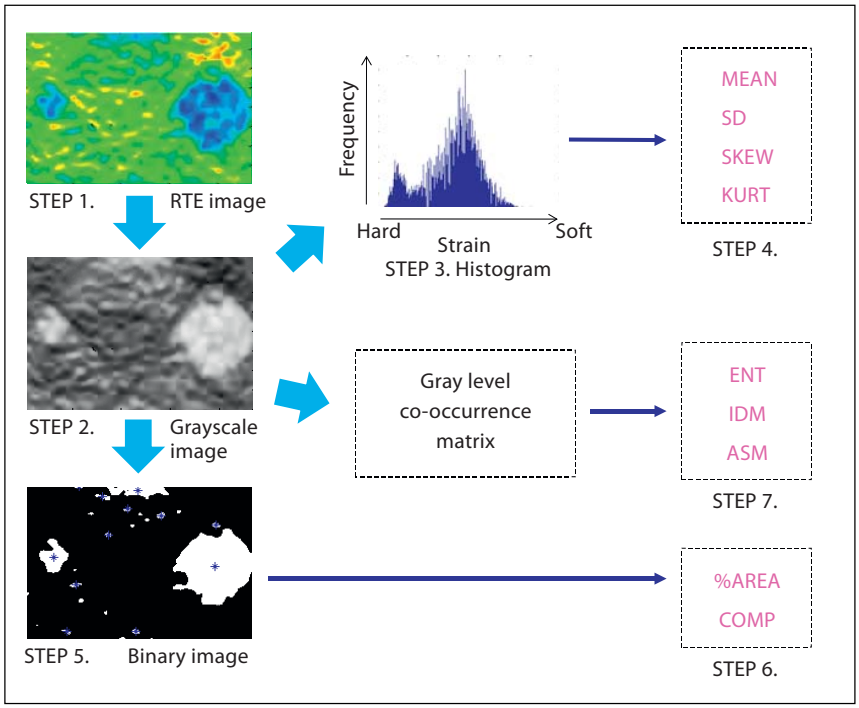

Fig. 1. Flow of calculations.

relaxation of the liver induced by the cardiac motion is easily detected to compute strain images. The ultrasound system parameters such as depth, ROI and gain were set for optimum RTE image quality. RTE images obtained by the lateral movements of the heart were avoided. One to two RTE images are displayed in 1 heartbeat, and the best RTE image was selected for final analysis. In total 3–5 RTE images obtained from different heart cycles without lateral motion were selected. The average of these 3–5 images for each patient was then used in regression analysis.

We extracted the following 9 image features to quantify the patchy pattern of the RTE images. More details about these features can also be found in the literature [41].

All 9 parameters have been found in the literature to be very useful for characterizing the imaging pattern in many different applications, e.g. satellite imaging, geothermal imaging and machine visions [42]. For liver fibrosis staging using RTE images, we employ these features for characterizing the image and correlating them with fibrosis staging. Analysis of RTE image features were performed with the prototype analysis software shown in figure 1. This software converts the selected analysis area of the RTE image (STEP 1) into a 256-step grayscale image (STEP 2), plots the strain histogram (STEP 3), and calculates the mean of relative strain (MEAN), standard deviation of relative strain (SD), skewness of strain histogram (SKEW) and kurtosis of strain histogram (KURT; STEP 4). Moreover, it binarizes the RTE image into black and white regions: white as low strain (blue) regions and black as all other regions (STEP 5). To characterize the low strain (blue) regions of the binary image, it calculates the ratio of low strain regions within the selected analysis area (%AREA), and the complexity of the low strain region (COMP; STEP 6). Furthermore, it also calculates entropy (ENT), inverse difference moment (IDM), and angular second moment (ASM) to evaluate the texture of the RTE image (STEP 7). Multiple regression analysis was then performed to improve the diagnostic accuracy using all these 9 image features instead of diagnosing with individual image features.

The LFI was estimated using these 9 image features as independent variables and the hepatic fibrosis stage as a dependent variable, as shown in the following multiple regression equation:

$$\begin{aligned}\text{LFI} = {} & -0.009 \times \text{MEAN} - 0.005 \times \text{SD} + 0.023 \times \%\text{AREA} \\ & + 0.025 \times \text{COMP} + 0.775 \times \text{SKEW} - 0.281 \times \text{KURT} \\ & + 2.083 \times \text{ENT} + 3.042 \times \text{IDM} + 39.979 \times \text{ASM} - 5.542.\end{aligned}$$

Multiple regression analysis was also performed to estimate the Liver Activity Index (LAI) using 9 image features as independent variables and grade of inflammatory activity as a dependent variable. LFI and LAI were calculated for all patients and compared with the stage of hepatic fibrosis and grade of inflammatory activity. Then, to eliminate the inflammatory activity from hepatic fibrosis, LAI and grade of inflammatory activity were compared for each stage of hepatic fibrosis. Receiver operating characteristic (ROC) analysis was performed for LFI to obtain a cutoff value for the identification of F0–1/F2–4 and F0–3/F4, and also to calculate sensitivity, specificity, accuracy and area under ROC (AUROC).

Statistical Analysis

All of the statistical analysis, such as multiple regression analysis and ROC analysis were carried out using the JMP statistical discovery software, version 8.0 (SAS Institute Inc., Cary, N.C., USA) for windows.

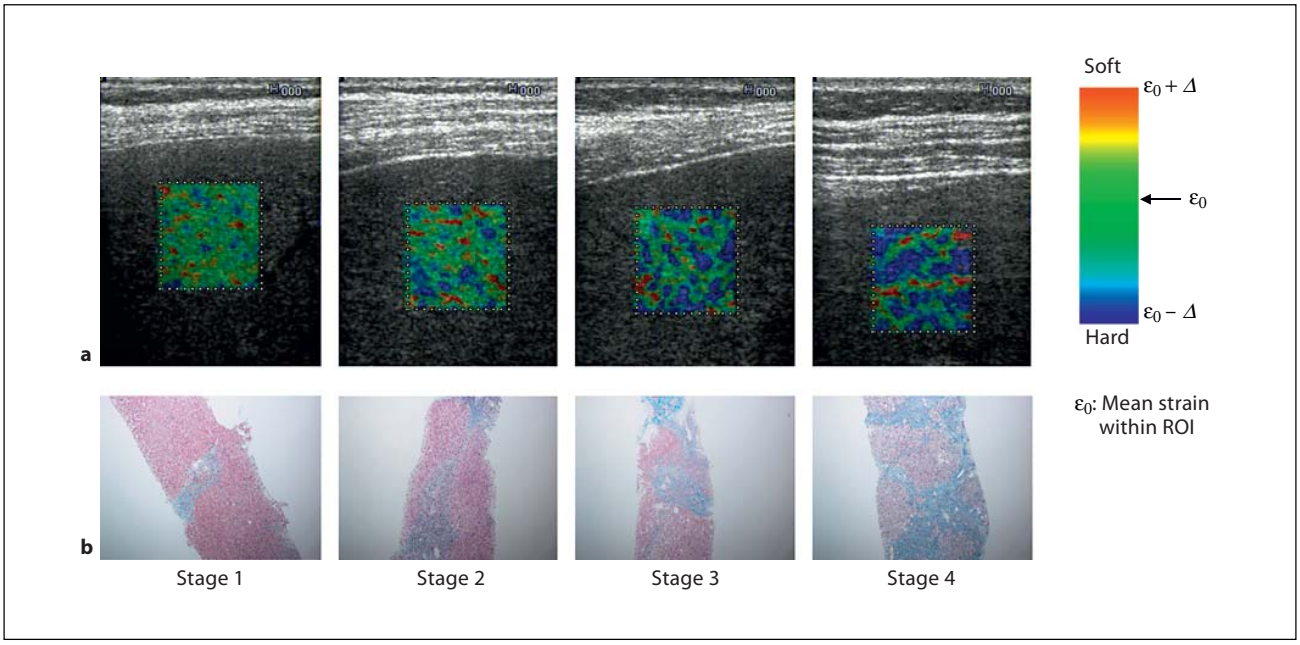

Fig. 2. RTE images (**a**) and pathological images, Masson trichrome stain, ×100 (**b**).

Results

Patients

We performed liver elastography in 365 patients (including 15 healthy volunteers) between April 2005 and November 2009. We excluded 55 patients from our study because more than 3 stable RTE images could not be acquired for these patients. Most of the reasons of exclusion were related to RTE skill of the clinicians, which improved significantly with more experience. Table 1 shows the characteristics of the 295 patients (excluding 15 healthy volunteers out of 310 patients). The indicated stages of hepatic fibrosis in the study patients were: F0 in 1 subject, F1 in 84 subjects, F2 in 97 subjects, F3 in 65 subjects and F4 in 48 subjects. The stage of hepatic fibrosis in all healthy volunteers was F0. Typical RTE images and pathological images for each fibrosis stage are shown in figure 2.

Correlation between Features and Stage

In the present study, as described previously, we extracted 9 image features. Correlation coefficients between 9 image features, such as MEAN, SD, %AREA, COMP, SKEW, KURT, ENT, IDM and ASM and stage of hepatic fibrosis were –0.63, 0.53, 0.65, 0.58, 0.59, 0.02, –0.22, 0.34 and 0.21, respectively. Thus, 5 of 9 image features, i.e. MEAN, SD, %AREA, COMP and SKEW, highly correlated with the stage of hepatic fibrosis (fig. 3).

Accuracy of Staging Fibrosis by LFI

Figure 4 shows the relationship between hepatic fibrosis stages and LFI calculated from 9 image features using multiple regression analysis. LFI highly correlates with the fibrosis stages ($r = 0.68$ with $p < 0.001$), and significant differences exist between all different stages. Figure 5 shows the ROC analysis. When the cutoff value of LFI was set to 1.92, the AUROC of LFI for F0–1 versus F2–4 was 0.82, and sensitivity, specificity and accuracy were 78.6, 78.0 and 78.4%, respectively. For F0–3 versus F4, when the cutoff value was 2.56, the AUROC was 0.87, and sensitivity, specificity and accuracy were 79.2, 80.5 and 80.3%, respectively (fig. 5). In this study, LFI clearly differentiates either F0–1 and F2–4 or F0–3 and F4.

Effect of Inflammation

Figure 6 shows the comparison between grades and the 9 image features for evaluating the effect of inflammation on RTE image. None of the 9 image features have a correlation with grades, and LAI, which was calculated by multiple regression analysis similar to LFI, also did not correlate with grades ($r = 0.30$; fig. 6j).

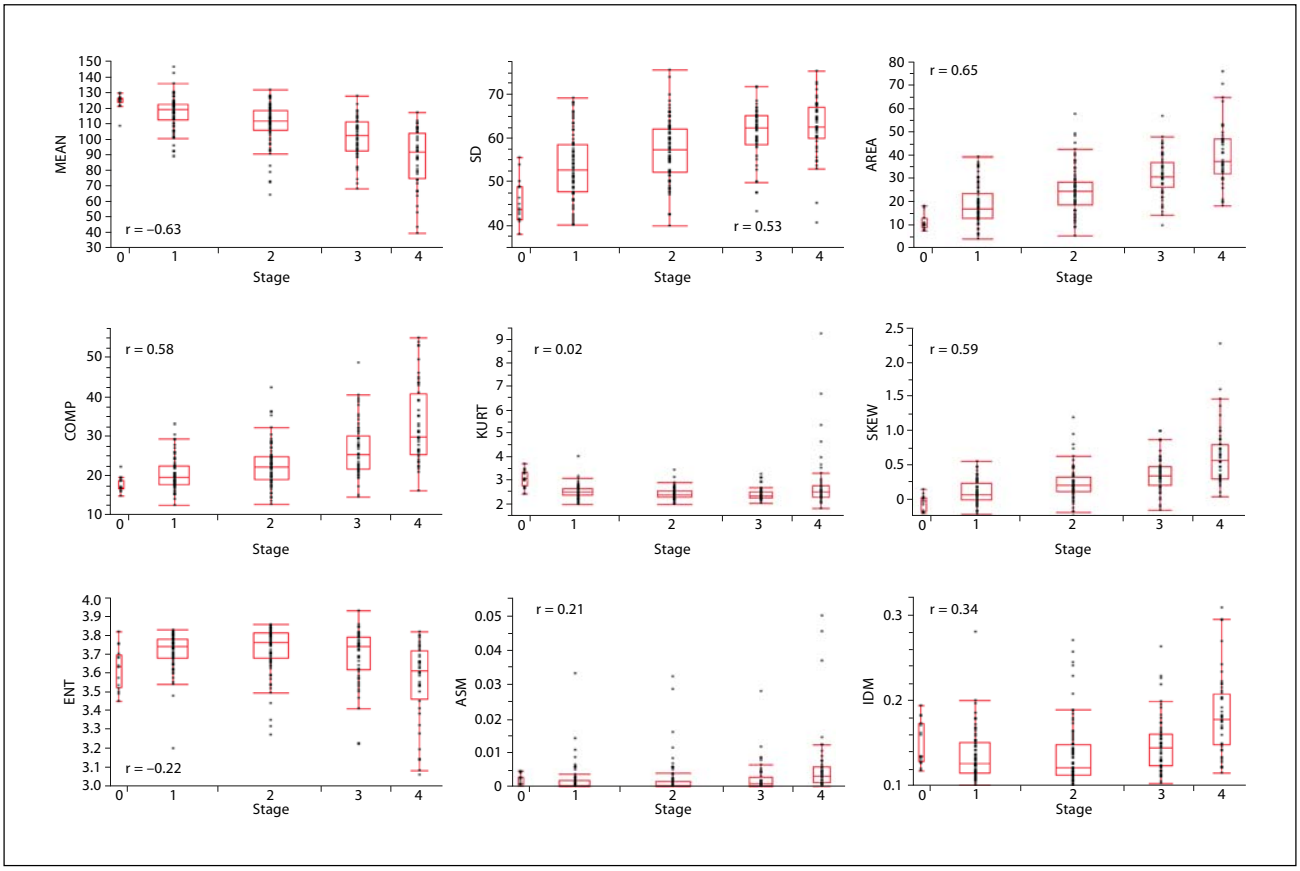

Color version available online

Fig. 3. Comparisons of stage of hepatic fibrosis and image features.

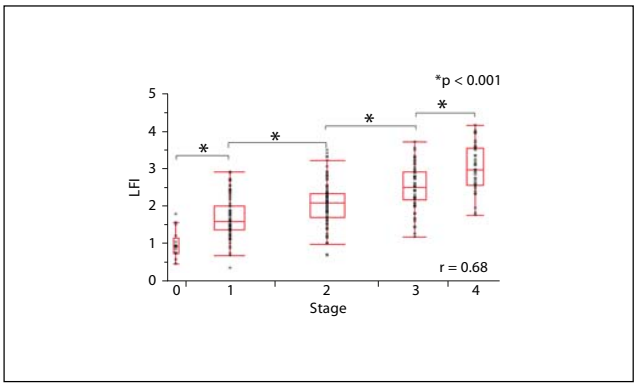

Color version available online

Fig. 4. Comparison of stage of hepatic fibrosis and LFI.

Discussion

Results of Estimation

To improve the accuracy of estimation of hepatic fibrosis and to make it automatic, we performed multiple regression analysis using 9 image features and obtained the estimated LFI. This index highly correlated with the stage of hepatic fibrosis ($r = 0.68$, $p < 0.001$) and significant differences were also observed between each stage. Furthermore, ROC analysis indicated that LFI has a high ability to differentiate each stage.

All 9 image features we used are independent and do not include confounding factors. Out of the 9 image features we analyzed, 5 (%AREA, MEAN, SD, COMP and SKEW) had a high correlation with the stages of hepatic fibrosis. This strong correlation, we believe, is mainly due to following reasons:

– AREA: hard area increases as a hepatic fibrosis progresses.

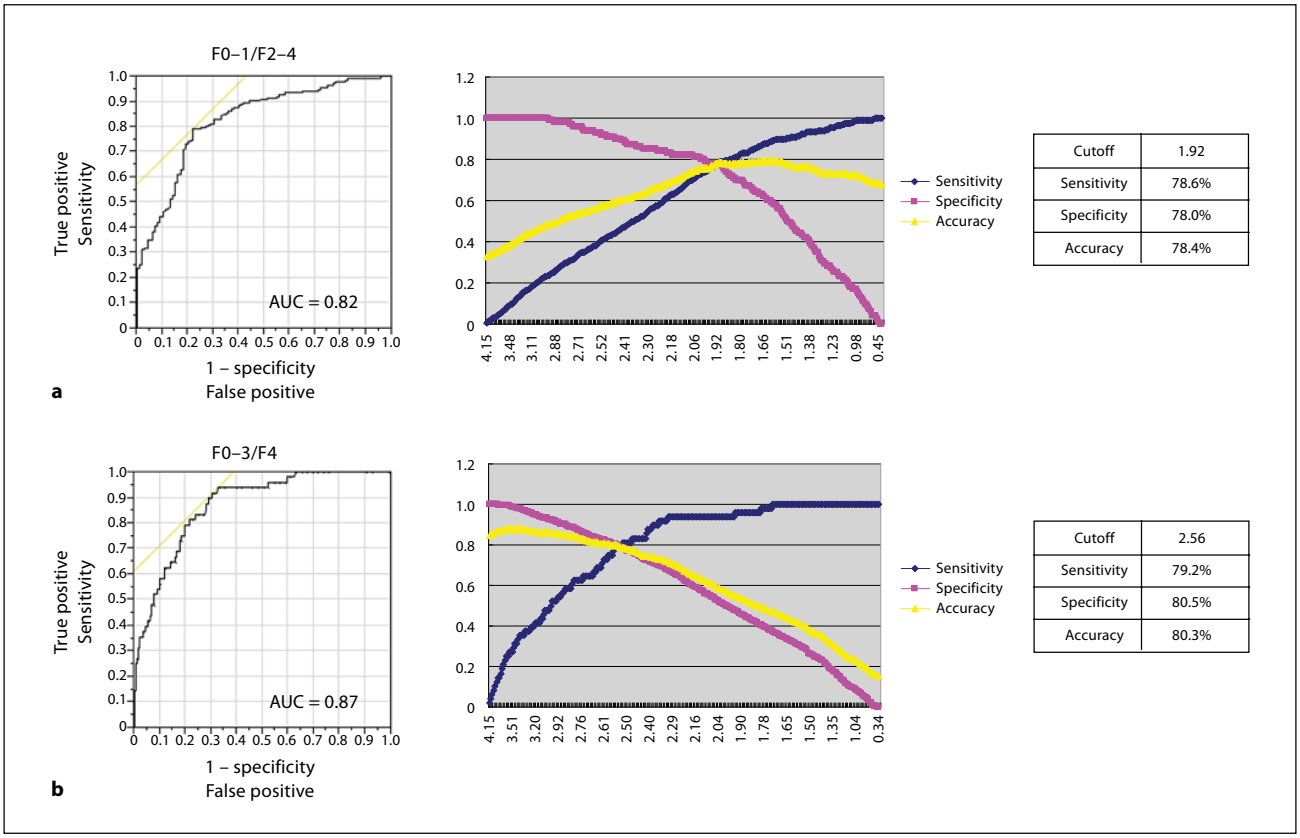

Fig. 5. ROC analysis differentiating F2–4 from F0–1 (**a**) and F4 from F0–3 (**b**).

- MEAN: liver parenchyma becomes stiffer as hepatic fibrosis progresses.
- SD: stiffness of liver parenchyma becomes heterogeneous as hepatic fibrosis progresses.
- COMP: figure of hard area becomes more complex as hepatic fibrosis progresses.
- SKEW: histogram skew towards the lower value of strain (harder) as hepatic fibrosis progresses.

Histopathological tissue evaluation using liver biopsy has been the gold standard for evaluation of hepatic fibrosis. However, this procedure is invasive, painful and could cause complications, such as hemorrhage, due to which many patients hesitate over the procedure. In addition, if the platelet count is low, partial thromboplastin time is greater than 3 s, the liver presents with a tumor and there is presence of ascites, then liver biopsy is also difficult to perform. This liver biopsy is also an economic burden due to the hospitalization required after the procedure. Currently, in such patients where a liver biopsy cannot be performed it is substituted with blood tests, which have significantly lower accuracy. Thus, our LFI based on RTE images, which is painless, cost-effective and can be performed in the presence of any of the above conditions can be a good addition to the clinicians tools for the noninvasive evaluation of liver fibrosis.

Effect of Inflammation

We did not find any correlation between any of the 9 features we used and inflammation grades. The RTE image, we believe, thus reflects the hepatic fibrosis and does not reflect the inflammatory factors such as intracellular pressure and change in blood flow due to inflammation. In addition, the spatial resolution of RTE images is 0.5–2 mm [43], which can completely capture the regenerating nodules in liver cirrhosis, which are 3–10 mm in size [44]. Thus, we can conclude that the LFI we have developed is not influenced by inflammation and it depends mainly upon liver fibrosis. Compared to RTE, other shear wave elastogra-

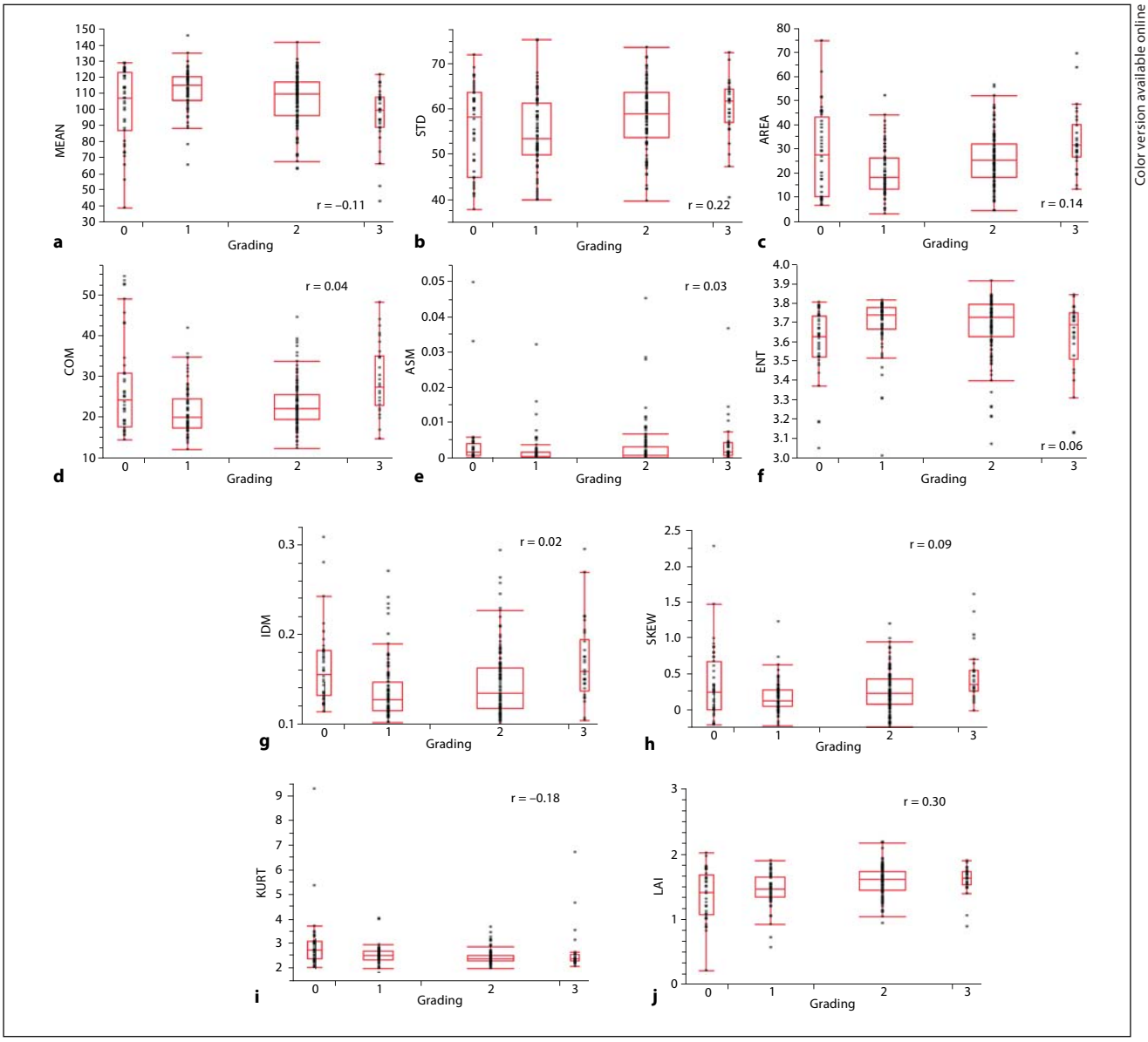

Color version available online

Fig. 6. a–j Comparison of grade and image features.

phy-based techniques, such as Fibroscan and ARFI, have been reported showing strong correlation with inflammation [45–47]. This correlation could be mainly because shear wave elastography adopts the principle of measuring the velocity of shear wave. Inflammatory factors such as intracellular pressure and condition of blood flow may change the velocity of shear waves, thus resulting in bias in the estimate.

Acquisition of RTE

We utilized compression/relaxation induced by the cardiac motion to obtain our RTE images for liver index computation. This helped to simplify RTE image acquisition and made it easier for clinicians to acquire RTE images. However, for some patients with weak pulsation and/or who are obese, it was difficult to perform liver elastography accurately. Training of clinicians was needed to avoid artifacts related to obesity, to set the ROI not

to include vessels and to adjust the position of the probe to image the liver where compression/relaxation was homogeneous and axial to the probe. RTE data were collected in 3 hospitals and 2 experts performed liver elastography. Image features were extracted from multiple RTE images and the average value from the acquired RTE images were used for our analysis.

Patient Selection Bias

In our study we did not include patients who had difficulty holding their breath or for whom it was difficult to image the liver through the intercostal spaces due to overlying bowel gases. Moreover, we excluded 55 cases with difficulty in analysis, the reasons for which are shown in table 1. The acquisition rate was 84.9% (310/365), which is still quite impressive in spite of these exclusions. Most of the exclusions happened at the beginning of the study. As the clinician gained experience, the failure rate reduced significantly and the success rate increased up to 98.0% (98/100). This implies that with some education and training the acquisition failure rate can be decreased significantly.

Limitations

We compared the results of LFI derived from RTE images with histopathological results of liver biopsy. However, liver biopsy results themselves have bias due to sampling error and due to the histopathological image being classified not by continuous quantity but staged by the progression of hepatic fibrosis. Moreover, there are large differences in the progression of hepatic fibrosis between 4 stages of liver fibrosis [40], thus the accuracy of liver biopsy is limited. Since liver biopsy results are used as a training set for our LFI computation, we speculate that there is also some bias in our estimate of liver fibrosis. A new index is needed as training data to derive a multiple regression equation to reduce the variation in results.

As a future subject for increasing the accuracy of the LFI, fibrosis staging by two or more pathologists is due to be judged using the block specimen by a surgical resection. Thereby, since the variation in a pathology result can be decreased, we think that better equation estimates of LFI can be derived.

Prospects of RTE

Our results of liver fibrosis staging are very impressive. It is automatic, consistent and agrees very well with current liver biopsy results. Thus, in the near future, we expect that the RTE could be used as a first-choice imaging tool for fibrosis screening. If considered suspicious, then liver biopsy can be performed for further confirmation. In addition, RTE imaging could be the only choice available along with blood tests for patients in whom liver biopsy cannot be performed. RTE can also be used for monitoring the progress or resolution of fibrosis in patients treated with interferon. It can also be used to monitor the progress in fibrosis in patients where interferon treatment was not done. RTE imaging is easy to use, cost-effective and, moreover, painless. It is readily available with the ultrasound machine as an additional mode making the technique easily available and easy to use when liver screening is being done to monitor cirrhosis and rule out HCC. It can also be used in patients with hepatitis other than viral, such as nonalcoholic steatohepatitis, etc.

Conclusion

LFI computed from RTE images highly correlates with stages of hepatic fibrosis and accurately reflects the underlying hepatic fibrosis, even with the presence of inflammation. Thus, it can be used for screening, monitoring and at times diagnosis of hepatic fibrosis. We believe our results and our techniques are superior to other techniques such as transient elastography. In the near future we plan to conduct more extensive clinical studies both for substantiating our results as well as to prove the clinical utility of RTE imaging for liver fibrosis staging.

Acknowledgments

We would like to thank Akiko Tonomura, Tsuyoshi Mitake, Mitsuru Motoki, Tomoko Furuta, MD, Chie Tatsumi, MD, Shigeo Wada, MD and Masahide Oshita, MD, for valuable contributions to this study.

Disclosure Statement

The authors declare that no conflicts of interest exist.

References

1 WHO International Agency for Research on Cancer: World Cancer Report 2008. Section 1 – global cancer control, chapter 1.3: worldwide cancer burden. http://www.iarc.fr/en/publications/pdfs-online/wcr/2008/index.php.
2 WHO International Agency for Research on Cancer: World Cancer Report 2008. Section 2 – etiology of cancer, chapter 2.5: chronic Infections.

3 Yoshida H, Shiratori Y, Moriyama M, et al: Interferon therapy reduces the risk for hepatocellular carcinoma: national surveillance program of cirrhotic and noncirrhotic patients with chronic hepatitis C in Japan. Ann Intern Med 1999;131:174–181.
4 Shiratori Y, Imazeki F, Moriyama M, et al: Histologic improvement of fibrosis in patients with hepatitis C who have sustained response to interferon therapy. Ann Intern Med 2000;132:517–524.
5 Desmet VJ, Gerber M, Hoofnagle JH, et al: Classification of chronic hepatitis: diagnosis, grading and staging. Hepatology 1994; 19:1513–1520.
6 Ichida F, Tsuji T, Omata M, et al: Classification report: new inuyama classification for histological assessment of chronic hepatitis. Internat Hepatol Comm 1996;6:112–119.
7 Ishak K, Baptista A, Bianchi L, et al: Histological grading and staging of chronic hepatitis. J Hepatol 1995;22:696.
8 Bataller R, Brenner DA: Liver fibrosis. J Clin Invest 2005;115:209–218.
9 Pinzani M, Rombouts K, Colagrande S: Fibrosis in chronic liver diseases: diagnosis and management. J Hepatol 2005;42:S22–S26.
10 Dienstag JL: The role of liver biopsy in chronic hepatitis C. Hepatology 2002;36: S152–S160.
11 Gebo KA, Herlong HF, Torbenson MS, et al: Role of liver biopsy in management of chronic hepatitis C: a systemic review. Hepatology 2002;36:161–172.
12 Regev A, Berho M, Jeffers LJ, Milikowski C, et al: Sampling error and intraobserver variation in liver biopsy in patients with chronic HCV infection. Am J Gastroenterol 2002;97: 2614–2618.
13 Bedossa P, Dargère D, Paradis V: Sampling variability of liver fibrosis in chronic hepatitis C. Hepatology 2003;38:1449–1457.
14 Omata M: A strategy of the treatment for the viral hepatitis (in Japanese). J Jpn Soc Int Med 2004;93:269–276.
15 Manning DS, Afdhai NH: Diagnosis and quantitation of fibrosis. Gastroenterology, 2008;134:1670–1681.
16 Wai CT, Greenson JK, Fontana RJ, et al: A simple noninvasive index can predict both significant fibrosis and cirrhosis in patients with chronic hepatitis C. Hepatology 2003; 38:518–526.
17 Imbert-Bismut F, Ratziu, Pieroni L, Charlotte F, et al: Biochemical markers of liver fibrosis in patients with hepatitis C virus infection: a prospective study. Lancet 2001;357: 1069–1075.
18 Forns X, Ampurdanes S, Llovet JM, et al: Indentification of chronic hepatitis C patients without hepatic fibrosis by a simple predictive model. Hepatology 2001;36:986–992.
19 Freeman MP, Vick CW, Taylor KJ, et al: Regenerating nodules in cirrhosis: sonographic appearance with anatomic correlation. AJR Am J Roentgenol 1986;146:533–536.
20 Ishikawa H, Ono M, Goto M, et al: Ultrasonographic findings in patients with liver cirrhosis; relationships between parenchymal, superficial echo patterns, and histological findings (in Japanese). Jpn J Med Ultrason 1990;17:522–529.
21 Fujimoto K, Yamamoto Y, Waki H, et al: Tissue characterization using integrated backscatter in viral chronic liver disease. J Ultrasound Med 1999;18(suppl):472.
22 Kumada T, Toyoda H, Ogawa S, et al: Quantification of fibrosis in hepatitis C using statistics analysis tool of ultrasonics (2nd report). Jpn J Med Ultrasonics 2007;34:S641.
23 Ziol M, Handra-Luca A, Kettaneh A, et al: Noninvasive assessment of liver fibrosis by measurement of stiffness in patients with chronic hepatitis C. Hepatology 2005;41:48–54.
24 Joo I, Choi BI: New Paradigm for management of hepatocellular carcinoma by imaging. Liver Cancer 2012;1:94–109.
25 Sandrin L, Fourquet B, Hasquenoph JM, et al: Transient elastography: a new noninvasive method for assessment of hepatic fibrosis. Ultrasound Med Biol 2003;29:1705–1713.
26 Foucher J, Chanteloup E, Vergniol J, et al: Diagnosis of cirrhosis by transient elastography (FibroScan): a prospective study. Gut 2006;55:403–408.
27 Fraquelli M, Rigamonti C, Casazza G, et al: Reproducibility of transient elastography in the evaluation of liver fibrosis in patients with chronic liver disease. Gut 2007;56:968–973.
28 Kim DY, Kim SU, Park JY, Ahn SH, Song KJ, Han KH: FibroScan based risk estimation of HBV-related HCC occurrence: development and validation of a predictive model. Liver Cancer 2012;1:123.
29 Friedrich-Rust M, Wunder K, Kriener S, et al: Liver fibrosis in viral hepatitis: noninvasive assessment with acoustic radiation force impulse imaging versus transient elastography. Radiology 2009;252:595–604.
30 Shiina T, Nitta N, Ueno E, et al: Real time tissue elasticity imaging using the combined autocorrelation method. J Med Ultrasonics 1999;26:57–66.
31 Shiina T, Nitta N, Ueno E, et al: Real time tissue elasticity imaging using the combined autocorrelation method. J Med Ultrasonics 2002;29:119–128.
32 Joo I, Choi BI: New paradigm for management of hepatocellular carcinoma by imaging. Liver Cancer 2012;1:94–109.
33 Itoh A, Ueno E, Tohno E, et al: Breast disease: clinical application of US elastography for diagnosis. Radiology 2006;239:341–350.
34 Fukunari N: More accurate and sensitive diagnosis for thyroid tumors with elastography – detection and differential diagnosis of thyroid cancers. MEDIX Suppl. 2007. http://www.hitachi-medical.co.jp/tech/medix/pdf/supple/sup_05.pdf.
35 Tsutsumi M, Miyagawa T, Matsumura T, et al: Real-time balloon inflation elastography for prostate cancer detection and initial evaluation of clinic pathologic analysis, AJR Am J Roentgenol 2010;194:W471–W476.
36 Hirooka Y, Itoh A, Kawashima H, et al: Diagnosis of pancreatic disorders using contrast-enhanced endoscopic ultrasonography and endoscopic elastography. Clin Gastroenterol Hepatol 2009;7:S63–S67.
37 Fujimoto K, Wada S, Oshita M, et al: Noninvasive evaluation of hepatic fibrosis in patients with chronic hepatitis C using elastography. MEDIX Suppl. 2007. http://www.hitachi-medical.co.jp/tech/medix/pdf/supple/sup_07.pdf.
38 Tatsumi C, Kudo M, Ueshima K, et al: Noninvasive evaluation of hepatic fibrosis using serum fibrotic markers, transient elastography (FibroScan), and real-time tissue elastography. Intervirology 2008;1:S27–S33.
39 Tatsumi C, Kudo M, Ueshima K, et al: Noninvasive evaluation of hepatic fibrosis for type C chronic hepatitis. Intervirology 2010; 53:76–81.
40 Fujimoto K, Kato M, Tonomura A, et al: Non-invasive evaluation method of the liver fibrosis using real-time tissue elastography – usefulness of judgment liver fibrosis stage by Liver Fibrosis Index (LF Index) (in Japanese). Kanzo 2010;51:539–541.
41 Haralick RM, Shanmugan K, Dinstein I: Textural features for image classification. IEEE Trans Syst Man Cybern 1973;3:610–621.
42 Mittal D, Kumara V, et al: Neural network based focal liver lesion diagnosis using ultrasound images. Comp Med Imaging Graphics 2011;35:315–323.
43 Matsumura T, Shiina T, Oosaka T, et al: Development of real-time tissue elastography (in Japanese). MEDIX 2004;41:30–35.
44 Hoon L, Kim Y, Lee J: Regenerative nodules in liver cirrhosis: findings at CT during arterial portography and CT hepatic arteriography with histopathologic correlation. Radiology 1999;210:451–458.
45 Arena U, Vizzutti F, Abraldes JG, et al: Reliability of transient elastography for the diagnosis of advanced fibrosis in chronic hepatitis C. Gut 2008;57:1288–1293.
46 Vispo E, Barreiro P, Del Valle J, et al: Overestimation of liver fibrosis staging using transient elastography in patients with chronic hepatitis C and significant liver inflammation. Antivir Ther 2009;14:187–193.
47 Rifai K, Cornberg J, Mederacke I, et al: Clinical feasibility of liver elastography by acoustic radiation force impulse imaging (ARFI). Dig Liver Dis 2011;43:491–497.

Oncology

Oncology 2013;84(suppl 1):13–20
DOI: 10.1159/000345884

Published online: February 20, 2013

Assessment of Liver Fibrosis with Real-Time Tissue Elastography in Chronic Viral Hepatitis

Norihisa Yada[a] Masatoshi Kudo[a] Hiroyasu Morikawa[b] Kenji Fujimoto[c, d] Michio Kato[d] Norifumi Kawada[b]

[a]Department of Gastroenterology and Hepatology, Kinki University Faculty of Medicine, Osakasayama, [b]Department of Hepatology, Graduate School of Medicine, Osaka City University, Osaka, and [c]Division of Clinical Research and [d]Department of Internal Medicine, National Hospital Organization, Minamiwakayama Medical Center, Tanabe, Japan

Key Words
Real-time tissue elastography · FibroScan · Liver fibrosis · Liver stiffness

Abstract
Objective: The aim of this study was to assess prospectively the accuracy of measurement of liver fibrosis with real-time tissue elastography (RTE) in patients with chronic viral hepatitis. ***Methods:*** Two hundred and forty-five patients were prospectively enrolled. Nine image features were measured from strain images, and Liver Fibrosis Index (LFI) was calculated from these features. Fibrosis stage was diagnosed from pathological specimens obtained by ultrasound-guided biopsy. LFI and serological markers were compared with pathological diagnosis, and the diagnostic performance of RTE was compared. ***Results:*** LFI in stages F0–F1, F2, F3 and F4 was 1.58, 2.03, 2.40 and 2.86, respectively, demonstrating a stepwise increase with increasing severity of liver fibrosis ($p < 0.001$). LFI in F2 did not significantly differ from that in F3, whereas for all other combinations of stages, there were significant differences. The area under the receiver operating characteristic curve of the LFI, platelet count, aspartate/alanine aminotransferase ratio, aspartate aminotransferase-to-platelet ratio, and FibroIndex for predicting F3 stage or higher (F0–F2 vs. F3–F4) was 0.865, 0.824, 0.708, 0.789 and 0.828, respectively. ***Conclusions:*** RTE is useful for diagnosis of liver fibrosis, regardless of stage, in patients with chronic viral hepatitis.

Introduction

The assessment of liver fibrosis is an important factor in deciding on therapeutic options and for predicting the prognosis of chronic hepatitis. Biopsy is the gold standard for assessment of liver fibrosis; however, it carries risks such as bleeding and pain. Furthermore, needle biopsy of the liver has been shown to be associated with a high rate of sampling error in patients with diffuse parenchymal liver diseases. The possibility of sampling error with liver biopsy arises because the tissue obtained represents only a small portion (approx. one part in 50,000) of the entire liver mass [1–3].

Elastography is reported to be useful for diagnosis of liver fibrosis and has a variety of measurement methods [4, 5]. FibroScan, virtual-touch tissue quantification, and shear wave elastography measure the propagation speed

KARGER

Fax +41 61 306 12 34
E-Mail karger@karger.com
www.karger.com

0030–2414/13/0847–0013$38.00/0

Accessible online at:
www.karger.com/ocl

Masatoshi Kudo, MD, PhD
Division of Gastroenterology and Hepatology, Department of Internal Medicine
Kinki University Faculty of Medicine
377-2 Ohno-Higashi, Osakasayama, Osaka 589-8511 (Japan)
E-Mail m-kudo@med.kindai.ac.jp

of the shear wave [6–8]. The more severe hepatic fibrosis progresses, the faster propagation speed increases. They are said to be useful for the diagnosis of liver fibrosis, especially in advanced fibrosis cases. However, the propagation speed of the shear wave is not only affected by liver fibrosis, but also hepatic activity, jaundice and hepatic congestion [9–12]. The other method measures tissue distortion. Real-time tissue elastography (RTE) shows in real time the strain of the tissue. It has been reported that RTE is useful for evaluation of malignant tumors in the mammary gland and thyroid [13, 14].

In the present study, we investigated the performance of RTE for diagnosis of liver fibrosis. We also compared the diagnostic performance of RTE and serum markers of fibrosis.

Patients and Methods

Patients

This was a multicenter, cross-sectional study that was performed at Kinki University Hospital (Osaka, Japan), Osaka City University Hospital (Osaka, Japan) and Minamiwakayama Medical Center (Wakayama, Japan). Consecutive patients with chronic hepatitis C virus (HCV) or chronic by hepatitis B virus (HBV) infection, who underwent percutaneous ultrasound-guided liver biopsy before treatment, were enrolled. Only patients with HCV or HBV, whose disease was defined by the presence of serum anti-HCV antibody and serum HCV RNA, or the presence of serum hepatitis B surface antibody and serum HBV DNA, were included. Percutaneous ultrasound-guided liver biopsy was performed within 2 weeks before or after RTE. Clinical and laboratory data were collected at the time of liver biopsy. Patients were excluded if they consumed >20 g alcohol per day. Patients with a history of autoimmune hepatitis, primary biliary hepatitis, primary sclerosing cholangitis, hemochromatosis, α1-antitrypsin deficiency, or Wilson's disease were also excluded. The study protocol conformed to the Declaration of Helsinki and was approved by the local ethics committee. Informed consent to participate in the study was obtained from each patient.

Clinical and Laboratory Assessments

Relevant clinical data recorded were age, sex, weight, height, waist circumference and cause of chronic liver disease. Body Mass Index was calculated as weight (kg) divided by height (m) squared. Blood samples were taken after overnight fasting on the day of biopsy. Laboratory tests including platelet count, cholesterol, bilirubin, aspartate aminotransferase (AST), alanine aminotransferase (ALT), γ-glutamyl transpeptidase, bilirubin, albumin, γ-globulins, prothrombin time and international normalized ratio were assessed using automated methods. From these single variables, three ratio indexes were calculated using classical ratios: AST/ALT [15]; AST-to-platelet ratio index [APRI; AST/upper limit of normal 100/platelet count (10^4/mm^3)] [16], and FibroIndex [1.738 – 0.064 × platelet count (10^4/mm^3) + 0.005 × AST (U/l) + 0.463 × γ-globulin (g/dl)] [17].

Liver Histological Assessment

Percutaneous ultrasound-guided liver biopsy was performed on the liver right lobe with a Tru-Cut semiautomatic 18-gauge needle apparatus (Monopty; C.R. Bard, Tempe, Ariz., USA). The liver biopsy specimens were fixed in formalin, embedded in paraffin and stained with hematoxylin and eosin, Masson's trichrome or Azan stain. All biopsy specimens were examined by pathologists who were blinded to the patient characteristics. Liver fibrosis was scored by the New Inuyama classification. The stage of fibrosis was classified from F0 to F4 as follows: F0, no fibrosis; F1, fibrosis portal expansion; F2, bridging fibrosis (portal–portal or portal–central linkage); F3, bridging fibrosis with lobular distortion (disorganization), and F4, cirrhosis.

Real-Time Tissue Elastography

RTE was performed using ultrasonography (EUS-8500, HI-VISION 900 and HI-VISION Ascendus; Hitachi Aloka Medical, Tokyo, Japan) and the EUP-L52 linear probe (3–7 MHz; Hitachi Aloka Medical). Patients were examined in the spine position with the right arm in maximal abduction and were instructed to hold their breath. The examinations were performed on the right lobe of the liver through the intercostal spaces, holding firmly the transducer without applying compression on the skin. The B-mode and static image superimposed on B-mode were both visualized in real-time; therefore, the best position could be easily selected. The region of interest (ROI) of the strain image was 2.5 cm^2 and located about 1 cm below the surface of the liver. In addition, to obtain good images, scanning was performed to avoid large vessels and attenuation by lungs and ribs. RTE shows a relative strain image, thus, there should be no artifacts in the ROI of the strain image.

Nine image features were extracted from each RTE image: mean relative strain value (MEAN); standard deviation of relative strain value (SD); percentage of low strain area (percentage of blue color area – %AREA); complexity of low strain area (calculated as perimeter^2/area – COMP); skewness (SKEW); kurtosis (KURT); entropy (ENT); textural complexity, inverse difference moment (IDM), and angular second moment (ASM). For stable extracting of image features, the extraction area approximately matched or was slightly smaller than the ROI of the strain image (fig. 1). To perform a quantitative evaluation, Liver Fibrosis Index (LFI) was calculated as follows: –0.009 × MEAN – 0.005 × SD + 0.023 × %AREA + 0.025 × COMP + 0.775 × SKEW – 0.281 × KURT + 2.083 × ENT + 3.042 × IDM + 39.979 × ASM – 5.542 [18, 19]. The median LFI was calculated from 10 images.

Statistical Analysis

Descriptive statistics are shown as the mean ± SD, median or percentage, as appropriate. Comparisons between groups were determined by Wilcoxon's signed rank test and confirmed by the nonparametric Mann-Whitney U test between groups. Correlation between data was tested using the nonparametric Spearman rank correlation analysis. Differences were considered statistically significant at $p < 0.05$. Tukey's Honestly Significant Difference test was used to compare the data among each fibrosis stage of chronic hepatitis. The diagnostic performance for liver fibrosis was determined in terms of sensitivity, specificity, positive predictive value, negative predictive value, diagnostic accuracy and area under the receiver operating characteristic curve (AUROC). Analysis was performed using SPSS Statistics 20 (IBM, Armonk, N.Y., USA).

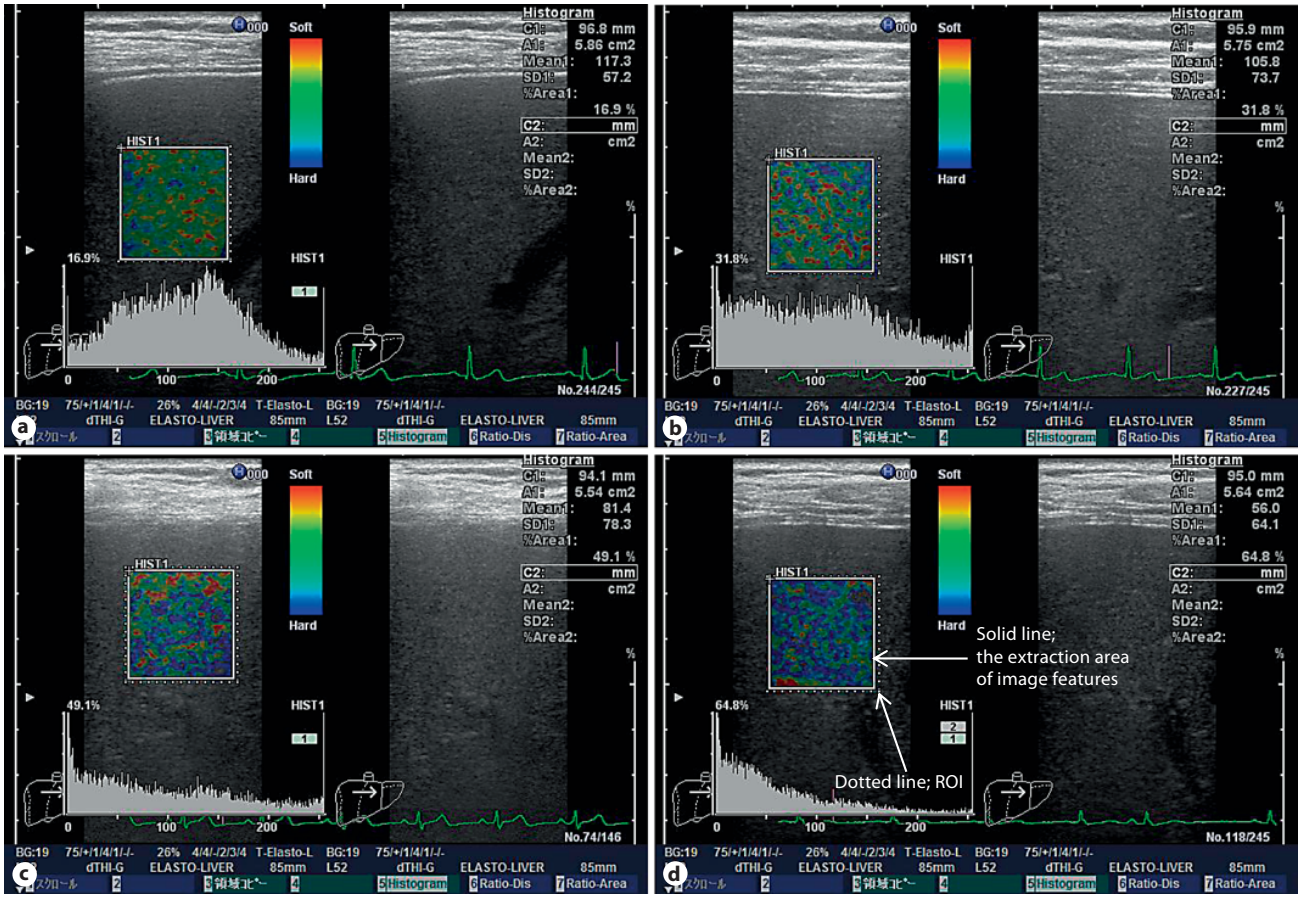

Fig. 1. RTE images in patients with chronic viral hepatitis. With fibrosis associated to progress, strain elastogram increases color variation between relatively low strain regions and generates a patched image pattern. F1 stage (**a**), F2 stage (**b**), F3 stage (**c**), F4 stage (**d**).

Results

Demographics and Baseline Features

In 4 patients, the liver biopsy specimen was too small to be used for pathological diagnosis. The remaining 245 patients, 137 (56.1%) men and 108 women (43.9%) who met the requirements were enrolled in the study. The clinical characteristics and laboratory data are shown in table 1. One hundred and eighty-nine patients (77.1%) had HCV and the other 56 (22.9%) had HBV. Four, 95, 77, 27 and 42 patients were respectively diagnosed with stage F0, F1, F2, F3 and F4 fibrosis. AST and alkaline phosphatase were significantly elevated with increasing severity of fibrosis ($p < 0.001$). Serum albumin, cholinesterase, total cholesterol, prothrombin time and platelet count were significantly decreased with increasing severity of fibrosis ($p < 0.001$).

Comparison of Serological Markers and Pathological Diagnosis

Serological fibrosis makers, platelet count, AST/ALT ratio, APRI and FibroIndex were compared with the pathological diagnosis of hepatic fibrosis. Platelet count in patients with F0–F1, F2, F3 and F4 stage fibrosis was 21.0, 15.7, 14.1 and 10.6 $\times$ 10^4/mm^3, respectively, demonstrating a stepwise decrease with increasing severity of liver fibrosis ($p < 0.001$). AST/ALT ratio in patients with F0–F1, F2, F3 and F4 stage fibrosis was 1.09, 1.01, 1.59 and 1.33, respectively, and showed a slightly upward trend with increasing severity of liver fibrosis ($p = 0.001$). APRI in patients with F0–F1, F2, F3, and F4 stage fibrosis was 5.49, 11.37, 12.52 and 23.79, respectively, and FibroIndex in patients with F0–F1, F2, F3 and F4 stage was 1.21, 1.78, 1.82, and 2.31, respectively. Both APRI and FibroIndex

Table 1. Clinical characteristics and laboratory data of patients

Fibrosis stage	F0–F1	F2	F3	F4	Total	p value
Etiology (HCV/HBV)	70/30	63/16	20/7	39/3	189/56	
Sex (male/female)	55/44	45/32	15/12	22/20	137/108	
Age, years	51.4 ± 12.8	59.6 ± 14.0	59.6 ± 14.9	66.7 ± 11.6	57.7 ± 14.3	<0.001
Height, m	162.1 ± 8.2	165.3 ± 8.7	161.5 ± 7.5	160.1 ± 9.2	162.5 ± 8.4	NS
Weight, kg	60.7 ± 10.9	65.5 ± 14.7	59.4 ± 9.4	61.2 ± 14.2	61.7 ± 12.1	NS
Waist circumference, cm	82.8 ± 8.6	90.1 ± 14.1	87.9 ± 12.4	87.2 ± 10.6	85.7 ± 10.6	NS
Body mass index	23.1 ± 3.5	23.8 ± 4.2	22.8 ± 3.5	23.6 ± 3.7	23.3 ± 3.7	NS
AST, IU/l	43.6 ± 33.8	58.3 ± 48.2	63.3 ± 42.2	70.0 ± 47.2	54.0 ± 41.8	<0.001
ALT, IU/l	57.0 ± 63.3	69.6 ± 55.7	57.6 ± 46.7	59.7 ± 45.3	60.1 ± 56.6	NS
GGT, IU/l	42.3 ± 48.8	62.1 ± 70.1	45.2 ± 44.2	61.8 ± 86.6	50.4 ± 62.2	NS
ALP, IU/l	238.2 ± 83.4	266.6 ± 95.3	307.0 ± 169.8	376.7 ± 209.5	280.4 ± 141.4	<0.001
Total bilirubin, mg/dl	0.72 ± 0.49	0.92 ± 1.48	0.78 ± 0.58	1.09 ± 0.63	0.84 ± 0.82	<0.001
Total protein, g/dl	7.8 ± 7.1	7.2 ± 0.7	7.1 ± 0.9	7.1 ± 0.8	7.5 ± 4.9	NS
Serum albumin, g/dl	4.2 ± 0.4	4.1 ± 0.4	4.1 ± 0.7	3.6 ± 0.6	4.1 ± 0.5	<0.001
Gamma globulin, g/dl	1.4 ± 0.4	1.6 ± 0.4	1.7 ± 0.5	2.0 ± 0.5	1.6 ± 0.5	<0.001
Cholinesterase, IU/l	353.9 ± 99.8	288.3 ± 47.4	273.9 ± 76.5	157.4 ± 80.0	313.8 ± 105.0	<0.001
Total cholesterol, mg/dl	185.3 ± 32.7	172.2 ± 31.2	161.5 ± 34.9	149.7 ± 26.8	172.8 ± 34.4	<0.001
Prothrombin time, %	100.4 ± 11.7	95.8 ± 15.6	89.1 ± 14.9	76.6 ± 15.4	93.2 ± 16.4	<0.001
Platelets, $10^4/mm^3$	21.0 ± 6.0	15.7 ± 5.0	14.1 ± 4.7	10.6 ± 7.5	17.1 ± 7.3	<0.001
AST/ALT ratio	1.09 ± 0.92	1.01 ± 0.45	1.59 ± 1.46	1.33 ± 0.53	1.18 ± 0.88	0.001
APRI	5.49 ± 4.14	11.37 ± 13.68	12.52 ± 7.87	23.79 ± 26.23	11.05 ± 15.14	<0.001
FibroIndex	1.21 ± 0.45	1.78 ± 0.60	1.82 ± 0.55	2.31 ± 0.66	1.63 ± 0.70	<0.001
LFI	1.58 ± 0.67	2.03 ± 0.71	2.40 ± 0.64	2.86 ± 0.64	2.02 ± 0.82	<0.001
Total, n	99	77	27	42	245	

GGT = γ-Glutamyl transpeptidase; ALP = alkaline phosphatase.

showed a significant stepwise increase with severity of liver fibrosis ($p < 0.001$). However, there were a number of outliers in these serological markers (fig. 2).

Comparison between each F stage group was performed. Platelet count showed a significant decrease with severity of liver fibrosis between F0–F1 and F2, F0–F1 and F3, F0–F1 and F4, and F2 and F4. APRI showed a significant increase with severity of liver fibrosis between F0–F1 and F4, F2 and F4, and F3 and F4. FibroIndex showed a significant increase with severity of liver fibrosis between F0–F1 and F2, F0–F1 and F3, F0–F1 and F4, F2 and F4, and F3 and F4 (fig. 2).

Relationship between LFI and Pathological Liver Fibrosis

RTE was performed in all the enrolled patients. LFI was calculated as the median from 10 images. The median LFI in patients with F0–F1, F2, F3 and F4 stage fibrosis was 1.58, 2.03, 2.40 and 2.86, respectively, demonstrating a stepwise increase with increasing severity of liver fibrosis ($p < 0.001$). Comparison between each F stage group was performed. There was a significant increase between F0–F1 and F2, F0–F1 and F3, F0–F1 and F4, F2 and F4, and F3 and F4. The best cutoff of LFI for diagnosis of F2 or higher stage fibrosis (differentiating F2–F4 from F0–F1) was 2.05, and the accuracy was 73.0%. The best cutoff of LFI for diagnosis of F3 or higher stage fibrosis (differentiating F3–F4 from F0–F2) was 2.28, and the accuracy was 79.6%. The best cutoff of LFI for diagnosis of F4 stage fibrosis (differentiating F4 from F0–F3) was 2.36, and the accuracy was 78.3 (table 2).

Correlation with LFI and Serum Markers

The AUROC of the LFI, platelet count, AST/ALT ratio, APRI and FibroIndex for predicting F2 or higher stage fibrosis (F0–F1 vs. F2–F4) was 0.800, 0.832, 0.646, 0.820 and 0.853, respectively. Similarly, the AUROC for predicting F3 or higher stage fibrosis (F0–F2 vs. F3–F4) was 0.865, 0.824, 0.708, 0.789 and 0.828, respectively.

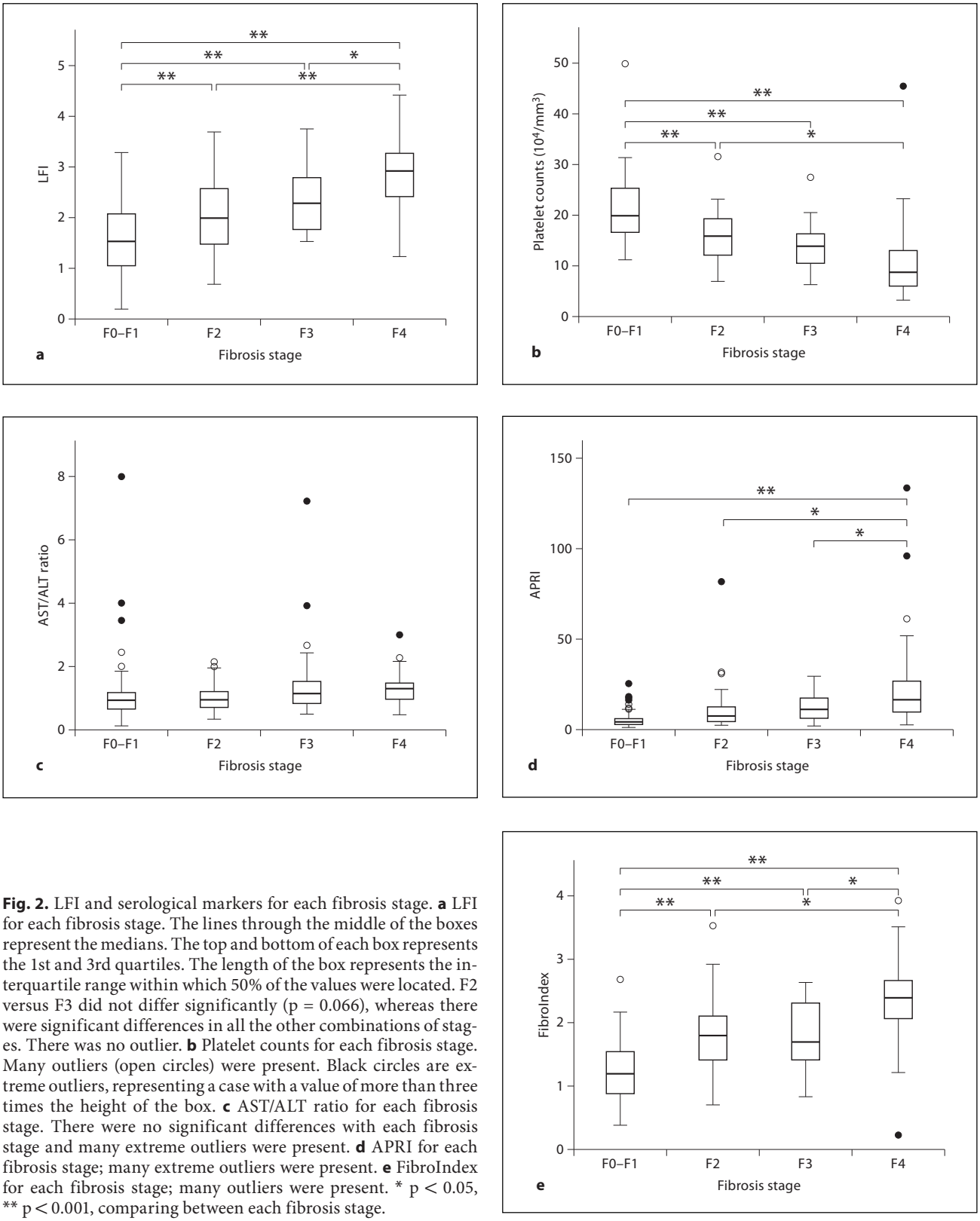

Fig. 2. LFI and serological markers for each fibrosis stage. **a** LFI for each fibrosis stage. The lines through the middle of the boxes represent the medians. The top and bottom of each box represents the 1st and 3rd quartiles. The length of the box represents the interquartile range within which 50% of the values were located. F2 versus F3 did not differ significantly ($p = 0.066$), whereas there were significant differences in all the other combinations of stages. There was no outlier. **b** Platelet counts for each fibrosis stage. Many outliers (open circles) were present. Black circles are extreme outliers, representing a case with a value of more than three times the height of the box. **c** AST/ALT ratio for each fibrosis stage. There were no significant differences with each fibrosis stage and many extreme outliers were present. **d** APRI for each fibrosis stage; many extreme outliers were present. **e** FibroIndex for each fibrosis stage; many outliers were present. * $p < 0.05$, ** $p < 0.001$, comparing between each fibrosis stage.

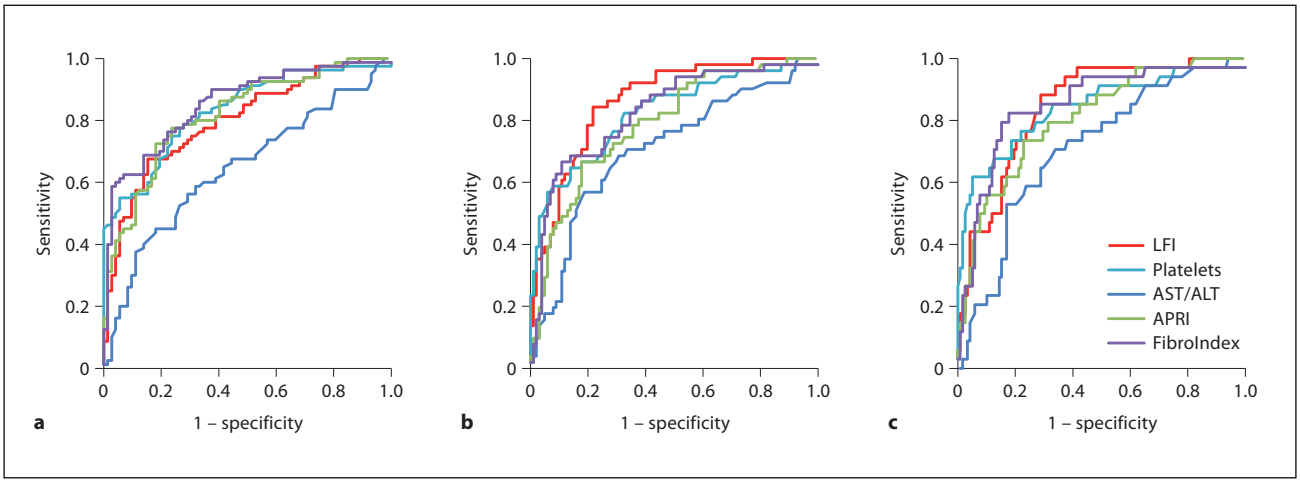

Fig. 3. a ROC curve of the LFI, platelet count, AST/ALT ratio, APRI, and FibroIndex for predicting F2 stage or higher fibrosis (F0–F1 vs. F2–F4). **b** ROC of predicting F3 stage or higher fibrosis. **c** ROC of predicting stage F4 fibrosis.

Table 2. Sensitivity, specificity, positive predictive value, negative predictive value and accuracy of cutoff values of LFI for predicting hepatic fibrosis stage

	Fibrosis stage		
	F0–F1 vs. F2–F4	F0–F2 vs. F3–F4	F0–F3 vs. F4
AUROC	0.800	0.865	0.846
Cutoff value	2.049	2.278	2.357
Sensitivity, %	70.0	78.4	73.5
Specificity, %	76.4	80.2	79.7
Positive predictive value, %	76.7	66.7	51.0
Negative predictive value, %	69.6	88.0	91.3
Accuracy, %	73.0	79.6	78.3

Table 3. AUROC of LFI and several serological makers for predicting liver fibrosis stage

	LFI	Platelets	AST/ALT	APRI	FibroIndex
F0–F1 vs. F2–F4	0.800	0.832	0.646	0.820	0.853
F0–F2 vs. F3–F4	0.865	0.824	0.708	0.789	0.828
F0–F3 vs. F4	0.846	0.840	0.710	0.809	0.850

For diagnosis of cirrhosis (F0–F3 vs. F4), AUROC was 0.846, 0.840, 0.710, 0.809 and 0.850, respectively (table 3, fig. 3). Regardless of the degree of fibrosis progression, RTE has a very good diagnostic capability for liver fibrosis.

Discussion

There is a variety of methods for performing elastography. FibroScan, virtual-touch tissue quantification and shear wave elastography measure the velocity of propagation of the shear wave, which is displayed as elastic modulus or velocity. As the liver becomes hard, the speed of propagation increases. However, the hardness of the liver is also affected by inflammation, jaundice and congestion, as well as fibrosis. FibroScan has been most frequently used in clinical practice to evaluate advanced fibrosis without liver biopsy. However, FibroScan cannot be performed in patients with ascites, narrow intercostal space or severe obesity. Furthermore, it has the disadvantage of low accuracy because there is no B-mode.

RTE displays in real time the relative strain of the tissue by measuring its displacement and does not have the limitations of FibroScan. In the mammary gland, thyroid and prostate, the relative degree of elastic modulus can distinguish malignant space-occupying lesions [13, 14, 20]. As mentioned previously, as liver fibrosis pro-

gresses, the blue portion of the strain image tends to increase in RTE [21]. Shiina et al. [22] have indicated that this pattern of strain images is related to the fibrous structure changes of fibrosis. Several previous studies have focused on the diagnostic accuracy of RTE for liver fibrosis. There are few reports representing a poor accuracy of liver fibrosis. However, the reason for the poor diagnostic accuracy may be the lack of experience of the examiners. To the best of our knowledge, we have been one of the first groups worldwide to perform RTE in patients with liver fibrosis [18, 21, 23, 24]. It is slightly difficult to visualize strain images well. Artifacts such as multiple reflections at the surface of the liver, echo-free areas by thick blood vessels, ribs and lungs, and lack of penetration should be avoided if possible. These are important issues when performing RTE. Although manipulative pressure is used during RTE of the mammary gland and thyroid gland, we performed RTE of the liver without using such pressure. If manipulative pressure is too strong, there is a possibility that the elastic relationship will vary due to the elastic nonlinearity. In addition, there is a possibility that the pressure is not uniformly transmitted to the liver. On the other hand, the liver is deformed slightly by the steady rhythm of the heartbeat. Good images can be obtained merely by light application of the probe to the right intercostal region. Furthermore, because manipulative pressure is not used, human error can be minimized.

LFI in stage F2 fibrosis did not significantly differ from that in stage F3, whereas in all other combinations of stages there were significant differences. The AUROC for prediction of ≥F4 and ≥F2 of LFI was higher than that of serological markers. Our study confirmed that RTE is useful for distinguishing not only advanced fibrosis patients but also mild fibrosis patients from others. Moreover, our study showed that RTE can be performed in all cases, with good discrimination of each fibrosis stage.

In summary, we demonstrated a convenient and noninvasive tool, RTE, for relative strain imaging of the liver. We found that LFI measured by RTE is a useful predictive factor for diagnosis of liver fibrosis stage in patients with chronic viral hepatitis. Our study was based on the gold standard of diagnosis by liver biopsy; therefore, there was a possibility of sampling error. Further studies are desirable on a large number of patients with diagnosis of fibrosis using surgical specimens.

Disclosure Statement

The authors declare that no conflicts of interests exist.

References

1 Nord HJ: Biopsy diagnosis of cirrhosis: blind percutaneous versus guided direct vision techniques – a review. Gastrointest Endosc 1982;28:102–104.

2 Regev A, Berho M, Jeffers LJ, Milikowski C, Molina EG, Pyrsopoulos NT, Feng ZZ, Reddy KR, Schiff ER: Sampling error and intraobserver variation in liver biopsy in patients with chronic HCV infection. Am J Gastroenterol 2002;97:2614–2618.

3 Bedossa P, Dargere D, Paradis V: Sampling variability of liver fibrosis in chronic hepatitis C. Hepatology 2003;38:1449–1457.

4 Joo I, Choi BI: New paradigm for management of hepatocellular carcinoma by imaging. Liver Cancer 2012;1:94–109.

5 Kim DY, Kim SU, Park JY, Ahn SH, Song KJ, Han KH: FibroScan based risk estimation of HBV-related HCC occurrence: development and validation of a predictive model. Liver Cancer 2012;1:123.

6 Sandrin L, Fourquet B, Hasquenoph JM, Yon S, Fournier C, Mal F, Christidis C, Ziol M, Poulet B, Kazemi F, Beaugrand M, Palau R: Transient elastography: a new noninvasive method for assessment of hepatic fibrosis. Ultras Med Biol 2003;29:1705–1713.

7 Friedrich-Rust M, Wunder K, Kriener S, Sotoudeh F, Richter S, Bojunga J, Herrmann E, Poynard T, Dietrich CF, Vermehren J, Zeuzem S, Sarrazin C: Liver fibrosis in viral hepatitis: noninvasive assessment with acoustic radiation force impulse imaging versus transient elastography. Radiology 2009;252:595–604.

8 Ferraioli G, Tinelli C, Dal Bello B, Zicchetti M, Filice G, Filice C: Accuracy of real-time shear wave elastography for assessing liver fibrosis in chronic hepatitis C: a pilot study. Hepatology 2012, E-pub ahead of print.

9 Arena U, Vizzutti F, Corti G, Ambu S, Stasi C, Bresci S, Moscarella S, Boddi V, Petrarca A, Laffi G, Marra F, Pinzani M: Acute viral hepatitis increases liver stiffness values measured by transient elastography. Hepatology 2008;47:380–384.

10 Cobbold JF, Taylor-Robinson SD: Transient elastography in acute hepatitis: all that's stiff is not fibrosis. Hepatology 2008;47:370–372.

11 Millonig G, Reimann FM, Friedrich S, Fonouni H, Mehrabi A, Buchler MW, Seitz HK, Mueller S: Extrahepatic cholestasis increases liver stiffness (FibroScan) irrespective of fibrosis. Hepatology 2008;48:1718–1723.

12 Colli A, Pozzoni P, Berzuini A, Gerosa A, Canovi C, Molteni EE, Barbarini M, Bonino F, Prati D: Decompensated chronic heart failure: increased liver stiffness measured by means of transient elastography. Radiology 2010;257:872–878.

13 Itoh A, Ueno E, Tohno E, Kamma H, Takahashi H, Shiina T, Yamakawa M, Matsumura T: Breast disease: clinical application of US elastography for diagnosis. Radiology 2006; 239:341–350.

14 Fukunari N: More accurate and sensitive diagnosis for thyroid tumors with elastography – detection and differential diagnosis of thyroid cancers. MEDIX Suppl. 2007. http://www.hitachi-medical.co.jp/tech/medix/pdf/supple/sup_05.pdf.

15 Williams AL, Hoofnagle JH: Ratio of serum aspartate to alanine aminotransferase in chronic hepatitis: relationship to cirrhosis. Gastroenterology 1988;95:734–739.
16 Wai CT, Greenson JK, Fontana RJ, Kalbfleisch JD, Marrero JA, Conjeevaram HS, Lok AS: A simple noninvasive index can predict both significant fibrosis and cirrhosis in patients with chronic hepatitis C. Hepatology 2003;38:518–526.
17 Koda M, Matunaga Y, Kawakami M, Kishimoto Y, Suou T, Murawaki Y: FibroIndex, a practical index for predicting significant fibrosis in patients with chronic hepatitis C. Hepatology 2007;45:297–306.
18 Tatsumi C, Kudo M, Ueshima K, Kitai S, Ishikawa E, Yada N, Hagiwara S, Inoue T, Minami Y, Chung H, Maekawa K, Fujimoto K, Kato M, Tonomura A, Mitake T, Shiina T: Non-invasive evaluation of hepatic fibrosis for type C chronic hepatitis. Intervirology 2010;53:76–81.
19 Fujimoto K, Kato M, Tonomura A, Yada N, Tatsumi C, Oshita M, Wada S, Ueshima K, Ishida T, Furuta T, Yamasaki M, Tsujimoto M, Motoki M, Mitake T, Shiina T, Kudo M, Hayashi N: Non-invasive evaluation method of the liver fibrosis using real-time tissue elastograpy: usefulness of judgment liver fibrosis stage by liver fibrosis index (LF index). Kanzo 2010;59:539–541.
20 Miyanaga N, Akaza H, Yamakawa M, Oikawa T, Sekido N, Hinotsu S, Kawai K, Shimazui T, Shiina T: Tissue elasticity imaging for diagnosis of prostate cancer: a preliminary report. Int J Urol 2006;13:1514–1518.
21 Fujimoto K, Wada S, Oshita M, Kato M, Tonomura A, Mitake T: Non-invasive evaluation of hepatic fibrosis in patients with chronic hepatitis C using elastography. MEDIX Suppl. 2007. http://www.hitachi-medical.co.jp/tech/medix/pdf/supple/sup_07.pdf.
22 Shiina T, Maki T, Yamakawa M, Mitake T, Kudo M, Fujimoto K: Mechanical model analysis for quantitative evaluation of liver fibrosis based on ultrasound tissue elasticity imaging. Jpn J Appl Phys 2012; DOI: 10.1143/JJAP.51.07GF11.
23 Morikawa H, Fukuda K, Kobayashi S, Fujii H, Iwai S, Enomoto M, Tamori A, Sakaguchi H, Kawada N: Real-time tissue elastography as a tool for the noninvasive assessment of liver stiffness in patients with chronic hepatitis C. J Gastroenterol 2011; 46:350–358.
24 Tatsumi C, Kudo M, Ueshima K, Kitai S, Takahashi S, Inoue T, Minami Y, Chung H, Maekawa K, Fujimoto K, Akiko T, Takeshi M: Noninvasive evaluation of hepatic fibrosis using serum fibrotic markers, transient elastography (FibroScan) and real-time tissue elastography. Intervirology 2008;51 (suppl 1):27–33.

Oncology

Oncology 2013;84(suppl 1):21–27
DOI: 10.1159/000345885

Published online: February 20, 2013

Role of Gadolinium-Ethoxybenzyl-Diethylenetriamine Pentaacetic Acid-Enhanced Magnetic Resonance Imaging in the Management of Hepatocellular Carcinoma: Consensus at the Symposium of the 48th Annual Meeting of the Liver Cancer Study Group of Japan

Masatoshi Kudo[a] Osamu Matsui[b] Michiie Sakamoto[c] Azusa Kitao[b] Tonsok Kim[e] Shun-ichi Ariizumi[d] Tomoaki Ichikawa[f] Satoshi Kobayashi[b] Yasuharu Imai[g] Namiki Izumi[h] Yasunari Fujinaga[i] Shigeki Arii[j]

[a]Department of Gastroenterology and Hepatology, Kinki University School of Medicine, Osakasayama, [b]Department of Radiology, Kanazawa University Graduate School of Medical Science, Kanazawa, [c]Department of Pathology, Keio University School of Medicine, and [d]Department of Surgery, Institute of Gastroenterology, Tokyo Women's Medical University, Tokyo, [e]Department of Radiology, Osaka University Graduate School of Medicine, Osaka, [f]Department of Radiology, University of Yamanashi, Yamanashi, [g]Department of Gastroenterology, Ikeda Municipal Hospital, Ikeda, [h]Division of Gastroenterology and Hepatology, Musashino Red Cross Hospital, Musashino, [i]Department of Radiology, Shinshu University School of Medicine, Matsumoto, and [j]Department of Surgery, Hamamatsu Rosai Hospital, Hamamatsu, Japan

Key Words
Hepatocellular carcinoma · EOB-MRI · Expert consensus

Abstract
We summarize here the consensus reached at the Symposium of the 48th Annual Meeting of the Liver Cancer Study Group of Japan held in Kanazawa on July 20th and 21st, 2012, on the role of gadolinium-ethoxybenzyl-diethylenetriamine pentaacetic acid-enhanced magnetic resonance imaging (EOB-MRI) in the management of hepatocellular carcinoma (HCC). Currently, dynamic CT is the first choice of imaging modality when HCC is suspected. EOB-MRI is useful for differentiation and definitive diagnosis of HCC when dynamic CT/MRI does not show conclusive findings for HCC. In addition, contrast- enhanced ultrasound with Sonazoid is useful for making a decision on whether or not to treat a hypovascular lesion <1 cm when the nodules are shown with low intensity in the hepatocyte phase of EOB-MRI. Furthermore, EOB-MRI should be performed in selected cases of HCC ultrahigh-risk groups every 3–4 months, or EOB-MRI should be performed at least once at the first visit in all HCC ultrahigh-risk groups.

Introduction

Gadolinium-ethoxybenzyl-diethylenetriamine pentaacetic acid (Gd-EOB-DTPA; Primovist, Bayer Healthcare, Leverkusen, Germany) [1–5] has been available in Japan as a magnetic resonance imaging (MRI) contrast agent for more than 4 years since its release in January 2008. This contrast agent, consisting of Gd-DTPA conjugated with an ethoxybenzyl (EOB) group, has the characteristics of both an extracellular Gd contrast agent and a hepatocyte-specific contrast agent. Because Gd-EOB-DTPA-enhanced MRI (EOB-MRI) allow for the observa-

KARGER

Fax +41 61 306 12 34
E-Mail karger@karger.com
www.karger.com

0030–2414/13/0847–0021$38.00/0

Accessible online at:
www.karger.com/ocl

Masatoshi Kudo, MD, PhD
Division of Gastroenterology and Hepatology, Department of Internal Medicine
Kinki University School of Medicine
377-2 Ohno-Higashi, Osakasayama, Osaka 589-8511 (Japan)
E-Mail m-kudo@med.kindai.ac.jp

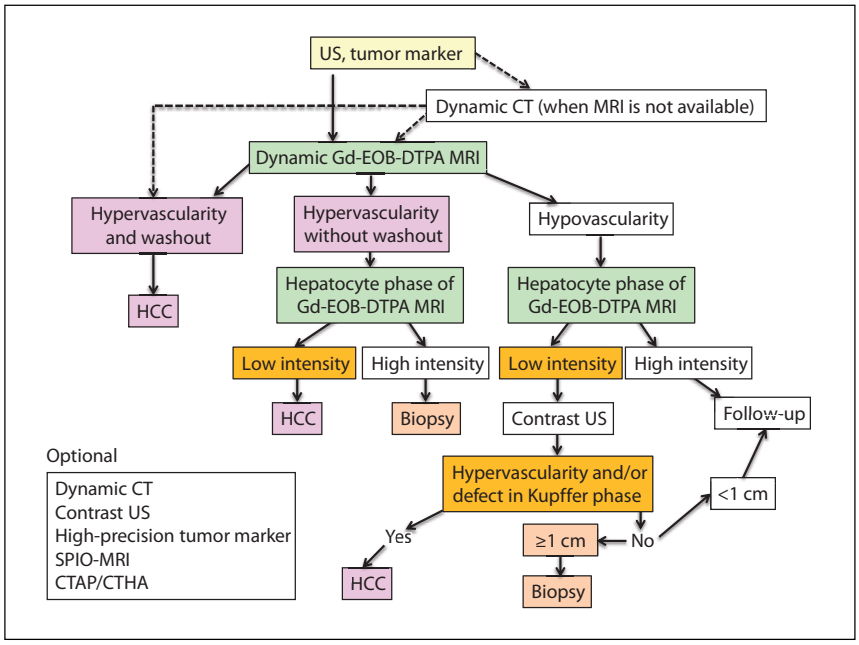

Fig. 1. New diagnostic algorithm proposed by the research group (headed by Shigeki Arii) supported by the Japan Ministry of Health, Labour and Welfare.

tion of blood flow in hepatocellular carcinoma (HCC) and the function of hepatocyte, diagnosis made by EOB-MRI is reportedly superior to diagnosis of hepatic blood flow either by dynamic computed tomography (CT) using multi-detector CT, dynamic MRI using an extracellular Gd contrast agent, or functional diagnosis of hepatic Kupffer cells by superparamagnetic iron oxide (SPIO)-MRI [6–13]. EOB-MRI is highly capable of detecting not only typical hypervascular HCC but also early-stage hypovascular HCC [11–13], greatly influencing early diagnosis and treatment for HCC. However, MRI is not as widespread as CT and it takes longer to complete EOB-MRI than dynamic CT, thus limiting the number of EOB-MRI scans performed in daily clinical practice.

Based on this background, the Symposium of the 48th Annual Meeting of the Liver Cancer Study Group of Japan was held on July 20th, 2012, to address the role of EOB-MRI in the management of HCC. Here, we report the consensus reached using a key-pad answering system in the meeting. Votes were cast by 144 experts specialized in internal medicine (57%), radiology (24%), surgery (12%), pathology (4%) and other fields (3%). This report describes consensus of current clinical practice for patients with HCC in Japan. The consensuses that achieved more than 67% agreement were summarized as 'consensus statements'. Furthermore, issues obtaining more than 50% agreement were summarized as 'informative statements'.

Novel Diagnostic Algorithm Proposed for the Management of HCC

In Japan, HCC diagnostic algorithms have been proposed in the EBM-based 'HCC Clinical Practice Guidelines' [14] and the 'HCC Clinical Practice Manual' [15] based on EBM plus consensus reached by HCC experts. The algorithm in the 'HCC Clinical Practice Manual' reflects Japan's sophisticated approach to the detection of early HCC and is in line with the actual clinical situation; however, the algorithm is somewhat complicated to use as a clinical practice guideline. Moreover, there is an increasing need to develop a simple HCC diagnostic algorithm centered on EOB-MRI, owing to its good diagnostic capability, simplicity and highly objective nature. Accordingly, a new HCC diagnostic algorithm was proposed in March 2012 by the research group (headed by Dr. Shigeki Arii) funded by the Ministry of Health, Labour and Welfare for the 'development of molecular markers and diagnostic imaging systems for the early detection of HCC' (fig. 1).

This algorithm basically recommends the implementation of EOB-MRI in cases where HCC is suspected by B-mode ultrasound findings and tumor marker measurements. The diagnosis of HCC is made when a nodular lesion is hypervascular in the arterial phase and washed out in the late phase on EOB-MRI images. HCC is also diagnosed when nodular lesions are hypervascular

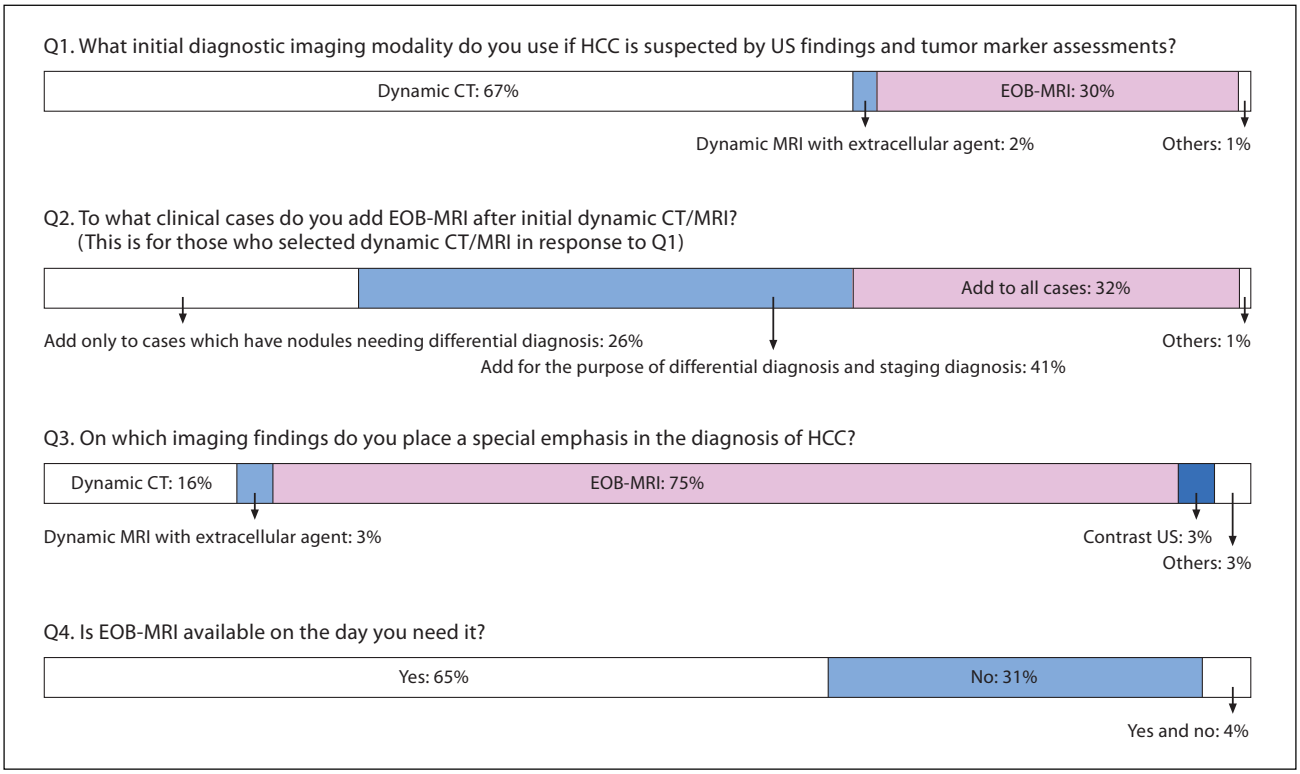

Color version available online

Fig. 2. Questions 1–4 and responses.

in the arterial phase and hypointense in the hepatocyte phase of EOB-MRI, even if it is difficult to determine the degree of washout in the portal phase (with the exclusion of hemangioma by another imaging modality). When hypervascular nodular lesions are hyperintense in the hepatocyte phase on EOB-MRI imaging, they are difficult to diagnose as HCC, but can be diagnosed as HCC when the capsule or mosaic structure is apparent. Biopsy is recommended if the diagnosis is not definitive.

On the other hand, if nodular lesions are hypovascular in the arterial phase and hypointense in the hepatocyte phase on EOB-MRI images, contrast-enhanced ultrasonography (US) using Sonazoid is required to confirm hypervascularity or defects in the Kupffer phase in order to make a definitive diagnosis of HCC. If hypervascularity or defects in the Kupffer phase are absent, lesions ≥1 cm in diameter should be biopsied and those <1 cm need to be followed up. Follow-up observations are also recommended for nodular lesions that are hypovascular in the arterial phase and hyperintense in the hepatocyte phase on EOB-MRI images. Furthermore, institutions unable to conduct MRI as initial diagnostic imaging need to perform dynamic CT first, followed by EOB-MRI as the recommended diagnostic method. CT arterial portography/CT hepatic arteriography (CTAP/CTHA), SPIO-MRI and high-precision tumor marker assessments should be performed as needed at each institution. At the symposium, we evaluated HCC management on the basis of this algorithm and voted for the consensus.

Consensus Voting Results

Selection of Diagnostic Imaging Modality: Questions 1–4

When HCC is suspected based on US and tumor marker findings, 67% of physicians would select dynamic CT as the initial diagnostic imaging, 30% EOB-MRI and 2% dynamic MRI. When those who had selected dynamic CT/MRI were asked to which clinical cases they would add EOB-MRI, 41% selected 'cases requiring differential diagnosis and staging' and 32% responded with 'all cases'. When asked on what imaging findings they would place a special emphasis in the diagnosis of HCC, 75% of physi-

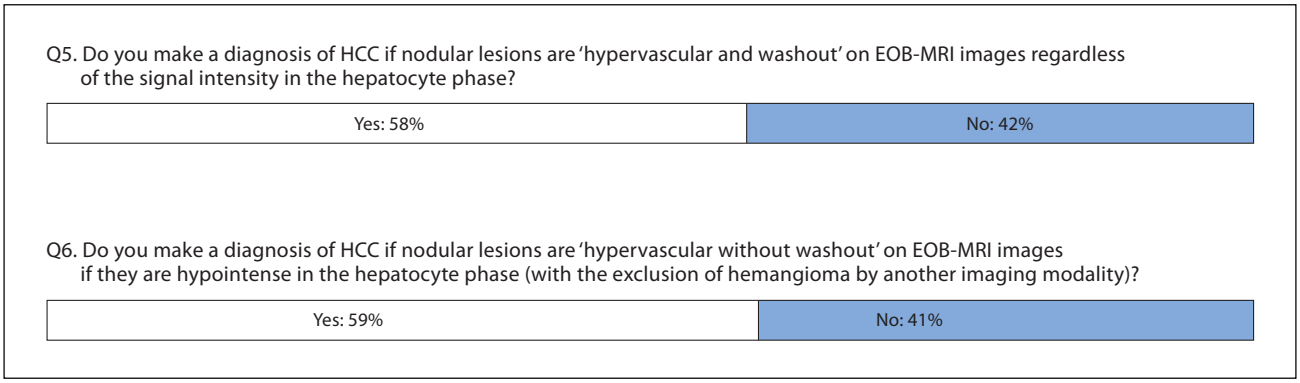

Color version available online

Fig. 3. Questions 5–6 and responses.

cians selected EOB-MRI and 16% dynamic CT. However, because only 65% of physicians answered that EOB-MRI was available on the day they needed it, availability of MRI at each institution might have affected the selection of initial diagnostic imaging modality (fig. 2).

Diagnosis of Hypervascular HCC by EOB-MRI: Questions 5–6

'HCC is diagnosed if nodular lesions are hypervascular in the arterial phase and washed out in the portal/equilibrium phase on EOB-MRI images regardless of the signal intensity in the hepatocyte phase' was selected by 58% of physicians. Similarly, 'HCC is diagnosed if nodular lesions are hypervascular in the arterial phase and hypointense in the hepatocyte phase of EOB-MRI even if no washout is observed (with the exclusion of hemangioma by another imaging modality)' was selected by 59% of physicians. We think that the answer to this question was affected by the fact that the patients in question are not restricted to those with cirrhosis, that washout is interpreted differently between EOB-MRI and dynamic MRI using extracellular Gd contrast agents, and that some pseudotumors such as arterioportal shunt exhibit low signals in the hepatocyte phase (fig. 3).

Diagnosis and Treatment of Hypovascular HCC: Questions 7–14

When asked if they would treat hypovascular nodular lesions ≥1.5 cm in diameter with hypointense signals in the hepatocyte phase of EOB-MRI, 55% of physicians voted for 'treat based on the results of additional imaging', 23% selected 'treat if biopsy confirms cancer', 17% chose 'treat with no additional imaging' and only 5% selected 'assign to follow-up observation'. As additional imaging, 52% of physicians would select contrast-enhanced US with Sonazoid and 45% CTAP/CTHA. When nodular lesions are ≥1.0 cm but <1.5 cm, 72% would 'treat based on the results of additional imaging', 18% would 'treat if biopsy confirms cancer', 5% would 'treat with no additional imaging' and another 5% would 'assign to follow-up observation'. For nodular lesions <1.0 cm, 9% of physicians would consider the option 'assign to follow-up observations'. In summary, a certain number of physicians would treat hypointense nodular lesions in the hepatocyte phase even if the lesions were hypovascular.

When asked about the most appropriate diagnostic imaging to perform when deciding whether to follow up hypovascular nodular lesions with hypointense signals in the hepatocyte phase of EOB-MRI, 63% of physicians selected EOB-MRI, 9% chose contrast-enhanced US with Sonazoid, 6% nominated dynamic CT, 2% indicated dynamic MRI and 20% suggested combinations of these imaging modalities. Physicians considered 6 months (56%) and 3 months (41%) to be the most appropriate interval for follow-up observations (fig. 4).

HCC Screening: Questions 15–17

When asked whether EOB-MRI should be performed for ultrahigh-risk groups (patients with cirrhosis due to hepatitis B or C) as a screening tool, 49% of physicians selected 'in all cases' and 42% 'depending on the case'. To clarify the definition of 'a screening tool', physicians were further asked whether such high-risk individuals should undergo EOB-MRI every 3–4 months: overwhelmingly, 71% selected 'depending on the case'. In addition, the majority of physicians (83%) answered 'in all cases' to the question of whether 'EOB-MRI should be used at least once in patients at ultrahigh-risk for HCC' (fig. 5).

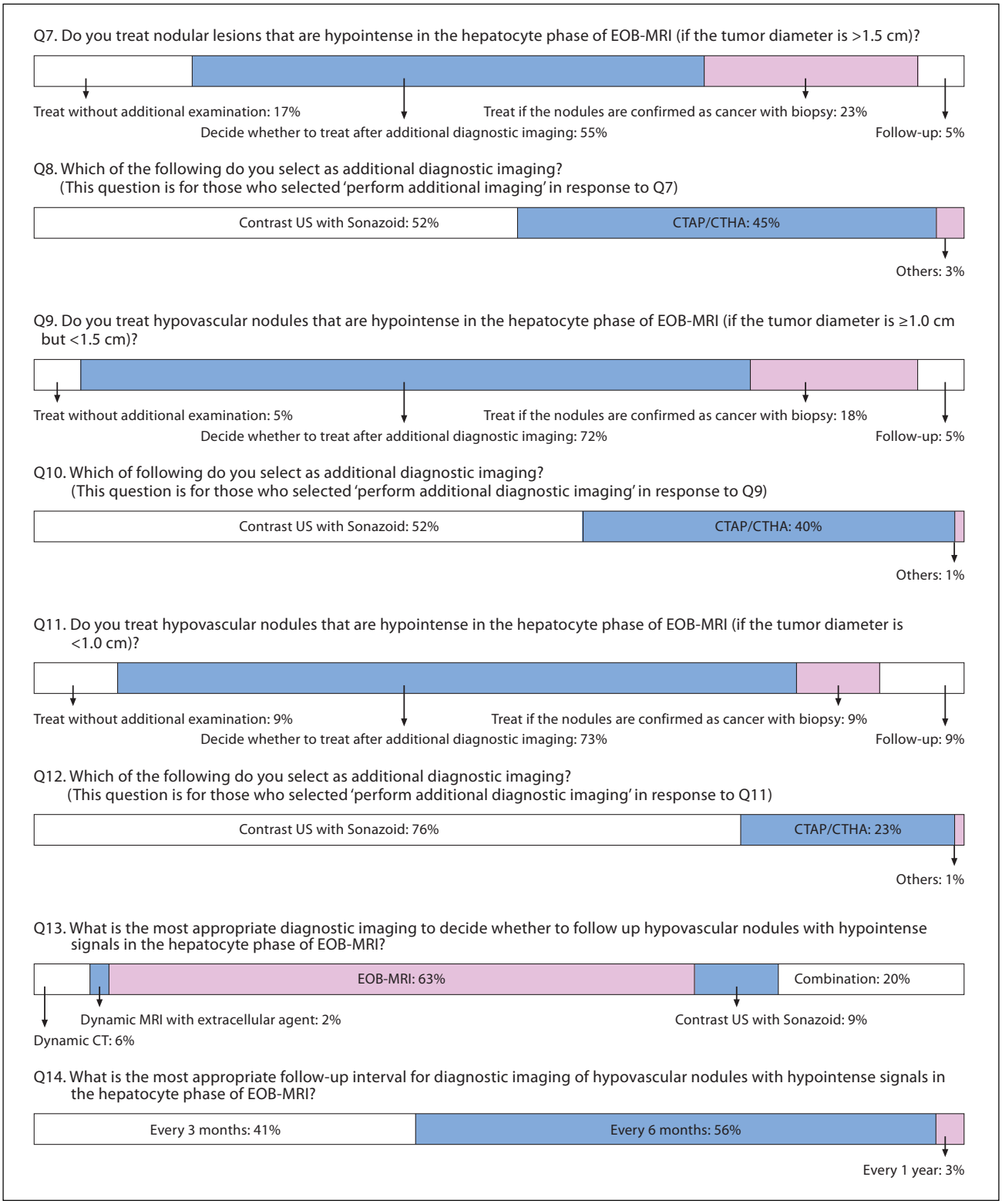

Color version available online

Fig. 4. Questions 7–14 and responses.

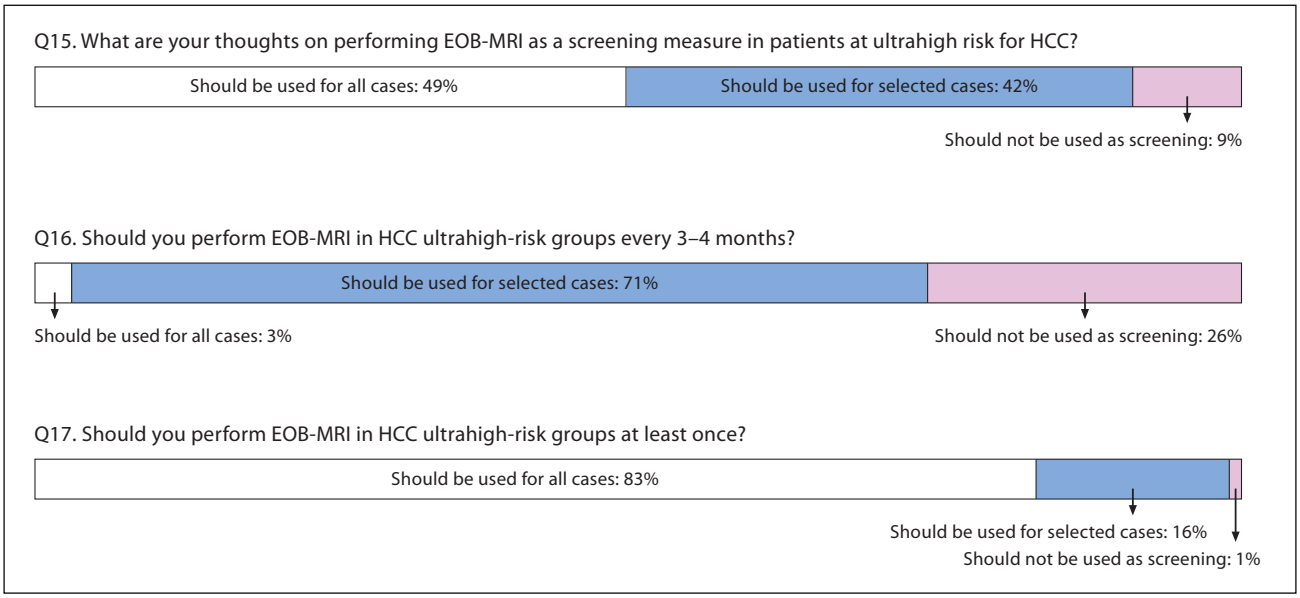

Fig. 5. Questions 15–17 and responses.

Consensus Statements

(1) Currently, dynamic CT is the first choice of imaging modality when HCC is suspected (agreement: 67%).
(2) EOB-MRI is useful for differentiation and definitive diagnosis of HCC when dynamic CT/MRI does not show conclusive findings for HCC (agreement: 75%).
(3) Contrast-enhanced US with Sonazoid is useful for making a decision on whether or not to treat hypovascular lesions <1 cm when the nodules are shown with low intensity in the hepatocyte phase (agreement: 76%).
(4) EOB-MRI should be performed in selected cases of HCC ultrahigh-risk groups every 3–4 months (agreement: 71%).
(5) EOB-MRI should be performed at least once in all HCC ultrahigh-risk groups (agreement: 83%).

Informative Statements

(1) HCC can be confirmed by EOB-MRI when nodular lesions show arterial hypervascularity with venous washout (agreement: 58%).
(2) HCC can be confirmed by EOB-MRI when nodular lesions show arterial hypervascularity with low intensity on hepatocyte phase (agreement: 59%).
(3) Contrast-enhanced US with Sonazoid is useful for making a decision on whether or not to treat nodules >1 cm when the hypovascular nodules are shown with low intensity in the hepatocyte phase of EOB-MRI (agreement: 59%).
(4) EOB-MRI is the most appropriate diagnostic tool to decide whether to treat or to follow up hypovascular nodules with hypointense in the hepatocyte phase EOB-MRI (agreement: 63%).
(5) Hypovascular nodules with hypointense signals in the hepatocyte phase of EOB-MRI should be followed up every 6 months (agreement: 56%).

Conclusion

The above results clearly show that EOB-MRI has become a crucial diagnostic imaging tool for HCC despite the problems associated with insufficient MRI availability. It is also clear that it is considered that hypointense nodular lesions in the hepatocyte phase on EOB-MRI images should be treated, even if the nodule is hypovascular, in current clinical practice in Japan.

Disclosure Statement

This symposium was sponsored by Bayer Yakuhin Ltd., Osaka, Japan.

References

1 Ricke J, Seidensticker M, Mohnike K: Noninvasive diagnosis of hepatocellular carcinoma in cirrhotic liver: current guidelines and future prospects for radiological imaging. Liver Cancer 2012;1:51–58.

2 Choi D: Imaging diagnosis of very small hepatocellular carcinoma in Gd-EOB-DTPA-enhanced and diffusion-weighted MRI. Liver Cancer 2012;1:115.

3 Lee JM, Phongkitrarun S, Bergmann K, Jeong M, Liamsuwa S, Luong B: Effectiveness of using Gd-EOB-DTPA-enhanced MRI for confirmation of hepatocellular carcinoma in Thailand and Korea as compared to extracellular contrast media-enhanced MRI and 3-phase MD-CT. Liver Cancer 2012;1:126.

4 Min YW, Paik SW, Gwak GY, Paik YH, Choi MS, Lee JH, et al: Utility of gadoxetic acid-enhanced MRI in the surveillance for postoperative recurrence of hepatocellular carcinoma. Liver Cancer 2012;1:129.

5 Choi JI, Jang HY, Lee YJ: Diagnostic accurary of gadoxetic acid enhanced magnetic resonance imaging in predicting the appropriateness of a transplant recipient based on the Milan criteria. Liver Cancer, in press.

6 Di Martino M, Marin D, Guerrisi A, Baski M, Galati F, Rossi M, et al: Intraindividual comparison of gadoxetate disodium-enhanced MR imaging and 64-section multidetector CT in the detection of hepatocellular carcinoma in patients with cirrhosis. Radiology 2010;256:806–816.

7 Haradome H, Grazioli L, Tinti R, Morone M, Motosugi U, Sano K, et al: Additional value of gadoxetic acid-DTPA-enhanced hepatobiliary phase MR imaging in the diagnosis of early-stage hepatocellular carcinoma: comparison with dynamic triple-phase multidetector CT imaging. J Magn Reson Imaging 2011;34:69–78.

8 Onishi H, Kim T, Imai Y, Hori M, Nagano H, Nakaya Y, et al: Hypervascular hepatocellular carcinomas: detection with gadoxetate disodium-enhanced MR imaging and multiphasic multidetector CT. Eur Radiol 2012;22:845–854.

9 Park G, Kim YK, Kim CS, Yu HC, Hwang SB: Diagnostic efficacy of gadoxetic acid-enhanced MRI in the detection of hepatocellular carcinomas: comparison with gadopentetate dimeglumine. Br J Radiol 2010;83:1010–1016.

10 Kim YK, Kim CS, Han YM, Park G, Hwang SB, Yu HC: Comparison of gadoxetic acid-enhanced MRI and superparamagnetic iron oxide-enhanced MRI for the detection of hepatocellular carcinoma. Clin Radiol 2010;65:358–365.

11 Okada M, Imai Y, Kim T, Kogita S, Takamura M, Kumano S, et al: Comparison of enhancement patterns of histologically confirmed hepatocellular carcinoma between gadoxetate- and ferucarbotran-enhanced magnetic resonance imaging. J Magn Reson Imaging 2010;32:903–913.

12 Kogita S, Imai Y, Okada M, Kim T, Onishi H, Takamura M, et al: Gd-EOB-DTPA-enhanced magnetic resonance images of hepatocellular carcinoma: correlation with histological grading and portal blood flow. Eur Radiol 2010;20:2405–2413.

13 Sano K, Ichikawa T, Motosugi U, Sou H, Muhi AM, Matsuda M, et al: Imaging study of early hepatocellular carcinoma: usefulness of gadoxetic acid-enhanced MR imaging. Radiology 2011;261:834–844.

14 Makuuchi M, Kokudo N, Arii S, Igaki H, Ikai I, Kaneko S, et al: Surveillance algorithm and diagnostic algorithm for hepatocellular carcinoma. Hepatology Research 2010;40(suppl 1):1–144.

15 Kudo M, Izumi N, Kokudo N, Matsui O, Sakamoto M, Nakashima O, et al: Management of hepatocellular carcinoma in Japan: Consensus-Based Clinical Practice Guidelines proposed by the Japan Society of Hepatology (JSH) 2010 updated version. Dig Dis 2011;29:339–364.

Oncology

Oncology 2013;84(suppl 1):51–57
DOI: 10.1159/000345890

Published online: February 20, 2013

Usefulness of Contrast-Enhanced Ultrasonography to Evaluate the Post-Treatment Responses of Radiofrequency Ablation for Hepatocellular Carcinoma: Comparison with Dynamic CT

Tatsuo Inoue Masatoshi Kudo Kinuyo Hatanaka Tadaaki Arizumi
Masahiro Takita Satoshi Kitai Norihisa Yada Satoru Hagiwara
Yasunori Minami Toshiharu Sakurai Kazuomi Ueshima Naoshi Nishida

Division of Gastroenterology and Hepatology, Department of Internal Medicine, Kinki University Faculty of Medicine, Osakasayama, Japan

Key Words
Hepatocellular carcinoma · Radiofrequency ablation · Treatment response · Contrast-enhanced ultrasonography · Defect-reperfusion imaging

Abstract
Objective: Contrast-enhanced ultrasonography (CEUS) with Sonazoid® and dynamic computed tomography (CT) were used to evaluate radiofrequency ablation (RFA) for hepatocellular carcinoma (HCC). Local recurrence rate was used as the gold standard of evaluation. ***Methods:*** From January 2007 to December 2011, 86 HCCs from 70 patients were treated with RFA. CEUS with Sonazoid and dynamic CT were then used to evaluate the effect of RFA. For CEUS and dynamic CT, effects were classified as follows: (1) complete ablated response with safety margin >5 mm (CRSM+); (2) complete ablated response but with safety margin <5 mm (CRSM–); (3) incomplete, residual tumor detected after treatment. ***Results:*** CEUS judged 33 cases as CRSM+, while dynamic CT identified 49 cases. None of these 33 cases from the CEUS group had local recurrences, while dynamic CT had 1 case. CEUS judged 49 cases as CRSM–, compared to 34 cases with dynamic CT. Of these, 9 cases of CEUS and 8 cases of dynamic CT showed local recurrences. Two cases diagnosed as 'incomplete' by CEUS and dynamic CT had recurrences within 1 year. ***Conclusion:*** CEUS can be used to assess the efficacy of RFA for HCC, with the potential to reduce the number of CT scans required for confirmation.

Introduction

Hepatocellular carcinoma (HCC) ranks worldwide as the sixth most common cancer and as the third most common cause of cancer deaths. For patients with HCC, percutaneous radiofrequency ablation (RFA) has recently been established as a promising and safe technique [1–4]. RFA has steadily become a first-line ablative procedure for small- to intermediate-sized (3 cm) HCCs at many centers. It has a primary effectiveness rate of 88–99% in treating HCC [5–9]. Dynamic computed tomography (CT) is commonly used for evaluating the response of HCC after RFA [10–12]. However, the use of dynamic CT is prohibited for patients with renal dysfunction and iodine allergy. Another concern for patients is to minimize the exposure to radiation.

KARGER

Fax +41 61 306 12 34
E-Mail karger@karger.com
www.karger.com

0030–2414/13/0847–0051$38.00/0

Accessible online at:
www.karger.com/ocl

Masatoshi Kudo, MD, PhD
Division of Gastroenterology and Hepatology, Department of Internal Medicine
Kinki University Faculty of Medicine
377-2 Ohno-Higashi, Osakasayama, Osaka 589-8511 (Japan)
E-Mail m-kudo@med.kindai.ac.jp

Sonazoid® (Daiichi-Sankyo, Tokyo, Japan; GE Healthcare, Milwaukee, Wisc., USA), a lipid-stabilized suspension of perfluorobutane gas microbubbles was approved exclusively in Japan in January 2007. It facilitates obtaining a real-time blood flow image in addition to a stable Kupffer phase [13]. Sonazoid is a second-generation contrast agent possessing superior qualities over other agents that enabled the acquisition of a good real-time vascular image and a very stable Kupffer-phase image lasting up to 120 min after injection [14, 15]. Defect reperfusion imaging is an innovative technique by which the arterial blood flow can be demonstrated in nodules that show a defect in the Kupffer phase owing to the stability of the Kupffer image with Sonazoid. This is a unique property of Sonazoid and dual phase contrast ultrasound is now a breakthrough in the diagnostic imaging of HCC [14, 16]. By using defect reperfusion imaging in the assessment of RFA, an ablated area can be visualized clearly. Furthermore, a residual nodule or recurrence can be diagnosed by assuming that the defect reinjection sign was positive when arterial vascularity was noted inside a Kupffer defect area. In the present study, the defect reperfusion imaging procedure with Sonazoid was used in assessing the response to RFA. The results were then compared with dynamic CT.

Materials and Methods

Patients

From January 2007 to December 2011, 70 patients (41 males and 29 females; age range 52–83 years) with HCC underwent RFA. Sixty-two patients had cirrhosis (56 with Child-Pugh A and 6 with Child-Pugh B), and 8 patients had chronic hepatitis. Baseline features of the study population are summarized in table 1. All patients met the following criteria for treatment with percutaneous RFA: percutaneous accessibility of the tumor; absence of portal venous and extrahepatic metastases; prothrombin time ratio >50%; total bilirubin concentration <3.0 mg/dl, and platelet count >50,000/μl. Patients were excluded if they had an excessive bleeding tendency (platelet count <50,000/μl or prothrombin activity <50%) or refractory ascites. The study was performed according to the guidelines of the Helsinki Declaration and was approved by our institution's ethics committee. Written, fully informed consent was obtained from each patient before treatment.

Diagnosis of HCC

The diagnosis of HCC was made by the presence of typical tumor features, such as hyperattenuations in the arterial phase and hypoattenuations in the portal phase, using dynamic CT with 64 detectors (LightSpeed VCT; GE Healthcare) [17, 18]. The median diameter of HCC was 16.5 ± 7.1 mm on B-mode ultrasonography (US). All patients underwent dynamic CT during the month before RFA.

Table 1. Baseline features of study population

Patients, n	70
Tumors, n	86
Mean age, years	70.7 ± 7.1
Sex (male/female)	41/29
Size of tumors, cm	16.5 ± 7.1
Follow-up, days	873 ± 426
Child-Pugh (A/B/C)	64/6/0

RFA Technique

All RFAs were performed percutaneously by experienced hepatologists, each of whom had more than 5 years of experience in US-guided interventional procedures and RFA. The treatments were performed under local anesthesia and conscious sedation. Patients were treated with a cooled-tip needle RFA system (Cooltip, Covidien, Dublin, Ireland), which is a 480-kHz alternative current generator that can produce a maximum power of 180 W through a 17-gauge monopolar cooled-tip needle electrode. A single 2-cm exposed tip was selected for nodules <2 cm in diameter and a single 3-cm exposed tip for larger nodules.

Evaluation of Post-Treatment Effect of RFA

Evaluation of the Effect of RFA Using Contrast-Enhanced US (CEUS). CEUS was performed using a GE LOGIQ 7 ultrasound scanner with a 4.0- or 6.5-MHz convex transducer. The acoustic power of contrast-enhanced harmonic US was set at the default setting with a mechanical index of 0.2; the dynamic range was fixed at 60–65 dB. A single focus point was set at a depth of 10 cm. Data were analyzed and defined by consensus of two hepatologists (T.I., K.H.) who were blinded to the results of evaluation by dynamic CT. In case of discrepancy, the reviewers assessed the saved images together and their findings were re-evaluated to reach an agreement. Defect reperfusion imaging [14, 19] was used to evaluate the Kupffer phase of CEUS with Sonazoid (fig. 1, 2). When the tumor was completely ablated with a safe margin of more than 5 mm, the effectiveness was graded as (CRSM+). When the tumor was completely ablated but with a safe margin less than 5 mm, the effectiveness was graded as (CRSM–). When there were residual tumors (reperfusion areas adjacent to the ablated tumor in the defect reperfusion test), the grading was recorded as 'incomplete', indicative of a residual tumor after treatment. All CEUS studies were performed within 1–3 days of RFA.

Evaluation of Treatment Effect of RFA Using Dynamic CT. Dynamic CT data were analyzed and defined by consensus of two hepatologists (M.K., T.A.) who were blinded to the results of contrast-enhanced US. In case of discrepancy, the reviewers assessed the saved images together and their findings were re-evaluated to reach an agreement. A CT scan with a 5-mm section thickness was performed 1–3 days after RFA to evaluate its effectiveness [1]. When the tumor was completely ablated with a safe margin of more than 5 mm, the effectiveness was graded as CRSM+. When the tumor was completely ablated but with a safe margin less than 5 mm, the effectiveness was graded as (CRSM–). When there were residual tumors (hyperattenuations in the arterial phase and hypoattenuation areas in the portal phase adjacent to the tumor) the grading was recorded as 'incomplete', indicating a residual tumor after treatment.

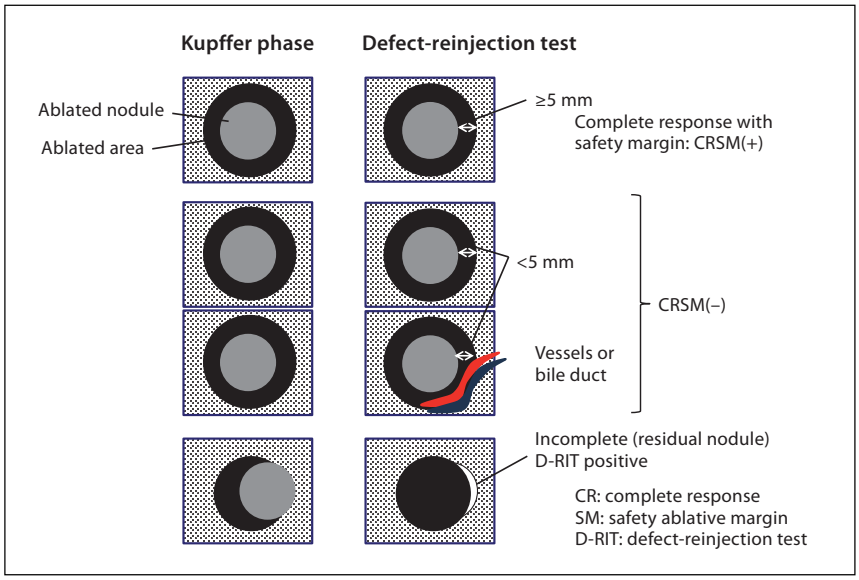

Fig. 1. Evaluation of post-treatment effect of RFA using defect reperfusion test 1. When the ablated tumor was detected on Kupffer-phase image, post-treatment effect was evaluated using the technique shown here. Briefly, in Kupffer phase, the ablated area was observed after reinjection of Sonazoid. If the tumor was completely ablated with adequate safety margin (>5 mm), the therapeutic effect was judged as CRSM(+). If the tumor was ablated without adequate safety margin (<5 mm) or there were some vessels close to tumors within 5 mm, the therapeutic effect was judged as CRSM(–). If there were reperfusion areas on the defect reperfusion test, they were judged as incomplete (residual tumor).

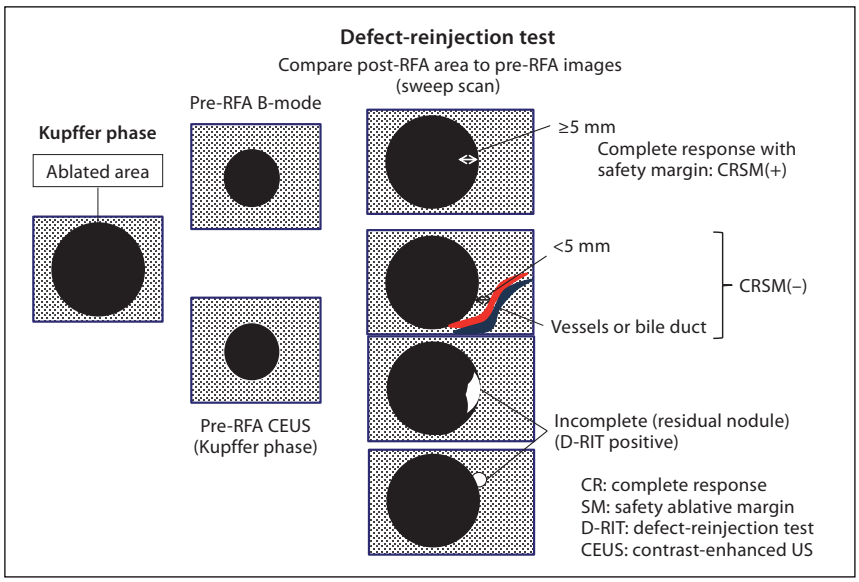

Fig. 2. Evaluation of post-treatment effect of RFA using defect reperfusion test 2. When the ablated tumor cannot be detected on Kupffer-phase image, the safety margin was evaluated by comparing images of pre-B-mode or Kupffer-phase images of HCCs with postablated areas side by side on the US screen.

Assessment of Local Recurrence

Tumor recurrence rates were assessed by performing dynamic CT every 3–4 months after RFA. Local tumor recurrence was defined as the appearance of a viable tumor during follow-up that was contiguous with the zone that had been ablated.

Statistical Analysis

Cumulative incidence of local tumor recurrence was calculated using the Kaplan-Meier test and Fisher's exact test was used to analyze the data. The level of significance was set at $p < 0.05$. All analyses were performed with statistical software (SPSS version 11, SPSS Inc., Chicago, Ill., USA) for Microsoft Windows.

Results

Post-Treatment Evaluation of RFA for HCC Using Each Modality

At the initial evaluation of post-treatment effect of RFA there were 33 and 49 cases judged CRSM+ by CEUS and dynamic CT, respectively. Also, there were 49 and 34 cases judged CRSM– by CEUS and dynamic CT, respectively. CEUS and multidetector CT each judged 3 cases as 'incomplete'. Two cases out of 3 were judged 'incomplete' on both contrast-enhanced US and dynamic CT.

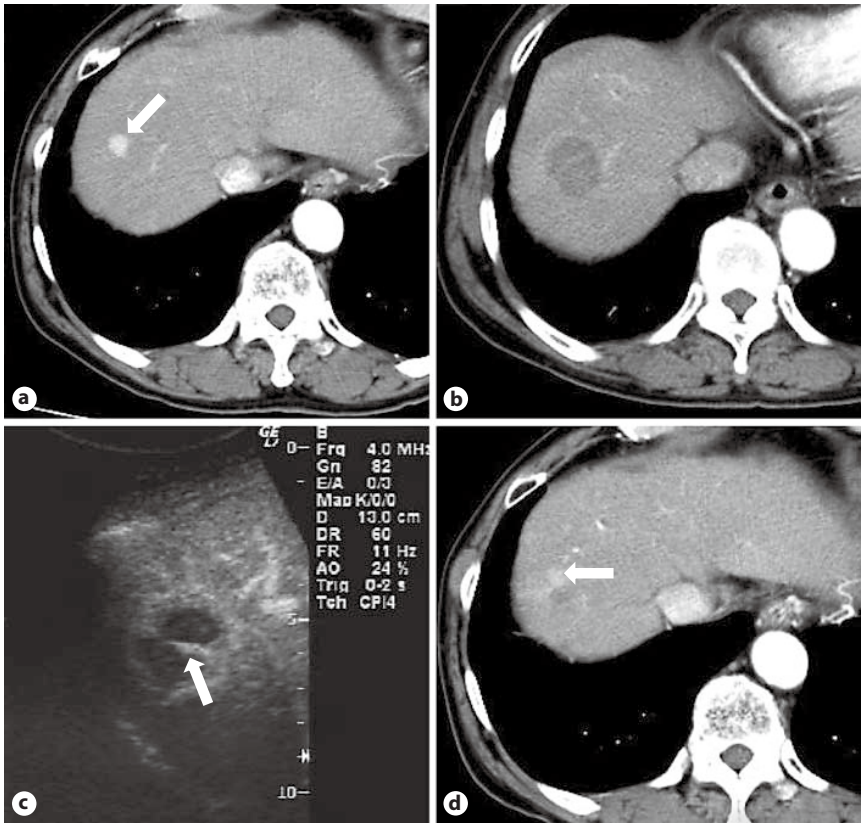

Fig. 3. Case presentation of local tumor recurrence after RFA. **a** A 62-year-old man with a 1.3-cm HCC; Dynamic CT shows a hypervascular tumor (arrow) in segment VIII; RFA was performed on 25th July, 2007. **b** On dynamic CT, the effect of RFA was judged as complete response with a safety margin >5 mm (CRSM+). **c** By using a defect reperfusion test in Kupffer phase, there was a vessel in the ablated area (arrow); the judgment by CEUS was complete response without a safety ablative margin (CRSM–). **d** Local tumor recurrence was observed on 4th June 2008 (arrow).

Table 2. Post-treatment evaluation of RFA for HCC using each modality

Dynamic CT	Contrast-enhanced US			
	CRSM(+)	CRSM(–)	incomplete	N/A
CRSM(+)	30	19	0	0
CRSM(–)	3	29	1	1
Incomplete	0	1	2	0

N/A = Not available.

Table 3. Result of the local recurrence rate according to the therapeutic evaluation of each modality

	Post-treatment evaluation			
	CRSM(+)	CRSM(–)	incomplete	N/A
Dynamic CT	1/49 (2.5%)[1]	8/34 (30%)[1]	3/3	0
Contrast-enhanced US	0/33 (0%)[1]	9/49 (18%)[1]	3/3	0/1

N/A = Not available. [1] Fisher's exact test.

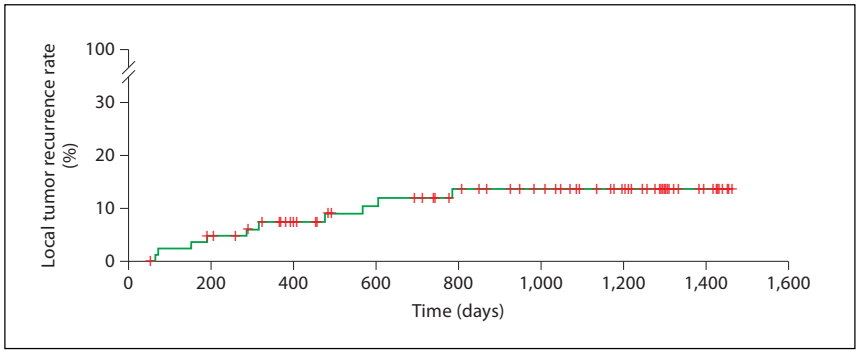

Fig. 4. Cumulative local tumor recurrence rate after RFA of the present study: 9% in 1 year and 12% in 2 years.

One case which could not be evaluated by CEUS was judged as CRSM– by dynamic CT. The consistency of the evaluation result of each modality was 71% (61/86) (table 2).

Local Tumor Recurrence

Two cases were judged 'incomplete' on both contrast-enhanced US and dynamic CT and these were eliminated from the calculation of the cumulative local tumor recurrence rate. Finally, local tumor recurrence was investigated in 84 nodules of 68 patients. Ten of the 84 nodules developed a local tumor recurrence (fig. 3). The cumulative local tumor recurrence rates were 9 and 12% in 1 and 2 years, respectively (fig. 4).

Evaluation of Local Recurrence Rates for Each Modality

Recurrence rates in the CRSM+ and CRSM– groups of dynamic CT were 2.5% (1/49) and 30% (8/34), respectively. Recurrence rates in the CRSM+ and CRSM– groups of CEUS were 0% (0/33) and 18% (9/49), respectively. There were no differences between dynamic CT and CEUS for each of the 3 evaluations, i.e. CRSM+, CRSM– and 'incomplete' (not significant by Fisher's exact test; table 3).

Discussion

Post-treatment responses of percutaneous ethanol injection and RFA for HCC using CEUS have been evaluated in several studies [20–24]. However, precise evaluation was difficult because Doppler US studies with contrast agents were affected by blooming artifacts, poor spatial resolution and low sensitivity to slow flow [20]. Levovist (SH U 508A; Schering AG, Berlin, Germany), was effective only when imaging was performed at high acoustic power using a high mechanical index, but the effect was transient [21, 22]. SonoVue (Bracco, Milan, Italy) is widely available for contrast visualization in Europe and China and is thought to be a truly intravascular, blood-pool contrast agent, with no interstitial equilibrium phase. When parenchyma-specific contrast images can be seen only 3–5 min after the injection, a precise post-treatment evaluation is difficult [23, 24]. Unlike Levovist and SonoVue, Sonazoid has a very stable Kupffer-phase image that may last up to 120 min after its injection. Therefore, in the present study, post-RFA areas were easily detected as perfusion defects in the Kupffer phase. If tumors inside the ablated areas can be detected in the Kupffer phase, safe margins can be clearly seen by using defect reperfusion imaging. Even if tumors cannot be detected in the ablated areas after RFA, safe margins can be evaluated by carefully comparing images of pre-B-mode or Kupffer-phase images of HCCs with postablated areas in the Kupffer phase side by side on the US screen. If arterial perfusion within the defect is demonstrated by the reinjection test of Sonazoid, it can easily define a residual tumor, or if some vessels recognized by the reinjection test are inside ablated areas, the adequacy of the safety margin can be determined. Kim et al. [25] and Nakazawa et al. [26] reported that an ablation zone with a margin of 5 mm or greater was the most important factor for local control of HCC. Therefore, we evaluated the local recurrence rate with or without adequate margins (more than 5 mm). Local recurrence rates between contrast-enhanced US and dynamic CT on each evaluation showed no difference and the consistency of the evaluation result of each modality was 71%. This indicated that CEUS is also useful to evaluate the response of RFA. To date, dynamic CT has been used most frequently to assess the effectiveness of RFA for HCC treatment. However, dynamic CT is prohibited for patients with renal dysfunction

and iodine allergy. It is also preferable for the patients to refrain from exposure to radiation. MRI has also been used for evaluating the therapeutic effect of RFA [27, 28]. However, patients who have a heart pacemaker, a metallic foreign body (metal sliver) in the eye or an aneurysm clip in the brain, cannot have an MRI scan because the magnetic field may dislodge the metal. It has been reported that another contrast agent like gadolinium sometimes causes nephrogenic systemic sclerosis [29].

Compared with dynamic CT and MRI [12], Sonazoid enhanced US has none of the risks mentioned above for the patients. Furthermore, CEUS is less expensive than CT and MRI and can be performed numerous times [30, 31].

This study had several limitations. First, it was a retrospective review of HCCs examined by CEUS using Sonazoid and dynamic CT nearly simultaneously after treatment, and there was a bias in the selection of the lesions. Second, the number of evaluated lesions was small. Third, histopathologic findings were not obtained from all patients for the diagnosis of local recurrence. To evaluate the true usefulness of CEUS using Sonazoid for the detection of local recurrence after treatment for HCC, further prospective randomized studies with a larger number of patients are warranted. In conclusion, CEUS with Sonazoid can be used to assess the efficacy of RFA for HCC, with the potential of reducing the number of CT scans required for confirmation.

Disclosure Statement

The authors declare that no conflicts of interests exist.

References

1 Shiina S, Tateishi R, Arano T, Uchino K, Enooku K, Nakagawa H, et al: Radiofrequency ablation for hepatocellular carcinoma: 10-year outcome and prognostic factors. Am J Gastroenterol 2012;107:569–578.

2 Shibata T, Iimuro Y, Yamamoto Y, Maetani Y, Ametani F, Itoh K, et al: Small hepatocellular carcinoma: comparison of radio-frequency ablation and percutaneous microwave coagulation therapy. Radiology 2002; 223:331–337.

3 Wood TF, Rose DM, Chung M, Allegra DP, Foshag LJ, Bilchik AJ: Radiofrequency ablation of 231 unresectable hepatic tumors: indications, limitations, and complications. Ann Surg Oncol 2000;7:593–600.

4 Livraghi T, Goldberg SN, Lazzaroni S, Meloni F, Solbiati L, Gazelle GS: Small hepatocellular carcinoma: treatment with radio-frequency ablation versus ethanol injection. Radiology 1999;210:655–661.

5 Tateishi R, Shiina S, Teratani T, Obi S, Sato S, Koike Y, et al: Percutaneous radiofrequency ablation for hepatocellular carcinoma: an analysis of 1,000 cases. Cancer 2005;103: 1201–1209.

6 Teratani T, Yoshida H, Shiina S, Obi S, Sato S, Tateishi R, et al: Radiofrequency ablation for hepatocellular carcinoma in so-called high-risk locations. Hepatology 2006;43: 1101–1108.

7 Camma C, Di Marco V, Orlando A, Sandonato L, Casaril A, Parisi P, et al: Treatment of hepatocellular carcinoma in compensated cirrhosis with radio-frequency thermal ablation (RFTA): a prospective study. J Hepatol 2005;42:535–540.

8 Lencioni RA, Allgaier HP, Cioni D, Olschewski M, Deibert P, Crocetti L, et al: Small hepatocellular carcinoma in cirrhosis: randomized comparison of radio-frequency thermal ablation versus percutaneous ethanol injection. Radiology 2003;228:235–240.

9 Tiong L, Maddern GJ: Systematic review and meta-analysis of survival and disease recurrence after radiofrequency ablation for hepatocellular carcinoma. Br J Surg 2011;98: 1210–1224.

10 Lim HK, Choi D, Lee WJ, Kim SH, Lee SJ, Jang HJ, et al: Hepatocellular carcinoma treated with percutaneous radio-frequency ablation: evaluation with follow-up multiphase helical CT. Radiology 2001;221:447–454.

11 Chopra S, Dodd GD 3rd, Chintapalli KN, Leyendecker JR, Karahan OI, Rhim H: Tumor recurrence after radiofrequency thermal ablation of hepatic tumors: spectrum of findings on dual-phase contrast-enhanced CT. AJR Am J Roentgenol 2001;177:381–387.

12 Lee JM, Yoon JH, Joo I, Woo HS: Rencet advances in CT and MR imaging for evaluation of hepatocellular carcinoma. Liver Cancer 2012;1:22–40.

13 Halpern EJ, McCue PA, Aksnes AK, Hagen EK, Frauscher F, Gomella LG: Contrast-enhanced US of the prostate with Sonazoid: comparison with whole-mount prostatectomy specimens in 12 patients. Radiology 2002;222:361–366.

14 Kudo M, Hatanaka K, Kumada T, Toyoda H, Tada T: Double-contrast ultrasound: a novel surveillance tool for hepatocellular carcinoma. Am J Gastroenterol 2011;106:368–370.

15 Hatanaka K, Kudo M, Minami Y, Maekawa K: Sonazoid-enhanced ultrasonography for diagnosis of hepatic malignancies: comparison with contrast-enhanced CT. Oncology 2008;75(suppl 1):42–47.

16 Kudo M, Hatanaka K, Maekawa K: Newly developed novel ultrasound technique, defect reperfusion ultrasound imaging, using sonazoid in the management of hepatocellular carcinoma. Oncology 2010;78(suppl 1): 40–45.

17 Kudo M, Okanoue T, Japan Society of Hepatology: Management of hepatocellular carcinoma in Japan: consensus-based clinical practice manual proposed by the Japan Society of Hepatology. Oncology 2007;72(suppl 1):2–15.

18 Bruix J, Sherman M: Management of hepatocellular carcinoma: an update. Hepatology 2011;53:1020–1022.

19 Kudo M, Hatanaka K, Maekawa K: Defect reperfusion imaging, a newly developed novel technology using Sonazoid in the treatment of hepatocellular carcinoma. J Med Ultrasound 2008;16:169–175.

20 Bartolozzi C, Lencioni R, Ricci P, Paolicchi A, Rossi P, Passariello R: Hepatocellular carcinoma treatment with percutaneous ethanol injection: evaluation with contrast-enhanced color Doppler US. Radiology 1998; 209:387–393.

21 Ding H, Kudo M, Onda H, Suetomi Y, Minami Y, Chung H, et al: Evaluation of post-treatment response of hepatocellular carcinoma with contrast-enhanced coded phase-inversion harmonic US: comparison with dynamic CT. Radiology 2001;221:721–730.

22 Ding H, Kudo M, Onda H, Suetomi Y, Minami Y, Maekawa K: Contrast-enhanced subtraction harmonic sonography for evaluating treatment response in patients with hepatocellular carcinoma. AJR Am J Roentgenol 2001;176:661–666.
23 Frieser M, Kiesel J, Lindner A, Bernatik T, Haensler JM, Janka R, et al: Efficacy of contrast-enhanced US versus CT or MRI for the therapeutic control of percutaneous radiofrequency ablation in the case of hepatic malignancies. Ultraschall Med 2011;32:148–153.
24 Ricci P, Cantisani V, Drudi F, Pagliara E, Bezzi M, Meloni F, et al: Is contrast-enhanced US alternative to spiral CT in the assessment of treatment outcome of radiofrequency ablation in hepatocellular carcinoma? Ultraschall Med 2009;30:252–258.
25 Kim YS, Rhim H, Cho OK, Koh BH, Kim Y: Intrahepatic recurrence after percutaneous radiofrequency ablation of hepatocellular carcinoma: analysis of the pattern and risk factors. Eur J Radiol 2006;59:432–441.
26 Nakazawa T, Kokubu S, Shibuya A, Ono K, Watanabe M, Hidaka H, et al: Radiofrequency ablation of hepatocellular carcinoma: correlation between local tumor progression after ablation and ablative margin. AJR Am J Roentgenol 2007;188:480–448.
27 Tokunaga S, Koda M, Matono T, Sugihara T, Nagahara T, Ueki M, et al: Assessment of ablative margin by MRI with ferucarbotran in radiofrequency ablation for liver cancer: comparison with enhanced CT. Br J Radiol 2012;85:745–752.
28 Koda M, Tokunaga S, Miyoshi K, Kishina M, Fujise Y, Kato J, et al: Assessment of ablative margin by unenhanced magnetic resonance imaging after radiofrequency ablation for hepatocellular carcinoma. Eur J Radiol 2012;81:2730–2736.
29 Grobner T, Prischl FC: Gadolinium and nephrogenic systemic fibrosis. Kidney Int 2007;72:260–264.
30 Joo I, Choi BI: New paradigm for management of hepatocellular carcinoma by imaging. Liver Cancer 2012;1:94–109.
31 Salvatore V, Bolondi L: Clinical impact of ultrasound-related techniques in the diagnosis of focal liver lesions. Liver Cancer, 2012;1:238–246.

Oncology

Oncology 2013;84(suppl 1):58–63
DOI: 10.1159/000345891

Published online: February 20, 2013

Therapeutic Response Assessment of Transcatheter Arterial Chemoembolization for Hepatocellular Carcinoma: Ultrasonography, CT and MR Imaging

Yasunori Minami Masatoshi Kudo

Department of Gastroenterology and Hepatology, Kinki University Faculty of Medicine, Osakasayama, Japan

Key Words
Computed tomography · Hepatocellular carcinoma · Magnetic resonance imaging · Transcatheter arterial chemoembolization · Ultrasonography

Abstract
Two randomized controlled trials identified that transcatheter arterial chemoembolization (TACE) for hepatocellular carcinoma (HCC) shows a significant survival benefit compared with controls, after a long-term controversy. Thus, TACE is the current standard of care for patients presenting with multinodular HCC. Monitoring tumor response to TACE is part of the clinical management of HCC patients. Imaging, including ultrasonography, computed tomography and magnetic resonance imaging, has an important role in assessing therapeutic effects earlier and more objectively. Imaging assessment needs to detect not only a reduction in overall tumor load but also a reduction in viable tumor. Here, we give an overview of the current status of the imaging assessment of HCC response to TACE.

Introduction

The primary goal of cancer treatment is to produce a complete and sustained remission. Monitoring tumor response to therapy is part of the clinical management of cancer patients. Imaging is generally used to assess therapeutic effects earlier and more objectively.

Hepatocellular carcinoma (HCC) is a main leading cause of cancer-related death worldwide [1–4]. HCC may also develop in more than one site in the liver and may grow into multiple tumors. In addition, in a high proportion of cases the disease recurs after radical therapy. Transcatheter arterial chemoembolization (TACE) is the current standard of care for patients presenting with multinodular HCC and relatively preserved liver function, absence of cancer-related symptoms, and no evidence of vascular invasion or extrahepatic spread [5–10]. In 2002, two randomized controlled trials [11–14] identified that TACE showed a significant survival benefit compared with controls after a long-term controversy. TACE has often been performed repeatedly during effective monitoring [15]. However, repetitive TACE treatments might reduce liver function and induce stenosis of the hepatic artery. Furthermore, repetitive TACE treatments can become less effective in patients with relapsed HCC. These cases are considered TACE-refractory in clinical practice [16–18]. It is essential to assess tumor response accurately in order to discontinue ineffective therapies and avoid complications caused by tumor progression. Imaging, including ultrasonography (US), computed tomography (CT) and magnetic resonance imaging (MRI) [19], has an important role in assessing the effectiveness of tumor response of HCC. Therefore, we need to understand the characteristics of each imag-

KARGER

Fax +41 61 306 12 34
E-Mail karger@karger.com
www.karger.com

0030–2414/13/0847–0058$38.00/0

Accessible online at:
www.karger.com/ocl

Masatoshi Kudo, MD, PhD
Division of Gastroenterology and Hepatology, Department of Internal Medicine
Kinki University Faculty of Medicine
377-2 Ohno-Higashi, Osakasayama, Osaka 589-8511 (Japan)
E-Mail m-kudo@med.kindai.ac.jp

ing modality for reading images. In this review, we focus our discussion on the imaging assessment of HCC response to TACE.

Principle of Tumor Response Assessment to TACE for HCC

Tumor shrinkage after therapy is only one parameter affecting patient survival. Conventional methods for response assessment, such as the World Health Organization (WHO) criteria and the Response Evaluation Criteria In Solid Tumors (RECIST), have limited predictive value in HCC patients treated with TACE [20–22]. TACE induces direct tumor necrosis and its anticancer efficacy is not paralleled by a reduction in overall tumor load but rather by a reduction in viable tumor, as recognized by contrast-enhanced radiologic imaging [21, 22]. The guidelines state that assessment of response in HCC should be based on performing contrast-enhanced imaging 1 month after initial treatment and at least every 3 months during follow-up [22, 23]. These criteria rely only on tumor shrinkage as a measure of antitumor activity.

Imaging

Computed Tomography

Recently, drug-eluting beads have provided an attractive alternative to iodized oil-based regimens. However, conventional TACE with administration of an anticancer agent-in-oil emulsion followed by embolic agents has been the most popular technique. Lipiodol (Lipiodol Ultrafluide, Laboratoire Guerbet, Aulnay-Sous-Bois, France) is an oily contrast medium in radiography, and Lipiodol accumulation in the tumor can be regarded as representing a necrotic area [24, 25]. Therefore, CT is commonly used as the standard imaging technique for evaluating the therapeutic response in patients with HCC after TACE (table 1) [26–38].

The accumulation pattern of Lipiodol observed on CT can be classified, and the pattern and distribution of Lipiodol in the tumor are useful for assessing the therapeutic effects of TACE. A greater amount of accumulation of Lipiodol within a tumor indicates a greater area of necrosis. During follow-up, the focal defect or washout of Lipiodol in the mass with the contrast-enhanced area suggests the presence of a viable tumor and that additional treatment is needed. However, Lipiodol can be more difficult to assess on CT because accumulation of Lipiodol in tumors can mask the enhancement of a residual tumor. At least a few weeks are required to evaluate whether Lipiodol accumulation corresponds to the necrotic area on CT because Lipiodol gradually washes out of the viable area in the tumor [25]. Thus, it is considered that early assessment of response of TACE is difficult on contrast-enhanced CT.

Recent developments in flat panel detector technology and rotational angiography techniques can provide 3D imaging information that offers a quality similar to that of CT images. Several studies have shown that cone-beam CT angiography can be extremely helpful during TACE [39–42]. Cone-beam CT would potentially be a convenient tool for very early assessment of response by Lipiodol retention in HCCs immediately after TACE [43].

Ultrasonography

A recent advance in US imaging is the development of microbubble contrast agents, which consist of a gas core that is encapsulated by a shell constructed of a lipid monolayer or cross-linked albumin. Each bubble acts as a harmonic oscillator and contrast-enhanced echo signals contain significant energy components at higher harmonics, while tissue echoes do not. With the use of a contrast agent, contrast harmonic imaging possesses not only a very high sensitivity to the contrast agent but also a high spatial resolution, and can depict signals from microbubbles in very slow flow without Doppler-related artifacts. Consequently, it could be a more accurate way to demonstrate residual viable tumor flow in HCC after therapy. Several researchers have reported that contrast harmonic imaging is a useful tool for assessing vascularity in comparison with contrast-enhanced CT because the tumor vascularity depiction is not affected by Lipiodol accumulation (table 2) [44–52]. Residual tumor blood flow on contrast-enhanced US performed within days to 2 weeks after TACE could be predictive of tumor outcome as an early assessment of response to TACE. Use of contrast-enhanced US permits the proper selection of patients who would benefit from additional focal therapy after TACE earlier, as well as helping to guide focal ablation to the viable portion of HCC [46, 49]. However, contrast-enhanced US has technical limitations imposed by body habitus and the difficulty involved in the accessibility to lesions near the hemidiaphragm and to lesions in some small or diseased livers. Additionally, contrast-enhanced US examinations used to be performed on a solitary mass or on a dominant mass in patients with multiple lesions.

Magnetic Resonance Imaging

MRI provides better contrast between the different soft tissues and higher spatial resolution with sensitivity

Table 1. Assessment of treatment response to TAE/TACE using CT

First author, year	n (patients/ nodules)	Mean tumor size, cm	Procedure	Assessment of response
Takayasu, 1984 [26]	18/ND	ND	TAE	Contrast-enhanced area
Furui, 1984 [27]	50/65	ND	TAE	Contrast-enhanced area
Matsuo, 1993 [28]	12/ND	ND	Lip-TACE	Lipiodol uptake
Nishimine, 1994 [29]	98/ND	ND	Lip-TACE	Lipiodol uptake
Tsushima, 1998 [30]	22/ND	ND	Lip-TACE	Lipiodol uptake + contrast-enhanced area
Ernst, 1999 [31]	160/ND	ND	Lip-TACE	Lipiodol uptake only
Sumi, 1999 [32]	45/142	ND	Lip-TACE	Lipiodol uptake + contrast-enhanced area
Okusaka, 2000 [33]	88/ND	ND	Lip-TACE	Lipiodol uptake + contrast-enhanced area
Cioni, 2000 [34]	47/68	4.3	Lip-TACE	Lipiodol uptake + contrast-enhanced area
Katyal, 2000 [35]	57/ND	ND	TACE	Contrast-enhanced area
Kubota, 2001 [36]	54/84	2.2	Lip-TACE	Lipiodol uptake + contrast-enhanced area
Kim, 2002 [37]	54/129	ND	Lip-TACE	Lipiodol uptake + contrast-enhanced area
Ebied, 2003 [38]	72/186	ND	Lip-TACE	Lipiodol uptake + contrast-enhanced area

Lip = Lipiodol; ND = not described; TAE = transcatheter arterial embolization.

Table 2. Assessment of treatment response to TACE: contrast harmonic US versus contrast-enhanced CT

First author, year	n (patients/ nodules)	Mean tumor size, cm	Contrast agent	Viable area detection rate (US/CT), %
Catalano, 1999 [44]	28/43	3.4	Levovist	91/72
Cioni, 2000 [34]	47/68	4.3	Levovist	88/34
Numata, 2001 [45]	29/39	ND	Levovist	92/33
Minami, 2003 [46]	40/44	3.9	Levovist	86/43
Morimoto, 2003 [47]	29/29	ND	Levovist	57/ND
Kim, 2006 [48]	29/29	2.5	Levovist	61/39
Kono, 2007 [49]	33/42	ND	Optison	78/ND
Xia, 2008 [50]	28/43	1.7	Sonazoid	58/40
Schacherer, 2010 [51]	15/15	4.8	SonoVue	93/73

ND = Not described.

Table 3. Assessment of treatment response to TACE: MRI versus CT

First author, year	n (patients/ nodules)	Mean tumor size, cm	Contrast agent	Viable area detection rate (MRI/CT), %
Yamashita, 1993 [53]	37/44	ND	Gd-DTPA	100/ND
Ito, 1995 [54]	13/13	ND	Gd-DTPA	77/ND
Kubota, 2001 [55]	54/84	2.2	Gd-DTPA	100/76
Minami, 2003 [46]	40/44	3.9	Gd-DTPA	50/43
Chen, 2006 [56]	20/20	ND	none (diffusion-weighted MRI)	100/ND
Kubota, 2010 [57]	25/36	2.0	none (diffusion-weighted MRI)	92/92

ND = Not described.

than CT. Recent advances in MRI, including breath-hold 3D imaging and rapid half-Fourier acquisition, allow imaging of the liver in a single breath-hold with a high spatial resolution. Various contrast agents are available to image the liver. A paramagnetic ion, gadolinium-diethylenetriamine pentaacetic acid, is the most commonly used MRI contrast agent; it has an extracellular distribution and behaves similarly to the iodinated contrast agents used in CT. The presence of gadolinium can strongly influence the relaxation properties of nearby protons, leading to changes in tissue contrast. Liver-specific contrast media, such as mangafodipir trisodium (taken up by hepatocytes) and ferrum oxides (taken up by Kupffer cells), demonstrate selective uptake in the liver and are primarily used for lesion detection.

Lipiodol causes variable signal intensity changes on unenhanced MRI, and it is difficult to detect accurately [24]. Enhanced areas in the embolization site on gadolinium-enhanced MRI presumably represent viable tumor (table 3) [53–57] but could also result from post-treatment granulation tissue [58]. In addition, diffusion-weighted MRI is a new kind of functional imaging technology that can explore the random diffusion motion of water molecules in vivo. Diffusion-weighted MRI has been found to be useful for lesion detection with higher accuracy compared with superparamagnetic iron oxide-enhanced MRI [59]. However, diffusion-weighted MRI is known to have limitations such as a relatively poor signal-to-noise ratio and high sensitivity to pulsatile or susceptibility artifacts, degrading the ability to detect lesions. A new quantitative measurement on diffusion-weighted MRI may allow effective evaluation of the efficacy of TACE for HCC and correctly reveal recurrent tumors [56, 57].

Conclusion

Conventional TACE with administration of an anticancer agent-in-oil emulsion followed by embolic agents has been the most popular technique. Imaging, including US, CT and MRI, has an important role in assessing the effectiveness of tumor response of HCC. Imaging assessment needs to detect not only a reduction in overall tumor load, but also a reduction in viable tumor.

CT is commonly used as the standard imaging technique because the accumulation of Lipiodol is observed easily on plain CT. Distribution of Lipiodol in the tumor is useful for assessing the therapeutic effects on CT. However, Lipiodol often makes it difficult to detect the residual tumor on CT because accumulation of intratumoral Lipiodol can mask its enhancement. Contrast-enhanced US is a useful tool for assessing the vascularity in comparison with contrast-enhanced CT because the tumor vascularity depiction is not affected by Lipiodol accumulation. However, US examinations used to be performed on a solitary mass or on a dominant mass in patients with multiple lesions. MRI provides better contrast between the different soft tissues and higher spatial resolution than that of CT. Enhanced areas in the embolization site on gadolinium-enhanced MRI presumably represent viable tumor with high sensitivity but low specificity.

Disclosure Statement

The authors declare that no conflicts of interest exist.

References

1 El-Serag HB: Hepatocellular carcinoma. N Engl J Med 2011;365:1118–1127.
2 Parkin DM, Bray F, Ferlay J, Pisani P: Estimating the world cancer burden: Globocan 2000. Int J Cancer 2001;94:153–156.
3 Altekruse SF, McGlynn KA, Reichman ME: Hepatocellular carcinoma incidence, mortality, and survival trends in the United States from 1975 to 2005. J Clin Oncol 2009; 27:1485–1491.
4 Kim DY, Han KH: Epidemiology and surveillance of hepatocellular carcinoma. Liver Cancer 2012;1:2–14.
5 Yamada R, Sato M, Kawabata M, Nakatsuka H, Nakamura K, Takashima S: Hepatic artery embolization in 120 patients with unresectable hepatoma. Radiology 1983;148:397–401.
6 Ohishi H, Uchida H, Yoshimura H, Ohue S, Ueda J, Katsuragi M, Matsuo N, Hosogi Y: Hepatocellular carcinoma detected by iodized oil: use of anticancer agents. Radiology 1985;154:25–29.
7 Takayasu K, Shima Y, Muramatsu Y, Moriyama N, Yamada T, Makuuchi M, Hasegawa H, Hirohashi S: Hepatocellular carcinoma: treatment with intraarterial iodized oil with and without chemotherapeutic agents. Radiology 1987;163:345–351.
8 Matsui O, Kadoya M, Yoshikawa J, Gabata T, Arai K, Demachi H, Miyayama S, Takashima T, Unoura M, Kogayashi K: Small hepatocellular carcinoma: treatment with subsegmental transcatheter arterial embolization. Radiology 1993;188:79–83.
9 Takayasu K: Transarterial chemoembolization for hepatocellular carcinoma over three decades: current progress and perspective. Jpn J Clin Oncol 2012;42:247–255.
10 Lencioni R: Chemoembolization for hepatocellular carcinoma. Semin Oncol 2012;39: 503–509.
11 Llovet JM, Real MI, Montaña X, Planas R, Coll S, Aponte J, Ayuso C, Sala M, Muchart J, Solà R, Rodés J, Bruix J, Barcelona Liver Cancer Group: Arterial embolisation or chemoembolisation versus symptomatic treatment in patients with unresectable hepatocellular carcinoma: a randomised controlled trial. Lancet 2002;359:1734–1739.

12 Lo CM, Ngan H, Tso WK, Liu CL, Lam CM, Poon RT, Fan ST, Wong J: Randomized controlled trial of transarterial Lipiodol chemoembolization for unresectable hepatocellular carcinoma. Hepatology 2002;35:1164–1171.
13 Lencioni R: Chemoembolization in patients with hepatocellular carcinoma. Liver Cancer 2012;1:41–50.
14 Lin S, Hoffmann K, Schemmer P: Treatment of hepatocellular carcinoma: a systematic review. Liver Cancer 2012;1:144–158.
15 Ikeda K, Kumada H, Saitoh S, Arase Y, Chayama K: Effect of repeated transcatheter arterial embolization on the survival time in patients with hepatocellular carcinoma: an analysis by the Cox proportional hazard model. Cancer 1991;68:2150–2154.
16 Yamanaka K, Hatano E, Kitamura K, Iida T, Ishii T, Machimito T, Taura K, Yasuchika K, Isoda H, Shibata T, Uemoto S: Early evaluation of transcatheter arterial chemoembolization-refractory hepatocellular carcinoma. J Gastroenterol 2012;47:343–346.
17 Kudo M: Treatment of advanced hepatocellular carcinoma with emphasis on hepatic arterial infusion chemotherapy and molecular targeted therapy. Liver Cancer 2012;1:62–70.
18 Kudo M, Izumi N, Kokudo N, Matsui O, Sakamoto M, Nakashima O, Kojiro M, Makuuchi M: Management of hepatocellular carcinoma in Japan: consensus-based clinical practice guidelines proposed by the Japan Society of Hepatology (JSH) 2010 updated version. Dig Dis 2011;29:339–364.
19 Lee JM, Yoon JH, Joo I, Woo HS: Recent advances in CT and MR imaging for evaluation of hepatocellular carcinoma. Liver Cancer 2012;1:22–40.
20 Forner A, Ayuso C, Varela M, Rimola J, Hessheimer AJ, de Lope CR, Reig M, Bianchi L, Llovet JM, Bruix J: Evaluation of tumor response after locoregional therapies in hepatocellular carcinoma: are response evaluation criteria in solid tumors reliable? Cancer 2009;115:616–623.
21 Takayasu K: Transarterial chemoembolization for hepatocellular carcinoma over three decades: current progress and perspective. Jpn J Clin Oncol 2012;42:247–255.
22 Kudo M, Kubo S, Takayasu K, Sakamoto M, Tanaka M, Ikai I, Furuse J, Nakamura K, Makuuchi M, Liver Cancer Study Group of Japan (Committee for Response Evaluation Criteria in Cancer of the Liver): Response Evaluation Criteria in Cancer of the Liver (RECICL) proposed by the Liver Cancer Study Group of Japan (2009 revised version). Hepatol Res 2010;40:686–692.
23 European Association for the Study of the Liver, European Organization for Research and Treatment of Cancer: EASL–EORTC clinical practice guidelines: management of hepatocellular carcinoma. J Hepatol 2012;56:908–943.
24 Imaeda T, Yamawaki Y, Seki M, Goto H, Iinuma G, Kanematsu M, Mochizuki R, Doi H, Saji S, Shimokawa K: Lipiodol retention and massive necrosis after Lipiodol-chemoembolization of hepatocellular carcinoma: correlation between computed tomography and histopathology. Cardiovasc Intervent Radiol 1993;16:209–213.
25 Takayasu K, Arii S, Matsuo N, Yoshikawa M, Ryu M, Takasaki K, Sato M, Yamanaka N, Shimamura Y, Ohto M: Comparison of CT findings with resected specimens after chemonmbolization with iodized oil for hepatocellular carcinoma. AJR Am J Roentogenol 2000;175:699–704.
26 Takayasu K, Moriyama N, Muramatsu Y, Suzuki M, Yamada T, Kishi K, Hasagawa H, Okazaki N: Hepatic arterial embolization for hepatocellular carcinoma: comparison of CT scans and resected specimens. Radiology 1984;150:661–665.
27 Furui S, Otomo K, Itai Y, Iio M: Hepatocellular carcinoma treated by transcatheter arterial embolization: progress evaluated by computed tomography. Radiology 1984;150:773–778.
28 Matsuo N, Uchida H, Nishimine K, Soda S, Oshima M, Nakano H, Nagano N, Nishimura Y, Yoshioka T, Guo Q, et al: Segmental transcatheter hepatic artery chemoembolization with iodized oil for hepatocellular carcinoma: antitumor effect and influence on normal tissue. J Vasc Interv Radiol 1993;4:543–549.
29 Nishimine K, Uchida H, Matsuo N, Sakaguchi H, Hirohashi S, Nishimura Y, Guo Q, Ohishi H, Nagano N, Yoshioka T, et al: Segmental transarterial chemoembolization with Lipiodol mixed with anticancer drugs for nonresectable hepatocellular carcinoma: follow-up CT and therapeutic results. Cancer Chemother Pharmacol 1994;33(suppl):S60–S68.
30 Tsushima Y, Unno Y, Koizumi J, Kusano S: Hepatic perfusion changes after transcatheter arterial embolization (TAE) of hepatocellular carcinoma: measurement by dynamic computed tomography (CT). Dig Dis Sci 1998;43:317–322.
31 Ernst O, Sergent G, Mizrahi D, Delemazure O, Paris JC, L'Herminé C: Treatment of hepatocellular carcinoma by transcatheter arterial chemoembolization: comparison of planned periodic chemoembolization and chemoembolization based on tumor response. AJR Am J Roentgenol 1999;172:59–64.
32 Sumi S, Yamashita Y, Mitsuzaki K, Yamamoto H, Urata J, Nishiharu T, Takahashi M: Power Doppler sonography assessment of tumor recurrence after chemoembolization therapy for hepatocellular carcinoma. AJR Am J Roentgenol 1999;172:67–71.
33 Okusaka T, Okada S, Ueno H, Ikeda M, Yoshimori M, Shimada K, Yamamoto J, Kosuge T, Yamasaki S, Iwata R, Furukawa H, Moriyama N, Sakamoto M, Hirohashi S: Evaluation of the therapeutic effect of transcatheter arterial embolization for hepatocellular carcinoma. Oncology 2000;58:293–299.
34 Cioni D, Lencioni R, Bartolozzi C: Therapeutic effect of transcatheter arterial chemoembolization on hepatocellular carcinoma: evaluation with contrast-enhanced harmonic power Doppler ultrasound. Eur Radiol 2000;10:1570–1575.
35 Katyal S, Oliver JH, Peterson MS, Chang PJ, Baron RL, Carr BI: Prognostic significance of arterial phase CT for prediction of response to transcatheter arterial chemoembolization in unresectable hepatocellular carcinoma: a retrospective analysis. AJR Am J Roentgenol 2000;175:1665–1672.
36 Kubota K, Hisa N, Nishikawa T, Fujiwara Y, Murata Y, Itoh S, Yoshida D, Yoshida S: Evaluation of hepatocellular carcinoma after treatment with transcatheter arterial chemoembolization: comparison of Lipiodol-CT, power Doppler sonography, and dynamic MRI. Abdom Imaging 2001;26:184–190.
37 Kim HC, Kim AY, Han JK, Chung JW, Lee JY, Park JH, Choi BI: Hepatic arterial and portal venous phase helical CT in patients treated with transcatheter arterial chemoembolization for hepatocellular carcinoma: added value of unenhanced images. Radiology 2002;225:773–780.
38 Ebied OM, Federle MP, Carr BI, Pealer KM, Li W, Amesur N, Zajko A: Evaluation of responses to chemoembolization in patients with unresectable hepatocellular carcinoma. Cancer 2003;97:1042–1050.
39 Hirota S, Nakao N, Yamamoto S, Kobayashi K, Maeda H, Ishikura R, Miura K, Sakamoto K, Ueda K, Baba R: Cone-beam CT with flat-panel-detector digital angiography system: early experience in abdominal interventional procedures. Cardiovasc Intervent Radiol 2006;29:1034–1038.
40 Kakeda S, Korogi Y, Ohnari N, Moriya J, Oda N, Nishino K, Miyamoto W: Usefulness of cone-beam volume CT with flat panel detectors in conjunction with catheter angiography for transcatheter arterial embolization. J Vasc Interv Radiol 2007;18:1508–1516.
41 Miyayama S, Yamashiro M, Okuda M, Yoshie Y, Sugimori N, Igarashi S, Nakashima Y, Matsui O: Usefulness of cone-beam computed tomography during ultraselective transcatheter arterial chemoembolization for small hepatocellular carcinomas that cannot be demonstrated on angiography. Cardiovasc Intervent Radiol 2009;32:255–264.
42 Higashihara H, Osuga K, Onishi H, Nakamoto A, Tsuboyama T, Maeda N, Hori M, Kim T, Tomiyama N: Diagnostic accuracy of C-arm CT during selective transcatheter angiography for hepatocellular carcinoma: comparison with intravenous contrast-enhanced, biphasic, dynamic MDCT. Eur Radiol 2012;22:872–879.
43 Jeon UB, Lee JW, Choo KS, Kim CW, Kim S, Lee TH, Jeong YJ, Kang DH: Iodized oil uptake assessment with cone-beam CT in chemoembolization of small hepatocellular carcinomas. World J Gastroenterol 2009;15:5833–5837.

44 Catalano O, Esposito M, Lobianco R, Cusati B, Altei F, Siani A: Hepatocellular carcinoma treated with chemoembolization: assessment with contrast-enhanced doppler ultrasonography. Cardiovasc Intervent Radiol 1999;22:486–492.
45 Numata K, Tanaka K, Kiba T, Saito S, Isozaki T, Hara K, Morimoto M, Sekihara H, Yonezawa H, Kubota T: Using contrast-enhanced sonography to assess the effectiveness of transcatheter arterial embolization for hepatocellular carcinoma. AJR Am J Roentgenol 2001;176:1199–1205.
46 Minami Y, Kudo M, Kawasaki T, Kitano M, Chung H, Maekawa K, Shiozaki H: Transcatheter arterial chemoembolization of hepatocellular carcinoma: usefulness of coded phase-inversion harmonic sonography. AJR Am J Roentgenol 2003;180:703–708.
47 Morimoto M, Shirato K, Sugimori K, Kokawa A, Tomita N, Saito T, Imada T, Tanaka N, Nozawa A, Numata K, Tanaka K: Contrast-enhanced harmonic gray-scale sonographic-histologic correlation of the therapeutic effects of transcatheter arterial chemoembolization in patients with hepatocellular carcinoma. AJR Am J Roentgenol 2003;181:65–69.
48 Kim HJ, Kim TK, Kim PN, Kim AY, Ko EY, Kim KW, Sung KB, Ha HK, Kim HC, Lee MG: Assessment of the therapeutic response of hepatocellular carcinoma treated with transcatheter arterial chemoembolization: comparison of contrast-enhanced sonography and 3-phase computed tomography. J Ultrasound Med 2006;25:477–486.
49 Kono Y, Lucidarme O, Choi SH, Rose SC, Hassanein TI, Alpert E, Mattrey RF: Contrast-enhanced ultrasound as a predictor of treatment efficacy within 2 weeks after transarterial chemoembolization of hepatocellular carcinoma. J Vasc Interv Radiol 2007;18:57–65.
50 Xia Y, Kudo M, Minami Y, Hatanaka K, Ueshima K, Chung H, Hagiwara S, Inoue T, Ishikawa E, Kitai S, Takahashi S, Tatsumi C, Ueda T, Hayaishi S, Maekawa K: Response evaluation of transcatheter arterial chemoembolization in hepatocellular carcinomas: the usefulness of sonazoid-enhanced harmonic sonography. Oncology 2008;75(suppl 1):99–105.
51 Schacherer D, Girlich C, Zorger N, Wiest R, Schoelmerich J, Feuerbach S, Jung EM: Sono-hepatic-arteriography (Sono-HA) in the assessment of hepatocellular carcinoma in patients undergoing transcatheter arterial chemoembolization (TACE). Ultraschall Med 2010;31:270–275.
52 Salvatore V, Bolondi L: Clinical impact of ultrasound-related techniques in the diagnosis of focal liver lesions. Liver Cancer, in press.
53 Yamashita Y, Yoshimatsu S, Sumi M, Harada M, Takahashi M: Dynamic MR imaging of hepatoma treated by transcatheter arterial embolization therapy: assessment of treatment effect. Acta Radiol 1993;34:303–308.
54 Ito K, Honjo K, Fujita T, Matsui M, Awaya H, Matsumoto T, Matsunaga N, Nakanishi T: Therapeutic efficacy of transcatheter arterial chemoembolization for hepatocellular carcinoma: MRI and pathology. J Comput Assist Tomogr 1995;19:198–203.
55 Kubota K, Hisa N, Nishikawa T, Fujiwara Y, Murata Y, Itoh S, Yoshida D, Yoshida S: Evaluation of hepatocellular carcinoma after treatment with transcatheter arterial chemoembolization: comparison of Lipiodol-CT, power Doppler sonography, and dynamic MRI. Abdom Imaging 2001;26:184–190.
56 Chen CY, Li CW, Kuo YT, Jaw TS, Wu DK, Jao JC, Hsu JS, Liu GC: Early response of hepatocellular carcinoma to transcatheter arterial chemoembolization: choline levels and MR diffusion constants – initial experience. Radiology 2006;239:448–456.
57 Kubota K, Yamanishi T, Itoh S, Murata Y, Miyatake K, Yasunami H, Morio K, Hamada N, Nishioka A, Ogawa Y: Role of diffusion-weighted imaging in evaluating therapeutic efficacy after transcatheter arterial chemoembolization for hepatocellular carcinoma. Oncol Rep 2010;24:727–732.
58 De Santis M, Alborino S, Tartoni PL, Torricelli P, Casolo A, Romagnoli R: Effects of lipiodol retention on MRI signal intensity from hepatocellular carcinoma and surrounding liver treated by chemoembolization. Eur Radiol 1997;7:10–16.
59 Nasu K, Kuroki Y, Nawano S, Kuroki S, Tsukamoto T, Yamamoto S, Motoori K, Ueda T: Hepatic metastases: diffusion-weighted sensitivity-encoding versus SPIO-enhanced MR imaging. Radiology 2006;239:122–130.

Oncology

Oncology 2013;84(suppl 1):75–81
DOI: 10.1159/000345894

Published online: February 20, 2013

The Prognostic Value of Vascular Endothelial Growth Factor in Hepatocellular Carcinoma for Predicting Metastasis after Curative Resection

Mutsuko Minata[a, e] Kouji H. Harada[b] Masatoshi Kudo[d] Iwao Ikai[c]
Naoshi Nishida[a, d]

[a]Department of Medicine and Clinical Science, Kyoto University Graduate School of Medicine, [b]Kyoto University School of Public Health, and [c]Department of Surgery, National Hospital Organization Kyoto Medical Center, Kyoto, and [d]Department of Gastroenterology and Hepatology, Kinki University Faculty of Medicine, Osakasayama, Japan; [e]Department of Molecular and Cellular Biology, Beckman Research Institute of City of Hope, Duarte, Calif., USA

Key Words
Hepatocellular carcinoma · Vascular endothelial growth factor · E-cadherin · Recurrence

Abstract
Objectives: Hepatocellular carcinoma (HCC) frequently recurs even after curative resection. The purpose of this study was to identify factors predictive for postoperative recurrence of HCC in patients who underwent curative resection using immunohistochemistry. ***Methods:*** Expression of vascular endothelial growth factor (VEGF), E-cadherin and cyclin D1 in HCC tissue were analyzed for 133 HCC patients who underwent curative resection of tumors using immunohistochemical analysis. Relationships of expressions and disease-free survival of HCC were evaluated using univariate and multivariate analyses. ***Results:*** The average period of follow-up of the patients was 6.7 years. Multivariate analyses revealed that only strong expression of VEGF in HCC tissue was significantly associated with metastatic recurrence ($p < 0.001$, hazard ratio, HR, 3.32). ***Conclusions:*** Evaluating VEGF in HCC tissue after surgical resection has predictive value for metastatic HCC recurrence. The ability to risk stratify should improve the treatment strategies after hepatectomy.

Introduction

Postoperative recurrence of hepatocellular carcinoma (HCC) is common and limits long-term survival following otherwise successful surgery [1–3]. Rates of recurrence within 3 years after initial resection have ranged from approximately 60 to 80%, even in HCC tumors smaller than 4 cm or curative resection [4, 5]. A high recurrence rate of HCC is attributed to frequent occurrence of microvascular invasion, occult metastases [6] and multicentric recurrence within a background liver of liver cirrhosis [7]. On the other hand, it was previously demonstrated that metastatic recurrence is associated with angiogenesis and invasiveness of the tumor [8]. Vascular endothelial growth factor (VEGF) is frequently implicated in metastasis by promoting an angiogenic phenotype [9]. Besides, transcriptional inactivation of E-cadherin was shown to occur frequently in tumor progression [10]. From this standpoint, molecular analyses based on genetic profiles of HCC could be useful for predicting the clinical behavior of HCC. However, highly specialized molecular analyses, such as expression microarrays, could not be applicable for clinical setting because of the cost and complexity on analyses. In this study, we investigated an alternative method of molecu-

KARGER

Fax +41 61 306 12 34
E-Mail karger@karger.com
www.karger.com

0030–2414/13/0847–0075$38.00/0

Accessible online at:
www.karger.com/ocl

Naoshi Nishida, MD
Department of Gastroenterology and Hepatology
Kinki University Faculty of Medicine
377-2 Ohno-higashi, Osakasayama, Osaka 589-8511 (Japan)
E-Mail naoshi@med.kindai.ac.jp

lar analysis using immunohistochemical analysis of cancer-related molecules. Specifically, we sought to identify relationships between patterns of recurrence in the expression of VEGF in HCC after curative hepatectomy.

Materials and Methods

Patients

We retrospectively analyzed the relationship between the recurrence of HCCs and clinicopathological parameters in 133 patients who were diagnosed with HCC of stage I or II and underwent curative hepatectomy at Kyoto University Hospital between 1985 and 1993. The mean follow-up period was 6.7 ± 5.2 years (range 0–21) and the patients consisted of 89 men and 44 women with a mean age of 61.4 years. The study was approved by the institutional review board of involved institutions and informed consent was obtained from each patient. The stage of HCC and the curability of surgery were classified according to general rules for the clinical and pathological study of primary liver cancer established by the Liver Cancer Study Group of Japan [11]. After surgery, each patient was monitored every 3 months with serum α-fetoprotein levels and radiological examination of computed tomography or magnetic resonance imaging until September 2008. Abdominal echogram and chest radiograms were also performed every 3 months. Outcome of the patients was classified into 3 groups: recurrence-free (n = 37), multicentric recurrence (n = 22) and metastatic recurrence (n = 74). The patterns of recurrence were assessed morphologically from computed tomography images, angiography, bone scintigrams and pathological findings. Intrahepatic metastatic recurrence was diagnosed as follows: emergence of multiple hypervascular tumors appeared in a localized segment that had contained the original tumor, emergence of a large tumor situated near the original site, emergence of additional smaller tumors in distant parts of the liver [12].

Additional clinicopathological information of the patients are as follows (some data were not available for all patients): status of hepatitis virus, positive for hepatitis B surface antigen (HBsAg; n = 17), positive for hepatitis C virus antibody (HCVAb) or HCV-RNA (n = 77), negative for both HBsAg and HCVAb (n = 5); clinical stage of HCC I (n = 34), II (n = 97); serum alanine aminotransferase (ALT) level ≤80 IU/l (n = 81), >80 IU/l (n = 50); platelet count ($10^3/mm^3$) ≥10×10^4 (n = 76), <10×10^4 (n = 56); serum α-fetoprotein level ≤400 ng/ml (n = 95), >400 ng/ml (n = 34); histology of noncancerous liver normal (n = 5), chronic hepatitis (n = 35), cirrhosis (n = 89); tumor size <2 cm (n = 47), 2–5 cm (n = 75), >5 cm (n = 11); histological differentiation of HCC well (n = 13), moderate (n = 90), poor (n = 30); vascular invasion positive (n = 2), negative (n = 131). There was no significant correlation between each item of clinicopathological data and patient outcome.

Immunohistochemical Analyses

Immunohistochemical staining for VEGF, E-cadherin and cyclin D1 were performed using the avidin-biotin complex method (Vecstatin ABC kit, Vector Laboratories, Burlingame, Calif., USA). Antibodies used were a rabbit polyclonal antibody for VEGF (Santa Cruz Biotechnology, Santa Cruz, Calif., USA) at a 1:200 dilution, a mouse monoclonal antibody for E-cadherin (Takara Shuzo Co., Shiga, Japan) at a 1:20 dilution and a mouse monoclonal antibody for cyclin D1 (Progen Biotechnik GmbH, Heidelberg, Germany) at a 1:20 dilution. VEGF expression level was scored semi-quantitatively based on staining intensity and distribution using the immunoreactive score (IRS) as described before [13, 14]: IRS = SI (staining intensity) × PP (percentage of positive cells). SI was determined as 0 (negative), 1 (weak), 2 (moderate) and 3 (strong). PP was defined as 0 (negative), 1 (10% positive cells), 2 (11–50% positive cells), 3 (51–80% positive cells) and 4 (more than 80% positive cells). Ten visual fields from different areas of each tumor were used for IRS evaluation. Based on the IRS score, staining intensity was graded into 4 categories of grade 0 (–) (IRS 0–3), grade 1 (+) (IRS 4–6), grade 2 (++) (IRS 7–9) or grade 3 (+++) (IRS 10–12; fig. 1a, b).

To evaluate E-cadherin expression, the immunostaining pattern in normal disease-free liver was used as a positive control. E-cadherin staining was observed at cell-cell borders of all epithelial cells in normal liver; discontinuous or negative membrane staining was defined as abnormal. The approximate intensity of E-cadherin staining in the membrane of each specimen was scored and arranged into three categories: equivalent staining intensity to that of normal hepatic cells was regarded as positive (+), recognizable albeit weaker staining than present in normal cells was classified as weak positive (±) and complete loss of staining was determined as negative (–) (fig. 1c, d).

The expression of cyclin D1 was categorized it as either positive (+) or negative (–). Cyclin D1 expression in cancer was classified as positive staining when more than 30% of tumor cells were positive in high intensity (fig. 1e, f). IHC staining was evaluated independently by two pathologists who were blinded to the patient profiles.

Statistics

Correlations between the expressions of VEGF, E-cadherin and cyclin D1, and clinicopathological features were evaluated using χ^2 tests or Fisher's exact tests. Disease-free survival (DFS) of the patients with each pattern of immunohistochemical staining was estimated using the Kaplan-Meier method and p value of the log-rank tests were calculated. Death was treated as censored at that time. To clarify the relationship between expression of each molecule and metastatic recurrence, we also verified the hazard ratios (HR) of emergence of recurrence within 2 years for each patient group, which were classified according to the intensity of immunohistochemical staining. HR and 95% confidence intervals (95% CI) were calculated with the Cox proportional hazards regression model and each analysis was performed so as to compare different groups (i.e. metastatic recurrence vs. multicentric recurrence, and multicentric recurrence vs. recurrence-free). p values <0.05 were considered statistically significant. The data were managed and analyzed using SAS software (version 9.1, SAS Institute Inc., Cary, N.C., USA).

Results

Correlation between VEGF Expression and Clinical Outcome

VEGF staining was primarily cytoplasmic (fig. 1a, b). The proportion of HCC exhibiting grade 2 or 3 expression of VEGF was significantly higher in patients with

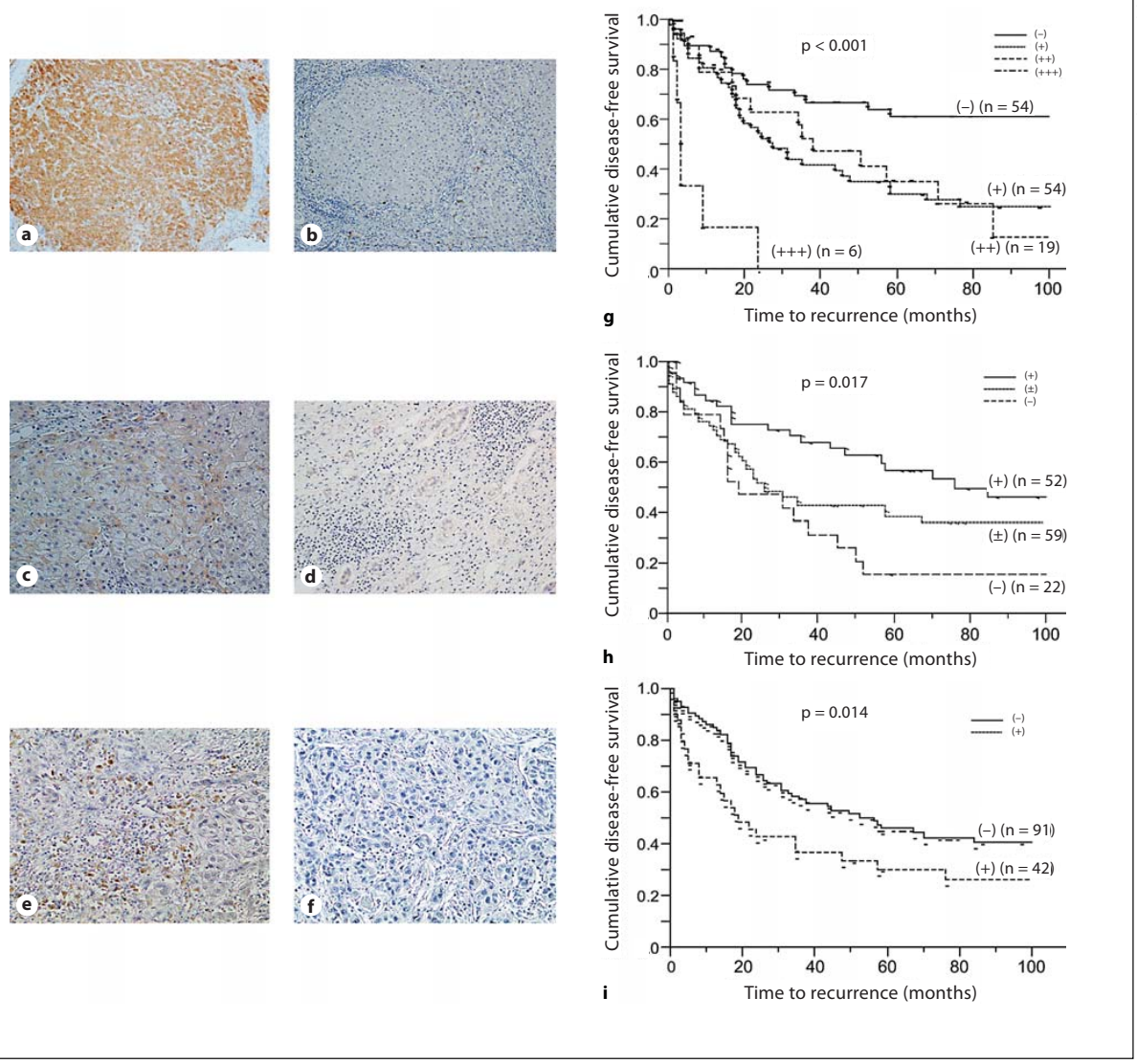

Color version available online

Fig. 1. Immunostaining with a VEGF antibody in HCCs with chronic hepatitis or early cirrhosis: grade 3 (+++) (**a**), negative (–) (**b**). Immunostaining with an E-cadherin antibody in HCCs with chronic hepatitis or early cirrhosis; E-cadherin was observed at cell-cell boundaries: positive (+) (**c**), negative (–) (**d**). Immunostaining with a cyclin D1 antibody in HCCs; cyclin D1 was primarily located in the nucleus: positive (+) (**e**), negative (–) (**f**). **a–f** Original magnification ×200. **g–i** Comparison of cumulative postoperative DFS curves according to intensity. VEGF expression in cancerous tissue (**g**), E-cadherin expression in cancerous tissue (**h**), cyclin D1 expression in cancerous tissue (**i**). Immunostaining intensity was evaluated by the Kaplan-Meier method. All patients with grade 3 (+++) expression of VEGF in cancerous tissues exhibited recurrence within 2 years. The group with grade 1 (+), grade 2 (++) or grade 3 (+++) expression of VEGF in cancerous tissues exhibited higher recurrence rates than those with negative (–) expression of VEGF ($p < 0.001$; log-rank). The group with negative (–) E-cadherin expression in cancerous tissues exhibited shorter periods of DFS than those with weak positive (±) or positive (+) expression. In accordance with reduced E-cadherin expression, the group with reduced E-cadherin expression exhibited higher recurrence rates than those with positive (+) expression of E-cadherin ($p = 0.017$; log-rank). The group with positive (+) expression of cyclin D1 in cancerous tissue exhibited higher recurrence rates than those with negative (–) expression of cyclin D1 ($p = 0.013$; log-rank).

Table 1. Univariate and multivariate analyses

Variable	Univariate			Multivariate		
	HR	95% CI	p	HR	95% CI	p
a *Factors associated with metastatic recurrence (metastatic recurrence vs. multicentric carcinoma and recurrence-free) using univariate and multivariate Cox proportional analysis*						
Platelet count, $10^3/mm^3$						
$\geq 10 \times 10^4$	1.00		–			
$<10 \times 10^4$	1.30	1.03–1.64	0.029			
VEGF expression in HCC tissue						
Negative	1.00		–			
Grade 1	1.54	1.17–2.08	0.002	1.57	1.18–2.13	0.002
Grade 2	1.51	1.05–2.14	0.027	1.52	1.05–2.17	0.027
Grade 3	3.54	2.10–5.60	<0.001	3.32	1.93–5.41	<0.001
E-cadherin expression in HCC tissue						
Positive	1.00		–			
Weak positive	1.29	0.99–1.70	0.056			
Negative	1.58	1.13–2.18	0.008			
Cyclin D1 expression in HCC tissue						
Negative	1.00		–			
Positive	1.34	1.05–1.69	0.019			
b *Factors associated with multicentric carcinoma (multicentric carcinoma vs. recurrence-free) using univariate and multivariate Cox proportional analysis*						
Hepatitis status						
Non-B non-C	1.00		–			
HCV	1.91	1.16–3.57	0.010	1.83	1.11–3.25	0.017
HBV	0.80	0.18–2.08	0.671			
Clinical stage						
I	1.00		–			
II	1.76	1.10–2.78	0.020			
ALT, IU/l						
≤80	1.00		–			
>80	1.58	1.03–2.45	0.035	1.59	1.03–2.48	0.037
Cyclin D1 expression in HCC tissue						
Negative	1.00		–			
Positive	1.46	1.11–1.39	0.18			

p values were calculated for continuous values by ANOVA and for categorical values for the χ^2 test or Fisher's exact test. The patients who had incomplete data were excluded. Non-B non-C denotes negative for HBsAg and HCVAb or HCV-RNA (–); HCV denotes positive for HCVAb or HCV-RNA; HBV denotes positive for HBsAg.

metastatic recurrence (27%; 20/74) than those with multicentric recurrence (9.1%; 2/22) or as recurrence-free (8.1%; 3/37; $p < 0.001$). Notably, all cases of grade 3 VEGF expression were observed exclusively in patients with metastatic recurrence (100%; 6/6).

Table 1 compares HR of metastatic versus multicentric recurrence and recurrence-free, and multicentric recurrence versus recurrence-free. These comparisons were made in relation to clinicopathological data from univariate and multivariate analyses, which were performed to evaluate variables that could affect metastatic recurrence or the emergence of multicentric recurrence after curative surgery. For the onset of metastatic recurrence, the extent of VEGF staining correlated significantly with an increased HR for grade 3 ($p < 0.001$, HR 3.54, 95% CI 2.10–5.60), grade 2 ($p = 0.027$, HR 1.51, 95% CI 1.05–2.14) and grade 1 ($p = 0.002$, HR 1.54, 95% CI 1.17–2.08) by univariate analysis. Multivariate analysis comparing between metastatic recurrence and multicentric recurrence and recurrence-free revealed significantly elevated risk of metastatic recurrence for each grade of VEGF expression (grade 1: $p = 0.002$, HR 1.57, 95% CI 1.18–2.13; grade 2:

p = 0.027, HR 1.52, 95% CI 1.05–2.17; grade 3: $p < 0.001$, HR 3.32, 95% CI 1.93–5.41; table 1); however, no significant relationship existed between VEGF expression and multicentric recurrence.

Correlation between E-Cadherin Expression and Clinical Outcome

E-cadherin staining was detected at the cell-cell boundary (fig. 1c, d). Negative E-cadherin expression was observed more frequently in patients with metastatic recurrence (21.6%; 16/74) than in patients with multicentric recurrence (4.5%; 1/22) or recurrence-free (13.5%; 5/37). According to univariate analysis, negative E-cadherin expression indicated increased risk for metastatic recurrence (p = 0.008, HR 1.58, 95% CI 1.13–2.18; table 1). However, no significant relationship existed between metastatic recurrence and E-cadherin expression by multivariate analysis. Moreover, there was no significant relationship between E-cadherin expression and multicentric recurrence.

Correlation between Cyclin D1 Expression and Clinical Outcome

Cyclin D1 staining was observed primarily in the nucleus (fig. 1e, f). The positive rate was higher in patients with metastatic recurrence (36.5%; 27/74) than for patients with multicentric recurrence (13.6%; 3/22) or recurrence (32.4%; 12/37), although this was not significant. Univariate analysis demonstrated that expression of cyclin D1 correlated with metastatic recurrence (p = 0.019, HR 1.34, 95% CI 1.05–1.69); however, multivariate analysis did not demonstrate a correlation between cyclin D1 expression and metastatic recurrence or multicentric carcinoma (table 1).

Clinical Features of the Patients and Outcome

For metastatic recurrence, low platelet count ($<10 \times 10^4$) was revealed to be the significant correlation in univariate analysis (p = 0.029, HR 1.30, 95% CI 1.03–1.64) but not in multivariate analysis. For multicentric recurrence, positivity for HCV (p = 0.010, HR 1.91, 95% CI 1.16–3.57), advanced clinical stage of HCC (p = 0.020, HR 1.76, 95% CI 1.10–2.78) and serum ALT level (>80; p = 0.035, HR 1.58, 95% CI 1.03–2.45) were revealed as the significant relationships by univariate analysis, and the presence of HCV and serum ALT level were selected as independent factors for emergence of multicentric recurrence by multivariate analysis (p = 0.017, HR 1.83, 95% CI 1.11–3.25 and p = 0.037, HR 1.59, 95% CI 1.03–2.48, respectively; table 1).

DFS, Expression of VEGF, E-Cadherin and Cyclin D1

The median duration of DFS in patients with multicentric recurrence was significantly longer (87.3 ± 56.7 months) than in patients with metastatic recurrence (22.9 ± 20.5 months; $p < 0.001$). The recurrence rate was positively correlated with the extent of VEGF expression ($p < 0.001$; fig. 1g). Notably, all patients with grade 3 VEGF expression occurred recurrence within 2 years and HR of recurrence within 2 years was much higher in grade 3 VEGF expression than the other groups ($p < 0.001$, HR 3.20, 95% CI 1.87–5.17).

Negative or weak E-cadherin expression correlated with shorter periods of DFS, the recurrence rate correlated negatively with the extent of E-cadherin expression (p = 0.017; fig. 1h). Moreover, HRs of recurrence within 2 years for negative as well as weak E-cadherin expression were higher than the normal expression group ($p < 0.040$, HR 1.57, 95% CI 1.01–2.42 and $p < 0.02$, HR 1.46, 95% CI 1.04–2.11, respectively). Additionally, positive cyclin D1 expression was correlated with a high rate of recurrence (p = 0.014; fig. 1i). HR of recurrence within 2 years for patients with positive cyclin D1 expression was higher than the other groups ($p < 0.005$, HR 1.51, 95% CI 1.13–2.01).

Discussion

Our results confirm the findings of prior studies that evaluated the prognostic value of measuring the expression of cancer-related genes, such as VEGF in HCC [15, 16]. We compared the significance of expression of VEGF, E-cadherin and cyclin D1 on the risk of HCC recurrence after curative resection using immunohistochemical analyses. We found that the extent of VEGF expression in HCC provides the important prognostic information that can be used to evaluate the risk of metastasis following curative hepatic surgery. An interesting dosage-effect of VEGF expression was identified in which HCC patients with grade 3 expression demonstrated the shortest periods of DFS (fig. 1g), which reinforced the notion that angiogenesis plays a pivotal role in metastasis. It is known that metastatic recurrence is early-phase recurrence (within 2 years), whereas those associated with multicentric recurrence contributed to late-phase recurrence (after 2 years) [17], which was consistent with the fact that VEGF expression was associated with metastatic recurrence.

We also found that E-cadherin (reduced expression) and cyclin D1 expression in HCC correlated with metastatic recurrence (table 1). Recent studies suggest that the loss of E-cadherin expression in HCC plays an important role for metastasis by inducing an epithelial-to-mesenchymal transition and disrupting intercellular contacts [18]. Gene expression analysis has also revealed that the loss of E-cadherin contributes to metastatic dissemination by inducing wide-ranging transcriptional and functional changes [19]. On the other hand, overexpression of cyclin D1 reportedly associates with aggressive forms of HCC [20]. Our results suggest that positive expression of cyclin D1 confers an additional growth advantage to the tumor by disrupting cell cycle checkpoints.

Here we have demonstrated the utility of immunohistochemical profiling of VEGF expression in HCC as a predictive biomarker in patients who undergo curative HCC resection. Such analyses can theoretically be performed preoperatively to identify patients most likely to benefit from curative resection. These findings could become important in planning strategies to prevent or reduce HCC recurrence after surgical resection. Recently it has been shown that the treatments to prevent recurrence (including intrahepatic metastasis and multicentric carcinogenesis) are extremely effective for improving the prognosis of HCC patients. For instance, the molecular targeted agent sorafenib, multikinase inhibitors and VEGF inhibitors, significantly prolonged the survival of patients with advanced HCC [21]. Furthermore, another article reported an antibody against placental growth factor (PlGF), a VEGF homolog, which regulates the angiogenic switched in disease, but not in health. αPlGF inhibited growth and metastasis of various tumors [22]. Predicting the recurrence earlier should be important for prolonged prognosis owing to these agents. The IHC expression profiles using HCC tissue revealed high-risk patterns of metastatic recurrence. The results of the current study will contribute to the development of comprehensive adjuvant prevention strategies for postoperative management of HCC.

Disclosure Statement

The authors have no competing interests to declare. This work was supported in part by a grant from the Smoking Research Foundation.

References

1 Zhou XD, Tang ZY, Yang BH, Lin ZY, Ma ZC, Ye SL, Wu ZQ, Fan J, Qin LX, Zheng BH: Experience of 1,000 patients who underwent hepatectomy for small hepatocellular carcinoma. Cancer 2001;91:1479–1486.

2 Nathan H, Schulick RD, Choti MA, Pawlik TM: Predictors of survival after resection of early hepatocellular carcinoma. Ann Surg 2009;249:799–805.

3 Belghiti J, Fuks D: Liver resection and transplantation in hepatocellular carcinoma. Liver Cancer 2012;2:71–82.

4 Nishikawa H, Inuzuka T, Takeda H: Comparison of percutaneous radiofrequency thermal ablation and surgical resection for small hepatocellular carcinoma. BMC Gastroenterol 2011;28:143–154.

5 Choi GH, Kim DH, Kang CM, Kim KS, Choi JS, Lee WJ, Kim BR: Prognostic factors and optimal treatment strategy for intrahepatic nodular recurrence after curative resection of hepatocellular carcinoma. Ann Surg Oncol 2008;15:618–629.

6 Nanashima A, Tobinaga S, Abo T, Kunizaki M, Takeshita H, Hidaka S, Taura N, Ichikawa T, Sawai T, Nakao K, Nagayasu T: Usefulness of sonazoid-ultrasonography during hepatectomy in patients with liver tumors: a preliminary study. J Surg Oncol 2011;103:152–157.

7 Okuda K: Hepatocellular carcinoma: recent progress. Hepatology 1992;15:948–963.

8 Poon RT, Lau CP, Ho JW, Yu WC, Fan ST, Wong J: Tissue factor expression correlates with tumor angiogenesis and invasiveness in human hepatocellular carcinoma. Clin Cancer Res 2003;9:5339–5345.

9 Shibuya M: Vascular endothelial growth factor receptor-1 (VEGFR-1/Flt-1): a dual regulator for angiogenesis. Angiogenesis 2006;9:225–231.

10 Hirohashi S: Inactivation of the E-cadherin-mediated cell adhesion system in human cancers. Am J Pathol 1998;153:333–339.

11 Liver cancer study group of Japan: The general rules for the clinical and pathological study of primary liver cancer. Jpn J Surg 1989;19:98–129.

12 Ikeda K, Arase Y, Kobayashi M, Saitoh S, Someya T, Hosaka T, Suzuki Y, Suzuki F, Tsubota A, Akuta N, Kumada H: Significance of multicentric cancer recurrence after potentially curative ablation of hepatocellular carcinoma: a longterm cohort study of 892 patients with viral cirrhosis. J Gastroenterol 2003;38:865–876.

13 Chui X, Egami H, Yamashita J, Kurizaki T, Ohmachi H, Yamamoto S, Ogawa M: Immunohistochemical expression of the c-kit proto-oncogene product in human malignant and non-malignant breast tissues. Br J Cancer 1996;73:1233–1236.

14 Friedrichs K, Gluba S, Eidtmann H, Jonat W: Overexpression of p53 and prognosis in breast cancer. Cancer 1993;72:3641–3647.

15 Yang JC, Teng CF, Wu HC, Tsai HW, Chuang HC, Tsai TF, Hsu YH, Huang W, Wu LW, Su IJ: Enhanced expression of vascular endothelial growth factor-A in ground glass hepatocytes and its implication in hepatitis B virus hepatocarcinogenesis. Hepatology 2009;49:1962–1971.

16 Schoenleber SJ, Kurtz DM, Talwalkar JA, Roberts LR, Gores GJ: Prognostic role of vascular endothelial growth factor in hepatocellular carcinoma: systematic review and meta-analysis. Br J Cancer 2009;100:1385–1392.
17 Imamura H, Matsuyama Y, Tanaka E, Ohkubo T, Hasegawa K, Miyagawa S, Sugawara Y, Minagawa M, Takayama T, Kawasaki S, Makuuchi M: Risk factors contributing to early and late phase intrahepatic recurrence of hepatocellular carcinoma after hepatectomy. J Hepatol 2003;38:200–207.
18 Schmalhofer O, Brabletz S, Brabletz T: E-cadherin, β-catenin, and ZEB1 in malignant progression of cancer. Cancer Metastasis Rev 2009;28:151–166.
19 Onder TT, Gupta PB, Mani SA, Yang J, Lander ES, Weinberg RA: Loss of E-cadherin promotes metastasis via multiple downstream transcriptional pathways. Cancer Res 2008;68:3645–3654.
20 Nishida N, Fukuda Y, Komeda T, Kita R, Sando T, Furukawa M, Amenomori M, Shibagaki I, Nakao K, Ikenaga M, et al: Amplification and overexpression of the cyclin D1 gene in aggressive human hepatocellular carcinoma. Cancer Res 1994;54:3107–3110.
21 Kudo M: Adjuvant therapy after curative treatment for hepatocellular carcinoma. Oncology 2011;81(suppl 1):50–55.
22 Fischer C, Jonckx B, Mazzone M, Zacchigna S, Loges S, Pattarini L, Chorianopoulos E, Liesenborghs L, Koch M, De Mol M, Autiero M, Wyns S, Plaisance S, Moons L, van Rooijen N, Giacca M, Stassen JM, Dewerchin M, Collen D, Carmeliet P: Anti-PlGF inhibits growth of VEGF(R)-inhibitor-resistant tumors without affecting healthy vessels. Cell 2007;131:463–475.

Oncology

Oncology 2013;84(suppl 1):82–87
DOI: 10.1159/000345895

Published online: February 20, 2013

Quantification of Tumor DNA in Serum and Vascular Invasion of Human Hepatocellular Carcinoma

Naoshi Nishida[a, b] Tadaaki Arizumi[a] Masahiro Takita[a] Tomoyuki Nagai[a] Satoshi Kitai[a] Norihisa Yada[a] Satoru Hagiwara[a] Tatsuo Inoue[a] Yasunori Minami[a] Kazuomi Ueshima[a] Toshiharu Sakurai[a] Hiroshi Ida[b] Masatoshi Kudo[a]

[a]Department of Gastroenterology and Hepatology, Kinki University Faculty of Medicine, Osakasayama, and
[b]Department of Gastroenterology and Hepatology, Kyoto University Graduate School of Medicine, Kyoto, Japan

Key Words
Hepatocellular carcinoma · Tumor suppressor gene · DNA methylation · Epigenetics · Molecular diagnosis

Abstract
Objectives: Hepatocellular carcinoma (HCC) is one of the common cancers worldwide. Accurate diagnosis of tumor progression is critical for the appropriate management of HCC. Here, we established a sensitive assay to detect and quantify tumor-derived DNA in the serum of HCC patients. ***Methods:*** Aberrant methylation of the *APC* gene was quantified in 23 HCC patients and 8 healthy volunteers using 100 μl of serum. For sensitive detection and accurate quantification of tumor DNA, we combined seminested polymerase chain reaction (PCR) with TaqMan PCR, which could amplify the *APC* gene regardless of the methylation status and detect the methylated and unmethylated sequences separately. The ratio of methylated to unmethylated sequences was quantified. ***Results:*** The methylated *APC* gene was detected in all HCC patients examined, but no healthy volunteers showed amplification of methylated sequences in serum. HCC patients with portal vein thrombosis showed a significantly higher methylated to unmethylated *APC* gene ratio in serum than those without portal vein thrombosis ($p = 0.0029$). ***Conclusions:*** Considering the strong association between the ratio of the methylated to unmethylated *APC* sequences in serum and the presence of portal vein thrombosis, methylation status of *APC* sequences could be a promising marker for improving HCC management.

Introduction

Hepatocellular carcinoma (HCC) is one of the most common cancers in the world, and infection with hepatitis B virus or hepatitis C virus is a critical risk for the emergence of this type of malignancy. The number of HCC patients is expected to increase after recent studies revealed that several types of common metabolic disorder such as diabetes mellitus and obesity could also act as important factors for accelerating HCC development [1]. Surgical treatment [2], radiofrequency ablation [3] and trance catheter arterial chemoembolization [4] are well-known major treatment options; however, the prognosis of advanced HCC is unsatisfactory because of the lack of effective therapeutic alternatives [1].

KARGER

Fax +41 61 306 12 34
E-Mail karger@karger.com
www.karger.com

0030–2414/13/0847–0082$38.00/0

Accessible online at:
www.karger.com/ocl

Naoshi Nishida, MD
Department of Gastroenterology and Hepatology
Kinki University Faculty of Medicine
377-2 Ohno-higashi, Osakasayama, Osaka 589-8511 (Japan)
E-Mail naoshi@med.kindai.ac.jp

Recent advancements in the study of molecular targeted agents such as sorafenib have resulted in improved survival rates of patients with advanced HCC and increased time to progression, even in cases that failed to achieve tumor regression [5]. However, estimation of this type of tumor response, or response to 'dormant therapy', is sometimes difficult because the lack of tumor regression identified through imaging studies could be regarded as treatment failure, even in cases of stable disease with prolonged time to progression, which could be a benefit of treatment with sorafenib. Imaging studies are also inadequate for estimating a total tumor burden because the advanced tumors are usually associated with multiple small metastatic lesions. Therefore, in addition to imaging studies, conventional tumor markers such as α-fetoproteins (AFP) and des-γ-carboxy prothrombin (DCP) have been examined to evaluate the dynamics of tumor volume during treatment [6]. Although a combination of AFP and DCP reportedly improved the sensitivity of diagnosing HCC, a considerable number of HCC patients failed to show an increase in tumor marker levels [7]. In these patients, conventional tumor markers were not useful for the estimation of tumor response during the course of HCC treatment.

Generally, the molecular pathogenesis of cancer development involves multiple genetic and epigenetic aberrations, which lead to activation of oncogenes and inactivation of tumor suppressor genes (TSGs) [8]. Recent reports have suggested that quantification of circulating mutant genes from tumor cells could be useful in assessing the tumor dynamics of colon cancer during treatment and that this personalized genetic approach could be generally applied to patients with other types of cancer [9]. So far, we have intensively analyzed genetic and epigenetic alterations in oncogenes and TSGs in human HCC tissues [10–13]. Although recurrent genetic alterations of individual genes are not frequent, epigenetic alterations such as methylation of the promoter of TSGs occur far more frequently. In particular, we found that abnormal methylation of the promoter of the adenomatous polyposis coli *(APC)* gene was seen in a majority of HCC tissues, and the methylation level of the *APC* gene was considerably different between HCC tissue and the corresponding noncancerous liver tissue [14].

In this study, we developed a sensitive assay for the quantification of cancer-specific DNA in serum of HCC patients, based on the methylated *APC* gene. We explored the possible diagnostic value of this tumor-specific DNA alteration for tumor detection. We found the amount of the methylated *APC* gene in serum to be strongly correlated with vascular invasion of HCC. In addition, quantification of this epigenetic alteration could be a powerful tool to estimate the aggressiveness of the tumor as well as tumor dynamics during the treatment of HCC.

Materials and Methods

Patients

Twenty-three HCC patients and 8 healthy volunteers were analyzed to quantify promoter methylation of the *APC* gene using serum DNA. The clinical backgrounds of the HCC patients were as follows: median age was 71 years (25th and 75th percentiles: 66 and 73); 14 were male and 9 were female, and 4 were hepatitis B virus surface antigen (HBsAg) positive, 13 were hepatitis C virus antibody (HCVAb) positive, 2 were positive for both HBsAg and HCVAb, and 4 were negative for both. Among 23 patients, 7 showed portal vein invasion and 19 showed multiple HCCs (2 or more) on contrast enhanced-computed tomography. Three HCC patients were classified as stage 1, 2 as stage 2, 11 as stage 3 and 7 as stage 4. Median serum AFP and DCP levels were 76 ng/ml (25th and 75th percentiles: 21 and 778) and 307 mAU/ml (25 and 1,169), respectively. Informed consent was obtained from each patient and the study was approved by the institutional review board of the involved institution.

Quantification of Methylation Levels in Serum DNA

DNA was extracted from 100 μl of serum using the DNA Extractor SP Kit according to the manufacturer's protocol (Wako Pure Chemical Industries Ltd., Osaka, Japan). The serum DNA samples were subjected to bisulfite treatment using the EpiTect™ Bisulfite kit (QIAGEN Inc., Valencia, Calif., USA). We selected the methylated *APC* gene as a target for the detection of tumor DNA because our previous analysis indicated aberrant methylation of the *APC* gene in 84% of HCC cases [14, 15]. In addition, the difference in the methylation level between HCC and noncancerous liver tissues was most prominent in the promoter of the *APC* gene among the CpG loci examined. HCC tissues showed a high level of methylation, but methylation was extremely low in noncancerous tissues [14, 15]. Thus, the methylation level of this gene made it an ideal candidate for quantification of tumor-derived DNA in serum of HCC patients in the context of minimizing false-positive and false-negative errors. For the quantification of methylated *APC* genes, the ratio of amount of the methylated to unmethylated *APC* gene was determined using the StepOne™ real-time detection system (Applied Biosystems, Foster City, Calif., USA). In order to increase the sensitivity for detecting small amounts of methylated DNA, we used semi-nested PCR with setting TaqMan probes for the detection of inner PCR products that are specific for the methylated or unmethylated *APC* gene (fig. 1a). These primers and probes were designed to amplify the promoter of the *APC* gene. The PCR primers and probes used in this assay were as follows: forward outer PCR primer, 5′-GGTTATGTGTGTTTATATTTAGTTAATTGGTG-3′ and reverse outer PCR primer, 5′-AAATACAAACCAAAACACTCCCC-3′. The inner forward nested-PCR primer and TaqMan probe for detecting the methylated *APC* gene pro-

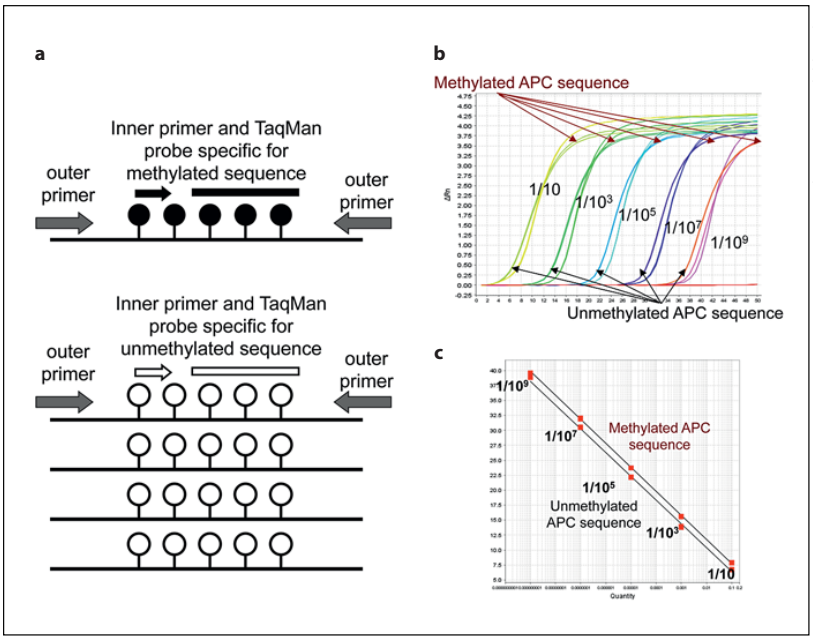

Color version available online

Fig. 1. Sensitive detection and quantification of the ratio of methylated to unmethylated *APC* genes. **a** Heminested PCR for the methylated and unmethylated *APC* genes. Using outer primers, which do not contain a CpG site, the *APC* gene was amplified regardless of methylation status. However, methylated and unmethylated *APC* genes can be detected separately by using the inner heminested primer and TaqMan probe specific for the methylated and unmethylated sequences, respectively. A filled circle and an empty circle represent a methylated and unmethylated CpG site, respectively. Amplification curve (**b**) and standard curve (**c**) for PCR of the methylated and unmethylated *APC* genes; the efficiency of PCR amplification of the methylated and unmethylated *APC* genes was almost equal.

moter were 5′-TTATATGTCGGTTACGTGCGTTTATAT-3′ and FAM-CCCGTCGAAAACCCGCCGATTA-MBG, respectively. The inner PCR forward primer and TaqMan probe specific for the unmethylated promoter were 5′-GGTTATGTGTGTTTATA-TTTAGTTAATTGGTG-3′ and FAM-TTCCCATCAAAAAC-MGB, respectively. We expected that both methylated and unmethylated promoters would be equally amplified on using the outer primer pairs, which do not contain the CpG sequence. However, the methylated and unmethylated promoters would be quantified separately on using the specific inner primer pairs and TaqMan probes for methylated or unmethylated DNA (fig. 1a). The PCR was performed according to the manufacturer's protocol using TaqMan® Fast Universal PCR Master Mix (Applied Biosystems). A standard curve for each assay was generated by the serial dilution of bisulfite-treated CpGenome™ Universal Methylated DNA (Chemicon International Inc., Temecula, Calif., USA). The ratio of amount of the methylated to unmethylated *APC* gene was calculated using the StepOne™ real-time detection system (Applied Biosystems).

Statistical Analysis

The Wilcoxon rank-sum test was applied to compare the differences in the ratio of methylated to unmethylated *APC* gene levels between any 2 categorical variables of clinical factors. Continuous variables such as age, serum AFP levels and serum DCP levels were each categorized into 2 subgroups: <70 or ≥70 years, <100 or ≥100 ng/ml, and <400 or >400 mAU/ml, respectively. All p values were two-sided and $p < 0.05$ was considered statistically significant. All statistical analyses were performed using JMP version 9.0 software (SAS Institute Inc., Cary, N.C., USA).

Results

Amplification of the Methylated and Unmethylated APC Genes

Using the sensitive assay, a combined seminested and real-time PCR-detection system, we successfully amplified both the methylated and unmethylated *APC* gene from serum DNA. Figure 1b, c shows the amplification and standard curve of the methylated and unmethylated gene products, respectively. The 2 standard curves for the amplification of the methylated and unmethylated genes revealed that amplification efficiency should be similar for the 2 heminested PCR products of the methylated and unmethylated genes. The serum DNA of 8 healthy volunteers showed amplification of the unmethylated gene, but no amplification of the methylated gene. In contrast, serum DNA samples from all 23 HCC patients showed amplification of the methylated as well as the unmethylated gene, and we were able to calculate the ratio of methylated to unmethylated DNA in 20 of 23 samples. The mean value was 9% (25th and 75th percentiles: 8.0 and 18.8%). For 3 of 23 serum DNA samples, the ratio of methylated to unmethylated DNA could not be determined because of the low level (less than 1%) of the methylated APC allele.

Table 1. Association between the ratio of the methylated to unmethylated *APC* gene in serum DNA and clinical background of HCC patients

Clinical background (number of cases)	Mean ratio, % (25–75th percentiles)	p value
Age		
<70 years (10)	11 (7–18.25)	0.2256
≥70 years (10)	5.5 (3.75–23.5)	
Gender		
Male (11)	11 (7–18)	0.2697
Female (9)	5 (3.5–23)	
Viral status		
HBV (4)	21 (11.25–27)	0.2626
HCV (11)	7 (4–19)	
HBV and HCV (2)	8 (5–11)	
Virus negative (3)	7 (2–13)	
Tumors, n		
<2 (4)	11 (5.5–25)	0.3066
≥2 (16)	8 (4.5–18.25)	
Maximal tumor size		
<3 cm (10)	9 (6.25–12.5)	1.0000
≥3 cm (10)	9 (4.25–21.25)	
Portal vein thrombosis		
Presence (7)	19 (11–28)	0.0029*
Absence (13)	6 (4–10)	
Serum AFP level		
<100 ng/ml (8)	7 (3.25–10.5)	0.1527
≥100 ng/ml (12)	12 (6.25–21.25)	
Serum DCP level		
<400 mAU/ml (11)	9 (5–22)	0.7320
≥400 mAU/ml (9)	7 (5–2)	

Three patients who showed a ratio of less than 1% were excluded from the analysis. Continuous variables of age, serum AFP and DCP level were categorized into two subgroups of <70 or ≥70 years, <100 or ≥100 ng/ml, and <400 or ≥400 mAU/ml, respectively. p values calculated by the Wilcoxon rank-sum test. * $p < 0.05$.

Relationship between the Ratio of Methylated to Unmethylated Gene Sequences and Clinical Backgrounds of HCC Patients

Table 1 shows the relationship between the ratio of the methylated to unmethylated *APC* genes in serum and the clinical background of each HCC patient. Clinical background variables such as age, gender and status of hepatitis virus were not associated with this ratio. In addition, no significant association was noted between the levels of conventional tumor markers AFP and DCP and the degree of the methylated *APC* gene. In contrast, although the factors of tumor size and number did not affect the ratio of the methylated to unmethylated genes, HCC patients with portal vein thrombosis showed a significantly higher degree of the methylated *APC* gene in serum DNA ($p = 0.0029$ by the Wilcoxon rank-sum test; table 1). The mean values of the ratio of methylated to unmethylated genes in patients with and without portal vein thrombosis were 19% (25th and 75th percentiles: 11 and 28%) and 6% (4 and 10%), respectively (table 1).

Discussion

HCC is one of the most common malignancies worldwide, and the overall prevalence of the at-risk population is still growing. Although the definitive molecular pathogenesis of HCC still needs to be clarified, several reports describe different forms of genetic and epigenetic alterations in HCC [8]. Recent genome-wide analysis of human HCC tissues revealed that a variety of genes harbored several types of genetic alterations; however, the frequency of alteration types in individual cancer-related genes was low compared with epigenetic changes such as promoter methylation of TSGs [8, 16]. Therefore, we hypothesized that the evolution and progression of this disease may involve epigenetic alterations, which could be a target for the detection of tumor DNA in serum.

So far, many studies have tried to detect tumor-associated aberrant methylation of TSGs in the circulation of patients with HCC. Wong et al. [17] reported that the methylated *CDKN2A* sequence was found in the serum of HCC patients, and that methylation was evident in the *CDKN2A* gene in the tumor. More recently, it was reported that the quantification of tumor-specific methylated genes in the serum of HCC patients could be applied to predict disease-free survival after hepatectomy [18], and as a valuable biomarker for early detection in populations at high risk of HCC [19]. These results suggest that circulating tumor-derived DNA could be detected using tumor-associated DNA methylation changes and that this approach may have implications for the noninvasive detection of HCCs as well as the prediction of aggressive tumor behavior.

Treatment of advanced HCC is still unsatisfactory because of high tumor recurrence rates. In particular, invasion into the portal vein is a characteristic feature of advanced HCC, which limits treatment options. However, advances in molecular targeted therapy, such as the use of sorafenib, can possibly play an important role in the treatment of this refractory tumor, especially a tumor with metastasis or portal vein thrombosis [5]. Predictive biomarkers for sorafenib treatment are still undetermined, making early detection of vascular invasion criti-

cal in determining the timing of the administration of sorafenib [20]. Consequently, the results obtained from our study are clinically important because we found a significant association between increase of methylated *APC* gene in serum and the presence of portal vein thrombosis. As tumor-derived DNA in serum should be a result of the moving out of DNA from HCC tissue to circulation [9], the results of this study are reasonable; high levels of methylated sequences of tumor DNA were observed in HCC patients, especially in those with vascular invasion. In addition, the results indicated that the ratio of methylated to unmethylated DNA did not significantly correlate with the levels of other conventional tumor markers such as AFP and DCP. Because these conventional markers are also associated with tumor growth [6], the combination of tumor-derived methylated DNA measurement and AFP and DCP level evaluation could provide a powerful tool for early detection and prediction of portal vein thrombosis in HCC patients [21]. This information can be applied to HCC management in the context of treatment selection [20]. Furthermore, measurements of circulating tumor DNA can possibly be applied to reliably monitor tumor dynamics in patients undergoing cancer therapy [18]. Reduction in tumor-derived DNA levels occurred faster than the reduction in conventional tumor marker levels after effective treatment [9], so we concluded that the measurement of circulating tumor DNA, such as the methylated *APC* sequence, in the serum of HCC patients could be critical for early determination of therapy effectiveness [22]. This is of importance because the establishment of second-line therapy for refractory HCC cases is currently under investigation.

In this study, we established a novel assay for the sensitive detection and quantification of tumor-derived DNA in the peripheral blood of HCC patients based on the aberrant methylation of the *APC* gene. We successfully quantified tumor DNA in the peripheral blood of these patients using small amounts of serum. Our previous study revealed that methylation of the *APC* gene was detected in a majority of HCC cases and could discriminate HCC from noncancerous liver tissue. Therefore, the methylated *APC* sequence is an ideal target for the detection of tumorous DNA in peripheral blood. Considering the strong association between the ratio of methylated to unmethylated *APC* sequences in serum and the presence of portal vein thrombosis in HCC, quantification of the methylated sequence of the *APC* gene could be a promising approach for the management of advanced HCC.

Disclosure Statement

The authors have no competing interests to declare. This work was supported in part by a grant from the Smoking Research Foundation.

References

1 Kim DY, Han K-H: Epidemiology and surveillance of hepatocellular carcinoma. Liver Cancer 2012;1:2–14.
2 Belghiti J, Fuks D: Liver resection and transplantation in hepatocellular carcinoma. Liver Cancer 2012;1:71–82.
3 Kuang M, Wang Y, Jiang C, Xie XY, Lu MD: A precise safety margin of 1.0 cm is required for best local efficacy of radiofrequency ablation of hepatocellular carcinoma: assessment with a novel three dimensional reconstruction software. Liver Cancer 2012;1:125.
4 Lencioni R: Chemoembolization in patients with hepatocellular carcinoma. Liver Cancer 2012;1:41–50.
5 Llovet JM, Ricci S, Mazzaferro V, Hilgard P, Gane E, Blanc JF, de Oliveira AC, Santoro A, Raoul JL, Forner A, Schwartz M, Porta C, Zeuzem S, Bolondi L, Greten TF, Galle PR, Seitz JF, Borbath I, Haussinger D, Giannaris T, Shan M, Moscovici M, Voliotis D, Bruix J: Sorafenib in advanced hepatocellular carcinoma. N Engl J Med 2008;359:378–390.
6 Koike Y, Shiratori Y, Sato S, Obi S, Teratani T, Imamura M, Yoshida H, Shiina S, Omata M: Des-gamma-carboxy prothrombin as a useful predisposing factor for the development of portal venous invasion in patients with hepatocellular carcinoma: a prospective analysis of 227 patients. Cancer 2001;91:561–569.
7 Lok AS, Sterling RK, Everhart JE, Wright EC, Hoefs JC, Di Bisceglie AM, Morgan TR, Kim HY, Lee WM, Bonkovsky HL, Dienstag JL: Des-γ-carboxy prothrombin and α-fetoprotein as biomarkers for the early detection of hepatocellular carcinoma. Gastroenterology 2010;138:493–502.
8 Nishida N, Goel A: Genetic and epigenetic signatures in human hepatocellular carcinoma: a systematic review. Curr Genomics 2011;12:130–137.
9 Diehl F, Schmidt K, Choti MA, Romans K, Goodman S, Li M, Thornton K, Agrawal N, Sokoll L, Szabo SA, Kinzler KW, Vogelstein B, Diaz LA Jr: Circulating mutant DNA to assess tumor dynamics. Nat Med 2008;14:985–990.
10 Nishida N, Fukuda Y, Kokuryu H, Toguchida J, Yandell DW, Ikenega M, Imura H, Ishizaki K: Role and mutational heterogeneity of the p53 gene in hepatocellular carcinoma. Cancer Res 1993;53:368–372.
11 Nishida N, Fukuda Y, Komeda T, Kita R, Sando T, Furukawa M, Amenomori M, Shibagaki I, Nakao K, Ikenaga M, et al: Amplification and overexpression of the cyclin d1 gene in aggressive human hepatocellular carcinoma. Cancer Res 1994;54:3107–3110.
12 Nishida N: Impact of hepatitis virus and aging on DNA methylation in human hepatocarcinogenesis. Histol Histopathol 2010;25:647–654.
13 Nishida N, Kudo M, Nagasaka T, Ikai I, Goel A: Characteristic patterns of altered DNA methylation predict emergence of human hepatocellular carcinoma. Hepatology 2012;56:994–1003.

14 Nishida N, Nagasaka T, Nishimura T, Ikai I, Boland CR, Goel A: Aberrant methylation of multiple tumor suppressor genes in aging liver, chronic hepatitis, and hepatocellular carcinoma. Hepatology 2008;47:908–918.
15 Nishida N, Nishimura T, Nagasaka T, Ikai I, Goel A, Boland CR: Extensive methylation is associated with beta-catenin mutations in hepatocellular carcinoma: evidence for two distinct pathways of human hepatocarcinogenesis. Cancer Res 2007;67:4586–4594.
16 Fujimoto A, Totoki Y, Abe T, Boroevich KA, Hosoda F, Nguyen HH, Aoki M, Hosono N, Kubo M, Miya F, Arai Y, Takahashi H, Shirakihara T, Nagasaki M, Shibuya T, Nakano K, Watanabe-Makino K, Tanaka H, Nakamura H, Kusuda J, Ojima H, Shimada K, Okusaka T, Ueno M, Shigekawa Y, Kawakami Y, Arihiro K, Ohdan H, Gotoh K, Ishikawa O, Ariizumi S, Yamamoto M, Yamada T, Chayama K, Kosuge T, Yamaue H, Kamatani N, Miyano S, Nakagama H, Nakamura Y, Tsunoda T, Shibata T, Nakagawa H: Whole-genome sequencing of liver cancers identifies etiological influences on mutation patterns and recurrent mutations in chromatin regulators. Nat Genet 2012;44:760–764.
17 Wong IH, Lo YM, Zhang J, Liew CT, Ng MH, Wong N, Lai PB, Lau WY, Hjelm NM, Johnson PJ: Detection of aberrant p16 methylation in the plasma and serum of liver cancer patients. Cancer Res 1999;59:71–73.
18 Wong IH, Zhang J, Lai PB, Lau WY, Lo YM: Quantitative analysis of tumor-derived methylated *p16ink4a* sequences in plasma, serum, and blood cells of hepatocellular carcinoma patients. Clin Cancer Res 2003;9:1047–1052.
19 Zhang YJ, Wu HC, Shen J, Ahsan H, Tsai WY, Yang HI, Wang LY, Chen SY, Chen CJ, Santella RM: Predicting hepatocellular carcinoma by detection of aberrant promoter methylation in serum DNA. Clin Cancer Res 2007;13:2378–2384.
20 Llovet JM, Pena CE, Lathia CD, Shan M, Meinhardt G, Bruix J: Plasma biomarkers as predictors of outcome in patients with advanced hepatocellular carcinoma. Clin Cancer Res 2012;18:2290–2300.
21 Iizuka N, Oka M, Sakaida I, Moribe T, Miura T, Kimura N, Tamatsukuri S, Ishitsuka H, Uchida K, Terai S, Yamashita S, Okita K, Sakata K, Karino Y, Toyota J, Ando E, Ide T, Sata M, Tsunedomi R, Tsutsui M, Iida M, Tokuhisa Y, Sakamoto K, Tamesa T, Fujita Y, Hamamoto Y: Efficient detection of hepatocellular carcinoma by a hybrid blood test of epigenetic and classical protein markers. Clin Chim Acta 2011;412:152–158.
22 Kawakami K, Brabender J, Lord RV, Groshen S, Greenwald BD, Krasna MJ, Yin J, Fleisher AS, Abraham JM, Beer DG, Sidransky D, Huss HT, Demeester TR, Eads C, Laird PW, Ilson DH, Kelsen DP, Harpole D, Moore MB, Danenberg KD, Danenberg PV, Meltzer SJ: Hypermethylated APC DNA in plasma and prognosis of patients with esophageal adenocarcinoma. J Natl Cancer Inst 2000;92:1805–1811.

Oncology

Oncology 2013;84(suppl 1):88–92
DOI: 10.1159/000345896

Published online: February 20, 2013

Expression of E-Cadherin and Vascular Endothelial Growth Factor in Noncancerous Liver Is Associated with Recurrence of Hepatocellular Carcinoma after Curative Resection

Mutsuko Minata[a, e] Masatoshi Kudo[d] Kouji H. Harada[b] Iwao Ikai[c]
Naoshi Nishida[a, d]

[a]Department of Medicine and Clinical Science, Kyoto University Graduate School of Medicine, [b]Kyoto University School of Public Health, and [c]Department of Surgery, National Hospital Organization Kyoto Medical Center, Kyoto, and [d]Department of Gastroenterology and Hepatology, Kinki University Faculty of Medicine, Osakasayama, Japan; [e]Department of Molecular and Cellular Biology, Beckman Research Institute of City of Hope, Duarte, Calif., USA

Key Words
Hepatocellular carcinoma · E-cadherin · Recurrence · Vascular endothelial growth factor · Metastasis

Abstract
Objectives: Hepatocellular carcinoma (HCC) frequently recurs even after curative resection. The purpose of this study was to examine how background liver affects postoperative recurrence of HCC that underwent curative resection using expression of cancer-related molecules in the adjacent noncancerous liver of HCC patients. ***Methods:*** We examined expression of E-cadherin and vascular endothelial growth factor in noncancerous liver tissues of 133 HCC patients who underwent curative resection of tumors using immunohistochemical analysis. Associations between expressions of these molecules and disease-free survival of HCC were analyzed using the Kaplan-Meier method. ***Results:*** The average period of follow-up of the patients was 6.7 years. Multivariate analyses revealed that low platelet count and negative expression of E-cadherin in adjacent noncancerous liver were significantly associated with metastatic recurrence [p = 0.017, hazard ratio (HR) = 1.31 for low platelet count, and p = 0.009, HR = 1.43 for negative expression of E-cadherin, respectively]. ***Conclusions:*** Expression levels of E-cadherin in adjacent noncancerous liver after surgical resection was associated with metastatic HCC recurrence later on. Analysis of E-cadherin expression should provide important information for predicting recurrence after curative resection of HCC.

Introduction

Despite significant advances in early detection and therapy for hepatocellular carcinoma (HCC), recurrence rate of this tumor is still high and long-term survival remains poor [1]. Recurrence of HCC can be divided into metastasis and multicentric recurrence [2]. However, so far, more than 90% of cancer-related deaths are attributed to the recurrence of tumor metastasis [3]. In addition, recent studies have revealed that epithelial-mesenchymal transition (EMT) is critically involved in invasion and metastasis in cancer, and loss of E-cadherin expression reportedly plays a critical role for phenotype of EMT [4]. Besides, it has also been reported that vascular endothelial growth factor (VEGF)-responsive precursor cells are necessary for neovascularization in the premetastatic

KARGER

Fax +41 61 306 12 34
E-Mail karger@karger.com
www.karger.com

0030–2414/13/0847–0088$38.00/0

Accessible online at:
www.karger.com/ocl

Naoshi Nishida, MD
Department of Gastroenterology and Hepatology
Kinki University Faculty of Medicine
377-2 Ohno-higashi, Osakasayama, Osaka 589-8511 (Japan)
E-Mail naoshi@med.kindai.ac.jp

niche [5]. From this standpoint, analyses of E-cadherin and VEGF based on genetic profiles in the background liver of HCC patients should be important for predicting the biological behavior of HCC. We investigated the relationships between patterns of recurrence and the expression of E-cadherin or VEGF in noncancerous liver tissue of HCC patients after curative hepatectomy using an immunohistochemical analysis.

Material and Methods

Patients

The tissue samples were collected from 133 HCC patients who were consecutively treated with surgery for primary HCC between 1985 and 1993 at Kyoto University Hospital. We specifically selected and focused on the patients who curatively resected of HCC with stage I or II and retrospectively analyzed the correlation between the recurrence of HCC and their clinicopathological parameters (over a median follow-up period of 6.7 ± 5.2 years). This study was performed based on the consent of the institutional review board of involved institutions and informed consent was obtained from each patient. We classified the stage of HCC and the surgical curability according to the criteria of general rules established by the Liver Cancer Study Group of Japan for the clinical and pathological study of primary liver cancer [6]. Every 3 months until September 2008, all patients were followed up with regular monitoring for serum α-fetoprotein level, and computerized tomographic (CT) scan or magnetic resonance imaging (MRI) of the liver in addition to abdominal echogram and chest radiograms. The diagnosis of recurrence was based on CT or angiography and, if necessary, bone scintigram was performed. Pathological findings of recurrent tumor tissues were also taken into consideration if available. Intrahepatic metastatic recurrence was diagnosed as follows: emergence of multiple hypervascular tumors appeared in a localized segment that had contained the original tumor, emergence of a large tumor situated near the original site and emergence of additional smaller tumors in distant parts of the liver [7]. Finally, the outcome of the patients was categorized into 3 groups of recurrence-free (n = 37), multicentric recurrence (n = 22) and metastatic recurrence (n = 74).

Additional clinicopathological information of the patients are as follows: sex, male (n = 89), female (n = 44) with a mean age of 61.4 years; status of hepatitis virus, positive for hepatitis B virus antigen (n = 17), positive for hepatitis C virus antibody or hepatitis C virus RNA (n = 77), negative for both hepatitis B virus antigen and hepatitis C virus (n = 5); clinical stage of HCC, I (n = 34), II (n = 97); serum alanine aminotransferase (ALT) level ≤80 IU/l (n = 81), >80 IU/l (n = 50); platelet count (10^3/mm^3) ≥10×10^4 (n = 76), <10×10^4 (n = 56); serum α-fetoprotein level ≤400 ng/ml (n = 95), >400 ng/ml (n = 34); histology of noncancerous liver, normal (n = 5), chronic hepatitis (n = 35), cirrhosis (n = 89); tumor size <2 cm (n = 47), 2–5 cm (n = 75), >5 cm (n = 11); histological differentiation of HCC, well (n = 13), moderate (n = 90), poor (n = 30); vascular invasion, positive (n = 2), negative (n = 131). No significant correlation was observed between each clinicopathological category and patient outcome.

Immunohistochemical Analyses

We performed immunohistochemical staining for E-cadherin and VEGF using the avidin-biotin complex method (Vecstatin ABC kit, Vector Laboratories, Burlingame, Calif., USA). Antibodies were: E-cadherin, a rabbit polyclonal (Takara Shuzo Co., Shiga, Japan) at a 1:20 dilution and VEGF, a mouse monoclonal (Santa Cruz Biotechnology, Santa Cruz, Calif., USA) at a 1:200 dilution. E-cadherin staining was observed at cell-cell borders of all epithelial cells in normal liver, discontinuous or negative membrane staining was defined as abnormal. The E-cadherin expression patterns were divided into three groups as follows: (1) positive (+), E-cadherin staining was similar to that of normal hepatic cells; (2) weak positive (±), staining was weaker than present in normal cells; (3) negative (–), complete loss of staining was discerned. VEGF staining was primarily cytoplasmic, the percentage of positive cells was semi-quantitatively counted based on staining intensity and distribution using the immunoreactive score (IRS) as described in previous studies [8, 9]. Based on the IRS score, VEGF staining intensity was divided into four groups as follows: (1) grade 0 (–), IRS 0–3; (2) grade 1 (+), IRS 4–6; (3) grade 2 (++), IRS 7–9; (4) grade 3 (+++), IRS 10–12. For IRS evaluation, ten visual fields from different areas were recorded.

Statistics

All the data in this study were evaluated using SAS software (version 9.1, SAS Institute Inc., Cary, N.C., USA). Differences were considered significant at values of $p < 0.05$. Fisher's exact tests or χ^2 test was used for the analysis of relationships between the expressions of E-cadherin or VEGF, and clinicopathological characters. Cumulative disease-free survival (DFS) was computed using the Kaplan-Meier method and compared between groups by the log-rank test. DFS was measured from the date of liver surgery to the date when recurrent disease was diagnosed or, in the absence of detectable tumor, to the date of death or the last follow-up. To elucidate the relationship between each expression and metastatic recurrence, we also analyzed the hazard ratios (HR) of recurrence within 2 years for each patient group, which were classified according to the intensity of immunohistochemical staining. Using the Cox proportional hazards regression model, HR and 95% CI were calculated and each analysis was performed so as to compare different groups (i.e. metastatic recurrence vs. multicentric recurrence, and multicentric recurrence vs. recurrence-free).

Results

Correlation between E-Cadherin Expression in Noncancerous Liver and Clinical Outcome

E-cadherin staining was specifically observed at the cell boundary. Negative E-cadherin expression was observed more frequently in patients with metastatic recurrence (32.4%; 24/74) than in patients with multicentric recurrence (13.6%; 3/22) or recurrence-free (13.5%; 5/37).

Table 1 compares HR for patients between metastatic recurrence versus multicentric recurrence and recurrence-free and multicentric recurrence versus recurrence-

Table 1. Univariate and multivariate Cox proportional analyses

a Factors associated with metastatic recurrence (metastatic recurrence vs. multicentric carcinoma and recurrence-free)

Variable	Univariate			Multivariate		
	HR	95% CI	p	HR	95% CI	p
Platelet count, $10^3/mm^3$						
≥10 × 10^4	1.00		–			
<10 × 10^4	1.30	1.03–1.64	0.029	1.31	1.05–1.68	0.017
E-cadherin expression in noncancerous liver						
Positive	1.00					
Weak positive	1.04	0.79–1.37	0.076			
Negative	1.41	1.06–1.87	0.020	1.43	1.10–1.84	0.009
VEGF expression in noncancerous liver						
Negative	1.00					
Grade 1	1.20	0.82–1.65	0.210			
Grade 2 or Grade 3	1.43	1.02–2.03	0.038			

The patients with grade 3 and grade 2 expression of VEGF in noncancerous tissues are combined for statistical analysis.

b Factors associated with multicentric carcinoma (multicentric carcinoma vs. recurrence-free)

Variable	Univariate			Multivariate		
	HR	95% CI	p	HR	95% CI	p
Hepatitis status			–			
Non-B non-C	1.00					
HCV	1.91	1.16–3.57	0.010	1.83	1.11–3.25	0.017
HBV	0.80	0.18–2.08	0.671			
Clinical stage						
I	1.00		–			
II	1.76	1.10–2.78	0.020			
ALT, IU/l						
≤80	1.00		–			
>80	1.58	1.03–2.45	0.035	1.59	1.03–2.48	0.037

p values were calculated for continuous values by ANOVA and for categorical values for the χ^2 test or Fisher's exact test.

The patients with incomplete data were excluded.

Non-B non-C hepatitis = Negative for hepatitis B surface antigen (HBsAg) and hepatitis C virus antibody (HCVAb) or RNA (–); HCV = positive for HCVAb or HCV-RNA; HBV = positive for HBsAg.

free. These comparisons were made in relation to clinicopathological data from univariate and multivariate analyses, which were performed to evaluate variables that could affect metastatic recurrence or the emergence of multicentric recurrence after curative surgery. According to univariate and multivariate analyses, negative E-cadherin expression in noncancerous liver was associated with increased risk for metastatic recurrence (p = 0.020, HR 1.41, 95% CI 1.06–1.87; p = 0.009, HR 1.43, 95% CI 1.10–1.84 by univariate and multivariate analyses, respectively; table 1). However, no significant relationship existed between multicentric recurrence and expression of E-cadherin by both univariate and multivariate analyses.

Correlation between VEGF Expression in Noncancerous Liver and Clinical Outcome

The proportion of HCC exhibiting grade 2 or 3 expression of VEGF in noncancerous liver was significantly higher in patients with metastatic recurrence (28.4%; 21/74) than those with multicentric recurrence (9.1%; 2/22) or as recurrence-free (10.8%; 4/37, p = 0.038). All cases of grade 3 VEGF expression, even though the number was only 2 patients, experienced metastatic recurrence (100%; 2/2).

For the onset of metastatic recurrence, the degree of VEGF staining in noncancerous liver was significantly correlated with an increased HR for grade 2 or grade 3 expression (p = 0.038, HR 1.43, 95% CI 1.02–2.03) than grade 1 (p = 0.210, HR 1.20, 95% CI 0.82–1.65) by univariate analysis; however, there was no correlation with multivariate analysis (table 1). On the contrary, no significant relationship was observed between VEGF expression and multicentric recurrence.

Clinical Features of the Patients and Outcome

For metastatic recurrence, low platelet count (<10 × 10^4) was revealed to be the significant correlation in both univariate and multivariate analyses (p = 0.029, HR 1.30, 95% CI 1.03–1.64; p = 0.017, HR 1.31, 95% CI 1.05–1.68 by univariate and multivariate analyses, respectively). For multicentric recurrence, the positive for hepatitis C virus antibody (p = 0.010, HR 1.91, 95% CI 1.16–3.57), advanced clinical stage of HCC (p = 0.020, HR 1.76, 95% CI 1.10–2.78) and serum ALT level (>80; p = 0.035, HR 1.58, 95% CI 1.03–2.45) were revealed as significant risk factors in univariate analysis, and the presence of hepatitis C virus and serum ALT level were the independent prognostic factors for emergence of multicentric recurrence by multivariate analysis (p = 0.017, HR = 1.83, 95% CI 1.11–3.25; p = 0.037, HR 1.59, 95% CI 1.03–2.48, respectively; table 1).

DFS of HCC, and Expression of E-Cadherin and VEGF in Noncancerous Liver

The median duration of DFS in patients with multicentric recurrence was significantly longer (87.3 ± 56.7 months) than in patients with metastatic recurrence (22.9 ± 20.5 months; p < 0.001). Negative E-cadherin expres-

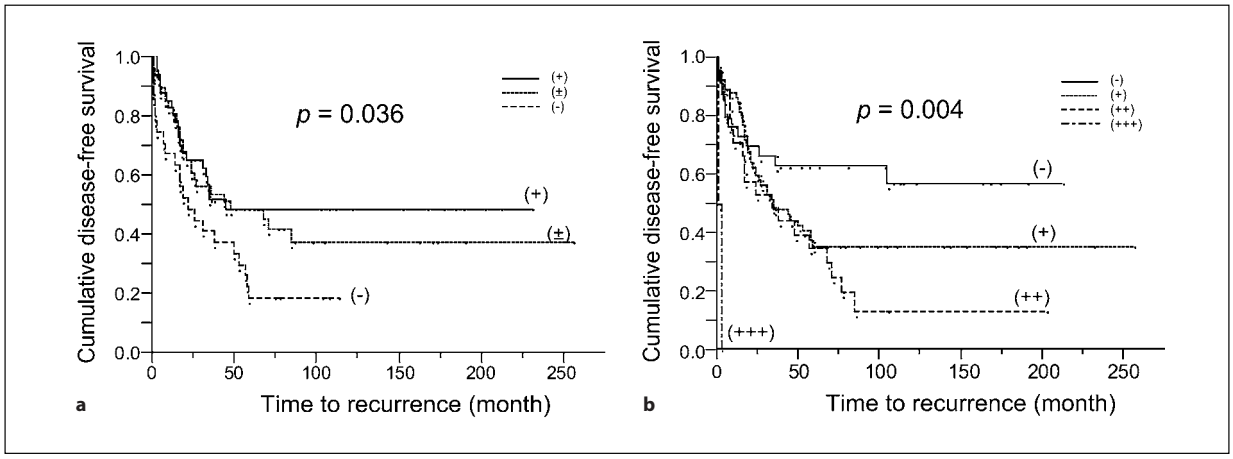

Fig. 1. Comparison of cumulative postoperative DFS curves according to intensity of immunohistochemistry. E-cadherin expression in noncancerous tissue (**a**) and VEGF expression in noncancerous tissue (**b**). Immunostaining intensity was evaluated by the Kaplan-Meier method. The group with negative (–) E-cadherin expression in noncancerous liver tissues exhibited shorter periods of DFS than those with weak positive (±) or positive (+) expression (p = 0.036 by log-rank test). All patients with grade 3 (+++) expression of VEGF in noncancerous tissues exhibited recurrence within 2 years. The group with grade 1 (+), grade 2 (++) or grade 3 (+++) expression of VEGF in noncancerous liver tissues exhibited higher recurrence rates than those with negative (–) expression of VEGF (p = 0.004 by log-rank test).

sion in noncancerous liver correlated with reduced time of DFS, and the recurrence rate correlated negatively with the extent of E-cadherin expression (p = 0.036; fig. 1a). Moreover, HR of recurrence within 2 years for negative E-cadherin expression was higher than the normal expression, although not statistically significant.

All patients with grade 3 for VEGF expression occurred recurrence within 2 years, and HR of recurrence within 2 years was much higher in grade 3 VEGF expression than the other groups (p = 0.004, HR 4.68, 95% CI 1.78–9.70). Furthermore, patients with grade 2 or 3 VEGF expression exhibited higher recurrence rates than those with negative VEGF expression (p = 0.030, HR 2.05, 95% CI 1.04–4.11). The reduced DFS was positively correlated with degree of VEGF expression in noncancerous liver (p = 0.004; fig. 1b).

Discussion

Surgical resection offers good overall survival for patients with HCC [10], although recurrence rates remain high [11]. In the cases of multicentric recurrence, surgical resection of tumor [12], radiofrequency ablation [13] and transplantation [1, 14] should be effective for treatment of recurrent tumor; however, there are few effective treatment options for patients with metastasis. In this study, we found an interesting association between expression of E-cadherin in noncancerous liver and occurrence of metastatic recurrence after curative resection of HCC.

The mechanism of metastasis is, as yet, not fully understood. Increasing evidence suggests that the role of the microenvironment surrounding metastasis appears critical for 'self-seeding' of cancer cells [15, 16], evaluating the 'soil' (premetastatic niche) seems to play an important role for establishment of metastasis. Nonetheless, the relationship between the status of adjacent nontumor liver tissue and metastatic recurrence has not been clarified yet. In this study we focused on the relationship between the supporting noncancerous liver tissue and recurrence signature after curative resection of HCC. It is clear that EMT is involved in metastatic events in cancer [4], besides which, reduced E-cadherin expression is one of the EMT markers [17, 18]. We observed a positive relationship between metastatic recurrence and reduced E-cadherin expression in adjacent noncancerous liver (table 1). For this finding, it is possible to speculate over the two possible roles of E-cadherin expression in the liver. First, reduced E-cadherin in adjacent nontumor liver is associated with presence of microvascular invasion or micrometastasis of primary tumor at the time of surgery. Second, noncancerous liver with reduced E-cadherin ex-

pression might be suitable for homing of HCC cells in the circulation, which might lead to loosening of cell-cell contacts of epithelium [19, 20]. In chronic hepatitis and liver cirrhosis, downregulation of E-cadherin by aberrant DNA methylation has been reported [21]. Therefore, epigenetic inactivation of E-cadherin in noncancerous liver might be a risk of metastatic recurrence after curative resection of HCC. Our result also revealed that the only clinical independent factor for predicting emergence of metastatic recurrence was reduced platelet count.

Moreover, we observed that reduced E-cadherin expressions as well as increased VEGF expressions in noncancerous liver were associated with the shorter periods of DFS (fig. 1a, b). It is reported that reduced E-cadherin was associated with increases in HIF-1α and VEGF expression, and elevated microvessel density [22]. Therefore, reduced E-cadherin and increased VEGF expression should be correlated with each other and this association seems to be one of the hallmarks of metastasis in the context of status of background noncancerous liver of HCC. From this standpoint, blocking reductions or improving the expression of E-cadherin might have potential therapeutic implications by suppressing invasiveness and inhibiting the formation of HCC metastases [23].

The IHC expression profiles of E-cadherin in adjacent noncancerous liver tissue revealed high-risk patterns of metastatic recurrence. These results could suggest a promising approach to suppression of metastasis for patients with high risk of postoperative recurrence whose tumors are completely resected.

Disclosure Statement

The authors have no competing interests to declare. This work was supported in part by a grant from the Smoking Research Foundation.

References

1 Poon RT, Fan ST, Lo CM, Liu CL, Wong J: Long-term survival and pattern of recurrence after resection of small hepatocellular carcinoma in patients with preserved liver function: implications for a strategy of salvage transplantation. Ann Surg 2002;235:373–382.
2 Kumada T, Nakano S, Takeda I, Sugiyama K, Osada T, Kiriyama S, Sone Y, Toyoda H, Shimada S, Takahashi M, Sassa T: Patterns of recurrence after initial treatment in patients with small hepatocellular carcinoma. Hepatology 1997;25:87–92.
3 Gupta R: Building patient confidence through effective communication. Br J Hosp Med (Lond) 2006;67:M2–M4.
4 Thiery JP, Acloque H, Huang RY, Nieto MA: Epithelial-mesenchymal transitions in development and disease. Cell 2009;139:871–890.
5 Lyden D, Hattori K, Dias S, Costa C, Blaikie P, Butros L, Chadburn A, Heissig B, Marks W, Witte L, Wu Y, Hicklin D, Zhu Z, Hackett NR, Crystal RG, Moore MA, Hajjar KA, Manova K, Benezra R, Rafii S: Impaired recruitment of bone-marrow-derived endothelial and hematopoietic precursor cells blocks tumor angiogenesis and growth. Nat Med 2001;7:1194–1201.
6 Liver Cancer Study Group of Japan: The general rules for the clinical and pathological study of primary liver cancer. Jpn J Surg 1989;19:98–129.
7 Ikeda K, Arase Y, Kobayashi M, Saitoh S, Someya T, Hosaka T, Suzuki Y, Suzuki F, Tsubota A, Akuta N, Kumada H: Significance of multicentric cancer recurrence after potentially curative ablation of hepatocellular carcinoma: a long-term cohort study of 892 patients with viral cirrhosis. J Gastroenterol 2003;38:865–876.
8 Chui X, Egami H, Yamashita J, Kurizaki T, Ohmachi H, Yamamoto S, Ogawa M: Immunohistochemical expression of the c-kit proto-oncogene product in human malignant and non-malignant breast tissues. Br J Cancer 1996;73:1233–1236.
9 Friedrichs K, Gluba S, Eidtmann H, Jonat W: Overexpression of p53 and prognosis in breast cancer. Cancer 1993;72:3641–3647.
10 Belghiti J, Fuks D: Liver resection and transplantation in hepatocellular carcinoma. Liver Cancer 2012;1:71–82.
11 Lim KC, Chow PK, Allen JC, Siddiqui FJ, Chan ES, Tan SB: Systematic review of outcomes of liver resection for early hepatocellular carcinoma within the Milan criteria. Br J Surg 2012;99:1622–1629.
12 Minagawa M, Makuuchi M, Takayama T, Kokudo N: Selection criteria for repeat hepatectomy in patients with recurrent hepatocellular carcinoma. Ann Surg 2003;238:703–710.
13 Cho YK, Rhim H, Noh S: Radiofrequency ablation versus surgical resection as primary treatment of hepatocellular carcinoma meeting the Milan criteria: a systematic review. J Gastroenterol Hepatol 2011;26:1354–1360.
14 Cheah YL, Chow P: Liver transplantation for heptatocellular carcinoma: an appraisal of the current controversies. Liver Cancer, in press.
15 Erler JT, Bennewith KL, Cox TR, Lang G, Bird D, Koong A, Le QT, Giaccia AJ: Hypoxia-induced lysyl oxidase is a critical mediator of bone marrow cell recruitment to form the premetastatic niche. Cancer Cell 2009;15:35–44.
16 Valastyan S, Weinberg RA: Tumor metastasis: molecular insights and evolving paradigms. Cell 2011;147:275–292.
17 Schmalhofer O, Brabletz S, Brabletz T: E-cadherin, beta-catenin, and ZEB1 in malignant progression of cancer. Cancer Metastasis Rev 2009;28:151–166.
18 Onder TT, Gupta PB, Mani SA, Yang J, Lander ES, Weinberg RA: Loss of E-cadherin promotes metastasis via multiple downstream transcriptional pathways. Cancer Res 2008;68:3645–3654.
19 Paschos KA, Canovas D, Bird NC: The role of cell adhesion molecules in the progression of colorectal cancer and the development of liver metastasis. Cell Signal 2009;21:665–674.
20 Ramis-Conde I, Chaplain MA, Anderson AR, Drasdo D: Multi-scale modelling of cancer cell intravasation: the role of cadherins in metastasis. Phys Biol 2009;6:016008.
21 Kanai Y, Ushijima S, Tsuda H, Sakamoto M, Hirohashi S: Aberrant DNA methylation precedes loss of heterozygosity on chromosome 16 in chronic hepatitis and liver cirrhosis. Cancer Lett 2000;148:73–80.
22 Calvisi DF, Ladu S, Conner EA, Factor VM, Thorgeirsson SS: Disregulation of E-cadherin in transgenic mouse models of liver cancer. Lab Invest 2004;84:1137–1147.
23 Fransvea E, Angelotti U, Antonaci S, Giannelli G: Blocking transforming growth factor-beta up-regulates E-cadherin and reduces migration and invasion of hepatocellular carcinoma cells. Hepatology 2008;47:1557–1566.

Oncology

Oncology 2013;84(suppl 1):93–97
DOI: 10.1159/000345897

Published online: February 20, 2013

Recent Advancements in Comprehensive Genetic Analyses for Human Hepatocellular Carcinoma

Naoshi Nishida Masatoshi Kudo

Department of Gastroenterology and Hepatology, Kinki University Faculty of Medicine, Osakasayama, Japan

Key Words
Hepatocellular carcinoma · Whole-genome sequencing · Exome analysis · Genome-wide association study

Abstract
Hepatocellular carcinoma (HCC) typically develops in the liver with chronic hepatitis and cirrhosis, and activation of oncogenes and inactivation of tumor suppressor genes occurs during carcinogenesis via genetic and epigenetic mechanisms. Recent advancements in the development of analyses for examining the cancer genome have revealed information regarding genetic alterations in HCC tissues. According to previous studies, the incidence of recurrent genetic alterations in individual genes was thought to be relatively rare and limited to a subset of a few cancer-specific genes such as tumor suppressor *p53*, *RB* genes and oncogenes such as *CTNNB1*. However, recent whole-genome analyses and exome sequencing of tumor DNA have revealed numerous novel alterations of cancer-related genes and pathways critical for HCC development. In addition, various risk factors for HCC, such as the presence or absence of hepatitis B and C virus, may affect the mutation profile of the corresponding cancer genome. On the other hand, genome-wide association studies have also identified important single-nucleotide polymorphisms involved in HCC development, which may allow detection of a group at high risk of HCC emergence. Such analyses will clarify how this malignancy can be treated, diagnosed and prevented more effectively.

Introduction

Hepatocellular carcinoma (HCC) is one of the most common cancers worldwide, and multiple risk factors, such as chronic infection of hepatitis B virus and hepatitis C virus (HCV), alcohol intake and exposure to carcinogens such as aflatoxin B1 are known to be involved in the development of this disease [1]. Thus far, several studies have examined the analytical methods used for determining the molecular characteristics of HCC [2–8]. However, because of the limited number of genes and genomic regions analyzed, genomic alterations and critical pathways involved during hepatocarcinogenesis remains unclear. In contrast, a recent report involving whole-genome and exome analyses of human HCC revealed a novel landscape of genetic alterations, which had not been previously recognized [9, 10]. In this review, we focus on the recent exome analysis and whole-genome DNA sequencing of HCC tissues. We also dis-

KARGER

Fax +41 61 306 12 34
E-Mail karger@karger.com
www.karger.com

0030–2414/13/0847–0093$38.00/0

Accessible online at:
www.karger.com/ocl

Naoshi Nishida, MD
Department of Gastroenterology and Hepatology
Kinki University Faculty of Medicine
377-2 Ohno-higashi, Osakasayama, Osaka 589-8511 (Japan)
E-Mail naoshi@med.kindai.ac.jp

cuss a genome-wide association study (GWAS) involving the somatic cells of HCC patients, which revealed critical single-nucleotide polymorphisms (SNPs) important for identifying patients at high risk of HCC emergence [11].

Base Substitution and Etiology of HCC

A profile of base substitutions resulting in mutations in HCC has been reported on the basis of mutation analyses of the tumor suppressor *TP53* gene, in which G>T/C>A transversions were predominant [2, 12]. Most base substitutions were detected on the nontranscribed strand, which may be attributed to preferential repair of the transcribed strand [2]. Further, aflatoxin B1 is known to induce G>T/C>A transversions at codon 249, and many HCCs in China and South Africa reportedly carry this mutation [12, 13]. Recently, Guichard et al. [14] performed whole-exome sequencing and reported that G>T/C>A transversions were significantly more frequent in tumors that developed on noncirrhotic liver. This suggests that specific genotoxic agents, such as aflatoxin B1, may contribute in part to HCC emergence without the background condition of liver cirrhosis. Most HCC cases in this cohort were in patients from France and not likely associated with aflatoxin B1; therefore, another genotoxin may be involved in HCC carcinogenesis [14]. Substitutions of G>T/C>A and T>A>A>T transversions were also frequently detected in HBV-related HCCs with portal vein thrombosis (PVTT) [15].

In contrast, Totoki et al. [16] performed a massive parallel sequencing of HCV-positive HCC and found a predominance of T>C/A>G substitutions at the ApT site in the genomes of HCV-related HCCs compared to smoking- and ultraviolet-related cancers. A study by Fujimoto et al. [17] showed that the C>T/G>A at the CpG site was also important. However, because this type of transition was also predominant in other cancers, they concluded that T>C/A>G and C>A/G>T substitutions may be characteristic of HCCs in Japan, where most HCCs were HCV-related [17]. They also reported that habitual alcohol consumption and occurrence of synchronous or metachronous multiple liver nodules were significantly associated with components of the somatic substitution profile of HCC [17]. Therefore, variations in somatic substitution patterns in HCCs may reflect a difference in status of hepatitis virus and exposure to various carcinogens.

Mutational Profile of Cancer-Related Genes and Etiology of HCC

By analyzing HCV-related HCCs, several somatic mutations have been reported, including the *TP53*, *AXIN1*, *ADAM22*, *JAK2*, *KHDRBS2*, *NEK8* and *TRRAP* genes, as well as a large number of somatic mutations in genes encoding phosphoproteins and those with bipartite nuclear signals [16]. Through high-resolution characterization, they also identified intratumor heterogeneity of the mutations, including inactivation of the *TSC* complex in a subpopulation of the tumors [16]. Li et al. [18] also reported differences in mutated genes among HCCs with several etiologies, focusing on 5 genes: *ARID2*, *CTNNB1*, *TP53*, *DMXL1* and *NLRP1*. Mutations in the *ARID2* gene, which encodes a subunit of the chromatin remodeling complex, were more frequently detected in HCV-related HCC compared with HBV-related HCC [18]. In addition, mutations in the *ARID2* gene were correlated with *CTNNB1* mutations and were mutually exclusive with *TP53* mutations [18]. *CTNNB1* mutations were also more frequently observed in HCV-related HCCs than in HBV-related tumors. In contrast, the prevalence of *TP53* mutations was significantly higher in patients from China [18], where HBV infection is the leading cause of hepatocarcinogenesis.

Huang et al. [19] performed RNA sequence analysis of HBV-related HCC and identified a novel, highly unregulated exon-exon junction in the *ATAD2* gene. According to high-resolution copy number analysis and whole genome sequencing, novel recurrent alterations in the *ARID1A*, *RPS6KA3*, *NFE2L2* and *IRF2* genes were detected [14]. Interestingly, inactivation of the *IRF2* gene was exclusively observed in HBV-related HCC, which led to disruption of *TP53* function [14]. However, mutations in chromatin remodelers were observed in association with alcohol-related HCC [14]. They also reported an association between highly rearranged copy number profile and HCC progression, such as high serum tumor markers, larger size and tumor dedifferentiation [14], which was suggested previously [20, 21]. Further, a high degree of copy number alterations was more frequently observed in HBV-related tumor, tumors developed in noncirrhotic liver and tumors with the *TP53* mutation [14, 22]. They described the 5 major pathways commonly altered by somatic mutations and homozygous deletions, including the Wnt/beta-catenin, p53/cell cycle control, chromatin remodeling, PI3K/Ras signaling and oxidative and endoplasmic reticulum stress pathways. Among these, the Wnt/beta-catenin pathway was the most fre-

quently altered pathway according to whole-genome sequencing [14]. This study also revealed that most *CTNNB1* mutations were present in tumors without HBV infection and were mutually exclusive to the*TP53* mutation [14], which is consistent with the results of Li et al. [18]. In contrast, mutations in the *AXIN1* and *APC* genes were detected in tumors with various etiologies and showed no relationship with*TP53* mutations. Alterations in *IRF2*, which is involved in the p53 pathway, are associated with HBV infection and high chromosomal instability [14]. Mutations of the chromatin remodeling-related genes *ARID1A* were significantly more frequent in alcohol-related HCC and showed an association with the *CTNNB1* mutation [14]. Overall, >24% of HCCs possessed mutations in at least one of the genes involved in the chromatin remodeling pathway. Mutations of the *RPS6KA3* gene, which encodes a component involved in PI3K/Ras signaling, were detected predominantly in HCC without cirrhosis and associated with *AXIN1* mutations [14]. Mutations in the *NFE2L2* gene, which encodes a component of the oxidative and endoplasmic reticulum stress pathways, showed an association with alterations in the Wnt/beta-catenin pathway [14].

Fujimoto et al. [17] also analyzed HCC with various etiologies and showed that 52% of HCCs carried mutations in at least one of the genes associated with chromatin regulation, including *ARID1A*, *ARID1B*, *ARID2*, *MLL*, *MLL3*, *BAZ2B*, *BRD8*, *BPTF*, *BRE* and *HIST1H4B*. These mutations were marginally associated with the stage of liver fibrosis and hepatic invasion. Huang et al. [15] also analyzed HBV-related HCC with PVTT and intrahepatic metastasis by using exome sequencing. The gene that encodes the component of the chromatin remodeling complex, *ARID1A*, was mutated in 13% of subjects in the HBV-related HCC cohort [15]. However, mutations in this gene were also observed in HCV-related and non-virus-infected HCCs. They also described that mutations in *VCAM1* and *TMEM35* genes may be potential driver mutations for hepatocarcinogenesis [15].

Integration of HBV Genome into Host DNA

For HCC cases with HBV infection, HBV integration was reportedly observed within or upstream of the *TERT* gene in tumor tissues [17]. Recurrent integration of HBV was also detected in the *FAR2*, *ITPR1*, *IRAK2*, *MAPK1*, *MLL* and *MLL4* genes [23–26]. In addition to integration of HBV into the *TERT* gene, Sung et al. [27] reported integration events at the *MLL4* and *CCNE1*, and *SENP5* and *ROCK1* genes. They found that most HBV breakpoints in HCC were close to active coding genes, potentially allowing HBV to integrate into the open chromatin region more effectively [27]. Breakpoints in HBV were over-represented in exon and promoter in HCC issues, but these were primarily detected in introns in noncancerous liver tissues, which may be attributed to positive selective pressure induced by integration of HBV into exons and promoters of active genes [27].

Jiang et al. [28] also performed comprehensive analyses of HBV-related HCC and their corresponding normal tissues using Alu-PCR, ligation-mediated PCR and an array-based comparative genomic hybridization assay. Nontumor liver tissues carried many viral integration sites randomly scattered throughout the genome. However, clonal and high-abundance viral integrations were detected in tumor tissue [27, 28]. Integration events may lead to abnormal expression of genes close to the integration sites, emergence of fusion genes and alterations of DNA copy number [28], which has also been suggested in another study [27].

A larger number of HBV integration events is reportedly associated with a high serum level of hepatitis surface antigen, α-fetoprotein, younger age of HCC emergence and chromosome copy number [14, 27]. Interestingly, it is also associated with patient survival and tumor aggressiveness [27].

Evolution of Genetic Alteration during Tumor Progression

Whole-genome sequencing is a powerful tool that can be used to identify candidate driver mutations of carcinogenesis using human tissue samples. Tao et al. [29] analyzed the evolution of HCC using 9 different sections of 3 tumors, including original and metastatic lesions and 7 sections of adjacent nontumor tissues by using whole-genome sequencing. In these analyses, somatic mutations were used to define 4 evolutionary linkages among tumor cells and candidate diver mutations of tumor progression of these HCC cases were speculated. Huang et al. [15] compared primary tumors and their PVTT lesions and reported that 94.2% of mutations were identical among primary tumors and PVTT. However, PVTT cases are thought to be derived from primary tumors, and mutations in the *KDM6A* and *CUL9* genes were exclusively detected in PVTT, suggesting that these mutations play a role in tumor progression [15].

Genetic Risk of HCC

Although hepatitis virus infection, alcohol consumption, obesity, diabetes mellitus and intake of genotoxic agents such as aflatoxin B1 are known critical risk factors for developing HCC, genetic factors determined on the basis of the nucleotide sequence of the host genome may also play a role in malignancy [11]. Several reports have suggested the association between polymorphisms in individual genes and the risk of HCC. For example, SNPs of the *SCBY14*, *CRHR2*, *GFRA1*, *CCND2*, *RAD23B*, *GRP78*, *CEP164*, *MDM2* and *ALDH2* genes were reportedly associated with an increased risk of HCC in Japanese patients with HCV infection [30, 31].

Recently, a GWAS revealed that intronic SNPs in the *DEPDC5* locus on chromosome 22 are associated with HCC risk in Japanese patients with chronic hepatitis C [32]. The *DEPDC5* gene is known to be involved in bladder carcinogenesis, but the function of this gene remains debatable [33]. Kumar et al. [34] also performed a GWAS on HCV-related HCCs and found a novel SNP of rs2596542 located in the 5′-region of the *MICA* gene on chromosome 6p. According to the GWAS conducted to identify risk of HBV-related hepatocarcinogenesis, an intronic SNP of the *KIF1B* gene on chromosome 1p was reported, and SNPs in the *UBE4B* and *PGD* genes were also shown to be significant for HCC emergence among HBV-positive patients [35].

Conclusion

Through comprehensive and precise analyses of cancer genomes, novel mutations and alterations in individual pathways involved in HCC development have been clarified. This information may be critical for establishing novel biomarkers for cancer therapy. Furthermore, these analyses will provide useful information for developing novel molecular-targeted therapy of this refractory cancer. Also, GWAS using DNA of somatic cells will be important for specifically identifying those at high risk of developing HCC. Accumulation of genetic information regarding cancer and somatic cells may help clarify how HCC should be managed to prevent HCC more effectively in the future.

Disclosure Statement

The authors have no competing interests to declare. This work was supported in part by a grant from the Smoking Research Foundation.

References

1 Kim DY, Han K: Epidemiology and surveilance of hepatocellular carcinoma. Liver Cancer 2012;1:2–14.
2 Nishida N, Fukuda Y, Kokuryu H, Toguchida J, Yandell DW, Ikenega M, Imura H, Ishizaki K: Role and mutational heterogeneity of the p53 gene in hepatocellular carcinoma. Cancer Res 1993;53:368–372.
3 Nishida N, Fukuda Y, Komeda T, Kita R, Sando T, Furukawa M, Amenomori M, Shibagaki I, Nakao K, Ikenaga M, et al: Amplification and overexpression of the cyclin D1 gene in aggressive human hepatocellular carcinoma. Cancer Res 1994;54:3107–3110.
4 Nishida N, Fukuda Y, Ishizaki K, Nakao K: Alteration of cell cycle-related genes in hepatocarcinogenesis. Histol Histopathol 1997;12:1019–1025.
5 Nishida N, Nishimura T, Ito T, Komeda T, Fukuda Y, Nakao K: Chromosomal instability and human hepatocarcinogenesis. Histol Histopathol 2003;18:897–909.
6 Nishida N, Nagasaka T, Nishimura T, Ikai I, Boland CR, Goel A: Aberrant methylation of multiple tumor suppressor genes in aging liver, chronic hepatitis, and hepatocellular carcinoma. Hepatology 2008;47:908–918.
7 Nishida N: Impact of hepatitis virus and aging on DNA methylation in human hepatocarcinogenesis. Histol Histopathol 2010;25:647–654.
8 Nishida N, Goel A: Genetic and epigenetic signatures in human hepatocellular carcinoma: a systematic review. Curr Genomics 2011;12:130–137.
9 Toffanin S, Cornella H, Harrington A, Llovet JM: Next-generation sequencing: path for driver discovery in hepatocellular carcinoma. Gastroenterology 2012;143:1391–1393.
10 Zhang Z: Genomic landscape of liver cancer. Nat Genet 2012;44:1075–1077.
11 Hoshida Y, Fuchs BC, Tanabe KK: Genomic risk of hepatitis C-related hepatocellular carcinoma. J Hepatol 2012;56:729–730.
12 Hsu IC, Metcalf RA, Sun T, Welsh JA, Wang NJ, Harris CC: Mutational hotspot in the p53 gene in human hepatocellular carcinomas. Nature 1991;350:427–428.
13 Bressac B, Kew M, Wands J, Ozturk M: Selective G to T mutations of p53 gene in hepatocellular carcinoma from southern Africa. Nature 1991;350:429–431.
14 Guichard C, Amaddeo G, Imbeaud S, Ladeiro Y, Pelletier L, Maad IB, Calderaro J, Bioulac-Sage P, Letexier M, Degos F, Clement B, Balabaud C, Chevet E, Laurent A, Couchy G, Letouze E, Calvo F, Zucman-Rossi J: Integrated analysis of somatic mutations and focal copy-number changes identifies key genes and pathways in hepatocellular carcinoma. Nat Genet 2012;44:694–698.
15 Huang J, Deng Q, Wang Q, Li KY, Dai JH, Li N, Zhu ZD, Zhou B, Liu XY, Liu RF, Fei QL, Chen H, Cai B, Xiao HS, Qin LX, Han ZG: Exome sequencing of hepatitis B virus-associated hepatocellular carcinoma. Nat Genet 2012;44:1117–1121.

16 Totoki Y, Tatsuno K, Yamamoto S, Arai Y, Hosoda F, Ishikawa S, Tsutsumi S, Sonoda K, Totsuka H, Shirakihara T, Sakamoto H, Wang L, Ojima H, Shimada K, Kosuge T, Okusaka T, Kato K, Kusuda J, Yoshida T, Aburatani H, Shibata T: High-resolution characterization of a hepatocellular carcinoma genome. Nat Genet 2011;43:464–469.
17 Fujimoto A, Totoki Y, Abe T, Boroevich KA, Hosoda F, Nguyen HH, Aoki M, Hosono N, Kubo M, Miya F, Arai Y, Takahashi H, Shirakihara T, Nagasaki M, Shibuya T, Nakano K, Watanabe-Makino K, Tanaka H, Nakamura H, Kusuda J, Ojima H, Shimada K, Okusaka T, Ueno M, Shigekawa Y, Kawakami Y, Arihiro K, Ohdan H, Gotoh K, Ishikawa O, Ariizumi S, Yamamoto M, Yamada T, Chayama K, Kosuge T, Yamaue H, Kamatani N, Miyano S, Nakagama H, Nakamura Y, Tsunoda T, Shibata T, Nakagawa H: Whole-genome sequencing of liver cancers identifies etiological influences on mutation patterns and recurrent mutations in chromatin regulators. Nat Genet 2012;44:760–764.
18 Li M, Zhao H, Zhang X, Wood LD, Anders RA, Choti MA, Pawlik TM, Daniel HD, Kannangai R, Offerhaus GJ, Velculescu VE, Wang L, Zhou S, Vogelstein B, Hruban RH, Papadopoulos N, Cai J, Torbenson MS, Kinzler KW: Inactivating mutations of the chromatin remodeling gene ARID2 in hepatocellular carcinoma. Nat Genet 2011;43:828–829.
19 Huang Q, Lin B, Liu H, Ma X, Mo F, Yu W, Li L, Li H, Tian T, Wu D, Shen F, Xing J, Chen ZN: RNA-Seq analyses generate comprehensive transcriptomic landscape and reveal complex transcript patterns in hepatocellular carcinoma. PLoS One 2011;6:e26168.
20 Nishida N, Fukuda Y, Kokuryu H, Sadamoto T, Isowa G, Honda K, Yamaoka Y, Ikenaga M, Imura H, Ishizaki K: Accumulation of allelic loss on arms of chromosomes 13q, 16q and 17p in the advanced stages of human hepatocellular carcinoma. Int J Cancer 1992;51:862–868.
21 Nishida N, Fukuda Y, Komeda T, Ito T, Nishimura T, Minata M, Kuno M, Katsuma H, Ikai I, Yamaoka Y, Nakao K: Prognostic impact of multiple allelic losses on metastatic recurrence in hepatocellular carcinoma after curative resection. Oncology 2002;62:141–148.
22 Nishida N, Nishimura T, Nagasaka T, Ikai I, Goel A, Boland CR: Extensive methylation is associated with beta-catenin mutations in hepatocellular carcinoma: evidence for two distinct pathways of human hepatocarcinogenesis. Cancer Res 2007;67:4586–4594.
23 Gozuacik D, Murakami Y, Saigo K, Chami M, Mugnier C, Lagorce D, Okanoue T, Urashima T, Brechot C, Paterlini-Brechot P: Identification of human cancer-related genes by naturally occurring hepatitis B virus DNA tagging. Oncogene 2001;20:6233–6240.
24 Paterlini-Brechot P, Saigo K, Murakami Y, Chami M, Gozuacik D, Mugnier C, Lagorce D, Brechot C: Hepatitis B virus-related insertional mutagenesis occurs frequently in human liver cancers and recurrently targets human telomerase gene. Oncogene 2003;22:3911–3916.
25 Murakami Y, Saigo K, Takashima H, Minami M, Okanoue T, Brechot C, Paterlini-Brechot P: Large scaled analysis of hepatitis B virus (HBV) DNA integration in HBV related hepatocellular carcinomas. Gut 2005;54:1162–1168.
26 Saigo K, Yoshida K, Ikeda R, Sakamoto Y, Murakami Y, Urashima T, Asano T, Kenmochi T, Inoue I: Integration of hepatitis B virus DNA into the myeloid/lymphoid or mixed-lineage leukemia (MLL4) gene and rearrangements of MLL4 in human hepatocellular carcinoma. Hum Mutat 2008;29:703–708.
27 Sung WK, Zheng H, Li S, Chen R, Liu X, Li Y, Lee NP, Lee WH, Ariyaratne PN, Tennakoon C, Mulawadi FH, Wong KF, Liu AM, Poon RT, Fan ST, Chan KL, Gong Z, Hu Y, Lin Z, Wang G, Zhang Q, Barber TD, Chou WC, Aggarwal A, Hao K, Zhou W, Zhang C, Hardwick J, Buser C, Xu J, Kan Z, Dai H, Mao M, Reinhard C, Wang J, Luk JM: Genome-wide survey of recurrent HBV integration in hepatocellular carcinoma. Nat Genet 2012;44:765–769.
28 Jiang S, Yang Z, Li W, Li X, Wang Y, Zhang J, Xu C, Chen PJ, Hou J, McCrae MA, Chen X, Zhuang H, Lu F: Re-evaluation of the carcinogenic significance of hepatitis B virus integration in hepatocarcinogenesis. PLoS One 2012;7:e40363.
29 Tao Y, Ruan J, Yeh SH, Lu X, Wang Y, Zhai W, Cai J, Ling S, Gong Q, Chong Z, Qu Z, Li Q, Liu J, Yang J, Zheng C, Zeng C, Wang HY, Zhang J, Wang SH, Hao L, Dong L, Li W, Sun M, Zou W, Yu C, Li C, Liu G, Jiang L, Xu J, Huang H, Mi S, Zhang B, Chen B, Zhao W, Hu S, Zhuang SM, Shen Y, Shi S, Brown C, White KP, Chen DS, Chen PJ, Wu CI: Rapid growth of a hepatocellular carcinoma and the driving mutations revealed by cell-population genetic analysis of whole-genome data. Proc Natl Acad Sci USA 2011;108:12042–12047.
30 Kato N, Ji G, Wang Y, Baba M, Hoshida Y, Otsuka M, Taniguchi H, Moriyama M, Dharel N, Goto T, Shao RX, Matsuura T, Ishii K, Shiina S, Kawabe T, Muramatsu M, Omata M: Large-scale search of single nucleotide polymorphisms for hepatocellular carcinoma susceptibility genes in patients with hepatitis C. Hepatology 2005;42:846–853.
31 Tomoda T, Nouso K, Sakai A, Ouchida M, Kobayashi S, Miyahara K, Onishi H, Nakamura S, Yamamoto K, Shimizu K: Genetic risk of hepatocellular carcinoma in patients with hepatitis C virus: a case control study. J Gastroenterol Hepatol 2012;27:797–804.
32 Miki D, Ochi H, Hayes CN, Abe H, Yoshima T, Aikata H, Ikeda K, Kumada H, Toyota J, Morizono T, Tsunoda T, Kubo M, Nakamura Y, Kamatani N, Chayama K: Variation in the DEPDC5 locus is associated with progression to hepatocellular carcinoma in chronic hepatitis C virus carriers. Nat Genet 2011;43:797–800.
33 Kanehira M, Harada Y, Takata R, Shuin T, Miki T, Fujioka T, Nakamura Y, Katagiri T: Involvement of upregulation of DEPDC1 (dep domain containing 1) in bladder carcinogenesis. Oncogene 2007;26:6448–6455.
34 Kumar V, Kato N, Urabe Y, Takahashi A, Muroyama R, Hosono N, Otsuka M, Tateishi R, Omata M, Nakagawa H, Koike K, Kamatani N, Kubo M, Nakamura Y, Matsuda K: Genome-wide association study identifies a susceptibility locus for HCV-induced hepatocellular carcinoma. Nat Genet 2011;43:455–458.
35 Zhang H, Zhai Y, Hu Z, Wu C, Qian J, Jia W, Ma F, Huang W, Yu L, Yue W, Wang Z, Li P, Zhang Y, Liang R, Wei Z, Cui Y, Xie W, Cai M, Yu X, Yuan Y, Xia X, Zhang X, Yang H, Qiu W, Yang J, Gong F, Chen M, Shen H, Lin D, Zeng YX, He F, Zhou G: Genome-wide association study identifies 1p36.22 as a new susceptibility locus for hepatocellular carcinoma in chronic hepatitis B virus carriers. Nat Genet 2010;42:755–758.

Ultrasound in Med. & Biol., Vol. 39, No. 2, pp. 187–210, 2013

0301-5629/$ - see front matter

http://dx.doi.org/10.1016/j.ultrasmedbio.2012.09.002

● *Guideline*

GUIDELINES AND GOOD CLINICAL PRACTICE RECOMMENDATIONS FOR CONTRAST ENHANCED ULTRASOUND (CEUS) IN THE LIVER – UPDATE 2012 A WFUMB-EFSUMB INITIATIVE IN COOPERATION WITH REPRESENTATIVES OF AFSUMB, AIUM, ASUM, FLAUS AND ICUS

Michel Claudon,[1,*] Christoph F. Dietrich,[2,*] Byung Ihn Choi,[3] David O. Cosgrove,[4] Masatoshi Kudo,[5] Christian P. Nolsøe,[6] Fabio Piscaglia,[7] Stephanie R. Wilson,[8] Richard G. Barr,[9] Maria C. Chammas,[10] Nitin G. Chaubal,[11] Min-Hua Chen,[12] Dirk Andre Clevert,[13] Jean Michel Correas,[14] Hong Ding,[15] Flemming Forsberg,[16] J. Brian Fowlkes,[17] Robert N. Gibson,[18] Barry B. Goldberg,[19] Nathalie Lassau,[20] Edward L. S. Leen,[21] Robert F. Mattrey,[22] Fuminori Moriyasu,[23] Luigi Solbiati,[24] Hans-Peter Weskott,[25] and Hui-Xiong Xu[26]

[1]Department of Pediatric Radiology, INSERM U947, Centre Hospitalier Universitaire de Nancy and Université de Lorraine, Vandoeuvre, France; [2]Medizinische Klinik 2, Caritas-Krankenhaus Bad Mergentheim, Germany; [3]Department of Radiology, Seoul National University Hospital, Seoul, Korea; [4]Imaging Sciences Department, Imperial College, Hammersmith Hospital, London, United Kingdom; [5]Department of Gastroenterology and Hepatology, Kinki University School of Medicine, Osaka, Japan; [6]Ultrasound Section, Division of Surgery, Department of Gastroenterology, Herlev Hospital, University of Copenhagen, Copenhagen, Denmark; [7]Division of Internal Medicine, University of Bologna, Bologna, Italy; [8]Division of Gastroenterology, University of Calgary, Calgary, Alberta, Canada; [9]Northeastern Ohio Medical University, Rootstown, Ohio, United States of America; [10]Institute of Radiology, School of Medicine, University of São Paulo, São Paulo, Brazil; [11]Thane Ultrasound Centre, Jaslok Hospital, Mumbai, India; [12]Peking University Cancer Hospital, Peking, China; [13]Interdisciplinary Ultrasound Center, Department of Clinical Radiology, University of Munich-Grosshadern Campus, Munich, Germany; [14]Service de Radiologie Adultes, Hôpital Necker, Université Paris Descartes, Paris, France; [15]Department of Ultrasound, Zhongshan Hospital, Fudan University, Shanghai, China; [16]Department of Radiology, Thomas Jefferson University, Philadelphia, Pennsylvania, United States of America; [17]Department of Radiology, University of Michigan, Ann Arbor, Michigan, United States of America; [18]Department of Radiology, Royal Melbourne Hospital, University of Melbourne, Melbourne, Australia; [19]Division of Diagnostic Ultrasound, Department of Radiology, Thomas Jefferson University Hospital, Philadelphia, Pennsylvania, United States of America; [20]Integrated Research Cancer Institute in Villejuif, Gustave Roussy Institute, Villejuif, France; [21]Imaging Department, Imperial College, London, United Kingdom; [22]MRI Institute, University of California San Diego, San Diego, California, United States of America; [23]Department of Gastroenterology and Hepatology, Tokyo Medical University, Tokyo, Japan; [24]Department of Interventional Oncologic Radiology, General Hospital of Busto Arsizio, Busto Arsizio, Italy; [25]Central Ultrasound Department, Klinikum Siloah, Klinikum Region Hannover, Hannover, Germany; and [26]Department of Medical Ultrasound, Tenth People's Hospital of Tongji University, Shanghai, China

Abstract—Initially, a set of guidelines for the use of ultrasound contrast agents was published in 2004 dealing only with liver applications. A second edition of the guidelines in 2008 reflected changes in the available contrast agents and updated the guidelines for the liver, as well as implementing some non-liver applications. Time has moved on, and the need for international guidelines on the use of CEUS in the liver has become apparent. The present document describes the third iteration of recommendations for the hepatic use of contrast enhanced ultrasound (CEUS) using contrast specific imaging techniques. This joint WFUMB-EFSUMB initiative has implicated experts from major leading ultrasound societies worldwide. These liver CEUS guidelines are simultaneously published in the official journals of both organizing federations (i.e., Ultrasound in Medicine and Biology for WFUMB and Ultraschall in der Medizin/European Journal of Ultrasound for EFSUMB). These guidelines and recommendations provide general advice on the use of all currently clinically available ultrasound contrast agents (UCA). They are intended to create standard protocols for the use and administration of UCA in liver applications on an international basis and improve the management of patients worldwide. (E-mail: Christoph.dietrich@ckbm.de) **© 2013 World Federation for Ultrasound in Medicine & Biology.**

Key Words: **Diagnosis, Metastases, Hepatocellular carcinoma, Focal nodular hyperplasia, Hemangioma, Microbubble.**

Address correspondence to: Prof. Dr. med. Christoph F. Dietrich, Caritas Krankenhaus Bad Mergentheim, Med. Klinik 2, Uhlandstr. 7, 97980 Bad Mergentheim. E-mail: Christoph.dietrich@ckbm.de

[*]Both authors equally contributed to the manuscript (as co-first authors).

LIST OF ABBREVIATIONS:

AASLD – American Association for the Study of Liver Diseases
AFSUMB – Asian Federation of Societies for Ultrasound in Medicine and Biology
AIUM – American Institute of Ultrasound in Medicine
ASUM – Australasian Society for Ultrasound in Medicine
AUC – area under the curve
AUWI – area under the wash in
AUWO – area under the wash out
CCC – cholangiocellular carcinoma
CT – computed tomography
CECT – contrast enhanced computed tomography
CEMRI – contrast enhanced magnetic resonance imaging
CEUS – contrast enhanced ultrasound
DCE-US – dynamic contrast enhanced ultrasound
ECG – electrocardiogram
EMA – European Medicines Agency
EFSUMB – European Federation of Societies for Ultrasound in Medicine and Biology
FLAUS – Latin-American Federation of Societies for Ultrasound in Medicine and Biology
FLL – focal liver lesion(s)
FNH – focal nodular hyperplasia
HA – hepatic artery
HCA – hepatocellular adenoma
HCC – hepatocellular carcinoma
ICU – intensive care unit
ICUS – International Contrast Ultrasound Society
IO-CEUS – intraoperative contrast enhanced ultrasound
IOUS – intraoperative ultrasound
IVC – inferior vena cava
MI – mechanical index
MIP – maximum intensity projection
MRI – magnetic resonance imaging
MTT – mean transit time (TIC parameter)
PI – peak intensity
PV – portal vein (portal venous)
RECIST – response evaluation criteria in solid tumors
RF – radio-frequency
SPIO – superparamagnetic iron oxide
SWI – slope of the wash in (TIC parameter)
TIC – time intensity curve(s)
TPI – time to peak intensity (TIC parameter)
UCA – ultrasound contrast agent(s)
US – ultrasound or ultrasonography
USA-FDA – United States of America Food and Drug Administration
WFUMB – World Federation for Ultrasound in Medicine and Biology
WHO – World Health Organization

CONTENT

General overview, steering committee and contributions

PREAMBLE

The present document describes the third iteration of recommendations for the hepatic use of contrast enhanced ultrasound (CEUS) and contrast specific imaging techniques introduced ten years ago in Europe and Canada.

Initially, a set of guidelines for the use of ultrasound contrast agents (UCA) was published in the 2004 edition of Ultraschall in der Medizin (European Journal of Ultrasound) dealing only with liver applications (Albrecht et al. 2004). Subsequently, CEUS was introduced into other important guidelines and recommendations for the diagnostic strategy of focal liver lesions (FLL) in cirrhosis, including the guidelines of the American Association for the Study of Liver Diseases (AASLD) 2005 (Bruix and Sherman 2005), the Asian Pacific Association for the Study of the Liver consensus recommendations on hepatocellular carcinoma (HCC) (Omata et al. 2010) and the recommendations of the Japan Society of Hepatology (Kudo et al. 2011b). A second edition of the guidelines in 2008 reflected changes in the available contrast agents and updated the guidelines for the liver (Claudon et al. 2008). CEUS has also been recommended in guidelines for several non-liver applications, which have recently been updated under the auspices of European Federation of Societies for Ultrasound in Medicine and Biology (EFSUMB) as non-liver guidelines (Piscaglia et al. 2011).

Time has moved on, and the need for worldwide guidelines on the use of CEUS in the liver has become apparent. World Federation for Ultrasound in Medicine and Biology (WFUMB) and EFSUMB initiated further discussions in 2010, in conjunction with the Asian Federation of Societies for Ultrasound in Medicine and Biology (AFSUMB), American Institute of Ultrasound in Medicine (AIUM), Australasian Society for Ultrasound in Medicine (ASUM) and International Contrast Ultrasound Society (ICUS) to bring the 2008 liver guidelines up-to-date, recognizing the fact that contrast agents are now licensed in many parts of the world, including Australasia, Brazil, Canada, China, Europe, India, Japan and Korea.

This joint WFUMB-EFSUMB venture has resulted in a liver CEUS simultaneous duplicate on liver CEUS in the official journals of WFUMB and EFSUMB (*i.e.*, Ultrasound in Medicine and Biology and Ultraschall in der Medizin/European Journal of Ultrasound).

To produce the new CEUS liver guidelines and recommendations, a meeting of representatives from 36 European (France, Denmark, Germany, Italy and the UK), North American (Canada and the USA), Asian (China, India, Japan and Korea) and Australian experts was held in Chicago in December 2010. While a significant portion of the work was accomplished at the meeting, the group continued to meet *via* conference calls and at local meetings.

As before, these guidelines are based on comprehensive literature surveys, including results from prospective clinical trials. On topics where no significant study data were available, evidence was obtained from expert committee reports or was based on the consensus of experts in the field of ultrasound (US) and CEUS during the consensus conferences. During the meeting of experts in Chicago, many additional new developments were discussed and included. Others were believed to be too early in their development to be included in the current recommendations.

These guidelines and recommendations provide general advice on the use of UCA. They are intended to create standard protocols for the use and administration of UCA in liver applications on an international basis and improve the management of patients. Individual cases must be managed on the basis of all clinical data available.

1. GENERAL CONSIDERATIONS (TECHNICAL ASPECTS)

1.1. Introduction

The development of microbubble ultrasound contrast agents has overcome some of the limitations of conventional B-mode and Doppler ultrasound techniques for the liver and enabled the display of the parenchymal microvasculature (Claudon et al. 2008). The enhancement patterns of lesions can be studied during all vascular phases (arterial, portal venous, late and postvascular phases), in a similar fashion to contrast enhanced computed tomography (CECT) and contrast enhanced magnetic resonance imaging (CEMRI) but in real time and under full control of the ultrasound operator. UCA have different pharmacokinetics from commonly used contrast agents for computed tomography (CT) and magnetic resonance imaging (MRI) in that they are confined to the vascular space whereas the majority of contrast agents for CT and MRI are rapidly cleared from the blood pool into the extravascular space (Dawson et al. 1999). In addition, some UCA have a late or a postvascular phase during which they are retained in the liver (and in the spleen) (Dawson et al. 1999).

An inherent advantage of CEUS is the opportunity to assess the contrast enhancement patterns in real time, with a much higher temporal resolution than is possible with other imaging modalities, so that the enhancement dynamics of lesions can be studied. There is no need to predefine scan time points or to perform bolus tracking. Furthermore, the excellent tolerance and safety profiles of UCA allow for their repeated administrations in the same session when needed. Regrettably, UCA studies are subject to the same limitations as other types of ultrasound imaging: as a general rule, if the baseline ultrasound is suboptimal, CEUS may be disappointing.

There are limitations in the use of CEUS in the liver:

- Limitations of resolution of CEUS or particular scanning conditions mean that the smallest detectable lesions range between 3 and 5 mm in diameter (Leoni et al. 2010).
- Very small FLL may be overlooked.
- Subdiaphragmatic lesions, especially those in segment VIII, may not be accessible to conventional US or CEUS. Intercostal scanning and positioning the patient in the left decubitus position can help reduce this limitation.
- Since CEUS has limited penetration, especially in steatosis, deep-seated lesions may not be accessible. Again, scanning in the left lateral decubitus position brings the liver forward and closer to the transducer and can help to reduce this limitation; it should be part of the routine survey.
- The falciform ligament and surrounding fat can cause an enhancement defect that may be confused with a FLL.

1.2. Commercially available UCA for the liver

The UCA currently used in diagnostic US of the liver are microbubbles consisting of gas bubbles

stabilized by a shell (Claudon et al. 2008). Three are in common use today as follows:

- SonoVue® (sulfur hexafluoride with a phospholipid shell) Bracco SpA, Milan, Italy, introduced in 2001. Licensed in Europe, China, India, Korea, Hong Kong, New Zealand, Singapore and Brazil.
- Definity®/Luminity® (octafluoropropane [perflutren] with a lipid shell) Lantheus Medical, Billerica, MA, USA, introduced in 2001. Licensed in Canada and Australia.
- Sonazoid® (perfluorobutane with a phospholipid shell: hydrogenated egg phosphatidyl serine). Daiichi-Sankyo, GE Tokyo, Japan, introduced in 2007. Licensed in Japan and now South Korea.

There are several other UCA which may be useful in liver studies but they are either not licensed for the liver in any country or, in the case of Levovist® (Bayer Schering AG, Germany), production has ceased.

For product information regarding handling, composition, packaging, storage, indications and contraindications of these agents, contact the manufacturing company.

1.3. Background on UCA and contrast specific modes

UCA strongly increase the backscatter of US regardless of whether the microbubbles are flowing or stationary. The low solubility of the gases in currently licensed UCA improves their stability and provides good resonance behavior at low acoustic pressures. This allows minimally disruptive contrast-specific imaging and enables effective investigation over several minutes to visualize their dynamic enhancement patterns in real time.

Because of their physical size (equal to or smaller than red blood cells), UCA act as blood pool agents and allow depiction of both the macrovasculature and the microvasculature (Cosgrove and Harvey 2009). Despite their varied physicochemical composition, all UCA have similar behaviors for CEUS imaging, rapidly enhancing the vascular pool after intravenous injection, with slow dissipation over about 5 min. An exception to this behavior occurs with Sonazoid®, which has an extended late phase, herein termed the "postvascular phase" in which it persists for several hours in the liver and spleen, long after it has disappeared from the detectable vascular pool. Sonazoid® is phagocytozed by Kupffer cells and this undoubtedly contributes to its persistence in the liver. This postvascular phase is often referred to as "the Kupffer phase" (Yanagisawa et al. 2007).

Contrast-specific US modes cancel the linear US signals from tissue and utilize the nonlinear responses from the microbubbles to form images (Claudon et al. 2008). This nonlinear microbubble response can be produced by two different mechanisms:

- Stable nonlinear oscillations at low acoustic pressure, which is nowadays the standard modality for most CEUS examinations.
- Disruption at higher acoustic pressures to give broadband nonlinear responses.

Nonlinear harmonic US signals also arise from tissue because the sound waves become distorted during their propagation. These "tissues harmonics" increase with increasing acoustic pressure, which is roughly indicated by the mechanical index (MI), [see section 1.8] (Simpson et al. 1999; Tiemann et al. 1999; Averkiou et al. 2003; Szabo 2004). However, a low MI is usually chosen for continuous real-time imaging, and for minimizing microbubble destruction. MI is considered as "low" when $\leq$0.3 but most systems work optimally with MI far below 0.3 (as low as 0.05).

Current contrast specific imaging enables effective tissue cancellation to generate almost pure microbubble images. Each manufacturer has developed proprietary techniques for this and adequate cancellation is indicated by near-disappearance of the ultrasound parenchymal liver structures (the screen goes black), though strong reflectors, such as vascular structures and the diaphragm/lung interface, remain barely visible. Correct settings on the ultrasound scanner and the scanning mode are important to avoid artifacts (Dietrich et al. 2011). Inappropriately high MI and gain are the two most common causes of tissue signals being wrongly displayed.

1.4. Intermodality comparison

For characterization of FLL, the enhancement patterns observed during the arterial, portal venous and late phases are generally similar among CEUS, CECT and CEMRI. The real-time nature of US allows depiction of early arterial phase enhancement which is sometimes missed on CT and MRI because they have lower frame rates. Discordance has also been shown in some lesions during the portal venous and late phases when CT and MRI contrast materials diffuse into the tumor interstitium and may conceal wash out (Wilson et al. 2007). On the other hand, postvascular phase imaging with Sonazoid® shows patterns similar to those described with superparamagnetic iron oxide (SPIO)-MRI (Korenaga et al. 2009).

1.5. Equipment and contrast signal detection

See companies' websites for references and specification.

1.6. Clinical practitioner training

Investigators wishing to perform CEUS examinations are recommended to gain experience by observing contrast studies being performed by experts in this field. EFSUMB has defined three levels of training in its

minimal training requirements (EFSUMB 2006) and recommends that CEUS should be performed by operators at a competence level higher than level 1 (EFSUMB 2010: Appendix 14).

They should also ensure that their equipment is optimized for CEUS by discussion with their equipment manufacturer. In addition, a sufficient volume and variety of pathology are essential to acquire and maintain an adequate level of skill. Practitioners need competence in the intravenous administration of contrast agents, familiarity with any contraindications and ability to deal with any possible adverse effects within the medical and legal framework of their country.

1.7. Safety considerations

In general, UCA are safe with a very low incidence of side effects. There are no cardio-, hepato- or nephrotoxic effects. Therefore, it is not necessary to perform laboratory tests to assess liver or kidney function before their administration.

The incidence of severe hypersensitivity events is lower than with current X-ray contrast agents and is comparable to those encountered with MRI contrast agents. Life-threatening anaphylactoid reactions in abdominal applications have been reported with a rate of 0.001%, with no deaths in a series of >23,000 patients (Piscaglia and Bolondi 2006). Nonetheless, investigators should be trained in resuscitation and have the appropriate facilities available.

Deaths in critically ill patients who have undergone contrast echocardiography examinations have been reported but with no evidence of a causal relationship (Main et al. 2009). Contraindications for the use of SonoVue® were defined by the European Medicines Agency (EMA) in 2004. In 2007, the United States of America Food and Drug Administration (US-FDA) issued contraindications for the use of Definity® and Optison® (GE Healthcare, licensed for cardiac use) in patients with severe cardiopulmonary disease, and imposed echocardiogram (ECG) monitoring for 30 min after injection (US-FDA Alert 10/2007). The contraindications were downgraded to warnings in May 2008 following review of recent studies on contrast reactions and postmarketing studies supplied by the manufacturers at the request of the FDA (Exuzides et al. 2010); in 2011, the requirement to observe the patient for 30 min after injection was removed. Numerous subsequent studies have been conducted to examine adverse reactions to UCA in cardiac applications (Khawaja et al. 2010) and these have indicated an excellent safety profile. One study (Kurt et al. 2009) demonstrated the positive impact of the use of UCA in cardiac examinations: additional procedures were avoided or therapy changed in over 35% of patients. Another large study reported better survival in acute cardiac disorders undergoing UCA administration in comparison to those receiving echocardiography without UCA (Main et al. 2008).

Although there is a theoretical possibility that the interaction of diagnostic ultrasound and UCA could produce bioeffects, there is no clinical evidence for adverse effects on the human liver. Cellular effects that have been observed *in vitro* include sonoporation, hemolysis and cell death (Skyba et al. 1998). Data from small animal models suggest that microvascular disruption can occur when microbubbles are insonated (Skyba et al. 1998). Thus, in general, low MI should be preferred for CEUS of the liver. Where diagnostic information can only be obtained using high MI sequences, the benefits vs. the risks of the procedure should be assessed and the mode selected for the benefit of the patient.

There is limited data on the use of UCA in pregnancy, during breastfeeding or in pediatrics (Piskunowicz et al. 2011). The implied contraindications can be overridden according to clinical judgment and with dedicated informed consent in case of need.

All administration decisions and procedures for the use of UCA should be made with the local regulatory restrictions in mind.

Some general recommendations include:

- As in all diagnostic ultrasound procedures, the operator should be mindful of the desirability of keeping the displayed MI low and of avoiding unduly long exposure times.
- Caution should be exercised when using UCA in patients with severe coronary artery disease.
- As with all contrast agents, resuscitation facilities must be available.
- The use of UCA should be avoided 24 h prior to extracorporeal shock wave therapy.

1.8. Terminology

The appearance of a lesion or region-of-interest in the liver should be described in terms of the degree and timing (phase) of enhancement.

Degree of enhancement: describing the region in terms of vascularity (*e.g.*, hypervascular, hypovascular) may be incorrect from a histologic point of view and describing the degree of enhancement is preferred.

- *Enhancement* refers to the intensity of the signal relative to that of the adjacent parenchyma: either equal to, *isoenhancing*; greater than, *hyperenhancing*; or less than, *hypoenhancing*.
- *Sustained enhancement* usually refers to continuance of enhancement in the lesion over time.
- *Complete absence of enhancement* can be described as nonenhancing. When a region is nonenhancing in the postvascular phase with Sonazoid®, the term

"*enhancement defect*" is often used in clinical practice.

Phase of enhancement

- The enhancement pattern should be described separately for the different phases, which for the liver comprise the arterial, the portal venous, the late phases and, in case of Sonazoid®, also the postvascular phase. Conventional, but imprecise time points, separate these different phases [see section 2.1.1].
- "*Wash in*" used for both qualitative and quantitative analysis, refers to the period of progressive enhancement within a region of interest from the arrival of microbubbles in the field of view to "peak enhancement" and "*wash out phase*" refers to the period of reduction in enhancement which follows peak enhancement.

Mechanical index

MI refers to the mechanical index of an ultrasound system, which is an estimate of the maximum amplitude of the pressure pulse in tissue, reflecting the power of the system. In very simple terms, higher MI tends to correspond to higher acoustic pressure emission and consequently to more rapid disruption of microbubbles. In physical terms, the MI is defined as:

$$MI = \frac{PNP}{\sqrt{(F_c)}}$$

where PNP is the peak negative pressure of the ultrasound wave (in MPa and derated for modeled attenuation) and F_c is the center frequency of the ultrasound wave (MHz).

Data types

Different types of data have been used in CEUS studies (Szabo 2004):

- *RF data* refers to the radiofrequency information after the beam former.
- *Raw data* refers to the data after the phase information in the RF data has been removed.
- *Linear data* refers to the RF or Raw data, before compression.
- *Video data* refers to the data after log (or quasi log) compression for video display.

2. CEUS FOR CHARACTERIZATION OF FOCAL LIVER LESIONS

CEUS should be performed with knowledge of all prior imaging, the patient's demographics and the clinical history, exactly as for a conventional ultrasound examination. This is particularly important for lesion characterization because the range of tumor types differs between cirrhotic and noncirrhotic livers. Accordingly, in these guidelines the characterization of FLL is described separately for patients with and without cirrhosis.

Table 1. Vascular phases in CEUS of the liver (visualization postinjection time)

Phase	Start (s)	End (s)
Arterial	10–20	30–45
Portal venous (PV)	30–45	120
Late	>120	Bubble disappearance (approx. 4–6 min)

The portal and late phases start at the end of the preceding one. Individual hemodynamic and other factors (*e.g.*, site of injection) may influence their time of onset.

2.1. Characterization of FLL in the noncirrhotic liver

2.1.1. Background. The dual blood supply of the liver from the hepatic artery (25%–30%) and the portal vein (70%–75%) gives rise to three overlapping vascular phases on CEUS study (Table 1):

- The *arterial phase* provides information on the degree and pattern of the arterial vascular supply. Depending on the individual's circulatory status, the hepatic arterial phase generally starts within 20 s after injection and continues to 30–45 s. This phase may occur very rapidly and the real-time nature of CEUS is needed to capture them, often best seen in a slow replay of a stored cine loop.
- The *portal venous phase* usually lasts until 2 min after injection. These two early phases are very similar between the different available UCA (SonoVue®, Definity®, Sonazoid®).
- *The late phase lasts* until the clearance of the UCA from the circulation and is limited to 4–6 min.

The additional *postvascular* (or Kupffer) *phase* for Sonazoid® begins 10 min after injection and lasts for an hour or more. To ensure that there is no overlap with the late phase, postvascular phase scanning should not be performed sooner than 10 min after injection.

All of these times may be shortened by microbubble disruption if the liver is imaged continuously, even at a low MI.

Late and postvascular phase enhancement provide important information regarding the character of a lesion as most malignant lesions are hypoenhancing while the majority of solid benign lesions are iso- or hyperenhancing (Wilson and Burns 2006; Claudon et al. 2008; Strobel et al. 2008; Trillaud et al. 2009; Bernatik et al. 2010; Seitz et al. 2010; Seitz et al. 2011).

2.1.2. Study procedure. Low MI contrast-specific techniques allow dynamic evaluation of the three vascular phases for all UCA and also of the postvascular phase for Sonazoid®:

- Any investigation should start with conventional B-mode and Doppler techniques.

- After identification of the target lesion, the transducer is held still while the scanner is switched to low MI contrast-specific imaging.
- A dual screen format showing a low MI B-mode image alongside the contrast-only display aids anatomic guidance. This is useful for small lesions to ensure that the target is kept within the field of view during CEUS. A difficulty with the split screen method is that a low MI is used for both panels and this means that the gray scale display is noisy so that smaller and low contrast lesions may be difficult to image. On some scanners, conventional and CEUS images are not split onto two screens but overlaid with different color scales.
- UCA is administered as a bolus injection followed by a flush of normal saline 0.9%.
- Ideally, the diameter of the venous line should not be smaller than 20 G to avoid destruction of microbubbles during injection. Central line and port systems can be used as long as there is no filter requiring a high injection pressure but contrast arrival time will be shorter.
- A stop clock should be started at the time of UCA injection.
- Because of the dynamic nature of real-time CEUS, essential clips for each vascular phase should be recorded.
- Assessment of the arterial and portal venous phases should be carried out without interruption. For the late phase, intermittent scanning may be used until the disappearance of the UCA from the liver's microvasculature. Under some circumstances, especially for HCC, the examination may need to be continued for up to 5 min because wash out may be delayed (Mork et al. 2007).
- Injection can be repeated when a lesion has been detected in the portal venous phase or in the late/postvascular phase to study the arterial phase and in the case of multiple FLL. Reinjection should be postponed until most microbubbles have vanished and the CEUS screen is almost black again, which can be expected after 6–10 min using SonoVue® and Definity®.

2.1.3. Image interpretation and differentiation of benign from malignant lesions. CEUS can often establish a definitive diagnosis or otherwise facilitate the clinical decision as to whether a sonographically detected liver lesion needs further investigation.

2.1.4. Benign liver lesions. Sustained enhancement in the portal and late phases is typically observed in almost all solid benign liver lesions. They can be further characterized by their enhancement patterns during the arterial phase, (*e.g.*, enhancement of the whole lesion [typical of focal nodular hyperplasia] or initial peripheral globular/nodular enhancement [in hemangiomas]).

The enhancement patterns are summarized in Table 2.

Hemangioma. CEUS has markedly improved the accurate diagnosis of hemangiomas, which is now possible in about 95% of cases (Strobel et al. 2008). The typical CEUS features of a hemangioma are peripheral nodular enhancement in the arterial phase, progressing in a centripetal direction to partial or complete fill-in. The filling lasts from seconds to minutes and is more rapid in smaller lesions. Enhancement is sustained through the late and postvascular phases.

High flow (or shunt) hemangiomas show rapid homogeneous hyperenhancement in the arterial phase and can be confused with focal nodular hyperplasia (FNH), or rarely with hepatocellular adenomas or carcinomas. Thrombosed hemangiomas can be confused with malignancies because of the lack of enhancement in the thrombosed portions, which may be misinterpreted as wash out (Dietrich et al. 2007b).

Focal nodular hyperplasia. FNH is a benign hepatic lesion that is usually discovered incidentally. It can be managed conservatively in most patients. Color Doppler techniques are helpful to visualize the spoke-wheel vascular pattern which strongly supports the diagnosis of FNH (Dietrich et al. 2005; Piscaglia et al. 2010) more sensitively shown on CEUS, especially with maximum intensity projection (MIP) technique. On CEUS, FNH typically appears as a hyperenhancing homogeneous lesion in all phases. Hyperenhancement is obvious and usually marked in the arterial phase, with a rapid fill-in from the center outwards (70%) or with an eccentric vascular supply (30%) (Dietrich et al. 2005). During the portal venous and late phases, FNH may remain slightly hyperenhancing or become isoenhancing (Piscaglia et al. 2010) and a centrally located scar may be seen, hypoenhancing in the late phase. In small or deeply located lesions, it can be helpful to switch to color Doppler techniques after the CEUS study and use the remaining circulating microbubbles to enhance the Doppler signals for improved recognition of the typical spoke-wheel vascular pattern. Postvascular phase imaging (Sonazoid®) shows iso or hyperenhancement (Hatanaka et al. 2008b).

Hepatocellular adenoma. Hepatocellular adenoma (HCA) is a benign estrogen-dependent tumor, which is often discovered incidentally (Dietrich et al. 2005). HCA is an indication for surgery, particularly when larger than 5 cm (risk of hemorrhage and possible malignant transformation). On CEUS, HCA exhibit arterial hyperenhancement, usually initially at the periphery with subsequent very rapid centripetal filling, the opposite direction to that seen in FNH. However, this arterial

Table 2. Enhancement patterns of benign focal liver lesions in the non cirrhotic and cirrhotic liver

Lesion	Arterial phase	Portal venous phase	Late phase
A. Noncirrhotic liver			
Hemangioma			
Typical features	Peripheral nodular enhancement	Partial/complete centripetal fill in	Complete enhancement
Additional features	Small lesion: complete, rapid centripetal enhancement		Nonenhancing regions
FNH			
Typical features	Hyperenhancing from the center, complete, early	Hyperenhancing	Iso/hyperenhancing
Additional features	Spoke-wheel arteries Feeding artery	Unenhanced central scar	Unenhanced central scar
Hepatocellular adenoma			
Typical features	Hyperenhancing, complete	Isoenhancing	Isoenhancing
Additional features	Nonenhancing regions	Hyperenhancing Nonenhancing regions	Slightly hypoenhancing Nonenhancing regions
Focal fatty infiltration			
Typical features	Isoenhancing	Isoenhancing	Isoenhancing
Focal fatty sparing			
Typical features	Isoenhancing	Isoenhancing	Isoenhancing
Abscess			
Typical features	Peripheral enhancement, no central enhancement	Hyper-/isoenhancing rim, no central enhancement	Hypoenhancing rim, no central enhancement
Additional features		Hypoenhancing rim	
	Enhanced septa	Enhanced septa	
	Hyperenhanced liver segment	Hyperenhanced liver segment	
Simple cyst			
Typical features	Nonenhancing	Nonenhancing	Nonenhancing
B. Cirrhotic liver			
Regenerative nodule (±dysplastic)			
Typical features (not diagnostic)	Isoenhancing	Isoenhancing	Isoenhancing
Additional features	Hypoenhancing		

In cirrhotic liver simple cysts, hemangiomas and abscesses may also be found and show the same enhancement pattern as in noncirrhotic livers. All other entities are rare findings in cirrhotic livers.

enhancement pattern can also be encountered in HCC and hyperenhancing metastases and is not pathognomonic of HCA. The transition from the arterial hyperenhancing to the isoenhancing appearance occurs at the beginning of the portal venous phase, usually earlier than in FNH (Dietrich et al. 2005; Piscaglia et al. 2010). In most cases, the enhancement patterns of HCA may suggest malignancy when wash out occurs in the late phase, one of the few causes of false positives on CEUS.

Focal fatty change. Focal fatty change, either fat infiltration or fatty sparing, may simulate masses on conventional B-mode US. Differential diagnosis is important, especially in patients with underlying malignant disease or with an atypical location of suspected focal fatty changes. Focal fatty change shows exactly the same enhancement patterns as the adjacent liver parenchyma in all phases (Hirche et al. 2007).

Infection. Phlegmonous inflammation has variable and sometimes confusing CEUS appearances, which change as they evolve, early lesions being hyperenhancing, while mature lesions develop hypoenhancing foci as liquefaction progresses.

Mature abscesses typically show marginal enhancement in the arterial phase, sometimes with enhancement of septae followed by venous hypoenhancement. Lack of enhancement in the liquefied portions is the most prominent feature (Catalano et al. 2004; Catalano et al. 2007; Liu et al. 2008a).

The appearances of granulomas and focal tuberculosis on CEUS are variable but the majority show peripheral enhancement in the arterial phase with wash out in the portal and late phases, which may be difficult or impossible to differentiate from malignancies. The clinical history is important and the diagnosis is usually obtained on histopathology or microbiology (Liu et al. 2008a; Cao et al. 2010).

Other benign lesions. *Active hemorrhage* demonstrates contrast extravasation whereas hematomas show no enhancement.

Cysts show no contrast enhancement at all. CEUS is not needed for simple cysts but is useful to evaluate complicated or atypical cysts.

Inflammatory pseudotumor is a rare disease whose definite diagnosis is usually only made at surgery. It may show arterial enhancement and late phase hypoenhancement, falsely suggesting malignancy (Dietrich et al. 2007b).

Hepatic angiomyolipoma is a rare benign mesenchymal tumor with heterogeneous echogenicity on

Table 3. Enhancement patterns of malignant focal liver lesions in the noncirrhotic and cirrhotic liver

Lesion	Arterial phase	Portal venous phase	Late phase
A. Noncirrhotic liver			
Metastasis			
Typical features	Rim-enhancement	Hypoenhancing	Hypo/nonenhancing
Additional features	Complete enhancement Hyperenhancement Nonenhancing regions	Nonenhancing regions	Nonenhancing regions
HCC			
Typical features	Hyperenhancing	Isoenhancing	Hypo/nonenhancing
Additional features	Nonenhancing regions	Nonenhancing regions	Nonenhancing regions
Cholangiocarcinoma			
Typical features	Rim-like hyperenhancement, central hypoenhancement	Hypoenhancing	Nonenhancing
Additional features	Nonenhancing regions Inhomogeneous Hyperenhancement	Nonenhancing regions	Nonenhancing regions
B. Cirrhotic liver			
HCC			
Typical features	Hyperenhancing, complete Nonenhancing areas (if large)	Isoenhancing Nonenhancing regions	Hypoenhancing (slightly or moderately)
Additional features	Basket pattern, chaotic vessels Enhancing tumor thrombus		Isoenhancing
	Hypo/nonenhancing	Nonenhancing	Nonenhancing

Explanation: Other malignancies in cirrhosis have the same patterns as in noncirrhotic livers.

baseline ultrasound. CEUS shows arterial hyperenhancement (Wang et al. 2010).

Cholangiocellular adenomas (CCA or bile duct adenoma) are rare lesions that are usually small (90% <1 cm). CEUS may show strong arterial enhancement and early wash out in the portal and late phases (they lack portal veins), falsely suggesting malignancy (Ignee et al. 2009).

2.1.5. Malignant liver lesions. Hypoenhancement of solid lesions in the late and postvascular phases, corresponding to the wash out phenomenon characterizes malignancies. Almost all metastases show this feature, regardless of their enhancement pattern in the arterial phase. Very few exceptions to this rule have been reported, mainly in atypical HCC (Table 3).

HCC in the noncirrhotic liver. HCC are usually hyperenhancing in the arterial phase, typically with a chaotic vascular pattern. In the portal venous and late phases, HCC usually shows hypoenhancement apart from well-differentiated HCC that may be isoenhancing. Hyperenhancement in the arterial phase is believed to be homogeneous with fill from the periphery. However, this information is based only on expert opinion. The fibrolamellar variant of HCC has nonspecific appearances on B-mode. According to expert opinion and a single case report, they show rapid hyperenhancement with a heterogeneous pattern in the arterial phase and rapid wash out (Mandry et al. 2007).

Cholangiocarcinoma (intrahepatic cholangiocellular carcinoma). Intrahepatic cholangiocarcinomas have a variety of patterns in the arterial phase but all show late phase wash out, in contrast to the late enhancement on CECT or CEMRI (Xu et al. 2006b; Chen et al. 2008; Chen et al. 2010). The typical pattern of malignancy is better displayed by CEUS than by CECT or CEMRI. Peripheral cholangiocarcinoma may also be suspected on baseline US as surface retraction is a characteristic feature.

Metastases. Liver metastases can be detected and characterized reliably as hypoenhancing lesions during the portal venous and late phases, with very few exceptions. Wash out starts early, usually in the portal venous phase, and is marked. Thus, they appear as punched-out "black foci" against the background of the uniformly enhanced normal liver. Larger traversing vessels can sometimes be seen as enhancing lines within the lesion but these are not tumor tissue and, thus, have the hemodynamics of the vascular tree, disappearing in parallel with the main liver vessels rather than being retained, as occurs in the normal liver parenchyma. In the late phase, very small metastases may be conspicuous and lesions that were occult on B-mode ultrasound can be detected (Dietrich et al. 2006).

Metastases usually show at least some contrast enhancement in the arterial phase and sometimes this is marked and often it is chaotic. Rim or halo enhancement is often seen. Only a few false positive results have been observed, mainly from abscesses or necrosis, old fibrous FNH, granulomas and inflammatory pseudotumors (Ding et al. 2005; Schuessler et al. 2006; Dietrich et al. 2008).

Benign lesions such as cysts, calcifications, hemangiomas, FNH and adenomas are found with the same frequency (5%–20%) in the metastatic liver as in a healthy

population. Thus, the possibility of a benign FLL must be kept in mind when the liver is first staged after the diagnosis of a cancer, especially with lesions <2 cm.

Lymphoma. Lymphoma shows variable arterial enhancement but characteristic wash out in the portal venous and late phases, predictive of malignancy (Foschi et al. 2010).

2.1.6. Recommended uses and indications. CEUS should be performed and interpreted with knowledge of the patient's clinical history and investigations findings. When the enhancement patterns are typical (in appropriate clinical settings) hemangiomas, FNH, focal fatty change and malignancies can all be characterized with confidence. FLL with atypical enhancement patterns or studies that are technically suboptimal require further investigation, mainly with CECT and/or CEMRI.

CEUS is indicated for lesion characterization in the following clinical situations:

- Incidental findings on routine ultrasound.
- Lesion(s) or suspected lesion(s) detected with US in patients with a known history of a malignancy, as an alternative to CT or MRI.
- Need for a contrast study when CT and MRI contrast are contraindicated.
- Inconclusive MRI/CT.
- Inconclusive cytology/histology results.

Specificity and sensitivity are reduced in moderately or markedly fatty livers and with deeply positioned lesions.

2.2. Characterization of FLL in the cirrhotic liver

2.2.1. Background. ***Types of FLL in cirrhosis.*** The FLL that occur in the cirrhotic liver are hepatocellular lesions (>95% of cases), peripheral cholangiocellular carcinomas (CCC), lymphomas and hemangiomas. Other diagnoses may be considered, but they are very rare, for unknown reasons.

B-mode ultrasound may detect features of malignancy (such as infiltration of adjacent structures, including vessels) but these features are usually only seen in large nodules (>5 cm) and do not help characterize smaller nodules.

Carcinogenic mechanism in HCC. The development of HCC is thought to occur through a multistep pathway in about 90% of cases (International Consensus Group for Hepatocellular Neoplasia 2009) in the following sequence:

- Large regenerative nodule.
- Low- or high-grade dysplastic nodule.
- Dysplastic nodule with a focus of HCC.
- Well differentiated HCC.
- Moderately to poorly differentiated HCC.

Progression along this pathway is accompanied by a decrease in both normal arterial and portal blood flow and a concurrent disappearance of normal intranodular vessels (Matsui 2005). Simultaneous with this decline in normal vascularity, there is a progressive increase in arterial flow from newly formed tumor vessels (neoangiogenesis). Therefore, hyperenhancement in the arterial phase can be seen in HCC of all stages of differentiation (Matsui 2005). These changes are key elements for the characterization of hepatocellular nodules in cirrhosis during the vascular phases of contrast enhancement.

Beside the vascular changes, HCC nodules tend to be devoid of reticuloendothelial cells (Kupffer cells), particularly with progressive dedifferentiation from well to moderately and poorly differentiated grades. This has become of particular importance with the introduction of contrast agents with a postvascular phase, where HCC shows as an enhancement defect.

The probability of HCC increases with nodule size. Nodules <1 cm are rarely malignant and ultrasound follow up (at 3-month intervals) is sufficient, according to the AASLD guidelines (Bruix and Sherman 2011). Further investigations should be started when the nodule enlarges to over 1 cm. The rate of HCC is 66% in nodules 1–2 cm (Forner et al. 2008; Iavarone et al. 2010), increasing to about 80% in nodules of 2–3 cm in size (Bolondi et al. 2005) and is above 92%–95% for nodules larger than 3 cm. The most challenging situation for imaging techniques is, therefore, the diagnosis of nodules of 1–3 cm in diameter.

2.2.2. Study procedure. General recommendations for the study of FLL are summarized above [see section 2.1.2]. In addition, if the liver is cirrhotic, the following points should be kept in mind:

Since the arterial phase is the most important in the setting of cirrhosis, good visualization of the nodule during normal breathing is desirable. If this is impossible, it is important to practice cooperation with the patient so that the nodule can be visualized during a breath hold, best taken about 10 s after contrast injection and maintained for 15–30 s.

As microbubbles are disrupted despite the use of a low mechanical index, acoustic output power should be reduced as much as possible, while maintaining sufficient signal intensity, to allow contrast persistence until the very late phase (beyond 3–4 min), which is often critical for the diagnosis of HCC. Furthermore, when the arterial phase is over, the lesion should be scanned intermittently, not continuously, to minimize bubble disruption that may cause difficulties in interpretation of subtle wash out.

2.2.3. Image interpretation and evaluation. ***CEUS pattern and diagnosis of HCC (Table 3).*** The key feature for the diagnosis of HCC in liver cirrhosis is hyperenhancement in the arterial phase, followed by wash out in the late phase (Bruix and Sherman 2011). This pattern corresponds to HCC in more than 97% of cases (Fan et al. 2006; Foschi et al. 2010; Vilana et al. 2010; Boozari et al. 2011). However, it has also been reported in peripheral CCC and hepatic lymphoma, which comprise the remaining 1%–3% of cases. The timing and intensity of wash out in the latter lesions have not yet been described precisely (Fan et al. 2006; Foschi et al. 2010; Vilana et al. 2010; Boozari et al. 2011).

Arterial hyperenhancement is usually homogeneous and intense in HCC, but may be inhomogeneous in larger nodules (>5 cm), which contain regions of necrosis. Rim enhancement is atypical for HCC.

Wash out is observed overall in about half the cases of HCC but more rarely in very small nodules (20%–30% in those 1–2 cm, 40%–60% in those 2–3 cm) (Forner et al. 2008; Leoni et al. 2010; Sangiovanni et al. 2010). Wash out is observed more frequently in HCC with poorer grades of differentiation than in well-differentiated HCC, which tend to be isoechoic in the late phase (Fan et al. 2006; Jang et al. 2007; Iavarone et al. 2010; Boozari et al. 2011).

The hypoenhancement in the late phase is usually less marked in HCC than in other primary tumors or in liver metastases. Furthermore, the wash out tends to start later in HCC, usually not before 60 s after injection and, in up to 25% of cases, appearing only after 180 s (Chen et al. 2006a; Boozari et al. 2011); consequently it is important to observe nodules in cirrhosis until very late (>4 min) to increase sensitivity for the diagnosis of HCC. Early wash out (<60 s) has been reported to occur in poorly differentiated HCC or to suggest a nonhepatocellular malignancy (Chen et al. 2006a; Fan et al. 2006; Jang et al. 2007; Boozari et al. 2011), most often a peripheral CCC. Wash out in HCC is observed less often with CEUS compared with MRI or CT because of their different contrast pharmacokinetics (Strobel et al. 2005; Forner et al. 2008; Leoni et al. 2010; Sangiovanni et al. 2010).

Arterial hyperenhancement not followed by wash out is also highly suspicious for HCC, mainly for the well-differentiated variants but is not definitive (Bolondi et al. 2005; Fan et al. 2006; Jang et al. 2007; Iavarone et al. 2010; Boozari et al. 2011).

An inconclusive CEUS pattern does not rule out malignancy and should prompt other imaging (CT or MRI) and, if these are also inconclusive, biopsy is needed. If this is negative, the nodule should be followed up every 3 months (at least for the first 2 years) and, if it enlarges or the enhancement pattern changes, diagnostic investigations must be resumed. If arterial enhancement is present on any imaging technique, repeated biopsy should be considered even in the absence of changes in size or enhancement.

Hemangioma has the same CEUS pattern in cirrhosis as in the noncirrhotic liver but an additional MRI scan is preferable to confirm the diagnosis in this clinical setting. Abscesses may occur in cirrhosis, usually as a complication of interventional procedures. CEUS shows typical findings of malignancy in CCC, whereas the enhancement pattern at MRI and CT may be inconclusive (Vilana et al. 2010).

Staging of cirrhotic patients with HCC and the role of CEUS. Examining the entire liver during the arterial phase to look for hyperenhancing nodules is difficult or impossible with CEUS, so CECT or CEMRI must be used to stage patients with HCC (Bruix and Sherman 2011). For Sonazoid®, the postvascular phase may improve staging of the disease.

A diagnostic flowchart for CEUS of nodules in cirrhosis is given in Figure 1.

2.2.4. Recommended uses, indications and limitations

CEUS is recommended:

- To characterize all nodules found on surveillance and routine US.
- To characterize nodules in cirrhosis and establish a diagnosis of HCC. It is a strong belief of the expert panel that CEUS is extremely useful, especially when performed immediately after nodule detection, to make a rapid diagnosis. However, CT or MRI are needed (unless contraindicated) to stage the disease before the treatment strategy is decided.
- Whether CEUS has a role as first line investigation at the same level as CT or MRI is variably accepted in national and international guidelines. For example, CEUS is part of the Japanese guidelines on HCC (Kudo and Okanoue 2007; Kudo et al. 2011b) but has been removed from the American guidelines (Bruix and Sherman 2011). This was partly justified by the fact that no UCA is licensed for the liver in the USA and additionally because of the risk of misdiagnosing CCC for HCC when CEUS is used alone (1%–2%). In practice, the likelihood of misdiagnosis is minimal when CEUS is performed by skilled operators (Barreiros et al. 2012).
- When CT or MRI is inconclusive, especially in nodules not suitable for biopsy.
- To contribute to the selection of nodule(s) for biopsy when they are multiple or have different contrast patterns.
- To monitor changes in size and enhancement patterns over time when a nodule is not diagnostic for HCC and is being followed.
- After inconclusive histology.

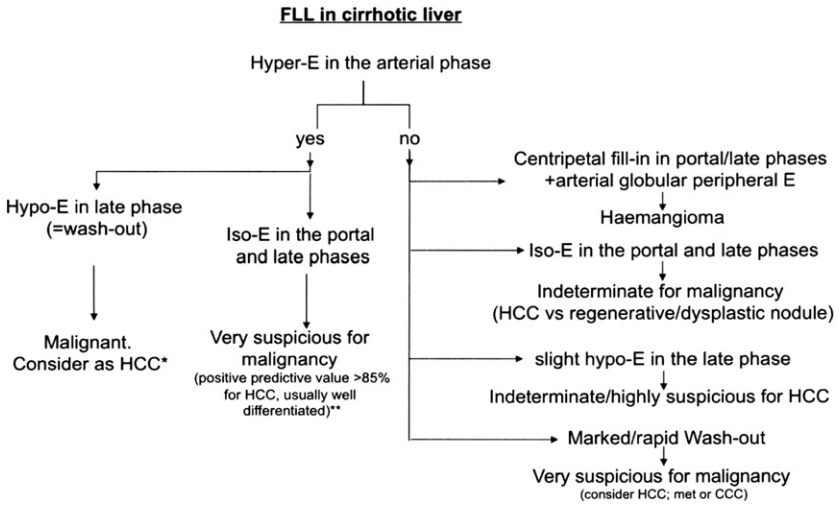

Fig. 1. * In cases with marked and rapid wash out in portal/late phase, consider the possibility of peripheral cholangiocarcinoma, especially if the pattern with MRI or CT does not confirm late wash out, or (exceptionally) metastasis or lymphoma. CEUS alone with a typical pattern is enough to establish a diagnosis of malignancy in nodules >1 cm, but a panoramic imaging technique (CT or MRI) is required to stage the patient before treatment. **When Sonazoid® is used, the postvascular phase may allow diagnosis of malignancy if the lesion becomes hypoenhancing in the postvascular phase, even though it appeared isoenhancing in the portal/late phases. E = enhancement; HCC = hepatocellular carcinoma; CCC = cholangiocellular carcinoma; met = metastasis.

2.2.5. CEUS with postvascular phase agents in cirrhotic liver nodules. ***Technical aspects and diagnostic features.*** Sonazoid® is different from pure blood-pool ultrasound contrast agents in that, in addition to the arterial and portal venous phases, there is a postvascular phase starting from 10 minutes after injection. Sonazoid® is taken up by the reticuloendothelial cells, particularly the Kupffer cells, similarly to SPIO MRI contrast agents (Korenaga et al. 2009). The microbubbles can be detected even when located within cells.

The mesenchymal meshwork of malignant lesions usually does not harbor reticuloendothelial (Kupffer) cells, at variance from normal and cirrhotic liver parenchyma and from most solid benign liver lesions. The absence of Kupffer cells causes a defect in Sonazoid® uptake in the postvascular phase (Hatanaka et al. 2008b; Inoue et al. 2008), which is, thus, a molecular imaging modality. The diagnostic capability of CEUS with Sonazoid® in the postvascular phase is similar to that of MRI with an SPIO (Korenaga et al. 2009) and has been endorsed in the Japanese guidelines for the management of HCC (Kudo et al. 2011b).

Study procedures specific to postvascular phase agents.

- After intravenous injection of Sonazoid®, continuous scanning for 30–60 s is recommended to assess the arterial and portal venous phases.
- The late vascular phase is deemed less relevant by Japanese authors, as this is replaced by the postvascular phase. For assessment of the postvascular (Kupffer) phase, scanning is begun not earlier than 10 min post-injection of Sonazoid® to allow clearance of contrast from the blood pool (Kudo et al. 2010).
- After the end of the portal venous phase, insonation of the liver should be stopped to limit acoustic disruption of microbubbles before the postvascular phase.
- The postvascular phase lasts until the microbubbles have disappeared; thus, there is usually enough time for a thorough assessment of the whole liver to detect enhancement defects that suggest malignant nodules.
- When an enhancement defect is identified in the postvascular phase, a repeat contrast injection can be performed, superimposed on the original enhancement, to assess the arterial phase in this region. This procedure is termed "defect reperfusion imaging" or "defect reinjection technique" (Kudo et al. 2010).

Image interpretation. Image interpretation in the postvascular phase with Sonazoid® is reported in Table 4. A contrast defect, corresponding to hypoenhancement in the postvascular phase should be regarded as highly suggestive of malignancy in the setting of nodules in cirrhosis (Hatanaka et al. 2008b). Very well differentiated, early HCC, are isoenhancing in both the arterial and the postvascular phases in approximately 70% of cases (Arita et al. 2011). Nodule characterization cannot be performed in the postvascular phase alone, for which arterial phase assessment remains the cornerstone.

Table 4. Enhancement patterns of focal liver lesions in liver cirrhosis during the postvascular phase (Kupffer phase) with Sonazoid®

Lesion	Post-vascular phase with Sonazoid® (Kupffer phase)
Cyst	Nonenhancing
Hemangioma	Nonenhancing
FNH	Iso to hyperenhancing
Regenerative nodule	
Typical features (but not diagnostic)	Isoenhancing
Additional features (but not diagnostic)	Slightly hypo- or hyperenhancing
Dysplastic nodule	Isoenhancing
HCC	
Typical features	Nonenhancing or hypoenhancing
Additional features	Isoenhancing (well differentiated HCC)
Cholangiocarcinoma	
Typical features	Nonenhancing or hypoenhancing
Additional features	Not reported
Metastasis	
Typical features	Nonenhancing or hypoenhancing
Additional features	Not reported

The arterial and portal venous phases are the same as for other agents. Cholangiocarcinoma may mimic metastasis and poorly differentiated HCC. Metastasis may mimic cholangiocarcinoma and poorly differentiated HCC.

Recommended uses and indications. CEUS with Sonazoid® is recommended:

- To characterize nodules in cirrhosis, allowing assessment of both the vascular and postvascular phases. CEUS has been adopted in the Japanese guidelines for the management of HCC (Kudo and Okanoue 2007; Kudo 2010; Kudo et al. 2011b) to search for nodules seen on CT or MRI but unidentifiable on B-mode ultrasound.
- To screen for HCC in a cirrhotic liver (Kudo et al. 2011a); however, there is no evidence to date that this procedure is cost-effective.
- To stage HCC in livers in which US imaging is satisfactory; however, there is no evidence to date that CEUS can replace CT or MRI.

2.2.6. Tips for all contrast agents

- When a nodule is deeply located (>8 cm) and suboptimally visualized with conventional B-mode ultrasound, its evaluation can become even worse during CEUS because of attenuation by contrast microbubbles. Use of greater amounts of contrast increases the signals both from nodules and from superficial tissues, usually failing to improve or even worsening target evaluation. Irrespective of the contrast agent used, high doses should be avoided because this limits CEUS penetration in all phases.
- When the liver parenchyma is coarse on B-mode ultrasound, it may be extremely difficult to detect small nodules making it difficult to choose the region to be scanned during CEUS in the arterial phase.
- In case of liver nodules in patients with complete portal thrombosis, perfusion of the parenchyma depends on the arterial supply. Reducing the contrast dose (half the usual dose or less) can reduce signal saturation and improve tumor conspicuity.

2.3. Characterization of portal vein thrombosis

2.3.1. Definition. Portal vein thrombosis refers to the development of solid material within the lumen of any portion of the portal vein. The thrombus may be occlusive or nonocclusive and may involve the entire portal venous system or any segment. There are two main forms (Piscaglia et al. 2010):

- Bland (appositional) thrombosis refers to the presence of a simple clot within the vein. It is often silent and may be clinically inapparent.
- Malignant (neoplastic) thrombosis occurs almost always as a complication of HCC in the liver. Its identification is of prognostic significance as it negatively alters therapy options and upstages disease.

2.3.2 Imaging of portal vein thrombosis. ***Baseline ultrasound and Doppler techniques.*** The thrombosed portal vein may look normal and yet be filled with thrombus. However, more often the thrombus has variable echogenicity, making the lumen appear hypoechoic rather than anechoic. The baseline scan should include color and spectral Doppler interrogation of the portal veins. Complete thrombosis shows no detectable signal from the portal vein, even when optimized for slow flow. The presence of intrathrombus signal with an arterial waveform on Doppler spectral examination is a highly specific sign of malignancy but its sensitivity is only moderate.

CEUS. Bland thrombus is avascular and shows as a void within the enhancing liver in all phases of CEUS but best visualized during the portal venous phase. A malignant thrombus has the same enhancement characteristics as the tumor from which it originated, including rapid arterial phase hyperenhancement (Rossi et al. 2006; Sorrentino et al. 2009; Piscaglia et al. 2010). While slow and weak portal venous wash out may be seen, the wash out is usually more rapid.

To perform the scans, the suspect thrombus within the vein should be studied during the wash in of the UCA, as the vascularization of the clot should parallel the arrival of the microbubbles within the hepatic artery in the liver in case of neoplastic thrombus. Sweeping through the liver in sagittal and axial planes in the portal venous phase will often depict the washed out tumor within the portal vein branches optimally.

The tumor source of a malignant portal vein thrombus may be obvious or it may be invisible on ultrasound, even with the assistance of CEUS. Sweeping through the liver in both the arterial and the portal venous phases of enhancement may be enlightening. Washed out regions of the liver should undergo reinjection with arterial phase imaging to show their arterial enhancement. A suspicious clot within the portal vein may be amenable to biopsy with US guidance, targeting, whenever possible, enhancing regions within the thrombus (Sorrentino et al. 2009).

2.4. CEUS for biopsy planning in cirrhotic and normal livers

CEUS prior to biopsy procedures can increase the diagnostic yield by 10% and decrease the false negative rate especially in large tumors with areas of necrosis. CEUS can localize the site for biopsy more accurately by demonstrating regions of vascularized viable tumor, which should be targeted, and regions of necrosis, which should be avoided (Wu et al. 2006). These two entities cannot be distinguished by conventional ultrasound alone. CEUS may also locate occult lesions on nonenhanced US (Schlottmann et al. 2004).

3. DETECTION OF MALIGNANT FLL: TRANSABDOMINAL APPROACH

3.1. Background

Conventional US is the most frequently used modality for the primary imaging of abdominal organs, including the liver but is less sensitive in the detection of liver lesions than CECT, CEMRI or intraoperative US. The main reasons for this are difficulties in detecting small and isoechoic lesions, especially when they are deep or in difficult anatomic locations.

The published literature (Dietrich et al. 2006; Quaia et al. 2006; Konopke et al. 2007; Larsen et al. 2007; Piscaglia et al. 2007; Chami et al. 2008; Inoue et al. 2008; Cantisani et al. 2010) provides strong evidence that CEUS significantly improves the detection of metastases compared with conventional US. The most important CEUS feature for detecting a malignant liver lesion is the identification of a focal region of wash out occurring as early as the late arterial phase but mostly during the portal venous and late or postvascular phases.

3.2. Study procedures

The study procedure is similar to the study procedure described in section 2.1.2 but the following points should be borne in mind:

- With all agents, lesion detection requires an examination time of at least 3–4 min, which is the useful persistence of most microbubbles.
- With agents presenting a postvascular phase (Sonazoid®), it is possible to detect lesions that wash out very late (Hatanaka et al. 2008b; Moriyasu and Itoh 2009).
- A second administration (reinjection technique) can be used to confirm the metastatic nature of any detected contrast defect by demonstrating arterial enhancement followed by wash out [see section 2.2.6].

3.3. Detection of metastatic lesions

The typical and almost invariable appearance of metastases is focal hypoenhancement in the portal venous, late and postvascular phases. The enhancement patterns observed during the arterial phase are variable and help to characterize lesions but aid only minimally in their detection [see section 2.1.3].

With vascular phase agents (SonoVue®, Definity®), several studies have shown that the accuracy in the detection of liver metastases is comparable to that of CECT and CEMRI, when scanning conditions allow a complete investigation of all liver segments (Larsen et al. 2007).

3.4. Detection of HCC and CCC

With all agents (SonoVue®, Definity®, Sonazoid®), most HCC show increased enhancement in the arterial phase but the short duration of this phase makes adequate assessment of the whole liver impossible, at least with current technology. The late phase lasts long enough for thorough exploration, but the appearances of HCC are variable, as described in section 2.2.3, and, importantly, not all HCC wash out in the late phase, limiting the sensitivity of CEUS for the detection of HCC. Consequently, routine use of UCA in the detection of HCC with vascular phase agents cannot be recommended.

With agents presenting a postvascular phase (Sonazoid®), scanning the entire liver at 10 min or later after injection helps to detect malignant nodules since typical HCC show as an enhancement defect (Hatanaka et al. 2008a; Maruyama et al. 2009; Moriyasu and Itoh 2009). However, postvascular defects are not specific findings and demonstration of homogeneous arterial enhancement requires a second administration of Sonazoid® to confirm the diagnosis of HCC. Moreover, approximately half of well differentiated HCC do not show enhancement defects in the postvascular phase (Arita et al. 2011).

Depiction of local tumor recurrence and residual tumor after ablation using B-mode alone is difficult. With vascular phase agents, scanning in the arterial phase with repeated injections demonstrates the hypervascularity in the recurrence, which usually lies adjacent to the previously ablated tumor. The same technique is useful for demonstrating new HCC and, in both cases, helps identify the target and guide treatment [see section 5.1].

Cholangiocarcinomas behave in the same way as metastases, washing out rapidly and appearing as defects in the late phase, regardless of the appearance in the arterial phase (Xu et al. 2006a). This pattern may facilitate detection of satellite nodules adjacent to a larger lesion that were not visualized on conventional US.

3.5. Recommended uses, indications and limitations

Use of CEUS is recommended for the following indications:

- To characterize indeterminate (usually small) lesions shown on either CECT or CEMRI.
- To "rule out" liver metastases or abscesses, unless conventional ultrasound shows typical findings.
- For treatment planning in selected cases to assess the number and location of liver metastases, either alone or as complementary to CECT and/or CEMRI.
- Surveillance of oncology patients where CEUS has been useful previously. Recommended to replace unenhanced US with CEUS for the evaluation of liver metastases in colorectal cancer after chemotherapy (Konopke et al. 2008).
- CEUS with vascular phase agents is not indicated for the detection and staging of HCC. With the use of Sonazoid® and postvascular phase scanning, CEUS may be used to stage HCC in the liver where imaging is good. However, there is no evidence to date that CEUS can replace CT or MRI.
- A potential pitfall is that small cysts, which were not seen on unenhanced US, are sometimes detected in late or postvascular phase scanning. Careful re-evaluation with conventional US may help to show their cystic nature. In doubtful situations, a second contrast agent injection is recommended, looking for arterial phase enhancement, which indicates viable tumor tissue.

4. INTRAOPERATIVE CONTRAST ENHANCED ULTRASOUND

4.1. Background

Standard preoperative imaging remains limited in selecting patients who may benefit from liver surgery (Ellsmere et al. 2007; Mazzoni et al. 2008). Intraoperative ultrasound (IOUS) is recognized as the gold standard, which ultimately dictates the surgical management of those undergoing resection (Charnley et al. 1991; Cervone et al. 2000; Jarnagin et al. 2001; Conlon et al. 2003). Patients with early stage HCC are offered transplantation or resection (Bruix et al. 2001), which can be curative procedures. Similarly, for patients with colorectal liver metastases, resection is the treatment of choice, with 5-year survival rates of up to 60% (Scheele et al. 1995; Fong 2000). However, 75% of patients who undergo resection develop recurrences (50% in the liver). The majority of recurrences appear within 2 years (Finlay et al. 1988; Scheele et al. 1995; Adam et al. 1997). Thus, more accurate imaging is required.

Recent studies of intraoperative contrast enhanced ultrasound (IO-CEUS) with different contrast agents have shown that it is more sensitive, specific and accurate than IOUS, CT or MRI in defining whether tumor resection (metastases or HCC) is appropriate. Furthermore, surgical management is altered in up to 30% of cases (Torzilli et al. 2005; Leen et al. 2006; Torzilli et al. 2007; Fioole et al. 2008; Nakano et al. 2008; Qiang et al. 2008). It is now recognized that the more aggressive the surgical approach adopted, the higher the impact of IO-CEUS becomes (Leen et al. 2006).

4.2. IO-CEUS technique

Dedicated high frequency intraoperative probes with contrast specific capability are needed. Covering the transducer and cable with a long sterile sheath containing coupling gel, and the control panel with a large sterile membrane ensures sterility. Some ultrasound systems provide intraoperative transducers that can be sterilized by gas and, thus, need no cover.

At surgery, all patients undergo a manual abdominal and pelvic exploration for extra-hepatic disease, followed by mobilization of the liver from the diaphragm to improve sonographic access. Bimanual palpation of the liver is then performed, followed by systematic IOUS of the entire liver, looking for previously diagnosed as well as for new lesions and to identify involvement of major vessels or bile ducts.

With vascular phase agents (SonoVue® and Definity®) CEUS is used as explained for the transabdominal approach [see section 2.1.2]. The duration of enhancement in normal liver in the late phase is shorter than with percutaneous US. Injections may be repeated for global assessment, or to assess the arterial phase enhancement of identified lesions for their characterization. Irrespective of the contrast agent used, high doses should be avoided because this limits US penetration in all phases.

With postvascular phase agents (Sonazoid®), detection of malignant FLL starts 10 min postinjection (Hatanaka et al. 2008b; Moriyasu and Itoh 2009). A second injection can be used to confirm the metastatic nature of a lesion by demonstrating arterial enhancement [see section 2.1.6].

4.3. Image interpretation

Image interpretation is the same as for the transabdominal approach reported in section 2.1.5.

4.4. Recommended use and limitations

IO-CEUS is recommended for:

- The detection of liver metastases in all patients undergoing liver resection.

- The characterization of focal liver nodules in cirrhotic patients undergoing liver resection for HCC, especially of new nodules detected at IOUS (Torzilli et al. 2007).
- The targeting of occult lesions for ablation therapy for patients undergoing combined liver resection and ablative therapy.

The shorter duration of contrast enhancement is a limitation of IO-CEUS.

5. MONITORING ABLATION TREATMENT

5.1. Monitoring local ablation treatment

5.1.1. Background. Locoregional therapies, which conventionally include ablation, whatever the modality used, and transarterial chemo/radioembolization, play a key role in the management of patients with liver malignancies, both HCC and metastases (Livraghi et al. 2000; Gillams and Lees 2009).

Unenhanced US is commonly used to guide ablation. It is easy to use and widely available but, even when combined with Doppler, it does not provide useful information on the extent of the ablation. Assessment of tissue perfusion is crucial to differentiate necrotic from viable residual tumor.

The addition of CEUS can provide important information in each of the following procedures (Choi et al. 2003; Minami et al. 2007):

- Assessment of the lesions to be treated by ablation (number and size and homogeneity of enhancement of the lesions, and the presence of feeding vessels) to define the eligibility of the patient for treatment and the best ablation strategy.
- Depict previously undetectable lesions with the support of fusion imaging, enabling needle/probe guidance.
- Detecting viable tumor persistence following locoregional treatment (either ablation or chemo/radioembolization).

5.1.2. Study procedures [see also section 2.1.2]. ***Pretreatment CEUS.*** Particularly for metastases, assessment of size must include the perilesional hypervascular halo with wash out. Tumor margins are better detected by CEUS than unenhanced US (Chen et al. 2007) because definition of its relationships with surrounding structures is improved, thus, helping develop appropriate treatment strategies and reducing the risks of complications (Chen et al. 2006b; Chen et al. 2007).

Accurate pretreatment planning can be improved by real-time fusion imaging with CT, MRI or CEUS, which provides an accurate volumetric map of the tumor and graphically depicts the number and sites of the ablation volumes needed to cover the whole mass and achieve an adequate perilesion "safety margin" (Chen et al. 2004; Liu et al. 2005).

Pretreatment CEUS is very helpful for comparison of the patterns before and after treatment.

The field depth, selected scan plane, acoustic gain and MI used for the pretreatment CEUS study of each lesion must be predefined. Images and/or video clips should be stored for precise comparison with immediate postablation studies.

Positioning of ablation device. The ablation device is inserted when the target is optimally depicted. When lesion targeting is particularly difficult (*e.g.*, small lesion size, difficult location), fusion imaging with CT/MRI may allow "targeted" CEUS in some instances (Crocetti et al. 2008) and consequent improvement of ablation needle/probe guidance. Depiction of a "virtual needle" during CEUS provided by fusion imaging may facilitate the procedure.

5.1.3. Image interpretation—definition of complete treatment response. The Response Evaluation Criteria in Solid Tumors (RECIST) guidelines (Therasse et al. 2000) for the assessment of tumor response are no longer considered adequate for locoregional treatment because of the poor relationship between necrosis and tumor size. After thermal ablations, completely necrotic tumors may remain unchanged in size, whereas tumors that shrink may still be partially viable.

Accordingly, the RECIST criteria have been amended, at least for HCC (Lencioni and Llovet 2010), to stress that the imaging indicator of complete ablation is the disappearance of any previously visualized intralesional enhancement on CEUS. This must be assessed throughout the whole volume of each tumor which has undergone ablation (Choi et al. 2003; Shiozawa et al. 2010). The volume of the necrosis achieved should be compared with the pretreatment volume of the tumor(s). Simultaneous display of tissue and contrast is of particular value for follow-up of treated lesions. The volume of necrosis achieved can be compared with the pretreatment volume of the same lesion on CECT or CEMRI using real-time fusion imaging (Kisaka et al. 2006).

Completeness of treatment of hypoenhancing lesions (mostly liver metastases) can be assessed by comparing the volume and location of pretreatment lesions with those of the ablated region. This also determines whether a sufficient safety margin around the lesion has been achieved. The frequent occurrence of satellite nodules around small HCC (5–10 mm from the main tumor [Sasaki et al. 2005]), dictates that the thickness of the safety margin following ablation should be assessed not only for liver metastases but also for HCC.

5.2. Periprocedural assessment of treatment response

Unenhanced US is used to monitor the reduction of the hyperechoic "cloud" of gas caused by heating immediately after ablation. This usually takes 5–15 min to dissipate.

For each treated lesion, the same system settings and scan planes must be used as for the preablation assessment. Images and/or video clips should be stored for comparison with previously stored preablation images. If additional probe/needle insertions are performed, repeated doses of UCA can be given.

5.2.1. Follow-up investigation to assess tumor recurrence. It is often difficult to depict local tumor recurrence after ablation using B-mode alone. Here, scanning in the late or postvascular phase, with subsequent reinjection to confirm tumor enhancement in any suspicious region is useful to identify the viable tumor adjacent to the ablated volume. This can be used to guide biopsy and additional treatment. While CEUS may be extremely useful to define local recurrence in a treated nodule, CT and MRI provide a better overview of the liver to detect distant intra- and extrahepatic tumor and cannot be replaced by CEUS.

In the early postablative evaluation (within the first 30 days), a thin, uniform enhancing rim can be visible along the periphery of the necrotic region, similar to the findings on CECT. Misinterpretation of this perilesional hyperemic halo as residual viable tumor can be avoided by comparing postablation images with preablation scans.

5.2.2. Recommended uses and indications

- As a complement to CECT and/or CEMRI for pretreatment staging and assessment of target lesion vascularity.
- Facilitation of needle positioning in cases of incomplete or poor lesion delineation on unenhanced US.
- Evaluation of the immediate treatment effect after ablation and guidance for immediate re-treatment of residual unablated tumor. Using this strategy, the rate of incomplete ablation in the first session is reported to decrease from 16% to 6% (Chen et al. 2004).
- Assessment of local tumor progression when follow-up CECT or CEMRI are contraindicated or not conclusive. In addition to CECT and/or CEMRI, CEUS may be used in follow-up protocols.

6. LIVER TRANSPLANTATION

6.1. Background

Liver transplantation is currently an established first-line treatment for patients with end-stage acute or chronic liver disease but postoperative complications may limit its long-term success and their early detection is extremely important for graft and patient survival. Hepatic artery (HA) thrombosis, which is the most common and severe vascular complication, occurs in 3%–8% of transplants in adults (Jain et al. 2000; Shaw et al. 2003). Acute HA thrombosis almost invariably leads to graft loss from infarction and eventual abscess formation. Hepatic artery stenosis may proceed to thrombosis and may cause ischemic liver and biliary injuries if not promptly corrected. Although portal vein (PV) and hepatic vein or caval thrombosis are less frequent, they are also serious complications that may lead to graft loss (Langnas et al. 1991). Clinical signs of vascular complications are often nonspecific, and the diagnosis, best made at the presymptomatic stage, depends on imaging. Ultrasound is usually used first to detect vascular complications as well as for long-term follow-up (Flint et al. 1988; Langnas et al. 1991; Dodd et al. 1994).

Though Doppler is useful, it may be not sensitive enough to depict slow flow in a patent HA, particularly in patients with postoperative edema, inaccessible hepatic arteries, or inability to cooperate (Sidhu et al. 2004). When flow cannot be identified in the HA, CECT or angiography, with their attendant risks, were hitherto required to obtain a definitive answer; CEUS can be used instead and is often able to overcome the limitations of Doppler.

6.2. Study procedure

The study procedure is as described in section 2.1.2. The intrahepatic arterial tree is well visualized at the time of its enhancement in the early arterial phase, before arrival of contrast microbubbles in the portal system. The right hepatic artery is usually visible anteriorly alongside the right portal branch through a right intercostal scan and the left hepatic artery at the bifurcation of the left portal branch, optimally seen with a supine epigastric approach. The portal vein and its branches are visualized in the portal venous phase, following which the enhancement of the parenchyma can be studied looking for infarcts, which appear as nonenhancing regions. Later the hepatic veins fill and can be studied. When only the vessels are to be explored, a reduced amount of injected contrast may improve their visualization by preventing signal saturation.

6.3. Image interpretation

Lack of visualization of the arterial tree, expected to be seen before portal enhancement, indicates complete arterial thrombosis with very high positive predictive values (Sidhu et al. 2004; Berstad et al. 2009; Clevert et al. 2009; Lu et al. 2012). Identification of the arterial branches when conventional Doppler has failed (Sidhu et al. 2004), may allow subsequent

targeted Doppler reassessment, which is needed to distinguish thrombosis from slow flow caused by vasoconstriction or splenic steal from post-thrombotic/stenotic recanalization, tasks not achievable using CEUS alone. When the main hepatic artery is visible, CEUS depicts the shape of the lumen and its course, possibly identifying stenoses, which usually occur at the site of the surgical anastomosis (Zheng et al. 2010). CEUS may also allow study of the shape and patency of the caval and portal anastomoses.

6.4. Recommended Indications and Limitations

6.4.1. Indications. Before liver transplantation, CEUS is indicated to assess portal vein thrombosis and characterize focal liver lesions in cirrhosis. After liver transplantation, CEUS can be performed at the bedside or in the intensive care unit, avoiding most of the risks associated with CECT or angiography (Huang et al. 2008; Berstad et al. 2009; Clevert et al. 2009; Luo et al. 2009; Zheng et al. 2010). CEUS is indicated for:

- Confirmation of occlusion of the intrahepatic hepatic arteries, portal veins, hepatic veins or inferior vena cava (IVC) after an inconclusive Doppler evaluation of the liver vasculature. The extrahepatic arterial tree cannot always be studied in its entirety and complete patency cannot be confirmed with certainty without the addition of the finding of normal flow tracings from the intrahepatic arteries on Doppler US. In the late phase, the ultrasound can be switched to Doppler to exploit the remaining microbubbles to enhance the Doppler signals and investigate small vessels missed without contrast.
- Confirmation of the presence and assessment of the nature of fluid collections and, in case of recent hematomas, to search for active bleeding.
- Exclusion of perfusion defects when infarction is suspected.
- For monitoring the success of thrombolysis in the intensive care unit (ICU) after interventions for hepatic artery occlusion.

6.4.2. Limitations

- In the early postoperative period, wounds and surgical dressings or subcutaneous emphysema, may limit examination windows.
- In patients with split liver transplantation or after living donor liver transplantation, the examination may be more difficult because of the complex anatomy.
- Imaging the prehepatic portions of the hepatic artery and portal vein may be precluded by the surgical wound or intervening bowel gas.

6.4.3. Tips and tricks

- When a side-to-side caval (piggyback) anastomosis is used, the distal part of the donor cava may thrombose and simulate a small subcapsular hematoma.
- Ascites may collect alongside the ligament teres and may simulate a complex cyst on follow-up examinations.
- Knowledge of the surgical procedures including the presence of jump grafts, difficult anastomoses and the status of the donor liver may be helpful to interpretation.
- While CEUS shows the morphology of the vessel lumen, integration with Doppler US is required to confirm the presence of a hemodynamically significant stenosis.

7. CONTRAST QUANTIFICATION AND MONITORING SYSTEMIC TREATMENT OF MALIGNANCIES

7.1. Background

Neovascularization is a key stage in the growth of malignancies beyond 2–3 mm^3. This neoangiogenesis is an important target for novel anticancer treatments and many new antiangiogenesis or antivascular treatments aim at destroying or limiting the growth of tumor vessels (Ferrara and Kerbel 2005; Kessler et al. 2010). A new area of clinical utility for dynamic contrast enhanced ultrasound (DCE-US) has emerged for monitoring the response to these drugs. Initially, such monitoring relied on qualitative analyses only. More recently, robust and quantitative features have been developed. To achieve successful results, standardization and strict control of scanner settings are needed (Dietrich et al. 2012).

7.2. Methodology and equipment for quantification

7.2.1. Data acquisition. Contrast specific imaging is used to distinguish microbubble signals from tissue. The best temporal and spatial resolution is provided by nonlinear gray scale modes [see section 1.3]. Conventional Doppler imaging techniques cannot visualize vessels smaller than approximately 100 μm but CEUS can detect signals from vessels up to 40 μm (Forsberg et al. 2008) and, thus, provides a better assessment of the extent of angiogenesis.

7.2.2. Quantification software. Early measurements of contrast kinetics (*i.e.*, time-intensity curves, TIC) were performed using video data because it was readily available. Background subtraction was necessary to compensate for attenuation effects (Bos et al. 1995) and extract reliable time-based features, such as time to peak intensity, mean transit time, *etc.* However, the

nonlinear compression applied to the original signals (required to display them on video monitors) distorts amplitude-based TIC features (*e.g.*, peak intensity and area under the curve) (Peronneau et al. 2010).

The majority of reports have used uncompressed, post beam formed data (radio-frequency data are not required since the phase information is not essential). TIC based on such raw data sets allow for accurate assessment of both time-based and amplitude-dependent features. All manufacturers that supply built-in analysis packages on their scanners use this type of data but off-line software packages are also available (Cosgrove and Lassau 2010).

7.3. Administration of UCA and quantitative analysis

7.3.1. Bolus injection. Functional ultrasound studies are based on measuring the time sequence of signal enhancement, typically over the initial 1–3 min after an intravenous bolus injection, either across a large region-of-interest such as an entire tumor or on a pixel-by-pixel basis. The resulting TIC follows the wash in and wash out of the contrast agent and features linked to blood flow and blood volume can be extracted from them. Quantitative analyses of the TIC can be performed to determine functional features that characterize the TIC with or without curve fitting. Several functional features can be studied (Lassau et al. 2010a):

- Related to fractional blood volume: peak intensity (PI); area under the curve (AUC) (Clevert et al. 2009); area under the wash in (AUWI); under the wash out (AUWO).
- Related to blood flow: time to peak intensity (TPI); slope of the wash in (SWI).
- Related to transit time: mean transit time (MTT).

It is also possible to map the changes in TIC features over time and show these as colorized functional images.

7.3.2. The disruption-replenishment or reperfusion method. In this method, originally described for the heart (Wei et al. 1998), a high intensity diagnostic series of pulses is transmitted to a tissue slice filled with microbubbles following bolus or infusion injection, to destroy the bubbles within it. The scanner then switches to a low MI and the refill of the slice with microbubbles is monitored with a contrast-specific imaging mode. The refill takes the form of a rising exponential curve whose slope, β, relates to the velocity of blood inflow while the maximum enhancement, A, relates to the fractional blood volume. Their product forms an estimate of tissue perfusion (Guibal et al. 2010).

The advantage of an infusion of UCA is that a concentration equilibrium can be achieved, which makes it easier to compare different tissue regions directly (Liu et al. 2008b; Su et al. 2009). With the destruction-reperfusion method only the wash in phase can be assessed, which may limit its utility.

7.3.3. Hepatic vein transit times. The arrival times of a UCA bolus in the hepatic artery, portal vein and hepatic veins can be measured and transit times calculated. Shortening of the transit time between the hepatic artery/portal vein and the hepatic veins occurs in the presence of liver malignancies, presumably because of intrahepatic shunting. However, this also occurs in cirrhosis (Lim et al. 2005; Li et al. 2010), resulting in a nonspecific finding which limits its use in liver malignancy. Its use to stage chronic hepatitis is also limited by the substantial overlap between different stages despite statistically significant differences among groups (Ridolfi et al. 2007).

7.4. Assessment of antiangiogenic treatment

Since antiangiogenic treatment frequently induces necrosis without causing tumor shrinkage, functional imaging techniques are particularly suitable for the early assessment of response, a task for which both the RECIST and World Health Organization (WHO) size criteria (World Health Organisation Offset Publication 1979; Therasse et al. 2000) are unsatisfactory (Lencioni and Llovet 2010).

Studies of various types of tumors treated with antiangiogenic therapies have confirmed that DCE-US may enable early prediction of response to treatment (De Giorgi et al. 2005; Lamuraglia et al. 2006; Lassau et al. 2006; Lassau et al. 2010b; Lassau et al. 2011; Lassau et al. 2012).

Acknowledgments—The authors acknowledge the educational contributions provided by the following companies: Bracco; GE Healthcare; Hitachi Medical Systems; Lantheus Medical Imaging; Medison; Philips Medical Systems; Siemens Healthcare; Toshiba Medical Systems; and Supersonic Imagine. The authors gratefully acknowledge Glynis Harvey from the WFUMB office for her efficient management.

REFERENCES

Adam R, Bismuth H, Castaing D, Waechter F, Navarro F, Abascal A, Majno P, Engerran L. Repeat hepatectomy for colorectal liver metastases. Ann Surg 1997;225:51–60. discussion -2.

Albrecht T, Blomley M, Bolondi L, Claudon M, Correas JM, Cosgrove D, Greiner L, Jager K, Jong ND, Leen E, Lencioni R, Lindsell D, Martegani A, Solbiati L, Thorelius L, Tranquart F, Weskott HP, Whittingham T. Guidelines for the use of contrast agents in ultrasound. January 2004. Ultraschall Med 2004;25: 249–256.

Arita J, Hasegawa K, Takahashi M, Hata S, Shindoh J, Sugawara Y, Kokudo N. Correlation between contrast-enhanced intraoperative ultrasound using Sonazoid and histologic grade of resected hepatocellular carcinoma. AJR Am J Roentgenol 2011;196:1314–1321.

Averkiou M, Powers J, Skyba D, Bruce M, Jensen S. Ultrasound contrast imaging research. Ultrasound Q 2003;19:27–37.

Barreiros AP, Piscaglia F, Dietrich CF. Contrast enhanced ultrasound for the diagnosis of hepatocellular carcinoma (HCC): Comments on AASLD guidelines. J Hepatol 2012;57:930–932.

Bernatik T, Seitz K, Blank W, Schuler A, Dietrich CF, Strobel D. Unclear focal liver lesions in contrast-enhanced ultrasonography–lessons to be learned from the DEGUM multicenter study for the characterization of liver tumors. Ultraschall Med 2010;31:577–581.

Berstad AE, Brabrand K, Foss A. Clinical utility of microbubble contrast-enhanced ultrasound in the diagnosis of hepatic artery occlusion after liver transplantation. Transpl Int 2009;22:954–960.

Bolondi L, Gaiani S, Celli N, Golfieri R, Grigioni WF, Leoni S, Venturi AM, Piscaglia F. Characterization of small nodules in cirrhosis by assessment of vascularity: the problem of hypovascular hepatocellular carcinoma. Hepatology 2005;42:27–34.

Boozari B, Soudah B, Rifai K, Schneidewind S, Vogel A, Hecker H, Hahn A, Schlue J, Dietrich CF, Bahr MJ, Kubicka S, Manns MP, Gebel M. Grading of hypervascular hepatocellular carcinoma using late phase of contrast enhanced sonography - a prospective study. Dig Liver Dis 2011;43:484–490.

Bos LJ, Piek JJ, Spaan JA. Background subtraction from time-intensity curves in videodensitometry: a pitfall in flow assessment using contrast echocardiography. Ultrasound Med Biol 1995;21: 1211–1218.

Bruix J, Sherman M. Management of hepatocellular carcinoma. Hepatology 2005;42:1208–1236.

Bruix J, Sherman M. Management of hepatocellular carcinoma: an update. Hepatology 2011;53:1020–1022.

Bruix J, Sherman M, Llovet JM, Beaugrand M, Lencioni R, Burroughs AK, Christensen E, Pagliaro L, Colombo M, Rodes J. Clinical management of hepatocellular carcinoma. Conclusions of the Barcelona-2000 EASL conference. European Association for the Study of the Liver. J Hepatol 2001;35:421–430.

Cantisani V, Ricci P, Erturk M, Pagliara E, Drudi F, Calliada F, Mortele K, D'Ambrosio U, Marigliano C, Catalano C, Marin D, Di Seri M, Longo F, Passariello R. Detection of hepatic metastases from colorectal cancer: prospective evaluation of gray scale US versus SonoVue(R) low mechanical index real time-enhanced US as compared with multidetector-CT or Gd-BOPTA-MRI. Ultraschall Med 2010;31:500–505.

Cao BS, Li XL, Li N, Wang ZY. The nodular form of hepatic tuberculosis: contrast-enhanced ultrasonographic findings with pathologic correlation. J Ultrasound Med 2010;29:881–888.

Catalano O, Sandomenico F, Nunziata A, Raso MM, Vallone P, Siani A. Transient hepatic echogenicity difference on contrast-enhanced ultrasonography: sonographic sign and pitfall. J Ultrasound Med 2007;26:337–345.

Catalano O, Sandomenico F, Raso MM, Siani A. Low mechanical index contrast-enhanced sonographic findings of pyogenic hepatic abscesses. AJR Am J Roentgenol 2004;182:447–450.

Cervone A, Sardi A, Conaway GL. Intraoperative ultrasound (IOUS) is essential in the management of metastatic colorectal liver lesions. Am Surg 2000;66:611–615.

Chami L, Lassau N, Malka D, Ducreux M, Bidault S, Roche A, Elias D. Benefits of contrast-enhanced sonography for the detection of liver lesions: comparison with histologic findings. AJR Am J Roentgenol 2008;190:683–690.

Charnley RM, Morris DL, Dennison AR, Amar SS, Hardcastle JD. Detection of colorectal liver metastases using intraoperative ultrasonography. Br J Surg 1991;78:45–48.

Chen LD, Xu HX, Xie XY, Lu MD, Xu ZF, Liu GJ, Liang JY, Lin MX. Enhancement patterns of intrahepatic cholangiocarcinoma: comparison between contrast-enhanced ultrasound and contrast-enhanced CT. Br J Radiol 2008;81:881–889.

Chen LD, Xu HX, Xie XY, Xie XH, Xu ZF, Liu GJ, Wang Z, Lin MX, Lu MD. Intrahepatic cholangiocarcinoma and hepatocellular carcinoma: differential diagnosis with contrast-enhanced ultrasound. Eur Radiol 2010;20:743–753.

Chen MH, Dai Y, Yan K, Fan ZH, Yin SS, Yang W, Wu W, Wang YB, Li JY. The role of contrast-enhanced ultrasound on the diagnosis of small hepatocellular carcinoma (</=3cm) in patients with cirrhosis. Hepatol Res 2006a;35:281–288.

Chen MH, Wei Y, Yan K, Gao W, Dai Y, Huo L, Yin SS, Zhang H, Poon RT. Treatment strategy to optimize radiofrequency ablation for liver malignancies. J Vasc Interv Radiol 2006b;17:671–683.

Chen MH, Yang W, Yan K, Dai Y, Wu W, Fan ZH, Callstrom MR, Charboneau JW. The role of contrast-enhanced ultrasound in planning treatment protocols for hepatocellular carcinoma before radiofrequency ablation. Clin Radiol 2007;62:752–760.

Chen MH, Yang W, Yan K, Zou MW, Solbiati L, Liu JB, Dai Y. Large liver tumors: protocol for radiofrequency ablation and its clinical application in 110 patients–mathematic model, overlapping mode, and electrode placement process. Radiology 2004;232:260–271.

Choi D, Lim HK, Lee WJ, Kim SH, Kim YH, Kim SH, Lim JH. Early assessment of the therapeutic response to radio frequency ablation for hepatocellular carcinoma: utility of gray scale harmonic ultrasonography with a microbubble contrast agent. J Ultrasound Med 2003;22:1163–1172.

Claudon M, Cosgrove D, Albrecht T, Bolondi L, Bosio M, Calliada F, Correas JM, Darge K, Dietrich C, D'Onofrio M, Evans DH, Filice C, Greiner L, Jager K, Jong N, Leen E, Lencioni R, Lindsell D, Martegani A, Meairs S, Nolsoe C, Piscaglia F, Ricci P, Seidel G, Skjoldbye B, Solbiati L, Thorelius L, Tranquart F, Weskott HP, Whittingham T. Guidelines and good clinical practice recommendations for contrast enhanced ultrasound (CEUS) - update 2008. Ultraschall Med 2008;29:28–44.

Clevert DA, Stickel M, Minaifar N, Lohe F, Graeb C, Jauch KW, Reiser M. Contrast-enhanced ultrasound in liver transplant: first results and potential for complications in the postoperative period. Clin Hemorheol Microcirc 2009;43:83–94.

Conlon R, Jacobs M, Dasgupta D, Lodge JP. The value of intraoperative ultrasound during hepatic resection compared with improved preoperative magnetic resonance imaging. Eur J Ultrasound 2003;16: 211–216.

Cosgrove D, Harvey C. Clinical uses of microbubbles in diagnosis and treatment. Med Biol Eng Comput 2009;47:813–826.

Cosgrove D, Lassau N. Imaging of perfusion using ultrasound. Eur J Nucl Med Mol Imaging 2010;37(Suppl 1):S65–S85.

Crocetti L, Lencioni R, Debeni S, See TC, Pina CD, Bartolozzi C. Targeting liver lesions for radiofrequency ablation: an experimental feasibility study using a CT-US fusion imaging system. Invest Radiol 2008;43:33–39.

Dawson P, Cosgrove D, Grainger R. Textbook of contrast media. Oxford: ISIS Medical Media; 1999.

De Giorgi U, Aliberti C, Benea G, Conti M, Marangolo M. Effect of angiosonography to monitor response during imatinib treatment in patients with metastatic gastrointestinal stromal tumors. Clin Cancer Res 2005;11:6171–6176.

Dietrich CF, Averkioui MA, Correas JM, Lassau N, Leen E, Piscaglia F. An EFSUMB introduction into dynamic contrast-enhanced ultrasound (DCE-US) for quantification of tumour perfusion. Ultraschall Med 2012;33:344–351.

Dietrich CF, Braden B, Hocke M, Ott M, Ignee A. Improved characterisation of solitary solid pancreatic tumours using contrast enhanced transabdominal ultrasound. J Cancer Res Clin Oncol 2008;134: 635–643.

Dietrich CF, Ignee A, Hocke M, Schreiber-Dietrich D, Greis C. Pitfalls and artefacts using contrast enhanced ultrasound. Z Gastroenterol 2011;49:350–356.

Dietrich CF, Kratzer W, Strobe D, Danse E, Fessl R, Bunk A, Vossas U, Hauenstein K, Koch W, Blank W, Oudkerk M, Hahn D, Greis C. Assessment of metastatic liver disease in patients with primary extrahepatic tumors by contrast-enhanced sonography versus CT and MRI. World J Gastroenterol 2006;12:1699–1705.

Dietrich CF, Mertens JC, Braden B, Schuessler G, Ott M, Ignee A. Contrast-enhanced ultrasound of histologically proven liver hemangiomas. Hepatology 2007b;45:1139–1145.

Dietrich CF, Schuessler G, Trojan J, Fellbaum C, Ignee A. Differentiation of focal nodular hyperplasia and hepatocellular adenoma by contrast-enhanced ultrasound. Br J Radiol 2005;78:704–707.

Ding H, Wang WP, Huang BJ, Wei RX, He NA, Qi Q, Li CL. Imaging of focal liver lesions: low-mechanical-index real-time ultrasonography with SonoVue. J Ultrasound Med 2005;24:285–297.

Dodd GD 3rd, Memel DS, Zajko AB, Baron RL, Santaguida LA. Hepatic artery stenosis and thrombosis in transplant recipients: Doppler diagnosis with resistive index and systolic acceleration time. Radiology 1994;192:657–661.

EFSUMB (European Federation of Societies for Ultrasound in Medicine and Biology). Minimum training recommendations for the practice of medical ultrasound. Ultraschall in Med 2006;27:79–105.

EFSUMB (European Federation of Societies for Ultrasound in Medicine and Biology). Minimum training requirements for the practice of Medical Ultrasound in Europe. Ultraschall Med 2010;31:426–427.

Ellsmere J, Kane R, Grinbaum R, Edwards M, Schneider B, Jones D. Intraoperative ultrasonography during planned liver resections: why are we still performing it? Surg Endosc 2007;21:1280–1283.

Exuzides A, Main ML, Colby C, Grayburn PA, Feinstein SB, Goldman JH. A retrospective comparison of mortality in critically ill hospitalized patients undergoing echocardiography with and without an ultrasound contrast agent. JACC Cardiovasc Imaging 2010;3:578–585.

Fan ZH, Chen MH, Dai Y, Wang YB, Yan K, Wu W, Yang W, Yin SS. Evaluation of primary malignancies of the liver using contrast-enhanced sonography: correlation with pathology. AJR Am J Roentgenol 2006;186:1512–1519.

Ferrara N, Kerbel RS. Angiogenesis as a therapeutic target. Nature 2005;438:967–974.

Finlay IG, Meek D, Brunton F, McArdle CS. Growth rate of hepatic metastases in colorectal carcinoma. Br J Surg 1988;75:641–644.

Fioole B, de Haas RJ, Wicherts DA, Elias SG, Scheffers JM, van Hillegersberg R, van Leeuwen MS, Borel Rinkes IH. Additional value of contrast enhanced intraoperative ultrasound for colorectal liver metastases. Eur J Radiol 2008;67:169–176.

Flint EW, Sumkin JH, Zajko AB, Bowen A. Duplex sonography of hepatic artery thrombosis after liver transplantation. AJR Am J Roentgenol 1988;151:481–483.

Fong Y. Hepatic colorectal metastasis: current surgical therapy, selection criteria for hepatectomy, and role for adjuvant therapy. Adv Surg 2000;34:351–381.

Forner A, Vilana R, Ayuso C, Bianchi L, Sole M, Ayuso JR, Boix L, Sala M, Varela M, Llovet JM, Bru C, Bruix J. Diagnosis of hepatic nodules 20 mm or smaller in cirrhosis: Prospective validation of the noninvasive diagnostic criteria for hepatocellular carcinoma. Hepatology 2008;47:97–104.

Forsberg F, Kuruvilla B, Pascua MB, Chaudhari MH, Merton DA, Palazzo JP, Goldberg BB. Comparing contrast-enhanced color flow imaging and pathological measures of breast lesion vascularity. Ultrasound Med Biol 2008;34:1365–1372.

Foschi FG, Dall'Aglio AC, Marano G, Lanzi A, Savini P, Piscaglia F, Serra C, Cursaro C, Bernardi M, Andreone P, Stefanini GF. Role of contrast-enhanced ultrasonography in primary hepatic lymphoma. J Ultrasound Med 2010;29:1353–1356.

Gillams AR, Lees WR. Five-year survival in 309 patients with colorectal liver metastases treated with radiofrequency ablation. Eur Radiol 2009;19:1206–1213.

Guibal A, Taillade L, Mule S, Comperat E, Badachi Y, Golmard JL, Le Guillou-Buffello D, Rixe O, Bridal SL, Lucidarme O. Noninvasive contrast-enhanced US quantitative assessment of tumor microcirculation in a murine model: effect of discontinuing anti-VEGF therapy. Radiology 2010;254:420–429.

Hatanaka K, Kudo M, Minami Y, Maekawa K. Sonazoid-enhanced ultrasonography for diagnosis of hepatic malignancies: comparison with contrast-enhanced CT. Oncology 2008a;75(Suppl 1):42–47.

Hatanaka K, Kudo M, Minami Y, Ueda T, Tatsumi C, Kitai S, Takahashi S, Inoue T, Hagiwara S, Chung H, Ueshima K, Maekawa K. Differential diagnosis of hepatic tumors: value of contrast-enhanced harmonic sonography using the newly developed contrast agent. Sonazoid. Intervirology 2008b;51(Suppl 1):61–69.

Hirche TO, Ignee A, Hirche H, Schneider A, Dietrich CF. Evaluation of hepatic steatosis by ultrasound in patients with chronic hepatitis C virus infection. Liver Int 2007;27:748–757.

Huang D, Chen Y, Li K, Zhang Q. Hemodynamic changes on color Doppler flow imaging and intravenous contrast-enhanced ultrasound for assessing transplanted liver and early diagnosis of complications. J Huazhong Univ Sci Technolog Med Sci 2008;28:284–286.

Iavarone M, Sangiovanni A, Forzenigo LV, Massironi S, Fraquelli M, Aghemo A, Ronchi G, Biondetti P, Roncalli M, Colombo M. Diagnosis of hepatocellular carcinoma in cirrhosis by dynamic contrast imaging: the importance of tumor cell differentiation. Hepatology 2010;52:1723–1730.

Ignee A, Piscaglia F, Ott M, Salvatore V, Dietrich CF. A benign tumour of the liver mimicking malignant liver disease–cholangiocellular adenoma. Scand J Gastroenterol 2009;44:633–636.

Inoue T, Kudo M, Hatanaka K, Takahashi S, Kitai S, Ueda T, Ishikawa E, Hagiwara S, Minami Y, Chung H, Ueshima K, Maekawa K. Imaging of hepatocellular carcinoma: qualitative and quantitative analysis of postvascular phase contrast-enhanced ultrasonography with sonazoid. Comparison with superparamagnetic iron oxide magnetic resonance images. Oncology 2008;75(Suppl 1):48–54.

International Consensus Group for Hepatocellular Neoplasia. Pathologic diagnosis of early hepatocellular carcinoma: a report of the international consensus group for hepatocellular neoplasia. Hepatology 2009;49:658–664.

Jain A, Reyes J, Kashyap R, Dodson SF, Demetris AJ, Ruppert K, Abu-Elmagd K, Marsh W, Madariaga J, Mazariegos G, Geller D, Bonham CA, Gayowski T, Cacciarelli T, Fontes P, Starzl TE, Fung JJ. Long-term survival after liver transplantation in 4,000 consecutive patients at a single center. Ann Surg 2000;232:490–500.

Jang HJ, Kim TK, Burns PN, Wilson SR. Enhancement patterns of hepatocellular carcinoma at contrast-enhanced US: comparison with histologic differentiation. Radiology 2007;244:898–906.

Jarnagin WR, Bach AM, Winston CB, Hann LE, Heffernan N, Loumeau T, DeMatteo RP, Fong Y, Blumgart LH. What is the yield of intraoperative ultrasonography during partial hepatectomy for malignant disease? J Am Coll Surg 2001;192:577–583.

Kessler T, Bayer M, Schwoppe C, Liersch R, Mesters RM, Berdel WE. Compounds in clinical Phase III and beyond. Recent Results Cancer Res 2010;180:137–163.

Khawaja OA, Shaikh KA, Al-Mallah MH. Meta-analysis of adverse cardiovascular events associated with echocardiographic contrast agents. Am J Cardiol 2010;106:742–747.

Kisaka Y, Hirooka M, Kumagi T, Uehara T, Hiasa Y, Kumano S, Tanaka H, Michitaka K, Horiike N, Mochizuki T, Onji M. Usefulness of contrast-enhanced ultrasonography with abdominal virtual ultrasonography in assessing therapeutic response in hepatocellular carcinoma treated with radiofrequency ablation. Liver Int 2006;26:1241–1247.

Konopke R, Bunk A, Kersting S. Contrast-enhanced ultrasonography in patients with colorectal liver metastases after chemotherapy. Ultraschall Med 2008;29(Suppl 4):S203–S209.

Konopke R, Kersting S, Bergert H, Bloomenthal A, Gastmeier J, Saeger HD, Bunk A. Contrast-enhanced ultrasonography to detect liver metastases: A prospective trial to compare transcutaneous unenhanced and contrast-enhanced ultrasonography in patients undergoing laparotomy. Int J Colorectal Dis 2007;22:201–207.

Korenaga K, Korenaga M, Furukawa M, Yamasaki T, Sakaida I. Usefulness of Sonazoid contrast-enhanced ultrasonography for hepatocellular carcinoma: comparison with pathological diagnosis and superparamagnetic iron oxide magnetic resonance images. J Gastroenterol 2009;44:733–741.

Kudo M. The 2008 Okuda lecture: Management of hepatocellular carcinoma: from surveillance to molecular targeted therapy. J Gastroenterol Hepatol 2010;25:439–452.

Kudo M, Hatanaka K, Kumada T, Toyoda H, Tada T. Double-contrast ultrasound: a novel surveillance tool for hepatocellular carcinoma. Am J Gastroenterol 2011a;106:368–370.

Kudo M, Hatanaka K, Maekawa K. Newly developed novel ultrasound technique, defect reperfusion ultrasound imaging, using sonazoid in the management of hepatocellular carcinoma. Oncology 2010;78(Suppl 1):40–45.

Kudo M, Izumi N, Kokudo N, Matsui O, Sakamoto M, Nakashima O, Kojiro M, Makuuchi M. Management of hepatocellular carcinoma in Japan: Consensus-Based Clinical Practice Guidelines proposed by the Japan Society of Hepatology (JSH) 2010 updated version. Dig Dis 2011b;29:339–364.

Kudo M, Okanoue T. Management of hepatocellular carcinoma in Japan: consensus-based clinical practice manual proposed by the Japan Society of Hepatology. Oncology 2007;72(Suppl 1):2–15.

Kurt M, Shaikh KA, Peterson L, Kurrelmeyer KM, Shah G, Nagueh SF, Fromm R, Quinones MA, Zoghbi WA. Impact of contrast

echocardiography on evaluation of ventricular function and clinical management in a large prospective cohort. J Am Coll Cardiol 2009; 53:802–810.

Lamuraglia M, Escudier B, Chami L, Schwartz B, Leclere J, Roche A, Lassau N. To predict progression-free survival and overall survival in metastatic renal cancer treated with sorafenib: pilot study using dynamic contrast-enhanced Doppler ultrasound. Eur J Cancer 2006;42:2472–2479.

Langnas AN, Marujo W, Stratta RJ, Wood RP, Shaw BW Jr. Vascular complications after orthotopic liver transplantation. Am J Surg 1991;161:76–82; discussion-3.

Larsen LP, Rosenkilde M, Christensen H, Bang N, Bolvig L, Christiansen T, Laurberg S. The value of contrast enhanced ultrasonography in detection of liver metastases from colorectal cancer: a prospective double-blinded study. Eur J Radiol 2007;62:302–307.

Lassau N, Chami L, Chebil M, Benatsou B, Bidault S, Girard E, Abboud G, Roche A. Dynamic contrast-enhanced ultrasonography (DCE-US) and anti-angiogenic treatments. Discov Med 2011;11: 18–24.

Lassau N, Chami L, Koscielny S, Chebil M, Massard C, Benatsou B, Bidault S, Cioffi A, Blay JY, Le Cesne A. Quantitative functional imaging by Dynamic Contrast Enhanced Ultrasonography (DCE-US) in GIST patients treated with masatinib. Invest New Drugs 2012;30:765–771.

Lassau N, Koscielny S, Albiges L, Chami L, Benatsou B, Chebil M, Roche A, Escudier BJ. Metastatic renal cell carcinoma treated with sunitinib: early evaluation of treatment response using dynamic contrast-enhanced ultrasonography. Clin Cancer Res 2010a;16: 1216–1225.

Lassau N, Koscielny S, Chami L, Chebil M, Benatsou B, Roche A, Ducreux M, Malka D, Boige V. Advanced Hepatocellular Carcinoma: Early Evaluation of Response to Bevacizumab Therapy at Dynamic Contrast-enhanced US with Quantification–Preliminary Results. Radiology 2010b;258:291–300.

Lassau N, Lamuraglia M, Chami L, Leclere J, Bonvalot S, Terrier P, Roche A, Le Cesne A. Gastrointestinal stromal tumors treated with imatinib: monitoring response with contrast-enhanced sonography. AJR Am J Roentgenol 2006;187:1267–1273.

Leen E, Ceccotti P, Moug SJ, Glen P, MacQuarrie J, Angerson WJ, Albrecht T, Hohmann J, Oldenburg A, Ritz JP, Horgan PG. Potential value of contrast-enhanced intraoperative ultrasonography during partial hepatectomy for metastases: an essential investigation before resection? Ann Surg 2006;243:236–240.

Lencioni R, Llovet JM. Modified RECIST (mRECIST) assessment for hepatocellular carcinoma. Semin Liver Dis 2010;30:52–60.

Leoni S, Piscaglia F, Golfieri R, Camaggi V, Vidili G, Pini P, Bolondi L. The impact of vascular and nonvascular findings on the noninvasive diagnosis of small hepatocellular carcinoma based on the EASL and AASLD criteria. Am J Gastroenterol 2010;105:599–609.

Li N, Ding H, Fan P, Lin X, Xu C, Wang W, Xu Z, Wang J. Intrahepatic transit time predicts liver fibrosis in patients with chronic hepatitis B: quantitative assessment with contrast-enhanced ultrasonography. Ultrasound Med Biol 2010;36:1066–1075.

Lim AK, Taylor-Robinson SD, Patel N, Eckersley RJ, Goldin RD, Hamilton G, Foster GR, Thomas HC, Cosgrove DO, Blomley MJ. Hepatic vein transit times using a microbubble agent can predict disease severity non-invasively in patients with hepatitis C. Gut 2005;54:128–133.

Liu GJ, Lu MD, Xie XY, Xu HX, Xu ZF, Zheng YL, Liang JY, Wang W. Real-time contrast-enhanced ultrasound imaging of infected focal liver lesions. J Ultrasound Med 2008a;27:657–666.

Liu JB, Wansaicheong G, Merton DA, Chiou SY, Sun Y, Li K, Forsberg F, Edmonds PR, Needleman L, Halpern EJ. Canine prostate: contrast-enhanced US-guided radiofrequency ablation with urethral and neurovascular cooling–initial experience. Radiology 2008b;247:717–725.

Liu Z, Lobo SM, Humphries S, Horkan C, Solazzo SA, Hines-Peralta AU, Lenkinski RE, Goldberg SN. Radiofrequency tumor ablation: insight into improved efficacy using computer modeling. AJR Am J Roentgenol 2005;184:1347–1352.

Livraghi T, Goldberg SN, Lazzaroni S, Meloni F, Ierace T, Solbiati L, Gazelle GS. Hepatocellular carcinoma: radio-frequency ablation of medium and large lesions. Radiology 2000;214:761–768.

Lu Q, Zhong XF, Huang ZX, Yu BY, Ma BY, Ling WW, Wu H, Yang JY, Luo Y. Role of contrast-enhanced ultrasound in decision support for diagnosis and treatment of hepatic artery thrombosis after liver transplantation. Eur J Radiol 2012;81:e338–e343.

Luo Y, Fan YT, Lu Q, Li B, Wen TF, Zhang ZW. CEUS: a new imaging approach for postoperative vascular complications after right-lobe LDLT. World J Gastroenterol 2009;15:3670–3675.

Main ML, Goldman JH, Grayburn PA. Ultrasound contrast agents: balancing safety versus efficacy. Expert Opin Drug Saf 2009;8: 49–56.

Main ML, Ryan AC, Davis TE, Albano MP, Kusnetzky LL, Hibberd M. Acute mortality in hospitalized patients undergoing echocardiography with and without an ultrasound contrast agent (multicenter registry results in 4,300,966 consecutive patients). Am J Cardiol 2008;102:1742–1746.

Mandry D, Bressenot A, Galloy MA, Chastagner P, Branchereau S, Claudon M. Contrast-enhanced ultrasound in fibro-lamellar hepatocellular carcinoma: a case report. Ultraschall Med 2007;28: 547–552.

Maruyama H, Takahashi M, Ishibashi H, Okugawa H, Okabe S, Yoshikawa M, Yokosuka O. Ultrasound-guided treatments under low acoustic power contrast harmonic imaging for hepatocellular carcinomas undetected by B-mode ultrasonography. Liver Int 2009;29:708–714.

Matsui O. Detection and characterization of hepatocellular carcinoma by imaging. Clin Gastroenterol Hepatol 2005;3:S136–S140.

Mazzoni G, Napoli A, Mandetta S, Miccini M, Cassini D, Gregori M, Colace L, Tocchi A. Intra-operative ultrasound for detection of liver metastases from colorectal cancer. Liver Int 2008;28:88–94.

Minami Y, Kudo M, Chung H, Kawasaki T, Yagyu Y, Shimono T, Shiozaki H. Contrast harmonic sonography-guided radiofrequency ablation therapy versus B-mode sonography in hepatocellular carcinoma: prospective randomized controlled trial. AJR Am J Roentgenol 2007;188:489–494.

Moriyasu F, Itoh K. Efficacy of perflubutane microbubble-enhanced ultrasound in the characterization and detection of focal liver lesions: phase 3 multicenter clinical trial. AJR Am J Roentgenol 2009;193:86–95.

Mork H, Ignee A, Schuessler G, Ott M, Dietrich CF. Analysis of neuroendocrine tumour metastases in the liver using contrast enhanced ultrasonography. Scand J Gastroenterol 2007;42:652–662.

Nakano H, Ishida Y, Hatakeyama T, Sakuraba K, Hayashi M, Sakurai O, Hataya K. Contrast-enhanced intraoperative ultrasonography equipped with late Kupffer-phase image obtained by sonazoid in patients with colorectal liver metastases. World J Gastroenterol 2008;14: 3207–3211.

Omata M, Lesmana LA, Tateishi R, Chen PJ, Lin SM, Yoshida H, Kudo M, Lee JM, Choi BI, Poon RT, Shiina S, Cheng AL, Jia JD, Obi S, Han KH, Jafri W, Chow P, Lim SG, Chawla YK, Budihusodo U, Gani RA, Lesmana CR, Putranto TA, Liaw YF, Sarin SK. Asian Pacific Association for the Study of the Liver consensus recommendations on hepatocellular carcinoma. Hepatol Int 2010;4:439–474.

Peronneau P, Lassau N, Leguerney I, Roche A, Cosgrove D. Contrast ultrasonography: necessity of linear data processing for the quantification of tumor vascularization. Ultraschall Med 2010;31: 370–378.

Piscaglia F, Bolondi L. The safety of Sonovue in abdominal applications: retrospective analysis of 23188 investigations. Ultrasound Med Biol 2006;32:1369–1375.

Piscaglia F, Corradi F, Mancini M, Giangregorio F, Tamberi S, Ugolini G, Cola B, Bazzocchi A, Righini R, Pini P, Fornari F, Bolondi L. Real time contrast enhanced ultrasonography in detection of liver metastases from gastrointestinal cancer. BMC Cancer 2007;7:171.

Piscaglia F, Gianstefani A, Ravaioli M, Golfieri R, Cappelli A, Giampalma E, Sagrini E, Imbriaco G, Pinna AD, Bolondi L. Criteria for diagnosing benign portal vein thrombosis in the assessment of

patients with cirrhosis and hepatocellular carcinoma for liver transplantation. Liver Transpl 2010;16:658–667.
Piscaglia F, Nolsoe C, Dietrich CF, Cosgrove DO, Gilja OH, Bachmann Nielsen M, Albrecht T, Barozzi L, Bertolotto M, Catalano O, Claudon M, Clevert DA, Correas JM, D'Onofrio M, Drudi FM, Eyding J, Giovannini M, Hocke M, Ignee A, Jung EM, Klauser AS, Lassau N, Leen E, Mathis G, Saftoiu A, Seidel G, Sidhu PS, ter Haar G, Timmerman D, Weskott HP. The EFSUMB Guidelines and Recommendations on the Clinical Practice of Contrast Enhanced Ultrasound (CEUS): update 2011 on non-hepatic applications. Ultraschall Med 2011;33:33–59.
Piskunowicz M, Kosiak W, Irga N. Primum non nocere? Why can't we use second generation ultrasound contrast agents for the examination of children? Ultraschall Med 2011;32:83–86.
Qiang L, Yan L, Chao-Xin Y, Zeng Y, Wu H, Lei Z, Zhong Y, Fan YT, Wang HH, Luo Y. Value of contrast-enhanced intraoperative ultrasound for cirrhotic patients with hepatocellular carcinoma: A report of 20 cases. World J Gastroenterol 2008;14:4005–4010.
Quaia E, D'Onofrio M, Palumbo A, Rossi S, Bruni S, Cova M. Comparison of contrast-enhanced ultrasonography versus baseline ultrasound and contrast-enhanced computed tomography in metastatic disease of the liver: diagnostic performance and confidence. Eur Radiol 2006;16:1599–1609.
Ridolfi F, Abbattista T, Marini F, Vedovelli A, Quagliarini P, Busilacchi P, Brunelli E. Contrast-enhanced ultrasound to evaluate the severity of chronic hepatitis C. Dig Liver Dis 2007;39:929–935.
Rossi S, Rosa L, Ravetta V, Cascina A, Quaretti P, Azzaretti A, Scagnelli P, Tinelli C, Dionigi P, Calliada F. Contrast-enhanced versus conventional and color Doppler sonography for the detection of thrombosis of the portal and hepatic venous systems. AJR Am J Roentgenol 2006;186:763–773.
Sangiovanni A, Manini MA, Iavarone M, Romeo R, Forzenigo LV, Fraquelli M, Massironi S, Della Corte C, Ronchi G, Rumi MG, Biondetti P, Colombo M. The diagnostic and economic impact of contrast imaging techniques in the diagnosis of small hepatocellular carcinoma in cirrhosis. Gut 2010;59:638–644.
Sasaki A, Kai S, Iwashita Y, Hirano S, Ohta M, Kitano S. Microsatellite distribution and indication for locoregional therapy in small hepatocellular carcinoma. Cancer 2005;103:299–306.
Scheele J, Stang R, Altendorf-Hofmann A, Paul M. Resection of colorectal liver metastases. World J Surg 1995;19:59–71.
Schlottmann K, Klebl F, Zorger N, Feuerbach S, Scholmerich J. Contrast-enhanced ultrasound allows for interventions of hepatic lesions which are invisible on convential B-mode. Z Gastroenterol 2004;42:303–310.
Schuessler G, Fellbaum C, Fauth F, Jacobi V, Schmidt-Matthiesen A, Ignee A, Dietrich CF. [The infammatory pseudotumour – an unusual liver tumour]. Ultraschall Med 2006;27:273–279.
Seitz K, Bernatik T, Strobel D, Blank W, Friedrich-Rust M, Strunk H, Greis C, Kratzer W, Schuler A. Contrast-enhanced ultrasound (CEUS) for the characterization of focal liver lesions in clinical practice (DEGUM Multicenter Trial): CEUS vs. MRI–a prospective comparison in 269 patients. Ultraschall Med 2010;31:492–499.
Seitz K, Greis C, Schuler A, Bernatik T, Blank W, Dietrich CF, Strobel D. Frequency of tumor entities among liver tumors of unclear etiology initially detected by sonography in the noncirrhotic or cirrhotic livers of 1349 patients. Results of the DEGUM multicenter study. Ultraschall Med 2011;32:598–603.
Shaw AS, Ryan SM, Beese RC, Sidhu PS. Ultrasound of non-vascular complications in the post liver transplant patient. Clin Radiol 2003;58:672–680.
Shiozawa K, Watanabe M, Takayama R, Takahashi M, Wakui N, Iida K, Sumino Y. Evaluation of local recurrence after treatment for hepatocellular carcinoma by contrast-enhanced ultrasonography using Sonazoid: comparison with dynamic computed tomography. J Clin Ultrasound 2010;38:182–189.
Sidhu PS, Shaw AS, Ellis SM, Karani JB, Ryan SM. Microbubble ultrasound contrast in the assessment of hepatic artery patency following liver transplantation: role in reducing frequency of hepatic artery arteriography. Eur Radiol 2004;14:21–30.
Simpson DH, Chin CT, Burns PN. Pulse inversion Doppler: a new method for detecting nonlinear echoes from microbubble contrast agents. IEEE Trans on Ultrasonics, Ferroelectrics, and Freq Control 1999;46:372–382.
Skyba DM, Price RJ, Linka AZ, Skalak TC, Kaul S. Direct in vivo visualization of intravascular destruction of microbubbles by ultrasound and its local effects on tissue. Circulation 1998;98:290–293.
Sorrentino P, D'Angelo S, Tarantino L, Ferbo U, Bracigliano A, Vecchione R. Contrast-enhanced sonography versus biopsy for the differential diagnosis of thrombosis in hepatocellular carcinoma patients. World J Gastroenterol 2009;15:2245–2251.
Strobel D, Kleinecke C, Hansler J, Frieser M, Handl T, Hahn EG, Bernatik T. Contrast-enhanced sonography for the characterisation of hepatocellular carcinomas–correlation with histological differentiation. Ultraschall Med 2005;26:270–276.
Strobel D, Seitz K, Blank W, Schuler A, Dietrich C, von Herbay A, Friedrich-Rust M, Kunze G, Becker D, Will U, Kratzer W, Albert FW, Pachmann C, Dirks K, Strunk H, Greis C, Bernatik T. Contrast-enhanced ultrasound for the characterization of focal liver lesions–diagnostic accuracy in clinical practice (DEGUM multicenter trial). Ultraschall Med 2008;29:499–505.
Su HL, Qian YQ, Wei ZR, He JG, Li GQ, Zhang J, Zhou XD, Jing W. Real-time myocardial contrast echocardiography in rat: infusion versus bolus administration. Ultrasound Med Biol 2009;35:748–755.
Szabo T. Diagnostic Ultrasound Imaging. Insite Out (Biomedical Engineering) ISBN 0126801452. Ed./Academic Press 2004.
Therasse P, Arbuck SG, Eisenhauer EA, Wanders J, Kaplan RS, Rubinstein L, Verweij J, Van Glabbeke M, van Oosterom AT, Christian MC, Gwyther SG. New guidelines to evaluate the response to treatment in solid tumors. European Organization for Research and Treatment of Cancer, National Cancer Institute of the United States, National Cancer Institute of Canada. J Natl Cancer Inst 2000;92:205–216.
Tiemann K, Lohmeier S, Kuntz S, Köster J, Pohl C, Burns P, Porter TR, Nanda NC, Lüderitz B, Becher H. Real-time contrast echo assessment of myocardial perfusion at low emission power: First experimental and clinical results using power pulse inversion imaging. Echocardiography 1999;16:799–809.
Torzilli G, Del Fabbro D, Palmisano A, Donadon M, Bianchi P, Roncalli M, Balzarini L, Montorsi M. Contrast-enhanced intraoperative ultrasonography during hepatectomies for colorectal cancer liver metastases. J Gastrointest Surg 2005;9:1148–1153; discussion 53–4.
Torzilli G, Del Fabbro D, Palmisano A, Donadon M, Montorsi M. Contrast-enhanced intraoperative ultrasonography: a valuable and not any more monocentric diagnostic technique performed in different ways. Ann Surg 2007;245:152–153; author reply-3.
Trillaud H, Bruel JM, Valette PJ, Vilgrain V, Schmutz G, Oyen R, Jakubowski W, Danes J, Valek V, Greis C. Characterization of focal liver lesions with SonoVue-enhanced sonography: international multicenter-study in comparison to CT and MRI. World J Gastroenterol 2009;15:3748–3756.
Vilana R, Forner A, Bianchi L, Garcia-Criado A, Rimola J, de Lope CR, Reig M, Ayuso C, Bru C, Bruix J. Intrahepatic peripheral cholangiocarcinoma in cirrhosis patients may display a vascular pattern similar to hepatocellular carcinoma on contrast-enhanced ultrasound. Hepatology 2010;51:2020–2029.
Wang Z, Xu HX, Xie XY, Xie XH, Kuang M, Xu ZF, Liu GJ, Chen LD, Lin MX, Lu MD. Imaging features of hepatic angiomyolipomas on real-time contrast-enhanced ultrasound. Br J Radiol 2010;83:411–418.
Wei K, Jayaweera AR, Firoozan S, Linka A, Skyba DM, Kaul S. Quantification of myocardial blood flow with ultrasound-induced destruction of microbubbles administered as a constant venous infusion. Circulation 1998;97:473–483.
Wilson SR, Burns PN. An algorithm for the diagnosis of focal liver masses using microbubble contrast-enhanced pulse-inversion sonography. AJR Am J Roentgenol 2006;186:1401–1412.
Wilson SR, Kim TK, Jang HJ, Burns PN. Enhancement patterns of focal liver masses: discordance between contrast-enhanced sonography and contrast-enhanced CT and MRI. AJR Am J Roentgenol 2007; 189:W7–W12.
World Health Organisation Offset Publication. WHO Handbook for Reporting Results of Cancer Treatment (Geneva, Switzerland). ISBN 92 4 170048 3. Ed World Health Organisation, 1979.

Wu W, Chen MH, Yin SS, Yan K, Fan ZH, Yang W, Dai Y, Huo L, Li JY. The role of contrast-enhanced sonography of focal liver lesions before percutaneous biopsy. AJR Am J Roentgenol 2006;187: 752–761.

Xu HX, Liu GJ, Lu MD, Xie XY, Xu ZF, Zheng YL, Liang JY. Characterization of small focal liver lesions using real-time contrast-enhanced sonography: diagnostic performance analysis in 200 patients. J Ultrasound Med 2006a;25:349–361.

Xu HX, Lu MD, Liu GJ, Xie XY, Xu ZF, Zheng YL, Liang JY. Imaging of peripheral cholangiocarcinoma with low-mechanical index contrast-enhanced sonography and SonoVue: initial experience. J Ultrasound Med 2006b;25:23–33.

Yanagisawa K, Moriyasu F, Miyahara T, Yuki M, Iijima H. Phagocytosis of ultrasound contrast agent microbubbles by Kupffer cells. Ultrasound Med Biol 2007;33:318–325.

Zheng RQ, Mao R, Ren J, Xu EJ, Liao M, Wang P, Lu MQ, Yang Y, Cai CJ, Chen GH. Contrast-enhanced ultrasound for the evaluation of hepatic artery stenosis after liver transplantation: potential role in changing the clinical algorithm. Liver Transpl 2010;16: 729–735.

Research Article

EASL EUROPEAN ASSOCIATION FOR THE STUDY OF THE LIVER | JOURNAL OF HEPATOLOGY

Comparison of resection and ablation for hepatocellular carcinoma: A cohort study based on a Japanese nationwide survey

Kiyoshi Hasegawa[1,†], Norihiro Kokudo[1,*,†], Masatoshi Makuuchi[2,†], Namiki Izumi[3,†], Takafumi Ichida[4,†], Masatoshi Kudo[5,†], Yonson Ku[6,†], Michiie Sakamoto[7,†], Osamu Nakashima[8,†], Osamu Matsui[9,†], Yutaka Matsuyama[10,†]

[1]*Hepato-Biliary-Pancreatic Surgery Division, Department of Surgery, Graduate School of Medicine, University of Tokyo, Japan;* [2]*Department of Hepato-Biliary-Pancreatic Surgery, Japanese Red Cross Medical Center, Japan;* [3]*Department of Gastroenterology, Musashino Red Cross Hospital, Japan;* [4]*Department of Gastroenterology, Juntendo University Shizuoka Hospital, Japan;* [5]*Department of Gastroenterology and Hepatology, Kinki University School of Medicine, Japan;* [6]*Division of Hepato-Biliary-Pancreatic Surgery, Kobe University Graduate School of Medicine, Japan;* [7]*Department of Pathology, Keio University School of Medicine, Japan;* [8]*Department of Clinical Laboratory Medicine, Kurume University Hospital, Japan;* [9]*Department of Radiology, Kanazawa University Graduate School of Medical Science, Japan;* [10]*Department of Biostatics, School of Public Health University of Tokyo, Japan*

Background & Aims: The treatment of choice for early or moderately advanced hepatocellular carcinoma (HCC) with good liver function remains controversial. We evaluated the therapeutic impacts of surgical resection (SR), percutaneous ethanol injection (PEI), and radiofrequency ablation (RFA) on long-term outcomes in patients with HCC.

Methods: A database constructed on the basis of a Japanese nationwide survey of 28,510 patients with HCC treated by SR, PEI, or RFA between 2000 and 2005 was used to identify 12,968 patients who had no more than 3 tumors (⩽3 cm) and liver damage of class A or B. The patients were divided into SR (n = 5361), RFA (n = 5548), and PEI groups (n = 2059). Overall survival and time to recurrence were compared among them.

Results: Median follow-up was 2.16 years. Overall survival at 3 and 5 years was respectively 85.3%/71.1% in the SR group, 81.0%/61.1% in the RFA, and 78.9%/56.3% in the PEI. Time to recurrence at 3 and 5 years was 43.3%/63.8%, 57.2%/71.7%, and 64.3%/76.9%, respectively. On multivariate analysis, the hazard ratio for death was significantly lower in the SR group than in the RFA (SR *vs.* RFA:0.84, 95% confidence interval, 0.74–0.95; $p = 0.006$) and PEI groups (SR *vs.* PEI:0.75, 0.64–0.86; $p = 0.0001$). The hazard ratios for recurrence were also lower in the SR group than in the RFA (SR *vs.* RFA:0.74, 0.68–0.79; $p = 0.0001$) and PEI groups (SR *vs.* PEI:0.59, 0.54–0.65; $p = 0.0001$).

Conclusions: Our findings suggest that surgical resection results in longer overall survival and shorter time to recurrence than either RFA or PEI in patients with HCC.

Keywords: Hepatectomy; Surgical resection; Radiofrequency ablation; Percutaneous ethanol injection.

Received 3 October 2012; received in revised form 2 November 2012; accepted 7 November 2012; available online 21 November 2012

* Corresponding author. Address: Hepato-Biliary-Pancreatic Surgery Division, Department of Surgery, Graduate School of Medicine, University of Tokyo, 7-3-1 Hongo, Bunkyo-ku, Tokyo 113-0033, Japan. Tel.: +81 3 5800 8841; fax: +81 3 5684 3989.

E-mail address: KOKUDO-2SU@h.u-tokyo.ac.jp (N. Kokudo).

† For the Liver Cancer Study Group of Japan.

Abbreviations: HCC, hepatocellular carcinoma; SR, surgical resection; RFA, radiofrequency ablation; PEI, percutaneous ethanol injection; TACE, transcatheter hepatic arterial chemoembolization.

Cancer

Introduction

Hepatocellular carcinoma (HCC) is the fifth most common cancer in men and the seventh in women, worldwide [1]. Outcomes remain disappointing, despite recent progress in the techniques of diagnosis and therapy. Japanese [2], European [3] and American [4] clinical practice guidelines strongly recommend surgical resection (SR) and percutaneous ablation, including radiofrequency ablation (RFA) and percutaneous ethanol injection (PEI), for the management of early or moderately advanced HCC (i.e., up to 3 tumors 3 cm or less in diameter) in patients with adequately maintained liver function. Although comparative studies of these treatments have been conducted previously [5–7], the most suitable treatment strategy still remains controversial.

By nationwide surveys initiated in 1965, the Liver Cancer Study Group of Japan has prospectively collected data on patients with HCC in Japan. The Group conducted two retrospective analyses to define the treatment with the best outcomes [8,9]. However, each of the analyses was flawed, and had several problems: data on RFA were not included in the first report [8], and the follow-up period was short in the second one [9]. Although the second analysis demonstrated that surgical resection was superior to RFA and PEI for preventing recurrence [9], no apparent difference in the overall survival could be discerned between surgery and percutaneous ablation therapies (RFA and PEI). Thus, the treatment of choice for less advanced HCC still remains under debate.

Before starting this study, the results of 2 randomized controlled trials (RCT) were available [10,11]. As we pointed out in a previous report [12], however, the study designs of these 2

trials were critically flawed by factors such as insufficient sample size, excessively optimistic hypotheses, and high conversion ratios. Because of these problems, the results of the two RCTs do not allow firm conclusions to be drawn concerning the important clinical question: is surgery or percutaneous ablation the treatment of choice for early or moderately advanced HCC? To answer this question, we conducted this cohort study based on the latest data available from a Japanese nationwide survey.

Patients and methods

Patients and settings

The Liver Cancer Study Group of Japan has performed nationwide surveys of patients with primary liver cancer since 1965. Patients are registered and followed up, as reported previously [9]. Although this study protocol was not submitted to the Institutional Review Board of each institution participating in the nationwide survey, the collection and registration of data of patients with HCC were performed with the approval of each institution. Because RFA has been available for clinical use since 1999 in Japan, we set the study period from 2000 to 2005, to exclude preliminary experiences with RFA. During this period, a total of 28,510 patients with HCC were registered and received surgical resection, RFA or PEI as the primary treatment with curative intent for HCC. We identified 12,968 patients who met the following criteria: (1) liver function classified as liver damage A or B defined by the Liver cancer Study Group of Japan [13]; (2) number of tumors 3 or less; (3) maximum tumor diameter $\leqslant$3 cm. The 12,968 patients were divided into 3 groups according to the treatment received: SR group (n = 5361, 41.3%), RFA group (n = 5548, 42.8%), and PEI group (n = 2059, 15.9%). The diagnostic criteria and details of follow-up were described previously [8]. Because it has been unusual for biopsies to be performed in cases treated by percutaneous ablation in Japan, histological findings such as microscopic vascular invasion, tumor grading, and microscopic intrahepatic metastasis were not evaluated in this study. Relevant clinical data were collected and analyzed.

Statistical analyses

The baseline characteristics of the three groups (Table 1) were compared by analysis of variance for continuous variables and by Chi-square or Mantel-trend tests for categorical variables. Consistent with our preliminary report [9], the SR group had a higher proportion of younger patients and male patients than the RFA and PEI groups. Hepatitis C virus infection was less prevalent in the SR group than in the RFA and PEI groups. Based on the liver damage class, serum albumin and total bilirubin levels, platelet counts, and the indocyanine green retention rate at 15 min, liver function was better in the SR group than in the RFA and PEI groups, consistent with our previous report [9]. As for tumor-related factors, the number of tumors was smaller, and the maximum tumor diameter was larger in the SR group than in the RFA or PEI group. The SR group had the lowest proportion of patients with abnormally elevated alpha-fetoprotein levels ($\geqslant$15 ng/ml) and the highest proportion of patients with abnormally elevated des-γ-carboxy prothrombin levels ($\geqslant$40 AU/ml).

Overall survival and time to recurrence curves were plotted using the Kaplan–Meier method and compared with the use of the log-rank test. Recurrence was diagnosed on the basis of imaging studies, clinical data, and/or histopathological studies at each institution [9].

The therapeutic impacts of surgical resection, RFA and PEI were estimated using a Cox proportional hazards model including the following 10 covariates: age, gender, liver damage class, hepatitis C virus antibody, hepatitis B surface antigen, platelet count, number of tumors, tumor size, and serum alpha-fetoprotein and des-γ-carboxy prothrombin levels. The results of multivariate analysis were expressed as hazard ratios with 95% confidence intervals. p values of <0.05 were considered to indicate statistical significance.

For the subgroup analyses, the study populations were classified into 8 subgroups according to the tumor size (< or $\geqslant$2 cm), tumor number (single or multiple), and liver damage class (A or B). Macroscopic vascular invasion was excluded from the subgroup analyses because its presence is a contraindication to percutaneous ablation therapies. The therapeutic impacts of the three treatments were evaluated in each of these subgroups, and hazard ratios with 95% confidence intervals and p values were calculated according to the above three factors (tumor size, number of tumors, and liver damage class).

Results

The median follow-up after treatment was 2.16 years, and the 5th and 95th percentiles were 0.14 and 5.19 years, respectively. The overall survival rates at 3/5 years were 85.3%/71.1% in the SR group, 81.0%/61.1% in the RFA group, and 78.9%/56.3% in the PEI group (Fig. 1). The median survival times were 8.4, 5.9, and 5.6 years in the three groups, respectively. The time to recurrence rates at 3/5 years in the 3 groups were 43.3%/63.8%, 57.2%/71.7%, and 64.3%/76.9%, respectively (Fig. 2).

According to the results of the multivariate analysis, the hazard ratio for death in the SR group was 0.84 (0.74–0.95, p = 0.006) relative to that in the RFA group, and 0.75 (0.64–0.86, p = 0.0001) relative to that in the PEI group (Table 2A). The hazard ratios for recurrence in the SR group were 0.74 (0.68–0.79, p = 0.0001) and 0.59 (0.54–0.65, p = 0.0001) relative to those in the RFA and PEI groups, respectively (Table 2B). These results indicated that the overall survival and time to recurrence rates were both significantly better in the SR group than in the RFA and PEI groups.

The overall survival rates following surgical resection, RFA and PEI in the 4 subgroups with a single tumor are shown in Fig. 3A–D. The results of the subgroup analyses (summarized in Fig. 4A) showed that the overall survival was significantly longer in the SR group than in the RFA group in 2 subgroups of patients, namely, those who had a single tumor smaller than 2 cm in diameter with liver damage class A, and those who had a single tumor 2 cm or larger in diameter with liver damage class B.

As shown in Fig. 4B, the time to recurrence was shorter in the SR group than that in the RFA group in the 4 following subgroups: patients with a single tumor with liver damage class A (regardless of the tumor size), those with multiple tumors 2 cm or larger in diameter with liver damage class A, and those with a single tumor 2 cm or larger in diameter with liver damage class B.

Discussion

Our study showed that surgical resection was associated with significantly lower risk of both death and recurrence as compared to RFA and PEI in patients with early or moderately advanced HCC. Our previous preliminary report [9] suggested that surgery reduces the risk of recurrence, but failed to demonstrate any difference in the overall survival between surgery and percutaneous ablation therapies in patients with early or moderately advanced HCC. The present study reconfirms that surgery is associated with a reduced recurrence rate and newly shows that surgery yields a longer overall survival than percutaneous ablation therapies.

Differences in the results between the present study and previous investigations are most likely related to the sample size and length of follow-up. The total number of subjects increased markedly from 7185 in our previous study to 12,968 in this study, and the median follow-up period increased from 10.4 months to 2.16 years (25.9 months). These factors are considered not only to have enhanced the reliability of our findings, but also to have strengthened our conclusions. We believe that our results, which are, of course, subject to the inherent drawbacks of the study design, are meaningful, given the current lack of credible data derived from well-designed RCTs.

The large sample size and prolonged follow-up period also allowed us to perform several subgroup analyses, which were not feasible in our previous study [9]. We classified the patients

Table 1. Baseline characteristics.

Variables	SR n = 5361	RFA n = 5548	PEI n = 2059	*p* value
Age, median (5, 95 percentile), yr	66 (48, 77)	69 (52, 80)	69 (52, 80)	<0.0001[a]
Sex				<0.0001[b]
Male, No. (%)	3967 (74.0)	3569 (64.3)	1303 (63.3)	
Female, No. (%)	1394 (26.0)	1979 (35.7)	756 (36.7)	
Hepatitis virus infection				<0.0001[b]
HBs Ag(+)/HCV-Ab(-), No. (%)	908 (16.9)	462 (8.3)	141 (6.8)	
HBs Ag(-)/HCV-Ab(+), No. (%)	3393 (63.3)	4263 (76.8)	1632 (79.3)	
HBs Ag(+)/HCV-Ab(+), No. (%)	106 (2.0)	87 (1.6)	32 (1.6)	
HBs Ag(-)/HCV-Ab(-), No. (%)	760 (14.2)	512 (9.2)	160 (7.8)	
Unknown	194 (3.6)	224 (4.0)	94 (4.6)	
Liver damage				<0.0001[b]
A, No. (%)	4000 (74.6)	3349 (60.4)	1204 (58.5)	
B, No. (%)	1361 (25.4)	2199 (39.6)	855 (41.5)	
Serum albumin, median (5, 95 percentile), g/dl	3.9 (3.1, 4.6)	3.7 (2.9, 4.4)	3.7 (2.8, 4.4)	<0.0001[a]
Serum total bilirubin, median (5, 95 percentile), mg/dl	0.8 (0.4, 1.5)	0.9 (0.4, 1.9)	0.9 (0.4, 2.2)	<0.0001[a]
Platelet count, median (5, 95 percentile), x 10^4/μl	12.6 (5.8, 24.0)	9.9 (4.5, 20.4)	9.5 (4.4, 19.6)	<0.0001[a]
ICG R15, median (5, 95 percentile), %	15 (5, 35)	22 (7, 51)	24 (8, 51)	<0.0001[a]
Tumor number				<0.0001[c]
Single, No. (%)	4458 (83.2)	4068 (73.3)	1449 (70.4)	
Two, No. (%)	706 (13.2)	1096 (19.8)	443 (21.5)	
Three, No. (%)	197 (3.7)	384 (6.9)	167 (8.1)	
Tumor size, median (5, 95 percentile), mm	23 (12, 30)	20 (10, 30)	17 (10, 30)	<0.0001[a]
Alpha-fetoprotein				<0.0001[b]
≥15 ng/ml, No. (%)	2726 (50.9)	3028 (54.6)	1125 (54.6)	
<15 ng/ml, No. (%)	2457 (45.8)	2301 (41.5)	828 (40.2)	
Unknown, No. (%)	178 (3.3)	219 (3.9)	106 (5.2)	
Des-γ-carboxy prothrombin				<0.0001[b]
≥40 AU/ml, No. (%)	2182 (40.7)	1593 (28.7)	541 (26.3)	
<40 AU/ml, No. (%)	2651 (49.5)	3322 (59.9)	1169 (56.8)	
Unknown, No. (%)	528 (9.9)	633 (11.4)	349 (17.0)	

HBsAg, hepatitis B virus antigen; HCV-Ab, hepatitis C virus antibody; ICG R15, indocyanine green retention rate at 15 min.
[a]ANOVA.
[b]Chi-square.
[c]Mante-trend test.

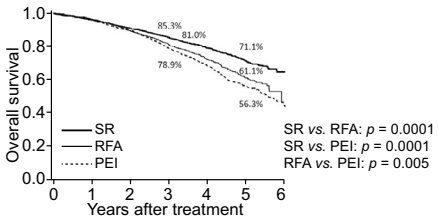

Patients at risk

SR	5361	3833	2570	1680	894	400	29
RFA	5548	3780	2328	1264	569	160	5
PEI	2059	1595	1112	718	444	247	58

Fig. 1. Overall survival curves after surgical resection (SR), radiofrequency ablation (RFA), and percutaneous ethanol injection (PEI).

into 8 subgroups according to 3 factors (liver damage class, tumor size, and number of tumors), which have repeatedly been shown to be clinically relevant prognostic factors. The results of the subgroup analyses indicated that surgical resection would effectively prevent recurrence in patients with relatively advanced HCC (2–3 cm in diameter) among the study populations, irrespective of liver damage class or number of tumors. This finding suggests that surgery might be superior to percutaneous ablation therapies in patients with a more advanced tumor stage. As for the subgroups with a single tumor, surgical resection yielded better overall survival and time to recurrence rates than RFA or PEI. Especially in the subgroup with a single tumor smaller than 2 cm in diameter, both the overall and time to recurrence rates were statistically significantly better after surgery than after RFA, whereas no such statistically significant differences in these two parameters between the two treatment groups were detected in a few subgroups with a single tumor, maybe due to the insufficient sample size of the subgroups. Thus, surgical resection would be considered as the treatment modality of first choice for a single HCC, as recommended by the Japanese clinical practice guideline [2]. Overall, there was a trend toward superior

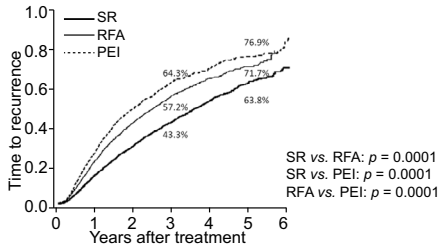

Patients at risk							
SR	5361	3265	1844	1039	451	189	15
RFA	5548	2954	1396	591	225	62	4
PEI	2059	1154	583	304	172	90	15

Fig. 2. Time to recurrence curves after surgical resection (SR), radiofrequency ablation (RFA), and percutaneous ethanol injection (PEI).

overall and time to recurrence rates after surgery than after RFA and PEI.

The reason why the long-term outcomes of the SR group were better than those of the PEI and RFA groups cannot be definitely clarified from the results of this study, however, in theory, surgical resection has the advantage of offering better local control of HCC over PEI and RFA, both of which have some potential risks of local recurrence associated with insufficient ablation. In addition, anatomic resection to remove minute tumor satellites [14] might have decreased the recurrence rate in the SR group, although this remains a speculation.

Recently, the latest trial from China [15], which had an adequate sample size (total 230 patients), reported that surgical resection yielded significantly better long-term outcomes than RFA. Although the study design was better than that of the two previously reported RCTs [10,11], it appeared to have limitations with respect to the results, such as drop in the overall survival in the RFA group as compared with that in the surgery group during the early period after treatment. The early deaths in the RFA group could have been treatment-related rather than cancer-related. Thus, no conclusion can be drawn from the three currently available RCTs.

One of the limitations of our study is the diversity of demographic factors in the study population, which would have been caused by the selection process of treatment modalities. As sim-

Table 2. Hazard ratios for death and recurrence adjusted by multivariate analysis.

A For death

Variables		Hazard ratio	95% CI	*p* value
Treatments	SR *vs.* RFA	0.84	0.74, 0.95	0.006
	SR *vs.* PEI	0.75	0.64, 0.86	0.0001
	RFA *vs.* PEI	0.88	0.77, 1.01	0.08
Age	<65 *vs.* ≥65	0.71	0.63, 0.79	0.0001
Sex	Female *vs.* male	0.87	0.78, 0.98	0.03
HBsAg	Positive *vs.* negative	0.91	0.74, 1.11	0.34
HCV Ab	Positive *vs.* negative	0.93	0.79, 1.10	0.40
Liver damage	A *vs.* B	0.62	0.56, 0.69	0.0001
Platelet count	$\geq 10^4$ *vs.* $<10^4/\mu l$	0.76	0.68, 0.85	0.0001
Tumor size	<2 *vs.* ≥2 cm	0.82	0.73, 0.92	0.0007
Tumor number	Single *vs.* multiple	0.72	0.64, 0.80	0.0001
AFP	<15 *vs.* ≥15 ng/ml	0.66	0.59, 0.74	0.0001
DCP	<40 *vs.* ≥40 AU/ml	0.59	0.53, 0.66	0.0001

B For recurrence

Variables		Hazard ratio	95% CI	*p* value
Treatments	SR *vs.* RFA	0.74	0.68, 0.79	0.0001
	SR *vs.* PEI	0.59	0.54, 0.65	0.0001
	RFA *vs.* PEI	0.81	0.74, 0.88	0.0001
Age	<65 *vs.* ≥65	0.83	0.78, 0.89	0.0001
Sex	Female *vs.* male	0.88	0.82, 0.95	0.0001
HBsAg	Positive *vs.* negative	1.04	0.92, 1.17	0.53
HCV Ab	Positive *vs.* negative	1.15	1.04, 1.27	0.007
Liver damage	A *vs.* B	0.87	0.81, 0.93	0.0001
Platelet count	$\geq 10^4$ *vs.* $<10^4/\mu l$	0.92	0.86, 0.98	0.02
Tumor size	<2 *vs.* ≥2 cm	0.84	0.79, 0.90	0.0001
Tumor number	Single *vs.* multiple	0.69	0.64, 0.74	0.0001
AFP	<15 *vs.* ≥15 ng/ml	0.71	0.67, 0.76	0.0001
DCP	<40 *vs.* ≥40 AU/ml	0.72	0.67, 0.77	0.0001

HBsAg, hepatitis B virus surface antigen; HCV, hepatitis C virus; Ab, antibody; AFP, alpha-fetoprotein; DCP, des-γ-carboxy prothrombin; SR, surgical resection; RFA, radiofrequency ablation; PEI, percutaneous ethanol injection; CI, confidence interval.

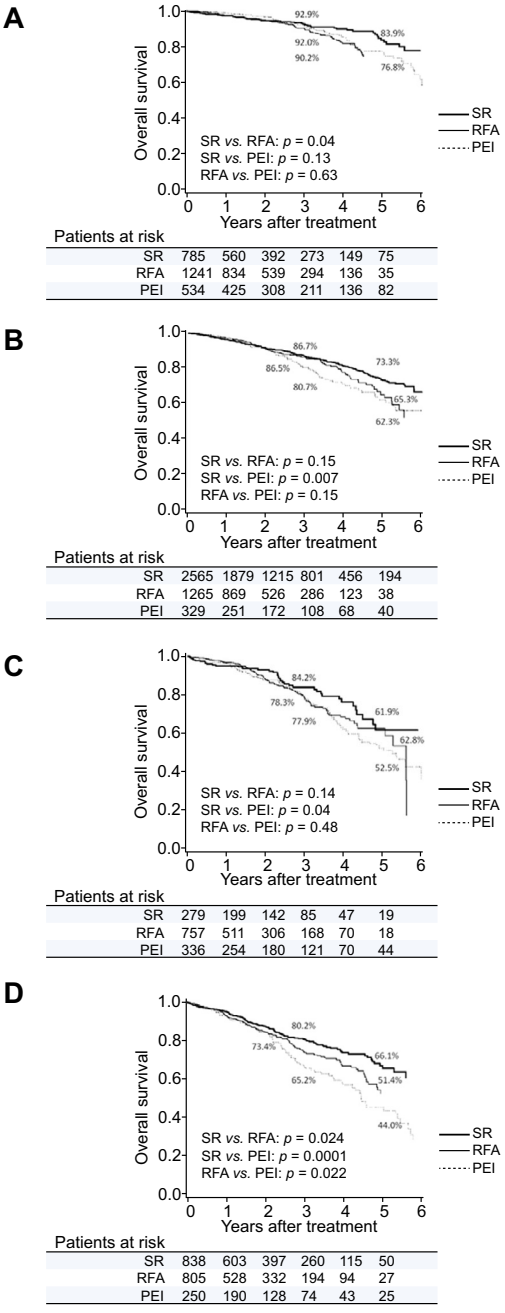

Fig. 3. Overall survival rates after surgical resection (SR), radiofrequency ablation (RFA), and percutaneous ethanol injection (PEI) in the subgroup of cases with single tumor and liver damage class A and B. (A) Liver damage class A, a single tumor (<2 cm); (B) liver damage class A, a single tumor (2–3 cm); (C) liver damage class B, a single tumor (<2 cm); (D) liver damage class B, a single tumor (2–3 cm).

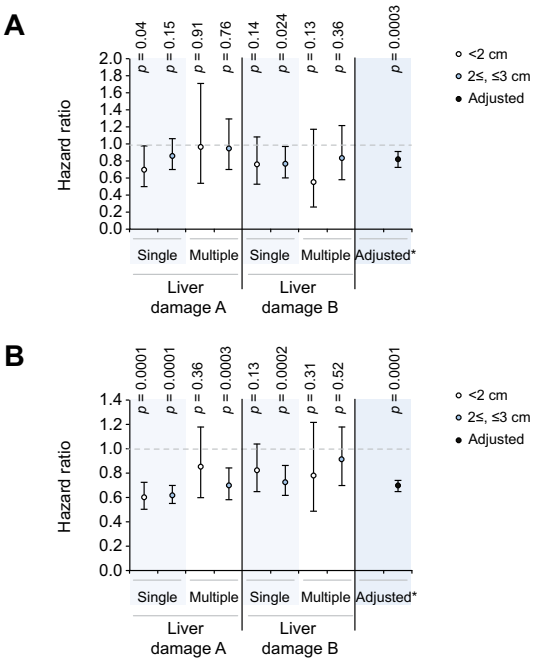

Fig. 4. Hazard ratios for death and recurrence with 95% confidence intervals and *p* values after surgical resection relative to those after radiofrequency ablation in the 8 subgroups. *The adjusted values for death and recurrence were calculated according to the three factors (tumor size, number of tumors, and liver damage class), as done in each subgroup. (A) Hazard ratios for death; (B) hazard ratios for recurrence.

ilar to the previous retrospective studies [5–9], the patients amenable to surgery had had younger age, less prevalence of hepatitis C virus infection, better liver function, less association with portal hypertension, fewer number of tumors and lower alpha-fetoprotein level, whereas their tumor size was larger and their des-γ-carboxy prothrombin level was higher. To minimize potential effects of confounding factors, we studied patients who had similar tumor-related and liver function-related factors and performed multivariate analysis using 10 clinically important factors, similar to our previous study [9]. Although it is impossible to completely eliminate potential negative impacts of demographic diversity, we believe that our results are clinically meaningful, because of the large sample size of our study. In Japan, a nationwide RCT in patients with HCC is now ongoing, and the results are expected to lead to more definitive conclusions [16].

Another potential limitation of our study is the lack of data on liver function during the follow-up, which precluded assessment of the relationship between the liver function status and the choice of treatment at recurrence. In HCC, the influence of the first treatment is considered to be smaller than that in other primary malignant diseases, because the liver function remarkably affects the recurrence rate. Further investigations, particularly prospective clinical trials, are needed to address these issues.

In conclusion, this large cohort study based on data obtained by a nationwide survey in Japan, suggests that surgical resection may offer some advantage over RFA and PEI in terms of both overall survival and time to recurrence in patients with less advanced HCC. Although our results are considered as being more reliable than those of previous studies comparing the treatment

outcomes in HCC, our conclusions need to be confirmed by future RCTs.

Financial support

This study was supported by the Liver Cancer Study Group of Japan. There were no other sources of funding for any authors.

Conflicts of interest

The authors who have taken part in this study declared that they do not have anything to disclose regarding funding or conflict of interest with respect to this manuscript.

Acknowledgements

We all express our sincere thanks to Mr. Tomohiro Shinozaki, Ph.D. for his great contribution to the preparation of the data for statistical analyses.

References

[1] El-Serag HB. Hepatocellular carcinoma. N Engl J Med 2011;365:1118–1127.
[2] Makuuchi M, Kokudo N. Clinical practice guidelines for hepatocellular carcinoma: the first evidence based guidelines from Japan. World J Gastroenterol 2006;12:828–829.
[3] Bruix J, Sherman M, Llovet JM, Beaugrand M, Lencioni R, Burroughs AK, et al. Clinical management of hepatocellular carcinoma. Conclusions of the Barcelona-2000 EASL Conference. European association for the study of the liver. J Hepatol 2001;35:421–430.
[4] Bruix J, Sherman M. Management of hepatocellular carcinoma. Hepatology 2005;42:1208–1236.
[5] Montorsi M, Santambrogio R, Bianchi P, Donadon M, Moroni E, Spinelli A, et al. Survival and recurrences after hepatic resection or radiofrequency for hepatocellular carcinoma in cirrhotic patients: a multivariate analysis. J Gastrointest Surg 2005;9:62–67.
[6] Hong SN, Lee SY, Choi MS, Lee JH, Koh KC, Paik SW, et al. Comparing the outcomes of radiofrequency ablation and surgery in patients with a single small hepatocellular carcinoma and well-preserved hepatic function. J Clin Gastroenterol 2005;39:247–252.
[7] Guglielmi A, Ruzzenente A, Valdegamberi A, Pachera S, Campagnaro T, D'Onofrio M, et al. Radiofrequency ablation versus surgical resection for the treatment of hepatocellular carcinoma in cirrhosis. J Gastrointest Surg 2008;12:192–198.
[8] Arii S, Yamaoka Y, Futagawa S, Inoue K, Kobayashi K, Kojiro M, et al. Results of surgical and nonsurgical treatment for small-sized hepatocellular carcinomas: a retrospective and nationwide survey in Japan. The Liver Cancer Study Group of Japan. Hepatology 2000;32:1224–1229.
[9] Hasegawa K, Makuuchi M, Takayama T, Kokudo N, Arii S, Okazaki M, et al. Surgical resection vs. percutaneous ablation for hepatocellular carcinoma: a preliminary report of the Japanese nationwide survey. J Hepatol 2008;49:589–594.
[10] Huang GT, Lee PH, Tsang YM, Lai MY, Yang PM, Hu RH, et al. Percutaneous ethanol injection versus surgical resection for the treatment of small hepatocellular carcinoma: a prospective study. Ann Surg 2005;242:36–42.
[11] Chen MS, Li JQ, Zheng Y, Guo RP, Liang HH, Zhang YQ, et al. A prospective randomized trial comparing percutaneous local ablative therapy and partial hepatectomy for hepatocellular carcinoma. Ann Surg 2006;243:321–328.
[12] Hasegawa K, Kokudo N, Makuuchi M. Surgery or ablation for hepatocellular carcinoma. Ann Surg 2008;247:557–558.
[13] Ikai I, Arii S, Kojiro M, Ichida T, Makuuchi M, Matsuyama Y, et al. Reevaluation of prognostic factors for survival after liver resection in patients with hepatocellular carcinoma in a Japanese nationwide survey. Cancer 2004;101:796–802.
[14] Makuuchi M, Hasegawa H, Yamazaki S. Ultrasonically guided subsegmentectomy. Surg Gynecol Obstet 1986;161:346–350.
[15] Huang J, Yan L, Cheng Z, Du L, Wang J, Xu Y, et al. A randomized trial comparing radiofrequency ablation and surgical resection for HCC conforming to the Milan criteria. Ann Surg 2010;252:903–912.
[16] Hasegawa K, Kokudo N, Shiina S, Tateishi R, Makuuchi M. Surgery vs. radiofrequency ablation for small hepatocellular carcinoma: start of a randomized controlled trial (SURF trial). Hepatol Res 2010;40:851–852.

Published in final edited form as:
Cancer Res. 2013 January 1; 73(1): 215–224. doi:10.1158/0008-5472.CAN-12-1602.

p38α inhibits liver fibrogenesis and consequent hepatocarcinogenesis by curtailing accumulation of reactive oxygen species

Toshiharu Sakurai[1,2], **Masatoshi Kudo**[1], **Atsushi Umemura**[2], **Guobin He**[2], **Ahmed M. Elsharkawy**[2,3], **Ekihiro Seki**[4], and **Michael Karin**[2]

[1]Department of Gastroenterology and Hepatology, Faculty of Medicine, Kinki University, 377-2 Ohnohigashi, Osaka-Sayama, Osaka, Japan

[2]Laboratory of Gene Regulation and Signal Transduction, Departments of Pharmacology and Pathology, School of Medicine, University of California, San Diego, 9500 Gilman Drive MC 0723, La Jolla, CA, USA

[3]Liver Group, Institute of Cellular Medicine, 4th Floor, Cookson Building, Medical School, Newcastle University, Newcastle upon Tyne NE2 4HH, United Kingdom

[4]Department of Medicine, University of California, San Diego, School of Medicine, La Jolla, CA, USA

Abstract

Most hepatocellular carcinomas (HCCs) develop in the context of severe liver fibrosis and cirrhosis caused by chronic liver inflammation, which also results in accumulation of reactive oxygen species (ROS). In this study, we examined whether the stress activated protein kinase p38α (Mapk14) controls ROS metabolism and development of fibrosis and cancer in mice given thioacetamide (TAA) to induce chronic liver injury. Liver-specific p38α ablation was found to enhance ROS accumulation, which appears to be exerted through the reduced expression of anti-oxidant protein heat shock protein (HSP) 25 (Hspb1), a mouse homologue of HSP27. Its re-expression in p38α-deficient liver prevents ROS accumulation and TAA-induced fibrosis. p38α-deficiency increased expression of SOX2, a marker for cancer stem cells, and the liver oncoproteins c-Jun (Jun) and Gankyrin (Psmd10) and led to enhanced TAA-induced hepatocarcinogenesis. The up-regulation of SOX2 and c-Jun was prevented by administration of the antioxidant butylated hydroxyanisole. Intriguingly, the risk of human HCC recurrence is positively correlated with ROS accumulation in liver. Thus, p38α and its target HSP25/HSP27 appear to play a conserved and critical hepatoprotective function by curtailing ROS accumulation in liver parenchymal cells engaged in oxidative metabolism of exogenous chemicals. Augmented oxidative stress of liver parenchymal cells may explain the close relationship between liver fibrosis and hepatocarcinogenesis.

Corresponding author: Dr. M. Karin. Laboratory of Gene Regulation and Signal Transduction, Departments of Pharmacology and Pathology, School of Medicine, University of California, San Diego, 9500 Gilman Drive MC 0723, La Jolla, CA 92093-0723, USA, karinoffice@ucsd.edu; Phone: (858) 534-1361; Fax: (858) 534-8158.; Dr. T. Sakurai. Department of Gastroenterology and Hepatology, Faculty of Medicine, Kinki University, 377-2 Ohnohigashi, Osakasayama, Osaka, Japan, sakurai@med.kindai.ac.jp; Phone: +81-75-751-4302; Fax: +81-75-751-4303.

Conflict of Interest:
The authors declare no conflict of interest.

Europe PMC Funders Author Manuscripts

Keywords

HSP27; liver fibrosis; ROS; SOX2; Gankyrin

Introduction

The liver plays an important role in oxidative metabolism and detoxification of endogenous and exogenous chemicals. The most common detoxification mechanism depends on cytochrome p450-mixed function oxidases (1). As a result, extensive and repetitive exposure to toxic chemicals can lead to accumulation of reactive oxygen species (ROS) in hepatocytes that are actively engaged in the detoxification of such chemicals. ROS accumulation can cause liver injury, which often progresses to liver fibrosis, cirrhosis and cancer.

Hepatocellular carcinoma (HCC) is the most common form of liver cancer and the third leading cause of cancer deaths worldwide and is usually associated with a very poor prognosis (2). In addition to chronic exposure to toxic chemicals, chronic infections with hepatitis B virus (HBV) or hepatitis C virus (HCV) as well as hepatosteatosis are the major risk factors for both liver fibrosis and HCC (3). In the case of HCV, a virus estimated to infect 4-5 million Americans (4), HCC develops only after one or more decades of chronic infection, and elevated risk of HCC progression is restricted largely to patients with cirrhosis or advanced fibrosis (5, 6). Although HCV-infected individuals with mild or nonhepatic fibrosis are unlikely to develop HCC, once cirrhosis is established, HCC develops at a rate of 1-4% per year (6). Thus, the risk of hepatocarcinogenesis depends on background liver factors, of which fibrosis is a major one. Development and progression of liver fibrosis is associated with hepatocyte death and a subsequent inflammatory response (7), both of which involve ROS accumulation in injured hepatocytes (8). Hence, a better understanding of hepatoprotective mechanisms that prevent ROS accumulation and their impact on fibrogenesis and carcinogenesis is of great importance.

The chemical thioacetamide (TAA) can induce liver cirrhosis and cancer of the bile ducts when given to rats over a period of several months (9). However, as described here we found that mice given TAA for 10 months develop HCC rather than cholangiocellular carcinoma subsequent to appearance of severe liver fibrosis, thus providing a model that closely mimics the natural history of human HCV-related liver disease. In addition, the histology of the TAA-exposed rat liver was reported to resemble human liver cirrhosis (10). Thus, the mouse TAA model may be suitable for studying the relationship between ROS accumulation, liver fibrogenesis and hepatocarcinogenesis and allows studies to be carried out that are of relevance to human HCV-related liver disease.

Mitogen and stress activated protein kinases (MAPK/SAPK) play a pivotal role in the transduction of extracellular signals to the nucleus, thereby modulating numerous cellular responses, including cell survival, proliferation, differentiation, and metabolism (11, 12). One of the SAPKs, p38α, the major p38 MAPK isoform, is activated in response to inflammation and oxidative stress and in turn controls expression of cytokines, inflammatory mediators, survival genes and anti-oxidants (13-16). As ubiquitous p38α ablation in all cells results in midgestational lethality, mainly due to placental insufficiency (17-20), we used a conditional *p38α* "floxed" ($p38\alpha^{F/F}$) strain (21) to generate $p38\alpha^{\Delta hep}$ mice, lacking p38α in liver parenchymal cells, to assess the role of this kinase in development of liver cancer (15). In the course of these studies we found that p38α prevented the accumulation of ROS in liver parenchymal cells exposed to the hepatic carcinogen diethylnitrosamine (DEN). We now describe that p38α also prevents ROS accumulation, liver fibrogenesis and subsequent hepatocarcinogenesis in mice exposed to

Europe PMC Funders Author Manuscripts

TAA. In both models, p38α prevents ROS accumulation by controlling the expression of heat shock protein (HSP) 25, the mouse homolog of human HSP27. Restoration of HSP25 expression in the p38α-deficient liver prevents TAA-induced ROS accumulation and fibrogenesis. We also show that the risk of HCC recurrence in post-hepatectomy patients is positively associated with ROS accumulation in the non-tumor liver tissue.

Materials and Methods

Animals, tumor induction and analysis

*p38*α$^{F/F}$ mice (21) were crossed with *Alb-Cre* mice (Jackson lab, Bar Harbor, Maine) to generate *p38*α$^{\Delta hep}$ mice (15). All mice were maintained in the C57BL/6 background in filter-topped cages on autoclaved or non-autoclaved food at UCSD and Kinki University, respectively. Mice were given 0.03% TAA in drinking water. After 10 months on normal chow, mice were sacrificed and analyzed for presence of HCCs. Tumor-occupied areas were measured using Image J software.

Biochemical and immunochemical analyses

JNK assays, real time Q-PCR, immunoblotting, and immunohistochemistry were previously described (15). The primer sequences for TIMP-1, PDGF-b, SOX2 and gankyrin were; forward primer 5′-CCAGAACCGCAGTGAAGAGT-3′, reverse primer 5′-AAGAAGCTGCAGGCATTGAT-3′; and forward primer 5′-CCTCGGCCTGTGACTAGAAG-3′, reverse primer 5′-AAGGCTCCTGCACACTTGTT-3′; forward primer 5′-GAACGCCTTCATGGTATGGT-3′, reverse primer 5′-TTGCTGATTCTCCGAGTTGTG-3′; respectively. Antibodies used were: anti-HSP27/25, anti-α-fetoprotein (Santa Cruz Biotechnology, Santa Cruz, CA); anti-actin (Sigma, St. Louis, MO); anti-α-smooth muscle actin (α-SMA) (Dako, Glostrup, Denmark); anti-p38α, anti-MAPKAPK2, anti-phospho-MAPKAPK2, anti-SOX2 (Cell Signaling, Danvers, MA); anti-PRMO1 (CD133, Abnova, Newmarket Suffolk, England); anti-c-kit (R&D systems); anti-JNK1, (Pharmingen, San Diego, CA). Immunohistochemistry was performed using ABC staining kit (Vector Laboratory, Burlingame, CA) according to manufacturer's recommendations. TUNEL staining was performed on tissue sections using In Situ Apoptosis Detection Kit (Takara, Tokyo, Japan). To examine accumulation of superoxide anions or H_2O_2, freshly prepared frozen liver sections were incubated with 2 μM dihydroethidine hydrochloride (Invitrogen, Carlsbad, CA) or 5 μM 5-[and-6]-chloromethyl-2′,7′-dichlorodihydrofluorescein diacetate (Invitrogen), respectively for 30 min at 37°C, after which they were observed by fluorescent microscopy and quantified with Metamorph software. Protein oxidation was assessed by the OxyBlot Protein Oxidation Detection Kit (Millipore, Billerica, MA). Sirius Red staining was performed to quantitate the amount of collagen present. To analyze the relative fibrotic area, the Sirius Red positive areas were measured in six random fields (100×) on each slide and quantified using NIH imaging software. Myeloperoxidase (MPO) activity was measured using MPO Activity Assay Kit (Invitrogen). Livers were homogenized in MPO buffer (0.5% hexadecyl trimethyl ammonium bromide, 10 mM EDTA, 50 mM Na_2HPO_4, pH 5.4). Hydroxyproline content was measured as described (22).

Adenoviral transduction

Adenovirus expressing HSP25 was prepared as described (15). Adenovirus stocks were injected via the tail vein at 1×10^9 plaque-forming units (PFU)/mouse. Before infection, virus stocks were dialyzed against PBS containing 10% glycerol.

Patients and specimens

HCC tissues and non-cancerous liver tissues were obtained from 43 patients, respectively, who had undergone curative hepatectomy for HCC at the Kinki University Hospital between 2004 and 2010. The specimens used were routinely processed, formalin-fixed, and paraffin-embedded. After hematoxylin-eosin staining, all samples were diagnosed as HCC. Non-cancerous tissue and HCC specimens were frozen and stocked at −80. The demographic profiles of the patients are summarized in Supplementary Table. The study protocol conformed to the ethical guidelines of the 1975 Declaration of Helsinki and was approved by the institutional review boards. Written informed consents were obtained from all patients for subsequent use of their resected tissues.

Statistical analysis

Data are presented as means ± SEM. Differences were analyzed by Fisher's exact test or Student's t test. Recurrence free survival curves were calculated by the Kaplan-Meier method and analyzed by the log-rank test. P values < 0.05 were considered significant.

Results

Enhanced fibrogenesis in p38α$^{\Delta hep}$ mice

Hepatic stellate cells (HSCs) which undergo a transition from a quiescent to an activated state after liver injury play an important part in the pathogenesis of liver fibrosis (23). HSC activation includes increased proliferation rate, a phenotypic transition to a myofibroblast-like, smooth muscle α-actin (α-SMA) expression, and a dramatic increase in the synthesis of extracellular matrix proteins. After 8 weeks of TAA treatment, we observed inflammation, HSC activation and formation of fibrotic septa as assessed histologically or by immunohistochemistry with a specific antibody against α-SMA (Fig. 1A). *p38*α$^{\Delta hep}$ mice exhibited more TAA-induced liver damage assessed by ALT release, and hepatocyte apoptosis measured by a TUNEL assay, relative to controls (Fig. 1A and B). Neutrophil infiltration was enhanced, based on measurement of myeloperoxidase (MPO) activity (Fig. 1C). In addition, there were higher numbers of α-SMA-positive cells, higher levels of hydroxyproline and larger fibrotic areas in *p38*α$^{\Delta hep}$ mice compared with control mice (Fig. 1D-F). No significant difference in serum ALT levels or fibrotic areas was found between male and female *p38*α$^{\Delta hep}$ mice (data not shown).

We examined the consequences of p38α deletion in liver parenchymal cells on expression of fibrogenic markers. Loss of p38α significantly enhanced expression of the mRNAs for col1α1, TIMP1, TGF-β1 and PDGFb (Fig. 1G). No difference in the expression of these fibrogenic markers was found in uninjured livers taken from *p38*α$^{F/F}$ and *p38*α$^{\Delta hep}$ mice (data not shown).

Enhanced ROS accumulation in p38α$^{\Delta hep}$ mice accounts for increased liver injury and fibrogenesis

A causal link between oxidative stress and liver fibrosis was proposed (24). We assessed the accumulation of hepatocyte superoxides by staining freshly frozen liver sections with dihydroethidine (DHE), whose oxidation gives rise to the fluorescent derivative ethidine. More extensive fluorescence was seen in periportal areas (zone 1) after TAA administration in *p38*α$^{\Delta hep}$ mice than in control mice (Fig. 2A, B). Notably, the histological location of TAA-induced ROS accumulation differs from that of DEN-induced ROS, which are mainly detected in centrilobular (zone 3) hepatocytes (15, 25). This differential distribution of ROS positive hepatocytes is likely to be due to a difference in the metabolism of the two compounds. Whereas DEN is metabolically activated by Cyp2E1 which is more abundant in zone 3 hepatocytes (26), TAA can be converted to more toxic metabolites via a

Europe PMC Funders Author Manuscripts

thioacetamide S-oxide intermediate by several enzymes including Cyp2B (27), whose spatial distribution in the liver is affected by exposure to different chemicals and growth factors (28). Increased H_2O_2 accumulation in livers of TAA-treated *p38*α$^{\Delta hep}$ mice was also detected using the ROS indicator 5-[and-6]-chloromethyl-2′,7′-dichlorodihydrofluorescein diacetate (CM-H_2DCFDA) (Fig. 2A). *p38*α$^{\Delta hep}$ mice were found to have higher levels of oxidized protein in comparison to *p38*α$^{F/F}$ mice (Fig. 2B).

To evaluate the contribution of oxidative stress to TAA-induced liver damage and fibrosis, we placed a group of mice on chow diet supplemented with the antioxidant butylated hydroxyanisole (BHA). *p38*α$^{\Delta hep}$ mice kept on this diet showed a significant reduction in TAA-induced liver injury (Fig. 2C) and fibrosis (Fig. 2D). Thus, loss of p38α enhances TAA-induced cell death and fibrogenesis through mechanisms that may depend on ROS accumulation.

The p38α-induced anti-oxidant gene HSP25 inhibits TAA-induced fibrosis

As previously described for DEN-treated mice (15), HSP25 expression was also induced by TAA administration and the extent of induction was much lower in *p38*α$^{\Delta hep}$ mice relative to *p38*α$^{F/F}$ controls (Fig. 3A, B). HSP25 was reported to inhibit ROS accumulation (29, 30). Adenoviral transduction of HSP25 into *p38*α$^{\Delta hep}$ liver (Supplementary Fig. 1) prevented TAA-induced ROS accumulation, protein oxidation (Fig. 3C, D), liver damage (Fig. 3E) and fibrogenesis (Fig. 3F, G). These results provide further support to the notion that the enhanced accumulation of ROS in the *p38*α-deficient liver is responsible for the enhanced fibrogenic response of *p38*α$^{\Delta hep}$ mice.

Decreased expression of MAPKAP kinase-2 and increased expression of SOX2, c-Jun and Gankyrin in TAA-treated p38α$^{\Delta hep}$ mice

Previous studies have described a critical role for c-Jun and JNK in mediating HCC development (31, 32). In the TAA model, p38α deficient livers exhibited elevated c-Jun expression and increased JNK activity (Fig. 4A, B). Whereas cytokine-driven compensatory proliferation was suggested to promote DEN-induced hepatocarcinogenesis (15, 25, 33), there was no significant increase in IL-6, and TNFα and IL-1β expression in TAA-treated *p38*α$^{\Delta hep}$ mice relative to *p38*α$^{F/F}$ controls (Fig. 4B). An important downstream target for p38 is MAPKAP kinase-2 (MAPKAPK2) and MAPKAPK2-deficient cells are more sensitive to DNA damage-induced cell death (34). As shown in Fig. 4C, MAPKAPK2 expression and phosphorylation is down-regulated in p38α deficient livers. Pluripetency-associated transcription factors like SOX2 and Nanog are known as regulators of cellular identity in embryonic stem cells. More recently SOX2 has been shown to participate in reprogramming of adult somatic cells to a pluripotent stem cell state and has been implicated in tumorigenesis in various organs (35). Loss of p38α significantly enhanced the expression of SOX2 mRNA and protein in TAA-treated mice (Fig. 4D and 4F). Gankyrin, a liver oncoprotein, was reported to mediate dedifferentiation and facilitate the tumorigenecity of rat hepatocytes (36). *p38*α$^{\Delta hep}$ miceexhibited a significant increase in gankyrin expression after TAA administration (Fig. 4E, F). No difference in the expression of Gankyrin was found in uninjured livers taken from *p38*α$^{F/F}$ and *p38*α$^{\Delta hep}$ mice (data not shown). To evaluate the contribution of oxidative stress to the increase in expression of these genes, we placed a group of mice on chow diet supplemented with the antioxidant BHA. *p38*α$^{\Delta hep}$ mice kept on this diet showed a significant reduction in SOX2 and c-Jun expression, but not the Gankyrin expression (Fig. 4G). Immunohistochemical analysis revealed that putative hematopoietic stem cells, c-kit-positive cells, were recruited to TAA treated livers (Fig. 4H) but not in non-treated livers (data not shown). We confirmed that c-kit-positive cells expressed p38α in *p38*α$^{\Delta hep}$ mice (Fig. 4H). Between *p38*α$^{F/F}$ and *p38*α$^{\Delta hep}$ livers, there was no significant difference in the number of c-kit-positive cells (data not shown),

Europe PMC Funders Author Manuscripts

indicating that hepatic p38α deficiency does not increase hematopoietic stem cell recruitment.

Enhanced hepatocarcinogenesis in p38α$^{\Delta hep}$ mice

p38α$^{F/F}$ and *p38α*$^{\Delta hep}$ mice were given TAA in drinking water for 10 months. When sacrificed, all *p38α*$^{\Delta hep}$ mice given TAA developed typical liver cirrhosis and 50% of *p38α*$^{\Delta hep}$ mice had ascites, a common clinical finding indicative of portal hypertension. The liver surface was irregular, closely resembling human cirrhotic liver (Fig. 5A). All the *p38α*$^{F/F}$ and *p38α*$^{\Delta hep}$ mice given TAA for 10 months developed well-differentiated HCCs (Fig 5B), whereas only a few and small number of cholangiocellular carcinomas were found. Many tumors were positive for α-fetoprotein (AFP) expression, a tumor marker specific for HCC (Fig. 5C). Tumor sizes and areas were considerably larger in *p38α*$^{\Delta hep}$ mice relative to similarly treated *p38α*$^{F/F}$ controls (Fig. 5D). In contrast to mice, TAA-treated rats develop cholangiecellular carcinoma (9). This may be because CD133-positive stem cells are induced by TAA in mice but not in rats (Fig. 5E).

Association between risk of HCC recurrence and protein oxidation in human liver

Forty-two patients with HCC were recruited in this study. Clinocopathological profiles of the patients and their HCCs are shown in Supplementary Table. Intrahepatic HCC development after hepatectomy is caused by de novo HCC development and/or metastasis from the resected HCC. The risk of the former depends on background liver factors such as liver fibrosis, while the risk of the latter mainly depends on the characteristics of the resected HCC (37). In mouse models, HSP25-mediated inhibition of ROS accumulation is involved in control of liver fibrogenesis and can subsequently attenuate de novo HCC development. We examined whether this hypothesis is applicable to humans, focusing on non-cancerous liver tissues rather than cancers to assess the potential for de novo HCC development or rapid progression of lesions that were undetectable or pre-neoplastic at the time of resection. In patients exhibiting HCC recurrence after hepatectomy, protein oxidation levels in the non-tumor tissues, but not in tumors, were significantly higher than in those without HCC recurrence (Fig. 6A). In addition, patients with low protein oxidation in non-cancerous liver had a prolonged recurrence-free survival (Fig. 6B). In conclusion, elevated ROS accumulation in the liver is associated with increased risk of human HCC development or recurrence.

Discussion

Oxidative stress is thought to play a major role in the pathogenesis of hepatic fibrosis (8) and cancer development (38, 39), exerting many effects, including alteration of gene expression (40), enhanced cell death and proliferation as well as genomic instability (39). However, the exact impact of oxidative stress and anti-oxidant responses on hepatic fibrosis and subsequent HCC development needs to be better understood. We previously found that the p38α MAPK pathway prevents ROS accumulation in mice exposed to the non-fibrogenic hepatic carcinogen DEN (15). Here we describe that p38α activity is also important for suppression of ROS accumulation upon TAA administration, which leads to induction of fibrosis, cirrhosis and HCC. In the absence of the p38α target HSP25, the TAA-exposed *p38α*$^{\Delta hep}$ liver shows elevated ROS accumulation that correlates with augmented liver damage in these mice. Increased susceptibility to liver damage in *p38α*$^{\Delta hep}$ mice is reversed by administration of the small molecule antioxidant BHA or restoration of HSP25 expression. These results support the hypothesis that increased ROS accumulation may be the main cause of hepatocyte death in p38α-deficient mice regardless of the hepatotoxic chemical to which they were exposed. Expression levels of MAPKAPK2 and phospho-MAPKAPK2 were decreased in the p38α depleted livers. Given the protective role

of MAPKAPK2 in DNA damage-induced cell death (34), the down-regulation of MAPKAPK2 expression and phosphorylation that take place in the absence of p38α, are likely to contribute, at least in part, to increased liver damage in $p38\alpha^{\Delta hep}$ mice. Hepatocyte death activates an inflammatory response, which promotes HSC activation via a paracrine mechanism (24), which we and others have suggested to involve IL-1α release (15, 41). This inflammatory response results in excessive synthesis of extracellular matrix proteins and fibrosis development (23). Correspondingly, BHA administration or restoration of HSP25 expression reverses enhanced thioacetamide-induced fibrogenesis caused by the p38α deficiency. A strong correlation between liver fibrogenesis and hepatocarcinogenesis has been reported in patients infected with HCV (6) and HCV infection has been demonstrated to cause ROS accumulation and oxidative stress (42). We find that enhanced protein oxidation in the non-cancerous portion of human liver is associated with a high risk of HCC recurrence after hepatectomy. These data support an important role of ROS accumulation within liver parenchymal cells in liver fibrogenesis and subsequent hepatocarcninogenesis.

HSP25/HSP27 has anti-oxidant properties (29, 30). Mice given TAA showed an inverse correlation between HSP25 expression and ROS accumulation in the liver. In addition, we found that elevated ROS accumulation correlated with the presence of HCC recurrence after hepatectomy. However, we did not observe a statistically significant relationship between HSP27 expression and ROS accumulation in human livers (data not shown). Whilst elevated HSP27 expression reduces ROS accumulation, HSP27 expression itself is up-regulated following oxidative stress (43). Most probably, our findings may reflect complex mechanisms regulating ROS accumulation via several molecules in the human liver. The exact relationship between HSP27 and oxidative stress in human parenchymal cells remains to be elucidated. In the mouse liver, however, it is quite clear that p38α negatively regulates ROS accumulation through induction of HSP25, which maintains parenchymal cell viability and suppresses liver fibrogenesis. Enhanced cell death caused by the absence of p38α results in increased inflammation and hepatic fibrogenesis, which eventually augments HCC development, as seen before in DEN-treated mice (15, 32). Thus, the anti-tumorigenic activity of hepatocyte p38α is not model specific and may also apply to human liver.

Stem cell function is central for the maintenance of normal tissue homeostasis. SOX2 forms the core of the self-renewal transcription network in embryonic stem cells. Selective downregulation of SOX2 induces embryonic stem cell differentiation and exit from the pluripotent stem cell state. By contrast, combinatorial overexpression of SOX2, Nanog and other transcription factors was shown to reprogram several types of adult somatic cells to a pluripotent stem cell like state (44-46). In these experiments, cells were reprogrammed fully or only partially (47), possibly due to heterogeneous exposure to reprogramming factors. It is tempting to speculate that acquisition or overexpression of SOX2 can promote tumorigenesis by processes that resemble partial reprogramming (35, 44, 47). In our study, we showed that p38α deletion increased expression of SOX2 through enhanced ROS accumulation. Hepatocyte dedifferentiation has been reviewed as a key cellular event during hepatocarcinogenesis (48). Gankyrin, also named 26S proteasome non-ATPase regulatory subunit 10, is a critical oncoprotein overexpressed in human HCC. A close association of Gankyrin expression with hepatocyte dedifferentiation were observed and differentiation induced by Gankyrin interference reduced the population of cancer stem cells in hepatoma cell lines (36), suggesting that Gankyrin promotes HCC development by driving dedifferentiation of hepatocytes and facilitating HCC stem/progenitor cell generation. We found that the p38α deficiency enhances the induction of Gankyrin expression in livers of TAA-treated mice. Recently, JNK activation was reported to be involved in stem cell expansion in human HCC (49). JNK activity was significantly enhanced in p38α-deficient liver. The inactivation of p38α also leads to an immature and hyperproliferative lung

Europe PMC Funders Author Manuscripts

epithelium that is highly sensitized to tumorigenesis (50). It has been shown that the Albumin-Cre driver does not only lead to deletion of genes in hepatocytes, but also deletes genes in hepatic precursor cells. These data suggest an important role of p38α in regulating hepatic stem/precursor cell behavior.

In conclusion, p38α plays a critical role in liver fibrogenesis and hepatocarcinogenesis through the control of HSP27 expression and ROS accumulation in the mouse TAA model which may be suitable for studying the pathogenesis of HCV-related HCC development. Importantly, the risk of human HCC recurrence after hepatectomy is positively correlated with protein oxidation in liver. Deletion of p38α upregulates expression of SOX2 and Gankyrin, which may be involved in cancer stem cell maintenance.

Supplementary Material

Refer to Web version on PubMed Central for supplementary material.

Acknowledgments

We thank J. Feramisco for help with image capture and analysis, S. Baird and D. Herold for review on pathology of the liver and J. Fujita for providing anti-Gankyrin antibody.

Grant Support

T.S. was supported by Mitsui Life Social Welfare Foundation, Osaka Community Foundation, Yasuda Medical Foundation, Novartis Foundation and the Ministry of Education, Science, Sport and Culture of Japan. A.M.E is a Wellcome Trust Clinical Research Fellow. Research was supported by grants from the Welcome Trust (WT086755) and the National Institute of Health (ES004151, ES006376 and CA118165) and the Superfund Basic Research Program (ES0100337). M. Karin is an American Cancer Society Research Professor.

References

1. Rooney PH, Telfer C, McFadyen MC, Melvin WT, Murray GI. The role of cytochrome P450 in cytotoxic bioactivation: future therapeutic directions. Curr Cancer Drug Targets. 2004; 4:257–65. [PubMed: 15134533]
2. Thorgeirsson SS, Grisham JW. Molecular pathogenesis of human hepatocellular carcinoma. Nat Genet. 2002; 31:339–46. [PubMed: 12149612]
3. Bosch FX, Ribes J, Diaz M, Cleries R. Primary liver cancer: worldwide incidence and trends. Gastroenterology. 2004; 127:S5–16. [PubMed: 15508102]
4. Ginick G. Hepatitis C: controversies, strategies and challenges. Eur J Surg. 1998; S582(Suppl):65–70.
5. Ikeda K, Saitoh S, Suzuki Y, Kobayashi M, Tsubota A, Koida I, et al. Disease progression and hepatocellular carcinogenesis in patients with chronic viral hepatitis: a prospective observation of 2215 patients. J Hepatol. 1998; 28:930–8. [PubMed: 9672166]
6. Hoshida Y, Ikeda K, Kobayashi M, Suzuki Y, Tsubota A, Saitoh S, et al. Chronic liver disease in the extremely elderly of 80 years or more: clinical characteristics, prognosis and patient survival analysis. J Hepatol. 1999; 31:860–6. [PubMed: 10580583]
7. Ghany MG, Kleiner DE, Alter H, Doo E, Khokar F, Promrat K, et al. Progression of fibrosis in chronic hepatitis C. Gastroenterology. 2003; 124:97–104. [PubMed: 12512034]
8. Parola M, Robino G. Oxidative stress-related molecules and liver fibrosis. J Hepatol. 2001; 35:297–306. [PubMed: 11580156]
9. Gupta DN. Production of cancer of the bile ducts with thioacetamide. Nature. 1955; 175:257. [PubMed: 13235865]
10. Zimmermann T, Müller A, Machnik G, Franke H, Schubert H, Dargel R. Biochemical and morphological studies on production and regression of experimental liver cirrhosis induced by thioacetamide in Uje: WIST rats. Z Versuchstierkd. 1987; 30:165–80. [PubMed: 3445704]

Europe PMC Funders Author Manuscripts

11. Chang L, Karin M. Mammalian MAP kinase signalling cascades. Nature. 2001; 410:37–40. [PubMed: 11242034]
12. Dhillon AS, Hagan S, Rath O, Kolch W. MAP kinase signalling pathways in cancer. Oncogene. 2007; 26:3279–90. [PubMed: 17496922]
13. Cuenda A, Rousseau S. p38 MAP-kinases pathway regulation, function and role in human diseases. Biochim Biophys Acta. 2007; 1773:1358–75. [PubMed: 17481747]
14. Park JM, Greten FR, Wong A, Westrick RJ, Arthur JS, Otsu K, et al. Signaling pathways and genes that inhibit pathogen-induced macrophage apoptosis--CREB and NF-kappaB as key regulators. Immunity. 2005; 23:319–29. [PubMed: 16169504]
15. Sakurai T, He G, Matsuzawa A, Yu GY, Maeda S, Hardiman G, Karin M. Hepatocyte necrosis induced by oxidative stress and IL-1α release mediate carcinogen-induced compensatory proliferation and liver tumorigenesis. Cancer Cell. 2008; 14:156–65. [PubMed: 18691550]
16. Wagner EF, Nebreda AR. Signal integration by JNK and p38 MAPK pathways in cancer development. Nat Rev Cancer. 2009; 9:537–49. [PubMed: 19629069]
17. Tamura K, Sudo T, Senftleben U, Dadak AM, Johnson R, Karin M. Requirement for p38alpha in erythropoietin expression: a role for stress kinases in erythropoiesis. Cell. 2000; 102:221–31. [PubMed: 10943842]
18. Adams RH, Porras A, Alonso G, Jones M, Vintersten K, Panelli S, et al. Essential role of p38alpha MAP kinase in placental but not embryonic cardiovascular development. Mol Cell. 2000; 6:109–16. [PubMed: 10949032]
19. Mudgett JS, Ding J, Guh-Siesel L, Chartrain NA, Yang L, Gopal S, et al. Essential role for p38alpha mitogen-activated protein kinase in placental angiogenesis. Proc Natl Acad Sci U S A. 2000; 97:10454–59. [PubMed: 10973481]
20. Allen M, Svensson L, Roach M, Hambor J, McNeish J, Gabel CA. Deficiency of the stress kinase p38alpha results in embryonic lethality: characterization of the kinase dependence of stress responses of enzyme-deficient embryonic stem cells. J Exp Med. 2000; 191:859–70. [PubMed: 10704466]
21. Nishida K, Yamaguchi O, Hirotani S, Hikoso S, Higuchi Y, Watanabe T, et al. p38alpha mitogen-activated protein kinase plays a critical role in cardiomyocyte survival but not in cardiac hypertrophic growth in response to pressure overload. Mol Cell Biol. 2004; 24:10611–10620. [PubMed: 15572667]
22. Seki E, de Minicis S, Inokuchi S, Taura K, Miyai K, van Rooijen N, et al. CCR2 promotes hepatic fibrosis in mice. Hepatology. 2009; 50:185–97. [PubMed: 19441102]
23. Bataller R, Brenner DA. Liver fibrosis. J Clin Invest. 2005; 115:209–18. [PubMed: 15690074]
24. Casini A, Ceni E, Salzano R, Biondi P, Parola M, Galli A, et al. Neutrophil-derived superoxide anion induces lipid peroxidation and stimulates collagen synthesis in human hepatic stellate cells: role of nitric oxide. Hepatology. 1997; 25:361–67. [PubMed: 9021948]
25. Maeda S, Kamata H, Luo JL, Leffert H, Karin M. IKKbeta couples hepatocyte death to cytokine-driven compensatory proliferation that promotes chemical hepatocarcinogenesis. Cell. 2005; 121:977–90. [PubMed: 15989949]
26. Yang CS, Yoo JS, Ishizaki H, Hong JY. Cytochrome P450IIE1: roles in nitrosamine metabolism and mechanisms of regulation. Drug Metab Rev. 1990; 22:147–59. [PubMed: 2272285]
27. Jeong TC, Gu HK, Park JI, Yun HI, Kim HC, Ha CS, et al. Pretreatment of male BALB/c mice with beta-ionone potentiates thioacetamide-induced hepatotoxicity. Toxicol Lett. 1999; 105:39–46. [PubMed: 10092055]
28. Allen JW, Khetani SR, Bhatia SN. In vitro zonation and toxicity in a hepatocyte bioreactor. Toxicol Sci. 2005; 84:110–19. [PubMed: 15590888]
29. Escobedo J, Pucci AM, Koh TJ. HSP25 protects skeletal muscle cells against oxidative stress. Free Radic Biol Med. 2004; 37:1455–62. [PubMed: 15454285]
30. Garrido C, Brunet M, Didelot C, Zermati Y, Schmitt E, Kroemer G. Heat shock proteins 27 and 70: anti-apoptotic proteins with tumorigenic properties. Cell Cycle. 2006; 5:2592–01. [PubMed: 17106261]

Europe PMC Funders Author Manuscripts

31. Sakurai T, Maeda S, Chang L, Karin M. Loss of hepatic NF-kappa B activity enhances chemical hepatocarcinogenesis through sustained c-Jun N-terminal kinase 1 activation. Proc Natl Acad Sci U S A. 2006; 103:10544–51. [PubMed: 16807293]
32. Hui L, Bakiri L, Mairhorfer A, Schweifer N, Haslinger C, Kenner L, et al. p38alpha suppresses normal and cancer cell proliferation by antagonizing the JNK-c-Jun pathway. Nat Genet. 2007; 39:741–49. [PubMed: 17468757]
33. Naugler WE, Sakurai T, Kim S, Maeda S, Kim K, Elsharkawy AM, Karin M. Gender disparity in liver cancer due to sex differences in MyD88-dependent IL-6 production. Science. 2007; 317:121–4. [PubMed: 17615358]
34. Jackson RM, Garcia-Rojas R. Kinase activity, heat shock protein 27 phosphorylation, and lung epithelial cell glutathione. Exp Lung Res. 2008; 34:245–62. [PubMed: 18465403]
35. Lengerke C, Fehm T, Kurth R, Neubauer H, Scheble V, Müller F, et al. Expression of the embryonic stem cell marker SOX2 in early-stage breast carcinoma. BMC Cancer. 2011; 11:42. [PubMed: 21276239]
36. Sun W, Ding J, Wu K, Ning BF, Wen W, Sun HY, et al. Gankyrin-mediated dedifferentiation facilitates the tumorigenicity of rat hepatocytes and hepatoma cells. Hepatology. 2011; 54:1259–72. [PubMed: 21735473]
37. Imamura H, Matsuyama Y, Tanaka E, Ohkubo T, Hasegawa K, Miyagawa S, et al. Risk factors contributing to early and late phase intrahepatic recurrence of hepatocellular carcinoma after hepatectomy. J Hepatol. 2003; 38:200–7. [PubMed: 12547409]
38. Ames BN. Dietary carcinogens and anticarcinogens. Oxygen radicals and degenerative diseases. Science. 1983; 221:1256–64. [PubMed: 6351251]
39. Woo RA, Poon RY. Activated oncogenes promote and cooperate with chromosomal instability for neoplastic transformation. Genes Dev. 2004; 18:1317–30. [PubMed: 15175263]
40. Allen RG, Tresini M. Oxidative stress and gene regulation. Free Radic Biol Med. 2000; 28:463–99. [PubMed: 10699758]
41. Chen CJ, Kono H, Golenbock D, Reed G, Akira S, Rock KL. Identification of a key pathway required for the sterile inflammatory response triggered by dying cells. Nat Med. 2007; 13:851–6. [PubMed: 17572686]
42. Kato J, Kobune M, Nakamura T, Kuroiwa G, Takada K, Takimoto R, et al. Normalization of elevated hepatic 8-hydroxy-2′-deoxyguanosine levels in chronic hepatitis C patients by phlebotomy and low iron diet. Cancer Res. 2001; 61:8697–702. [PubMed: 11751387]
43. Fulop, T.; Franceschi, C.; Hirokawa, K.; Pawelec, G. Handbook on Immunosenescence: Basic understanding and clinical applications. Springe□2009. p. 519
44. Park IH, Zhao R, West JA, Yabuuchi A, Huo H, Ince TA, et al. Reprogramming of human somatic cells to pluripotency with defined factors. Nature. 2008; 451:141–6. [PubMed: 18157115]
45. Takahashi K, Tanabe K, Ohnuki M, Narita M, Ichisaka T, Tomoda K, Yamanaka S. Induction of pluripotent stem cells from adult human fibroblasts by defined factors. Cell. 2007; 131:861–72. [PubMed: 18035408]
46. Yu J, Vodyanik MA, Smuga-Otto K, Antosiewicz-Bourget J, Frane JL, Tian S, et al. Induced pluripotent stem cell lines derived from human somatic cells. Science. 2007; 318:1917–20. [PubMed: 18029452]
47. Chan EM, Ratanasirintrawoot S, Park IH, Manos PD, Loh YH, Huo H, et al. Live cell imaging distinguishes bona fide human iPS cells from partially reprogrammed cells. Nat Biotechnol. 2009; 27:1033–7. [PubMed: 19826408]
48. Lazarevich NL, Cheremnova OA, Varga EV, Ovchinnikov DA, Kudrjavtseva EI, Morozova OV, et al. Progression of HCC in mice is associated with a downregulation in the expression of hepatocyte nuclear factors. Hepatology. 2004; 39:1038–47. [PubMed: 15057908]
49. Hagiwara S, Kudo M, Nagai T, Inoue T, Ueshima K, Nishida N, Watanabe T, Sakurai T. Activation of JNK and high expression level of CD133 predict a poor response to sorafenib in hepatocellular carcinoma. Br J Cancer. 2012; 106:1997–2003. [PubMed: 22596232]
50. Ventura JJ, Tenbaum S, Perdiguero E, Huth M, Guerra C, Barbacid M, Pasparakis M, Nebreda AR. p38alpha MAP kinase is essential in lung stem and progenitor cell proliferation and differentiation. Nat Genet. 2007; 39:750–8. [PubMed: 17468755]

Europe PMC Funders Author Manuscripts

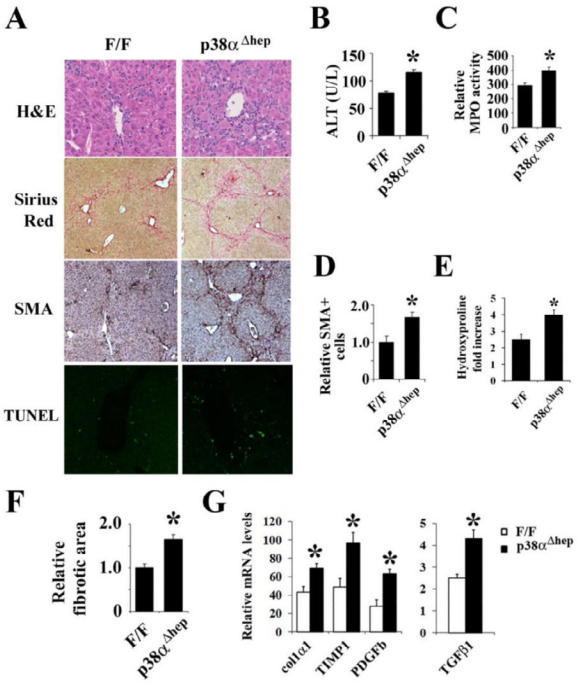

Figure 1.

Enhanced fibrogenesis in *p38*$\alpha^{\Delta hep}$ mice.

(A) Histological and immunohistological analysis of livers from mice treated with TAA for 8 weeks. Liver sections were examined using H&E and Sirius Red staining, immunohistochemistry with α-SMA specific antibody and TUNEL staining. (B) ALT levels in serum were determined after 8 weeks of TAA treatment. Results are means ± SEM (n=8). *, $p<0.05$ vs. control (F/F) mice. (C) Extent of neutrophil infiltration was determined by MPO assay. MPO activity in untreated liver was given an arbitrary value of 1.0. Results are means ± SEM (n=8). (D-F) The surface area stained with Sirius Red or antibody against α-SMA was quantified. Hepatic hydroxyproline content was measured. Results are means ± SEM (n=6). (G) Mice were treated with TAA for 8 weeks and liver RNA was extracted. Relative mRNA amounts of the indicated genes were determined by real time Q-PCR and normalized to the amount of actin mRNA. The amount of each mRNA in untreated liver was given an arbitrary value of 1.0. Results are means ± SEM (n=8).

Europe PMC Funders Author Manuscripts

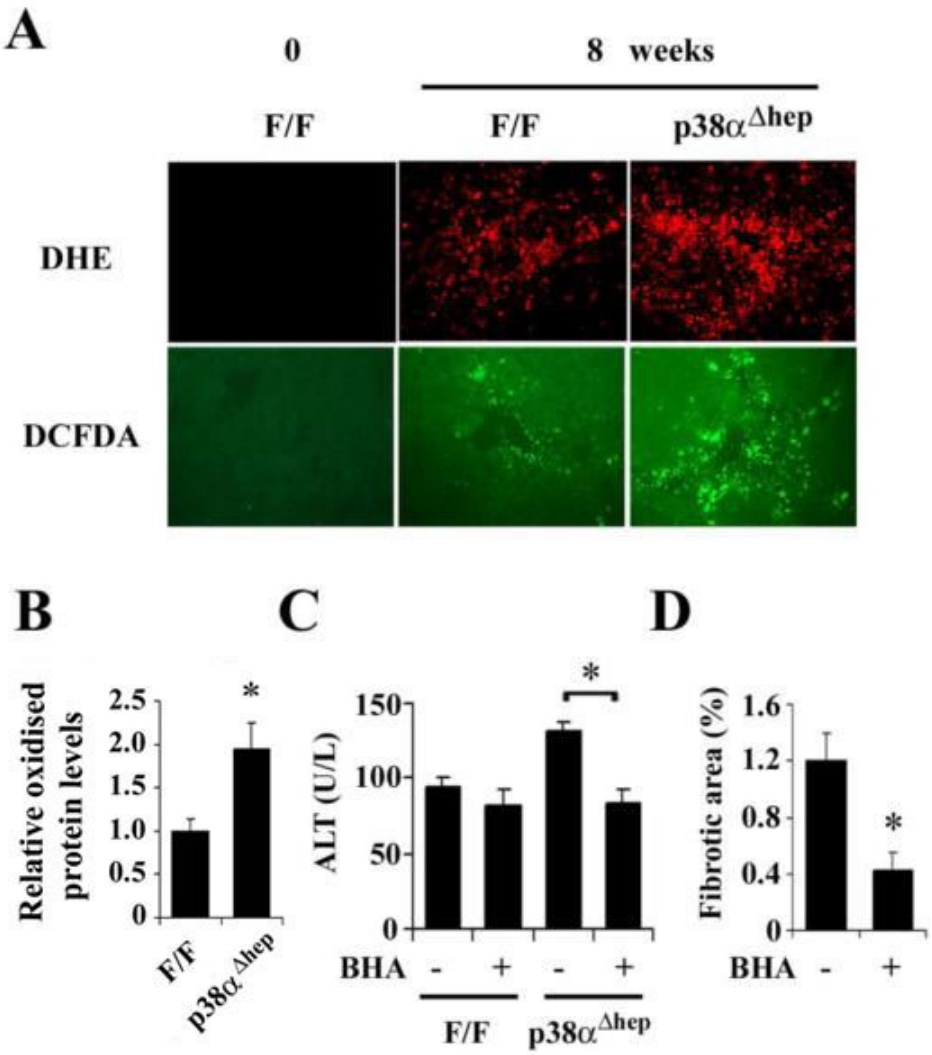

Figure 2.

Enhanced ROS accumulation in *p38*α$^{\Delta hep}$ mice accounts for increased liver injury and fibrogenesis.

(A) Frozen liver sections prepared after 8 weeks of TAA treatment were incubated with 2 μM dihydroethidine hydrochloride (DHE) or 5 μM 5-[and-6]-chloromethyl-2′,7′-dichlorodihydrofluorescein diacetate (DCFDA) for 30 min at 37°C. Cells staining positively for the oxidized dyes were identified by fluorescent microscopy (original magnification ×100). (B) Protein oxidation was assessed by immunoblotting (OxyBlot) and quantified using NIH image analysis software. Results are means ± SEM (n=6). *, p<0.05 vs. control (F/F) mice. (C, D) Mice were fed either BHA-supplemented (0.7%) or regular chow. After 4 weeks of TAA treatment, serum ALT was measured in *p38*α$^{F/F}$ (F/F) and *p38*α$^{\Delta hep}$ mice (C) and the surface area stained with Sirius Red was quantified in *p38*α$^{\Delta hep}$ mice (D). Results are means ± SEM (n=6). *, p<0.05.

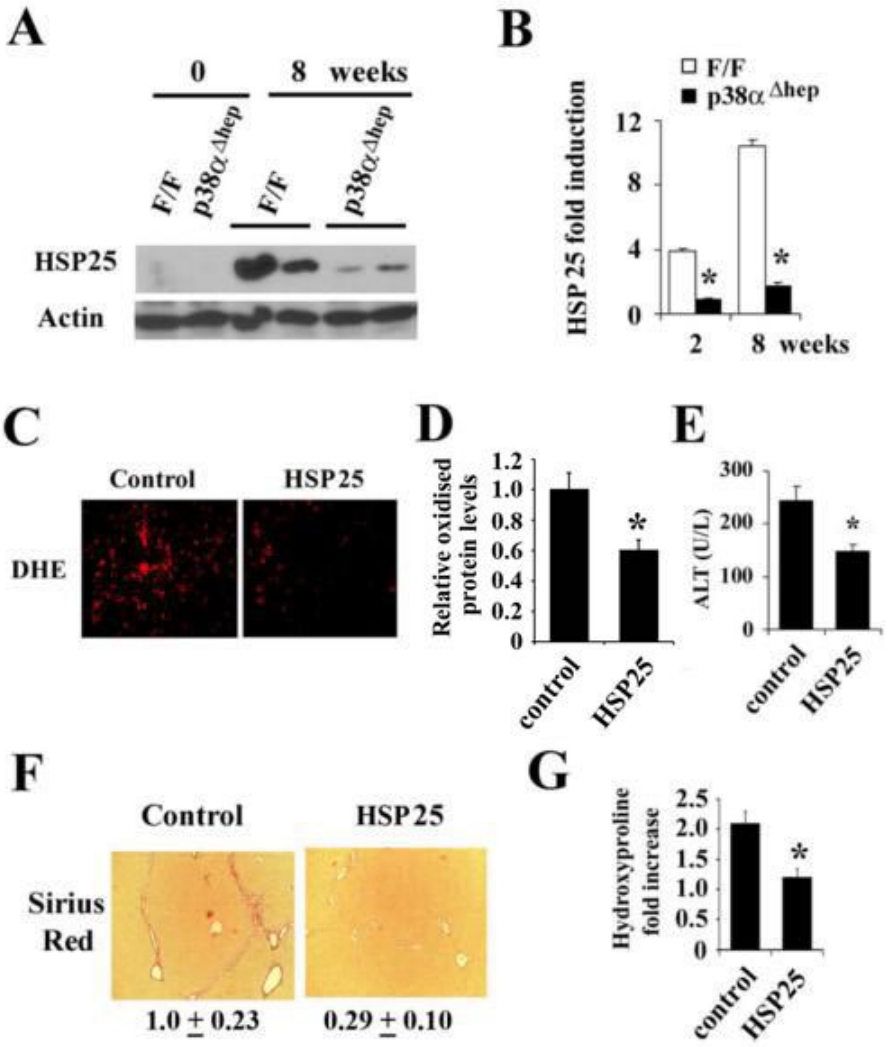

Figure 3.

The p38α-induced anti-oxidant gene HSP25 inhibits TAA-induced fibrosis.

(A) Mice were treated with TAA for 8 weeks and their livers isolated and homogenized. Homogenates were gel-separated and immunoblotted with the indicated antibodies. (B) Mice were treated as above and total liver RNA was extracted at the indicated times. Amounts of mRNA relative to those in untreated $p38\alpha^{F/F}$ livers were determined by real time Q-PCR. Results are means ± SEM (n=6). *, $p<0.05$ vs. control (F/F) mice. (C-G) $p38\alpha^{\Delta hep}$ mice were infected with an adenovirus-expressing HSP25 or a control adenovirus 20 hrs before TAA treatment. Frozen liver sections prepared after 4 weeks of TAA treatment were incubated with 2 μM DHE for 30 min at 37°C and photographed. (C). Protein oxidation was assessed by immunoblotting (OxyBlot) and quantified using NIH image analysis software (D). ALT levels in serum were determined after 4 weeks of TAA treatment (E). Sections of livers prepared after 4 weeks of TAA treatment were examined by Sirius Red staining. The numbers below the panels indicate relative fibrotic areas (F).

Hepatic hydroxyproline content was measured (G). Results are means ± SEM (n=6). *, $p<0.05$.

Europe PMC Funders Author Manuscripts

Europe PMC Funders Author Manuscripts

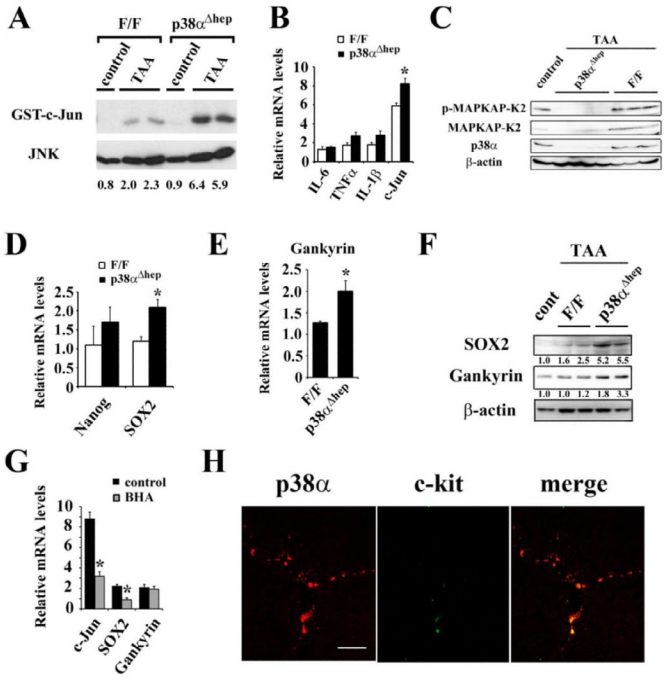

Figure 4.

Decreased expression of MAPKAP kinase-2 and increased expression of SOX2, c-Jun and gankyrin in TAA-treated p38α$^{\Delta hep}$ mice.

Mice of the indicated genotypes were given TAA for 8 weeks and their livers isolated, homogenized. (A) JNK activity was determined by immunecomplex kinase assay. Protein recovery was determined by immunoblotting with JNK1 antibody. The numbers below the panels indicate relative JNK activities determined by densitometry. (B, D, E) Liver RNA was extracted. Relative amounts of cytokine, Nanog, SOX2 and Gankyrin mRNAs were determined by real time Q-PCR and normalized to the amount of actin mRNA. The amount of each mRNA in untreated liver was given an arbitrary value of 1.0. Results are means ± SEM (n=6). (C, F) Homogenates of liver tissues were gel-separated and immunoblotted with the indicated antibodies. Representative data are shown. The numbers below the panels indicate relative expression levels determined by densitometry. (G) *p38*α$^{\Delta hep}$ mice were fed either BHA-containing (0.7%) or regular chow and treated with TAA for 8 weeks. Relative amounts of mRNAs were determined by real time Q-PCR and normalized to the amount of actin mRNA. The amount of each mRNA in untreated liver was given an arbitrary value of 1.0. Results are means ± SEM (n=6). (H) Immunohistochemistry was performed on frozen liver sections of TAA-treated *p38*α$^{\Delta hep}$ mice. Cells stained with indicated antibodies were identified by confocal microscopy. Scale bar = 50μm.

Europe PMC Funders Author Manuscripts

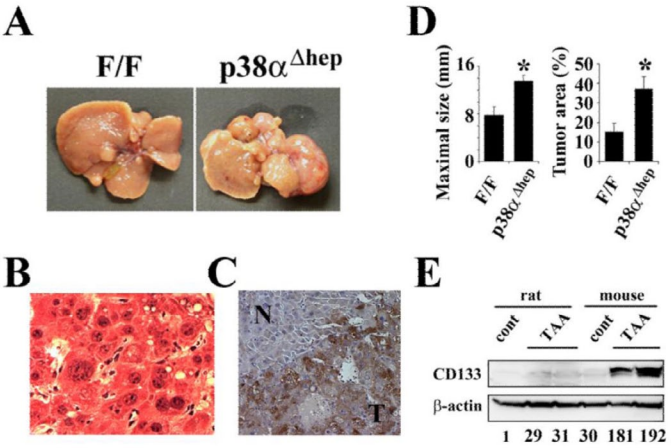

Figure 5.

Enhanced hepatocarcinogenesis in *p38*α$^{\Delta hep}$ mice.

(A) Livers of *p38*α$^{\Delta hep}$ and *p38*α$^{F/F}$ mice after 10 months of TAA treatment. (B, C) Sections of livers were examined using H&E staining (B) and by immunohistochemistry with α-fetoprotein (AFP) specific antibody (C). Original magnification: 200×. N, non-cancerous liver tissues; T, tumors. Distinction between tumor and non-cancerous liver tissue was made by H&E staining. (D) Maximal tumor sizes (diameters) and percentages of liver area occupied by tumors in *p38*α$^{F/F}$ (F/F, n=8) and *p38*α$^{\Delta hep}$ (n=8) mice. *, $p<0.05$ vs. control mice (F/F). (E) Sprague-Dawley rats and *p38*α$^{F/F}$ control mice were given TAA (0.03%) for 5 weeks and their livers isolated. Homogenates of rat and mouse liver tissues were gel-separated and immunoblotted with the indicated antibodies. The numbers below the panels indicate relative CD133 expression levels..

Europe PMC Funders Author Manuscripts

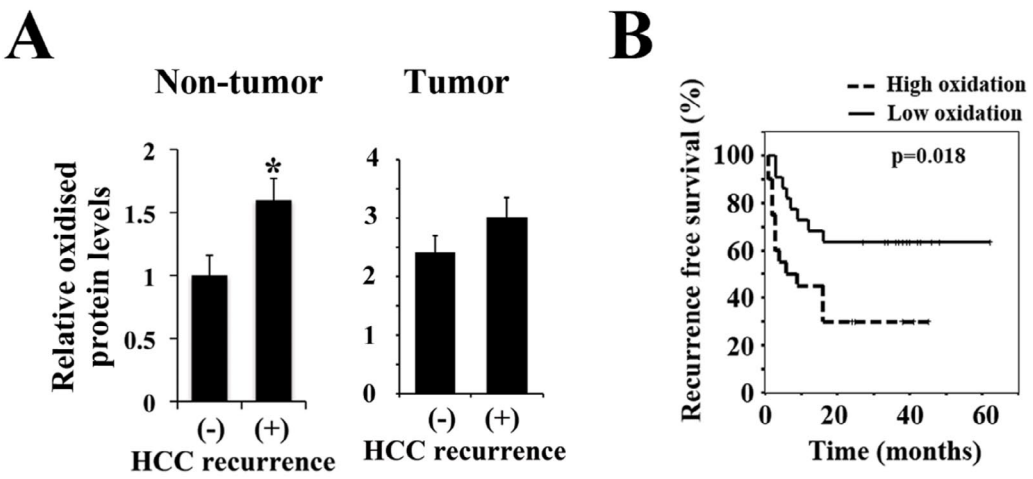

Figure 6.

Associations between the risk of HCC recurrence and protein oxidation in human liver. (A) Protein oxidation was assessed in tumors and non-tumorous human liver tissues by immunoblotting (OxyBlot) and quantified using NIH image analysis software. *, $p<0.05$ vs. patients without HCC recurrence. (B) Recurrence free survival vs protein oxidation. The Kaplan-Meier method was used to determine recurrence free survival and the log-rank test was used to compare recurrence free survival between patients grouped according to amount of protein oxidation in liver.

Guidelines and Good Clinical Practice Recommendations for Contrast Enhanced Ultrasound (CEUS) in the Liver – Update 2012

A WFUMB-EFSUMB Initiative in Cooperation With Representatives of AFSUMB, AIUM, ASUM, FLAUS and ICUS

Authors

M. Claudon[1*], C. F. Dietrich[2*], B. I. Choi[3], D. O. Cosgrove[4], M. Kudo[5], C. P. Nolsøe[6], F. Piscaglia[7], S. R. Wilson[8], R. G. Barr[9], M. C. Chammas[10], N. G. Chaubal[11], M.-H. Chen[12], D. A. Clevert[13], J. M. Correas[14], H. Ding[15], F. Forsberg[16], J. B. Fowlkes[17], R. N. Gibson[18], B. B. Goldberg[19], N. Lassau[20], E. L. S. Leen[21], R. F. Mattrey[22], F. Moriyasu[23], L. Solbiati[24], H.-P. Weskott[25], H.-X. Xu[26]

Affiliations

Affiliation addresses are listed at the end of the article.

Key words

- diagnosis
- metastases
- hepatocellular carcinoma
- focal nodular hyperplasia
- hemangioma
- microbubble

Abstract

Initially, a set of guidelines for the use of ultrasound contrast agents was published in 2004 dealing only with liver applications. A second edition of the guidelines in 2008 reflected changes in the available contrast agents and updated the guidelines for the liver, as well as implementing some non-liver applications. Time has moved on, and the need for international guidelines on the use of CEUS in the liver has become apparent. The present document describes the third iteration of recommendations for the hepatic use of contrast enhanced ultrasound (CEUS) using contrast specific imaging techniques. This joint WFUMB-EFSUMB initiative has implicated experts from major leading ultrasound societies worldwide. These liver CEUS guidelines are simultaneously published in the official journals of both organizing federations (i.e., Ultrasound in Medicine and Biology for WFUMB and Ultraschall in der Medizin/European Journal of Ultrasound for EFSUMB). These guidelines and recommendations provide general advice on the use of all currently clinically available ultrasound contrast agents (UCA). They are intended to create standard protocols for the use and administration of UCA in liver applications on an international basis and improve the management of patients worldwide.

Content

List of abbreviations

AASLD	American Association for the Study of Liver Diseases
AFSUMB	Asian Federation of Societies for Ultrasound in Medicine and Biology
AIUM	American Institute of Ultrasound in Medicine
ASUM	Australasian Society for Ultrasound in Medicine

Bibliography

DOI http://dx.doi.org/10.1055/s-0032-1325499
Published online: November 5, 2012
Ultraschall in Med 2013; 34: 11–29 © Georg Thieme Verlag KG Stuttgart · New York ·
ISSN 0172-4614

Correspondence

Prof. Dr. med. Christoph F. Dietrich
Caritas Krankenhaus
Bad Mergentheim,
Med. Klinik 2
Uhlandstr. 7
97980 Bad Mergentheim
Germany
christoph.dietrich@ckbm.de

* Both authors equally contributed to the manuscript (as co-first authors).

AUC	area under the curve
AUWI	area under the wash in
AUWO	area under the wash out
CCC	cholangiocellular carcinoma
CT	computed tomography
CECT	contrast enhanced computed tomography
CEMRI	contrast enhanced magnetic resonance imaging
CEUS	contrast enhanced ultrasound
DCE-US	dynamic contrast enhanced ultrasound
ECG	electrocardiogram
EMA	European Medicines Agency
EFSUMB	European Federation of Societies for Ultrasound in Medicine and Biology
FLAUS	Latin-American Federation of Societies for Ultrasound in Medicine and Biology
FLL	focal liver lesion(s)
FNH	focal nodular hyperplasia
HA	hepatic artery
HCA	hepatocellular adenoma
HCC	hepatocellular carcinoma
ICU	intensive care unit
ICUS	International Contrast Ultrasound Society
IO-CEUS	intraoperative contrast enhanced ultrasound
IOUS	intraoperative ultrasound
IVC	inferior vena cava
MI	mechanical index
MIP	maximum intensity projection
MRI	magnetic resonance imaging
MTT	mean transit time (TIC parameter)
PI	peak intensity
PV	portal vein (portal venous)
RECIST	response evaluation criteria in solid tumors
RF	radio-frequency
SPIO	superparamagnetic iron oxide
SWI	slope of the wash in (TIC parameter)
TIC	time intensity curve(s)
TPI	time to peak intensity (TIC parameter)
UCA	ultrasound contrast agent(s)
US	ultrasound or ultrasonography
USA-FDA	United States of America Food and Drug Administration
WFUMB	World Federation for Ultrasound in Medicine and Biology
WHO	World Health Organization

Preamble

The present document describes the third iteration of recommendations for the hepatic use of contrast enhanced ultrasound (CEUS) and contrast specific imaging techniques introduced ten years ago in Europe and Canada.

Initially, a set of guidelines for the use of ultrasound contrast agents (UCA) was published in the 2004 edition of Ultraschall in der Medizin (European Journal of Ultrasound) dealing only with liver applications [5]. Subsequently, CEUS was introduced into other important guidelines and recommendations for the diagnostic strategy of focal liver lesions (FLL) in cirrhosis, including the guidelines of the American Association for the Study of Liver Diseases (AASLD) 2005 [14], the Asian Pacific Association for the Study of the Liver consensus recommendations on hepatocellular carcinoma (HCC) [111] and the recommendations of the Japan Society of Hepatology [79]. A second edition of the guidelines in 2008 reflected changes in the available contrast agents and updated the guidelines for the liver [31]. CEUS has also been recommended in guidelines for several non-liver applications, which have recently been updated under the auspices of European Federation of Societies for Ultrasound in Medicine and Biology (EFSUMB) as non-liver guidelines [116].

Time has moved on, and the need for worldwide guidelines on the use of CEUS in the liver has become apparent. World Federation for Ultrasound in Medicine and Biology (WFUMB) and EFSUMB initiated further discussions in 2010, in conjunction with the Asian Federation of Societies for Ultrasound in Medicine and Biology (AFSUMB), American Institute of Ultrasound in Medicine (AIUM), Australasian Society for Ultrasound in Medicine (ASUM) and International Contrast Ultrasound Society (ICUS) to bring the 2008 liver guidelines up-to-date, recognizing the fact that contrast agents are now licensed in many parts of the world, including Australasia, Brazil, Canada, China, Europe, India, Japan and Korea.

This joint WFUMB-EFSUMB venture has resulted in a liver CEUS simultaneous duplicate on liver CEUS in the official journals of WFUMB and EFSUMB (i. e., Ultrasound in Medicine and Biology and Ultraschall in der Medizin/European Journal of Ultrasound).

To produce the new CEUS liver guidelines and recommendations, a meeting of representatives from 36 European (France, Denmark, Germany, Italy and the UK), North American (Canada and the USA), Asian (China, India, Japan and Korea) and Australian experts was held in Chicago in December 2010. While a significant portion of the work was accomplished at the meeting, the group continued to meet via conference calls and at local meetings.

As before, these guidelines are based on comprehensive literature surveys, including results from prospective clinical trials. On topics where no significant study data were available, evidence was obtained from expert committee reports or was based on the consensus of experts in the field of ultrasound (US) and CEUS during the consensus conferences. During the meeting of experts in Chicago, many additional new developments were discussed and included. Others were believed to be too early in their development to be included in the current recommendations.

These guidelines and recommendations provide general advice on the use of UCA. They are intended to create standard protocols for the use and administration of UCA in liver applications on an international basis and improve the management of patients. Individual cases must be managed on the basis of all clinical data available.

1. General Considerations (Technical Aspects)

1.1. Introduction

The development of microbubble ultrasound contrast agents has overcome some of the limitations of conventional B-mode and Doppler ultrasound techniques for the liver and enabled the display of the parenchymal microvasculature [31]. The enhancement patterns of lesions can be studied during all vascular phases (arterial, portal venous, late and postvascular phases), in a similar fashion to contrast enhanced computed tomography (CECT) and contrast enhanced magnetic resonance imaging (CEMRI) but in real time and under full control of the ultrasound operator. UCA have different pharmacokinetics from commonly used contrast agents for computed tomography (CT) and magnetic resonance imaging (MRI) in that they are confined to the vas-

cular space whereas the majority of contrast agents for CT and MRI are rapidly cleared from the blood pool into the extravascular space [37]. In addition, some UCA have a late or a postvascular phase during which they are retained in the liver (and in the spleen) [37].

An inherent advantage of CEUS is the opportunity to assess the contrast enhancement patterns in real time, with a much higher temporal resolution than is possible with other imaging modalities, so that the enhancement dynamics of lesions can be studied. There is no need to predefine scan time points or to perform bolus tracking. Furthermore, the excellent tolerance and safety profiles of UCA allow for their repeated administrations in the same session when needed. Regrettably, UCA studies are subject to the same limitations as other types of ultrasound imaging: as a general rule, if the baseline ultrasound is suboptimal, CEUS may be disappointing.

There are limitations in the use of CEUS in the liver:

- Limitations of resolution of CEUS or particular scanning conditions mean that the smallest detectable lesions range between 3 and 5 mm in diameter [92].
- Very small FLL may be overlooked.
- Subdiaphragmatic lesions, especially those in segment VIII, may not be accessible to conventional US or CEUS. Intercostal scanning and positioning the patient in the left decubitus position can help reduce this limitation.
- Since CEUS has limited penetration, especially in steatosis, deep-seated lesions may not be accessible. Again, scanning in the left lateral decubitus position brings the liver forward and closer to the transducer and can help to reduce this limitation; it should be part of the routine survey.
- The falciform ligament and surrounding fat can cause an enhancement defect that may be confused with a FLL.

1.2. Commercially available UCA for the liver

The UCA currently used in diagnostic US of the liver are microbubbles consisting of gas bubbles stabilized by a shell [31]. Three are in common use today as follows:

- SonoVue® (sulfur hexafluoride with a phospholipid shell) Bracco SpA, Milan, Italy, introduced in 2001. Licensed in Europe, China, India, Korea, Hong Kong, New Zealand, Singapore and Brazil.
- Definity®/Luminity® (octafluoropropane [perflutren] with a lipid shell) Lantheus Medical, Billerica, MA, USA, introduced in 2001. Licensed in Canada and Australia.
- Sonazoid® (perfluorobutane with a phospholipid shell: hydrogenated egg phosphatidyl serine). Daiichi-Sankyo, GE Tokyo, Japan, introduced in 2007. Licensed in Japan and now South Korea.

There are several other UCA which may be useful in liver studies but they are either not licensed for the liver in any country or, in the case of Levovist® (Bayer Schering AG, Germany), production has ceased.

For product information regarding handling, composition, packaging, storage, indications and contraindications of these agents, contact the manufacturing company.

1.3. Background on UCA and contrast specific modes

UCA strongly increase the backscatter of US regardless of whether the microbubbles are flowing or stationary. The low solubility of the gases in currently licensed UCA improves their stability and provides good resonance behavior at low acoustic pressures. This allows minimally disruptive contrast-specific imaging and enables effective investigation over several minutes to visualize their dynamic enhancement patterns in real time.

Because of their physical size (equal to or smaller than red blood cells), UCA act as blood pool agents and allow depiction of both the macrovasculature and the microvasculature [34]. Despite their varied physicochemical composition, all UCA have similar behaviors for CEUS imaging, rapidly enhancing the vascular pool after intravenous injection, with slow dissipation over about 5 min. An exception to this behavior occurs with Sonazoid®, which has an extended late phase, herein termed the "postvascular phase" in which it persists for several hours in the liver and spleen, long after it has disappeared from the detectable vascular pool. Sonazoid® is phagocytozed by Kupffer cells and this undoubtedly contributes to its persistence in the liver. This postvascular phase is often referred to as "the Kupffer phase" [153].

Contrast-specific US modes cancel the linear US signals from tissue and utilize the nonlinear responses from the microbubbles to form images [31]. This nonlinear microbubble response can be produced by two different mechanisms:

- Stable nonlinear oscillations at low acoustic pressure, which is nowadays the standard modality for most CEUS examinations.
- Disruption at higher acoustic pressures to give broadband nonlinear responses.

Nonlinear harmonic US signals also arise from tissue because the sound waves become distorted during their propagation. These "tissues harmonics" increase with increasing acoustic pressure, which is roughly indicated by the mechanical index (MI), (see section 1.8) [7, 132, 138, 140]. However, a low MI is usually chosen for continuous real-time imaging, and for minimizing microbubble destruction. MI is considered as "low" when ≤0.3 but most systems work optimally with MI far below 0.3 (as low as 0.05).

Current contrast specific imaging enables effective tissue cancellation to generate almost pure microbubble images. Each manufacturer has developed proprietary techniques for this and adequate cancellation is indicated by near-disappearance of the ultrasound parenchymal liver structures (the screen goes black), though strong reflectors, such as vascular structures and the diaphragm/lung interface, remain barely visible. Correct settings on the ultrasound scanner and the scanning mode are important to avoid artifacts [41]. Inappropriately high MI and gain are the two most common causes of tissue signals being wrongly displayed.

1.4. Intermodality comparison

For characterization of FLL, the enhancement patterns observed during the arterial, portal venous and late phases are generally similar among CEUS, CECT and CEMRI. The real-time nature of US allows depiction of early arterial phase enhancement which is sometimes missed on CT and MRI because they have lower frame rates. Discordance has also been shown in some lesions during the portal venous and late phases when CT and MRI contrast materials diffuse into the tumor interstitium and may conceal wash out [148]. On the other hand, postvascular phase imaging with Sonazoid® shows patterns similar to those described with superparamagnetic iron oxide (SPIO)-MRI [75].

1.5. Equipment and contrast signal detection

See companies' websites for references and specification.

1.6. Clinical practitioner training

Investigators wishing to perform CEUS examinations are recommended to gain experience by observing contrast studies being

performed by experts in this field. EFSUMB has defined three levels of training in its minimal training requirements (EFSUMB 2006) [1] and recommends that CEUS should be performed by operators at a competence level higher than level 1 (EFSUMB 2010: Appendix 14) [3].
They should also ensure that their equipment is optimized for CEUS by discussion with their equipment manufacturer. In addition, a sufficient volume and variety of pathology are essential to acquire and maintain an adequate level of skill. Practitioners need competence in the intravenous administration of contrast agents, familiarity with any contraindications and ability to deal with any possible adverse effects within the medical and legal framework of their country.

1.7. Safety considerations

In general, UCA are safe with a very low incidence of side effects. There are no cardio-, hepato- or nephrotoxic effects. Therefore, it is not necessary to perform laboratory tests to assess liver or kidney function before their administration.
The incidence of severe hypersensitivity events is lower than with current X-ray contrast agents and is comparable to those encountered with MRI contrast agents. Life-threatening anaphylactoid reactions in abdominal applications have been reported with a rate of 0.001 %, with no deaths in a series of > 23 000 patients [113]. Nonetheless, investigators should be trained in resuscitation and have the appropriate facilities available.
Deaths in critically ill patients who have undergone contrast echocardiography examinations have been reported but with no evidence of a causal relationship [101]. Contraindications for the use of SonoVue® were defined by the European Medicines Agency (EMA) in 2004. In 2007, the United States of America Food and Drug Administration (US-FDA) issued contraindications for the use of Definity® and Optison® (GE Healthcare, licensed for cardiac use) in patients with severe cardiopulmonary disease, and imposed echocardiogram (ECG) monitoring for 30 min after injection (US-FDA Alert 10/2007). The contraindications were downgraded to warnings in May 2008 following review of recent studies on contrast reactions and postmarketing studies supplied by the manufacturers at the request of the FDA [48]; in 2011, the requirement to observe the patient for 30 min after injection was removed. Numerous subsequent studies have been conducted to examine adverse reactions to UCA in cardiac applications [71] and these have indicated an excellent safety profile. One study [81] demonstrated the positive impact of the use of UCA in cardiac examinations: additional procedures were avoided or therapy changed in over 35 % of patients. Another large study reported better survival in acute cardiac disorders undergoing UCA administration in comparison to those receiving echocardiography without UCA [102].
Although there is a theoretical possibility that the interaction of diagnostic ultrasound and UCA could produce bioeffects, there is no clinical evidence for adverse effects on the human liver. Cellular effects that have been observed in vitro include sonoporation, hemolysis and cell death [133]. Data from small animal models suggest that microvascular disruption can occur when microbubbles are insonated [133]. Thus, in general, low MI should be preferred for CEUS of the liver. Where diagnostic information can only be obtained using high MI sequences, the benefits vs. the risks of the procedure should be assessed and the mode selected for the benefit of the patient.
There is limited data on the use of UCA in pregnancy, during breastfeeding or in pediatrics [117]. The implied contraindications can be overridden according to clinical judgment and with dedicated informed consent in case of need.
All administration decisions and procedures for the use of UCA should be made with the local regulatory restrictions in mind.
Some general recommendations include:

- As in all diagnostic ultrasound procedures, the operator should be mindful of the desirability of keeping the displayed MI low and of avoiding unduly long exposure times.
- Caution should be exercised when using UCA in patients with severe coronary artery disease.
- As with all contrast agents, resuscitation facilities must be available.
- The use of UCA should be avoided 24 h prior to extracorporeal shock wave therapy.

1.8. Terminology

The appearance of a lesion or region-of-interest in the liver should be described in terms of the degree and timing (phase) of enhancement.
Degree of enhancement: describing the region in terms of vascularity (e. g., hypervascular, hypovascular) may be incorrect from a histologic point of view and describing the degree of enhancement is preferred.

- Enhancement refers to the intensity of the signal relative to that of the adjacent parenchyma: either equal to, isoenhancing; greater than, hyperenhancing; or less than, hypoenhancing.
- Sustained enhancement usually refers to continuance of enhancement in the lesion over time.
- Complete absence of enhancement can be described as nonenhancing. When a region is nonenhancing in the postvascular phase with Sonazoid®, the term “enhancement defect” is often used in clinical practice.

Phase of enhancement

- The enhancement pattern should be described separately for the different phases, which for the liver comprise the arterial, the portal venous, the late phases and, in case of Sonazoid®, also the postvascular phase. Conventional, but imprecise time points, separate these different phases (see section 2.1.1).
- “Wash in” used for both qualitative and quantitative analysis, refers to the period of progressive enhancement within a region of interest from the arrival of microbubbles in the field of view to “peak enhancement” and “wash out phase” refers to the period of reduction in enhancement which follows peak enhancement.

Mechanical index

MI refers to the mechanical index of an ultrasound system, which is an estimate of the maximum amplitude of the pressure pulse in tissue, reflecting the power of the system. In very simple terms, higher MI tends to correspond to higher acoustic pressure emission and consequently to more rapid disruption of microbubbles. In physical terms, the MI is defined as:

$$MI = \frac{PNP}{\sqrt{(F_c)}}$$

where PNP is the peak negative pressure of the ultrasound wave (in MPa and derated for modeled attenuation) and F_c is the center frequency of the ultrasound wave (MHz).

Data types

Different types of data have been used in CEUS studies [138]:

- RF data refers to the radiofrequency information after the beam former.
- Raw data refers to the data after the phase information in the RF data has been removed.
- Linear data refers to the RF or Raw data, before compression.
- Video data refers to the data after log (or quasi log) compression for video display.

2. CEUS for Characterization of Focal Liver Lesions

▼

CEUS should be performed with knowledge of all prior imaging, the patient's demographics and the clinical history, exactly as for a conventional ultrasound examination. This is particularly important for lesion characterization because the range of tumor types differs between cirrhotic and noncirrhotic livers. Accordingly, in these guidelines the characterization of FLL is described separately for patients with and without cirrhosis.

2.1. Characterization of FLL in the noncirrhotic liver

2.1.1. Background

The dual blood supply of the liver from the hepatic artery (25 – 30 %) and the portal vein (70 – 75 %) gives rise to three overlapping vascular phases on CEUS study (**Table 1**):

- The arterial phase provides information on the degree and pattern of the arterial vascular supply. Depending on the individual's circulatory status, the hepatic arterial phase generally starts within 20 s after injection and continues to 30 – 45 s. This phase may occur very rapidly and the real-time nature of CEUS is needed to capture them, often best seen in a slow replay of a stored cine loop.
- The portal venous phase usually lasts until 2 min after injection. These two early phases are very similar between the different available UCA (SonoVue®, Definity®, Sonazoid®).
- The late phase lasts until the clearance of the UCA from the circulation and is limited to 4 – 6 min.

The additional postvascular (or Kupffer) phase for Sonazoid® begins 10 min after injection and lasts for an hour or more. To ensure that there is no overlap with the late phase, postvascular phase scanning should not be performed sooner than 10 min after injection.

All of these times may be shortened by microbubble disruption if the liver is imaged continuously, even at a low MI.

Late and postvascular phase enhancement provide important information regarding the character of a lesion as most malignant lesions are hypoenhancing while the majority of solid benign lesions are iso- or hyperenhancing [9, 31, 127, 128, 136, 143, 147].

Table 1 Vascular phases in CEUS of the liver (visualization postinjection time).

phase	start (s)	end (s)
arterial	10 – 20	30 – 45
portal venous (PV)	30 – 45	120
late	> 120	bubble disappearance (approx. 4 – 6 min)

The portal and late phases start at the end of the preceding one. Individual hemodynamic and other factors (e. g., site of injection) may influence their time of onset.

2.1.2. Study procedure

Low MI contrast-specific techniques allow dynamic evaluation of the three vascular phases for all UCA and also of the postvascular phase for Sonazoid®:

- Any investigation should start with conventional B-mode and Doppler techniques.
- After identification of the target lesion, the transducer is held still while the scanner is switched to low MI contrast-specific imaging.
- A dual screen format showing a low MI B-mode image alongside the contrast-only display aids anatomic guidance. This is useful for small lesions to ensure that the target is kept within the field of view during CEUS. A difficulty with the split screen method is that a low MI is used for both panels and this means that the gray scale display is noisy so that smaller and low contrast lesions may be difficult to image. On some scanners, conventional and CEUS images are not split onto two screens but overlaid with different color scales.
- UCA is administered as a bolus injection followed by a flush of normal saline 0.9 %.
- Ideally, the diameter of the venous line should not be smaller than 20 G to avoid destruction of microbubbles during injection. Central line and port systems can be used as long as there is no filter requiring a high injection pressure but contrast arrival time will be shorter.
- A stop clock should be started at the time of UCA injection.
- Because of the dynamic nature of real-time CEUS, essential clips for each vascular phase should be recorded.
- Assessment of the arterial and portal venous phases should be carried out without interruption. For the late phase, intermittent scanning may be used until the disappearance of the UCA from the liver's microvasculature. Under some circumstances, especially for HCC, the examination may need to be continued for up to 5 min because wash out may be delayed [109].
- Injection can be repeated when a lesion has been detected in the portal venous phase or in the late/postvascular phase to study the arterial phase and in the case of multiple FLL. Reinjection should be postponed until most microbubbles have vanished and the CEUS screen is almost black again, which can be expected after 6 – 10 min using SonoVue® and Definity®.

2.1.3. Image interpretation and differentiation of benign from malignant lesions

CEUS can often establish a definitive diagnosis or otherwise facilitate the clinical decision as to whether a sonographically detected liver lesion needs further investigation.

2.1.4. Benign liver lesions

Sustained enhancement in the portal and late phases is typically observed in almost all solid benign liver lesions. They can be further characterized by their enhancement patterns during the arterial phase, (e. g., enhancement of the whole lesion [typical of focal nodular hyperplasia] or initial peripheral globular/nodular enhancement [in hemangiomas]).

The enhancement patterns are summarized in **Table 2**.

Hemangioma

CEUS has markedly improved the accurate diagnosis of hemangiomas, which is now possible in about 95 % of cases [136]. The typical CEUS features of a hemangioma are peripheral nodular enhancement in the arterial phase, progressing in a centripetal

lesion	arterial phase	portal venous phase	late phase
A. noncirrhotic liver			
hemangioma			
typical features	peripheral nodular enhancement	partial/complete centripetal fill in	complete enhancement
additional features	small lesion: complete, rapid centripetal enhancement		nonenhancing regions
FNH			
typical features	hyperenhancing from the center, complete, early	hyperenhancing	iso/hyperenhancing
additional features	spoke-wheel arteries	unenhanced central scar	unenhanced central scar
	feeding artery		
hepatocellular adenoma			
typical features	hyperenhancing, complete	isoenhancing	isoenhancing
additional features	nonenhancing regions	hyperenhancing	slightly hypoenhancing
		nonenhancing regions	nonenhancing regions
focal fatty infiltration			
typical features	isoenhancing	isoenhancing	isoenhancing
focal fatty sparing			
typical features	isoenhancing	isoenhancing	isoenhancing
abscess			
typical features	peripheral enhancement, no central enhancement	hyper-/isoenhancing rim, no central enhancement	hypoenhancing rim, no central enhancement
additional features		hypoenhancing rim	
	enhanced septa	enhanced septa	
	hyperenhanced liver segment	hyperenhanced liver segment	
simple cyst			
typical features	nonenhancing	nonenhancing	nonenhancing
B. cirrhotic liver			
regenerative nodule (±dysplastic)			
typical features (not diagnostic)	isoenhancing	isoenhancing	isoenhancing
additional features	hypoenhancing		

Table 2 Enhancement patterns of benign focal liver lesions in the non cirrhotic and cirrhotic liver.

In cirrhotic liver simple cysts, hemangiomas and abscesses may also be found and show the same enhancement pattern as in noncirrhotic livers. All other entities are rare findings in cirrhotic livers.

direction to partial or complete fill-in. The filling lasts from seconds to minutes and is more rapid in smaller lesions. Enhancement is sustained through the late and postvascular phases.
High flow (or shunt) hemangiomas show rapid homogeneous hyperenhancement in the arterial phase and can be confused with focal nodular hyperplasia (FNH), or rarely with hepatocellular adenomas or carcinomas. Thrombosed hemangiomas can be confused with malignancies because of the lack of enhancement in the thrombosed portions, which may be misinterpreted as wash out [43].

Focal nodular hyperplasia

FNH is a benign hepatic lesion that is usually discovered incidentally. It can be managed conservatively in most patients. Color Doppler techniques are helpful to visualize the spoke-wheel vascular pattern which strongly supports the diagnosis of FNH [44, 115] more sensitively shown on CEUS, especially with maximum intensity projection (MIP) technique. On CEUS, FNH typically appears as a hyperenhancing homogeneous lesion in all phases. Hyperenhancement is obvious and usually marked in the arterial phase, with a rapid fill-in from the center outwards (70 %) or with an eccentric vascular supply (30 %) [44]. During the portal venous and late phases, FNH may remain slightly hyperenhancing or become isoenhancing [115] and a centrally located scar may be seen, hypoenhancing in the late phase. In small or deeply located lesions, it can be helpful to switch to color Doppler techniques after the CEUS study and use the remaining circulating microbubbles to enhance the Doppler signals for improved recognition of the typical spoke-wheel vascular pattern. Postvascular phase imaging (Sonazoid®) shows iso- or hyperenhancement [61].

Hepatocellular adenoma

Hepatocellular adenoma (HCA) is a benign estrogen-dependent tumor, which is often discovered incidentally [44]. HCA is an indication for surgery, particularly when larger than 5 cm (risk of hemorrhage and possible malignant transformation). On CEUS, HCA exhibit arterial hyperenhancement, usually initially at the periphery with subsequent very rapid centripetal filling, the opposite direction to that seen in FNH. However, this arterial enhancement pattern can also be encountered in HCC and hyperenhancing metastases and is not pathognomonic of HCA. The transition from the arterial hyperenhancing to the isoenhancing appearance occurs at the beginning of the portal venous phase, usually earlier than in FNH [44, 115]. In most cases, the enhancement patterns of HCA may suggest malignancy when wash out occurs in the late phase, one of the few causes of false positives on CEUS.

lesion	arterial phase	portal venous phase	late phase
A. noncirrhotic liver			
metastasis			
typical features	rim-enhancement	hypoenhancing	hypo/nonenhancing
additional features	complete enhancement	nonenhancing regions	nonenhancing regions
	hyperenhancement		
	nonenhancing regions		
HCC			
typical features	hyperenhancing	isoenhancing	hypo/nonenhancing
additional features	nonenhancing regions	nonenhancing regions	nonenhancing regions
cholangiocarcinoma			
typical features	rim-like hyperenhancement, central hypoenhancement	hypoenhancing	nonenhancing
additional features	nonenhancing regions	nonenhancing regions	nonenhancing regions
	inhomogeneous		
	hyperenhancement		
B. cirrhotic liver			
HCC			
typical features	hyperenhancing, complete	isoenhancing	hypoenhancing (slightly or moderately)
	nonenhancing areas (if large)	nonenhancing regions	
additional features	basket pattern, chaotic vessels		isoenhancing
	enhancing tumor thrombus		
	hypo/nonenhancing	nonenhancing	nonenhancing

Table 3 Enhancement patterns of malignant focal liver lesions in the noncirrhotic and cirrhotic liver.

Explanation: Other malignancies in cirrhosis have the same patterns as in noncirrhotic livers.

Focal fatty change

Focal fatty change, either fat infiltration or fatty sparing, may simulate masses on conventional B-mode US. Differential diagnosis is important, especially in patients with underlying malignant disease or with an atypical location of suspected focal fatty changes. Focal fatty change shows exactly the same enhancement patterns as the adjacent liver parenchyma in all phases [62].

Infection

Phlegmonous inflammation has variable and sometimes confusing CEUS appearances, which change as they evolve, early lesions being hyperenhancing, while mature lesions develop hypoenhancing foci as liquefaction progresses.

Mature abscesses typically show marginal enhancement in the arterial phase, sometimes with enhancement of septae followed by venous hypoenhancement. Lack of enhancement in the liquefied portions is the most prominent feature [19, 20, 95].

The appearances of granulomas and focal tuberculosis on CEUS are variable but the majority show peripheral enhancement in the arterial phase with wash out in the portal and late phases, which may be difficult or impossible to differentiate from malignancies. The clinical history is important and the diagnosis is usually obtained on histopathology or microbiology [18, 95].

Other benign lesions

Active hemorrhage demonstrates contrast extravasation whereas hematomas show no enhancement.

Cysts show no contrast enhancement at all. CEUS is not needed for simple cysts but is useful to evaluate complicated or atypical cysts.

Inflammatory pseudotumor is a rare disease whose definite diagnosis is usually only made at surgery. It may show arterial enhancement and late phase hypoenhancement, falsely suggesting malignancy [43].

Hepatic angiomyolipoma is a rare benign mesenchymal tumor with heterogeneous echogenicity on baseline ultrasound. CEUS shows arterial hyperenhancement [145].

Cholangiocellular adenomas (CCA or bile duct adenoma) are rare lesions that are usually small (90 % < 1 cm). CEUS may show strong arterial enhancement and early wash out in the portal and late phases (they lack portal veins), falsely suggesting malignancy [65].

2.1.5. Malignant liver lesions

Hypoenhancement of solid lesions in the late and postvascular phases, corresponding to the wash out phenomenon characterizes malignancies. Almost all metastases show this feature, regardless of their enhancement pattern in the arterial phase. Very few exceptions to this rule have been reported, mainly in atypical HCC (**Table 3**).

HCC in the noncirrhotic liver

HCC are usually hyperenhancing in the arterial phase, typically with a chaotic vascular pattern. In the portal venous and late phases, HCC usually shows hypoenhancement apart from well-differentiated HCC that may be isoenhancing. Hyperenhancement in the arterial phase is believed to be homogeneous with fill from the periphery. However, this information is based only on expert opinion. The fibrolamellar variant of HCC has nonspecific appearances on B-mode. According to expert opinion and a single case report, they show rapid hyperenhancement with a heterogeneous pattern in the arterial phase and rapid wash out [103].

Cholangiocarcinoma (intrahepatic cholangiocellular carcinoma)

Intrahepatic cholangiocarcinomas have a variety of patterns in the arterial phase but all show late phase wash out, in contrast to the late enhancement on CECT or CEMRI [24, 25, 152]. The typical pattern of malignancy is better displayed by CEUS than by CECT or CEMRI. Peripheral cholangiocarcinoma may also be sus-

pected on baseline US as surface retraction is a characteristic feature.

Metastases

Liver metastases can be detected and characterized reliably as hypoenhancing lesions during the portal venous and late phases, with very few exceptions. Wash out starts early, usually in the portal venous phase, and is marked. Thus, they appear as punched-out "black foci" against the background of the uniformly enhanced normal liver. Larger traversing vessels can sometimes be seen as enhancing lines within the lesion but these are not tumor tissue and, thus, have the hemodynamics of the vascular tree, disappearing in parallel with the main liver vessels rather than being retained, as occurs in the normal liver parenchyma. In the late phase, very small metastases may be conspicuous and lesions that were occult on B-mode ultrasound can be detected [42].

Metastases usually show at least some contrast enhancement in the arterial phase and sometimes this is marked and often it is chaotic. Rim or halo enhancement is often seen. Only a few false positive results have been observed, mainly from abscesses or necrosis, old fibrous FNH, granulomas and inflammatory pseudotumors [40, 45, 126].

Benign lesions such as cysts, calcifications, hemangiomas, FNH and adenomas are found with the same frequency (5 – 20 %) in the metastatic liver as in a healthy population. Thus, the possibility of a benign FLL must be kept in mind when the liver is first staged after the diagnosis of a cancer, especially with lesions < 2 cm.

Lymphoma

Lymphoma shows variable arterial enhancement but characteristic wash out in the portal venous and late phases, predictive of malignancy [57].

2.1.6. Recommended uses and indications

CEUS should be performed and interpreted with knowledge of the patient's clinical history and investigations findings. When the enhancement patterns are typical (in appropriate clinical settings) hemangiomas, FNH, focal fatty change and malignancies can all be characterized with confidence. FLL with atypical enhancement patterns or studies that are technically suboptimal require further investigation, mainly with CECT and/or CEMRI.

CEUS is indicated for lesion characterization in the following clinical situations:

- Incidental findings on routine ultrasound.
- Lesion(s) or suspected lesion(s) detected with US in patients with a known history of a malignancy, as an alternative to CT or MRI.
- Need for a contrast study when CT and MRI contrast are contraindicated.
- Inconclusive MRI/CT.
- Inconclusive cytology/histology results.

Specificity and sensitivity are reduced in moderately or markedly fatty livers and with deeply positioned lesions.

2.2. Characterization of FLL in the cirrhotic liver

2.2.1. Background

Types of FLL in cirrhosis

The FLL that occur in the cirrhotic liver are hepatocellular lesions (> 95 % of cases), peripheral cholangiocellular carcinomas (CCC), lymphomas and hemangiomas. Other diagnoses may be considered, but they are very rare, for unknown reasons.

B-mode ultrasound may detect features of malignancy (such as infiltration of adjacent structures, including vessels) but these features are usually only seen in large nodules (> 5 cm) and do not help characterize smaller nodules.

Carcinogenic mechanism in HCC

The development of HCC is thought to occur through a multistep pathway in about 90 % of cases (International Consensus Group for Hepatocellular Neoplasia 2009) [2] in the following sequence:

- Large regenerative nodule.
- Low- or high-grade dysplastic nodule.
- Dysplastic nodule with a focus of HCC.
- Well differentiated HCC.
- Moderately to poorly differentiated HCC.

Progression along this pathway is accompanied by a decrease in both normal arterial and portal blood flow and a concurrent disappearance of normal intranodular vessels [105]. Simultaneous with this decline in normal vascularity, there is a progressive increase in arterial flow from newly formed tumor vessels (neoangiogenesis). Therefore, hyperenhancement in the arterial phase can be seen in HCC of all stages of differentiation [105]. These changes are key elements for the characterization of hepatocellular nodules in cirrhosis during the vascular phases of contrast enhancement.

Beside the vascular changes, HCC nodules tend to be devoid of reticuloendothelial cells (Kupffer cells), particularly with progressive dedifferentiation from well to moderately and poorly differentiated grades. This has become of particular importance with the introduction of contrast agents with a postvascular phase, where HCC shows as an enhancement defect.

The probability of HCC increases with nodule size. Nodules < 1 cm are rarely malignant and ultrasound follow up (at 3-month intervals) is sufficient, according to the AASLD guidelines [15]. Further investigations should be started when the nodule enlarges to over 1 cm. The rate of HCC is 66 % in nodules 1 – 2 cm [55, 64], increasing to about 80 % in nodules of 2 – 3 cm in size [11] and is above 92 – 95 % for nodules larger than 3 cm. The most challenging situation for imaging techniques is, therefore, the diagnosis of nodules of 1 – 3 cm in diameter.

2.2.2. Study procedure

General recommendations for the study of FLL are summarized above (see section 2.1.2). In addition, if the liver is cirrhotic, the following points should be kept in mind.

Since the arterial phase is the most important in the setting of cirrhosis, good visualization of the nodule during normal breathing is desirable. If this is impossible, it is important to practice cooperation with the patient so that the nodule can be visualized during a breath hold, best taken about 10 s after contrast injection and maintained for 15 – 30 s.

As microbubbles are disrupted despite the use of a low mechanical index, acoustic output power should be reduced as much as possible, while maintaining sufficient signal intensity, to allow contrast persistence until the very late phase (beyond 3 – 4 min), which is often critical for the diagnosis of HCC. Furthermore, when the arterial phase is over, the lesion should be scanned intermittently, not continuously, to minimize bubble disruption that may cause difficulties in interpretation of subtle wash out.

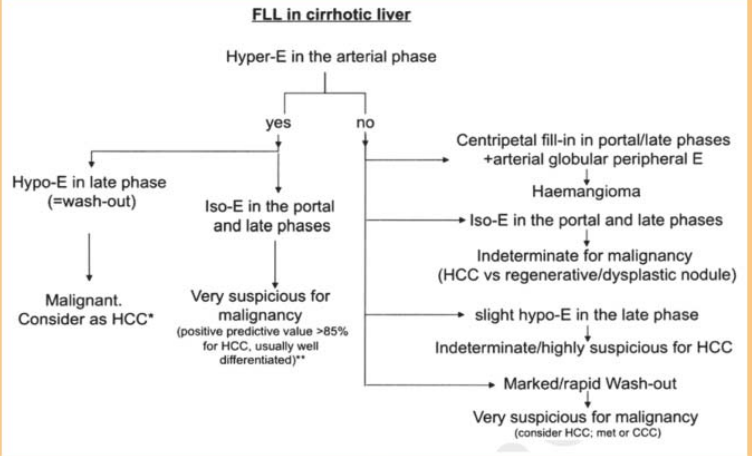

Fig. 1 *In cases with marked and rapid wash out in portal/late phase, consider the possibility of peripheral cholangiocarcinoma, especially if the pattern with MRI or CT does not confirm late wash out, or (exceptionally) metastasis or lymphoma. CEUS alone with a typical pattern is enough to establish a diagnosis of malignancy in nodules > 1 cm, but a panoramic imaging technique (CT or MRI) is required to stage the patient before treatment. **When Sonazoid is used, the postvascular phase may allow diagnosis of malignancy if the lesion becomes hypoenhancing in the postvascular phase, even though it appeared isoenhancing in the portal/late phases. E = enhancement; HCC = hepatocellular carcinoma; CCC = cholangiocellular carcinoma; met = metastasis.

2.2.3. Image interpretation and evaluation

CEUS pattern and diagnosis of HCC (Table 3)

The key feature for the diagnosis of HCC in liver cirrhosis is hyperenhancement in the arterial phase, followed by wash out in the late phase [15]. This pattern corresponds to HCC in more than 97 % of cases [12, 49, 57, 144]. However, it has also been reported in peripheral CCC and hepatic lymphoma, which comprise the remaining 1 – 3 % of cases. The timing and intensity of wash out in the latter lesions have not yet been described precisely [12, 49, 57, 144].

Arterial hyperenhancement is usually homogeneous and intense in HCC, but may be inhomogeneous in larger nodules (> 5 cm), which contain regions of necrosis. Rim enhancement is atypical for HCC.

Wash out is observed overall in about half the cases of HCC but more rarely in very small nodules (20 – 30 % in those 1 – 2 cm, 40 – 60 % in those 2 – 3 cm) [55, 92, 122]. Wash out is observed more frequently in HCC with poorer grades of differentiation than in well-differentiated HCC, which tend to be isoechoic in the late phase [12, 49, 64, 68].

The hypoenhancement in the late phase is usually less marked in HCC than in other primary tumors or in liver metastases. Furthermore, the wash out tends to start later in HCC, usually not before 60 s after injection and, in up to 25 % of cases, appearing only after 180 s [12, 26]; consequently it is important to observe nodules in cirrhosis until very late (> 4 min) to increase sensitivity for the diagnosis of HCC. Early wash out (< 60 s) has been reported to occur in poorly differentiated HCC or to suggest a nonhepatocellular malignancy [12, 26, 49, 68], most often a peripheral CCC. Wash out in HCC is observed less often with CEUS compared with MRI or CT because of their different contrast pharmacokinetics [55, 92, 122, 135].

Arterial hyperenhancement not followed by wash out is also highly suspicious for HCC, mainly for the well-differentiated variants but is not definitive [11, 12, 49, 64, 68].

An inconclusive CEUS pattern does not rule out malignancy and should prompt other imaging (CT or MRI) and, if these are also inconclusive, biopsy is needed. If this is negative, the nodule should be followed up every 3 months (at least for the first 2 years) and, if it enlarges or the enhancement pattern changes, diagnostic investigations must be resumed. If arterial enhancement is present on any imaging technique, repeated biopsy should be considered even in the absence of changes in size or enhancement.

Hemangioma has the same CEUS pattern in cirrhosis as in the noncirrhotic liver but an additional MRI scan is preferable to confirm the diagnosis in this clinical setting. Abscesses may occur in cirrhosis, usually as a complication of interventional procedures. CEUS shows typical findings of malignancy in CCC, whereas the enhancement pattern at MRI and CT may be inconclusive [144].

Staging of cirrhotic patients with HCC and the role of CEUS

Examining the entire liver during the arterial phase to look for hyperenhancing nodules is difficult or impossible with CEUS, so CECT or CEMRI must be used to stage patients with HCC [15]. For Sonazoid®, the postvascular phase may improve staging of the disease.

A diagnostic flowchart for CEUS of nodules in cirrhosis is given in **Fig. 1**.

2.2.4. Recommended uses, indications and limitations

CEUS is recommended:

- To characterize all nodules found on surveillance and routine US.
- To characterize nodules in cirrhosis and establish a diagnosis of HCC. It is a strong belief of the expert panel that CEUS is extremely useful, especially when performed immediately after nodule detection, to make a rapid diagnosis. However, CT or MRI are needed (unless contraindicated) to stage the disease before the treatment strategy is decided.
- Whether CEUS has a role as first line investigation at the same level as CT or MRI is variably accepted in national and international guidelines. For example, CEUS is part of the Japanese guidelines on HCC [79, 80] but has been removed from the American guidelines [15]. This was partly justified by the fact that no UCA is licensed for the liver in the USA and additionally because of the risk of misdiagnosing CCC for HCC when CEUS is used alone (1 – 2 %). In practice, the likelihood of misdiagnosis is minimal when CEUS is performed by skilled operators [8].
- When CT or MRI is inconclusive, especially in nodules not suitable for biopsy.
- To contribute to the selection of nodule(s) for biopsy when they are multiple or have different contrast patterns.

- To monitor changes in size and enhancement patterns over time when a nodule is not diagnostic for HCC and is being followed.
- After inconclusive histology.

2.2.5. CEUS with postvascular phase agents in cirrhotic liver nodules

Technical aspects and diagnostic features

Sonazoid® is different from pure blood-pool ultrasound contrast agents in that, in addition to the arterial and portal venous phases, there is a postvascular phase starting from 10 minutes after injection. Sonazoid® is taken up by the reticuloendothelial cells, particularly the Kupffer cells, similarly to SPIO MRI contrast agents [75]. The microbubbles can be detected even when located within cells.

The mesenchymal meshwork of malignant lesions usually does not harbor reticuloendothelial (Kupffer) cells, at variance from normal and cirrhotic liver parenchyma and from most solid benign liver lesions. The absence of Kupffer cells causes a defect in Sonazoid® uptake in the postvascular phase [61, 66], which is, thus, a molecular imaging modality. The diagnostic capability of CEUS with Sonazoid® in the postvascular phase is similar to that of MRI with an SPIO [75] and has been endorsed in the Japanese guidelines for the management of HCC [79].

Study procedures specific to postvascular phase agents

- After intravenous injection of Sonazoid®, continuous scanning for 30 – 60 s is recommended to assess the arterial and portal venous phases.
- The late vascular phase is deemed less relevant by Japanese authors, as this is replaced by the postvascular phase. For assessment of the postvascular (Kupffer) phase, scanning is begun not earlier than 10 min postinjection of Sonazoid® to allow clearance of contrast from the blood pool [78].
- After the end of the portal venous phase, insonation of the liver should be stopped to limit acoustic disruption of microbubbles before the postvascular phase.
- The postvascular phase lasts until the microbubbles have disappeared; thus, there is usually enough time for a thorough assessment of the whole liver to detect enhancement defects that suggest malignant nodules.
- When an enhancement defect is identified in the postvascular phase, a repeat contrast injection can be performed, superimposed on the original enhancement, to assess the arterial phase in this region. This procedure is termed “defect reperfusion imaging” or “defect reinjection technique” [78].

Image interpretation

Image interpretation in the postvascular phase with Sonazoid® is reported in **Table 4**. A contrast defect, corresponding to hypoenhancement in the postvascular phase should be regarded as highly suggestive of malignancy in the setting of nodules in cirrhosis [61]. Very well differentiated, early HCC, are isoenhancing in both the arterial and the postvascular phases in approximately 70 % of cases [6]. Nodule characterization cannot be performed in the postvascular phase alone, for which arterial phase assessment remains the cornerstone.

Recommended uses and indications

CEUS with Sonazoid® is recommended:

- To characterize nodules in cirrhosis, allowing assessment of both the vascular and postvascular phases. CEUS has been adopted in the Japanese guidelines for the management of HCC [76, 79, 80] to search for nodules seen on CT or MRI but unidentifiable on B-mode ultrasound.
- To screen for HCC in a cirrhotic liver [77]; however, there is no evidence to date that this procedure is cost-effective.
- To stage HCC in livers in which US imaging is satisfactory; however, there is no evidence to date that CEUS can replace CT or MRI.

2.2.6. Tips for all contrast agents

- When a nodule is deeply located (> 8 cm) and suboptimally visualized with conventional B-mode ultrasound, its evaluation can become even worse during CEUS because of attenuation by contrast microbubbles. Use of greater amounts of contrast increases the signals both from nodules and from superficial tissues, usually failing to improve or even worsening target evaluation. Irrespective of the contrast agent used, high doses should be avoided because this limits CEUS penetration in all phases.
- When the liver parenchyma is coarse on B-mode ultrasound, it may be extremely difficult to detect small nodules making it difficult to choose the region to be scanned during CEUS in the arterial phase.
- In case of liver nodules in patients with complete portal thrombosis, perfusion of the parenchyma depends on the arterial supply. Reducing the contrast dose (half the usual dose or less) can reduce signal saturation and improve tumor conspicuity.

Table 4 Enhancement patterns of focal liver lesions in liver cirrhosis during the postvascular phase (Kupffer phase) with Sonazoid®.

lesion	post-vascular phase with Sonazoid® (Kupffer phase)
cyst	nonenhancing
hemangioma	nonenhancing
FNH	iso to hyperenhancing
regenerative nodule	
typical features (but not diagnostic)	isoenhancing
additional features (but not diagnostic)	slightly hypo- or hyperenhancing
dysplastic nodule	isoenhancing
HCC	
typical features	nonenhancing or hypoenhancing
additional features	isoenhancing (well differentiated HCC)
cholangiocarcinoma	
typical features	nonenhancing or hypoenhancing
additional features	not reported
metastasis	
typical features	nonenhancing or hypoenhancing
additional features	not reported

The arterial and portal venous phases are the same as for other agents. Cholangiocarcinoma may mimic metastasis and poorly differentiated HCC. Metastasis may mimic cholangiocarcinoma and poorly differentiated HCC.

2.3. Characterization of portal vein thrombosis

2.3.1. Definition

Portal vein thrombosis refers to the development of solid material within the lumen of any portion of the portal vein. The thrombus may be occlusive or nonocclusive and may involve the entire portal venous system or any segment. There are two main forms [115]:

- Bland (appositional) thrombosis refers to the presence of a simple clot within the vein. It is often silent and may be clinically inapparent.
- Malignant (neoplastic) thrombosis occurs almost always as a complication of HCC in the liver. Its identification is of prognostic significance as it negatively alters therapy options and upstages disease.

2.3.2 Imaging of portal vein thrombosis

Baseline ultrasound and Doppler techniques

The thrombosed portal vein may look normal and yet be filled with thrombus. However, more often the thrombus has variable echogenicity, making the lumen appear hypoechoic rather than anechoic. The baseline scan should include color and spectral Doppler interrogation of the portal veins. Complete thrombosis shows no detectable signal from the portal vein, even when optimized for slow flow. The presence of intrathrombus signal with an arterial waveform on Doppler spectral examination is a highly specific sign of malignancy but its sensitivity is only moderate.

CEUS

Bland thrombus is avascular and shows as a void within the enhancing liver in all phases of CEUS but best visualized during the portal venous phase. A malignant thrombus has the same enhancement characteristics as the tumor from which it originated, including rapid arterial phase hyperenhancement [115, 121, 134]. While slow and weak portal venous wash out may be seen, the wash out is usually more rapid.

To perform the scans, the suspect thrombus within the vein should be studied during the wash in of the UCA, as the vascularization of the clot should parallel the arrival of the microbubbles within the hepatic artery in the liver in case of neoplastic thrombus. Sweeping through the liver in sagittal and axial planes in the portal venous phase will often depict the washed out tumor within the portal vein branches optimally.

The tumor source of a malignant portal vein thrombus may be obvious or it may be invisible on ultrasound, even with the assistance of CEUS. Sweeping through the liver in both the arterial and the portal venous phases of enhancement may be enlightening. Washed out regions of the liver should undergo reinjection with arterial phase imaging to show their arterial enhancement. A suspicious clot within the portal vein may be amenable to biopsy with US guidance, targeting, whenever possible, enhancing regions within the thrombus [134].

2.4. CEUS for biopsy planning in cirrhotic and normal livers

CEUS prior to biopsy procedures can increase the diagnostic yield by 10 % and decrease the false negative rate especially in large tumors with areas of necrosis. CEUS can localize the site for biopsy more accurately by demonstrating regions of vascularized viable tumor, which should be targeted, and regions of necrosis, which should be avoided [150]. These two entities cannot be distinguished by conventional ultrasound alone. CEUS may also locate occult lesions on nonenhanced US [125].

3. Detection of Malignant FLL: Transabdominal Approach

▼

3.1. Background

Conventional US is the most frequently used modality for the primary imaging of abdominal organs, including the liver but is less sensitive in the detection of liver lesions than CECT, CEMRI or intraoperative US. The main reasons for this are difficulties in detecting small and isoechoic lesions, especially when they are deep or in difficult anatomic locations.

The published literature [17, 22, 42, 66, 74, 84, 114, 119] provides strong evidence that CEUS significantly improves the detection of metastases compared with conventional US. The most important CEUS feature for detecting a malignant liver lesion is the identification of a focal region of wash out occurring as early as the late arterial phase but mostly during the portal venous and late or postvascular phases.

3.2. Study procedures

The study procedure is similar to the study procedure described in section 2.1.2 but the following points should be borne in mind:

- With all agents, lesion detection requires an examination time of at least 3 – 4 min, which is the useful persistence of most microbubbles.
- With agents presenting a postvascular phase (Sonazoid®), it is possible to detect lesions that wash out very late [61, 108].
- A second administration (reinjection technique) can be used to confirm the metastatic nature of any detected contrast defect by demonstrating arterial enhancement followed by wash out (see section 2.2.6).

3.3. Detection of metastatic lesions

The typical and almost invariable appearance of metastases is focal hypoenhancement in the portal venous, late and postvascular phases. The enhancement patterns observed during the arterial phase are variable and help to characterize lesions but aid only minimally in their detection (see section 2.1.3).

With vascular phase agents (SonoVue®, Definity®), several studies have shown that the accuracy in the detection of liver metastases is comparable to that of CECT and CEMRI, when scanning conditions allow a complete investigation of all liver segments [84].

3.4. Detection of HCC and CCC

With all agents (SonoVue®, Definity®, Sonazoid®), most HCC show increased enhancement in the arterial phase but the short duration of this phase makes adequate assessment of the whole liver impossible, at least with current technology. The late phase lasts long enough for thorough exploration, but the appearances of HCC are variable, as described in section 2.2.3, and, importantly, not all HCC wash out in the late phase, limiting the sensitivity of CEUS for the detection of HCC. Consequently, routine use of UCA in the detection of HCC with vascular phase agents cannot be recommended.

With agents presenting a postvascular phase (Sonazoid®), scanning the entire liver at 10 min or later after injection helps to detect malignant nodules since typical HCC show as an enhancement defect [60, 104, 108]. However, postvascular defects are not specific findings and demonstration of homogeneous arterial enhancement requires a second administration of Sonazoid® to confirm the diagnosis of HCC. Moreover, approximately half of

well differentiated HCC do not show enhancement defects in the postvascular phase [6].
Depiction of local tumor recurrence and residual tumor after ablation using B-mode alone is difficult. With vascular phase agents, scanning in the arterial phase with repeated injections demonstrates the hypervascularity in the recurrence, which usually lies adjacent to the previously ablated tumor. The same technique is useful for demonstrating new HCC and, in both cases, helps identify the target and guide treatment (see section 5.1).
Cholangiocarcinomas behave in the same way as metastases, washing out rapidly and appearing as defects in the late phase, regardless of the appearance in the arterial phase [151]. This pattern may facilitate detection of satellite nodules adjacent to a larger lesion that were not visualized on conventional US.

3.5. Recommended uses, indications and limitations

Use of CEUS is recommended for the following indications:

- To characterize indeterminate (usually small) lesions shown on either CECT or CEMRI.
- To "rule out" liver metastases or abscesses, unless conventional ultrasound shows typical findings.
- For treatment planning in selected cases to assess the number and location of liver metastases, either alone or as complementary to CECT and/or CEMRI.
- Surveillance of oncology patients where CEUS has been useful previously. Recommended to replace unenhanced US with CEUS for the evaluation of liver metastases in colorectal cancer after chemotherapy [73].
- CEUS with vascular phase agents is not indicated for the detection and staging of HCC. With the use of Sonazoid® and postvascular phase scanning, CEUS may be used to stage HCC in the liver where imaging is good. However, there is no evidence to date that CEUS can replace CT or MRI.
- A potential pitfall is that small cysts, which were not seen on unenhanced US, are sometimes detected in late or postvascular phase scanning. Careful re-evaluation with conventional US may help to show their cystic nature. In doubtful situations, a second contrast agent injection is recommended, looking for arterial phase enhancement, which indicates viable tumor tissue.

4. Intraoperative Contrast Enhanced Ultrasound

▼

4.1. Background

Standard preoperative imaging remains limited in selecting patients who may benefit from liver surgery [47, 106]. Intraoperative ultrasound (IOUS) is recognized as the gold standard, which ultimately dictates the surgical management of those undergoing resection [21, 23, 33, 69]. Patients with early stage HCC are offered transplantation or resection [16], which can be curative procedures. Similarly, for patients with colorectal liver metastases, resection is the treatment of choice, with 5-year survival rates of up to 60 % [54, 124]. However, 75 % of patients who undergo resection develop recurrences (50 % in the liver). The majority of recurrences appear within 2 years [4, 51, 124]. Thus, more accurate imaging is required.
Recent studies of intraoperative contrast enhanced ultrasound (IO-CEUS) with different contrast agents have shown that it is more sensitive, specific and accurate than IOUS, CT or MRI in defining whether tumor resection (metastases or HCC) is appropriate. Furthermore, surgical management is altered in up to 30 % of cases [52, 90, 110, 118, 141, 142]. It is now recognized that the more aggressive the surgical approach adopted, the higher the impact of IO-CEUS becomes [90].

4.2. IO-CEUS technique

Dedicated high frequency intraoperative probes with contrast specific capability are needed. Covering the transducer and cable with a long sterile sheath containing coupling gel, and the control panel with a large sterile membrane ensures sterility. Some ultrasound systems provide intraoperative transducers that can be sterilized by gas and, thus, need no cover.
At surgery, all patients undergo a manual abdominal and pelvic exploration for extra-hepatic disease followed by mobilization of the liver from the diaphragm to improve sonographic access. Bimanual palpation of the liver is then performed, followed by systematic IOUS of the entire liver, looking for previously diagnosed as well as for new lesions and to identify involvement of major vessels or bile ducts.
With vascular phase agents (SonoVue® and Definity®) CEUS is used as explained for the transabdominal approach (see section 2.1.2). The duration of enhancement in normal liver in the late phase is shorter than with percutaneous US. Injections may be repeated for global assessment, or to assess the arterial phase enhancement of identified lesions for their characterization. Irrespective of the contrast agent used, high doses should be avoided because this limits US penetration in all phases.
With postvascular phase agents (Sonazoid®), detection of malignant FLL starts 10 min postinjection [61, 108]. A second injection can be used to confirm the metastatic nature of a lesion by demonstrating arterial enhancement (see section 2.1.6).

4.3. Image interpretation

Image interpretation is the same as for the transabdominal approach reported in section 2.1.5.

4.4. Recommended use and limitations

IO-CEUS is recommended for:

- The detection of liver metastases in all patients undergoing liver resection.
- The characterization of focal liver nodules in cirrhotic patients undergoing liver resection for HCC, especially of new nodules detected at IOUS [142].
- The targeting of occult lesions for ablation therapy for patients undergoing combined liver resection and ablative therapy.

The shorter duration of contrast enhancement is a limitation of IO-CEUS.

5. Monitoring Ablation Treatment

▼

5.1. Monitoring local ablation treatment

5.1.1. Background

Locoregional therapies, which conventionally include ablation, whatever the modality used, and transarterial chemo/radioembolization, play a key role in the management of patients with liver malignancies, both HCC and metastases [58, 98].
Unenhanced US is commonly used to guide ablation. It is easy to use and widely available but, even when combined with Doppler, it does not provide useful information on the extent of the ablation. Assessment of tissue perfusion is crucial to differentiate necrotic from viable residual tumor.

The addition of CEUS can provide important information in each of the following procedures [30, 107]:

- Assessment of the lesions to be treated by ablation (number and size and homogeneity of enhancement of the lesions, and the presence of feeding vessels) to define the eligibility of the patient for treatment and the best ablation strategy.
- Depict previously undetectable lesions with the support of fusion imaging, enabling needle/probe guidance.
- Detecting viable tumor persistence following locoregional treatment (either ablation or chemo/radioembolization).

5.1.2. Study procedures (see also section 2.1.2)

Pretreatment CEUS

Particularly for metastases, assessment of size must include the perilesional hypervascular halo with wash out. Tumor margins are better detected by CEUS than unenhanced US [28] because definition of its relationships with surrounding structures is improved, thus, helping develop appropriate treatment strategies and reducing the risks of complications [27, 28].

Accurate pretreatment planning can be improved by real-time fusion imaging with CT, MRI or CEUS, which provides an accurate volumetric map of the tumor and graphically depicts the number and sites of the ablation volumes needed to cover the whole mass and achieve an adequate perilesion "safety margin" [29, 97].

Pretreatment CEUS is very helpful for comparison of the patterns before and after treatment.

The field depth, selected scan plane, acoustic gain and MI used for the pretreatment CEUS study of each lesion must be predefined. Images and/or video clips should be stored for precise comparison with immediate postablation studies.

Positioning of ablation device

The ablation device is inserted when the target is optimally depicted. When lesion targeting is particularly difficult (e. g., small lesion size, difficult location), fusion imaging with CT/MRI may allow "targeted" CEUS in some instances [36] and consequent improvement of ablation needle/probe guidance. Depiction of a "virtual needle" during CEUS provided by fusion imaging may facilitate the procedure.

5.1.3. Image interpretation – definition of complete treatment response

The Response Evaluation Criteria in Solid Tumors (RECIST) guidelines [139] for the assessment of tumor response are no longer considered adequate for locoregional treatment because of the poor relationship between necrosis and tumor size. After thermal ablations, completely necrotic tumors may remain unchanged in size, whereas tumors that shrink may still be partially viable.

Accordingly, the RECIST criteria have been amended, at least for HCC [91], to stress that the imaging indicator of complete ablation is the disappearance of any previously visualized intralesional enhancement on CEUS. This must be assessed throughout the whole volume of each tumor which has undergone ablation [30, 130]. The volume of the necrosis achieved should be compared with the pretreatment volume of the tumor(s). Simultaneous display of tissue and contrast is of particular value for follow-up of treated lesions. The volume of necrosis achieved can be compared with the pretreatment volume of the same lesion on CECT or CEMRI using real-time fusion imaging [72].

Completeness of treatment of hypoenhancing lesions (mostly liver metastases) can be assessed by comparing the volume and location of pretreatment lesions with those of the ablated region. This also determines whether a sufficient safety margin around the lesion has been achieved. The frequent occurrence of satellite nodules around small HCC (5 – 10 mm from the main tumor [123]), dictates that the thickness of the safety margin following ablation should be assessed not only for liver metastases but also for HCC.

5.2. Periprocedural assessment of treatment response

Unenhanced US is used to monitor the reduction of the hyperechoic "cloud" of gas caused by heating immediately after ablation. This usually takes 5 – 15 min to dissipate.

For each treated lesion, the same system settings and scan planes must be used as for the preablation assessment. Images and/or video clips should be stored for comparison with previously stored preablation images. If additional probe/needle insertions are performed, repeated doses of UCA can be given.

5.2.1. Follow-up investigation to assess tumor recurrence

It is often difficult to depict local tumor recurrence after ablation using B-mode alone. Here, scanning in the late or postvascular phase, with subsequent reinjection to confirm tumor enhancement in any suspicious region is useful to identify the viable tumor adjacent to the ablated volume. This can be used to guide biopsy and additional treatment. While CEUS may be extremely useful to define local recurrence in a treated nodule, CT and MRI provide a better overview of the liver to detect distant intra- and extrahepatic tumor and cannot be replaced by CEUS.

In the early postablative evaluation (within the first 30 days), a thin, uniform enhancing rim can be visible along the periphery of the necrotic region, similar to the findings on CECT. Misinterpretation of this perilesional hyperemic halo as residual viable tumor can be avoided by comparing postablation images with preablation scans.

5.2.2. Recommended uses and indications

- As a complement to CECT and/or CEMRI for pretreatment staging and assessment of target lesion vascularity.
- Facilitation of needle positioning in cases of incomplete or poor lesion delineation on unenhanced US.
- Evaluation of the immediate treatment effect after ablation and guidance for immediate re-treatment of residual unablated tumor. Using this strategy, the rate of incomplete ablation in the first session is reported to decrease from 16 to 6 % [29].
- Assessment of local tumor progression when follow-up CECT or CEMRI are contraindicated or not conclusive. In addition to CECT and/or CEMRI, CEUS may be used in follow-up protocols.

6. Liver Transplantation

▼

6.1. Background

Liver transplantation is currently an established first-line treatment for patients with end-stage acute or chronic liver disease but postoperative complications may limit its long-term success and their early detection is extremely important for graft and patient survival. Hepatic artery (HA) thrombosis, which is the most common and severe vascular complication, occurs in 3 – 8 % of transplants in adults [67, 129]. Acute HA thrombosis almost invariably leads to graft loss from infarction and eventual abscess formation. Hepatic artery stenosis may proceed to thrombosis and may cause ischemic liver and biliary injuries if not promptly

corrected. Although portal vein (PV) and hepatic vein or caval thrombosis are less frequent, they are also serious complications that may lead to graft loss [83]. Clinical signs of vascular complications are often nonspecific, and the diagnosis, best made at the presymptomatic stage, depends on imaging. Ultrasound is usually used first to detect vascular complications as well as for long-term follow-up [46, 53, 83].

Though Doppler is useful, it may be not sensitive enough to depict slow flow in a patent HA, particularly in patients with postoperative edema, inaccessible hepatic arteries, or inability to cooperate [131]. When flow cannot be identified in the HA, CECT or angiography, with their attendant risks, were hitherto required to obtain a definitive answer; CEUS can be used instead and is often able to overcome the limitations of Doppler.

6.2. Study procedure

The study procedure is as described in section 2.1.2. The intrahepatic arterial tree is well visualized at the time of its enhancement in the early arterial phase, before arrival of contrast microbubbles in the portal system. The right hepatic artery is usually visible anteriorly alongside the right portal branch through a right intercostal scan and the left hepatic artery at the bifurcation of the left portal branch, optimally seen with a supine epigastric approach. The portal vein and its branches are visualized in the portal venous phase, following which the enhancement of the parenchyma can be studied looking for infarcts, which appear as nonenhancing regions. Later the hepatic veins fill and can be studied. When only the vessels are to be explored, a reduced amount of injected contrast may improve their visualization by preventing signal saturation.

6.3. Image interpretation

Lack of visualization of the arterial tree, expected to be seen before portal enhancement, indicates complete arterial thrombosis with very high positive predictive values [10, 32, 99, 131]. Identification of the arterial branches when conventional Doppler has failed [131], may allow subsequent targeted Doppler reassessment, which is needed to distinguish thrombosis from slow flow caused by vasoconstriction or splenic steal from post-thrombotic/stenotic recanalization, tasks not achievable using CEUS alone. When the main hepatic artery is visible, CEUS depicts the shape of the lumen and its course, possibly identifying stenoses, which usually occur at the site of the surgical anastomosis [154]. CEUS may also allow study of the shape and patency of the caval and portal anastomoses.

6.4. Recommended Indications and Limitations

6.4.1. Indications

Before liver transplantation, CEUS is indicated to assess portal vein thrombosis and characterize focal liver lesions in cirrhosis. After liver transplantation, CEUS can be performed at the bedside or in the intensive care unit, avoiding most of the risks associated with CECT or angiography [10, 32, 63, 100, 154]. CEUS is indicated for:

- Confirmation of occlusion of the intrahepatic hepatic arteries, portal veins, hepatic veins or inferior vena cava (IVC) after an inconclusive Doppler evaluation of the liver vasculature. The extrahepatic arterial tree cannot always be studied in its entirety and complete patency cannot be confirmed with certainty without the addition of the finding of normal flow tracings from the intrahepatic arteries on Doppler US. In the late phase, the ultrasound can be switched to Doppler to exploit the remaining microbubbles to enhance the Doppler signals and investigate small vessels missed without contrast.
- Confirmation of the presence and assessment of the nature of fluid collections and, in case of recent hematomas, to search for active bleeding.
- Exclusion of perfusion defects when infarction is suspected.
- For monitoring the success of thrombolysis in the intensive care unit (ICU) after interventions for hepatic artery occlusion.

6.4.2. Limitations

- In the early postoperative period, wounds and surgical dressings or subcutaneous emphysema, may limit examination windows.
- In patients with split liver transplantation or after living donor liver transplantation, the examination may be more difficult because of the complex anatomy.
- Imaging the prehepatic portions of the hepatic artery and portal vein may be precluded by the surgical wound or intervening bowel gas.

6.4.3. Tips and tricks

- When a side-to-side caval (piggyback) anastomosis is used, the distal part of the donor cava may thrombose and simulate a small subcapsular hematoma.
- Ascites may collect alongside the ligament teres and may simulate a complex cyst on follow-up examinations.
- Knowledge of the surgical procedures including the presence of jump grafts, difficult anastomoses and the status of the donor liver may be helpful to interpretation.
- While CEUS shows the morphology of the vessel lumen, integration with Doppler US is required to confirm the presence of a hemodynamically significant stenosis.

7. Contrast Quantification and Monitoring Systemic Treatment of Malignancies

7.1. Background

Neovascularization is a key stage in the growth of malignancies beyond 2 – 3 mm^3. This neoangiogenesis is an important target for novel anticancer treatments and many new antiangiogenesis or antivascular treatments aim at destroying or limiting the growth of tumor vessels [50, 70]. A new area of clinical utility for dynamic contrast enhanced ultrasound (DCE-US) has emerged for monitoring the response to these drugs. Initially, such monitoring relied on qualitative analyses only. More recently, robust and quantitative features have been developed. To achieve successful results, standardization and strict control of scanner settings are needed [39].

7.2. Methodology and equipment for quantification

7.2.1. Data acquisition

Contrast specific imaging is used to distinguish microbubble signals from tissue. The best temporal and spatial resolution is provided by nonlinear gray scale modes (see section 1.3). Conventional Doppler imaging techniques cannot visualize vessels smaller than approximately 100 µm but CEUS can detect signals from vessels up to 40 µm [56] and, thus, provides a better assessment of the extent of angiogenesis.

7.2.2. Quantification software

Early measurements of contrast kinetics (i.e., time-intensity curves, TIC) were performed using video data because it was readily available. Background subtraction was necessary to compensate for attenuation effects [13] and extract reliable time-based features, such as time to peak intensity, mean transit time, etc. However, the nonlinear compression applied to the original signals (required to display them on video monitors) distorts amplitude-based TIC features (e.g., peak intensity and area under the curve) [112].

The majority of reports have used uncompressed, post beam formed data (radio-frequency data are not required since the phase information is not essential). TIC based on such raw data sets allow for accurate assessment of both time-based and amplitude-dependent features. All manufacturers that supply built-in analysis packages on their scanners use this type of data but off-line software packages are also available [35].

7.3. Administration of UCA and quantitative analysis

7.3.1. Bolus injection

Functional ultrasound studies are based on measuring the time sequence of signal enhancement, typically over the initial 1 – 3 min after an intravenous bolus injection, either across a large region-of-interest such as an entire tumor or on a pixel-by-pixel basis. The resulting TIC follows the wash in and wash out of the contrast agent and features linked to blood flow and blood volume can be extracted from them. Quantitative analyses of the TIC can be performed to determine functional features that characterize the TIC with or without curve fitting. Several functional features can be studied [87]:

- Related to fractional blood volume: peak intensity (PI); area under the curve (AUC) [32]; area under the wash in (AUWI); under the wash out (AUWO).
- Related to blood flow: time to peak intensity (TPI); slope of the wash in (SWI).
- Related to transit time: mean transit time (MTT).

It is also possible to map the changes in TIC features over time and show these as colorized functional images.

7.3.2. The disruption-replenishment or reperfusion method

In this method, originally described for the heart [146], a high intensity diagnostic series of pulses is transmitted to a tissue slice filled with microbubbles following bolus or infusion injection, to destroy the bubbles within it. The scanner then switches to a low MI and the refill of the slice with microbubbles is monitored with a contrast-specific imaging mode. The refill takes the form of a rising exponential curve whose slope, β, relates to the velocity of blood inflow while the maximum enhancement, A, relates to the fractional blood volume. Their product forms an estimate of tissue perfusion [59].

The advantage of an infusion of UCA is that a concentration equilibrium can be achieved, which makes it easier to compare different tissue regions directly [96, 137]. With the destruction-reperfusion method only the wash in phase can be assessed, which may limit its utility.

7.3.3. Hepatic vein transit times

The arrival times of a UCA bolus in the hepatic artery, portal vein and hepatic veins can be measured and transit times calculated. Shortening of the transit time between the hepatic artery/portal vein and the hepatic veins occurs in the presence of liver malignancies, presumably because of intrahepatic shunting. However, this also occurs in cirrhosis [93, 94], resulting in a nonspecific finding which limits its use in liver malignancy. Its use to stage chronic hepatitis is also limited by the substantial overlap between different stages despite statistically significant differences among groups [120].

7.4. Assessment of antiangiogenic treatment

Since antiangiogenic treatment frequently induces necrosis without causing tumor shrinkage, functional imaging techniques are particularly suitable for the early assessment of response, a task for which both the RECIST and World Health Organization (WHO) size criteria [139, 149] are unsatisfactory [91].

Studies of various types of tumors treated with antiangiogenic therapies have confirmed that DCE-US may enable early prediction of response to treatment [38, 82, 85, 86, 88, 89].

Affiliations

[1] Department of Pediatric Radiology, INSERM U947, Centre Hospitalier Universitaire de Nancy and Université de Lorraine, Vandoeuvre, France
[2] Medizinische Klinik 2, Caritas-Krankenhaus Bad Mergentheim, Germany
[3] Department of Radiology, Seoul National University Hospital, Seoul, Korea
[4] Imaging Sciences Department, Imperial College, Hammersmith Hospital, London, United Kingdom
[5] Department of Gastroenterology and Hepatology, Kinki University School of Medicine, Osaka, Japan
[6] Ultrasound Section, Division of Surgery, Department of Gastroenterology, Herlev Hospital, University of Copenhagen, Copenhagen, Denmark
[7] Division of Internal Medicine, University of Bologna, Bologna, Italy
[8] Division of Gastroenterology, University of Calgary, Calgary, Alberta, Canada
[9] Northeastern Ohio Medical University, Rootstown, Ohio, United States of America
[10] Institute of Radiology, School of Medicine, University of São Paulo, São Paulo, Brazil
[11] Thane Ultrasound Centre, Jaslok Hospital, Mumbai, India
[12] Peking University Cancer Hospital, Peking, China
[13] Interdisciplinary Ultrasound Center, Department of Clinical Radiology, University of Munich-Grosshadern Campus, Munich, Germany
[14] Service de Radiologie Adultes, Hôpital Necker, Université Paris Descartes, Paris, France
[15] Department of Ultrasound, Zhongshan Hospital, Fudan University, Shanghai, China
[16] Department of Radiology, Thomas Jefferson University, Philadelphia, Philadelphia, United States of America
[17] Department of Radiology, University of Michigan, Ann Arbor, Michigan, United States of America
[18] Department of Radiology, Royal Melbourne Hospital, University of Melbourne, Melbourne, Australia
[19] Division of Diagnostic Ultrasound, Department of Radiology, Thomas Jefferson University Hospital, Philadelphia, Pennsylvania, United States of America
[20] Integrated Research Cancer Institute in Villejuif, Gustave Roussy Institute, Villejuif, France
[21] Imaging Department, Imperial College, London, United Kingdom
[22] MRI Institute, University of California San Diego, San Diego, California, United States of America
[23] Department of Gastroenterology and Hepatology, Tokyo Medical University, Tokyo, Japan
[24] Department of Interventional Oncologic Radiology, General Hospital of Busto Arsizio, Busto Arsizio, Italy
[25] Central Ultrasound Department, Klinikum Siloah, Klinikum Region Hannover, Hannover, Germany
[26] Department of Medical Ultrasound, Tenth People's Hospital of Tongji University, Shanghai, China

Acknowledgments

The authors acknowledge the educational contributions provided by the following companies: Bracco; GE Healthcare; Hitachi Medical Systems; Lantheus Medical Imaging; Medison; Philips Medical Systems; Siemens Healthcare; Toshiba Medical Systems;

and Supersonic Imagine. The authors gratefully acknowledge Glynis Harvey from the WFUMB office for her efficient management.

References

1 EFSUMB (European Federation of Societies for Ultrasound in Medicine and Biology). Minimum training recommendations for the practice of medical ultrasound. Ultraschall in Med 2006; 27: 79 – 105
2 International Consensus Group for Hepatocellular Neoplasia. Pathologic diagnosis of early hepatocellular carcinoma: a report of the international consensus group for hepatocellular neoplasia. Hepatology 2009; 49: 658 – 664
3 EFSUMB (European Federation of Societies for Ultrasound in Medicine and Biology). Minimum training requirements for the practice of Medical Ultrasound in Europe. Ultraschall in Med 2010; 31: 426 – 427
4 *Adam R, Bismuth H, Castaing D et al.* Repeat hepatectomy for colorectal liver metastases. Ann Surg 1997; 225: 51 – 60, discussion 62
5 *Albrecht T, Blomley M, Bolondi L et al.* Guidelines for the use of contrast agents in ultrasound. January 2004. Ultraschall in Med 2004; 25: 249 – 256
6 *Arita J, Hasegawa K, Takahashi M et al.* Correlation between contrast-enhanced intraoperative ultrasound using Sonazoid and histologic grade of resected hepatocellular carcinoma. Am J Roentgenol 2011; 196: 1314 – 1321
7 *Averkiou M, Powers J, Skyba D et al.* Ultrasound contrast imaging research. Ultrasound Q 2003; 19: 27 – 37
8 *Barreiros AP, Piscaglia F, Dietrich CF.* Contrast enhanced ultrasound for the diagnosis of hepatocellular carcinoma (HCC): Comments on AASLD guidelines. J Hepatol 2012; 57: 930 – 932
9 *Bernatik T, Seitz K, Blank W et al.* Unclear focal liver lesions in contrast-enhanced ultrasonography – lessons to be learned from the DEGUM multicenter study for the characterization of liver tumors. Ultraschall in Med 2010; 31: 577 – 581
10 *Berstad AE, Brabrand K, Foss A.* Clinical utility of microbubble contrast-enhanced ultrasound in the diagnosis of hepatic artery occlusion after liver transplantation. Transpl Int 2009; 22: 954 – 960
11 *Bolondi L, Gaiani S, Celli N et al.* Characterization of small nodules in cirrhosis by assessment of vascularity: the problem of hypovascular hepatocellular carcinoma. Hepatology 2005; 42: 27 – 34
12 *Boozari B, Soudah B, Rifai K et al.* Grading of hypervascular hepatocellular carcinoma using late phase of contrast enhanced sonography – a prospective study. Dig Liver Dis 2011; 43: 484 – 490
13 *Bos LJ, Piek JJ, Spaan JA.* Background subtraction from time-intensity curves in videodensitometry: a pitfall in flow assessment using contrast echocardiography. Ultrasound Med Biol 1995; 21: 1211 – 1218
14 *Bruix J, Sherman M.* Management of hepatocellular carcinoma. Hepatology 2005; 42: 1208 – 1236
15 *Bruix J, Sherman M.* Management of hepatocellular carcinoma: an update. Hepatology 2011; 53: 1020 – 1022
16 *Bruix J, Sherman M, Llovet JM et al.* Clinical management of hepatocellular carcinoma. Conclusions of the Barcelona-2000 EASL conference. European Association for the Study of the Liver. J Hepatol 2001; 35: 421 – 430
17 *Cantisani V, Ricci P, Erturk M et al.* Detection of hepatic metastases from colorectal cancer: prospective evaluation of gray scale US versus SonoVue(R) low mechanical index real time-enhanced US as compared with multidetector-CT or Gd-BOPTA-MRI. Ultraschall in Med 2010; 31: 500 – 505
18 *Cao BS, Li XL, Li N et al.* The nodular form of hepatic tuberculosis: contrast-enhanced ultrasonographic findings with pathologic correlation. J Ultrasound Med 2010; 29: 881 – 888
19 *Catalano O, Sandomenico F, Nunziata A et al.* Transient hepatic echogenicity difference on contrast-enhanced ultrasonography: sonographic sign and pitfall. J Ultrasound Med 2007; 26: 337 – 345
20 *Catalano O, Sandomenico F, Raso MM et al.* Low mechanical index contrast-enhanced sonographic findings of pyogenic hepatic abscesses. Am J Roentgenol 2004; 182: 447 – 450
21 *Cervone A, Sardi A, Conaway GL.* Intraoperative ultrasound (IOUS) is essential in the management of metastatic colorectal liver lesions. Am Surg 2000; 66: 611 – 615
22 *Chami L, Lassau N, Malka D et al.* Benefits of contrast-enhanced sonography for the detection of liver lesions: comparison with histologic findings. Am J Roentgenol 2008; 190: 683 – 690
23 *Charnley RM, Morris DL, Dennison AR et al.* Detection of colorectal liver metastases using intraoperative ultrasonography. Br J Surg 1991; 78: 45 – 48
24 *Chen LD, Xu HX, Xie XY et al.* Enhancement patterns of intrahepatic cholangiocarcinoma: comparison between contrast-enhanced ultrasound and contrast-enhanced CT. Br J Radiol 2008; 81: 881 – 889
25 *Chen LD, Xu HX, Xie XY et al.* Intrahepatic cholangiocarcinoma and hepatocellular carcinoma: differential diagnosis with contrast-enhanced ultrasound. Eur Radiol 2010; 20: 743 – 753
26 *Chen MH, Dai Y, Yan K et al.* The role of contrast-enhanced ultrasound on the diagnosis of small hepatocellular carcinoma (≤ 3cm) in patients with cirrhosis. Hepatol Res 2006a; 35: 281 – 288
27 *Chen MH, Wei Y, Yan K et al.* Treatment strategy to optimize radiofrequency ablation for liver malignancies. J Vasc Interv Radiol 2006b; 17: 671 – 683
28 *Chen MH, Yang W, Yan K et al.* The role of contrast-enhanced ultrasound in planning treatment protocols for hepatocellular carcinoma before radiofrequency ablation. Clin Radiol 2007; 62: 752 – 760
29 *Chen MH, Yang W, Yan K et al.* Large liver tumors: protocol for radiofrequency ablation and its clinical application in 110 patients – mathematic model, overlapping mode, and electrode placement process. Radiology 2004; 232: 260 – 271
30 *Choi D, Lim HK, Lee WJ et al.* Early assessment of the therapeutic response to radio frequency ablation for hepatocellular carcinoma: utility of gray scale harmonic ultrasonography with a microbubble contrast agent. J Ultrasound Med 2003; 22: 1163 – 1172
31 *Claudon M, Cosgrove D, Albrecht T et al.* Guidelines and good clinical practice recommendations for contrast enhanced ultrasound (CEUS) – update 2008. Ultraschall in Med 2008; 29: 28 – 44
32 *Clevert DA, Stickel M, Minaifar N et al.* Contrast-enhanced ultrasound in liver transplant: first results and potential for complications in the postoperative period. Clin Hemorheol Microcirc 2009; 43: 83 – 94
33 *Conlon R, Jacobs M, Dasgupta D et al.* The value of intraoperative ultrasound during hepatic resection compared with improved preoperative magnetic resonance imaging. Eur J Ultrasound 2003; 16: 211 – 216
34 *Cosgrove D, Harvey C.* Clinical uses of microbubbles in diagnosis and treatment. Med Biol Eng Comput 2009; 47: 813 – 826
35 *Cosgrove D, Lassau N.* Imaging of perfusion using ultrasound. Eur J Nucl Med Mol Imaging 2010; 37 (Suppl 1): S65 – S85
36 *Crocetti L, Lencioni R, Debeni S et al.* Targeting liver lesions for radiofrequency ablation: an experimental feasibility study using a CT-US fusion imaging system. Invest Radiol 2008; 43: 33 – 39
37 *Dawson P, Cosgrove D, Grainger R.* Textbook of contrast media. Oxford: ISIS Medical Media; 1999
38 *De Giorgi U, Aliberti C, Benea G et al.* Effect of angiosonography to monitor response during imatinib treatment in patients with metastatic gastrointestinal stromal tumors. Clin Cancer Res 2005; 11: 6171 – 6176
39 *Dietrich CF, Averkioui MA, Correas JM et al.* An EFSUMB introduction into dynamic contrast-enhanced ultrasound (DCE-US) for quantification of tumour perfusion. Ultraschall in Med 2012; 33: 344 – 351
40 *Dietrich CF, Braden B, Hocke M et al.* Improved characterisation of solitary solid pancreatic tumours using contrast enhanced transabdominal ultrasound. J Cancer Res Clin Oncol 2008; 134: 635 – 643
41 *Dietrich CF, Ignee A, Hocke M et al.* Pitfalls and artefacts using contrast enhanced ultrasound. Z Gastroenterol 2011; 49: 350 – 356
42 *Dietrich CF, Kratzer W, Strobe D et al.* Assessment of metastatic liver disease in patients with primary extrahepatic tumors by contrast-enhanced sonography versus CT and MRI. World J Gastroenterol 2006; 12: 1699 – 1705
43 *Dietrich CF, Mertens JC, Braden B et al.* Contrast-enhanced ultrasound of histologically proven liver hemangiomas. Hepatology 2007b; 45: 1139 – 1145
44 *Dietrich CF, Schuessler G, Trojan J et al.* Differentiation of focal nodular hyperplasia and hepatocellular adenoma by contrast-enhanced ultrasound. Br J Radiol 2005; 78: 704 – 707
45 *Ding H, Wang WP, Huang BJ et al.* Imaging of focal liver lesions: low-mechanical-index real-time ultrasonography with SonoVue. J Ultrasound Med 2005; 24: 285 – 297
46 *Dodd GD 3rd, Memel DS, Zajko AB et al.* Hepatic artery stenosis and thrombosis in transplant recipients: Doppler diagnosis with resistive index and systolic acceleration time. Radiology 1994; 192: 657 – 661
47 *Ellsmere J, Kane R, Grinbaum R et al.* Intraoperative ultrasonography during planned liver resections: why are we still performing it? Surg Endosc 2007; 21: 1280 – 1283

48 *Exuzides A, Main ML, Colby C et al.* A retrospective comparison of mortality in critically ill hospitalized patients undergoing echocardiography with and without an ultrasound contrast agent. JACC Cardiovasc Imaging 2010; 3: 578 – 585
49 *Fan ZH, Chen MH, Dai Y et al.* Evaluation of primary malignancies of the liver using contrast- enhanced sonography: correlation with pathology. Am J Roentgenol 2006; 186: 1512 – 1519
50 *Ferrara N, Kerbel RS.* Angiogenesis as a therapeutic target. Nature 2005; 438: 967 – 974
51 *Finlay IG, Meek D, Brunton F et al.* Growth rate of hepatic metastases in colorectal carcinoma. Br J Surg 1988; 75: 641 – 644
52 *Fioole B, de Haas RJ, Wicherts DA et al.* Additional value of contrast enhanced intraoperative ultrasound for colorectal liver metastases. Eur J Radiol 2008; 67: 169 – 176
53 *Flint EW, Sumkin JH, Zajko AB et al.* Duplex sonography of hepatic artery thrombosis after liver transplantation. Am J Roentgenol 1988; 151: 481 – 483
54 *Fong Y.* Hepatic colorectal metastasis: current surgical therapy, selection criteria for hepatectomy, and role for adjuvant therapy. Adv Surg 2000; 34: 351 – 381
55 *Forner A, Vilana R, Ayuso C et al.* Diagnosis of hepatic nodules 20 mm or smaller in cirrhosis: Prospective validation of the noninvasive diagnostic criteria for hepatocellular carcinoma. Hepatology 2008; 47: 97 – 104
56 *Forsberg F, Kuruvilla B, Pascua MB et al.* Comparing contrast-enhanced color flow imaging and pathological measures of breast lesion vascularity. Ultrasound Med Biol 2008; 34: 1365 – 1372
57 *Foschi FG, Dall'Aglio AC, Marano G et al.* Role of contrast-enhanced ultrasonography in primary hepatic lymphoma. J Ultrasound Med 2010; 29: 1353 – 1356
58 *Gillams AR, Lees WR.* Five-year survival in 309 patients with colorectal liver metastases treated with radiofrequency ablation. Eur Radiol 2009; 19: 1206 – 1213
59 *Guibal A, Taillade L, Mule S et al.* Noninvasive contrast-enhanced US quantitative assessment of tumor microcirculation in a murine model: effect of discontinuing anti-VEGF therapy. Radiology 2010; 254: 420 – 429
60 *Hatanaka K, Kudo M, Minami Y et al.* Sonazoid-enhanced ultrasonography for diagnosis of hepatic malignancies: comparison with contrast-enhanced CT. Oncology 2008a; 75 (Suppl 1): 42 – 47
61 *Hatanaka K, Kudo M, Minami Y et al.* Differential diagnosis of hepatic tumors: value of contrast-enhanced harmonic sonography using the newly developed contrast agent. Sonazoid. Intervirology 2008b; 51 (Suppl 1): 61 – 69
62 *Hirche TO, Ignee A, Hirche H et al.* Evaluation of hepatic steatosis by ultrasound in patients with chronic hepatitis C virus infection. Liver Int 2007; 27: 748 – 757
63 *Huang D, Chen Y, Li K et al.* Hemodynamic changes on color Doppler flow imaging and intravenous contrast-enhanced ultrasound for assessing transplanted liver and early diagnosis of complications. J Huazhong Univ Sci Technolog Med Sci 2008; 28: 284 – 286
64 *Iavarone M, Sangiovanni A, Forzenigo LV et al.* Diagnosis of hepatocellular carcinoma in cirrhosis by dynamic contrast imaging: the importance of tumor cell differentiation. Hepatology 2010; 52: 1723 – 1730
65 *Ignee A, Piscaglia F, Ott M et al.* A benign tumour of the liver mimicking malignant liver disease – cholangiocellular adenoma. Scand J Gastroenterol 2009; 44: 633 – 636
66 *Inoue T, Kudo M, Hatanaka K et al.* Imaging of hepatocellular carcinoma: qualitative and quantitative analysis of postvascular phase contrast-enhanced ultrasonography with sonazoid. Comparison with superparamagnetic iron oxide magnetic resonance images. Oncology 2008; 75 (Suppl 1): 48 – 54
67 *Jain A, Reyes J, Kashyap R et al.* Long-term survival after liver transplantation in 4,000 consecutive patients at a single center. Ann Surg 2000; 232: 490 – 500
68 *Jang HJ, Kim TK, Burns PN et al.* Enhancement patterns of hepatocellular carcinoma at contrast-enhanced US: comparison with histologic differentiation. Radiology 2007; 244: 898 – 906
69 *Jarnagin WR, Bach AM, Winston CB et al.* What is the yield of intraoperative ultrasonography during partial hepatectomy for malignant disease? J Am Coll Surg 2001; 192: 577 – 583
70 *Kessler T, Bayer M, Schwoppe C et al.* Compounds in clinical Phase III and beyond. Recent Results Cancer Res 2010; 180: 137 – 163
71 *Khawaja OA, Shaikh KA, Al-Mallah MH.* Meta-analysis of adverse cardiovascular events associated with echocardiographic contrast agents. Am J Cardiol 2010; 106: 742 – 747
72 *Kisaka Y, Hirooka M, Kumagi T et al.* Usefulness of contrast-enhanced ultrasonography with abdominal virtual ultrasonography in assessing therapeutic response in hepatocellular carcinoma treated with radiofrequency ablation. Liver Int 2006; 26: 1241 – 1247
73 *Konopke R, Bunk A, Kersting S.* Contrast-enhanced ultrasonography in patients with colorectal liver metastases after chemotherapy. Ultraschall in Med 2008; 29 (Suppl 4): S203 – S209
74 *Konopke R, Kersting S, Bergert H et al.* Contrast-enhanced ultrasonography to detect liver metastases: A prospective trial to compare transcutaneous unenhanced and contrast-enhanced ultrasonography in patients undergoing laparotomy. Int J Colorectal Dis 2007; 22: 201 – 207
75 *Korenaga K, Korenaga M, Furukawa M et al.* Usefulness of Sonazoid contrast-enhanced ultrasonography for hepatocellular carcinoma: comparison with pathological diagnosis and superparamagnetic iron oxide magnetic resonance images. J Gastroenterol 2009; 44: 733 – 741
76 *Kudo M.* The 2008 Okuda lecture: Management of hepatocellular carcinoma: from surveillance to molecular targeted therapy. J Gastroenterol Hepatol 2010; 25: 439 – 452
77 *Kudo M, Hatanaka K, Kumada T et al.* Double-contrast ultrasound: a novel surveillance tool for hepatocellular carcinoma. Am J Gastroenterol 2011a; 106: 368 – 370
78 *Kudo M, Hatanaka K, Maekawa K.* Newly developed novel ultrasound technique, defect reperfusion ultrasound imaging, using sonazoid in the management of hepatocellular carcinoma. Oncology 2010; 78 (Suppl 1): 40 – 45
79 *Kudo M, Izumi N, Kokudo N et al.* Management of hepatocellular carcinoma in Japan: Consensus-Based Clinical Practice Guidelines proposed by the Japan Society of Hepatology (JSH) 2010 updated version. Dig Dis 2011b; 29: 339 – 364
80 *Kudo M, Okanoue T.* Management of hepatocellular carcinoma in Japan: consensus-based clinical practice manual proposed by the Japan Society of Hepatology. Oncology 2007; 72 (Suppl 1): 2 – 15
81 *Kurt M, Shaikh KA, Peterson L et al.* Impact of contrast echocardiography on evaluation of ventricular function and clinical management in a large prospective cohort. J Am Coll Cardiol 2009; 53: 802 – 810
82 *Lamuraglia M, Escudier B, Chami L et al.* To predict progression-free survival and overall survival in metastatic renal cancer treated with sorafenib: pilot study using dynamic contrast-enhanced Doppler ultrasound. Eur J Cancer 2006; 42: 2472 – 2479
83 *Langnas AN, Marujo W, Stratta RJ et al.* Vascular complications after orthotopic liver transplantation. Am J Surg 1991; 161: 76 – 82; discussion 83
84 *Larsen LP, Rosenkilde M, Christensen H et al.* The value of contrast enhanced ultrasonography in detection of liver metastases from colorectal cancer: a prospective double-blinded study. Eur J Radiol 2007; 62: 302 – 307
85 *Lassau N, Chami L, Chebil M et al.* Dynamic contrast-enhanced ultrasonography (DCE-US) and anti-angiogenic treatments. Discov Med 2011; 11: 18 – 24
86 *Lassau N, Chami L, Koscielny S et al.* Quantitative functional imaging by Dynamic Contrast Enhanced Ultrasonography (DCE- US) in GIST patients treated with masatinib. Invest New Drugs 2012; 30: 765 – 771
87 *Lassau N, Koscielny S, Albiges L et al.* Metastatic renal cell carcinoma treated with sunitinib: early evaluation of treatment response using dynamic contrast-enhanced ultrasonography. Clin Cancer Res 2010a; 16: 1216 – 1225
88 *Lassau N, Koscielny S, Chami L et al.* Advanced Hepatocellular Carcinoma: Early Evaluation of Response to Bevacizumab Therapy at Dynamic Contrast-enhanced US with Quantification–Preliminary Results. Radiology 2010b; 258: 291 – 300
89 *Lassau N, Lamuraglia M, Chami L et al.* Gastrointestinal stromal tumors treated with imatinib: monitoring response with contrast-enhanced sonography. Am J Roentgenol 2006; 187: 1267 – 1273
90 *Leen E, Ceccotti P, Moug SJ et al.* Potential value of contrast-enhanced intraoperative ultrasonography during partial hepatectomy for metastases: an essential investigation before resection? Ann Surg 2006; 243: 236 – 240
91 *Lencioni R, Llovet JM.* Modified RECIST (mRECIST) assessment for hepatocellular carcinoma. Semin Liver Dis 2010; 30: 52 – 60
92 *Leoni S, Piscaglia F, Golfieri R et al.* The impact of vascular and nonvascular findings on the noninvasive diagnosis of small hepatocellular

carcinoma based on the EASL and AASLD criteria. Am J Gastroenterol 2010; 105: 599 – 609
93 *Li N, Ding H, Fan P et al.* Intrahepatic transit time predicts liver fibrosis in patients with chronic hepatitis B: quantitative assessment with contrast-enhanced ultrasonography. Ultrasound Med Biol 2010; 36: 1066 – 1075
94 *Lim AK, Taylor-Robinson SD, Patel N et al.* Hepatic vein transit times using a microbubble agent can predict disease severity non-invasively in patients with hepatitis C. Gut 2005; 54: 128 – 133
95 *Liu GJ, Lu MD, Xie XY et al.* Real-time contrast-enhanced ultrasound imaging of infected focal liver lesions. J Ultrasound Med 2008a; 27: 657 – 666
96 *Liu JB, Wansaicheong G, Merton DA et al.* Canine prostate: contrast-enhanced US-guided radiofrequency ablation with urethral and neurovascular cooling–initial experience. Radiology 2008b; 247: 717 – 725
97 *Liu Z, Lobo SM, Humphries S et al.* Radiofrequency tumor ablation: insight into improved efficacy using computer modeling. Am J Roentgenol 2005; 184: 1347 – 1352
98 *Livraghi T, Goldberg SN, Lazzaroni S et al.* Hepatocellular carcinoma: radio-frequency ablation of medium and large lesions. Radiology 2000; 214: 761 – 768
99 *Lu Q, Zhong XF, Huang ZX et al.* Role of contrast-enhanced ultrasound in decision support for diagnosis and treatment of hepatic artery thrombosis after liver transplantation. Eur J Radiol 2012; 81: e338 – e343
100 *Luo Y, Fan YT, Lu Q et al.* CEUS: a new imaging approach for postoperative vascular complications after right-lobe LDLT. World J Gastroenterol 2009; 15: 3670 – 3675
101 *Main ML, Goldman JH, Grayburn PA.* Ultrasound contrast agents: balancing safety versus efficacy. Expert Opin Drug Saf 2009; 8: 49 – 56
102 *Main ML, Ryan AC, Davis TE et al.* Acute mortality in hospitalized patients undergoing echocardiography with and without an ultrasound contrast agent (multicenter registry results in 4,300,966 consecutive patients). Am J Cardiol 2008; 102: 1742 – 1746
103 *Mandry D, Bressenot A, Galloy MA et al.* Contrast-enhanced ultrasound in fibro-lamellar hepatocellular carcinoma: a case report. Ultraschall in Med 2007; 28: 547 – 552
104 *Maruyama H, Takahashi M, Ishibashi H et al.* Ultrasound-guided treatments under low acoustic power contrast harmonic imaging for hepatocellular carcinomas undetected by B-mode ultrasonography. Liver Int 2009; 29: 708 – 714
105 *Matsui O.* Detection and characterization of hepatocellular carcinoma by imaging. Clin Gastroenterol Hepatol 2005; 3: S136 – S140
106 *Mazzoni G, Napoli A, Mandetta S et al.* Intra-operative ultrasound for detection of liver metastases from colorectal cancer. Liver Int 2008; 28: 88 – 94
107 *Minami Y, Kudo M, Chung H et al.* Contrast harmonic sonography-guided radiofrequency ablation therapy versus B-mode sonography in hepatocellular carcinoma: prospective randomized controlled trial. Am J Roentgenol 2007; 188: 489 – 494
108 *Moriyasu F, Itoh K.* Efficacy of perflubutane microbubble-enhanced ultrasound in the characterization and detection of focal liver lesions: phase 3 multicenter clinical trial. Am J Roentgenol 2009; 193: 86 – 95
109 *Mork H, Ignee A, Schuessler G et al.* Analysis of neuroendocrine tumour metastases in the liver using contrast enhanced ultrasonography. Scand J Gastroenterol 2007; 42: 652 – 662
110 *Nakano H, Ishida Y, Hatakeyama T et al.* Contrast-enhanced intraoperative ultrasonography equipped with late Kupffer-phase image obtained by sonazoid in patients with colorectal liver metastases. World J Gastroenterol 2008; 14: 3207 – 3211
111 *Omata M, Lesmana LA, Tateishi R et al.* Asian Pacific Association for the Study of the Liver consensus recommendations on hepatocellular carcinoma. Hepatol Int 2010; 4: 439 – 474
112 *Peronneau P, Lassau N, Leguerney I et al.* Contrast ultrasonography: necessity of linear data processing for the quantification of tumor vascularization. Ultraschall in Med 2010; 31: 370 – 378
113 *Piscaglia F, Bolondi L.* The safety of Sonovue in abdominal applications: retrospective analysis of 23188 investigations. Ultrasound Med Biol 2006; 32: 1369 – 1375
114 *Piscaglia F, Corradi F, Mancini M et al.* Real time contrast enhanced ultrasonography in detection of liver metastases from gastrointestinal cancer. BMC Cancer 2007; 7: 171
115 *Piscaglia F, Gianstefani A, Ravaioli M et al.* Criteria for diagnosing benign portal vein thrombosis in the assessment of patients with cirrhosis and hepatocellular carcinoma for liver transplantation. Liver Transpl 2010; 16: 658 – 667
116 *Piscaglia F, Nolsoe C, Dietrich CF et al.* The EFSUMB Guidelines and Recommendations on the Clinical Practice of Contrast Enhanced Ultrasound (CEUS): update 2011 on non-hepatic applications. Ultraschall in Med 2011; 33: 33 – 59
117 *Piskunowicz M, Kosiak W, Irga N.* Primum non nocere? Why can't we use second generation ultrasound contrast agents for the examination of children? Ultraschall in Med 2011; 32: 83 – 86
118 *Qiang L, Yan L, Chao-Xin Y et al.* Value of contrast enhanced intraoperative ultrasound for cirrhotic patients with hepatocellular carcinoma. A report of 20 cases. World J Gastroenterol 2008; 14: 4005 – 4010
119 *Quaia E, D'Onofrio M, Palumbo A et al.* Comparison of contrast-enhanced ultrasonography versus baseline ultrasound and contrast-enhanced computed tomography in metastatic disease of the liver: diagnostic performance and confidence. Eur Radiol 2006; 16: 1599 – 1609
120 *Ridolfi F, Abbattista T, Marini F et al.* Contrast-enhanced ultrasound to evaluate the severity of chronic hepatitis C. Dig Liver Dis 2007; 39: 929 – 935
121 *Rossi S, Rosa L, Ravetta V et al.* Contrast-enhanced versus conventional and color Doppler sonography for the detection of thrombosis of the portal and hepatic venous systems. Am J Roentgenol 2006; 186: 763 – 773
122 *Sangiovanni A, Manini MA, Iavarone M et al.* The diagnostic and economic impact of contrast imaging techniques in the diagnosis of small hepatocellular carcinoma in cirrhosis. Gut 2010; 59: 638 – 644
123 *Sasaki A, Kai S, Iwashita Y et al.* Microsatellite distribution and indication for locoregional therapy in small hepatocellular carcinoma. Cancer 2005; 103: 299 – 306
124 *Scheele J, Stang R, Altendorf-Hofmann A et al.* Resection of colorectal liver metastases. World J Surg 1995; 19: 59 – 71
125 *Schlottmann K, Klebl F, Zorger N et al.* Contrast-enhanced ultrasound allows for interventions of hepatic lesions which are invisible on conventional B-mode. Z Gastroenterol 2004; 42: 303 – 310
126 *Schuessler G, Fellbaum C, Fauth F et al.* The infammatory pseudotumour – an unusual liver tumour. Ultraschall in Med 2006; 27: 273 – 279
127 *Seitz K, Bernatik T, Strobel D et al.* Contrast-enhanced ultrasound (CEUS) for the characterization of focal liver lesions in clinical practice (DEGUM Multicenter Trial): CEUS vs. MRI – a prospective comparison in 269 patients. Ultraschall in Med 2010; 31: 492 – 499
128 *Seitz K, Greis C, Schuler A et al.* Frequency of tumor entities among liver tumors of unclear etiology initially detected by sonography in the noncirrhotic or cirrhotic livers of 1349 patients. Results of the DEGUM multicenter study. Ultraschall in Med 2011; 32: 598 – 603
129 *Shaw AS, Ryan SM, Beese RC et al.* Ultrasound of non-vascular complications in the post liver transplant patient. Clin Radiol 2003; 58: 672 – 680
130 *Shiozawa K, Watanabe M, Takayama R et al.* Evaluation of local recurrence after treatment for hepatocellular carcinoma by contrast-enhanced ultrasonography using Sonazoid: comparison with dynamic computed tomography. J Clin Ultrasound 2010; 38: 182 – 189
131 *Sidhu PS, Shaw AS, Ellis SM et al.* Microbubble ultrasound contrast in the assessment of hepatic artery patency following liver transplantation: role in reducing frequency of hepatic artery arteriography. Eur Radiol 2004; 14: 21 – 30
132 *Simpson DH, Chin CT, Burns PN.* Pulse inversion Doppler: a new method for detecting nonlinear echoes from microbubble contrast agents. IEEE Trans on Ultrasonics, Ferroelectrics, and Freq Control 1999; 46: 372 – 382
133 *Skyba DM, Price RJ, Linka AZ et al.* Direct in vivo visualization of intravascular destruction of microbubbles by ultrasound and its local effects on tissue. Circulation 1998; 98: 290 – 293
134 *Sorrentino P, D'Angelo S, Tarantino L et al.* Contrast-enhanced sonography versus biopsy for the differential diagnosis of thrombosis in hepatocellular carcinoma patients. World J Gastroenterol 2009; 15: 2245 – 2251
135 *Strobel D, Kleinecke C, Hansler J et al.* Contrast-enhanced sonography for the characterisation of hepatocellular carcinomas–correlation with histological differentiation. Ultraschall in Med 2005; 26: 270 – 276
136 *Strobel D, Seitz K, Blank W et al.* Contrast-enhanced ultrasound for the characterization of focal liver lesions–diagnostic accuracy in clinical practice (DEGUM multicenter trial). Ultraschall in Med 2008; 29: 499 – 505

137 *Su HL, Qian YQ, Wei ZR et al.* Real-time myocardial contrast echocardiography in rat: infusion versus bolus administration. Ultrasound Med Biol 2009; 35: 748 – 755
138 *Szabo T.* Diagnostic Ultrasound Imaging. Insite Out (Biomedical Engineering) ISBN 0125801452. Ed./Academic Press 2004
139 *Therasse P, Arbuck SG, Eisenhauer EA et al.* New guidelines to evaluate the response to treatment in solid tumors. European Organization for Research and Treatment of Cancer, National Cancer Institute of the United States, National Cancer Institute of Canada. J Natl Cancer Inst 2000; 92: 205 – 216
140 *Tiemann K, Lohmeier S, Kuntz S et al.* Real-time contrast echo assessment of myocardial perfusion at low emission power: First experimental and clinical results using power pulse inversion imaging. Echocardiography 1999; 16: 799 – 809
141 *Torzilli G, Del Fabbro D, Palmisano A et al.* Contrast-enhanced intraoperative ultrasonography during hepatectomies for colorectal cancer liver metastases. J Gastrointest Surg 2005; 9: 1148 – 1153; discussion 53-54
142 *Torzilli G, Del Fabbro D, Palmisano A et al.* Contrast-enhanced intraoperative ultrasonography: a valuable and not any more monocentric diagnostic technique performed in different ways. Ann Surg 2007; 245: 152 – 153; author reply 153.
143 *Trillaud H, Bruel JM, Valette PJ et al.* Characterization of focal liver lesions with SonoVue-enhanced sonography: international multicenter-study in comparison to CT and MRI. World J Gastroenterol 2009; 15: 3748 – 3756
144 *Vilana R, Forner A, Bianchi L et al.* Intrahepatic peripheral cholangiocarcinoma in cirrhosis patients may display a vascular pattern similar to hepatocellular carcinoma on contrast-enhanced ultrasound. Hepatology 2010; 51: 2020 – 2029
145 *Wang Z, Xu HX, Xie XY et al.* Imaging features of hepatic angiomyolipomas on real-time contrast-enhanced ultrasound. Br J Radiol 2010; 83: 411 – 418
146 *Wei K, Jayaweera AR, Firoozan S et al.* Quantification of myocardial blood flow with ultrasound-induced destruction of microbubbles administered as a constant venous infusion. Circulation 1998; 97: 473 – 483
147 *Wilson SR, Burns PN.* An algorithm for the diagnosis of focal liver masses using microbubble contrast-enhanced pulse-inversion sonography. Am J Roentgenol 2006; 186: 1401 – 1412
148 *Wilson SR, Kim TK, Jang HJ et al.* Enhancement patterns of focal liver masses: discordance between contrast-enhanced sonography and contrast-enhanced CT and MRI. Am J Roentgenol 2007; 189: W7 – W12
149 World Health Organisation Offset Publication. WHO Handbook for Reporting Results of Cancer Treatment. Geneva, Switzerland: ISBN 92 4 170048 3. Ed World Health Organisation, 1979.
150 *Wu W, Chen MH, Yin SS et al.* The role of contrast-enhanced sonography of focal liver lesions before percutaneous biopsy. Am J Roentgenol 2006; 187: 752 – 761
151 *Xu HX, Liu GJ, Lu MD et al.* Characterization of small focal liver lesions using real-time contrast- enhanced sonography: diagnostic performance analysis in 200 patients. J Ultrasound Med 2006a; 25: 349 – 361
152 *Xu HX, Lu MD, Liu GJ et al.* Imaging of peripheral cholangiocarcinoma with low-mechanical index contrast-enhanced sonography and SonoVue: initial experience. J Ultrasound Med 2006b; 25: 23 – 33
153 *Yanagisawa K, Moriyasu F, Miyahara T et al.* Phagocytosis of ultrasound contrast agent microbubbles by Kupffer cells. Ultrasound Med Biol 2007; 33: 318 – 325
154 *Zheng RQ, Mao R, Ren J et al.* Contrast-enhanced ultrasound for the evaluation of hepatic artery stenosis after liver transplantation: potential role in changing the clinical algorithm. Liver Transpl 2010; 16: 729 – 735

J Gastroenterol (2013) 48:247–253
DOI 10.1007/s00535-012-0626-8

ORIGINAL ARTICLE—LIVER, PANCREAS, AND BILIARY TRACT

Toll-like receptor activation in basophils contributes to the development of IgG4-related disease

Tomohiro Watanabe · Kouhei Yamashita · Toshiharu Sakurai · Masatoshi Kudo · Masahiro Shiokawa · Norimitsu Uza · Yuzo Kodama · Kazushige Uchida · Kazuichi Okazaki · Tsutomu Chiba

Received: 17 January 2012 / Accepted: 11 June 2012 / Published online: 29 June 2012

Abstract
Background IgG4-related disease (IRD) is characterized by systemic IgG4 antibody responses and by infiltration of IgG4-expressing plasma cells into the affected organs. Although T helper type 2 (Th2) cytokines are implicated in enhanced IgG4 responses, molecular mechanisms accounting for the development of IgG4 antibody responses are poorly defined. Since basophils function as antigen-presenting cells for Th2 responses, we tried to clarify the role of basophils in the development of IgG4 responses in this study.
Methods IgG4 and cytokine responses to various nucleotide-binding oligomerization domain-like receptor and Toll-like receptor (TLR) ligands were examined by using basophils isolated from healthy controls and from patients with IgG4-related disease.
Results Activation of TLRs in basophils from healthy controls induced IgG4 production by B cells, which effect was associated with enhanced production of B cell activating factor (BAFF) and IL-13. In addition, activation of TLRs in basophils from patients with IRD induced a large amount of IgG4 by B cells from healthy controls. This enhancement of IgG4 production was again associated with BAFF and IL-13.
Conclusions These data suggest that innate immune responses mediated through TLRs may play a role in the development of IgG4-related disease, in part by production of BAFF from basophils.

Keywords IgG4-related disease · Basophil · TLR

Abbreviations

Ab	Antibody
Ag	Antigen
AIP	Autoimmune pancreatitis
APC	Antigen-presenting cell
BAFF	B cell activating factor
ELISA	Enzyme-linked immunosorbent assay
IRD	IgG4-related disease
LPS	Lipopolysaccharide
MDP	Muramyl dipeptide
NOD2	Nucleotide-binding oligomerization domain 2
NLR	NOD-like receptor
PAM	Pam_3CSK4
PBMC	Peripheral blood mononuclear cell
PGN	Peptidoglycan
TLR	Toll-like receptor
TSLP	Thymic stromal lymphopoietin

T. Watanabe
Center for Innovation in Immunoregulative Technology and Therapeutics, Kyoto University Graduate School of Medicine, Kyoto, Japan

T. Watanabe (✉) · M. Shiokawa · N. Uza · Y. Kodama · T. Chiba
Department of Gastroenterology and Hepatology, Kyoto University Graduate School of Medicine, 54 Shogoin Kawahara-cho, Sakyo-ku, Kyoto 606-8507, Japan
e-mail: tmhrwtnb@kuhp.kyoto-u.ac.jp

K. Yamashita
Department of Hematology and Oncology, Kyoto University Graduate School of Medicine, Kyoto, Japan

T. Sakurai · M. Kudo
Department of Gastroenterology and Hepatology, Kinki University Graduate School of Medicine, Osakasayama, Japan

K. Uchida · K. Okazaki
Third Department of Internal Medicine, Kansai Medical University, Moriguchi, Japan

Introduction

IgG4-related disease (IRD) is a newly proposed disease entity that is diagnosed based on enhanced systemic IgG4 antibody (Ab) responses [1, 2]. Patients with IRD exhibit a variety of symptoms associated with pancreatitis, cholangitis, sialoadenitis, nephritis, retroperitoneal fibrosis and inflammatory psuedotumors [1]. Thus, a variety of clinical manifestations related to involvement of multiple organs is one of the characteristic findings in patients with IRD. Importantly, infiltration of IgG4-expressing plasma cells is seen in the affected organs of IRD, which suggests possible involvement of systemic and local IgG4 responses in the pathophysiology of IRD [1].

Although autoimmune responses are considered to be involved in the development of IRD, the pathogenic antigens (Ags) have not been identified in this disorder. Given the fact that a significant population of patients with autoimmune pancreatitis (AIP), pancreatic manifestation of IRD, have a diagnosis of inflammatory bowel disease (IBD), the development and progression of which requires excessive immune reactions to intestinal microflora [3, 4], it is possible that enhanced immune responses toward microbial Ags underlie the immuno-pathogenesis of IRD. Compatible to this idea, we have previously shown that activation of toll-like receptors (TLRs) and nucleotide-binding oligomerization domain (NOD)-like receptors (NLRs) in monocytes by microbial Ags induce IgG4 production through activation of B cell-activation factor (BAFF)-mediated signaling pathways [5]. Thus, our previous data show the involvement of activation of TLRs and NLRs in the immunopathogeneis of IRD.

IgG4 production is regulated by T helper type 2 (Th2) cytokines such as IL-4, IL-10, and IL-13 [6]. Antigen-presenting cells (APCs) and T cells produce these Th2 cytokines to induce IgG4 secretion by B cells. Although basophils have been considered as Th2 effector cells, recent studies have now defined the role of basophils in the initiation of Th2 responses [7, 8]. Exposure of basophils to microbial Ags and protease allergen induce production of Th2 cytokines and BAFF, both of which are necessary for IgG production [9–11]. Therefore, it is possible that activation of basophils via microbial Ags contributes to the development of IRD via production of Th2 cytokines and BAFF.

In this study, we addressed the role of basophils in the development of IRD. Here we show evidence that basophil activation of TLRs enhances production of IgG4 from B cells in a BAFF-dependent manner. In addition, we found that basophils from patients with IRD induce IgG4 production from B cells more efficiently than those from healthy controls upon stimulation with TLR ligands. Thus, we propose that activation of TLRs in basophils contributes to the development of IRD.

Materials and methods

Stimulation of cells with microbial Ags

Basophils and B cells were isolated from peripheral blood mononuclear cells (PBMCs) by using a human basophil isolation kit (Miltenyi Biotech, Auburn, CA) and anti-CD19 microbead (Miltenyi Biotech), respectively. Basophils (1×10^6/mL) and $CD19^+$ B cells (1×10^6/mL) were stimulated with FK156 (Astellas, Tokyo, Japan, 20 μg/mL), muramyl dipeptide (MDP; 20 μg/mL, InvivoGen, San Diego, CA), Pam_3CSK4 (PAM; 10 μg/mL, InvivoGen), and lipopolysaccharide (LPS; 1 μg/mL, Sigma-Aldrich, St. Louis, MO) as described previously [5]. In some experiments, isolated cell populations were cultured with the indicated doses of a neutralizing anti-BAFF monoclonal Ab (R&D Systems, Minneapolis, MN), or anti-IL-13 monoclonal Ab (Pharmingen, San Jose, CA) or mouse IgG control Ab (eBioscience, San Diego, CA). Culture supernatants were collected at the indicated time points.

Enzyme-linked immunosorbent assays

Culture supernatants were assayed for the measurement of IL-8, IL-13, BAFF, and thymic stromal lymphopoietin (TSLP) by using enzyme linked immno-sorbent assay (ELISA) kits (Pharmingen, eBioscience) [5]. The production of IgG1, IgG4, IgE was determined by ELISAs as described previously [5].

Fluorescence-activated cell sorter analysis

Cells were pre-incubated with Fc-blocking solution (Miltenyi Biotech), stained with fluorescein isothiocyanate (FITC)-conjugated anti-human CD123 (Biolegend, San Diego, CA) and phycoerythrin-labeled anti-human CD203c, TLR2, and TLR4 (eBioscience). Stained cells were analyzed on an Accuri C6 cytometer (Accuri Cytometers, Ann Arbor, MI).

Studies using peripheral blood cells from patients

Ethical permission for this study was granted by the review board of Kyoto University. Healthy controls ($n = 8$) and treatment-naïve patients with IRD ($n = 5$) were enrolled in this study after informed consent was obtained. Basophils and $CD19^+$ B cells were isolated from the patients and stimulated with microbial Ags as described above. In some experiments, a neutralizing anti-BAFF monoclonal antibody (R&D systems) or mouse IgG control antibody (eBioscience) was used as described previously [5].

Statistical analysis

The Student's t test was used to evaluate statistical significance. A value of $p < 0.05$ was regarded as statistically significant.

Results

Activation of TLRs in basophils induces IgG4 production by B cells

Th2 responses are implicated in the development of IRD since Th2 cytokines such as IL-4, IL-10, and IL-13 enhance IgG4 production from B cells [6]. Although basophils have recently been identified as APCs necessary for optimal Th2 responses [7, 8], the role played by basophils in the development of IRD remains largely unknown. Our previous studies suggest possible involvement of TLR and NLR ligands in the immuno-pathogenesis of IRD. Given the fact that human primary basophils express functional TLRs [11], we investigated whether innate immune responses mediated by activation of TLRs and NLRs in basophils are involved in the development of IgG4 responses. To this end, basophils isolated from PBMCs from healthy controls were co-cultured with $CD19^+$ B cells in the presence of various TLR and NLR ligands (FK156, NOD1 ligand; MDP, NOD2 ligand; Pam_3CSK4, TLR2 ligand; LPS, TLR4 ligand) for 7 days. The purity of basophils, which are positive for CD203c and CD123 (IL-3Rα), are more than 90 % (Fig. 1a). As shown in Fig. 1b, stimulation of basophils with TLR2 and TLR4 ligands induced the production of IgG4, but not IgG1, by B cells in the absence of T cells. In contrast, the activation of NOD1 and NOD2 in basophils did not induce the production of IgG1 or IgG4. Thus, these data suggest that activation of TLR2 and TLR4 enhances the IgG4 response rather than the IgG1 response in a T cell-independent manner.

Activation of TLRs enhances production of BAFF and IL-13 by basophils

We next examined the effects of TLRs activation on mediator release and cytokine production by basophils. As shown in Fig. 2, basophils secret significant amounts of IL-8 upon stimulation with NOD1, TLR2, and TLR4 ligands. Th2 cytokines and BAFF are involved in the production of IgG4 [5, 6]. Consequently, we investigated whether NLR and TLR ligands induce these cytokines associated with IgG4 responses. TLR4 activation by LPS induced production of IL-13 and BAFF by basophils (Fig. 2a). In contrast, stimulation of basophil by LPS did not lead to the secretion of other Th2 cytokines such as IL-4 and TSLP. Similar results were obtained in basophils stimulated with PAM although not statistically significant. Thus, these data suggest that TLR4 activation in basophils induces production of BAFF and IL-13.

Activation of TLRs in basophils enhances IgG4 production via BAFF signaling pathways

We next addressed whether IgG4 production induced by basophil activation of TLRs depends upon signaling pathways via BAFF and/or IL-13. To this end, neutralizing Abs against BAFF and/or IL-13 were added to the co-culture containing $CD19^+$ B cells and basophils. Blockade of BAFF-signaling, but not IL-13 signaling, reduced IgG4 production induced by TLR4 activation in basophils (Fig. 2b). In contrast, neutralization of BAFF or IL-13 signaling did not change IgG1 production (data not shown). These data suggest that TLR4 activation of basophils induces IgG4 production by B cells via BAFF signaling pathways.

Basophils from patients with IgG4-related disease induces IgG4 production by B cells upon stimulation with TLR ligands

As mentioned above, we identified a novel pathway of TLR-mediated IgG4 production by utilizing peripheral blood basophils and B cells from healthy controls. To establish the significance of this finding in the immuno-pathogenesis of IRD, we compared the immune responses of basophils from patients with IgG4-related AIP with those from healthy controls. Three patients enrolled in this study met the criteria for the diagnosis of AIP [1] and were diagnosed with lymphoplasmacytic sclerosing pancreatitis type. These patients enrolled in this study show increased serum levels of IgG4 (948, 469, 262 mg/dL, normal range 4.8–105 mg/dL). For this purpose, basophils isolated from four healthy controls and three patients were co-cultured with $CD19^+$ B cells from healthy controls in the presence of MDP, PAM, and LPS. As shown in Fig. 3a, basophils from patients with IgG4-related AIP enhanced production of IgG1 and IgG4 by healthy $CD19^+$ B cells upon stimulation with TLR2 and TLR4 ligands as compared with basophils from healthy controls. It should be noted that induction of IgG4 production by patients' basophils was much greater than that of IgG1 production. This enhanced IgG4 production by patients' basophils was associated with increased production of BAFF and IL-13 (Fig. 3b). We also measured serum levels of BAFF and IL-13 in these patients. Although serum levels of IL-13 were below the detection limit in both patients and healthy controls, serum levels of BAFF were higher in patients as compared with those in healthy controls (patients versus controls,

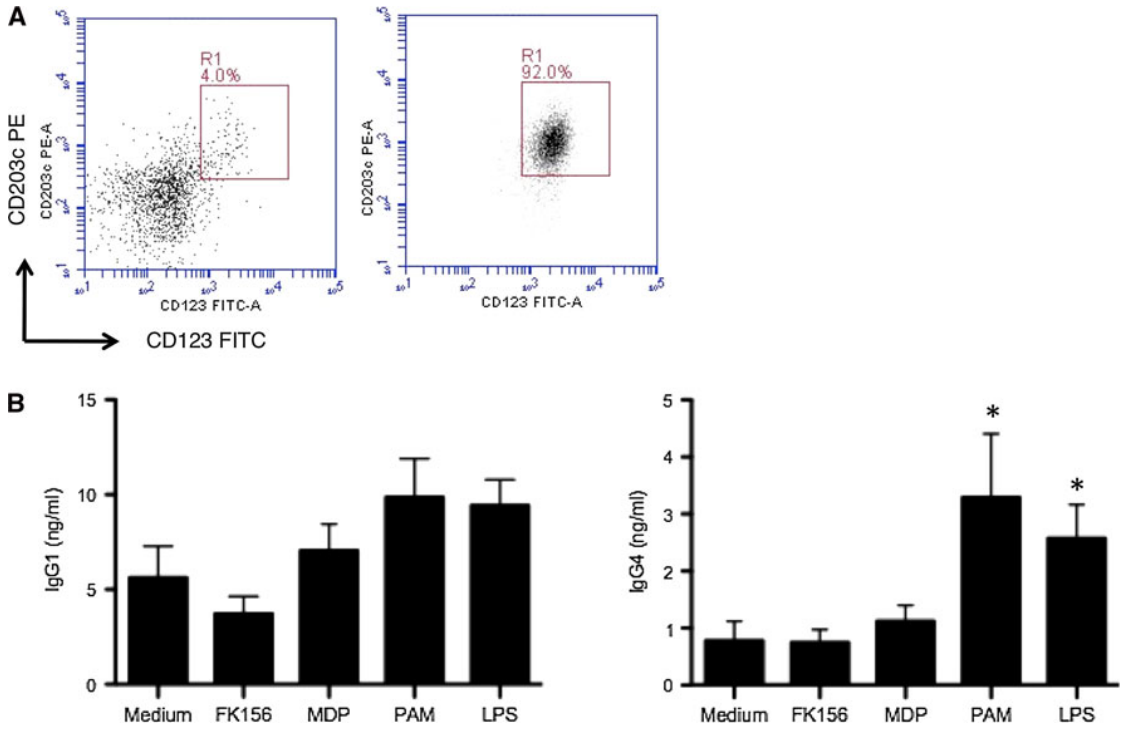

Fig. 1 Activation of TLRs in basophils enhances IgG4 production by the B cells. **a** Basophils were isolated from PBMCs from the healthy controls. The percentages of the basophils expressing CD203c and CD123 are shown in the plots (*left* before separation; *right* after separation). **b** The $CD19^+$ B cells (1×10^6/mL) from the healthy controls ($n = 4$) were co-cultured for 7 days with the basophils (1×10^6/mL) in the presence of FK156 (20 μg/mL), MDP (20 μg/mL), PAM (10 μg/mL), and LPS (1 μg/mL). The culture supernatants were analyzed for the production of IgG1 and IgG4. The results are expressed as mean ± SE. *$p < 0.05$, as compared with the medium alone

mean + standard deviation, 2.274 + 1.119 vs. 0.751 + 0.535 ng/mL).

BAFF-mediated signaling pathways are involved in IgG4 production induced by basophils from IRD patients

Finally, we addressed whether induction of IgG4 production by baosphils from IRD patients depends upon BAFF-mediated signaling pathways. As shown in Fig. 4, abrogation of BAFF signaling by its neutralizing Ab inhibited the production of IgG4. Thus, these data suggest that activation of TLRs in patients' basophils triggers IgG4 production by healthy $CD19^+$ B cells through signaling pathways mediated by BAFF.

Discussion

In this study we have reported that activation of TLRs in basophils induces IgG4 production by B cells through signaling pathways mediated by BAFF. More importantly, a marked increase in IgG4 production by healthy B cells is seen when B cells are co-cultured with basophils isolated from patients with IRD in the presence of TLR ligands as compared with those from healthy controls. Thus, these data suggest possible involvement of TLRs activation in basophils in the development of IRD. In our previous study, we showed that activation of NOD2 and TLRs in monocytes is involved in enhanced IgG4 responses in patients with IRD [5]. Our previous and present studies suggest that ligation of TLRs play roles in the development of enhanced IgG4 responses through activation of two different innate immune cells; monocytes and basophils. Interestingly, activation of these two different innate immune cells leads to T cell-independent IgG4 responses via BAFF-mediated signaling pathways, which highlights the importance of BAFF in the development of IRD. Therefore, two distinct innate immune cells utilize BAFF-mediated signaling pathways to achieve enhanced IgG4 production.

We previously showed that NOD2 activation in monocytes leads to a T cell-independent IgG4 production via BAFF-mediated signaling pathways [5]. Thus, BAFF-mediated signaling pathways induce T cell-independent IgG4 production either by activation of TLRs in basophils or by that of NOD2 in monocytes. Although serum levels of BAFF are higher in patients with IRD [12],

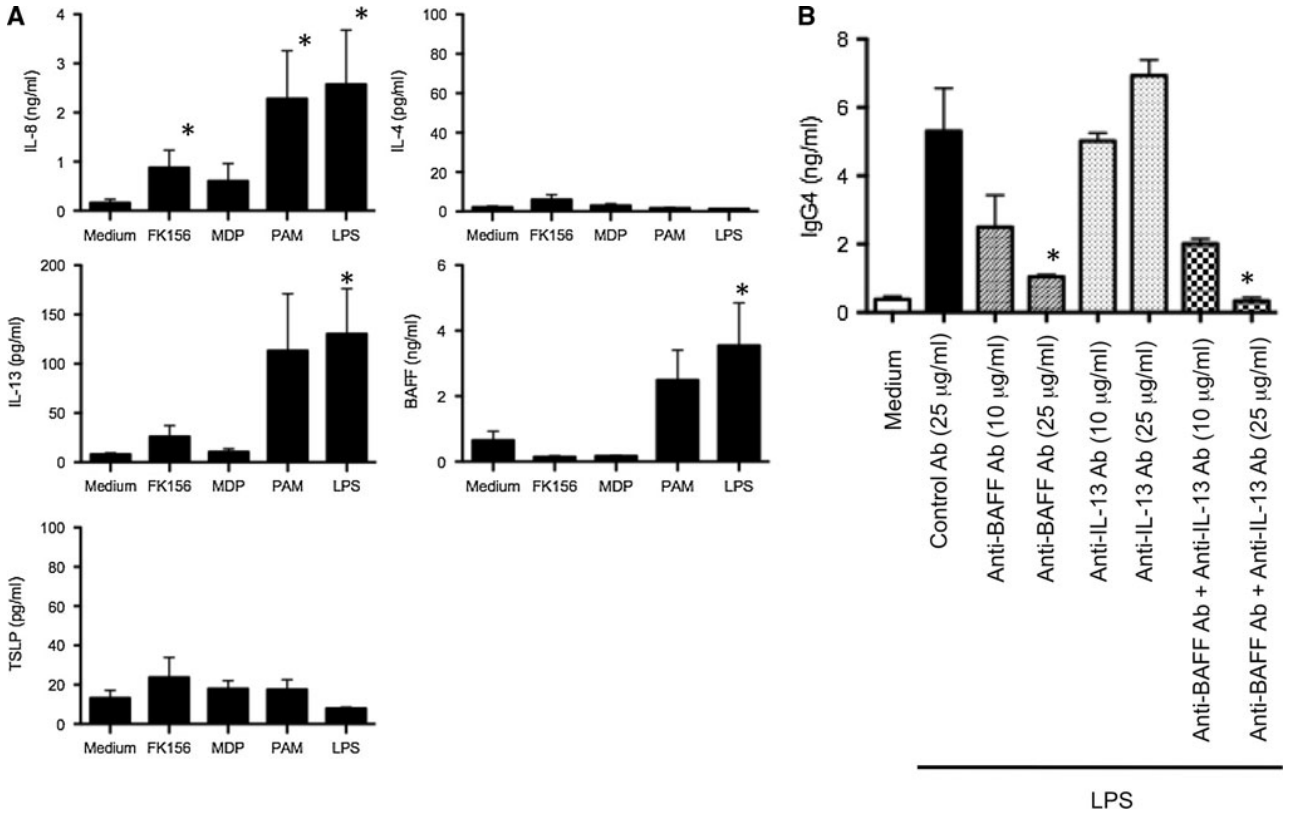

Fig. 2 Basophils produce IL-13 and BAFF upon stimulation with TLR ligands. **a** The basophils isolated from the PBMCs of the healthy controls ($n = 4$, 1×10^6/mL) were stimulated with the NLR and TLR ligands for 24 h as shown in Fig. 1. The culture supernatants were analyzed for the production of IL-8, IL-4, IL-13, BAFF, and TSLP. The results are expressed as mean ± SE. $^*p < 0.05$, as compared with the medium alone. **b** The $CD19^+$ B cells (1×10^6/mL) from the healthy controls ($n = 2$) were co-cultured for 7 days with basophils (1×10^6/mL) in the presence of LPS (1 μg/mL). The neutralizing Abs against BAFF and/or IL-13 were added to the co-culture. The culture supernatants were analyzed for the production of IgG4. The results are expressed as mean ± SE. $^*p < 0.05$, as compared with the control Ab

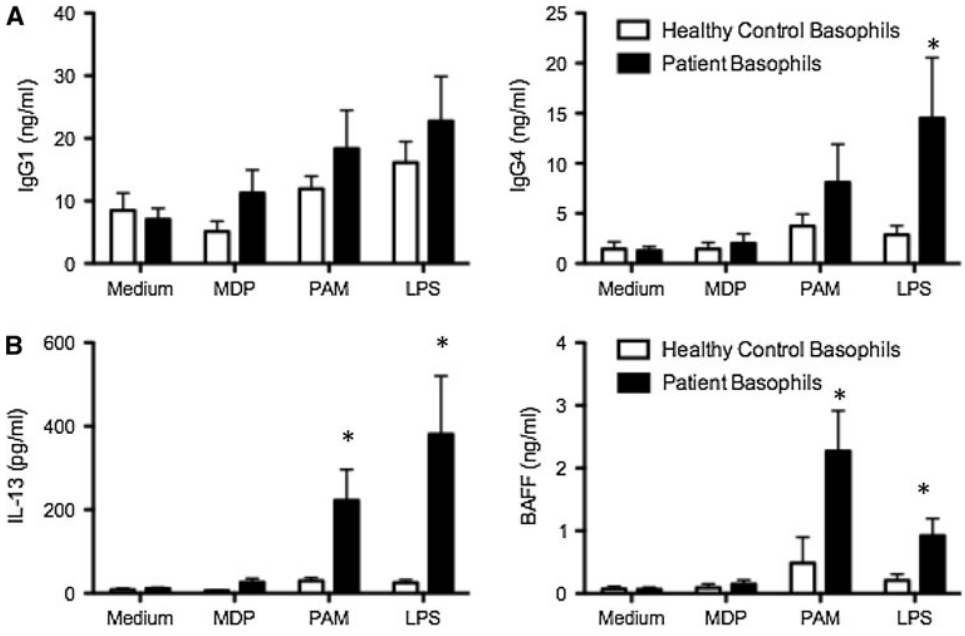

Fig. 3 Basophils isolated from the patients with IgG4-related AIP induce IgG4 production upon stimulation with TLR ligands by the B cells from the healthy controls. The $CD19^+$ B cells (1×10^6/mL) from the healthy controls ($n = 4$) were co-cultured with the basophils (1×10^6/mL) from the controls ($n = 4$) or the patients ($n = 3$) with IgG4-related AIP in the presence of MDP (20 μg/mL), PAM (10 μg/mL) or LPS (1 μg/mL) for 7 days. The culture supernatants obtained on day 7 were assayed for the presence of IgG1 (**a**), IgG4 (**a**), IL-13 (**b**), and BAFF (**b**). The results are expressed as means ± SE. $^*p < 0.05$, as compared with the culture conditions using the basophils from the healthy controls

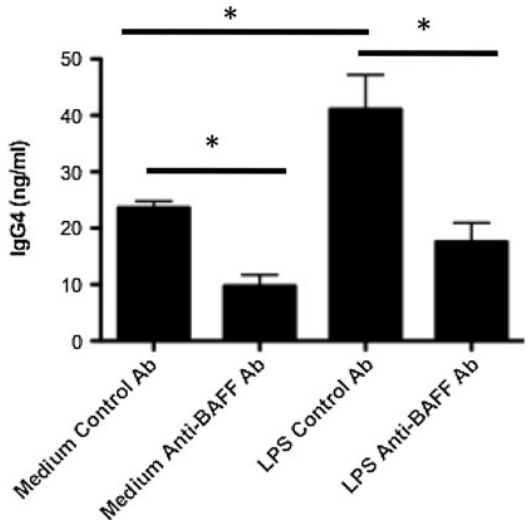

Fig. 4 BAFF-mediated IgG4 production by basophils from patients with IgG4-realted disease. The $CD19^+$ B cells (1×10^6/mL) from the healthy controls ($n = 2$) were co-cultured with the basophils (1×10^6/mL) from the patients ($n = 2$) with IgG4-related disease in the presence of LPS (1 μg/mL) for 7 days. The culture supernatants obtained on day 7 were assayed for the presence of IgG4. The neutralizing Ab against BAFF (25 μg/mL) was added to the co-culture. The results are expressed as means ± SE. $*p < 0.05$

the mechanisms accounting for enhanced BAFF production have been poorly understood. Our data suggest that activation of TLRs and NLRs in monocytes and basophils induces BAFF production and thereby causes systemic IgG4 responses. As for the mechanisms for enhanced BAFF production by monocytes, our previous study clearly shows that activation of NOD2 induces BAFF production via NF-κB-dependent signaling pathways [5]. It remains unknown whether BAFF production by basophils from IRD patients also requires activation of NF-κB as in the case of monocytes. Alternatively, circulating IgD may enhance BAFF production by basophils since binding of IgD to basophils induces the secretion of pro-inflammatory cytokines such as BAFF and IL-4 [9]. Further studies are necessary to elucidate the molecular mechanisms accounting for enhanced BAFF production by basophils isolated from IRD patients.

Although basophils have been considered as effectors cells for allergic Th2-IgE responses, recent studies show evidence that basophils with the ability to produce Th2 cytokines and to present Ags are inducers for these allergic reactions [7]. Thus, generation of allergic Th2-IgE responses depends upon activation of basophils not only at the effector phase but also at the induction phase. Patients with IRD often exhibit enhanced serum levels of IgE associated Th2 responses [2]. In this study, we clearly showed that activation of TLRs in basophils from IRD patients induce IgG4 production by B cells from healthy controls. Therefore, it is possible that microbial Ags trigger production of IgG4 and IgE through TLR activation in baosphils. However, we failed to detect IgE production (data not shown). This preferential induction of IgG4 responses rather than IgE responses by TLRs-activated basophils can be partially explained by the lack of IL-4 and TSLP production, both of which are necessary for IgE production [13, 14].

One question arising from the present study is the sites where basohil activation of TLRs occur. Given the fact that the mucosa of the gastrointestinal (GI) tract is always exposed to intestinal microflora [4, 15], it is possible that TLR ligands derived from intestinal microflora activate basophils in GI tract. Thus, the GI tract is one possible induction site for the development of systemic IgG4 responses. However, clinical analysis of patients with AIP show poor association between IgG4-related AIP and IBD [16], the latter of which requires excessive innate immune responses against intestinal microflora for the development of inflammation. In this regard, several mechanisms for preventing hyper-responsiveness to TLR ligands operate in the gut [4, 15]. Therefore, one possible explanation is that pathogenic immune reactions causing inflammation are suppressed in the gut by regulatory mechanisms whereas such reactions cause tissue injury in the other sterile organs such as pancreas and bile duct due to the lack of regulatory mechanisms. Confirmation of this idea awaits further investigation of immune responses occurring in the GI tract of patients with IRD.

In conclusion, it is important to note that the findings shown here have certain implications both with respect to possible mechanisms of IRD and with respect to a possible new approach to the treatment of this disease. Activation of TLR2 and TLR4 in basophils enhances IgG4 Ab responses by B cells from healthy controls and IRD, which suggests that abnormal innate immune responses through TLRs may be involved in the development of IRD. With respect to treatment, a link between BAFF and IgG4 implies that patients with IRD may be treated with the inhibition of BAFF signaling.

Acknowledgments This work is supported in part by grants from the Ministry of Education, Science and Culture, Japan, and the Japan Society for the Promotion of Science (21590532); Takeda Science Foundation; Astellas Foundation for Research on Metabolic Disorders; Yakult Bioscience Foundation; Cell Science Research Foundation; Kato Memorial Trust for Nambyo Research; Pancreas Research Foundation of Japan; Uehara Memorial Foundation (to T. W.); and Health and Labour Sciences Research Grants for research on intractable diseases from the Ministry of Health, Labour and Welfare of Japan (to T. C.).

Conflict of interest The authors have declared no conflicts of interest.

References

1. Okazaki K, Kawa S, Kamisawa T, et al. Japanese clinical guidelines for autoimmune pancreatitis. Pancreas. 2009;38: 849–66.
2. Masaki Y, Dong L, Kurose N, et al. Proposal for a new clinical entity, IgG4-positive multiorgan lymphoproliferative syndrome: analysis of 64 cases of IgG4-related disorders. Ann Rheum Dis. 2009;68:1310–5.
3. Ravi K, Chari ST, Vege SS, et al. Inflammatory bowel disease in the setting of autoimmune pancreatitis. Inflamm Bowel Dis. 2009;15:1326–30.
4. Strober W, Murray PJ, Kitani A, et al. Signalling pathways and molecular interactions of NOD1 and NOD2. Nat Rev Immunol. 2006;6:9–20.
5. Watanabe T, Yamashita K, Fujikawa S, et al. Activation of Toll-like receptors and NOD-like receptors is involved in enhanced IgG4 responses in autoimmune pancreatitis. Arthritis Rheum. 2012;64:914–24.
6. Jeannin P, Lecoanet S, Delneste Y, et al. IgE versus IgG4 production can be differentially regulated by IL-10. J Immunol. 1998;160:3555–61.
7. Sokol CL, Medzhitov R. Role of basophils in the initiation of Th2 responses. Curr Opin Immunol. 2010;22:73–7.
8. Paul WE, Zhu J. How are T(H)2-type immune responses initiated and amplified? Nat Rev Immunol. 2010;10:225–35.
9. Chen K, Xu W, Wilson M, et al. Immunoglobulin D enhances immune surveillance by activating antimicrobial, proinflammatory and B cell-stimulating programs in basophils. Nat Immunol. 2009;10:889–98.
10. Phillips C, Coward WR, Pritchard DI, et al. Basophils express a type 2 cytokine profile on exposure to proteases from helminths and house dust mites. J Leukoc Biol. 2003;73:165–71.
11. Bieneman AP, Chichester KL, Chen YH, et al. Toll-like receptor 2 ligands activate human basophils for both IgE-dependent and IgE-independent secretion. J Allergy Clin Immunol. 2005;115: 295–301.
12. Yamanishi H, Kumagi T, Yokota T, et al. Clinical significance of B cell-activating factor in autoimmune pancreatitis. Pancreas. 2011;40:840–5.
13. Siracusa MC, Saenz SA, Hill DA, et al. TSLP promotes interleukin-3-independent basophil haematopoiesis and type 2 inflammation. Nature. 2011;477:229–33.
14. Watanabe T, Katsukura H, Shirai Y, et al. Helper CD4+ T cells for IgE response to a dietary antigen develop in the liver. J Allergy Clin Immunol. 2003;111:1375–85.
15. Strober W, Fuss I, Mannon P. The fundamental basis of inflammatory bowel disease. J Clin Invest. 2007;117:514–21.
16. Sah RP, Chari ST, Pannala R, et al. Differences in clinical profile and relapse rate of type 1 versus type 2 autoimmune pancreatitis. Gastroenterology 2010;139:140–8 (quiz e12–3).

Dig Dis Sci (2013) 58:381–388
DOI 10.1007/s10620-012-2342-x

ORIGINAL ARTICLE

Heat Shock Protein 27 Expression is Inversely Correlated with Atrophic Gastritis and Intraepithelial Neoplasia

Yoshiaki Nagata · Masatoshi Kudo · Tomoyuki Nagai · Tomohiro Watanabe · Masanori Kawasaki · Yutaka Asakuma · Satoru Hagiwara · Naoshi Nishida · Shigenaga Matsui · Hiroshi Kashida · Toshiharu Sakurai

Received: 10 June 2012 / Accepted: 25 July 2012 / Published online: 11 August 2012

Abstract
Background Intestinal-type gastric carcinomas progress through several sequential steps, including atrophic gastritis, intestinal metaplasia, dysplasia, and cancer.
Aim We investigated heat shock protein 27 (HSP27) expression in gastric neoplasia and background gastric mucosa to assess its involvement in gastric carcinogenesis.
Methods We used real-time quantitative polymerase chain reaction to examine HSP27 expression in gastric neoplasias and background gastric mucosae of 30 patients with intraepithelial neoplasias and in gastric mucosae of 30 patients without gastric neoplasia. Immunohistochemical staining was performed on 30 advanced gastric cancer tissues.
Results HSP27 expression was negatively associated with atrophic gastritis. HSP27 expression in the background gastric mucosa of neoplasia-bearing patients was significantly lower than in the mucosa of those without gastric neoplasia. In tumor necrosis factor α-treated gastric cancer cells, HSP27 knockdown increased cell death and accumulation of the reactive oxygen species that link inflammation to cancer. Poorly differentiated tumors most frequently had high HSP27 levels. Dedifferentiation of cancer cells is associated with an epithelial–mesenchymal transition (EMT) signaling pathway. In gastric cancer MKN-1 cells, HSP27 knockdown upregulated E-cadherin and downregulated vimentin and smooth muscle actin, but this did not occur in MKN-74 cells.
Conclusion HSP27 expression in gastric mucosae is inversely correlated with intraepithelial neoplasia, a probable precursor to gastric cancer, and HSP27 expression in cancer is positively correlated with poor differentiation.

Keywords Gastric cancer · HSP27 · ROS
Inflammation · Atrophic gastritis · EMT · Stem cell

Introduction

The incidence of gastric cancer has decreased over the past few decades [1]. However, gastric adenocarcinoma remains one of the most frequent causes of cancer-related death worldwide [2]. Because it is frequently diagnosed late, it is associated with significant mortality. Overall 5-year survival for this type of cancer is only 35–45 % [3, 4]. Survival can only be improved if the disease is diagnosed early, because endoscopic or surgical resection can be curative when performed at an early stage. Therefore, it is important that new biomarkers are established to identify patients who are at high risk and to diagnose gastric cancer early.

In the Correa model, the currently accepted model of intestinal-type gastric carcinogenesis, development of intestinal-type gastric cancer is preceded by a number of sequential steps. These steps are atrophic gastritis, followed by intestinal metaplasia, dysplasia, and invasive neoplasia.

Electronic supplementary material The online version of this article (doi:10.1007/s10620-012-2342-x) contains supplementary material, which is available to authorized users.

Y. Nagata · M. Kudo · T. Nagai · M. Kawasaki · Y. Asakuma · S. Hagiwara · N. Nishida · S. Matsui · H. Kashida · T. Sakurai (✉)
Department of Gastroenterology and Hepatology, Faculty of Medicine, Kinki University, 377-2, Ohno-Higashi, Osaka-Sayama, Osaka 589-8511, Japan
e-mail: sakurai@med.kindai.ac.jp

T. Watanabe
Center for Innovation in Immunoregulative Technology and Therapeutics, Kyoto University Graduate School of Medicine, 54 Kawahara-cho, Shogoin, Sakyo-ku, Kyoto 606-8507, Japan

Atrophic gastritis is characterized by the atrophy of gastric mucosa because of chronic inflammation. Chronic inflammation and oxidative stress are related to human cancers as a result of the production of reactive oxygen species (ROS) by inflammatory cells such as neutrophils, eosinophils, and macrophages [5]. The ROS induce necrosis of neighboring cells, leading to further ROS accumulation and greater inflammatory response. Oxidative stress has many effects, including alteration of gene expression [6], an increase in cell death, and increased proliferation and induction of DNA mutation [7]. Although chronic inflammation may act as an initiator of gastric carcinogenesis, via the induction of oxidative stress, little is known about the molecular link between chronic gastritis and gastric cancer.

Tissue homeostasis in multicellular organisms requires a balance between cell death and proliferation. Homeostatic imbalance leads to many pathological conditions, for example chronic inflammation and cancer. Cellular necrosis leads to oxidative stress and a strong inflammatory response [8]. Recent studies suggest that IL-1α acts as a mediator that monitors signals from necrotic cells and induces the recruitment of inflammatory cells to the site of injury [9, 10]. In adults, cancer frequently develops in the setting of chronic inflammation, conditions in which epithelial cells are killed and inflammatory cells are activated to produce cytokines that drive the compensatory proliferation of surviving cells. Although the precise molecular effect of chronic inflammation in the pathogenesis of cancer remains to be fully elucidated, it is likely to promote cancer development through cycles of cell death and compensatory proliferation [11, 12]. For instance, increased epithelial cell death in inhibitor of NF kappa-B kinase subunit beta (IKK-β) null mice increases the rate of gastric carcinogenesis. Early induction of cell death may drive the development of gastric cancer via increased inflammatory-cell infiltration and ROS accumulation [13].

Heat shock protein 27 (HSP27), a stress-induced molecular chaperone, has been reported to inhibit ROS accumulation [14, 15]. HSP27 is highly and uniformly expressed in cancers [16], and its level of expression is associated with metastasis and poor prognosis [17–20]. Although several mechanisms have been proposed to explain the effect of HSP27 on the promotion and progression events of carcinogenesis, including enhanced motility and invasion [21, 22] and inhibition of cell death [23, 24], little is known about the function of HSP27 in the gastric epithelial cell at the initiation of gastric carcinogenesis. Given the critical function of HSP27 in protecting the stomach mucosa [25], we hypothesized that HSP27 may attenuate cell death and ROS accumulation in the gastric mucosa, and subsequently have a protective effect against gastric carcinogenesis. Thus, we investigated expression of HSP27 in the background gastric mucosa of patients with and without gastric intraepithelial neoplasia, the potential precursor to gastric cancer, using real-time quantitative polymerase chain reaction (qPCR) to evaluate the relevance of HSP27 to the development of gastric cancer. The HSP27 level in background gastric mucosa was significantly lower in patients with atrophic gastritis and neoplasia than in those without them. HSP27 may be a biomarker of gastric cancer risk and a promising target for cancer prevention.

Materials and Methods

Patients

From April 2010 to October 2011, 231 patients underwent endoscopic and surgical curative resection for gastric carcinoma at Kinki University School of Medicine. None of these patients had been subjected previously to any other form of therapy, for example radiation or chemotherapy. Thirty sample pairs of neoplasia and adjacent non-neoplastic tissue, and 30 gastric mucosa specimens from patients without neoplasia were obtained by endoscopy. These patients were selected from among those who had given informed consent to use of the tissue collected from them, and were matched by age and gender with controls. All non-cancerous tissues were obtained more than 3 cm away from any tumors.

Patients with advanced gastric cancer were assigned to 1 of 2 groups that were matched by age and gender. One group contained 15 patients with intestinal-type (differentiated) carcinoma; the other group contained 15 patients with diffuse-type (poorly differentiated, signet-ring cell) carcinoma. The extent of tumor cell differentiation was assessed by use of Laurens's classification [26]. Upper gastrointestinal tract biopsy with culture or urea breath test was used to diagnose *Helicobacter pylori* (*H. pylori*) infection. The median level of HSP27 mRNA, as determined by real-time qPCR, was used to distinguish low and high-expression groups. The study protocols conformed to the guidelines of the 1975 Declaration of Helsinki and were approved by the institutional review boards of Kinki University.

Biochemical and Immunochemical Analysis

We used previously described methods for real time qPCR, immunoblotting, and immunohistochemical analysis [10]. Antibodies used were: anti-poly (ADP-ribose) polymerase (PARP; Santa Cruz Biotechnology, CA, USA), anti-α-smooth muscle actin (α-SMA; Dako, Glostrup, Denmark), anti-actin (Sigma, St Louis, MO, USA), anti-vimentin (Cell Signaling, Danvers, MA, USA), anti-E-cadherin (Cell

Signaling), anti-caspase 3 (Cell Signaling) and anti-HSP27 (Cell Signaling). Immunohistochemistry was performed by use of ABC staining kits (Vector Laboratory, Burlingame, CA, USA), in accordance with manufacturer's recommendations. HSP27 immunoreactivity was coded as follows: no positive cells (−), 1–25 % positive cells (+), 26–75 % positive cells (++), >75 % positive cells (+++). Protein carbonylation, a major form of protein oxidation, was analyzed by use of the Oxiselect protein carbonyl immunoblot kit (Cell Biolabs, San Diego, CA, USA), in accordance with the manufacturer's instructions. To evaluate signal intensity, western blot image data were quantified by use of Image J software (NIH, Bethesda, MD, USA).

Cell Culture

MKN-1 and MKN-74 cells were derived from adenosquamous carcinomas and differentiated adenocarcinomas, respectively. We used these two cell lines because they express HSP27. These cells were seeded in Dulbecco's Modified Eagle Medium (Gibco Invitrogen, Carlsbad, CA, USA) supplemented with 100 U/mL penicillin, 100 μg/mL streptomycin (Gibco), and 10 % fetal bovine serum. Cells were cultured at 37 °C under 5 % CO_2/95 % ambient air. HSP27 siRNA duplexes that target the sequences sense, 5′-UGAGAGACUGCCGCCAAGUAA-3′, and antisense, 5′-UUACUU GGCGGCAGUCUCAUU-3′, were synthesized by Genedesign (Osaka, Japan). MKN-1 and MKN-74 cells were transfected with HSP27 siRNA or non-targeting siRNA as a negative control (Fig. 2a). siRNA was transfected by use of Lipofectamine RNAiMAX reagent (Invitrogen). Twenty-four hours after transfection, cells were treated with tumor necrosis factor (TNF)-α (50 ng/mL) plus cycloheximide (10 μg/mL) to induce cell death. The number of viable cells was estimated by trypan blue extraction 24 h after exposure to the stressors and the number of untreated cells was given an arbitrary value of 1. To assess the causal link between HSP27 and dedifferentiation of cancer cells, we investigated the effect of HSP27 on the epithelial–mesenchymal transition (EMT). Transforming growth factor (TGF)-β, epidermal growth factor (EGF), fibroblast growth factor (FGF), and hepatocyte growth factor (HGF) are well-known inducers of EMT. Therefore, we treated MKN-1 and MKN-74 cells with TGF-β, EGF, FGF, or HGF (10 ng/mL) for 72 h and EMT was evaluated by western blot analysis.

Statistical Analysis

Data are presented as mean ± SEM. Differences were analyzed by use of Fisher's exact test or Student's t test. p values <0.05 were considered significant.

Table 1 Characteristics of patients with and without intraepithelial neoplasia

Variable	Patients without neoplasia ($n = 30$)	Patients with neoplasia ($n = 30$)	p value
Age-years	69.0 ± 1.40	69.4 ± 1.76	Matched
Sex-no. (%)			Matched
Male	23	23	
Female	7	7	
Atrophic gastritis			0.014
Mild	11	3	
Moderate	14	13	
Severe	5	14	
H. pylori infection			0.064
Negative	16	8	
Positive	14	22	
HSP27 expression			0.037
Low	12	21	
High	18	9	

The median value of HSP27 mRNA level, as determined by real time-qPCR, was used as a cut-off between the low and high-expression groups

Results

HSP27 Expression Was Inversely Related to Atrophic Gastritis and Intraepithelial Neoplasia

The initiating molecular events in gastric carcinogenesis are not completely known. To assess the effect of HSP27 on the initiation of gastric carcinogenesis, we examined the relationship between HSP27 expression in background gastric mucosa and the presence of intraepithelial neoplasia. The level of expression of HSP27 in background gastric mucosa was significantly lower in neoplasia-bearing patients than in patients without gastric neoplasia (Fig. 1a, Table 1; $p = 0.004$). c-Jun N-terminal kinase (JNK) activation and cytokine, for example interleukin (IL)-1β, IL-6 and TNFα production, have been reported to have crucial involvement in carcinogenesis [10, 12, 13, 27]. There was no difference in the expression of c-Jun (a downstream molecule of JNK), IL-1β, IL-6, or TNFα between neoplasia-bearing patients and those without gastric neoplasia (Fig. 1a). Cell proliferation is involved inextricably in the development of cancer. In human gastric mucosa, there was no significant relationship between HSP27 and cyclin D or E expression (data not shown).

Embryonic stem cells are defined as cells that have the ability to perpetuate themselves by self-renewal and to generate mature cells of a particular tissue by differentiation [28]. Cancer stem cells have been suggested to have characteristics similar to those of embryonic stem cells.

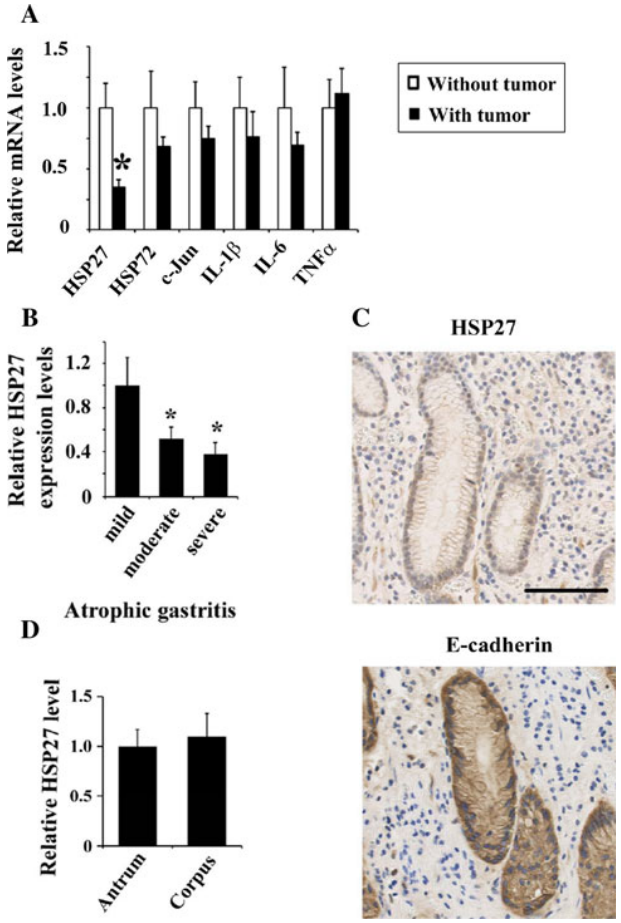

Fig. 1 HSP27 expression was inversely related to the presence of gastric neoplasia. **a** By real-time qPCR, mRNA levels of the indicated genes were quantified in the non-neoplastic gastric tissues of patients with intraepithelial neoplasias (*with tumor*) and in the gastric mucosae of those without gastric neoplasia (*without tumor*). Results are reported as the mean ± SEM. *$p < 0.05$ vs control. **b** mRNA levels of HSP27 in the gastric mucosae of patients with mild, moderate, and severe atrophic gastritis were quantified by real-time qPCR. *$p < 0.05$ vs mild atrophic gastritis. **c** Expression of HSP27 and E-cadherin, a marker for epithelial cells, in non-cancerous gastric tissue. Many epithelial cells were stained immunohistochemically with anti-HSP27 antibody, and a few non-epithelial cells were stained. **d** mRNA levels of HSP27 in the antrum and the corpus mucosae of the same patients were quantified by real-time qPCR

The stemness factors Sox2, Oct-4, and Nanog are associated with induced pluripotent stem cells. Some studies have suggested that these factors may be involved in human malignancy [29]. Therefore, we investigated the relationship between HSP27 and the stemness factors Sox2, Oct-4, and Nanog in human gastric mucosa by real-time qPCR. No significant association between them was found (data not shown).

One of the most frequently mentioned risk factors for gastric cancer development is atrophic gastritis because of *H. pylori* infection, which is consistent with our results (Table 1). We found a significant inverse relationship between HSP27 expression and severity of atrophic gastritis, but not between HSP27 expression and *H. pylori* infection (Table 2, Fig. 1b and Supplementary Table; $p = 0.015$). The significant relationship between the level of HSP27 expression in background gastric mucosa and the presence of atrophic gastritis and neoplasia was independent of *H. pylori* infection. As shown in Fig. 1c, HSP27 was mainly expressed in the epithelial cells of gastric mucosae which are positive for E-cadherin. Type B gastritis is a common type of atrophic gastritis in which more severe atrophy is present in the antrum than in the corpus mucosa. To assess the relationship between HSP27 expression and mucosal atrophy, we compared HSP27 expression in the antrum and corpus of the same patients. No significant difference in the level of expression of HSP27 was found between in the two regions (Fig. 1d). These data suggest that reduced HSP27 levels do not result from mucosal atrophy itself.

Table 2 Association between HSP27 expression and atrophic gastritis

	Atrophic gastritis			*p* value
	Mild	Moderate	Severe	
HSP27 expression				0.015
Low	4	15	15	
High	10	12	4	
H. pylori infection				0.057
Negative	11	14	5	
Positive	5	12	13	

The median value of HSP27 mRNA level, as determined from real time-qPCR, was used as a cut-off between the low and high-expression groups

HSP27 Prevented TNFα-Mediated Cell Death and ROS Accumulation in Gastric Cancer Cells

HSP27 has been shown to interact and inhibit components of both stress-induced and receptor-induced apoptotic pathways. HSP27 prevents the activation of caspases by sequestering cytochrome c in the cytoplasm [30]. Expression of TNFα was higher in neoplasia-bearing patients than in those without gastric neoplasia (Fig. 1a). We investigated whether HSP27 might provide a protection against TNFα in gastric cancer cells. As shown in Fig. 2b, TNFα induced significantly more cell death in HSP27 knockdown cells than in controls (MKN1, $p = 0.0005$; MKN74, $p = 0.017$). TNFα-treated HSP27 knockdown cells accumulated significantly more ROS than controls (Fig. 2c; MKN1, $p = 0.0012$; MKN74, $p = 0.0001$). Proteolytic cleavage of PARP and caspase 3 is a characteristic of apoptosis. There was slightly more PARP cleavage in TNFα-treated HSP27 knockdown cells than in controls and no difference in caspase 3 cleavage between TNFα-treated HSP27 knockdown

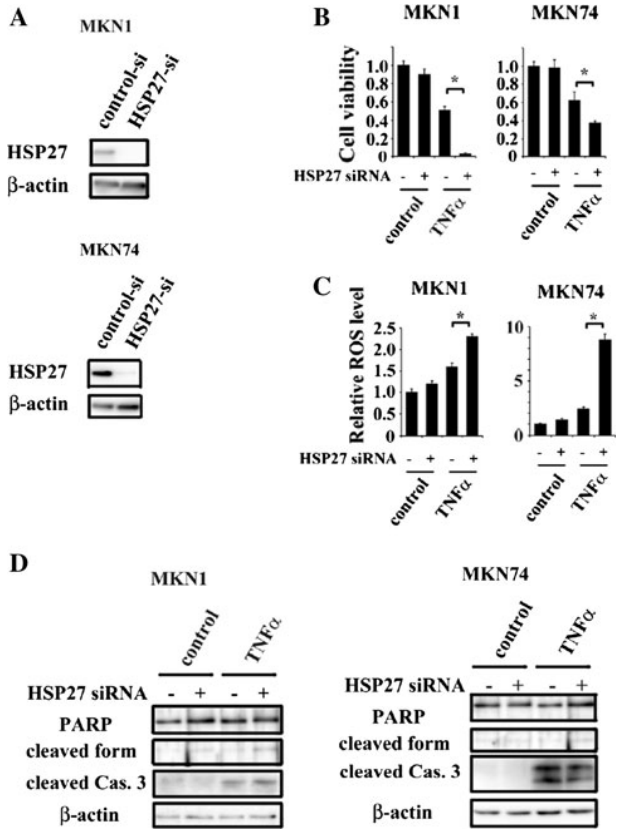

Fig. 2 HSP27 prevented TNFα-mediated cell death and ROS accumulation in gastric cancer cells. **a** MKN-1 and MKN-74 cells were transfected with HSP27 siRNA or non-targeting siRNA as negative control. Homogenates of cells were extracted 24 h after transfection, electrophoresed, and immunoblotted with anti-HSP27 antibody. **b**, **c** MKN1 and MKN74 cells were transfected with HSP27 siRNA or non-targeting siRNA. Culture with media that contained TNF-α (50 ng/mL) plus cycloheximide (10 μg/mL) was initiated 24 h after transfection. The number of viable cells was estimated by trypan blue extraction 24 h after exposure to the stressors and the number of untreated cells was given an arbitrary value of 1 (**b**). At 18 h after exposure to the stressors, protein carbonylation of cell lysate was examined by use of Oxiselect kits and the level of untreated controls was given an arbitrary value of 1 (**c**). Results are presented as mean ± SEM. $*p < 0.05$ vs control. **d** The protein levels of the uncleaved and cleaved forms of PARP and the cleaved form of caspase 3 (*Cas. 3*) were analyzed by western blotting

cells and controls (Fig. 2d), suggesting that HSP27 knock-down induces necrosis and apoptosis. HSP27 knock-down did not affect cell proliferation as assessed by trypan blue dye exclusion and MTT assays (data not shown).

Tumor Histology Grade Was Significantly Associated with HSP27 Expression

The level of HSP27 expression in the intraepithelial neoplasia was slightly higher than in the corresponding non-tumorous mucosa as assessed by real-time qPCR (Fig. 3). Next, we performed immunohistochemistry on 30 advanced gastric

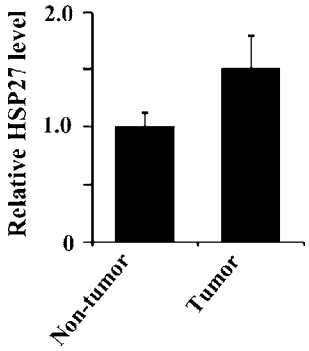

Fig. 3 Level of HSP27 expression in the intraepithelial neoplasia was slightly higher than in the corresponding non-tumorous mucosa. mRNA levels of HSP27 in intraepithelial neoplastic (*Tumor*) and non-neoplastic gastric tissues (*Non-tumor*) of the same patients were quantified by real-time qPCR

cancer tissues. HSP27 immunoreactivity occurred in 83.3 % (25 of 30) of gastric cancer specimens and 46.6 % (14 of 30) of the corresponding non-cancerous gastric mucosal specimens from 30 patients with advanced gastric cancer. The distribution of HSP27 expression in intestinal-type and diffuse-type carcinomas is reported in Fig. 4a–e and Table 3. We found significantly greater expression of HSP27 in diffuse-type (poorly differentiated) carcinomas than in intestinal-type (better differentiated) carcinomas ($p = 0.01$).

HSP27 Was Critical for EMT in Gastric Cancer MKN-1 Cells but Not in MKN-74 Cells

Because HSP27 expression was significantly higher in poorly differentiated gastric cancer than in better differentiated adenocarcinoma (Fig. 4, Table 3), we examined whether HSP27 is related to dedifferentiation of cancer cells. Epithelial–mesenchymal transition (EMT), defined as switching of polarized epithelial cells to a migratory fibroblastoid phenotype, is involved in dedifferentiation of cancer cells [31]. Western blot analysis revealed a decrease in E-cadherin level and an increase in SMA, vimentin, and HSP27 levels when MKN-1 cells were treated with TGF-β, an inducer of EMT (Fig. 5a). HSP27 expression is not associated with EMT induction in MKN74 cells (Fig. 5a). In MKN-1 cells, HSP27 knockdown resulted in an increase in E-cadherin level and a decrease in vimentin and SMA levels (Fig. 5b). In contrast, in MKN74 cells, there were no significant changes in E-cadherin, vimentin, or SMA levels (Fig. 5b). This implies that HSP27 modulates EMT in MKN-1 cells but not in MKN-74 cells.

Discussion

The gastrointestinal tract is continuously exposed to injurious agents that can lead to cellular stress and trigger

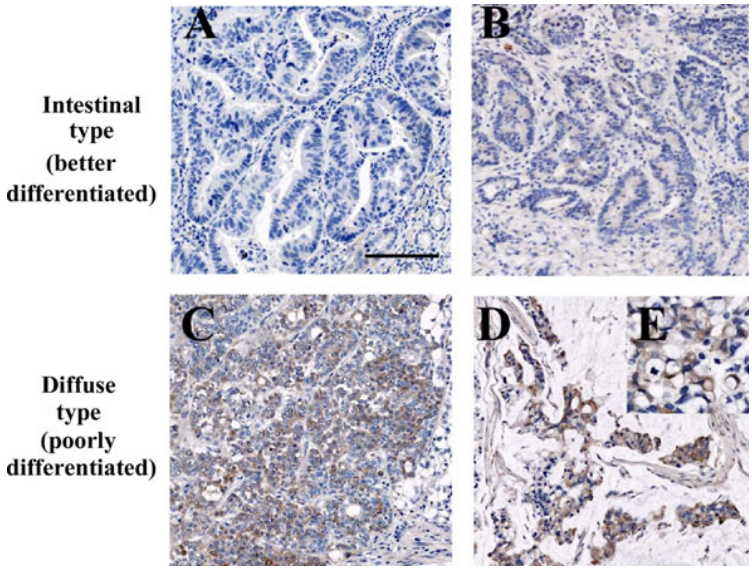

Fig. 4 Tumor histology grade was significantly associated with HSP27 expression. Representative immunostaining images of intestinal-type carcinoma (**a**, **b**) and diffuse-type carcinoma (**c**–**e**) are shown. *Scale bar* 100 μm

Table 3 HSP27 Expression in gastric cancer samples and its relationship to tumor differentiation

Histologic grade	Immunostaining distribution of HSP27				*p* value
	−	+	++	+++	
Intestinal type (better differentiated)	7	5	3	0	0.010
Diffuse type (poorly differentiated)	1	3	6	5	

HSP27 immunoreactivity was assessed as follows: −, no positive cells; +, 1–25 % positive cells; ++, 26–75 % positive cells; +++, >75 % positive cells

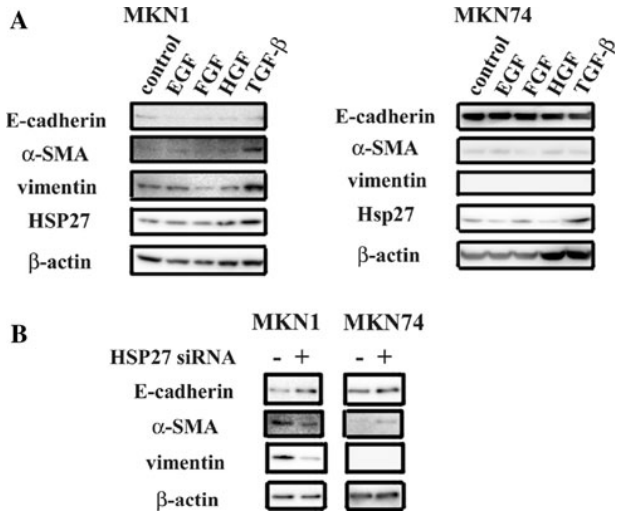

Fig. 5 HSP27 was critical for EMT in gastric cancer MKN-1 cells but not in MKN-74 cells. Representative western blots evaluating EMT and HSP27 are shown. **a** MKN-1 and MKN-74 cells treated with TGF-*β*, EGF, FGF, or HGF (10 ng/mL) for 72 h. Homogenates of cells were electrophoresed and immunoblotted with the indicated antibodies. **b** MKN-1 and MKN-74 cells were transfected with siRNA against HSP27 or control siRNA. Twenty-four hours after transfection, cell lysates were extracted and immunoblotted with the indicated antibodies

epithelial damage and cell death. The manner of epithelial cell death can be determined from cell morphology and intracellular signaling pathways [32]. Apoptosis is a naturally occurring form of cell death that can be initiated via either extrinsic or intrinsic pathways. In contrast, cellular necrosis lacks the features of apoptosis or autophagy and does not occur normally [33]. Cellular necrosis is induced by a variety of external factors, and typically leads to oxidative stress and a strong inflammatory response [8]. Recent studies suggest that IL-1α acts as a mediator that monitors signals from necrotic cells and induces the recruitment of immune cells to the site of injury [9, 10]. There may be a causal link between inflammation and cancer [5]. Especially in adults, cancer is frequently preceded by a long period of subclinical inflammatory disease and micronecrosis that provides a setting in which the epigenetic regulation of genes, cell death, cell proliferation, and mutagenesis occur [11]. Cancer results from rounds of disordered and unscheduled necrotic cell death and subsequent proliferation of surviving cells, rather than from a process that is determined solely by cell growth [11, 12].

Indeed, rapid progression to dysplasia or cancer is associated with greater susceptibility to gastric epithelial cell death after *H. felis* infection [13]. Here, we showed that HSP27 prevents cell death and ROS production and that HSP27 expression is inversely related to atrophic gastritis and intraepithelial neoplasia, the potential precursor to gastric cancer, in humans. HSP27 may protect against the initiation of gastric cancer by suppression of epithelial cell death, ROS accumulation, and the subsequent inflammatory response.

It has been widely reported that the major causative factor of chronic gastritis is infection with the bacterium *H. pylori* [34]. However, *H. pylori* tend to disappear as intestinal metaplasia, the final stage of atrophic gastritis, develops. This may be because of histological changes that create unfavorable environments for survival of the bacterium [35]. Epidemiologic studies have revealed an association between *H. pylori* infection and gastric cancer risk [36, 37], and the development of gastric cancer is also affected by other factors, for example diet and patient genetic factors [38]. In our study, there was a consistent correlation between *H. pylori* infection and the presence of atrophic gastritis and neoplasia (Tables 1, 2).

HSP27 is expressed in a variety of human cancers. For cancers such as rectal [19], gastric [18, 20], and hepatocellular carcinoma [17], high levels of HSP27 are associated with a poor prognosis. Poorly differentiated tumors are more invasive and patients with these tumors have worse prognoses than those with differentiated tumors. We demonstrated that HSP27 expression is related to poor differentiation of human gastric cancer. EMT is an active process driving tumor dedifferentiation and determining tumor histology, one of the major prognostic variables used in clinical practice for gastric cancer patients [38, 39]. HSP27 induces EMT in gastric cancer MKN-1 cells, but not in MKN-74 cells. In contrast with normal epithelial cells, cancer cells are phenotypically and functionally heterogeneous. In at least some types of gastric cancer, HSP27 is critical for EMT-related dedifferentiation. HSP27 expression in cancer is positively correlated with its poor differentiation although the cause–effect relationship between HSP27 and poor differentiation remains to be elucidated.

In conclusion, HSP27 expression in the background mucosa is inversely associated with atrophic gastritis and gastric intraepithelial neoplasia, whereas HSP27 expression in the tumor is positively associated with poor differentiation of tumor cells. HSP27 may have distinct effects in the initiation step of gastric carcinogenesis and the progression of gastric cancers. Although studies have suggested that HSP27 can inhibit cancer cell death, leading to increases in cancer cell growth and expansion, there have been only a few studies of the involvement of HSP27 in the initiation of carcinogenesis [10]. Further work using knock-out mice is necessary to validate these findings and to determine whether HSP27 is crucially involved in carcinogenesis in vivo.

Acknowledgments This research was supported by grants from the Yasuda Medical Foundation, the Novartis Foundation, and Grant-in-Aid for Scientific Research from the Ministry of Education, Science and Culture of Japan.

Conflict of interest None.

References

1. Pinheiro PS, Tyczyński JE, Bray F, Amado J, Matos E, Parkin DM. Cancer incidence and mortality in Portugal. *Eur J Cancer*. 2003;39:2507–2520.
2. Ferlay J, Shin HR, Bray F, Forman D, Mathers C and Parkin DM. GLOBOCAN 2008 v1.2, cancer incidence and mortality worldwide: IARC CancerBase No. 10. Lyon, France: International Agency for Research on Cancer; 2010.
3. Hartgrink HH, van de Velde CJ. Status of extended lymph node dissection: locoregional control is the only way to survive gastric cancer. *J Surg Oncol*. 2005;90:153–165.
4. Novotny AR, Schuhmacher C, Busch R, Kattan MW, Brennan MF, Siewert JR. Predicting individual survival after gastric cancer resection: validation of a US-derived nomogram at a single high-volume center in Europe. *Ann Surg*. 2006;243:74–81.
5. Balkwill F, Coussens LM. Cancer: an inflammatory link. *Nature*. 2004;431:540–550.
6. Allen RG, Tresini M. Oxidative stress and gene regulation. *Free Radic Biol Med*. 2000;28:463–499.
7. Toyokuni S. Novel aspects of oxidative stress-associated carcinogenesis. *Antioxid Redox Signal*. 2006;8:1373–1377.
8. Scaffidi P, Misteli T, Bianchi ME. Release of chromatin protein HMGB1 by necrotic cells triggers inflammation. *Nature*. 2002;418:191–195.
9. Chen CJ, Kono H, Golenbock D, Reed G, Akira S, Rock KL. Identification of a key pathway required for the sterile inflammatory response triggered by dying cells. *Nat Med*. 2007;13:851–856.
10. Sakurai T, He G, Matsuzawa A, et al. Hepatocyte necrosis induced by oxidative stress and IL-1 alpha release mediate carcinogen-induced compensatory proliferation and liver tumorigenesis. *Cancer Cell*. 2008;14:156–165.
11. Vakkila J, Lotze MT. Inflammation and necrosis promote tumor growth. *Nat Rev Immunol*. 2004;4:641–648.
12. Sakurai T, Maeda S, Chang L, Karin M. Loss of hepatic NF-κB activity enhances chemical hepatocarcinogenesis through sustained c-Jun N-terminal kinase 1 activation. *Proc Natl Acad Sci USA*. 2006;103:10544–10551.
13. Shibata W, Takaishi S, Muthupalani S, et al. Conditional deletion of IkappaB-kinase-beta accelerates Helicobacter-dependent gastric apoptosis, proliferation, and preneoplasia. *Gastroenterology*. 2010;138:1022–1034.
14. Garrido C, Brunet M, Didelot C, Zermati Y, Schmitt E, Kroemer G. Heat shock proteins 27 and 70: anti-apoptotic proteins with tumorigenic properties. *Cell Cycle*. 2006;5:2592–2601.
15. Sankhala KK, Mita MM, Mita AC, Takimoto CH. Heat shock proteins: a potential anticancer target. *Curr Drug Targets*. 2011;12:2001–2008.
16. Huang Q, Ye J, Huang Q, et al. Heat shock protein 27 is overexpressed in tumor tissues and increased in sera of patients with gastric adenocarcinoma. *Clin Chem Lab Med*. 2010;48:263–269.
17. King KL, Li AF, Chau GY, et al. Prognostic significance of heat shock protein-27 expression in hepatocellular carcinoma and its relation to histologic grading and survival. *Cancer*. 2000;88:2464–2470.
18. Kapranos N, Kominea A, Konstantinopoulos PA, et al. Expression of the 27-kDa heat shock protein (HSP27) in gastric carcinomas and adjacent normal, metaplastic, and dysplastic gastric mucosa, and its prognostic significance. *J Cancer Res Clin Oncol*. 2002;128:426–432.
19. Tweedle EM, Khattak I, Ang CW, et al. Low molecular weight heat shock protein HSP27 is a prognostic indicator in rectal cancer but not colon cancer. *Gut*. 2010;59:1501–1510.

20. Giaginis C, Daskalopoulou SS, Vgenopoulou S, Sfiniadakis I, Kouraklis G, Theocharis SE. Heat Shock Protein-27, -60 and -90 expression in gastric cancer: association with clinicopathological variables and patient survival. *BMC Gastroenterol*. 2009;9:14.
21. Xu L, Chen S, Bergan RC. MAPKAPK2 and HSP27 are downstream effectors of p38 MAP kinase-mediated matrix metalloproteinase type 2 activation and cell invasion in human prostate cancer. *Oncogene*. 2006;25:2987–2998.
22. Tak H, Jang E, Kim SB, et al. 14–3-3epsilon inhibits MK5-mediated cell migration by disrupting F-actin polymerization. *Cell Signal*. 2007;19:2379–2387.
23. Bruey JM, Ducasse C, Bonniaud P, et al. Hsp27 negatively regulates cell death by interacting with cytochrome c. *Nat Cell Biol*. 2000;2:645–652.
24. Schmitt E, Gehrmann M, Brunet M, Multhoff G, Garrido C. Intracellular and extracellular functions of heat shock proteins: repercussions in cancer therapy. *J Leukoc Biol*. 2007;81:15–27.
25. Ebert MP, Schäfer C, Chen J, et al. Protective role of heat shock protein 27 in gastric mucosal injury. *J Pathol*. 2005;207:177–184.
26. Ushijima T, Sasako M. Focus on gastric cancer. *Cancer Cell*. 2004;5:121–125.
27. Tu S, Bhagat G, Cui G, et al. Overexpression of interleukin-1beta induces gastric inflammation and cancer and mobilizes myeloid-derived suppressor cells in mice. *Cancer Cell*. 2008;14:408–419.
28. Reya T, Morrison SJ, Clarke MF, Weissman IL. Stem cells, cancer, and cancer stem cells. *Nature*. 2001;414:105–111.
29. Matsuoka J, Yashiro M, Sakurai K, et al. Role of the stemness factors sox2, oct3/4, and nanog in gastric carcinoma. *J Surg Res*. 2012;174:130–135.
30. Pandey P, Farber R, Nakazawa A, et al. Hsp27 functions as a negative regulator of cytochrome c-dependent activation of procaspase-3. *Oncogene*. 2000;19:1975–1981.
31. Savagner P. The epithelial–mesenchymal transition (EMT) phenomenon. *Ann Oncol*. 2010;21:vii89–vii92.
32. Galluzzi L, Maiuri MC, Vitale I, et al. Cell death modalities: classification and pathophysiological implications. *Cell Death Differ*. 2007;14:1237–1243.
33. Golstein P, Kroemer G. Cell death by necrosis: towards a molecular definition. *Trends Biochem Sci*. 2007;32:37–43.
34. Marshal BJ. Campylobacter pyloridis and gastritis. *J Infect Dis*. 1986;153:650–657.
35. Genta RM, Graham DY. Intestinal metaplasia, not atrophy or achlorhydria, creates a hostile environment for *Helicobacter pylori*. *Scand J Gastroenterol*. 1993;28:924–928.
36. Parsonnet J, Friedman GD, Vandersteen DP, et al. *Helicobacter pylori* infection and the risk of gastric carcinoma. *N Engl J Med*. 1991;325:1127–1131.
37. Peek RM Jr, Blaser MJ. *Helicobacter pylori* and gastrointestinal tract adenocarcinomas. *Nat Rev Cancer*. 2002;2:28–37.
38. Panani AD. Cytogenetic and molecular aspects of gastric cancer: clinical implications. *Cancer Lett*. 2008;266:99–115.
39. Thiery JP, Acloque H, Huang RY, Nieto MA. Epithelial–mesenchymal transitions in development and disease. *Cell*. 2009;139:871–890.

Liver INTERNATIONAL
OFFICIAL JOURNAL OF THE INTERNATIONAL ASSOCIATION FOR THE STUDY OF THE LIVER

Liver International ISSN 1478-3223

CONSENSUS

Consensus recommendations and review by an International Expert Panel on Interventions in Hepatocellular Carcinoma (EPOIHCC)

Joong-Won Park[1], Deepak Amarapurkar[2], Yee Chao[3], Pei-Jer Chen[4], Jean-Francois H. Geschwind[5], Khean Lee Goh[6], Kwang-Hyub Han[7], Masatoshi Kudo[8], Han Chu Lee[9], Rheun-Chuan Lee[10], Laurentius A. Lesmana[11], Ho Yeong Lim[12], Seung Woon Paik[13], Ronnie T Poon[14], Chee-Kiat Tan[15], Tawesak Tanwandee[16], Gaojun Teng[17] and Ann-Lii Cheng[18]

1 Centre for Liver Cancer, National Cancer Center Hospital, Seoul, Korea
2 Department of Gastroenterology, Bombay Hospital and Medical Research Centre, Mumbai, India
3 Division of Chemoradiotherapy, Cancer Centre Taipei Veterans General Hospital, Taipei, Taiwan
4 Graduate Institute of Clinical Medicine, College of Medicine, Taiwan National University, Taipei, Taiwan
5 Johns Hopkins University School of Medicine, Baltimore, USA
6 Division of Gastroenterology, Department of Medicine, University of Malaya, Kuala Lumpur, Malaysia
7 Department of Internal Medicine, Yonsei University College of Medicine, Seoul, Korea
8 Department of Hepatology and Gastroenterology, Kinki University School of Medicine, Osaka-Sayama, Japan
9 Department of Internal Medicine, Asan Medical Center, University of Ulsan College of Medicine, Seoul, Korea
10 Department of Radiology, Taipei Veterans General Hospital, Taipei, Taiwan
11 Hepatology Section, Department of Internal Medicine, Faculty of Medicine, University of Indonesia, Jakarta, Indonesia
12 Division of Hematology-Oncology, Department of Medicine, Samsung Medical Center, Seoul, Korea
13 Department of Medicine, Samsung Medical Center, Sungkyunkwan University School of Medicine, Seoul, Korea
14 Department of Surgery, Queen Mary Hospital, University of Hong Kong, Hong Kong
15 Department of Gastroenterology and Hepatology, Singapore General Hospital, Singapore
16 Division of Gastroenterology, Department of Medicine, Siriraj Hospital, Mahidol University, Bangkok, Thailand
17 Department of Radiology, Zhong-Da Hospital, Southeast University, Nanjing, China
18 Department of Oncology and Internal Medicine, National Taiwan University Hospital, Taipei, Taiwan

Keywords
Combination therapy – Hepatocellular carcinoma – Sorafenib – TACE

Correspondence
Ann-Lii Cheng, Department of Oncology and Internal Medicine, National Taiwan University Hospital, No. 7, Chung-Shan South Road, Taipei 10016, Taiwan, China
Tel: +886-2-23123456-7251
Fax: +886-2-23711174
e-mail: alcheng@ntu.edu.tw

DOI:10.1111/liv.12083
Liver Int. 2013: 33: 327–337

Abstract

Hepatocellular carcinoma (HCC) presents with a high burden of disease in East Asian countries. Intermediate-stage HCC as defined by the Barcelona Clinic Liver Cancer (BCLC) staging system poses a clinical challenge as it includes a heterogeneous population of patients that can vary widely in terms of tumour burden, liver function and disease aetiology. Intermediate HCC patients often have unsatisfactory clinical outcomes with repeated transarterial chemoembolization (TACE, due to non-response of the target tumour or the development of further metastasis indicating progressive disease. In September 2011, an Expert Panel Opinion on Interventions in Hepatocellular Carcinoma (EPOIHCC) was convened in HK in an attempt to provide a consensus on the practice of TACE. To that end, current clinical practice throughout Asia was reviewed in detail including safety and efficacy data on TACE alone as well as in combination with targeted systemic therapies. This review summarises the evidence discussed at the meeting and provides expert recommendation regarding the available therapeutic options for unresectable intermediate stage HCC. A key consensus of the Expert Panel was that in order to improve patient outcomes and long-term survival, the possibility of using TACE in combination with targeted agents given systemically should be explored. While the currently available clinical data is promising, the expected completion of several pivotal phase II and III RCTs will provide further evidence in support of the rationale for combination therapy regimens.

Globally, hepatocellular carcinoma (HCC) is the fifth most common form of cancer (1) with a particularly high burden of disease in east Asian countries, including China, Japan, Korea, and Taiwan (2, 3). There are a number of staging systems for HCC classification, often with different numbers of stages and different criteria for classification. While early stage HCC is commonly staged consistently between systems, the differentiation

of intermediate from advanced stage HCC is often not well defined. Differences arise depending on the underlying level of liver disease, the level of liver function and historical slant towards resectable versus non resectable tumours (Reviewed in(4)). As the prognosis of unresectable patients varies greatly, from weeks to years, depending on tumor extension and liver function, surgical unresectability alone is not suitable for prognostic staging or treatment decision. Studies have shown the degree of liver dysfunction is a determinant of both prognosis and appropriate treatment eligibility and treatments themselves may impact on liver function (4). The Barcelona Clinic Liver Cancer (BCLC)(5) staging system has been widely adopted as the staging system of choice in many countries across the world as it links different stages of HCC with appropriate therapeutic treatment options(6) and has been endorsed by the European Association for the Study of the Liver (EASL) (7) and the American Association for the Study of the Liver (AASLD) (8). The BCLC system has four stages with well defined early and advanced patient staging. Subsequently, intermediate stages are also more clearly defined and include criteria for tumor stage, liver functional status, physical status and cancer related symptoms (5).

Intermediate HCC

Intermediate-stage HCC includes a heterogeneous population of patients that can vary widely in terms of tumour burden, liver function and disease aetiology (6). The BCLC intermediate stage (BCLC-B) consists of Child-Pugh A and B patients with large/multifocal HCC (defined as >3 tumors whichever the size, or 2–3 tumor exceeding 3 cm in maximal diameter or one single unresectable tumor larger than 5 cm, who do not have cancer related symptoms, macrovascular invasion or extrahepatic spread) (5). Some cases with good liver function and small tumors of intermediate stage may reach 50% survival over 3 years without therapy (9). However, Child-Pugh B patients with large and multiple/diffuse HCC show worse prognosis. Therapeutically, intermediate stage HCC patients are considered optimal candidates for transarterial embolization (TAE) and chemoembolisation (TACE). Conventional TACE most often consists of arterial infusion of an emulsion of lipiodol with a chemotherapeutic agent (e.g. doxorubicin, cisplatin) followed by embolization. TAE has been shown to be effective in inducing tumour necrosis and in delaying tumour progression and revascularisation of the tumor bed in 15–55% of patients (10, 11). However, a recent study indicates the inclusion of a chemotherapeutic agent provided a better local tumor response, with lower recurrence and longer time to progression than TAE alone (12). Despite this, systemic chemotherapy alone is not particularly effective. The most active agents *in vitro* and *in vivo* are doxorubicin and cisplatin but a meta-analysis reported only partial responses in around 10% of cases, without any evidence of survival advantages (13). An early meta-analysis of six randomized control trials which compared TACE with best supportive care or suboptimal therapies, recommended TACE as the standard-of-care for intermediate-stage HCC (14). However, only two of these six studies reporting 2-year survival demonstrated a statistically significant improvement compared with conservative management reflecting significant differences between the individual study designs (Reviewed in(6)). A 2011 meta-analysis defined the evidence supporting the benefits of TACE as limited (15), however, there have been several criticisms of this analysis primarily related to the inclusion of inappropriate trial data (Reviewed in 6) (16). TACE has been reported to achieve a partial response in 15–62% of patients, with significantly delayed tumor progression and vascular invasion and an improvement of median survival from 16 to 20 months (14, 17). A recent expert opinion review of the indications/contraindications for TACE including technical issues relating to the procedure and follow up have been published and has highlighted the importance of patient selection in predicting favourable responses to TACE (18). While there is clear evidence for the effectiveness of conventional TACE in prolonging survival in intermediate patients with well preserved liver function (Child-Pugh A class) (14), <10% of the total population in this meta-analysis were Child-Pugh B patients (4). Child-Pugh B patients represent a highly heterogeneous population with limited evidence of benefit from TACE treatment with an inherent risk of deterioration of liver function. This view is further reinforced by a recent study utilising selective and sequential TACE reporting median survival of 46.1 months for Child-Pugh A and only 11.1 months for Child-Pugh B patients (19).

Currently, TACE procedures are not well standardised and the optimal chemotherapeutic/embolizing agent and the retreatment strategy, including standardisation of treatment schedule and indications, have to be determined (20). For example, gelatine sponge particles, or gelfoam, widely used in Asia and previously the most common embolizing agent used in trials, provide a heterogeneous and temporary arterial obstruction. In contrast, polyvinyl alcohol particles (PVA), not widely used in Asia but used in many Western centres, results in permanent artery occlusion (20). Additionally, the time lag between chemotherapy injection and vessel obstruction allows systemic release of the chemotherapy agent while another critical factor influencing the effectiveness of TACE is tumor burden and operator skill (4). The recent development of DEB-TACE enables a slow release of the chemotherapy agent following injection into the blood stream and systemic release is significantly reduced resulting in reduced toxicity as compared to conventional TACE (reviewed in(21)). Selective embolization is associated with a greater antitumor effect, as it preserves liver function and is associated with better overall outcome (22), however, very large tumors and

bilobar infiltration reduces the possibility of selective embolization or total tumor necrosis (4). A phase II RCT (Precision V) recently compared conventional TACE with TACE using drug-eluting beads (DEB-TACE) to enhance tumor drug delivery and reduce systemic availability (23, 24). While the Precision V study failed to show a statistically significant difference in the 6-month objective response rate, better 6-month objective response rates were seen in patients with more advanced liver impairment, performance status 1, bilobar and recurrent disease (24). Encouraging data have been provided by a recent evaluation of the survival of HCC patients treated with DEB-TACE with well preserved liver function, the absence of symptoms, extrahepatic spread or vascular invasion reported median survival times of 54.2 months in BCLC stage A patients and 47.7 months in stage B patients (21).

Transarterial radioembolization with the use of the radioisotope yttrium-90 (Y-90) has also produced results similar to TACE in small numbers of patients (25, 26). Internal radioembolization might be more advantageous than TACE in Child-Pugh A patients with very large tumors where TACE does not provide very effective treatment (25, 26). Unfortunately, these trials excluded Child-Pugh B patients limiting conclusions of efficacy in the broader class of intermediate HCC. This has been partially addressed by a recent retrospective analysis of 325 patients which reported considerable variation in median overall survival between tumour stage (BCLC A, 24.4 months, BCLC B, 16.9 months, BCLC C, 10.0 months) and Child status (BCLC A: 30.9 months (Child A) vs 19.4 months (Child B); BCLC B: 18.4 months (Child A) vs 3.6 months (Child B); BCLC C: 9.7 months (Child A) vs 10.0 months (Child B)) (27). An important advantage of radioembolization is that it is safe in patients with portal vein thrombosis in whom TACE may lead to complications such as liver abscess or decompensation of cirrhosis (28, 29). However, an important consideration for radioembolization in cirrhotic patients is the potential changes in the distribution of microspheres as a result of vascular changes that occur in the cirrhotic liver. This altered microvascular pattern and the presence of anatomical arterio-portal and arterio-venous shunts may modify the radiation dose absorbed by the tumor and the non-tumoral liver and therefore affect treatment tolerance and effectiveness (30). A major disadvantage of radioembolization is that in order to ensure Y-90-microspheres do not spread into gastroduodenal or gastric circulation resulting in severe clinical consequences, it is essential to carefully map the tumor perfusing vessels, to embolize collateral vessels and to assess portal vein patency before the administration of the treatment compound. Therefore, invasive hepatic angiography is an essential first step in planning a radiembolization treatment, adding additional risks and costs to therapy (31). While a number of scientific societies and groups of experts have acknowledged that radioembolization may have a role as a valuable form of locoregional therapy for HCC in recently issued treatment guidelines (reviewed in(30)), the recently updated guidelines of the American Association for the Study of Liver Diseases (AASLD) do not consider that radioembolization can be recommended as standard therapy for advanced HCC outside clinical trials (9).

Sorafenib is an oral multikinase inhibitor which blocks tumor cell proliferation and angiogenesis by inhibiting the serine/threonine kinases Raf-1/B-Raf and the tyrosine kinases of vascular endothelial growth factor receptor (VEGFR-2/-3) and platelet derived growth factor receptor (PDGFR) (32). In the landmark SHARP trial, the median overall survival (OS) was 10.7 months in the sorafenib group and 7.9 months in the placebo group in 602 patients with advanced HCC with well-preserved liver function (33). A phase III trial has also been conducted in Asia which showed a similar magnitude of benefit in the sorafenib arm compared with the placebo arm (34). These two phase III trials have established sorafenib as the preferred systemic therapy for advanced HCC although the role for sorafenib in intermediate HCC is less clear. It should be noted that both of these Phase III studies restricted enrolment to patients with Child-Pugh class A disease, because impairment of liver function associated with Child-Pugh class B or C could have potentially confounded the results (33, 34). To date there have only been small numbers of Child-Pugh B patients treated with sorafenib in a clinical trial setting so it is not possible to adequately assess efficacy and safety in this important patient group at this time.

TACE in Asia

Transarterial chemoembolization (TACE) has been used for almost 30 years in Asian countries in unresectable HCC patients without strong evidence of improved survival or quality of life (35). To date, seven randomized studies, including more than 500 patients, have compared TACE with best supportive care. Two of these reported a survival advantage for treated patients. A Spanish randomised controlled study demonstrated 1 and 2 year survival probabilities of 82 and 63%, respectively, for patients who underwent TACE vs 63 and 27% for the control group receiving supportive care only (36). Comparatively, a Hong Kong study indicated 1 and 2 year survival probabilities of 57% and 31%, respectively vs 32% and 11% for patients receiving symptomatic treatment only (37). A subsequent meta analysis demonstrated a beneficial survival effect of TACE compared with conservative treatment (14). While the difference in survival rates between these populations could be due to a number of factors, including protocol differences, there were considerable differences in hepatitis status with 81% of the Spanish patients having cirrhosis caused by the hepatitis C virus (HCV), while 85% of the Hong Kong patients had cirrhosis

predominantly due to the hepatitis B virus (HBV). There is still considerable debate about whether TACE can affect viral replication. Studies have reported that patients with decreased pre-TACE white blood cell counts (38), HBeAg seropositivity (39), increased serum total bilirubin coexisting with cirrhosis and the total number of cycles of TACE received(40) all have a potential risk of the reactivation of the replication of HBV or HCV after TACE. HBV-DNA load is a risk factor for HCC and IFN-α treatment will reduce the HBV-DNA load (41). The current EASL guidelines recommend antiviral therapies leading to maintained HBV suppression in chronic hepatitis B patients and sustained viral response in hepatitis C since they have been shown to prevent progression to cirrhosis, and hence HCC development (42). However, once cirrhosis is established, the benefits of anti-viral therapy in preventing HCC development are not robustly demonstrated (42).

Previous studies have indicated potential ethnic differences in HCC prognosis and survival after similar treatments (43). A North American study reported survival rates following TACE therapy intermediate between these two populations (76% at 1 year and 56% at 2 years) that could indicate a mixed ethnicity within this population but was also reflective of the mean tumour size of the treated lesions (5 cm for the Spanish study, 6.8 cm for the North American study and 7 cm for the Hong Kong study) (35). A large case series from Japanese patients treated with TACE reported median survival of 34 months with good stratification of survival by degree of liver damage and the tumor, node, metastasis system proposed by the Liver Cancer Study Group of Japan (44). A 13 year retrospective analysis of patients in China with unresectable HCC undergoing TACE as initial treatment identified tumor status, hepatic function reserve, AFP, and HBV status as independent prognostic factors (45). These studies indicate that TACE can effectively delay HCC progression and prevent recurrence early. However, 2 year survival rates are poor (46). Recent Asian trials of TACE with modified formulations of cisplatin, doxorubicin and epirubicin microspheres reported overall 2 year survival rates of 76%, 46% and 59%, respectively (47, 48). A recent Korean study of TACE in BCLC B/C patients reported a median TTP of 3.8 months (49).

Patient selection

As noted above, intermediate stage HCC includes a heterogeneous group of patients with significant variations in tumor and liver characteristics. In order to achieve the best outcomes, there must be careful selection of patients for each treatment option and the expert application of these treatments (9). A recent review suggests there are patients who are currently categorized within the intermediate patient segment for whom TACE may not be the optimal treatment option (50). Tumor stage is strongly associated with the prognosis of solid tumors and should also guide treatment decisions although the underlying liver function in many HCC patients makes the prediction of prognosis complex (9). The BCLC staging system has been used by a number of major trials of HCC therapy as it can define patient groups for therapies across the continuum of disease extent seen with HCC (9). This enables a more defined patient population to be recruited and stratified into separate prognosis categories based on published response rates to the various treatments (9, 50).

Repetition of TACE is based on evidence suggesting that one cycle of TACE may not be sufficient for effective treatment of intermediate-stage HCC and repeating TACE prolongs survival (reviewed in(50)). However, current treatment guidelines do not specify the criteria for repeating TACE providing unnecessary uncertainty. Consequently, TACE uptake rates in Asia are high accounting for 50–60% of all HCC procedures at institutions involved in the TACE Study Group of Japan (51). A recent study reported TACE was the most common first treatment in Asia and North America (52). In terms of scheduling repeat TACE sessions, it is unclear if on-demand TACE is more or less effective than scheduled TACE for improving patient survival although aggressive repetition of TACE increases the incidence of adverse events (reviewed in(50)). Raoul *et al.* recently proposed a treatment algorithm for the repetition of cTACE in patients with intermediate stage HCC repetition on-demand, with longer intervals between treatments, rather than regular repetition (50). Of note, the algorithm also considers sorafenib as a treatment option in this patient population when cTACE fails or is contraindicated.

Molecular targeted therapy in intermediate stage HCC

The current AASLD recommendations suggest TACE should be used as first line non-curative therapy for BCLC B patients (9). The recent development of sorafenib has provided a viable treatment option with demonstrable benefits in prolonging life in patients with advanced HCC. Two phase III trials comparing sorafenib with placebo in patients with advanced HCC reported median overall survival of 10.7 months and 6.5 months in the sorafenib groups vs7.9 months and 4.2 months in the placebo groups, respectively (33, 34). Sorafenib is recommended for those who have failed TACE or for TACE-refractory patients, but TACE failure or refractoriness has not been clearly defined. The need to define TACE refractory HCC is particularly important for the strategy of repeating multiple sessions of TACE for residual viable tumors or the development of new lesions as an on-demand basis, especially in Asian countries (53).

Despite promising results in patients with advanced HCC where sorafenib is the only systemic agent to have demonstrated an overall survival benefit (33), the role for sorafenib in intermediate HCC has not yet been

established. Currently, multifocal (intermediate BCLC stage B) HCC is treated primarily with TACE alone and more advanced (BCLC stage C) HCC is treated with sorafenib monotherapy (9). While these treatments produce modest survival benefits when used alone, the likely benefits of combination therapy are enticing. Recently, two prospective phase II studies and one case study which used drug eluting bead (DEB)-TACE (54, 55), yttrium-90 microspheres (54), or conventional TACE(56) plus sorafenib combination therapy, have reported promising efficacy results with both intermediate and advanced HCC (54–56). There are a substantial number of clinical trials assessing the combination of TACE with sorafenib that have either been completed or are currently underway (Table 1). Interim or final results have been presented for some of these trials and are summarised below (Table 2). The Study in Asia of the Combination of TACE with Sorafenib in Patients with HCC (START) study is a prospective Phase II, open label, trial that investigated the safety and efficacy of the combination of Sorafenib and conventional TACE in South East Asian patients with HCC, the majority of which were BCLC stage B. The preliminary results of START indicate concurrent sorafenib and TACE therapy is safe and effective with no unexpected side effects (57). The phase II randomized, double-blind, placebo-controlled sorafenib or placebo in combination with TACE in HCC (SPACE) trial incorporates a continuous sorafenib administration protocol concurrently with DEB-TACE (58). In 307 patients the median treatment duration in the treatment and placebo groups was 4.8 and 6.3 months, respectively, and the HR for TTP was 0.797. While median TTP reported was similar for both groups (Table 2), there were considerable differences in TTP at the 25th and 75th percentiles and the study met its primary endpoint of improving TTP when sorafenib was added to a regimen of TACE with DEBDOX, compared with TACE with

Table 1. Clinical trials evaluating the combination of TACE and sorafenib listed on clinicaltrials.gov (Accessed 23 August, 2012)

NCT Number	Status	Interventions	Sponsor/Collaborators	*N*	Study Design	Other IDs
NCT00478374	Completed	cTACE + continuous sorafenib	University of Bern	21	I Single Arm, Open label	S-TACE
NCT00494299	Completed	cTACE + sequential sorafenib	Bayer	458	III Randomized, Placebo controlled, Double Blind	11721
NCT00768937	Completed	cTACE + continuous sorafenib	Medical University of Vienna	22	I/II Single Arm, Open label	SORATACE1
NCT00844883	Active, not recruiting	DEB-TACE + continuous sorafenib	Johns Hopkins Hospital, Baltimore	50	II Single Arm, Open label	J08110
NCT00855218	Active, not recruiting	DEB-TACE + continuous sorafenib	Bayer	307	II Randomized, Placebo controlled, Double Blind	SPACE
NCT00919009	Completed	cTACE + continuous sorafenib	National Cancer Center, Korea	50	II Single Arm, Open label	COTSUN Korea Trial
NCT00990860	Active, not recruiting	cTACE + interrupted sorafenib	Taipei Veterans General Hospital, Taiwan	36	II Single Arm, Open label	START
NCT01004978	Recruiting	cTACE/DEB-TACE + continuous sorafenib	National Cancer Institute (NCI), Eastern Cooperative Oncology Group	400	III Randomized, Placebo controlled, Double Blind	ECOG-E1208
NCT01042041	Completed	cTACE + continuous sorafenib	Abramson Cancer Center of the University of Pennsylvania	18	I Single Arm, Open label	UPCC 08208
NCT01170104	Recruiting	cTACE + continuous sorafenib	Chung-Ang University, Gyeongsang National University Hospital	63	II Single Arm, Open label	CAUHHO 2009-1
NCT01217034	Recruiting	cTACE + interrupted sorafenib	Japan Liver Oncology Group	228	II Randomized, Parallel, Open label	TACTICS
NCT01324076	Recruiting	DEB-TACE + continuous sorafenib	National Cancer Institute (NCI), University College, London	412	III Randomized, Double Blind	CRUK-TACE-2
NCT01409499	Recruiting	cTACE + sequential sorafenib	Sun Yat-sen University	200	IV Parallel, Open label	2011PTAHCC
NCT01556815	Not yet recruiting	cTACE + continuous sorafenib	Shandong Cancer Hospital and Institute	40	II Parallel, Open label	ShandongCHI-001
NCT01605734	Not yet recruiting	cTACE + sequential sorafenib	Shandong Cancer Hospital and Institute	120	II Parallel, Open label	ShandongCHI-002
NCT00618384	Terminated	cTACE interrupted	Heinrich-Heine University, Duesseldorf	43	II Single Arm, Open label	SOCRATES-072

Table 2. Published trials evaluating the combination of TACE and sorafenib

Study Author	Study Design	*N*	TACE	Sorafenib Tx	Outcome Reported
Kudo *et al.*, 2011(61)	Phase III, Randomized, Placebo controlled, Double Blind	458	cTACE Epirubicin + cisplatin + doxorubicin + mitomycin + lipiodol + gelatin sponge	Sequential 400 mg po bid, Median start 9.3 weeks post TACE	Med TTP 5.4 mo (TACE + S) 3.7 mo (placebo) HR 0.87 6-mo PFR 45.7% (TACE + S) 33.5% (placebo)
Sansonno *et al.*, 2012(62)	Phase II, Randomized, Placebo controlled, Double Blind	80	cTACE Doxorubicin + mitomycin C + lipiodol + gelatin sponge	Sequential 400 mg po bid, Start 30 days post TACE	Med TTP 9.2 mo (TACE + S) 4.9 mo (placebo)
Lencioni *et al.*, 2012(58)	Phase II, Randomized, Placebo controlled, Double Blind	307	DEB-TACE doxorubicin	Continuous 400 mg po bid, Start 3–7 days pre TACE	Med TTP 5.6 mo (TACE + S) 5.5 mo (TACE) HR 0.797
Siegert *et al.*, 2012(63)	Phase I, Single Arm, Open label	15	cTACE Doxorubicin + lipiodol + gelatin sponge	Continuous 400 mg po bid, Start 2 weeks pre TACE	Med OS 10.6 mo
Pawlik *et al.*, 2011(55)	Phase II, Single Arm, Open label	35	DEB-TACE doxorubicin	Continuous 400 mg po bid, Start 1 week pre TACE	DCR 92% ORR 58%
Park *et al.*, 2012(56)	Phase II, Single Arm, Open label	50	cTACE Doxorubicin + lipiodol + gelatin sponge	Interrupted 400 mg po bid, Start 3 days post TACE Stop 1 day pre TACE	TTP 7.1 mo overall 7.3 mo BCLC B 5.0 mo BCLC C 6-mo PFS 52%
Qu *et al.*, 2012(64)	Phase II, Parallel (1:1), Open label	90	cTACE Oxaliplatin + Epirubicin + lipiodol + gelatin sponge	Interrupted 400 mg po bid, Start 3 days post TACE Stop 3 days pre TACE	Med OS 27 mo (TACE + S) 17 mo (TACE)
Chung *et al.*, 2010(57)	Phase II, ingle Arm, Open label	50	cTACE Doxorubicin + lipiodol + gelatin sponge	Interrupted 400 mg po bid, Start 3 days post TACE Stop 3 days pre TACE	CR 18/50 PD 2/50
Erhardt *et al.*, 2011(65)	Phase II, Single Arm, Open label	45	cTACE Doxorubicin + lipiodol + gelatin sponge	Interrupted 400 mg po bid, Start 1 day post TACE Stop 3 days pre TACE	TTP 18.9 mo Med OS 20.1 mo

DEBDOX alone. Considering the natural course of intermediate stage HCC, the optimal time for discontinuation of sorafenib in combination treatment strategies must still be determined given the possibility of rebound after discontinuation of sorafenib in patients who respond to this drug (56).

Therapeutic end points

There are a number of recommended primary and secondary endpoints for HCC clinical trials (Reviewed in (6)). These include survival, defined as time from randomization to death and time to progression (TTP), defined as time from initiation of therapy to progression by the Response Evaluation Criteria in Solid Tumors (RECIST). A number of composite endpoints have also been used in HCC research, such as disease-free and progression-free survival, defined as time from randomization to either recurrence or death (disease-free) or radiological progression or death (progression-free). In clinical practice however, there is less agreement about the measurement of treatment response. RECIST was created to assess tumor response to therapy by measuring tumor size (unidimensional longest diameter) thereby providing a quantitative simple measure of tumor response that could easily be reproduced throughout the world. (59). However, it was noted that liver tumors typically do not shrink after loco-regional therapy making RECIST somewhat obsolete as an imaging tool. This was also observed for anticancer drugs with alternate mechanisms of action, such as molecular targeted therapies, which do not cause tumor shrinkage (6). Treatments such as TACE and sorafenib for example, poorly correlate with the extent of tumor shrinkage. Rather, these types of therapies cause tumor necrosis which is reflected by a decrease in the enhancement of the tumors. This new type of tumor response assessment by imaging was endorsed by the European Association

Table 3. EPOIHCC pre-meeting survey questions and summary of responses

Question	No. of responses
Q1. Do you rely on specific guidelines to advise the use of TACE in HCC?	
Yes	8
No	4
Local/Hospital guidelines	3
AASLD HCC Practice Guidelines	3
British Society of Gastroenterology	1
APASL Guidelines	3
NICE Guidelines	1
Other	3
Q2. Which TACE regimen do you use routinely in clinical practice?	
DC Beads	4
cTACE-Doxorubicin	8
cTACE-Cisplatin	2
cTACE-Mitomycin	2
Other	3
Q3. In your experience, what is the optimal number of TACE procedures required in the treatment of intermediate HCC patients? Please specify average in your practice	
Q4. How do measure patient response to TACE in clinical practice?	
Response Evaluation Criteria in Solid Tumours (RECIST)	6
Modified RECIST (mRECIST)	6
WHO	0
EASL	2
Other (specify)	
Q5. What is the greatest challenge faced in the application of TACE in intermediate HCC patients?	
Liver Function	9
Vascular Access	5
Patient Selection	4
Evidence	
Other (specify)	
Q6. In your opinion, would improved patient outcomes with TACE, mean less procedures and preserve liver function?	
Yes	9
No	3
Q7. What current alternatives to TACE, would you consider in clinical practice?	
Yt-90	9
RFA	7
External beam radiotherapy	5
Other (specify)	
Q8. Which patients are unsuitable for TACE, what treatment options would you consider in these cases?	
Technical issues	9
Tumour size	9
Liver function	10
In your opinion there is insufficient evidence to support alternatives	2
Q9. In your opinion, which intermediate stage HCC patients would potentially benefit from molecular targeted therapy?	
Patients with tumour >10 cm	7
Patients with vascular invasion	9
Patients who have undergone $\geq$2 TACE procedures, without satisfactory response	11
Other (specify	3
Q10. In your opinion, is there sufficient evidence to support the use of sorafenib and TACE in combination therapy?	
I do use it in clinical practice currently	1
I do use it but only in special patient populations	4
I do not use it in clinical practice	5

for the Study of the Liver (EASL) and became known as the EASL amendment (60). It equated the lack of contrast enhancement with tumor necrosis. Since then, another modification was suggested whereby residual enhancement in tumors would be measured and equated with viable tumor. These criteria became known as the mRECIST (7).

Expert panel meeting

In September, 2011 the Expert Panel Opinion on Interventions in Hepatocellular Carcinoma (EPOIHCC) meeting was convened in Hong Kong bringing together 17 experts from Asia Pacific. The panel was intended to provide a multidisciplinary approach to optimizing HCC management incorporating input from specialists in gastroenterology, hepatology, surgery, transplant surgery, interventional and diagnostic radiology, medical oncology, radiation oncology and nuclear medicine. The objectives for the meeting were to review current clinical practice with TACE in Asia, the existing Asian guidelines and the available data for intermediate HCC including safety & efficacy data for TACE combination therapy from current clinical trials with a view to communicating consensus recommendations for intermediate HCC patients or in advanced HCC after TACE failure.

Pre-Meeting Survey: Current Clinical Practice with TACE in HCC in Asia

To provide a snapshot of current clinical practice in Asia, a pre-meeting survey was completed by 12 of the expert panel members (Table 3). The results indicated that the majority (8/12) clinicians refer to guidelines based on APASL/AASLD recommendations while country specific guidelines include the Korean Liver Cancer Study Group and the Japanese Society of Hepatology (JSH consensus-based treatment algorithm for HCC). Respondents indicated that conventional TACE-doxorubicin and DC beads are commonly used in clinical practice with an estimated median 2–5 procedures required, according to a case-by-case basis. Treatment responses are measured using both RECIST and mRECIST criteria with tumour size measured by imaging (CT or MRI) and biomarkers. The primary technical

challenges facing treatment are related to vascular access and liver function damage related to TACE outcomes. The majority (9/12) of clinicians agreed that improved patient outcomes will likely translate to fewer rounds of TACE required and will subsequently preserve liver function. Panel members suggested the measurement of hepatitis B virus DNA level is necessary for chronic hepatitis B control after TACE, with the aim of prolonging TTP, OS and delaying disease progression. The measurement of serum VEGF would assist with patient selection for TACE, but more studies are necessary for clinical use. Current alternatives to TACE in use include Yt-90, Radiofrequency Ablation (RFA) and external beam radiotherapy.

Summary of the Panel Discussions

The Barcelona Clinic Liver Cancer (BCLC)(5) staging system has been widely adopted as the staging system of choice. It links different stages of HCC with appropriate therapeutic treatment options with the result that intermediate stages are also more clearly defined. *For a given therapy, appropriate patient selection is essential to ensure optimal therapeutic efficacy*.

The survey conducted here indicates the use of RECIST guidelines to evaluate responses to treatment in Asia appears to be decreasing while there is increasing use of mRECIST for response evaluation in clinical practice. The panel acknowledges that the use of mRECIST takes into account reductions in the viable tumor area induced by treatment using contrast-enhanced radiological imaging, which may be more appropriate for the newer molecular targeted therapies (7). However, it is also noted that mRECIST was developed through consensus rather than via a rigorous clinical approach, and subsequently, there is no data which supports any correlation of staging with tumour necrosis. *The considerable heterogeneity of disease stages and ill-defined tumour borders complicate the management of intermediate HCC and the panel recommends both RECIST and mRECIST be used for accurate assessment of treatment response.*

According to current guidelines, the consensus for standard of care for intermediate stage unresectable HCC is TACE (conventional or DC beads). However, intermediate HCC patients represent a highly heterogeneous population with limited evidence of clear benefit from TACE treatment with an inherent risk of deterioration of liver function. *While TACE is associated with benefits in intermediate HCC, TACE procedures are not well standardised and the optimal chemotherapeutic/embolizing agent and the retreatment strategy, including standardisation of treatment schedule and indications, have to be determined (20)*.

HBV-DNA load is a risk factor for HCC and antiviral treatment will reduce the HBV-DNA load (41). The current EASL guidelines recommend antiviral therapies leading to maintained HBV suppression in chronic hepatitis B patients and sustained viral response in hepatitis C since they have been shown to prevent progression to cirrhosis, and hence HCC development (42). *The expert panel concurs with this recommendation with the aim of prolonging TTP, OS and delaying disease progression*.

Transarterial radioembolization has also produced results similar to TACE in small numbers of patients but may be more suited to specific patient populations unsuitable for other therapies. *Radioembolization is not yet widely endorsed in Asia*.

Sorafenib is currently the standard of care in advanced HCC. TACE combined with molecular targeted therapy is currently only considered in special populations or clinical trials. There have been recent positive results of a number of trials combining TACE with sorafenib to enhance efficacy in intermediate HCC patients. Differences in AE profile and efficacy are beginning to emerge between sequential, continuous and interrupted sorafenib administration. *The results of these ongoing trials are expected to provide important insights into the design of treatment protocols when sorafenib is administered in combination with TACE*.

Patients who remain TACE-refractory after repeated procedures should be considered for other types of treatment to improve OS. The panel members highlighted the fact that it is currently difficult to differentiate TACE-refractory patients from treatment failures. This complicates the definition of appropriate patient management. Recent expert opinion by other groups has indicated no response of the treated tumour after at least two sessions of TACE constitutes TACE failure (50). Reflecting the uncertainty in this field, there was considerable discussion among the panel members on the definition of TACE refractory or failure status. *The panel defined TACE-Failure as no response after 3 or more TACE procedures within a 6 month period, to the same area.*

TACE is limited in patients with complications of vascular access where there are difficulties delivering a catheter to the tumour site and for patients with hypovascular HCC. *For these populations Molecular targeted therapies, RFA or radiation therapy may also be considered, if appropriate.*

Summary

This expert panel meeting was convened to assess how intermediate stage unresectable HCC patients should be managed in clinical practice in Asia. This heterogeneous patient population often suffer from poor prognosis with repeated TACE, due to non-response of the target tumour or the development of further complications including metastasis from the primary tumour lesion. In order to improve patient outcomes and long-term survival TACE combination therapy can be considered with molecular targeted therapy, or treatment switching to systemic therapy. The expected completion of several pivotal phase II and III RCTs will provide further

evidence in support of the rationale for combination therapy regimens.

Acknowledgements

All authors received honoraria for participation in the expert panel meeting, but received no compensation for their authorship of this manuscript. The authors would also like to acknowledge Bruce Mungall BSc, PhD from UBM Medica Pte Ltd Singapore for providing editorial and writing support, which was supported by an educational grant from Bayer (South East Asia) Pte Ltd.

References

1. GLOBOCAN, International Agency for Cancer Research. 2008 Available at http://www-dep.iarc.fr. Accessed 20 November 2011.
2. El-Serag HB, Rudolph KL. Hepatocellular carcinoma: epidemiology and molecular carcinogenesis. *Gastroenterology* 2007; **132**: 2557–76.
3. Parkin DM, Bray F, Ferlay J, Pisani P. Global cancer statistics, 2002. *CA Cancer J Clin* 2005; **55**: 74–108.
4. Piscaglia F, Bolondi L. The intermediate hepatocellular carcinoma stage: should treatment be expanded? *Dig Liver Dis* 2010; **42**(Suppl. 3): S258–63.
5. Llovet JM, Bru C, Bruix J. Prognosis of hepatocellular carcinoma: the BCLC staging classification. *Semin Liver Dis* 1999; **19**: 329–38.
6. Llovet JM, Di Bisceglie AM, Bruix J, *et al.* Design and endpoints of clinical trials in hepatocellular carcinoma. *J Natl Cancer Inst* 2008a; **100**: 698–711.
7. Bruix J, Sherman M, Llovet JM, *et al.* Clinical management of hepatocellular carcinoma. Conclusions of the Barcelona-2000 EASL conference. European Association for the Study of the Liver. *J Hepatol* 2001; **35**: 421–30.
8. Bruix J, Sherman M. Management of hepatocellular carcinoma. *Hepatology* 2005; **42**: 1208–36.
9. Bruix J, Sherman M. Management of hepatocellular carcinoma: an update. *Hepatology* 2011; **53**: 1020–2.
10. Bruix J, Sala M, Llovet JM. Chemoembolization for hepatocellular carcinoma. *Gastroenterology* 2004; **127**(5 Suppl. 1): S179–88.
11. Llovet JM, Burroughs A, Bruix J. Hepatocellular carcinoma. *Lancet* 2003; **362**: 1907–17.
12. Malagari K, Pomoni M, Kelekis A, *et al.* Prospective randomized comparison of chemoembolization with doxorubicin-eluting beads and bland embolization with BeadBlock for hepatocellular carcinoma. *Cardiovasc Intervent Radiol* 2010; **33**: 541–51.
13. Lopez PM, Villanueva A, Llovet JM. Systematic review: evidence-based management of hepatocellular carcinoma–an updated analysis of randomized controlled trials. *Aliment Pharmacol Ther* 2006; **23**: 1535–47.
14. Llovet JM, Bruix J. Systematic review of randomized trials for unresectable hepatocellular carcinoma: chemoembolization improves survival. *Hepatology* 2003; **37**: 429–42.
15. Oliveri RS, Wetterslev J, Gluud C. Transarterial (chemo) embolisation for unresectable hepatocellular carcinoma. *Cochrane Database Syst Rev* 2011 (3): CD004787.
16. Forner A, Llovet JM, Bruix J. Hepatocellular carcinoma. *Lancet* 2012; **379**: 1245–55.
17. Lin DY, Liaw YF, Lee TY, Lai CM. Hepatic arterial embolization in patients with unresectable hepatocellular carcinoma–a randomized controlled trial. *Gastroenterology* 1988; **94**: 453–6.
18. Peck-Radosavljevic M, Sieghart W, Kolblinger C, *et al.* Austrian Joint OGGH-OGIR-OGHO-ASSO position statement on the use of transarterial chemoembolization (TACE) in hepatocellular carcinoma. *Wien Klin Wochenschr* 2012; **124**: 104–10.
19. Antoch G, Roelle G, Ladd SC, *et al.* Selective and sequential transarterial chemoembolization: survival in patients with hepatocellular carcinoma. *Eur J Radiol* 2012; **81**: 2290–7.
20. Marelli L, Stigliano R, Triantos C, *et al.* Transarterial therapy for hepatocellular carcinoma: which technique is more effective? A systematic review of cohort and randomized studies. *Cardiovasc Intervent Radiol* 2007; **30**: 6–25.
21. Burrel M, Reig M, Forner A, *et al.* Survival of patients with hepatocellular carcinoma treated by transarterial chemoembolisation (TACE) using Drug Eluting Beads. Implications for clinical practice and trial design. *J Hepatol* 2012; **56**: 1330–5.
22. Camma C, Schepis F, Orlando A, *et al.* Transarterial chemoembolization for unresectable hepatocellular carcinoma: meta-analysis of randomized controlled trials. *Radiology* 2002; **224**: 47–54.
23. Varela M, Real MI, Burrel M, *et al.* Chemoembolization of hepatocellular carcinoma with drug eluting beads: efficacy and doxorubicin pharmacokinetics. *J Hepatol* 2007; **46**: 474–81.
24. Lammer J, Malagari K, Vogl T, *et al.* Prospective randomized study of doxorubicin-eluting-bead embolization in the treatment of hepatocellular carcinoma: results of the PRECISION V study. *Cardiovasc Intervent Radiol* 2010; **33**: 41–52.
25. Carr BI, Kondragunta V, Buch SC, Branch RA. Therapeutic equivalence in survival for hepatic arterial chemoembolization and yttrium 90 microsphere treatments in unresectable hepatocellular carcinoma: a two-cohort study. *Cancer* 2010; **116**: 1305–14.
26. D'Avola D, Lnarrairaegui M, Bilbao JI, *et al.* A retrospective comparative analysis of the effect of Y90-radioembolization on the survival of patients with unresectable hepatocellular carcinoma. *Hepatogastroenterology* 2009; **56**: 1683–8.
27. Sangro B, Carpanese L, Cianni R, *et al.* Survival after yttrium-90 resin microsphere radioembolization of hepatocellular carcinoma across Barcelona clinic liver cancer stages: a European evaluation. *Hepatology* 2011; **54**: 868–78.
28. Inarrairaegui M, Thurston KG, Bilbao JI, *et al.* Radioembolization with use of yttrium-90 resin microspheres in patients with hepatocellular carcinoma and portal vein thrombosis. *J Vasc Interv Radiol* 2010; **21**: 1205–12.
29. Chan AO, Yuen MF, Hui CK, Tso WK, Lai CL. A prospective study regarding the complications of transcatheter intraarterial lipiodol chemoembolization in patients with hepatocellular carcinoma. *Cancer* 2002; **94**: 1747–52.
30. Sangro B, Inarrairaegui M, Bilbao JI. Radioembolization for hepatocellular carcinoma. *J Hepatol* 2012; **56**: 464–73.
31. Prompers L, Bucerius J, Brans B, *et al.* Selective internal radiation therapy (SIRT) in primary or secondary liver cancer. *Methods* 2011; **55**: 253–7.

32. Wilhelm SM, Carter C, Tang L, *et al.* BAY 43–9006 exhibits broad spectrum oral antitumor activity and targets the RAF/MEK/ERK pathway and receptor tyrosine kinases involved in tumor progression and angiogenesis. *Cancer Res* 2004; **64**: 7099–109.
33. Llovet JM, Ricci S, Mazzaferro V, *et al.* Sorafenib in advanced hepatocellular carcinoma. *N Engl J Med* 2008b; **359**: 378–90.
34. Cheng AL, Kang YK, Chen Z, *et al.* Efficacy and safety of sorafenib in patients in the Asia-Pacific region with advanced hepatocellular carcinoma: a phase III randomised, double-blind, placebo-controlled trial. *Lancet Oncol* 2009; **10**: 25–34.
35. Molinari M, Kachura JR, Dixon E, *et al.* Transarterial chemoembolisation for advanced hepatocellular carcinoma: results from a North American cancer centre. *Clin Oncol (R Coll Radiol)* 2006; **18**: 684–92.
36. Llovet JM, Real MI, Montana X, *et al.* Arterial embolisation or chemoembolisation versus symptomatic treatment in patients with unresectable hepatocellular carcinoma: a randomised controlled trial. *Lancet* 2002; **359**: 1734–9.
37. Lo CM, Ngan H, Tso WK, *et al.* Randomized controlled trial of transarterial lipiodol chemoembolization for unresectable hepatocellular carcinoma. *Hepatology* 2002; **35**: 1164–71.
38. Lin CI, Lin ZY, Hsieh MY, *et al.* Potential risk factors for the reactivation of the replication of hepatitis B and C viruses after transcatheter arterial chemoembolization of hepatocellular carcinoma. *Kaohsiung J Med Sci* 2011; **27**: 554–9.
39. Jang JW, Choi JY, Bae SH, *et al.* Transarterial chemo-lipiodolization can reactivate hepatitis B virus replication in patients with hepatocellular carcinoma. *J Hepatol* 2004; **41**: 427–35.
40. Peng JW, Lin GN, Xiao JJ, Jiang XM. Hepatitis B virus reactivation in hepatocellular carcinoma patients undergoing transcatheter arterial chemoembolization therapy. *Asia Pac J Clin Oncol* 2013; **8**: 356–61.
41. Ikeda K, Arase Y, Kobayashi M, *et al.* Hepatitis B virus-related hepatocellular carcinogenesis and its prevention. *Intervirology* 2005; **48**: 29–38.
42. EASL-EORTC clinical practice guidelines. management of hepatocellular carcinoma. *J Hepatol* 2012; **56**: 908–43.
43. Chin PL, Chu DZ, Clarke KG, *et al.* Ethnic differences in the behavior of hepatocellular carcinoma. *Cancer* 1999; **85**: 1931–6.
44. Takayasu K, Arii S, Ikai I, *et al.* Prospective cohort study of transarterial chemoembolization for unresectable hepatocellular carcinoma in 8510 patients. *Gastroenterology* 2006; **131**: 461–9.
45. Shi M, Chen JA, Lin XJ, *et al.* Transarterial chemoembolization as initial treatment for unresectable hepatocellular carcinoma in southern China. *World J Gastroenterol* 2010; **16**: 264–9.
46. Cheng HY, Wang X, Chen D, Xu AM, Jia YC. The value and limitation of transcatheter arterial chemoembolization in preventing recurrence of resected hepatocellular carcinoma. *World J Gastroenterol* 2005; **11**: 3644–6.
47. Kasai K, Ushio A, Sawara K, *et al.* Transcatheter arterial chemoembolization with a fine-powder formulation of cisplatin for hepatocellular carcinoma. *World J Gastroenterol* 2010; **16**: 3437–44.
48. Seki A, Hori S, Kobayashi K, Narumiya S. Transcatheter arterial chemoembolization with epirubicin-loaded superabsorbent polymer microspheres for 135 hepatocellular carcinoma patients: single-center experience. *Cardiovasc Intervent Radiol* 2011; **34**: 557–65.
49. Kim HW, Park JW, Park HK, *et al.* Outcome of transarterial chemoembolization in Korean patients with hepatocellular carcinoma: reference for a prospective combination study with molecular targeted agents. *Hepatology* 2010; **52** (suppl): 1183A.
50. Raoul JL, Sangro B, Forner A, *et al.* Evolving strategies for the management of intermediate-stage hepatocellular carcinoma: available evidence and expert opinion on the use of transarterial chemoembolization. *Cancer Treat Rev* 2011; **37**: 212–20.
51. Satake M, Uchida H, Arai Y, *et al.* Transcatheter arterial chemoembolization (TACE) with lipiodol to treat hepatocellular carcinoma: survey results from the TACE study group of Japan. *Cardiovasc Intervent Radiol* 2008; **31**: 756–61.
52. Park JW, Kim HW, Chen PJ, *et al.* Observations of HCC management patterns from the global HCC BRIDGE study: an interim analysis from a south Korean referral center. *APASL 9th Single Topic Conference.* 2011; GS3-4.
53. Kim HY, Park JW, Joo J, *et al.* Severity and timing of progression predict refractoriness to transarterial chemoembolization in hepatocellular carcinoma. *J Gastroenterol Hepatol* 2011; **27**: 1051–6.
54. Cabrera R, Pannu DS, Caridi J, *et al.* The combination of sorafenib with transarterial chemoembolisation for hepatocellular carcinoma. *Aliment Pharmacol Ther* 2011; **34**: 205–13.
55. Pawlik TM, Reyes DK, Cosgrove D, *et al.* Phase II trial of sorafenib combined with concurrent transarterial chemoembolization with Drug-Eluting Beads for hepatocellular carcinoma. *J Clin Oncol* 2011; **29**: 3960–7.
56. Park JW, Koh YH, Kim HB, *et al.* , Phase II study of concurrent transarterial chemoembolization and sorafenib in patients with unresectable hepatocellular carcinoma. *J Hepatol* 2012; **56**: 1336–42.
57. Chung YH, Han G, Yoon JH, *et al.* Interim analysis of start: Study in asia of the combination of TACE (Transcatheter arterial chemoembolization) with sorafenib in patients with hepatocellular carcinoma trial. *Int J Cancer* 2012; doi: 10.1002/ijc.27925.
58. Lencioni R, Llovet JM, Han G, *et al.* , Sorafenib or placebo in combination with transarterial chemoembolization (TACE) with doxorubicin-eluting beads (DEBDOX) for intermediate-stage hepatocellular carcinoma (HCC): phase II, randomized, double-blind SPACE trial. *J Clin Oncol* 2012. **30**(4 suppl): Abstract LBA 154.
59. Miller AB, Hoogstraten B, Staquet M, Winkler A. Reporting results of cancer treatment. *Cancer* 1981; **47**: 207–14.
60. Lencioni R, Llovet JM. Modified RECIST (mRECIST) assessment for hepatocellular carcinoma. *Semin Liver Dis* 2010; **30**: 52–60.
61. Kudo M, Imanaka K, Chida N, *et al.* Phase III study of sorafenib after transarterial chemoembolisation in Japanese and Korean patients with unresectable hepatocellular carcinoma. *Eur J Cancer* 2011; **47**: 2117–27.
62. Sansonno D, Lauletta G, Russi S, *et al.* Transarterial chemoembolization plus sorafenib: a sequential therapeutic

scheme for HCV-related intermediate-stage hepatocellular carcinoma: a randomized clinical trial. *Oncologist* 2012; **17**: 359–66.
63. Sieghart W, Pinter M, Reisegger M, *et al.* Conventional transarterial chemoembolisation in combination with sorafenib for patients with hepatocellular carcinoma: a pilot study. *Eur Radiol* 2012; **22**: 1214–23.
64. Qu XD, Chen CS, Wang JH, *et al.* The efficacy of TACE combined sorafenib in advanced stages hepatocellullar carcinoma. *BMC Cancer* 2012; **12**: 263.
65. Erhardt A, Kolligs FT, Dollinger M, *et al.* Sorafenib plus TACE for the treatment of advanced Hepatocellular carcinoma – final results of the SOCRATES trial. *J Hepatol* 2011; **54**: S25–44.

REVIEW

Gut and Liver, Vol. 7, No. 1, January 2013, pp. 1-6

Radiofrequency Ablation of Liver Metastases from Colorectal Cancer: A Literature Review

Yasunori Minami and Masatoshi Kudo

Department of Gastroenterology and Hepatology, Kinki University Faculty of Medicine, Osaka, Japan

Liver metastases occur in up to 60% of patients with colorectal cancer, and the control of liver metastases is considered to be of primary importance because it is a critical factor in determining prognosis. Radiofrequency ablation (RFA) therapy is one of the least invasive techniques for unresectable hepatic malignancies and can be performed safely using percutaneous, laparoscopic, or open surgical techniques. The local tumor progression rates after RFA for colorectal liver metastases range from 8.8% to 40.0%, and 5-year survival rates range from 20.0% to 48.5%. No prospective, randomized trials comparing the efficacy of RFA with that of surgical resection for colorectal liver metastases are currently available. However, some retrospective studies have reported that patients who received RFA had a survival rate similar to that observed in surgically treated groups, while other studies have reported better survival among patients who underwent surgical resection. The use of a laparoscopic or open surgical approach allows the repeated placement of RFA electrodes at multiple sites to ablate larger tumors. An accurate evaluation of treatment response is very important for the success of RFA therapy because a sufficient safety margin (at least 0.5 cm) can prevent local tumor progression. This review critically summarizes the current status of RFA for liver metastases from colorectal cancer. **(Gut Liver 2013;7:1-6)**

Key Words: Colorectal neoplasms; Liver metastasis; Safety margin; Radiofrequency ablation

INTRODUCTION

The liver is a common site for cancer metastasis, and liver metastases occur in up to 60% of patients with colorectal cancer (CRC).[1] As one of the critical factors determining the prognosis of the patients with advanced stage CRC is liver metastasis, adequate local control of liver metastasis must be achieved. Surgery provides the therapeutic choice for cure in patients with hepatic metastases, and it has been reported that hepatic resection provides a good prognosis and a favorable quality of life in the patients with colorectal liver metastasis (CRLM).[2] However, chemotherapy following the resection of primary CRC can cause hepatic injury.[3] Repeat hepatic resection for current CRLM would be confined to the patients with good liver function. Moreover, difficulties of surgical resection may be related to the size, site, and number of tumors, vascular, and extrahepatic involvement as well as poor liver function.

There is a need for an effective and less invasive technique for the treatment of unresectable hepatic malignancies. Recently, several local ablative techniques, such as, percutaneous ethanol injection, microwave coagulation therapy, and radiofrequency ablation (RFA) have been reported to be effective in the patients, considered for liver-directed therapies, expanding the pool of patients who can be treated.[4-7] RFA, in particular, has resulted in a higher rate of complete necrosis of the metastatic lesions in the liver and required fewer treatment sessions than the other ablation therapies.[6-8] The advantage of minimal invasiveness for RFA, combined with claims of good local control and good survival have had a positive impact on the clinical management of the patients with CRLM. However, there is a need to scientifically analyze in detail the potential advantages and disadvantages of resection versus RFA for resectable CRLM. Recently randomized controlled trials have been advocated to compare RFA and hepatic resection in resectable CRLM; but to date, this has not yet been performed. In this review, we focus our discussion on the efficacy of percutaneous, laparoscopic and open surgical RFA for CRLM, and the comparison between percutaneous RFA and surgical resection.

Correspondence to: Yasunori Minami
Department of Gastroenterology and Hepatology, Kinki University Faculty of Medicine, 377-2 Ohno-Higashi Osaka-Sayama, Osaka 589-8511, Japan
Tel: +81-72-366-0221, Fax: +81-72-367-2880, E-mail: m-kudo@med.kindai.ac.jp
Received on December 5, 2011. Revised on February 8, 2012. Accepted on February 27, 2012. Published online on December 5, 2012.
pISSN 1976-2283 eISSN 2005-1212 http://dx.doi.org/10.5009/gnl.2013.7.1.1

BACKGROUND

1. Localized application of radiofrequency energy

RFA is a localized thermal treatment technique designed to induce tumor destruction by heating the tumor tissue to temperatures that exceed 60°C.[5-7] The alternating current of radiofrequency waves passing down from an uninsulated electrode tip into the surrounding tissues generates changes in the direction of ions and creates ionic agitation and frictional heating. This tissue heating then drives extracellular and intracellular water out of the tissue, resulting in tissue destruction by coagulative necrosis. When tumor cells are heated above 45°C to 50°C, intracellular proteins are denatured and cell membranes are destroyed through dissolution and melting of lipid bilayers. As a result, successful ablations usually increase the temperature of the ablated tissue to above 60°C.

Percutaneous RFA under local anesthesia is feasible, although intraoperative RFA under general anesthesia has also been performed to prevent severe pain and discomfort during the procedure.

2. Treatment algorithm

RFA is recommended for liver metastases with a maximum diameter of 3 cm in patients with not more than three tumors who are contraindicated for surgery, according to hepatocellular carcinoma (HCC) treatment algorithm in Japan and the West.[9-11] This algorithm has often been applied in the treatment of liver metastases. However, the number of lesions should not be considered an absolute limiting consideration for RFA, if successful treatment of all metastasis deposits can be accomplished. Most centers preferentially treat patients with five or fewer lesions. The target tumor should not exceed 3 cm in the longest axis to achieve best rates of complete ablation with most of the currently available devices.

3. Imaging of liver metastasis from CRC

Ultrasonography (US) shows multiple round and/or hypoechoic masses with irregular borders.[12] A Bull's eye appearance represents histological findings of an area showing central coagulative necrosis surrounded by a zonal area of viable tumor. However, the poorly-differentiated adenocarcinoma often appears as infiltrative, without a capsule, and the tumor border can be shown irregular on B-mode US. Contrast enhanced US can show intratumoral vascurality in the peripheral hypoechoic zone, in which viable tumor cells are proliferating.[13] It has been reported that the presence of rim enhancement with peripheral tumor vessels (sensitivity, 88.1%; specificity, 100%) is the typical pattern.[14] Contrast enhanced US in the late phase provides marked improvement in the detection of hepatic metastases as areas of hypoenhancement, and can be advantageous in detecting small metastases compared with computed tomography (CT) and magnetic resonance imaging (MRI).[15,16]

Multidetector row helical CT have further improved the performance of CT scanners in terms of speed of acquisition, resolution, and the ability to image the liver during various phases of contrast enhancement more precisely than was possible previously. CRLM are detected as hypodense lesions in the late portal venous phase on contrast-enhanced CT. In this phase the attenuation of the normal liver parenchyma increases, revealing the relatively hypoattenuating metastases, sometimes with rim enhancement.[17]

The majority of CRLM show several typical findings on MRI. The lesions appear as low signal intensity on T1-weighted images and as moderately high signal intensity lesions on T2-weighted images with fat suppression.[18] Metastases with intratumoral hemorrhage or coagulative necrosis may exhibit mixed signal intensity on T1-weighted images, and those with a desmoplastic reaction may exhibit low signal intensity on T2-weighted images. Especially, gadolinium-ethoxybenzyl-diethylenetriamine-pentaacetic acid (Gd-EOB-DTPA) is a liver-specific hepatobiliary MR contrast agent that offers both dynamic imaging and static hepatocyte imaging. Gd-EOB-DTPA is taken up by hepatocytes in healthy liver tissue in an amount of about 50% of injected dose, and because malignant primary and secondary tumors usually do not contain functioning hepatocytes, the contrast effect the lesions will appear as dark areas against healthy liver parenchyma.[19]

4. Assessment of technical effectiveness

The area of perilesional rim enhancement shown in contrast-enhanced CT suggests microscopic tumor cell infiltration. The assessment of the therapeutic effect of RFA is very important. The technical effectiveness of ablation is commonly assessed by findings on contrast enhanced CT or MRI because of objectivity and reproducibility of the image. Contrast-enhanced US may also provide an alternative approach in assessing the therapeutic effect of RFA, in spite of having limitations in identifying the safety margin.[20] A tumor is considered to have been successfully ablated when there is at least a 0.5 cm margin of apparently normal hepatic tissue surrounding the tumor during the portal phase (Fig. 1).[21,22] Failure to establish a sufficient ablative safety margin is an independently significant risk factor for local tumor progression on multivariate analysis.[23] Basically, the local tumor progression rate following a single RFA treatment depends on how strictly the therapeutic effect is assessed.

CLINICAL OUTCOMES

1. Percutaneous approach

1) Local controllability (local tumor progression) and survival

The reported local recurrence rate after RFA for liver metastases ranges from 8.8% to 40% (Table 1).[23-35] Three-year and 5-year survival ranges from 22% to 57% and 20% to 48.5%, re-

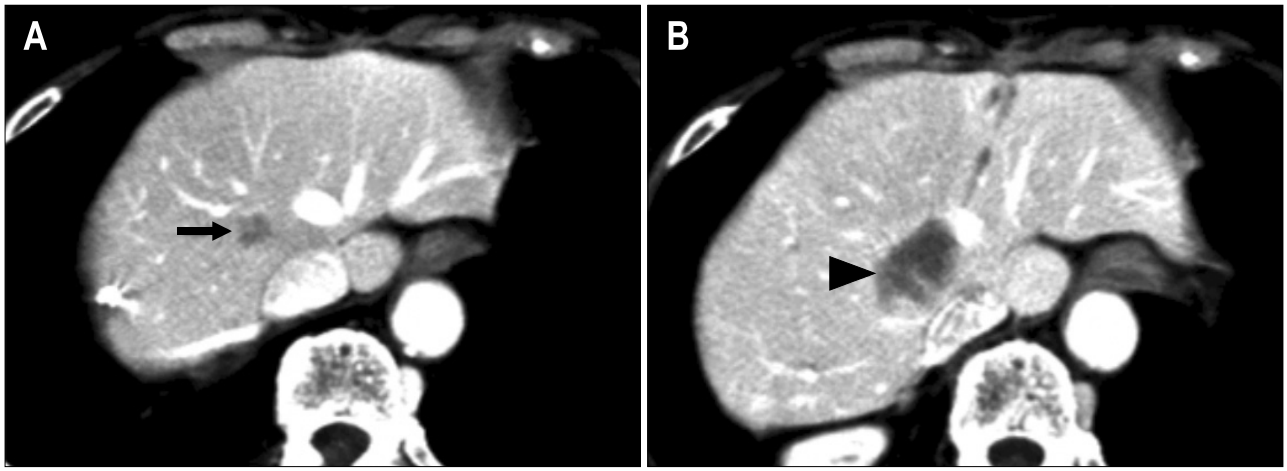

Fig. 1. An 86-year-old man with a liver metastasis from the colon measuring 1.5 cm in diameter. (A) A portal-phase dynamic computed tomography (CT) scan showing a hypovascular tumor (arrow) in segment eight of the liver. (B) A portal-phase dynamic CT scan obtained 2 days after RFA showing that the tumor and surrounding area (arrowhead) are not enhanced. Thus, this tumor is considered to have been successfully ablated.

Table 1. Local Tumor Progression Rate and Survival after Radiofrequency Ablation for Liver Metastases

Author (yr)	Origin	No.	Tumor size, mean, cm	Follow-up period, mean, mo	Local progression, %	Survival, %
Livraghi *et al*. (2003)[24]	C&R	88	2.1	33	40	-
Oshowo *et al*. (2003)[25]	C&R	25	-	-	-	53 (3-yr)
Abdalla *et al*. (2004)[26]	C&R	57	2.5	-	-	22 (3-yr)
Berber et al. (2005)[27]	C&R	135	4.1	-	-	36 (4-yr)
Aloia *et al*. (2006)[28]	C&R	27	3.0	50	31	27 (5-yr)
Machi *et al*. (2006)[29]	C&R	507	-	24.5	-	30.5 (5-yr)
Abitabile *et al*. (2007)[30]	C&R	147	-	33	8.8	57 (3-yr)
White *et al*. (2007)[23]	C&R	22	2.4	17	55	25 (3-yr)
Park *et al*. (2008)[31]	C&R	30	2.0	49	23	20 (5-yr)
Lee *et al*. (2008)[32]	C&R	37	-	-	-	48.5 (5-yr)
Reuter *et al*. (2009)[33]	C&R	66	3.2	-	17	21 (5-yr)
Gillams *et al*. (2009)[34]	C&R	309	3.7	-	-	34 (5-yr)
Knudsen *et al*. (2009)[35]	C&R	36	2.1	27	-	34 (3-yr)

C&R, colon and rectum.

spectively. Several factors can be correlated with the survival of the patients with untreated hepatic CRC metastases. The dominant effect of liver tumor involvement suggests that successful local therapy could increase life expectancy, decrease mortality, or both. Local tumor progression is related to incomplete tumor ablation. However, it is often difficult to obtain a specific safety margin in three dimensions all around a large tumor. Some researchers reported that the most important factor associated with failure of local tumor control could be tumor size.[36] Table 1 shows that local tumor progression does not necessarily depend on the tumor size; however, recurrence could occur even after a sufficient margin had been ensured. It is suggested that local tumor progression arises from the residual cancer after RFA, while recurrence from a microsatellite or by microvascular invasion other than the main nodule may also appear as a late local tumor progression. Therefore, a larger safety margin is necessary in order to obtain complete local ablation of liver metastases because of infiltrative invasion.

2) Survival: comparison with those after resection

At present, no prospective randomized trials have been reported. However, there are some retrospective reports of large numbers of patients regarding RFA versus surgical resection for hepatic colorectal metastasis (Table 2).[23,25,26,28,31-33] Some reported that patients who received RFA had survival rates similar to surgical groups, while others found that survival rates were better among patients undergoing surgical resection. Reuter *et al*.[33] conducted a comparative study on 192 patients with hepatic colorectal metastases who received either percutaneous RFA or surgical resection. Patients who underwent RFA were similar

Table 2. Survival Rates Associated with RFA versus Hepatic Resection for Liver Metastases

Author (yr)	No., RFA/resection	Mean tumor size, RFA/resection, cm	Overall survival, RFA vs resection, %	p-value
White *et al*. (2007)[23]	22/30	2.4/2.7	25 vs 82 (3-yr)	-
Oshowo *et al*. (2003)[25]	25/20	-/-	53 vs 55 (3-yr)	NS
Abdalla *et al*. (2004)[26]	57/190	2.5/-	22 vs 65 (3-yr)	<0.001
Aloia *et al*. (2006)[28]	27/147	-	27 vs 71 (5-yr)	<0.001
Park *et al*. (2008)[31]	30/59	2.0/3.1	20 vs 42 (5-yr)	0.0002
Lee *et al*. (2008)[32]	37/116	-	48.5 vs 65.7 (5-yr)	0.227
Reuter *et al*. (2009)[33]	66/126	3.2/5.3	21 vs 23 (5-yr)	NS

RFA, radiofrequency ablation; NS, not significant.

to resection patients based on mean number of hepatic lesions (2.8 vs 2.1, p=0.14), and prior chemotherapy (67% vs 60%, p=0.33). However, the median time to recurrence was shorter with ablation than with resection (12.2 months vs 31.1 months, p<0.001). Recurrence at the ablation-resection site was more common with ablation than with resection, occurring in 17% versus 2% (p<0.001) of cases, respectively. Distant recurrence in the liver was also more common with ablation, occurring in 33% of patients versus 14% for resection (p=0.002). Abdalla *et al*.[26] reported that local recurrence was most common after RFA (9% vs 2%, p<0.02). The overall survival rate was highest after resection (58% at 5 years); 4-year survival after resection and RFA only were 65% and 22%, respectively (p<0.0001). In both of the above studies, RFA alone for unresectable patients did not yield the survival rate comparable to the resected group. However, this difference probably reflects a selection bias since RFA was used in operative candidates who could not undergo complete resection of the disease. A subgroup of patients has been identified for whom local control after RFA was equivalent to the resected group. Further studies are necessary to determine the efficacy of RFA versus resection. We would suggest that the time has come for a randomized trial.

2. Laparoscopic/open surgical approach

The use of a laparoscopic or open surgical approach allows repeated placement of RFA electrodes at multiple sites to ablate larger tumors.[37-39] Berber *et al*.[39] reported that local recurrence was identified in 21.7% of tumors on CT scans with a mean follow-up of 17 months (median, 12 months; range, 3 to 68 months). The local recurrence rate per tumor was highest for colorectal metastasis (34%), followed by noncolorectal, nonneuroendocrine metastasis (22%), HCC (18%), and neuroendocrine metastasis (6%). The Cox proportional hazard model identified tumor type, tumor size, ablation margin, and blood vessel proximity to be independent predictors of local recurrrence. The next advantage is the use of intraoperative US, which provides better resolution of the number and location of liver tumors. Ibrahim reported that laparoscopic ultrasound identified 19 new malignant lesions (18.4%), in comparison with the result of preoperative imaging.[40] In general, great difficulty can be encountered during laparoscopic RFA of lesions in contact with the diaphragm. However, a hand-assisted technique can offer traction while the natural diaphragmatic attachments of the liver provides countertraction. Machi *et al*.[41] discussed that the hand-assisted laparoscopic method combines the advantages of both laparoscopic and open surgical approaches for RFA treatment of liver tumors. The hand-assisted laparoscopic surgery approach has several advantages; it facilitates and expedites the procedure, reduces the stress factor on the surgeon, greatly improves exposure, and facilitates immediate and efficient control of bleeding vessels with the internal hand.

Although more invasive, open surgical RFA can be performed more easily and the puncture course of the RF needle can be more widely selected than that during a laparoscopic approach.[42,43] Radical open surgical RFA has an advantage of few ablation site recurrences, even when the nodules measure more than 4 cm in diameter or there are more than three nodules, because of fewer limitations of RF needle puncture.

3. Complications

A recent review indicated that the complication rates for percutaneous, laparoscopic, and open surgical RFA of hepatic tumors in 3,670 patients are 7.2%, 9.5%, and 9.9%, respectively.[44] Overall, the frequency of major complications of percutaneous RFA ranges from 0.6% to 8.9%.[45] In RFA of HCC, Llovet *et al*.[46] reported that dissemination along the puncture route was observed in 12.5% of their patients, so dissemination might not occur at such a high frequency. However, this complication was almost absent in many reports from Japan.[45] On the other hand, neoplastic seeding can occur after RFA of liver metastases.[47] In comparison with RFA of HCC, there are no papers on whether or not the seeding on RFA of liver metastases is frequent.

SUMMARY

The successful management of liver metastases from CRC can be obtained with RFA. RFA has a potential to achieve the same overall and disease-free survival rate as surgical resection

for patients with liver metastases, while causing fewer side effects. The use of laparoscopic or open surgical approach allows repeated placement of RFA electrodes at multiple sites to ablate larger tumors. In addition, an accurate evaluation of treatment response is very important for successful RFA therapy, since a sufficient safety margin (at least 0.5 cm) can prevent local tumor progression. Finally, because early and accurate diagnosis is necessary for the appropriate management of the complications, physicians should be familiar with all the features of the complications of RFA therapy.

CONFLICTS OF INTEREST

No potential conflict of interest relevant to this article was reported.

REFERENCES

1. Geoghegan JG, Scheele J. Treatment of colorectal liver metastases. Br J Surg 1999;86:158-169.
2. de Jong MC, Mayo SC, Pulitano C, et al. Repeat curative intent liver surgery is safe and effective for recurrent colorectal liver metastasis: results from an international multi-institutional analysis. J Gastrointest Surg 2009;13:2141-2151.
3. Khan AZ, Morris-Stiff G, Makuuchi M. Patterns of chemotherapy-induced hepatic injury and their implications for patients undergoing liver resection for colorectal liver metastases. J Hepatobiliary Pancreat Surg 2009;16:137-144.
4. Bartolozzi C, Lencioni R. Ethanol injection for the treatment of hepatic tumours. Eur Radiol 1996;6:682-696.
5. Rossi S, Di Stasi M, Buscarini E, et al. Percutaneous radiofrequency interstitial thermal ablation in the treatment of small hepatocellular carcinoma. Cancer J Sci Am 1995;1:73-81.
6. Minami Y, Kudo M. Radiofrequency ablation of hepatocellular carcinoma: current status. World J Radiol 2010;2:417-424.
7. Rhim H, Lim HK. Radiofrequency ablation of hepatocellular carcinoma: pros and cons. Gut Liver 2010;4 Suppl 1:S113-S118.
8. Livraghi T, Goldberg SN, Lazzaroni S, Meloni F, Solbiati L, Gazelle GS. Small hepatocellular carcinoma: treatment with radio-frequency ablation versus ethanol injection. Radiology 1999;210:655-661.
9. Kudo M, Okanoue T; Japan Society of Hepatology. Management of hepatocellular carcinoma in Japan: consensus-based clinical practice manual proposed by the Japan Society of Hepatology. Oncology 2007;72 Suppl 1:2-15.
10. Bruix J, Sherman M; Practice Guidelines Committee, American Association for the Study of Liver Diseases. Management of hepatocellular carcinoma. Hepatology 2005;42:1208-1236.
11. Omata M, Lesmana LA, Tateishi R, et al. Asian Pacific Association for the Study of the Liver consensus recommendations on hepatocellular carcinoma. Hepatol Int 2010;4:439-474.
12. Yoshida T, Matsue H, Okazaki N, Yoshino M. Ultrasonographic differentiation of hepatocellular carcinoma from metastatic liver cancer. J Clin Ultrasound 1987;15:431-437.
13. Konopke R, Kersting S, Bergert H, et al. Contrast-enhanced ultrasonography to detect liver metastases: a prospective trial to compare transcutaneous unenhanced and contrast-enhanced ultrasonography in patients undergoing laparotomy. Int J Colorectal Dis 2007;22:201-207.
14. Hatanaka K, Kudo M, Minami Y, et al. Differential diagnosis of hepatic tumors: value of contrast-enhanced harmonic sonography using the newly developed contrast agent, Sonazoid. Intervirology 2008;51 Suppl 1:61-69.
15. Hatanaka K, Kudo M, Minami Y, Maekawa K. Sonazoid-enhanced ultrasonography for diagnosis of hepatic malignancies: comparison with contrast-enhanced CT. Oncology 2008;75 Suppl 1:42-47.
16. Dietrich CF, Ignee A, Trojan J, Fellbaum C, Schuessler G. Improved characterisation of histologically proven liver tumours by contrast enhanced ultrasonography during the portal venous and specific late phase of SHU 508A. Gut 2004;53:401-405.
17. Francis IR, Cohan RH, McNulty NJ, et al. Multidetector CT of the liver and hepatic neoplasms: effect of multiphasic imaging on tumor conspicuity and vascular enhancement. AJR Am J Roentgenol 2003;180:1217-1224.
18. Yu JS, Rofsky NM. Hepatic metastases: perilesional enhancement on dynamic MRI. AJR Am J Roentgenol 2006;186:1051-1058.
19. Sofue K, Tsurusaki M, Tokue H, Arai Y, Sugimura K. Gd-EOB-DTPA-enhanced 3.0 T MR imaging: quantitative and qualitative comparison of hepatocyte-phase images obtained 10 min and 20 min after injection for the detection of liver metastases from colorectal carcinoma. Eur Radiol 2011;21:2336-2343.
20. Wen YL, Kudo M, Zheng RQ, et al. Radiofrequency ablation of hepatocellular carcinoma: therapeutic response using contrast-enhanced coded phase-inversion harmonic sonography. AJR Am J Roentgenol 2003;181:57-63.
21. Ni Y, Chen F, Mulier S, et al. Magnetic resonance imaging after radiofrequency ablation in a rodent model of liver tumor: tissue characterization using a novel necrosis-avid contrast agent. Eur Radiol 2006;16:1031-1040.
22. Mori K, Fukuda K, Asaoka H, et al. Radiofrequency ablation of the liver: determination of ablative margin at MR imaging with impaired clearance of ferucarbotran: feasibility study. Radiology 2009;251:557-565.
23. White RR, Avital I, Sofocleous CT, et al. Rates and patterns of recurrence for percutaneous radiofrequency ablation and open wedge resection for solitary colorectal liver metastasis. J Gastrointest Surg 2007;11:256-263.
24. Livraghi T, Solbiati L, Meloni F, Ierace T, Goldberg SN, Gazelle GS. Percutaneous radiofrequency ablation of liver metastases in potential candidates for resection: the "test-of-time approach." Cancer 2003;97:3027-3035.
25. Oshowo A, Gillams A, Harrison E, Lees WR, Taylor I. Comparison of resection and radiofrequency ablation for treatment of solitary colorectal liver metastases. Br J Surg 2003;90:1240-1243.

26. Abdalla EK, Vauthey JN, Ellis LM, et al. Recurrence and outcomes following hepatic resection, radiofrequency ablation, and combined resection/ablation for colorectal liver metastases. Ann Surg 2004;239:818-825.
27. Berber E, Pelley R, Siperstein AE. Predictors of survival after radiofrequency thermal ablation of colorectal cancer metastases to the liver: a prospective study. J Clin Oncol 2005;23:1358-1364.
28. Aloia TA, Vauthey JN, Loyer EM, et al. Solitary colorectal liver metastasis: resection determines outcome. Arch Surg 2006;141:460-466.
29. Machi J, Oishi AJ, Sumida K, et al. Long-term outcome of radiofrequency ablation for unresectable liver metastases from colorectal cancer: evaluation of prognostic factors and effectiveness in first- and second-line management. Cancer J 2006;12:318-326.
30. Abitabile P, Hartl U, Lange J, Maurer CA. Radiofrequency ablation permits an effective treatment for colorectal liver metastasis. Eur J Surg Oncol 2007;33:67-71.
31. Park IJ, Kim HC, Yu CS, Kim PN, Won HJ, Kim JC. Radiofrequency ablation for metachronous liver metastasis from colorectal cancer after curative surgery. Ann Surg Oncol 2008;15:227-232.
32. Lee WS, Yun SH, Chun HK, et al. Clinical outcomes of hepatic resection and radiofrequency ablation in patients with solitary colorectal liver metastasis. J Clin Gastroenterol 2008;42:945-949.
33. Reuter NP, Woodall CE, Scoggins CR, McMasters KM, Martin RC. Radiofrequency ablation vs. resection for hepatic colorectal metastasis: therapeutically equivalent? J Gastrointest Surg 2009;13:486-491.
34. Gillams AR, Lees WR. Five-year survival in 309 patients with colorectal liver metastases treated with radiofrequency ablation. Eur Radiol 2009;19:1206-1213.
35. Knudsen AR, Kannerup AS, Mortensen FV, Nielsen DT. Radiofrequency ablation of colorectal liver metastases downstaged by chemotherapy. Acta Radiol 2009;50:716-721.
36. Mulier S, Ni Y, Jamart J, Ruers T, Marchal G, Michel L. Local recurrence after hepatic radiofrequency coagulation: multivariate meta-analysis and review of contributing factors. Ann Surg 2005;242:158-171.
37. Mulier S, Ruers T, Jamart J, Michel L, Marchal G, Ni Y. Radiofrequency ablation versus resection for resectable colorectal liver metastases: time for a randomized trial? An update. Dig Surg 2008;25:445-460.
38. Berber E, Tsinberg M, Tellioglu G, Simpfendorfer CH, Siperstein AE. Resection versus laparoscopic radiofrequency thermal ablation of solitary colorectal liver metastasis. J Gastrointest Surg 2008;12:1967-1972.
39. Berber E, Siperstein A. Local recurrence after laparoscopic radiofrequency ablation of liver tumors: an analysis of 1,032 tumors. Ann Surg Oncol 2008;15:2757-2764.
40. Salama IA, Korayem E, ElAbd O, El-Refaie A. Laparoscopic ultrasound with radiofrequency ablation of hepatic tumors in cirrhotic patients. J Laparoendosc Adv Surg Tech A 2010;20:39-46.
41. Machi J, Oishi AJ, Mossing AJ, Furumoto NL, Oishi RH. Hand-assisted laparoscopic ultrasound-guided radiofrequency thermal ablation of liver tumors: a technical report. Surg Laparosc Endosc Percutan Tech 2002;12:160-164.
42. Minami Y, Kawasaki T, Kudo M, et al. Treatment of large and/or multiple hepatic malignancies: open surgical approaches of radiofrequency ablation. Hepatogastroenterology 2007;54:2358-2360.
43. Topal B, Aerts R, Penninckx F. Laparoscopic radiofrequency ablation of unresectable liver malignancies: feasibility and clinical outcome. Surg Laparosc Endosc Percutan Tech 2003;13:11-15.
44. Mulier S, Mulier P, Ni Y, et al. Complications of radiofrequency coagulation of liver tumours. Br J Surg 2002;89:1206-1222.
45. Kudo M. Local ablation therapy for hepatocellular carcinoma: current status and future perspectives. J Gastroenterol 2004;39:205-214.
46. Llovet JM, Vilana R, Brú C, et al. Increased risk of tumor seeding after percutaneous radiofrequency ablation for single hepatocellular carcinoma. Hepatology 2001;33:1124-1129.
47. Liu SY, Lee KF, Lai PB. Needle track seeding: a real hazard after percutaneous radiofrequency ablation for colorectal liver metastasis. World J Gastroenterol 2009;15:1653-1655.

HEPATOLOGY
Official Journal of the American Association for the Study of Liver Diseases

FGF3/FGF4 Amplification and Multiple Lung Metastases in Responders to Sorafenib in Hepatocellular Carcinoma

Tokuzo Arao,[1]* Kazuomi Ueshima,[2]* Kazuko Matsumoto,[1]* Tomoyuki Nagai,[1,2] Hideharu Kimura,[1] Satoru Hagiwara,[2] Toshiharu Sakurai,[2] Seiji Haji,[3] Akishige Kanazawa,[4] Hisashi Hidaka,[5] Yukihiro Iso,[6] Keiichi Kubota,[6] Mitsuo Shimada,[7] Tohru Utsunomiya,[7] Masashi Hirooka,[8] Yoichi Hiasa,[8] Yoshikazu Toyoki,[9] Kenichi Hakamada,[9] Kohichiroh Yasui,[10] Takashi Kumada,[11] Hidenori Toyoda,[11] Shuichi Sato,[12] Hiroyuki Hisai,[13] Teiji Kuzuya,[14] Kaoru Tsuchiya,[14] Namiki Izumi,[14] Shigeki Arii,[15] Kazuto Nishio,[1] and Masatoshi Kudo[2]

The response rate to sorafenib in hepatocellular carcinoma (HCC) is relatively low (0.7%-3%), however, rapid and drastic tumor regression is occasionally observed. The molecular backgrounds and clinico-pathological features of these responders remain largely unclear. We analyzed the clinical and molecular backgrounds of 13 responders to sorafenib with significant tumor shrinkage in a retrospective study. A comparative genomic hybridization analysis using one frozen HCC sample from a responder demonstrated that the 11q13 region, a rare amplicon in HCC including the loci for *FGF3* and *FGF4*, was highly amplified. A real-time polymerase chain reaction–based copy number assay revealed that *FGF3*/*FGF4* amplification was observed in three of the 10 HCC samples from responders in which DNA was evaluable, whereas amplification was not observed in 38 patients with stable or progressive disease ($P = 0.006$). Fluorescence *in situ* hybridization analysis confirmed *FGF3* amplification. In addition, the clinico-pathological features showed that multiple lung metastases (5/13, $P = 0.006$) and a poorly differentiated histological type (5/13, $P = 0.13$) were frequently observed in responders. A growth inhibitory assay showed that only one *FGF3*/*FGF4*-amplified and three *FGFR2*-amplified cancer cell lines exhibited hypersensitivity to sorafenib *in vitro*. Finally, an *in vivo* study revealed that treatment with a low dose of sorafenib was partially effective for stably and exogenously expressed *FGF4* tumors, while being less effective in tumors expressing *EGFP* or *FGF3*. *Conclusion:* *FGF3*/*FGF4* amplification was observed in around 2% of HCCs. Although the sample size was relatively small, *FGF3*/*FGF4* amplification, a poorly differentiated histological type, and multiple lung metastases were frequently observed in responders to sorafenib. Our findings may provide a novel insight into the molecular background of HCC and sorafenib responders, warranting further prospective biomarker studies. (HEPATOLOGY 2013;57:1407-1415)

Abbreviations: 5FU, 5-fluorouracil; CGH, comparative genomic hybridization; DMEM, Dulbecco's modified Eagle's medium; EGFR, epidermal growth factor receptor; FBS, fetal bovine serum; FFPE, formalin-fixed, paraffin-embedded; FISH, fluorescence in situ *hybridization; HCC, hepatocellular carcinoma; IC_{50}, 50% inhibitory concentration; mRNA, messenger RNA; PCR, polymerase chain reaction; PIVKA-II, protein induced by vitamin K absence or antagonist-II; RPMI-1640, Roswell Park Memorial Institute 1640; RT-PCR, reverse-transcription PCR.*

From the [1]Department of Genome Biology, [2]Department of Gastroenterology and Hepatology, and [3]Department of Surgery, Kinki University Faculty of Medicine, Osaka, Japan; the [4]Department of Hepato-Biliary-Pancreatic Surgery, Osaka City General Hospital, Miyakojima-hondori, Miyakojima-ku, Osaka, Japan; the [5]Department of Gastroenterology, Internal Medicine, Kitasato University East Hospital, Sagamihara, Japan; the [6]Second Department of Surgery, Dokkyo Medical University, Mibu, Japan; the [7]Department of Surgery, The University of Tokushima, Tokushima, Japan; the [8]Department of Gastroenterology and Metabology, Ehime University Graduate School of Medicine, Ehime, Japan; the [9]Department of Gastroenterological Surgery, Hirosaki University Graduate School of Medicine, Hirosaki, Japan; the [10]Department of Molecular Gastroenterology and Hepatology, Graduate School of Medical Science, Kyoto Prefectural University of Medicine, Kyoto, Japan; the [11]Department of Gastroenterology, Ogaki Municipal Hospital, Ogaki, Japan; the [12]Department of Gastroenterology and Hepatology, Shimane University, Faculty of Medicine, Izumo, Japan; the [13]Department of Gastroenterology, Japan Red Cross Date General Hospital, Date, Japan; the [14]Division of Gastroenterology and Hepatology, Musashino Red Cross Hospital, Tokyo, Japan; and the [15]Department of Hepato-Biliary-Pancreatic Surgery, Tokyo Medical and Dental University, Graduate School of Medicine, Tokyo, Japan.

Received October 7, 2011; accepted June 25, 2012.

Supported by the Third-Term Comprehensive 10-Year Strategy for Cancer Control (K. N.), a National Cancer Center Research and Development Fund (H22-015, to M. K.), and a Grant-in-Aid for Scientific Research (23650627, to K. N.).

**These authors contributed equally to this work.*

See Editorial on Page 1291

Hepatocellular carcinoma (HCC) is the sixth most common cancer-related cause of death in the world annually, and the development of new primary tumors, recurrences, and metastasis are the most common causes of mortality among patients with HCC.[1,2] Sorafenib (Nexavar; Bayer Healthcare Pharmaceuticals Inc.) is a small molecule kinase inhibitor that is classified as an anti-angiogenic inhibitor.[3] Sorafenib inhibits the kinase activities of Raf-1 and B-Raf in addition to vascular endothelial growth factor receptors, platelet-derived growth factor receptor β, Flt-3, and c-KIT. Two large randomized controlled trials reported a significant clinical benefit of single-agent sorafenib in extending overall survival in both Western and Asian patients with advanced unresectable HCC.[4,5] Consequently, sorafenib is now used as a standard therapy for HCC. The mechanisms of action that lead to these remarkably prolonged overall survival periods are thought to result from the anti-angiogenic effects of sorafenib and its characteristic inhibitory effect on Raf-1 and B-Raf signaling. In these trials, a partial response was observed in 0.7% (2/299) and 3.3% (5/150) of the patients treated with sorafenib.[4-5]

Recently, emerging evidence has demonstrated that some responders exhibit rapid tumor regression as a result of sorafenib treatment for HCC. Complete responses were observed in two patients with advanced HCC and multiple lung metastases, with rapid tumor regression observed even after short-term treatment with sorafenib.[6,7] The drastic tumor response to sorafenib seems to be similar to the tumor response obtained using other tyrosine kinase inhibitors to target a deregulated signal in cancer cells. For example, constitutively active mutations of epidermal growth factor receptor (EGFR) tyrosine kinase in non–small cell lung cancer are associated with a striking treatment response to gefitinib, a selective EGFR tyrosine kinase inhibitor.[8,9] We hypothesized that these HCC cells may harbor a genetic background conducive to a drastic response to sorafenib, rather than the typical anti-angiogenic effect. In this study, we retrospectively searched for genetic changes using mainly formalin-fixed, paraffin-embedded (FFPE) samples from patients with HCC who had undergone sorafenib treatment.

Patients and Methods

Reagent and Cell Culture. Sorafenib was provided by Bayer Healthcare Pharmaceuticals Inc. (Montville, NJ). All cell lines used in this study were maintained in Roswell Park Memorial Institute 1640 (RPMI-1640) medium (Sigma, St. Louis, MO) except for IM95, OUMS23, Colo320, WiDr, HLF, HLE, Huh7, and HepG2 (Dulbecco's modified Eagle's medium [DMEM]; Nissui Pharmaceutical, Tokyo, Japan); LoVo (F12; Nissui Pharmaceutical, Tokyo, Japan); KYSE180, KYSE220, and KYSE270 (RPMI-1640:F12, 1:1); KYSE150 (F12); and KYSE70 (DMEM) supplemented with 10% heat-inactivated fetal bovine serum (FBS) (Gibco BRL, Grand Island, NY) or 2% FBS for the KYSE series plus penicillin and streptomycin in a humidified atmosphere of 5% CO_2 at 37°C. These cell lines were obtained from the American Type Culture Collection (Manassas, VA) and the Japanese Collection of Research Bioresources Collection (Sennan-shi, Osaka, Japan).

Patients and Samples. The inclusion criteria for the study were as follows: patients with histologically confirmed HCC who had been treated with sorafenib, from whom pretreatment tumor samples were available. Finally, the clinical characteristics of a total of 55 cases of HCC from 12 medical centers were evaluated retrospectively. In the gene copy number analysis, four samples were excluded because of an insufficient quantity of DNA, two samples were excluded because of the poor quality of the DNA and two samples were response not evaluable. One not evaluable sample was poor DNA quality. Thus, the copy number assay was performed using the remaining 48 samples. Meanwhile, a series of 82 HCC samples were obtained from frozen specimens of surgical specimens at the Kinki University Faculty of Medicine. The tumor response was evaluated using computerized tomography according to the Response Evaluation Criteria in Solid Tumors; the response was then classified as a complete response, a partial response, stable disease, progressive disease, or not evaluable. The clinico-pathological features evaluated included age, sex, viral infection, alpha-fetoprotein level, protein induced by vitamin K absence or antagonist-II (PIVKA-II), clinical stage, primary tumor size, metastatic lesion, histological type, treatment response, and duration of sorafenib

Address reprint requests to: Kazuto Nishio, Department of Genome Biology, Kinki University School of Medicine, 377-2 Ohno-higashi, Osaka-Sayama, Osaka 589-8511, Japan. E-mail: knishio@med.kindai.ac.jp; fax: (81)-72-367-6369..

View this article online at wileyonlinelibrary.com.

DOI 10.1002/hep.25956

Potential conflict of interest: Nothing to report.

treatment. The present study was approved by the institutional review boards of all the centers involved in the study, and informed consent was obtained from the patients.

Isolation of Genomic DNA. Genomic DNA samples were extracted from deparaffinized tissue sections preserved as FFPE tissue using a QIAamp DNA Micro kit (Qiagen, Hilden, Germany) according to the manufacturer's instructions. Genomic DNA samples were extracted from surgical frozen sections using a QIAamp DNA Mini kit (Qiagen) according to the manufacturer's instructions. The DNA concentration was determined using the NanoDrop2000 (Thermo Scientific, Waltham, MA).

Comparative Genomic Hybridization Analysis. The Genome-wide Human SNP Array 6.0 (Affymetrix, Santa Clara, CA) was used to perform array comparative genomic hybridization (CGH) on genomic DNA from HCC and paired liver samples according to the manufacturer's instructions. A total of 250 ng of genomic DNA was digested with both Nsp I and Sty I in independent parallel reactions, subjected to restriction enzymes, ligated to the adaptor, and amplified using polymerase chain reaction (PCR) with a universal primer and TITANIUM Taq DNA Polymerase (Clontech, Palo Alt, CA). The PCR products were quantified, fragmented, end-labeled, and hybridized onto a Genome-wide Human SNP6.0 Array. After washing and staining in Fluidics Station 450 (Affymetrix), the arrays were scanned to generate CEL files using the GeneChip Scanner 3000 and GeneChip Operating Software version 1.4. In the array CGH analysis, sample-specific copy number changes were analyzed using Partek Genomic Suite 6.4 software (Partek Inc., St. Louis, MO).

Copy Number Assay. The copy numbers for *FGF3* and *FGF4* were determined using commercially available and predesigned TaqMan Copy Number Assays according to the manufacturer's instructions (Applied Biosystems, Foster City, CA) as described.[10] The primer IDs used for the *FGFs* were as follows: *FGF3*, Hs06336027_cn; *FGF4*, HS01235235_cn. The *TERT* locus was used for the internal reference copy number. Human Genomic DNA (Clontech) and DNA from noncancerous FFPE tissue were used as a normal control.

Real-Time Reverse-Transcription PCR. Real-time reverse-transcription PCR (RT-PCR) was performed as described.[11] In brief, complementary DNA was prepared from the total RNA obtained from each surgical frozen section using a GeneAmp RNA-PCR kit (Applied Biosystems). Real-time RT-PCR amplification was performed using a Thermal Cycler Dice (TaKaRa, Otsu, Japan) in accordance with the manufacturer's instructions under the following conditions: 95°C for 5 minutes, followed by 50 cycles of 95°C for 10 seconds and 60°C for 30 seconds. The primers used for the real-time RT-PCR were as follows: *FGF3*, 5′-TTT GGA GAT AAC GGC AGT GGA-3′ (forward) and 5′-CGT ATT ATA GCC CAG CTC GTG GA-3′ (reverse); *FGF4*, 5′-GAG CAG CAA GGG CAA GCT CTA-3′ (forward) and 5′-ACC TTC ATG GTG GGC GAC A-3′ (reverse); *GAPD*, 5′-GCA CCG TCA AGG CTG AGA AC-3′ (forward) and 5′-ATG GTG GTG AAG ACG CCA GT-3′ (reverse). *GAPD* was used to normalize expression levels in the subsequent quantitative analyses.

Fluorescence* In Situ *Hybridization Analysis. Fluorescence *in situ* hybridization (FISH) was performed as described.[10] Probes designed to detect the *FGF3* gene and *CEN11p* on chromosome 11 were labeled with fluorescein isothiocyanate or Texas red and were designed to hybridize to the adjacent genomic sequence spanning approximately 0.32 Mb and 0.63 Mb, respectively. The probes were generated from appropriate clones from a library of human genomic clones (GSP Laboratory, Kawasaki, Japan).

Immunoblotting. Western blot analysis was performed as described.[11] The following antibodies were used: monoclonal FGF3 (R&D Systems, Minneapolis, MN), FGF4 and FGFR2 antibodies (Santa Cruz Biotechnology, Santa Cruz, CA), and phosphorylated FGFR and horseradish peroxidase–conjugated secondary antibodies (Cell Signaling Technology, Beverly, MA). NIH-3T3 cells were exposed to the indicated concentrations of sorafenib for 2 hours and were then stimulated with FGF4-conditioned medium for 20 minutes.

Cell Growth Inhibitory Assay. To evaluate growth inhibition in the presence of various concentrations of sorafenib, we used an MTT assay as described.[12]

Plasmid Construction, Viral Production, and Stable Transfectants. The methods used in this section have been described.[12] The complementary DNA fragment encoding human full-length *FGF3* or *FGF4* was isolated using PCR and Prime STAR HS DNA polymerase (TaKaRa, Otsu, Japan) with following primers: *FGF3*, 5′-GG GAA TTC GCC GCC ATG GGC CTA ATC TGG CTG CTA-3′ (forward) and 5′-CC CTC GAG GCC CAG CTA GTG CGC ACT GGC CTC-3′ (reverse); *FGF4*, 5′-GG GAA TTC GCC GCC ATG TCG GGG CCC GGG ACG GCC GCG GTA GCG C-3′ (forward) and 5′-CC CTC GAG

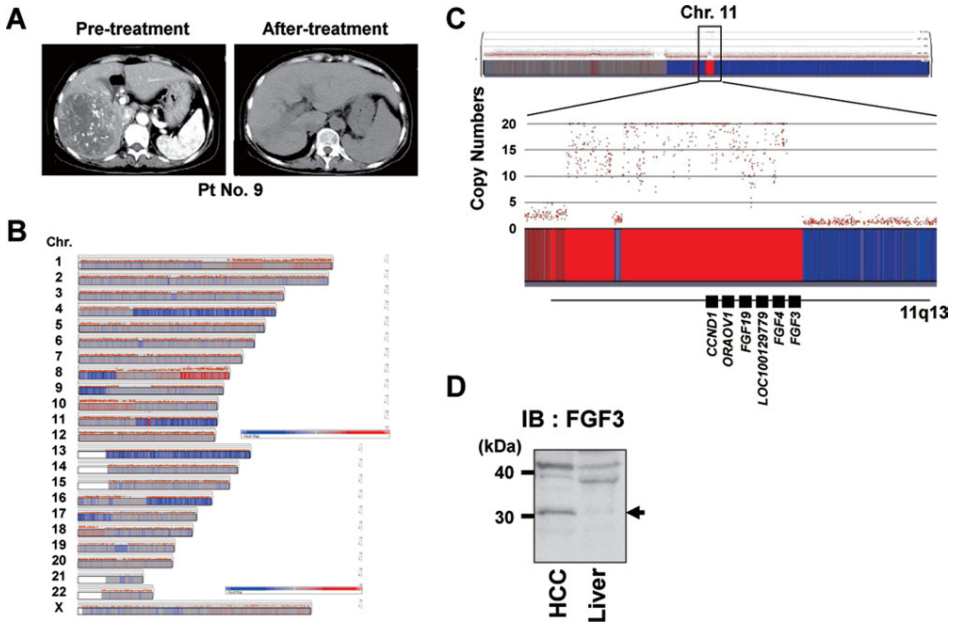

Fig. 1. HCC exhibiting a marked response to sorafenib treatment harbors *FGF3/FGF4* gene amplification. (A) Abdominal CT images obtained pretreatment (left panel) and 2 months after treatment (right panel). (B) CGH analysis of the tumor. Paired background liver tissue was used as a reference sample. A gain (>4 copies, red) and a loss (<0.5 copies, blue) of genomic copy number are shown. (C) Whole copy numbers of chromosome 11 are shown. A highly amplified region is described in the lower panel. (D) Western blot analysis of FGF3 (arrow) in HCC and paired background liver samples. IB, immunoblotting.

GGA GGG TCA CAG CCT GGG GAG GAA GTG GGT GAC CTT C-3′ (reverse). The stable transfectants expressing *EGFP* or *FGF3* or *FGF4* for each cell line were designated as A549/EGFP, A549/FGF3, and A549/FGF4.

Xenograft Studies. Nude mice (BALB/c nu/nu, 6-week-old females; CLEA Japan Inc., Tokyo) were used for *in vivo* studies and were cared for in accordance with the recommendations for the handling of laboratory animals for biomedical research compiled by the Committee on Safety and Ethical Handling Regulations for Laboratory Animal Experiments, Kinki University. Mice were subcutaneously inoculated with a total of 5×10^6 A549/EGFP, A549/FGF3, or A549/FGF4 cells. Two weeks after inoculation, the mice were randomized according to tumor size into two groups to equalize the mean pretreatment tumor size among the three groups (n = 20 mice per group). The mice were then treated with a low dose of oral sorafenib (n = 10, 15 mg/kg/day) or vehicle control (n = 10, Cremophor EL/ethanol/water) for 9 days. Tumor volume was calculated as length $\times$ width^2 $\times$ 0.5 and was assessed every 2 to 3 days.

Statistical Analysis. The statistical analyses were performed to test for differences between groups using the Student *t* test or Fisher's exact test. $P < 0.05$ was considered statistically significant. All analyses were performed using PAWS Statistics 18 (SPSS Japan Inc., Tokyo, Japan).

Results

Responder to Sorafenib Who Harbored* FGF3/FGF4 *Gene Amplification. A 58-year-old woman was diagnosed as having histologically confirmed advanced HCC (Fig. 1A, left panel) with multiple lung metastases. She received combination treatment with sorafenib, 5-fluorouracil (5FU), and interferon, and a subsequent treatment assessment revealed a partial response. Because the disease was well controlled with sorafenib treatment for 14 months (Fig. 1A, right panel), surgery was performed. To characterize this tumor molecularly, we performed array CGH analysis using frozen surgical specimens of the HCC region and paired background liver tissue as a reference control. The array CGH analysis revealed a low-level gain in the genomic DNA copy number for 1q, 8q, 10p, and 18p and a high level gain at 11q13 (Fig. 1B). Interestingly, the 11q13 region, a rare amplicons in HCC that contains several genes, including *FGF3*, *FGF4*, *CCND1*, and *FGF19*, was highly amplified over 20 copies (Fig. 1C). Western blot analysis revealed that FGF3 was overexpressed in the HCC specimen compared with the paired background liver specimen (Fig. 1D).

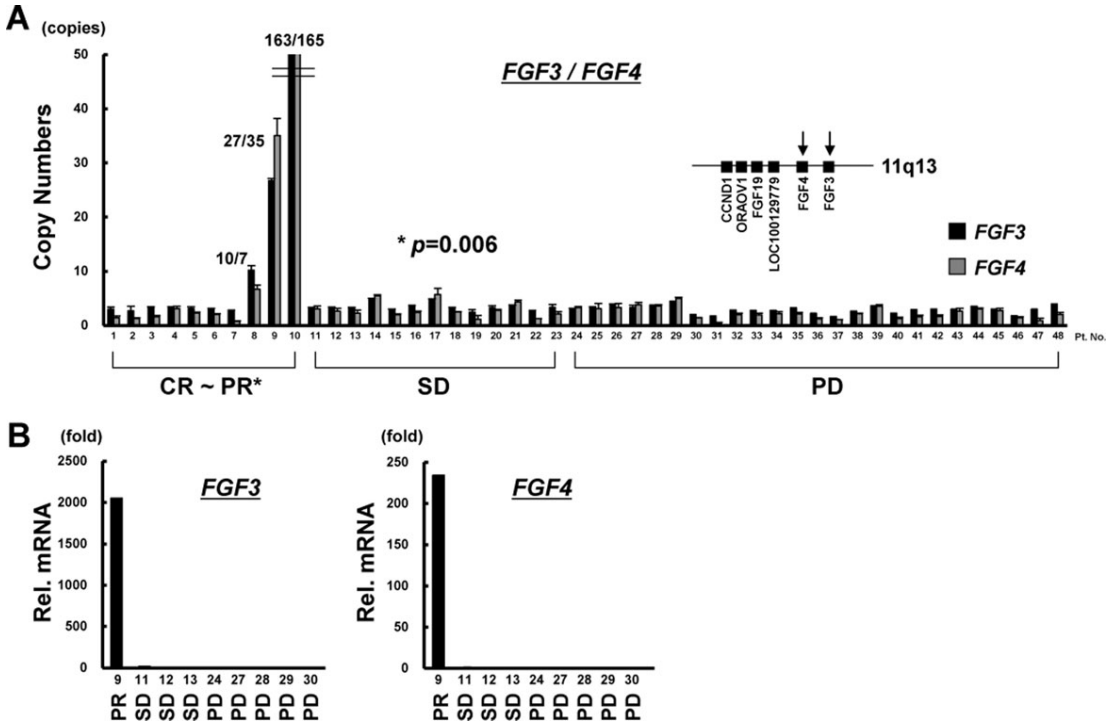

Fig. 2. *FGF3/FGF4* gene amplification is frequently observed in responders to sorafenib in HCC. (A) *FGF3/FGF4* gene amplification was determined using the TaqMan copy number assay in DNA samples obtained from 48 HCC samples that had been treated with sorafenib. *FGF3* amplification of >5 copies was observed in three of the sorafenib responders. *Complete response + partial response versus stable disease + progressive disease. (B) *FGF3/FGF4* gene amplification mediates the overexpression of *FGF3/FGF4* mRNA. The mRNA expression levels of *FGF3* and *FGF4* were examined in nine HCC samples that were available as frozen samples among 48 HCC samples that were treated with sorafenib. Rel. mRNA, *target gene/GAPD* $\times$ 10^6.

The 11q13 locus is known to be a frequently amplified region in several human cancers except HCC.[13] Thus, we hypothesized that the amplification of 11q13 may be involved in a marked response to sorafenib.

FGF3/FGF4 ***Gene Amplification Is Frequently Observed in Responders to Sorafenib.*** To address the question of whether *FGF3/FGF4* gene amplification is also found in the HCC of other responders to sorafenib, we examined HCC specimens collected from 11 other medical centers in Japan. Because most of the HCC samples were collected as FFPE samples, we used a TaqMan Copy number assay.[10] A copy number assay revealed that *FGF3/FGF4* amplification was observed in three of the 10 (30%) HCC samples that responded to sorafenib, whereas no amplification was observed in the 38 specimens from patients with stable or progressive disease ($P = 0.006$, Fig. 2A). The copy numbers for *FGF3/FGF4* were 10.2 $\pm$ 0.8/6.7 $\pm$ 0.8, 26.7 $\pm$ 0.4/35.1 $\pm$ 3.1, and 162.5 $\pm$ 9.0/165.0 $\pm$ 12.5 copies in the amplified samples, whereas the copy numbers of *FGF3* for all the other samples were below 5 copies. The correlation between the *FGF3* locus and the *FGF4* locus copy numbers was very high ($R = 0.998$), indicating that the DNA copy number assay for *FGF3/FGF4* was a sensitive and reproducible method.

FGF3/FGF4 ***Gene Amplification Mediates the Overexpression of*** **FGF3/FGF4** ***Messenger RNA.*** We examined the messenger RNA (mRNA) expression levels of *FGF3/FGF4* in nine HCC samples that were available as frozen samples among the 48 sorafenib-treated samples, as shown in Fig. 2A. One amplified sample expressed extremely high mRNA levels of *FGF3/FGF4* compared with nonamplified samples (Fig. 2B). The results demonstrated that *FGF3/FGF4* gene amplification mediates the overexpression of *FGF3/FGF4* mRNAs and proteins (Figs. 2B and 1D).

FISH Analysis Confirmed **FGF3/FGF4** ***Gene Amplification.*** We used FISH analysis to examine *FGF3/FGF4* amplification and to verify the results of the above-described PCR-based DNA copy number assay. All *FGF3/FGF4*-amplified clinical samples were confirmed as exhibiting high-level *FGF3* amplification using FISH analysis (Fig. 3). One patient showed multiple scattered signals, whereas two patients showed large clustered signals. Nonamplified HCC yielded a negative result for gene amplification. These results clearly demonstrate the presence of *FGF3/FGF4*-

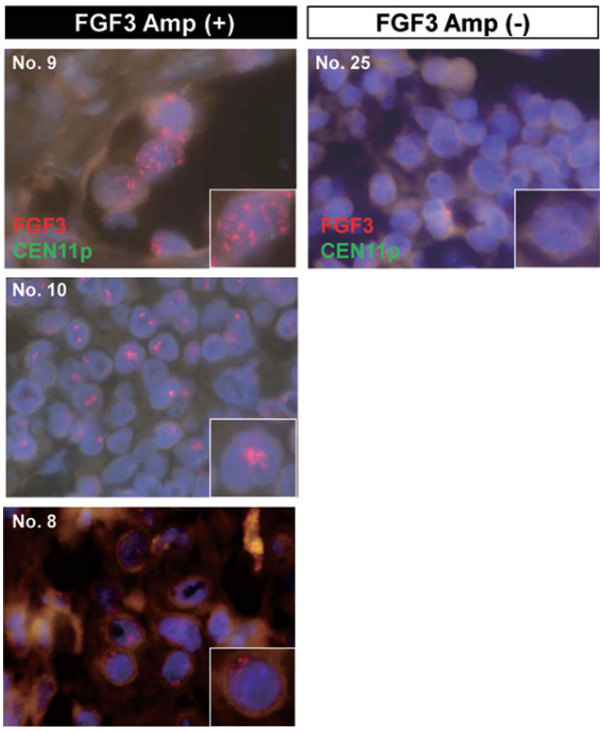

Fig. 3. FISH analysis of *FGF3*-amplified HCC. Patient numbers were indicated. Green staining indicates *CEN11P* loci; red staining indicates *FGF3* loci. High-power images are presented in each inset for a single cancer cell. Amp, gene amplification.

amplified HCC among the clinical samples, and the FISH analysis results were consistent with those for the copy number assay.

Frequency of* FGF3/FGF4 *Gene Amplification in HCC. To determine the frequency of *FGF3/FGF4* gene amplification in HCC, we performed a copy number assay for HCC samples without sorafenib treatment in a series of surgical specimens. Two of the 82 (2.4%) HCC samples exhibited *FGF3/FGF4* gene amplification, with copy numbers of 10.7/15.3 and 133.3/112.7 copies, respectively (Fig. 4). One amplified HCC was a poorly differentiated tumor, whereas the other was a moderately differentiated tumor.

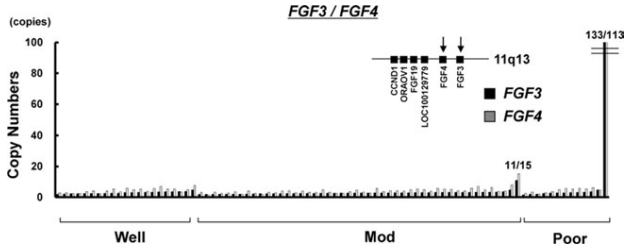

Fig. 4. *FGF3/FGF4* gene amplification in a series of HCC samples without sorafenib treatment. TaqMan copy number assay for *FGF3* and *FGF4* was used to examine DNA samples obtained from 82 surgical specimens. Human normal genomic DNA was used as a normal control. Well, well-differentiated HCC; Mod, moderately differentiated HCC; Poor, poorly differentiated HCC.

Clinicopathological Features of Responders to Sorafenib. The clinico-pathological features of the sorafenib responders are shown in Table 1. A comparison of clinical factors (age, sex, viral status, alpha-fetoprotein level, PIVKA-II, clinical stage, primary tumor size, metastatic status, histological type, and tumor response between responders and nonresponders) is given in Table 2. Notably, multiple lung metastases over five nodules was significantly higher among responders to sorafenib (responders, 5/13 [38%]; nonresponders, 2/42 [5%]; $P = 0.006$). Although the difference was not significant, poorly differentiated HCC tended to be

Table 1. Clinico-pathological Characteristics in Sorafenib Responders

Patient No.	Age, Years	Sex	Viral Status	AFP, ng/mL	PIVKA-II, mAU/mL	Clinical Stage	HCC in the Liver	Lung Metastasis	Other Metastases	Histological Type	Combination Treatment	Treatment Response	*FGF3/FGF4* Amplification
1	52	M	B	198	140	IV	2 cm, ×3	multi	Adrenal gland	Mod	(−)	PR	(−)
2	63	M	B	24	1,983	III	6 cm	(−)	(−)	Mod	(−)	CR	(−)
3	58	M	C	16	14	III	9 cm, multiple	(−)	(−)	Well	(−)	PR	(−)
4	62	M	B	8	130	IV	(−)	×3	(−)	Mod-Poor	(−)	PR	(−)
5	47	F	C	1,872	728	IV	2 cm, multiple	Multiple	(−)	Poor	+TAI	CR	(−)
6	66	M	C	290	18,507*	IV	5 cm	(−)	(−)	Mod	(−)	CR	(−)
7	71	M	C	404,100	1,328	IV	5 cm, multiple	Multiple	(−)	Poor	(−)	CR	(−)
8	66	M	Non	49	7,173	IV	(−)	×2	Pleural, LN	Mod	(−)	PR	Amplification
9	58	F	B	715	101	IV	11 cm	Multiple	(−)	Combination†	+5FU/IFN	PR	Amplification
10	80	F	C	378	21	III	3 cm, ×3	(−)	(−)	Poor, Mod‡	(−)	CR	Amplification
11	57	M	C	46,835	2,730	IV	14 cm, multiple	Multiple	(−)	Mod	(−)	CR	ND
12	77	M	B	435	71,000	IV	4 cm, multiple	(−)	(−)	Mod	(−)	PR	ND
13	84	M	Non	5,410	847,000*	IV	13 cm, multiple	(−)	(−)	Poor	(−)	PR	ND

Abbreviations: AFP, alpha-fetoprotein; CR, complete response; F, female; IFN, interferon; LN, lymph node; M, male; Mod, moderately differentiated; ND, not done; Non, non-B, non-C; Poor, poorly differentiated; PR, partial response; TAI, transcatheter arterial infusion; Well, well differentiated.

*Warfarin treatment (+).

†HCC with cholangiocarcinoma component.

‡From two different HCC nodules.

Table 2. Clinicopathological Characteristics and *FGF3/FGF4* Gene Amplification in Responders and Nonresponders to Sorafenib

Characteristic	Responders (n = 13)	Nonresponders (n = 42)	*P* Value*
Age, years (range)	63 (47-84)	66 (22-89)	0.98
Sex, M/F	10/3	30/12	0.97
Viral status, no.			0.69
HBV	5	10	
HCV	6	16	
B+C	0	1	
Non-B, non-C	2	15	
AFP, ng/mL (range)	378 (8-404,100)	56 (2-114,248)	0.33
PIVKA-II, mAU/mL (range)	728 (14-847,000)	81 (11-147,000)	0.78
Clinical stage, no.			0.73
II	0	1	
III	3	13	
IV	10	28	
Primary tumor, cm (range)	5 (0-14)	3 (0-15)	0.20
Lung metastasis, no.			0.13
(−)	6	31	
(+)	7	11	
Multiple lung metastases, no.			0.006
<5	8	40	
≥5	5	2	
Other metastases, no.			0.24
(−)	11	26	
(+)	2	16	
Histological type, no.			0.13
Well	1	7	
Moderate	6	26	
Poor	5	6	
Combination†	1	3	
Response, no.			ND
Complete response	6	–	
Partial response	7	–	
Stable disease	–	16	
Progressive disease	–	24	
Not evaluable	–	2	

Abbreviations: AFP, alpha-fetoprotein; HBV, hepatitis B virus; HCV, hepatitis C virus; ND, not done.

**P* values of viral status and histological type were calculated between HBV versus HCV and poorly differentiated versus nonpoorly differentiated.

†HCC with cholangiocarcinoma component.

more common among responders to sorafenib (responders, 5/13 [38%]; nonresponders, 6/42 [14%]; $P = 0.13$). These results suggest that multiple lung metastases and a poorly differentiated histology may be clinical biomarkers for sorafenib treatment in patients with HCC.

Sorafenib Potently Inhibits Cellular Growth in* FGF3/FGF4-*Amplified and* FGFR2-*Amplified Cell Lines. We examined the growth inhibitory effect of sorafenib in various cancer cell lines to evaluate whether activated FGFR signaling is involved in the response to sorafenib. Among 26 cell lines, KYSE220 was the only *FGF3/FGF4*-amplified cell line (data not shown), and HSC-43, HSC-39, and KATOIII were the only *FGFR2*-amplified cell lines.[14] Sorafenib potently inhibited cellular growth in these four cell lines at a sub-μM 50% inhibitory concentration (IC_{50}) (Fig. 5A). The IC_{50} values were as follows: HSC43, 0.8 μM; HSC39, 0.6 μM; KATOIII, 0.4 μM; and KYSE220, 0.18 μM. These results suggest that activated FGFR signaling may be involved in the response to sorafenib.

***Sorafenib Inhibits Tumor Growth in* FGF4-*Introducing Cell Lines* In Vivo.** Finally, we established cancer cell lines stably overexpressing *EGFP*, *FGF3*, or *FGF4* to examine the relationship between the gene function of *FGF3* or *FGF4* and drug sensitivity to sorafenib *in vivo*. Western blotting confirmed that exogenously expressed FGF3 and FGF4 were secreted into the culture medium (Fig. 5B). Sorafenib inhibited the FGF4-conditioned, medium-mediated expression levels of phosphorylated FGFR (Figure 5C). A similar result was obtained using recombinant FGF4 (data not shown). Mice inoculated with these cell lines were treated with a low dose of oral sorafenib (15 mg/kg/day) or without sorafenib (vehicle control). *FGF3* overexpression did not increase the tumor volume compared with EGFP tumors; however, *FGF4* overexpression aggressively increased tumor volume and clearly enhanced the malignant phenotype (Fig. 5D). Notably, the low-dose sorafenib treatment significantly inhibited the growth of the A549/FGF4 tumors, whereas it was not effective against A549/EGFP and A549/FGF3 tumors (Fig. 5D). These results suggest that overexpression of *FGF4* is partially involved in the response to sorafenib.

Discussion

The *FGF3* gene was first identified and characterized based on its similarity to the mouse *fgf3/int-2* gene, which is a proto-oncogene activated in virally induced mammary tumors in mice.[15] Meanwhile, the *FGF4* gene was first identified in gastric cancer as an oncogene *HST*, which has the ability to induce the neoplastic transformation of NIH-3T3 cells upon transfection.[16] These genes were initially regarded as proto-oncogenes. *FGF3* and *FGF4* genes are located side-by-side and are also closely located to the *FGF19* and *CCND1* genes (within 0.2 Mb of the 11q13 region).[13] The 11q13 region is known as a gene-dense region, and gene amplification of this region is frequently observed in various solid cancers (including breast cancer, squamous cell carcinoma of the head and neck, esophageal cancer, and melanoma) at frequencies of 13%-60%.[13] On the other hand, the frequency of *FGF3*/*FGF4* amplification in HCC remains

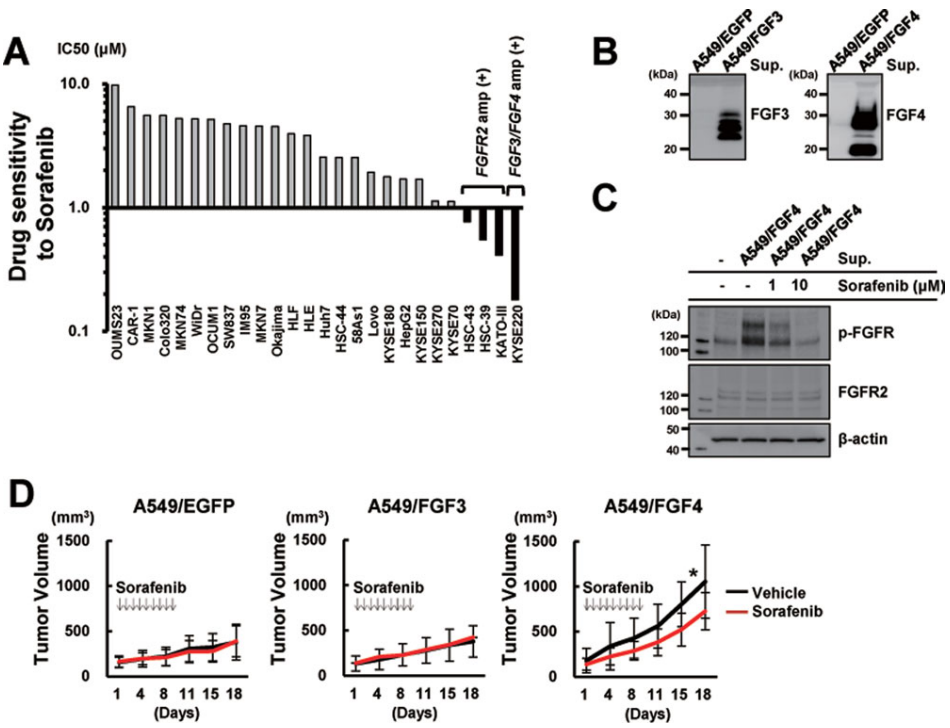

Fig. 5. FGF3 and FGF4 overexpression and drug sensitivity to sorafenib *in vitro* and *in vivo*. (A) Growth inhibitory assay examining sorafenib in various cancer cell lines *in vitro*. The growth inhibitory effect of sorafenib was examined using an MTT assay. The IC_{50} values of each cell line are shown in the graph. The black bars show that the IC_{50} values were below 1 μM. Amp, gene amplification. (B) Cancer cell lines stably overexpressing *EGFP*, *FGF3*, or *FGF4* were established and designated as A549/EGFP, A549/FGF3, and A549/FGF4. Western blot analysis confirmed that exogenously expressed FGF3 and FGF4 were secreted into the culture medium. Sup., supernatant. (C) NIH-3T3 cells were exposed to indicated concentrations of sorafenib for 2 hours and were then stimulated with FGF4-conditioned medium for 20 minutes. (D) Mice inoculated with A549/EGFP, A549/FGF3, or A549/FGF4 (n = 20 each) were treated with a low dose of oral sorafenib (n = 10, 15 mg/kg/day) or without (n = 10, vehicle control). $*P < 0.05$.

largely unclear. Relatively small cohort studies have reported that one out of 20 HCCs exhibited *FGF3* amplification as determined via CGH analysis,[17] and 3 out of 45 HCCs examined using Southern blot analysis had a copy number >5;[18] meanwhile, amplification was not detected in 0 out of 42 surgically resected HCCs.[19] In the present study, two of the 82 (2.4%) HCC samples exhibited *FGF3/FGF4* gene amplification in the HCC series. If only 2%-3% of HCC patients harbor the *FGF3*/*FGF4* amplification, its value as a biomarker seems to be limited in clinics because a frequency of 2%-3% is too low to stratify the patients for specific targeted therapy. However, a combination of biomarkers—including *FGF3*/*FGF4* amplification, lung metastasis, tumor differentiation, and other unrevealed dysregulation of FGFR signaling—may increase the response prediction. In addition, 2%-3% of *FGF3*/*FGF4* amplification may be a promising therapeutic target for future FGFR-targeted therapies in the treatment of HCC.

Tumor shrinkage might be due to the mixed effect (sorafenib + 5FU + interferon) of combination therapy in the initially described patient. However, during this patient's long clinical course, tumor regrowth was observed following withdrawal of sorafenib because of oral hemorrhage, and tumor reshrinkage was observed when sorafenib treatment recommenced. Thus, we considered that tumor shrinkage might be achieved by the effect of sorafenib on its own, rather than 5FU + interferon.

Regarding determinants of drug sensitivity to sorafenib, the mechanism of hypersensitivity in the gastric cancer cell lines HSC-39, HSC-43, and KATO-III is *FGFR2* gene amplification and is thought to be the addiction of these cell lines to this gene,[14] since sorafenib has a relatively weak but significant inhibitory effect on FGFR1 at a concentration of 580 ± 100 nM.[3] This result suggests that the blockade of FGFR signaling by sorafenib may lead to a significant treatment response, at least in *FGFR2*-amplified cells. In this study, we found that *FGF4*, but not *FGF3* overexpression, was partially involved in the sensitivity to sorafenib *in vivo*. The limitations of the study are the small number of responder patients and the potential bias in their selection because of the retrospective study design. Further clinical study of responders to

sorafenib is necessary. We are presently undertaking a prospective molecular translational study (2010-2012) in a cohort of Japanese patients with sorafenib-treated HCC.

Multiple lung metastases were frequently observed among responders to sorafenib (38%) but were less common among nonresponders (5%). Based on a Japanese follow-up survey of patients with primary HCC, lung metastasis was observed in 7% (169/2355) of the patients at the time of autopsy.[20] Another study demonstrated that 15% of patients were found to have extrahepatic metastases, and lung metastasis was detected in 6% of 995 consecutive HCC patients.[21] When compared with these data from large-scale studies, the frequency of lung metastasis among responders to sorafenib seems quite high. In addition, a poorly differentiated histological type tended to be more common among responders, although the correlation was not significant.

In conclusion, we found that *FGF3/FGF4* gene amplification, multiple lung metastases, and a poorly differentiated histological type may be involved in the response to sorafenib.

References

1. Jemal A, Murray T, Ward E, Samuels A, Tiwari RC, Ghafoor A, et al. Cancer statistics, 2005. Ca Cancer J Clin 2005;55:10-30.
2. Yamamoto J, Kosuge T, Takayama T, Shimada K, Yamasaki S, Ozaki H, et al. Recurrence of hepatocellular carcinoma after surgery. Br J Surg 1996;83:1219-1222.
3. Wilhelm SM, Carter C, Tang L, Wilkie D, McNabola A, Rong H, et al. BAY 43–9006 exhibits broad spectrum oral antitumor activity and targets the RAF/MEK/ERK pathway and receptor tyrosine kinases involved in tumor progression and angiogenesis. Cancer Res 2004;64:7099-7109.
4. Llovet JM, Ricci S, Mazzaferro V, Hilgard P, Gane E, Blanc JF, et al. SHARP Investigators Study Group. Sorafenib in advanced hepatocellular carcinoma. N Engl J Med 2008;359:378-390.
5. Cheng AL, Kang YK, Chen Z, Tsao CJ, Qin S, Kim JS, et al. Efficacy and safety of sorafenib in patients in the Asia-Pacific region with advanced hepatocellular carcinoma: a phase III randomised, double-blind, placebo-controlled trial. Lancet Oncol 2009;10:25-34.
6. So BJ, Bekaii-Saab T, Bloomston MA, Patel T. Complete clinical response of metastatic hepatocellular carcinoma to sorafenib in a patient with hemochromatosis: a case report. J Hematol Oncol 2008;1:18.
7. Nakazawa T, Hidaka H, Shibuya A, Koizumi W. Rapid regression of advanced hepatocellular carcinoma associated with elevation of des-gamma-carboxyprothrombin after short-term treatment with sorafenib—a report of two cases. Case Rep Oncol 2010;3:298-303.
8. Paez JG, Janne PA, Lee JC, Tracy S, Greulich H, Gabriel S, et al. EGFR mutations in lung cancer: correlation with clinical response to gefitinib therapy. Science 2004;304:1497-1500.
9. Lynch TJ, Bell DW, Sordella R, Gurubhagavatula S, Okimoto RA, Brannigan BW, et al. Activating mutations in the epidermal growth factor receptor underlying responsiveness of non-small-cell lung cancer to gefitinib. N Engl J Med 2004;350:2129-2139.
10. Matsumoto K, Arao T, Hamaguchi T, Shimada Y, Kato K, Oda I, et al. FGFR2 gene amplification and clinicopathological features in gastric cancer. Br J Cancer 2012;14:727-732.
11. Matsumoto K, Arao T, Tanaka K, Kaneda H, Kudo K, Fujita Y, et al. mTOR signal and hypoxia-inducible factor-1 alpha regulate CD133 expression in cancer cells. Cancer Res 2009;69:7160-7164.
12. Kaneda H, Arao T, Tanaka K, Tamura D, Aomatsu K, Kudo K, et al. FOXQ1 is overexpressed in colorectal cancer and enhances tumorigenicity and tumor growth. Cancer Res 2010;70:2053-2063.
13. Ormandy CJ, Musgrove EA, Hui R, Daly RJ, Sutherland RL. Cyclin D1, EMS1 and 11q13 amplification in breast cancer. Breast Cancer Res Treat 2003;78:323-335.
14. Takeda M, Arao T, Yokote H, Komatsu T, Yanagihara K, Sasaki H, et al. AZD2171 shows potent antitumor activity against gastric cancer over-expressing fibroblast growth factor receptor 2/keratinocyte growth factor receptor. Clin Cancer Res 2007;13:3051-3057.
15. Peters G, Brookes S, Smith R, Dickson C. Tumorigenesis by mouse mammary tumor virus: evidence for a common region for provirus integration in mammary tumors. Cell 1983;33:369-377.
16. Sakamoto H, Mori M, Taira M, Yoshida T, Matsukawa S, Shimizu K, et al. Transforming gene from human stomach cancers and a noncancerous portion of stomach mucosa. Proc Natl Acad Sci U S A 1986;83:3997-4001.
17. Takeo S, Arai H, Kusano N, Harada T, Furuya T, Kawauchi S, et al. Examination of oncogene amplification by genomic DNA microarray in hepatocellular carcinomas: comparison with comparative genomic hybridization analysis. Cancer Genet Cytogenet 2001;130:127-132.
18. Nishida N, Fukuda Y, Komeda T, Kita R, Sando T, Furukawa M, et al. Amplification and overexpression of the cyclin D1 gene in aggressive human hepatocellular carcinoma. Cancer Res 1994;54:3107-3110.
19. Chochi Y, Kawauchi S, Nakao M, Furuya T, Hashimoto K, Oga A, et al. A copy number gain of the 6p arm is linked with advanced hepatocellular carcinoma: an array-based comparative genomic hybridization study. J Pathol 2009;217:677-684.
20. Ikai I, Arii S, Ichida T, Okita K, Omata M, Kojiro M, et al. Report of the 16th follow-up survey of primary liver cancer. Hepatol Res 2005;32:163-172.
21. Uka K, Aikata H, Takaki S, Shirakawa H, Jeong SC, Yamashina K, et al. Clinical features and prognosis of patients with extrahepatic metastases from hepatocellular carcinoma. World J Gastroenterol 2007;13:414-420.

J Gastroenterol (2013) 48:382–390
DOI 10.1007/s00535-012-0641-9

ORIGINAL ARTICLE—LIVER, PANCREAS, AND BILIARY TRACT

Inhibition of hepatocellular carcinoma by PegIFNα-2a in patients with chronic hepatitis C: a nationwide multicenter cooperative study

Namiki Izumi · Yasuhiro Asahina · Masayuki Kurosaki · Gotaro Yamada · Tsutomu Kawai · Eiji Kajiwara · Yukishige Okamura · Takayuki Takeuchi · Osamu Yokosuka · Kazuya Kariyama · Joji Toyoda · Mie Inao · Eiji Tanaka · Hisataka Moriwaki · Hiroshi Adachi · Shinji Katsushima · Masatoshi Kudo · Kouichi Takaguchi · Yoichi Hiasa · Kazuaki Chayama · Hiroshi Yatsuhashi · Makoto Oketani · Hiromitsu Kumada

Received: 23 April 2012 / Accepted: 25 June 2012 / Published online: 9 August 2012

Abstract
Background We investigated whether the administration of maintenance doses of interferon prevented hepatocellular carcinoma (HCC) in patients with chronic hepatitis C.
Methods Study 1: A multicenter, retrospective, cooperative study was carried out to determine whether long-term administration of low-dose peginterferon alpha-2a (PegIFNα-2a) prevented HCC development in patients with chronic hepatitis C. In total, 594 chronic hepatitis C patients without a history of HCC were enrolled and treated with 90 μg PegIFNα-2a administered weekly or bi-weekly for at least 1 year. Study 2: HCC developed in 16 of 99 additional patients without PegIFNα-2a treatment during 3.8 years of observation. A propensity-matched control study was then carried out to compare the incidence of

N. Izumi (✉) · Y. Asahina · M. Kurosaki
Department of Gastroenterology and Hepatology, Musashino Red-Cross Hospital, Musashino, Japan
e-mail: nizumi@musashino.jrc.or.jp

G. Yamada
Department of Internal Medicine, Kawasaki Hospital of Kawasaki Medical University, Okayama, Japan

T. Kawai
Department of Gastroenterology, Kanbara General Hospital, Fuji, Japan

E. Kajiwara
Department of Gastroenterology, Shinnittetsu Yahata Memorial Hospital, Kitakyushu, Japan

Y. Okamura
Department of Gastroenterology, Sano Kousei Hospital, Kitakyushu, Japan

T. Takeuchi
Department of Gastroenterology, Notogawa Hospital, Higashioumi, Japan

O. Yokosuka
Department of Gastroenterology and Hepatology, Chiba University, Chiba, Japan

K. Kariyama
Department of Hepatology, Okayama Citizens' Hospital, Okayama, Japan

J. Toyoda
Department of Gastroenterology and Hepatology, Sapporo Kousei Hospital, Sapporo, Japan

M. Inao
Department of Gastroenterology and Hepatology, Saitama Medical University, Moroyama, Japan

E. Tanaka
Second Department of Internal Medicine, Shinshu University, Matsumoto, Japan

H. Moriwaki
Department of Gastroenterology and Hepatology, Gifu University, Gifu, Japan

H. Adachi
Department of Hepatology, Tonami General Hospital, Tonami, Japan

S. Katsushima
Department of Gastroenterology, Kyoto Medical Center, Kyoto, Japan

M. Kudo
Department of Gastroenterology and Hepatology, Kinki University, Higashiosaka, Japan

K. Takaguchi
Department of Gastroenterology, Kagawa Central Hospital, Takamatsu, Japan

HCC between the 59 patients who received low-dose PegIFNα-2a (PegIFNα-2a group) and 59 patients who did not receive PegIFNα-2a treatment (control group), matched for sex, age, platelet count, and total bilirubin levels.

Results Study 1: HCC developed in 49 patients. The risk of HCC was lower in patients with undetectable hepatitis C virus RNA, ≤40 IU/L alanine aminotransferase (ALT), or ≤10 ng/L alpha-fetoprotein (AFP) 24 weeks after the start of therapy. Study 2: The incidence of HCC was significantly lower in the PegIFNα-2a group than in the control group.

Conclusions Low-dose and long-term maintenance administration of PegIFNα-2a decreased the incidence of HCC in patients with normalized ALT and AFP levels at 24 weeks compared with patients without normal ALT and AFP levels.

Keywords Chronic hepatitis C · Hepatocellular carcinoma · Peginterferon

Introduction

Hepatocellular carcinoma (HCC), the sixth most common cancer worldwide, often develops because of long-term hepatitis B or C virus infection [1, 2]. In particular, chronic hepatitis C and hepatic cirrhosis increase the risk of HCC; the annual incidence of tumor development in such patients may be as high as 2–4 % [3–5]. The incidence of HCC decreases in patients who achieve a sustained virological response (SVR) to interferon (IFN) treatment, although the incidence remains high in non-SVR patients [6–9]. A detailed analysis of HCC development revealed that chronic hepatitis C patients aged 65 years or more, especially those with advanced fibrosis of the liver, were at an increased risk of developing HCC [10]. For patients 65 years or older with advanced liver fibrosis, the dose of ribavirin is often reduced or the agent is discontinued, resulting in lower SVR rates in those with discontinuation of ribavirin. Establishing an effective treatment strategy for preventing the development of HCC is important for these high-risk patients.

Factors related to the development of HCC have been analyzed in patients who did not achieve an SVR even after IFN treatment; advanced fibrosis of the liver and high levels of serum alanine aminotransferase (ALT), and alpha-fetoprotein (AFP) are risk factors for HCC development [11, 12]. A randomized controlled trial was conducted in Western countries to determine whether combined peginterferon and ribavirin treatment with weekly administration of 90 μg peginterferon alpha-2a (PegIFNα-2a) could prevent HCC in non-responders. A 3.5-year follow up showed that administration of a maintenance dose of PegIFNα-2a did not reduce tumor incidence in these patients [13]. However, after 8.5 years of observation, the incidence of HCC was decreased among those in the PegIFNα-2a group with cirrhosis [14]. Meanwhile, Bruix et al. [15] reported that maintenance therapy with PegIFNα-2b did not prevent HCC in chronic hepatitis C patients with cirrhosis. In Japan, long-term low-dose administration of natural IFN has been reported to decrease the incidence of HCC [16]. In light of these conflicting results, investigations should be carried out in a large number of patients with chronic hepatitis C to resolve the question of whether IFN treatment prevents the development of HCC.

We carried out a multicenter retrospective cooperative study of patients with chronic hepatitis C to determine whether those treated with 90 μg PegIFNα-2a without ribavirin had a reduced incidence of HCC compared with those not treated with IFN.

Patients and methods

Study 1: analysis of risk factors for HCC in patients treated with long-term low-dose-PegIFNα-2a

In total, at 21 hepatitis centers throughout Japan, 743 patients with hepatitis C who had received 90 μg of PegIFNα-2a therapy weekly or bi-weekly for 1 year or more without having received the full dose (180 μg) since December 2003 were examined retrospectively for the development of HCC. The end of enrollment in this study was the end of December 2008 and the end of follow up was the end of December 2010. Patients with a history of HCC before the start of therapy and those with a therapy period of less than 48 weeks were excluded, leaving 594 patients who had undergone long-term administration of PegIFNα-2a for analysis. At the 21 centers involved in this

Y. Hiasa
Department of Gastroenterology and Hepatology, Ehime University, Matsuyama, Japan

K. Chayama
Department of Gastroenterology and Hepatology, Hiroshima University, Hiroshima, Japan

H. Yatsuhashi
Department of Gastroenterology and Hepatology, Nagasaki Medical Center, Nagasaki, Japan

M. Oketani
Department of Gastroenterology and Hepatology, Kagoshima University, Kagoshima, Japan

H. Kumada
Department of Hepatology, Toranomon Hospital, Tokyo, Japan

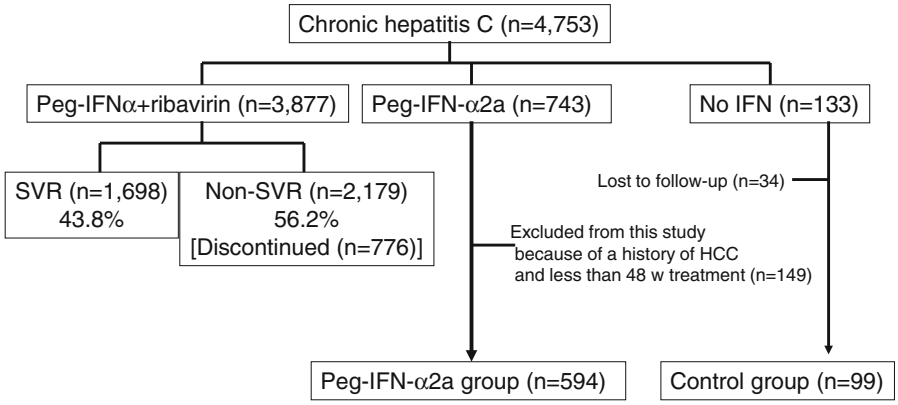

Fig. 1 Flow diagram of the patients' enrollment in the study. *Peg-IFNα* pegylated interferon α, *SVR* sustained viral response, *HCC* hepatocellular carcinoma, *w* week

study, 4,753 patients with chronic hepatitis C had been treated; Peg-IFN and ribavirin combination treatment had been administered to 3,877 patients, 743 patients had received Peg-IFN alone, and 133 patients had not agreed to receive IFN (a flow diagram of the enrollment of patients in this study is shown in Fig. 1). In the patients with Peg-IFN and ribavirin combination treatment, the SVR rate was 43.8 %; SVR was not achieved in 2,179 patients, and in 776 of these patients, the combination therapy was discontinued owing to adverse events or the patient's choice. Patients who failed to achieve an SVR were not included in this study, because the incidence of HCC is known to be reduced even in non-responders to IFN [17].

The backgrounds of the 594 patients studied are shown in Table 1. Findings from the liver biopsies of the patients were classified according to international standards [18]. Long-term PegIFNα-2a treatment is approved by the Japanese Medical Insurance system. Written informed consent was obtained from all patients prior to participation in this study. The study design was approved by the regional ethics committees of the 21 centers involved in this study, including the Musashino Red Cross Hospital, in accordance with the Helsinki Declaration. The 743 patients treated with PegIFNα-2a alone were not indicated for Peg-IFNα and ribavirin combination therapy because of anemia or heart disease. The 133 patients who did not agree to receive IFN served as the control group (see Fig. 1). A large proportion of the 594 study patients had advanced fibrosis of the liver and active inflammation. A dose of 90 μg PegIFNα-2a was administered to 512 and 82 patients weekly and biweekly, respectively, according to the patients' wishes. There were no significant differences between the weekly and biweekly groups in the patients' background data (data not shown).

The median duration of follow up in the PegIFNα-2a group was 1,273 days (range 228–2,768 days) and HCC was observed in 49 of the 594 patients (Table 1). Pre-treatment and on-treatment factors associated with the development of HCC were analyzed by Student's *t*-test, the Mann–Whitney *U*-test, and the χ^2 test (Table 2). Independent factors for the development of HCC were assessed by multivariate analysis using logistic regression. The

Table 1 Background data of patients treated with PegIFNα-2a ($n = 594$)

	$n = 594$
Age (years)	61.7 ± 11.7
Sex (male/female)	258/336
BMI	23.2 ± 3.3
Genotype (1/2)	443/151
Diagnosis (ASC/CH/LC)	4/460/130
History of excess alcohol consumption (≥60 g/day; yes/no)	118/376
Fibrosis (F0, 1, 2/F3, 4)	443/151
Inflammatory activity (A0, 1/A2, 3)	469/125
Diabetes mellitus (no/yes)	499/95
LDL cholesterol (mg/dL)	94.2 ± 31.1
Fasting blood sugar (mg/dL)	106.3 ± 28.5
White blood cell count (/mm^3)	4,360 ± 1,470
Red blood cell count ($\times 10^6$/μL)	423.8 ± 56.4
Hemoglobin (g/dL)	13.3 ± 1.8
Platelet count ($\times 10^3$/μL)	137 ± 56
Albumin (g/dL)	4.0 ± 0.5
Total bilirubin (mg/dL)	0.8 ± 0.6
AST (IU/L)	65.8 ± 47.8
ALT (IU/L)	72.1 ± 68.0
Gamma-GTP (IU/L)	55.2 ± 51.3
Esophageal varices (no/yes)	344/31
Alpha fetoprotein (ng/L)	6.9 (4.2–13.8)
Once weekly or biweekly PegIFNα-2a	512:82
Baseline HCV RNA (KIU/mL)	1,024 (73–2,130)
Development of HCC (no/yes)	545/49

PegIFN pegylated interferon, *BMI* body mass index, *ASC* asymtotomatic carrier, *CH* chronic hepatitis, *LC* liver cirrhosis, *LDL* low-density lipoprotein, *AST* aspartate aminotransferase, *ALT* alanine aminotransferase, *GTP* guanosine triphosphate, *HCV* hepatitis C virus, *HCC* hepatocellular carcinoma

Values are means ± SD, with ranges in parentheses

incidence of HCC was analyzed according to the ALT, AFP, and hepatitis C virus (HCV) RNA levels 24 weeks after the start of PegIFNα-2a administration by using the Kaplan–Meier method. The risk of HCC was analyzed, using the Kaplan–Meier method, only in the non-responders with detectable HCV RNA during PegIFNα-2a administration by dividing them according to the ALT and AFP levels 24 weeks after the start of therapy. The incidence of HCC was compared between the patients with ALT levels of <41 IU/L and those with levels of ≥41 IU/L, and between patients with serum AFP levels of <10 ng/L and those with levels of ≥10 ng/mL at 24 weeks after starting treatment, because at most of the centers participating in the this study, the upper normal range of serum ALT is set at 40 IU/L, and the most significant difference in the incidence of HCC was observed between the PegIFNα-2a and control group with the cut-off serum ALT set at 41 IU/L and cutoff serum AFP set at 10 ng/mL, 24 weeks after starting treatment. The HCV RNA level was measured using the Amplicor Monitor method with a lower detection limit of 50 IU/L (Roche Diagnostics, Tokyo, Japan). A history of excess alcohol consumption was determined as >60 g alcohol per day in order to exclude alcoholic liver disease.

An asymptomatic carrier was defined as a patient with a serum ALT level within the normal range and minimal inflammation or fibrosis in the biopsied tissues of the liver. Chronic hepatitis was defined as mild-to-severe fibrosis of the liver according to liver biopsy [18]. The diagnosis of liver cirrhosis was based on the results of histological examination of the biopsied liver tissues.

Study 2: incidence of HCC in the PegIFNα-2a therapy and non-administration (control) groups in comparison with propensity-matched controls

Ninety-nine of the 133 chronic hepatitis C patients who had not received IFN were examined as controls; patients in this group received liver-protective agents such as glycyrrhizin or were untreated, and the group was observed for more than 1 year. None of the individuals in the control groups had received IFN alone or PegIFNα and ribavirin combination treatment. They were treated for a median of 1,395 days (range 75–6,556 days). Fifty-nine of these patients underwent liver biopsy before the treatment and were considered the control group for the propensity-matched study. For the propensity-matched study, 59 patients were selected from the PegIFNα-2a group according to their age, sex, platelet count, and total bilirubin levels, which had been identified as independent pretreatment risk factors for the development of HCC in Study 1. The rates of HCC were analyzed using the Kaplan–Meier method, and the risk of HCC was analyzed particularly in patients with advanced fibrosis of the liver (F3 and F4).

Table 2 Comparison of HCC and non-HCC patients with long-term PegIFNα-2a administration ($n = 594$)

	Patients with or without development of HCC		*p* value
	With HCC ($n = 49$)	Without HCC ($n = 545$)	
Pretreatment parameters			
Age (years)	63.8 ± 1.7	61.3 ± 0.5	<0.05
Sex (male/female)	32/17	226/319	<0.01
BMI	24.0 ± 0.5	23.1 ± 0.2	n.s.
Genotype (1/2)	47/6	397/148	n.s.
History of excess alcohol consumption (≥60 g/day; yes/no)	11/38	107/338	n.s.
Fibrosis (F0, 1, 2/F3, 4)	25/24	418/127	<0.001
Inflammatory activity (A0, 1/A2, 3)	7/42	462/83	<0.001
Diabetes mellitus (no/yes)	38/11	461/84	n.s.
LDL cholesterol (mg/dL)	88.2 ± 9.0	94.7 ± 2.6	n.s.
White blood cell count (/mm^3)	4,355 ± 210	4,360 ± 64	n.s.
Red blood cell count ($\times 10^6$/μL)	420.8 ± 8.1	424.1 ± 2.6	n.s.
Hemoglobin (g/dL)	13.6 ± 0.3	13.3 ± 0.1	n.s.
Platelet count ($\times 10^3$/μL)	106 ± 8	140 ± 2	<0.001
Albumin (g/dL)	3.8 ± 0.1	4.0 ± 0.1	<0.001
Total bilirubin (mg/dL)	1.2 ± 0.1	0.8 ± 0.1	<0.001
AST (IU/L)	78.1 ± 6.8	64.6 ± 2.1	n.s.
ALT (IU/L)	72.8 ± 9.7	72.0 ± 2.9	n.s.
Gamma-GTP (IU/L)	68.7 ± 7.5	53.9 ± 2.3	n.s.
Alpha fetoprotein (ng/L)	17.1 (4.4–36.8)	16.7 (4.1–23.1)	n.s.
Esophageal varices	29.0 % (9/31)	6.4 % (22/344)	<0.01
On-treatment parameters			
ALT (IU/L)	59.4 ± 5.7	44.6 ± 1.8	<0.05
Alpha fetoprotein (ng/L)	9.8 (4.6–17.4)	5.5 (3.7–11.1)	<0.01
HCV RNA level (KIU/mL)	236 (<0.5–2,210)	21 (<0.5–1,780)	<0.05

n.s. not significant

Statistical analysis

Categorical data were compared using the χ^2 test or Fisher's exact test. The distributions of continuous variables were analyzed using Student's *t*-test and the Mann–Whitney *U*-test for two groups. Multivariate analysis was

conducted using logistic regression. The cumulative incidence curve was determined using the Kaplan–Meier method and differences between groups were assessed by the log-rank test. For all methods, the level of significance was set at $p < 0.05$. Multivariate analysis of the risk of HCC was carried out using the Cox proportional hazard model. Statistical analyses were performed using the Statistical Package for the Social Sciences software version 11.0 (SPSS, Chicago, IL, USA). In Study 1, age, sex, platelet count, and total bilirubin levels were identified as independent factors for the development of HCC; therefore, these factors were selected for the propensity-matched control study (Study 2) in which 59 patients from the PegIFNα-2a group were included.

Results

Study 1

We analyzed the factors involved in the development of HCC in patients who received 90 μg PegIFNα-2a weekly or biweekly for more than a year. The incidence of HCC did not differ significantly between the groups treated with PegIFNα-2a weekly and biweekly (34 of 512 vs. 15 of 82, respectively). As shown in Table 2, univariate analysis revealed statistically significant differences in the pretreatment parameters including age, sex, fibrosis of the liver, platelet count, albumin level, and total bilirubin, between patients who developed HCC and those who did not. Endoscopy was carried out in 375 patients, and esophageal varices were noted in 31 of them. The incidence of HCC was higher in patients with esophageal varices than in those without varices [29.0 % (9 of 31) vs. 6.4 % (22 of 344)]. Assessment of on-treatment factors by univariate analysis revealed statistically significant differences in serum ALT, AFP, and HCV RNA levels 24 weeks after the start of PegIFNα-2a maintenance treatment (Table 2).

Multivariate analysis including pretreatment parameters revealed that age, sex, fibrosis of the liver, platelet count, and total bilirubin were independent risk factors for HCC development (Table 3). Multivariate analysis including on-treatment parameters identified ALT levels of ≥41 IU/L and AFP levels of ≥10 ng/L 24 weeks after the start of the PegIFNα-2a therapy as independent risk factors for HCC development (Table 3).

The incidence of HCC was significantly lower in patients with ALT levels of ≤40 IU/L than in those with ALT levels of ≥41 IU/L 24 weeks after the start of observation (Fig. 2). The incidence of HCC was also significantly lower in patients with AFP concentrations of <10 ng/mL at 24 weeks after the start of observation than in those with AFP concentrations of ≥10 ng/mL (Fig. 3). The dose of PegIFNα-2a was reduced to 45 μg in 16 patients because of neutropenia and thrombocytopenia. In addition, PegIFNα-2a was discontinued in 18 patients because of adverse events, including depression (7 patients), interstitial pneumonitis (3 patients), thrombocytopenia (3 patients), neutropenia (1 patient), itching (1 patient), and ascites (3 patients). No statistically significant differences were found between the patients with reduced dosage or treatment interruption and those without treatment modifications with respect to overall survival, HCC incidence, ascites formation, variceal bleeding, hepatic encephalopathy, and 2-point increases in the Child-Pugh score. No patients underwent liver transplantation.

Table 3 Independent risk factors for HCC development in patients treated with 90 μg PegIFNα-2a weekly or bi-weekly, evaluated by multivariate analysis (logistic regression analysis)

	Multivariate analysis		
	Odds ratio	95 % Confidence interval (CI)	*p*
Age (years) (every 5 years)	2.24	1.76–9.33	<0.005
Sex (male/female)	3.16	1.56–10.7	<0.005
Fibrosis (F3, 4/F0, 1, 2)	1.69	1.18–5.2	<0.01
Platelet count (<120 × 10^3/μL vs. ≥120 × 10^3/μL)	3.24	1.44–27.6	<0.01
Total bilirubin (mg/dL)	1.59	1.09–2.58	<0.05
ALT (at 24 weeks) (≥41 vs. <40 IU/L)	2.49	1.51–8.28	<0.05
AFP (at 24 weeks) (≥10 vs. <10 ng/L)	3.78	1.92–11.8	<0.01

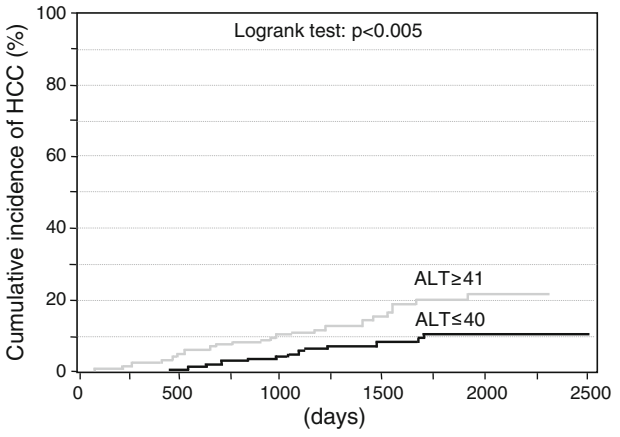

Fig. 2 Comparison of HCC rates in patients administered with PegIFNα-2a ($n = 594$) with respect to alanine aminotransferase (*ALT*) levels 24 weeks after the start of therapy. *Black line* patients with ALT ≥41 IU/L in the first 24 weeks, *gray line* patients with ALT ≤40 IU/L in the first 24 weeks

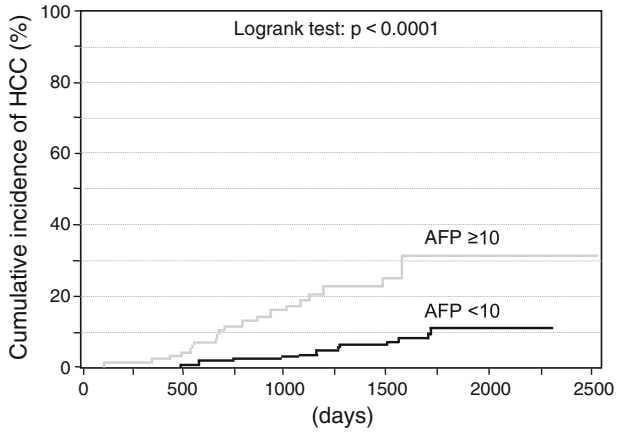

Fig. 3 Comparison of HCC rates in patients administered PegIFNα-2a ($n = 594$) with respect to alpha-fetoprotein (*AFP*) levels in the first 24 weeks after the start of therapy. *Black line* patients with AFP ≥10 ng/mL at 24 weeks, *gray line* patients with AFP <10 ng/mL at 24 weeks

Study 2

We compared the incidence of HCC between 59 patients in the control group and the same number of patients in the PegIFNα-2a group using the matched-pair test. The backgrounds of the patients are shown in Table 4. The PegIFNα-2a group had higher rates of advanced fibrosis (F3 and F4) and active inflammation (A2 and A3). No other differences were found between the two groups, except for the white blood cell count (Table 4).

Development of HCC was observed in 2 patients in the PegIFNα-2a group and 8 in the control group. The incidence of HCC was compared between the two groups, using the Kaplan–Meier method. The incidence of HCC in the PegIFNα-2a group was significantly lower than that in the control group (log-rank test, $p = 0.0187$; Fig. 4). Among the patients with advanced fibrosis of the liver (F3 and F4), those in the PegIFNα-2a group had a lower incidence of HCC than those in the control group. The independent risk factors for the development of HCC were analyzed using the stepwise Cox proportional hazard model. Only PegIFNα-2a administration and age were identified as independent risk factors for the development of HCC (Table 5).

Discussion

The number of HCC cases resulting from HCV infection continues to increase worldwide [19]. To date, IFN therapy is the most effective preventive measure against HCC in patients with chronic hepatitis C; furthermore, the incidence of HCC is reduced in patients who achieve an SVR to IFN [6–9] Therefore, achieving an SVR is the most effective approach for reducing the risk of developing HCC. In Japan, the incidence of HCC is elevated in older patients with hepatitis C. Corroborating this finding, the results of a Japanese study show a higher risk of HCC in patients aged 65 years and more [10]. Therefore, prevention of HCC in aged patients is an important challenge.

In the present multicenter, cooperative, retrospective study conducted in Japan, the incidence of HCC was reduced in patients who received 90 μg PegIFNα-2a weekly or biweekly and had AFP values of <10 ng/mL and ALT values of ≤40 IU/L 24 weeks after the start of the treatment. The results of the matched case–control study of the PegIFNα-2a group and the non-IFN control group show that the incidence of HCC was significantly lower in the PegIFNα-2a group than in the control group, especially in patients with advanced fibrosis of the liver (F3 and F4). However, there could have been a selection bias between

Table 4 Backgrounds of the patients in the propensity-matched control study (PegIFNα-2a group, $n = 59$; control group, $n = 59$)

	PegIFNα-2a group ($n = 59$)	Control group ($n = 59$)	p value
Age (years)	60.5 ± 13.0	63.3 ± 10.5	n.s.
Gender (male/female)	24/35	25/34	n.s.
BMI	22.9 ± 3.6	22.9 ± 3.4	n.s.
Genotype (1/2)	49/10	46/13	n.s.
History of excess alcohol consumption (60 g/day; yes/no)	10/49	4/55	n.s.
Fibrosis (F0, 1, 2/F3, 4)	37/22	43/16	<0.05
Development of HCC (F0–2/F3, 4)	1/1	1/7	n.s.
Inflammatory activity (A0,1/A2, 3)	19/40	30/29	<0.05
Diabetes mellitus (no/yes)	57/2	56/3	n.s.
LDL cholesterol (mg/dL)	95.3 ± 23.8	117.0 ± 4.2	n.s.
White blood cell count (/mm^3)	4,260 ± 1,239	5,193 ± 2,078	<0.05
Red blood cell count ($\times 10^{-4}$/μL)	430 ± 57.8	441 ± 44.9	n.s.
Hemoglobin (g/dL)	13.6 ± 1.5	13.6 ± 1.9	n.s.
Platelet count ($\times 10^{-3}$/μL)	14.5 ± 5.7	15.8 ± 5.7	n.s.
Albumin (g/dL)	4.1 ± 0.5	4.1 ± 0.4	n.s.
Total bilirubin (mg/dL)	0.7 ± 0.5	0.9 ± 0.7	n.s.
AST (IU/L)	58.3 ± 47.7	49.7 ± 26.6	n.s.
ALT (IU/L)	63.6 ± 68.7	58.0 ± 39.2	n.s.
Gamma-GTP (IU/L)	78.3 ± 81.3	55.3 ± 75.1	n.s.
Baseline alpha-fetoprotein (AFP) (ng/L)	7.2 (4.3–14.2)	7.7 (3.9–13.8)	n.s.
Baseline HCV RNA level (KIU/mL)	1,230 (24–3,870)	1,024 (38–3,110)	n.s.

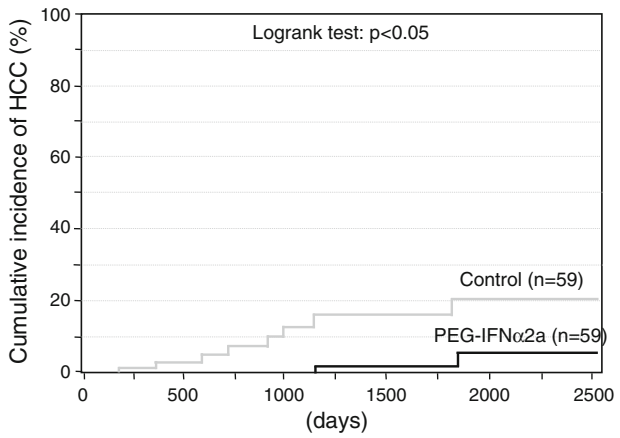

Fig. 4 Comparison of HCC rates between the long-term PegIFNα-2a administration group ($n = 59$) and non-administration group ($n = 59$) in the propensity-matched control study (Kaplan–Meier log-rank test, $p = 0.019$)

Table 5 Risk factors for HCC in the propensity-matched control study (Cox proportional hazard model)

Variables	Risk ratio	95 % CI	*p* value
PegIFN versus control	0.17	0.03–0.75	<0.05
Age (every 1 year)	1.12	1.02–1.25	<0.05
Fibrosis (F3, 4 vs. F0, 1, 2)	1.70	0.75–4.16	n.s.
Platelet count (every $10 \times 10^3/\mu L$)	0.89	0.73–1.09	n.s.
Albumin (every 1.0 g/dL)	0.80	0.10–6.68	n.s.
On-treatment AFP (<10 vs. ≥10 ng/L)	4.07	0.59–40.12	n.s.

the PegIFNα-2a group and the control group (patients who did not agree to receive IFN treatment), because this was a retrospective and non-randomized study. However, concordant with the findings of the HALT-C study [14], the present results show that PegIFNα-2a inhibits the development of HCC in patients with advanced fibrosis of the liver.

Recent studies show that polymorphisms in the host *IL28B* gene are important factors in the response to PegIFNα and ribavirin combination therapy [20, 21]. However, the mechanism of IL28B involvement in the response to PegIFNα and ribavirin has not been elucidated completely. A recent report has shown that IL28B is a significant factor in the development of HCC as well as in the response to IFN therapy [22]. Further studies are warranted to analyze the relationship between IL28B and inhibition of the development of HCC by PegIFNα in chronic hepatitis C.

Risk factors for the development of HCC have been discussed previously. Increased intrahepatic fat is involved in the development of HCC in chronic hepatitis C patients [23, 24]. In addition, diabetes-associated fat disorder [25, 26], hepatic iron overload [27], advanced fibrosis, older age, and fatty deposits in the liver are risk factors for HCC development [4]. Therefore, it is important to establish strategies to mitigate these risk factors to prevent the development of HCC and thus improve the outcomes of hepatitis C patients.

IFN therapy after HCC treatment is reported to inhibit the recurrence of tumors [28, 29], and a meta-analysis has revealed a trend toward inhibition of the recurrence of HCC [30, 31]. The prevention of HCC is an important issue that needs to be addressed to improve the survival of chronic hepatitis C patients. The findings of the present study and the HALT-C trial [14] indicate the effectiveness of long-term administration of maintenance IFN for preventing the development of HCC in chronic hepatitis C patients without an SVR. Improvement in ALT levels is also known to be an important predictor for the prevention of HCC [32]. A low AFP value during IFN administration is also recognized as a significant indicator of a lower risk of HCC [33, 34]. Recently, Osaki et al. [35] reported that a decrease of serum AFP during treatment with IFN was associated with a reduced incidence of HCC. Taking these findings and our own together, we conclude that maintenance administration of low-dose PegIFNα-2a weekly or biweekly to non-SVR patients with chronic hepatitis C decreases the incidence of HCC, especially in patients whose serum ALT and AFP levels are within the normal range 24 weeks after the start of treatment. The preventive effects of IFN against the development of HCC without elimination of the virus may be associated with its anticarcinogenic effects [16, 35]; however, the precise mechanism should be investigated.

The limitations of the present study are that it is retrospective and multicentric; therefore, potentially there may have been a selection bias. However, the reduction of the rate of development of HCC by maintenance administration of PegIFNα-2a in the patients in whom serum ALT and AFP levels were within the normal ranges 24 weeks after the start of treatment may be attributable to the anticarcinogenic effects of IFN without elimination of the virus.

Conclusion

The incidence of HCC was lower in non-SVR patients with chronic hepatitis C who were administered with maintenance low-dose PegIFNα-2a; especially in those whose serum ALT and AFP levels were within the normal ranges 24 weeks after the start of treatment.

Acknowledgments This study was supported by a Grant-in-Aid from the Japanese Ministry of Health, Welfare, and Labor.

Conflict of interest Namiki Izumi received lecture fees from Chugai Co. and MSD Co. in 2011.

References

1. Parkin DM, Bray F, Ferlay J, Pisani P. Global cancer statistics, 2002. CA Cancer J Clin. 2005;55:74–108. doi:10.3322/canjclin.55.2.74.
2. Llovet JM, Burroughs A, Bruix J. Hepatocellular carcinoma. Lancet. 2003;362:1907–17. doi:10.1016/S0140-6736(03)14964-1.
3. Kiyosawa K, Sodeyama T, Tanaka E, Gibo Y, Yoshizawa K, Nakano K, et al. Interrelationship of blood transfusion, non-A, non-B hepatitis and hepatocellular carcinoma: analysis by detection of antibody to hepatitis C virus. Hepatology. 1990;12:671–5. doi:10.1002/hep.1840120409.
4. Namiki I, Nishiguchi S, Hino K, Suzuki F, Kumada H, Itoh T, et al. Management of hepatitis C; Report of the consensus meeting at the 45th annual meeting of the Japan Society of Hepatology (2009). Hepatol Res. 2010;40:347–68. doi:10.1111/j.1872-034X.2010.00642.x.
5. Tanaka Y, Hanada K, Mizokami M, Yeo AE, Shin JW, Gojobori T, et al. A comparison of the molecular clock of hepatitis C virus in the United States and Japan predicts that hepatocellular carcinoma incidence in the United States will increase over the next two decades. Proc Natl Acad Sci USA. 2002;99:11584–9. doi:10.1073/pnas.242608099.
6. Ikeda K, Saitoh S, Arase Y, Chayama K, Suzuki Y, Kobayashi M, et al. Effect of interferon therapy on hepatocellular carcinoma in patients with chronic hepatitis type C: a long-term observation study of 1,643 patients using statistical bias correction with proportional hazard analysis. Hepatology. 1999;29:1124–30.
7. Imai Y, Kawata S, Tamura S, Yabuuchi I, Noda S, Inada M, et al. Relation of interferon therapy and hepatocellular carcinoma in patients with chronic hepatitis C. Ann Intern Med. 1998;129:94–9.
8. Bruno S, Stroffolini T, Colombo M, Bollani S, Benveguu L, Mazzella G, et al. Sustained virological response to interferon-alpha is associated with improved outcome in HCV-related cirrhosis: a retrospective study. Hepatology. 2007;45:579–87. doi:10.1002/hep.21492.
9. Veldt BJ, Heathcote EJ, Wedemeyer H, Reichen J, Hofmann WP, Zeuzem S, et al. Sustained virological response and clinical outcomes in patients with chronic hepatitis C and advanced fibrosis. Ann Intern Med. 2007;147:677–84.
10. Asahina Y, Tsuchiya K, Tamaki N, Hirayama I, Tanaka T, Sato M, et al. Effect of aging on risk for hepatocellular carcinoma in chronic hepatitis C virus infection. Hepatology. 2010;52:518–27. doi:10.1002/hep.23691.
11. Amarapurkar D, Han KH, Chan HL, Ueno Y, Asia-Pacific working party on prevention of hepatocellular carcinoma. Application of surveillance programs for hepatocellular carcinoma in the Asia-Pacific Region. J Gastroenterol Hepatol. 2009;24:955–61. doi:10.1111/j.1440-1746.2009.05805.x.
12. Tamura Y, Yamagiwa S, Aoki Y, Kurita S, Suda T, Ohkoshi S, et al. Serum alpha-fetoprotein levels during and after interferon therapy and the development of hepatocellular carcinoma in patients with chronic hepatitis C. Dig Dis Sci. 2009;54:2530–7.
13. Di Bisceglie AM, Shiffman ML, Everson GT, Lindsay KL, Everhart JE, Wright EC, et al. Prolonged therapy of advanced chronic hepatitis C with low-dose peginterferon. N Engl J Med. 2008;359:2429–41. doi:10.1056/NEJMoa0707615.
14. Lok AS, Everhart JE, Wright EC, Di Bischeglie AM, Kim HY, Stering RK, et al. Maintenance peginterferon therapy and other factors associated with hepatocellular carcinoma in patients with advanced hepatitis C. Gastroenterology. 2011;140:840–9. doi:10.1053/j.gastro.2010.11.050.
15. Bruix J, Poynard T, Colombo M, Schiff E, Burak K, Heathcote EJ, et al. Maintenance therapy with peginterferon alfa-2b does not prevent hepatocellular carcinoma in cirrhotic patients with chronic hepatitis C. Gastroenterology. 2011;140:1990–9. doi:10.1053/j.gastro.2010.11.050.
16. Arase Y, Ikeda K, Suzuki F, Suzuki Y, Kobayashi M, Akuta N, et al. Prolonged-interferon therapy reduces hepatocarcinogenesis in aged-patients with chronic hepatitis C. J Med Virol. 2007;79:1095–102. doi:10.1002/jmv.20866.
17. Poynard T, Moussali J, Ratziu V, Regimberu C, Opolan P. Effects of interferon therapy in "non-responder" patients with chronic hepatitis C. J Hepatol. 1999;31S:178–83. doi:10.1016/S0168-8278(99)80397-3.
18. Desmet VJ, Gerber M, Hoofnagle JH, Manns M, Scheuer P. Classification of chronic hepatitis: diagnosis, grading and staging. Hepatology. 1994;19:1513–20. doi:10.1016/0270-9139(94)90250-X, doi:10.1002/hep.1840190629.
19. Kanwal F, Hoang T, Kramer JR, Asch SM, Goetz MB, Zeringue A, et al. Increasing prevalence of HCC and cirrhosis in patients with chronic hepatitis C virus infection. Gastroenterology. 2011;140:1182–8. doi:10.1053/j.gastro.2010.12.032.
20. Ge D, Fellay J, Thompson AJ, Simon JS, Shianna KV, Urban TJ, et al. Genetic variation in IL28B predicts hepatitis C treatment-induced viral clearance. Nature. 2009;461:399–401. doi:10.1038/nature08309.
21. Tanaka Y, Nishida N, Sugiyama M, Kurosaki M, Matsuura K, Sakamoto N, et al. Genome-wide association of IL28B with response to pegylated interferon-alpha and ribavirin therapy for chronic hepatitis C. Nature. 2009;41:1105–9.
22. Fabris C, Falleti E, Cussigh A, Bitetto D, Fontanini E, Bignulin S, et al. IL-28B rs 12979860 C/T allele distribution in patients with liver cirrhosis: role in the course of chronic viral hepatitis and the development of HCC. J Hepatol. 2011;54:716–22. doi:10.1016/j.jhep.2010.07.019.
23. Kurosaki M, Hosokawa T, Matsunaga K, Hirayama I, Tanaka T, Sato M, et al. Hepatic steatosis in chronic hepatitis C is a significant risk factor for developing hepatocellular carcinoma independent of age, sex, obesity, fibrosis stage and response to interferon therapy. Hepatol Res. 2010;40:870–7. doi:10.1111/j.1872-034X.2010.00692.x.
24. Koike K. Steatosis, liver injury, and hepatocarcinogenesis in hepatitis C viral infection. J Gastroenterol. 2009;44(Suppl 19):82–8. doi:10.1007/s00535-008-2276-4.
25. Veldt BJ, Chen W, Heathcote EJ, Wedemeyer H, Reichen J, Hofman WP, et al. Increased risk of hepatocellular carcinoma among patients with hepatitis C cirrhosis and diabetes mellitus. Hepatology. 2008;47:1856–62. doi:10.1002/hep.22251.
26. Lai MS, Hsieh MS, Chiu YH, Chen TH. Type 2 diabetes and hepatocellular carcinoma: a cohort study in high prevalence area of hepatitis virus infection. Hepatology. 2006;43:1295–302. doi:10.1002/hep.21208.
27. Furutani T, Hino K, Okuda M, Gondo T, Nishina S, Kitase A, et al. Hepatic iron overload induces hepatocellular carcinoma in transgenic mice expressing the hepatitis C virus polyprotein. Gastroenterology. 2006;130:2087–98. doi:10.1053/j.gastro.2006.02.060.
28. Kubo S, Nishiguchi S, Hirohashi K, Tanaka H, Shuto T, Kinoshita H. Randomized clinical trial of long-term outcome after resection of hepatitis C virus-related hepatocellular carcinoma by

postoperative interferon therapy. Br J Surg. 2002;89:418–22. doi:10.1046/j.0007-1323.2001.02054.x.
29. Kudo M, Sakaguchi Y, Chung H, Hatanaka K, Hagiwara S, Ishikawa E, et al. Long-term interferon maintenance therapy improves survival in patients with HCV-related hepatocellular carcinoma after curative radiofrequency ablation. A matched case–control study. Oncology. 2007;72(Suppl 1):132–8. doi:10.1159/000111719.
30. Singal AK, Freeman DH Jr, Anand BS. Meta-analysis: interferon improves outcomes following ablation or resection of hepatocellular carcinoma. Aliment Pharmacol Ther. 2010;32:851–8. doi:10.1111/j.1365-2036.2010.04414.x.
31. Miyake Y, Takaki A, Iwasaki Y, Yamamoto K. Meta-analysis: interferon-alpha prevents the recurrence after curative treatment of hepatitis C virus-related hepatocellular carcinoma. J Viral Hepat. 2010;17:287–92. doi:10.1111/j.1365-2893.2009.01181.x.
32. Arase Y, Ikeda K, Suzuki F, Suzuki Y, Kobayashi M, Akuta N, et al. Interferon-induced prolonged biochemical response reduces hepatocarcinogenesis in hepatitis C virus infection. J Med Virol. 2007;79:1485–90. doi:10.1002/jmv.20925.
33. Nomura H, Kashiwagi Y, Hirano R, Tanimoto H, Tsutsumi N, Higashi M, et al. Efficacy of low dose long-term interferon monotherapy in aged patients with chronic hepatitis C genotype 1 and its relation to alpha-fetoprotein: a pilot study. Hepatol Res. 2007;37:490–7. doi:10.1111/j.1872-034X.2007.00073.x.
34. Chen TM, Huang PT, Tsai MH, Lin LF, Liu CC, Ho KS, et al. Predictors of alpha-fetoprotein elevation in patients with chronic hepatitis C, but not hepatocellular carcinoma, and its normalization after pegylated interferon alfa 2a-ribavirin combination therapy. J Gastroenterol Hepatol. 2007;22:669–75. doi:10.1111/j.1440-1746.2007.04898.x.
35. Osaki Y, Ueda Y, Marusawa H, Nakajima J, Kimura T, Kita R, et al. Decrease in alpha-fetoprotein levels predicts reduced incidence of hepatocellular carcinoma in patients with hepatitis C virus infection receiving interferon therapy: a single center study. J Gastroenterol. 2012;47:444–51.

Liver INTERNATIONAL
OFFICIAL JOURNAL OF THE INTERNATIONAL ASSOCIATION FOR THE STUDY OF THE LIVER

Liver International ISSN 1478-3223

LIVER CANCER

Clinical implication of hypovascular hepatocellular carcinoma studied in 4,474 patients with solitary tumour equal or less than 3 cm

Kenichi Takayasu[1], Shigeki Arii[2], Michiie Sakamoto[3], Yutaka Matsuyama[4], Masatoshi Kudo[5], Takafumi Ichida[6], Osamu Nakashima[7], Osamu Matsui[8], Namiki Izumi[9], Yonson Ku[10], Norihiro Kokudo[11] and Masatoshi Makuuchi[12] for the Liver Cancer Study Group of Japan

1 Department of Diagnostic Radiology, National Cancer Center Hospital, Tokyo, Japan
2 Hepato-Biliary-Pancreatic Surgery, Hamamatsu Rosai Hospital, Japan Labor Health and Welfare Organization, Hamamatsu, Japan
3 Department of Pathology, Keio University School of Medicine, Tokyo, Japan
4 Department of Biostatistics, School of Public Health, University of Tokyo, Tokyo, Japan
5 Department of Gastroenterology and Hepatology, Kinki University School of Medicine, Sayama, Japan
6 Department of Hepatology and Gastroenterology, Juntendo Shizuoka Hospital, Izunokuni, Japan
7 Department of Clinical Laboratory Medicine, Kurume University Hospital, Kurume, Japan
8 Department of Radiology, Kanazawa University Graduate School of Medical Science, Kanazawa, Japan
9 Department of Gastroenterology and Hepatology, Musashino Red Cross Hospital, Musashino, Japan
10 Department of Surgery, Kobe University Graduate School of Medicine, Kobe, Japan
11 Hepato-Biliary-Pancreatic Surgery Division, Artificial Organ and Transplantation Division, Department of Surgery, Graduate School of Medicine, University of Tokyo, Tokyo, Japan
12 Surgery, Japanese Red Cross Medical Center, Tokyo, Japan

Keywords
arterial tumour hypervascularization – des-γ-carboxy prothrombin (DCP) – histologic differentiation – hypovascular hepatocellular carcinoma (HCC) – multistep hepatocarcinogenesis

Correspondence
Kenichi Takayasu, Department of Diagnostic Radiology, National Cancer Center Hospital, 5-1-1, Tsukiji, Chuo-Ku Tokyo 104-0045, Japan
Tel: +81 3 3542 2511
Fax: +81 3 3542 3815
e-mail: ktakayas@ncc.go.jp

Received 18 August 2012
Accepted 21 January 2013

DOI:10.1111/liv.12130
Liver Int. 2013: 33: 762–770

Abstract

Background & Aims: To clarify the biological behaviour of small hypovascular hepatocellular carcinoma (HCC) because of insufficient evidence even though frequently encountered. *Methods:* The study covered naïve 4,474 patients who met solitary HCC $\leq$3 cm (mean, 2.1 cm), histopathologically proven and Child Pugh A or B. Macroscopic vascular invasion and distant metastasis were excluded. The hypovascularity of tumour was defined as hypo- or iso-enhancement in arterial phase of multiple dynamic imaging techniques. *Results:* Of them, 802 (18%) were hypovascular. The ratio of hypovascular HCC decreased as tumour size increased ($P < 0.001$) and most of them developed to hypervascular type when they grew over 1.5 cm. Hypovascular group showed a significantly higher ratio of well differentiated grade ($P < 0.001$) and marginally less incidence of microvascular invasion and metastases compared with hypervascular group. The histologic dedifferentiation (less differentiation) developed step-by-step as tumour size increased in hyper- and even hypovascular group. The des-γ-carboxy prothrombin (DCP) value $\geq$ 300mAU/ml was closely correlated with increase of tumour size in both groups. Logistic regression analysis revealed five variables were independent predictors for hypovascular HCC; tumour size $\leq$1.5 cm, alpha-fetoprotein < 200 ng/ml, DCP < 40mAU/ml, well differentiated grade, and positivity for hepatitis C virus antibody. *Conclusions:* Hypovascular HCC was biologically less aggressive and developed with stepwise dedifferentiation and transformation to hypervascular appearance along with tumour growth. These results will help in leading correct diagnosis of small hypovascular tumour and assessing optimal treatment for hypovascular HCC$\leq$3 cm.

Hepatocellular carcinoma (HCC) is the sixth most common malignancy and the third most common cause of cancer-related death in the world (1). With the prevalence of surveillance protocols for at-risk patients with chronic liver disease and the development of diagnostic imaging modalities, small HCC is easily found and curative treatment of resection, local ablation and liver transplantation has been undergone. During the last 10 years, the frequency of HCC $\leq$ 2 cm found in nation-wide surveillance has much improved from 25% to 34% in Japan (2, 3). Consequently, we have encountered not a few small hypo- or isovascular HCCs in the

arterial phase of dynamic imaging modalities (4–8) which is an atypical finding for definite HCC in the diagnostic algorithms proposed by the Japanese guidelines (9) and the American Association for the Study of Liver Diseases (AASLD) (10, 11).

To date, hypovascular HCC has been reported to be smaller in size and predominantly accounted for well differentiated grade compared with hypervascular HCC examined by radiological (4–6, 8, 12) and pathological (13) studies. More recently, the entity of early HCC was proposed to have vaguely nodular gross appearance with histopathologically well differentiated grade, portal tracts (14–16) and stromal invasion (17). Radiologically, almost early HCC was hypo- or isovascular in the arterial phase of dynamic enhanced CT and combination study of CT and hepatic arteriography (18,19). As a result, single hypovascular or early HCC was recommended to be intensively followed-up and treated with local ablation under some conditions; pathologically diagnosed as early HCC, decreased uptake on hepatobiliary phase of gadoxetic acid enhanced-MRI, or decreased portal flow on CT during arterial portography by Consensus Meeting of the Japan Society of Hepatology (20). To date, better survival of patients with early HCC (hypovascular) compared to those with progressed HCC (hypervascular) on resection was reported (21). However, which treatment is optimal for patient with small hypovascular HCC is not yet established. In addition, several queries of hypovascular HCC remain still unclear; the frequency, relation of tumour size and differentiation, transformation of tumour vascularity, biomarker and relevance of hypovascular HCC and early HCC.

Therefore, we conducted this study using a large population over 4,000 patients with histopathologically proved solitary HCC $\leq$ 3 cm. To our best knowledge, we were unable to find any previous study on this scale.

Patients and Methods

Patients

During the six years from January 2000 to December 2005, a total of 60,773 patients with primary liver cancer were diagnosed and prospectively registered nationwide every two years through more than 500 institutions by the Liver Cancer Study Group of Japan (LCSGJ). Of these, 53,008 patients were clinically diagnosed as HCC with multiple imaging modalities, tumour markers and/or needle biopsy. Finally, 4,474 patients were enrolled in this study who met the following inclusion criteria; Child-Pugh A or B, solitary HCC $\leq$3 cm in diameter histopathologically proven and tumour vascularity confirmed whether hyper- or hypovascular appearance in the arterial phase of multimodal dynamic techniques of CT/MRI/contrast enhanced ultrasonography (CE-US) and/or angiography. All of them underwent one of the following treatments as an initial therapy; resection (n = 2,445 patients), local ablation such as radiofrequency ablation (n = 1,345), percutaneous ethanol injection (n = 363) and microwave coagulation (n = 225), or transarterial chemoembolization (n = 96). Exclusion criteria were macroscopic vascular invasion of portal and hepatic veins, extrahepatic metastasis and previous history of HCC.

Diagnosis

For at-risk, patients with chronic liver disease mainly associated with hepatitis C virus (HCV) and/or B virus (HBV), surveillance protocol has been carried out with US and tumour markers of alpha-fetoprotein (AFP; normal <15 ng/ml) and des-γ-carboxy prothrombin (DCP; <40 mAU/ml) every 3–4 months. The typical vascular profile of HCC was defined to be hypervascular in the arterial phase followed by hypovascular or washout in portal or equilibrium phase on multidetector CT (MDCT, 4-detector scanner commercially available from 1999 in Japan) or helical CT, MRI with gadolinium- diethylenetriaminepenta-acetic acid (Gd-DTPA) and CE-US (Levovist, Schering AG, Berlin, Germany; available from 1999). If the tumour did not show typical vascular appearance and was larger than 2 cm in diameter, further examinations were recommended, i.e. angiography, combination study of CT and angiography, MRI with super-paramagnetic iron oxide and/or needle biopsy. If the tumour was less than 2 cm, follow-up study with US every three months was recommended by the Japanese guidelines (9).

In this study, hypovascular HCC included isovascular type and was defined not to show enhancement compared with surrounding liver parenchyma in the arterial phase of dynamic imaging technique(s). Overall, 4,119 (92%) of 4,474 patients in the study were available to evaluate the imaging modalities used. Namely, they had a total of 8,498 imaging studies with a mean of 2.1 (range, 1–4); CT was performed in 3,377 patients (82%), MRI in 840, CE-US in 2,664 and angiography in 1,617 (Table 1). The frequency of combination of imaging techniques was - in descending order - combination of CT and CE-US in 901 (22%) patients, CT alone in 863 (21%), combination of CT, CE-US and angiography in 693 (17%), combination of all four techniques in 453 (11%), and others. The 2,578 (63%) patients underwent multimodal imaging techniques and remaining 1,541 (37%) received single technique. For hypovascular HCC, imaging modalities used was available in 616 (77%) of 802 patients who underwent a total of 1,212 dynamic imaging modalities with a mean of 2.0. The breakdown of grouping of studies was in descending order; combination of CT and CE-US in 177 patients (29%), CE-US alone in 118 (19%), combination of CT, CE-US and angiography in 81 (13%), CT alone in 72 (12%), combination of all four modalities in 52 (8%) followed by angiography alone in 32 (6%) and others. Namely, 380 patients (62%) underwent multimodal

Table 1. Breakdown of combination study with 8,498 various dynamic imaging modalities to confirm the arterial tumor vascularity of HCC in 4,119 patients

No. of patients receiving combination or single modality (%)	Diagnostic modality			
	CT	MRI	CE-US*	Angiography
453 (11)	+	+	+	+
147 (4)	+	+	+	
49 (1)	+	+		+
693 (17)	+		+	+
6 (0.1)		+	+	+
65 (2)	+	+		
901 (22)	+		+	
206 (5)	+			+
33(1)		+	+	
7 (0.2)		+		+
18 (0.4)			+	+
863 (21)	+			
80(2)		+		
413 (10)			+	
185 (4)				+
Total no. of study (%)†	3,377 (82)	840 (20)	2,664 (65)	1,617 (39)

+, examination was performed.

*CE-US, contrast enhanced ultrasonography.

†Percentage calculated by a total no. of study divided by a total no. of patients (n = 4,119) × 100.

studies and remaining 236 (38%) had single study. The tumour vascular profile in portal/venous or equilibrium phase was not available because of lack of inclusion in the questionnaire sheet.

The histologic diagnosis of HCC was made with resected (n = 2,445 patients, 55%) and needle-biopsied specimens (n = 2,029). Of these, 4,196 (94%) were available for histologic differentiation with Edmondson-Steiner's classification (22). The histology of non-cancerous hepatic parenchyma was cirrhosis in 1,514 (56%) of 2,722 patients available, chronic hepatitis or liver fibrosis in 1,124 and normal liver in 84. In addition, fibrous capsule formation (fc), portal vein (vp) and hepatic vein invasions, and intrahepatic metastasis (im) were microscopically studied with resected specimens (n = 2,445 patients). The grade of vp1 ≤ is designated as invasion of distal to second order branches (second order branches not included) of the portal vein or more proximal (23). The grade of ims≤ means spread of metastasis of one subsegment (Couinaud's segment) or more.

Statistical analysis

A chi-squared test and Student's t-test were used to compare the discrete and continuous variables respectively. The Mantel-Haenszel trend test was used for ordinal variables. Multivariate analysis was performed with logistic regression. All significance tests were 2-tailed and a P-value <0.05 was considered statistically significant. Statistical analyses were performed with Statistical Analysis System version 9.1 (SAS Inc, Cary, NC).

Results

Of 4,474 HCCs, 802 (18%) were hypovascular and 3,672 (82%) were hypervascular (Table 2). The mean tumour size was 2.1 ± 0.6 cm (mean±standard deviation; range, 0.5–3.0, median, 2.0) in entire, 1.7 ± 0.6 cm in hypovascular and 2.1 ± 0.6 cm in hypervascular HCC groups. There was a significant difference between the latter two groups (P < 0.001).

Demographic finding of patients and multivariate logistic regression analysis

Concerning background factors of hypo- and hypervascular groups, univariate analysis revealed a significant difference in all eight variables (P = 0.016 to P < 0.001); the following was favourable for hypovascular HCC: age ≥60 years, female, Child-Pugh B, negative for HBs antigen and positive for HCV antibody, small tumour size ≤1.5 cm, low level of AFP <200 ng/ml, normal of DCP and well differentiated grade (Table 2). The multivariate logistic regression analysis with these eight variables disclosed the following four were unlikely and one was likely to associate with significant predictor for hypovascular HCC (Table 3)**:** for the former four, tumour size ≥1.6 cm (odd ratio (OR), 0.47; 95% confidence interval (CI), 0.34–0.64, P < 0.001), tumour 2.1–2.5 cm (0.24; 0.16–0.35, P < 0.001), and tumour 2.6–3 cm (0.18; 0.12–0.27, P < 0.001); AFP level ≥200 ng/ml (0.57; 0.39–0.85, P = 0.01) and DCP levels with 40–299 mAU/ml (0.47; 0.36–0.61, P < 0.001) and ≥ 300 mAU/ml (0.59; 0.36–0.98, P = 0.04) and moderate (0.18; 0.14–0.23, P < 0.001) and poor differentiation (0.18; 0.10–0.34, P < 0.001); and for the latter one, positivity for HCV antibody (1.57; 1.11–2.22, P = 0.01). Namely, tumour size ≤1.5 cm, AFP<200 ng/ml, DCP<40mAU/ml, well differentiated grade and positivity for HCV antibody were independent predictors for hypovascular HCC.

Histopathologic study of resected specimens disclosed that for hypovascular group, fibrous capsule formation was significantly less often seen (P < 0.001) and portal vein invasion and intrahepatic metastasis tended to be less frequently shown with marginally significant difference (P = 0.060 and P = 0.053, respectively; lower portion of Table 2). But no significant difference was seen for hepatic vein invasion (P = 0.555).

The relation of tumour vascularity and size

According to tumour size with a 5 mm-interval, the incidence of hypovascular group step-wisely decreased from 40% in tumours ≤1 cm to 7% in 2.6–3 cm, in

Table 2. Demographic details of 4,474 patients with solitary hypo- or hypervascular HCC ≤ 3 cm, histopathologically proven, and histologic findings of resected specimens

Background factors	No. of pts	%	Hypovascular (n = 802) No. of pts	%	Hypervascular (n = 3.672) No. of pts	%	*P*-value
Age (yr)							
<60	997	22	153	19	844	23	0.016
60 ≤	3,474	78	648	81	2,826	77	
Gender							
Male	3,025	68	492	61	2,533	69	<0.001
Female	1,449	32	310	39	1,139	31	
Child-Pugh classification							
A	3,775	84	641	80	3,134	85	<0.001
B	699	16	161	20	538	15	
HBV and HCV							
HBsAg−&HCVAb−	559	13	60	8	499	14	<0.001
HBsAg−&HCVAb +	3,104	71	628	81	2,476	69	
HBsAg + &HCVAb−	626	14	71	9	555	16	
HBsAg + &HCVAb +	80	2	18	2	62	2	
Tumor size (cm)							
≤ 1	298	7	119	15	179	5	<0.001
1.1–1.5	855	19	298	37	557	15	
1.6–2.0	1,417	32	238	30	1,179	32	
2.1–2.5	931	21	83	10	848	23	
2.6–3.0	973	22	64	8	909	25	
Alpha-fetoprotein (ng/ml)							
<15	2,076	48	369	47	1,707	48	0.003
15–199	1,672	38	357	46	1,315	37	
200 ≤	603	14	52	7	551	15	
des-γ-carboxy prothrombin (mAU/ml)							
<40	2,622	65	598	84	2,024	60	<0.001
40–299	1,088	27	93	13	995	30	
300 ≤	347	9	20	3	327	10	
Histologic differentiation							
Well	1,839	44	624	80	1,215	35	<0.001
Moderately	2,111	50	140	18	1,971	58	
Poorly	246	6	14	2	232	7	
Histopathologic findings of nesected specimens (n = 2445)							
Fibrous capsule formation (fc)							
Absent	757	32	77	52	680	31	<0.001
Present	1618	68	71	48	1547	70	
Portal vein invasion (vp)							
Absent (vp0)	2088	88	140	93	1948	88	0.060
Present (vpl ≤)	288	12	11	7	277	12	
Intrahepatic metastasis (im)							
Absent (im0)	2262	97	151	99	2111	96	0.053
Present (ims ≤)	80	3	1	1	79	4	

contrast that of the hypervascular group increased from 60% to 93% with a significant difference ($P < 0.001$, Table 4). Drawing a frequency distribution of tumour size with a 5 mm interval, hypovascular group showed peak percentage of 37% in tumours 1.1–1.5 cm and the hypervascular group demonstrated a peak of 32% in tumours 1.6–2 cm (Table 2 and Fig. 1). After the peak, the hypovascular group revealed a slight decline of 30% in 1.6–2 cm and finally to 8% in 2.6–3 cm. On the contrary, the hypervascular HCC group did show a slight decline and subsequently reached a plateau of 25%. These results suggest that hypovascular HCC was transformed to hypervascular HCC when it grew over 1.5 cm. Moreover, it was found that 5% of the hypervascular group were already hypervascular in the smallest tumours ≤ 1 cm, whereas 8% of hypovascular group still remained hypovascular even in the largest tumours 2.6–3 cm.

The relation of histologic differentiation and tumour size

In entire 4,196 HCCs, the histologic grade was well differentiated in 44%, moderately in 50% and poorly in 6% (Tables 2 and 5, upper portion). As tumour size

Table 3. Multivariate logistic regression analysis for predicting hypovascular HCC

Variables	Estimate	SE	OR (95% CI)	*P*-value
Age (yr)				
<60	Ref		Ref	
60 ≤	0.05	0.13	1.05 (0.81–1.35)	0.73
Gender				
Male	Ref		Ref	
Female	0.09	0.10	1.10 (0.90–1.35)	0.36
Child-Pugh classification				
A	Ref		Ref	
B	0.10	0.12	1.11 (0.87–1.41)	0.40
HBV and HCV				
HBsAg−& HCV Ab−	Ref		Ref	
HBsAg− & HCV Ab+	0.45	0.18	1.57 (1.11–2.22)	0.01
HBsAg+ & HCV Ab−	0.22	0.23	1.25 (0.79–1.96)	0.34
HBsAg+ & HCV Ab+	0.65	0.38	1.92 (0.92–4.00)	0.08
Tumor size (cm)				
≤1	Ref		Ref	
1.1–1.5	−0.06	0.16	0.94 (0.68–1.30)	0.71
1.6–2.0	−0.76	0.16	0.47 (0.34–0.64)	<0.001
2.1–2.5	−1.43	0.19	0.24 (0.16–0.35)	<0.001
2.6–3.0	−1.70	0.21	0.18 (0.12–0.27)	<0.001
Alpha-fetoprotein (ng/ml)				
<15	Ref		Ref	
15–199	0.10	0.10	1.11 (0.90–1.35)	0.33
200 ≤	−0.56	0.20	0.57 (0.39–0.85)	0.01
des-γ-carboxy prothrombin (mAU/ml)				
<40	Ref		Ref	
40–299	−0.75	0.13	0.47 (0.36–0.61)	<0.001
300 ≤	−0.53	0.26	0.59 (0.36–0.98)	0.04
Histologic differentiation				
Well	Ref		Ref	
Moderately	−1.71	0.11	0.18 (0.14–0.23)	<0.001
Poorly	−1.70	0.31	0.18 (0.10–0.34)	<0.001

SE, Standard Error; OR,Odds Ratio; CI, Confidence Interval.

Table 4. The relation of tumor size and arterial tumor vascularity of HCC

Size (cm)	No. of tumors	Tumor vascularity (%)		*P*-value
		Hypovascular	Hypervascularr	
≤1.0	298	119 (40)	179 (60)	<0.001
1.1–1.5	855	298 (35)	557 (65)	
1.6–2.0	1417	238 (17)	1179 (83)	
2.1–2.5	931	83 (9)	848 (91)	
2.6–3.0	973	64 (7)	909 (93)	
Total	4,474	802 (18)	3,672 (82)	

increased, the proportion of the well differentiated grade decreased from 69% in tumours ≤1 cm to 31% in 2.6–3 cm. In contrast, those of moderately and poorly differentiated grades increased from 29% to 61% and 2% to 8% respectively. Namely, dedifferentiation, i.e., less differentiation significantly progressed step by step with increase of tumour size ($P < 0.001$).

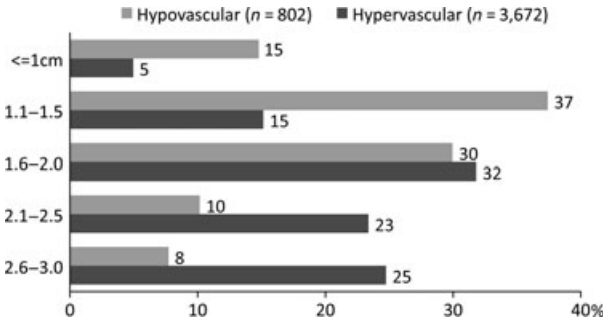

Fig. 1. Frequency distribution of hypo- and hypervascular HCCs according to tumours size. Hypovascular group shows peak percentage of 37% in 1.1–1.5 cm followed by decline to 8% in 2.6–3 cm. In contrast, hypervascular group demonstrates the peak of 32% in 1.6–2 cm and subsequently slight decline to plateau of 25% in 2.6–3 cm.

The similar dedifferentiation in relation to tumour size was recognized in both hypo- and hypervascular groups (both, $P < 0.001$, Table 5, middle and lower portions). However, the proportion of tumour differentiation was very different. Hypovascular group mainly composed of well differentiated grade and hypervascular group consisted of moderately and poorly differentiated grades. As a result, hypovascular HCCs ≤1.5 cm were well differentiated in more than 88%. By contrast, hypervascular HCC ≥2.1 cm were moderately differentiated in approximately two-thirds and poorly differentiated in more than 7%. Throughout both groups, the ratio of well vs. moderately to poorly differentiated grades was almost comparable between tumours 2.6–3 cm in hypovascular group and tumours ≤1 cm in hypervascular group; 58% and 42% vs. 56% and 44%respectively.

The relation of AFP and DCP level and tumour size

The 2,076 (48%) of 4,351 patients showed normal AFP level. The 7% of hypovascular and 15% of hypervascular group were positive for AFP level ≥200 ng/ml, The positive rate for AFP ≤15 ng/ml significantly increased with tumour size in entire group ($P = 0.03$), but not seen in hypo- and hypervascular groups ($P = 0.40$ and $P = 0.25$, respectively, Supplementary Table 1). On the other hand, 2,622 (65%) of 4,057 patients showed normal DCP level (Table 6). The positive rate for DCP ≥40mAU/ml significantly elevated with tumour size in entire, hypo- and hypervascular groups (all, $P < 0.001$). The positive relation between tumour size and incidence of patients was shown in entire and hypervascular groups with DCP >40mAU/ml and in hypovascular group with DCP ≥300mAU/ml.

Discussion

Whether a small nodule suspected HCC is hyper- or hypovascular is crucial for differentiating tumours in

Liver International (2013)

Table 5. Incidence of tumors according to tumor size and histopathologic grade in entire, hypo- and hypervascular HCC groups.

Group	Size (cm)	No. of tumor	Well (%)	Moderately (%)	Poorly (%)	*P*-value
Entire	≤ 1.0	284	196 (69)	82 (29)	6 (2)	<0.001
	1.1–1.5	808	478 (59)	295 (37)	35 (4)	
	1.6–2.0	1322	581 (44)	666 (50)	75 (6)	
	2.1–2.5	877	300 (34)	517 (59)	60 (7)	
	2.6–3.0	905	284 (31)	551 (61)	70 (8)	
	Total	4196	1839 (44)	2111 (50)	246 (6)	
Hypovascular	≤ 1.0	115	102 (89)	13 (11)	0 (0)	<0.001
	1.1–1.5	291	256 (88)	33 (11)	2 (1)	
	1.6–2.0	233	178 (76)	50 (22)	5 (2)	
	2.1–2.5	79	53 (67)	24 (30)	2 (3)	
	2.6–3.0	60	35 (58)	20 (34)	5 (8)	
	Total	778	624 (80)	140 (18)	14 (2)	
Hypervascular	≤ 1.0	169	94 (56)	69 (41)	6 (3)	<0.001
	1.1–1.5	517	222 (43)	262 (51)	33 (6)	
	1.6–2.0	1089	403 (37)	616 (57)	70 (6)	
	2.1–2.5	798	247 (31)	493 (62)	58 (7)	
	2.6–3.0	845	249 (29)	531 (63)	65 (8)	
	Total	3418	1215 (35)	1971 (58)	232 (7)	

Table 6. Distribution of patients according to tumor size and des-γ-carboxy prothrombin in entire, hypo- and hypervascular HCC groups

			des-γ-carboxy prothnrombin			
Group	Tumor size (cm)	No. of patient	<40 mAU/ml	40–299	300 ≤	*P*-value
Entire	≤ 1.0	262	214 (82)	46 (17)	2 (1)	<0 0001
	1.1–1.5	772	605 (78)	148 (19)	19 (3)	
	1.6–2.0	1289	863 (67)	342 (27)	84 (6)	
	2.1–2.5	861	502 (58)	271 (32)	88 (10)	
	2.6–3.0	873	438 (50)	281 (32)	154 (18)	
	Total	4057	2622 (65)	1088 (27)	347 (8)	
Hypovascular	≤ 1.0	101	84 (83)	17 (17)	0 (0)	<0.001
	1.1–1.5	266	237 (89)	26 (10)	3 (1)	
	1.6–2.0	220	183 (83)	31 (14)	6 (3)	
	2.1–2.5	74	60 (81)	10 (14)	4 (5)	
	2.6–3.0	50	34 (68)	9 (18)	7 (14)	
	Total	711	598 (84)	93 (13)	20 (3)	
Hypervascular	≤ 1.0	161	130 (81)	29 (18)	2 (1)	<0.001
	1.1–1.5	506	368 (73)	122 (24)	16 (3)	
	1.6–2.0	1069	680 (64)	311 (29)	78 (7)	
	2.1–2.5	787	442 (56)	261 (33)	84 (11)	
	2.6–3.0	823	404 (49)	272 (33)	147 (18)	
	Total	3346	2024 (60)	995 (30)	327 (10)	

Parentheses show percentage.

cirrhotic liver such as dysplastic nodule, early HCC, hypo- and hypervascular advanced HCC (12). Thus, much attention has been paid to obtain the optimal acquisition time to disclose tumour vascularity on dynamic imaging techniques. In this study, arterial tumour vascularity was carefully confirmed with combination of two or more dynamic imaging modalities in 63% of entire patient. It was strongly presumed that majority of 1,617 (39%) patients who underwent angiography alone concurrently had combination study of CT and hepatic arteriography as was one of the most sensitive techniques for identifying tumour vascularity.

The incidence of hypovascular HCC was 18% of 4,474 HCCs ≤ 3 cm, 25% of 2,570 ≤ 2 cm and 24% of 2,272 ranging 1.1–2 cm (Table 4). To date, wide range of incidence of hypovascular HCC has been reported using various imaging modalities; 6% by multiple dynamic imaging modalities (5), 14% by US angiography with intra-arterial CO_2 microbubbles (6) and 18% by digital subtraction angiography and in part by combination of CT and hepatic arteriography (4). And recent studies reported higher incidence than before, i.e., 32% in CE-US, 35% in CT and 34% in MRI for 34 HCCs 1–2 cm (24), 22% in CE-US and 15% in MRI for

60HCCs ≤ 2 cm (25), and 29% in MDCT for 204 HCCs ≤ 3 cm (8). Gadoxetic acid-enhanced MRI, more recently introduced has revealed to detect hypovascular HCC more frequently as a result of higher sensitivity for early stage HCC than combination of CT and arterial portography (26) and dynamic MRI (27).

A total of five variables were independent predictor for hypovascular HCC on logistic regression analysis: small tumour ≤ 1.5 cm, lower levels of AFP <200 ng/ml and DCP <40mAU/ml, well differentiated grade and positivity for HCV antibody. The positivity for HCV antibody is consistent with the previous result in which hypovascular HCC emerged more frequently in HCV related patients than HBV and non-B non-C virus related patients (28). On the other hand, microscopic study of resected specimens first revealed that hypovascular group had significantly less fibrous capsule formation and tended to have less portal invasion and intrahepatic metastasis, suggesting hypovascular group is pathologically in earlier stage and less aggressive compared with hypervascular group (Table 2).To date, microvascular invasion was reported to closely associate with poor outcome after resection (29) and liver transplantation (30).

Concerning tumour vascularity and size, there was a significantly negative correlation in hypovascular and positive association in hypervascular HCC in good order ($P < 0.001$). These findings were not inconsistent with previous studies with no more than 200 patients (4–6, 8). Present study revealed more precise and reliable relationship between these two factors with 5 mm-interval of tumour size and more than 4,000 patients.

The tumour size of 1.5 cm was first identified to be critical for hypovascular HCC to transform to hypervascularization, i.e., angiogenic switch confirmed by imaging techniques in this cross-sectional study (Fig. 1). The near tumour sizes ranging 1.0 to 1.5 cm were recently reported by longitudinal study with gadoxetic acid-enhanced MRI (31, 32). The cut-off value of 1.5 cm seems interested in patients with hypovascular tumour ranging 1–2 cm negative for sequential two dynamic contrast enhanced studies, because subsequent biopsy is recommended by the AASLD guidelines updated (11). First, intensive follow-up of hypovascular tumour would be acceptable to monitor the size and vascularity by ultrasonography with and without contrast medium because of high incidence of transition to hypervascularization with tumour growth over 1.5 cm and slow growing nature (33). Second, elevation of DCP level ≥ 300 mAU/ml is helpful in suspecting that tumors possibly obtain more aggressive nature even without transition to hypervascular type (Table 6). Third, biopsy could be safely performed in a case of hypovascular tumour ≤ 1.5 cm because of the highest incidence of well differentiated grade $\geq 88\%$ and the lowest ratio of poorly differentiated grade $\leq$ 1% (Table 5). The poorly differentiated grade was closely associated with neoplastic seeding after radiofrequency ablation (34, 35) and poor prognosis after transplantation (30). Our study revealed the ratio was 6% in entire population (Table 5), much lower than that of 12% in patients with advanced large HCC (36). While, 94% of 246 poorly differentiated HCCs were hyper- and only 6% were hypovascular.

The very close correlation was recognized between tumour size and dedifferentiation which reflects multistep progress of hepatocarcinogenesis in small HCC (15, 28). Interestingly, the ratio of well vs. moderately and poorly differentiated grades was almost same i.e., 58% vs. 42% in tumour 2.6–3.0 cm of hypovascular group and 56% vs.44% in tumour ≤ 1 cm of hypervascular group (Table 5). These results imply that hypovascular tumour would grow slowly and reached tumour 2.6–3.0 cm without emergence of vascular transformation, in contrast hypervascular tumour would rapidly progress and reach tumour ≤ 1 cm after obtaining neoangiogenesis. The reason why 5% of hypervascular group was already hypervascular even in tumour ≤ 1 cm (Fig. 1) could be explained by *de novo* carcinogenesis other than multistep progression. While, 8% of hypovascular group being still hypovascular in 2.6–3 cm lesions would depend on lack or delay of induction of angiogenic switch in molecular level.

The positive rate for DCP ≥ 40mAU/ml was significantly higher in hypervascular than hypovascular group ($P < 0.001$, Table 2). A significant correlation was recognized between tumour size and DCP level in both groups ($P < 0.001$, Table 6). Interestingly, better correlation was seen in ≥ 40mAU/ml in hypervascular group and in DCP level ≥ 300mAU/ml in hypovascular group. These results suggest that microvascular invasion and micro-metastases are associated with increase of tumour size in hypervascular group (37–39) and even in hypovascular group. On the other hand, AFP level <200 ng/ml was independent predictor for hypovascular group on multivariate analysis but there was no significant correlation between tumour size and AFP level in both groups. Prior study reported elevated AFP level showed significant predictor for poor prognosis after resection (40, 41).

The incidence of early HCC occupied in hypovascular HCC group was one of great interests in this study. However, it was hard to clarify it because inconsistency was not dissolved between gross appearance and histologic differentiation in early HCC resected. It might depend on in part the difficulty to differentiate gross type of early HCC/vaguely nodular type from other types such as infiltrative one. As another reason, pathologic findings specific to early HCC, such as portal triad and/or stromal invasion (17) were not available becaue of lack of inclusion in questionnaire sheet. Further study is needed with gadoxetic acid-enhanced MRI which could more often detect and characterize early HCC than dynamic CT and combination of CT and angiography (42).

As possible limitation of this study, single dynamic imaging modality seems insufficient to determine hypovascular tumour which was seen in 38% of hypovascular group, but one dynamic imaging technique had been recommended for tumours ≥ 2 cm by the original AASLD guidelines (10). One possible reason of less imaging modality could be speculated that first imaging modality performed in primary clinic or hospital was incidentally omitted and a total number of imaging techniques were undercounted by large volume centre hospitals where patients were finally treated. In any event, we believe that the tumour vascularity was correctly judged in the majority of hypovascular tumours by final institutions. As another limitation, lack of vascular profile in the portal/venous phase of dynamic imaging modalities could be given. However, it is not crucial to evaluate arterial tumour vascularity because all tumors were histopathologically diagnosed HCC.

In conclusion, hypovascular HCC accounted for 18% of solitary 4,474 HCCs ≤ 3 cm histologically proven and was confirmed to be biologically less aggressive caused by higher incidence of well differentiated grade, lower value of AFP and DCP, smaller tumour size, and lower incidence of microvascular invasion and micrometastasis. Most hypovascular HCCs seem to transform to hypervascular type when they grew over 1.5 cm. Logistic regression analysis revealed tumour size ≤ 1.5 cm, AFP <200 ng/ml and DCP <40mAU/ml, well differentiated grade and positivity for HVC antibody were independent predictor for hypovascular HCC. These results would practically help in determining an appropriate diagnostic algorithm and timely biopsy for small hypovascular tumours particularly after wide introduction of gadoxetic acid-enhanced MRI. Moreover, they will contribute to evaluate the outcome of treatments for small hypovascular HCC.

Acknowledgement

Funding: No support.
Competing interest: None.
Ethics approval: Approved by the ethics committee of each institution.

References

1. Kamangar F, Dores GM, Anderson WF. Patterns of cancer incidence, mortality, and prevalence across five continents: defining priorities to reduce cancer disparities in different geographic regions of the world. *J Clin Oncol* 2006; **24**: 2137–50.
2. The Liver Cancer Study Group of Japan. *Report of the 14th follow-up survey of primary liver cancer*. Kyoto: Shinkou-insatsu Press, 2000 (in Japanese): 38.
3. Ikai I, Kudo M, Arii S, *et al.* Report of the 18th follow-up survey of primary liver cancer in Japan. *Hepatol Res* 2010; **40**: 1043–59.
4. Takayasu K, Shima Y, Muramatsu Y, *et al.* Angiography of small hepatocellular carcinomas: analysis of 105 resected tumors. *AJR Am J Roentgenol* 1986; **147**: 525–9.
5. Matsui O, Kadoya M, Kameyama T, *et al.* Benign and malignant nodules in cirrhotic livers: distinction based on blood supply. *Radiology* 1991; **178**: 493–7.
6. Kudo M, Tomita S, Tochio H, *et al.* Small hepatocellular carcinoma: diagnosis with US angiography with intraarterial CO2 microbubbles. *Radiology* 1992; **182**: 155–60.
7. Bolondi L, Gaiani S, Celli N, *et al.* Characterization of small nodules in cirrhosis by assessment of vascularity: the problem of hypovascular hepatocellular carcinoma. *Hepatology* 2005; **42**: 27–34.
8. Yoon SH, Lee JM, So YH, *et al.* Multiphasic MDCT enhancement pattern of hepatocellular carcinoma smaller than 3 cm in diameter: tumor size and cellular differentiation. *AJR Am J Roentgenol* 2009; **193**: W482–9.
9. Makuuchi M, Kokudo N, Arii S, *et al.* Development of evidence-based clinical guidelines for the diagnosis and treatment of hepatocellular carcinoma in Japan. *Hepatol Res* 2008; **38**: 37–51.
10. Bruix J, Sherman M. Management of hepatocellular carcinoma. *Hepatology* 2005; **42**: 1208–36.
11. Bruix J, Sherman M. Management of hepatocellular carcinoma: an update. *Hepatology* 2011; **53**: 1020–2.
12. Hayashi M, Matsui O, Ueda K, *et al.* Correlation between the blood supply and grade of malignancy of hepatocellular nodules associated with liver cirrhosis: evaluation by CT during intraarterial injection of contrast medium. *AJR Am J Roentgenol* 1999; **172**: 969–76.
13. Kenmochi K, Sugihara S, Kojiro M. Relationship of histologic grade of hepatocellular carcinoma (HCC) to tumor size, and demonstration of tumor cells of multiple different grades in single small HCC. *Liver* 1987; **7**: 18–26.
14. Kanai T, Hirohashi S, Upton MP, *et al.* Pathology of small hepatocellular carcinoma. A proposal for a new gross classification. *Cancer* 1987; **60**: 810–19.
15. Sakamoto M, Hirohashi S, Shimosato Y. Early stages of multistep hepatocarcinogenesis: adenomatous hyperplasia and early hepatocellular carcinoma. *Hum Pathol* 1991; **22**: 172–8.
16. The Liver Cancer Study Group of Japan. *The General Rules for the Clinical and Pathological Study of Primary Liver Cancer*. 2nd English ed. Tokyo, Japan: Kanehara & Co., Ltd., 2003.
17. International Consensus Group for Hepatocellular Neoplasia. Pathologic diagnosis of early hepatocellular carcinoma: a report of the international consensus group for hepatocellular neoplasia. *Hepatology* 2009; **49**: 658–64.
18. Takayasu K, Furukawa H, Wakao F, *et al.* CT diagnosis of early hepatocellular carcinoma: sensitivity, findings, and CT-pathologic correlation. *AJR Am J Roentgenol* 1995; **164**: 885–90.
19. Takayasu K, Muramatsu Y, Furukawa H, *et al.* Early hepatocellular carcinoma: appearance at CT during arterial portography and CT arteriography with pathologic correlation. *Radiology* 1995; **194**: 101–5.
20. Arii S, Sata M, Sakamoto M, *et al.* Management of hepatocellular carcinoma: Report of Consensus Meeting in the 45th Annual Meeting of the Japan Society of Hepatology (2009). *Hepatol Res* 2010; **40**: 667–85.
21. Takayama T, Makuuchi M, Hirohashi S, *et al.* Early hepatocellular carcinoma as an entity with a high rate of surgical cure. *Hepatology* 1998; **28**: 1241–6.
22. Edmondson HA, Steiner PE. Primary carcinoma of the liver: a study of 100 cases among 48,900 necropsies. *Cancer* 1954; **7**: 462–503.

23. The Liver Cancer Study Group of Japan. *The General Rules for the Clinical and Pathological Study of Primary Liver Cancer*. 3rd English ed. Tokyo, Japan: Kanehara & Co., Ltd., 2010.
24. Sangiovanni A, Manini MA, Iavarone M, *et al.* The diagnostic and economic impact of contrast imaging techniques in the diagnosis of small hepatocellular carcinoma in cirrhosis. *Gut* 2010; **59**: 638–44.
25. Forner A, Vilana R, Ayuso C, *et al.* Diagnosis of hepatic nodules 20 mm or smaller in cirrhosis: Prospective validation of the noninvasive diagnostic criteria for hepatocellular carcinoma. *Hepatology* 2008; **47**: 97–104.
26. Kogita S, Imai Y, Okada M, *et al.* Gd-EOB-DTPA-enhanced magnetic resonance images of hepatocellular carcinoma: correlation with histological grading and portal blood flow. *Eur Radiol* 2010; **20**: 2405–13.
27. Golfieri R, Renzulli M, Lucidi V, *et al.* Contribution of the hepatobiliary phase of Gd-EOB-DTPA-enhanced MRI to dynamic MRI in the detection of hypovascular small ($\leq$ 2 cm) HCC in cirrhosis. *Eur Radiol* 2011; **21**: 1233–42.
28. Oikawa T, Ojima H, Yamasaki S, *et al.* Multistep and multicentric development of hepatocellular carcinoma: histological analysis of 980 resected nodules. *J Hepatol* 2005; **42**: 225–9.
29. Imamura H, Matsuyama Y, Tanaka E, *et al.* Risk factors contributing to early and late phase intrahepatic recurrence of hepatocellular carcinoma after hepatectomy. *J Hepatol* 2003; **38**: 200–7.
30. Jonas S, Bechstein WO, Steinmuller T, *et al.* Vascular invasion and histopathologic grading determine outcome after liver transplantation for hepatocellular carcinoma in cirrhosis. *Hepatology* 2001; **33**: 1080–6.
31. Motosugi U, Ichikawa T, Sano K, *et al.* Outcome of hypovascular hepatic nodules revealing no gadoxetic acid uptake in patients with chronic liver disease. *J Magn Reson Imaging* 2011; **34**: 88–94.
32. Kumada T, Toyoda H, Tada T, *et al.* Evolution of hypointense hepatocellular nodules observed only in the hepatobiliary phase of gadoxetate disodium-enhanced MRI. *AJR Am J Roentgenol* 2011; **197**: 58–63.
33. Tochio H, Tomita S, Kudo M, *et al.* Growth speed of hepatocellular carcinoma - relationship with arterial vascularity evaluated by US angiography. *Kanzo* (in Japanese) 1992; **33**: 758–65.
34. Llovet JM, Vilana R, Bru C, *et al.* Increased risk of tumor seeding after percutaneous radiofrequency ablation for single hepatocellular carcinoma. *Hepatology* 2001; **33**: 1124–9.
35. Imamura J, Tateishi R, Shiina S, *et al.* Neoplastic seeding after radiofrequency ablation for hepatocellular carcinoma. *Am J Gastroenterol* 2008; **103**: 3057–62.
36. Kudo M, Arii S, Ikai I, *et al.* Report of the 18th follow-up survey of primary liver cancer in Japan. *Kanzo* (in Japanese)2010; **51**: 460–84.
37. Koike Y, Shiratori Y, Sato S, *et al.* Des-gamma-carboxy prothrombin as a useful predisposing factor for the development of portal venous invasion in patients with hepatocellular carcinoma: a prospective analysis of 227 patients. *Cancer* 2001; **91**: 561–9.
38. Sakon M, Monden M, Gotoh M, *et al.* Relationship between pathologic prognostic factors and abnormal levels of des-gamma-carboxy prothrombin and alpha-fetoprotein in hepatocellular carcinoma. *Am J Surg* 1992; **163**: 251–6.
39. Okuda H, Nakanishi T, Takatsu K, *et al.* Serum levels of des-gamma-carboxy prothrombin measured using the revised enzyme immunoassay kit with increased sensitivity in relation to clinicopathologic features of solitary hepatocellular carcinoma. *Cancer* 2000; **88**: 544–9.
40. Ikai I, Arii S, Kojiro M, *et al.* Reevaluation of prognostic factors for survival after liver resection in patients with hepatocellular carcinoma in a Japanese nationwide survey. *Cancer* 2004; **101**: 796–802.
41. Imamura H, Matsuyama Y, Miyagawa Y, *et al.* Prognostic significance of anatomical resection and des-gamma-carboxy prothrombin in patients with hepatocellular carcinoma. *Br J Surg* 1999; **86**: 1032–8.
42. Sano K, Ichikawa T, Motosugi U, *et al.* Imaging study of early hepatocellular carcinoma: usefulness of gadoxetic acid-enhanced MR imaging. *Radiology* 2011; **261**: 834–44.

Supporting Information

Additional Supporting Information may be found in the online version of this article:

Table S1. Distribution of patients according to tumor size and alpha-fetoprotein level in entire, hypo- and hypervascular HCC groups

Hypovascular Nodules in Patients with Chronic Liver Disease: Risk Factors for Development of Hypervascular Hepatocellular Carcinoma[1]

Tomoko Hyodo, MD
Takamichi Murakami, MD, PhD
Yasuharu Imai, MD, PhD
Masahiro Okada, MD, PhD
Masatoshi Hori, MD, PhD
Yuki Kagawa, MD, PhD
Sachiyo Kogita, MD
Seishi Kumano, MD, PhD
Masatoshi Kudo, MD, PhD
Teruhito Mochizuki, MD

Purpose: To identify patient characteristics and magnetic resonance (MR) imaging findings associated with subsequent hypervascularization in hypovascular nodules that show hypointensity on hepatobiliary phase gadoxetic acid–enhanced MR images in patients with chronic liver diseases.

Materials and Methods: Institutional review board approval was obtained, and informed consent was waived. At multiple follow-up gadoxetic acid–enhanced MR imaging examinations of 68 patients, 160 hypovascular nodules were retrospectively reviewed. A Cox regression model for hypervascularization was developed to explore the association of baseline characteristics, including patient factors (Child-Pugh classification, etiology of liver disease, history of local therapy for hepatocellular carcinoma [HCC], and coexistence of hypervascular HCC) and MR imaging findings (fat content, signal intensity on T2-weighted images, and nodule size). In addition, the growth rate was calculated as the reciprocal of tumor volume doubling time to investigate its relationship with subsequent hypervascularization by using receiver operating characteristic and Kaplan-Meier analyses.

Results: The prevalence of subsequent hypervascularization was 31% (50 of 160 nodules). Independent Cox multivariable predictors of increased risk of hypervascularization were hyperintensity on T2-weighted images (hazard ratio [HR] = 8.7; 95% confidence interval [CI]: 3.6, 20.8), previous local therapy for hypervascular HCC (HR = 5.0; 95% CI: 1.8, 13.6), Child-Pugh B cirrhosis (HR = 3.6; 95% CI: 1.4, 9.5) and coexistence of hypervascular HCC (HR = 2.0; 95% CI: 1.0, 3.8). The mean growth rate was significantly higher in nodules that showed subsequent hypervascularization than in those without hypervascularization. Kaplan-Meier analysis based on the receiver operating characteristic cutoff level (1.8×10^{-3}/day [tumor volume doubling time, 542 days]) showed that nodules with a higher growth rate had a significantly higher incidence of hypervascularization ($P = 5.2 \times 10^{-8}$, log-rank test).

Conclusion: Hyperintensity on T2-weighted images is an independent and strong risk factor at baseline for subsequent hypervascularization in hypovascular nodules in patients with chronic liver disease. Tumor volume doubling time of less than 542 days was associated with a high rate of subsequent hypervascularization.

[1] From the Departments of Radiology (T.H., T. Murakami, M.O., Y.K.) and Internal Medicine (M.K.), Kinki University Faculty of Medicine, 377-2 Ohno-Higashi, Osaka-Sayama, Osaka 589-8511, Japan; Department of Gastroenterology, Ikeda Municipal Hospital, Osaka, Japan (Y.I., S. Kogita); Department of Radiology, Osaka University Graduate School of Medicine, Suita, Japan (M.H.); Department of Radiology, Osaka Medical College, Takatsuki, Japan (S. Kumano); and Department of Diagnostic and Therapeutic Radiology, Ehime University Graduate School of Medicine, Toon, Japan (T.H., T. Mochizuki). From the 2011 RSNA Annual Meeting. Received December 16, 2011; revision requested January 30, 2012; revision received July 30; accepted August 29; final version accepted September 18. Supported by an Osaka Cancer Foundation grant. **Address correspondence to** T.H. (e-mail: *neneth@m.ehim-u.ac.jp*).

Follow-up surveillance of patients with cirrhosis has been performed to detect hepatocellular carcinoma (HCC) early enough to allow curative treatment (1). The American Association for the Study of Liver Diseases practice guidelines outline a strategy for distinguishing HCCs from other hepatic lesions of smaller than 3 cm that are identified during ultrasound (US) screening of livers in patients with cirrhosis (2). The guidelines suggest that nodules greater than 1 cm in diameter be further investigated by using dynamic contrast material–enhanced computed tomography (CT) or magnetic resonance (MR) imaging. Thus, the detection of arterial hypervascularization can justify treating the nodule as if it were HCC. For hypovascular nodules, defined as lesions that appear less enhanced than the surrounding liver both on arterial and venous phase images (2), careful monitoring (eg, repeat US at 3 months and biopsy) is recommended. However, the existing treatment guidelines do not specify the patient and tumor attributes that accurately predict subsequent hypervascularization.

Advances in Knowledge

- In patients with chronic liver disease, 31% (50 of 160) of the hypovascular nodules that showed hypointensity in the hepatobiliary phase of gadoxetic acid–enhanced MR imaging became hypervascular, which is a 1-year cumulative incidence of 25%.
- Hepatic hypovascular nodules that showed hyperintensity on T2-weighted images were at the highest risk for development of hypervascular hepatocellular carcinoma (hazard ratio, 8.7; 95% CI: 3.6, 20.8; $P < .001$).
- The higher growth rate (tumor volume doubling time, < 542 days) of a hepatic hypovascular nodule was associated with its subsequent development to hypervascular hepatocellular carcinoma.

The hepatobiliary phase of gadoxetic acid–enhanced MR imaging can allow clear visualization of hepatic focal lesions (3–6). Along with the widespread use of advanced imaging techniques, including three-dimensional T1-weighted gradient-echo sequences with high spatial resolution (7), hypovascular small nodules that show hypointensity on gadoxetic acid–enhanced hepatobiliary phase MR images are increasingly detected during HCC screening of patients with cirrhosis. Such nodules may include hypovascular well-differentiated HCCs, dysplastic nodules, and other benign nodules (8), which are difficult to distinguish, even at needle biopsy. Of these, hypovascular HCC and dysplastic nodules grow and acquire a more extensive arterial supply, and show overt stromal invasion (invasive growth of tumor tissue in portal tracts and fibrous septa), during stepwise carcinogenesis of HCC (9,10).

Previously, image-based studies suggested that hypovascular nodules containing fat or those that were greater than 10–15 mm in diameter were at high risk for development of hypervascularization (11–13). Authors of a histopathologic study (14) reported that most borderline nodules (dysplastic nodules or well-differentiated HCCs) greater than 15 mm in diameter were early HCC. Because these results were taken from findings at a single time point, further research examining the time course of the development of this change is required for the development of a better approach to follow-up of these hypovascular nodules.

Implications for Patient Care

- MR imaging findings may provide useful diagnostic information for the development of a treatment strategy for patients with hepatic hypovascular nodules.
- The hepatic hypovascular nodules that show hyperintensity on T2-weighted images, or that show a higher growth rate should be considered for more frequent follow-up or biopsy.

The aims of our study were to identify patient characteristics and MR imaging findings associated with subsequent hypervascularization in hypovascular nodules that show hypointensity on gadoxetic acid–enhanced hepatobiliary phase MR images in patients with chronic liver diseases.

Materials and Methods

Study Group

Retrospective data collection and analysis were approved by the institutional review board of the two participating hospitals, and the requirement for informed consent was waived. The selection of the subjects is outlined in Figure 1. From February 2008 to October 2010, there were 238 patients who underwent multiple gadoxetic acid–enhanced MR imaging examinations for HCC surveillance. Of these, we excluded patients with *(a)* Child-Pugh class C, owing to insufficient enhancement on gadoxetic acid–enhanced hepatobiliary phase MR images (1), and *(b)* those who had undergone previous systemic chemotherapy or treatment with molecularly targeted agents against malignant tumors. One radiologist (S. Kumano, with 22 years of experience in abdominal imaging) and one gastroenterologist

Published online
10.1148/radiol.12112677 **Content code:** GI

Radiology 2013; 266:480–490

Abbreviations:
CI = confidence interval
HCC = hepatocellular carcinoma
HR = hazard ratio
TVDT = tumor volume doubling time

Author contributions:
Guarantors of integrity of entire study, T.H., T. Murakami; study concepts/study design or data acquisition or data analysis/interpretation, all authors; manuscript drafting or manuscript revision for important intellectual content, all authors; approval of final version of submitted manuscript, all authors; literature research, T.H., Y.I., M.O., Y.K., S. Kumano, M.K., T. Murakami; clinical studies, T.H., Y.I., M.O., Y.K., S. Kogita, M.K.; statistical analysis, T.H., Y.I., M.H.; and manuscript editing, T.H., T. Murakami, Y.I., M.O., M.H., T. Mochizuki.

Conflicts of interest are listed at the end of this article.

Figure 1

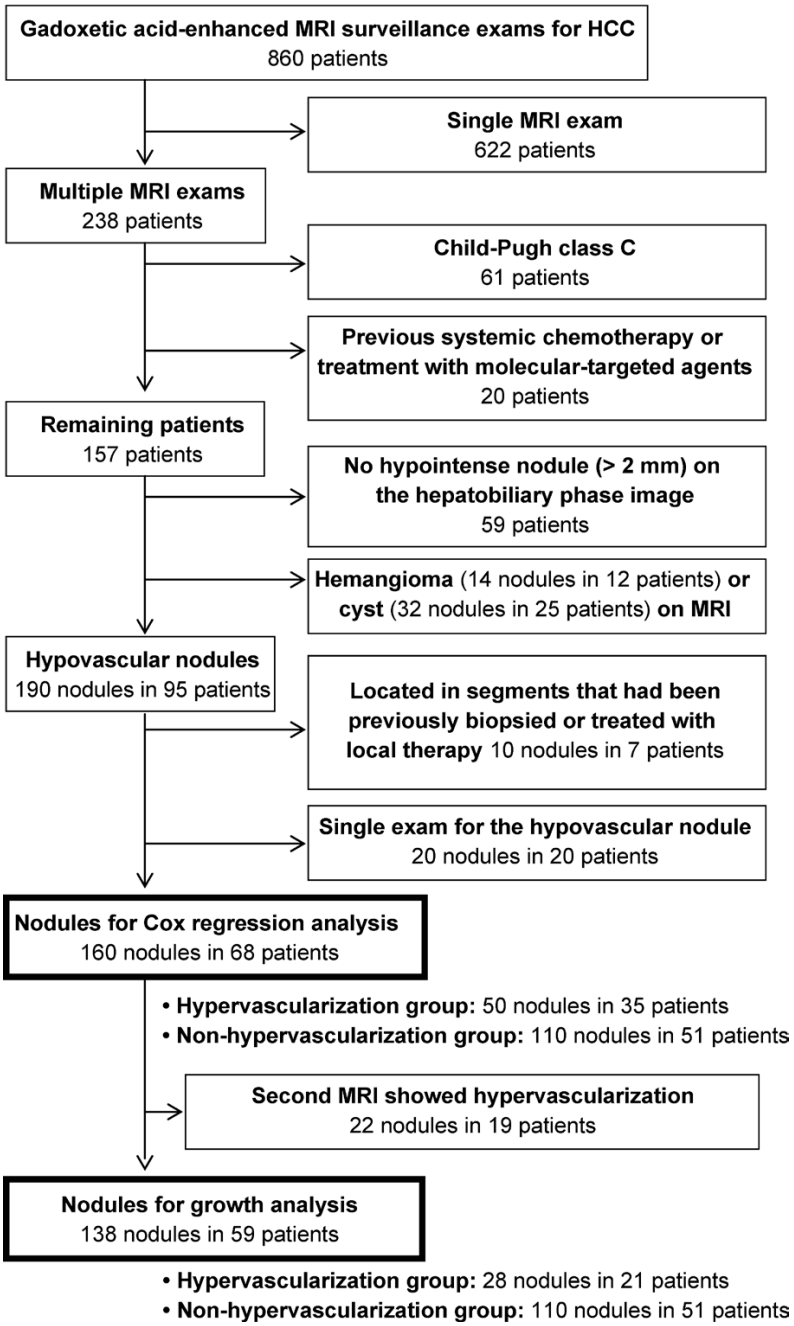

Figure 1: Flowchart of the study population.

specializing in hepatology (Y.I., with 30 years of experience) reviewed images to detect hypovascular nodules and to diagnose subsequent hypervascularization in consensus. A hypovascular nodule was defined as that in which all parts of the nodule showed lower signal intensity than the surrounding liver parenchyma during the arterial phase of dynamic imaging when any of the available modalities were used (intravenous contrast-enhanced CT, CT hepatic arteriography and contrast-enhanced ultrasound) compared with the corresponding site on the unenhanced image. The arterial enhancement was assessed by means of visual inspection. In addition, the subjects were limited to those with round hypointense lesions on gadoxetic acid–enhanced hepatobiliary phase MR images. Procedures involving all modalities were performed within 2 weeks of each other. Nodules were excluded if they were *(a)* less than 2 mm in diameter; *(b)* considered to be suspicious for hemangiomas, cysts or cystic tumors on the basis of other MR imaging sequences or modalities; or *(c)* located in segments that had been previously biopsied or treated with local therapy (including transcatheter arterial chemoembolization).

We identified 160 hypovascular nodules in 68 patients (mean patient age ± standard deviation, 70.0 ± 7.8 years; range, 51–85 years). Among these patients, 48 were men (mean age, 69.9 ± 7.7 years; range, 54–85 years), and 20 were women (mean age, 70.2 ± 8.4 years; range, 51–79 years). The presumed causes of chronic liver disease of the patients were chronic hepatitis C viral infection (n = 46), chronic hepatitis B viral infection (n = 12), alcohol abuse (n = 4), nonalcoholic steatohepatitis (n = 1) and unknown cause (n = 5). Forty (27%) patients had cirrhosis. The number of nodules per patient ranged from one to 10, with a mean value of 2.3. The date of entry into the study was defined as the date of the initial gadoxetic acid–enhanced MR imaging examination. All patients were treated according to the clinical guidelines for the diagnosis and treatment of HCC in Japan (15). During the study period, all patients

received follow-up gadoxetic acid–enhanced MR imaging examinations in combination with US, CT, or angiography at various times according to the degree of liver disease. One radiologist (S. Kumano) and one gastroenterologist who specializes in hepatology (Y.I.) reviewed images in consensus to verify lesion correspondence between the different imaging modalities. Each nodule was followed up until it showed early enhancement when imaged by means of any of the imaging modalities, until the segment containing the nodule was biopsied or treated, or until the final imaging examination of the study period. The number of gadoxetic acid–enhanced MR imaging examinations reviewed per patient was two for 32 patients (43%), three for 16 patients (28%), four for 12 patients (18%), five for three patients (4%), six for three patients (4%), seven for one patient (1%) and eight for one patient (1%). The mean interval between gadoxetic acid–enhanced MR imaging examinations was 186 days ± 110 (range, 57–619 days). Of the 110 nodules that did not develop into hypervascular nodules, 101 were censored at the date of the most recent consultation before November 1, 2010, and nine (in five patients) were censored at the date of the final imaging examination of the study period before therapy (six nodules for transarterial chemoembolization; one each for radiofrequency ablation, intra-arterial reservoir chemotherapy and whole-liver radiation therapy due to coexistent HCC) of the liver segment(s) involved.

We obtained the baseline clinical data by means of review of all available medical records for assessment of the association with the subsequent hypervascularization. The clinical data comprised seven patient characteristics at the time of baseline MR imaging and six initial gadoxetic acid–enhanced MR imaging findings from each nodule (see the Imaging Analysis subsection). Patient characteristics that were used in the study were age, sex, Child-Pugh classification, cause of liver disease, serum α-fetoprotein level, history of local therapy for HCC, and coexistence of hypervascular HCC. For patients with hepatitis B infections, we recorded information regarding the use of oral nucleotide analogs with activity against hepatitis B. The mean interval between the laboratory test and initial MR imaging examination was 9 days (range, 0–24 days).

Nodules were categorized into two groups according to the presence (hypervascularization group) or absence (nonhypervascularization group) of early enhancement at the final imaging examination. Needle biopsy specimens were reviewed by two expert pathologists who made a consensus diagnosis according to the International Working Party criteria (9).

Imaging Techniques

MR imaging studies were performed by using either a 3.0 T (Achieva; Philips Medical Systems, Best, Netherlands) or one of two 1.5 T systems (Signa Excite HDxt; GE Healthcare, Milwaukee, Wis; Gyroscan Intera Nova; Philips Medical Systems) (Table 1). First, a T1-weighted dual-echo sequence was performed. For dynamic imaging, T1-weighted three-dimensional fat-suppressed gradient-echo images were acquired before and after a bolus injection of 0.025 mmol/kg of body weight of gadoxetic acid (EOB-Primovist; Bayer Schering Pharma, Osaka, Japan) at a rate of 2 mL/sec with a saline flush through the antecubital vein. Arterial-phase imaging was performed by using a bolus tracking technique: the center of k-space was acquired 15 seconds after the contrast material appeared in the abdominal aorta (16). Portal venous and hepatobiliary phase images were acquired after an imaging delay of 70 seconds and 20 minutes, respectively. T2-weighted images were acquired with a fat-suppressed fast spin-echo sequence before or within 10 min after contrast-material injection. Although there were missing data from the fat-suppressed T2-weighted fast spin-echo images (not available owing to motion artifacts in two nodules; other T2-weighted sequences were obtained for 32 nodules), we included all subjects in the analysis. Dynamic contrast-enhanced CT, CT hepatic arteriography and contrast-enhanced US were performed as described in the literature (17–19).

Image Analysis

A consensus review of baseline MR images was performed by three radiologists (M.O., T.H., and Y.K., with 18, 11, and 6 years of experience in abdominal imaging, respectively), who were blinded to the outcomes and the biopsy results for each nodule. The fat content of each nodule was determined on the basis of T1-weighted dual-echo images according to apparent signal loss on opposed-phase images relative to in-phase images. On the T2-weighted images, each lesion was evaluated for signal intensity relative to that of the surrounding liver parenchyma and classified as hyperintense, isointense, hypointense or missing. On the T1-weighted three-dimensional fat-suppressed gradient-echo images of without and with contrast enhancement (hepatobiliary phase), signal intensities of the nodule and liver parenchyma were recorded to evaluate nodule-to-liver contrast ratios. For measurement of the nodule, one abdominal radiologist (T.H.) placed the largest possible region of interest but did not include the edges of the nodule to avoid edge artifacts. For the liver parenchyma, two regions of interest that avoided the major hepatic and portal vessels (size range, 200–400 mm^2) were selected, and then the mean value was calculated. The nodule-to-liver contrast ratios were calculated for each unenhanced and hepatobiliary phase image by dividing the signal intensity of the nodule by the signal intensity of the liver parenchyma. The contrast enhancement ratio was then calculated by dividing the contrast ratios of the hepatobiliary phase images by those of the unenhanced images.

One abdominal radiologist (T.H.) measured the maximum nodule diameter on axial gradient-echo T1-weighted gadoxetic acid–enhanced hepatobiliary–phase images of the baseline and the final MR imaging examinations. Only for the purpose of the growth analysis, the final MR imaging examination was defined as the last MR imaging examination before hypervascularization for each nodule. Twenty-two nodules in which the second MR imaging examination showed hypervascularization (19 pairs of examinations; median interval between the two examinations, 210 days;

Table 1

Pulse Sequence Parameters for 1.5-T and 3.0-T Imaging

	T1-weighted Dual-Echo GRE*		Fat-suppressed 3D T1-weighted GRE		Fat-suppressed T2-weighted Fast Spin-Echo	
Parameter	1.5 T 2D†	3.0 T 3D‡	1.5 T†	3.0 T‡	1.5 T†	3.0 T‡
Breathing	Breath hold	Breath hold	Breath hold	Breath hold	Respiratory-triggered technique	Respiratory-triggered technique
Matrix	256 × 256, 320 × 192	192, 176	320 × 512, 320 × 192	320 × 256, 320 × 192	512 × 272, 256 × 224	400, 400
Section thickness (mm)	8, 3.5	7, 7	5, 5	2.5, 3	8, 7	6, 6
Intersection gap (mm)	0.8, 0	0, 0	−2.5, −2.5	−1.25, −1.5	0.8, 1.4	1, 1
Repetition time (msec)	200, 200	3.9, 3.8	4.4, 4.3	3.5, 3.5	>2000, >2000	>3000, >3000
Echo time (msec) in/opposed	4.6/2.3, 4.3/2.1	1.17/2.5, 1.17/2.5	2.2, 2.1	1.7, 1.7	80, 105	80, 80
Flip angle/refocusing angle (degrees)	70, 70	10, 10	10, 12	10, 10	180, 180	160, 160
Reduction factor	1.8, 2	2, 2	1.8, 2	2, 1.9	0, 2	1.6, 2

Note.—Field of view was 250–270 mm × 350–380 mm (adjusted for each patient). 2D = two dimensional, 3D = three dimensional, GRE = gradient-recalled echo.

* Indicates in- and opposed-phase imaging.

† For the 1.5-T system, a 16-channel and an 8-channel phased-array body coil were used. Data are presented as 16 channel/8 channel.

‡ For the 3-T system, a 6-channel body coil and 32-channel cardiac coil were used and adjusted to the patient's physique. Data are presented as 6 channel/32 channel.

range, 91–410 days) were excluded from the growth analysis, because the growth rate before hypervascularization could not be calculated. Thus, 138 nodules from 59 patients were included in the growth analysis. First, the tumor volume doubling time (TVDT) was calculated as follows (20,21): TVDT = $T \times \log 2/[3 \times \log(D_2/D_1)]$, where T is the time interval between two measurements and D_1 and D_2 denote the maximum diameter of the nodule at the initial and last MR imaging examinations, respectively. Then, the growth rate of the nodules was calculated as the inverse of the TVDT.

Statistical Analysis

All analyses were conducted at the nodule level. R software (Version 2.12.0; R Foundation for Statistical Computing, Vienna, Austria) was used for statistical analysis (22). To evaluate the independent prognostic significance of baseline covariates for subsequent hypervascularization, a multivariate Cox proportional hazard model was used. Because 32 patients had multiple nodules detected at two or more follow-up examinations, we used the coxph function from the survival package in the R software, with the cluster option. This method allows accounting for correlation induced by having multiple nodules per patient and uses robust variance estimates (23). Before model selection, bivariate analysis was performed by using Spearman rank correlations to test for collinearity among independent variables. As a result, Spearman correlation coefficients for variables were generally below 0.5, which suggests that multicollinearity was not of concern. Hazard ratios (HRs) and 95% confidence intervals (CIs) were calculated. Because no factor (except intensity on T2-weighted images) was found to show a significant difference when univariate analysis was performed, preliminary multivariate Cox proportional hazards models were constructed by using all 13 variables. Candidate variables were then allowed to enter the final model (entry criterion, $P < .05$). Fat content and initial diameter were forced into the final model because they were considered important predictors (12). The Wald test was performed to determine an overall P value for each variable, and a robust score test was used to assess the significance of the final model as a whole. The model that was fitted by using missing data was not appreciably different from that with the missing data excluded.

The median time interval between the initial and final MR imaging examination was compared for the two groups by using the Mann-Whitney U test. For evaluation of initial diameter and growth rate of the nodules, continuous data differences between the two groups were tested with the Mann-Whitney U test, and categorical data were assessed by using the χ^2 test. Correlation between the initial diameter and the growth rate of the nodules was examined by using the Kendall tau rank test. The prognostic value of the growth rate was evaluated by means of the area under the receiver operating characteristic curve. By using the ROCR package in the R software, the cutoff value for the growth rate was determined at the optimal operating point, with the highest sensitivity and specificity combined (24). Cumulative event rates were estimated by using the Kaplan-Meier method and compared by using the log rank statistic. A P value of less than .05 was considered to indicate a statistically significant difference. All P values were two-sided.

Results

Study Population and Events

During the median follow-up time of 342 days (range, 64–948 days), arterial hypervascularization was observed in 31% (50 of 160) of the nodules in 52% (35 of 68) of the patients. The cumulative percentages of nodules that showed

Table 2

Baseline Patient Characteristics and MR Imaging Findings of 160 Nodules

Parameter	No. of Nodules	Hypervascularization at Follow-up		Preliminary Multivariate Cox Model	
		Yes ($n = 50$)	No ($n = 110$)	HR (95% CI)	*P* Value
Patient characteristic					
Age (y)	. . .	70.5 ± 7.6 (58–85)*	70.4 ± 8.3 (51–84)*	1.0 (0.9, 1.1)	.852
Sex	. . .				.326
Men	106	32 (30)	74 (70)	1.0	
Women	54	18 (33)	36 (67)	1.4 (0.7, 3.1)	
Child-Pugh class					.005
A or chronic hepatitis	146	44 (30)	102 (70)	1.0	
B	14	6 (43)	8 (57)	3.8 (1.5, 9.0)	
Etiology of liver disease					.019
Hepatitis C virus	107	35 (33)	72 (67)	1.0 (0.3, 3.1)	
Hepatitis B virus	26	6 (23)	20 (77)	0.2 (0.03, 0.8)	
Non-B, non-C (ref)	27	9 (33)	18 (67)	1.0	
Serum α-fetoprotein level > 20 ng/mL	66	24 (36)	42 (64)	0.9 (0.5, 2.0)	.948
History of local therapy for HCC	129	46 (36)	83 (64)	5.5 (2.1, 14.7)	<.001
Coexistence of hypervascular HCC	67	29 (43)	38 (57)	2.0 (1.1, 3.7)	.022
MR Imaging Finding					
Fat-suppressed T2-weighted fast spin echo†					<.001
Hyperintensity	18	10 (56)	8 (44)	9.4 (3.6, 24.5)	
Iso- or hypointensity (ref)	108	25 (23)	83 (77)	1.0	
Missing data	34	15 (34)	19 (56)	3.7 (1.7, 8.0)	
Fat containing on in- and opposed-phase images†	24	10 (42)	14 (58)	1.4 (0.6, 3.4)	.491
Noise-to-liver contrast on unenhanced fat-suppressed T1-weighted GRE images	. . .	0.95 ± 0.14 (0.66–1.3)*	0.97 ± 0.17 (0.49–1.9)*	0.05 (0.1×10^{-4}, 1.7×10^{2})	.464
Noise-to-liver contrast on hepatobiliary phase fat-suppressed T1-weighted GRE images	. . .	0.69 ± 0.13 (0.31–0.99)*	0.71 ± 0.11 (0.46–0.95)*	47.5 (6.8×10^{-4}, 3.3×10^{6})	.489
Gadoxetic acid contrast-enhancement ratio	. . .	0.74 ± 0.14 (0.40–0.98)*	0.75 ± 0.14 (0.42–1.5)*	0.07 (0.1×10^{-5}, 3.8×10^{3})	.629
Diameter (mm)	. . .	9.5 ± 5.1 (2–34)*	9.8 ± 3.7 (4–21)*	1.0 (0.9, 1.1)	.998

Note.—Unless otherwise indicated, data are numbers of patients, with percentages in parentheses. GRE = gradient-recalled echo, ref = referent category.

* Data are mean ± standard deviation, with range in parentheses.

† Qualitative assessment.

hypervascularization at 6, 12, 18, and 24 months were 10%, 25%, 36%, and 46%, respectively. Hypervascularization was diagnosed in 39 nodules on the basis of arterial-phase gadoxetic acid–enhanced MR images, eight nodules on the basis of dynamic CT images, two nodules on the basis of CT hepatic arteriographic images, and one nodule on the basis of contrast-enhanced US. In the hypervascularization group, the mean number of hypervascularized nodules was 1.5 (range, 1–7) per patient during the study period.

Histologic results from core needle biopsy were obtained for 13 nodules. Of these, nine nodules were in the hypervascularization group (eight well-differentiated HCCs and one moderately differentiated HCC). Three nodules in the nonhypervascularization group were diagnosed as dysplastic nodules and one as well-differentiated HCC.

Baseline Findings

Table 2 shows the baseline characteristics of the 160 nodules and results of the preliminary multivariate Cox regression. In the final model, five of the variables showed a statistically significant difference (robust score test, $P = .023$; Table 3). The factors associated with an increased risk of hypervascularization were hyperintensity on T2-weighted images (HR = 8.7; 95% CI: 3.6, 20.8), previous local therapy for HCC (HR = 5.0; 95% CI: 1.8, 13.6), Child-Pugh class B cirrhosis (HR = 3.6; 95% CI: 1.4, 9.5), and coexistence of hypervascular HCC (HR = 2.0; 95% CI: 1.0, 3.8). Hepatitis B infection was independently associated with a decreased risk (HR = 0.2; 95% CI: 0.04, 0.8). Of 26 nodules in 13 patients with chronic hepatitis B infections, 23 nodules in 11 patients were treated with oral nucleotide analogs with activity against hepatitis B at the point of entry (five of six nodules in the hypervascularization group and 18 of 20 nodules in the nonhypervascularization group). Fat content and the initial diameter of the nodule were not substantially different in the final model. Of 14 fat-containing nodules in the nonhypervascularization

group, four nodules in one patient were censored because the patient underwent transcatheter arterial chemoembolization for HCC in a different liver segment. Two nodules were censored because of biopsy; one was diagnosed as moderately differentiated HCC, and the other was a dysplastic nodule. The mean initial nodule diameter was not significantly different between the hypervascularization (9.5 mm ± 5.1 [range, 2–34 mm]) and the nonhypervascularization groups (9.8 mm ± 3.7 [range, 4–21 mm]) (P = .282). The numbers of nodules that were smaller than 5 mm, 5–10 mm, 10–15 mm, and greater than 15 mm in initial size were four, 28, 11, and seven in the hypervascularization group, and three, 60, 33, and 14 in the nonhypervascularization group, respectively. In addition, there was no difference in the percentage of nodules greater than or equal to 15 mm in size between the two groups (14% [seven of 50] vs 13% [14 of 110], respectively; P = .825).

Table 3

Multivariate Predictors of Subsequent Hypervascularization

Variable	HR (95% CI)	*P* Value
Significant independent predictors		
Child-Pugh classification		.008
A or chronic hepatitis	1.0	
B	3.6 (1.4, 9.5)	
Cause of liver disease		.017
Hepatitis C virus	1.1 (0.4, 3.1)	
Hepatitis B virus	0.2 (0.04, 0.8)	
Non-B and non-C liver disease (Ref)	1.0	
History of local therapy for HCC	5.0 (1.8, 13.6)	.002
Coexistence of hypervascular HCC	2.0 (1.0, 3.8)	.038
Fat-suppressed T2-weighted fast spin echo		<.001
Hyperintensity	8.7 (3.6, 20.8)	
Hypo- or isointensity (Ref)	1.0	
Missing data	3.4 (1.4, 7.9)	
Additional variables included in the model		
Fat containing on in- and opposed-phase images	1.3 (0.5, 3.7)	.567
Diameter (mm)	1.0 (0.9, 1.1)	.692

Growth Analysis

Twenty-eight lesions in the hypervascularization group (initial diameter, 9.7 mm ± 5.9 [range, 2–34 mm]) and 110 nodules (9.8 mm ± 3.7 [range, 4–21 mm]) in the nonhypervascularization group were evaluated. The median time between the initial and last MR imaging examination was not significantly different (P = .075) between the two groups (235 and 293 days, respectively). In the hypervascularization group, 27 nodules increased in diameter during follow-up (Fig 2) and one remained stable. The mean growth rate in the hypervascularization group (6.5×10^{-3}/day [TVDT, 154 days]) was significantly higher ($P = 1.8 \times 10^{-6}$) than that in the nonhypervascularization group (1.1×10^{-3}/day [TVDT, 946 days]) (Fig 3). There was no correlation between initial diameter and growth rate (Kendall tau = −0.066; P = .266) (Fig 4). Receiver operating characteristic analysis (area under the curve, 0.79) identified a growth rate cutoff value of 1.8×10^{-3} per day (TVDT, 542 days) with a positive predictive value of 89% (25 of 28 nodules) and a negative predictive value of 63% (70 of 110 nodules) for hypervascularization (Fig 5, *A*). The 1-year cumulative proportion of nodules showing hypervascularization was 0% for those with a growth rate of less than 1.8×10^{-3}/day and 53% for those with a growth rate greater than or equal to 1.8×10^{-3}/day (log-rank test, $P = 5.2 \times 10^{-8}$; Fig 5, *B*).

Discussion

We set out to determine risk factors associated with hypervascularization in hypovascular nodules in patients with chronic liver diseases by using time-to-event analysis. Among the baseline patient characteristics and MR imaging findings, the most important variable associated with an increased risk of hypervascularization was hyperintensity on T2-weighted images. In the hypervascularization group, higher signal intensity on T2-weighted images might reflect peliotic changes in the intratumoral sinusoids of HCC (25). Meanwhile, nodular regeneration, fibrosis, and scarring that occur in the course of cirrhosis occasionally appear as hyperintense round lesions on T2-weighted images. Dysplastic nodules can be hyperintense on T2-weighted images; the causes are considered to be varying degrees of fibrosis, or infarction (26,27). It has been reported that T2-weighted imaging does not provide added diagnostic value to gadoxetic acid–enhanced images for the detection and characterization of focal lesions in cirrhotic livers (28). Findings from our study suggest that the combination of T2-weighted images and gadoxetic acid–enhanced MR images could be useful in the prediction of hypervascularization of previously hypovascular nodules.

Child-Pugh class B cirrhosis increased the risk of hypervascularization compared with Child-Pugh class A or chronic hepatitis, and hepatitis B infection decreased the risk compared with hepatitis C infection. These results might reflect the epidemiologic features of HCC (29,30); Child-Pugh class B and C are associated with a three-fold increase in the risk of HCC. The annual incidence of HCC in patients with cirrhosis due to hepatitis B infection exceeds 2%, which is lower than that due to hepatitis C infection (3%–8%). In addition, there may be morphologic and histologic differences between hypovascular nodules associated with hepatitis B and those associated with hepatitis C infection.

Figure 2

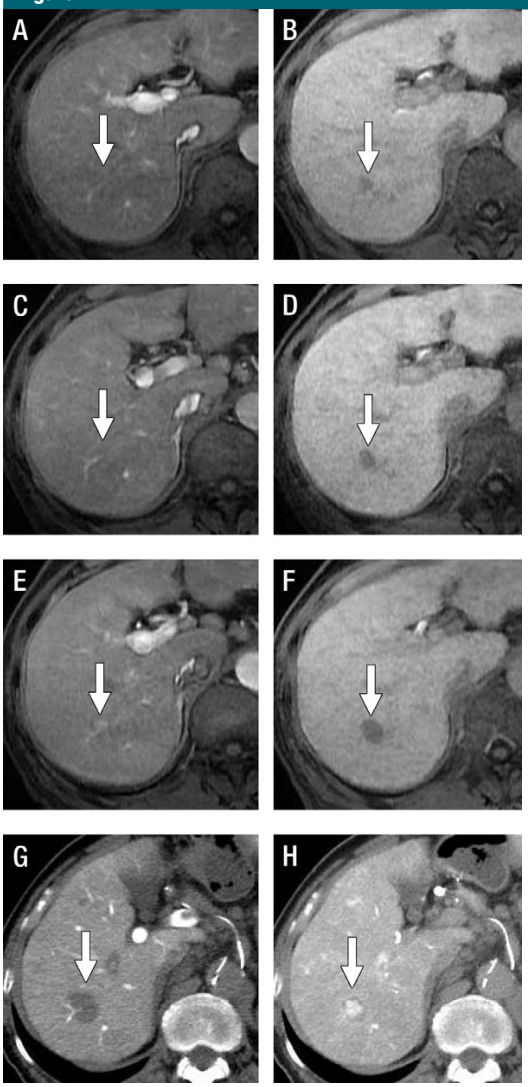

Figure 2: Growing hypovascular hepatic nodule (arrows) and subsequent hypervascularization in an 86-year-old man with hepatitis C and Child-Pugh class B cirrhosis. *A-F*, Axial gadoxetic acid–enhanced T1-weighted fat-suppressed three-dimensional gradient-recalled echo images obtained during (*A*, *C*, and *E*) arterial phase and (*B, D, F*) hepatobiliary phase obtained at (*A, B*) baseline, (*C, D*) day 94, and (*E, F*) day 176. At (*A*) baseline and (*C*) day 94, hepatic nodule in right posterior section showed neither arterial-phase enhancement nor portal-venous phase washout. Hepatobiliary phase images showed that maximum diameter increased from 8 mm at, *B*, baseline to 12 mm at, *D*, day 94, and TVDT was calculated as 170 days. *E*, Arterial-phase image at day 176 shows partial enhanceme of nodule. *G*, At day 194, CT arterial portographic image shows a well-defined, round perfusion defect and, *H*, CT hepatic arteriographic image shows marked enhancement corresponding to nodule. Nodule was diagnosed as HCC on the basis of image views and tumor markers.

Figure 3

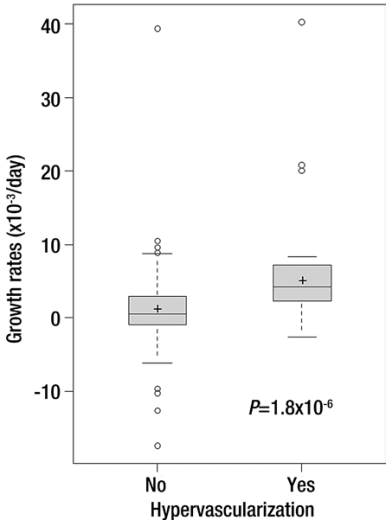

Figure 3: Box plot shows distribution of growth rates of 138 nodules. Median values and 25th and 75th percentiles are shown in each box plot. Vertical bars represent largest and smallest values that are not outliers. + = Mean; ○ = outlier of more than 1.5 times box length.

In comparison with hepatitis C infection or alcohol abuse, hepatitis B infection tends to induce macronodular (> 3 mm) cirrhosis (31). Thus, macronodular benign nodules in cases of hepatitis B cirrhosis might have been present in our subjects. Another possible reason why hepatitis B infection was a negative predictor for hypervascularization might be that antihepatitis B nucleoside analogs prevented the development of HCC (32).

The nodule-to-liver contrast ratios on unenhanced T1-weighted images and gadoxetic acid–enhanced hepatobiliary phase MR images were not a significant prognostic factor, which is consistent with previous reports (33). The signal intensity of nodules on T1-weighted images may be affected by intratumoral fat, metal, or glycogen in the surrounding hepatic parenchyma (1,34). The fat content of the nodules was also not a significant predictor of hypervascularization in our study. One possible reason for this was the fact that both early HCCs and dysplastic nodules could appear as intracellular lipid-containing lesions in cirrhotic livers (35). There was also no statistically significant association between initial diameter and hypervascularization in our study results. The probable reason for this was that most subjects (87%) had nodules of less than 15 mm in diameter (139 of 160 nodules).

The reported TVDT for HCC ranges from 18 to 605 days (1). The mean growth rate for HCCs smaller than 20 mm that showed no hyperintensity on T2-weighted MR images but that enhanced during arterial phase MR imaging was 10.5×10^{-3}/day (TVDT, 95 days; calculated by using data from Jeong et al [36]). The hypervascularization group, which was considered to be representative of an earlier stage of multistep carcinogenesis, showed the lower mean growth rate (6.5×10^{-3}/day [TVDT, 154

Figure 5

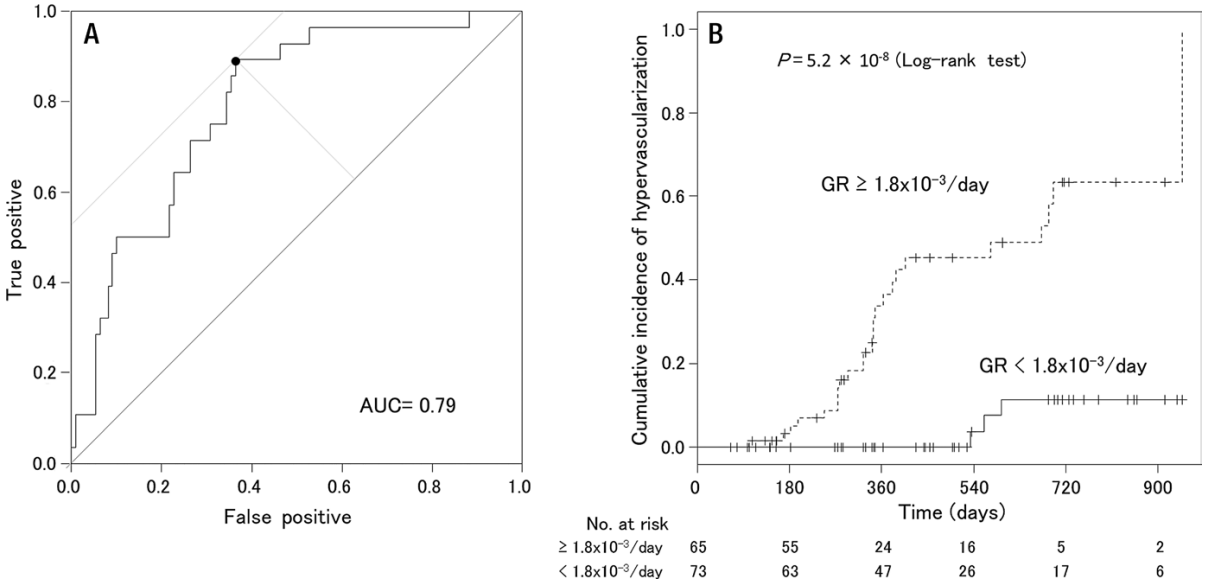

Figure 5: *A,* Graph shows receiver operating characteristic curve of growth rate *(GR)* for the prediction of hypervascularization (area under the curve *[AUC]*, 0.79). The optimal operating point on the receiver operating characteristic curve is marked with a black dot (growth rate, 1.8 × 10^{-3}/day). *B,* Kaplan-Meier analysis shows effect of growth rate on cumulative incidence of hypervascularization. Number of nodules at risk at each time point is shown at bottom of figure.

days]) than that reported in the Jeong et al study (36).

On the basis of these previous studies, hypovascular nodules larger than 15 mm are considered appropriate for biopsy. In cases with nodules less than 10 mm in diameter, the American Association for the Study of Liver Disease recommends imaging follow-up at 3–6 month intervals, with careful attention to increases in size or changes in vascular pattern. Repeated biopsy for nodules larger than 10 mm can be performed, but a needle liver biopsy has some disadvantages including inaccurate sampling caused by technical difficulties (eg, poor lesion or needle visualization, deeply located lesions, and hepatic fibrosis), risk of bleeding, and needle track seeding. Our growth analysis, along with baseline risk factors, might improve diagnostic discrimination with or without the need for biopsy, particularly for nodules measuring 10–15 mm. By using a cutoff growth rate of 1.8 × 10^{-3}/day (TVDT, 542 days), the calculated diameters at

Figure 4

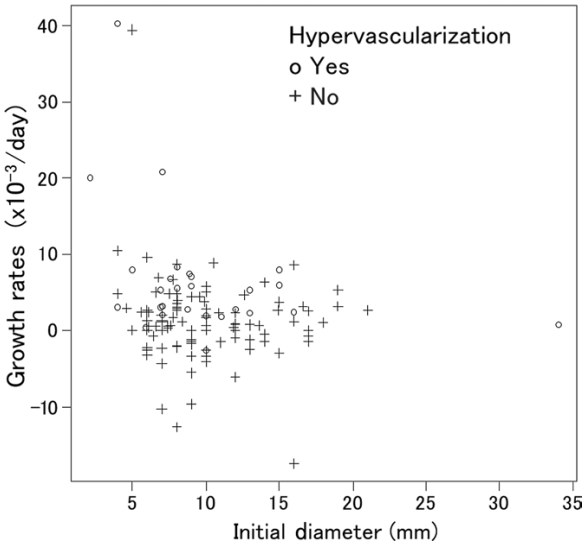

Figure 4: Scatterplot shows growth rate above the initial diameter. Individual nodules were coded according to whether they showed subsequent hypervascularization during the study period.

the 6-month follow-up examination for nodules with an initial diameter of 10, 11, 12, 13, and 14 mm were 10.8, 11.9, 13.0, 14.0, and 15.1 mm, respectively. We suggest that nodules with the risk factors for hypervascularization or those showing faster growth may justify more frequent follow-up or biopsy. If growth is slower, biopsy may not be needed, although the absence of growth does not rule out malignancy. According to expert opinion, nodules are declared benign only if they regress or remain stable for 2 years (37).

The reported incidence rates of hypervascularization vary throughout different studies. In our study, the overall 6- and 12-month cumulative percentages for hypervascularization were 10% and 25%, respectively, which is lower than the percentages calculated by Kumada et al (27.6% and 43.5%, respectively) (13). This may be partially explained by time frame, sample size, and/or follow-up policy of subjects in each study.

Our study had some limitations. It was a retrospective study, and this fact may have introduced bias in data homogeneity. To minimize sampling bias, we collected data from consecutive patients who underwent multiple gadoxetic acid–enhanced MR imaging examinations in two hospitals. Also, the duration of disease and date of diagnosis were potentially important confounders. However, they were not available for retrospective review.

Regarding the imaging technique, a relatively high rate (2 mL/sec) of injection of gadoxetic acid might reduce the performance of arterial-phase imaging. Some reports suggested that a lower injection rate might be appropriate owing to stretching the bolus without reducing the enhancement peak (38,39). However, we performed gadoxetic acid–enhanced MR imaging with optimized imaging technique (40) and timing (16) to acquire good images in the arterial phase.

On imaging analysis, our study was potentially limited by consensus review because we did not assess interobserver variability. Also, in the case of smaller nodules (< 10 mm), it might be difficult to obtain a clear correspondence between the MR images and those of the other modalities (CT, and in particular, contrast-enhanced US), even though well-trained radiologists and physicians reviewed the images.

Tumor growth kinetic calculations were based on the general assumption that tumor cells grow exponentially. This assumption might not hold true owing to fibrosis or to the intracellular lipid content of both the hepatic nodules and surrounding cirrhotic liver parenchyma. Because patients with Child-Pugh class C cirrhosis were excluded, the influence of fibrosis of the surrounding parenchyma is limited. Also, measurement errors associated with manual evaluation may have led to bias. However, to improve accuracy all measurements were performed in the same manner, by using T1-weighted three-dimensional gradient-echo images that provided high spatial resolution (7). A large-scale prospective validation study is necessary to confirm our proposed cutoff values.

In conclusion, hypervascularization occurs in about one-third of the hypovascular nodules that show hypointensity on gadoxetic acid–enhanced hepatobiliary phase MR images. MR imaging findings, including hyperintensity on T2-weighted images and a higher growth rate, may predict arterial hypervascularization, which may lead to early diagnosis and treatment of HCC.

Disclosures of Conflicts of Interest: T.H. Financial activities related to the present article: Received Osaka Cancer Foundation grant in 2010. Financial activities not related to the present article: none to disclose. Other relationships: none to disclose. **T. Murakami** No relevant conflicts of interest to disclose. **Y.I.** No relevant conflicts of interest to disclose. **M.O.** No relevant conflicts of interest to disclose. **M.H.** No relevant conflicts of interest to disclose. **Y.K.** No relevant conflicts of interest to disclose. **S. Kogita** No relevant conflicts of interest to disclose. **S. Kumano** No relevant conflicts of interest to disclose. **M.K.** No relevant conflicts of interest to disclose. **T. Mochizuki** No relevant conflicts of interest to disclose.

References

1. Willatt JM, Hussain HK, Adusumilli S, Marrero JA. MR Imaging of hepatocellular carcinoma in the cirrhotic liver: challenges and controversies. Radiology 2008;247(2):311–330.
2. Bruix J, Sherman M; American Association for the Study of Liver Diseases. Management of hepatocellular carcinoma: an update. Hepatology 2011;53(3):1020–1022.
3. Giovagnoni A, Paci E. Liver. III: Gadolinium-based hepatobiliary contrast agents (Gd-EOB-DTPA and Gd-BOPTA/Dimeg). Magn Reson Imaging Clin N Am 1996;4(1):61–72.
4. Bluemke DA, Sahani D, Amendola M, et al. Efficacy and safety of MR imaging with liver-specific contrast agent: U.S. multicenter phase III study. Radiology 2005;237(1):89–98.
5. Haradome H, Grazioli L, Tinti R, et al. Additional value of gadoxetic acid-DTPA-enhanced hepatobiliary phase MR imaging in the diagnosis of early-stage hepatocellular carcinoma: comparison with dynamic triple-phase multidetector CT imaging. J Magn Reson Imaging 2011;34(1):69–78.
6. Okada M, Imai Y, Kim T, et al. Comparison of enhancement patterns of histologically confirmed hepatocellular carcinoma between gadoxetate- and ferucarbotran-enhanced magnetic resonance imaging. J Magn Reson Imaging 2010;32(4):903–913.
7. Lee VS, Lavelle MT, Rofsky NM, et al. Hepatic MR imaging with a dynamic contrast-enhanced isotropic volumetric interpolated breath-hold examination: feasibility, reproducibility, and technical quality. Radiology 2000;215(2):365–372.
8. Golfieri R, Renzulli M, Lucidi V, Corcioni B, Trevisani F, Bolondi L. Contribution of the hepatobiliary phase of Gd-EOB-DTPA-enhanced MRI to Dynamic MRI in the detection of hypovascular small (≤ 2 cm) HCC in cirrhosis. Eur Radiol 2011;21(6):1233–1242.
9. International Consensus Group for Hepatocellular NeoplasiaThe International Consensus Group for Hepatocellular Neoplasia. Pathologic diagnosis of early hepatocellular carcinoma: a report of the international consensus group for hepatocellular neoplasia. Hepatology 2009;49(2):658–664.
10. Hayashi M, Matsui O, Ueda K, et al. Correlation between the blood supply and grade of malignancy of hepatocellular nodules associated with liver cirrhosis: evaluation by CT during intraarterial injection of contrast medium. AJR Am J Roentgenol 1999;172(4):969–976.
11. Yu JS, Chung JJ, Kim JH, Kim KW. Fat-containing nodules in the cirrhotic liver: chemical shift MRI features and clinical implications. AJR Am J Roentgenol 2007;188(4):1009–1016.
12. Motosugi U, Ichikawa T, Sano K, et al. Outcome of hypovascular hepatic nodules revealing no gadoxetic acid uptake in patients

with chronic liver disease. J Magn Reson Imaging 2011;34(1):88–94.

13. Kumada T, Toyoda H, Tada T, et al. Evolution of hypointense hepatocellular nodules observed only in the hepatobiliary phase of gadoxetate disodium-enhanced MRI. AJR Am J Roentgenol 2011;197(1):58–63.
14. Sakamoto M, Hirohashi S, Shimosato Y. Early stages of multistep hepatocarcinogenesis: adenomatous hyperplasia and early hepatocellular carcinoma. Hum Pathol 1991;22(2):172–178.
15. Makuuchi M, Kokudo N, Arii S, et al. Development of evidence-based clinical guidelines for the diagnosis and treatment of hepatocellular carcinoma in Japan. Hepatol Res 2008;38(1):37–51.
16. Kagawa Y, Okada M, Kumano S, et al. Optimal scanning protocol of arterial dominant phase for hypervascular hepatocellular carcinoma with gadolinium-ethoxybenzyl-diethylenetriamine pentaacetic acid-enhanced MR. J Magn Reson Imaging 2011;33(4):864–872.
17. Goshima S, Kanematsu M, Kondo H, et al. MDCT of the liver and hypervascular hepatocellular carcinomas: optimizing scan delays for bolus-tracking techniques of hepatic arterial and portal venous phases. AJR Am J Roentgenol 2006;187(1):W25–W32.
18. Hori M, Murakami T, Kim T, Nakamura H. Diagnosis of hepatic neoplasms using CT arterial portography and CT hepatic arteriography. Tech Vasc Interv Radiol 2002; 5(3):164–169.
19. Kudo M, Hatanaka K, Maekawa K. Newly developed novel ultrasound technique, defect reperfusion ultrasound imaging, using sonazoid in the management of hepatocellular carcinoma. Oncology 2010;78(Suppl 1):40–45.
20. Collins VP, Loeffler RK, Tivey H. Observations on growth rates of human tumors. Am J Roentgenol Radium Ther Nucl Med 1956;76(5):988–1000.
21. Schwartz M. A biomathematical approach to clinical tumor growth. Cancer 1961; 14:1272–1294.
22. R Development Core Team. R: A language and environment for statistical computing. Vienna, Austria: R Foundation for Statistical Computing, 2010.
23. Lin DY. Cox regression analysis of multivariate failure time data: the marginal approach. Stat Med 1994;13(21):2233–2247.
24. Fawcett T. An introduction to ROC analysis. Pattern Recognit Lett 2006;27(8):861–874.
25. Kadoya M, Matsui O, Takashima T, Nonomura A. Hepatocellular carcinoma: correlation of MR imaging and histopathologic findings. Radiology 1992;183(3):819–825.
26. Ohtomo K, Baron RL, Dodd GD 3rd, Federle MP, Ohtomo Y, Confer SR. Confluent hepatic fibrosis in advanced cirrhosis: evaluation with MR imaging. Radiology 1993;189(3):871–874.
27. Kim T, Baron RL, Nalesnik MA. Infarcted regenerative nodules in cirrhosis: CT and MR imaging findings with pathologic correlation. AJR Am J Roentgenol 2000;175(4): 1121–1125.
28. Hussain HK, Syed I, Nghiem HV, et al. T2-weighted MR imaging in the assessment of cirrhotic liver. Radiology 2004;230(3): 637–644.
29. Fattovich G, Stroffolini T, Zagni I, Donato F. Hepatocellular carcinoma in cirrhosis: incidence and risk factors. Gastroenterology 2004;127(5,Suppl 1):S35–S50.
30. Bolondi L, Sofia S, Siringo S, et al. Surveillance programme of cirrhotic patients for early diagnosis and treatment of hepatocellular carcinoma: a cost effectiveness analysis. Gut 2001;48(2):251–259.
31. Rozario R, Ramakrishna B. Histopathological study of chronic hepatitis B and C: a comparison of two scoring systems. J Hepatol 2003;38(2):223–229.
32. Matsumoto A, Tanaka E, Rokuhara A, et al. Efficacy of lamivudine for preventing hepatocellular carcinoma in chronic hepatitis B: A multicenter retrospective study of 2795 patients. Hepatol Res 2005;32(3): 173–184.
33. Kobayashi S, Matsui O, Gabata T, et al. Gadolinium ethoxybenzyl diethylenetriamine pentaacetic Acid-enhanced magnetic resonance imaging findings of borderline lesions at high risk for progression to hypervascular classic hepatocellular carcinoma. J Comput Assist Tomogr 2011;35(2): 181–186.
34. Ebara M, Fukuda H, Kojima Y, et al. Small hepatocellular carcinoma: relationship of signal intensity to histopathologic findings and metal content of the tumor and surrounding hepatic parenchyma. Radiology 1999; 210(1):81–88.
35. Basaran C, Karcaaltincaba M, Akata D, et al. Fat-containing lesions of the liver: cross-sectional imaging findings with emphasis on MRI. AJR Am J Roentgenol 2005; 184(4):1103–1110.
36. Jeong YY, Mitchell DG, Kamishima T. Small (<20 mm) enhancing hepatic nodules seen on arterial phase MR imaging of the cirrhotic liver: clinical implications. AJR Am J Roentgenol 2002;178(6):1327–1334.
37. Bruix J, Sherman M; Practice Guidelines Committee, American Association for the Study of Liver Diseases. Management of hepatocellular carcinoma. Hepatology 2005;42(5):1208–1236.
38. Zech CJ, Vos B, Nordell A, et al. Vascular enhancement in early dynamic liver MR imaging in an animal model: comparison of two injection regimen and two different doses Gd-EOB-DTPA (gadoxetic acid) with standard Gd-DTPA. Invest Radiol 2009;44(6):305–310.
39. Chung SH, Kim MJ, Choi JY, Hong HS. Comparison of two different injection rates of gadoxetic acid for arterial phase MRI of the liver. J Magn Reson Imaging 2010;31(2):365–372.
40. Kim KA, Herigault G, Kim MJ, Chung YE, Hong HS, Choi SY. Three-dimensional contrast-enhanced hepatic MR imaging: comparison between a centric technique and a linear approach with partial Fourier along both slice and phase directions. J Magn Reson Imaging 2011;33(1):160–166.

Journal of Medical Virology 85:987–995 (2013)

Impact of Peginterferon Alpha-2b and Entecavir Hydrate Combination Therapy on Persistent Viral Suppression in Patients with Chronic Hepatitis B

Satoru Hagiwara,[1] Masatoshi Kudo,[1] Yukio Osaki,[2] Hiroo Matsuo,[2] Tadashi Inuzuka,[2] Akihiro Matsumoto,[3] Eiji Tanaka,[3] Toshiharu Sakurai,[1]* Kazuomi Ueshima,[1] Tatsuo Inoue,[1] Norihisa Yada,[1] and Naoshi Nishida[1]*

[1]*Department of Gastroenterology and Hepatology, Kinki University School of Medicine, Osaka-Sayama, Japan*
[2]*Department of Gastroenterology and Hepatology, Osaka Red Cross Hospital, Osaka, Japan*
[3]*Department of Medicine, Shinshu University School of Medicine, Matsumoto, Japan*

The ideal approach to treat chronic hepatitis B remains controversial. This pilot study aimed to evaluate the effectiveness of peginterferon (PEG-IFN) α-2b and entecavir hydrate (ETV) as a combination therapy for patients with chronic hepatitis B, particularly in the context of virological response and the reduction of intrahepatic covalently closed circular DNA (cccDNA). A total of 17 patients with hepatitis B virus (HBV) genotype C were enrolled in this study. All subjects were treated with this combination therapy for 48 weeks and observed for an additional 24 weeks. All patients underwent liver biopsy before and after the therapy period. Changes in cccDNA levels and liver histology were monitored between biopsies. Among the 11 patients who exhibited pretherapy hepatitis B e antigen (HBeAg), 8 (73%) showed evidence of HBeAg seroconversion by the end of the follow-up period. Serum HBV DNA levels decreased by 5.2 and 3.3 log copies/ml (mean) by the end of the therapy and follow-up periods, respectively. In addition, intrahepatic cccDNA decreased significantly to 1.4 log copies/μg (mean) by the end of the therapy period. Among the 11 patients who did not experience viral relapse, only 2 (18%) exhibited high levels of cccDNA (>4.5 log copies/μg) by the end of the treatment period. In contrast, all relapsed subjects exhibited significantly higher levels of cccDNA than subjects who did not relapse ($P = 0.027$). The combination regimen is a promising approach to treat chronic hepatitis B and may achieve significant reduction in serum HBV DNA and intrahepatic cccDNA. ***J. Med. Virol. 85:987–995, 2013.*** © 2013 Wiley Periodicals, Inc.

KEY WORDS: hepatitis B virus; peginterferon α-2b; entecavir hydrate; combination therapy; covalently closed circular DNA

INTRODUCTION

Chronic infection with hepatitis B virus (HBV) occurs commonly and is associated with increased risk of cirrhosis and the development of hepatocellular carcinoma [Lai et al., 2003]. This type of hepatitis is a worldwide health problem, but achievement of sustained suppression of HBV replication by conventional antiviral agents is sometimes difficult because of the unique nature of HBV replication. For example, after it infects hepatocytes, linear HBV DNA transforms into covalently closed circular DNA (cccDNA), which represents the intracellular HBV template [Newbold et al., 1995; Arase et al., 2002]. Various nucleotide analogues, such as lamivudine (LVD) [Dienstag et al., 1995; Lai et al., 1998; Leung

Additional supporting information may be found in the online version of this article.

Conflicts of interest: The authors declare no conflicts of interest.

*Correspondence to: Naoshi Nishida, M.D., Ph.D., and Toshiharu Sakurai, M.D., Ph.D., Department of Gastroenterology and Hepatology, Kinki University School of Medicine, 377-2 Ohno-Higashi, Osaka-Sayama, Osaka 589-8511, Japan. E-mail: naoshi@med.kindai.ac.jp; sakurai@med.kindai.ac.jp

Accepted 28 January 2013

DOI 10.1002/jmv.23564
Published online in Wiley Online Library (wileyonlinelibrary.com).

et al., 2001], adefovir dipivoxil (ADV) [Hadziyannis et al., 2003; Marcellin et al., 2003], entecavir (ETV) [Chang et al., 2006; Lai et al., 2006], and tenofovir disoproxil fumarate have been approved as treatments to suppress HBV replication. However, the mechanism of action of nucleotide analogues is limited to reverse transcription and does not decrease the quantity of cccDNA; the cessation of this type of treatment frequently results in viral relapse. In addition, long-term use of nucleotide analogues is hampered by considerable emergence of resistant mutants [Yuen et al., 2001, 2007; Lok et al., 2003].

On the other hand, peginterferon (PEG-IFN) is known to reduce the quantity of cccDNA, presumably by inducing cytotoxic T lymphocytes (CTL), which destroy infected hepatocytes [Wursthorn et al., 2006]. Despite its rapid anti-viral effects, PEG-IFN monotherapy alone is less effective than nucleotide analogues [Wu et al., 1990]. From this perspective, a combination approach of immune modification (PEG-IFN) and blockade of reverse-transcription (nucleotide analogues) conceivably may compensate for the antiviral shortcomings inherent to each as a monotherapy, and thus, appears promising for achieving long-term suppression of viral replication that continues after the completion of antiviral therapy. However, a relatively low amount of data has been generated on the combined use of PEG-IFN and nucleotide analogues to treat chronic hepatitis B.

The present study evaluated prospectively the effectiveness of combined PEG-IFN α-2b and ETV treatment in patients with chronic hepatitis B. ETV was selected among several nucleotide analogue options because it exerts the strongest antiviral activity and has the lowest incidence of resistant mutation [Chang et al., 2006; Lai et al., 2006]. A systematic and comprehensive analysis was conducted to establish an HBV profile based on several related markers, which included serial measurements of HBeAg, anti-HBe antibody, serum HBV DNA and RNA, and intrahepatic cccDNA, and histological evaluations throughout the clinical course. This report offers profound insight on the antiviral impact of PEG-IFN and ETV combination therapy in patients with chronic hepatitis B.

METHODS

Patient Characteristics and Study Design

A total of 17 patients with chronic hepatitis B received combination therapy of PEG-IFN α-2b (PegIntron, Schering-Plough; Kenilworth, NJ) and ETV (Baraclude, Bristol-Myers Squibb; Princeton, NJ) between February 2008 and April 2010 in Kinki University Hospital or Osaka Red Cross Hospital. All patients were serum-positive for hepatitis B surface antigen (HBsAg) for at least 6 months. Additional inclusion criteria included serum HBV DNA levels greater than 5 log copies/ml at a measurement obtained 4 weeks before the first biopsy, serum alanine aminotransferase (ALT) levels greater than 31 IU/ml, and no treatment with nucleic acid analogues or IFN within 3 years prior to study initiation. Subjects with hepatitis C virus, hepatitis D virus, human immunodeficiency virus, a history of hepatocellular carcinoma, autoimmune hepatitis, primary biliary cirrhosis, or decompensated cirrhosis were excluded from the study. Patient characteristics are listed in Table I.

After patients provided informed consent, both drugs were administered throughout the 48-week treatment phase. Treatment consisted of daily doses of oral ETV (0.5 mg) and weekly subcutaneous injection of PEG-IFN α-2b (1.5 μg/kg body weight). PEG-IFN α-2b was selected for the IFN component of therapy because its dosing strategy is adjusted for body weight. For histological analysis and assessment of intrahepatic viral DNA, liver biopsy samples were obtained before and after the 48-week treatment period. All biopsies were performed percutaneously. The 48-week treatment phase was followed by a 24-week treatment-free phase. The protocol included ETV monotherapy after the 24-week follow-up phase for subjects who had relapsed after they received the full combination treatment of PEG-IFN α-2b and ETV. The schematic representation of schedule is shown in Supplementary Figure 1. The Medical Ethics Committee of Kinki University School of Medicine and Osaka Red Cross Hospital approved this study.

Response to Therapy

The virological response to combination therapy was defined as a decrease in serum HBV DNA

TABLE I. Characteristics of the Patients at Baseline

	HBeAg-positive (n = 11)	HBeAg-negative (n = 6)	Overall (n = 17)
Age (year, mean ± SD)	45 ± 12	50 ± 11	47 ± 12
Gender (male, no.; %)	9 (82)	4 (67)	13 (76)
Serum HBV DNA (log copies/ml, mean ± SD)	7.8 ± 1.3	6.8 ± 1.3	7.5 ± 1.4
ALT (IU/l, mean ± SD)	191 ± 161	93 ± 77	157 ± 143
Necroinflammation score (mean ± SD)	5.9 ± 2.3	5.5 ± 3.5	5.8 ± 2.7
No. of cases with F score >3 (%)	9 (82)	3 (50)	12 (71)
cccDNA (log copies/μg, mean ± SD)	5.8 ± 1.1	4.8 ± 0.5	5.4 ± 1.0

All patients analyzed were Asian with HBV of genotype C.
SD, standard deviation; HBeAg, hepatitis B e antigen; ALT, alanine aminotransferase; IU, international unit.

4.0 log copies/ml or less. The biological response was defined as a decrease in serum ALT to normal levels of 40 IU/L or less. A complete response was defined as the achievement of HBeAg seroconversion, which was indicated by the loss of HBeAg and appearance of anti-HBe antibody, and evidence of positive virological and biological response throughout the follow-up phase. For HBeAg-negative patients, a virological and biological response that did not include the appearance of HBeAg was considered a complete response.

Virological Analyses

Serum levels of HBsAg, anti-HBs, HBeAg, and anti-HBe were measured using the chemiluminescent immunoassay (CLIA) from the ARCHITECT kit (Abbott Japan; Tokyo, Japan). The serum hepatitis B core-related antigen (HBcrAg) was quantified using the chemiluminescent enzyme immunoassay (CLEIA) with Lumipulse HBcrAg (Fujirebio, Tokyo, Japan). Luminescence was detected using Lumipulse f (Fujirebio) [Kimura et al., 2002]. The HBV DNA genotype was determined by PCR-restriction fragment length polymorphism. Serum HBV DNA was quantified using TaqMan PCR (Roche Diagnostics, Mannheim, Germany); the lower limit of quantification for HBV DNA was 2.1 log copies/ml [Allice et al., 2007].

Quantitation of HBV RNA and Intrahepatic cccDNA

HBV RNA was quantified by the method reported by Rokuhara et al. [2006].

DNA was extracted from liver biopsy specimens using the QIAamp DNA mini kit (Qiagen, Hilder, Germany) according to the manufacturer's instructions. To quantify HBV cccDNA, real-time PCR on 500 ng DNA was performed. The DR1 and DR2 regions of HBV cccDNA were amplified using forward and reverse primer sequences that is 5'-CTGCTGTGC CTTCTCATCTGC-3' and 5'-GCTCAGCTTGGAGGCTT-GAC-3', respectively. The sequence of the TaqMan probe was 5' FAM-AACAATTTATGCCTACAG-MGB 3'. The quantitative real-time PCR procedure was performed in an ABI 7700 or 7900 system (Applied Biosystems, Foster City, CA). The real-time PCR procedure included 40 cycles, each of which began with 40 sec of denaturation at 95°C and 90 sec of annealing and polymerization at 60°C. The amplified gene was used as an endogenous control for quantification purposes. The standard curve was generated by serial dilution of plasmid DNA that contained HBV genotype C DNA.

Immunostaining of Hepatitis B Virus Core Antigen

Hepatitis activity was evaluated in liver biopsies by determining the Knodell necroinflammatory score [Knodell et al., 1981]. Fibrosis was scored according to the Ishak fibrosis scoring system [Ishak et al., 1995]. Formalin-fixed, paraffin-embedded sections were subjected to immunohistological staining with antiserum specific for hepatitis B virus core antigen (HBcAg) (Dako Cytomation, Carpinteria, CA). For quantification, the mean percentages of HBcAg-positive hepatocytes were determined. Five fields of images were obtained for each sample and stain-positive nuclei were enumerated by Image J software (NIH, Bethesda, MD).

Evaluation of Safety

Hematological and biochemical examinations were performed weekly during the first 12 weeks of the treatment phase. Thereafter, blood-based examinations were performed every 4 weeks until week 28, every 8 weeks until the end of the treatment (48 weeks), and 4, 8, 12, and 24 weeks after the treatment ended. The WHO Toxicity Grading Scale was used to assess adverse reactions.

Statistical Analyses

To determine significant differences between groups, the Fisher's exact test and paired t-test were used as appropriate. A P-value of less than 0.05 was considered significant. All analyses described above were performed using the SPSS program (version 11.5, SPSS, Inc.; Chicago, IL).

RESULTS

Virological and Biological Response to Combination Therapy

All patients enrolled in the study completed the combination therapy regimen. The dose of PEG-IFN α-2b was reduced to 40 μg for three patients, and in one case, PEG-IFN α-2b was suspended at week 46 because of adverse side effects. All patients received regular, oral doses of ETV (0.5 mg) every day for 48 weeks. Baseline levels of mean ALT and HBV DNA ($\pm$SD) were 157 $\pm$ 143 IU/ml and 7.5 $\pm$ 1.4 log copies/ml, respectively, and the mean necroinflammatory score was 5.8. An advanced F score of 3 or 4 was observed in 12 of 17 patients (71%) (Table I).

At the end of the 48-week treatment period, the mean level of serum HBV DNA in all patients was 2.3 log copies/ml, and the mean decrease in HBV DNA was 5.2 log copies/ml ($P < 0.01$). A virological response was achieved in 14 patients (14/17, 94%). By the conclusion of the follow-up phase, the mean level of serum HBV DNA was 4.1 log copies/ml and the mean decrease in HBV DNA was 3.3 log copies/ml less than the baseline ($P < 0.01$); 12 of 17 cases (71%) achieved virological response (Fig. 1A; Table II). Biological response was achieved in 13 patients (76%) by the end of the treatment period and in 14 patients (82%) by the end of the follow-up phase (Fig. 1B). Of the 11 HBeAg-positive patients, HBe seroconversion was observed in four patients (36%) by the end of the treatment period and in eight

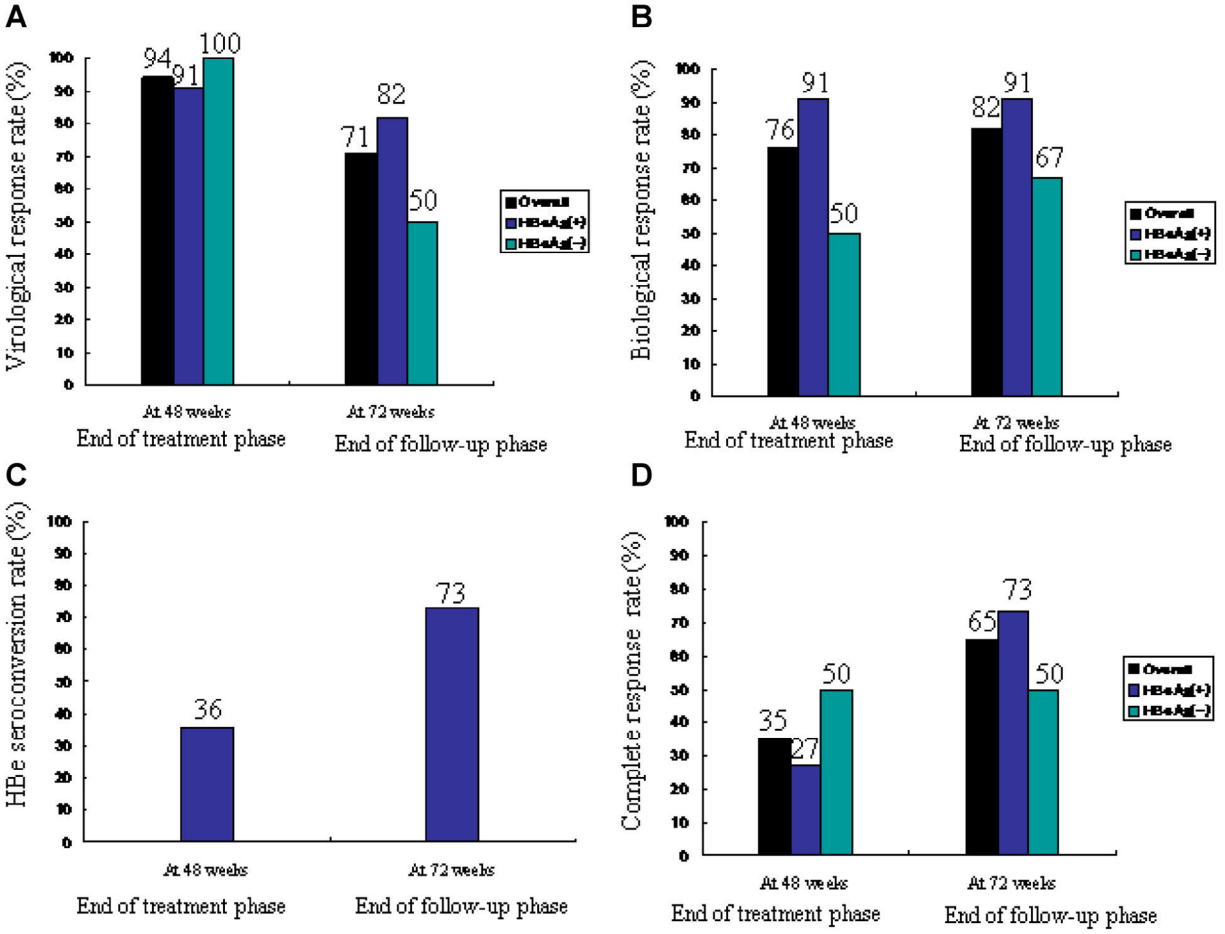

Fig. 1. Virological and biological response during and after combination therapy. **A**: Comparison of effective virological response (<4.0 log copies/ml) at the end of the treatment period with the response 24 weeks after treatment ended. **B**: Comparison of effective biological response (<40 IU/L) at the end of the treatment period with the response 24 weeks after treatment ended. **C**: Comparison of HBeAg seroconversion at the end of the treatment period with seroconversion 24 weeks after treatment. **D**: CR rates 24 weeks after the treatment period ended.

TABLE II. Summary of Therapy Effects at 48 and 72 Weeks

Serological and histological parameters	At 48 weeks	At 72 weeks
Serum HBV DNA reduction (log copies/ml, mean)	−5.2	−3.3
Serum HBV DNA <2.1 log copies/ml	14/17 (82%)	5/17 (29%)
Serum HBV DNA <4.0 log copies/ml	16/17 (94%)	12/17 (71%)
Serum HBsAg reduction (log IU/ml, mean)	−0.4	N.E.
Serum HBcrAg reduction (log U/ml, mean)	−0.7	N.E.
Serum HBV RNA reduction (log copies/ml, mean)	−2.0	N.E.
HBsAg seroconversion	0/17 (0%)	1/17 (6%)
HBeAg seroconversion	4/11 (36%)	8/11 (73%)
ALT improvement	14/17 (82%)	14/17 (82%)
ALT normalization	13/17 (76%)	14/17 (82%)
cccDNA reduction (log copies/μg, mean)	−1.4	N.E.
Inflammation score improved	14/17 (82%)	N.E.
Fibrosis score improved	5/17 (29%)	N.E.

HBsAg, hepatitis B surface antigen; IU, international unit; HBcrAg, hepatitis B core-related antigen; U, unit; HBeAg, hepatitis B e antigen; ALT, alanine aminotransferase; cccDNA, covalently closed circular DNA; N.E., not evaluable.

patients (73%) by the end of the follow-up phase (Fig. 1C); 65% achieved complete response (Fig. 1D).

Improved Histology and Decreased HBcAg-Positive Hepatocytes and cccDNA After Combination Therapy

Scores improved for inflammation in 14 patients (82%; Fig. 2A) and for fibrosis in five patients (29%; Fig. 2B) after combination treatment. These biopsies were used for simultaneous immunohistochemical analyses of HBcAg (Fig. 3). The median values and ranges of HBcAg-positive hepatocytes in each patient are listed in Supplementary Table I. The mean percentage of HBcAg-positive hepatocytes was 11.2% at baseline and 0.9% after the 48-week treatment phase. A decrease in hepatic cccDNA was observed in 14 of 17 patients (82%). The mean level of hepatocyte cccDNA decreased from 5.4 to 4.0 log copies/μg after the 48-week treatment period ($P = 0.007$, Fig. 4). In two patients, the level of cccDNA dropped dramatically by more than 3 log copies/μg after combination therapy. Each patient's chronic hepatitis B profile, including altered serum markers, HBV DNA, HBV RNA, and histological assessments, is listed in Supplementary Table I.

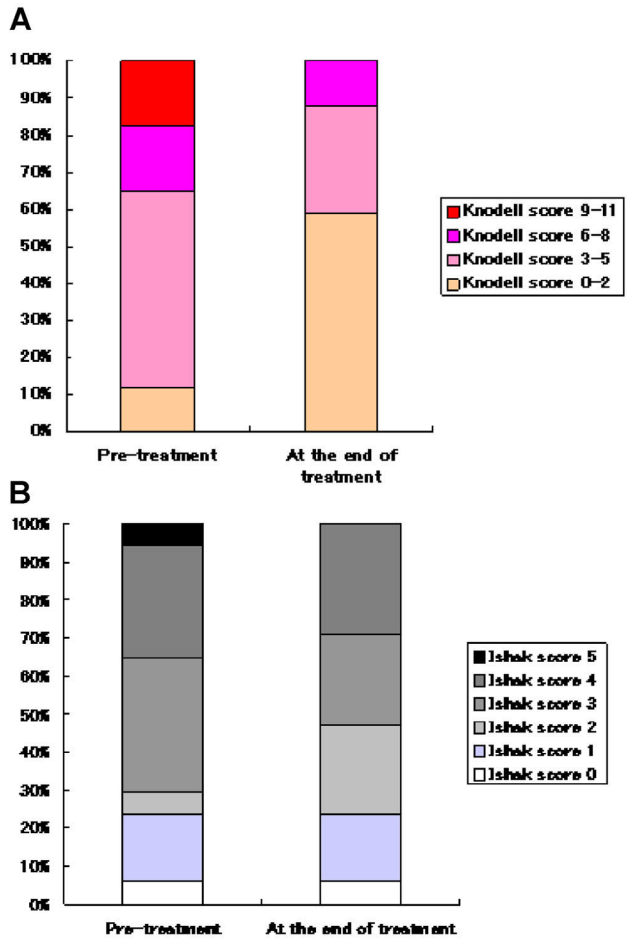

Fig. 2. Improved histology after combination therapy. Histology was evaluated before treatment initiation and at the end of the 48-week treatment period. Improved inflammation scores were evident in 14 patients (82%) (**A**), and improved fibrosis scores were evident in five patients (29%) (**B**).

Associations Among cccDNA, Relapse, and Serum Viral Markers at the End of the 48-week Treatment Period

The 14 patients who exhibited a decrease in serum DNA to less than 2.1 log copies/ml by the end of the 48-week treatment period were analyzed subsequently for associations between intrahepatic cccDNA and post-treatment relapse. Among the 14 patients with undetectable levels of serum HBV DNA at the end of treatment, 3 did not achieve virological response by the end of the follow-up phase; they were considered relapse cases of hepatitis. All three patients exhibited high levels of intrahepatic cccDNA (>4.5 log/copies/μg) by the end of the treatment. In contrast, only 2 of the 11 non-relapsed patients exhibited high levels of cccDNA by the end of the treatment period ($P = 0.027$, Table III). These data suggest that high levels of intrahepatic cccDNA can be interpreted as a risk factor for the relapse of hepatitis. However, by the end of the 48-week treatment period, cccDNA did not correlate significantly with serum viral markers (HBsAg, HBV RNA, and HBcrAg; date not shown).

Safety

The adverse effects in each patient are summarized in Supplementary Table I. During week 4 of the treatment period, patient No. 4 displayed obvious grade 3 neutropenia and the dose of PEG-IFN α-2b was reduced from 80 to 40 μg. During week 20 of the treatment period, patient No. 5 displayed obvious grade 3 thrombocytopenia and the dose of PEG-IFN α-2b also was reduced from 80 to 40 μg. Both patients were able to continue the treatment until week 48. During week 46, patient No. 10 experienced a grade 3 transient ischemic attack. Because the symptom potentially was caused by PEG-IFN α-2b, PEG-IFN α-2b administration was suspended in this patient and ETV was continued for the 2 weeks that remained in the treatment period. All adverse effects improved after the treatment was discontinued and no deaths occurred.

DISCUSSION

Thus far, several reports have described the effectiveness of combination therapies using PEG-IFN and either LVD or ADV to treat chronic hepatitis B [Chan et al., 2005; Lau et al., 2005; Wursthorn et al., 2006; Flink et al., 2007; Papadopoulos et al., 2009]. However, the therapeutic outcomes of the described approaches remain unsatisfactory. The objective of the present study was to evaluate the effectiveness of

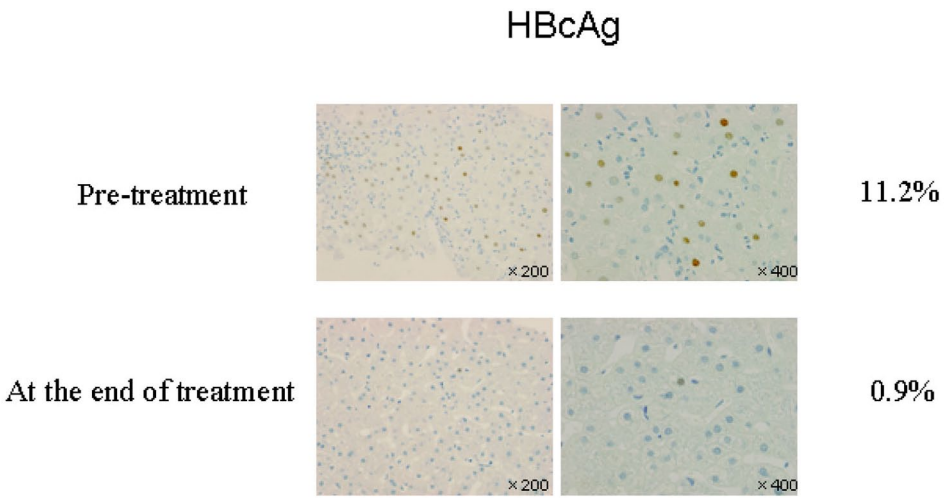

Fig. 3. Reduced quantity of HBcAg-positive hepatocytes after combination therapy. Liver biopsy samples were collected before and after the 48-week period of combination therapy; the data from a representative patient are shown. Liver sections were fixed with formalin, embedded in paraffin, and subjected to immunohistological staining with antiserum specific for HBcAg.

PEG-IFN α-2b and ETV combination therapy. The results indicated that combination therapy with ETV may bring about greater levels of HBV suppression than combination therapies that use other nucleotide analogues.

Among several potential nucleotide analogues, ETV was selected because reports have shown that it possesses stronger anti-viral activity and is less prone to resistant mutations than the other analogues [Chang et al., 2006; Colonno et al., 2006; Lai et al., 2006]. Thus, it is speculated that a combination approach with ETV presented significant promise for achieving persistent viral suppression after the completion of therapy, which is the ultimate goal of chronic hepatitis B treatment. In addition, the levels of intrahepatic cccDNA were evaluated because they may reflect the sustained antiviral effects of a drug directly, to determine the effects of combination therapy.

By the end of the treatment period, 94% of the patients achieved virological response. In addition, 76% (13/17) of the patients achieved biological response. Among the 11 patients who presented with HBeAg initially, 10 (91%) exhibited virological and biological response by the end of the therapy period. In addition, four patients (36%) exhibited HBe seroconversion, and thus, a complete response.

At the end of the follow-up phase, 12 patients (71%) exhibited a virological response, 82% exhibited a biological response rate, and the number of patients

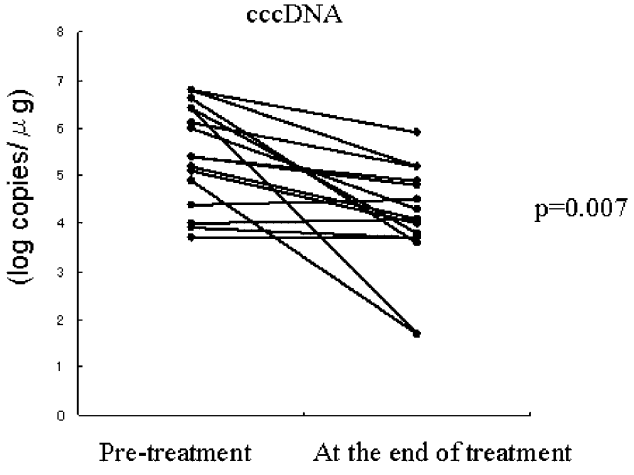

Fig. 4. Reduced levels of cccDNA after combination therapy. Each dot represents one patient, and each solid line represents the changed level of cccDNA in each patient.

TABLE III. Association Between Intrahepatic cccDNA Content and Relapse Rates

	Serum HBV DNA levels <2.1 log copies/ml at the end of the treatment (n = 14)		*P* value
	Cases with non-relapse (n = 11)	Cases with relapse (n = 3)	
No. of cases with high cccDNA level	2/11 (18%)	3/3 (100%)	0.027

Cases with a decrease in serum DNA concentrations to less than 2.1 log copies/ml at the end of the treatment were subjected to analysis. Relapse was defined as serum DNA ≥ 4.0 log at the end of follow-up.
Relapse: serum HBV DNA at 4.0 log copies/ml or higher at the end of follow-up.
Non-relapse: serum HBV DNA less than 4.0 log copies/ml at the end of follow-up.
P value by Fisher's exact test.
High cccDNA level: intrahepatic cccDNA ≥ 4.5 log at the end of treatment.

with a complete response increased to 65% (11/14). For HBeAg-positive patients, the number with a complete response increased from 3 of 11 (27%) at the end of the treatment phase to 8 of 11 (73%) at the end of the follow-up phase. It has been reported that IFN treatment can induce HBeAg seroconversion via immunological mechanisms during and after treatment [Lau, 2009]. From this perspective, the high percentage of patients who achieved complete response after the conclusion of combination therapy can be attributed primarily to the compensatory, immune-modulator effects of IFN.

Previously, the effectiveness of PEG-IFN α-2a monotherapy or combination therapy with LVD was compared among patients with HBeAg-positive chronic hepatitis B [Lau et al., 2005]. However, PEG-IFN α-2a monotherapy failed to reach the level of superiority of the combination therapy with regard to HBeAg seroconversion and virological response; HBeAg seroconversion occurred in 29–32% of patients treated with PEG-IFN α-2a monotherapy and in 27–29% of patients who received combination therapy (Supplementary Table II). Therefore, the authors concluded that combination therapy with LVD does not yield additive effects, and this conclusion supported the use of PEG-IFN α-2a monotherapy as the first-line treatment [Janssen et al., 2005; Lau et al., 2005]. In contrast, by replacing LVD with ETV, HBeAg seroconversion was observed in 73% of study patients at the end of the follow-up phase (week 72) and virological response in 82% of HBeAg-positive patients, which is significantly higher than that in the previous report. Furthermore, our definition of a "positive" virological response (<4.0 log copies/ml) was more strict than the previously reported definition (<5.0 log copies/ml), and therefore, it is speculated that the combination of PEG-IFN and EVT is more effective than the combination of PEG-IFN and LVD. The superiority of the PEG-IFN and ETV combination was observed even in HBeAg-negative patients. The biological and virological response rates of PEG-IFN alone was 59% and 43%, respectively, and the rates of a PEG-IFN and LVD combination were 60% and 44%, respectively (Supplementary Table II). In contrast, the biological and virological response rates to combined PEG-IFN and ETV treatment were 67% and 50%, respectively. Based on the response levels of ALT and HBV DNA in our cohort, all HBeAg-positive patients who had achieved virological and biological response also exhibited HBeAg seroconversion at the end of the follow-up phase and vice versa. From this perspective, achievement of both virological and biological response at the end of follow-up phase was considered to be critical to HBeAg-positive and HBeAg-negative patients. Therefore, the definition of complete response was modified to include HBeAg-negative patients and the overall complete response ratio was calculated. In the present cohort, 65% achieved complete response (Fig. 4D), which was considerably high for the treatment of chronic hepatitis B. Considering these data, it is speculated that PEG-IFN and ETV may function as a more powerful and ideal combination treatment that yields additive effects.

Recent studies have shown that relapse of hepatitis sometimes occurs after antiviral therapy is discontinued, even in patients who exhibited decreased levels of serum HBV DNA, because of the protracted half-life of cccDNA in infected hepatocytes [Moraleda et al., 1997; Le Guerhier et al., 2000; Mommeja-Marin et al., 2003; Werle-Lapostolle et al., 2004; Sung et al., 2005; Laras et al., 2006]. Therefore, a critical component of any assessment of anti-HBV therapy is the reduction of intrahepatic cccDNA. In the present study, intrahepatic cccDNA dropped by a mean of 1.4 log copies/μg by the end of the treatment period.

This study investigated the relationship between intrahepatic cccDNA at the end of the treatment period and viral reactivation at the end of the follow-up phase in patients with undetectable levels of serum HBV DNA at the end of the treatment period. All relapsed patients displayed high levels of intrahepatic cccDNA (≥4.5 log copies/μg) at the end of the treatment period, whereas, only 2 of the 11 non-relapse patients displayed high levels of intrahepatic cccDNA. The findings from both the present study and previous reports [Moraleda et al., 1997; Le Guerhier et al., 2000; Werle-Lapostolle et al., 2004; Laras et al., 2006] support the notion that cccDNA levels predict long-term suppression of HBV more accurately than serum HBV DNA. Subsequently, non-invasive serum markers that may reflect intrahepatic levels of cccDNA were evaluated. The mechanism of action of nucleotide analogues barely influences the transcription of cccDNA to mRNA or translation to various viral proteins. Therefore, treatment with nucleotide analogues should still allow HBsAg, HBcrAg [Rokuhara et al., 2003; Tanaka et al., 2008; Matsumoto et al., 2012], and HBV RNA levels to function as surrogate markers of intrahepatic cccDNA. Nevertheless, the levels of cccDNA did not correlate with any of these markers in this study. It is possible that maldistribution of cccDNA in liver tissue presents a critical issue to quantification. Therefore, the quantification of cccDNA from multiple liver biopsies from different sites would be ideal for determining the accurate level of cccDNA in each patient. However, because of ethical limitations, only one liver biopsy was performed on each patient and thus the distribution differences from single liver tissue samples could not be evaluated. Nevertheless, the amount of cccDNA observed before treatment initiation correlated significantly with serum HBV DNA ($r = 0.85$, $P < 0.001$) and serum HBsAg ($r = 0.70$, $P = 0.002$), and thus, the levels of cccDNA determined in this study are probably sound. Because of this study's limited number of patients, future studies may yield controversial results with regard to the levels of cccDNA, HBcrAg, and HBV RNA.

Further investigation should be conducted on a larger number of patients.

In summary, this study systematically analyzed the efficacy of a new combination therapy that consists of PEG-IFN α-2b and ETV administered over a 48-week period. In particular, the effectiveness of this combination approach was evident by decreases in intrahepatic cccDNA. Given the robustness of the data, these results are clinically significant with respect to the achievement of sustained viral response, which is the ultimate goal for chronic hepatitis B treatment. However, further investigation is needed on a larger number of patients and to compare combination therapy to PEG-IFN monotherapy. To address these important issues, and validate the results of the present study, a prospective multicenter trial of patients using combination therapy will be conducted.

REFERENCES

Allice T, Cerutti F, Pittaluga F, Varetto S, Gabella S, Marzano A, Franchello A, Colucci G, Ghisetti V. 2007. COBAS AmpliPrep-COBAS TaqMan hepatitis B virus (HBV) test: A novel automated real-time PCR assay for quantification of HBV DNA in plasma. J Clin Microbiol 45:828–834.

Arase Y, Tsubota A, Saitoh S, Suzuki Y, Kobayashi M, Suzuki F, Someya T, Akuta N, Ikeda K, Kobayashi M, Kumada H. 2002. Randomized, controlled trial of natural interferon-alpha therapy for e-antigen-positive chronic hepatitis B patients. Hepatol Res 23:98–104.

Chan HL, Leung NW, Hui AY, Wong VW, Liew CT, Chim AM, Chan FK, Hung LC, Lee YT, Tam JS, Lam CW, Sung JJ. 2005. A randomized, controlled trial of combination therapy for chronic hepatitis B: Comparing pegylated interferon-alpha2b and lamivudine with lamivudine alone. Ann Intern Med 142:240–250.

Chang TT, Gish RG, de Man R, Gadano A, Sollano J, Chao YC, Lok AS, Han KH, Goodman Z, Zhu J, Cross A, DeHertogh D, Wilber R, Colonno R, Apelian D. BEHoLD AI463022 Study Group. 2006. A comparison of entecavir and lamivudine for HBeAg-positive chronic hepatitis B. N Engl J Med 354:1001–1010.

Colonno RJ, Rose R, Baldick CJ, Levine S, Pokornowski K, Yu CF, Walsh A, Fang J, Hsu M, Mazzucco C, Eggers B, Zhang S, Plym M, Klesczewski K, Tenney DJ. 2006. Entecavir resistance is rare in nucleotide naïve patients with hepatitis B. Hepatology 44:1656–1665.

Dienstag JL, Perrillo RP, Schiff ER, Bartholomew M, Vicary C, Rubin M. 1995. A preliminary trial of lamivudine for chronic hepatitis B infection. N Engl J Med 333:1657–1661.

Flink HJ, Buster EH, Merican I, Nevens F, Kitis G, Cianciara J, de Vries RA, Hansen BE, Schalm SW, Janssen HL. 2007. Relapse after treatment with peginterferon alpha-2b alone or in combination with lamivudine in HBeAg positive chronic hepatitis B. Gut 56:1485–1486.

Hadziyannis SJ, Tassopoulos NC, Heathcote EJ, Chang TT, Kitis G, Rizzetto M, Marcellin P, Lim SG, Goodman Z, Wulfsohn MS, Xiong S, Fry J, Brosgart CL, Adefovir Dipivoxil 438 Study Group. 2003. Adefovir dipivoxil for the treatment of hepatitis B e antigen-negative chronic hepatitis B. N Engl J Med 348:800–807.

Ishak K, Baptista A, Bianchi L, Callea F, De Groote J, Gudat F, Denk H, Desmet V, Korb G, MacSween RN. 1995. Histological grading and staging of chronic hepatitis. J Hepatol 22:696–699.

Janssen HL, van Zonneveld M, Senturk H, Zeuzem S, Akarca US, Cakaloglu Y, Simon C, So TM, Gerken G, de Man RA, Niesters HG, Zondervan P, Hansen B, Schalm SW. 2005. Pegylated interferon alfa-2b alone or in combination with lamivudine for HBeAg-positive chronic hepatitis B: A randomised trial. Lancet 365:123–129.

Kimura T, Rokuhara A, Sakamoto Y, Yagi S, Tanaka E, Kiyosawa K, Maki N. 2002. Sensitive enzyme immunoassay for hepatitis B virus core-related antigens and their correlation to virus load. J Clin Microbiol 40:439–445.

Knodell RG, Ishak KG, Black WC, Chen TS, Craig R, Kaplowitz N, Kiernan TW, Wollman J. 1981. Formulation and application of a numerical scoring system for assessing histological activity in asymptomatic chronic active hepatitis. Hepatology 1:431–435.

Lai CL, Chien RN, Leung NW, Chang TT, Guan R, Tai DI, Ng KY, Wu PC, Dent JC, Barber J, Stephenson SL, Gray DF. 1998. A one-year trial of lamivudine for chronic hepatitis B. Asia Hepatitis Lamivudine Study Group. N Engl J Med 339:61–68.

Lai CL, Ratziu V, Yuen MF, Poynard T. 2003. Viral hepatitis B. Lancet 362:2089–2094.

Lai CL, Shouval D, Lok AS, Chang TT, Cheinquer H, Goodman Z, DeHertogh D, Wilber R, Zink RC, Cross A, Colonno R, Fernandes L, BEHoLD AI463027 Study Group. 2006. Entecavir versus lamivudine for patients with HBeAg-negative chronic hepatitis B. N Engl J Med 354:1011–1020.

Laras A, Koskinas J, Dimou E, Kostamena A, Hadziyannis SJ. 2006. Intrahepatic levels and replicative activity of covalently closed circular hepatitis B virus DNA in chronically infected patients. Hepatology 44:694–702.

Lau GK. 2009. HBeAg-positive chronic hepatitis B: Why do I treat my patients with pegylated interferon. Liver Int 29:125–129.

Lau GK, Piratvisuth T, Luo KX, Marcellin P, Thongsawat S, Cooksley G, Gane E, Fried MW, Chow WC, Paik SW, Chang WY, Berg T, Flisiak R, McCloud P, Pluck N, Peginterferon Alfa-2a HBeAg-Positive Chronic Hepatitis B Study Group. 2005. Peginterferon Alfa-2a, lamivudine, and the combination for HBeAg-positive chronic hepatitis B. N Engl J Med 352:2682–2695.

Le Guerhier F, Pichoud C, Guerret S, Chevallier M, Jamard C, Hantz O, Li XY, Chen SH, King I, Trépo C, Cheng YC, Zoulim F. 2000. Characterization of the antiviral effect of 2',3'-dideoxy-2', 3'-didehydro-beta-L-5-fluorocytidine in the duck hepatitis B virus infection model. Antimicrob Agents Chemother 44:111–122.

Leung NW, Lai CL, Chang TT, Guan R, Lee CM, Ng KY, Lim SG, Wu PC, Dent JC, Edmundson S, Condreay LD, Chien RN, Asia Hepatitis Lamivudine Study Group. 2001. Extended lamivudine treatment in patients with chronic hepatitis B enhances hepatitis B e antigen seroconversion rates: Results after 3 years of therapy. Hepatology 33:1527–1532.

Lok AS, Lai CL, Leung N, Yao GB, Cui ZY, Schiff ER, Dienstag JL, Heathcote EJ, Little NR, Griffiths DA, Gardner SD, Castiglia M. 2003. Long-term safety of lamivudine treatment in patients with chronic hepatitis B. Gastroenterology 125:1714–1722.

Marcellin P, Chang TT, Lim SG, Tong MJ, Sievert W, Shiffman ML, Jeffers L, Goodman Z, Wulfsohn MS, Xiong S, Fry J, Brosgart CL, Adefovir Dipivoxil 437 Study Group. 2003. Adefovir dipivoxil for the treatment of hepatitis B e antigen-positive chronic hepatitis B. N Engl J Med 348:808–816.

Matsumoto A, Tanaka E, Suzuki Y, Kobayashi M, Tanaka Y, Shinkai N, Hige S, Yatsuhashi H, Nagaoka S, Chayama K, Tsuge M, Yokosuka O, Imazeki F, Nishiguchi S, Saito M, Fujiwara K, Torii N, Hiramatsu N, Karino Y, Kumada H. 2012. Combination of hepatitis B viral antigens and DNA for prediction of relapse after discontinuation of nucleos(t)ide analogs in patients with chronic hepatitis B. Hepatol Res 42:139–149.

Mommeja-Marin H, Mondou E, Blum MR, Rousseau F. 2003. Serum HBV DNA as a marker of efficacy during therapy for chronic HBV infection: Analysis and review of the literature. Hepatology 37:1309–1319.

Moraleda G, Saputelli J, Aldrich CE, Averett D, Condreay L, Mason WS. 1997. Lack of effect of antiviral therapy in nondividing hepatocyte cultures on the closed circular DNA of woodchuck hepatitis virus. J Virol 71:9392–9399.

Newbold JE, Xin H, Tencza M, Sherman G, Dean J, Bowden S, Locarnini S. 1995. The covalently closed duplex from of the hepadnavirus genome exists in situ as a heterogeneous population of viral minichromosomes. J Virol 69:3350–3357.

Papadopoulos VP, Chrysagis DN, Protopapas AN, Goulis IG, Dimitriadis GT, Mimidis KP. 2009. Peginterferon alfa-2b as monotherapy or in combination with lamivudine in patients with HBeAg-negative chronic hepatitis B: A randomised study. Med Sci Monit 15:56–61.

Rokuhara A, Tanaka E, Matsumoto A, Kimura T, Yamaura T, Orii K, Sun X, Yagi S, Maki N, Kiyosawa K. 2003. Clinical evaluation of a new enzyme immunoassay for hepatitis B virus core-

related antigen; a marker distinct from viral DNA for monitoring lamivudine treatment. J Viral Hepat 10:324–330.

Rokuhara A, Matsumoto A, Tanaka E, Umemura T, Yoshizawa K, Kimura T, Maki N, Kiyosawa K. 2006. Hepatitis B virus RNA is measurable in serum and can be a new marker for monitoring lamivudine therapy. J Gastroenterol 41:785–790.

Sung JJ, Wong ML, Bowden S, Liew CT, Hui AY, Wong VW, Leung NW, Locarnini S, Chan HL. 2005. Intrahepatic hepatitis B virus covalently closed circular DNA can be a predictor of sustained response to therapy. Gastroenterology 128:1890–1897.

Tanaka E, Matsumoto A, Yoshizawa K, Maki N. 2008. Hepatitis B core-related antigen assay is useful for monitoring the antiviral effects of nucleoside analogue therapy. Intervirology 51:3–6.

Werle-Lapostolle B, Bowden S, Locarnini S, Wursthorn K, Petersen J, Lau G, Trepo C, Marcellin P, Goodman Z, Delaney WE IV, Xiong S, Brosgart CL, Chen SS, Gibbs CS, Zoulim F. 2004. Persistence of cccDNA during the natural history of chronic hepatitis B and decline during adefovir dipivoxil therapy. Gastroenterology 126:1750–1758.

Wu TT, Coates L, Aldrich CE, Summers J, Mason WS. 1990. In hepatocytes infected with duck hepatitis B virus, the template for viral RNA synthesis is amplified by an intracellular pathway. Virology 175:255–261.

Wursthorn K, Lutgehetmann M, Dandri M, Volz T, Buggisch P, Zollner B, Longerich T, Schirmacher P, Metzler F, Zankel M, Fischer C, Currie G, Brosgart C, Petersen J. 2006. Peginterferon alpha-2b plus adefovir induce strong cccDNA decline and HBsAg reduction in patients with chronic hepatitis B. Hepatology 44:675–684.

Yuen MF, Sablon E, Hui CK, Yuan HJ, Decraemer H, Lai CL. 2001. Factors associated with hepatitis B virus DNA breakthrough in patients receiving prolonged lamivudine therapy. Hepatology 34:785–791.

Yuen MF, Seto WK, Chow DH, Tsui K, Wong DK, Ngai VW, Wong BC, Fung J, Yuen JC, Lai CL. 2007. Long-term lamivudine therapy reduces the risk of long-term complications of chronic hepatitis B infection even in patients without advanced disease. Antivir Ther 12:1295–1303.

Liver Cancer

Liver Cancer 2013;2:69–72
DOI: 10.1159/000343842
Published online: April 15, 2013

2235-1795/13/0022-0069$38.00/0
www.karger.com/lic

Editorial

Early Hepatocellular Carcinoma: Definition and Diagnosis

Prof. M. Kudo

Editor *Liver Cancer*

Early hepatocellular carcinoma (HCC) can be described as "early" according to its pathological characteristics as well as its clinical characteristics. Taking the pathological approach first, the term "early" implies that a lesion is at a relatively early stage of carcinogenesis and prognosis is still good. Well-differentiated HCC is not necessarily early HCC. According to the clinical approach, the term "early" is used to differentiate HCC diagnosed in its early developmental stage from that diagnosed at more advanced stages. The clinical approach to diagnosing early HCC is used preferentially in the United States and Europe and, in general, this conceptualization of early HCC refers to tumors smaller than 3 cm and three or fewer in number at stage A (early stage) with respect to Barcelona Clinic Liver Cancer staging, although it sometimes includes solitary tumors up to 5 cm in size, as defined in the Milan criteria. Both very early and early stage tumors are relatively small, but both are hypervascular in the arterial phase and are regarded as classic HCC.

The pathological approach, however, defines early HCC as HCC in the early stage of carcinogenesis (generally ≤2 cm) that is often hypovascular with irregular boundaries on diagnostic imaging and contains portal elements without significantly affecting the original structure of the liver. The pathological characteristics of HCC include its multistep progression from a low-grade to a high-grade dysplastic nodule, to early HCC, and eventually to classic hypervascular HCC [1](fig.1). Accordingly, the accurate diagnosis and proper treatment of early HCC, a precursor of classic (typical) HCC, is extremely important. Therefore, I will discuss here the pathological aspects of early HCC.

According to the General Rules for the Clinical and Pathological Study of Primary Liver Cancer developed by the Liver Cancer Study Group of Japan [2], early HCC is defined as follows. Early HCC exhibits focal structural abnormalities such as acinar or pseudoglandular structures, broken or irregular trabecular alignment, and/or obvious invasion of the stromal tissue. Cellular atypia is usually unremarkable, but the nuclear–cytoplasmic ratio is increased due to decreased amounts of cytoplasm. The cytoplasm also shows eosinophilia or basophilia. The cell density may be more than twice that of the surrounding non-cancerous liver tissue. In addition, lesions often exhibit fatty changes or clear cell changes. Because the cancer cells of early HCCs do not grow expansively, they instead proliferate by replacing ad-

Liver Cancer

Liver Cancer 2013;2:69–72
DOI: 10.1159/000343842
Published online: April 15, 2013

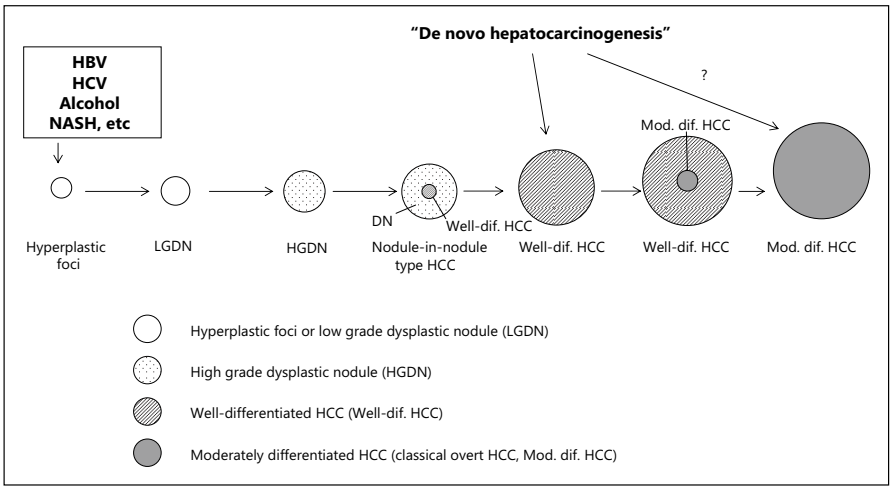

Fig. 1. Schematic representation of multistep progression of human hepatocarcinogenesis. HBV= hepatitis B virus; HCV=hepatitis C virus; NASH=nonalcoholic steatohe patitis.

jacent hepatocytes in a trabecular arrangement at the boundary with surrounding liver tissues, resulting in a poorly demarcated margin. Macroscopically, the lesions are classified as small nodules with indistinct margins [3]. These criteria for early HCC have already gained international consensus [4] and have been incorporated into the World Health Organization's latest "blue book" on digestive system tumors [5]. In addition, several molecular markers for the pathological diagnosis of early HCC have been identified, including heat-shock protein 70 (HSP70) [6], glypican-3 (GPC3) [7], glutamine synthetase (GS), cyclase-associated protein 2, and Bmi-1. Using HSP70, GPC3, and GS markers in combination, the sensitivity and specificity of early HCC diagnosis can be as high as 72 and 100%, respectively [8].

However, accurate differentiation of early HCC from dysplastic nodules is possible only when stromal invasion is found in resected specimens. In other words, differential diagnosis between early HCC and dysplastic nodules is often not possible without the findings of stromal invasion on biopsy. Differentiating between these two types of lesions with imaging used to be challenging, even when using computed tomography (CT) during hepatic arteriography/CT during arterial portography (CTHA/CTAP).

However, the subsequent introduction of gadolinium (Gd)-ethoxybenzyl (EOB)-diethylenetriamine pentaacetic acid (DTPA)-enhanced magnetic resonance imaging (Gd-EOB MRI) has proven to be a major breakthrough in the diagnosis of early HCC. Gd-EOB-DTPA is endocytosed into liver cells via organic anion transporter 8 [9, 10]. Because early HCC appears on Gd-EOB MRI images as a hypointense nodular lesion and a dysplastic nodule appears as an iso- or hyperintense lesion on the hepatobiliary phase, the diagnostic accuracy of early HCC is now generally ≥95% [11–13]. Moreover, previous studies have followed up the natural course of hypovascular nodules with hypointense signals on the Gd-EOB MRI hepatobiliary phase and reported that, even if early HCC is ruled out on biopsy, there is a high probability that this type of hypovascular nodule will undergo hypervascular change and transform into typical HCC [14–16]. In other words, even if biopsy excludes early HCC, hypovascular nodules that are hypointense on the Gd-EOB MRI hepatobiliary phase may be regarded as early HCC. At any rate, such lesions can be considered as nodular lesions with a high potential to transform to HCC.

Liver Cancer

Liver Cancer 2013;2:69–72

DOI: 10.1159/000343842
Published online: April 15, 2013

Reflecting this clinical background, the HCC clinical practice guidelines used in Japan [17] already include a specific algorithm for the diagnosis and treatment of early HCC, whereas the HCC clinical practice guidelines used in the United States and Europe (AASLD and EASL-EORTC guidelines [18, 19]), as well as those in other Asian countries [20], do not contain criteria for the diagnosis and treatment of early HCC. This is a clear indication that, compared with other countries, HCC screening and diagnostic skills are well advanced in Japan, owing in large part to the sophisticated nationwide surveillance system for HCC [21]. Developing measures to identify hypervascular HCCs while they are still curable is currently the biggest challenge facing the United States, Europe, and other Asian countries, where effective nationwide surveillance systems for HCC have not been established. In contrast, the current focus in Japan, where small hypervascular HCCs are routinely diagnosed, is to differentiate early HCC correctly from dysplastic nodules and to develop effective treatment for early HCC defined in accordance with its pathological conceptualization. It is not an overstatement to say that the large gap between Japan's HCC screening/diagnostic capabilities and those of other countries manifests as a large difference in awareness and management of early HCC.

In conclusion, we sincerely hope that other countries will follow the Japanese approach and develop effective nationwide surveillance systems for HCC and join us in constructive dialog aimed at improving the diagnosis and treatment of early HCC.

References

1 Kudo M: Multistep human hepatocarcinogenesis: correlation of imaging with pathology. J Gastroenterol 2009;44(Suppl 19):112–118.
2 Liver Cancer Study Group of Japan: General rules for the clinical and pathological study of primary liver cancer, 3rd English edition. Kanehara & Co., Ltd. Tokyo, 2010.
3 Sakamoto M, Hirohashi S, Shimosato Y: Early stages of multistep hepatocarcinogenesis: adenomatous hyperplasia and early hepatocellular carcinoma. Hum Pathol 1991;22:172–178.
4 Kojiro M, Wanless I, Alves V, et al: Pathologic diagnosis of early hepatocellular carcinoma: a report of the international consensus group for hepatocellular neoplasia. Hepatology 2009;49:658–664.
5 Theise ND, Park YN, Curado MP, Sakamoto M, Franceschi S, Torbenson M, Hytiroglou P, Wee A, Kudo M: Hepatocellular carcinoma. WHO Classification of tumours of the Digestive System, 4th Edition, International Agency for Research on Cancer, Lyon. 2010:205–216.
6 Chuma M, Sakamoto M, Yamazaki K, Ohta T, Ohki M, Asaka M, Hirohashi S: Expression profiling in multistage hepatocarcinogenesis: identification of HSP70 as a molecular marker of early hepatocellular carcinoma. Hepatology 2003;37:198–207.
7 Libbrecht L, Severi T, Cassiman D, Vander Borght S, Pirenne J, Nevens F, Verslype C, van Pelt J, Roskams T: Glypican-3 expression distinguishes small hepatocellular carcinomas from cirrhosis, dysplastic nodules, and focal nodular hyperplasia-like nodules. Am J Surg Pathol 2006;30:1405–1411.
8 Di Tommaso L, Franchi G, Park YN, Fiamengo B, Destro A, Morenghi E, Montorsi M, Torzilli G, Tommasini M, Terracciano L, Tornillo L, Vecchione R, Roncalli M: Diagnostic value of HSP70, glypican 3, and glutamine synthetase in hepatocellular nodules in cirrhosis. Hepatology 2007;45:725–734.
9 Narita M, Hatano E, Arizono S, Miyagawa-Hayashino A, Isoda H, Kitamura K, Taura K, Yasuchika K, Nitta T, Ikai I, Uemoto S: Expression of OATP1B3 determines uptake of Gd-EOB-DTPA in hepatocellular carcinoma. J Gastroenterol 2009;44:793–798.
10 Kitao A, Zen Y, Matsui O, Gabata T, Kobayashi S, Koda W, Kozaka K, Yoneda N, Yamashita T, Kaneko S, Nakanuma Y: Hepatocellular carcinoma: signal intensity at gadoxetic acid-enhanced MR Imaging–correlation with molecular transporters and histopathologic features. Radiology 2010;256:817–826.
11 Sano K, Ichikawa T, Motosugi U, Sou H, Muhi AM, Matsuda M, Nakano M, Sakamoto M, Nakazawa T, Asakawa M, Fujii H, Kitamura T, Enomoto N, Araki T: Imaging study of early hepatocellular carcinoma: usefulness of gadoxetic acid-enhanced MR imaging. Radiology 2011;261:834–844.
12 Kudo M: The 2008 Okuda lecture: Management of hepatocellular carcinoma: From surveillance to molecular targeted therapy. J Gastroenterol Hepatol 2010;25:439–452.
13 Kitao A, Matsui O, Yoneda N, Kozaka K, Shinmura R, Koda W, Kobayashi S, Gabata T, Zen Y, Yamashita T, Kaneko S, Nakanuma Y: The uptake transporter OATP8 expression decreases during multistep hepatocarcinogenesis: correlation with gadoxetic acid enhanced MR imaging. Eur Radiol 2011;21:2056–2066.
14 Motosugi U, Ichikawa T, Sano K, Sou H, Onohara K, Muhi A, Amemiya F, Enomoto N, Matsuda M, Fujii H, Araki T: Outcome of hypovascular hepatic nodules revealing no gadoxetic acid uptake in patients with chronic liver disease. J Magn Reson Imaging 2011;34:88–94.

Liver Cancer

Liver Cancer 2013;2:69–72
DOI: 10.1159/000343842
Published online: April 15, 2013

15 Kumada T, Toyoda H, Tada T, Sone Y, Fujimori M, Ogawa S, Ishikawa T: Evolution of hypointense hepatocellular nodules observed only in the hepatobiliary phase of gadoxetate disodium-enhanced MRI. AJR Am J Roentgenol 2011;197:58–63.
16 Kobayashi S, Matsui O, Gabata T, Koda W, Minami T, Ryu Y, Kawai K, Kozaka K: Gadolinium ethoxybenzyl diethylenetriamine pentaacetic acid-enhanced magnetic resonance imaging findings of borderline lesions at high risk for progression to hypervascular classic hepatocellular carcinoma. J Comput Assist Tomogr 2011;35:181–186.
17 Kudo M, Izumi N, Kokudo N, Matsui O, Sakamoto M, Nakashima O, Kojiro M, Makuuchi M: Management of hepatocellular carcinoma in Japan: Consensus-Based Clinical Practice Guidelines proposed by the Japan Society of Hepatology (JSH) 2010 updated version. Dig Dis 2011;29:339–364.
18 Bruix J, Sherman M: Management of hepatocellular carcinoma: An update. Hepatology 2011;53:1020–1022.
19 Llovet JM, Ducreux M, et al: EASL-EORTC clinical practice guidelines: management of hepatocellular carcinoma. J Hepatol 2012;56:908–943.
20 Omata M, Lesmana LA, Tateishi R, Chen PJ, Lin SM, Yoshida H, Kudo M, Lee JM, Choi BI, Poon RT, Shiina S, Cheng AL, Jia JD, Obi S, Han KH, Jafri W, Chow P, Lim SG, Chawla YK, Budihusodo U, Gani RA, Lesmana CR, Putranto TA, Liaw YF, Sarin SK: Asian Pacific Association for the Study of the Liver consensus recommendations on hepatocellular carcinoma. Hepatol Int 2010;4:439–474.
21 Kudo M: Japan's successful model of nationwide hepatocellular carcinoma surveillance highlighting the urgent need for global surveillance. Liver Cancer 2012;1:141–143.

Granulocytic sarcoma of the jejunum diagnosed by biopsies during double-balloon endoscopy before treatment (with video)

A 56-year-old man was admitted to Saku Central Hospital as a result of repeated vomiting. He was afebrile and tender in the upper abdomen. Computed tomography showed an enhancing mass lesion (well contrasted by a radiopaque substance), 50 mm in diameter, arising from the small intestine and dilatation of its oral side. Double-balloon endoscopy (DBE) with oral approach revealed a circumferential tumorous lesion with obstruction (Fig. 1, left panel). Indigocarmine dye spray enhanced swelling villi of different sizes (Fig. 1, right panel). Biopsy specimens revealed diffuse infiltration of tumor cells, including mononuclear cells with polymorphisms and large nuclei with a few eosinophils (Fig. 2, left panel). Immunohistochemical tests revealed a definitive diagnosis of granulocytic sarcoma (GS) as a result of positive staining of granulocyte markers such as CD45 and CD68 (Fig. 2b, right panel). Bone marrow examinations revealed that the patient did not have leukemia, so he underwent surgical resection of the jejunum. Pathological diagnosis of the resected specimen was GS that invaded into the subserosa, and surgical margins were negative. The patient received adjuvant chemotherapy that comprised cytarabine and daunorubicin hydrochloride. He survives without recurrence 54 months later.

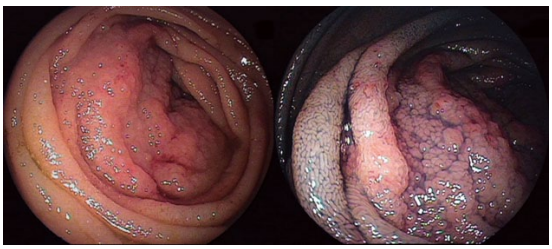

Figure 1 (Left panel) Double-balloon endoscopy with oral approach revealed circumferential tumorous lesion with obstruction. (Right panel) Indigocarmine dye spray enhanced swelling villi of different sizes.

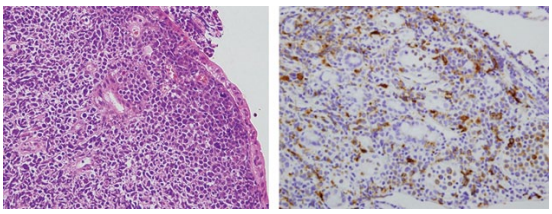

Figure 2 (Left panel) Biopsy specimens revealed diffuse infiltration of tumor cells, including mononuclear cells with polymorphisms and large nuclei with a few eosinophils (hematoxylin-eosin, original magnification ×400). (Right panel) Immunohistochemical tests of CD68 revealed a definitive diagnosis of granulocytic sarcoma as a result of positive staining of granulocyte markers (CD68, original magnification ×400).

GS is defined as a localized tumor composed of myeloid blasts and immature myeloid cells at an extramedullary site.[1] The proportion of GS found in the small intestine was reported to be approximately 10% of all sites. GS typically occurs concomitant with or after the onset of acute myeloid leukemia.[1] There has been only one case that was diagnosed by endoscopic biopsy before surgery.[2] To the best of our knowledge, this is the first case that could be diagnosed by biopsy using DBE before surgery.

Authors declare no conflict of interests for this article.

Kinichi Hotta[1,2] and Kenji Kunieda[2]
[1]Division of Endoscopy, Shizuoka Cancer Center, Shizuoka and [2]Department of Gastroenterology, Saku Central Hospital, Saku, Japan
doi: 10.1111/den.12107

REFERENCES

1 Yamauchi K, Yasuda M. Comparison in treatments of nonleukemic granulocytic sarcoma: Report of two cases and a review of 72 cases in the literature. *Cancer* 2002; **94**: 1739–46.
2 Corpechot C, Lemann M, Brocheriou I *et al*. Granulocytic sarcoma of the jejunum: a rare cause of small bowel obstruction. *Am. J. Gastroenterol.* 1998; **93**: 2586–8.

SUPPORTING INFORMATION

ADDITIONAL SUPPORTING INFORMATION may be found in the online version of this article at the publisher's web-site:
Video S1 Demonstrated observation of a granulocytic sarcoma by double-balloon endoscopy with oral approach.

Senile systemic amyloidosis localized to the stomach

A 71-year-old woman was admitted with a 3-month history of nausea and epigastric discomfort. Gastrointestinal endoscopy revealed a tumorous lesion that looked like gastric cancer at the lower gastric body (Fig. 1). Histological examination of the biopsy specimens showed deposition of amorphous, homogeneous and acidophilic material in the gastric

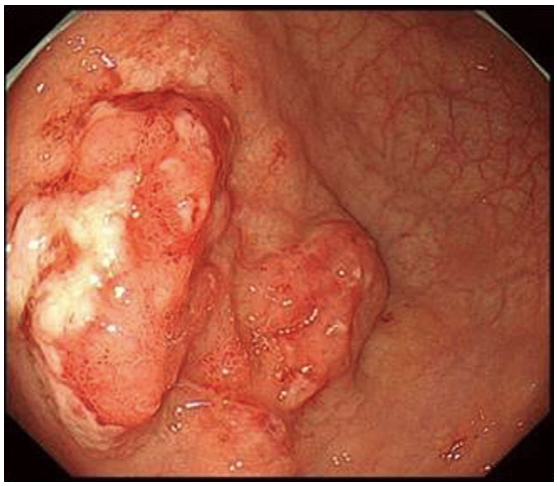

Figure 1 Endoscopy reveals a tumor at the inferior part of the gastric corpus mimicking an advanced gastric cancer.

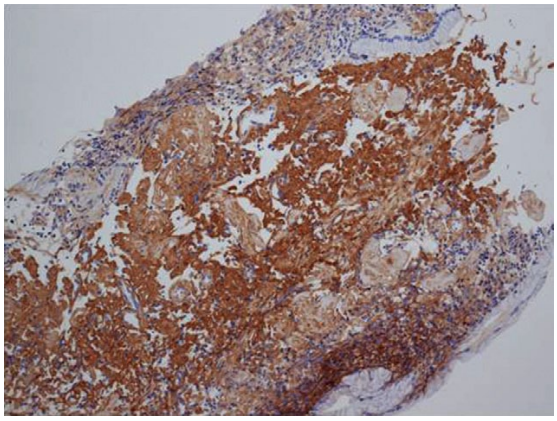

Figure 2 Tumor is strongly positive for transthyretin staining.

mucosa. This substance was proven to be amyloid as it was positive for Congo red staining and presented green birefringence under polarized light. Immunohistochemistry was strongly positive for transthyretin (Fig. 2) while being negative for kappa or lambda light chains, which was consistent with the diagnosis of senile systemic amyloidosis (SSA).

Endoscopic examination and biopsy sampling of the esophagus, duodenum, colon, and rectum excluded other gastrointestinal disorders. The liver and kidneys looked normal on computed tomography scan and on blood examination. A diagnosis of SSA was made, although the lesion was localized to the stomach. Amyloidosis is a disorder characterized by extracellular deposition of amyloid in various tissues and organs. It consists of at least four different types that are discriminated by the type of amyloid substance deposited: amyloid light-chain protein (AL), amyloid A (AA), amyloid β2-microglobulin (Aβ2M) in hemodialysis amyloidosis, and amyloidogenic transthyretin (ATTR) in some types of familial amyloidosis and senile systemic amyloidosis.[1]

Endoscopic findings in gastric amyloidosis are nonspecific, including erosion, ulcers, gastric cancer-mimicking lesions, and submucosal tumor-like lesions.[2,3] In the stomach, the deposition of AL amyloid as primary and solitary amyloidosis has been reported to be the most frequent.[4]

As far as the authors know, there has been no case report of senile systemic amyloidosis localized to the stomach. We suspect that such cases might have been misdiagnosed as AL amyloid if sufficient examination including staining for transthyretin had not been carried out.

Authors declare no conflict of interests for this article.

Shigenaga Matsui, Hiroshi Kashida and Masatoshi Kudo
Department of Gastroenterology and Hepatology, Kinki University, Osaka, Japan
doi: 10.1111/den.12121

REFERENCES

1 Sipe JD, Benson MD, Buxbaum JN *et al*. Amyloid fibril protein nomenclature: 2010 recommendations from the nomenclature committee of the International Society of Amyloid. *Amyloid* 2010; **17**: 101–4.
2 Tada S, Iida M, Iwashita A. Endoscopic and biopsy findings of the upper digestive tract in patients with amyloidosis. *Gastrointest. Endosc.* 1990; **36**: 10–4.
3 Ebert EC, Nagar M. Gastrointestinal manifestations of amyloidosis. *Am. J. Gastroenterol.* 2008; **103**: 776–87.
4 Yamada M, Hatakeyama S, Tsukagoshi H *et al*. Gastrointestinal amyloid deposition in AL (primary or myeloma-associated) and AA (secondary) amyloidosis: Diagnostic value of gastric biopsy. *Hum. Pathol.* 1985; **16**: 1206–11.

Unusual rectal bleeding caused by penetration of an intra-pelvic migrated guide pin

A 74-year-old man presented to our clinic because of intermittent episodes of blood per rectum for a week shortly after walking. The patient underwent open reduction and internal fixation for a left hip fracture 1 year ago. He had to walk on crutches after recovery from the surgery. There was no previous history of gastrointestinal hemorrhage or bowel habit change. Physical examination revealed no abdominal tenderness and no rebounding pain. Colonoscopy disclosed a metal wire piercing through the upper rectum resulting in a shallow

Dig Dis Sci (2013) 58:2337–2344
DOI 10.1007/s10620-013-2627-8

ORIGINAL ARTICLE

Association of Gankyrin and Stemness Factor Expression in Human Colorectal Cancer

Hiromasa Mine · Toshiharu Sakurai · Hiroshi Kashida · Shigenaga Matsui · Naoshi Nishida · Tomoyuki Nagai · Satoru Hagiwara · Tomohiro Watanabe · Masatoshi Kudo

Received: 7 December 2012 / Accepted: 26 February 2013 / Published online: 19 March 2013

Abstract
Background It is widely accepted that the adenoma-carcinoma sequence represents the process by which most colorectal cancers (CRCs) arise. Although gankyrin is overexpressed in CRC tissues, its roles in the initiation step of colorectal carcinogenesis remain largely unexplored.
Aim We investigated the expression of gankyrin and stemness factors in human colorectal adenomas, precancerous lesions, as well as CRC tissues to assess its involvement in colorectal carcinogenesis.
Methods Expression of several molecules including gankyrin and certain stemness factors was compared in 50 pairs of adenoma and surrounding normal mucosa using real-time quantitative polymerase chain reaction and in 30 CRC tissues using immunohistochemistry.
Results In CRC specimens, expression of CD133, a cancer stem cell marker, was significantly correlated with gankyrin expression. Gankyrin knockdown decreased the expression of vascular endothelial growth factor (VEGF) and stemness factors such as Nanog and Oct-4 in colorectal cancer cells. Expression of gankyrin and these stemness factors was significantly higher in adenomas than in the surrounding normal mucosa. Importantly, a significant correlation was observed between the expression of gankyrin, VEGF, and Nanog in colorectal adenomas.
Conclusion In CRC development, gankyrin would control stem cell behavior by regulating the expression of stemness factors.

Keywords Stem cell · Nanog · PSMD10 · VEGF · Colorectal adenoma

Abbreviations

CRC	Colorectal cancer
VEGF	Vascular endothelial growth factor
LST	Laterally spreading tumor

Introduction

Colorectal cancer (CRC) is an important global health problem. Worldwide, this tumor is the third most commonly diagnosed malignancy after lung and breast cancer [1]. According to the concept of adenoma-carcinoma sequence, a large colorectal adenoma is recognized as a premalignant lesion. Recent molecular analysis has proposed that there are two broad categories of colorectal adenomas, that is, superficial and conventional polypoid tumors. Laterally spreading tumors (LSTs), large superficial tumors, are characterized by several features such as lateral spread, size greater than 10 mm, and malignant potential [2–4]. Although LSTs were initially recognized only in Japan, they have also been detected and accepted in Western countries in recent years [5, 6].

Electronic supplementary material The online version of this article (doi:10.1007/s10620-013-2627-8) contains supplementary material, which is available to authorized users.

H. Mine · T. Sakurai (✉) · H. Kashida · S. Matsui · N. Nishida · T. Nagai · S. Hagiwara · M. Kudo (✉)
Department of Gastroenterology and Hepatology, Kinki University, 377-2 Ohno-Higashi, Osaka-Sayama, Osaka 589-8511, Japan
e-mail: sakurai@med.kindai.ac.jp

M. Kudo
e-mail: m-kudo@med.kindai.ac.jp

T. Watanabe
Center for Innovation in Immunoregulative Technology and Therapeutics, Kyoto University Graduate School of Medicine, Kyoto, Japan

The concept that tumors are maintained by dedicated stem cells, the so-called cancer stem cell hypothesis, has attracted a lot of interest. According to this hypothesis, cancer cannot be viewed as simple monoclonal expansions of functionally equal tumor cells. Instead, only a small minority of tumor cells, the cancer stem cells or tumor-initiating cells, have the ability to maintain the malignant population [7, 8]. CD133, a 120 kDa transmembrane glycoprotein, is one of the most representative and reliable molecular markers for the characterization of colon cancer stem cells [9]. The stemness factor Nanog is expressed in many kinds of tumors such as germ cell tumors [10], hepatocellular carcinomas (HCC) [11] and CRC [12]. This factor may play a crucial role in maintaining self-renewal of cancer stem cells and initiating tumors [11]. It was reported that Nanog affects the promotion and progression of colorectal carcinogenesis events through enhanced proliferation, motility, and migration [12].

Gankyrin (also known as PSMD10, p28 and Nas6p) has been identified as an oncoprotein that is frequently overexpressed in human cancers such as HCCs [13] and CRCs [14]. One tumorigenic effect of gankyrin, a regulator of the 26S proteasome, is associated with its antiapoptotic property that is attributable, at least in part, to increased proteasome-mediated degradation of p53, resulting in reduced expression of p53-dependent proapoptotic genes [15]. Overexpression of gankyrin could promote cell proliferation of colorectal cancer cells [14]. In addition, overexpression of gankyrin in HCC cells enhances epithelial-mesenchymal transition (EMT), defined as switching of polarized epithelial cells to a migratory fibroblastoid phenotype, and increases angiogenesis associated with vascular endothelial growth factor (VEGF) overexpression [16]. Thus, gankyrin acts as a critical driving force in carcinoma cells by overcoming a variety of barriers associated with limiting cancer growth; however, the association between gankyrin and stem cells in colorectal carcinogenesis has yet to be elucidated. In the present study, the expression of gankyrin and CD133 was immunohistochemically assessed in human CRC tissues. Furthermore, given that adenoma is a potential precursor to colorectal cancer, we also examined the expression levels of gankyrin and stemness factors in adenoma to evaluate the relevance of these molecules in the initiation step of colorectal carcinogenesis.

Materials and Methods

Patients

CRC tissues were obtained from 30 patients who had undergone curative colorectal resection at the University Hospital of Kinki University of Medicine between June 2011 and December 2011. Thirty patients with large colorectal adenoma ($\geq$10 mm) and 20 patients with small adenoma (<10 mm) underwent endoscopic curative resection at Kinki University from May 2011 to March 2012 and from March 2012 to May 2012, respectively, and 50 sample pairs of adenoma and adjacent non-neoplastic normal tissue were acquired by endoscopy. Informed consent was obtained prior to use of the collected tissues. The study protocols conformed to the ethical guidelines of the 1975 Declaration of Helsinki and were approved by the institutional review boards of Kinki University.

Biochemical and Immunochemical Analyses

Real-time qPCR and immunoblotting were performed as previously described [17]. The primer sequences are mentioned in the Supplementary Material. The following antibodies were used: anti-actin, anti-PSMD10 (gankyrin; Sigma, St. Louis, MO); anti-α-smooth muscle actin (α-SMA; Dako, Glostrup, Denmark); anti-CD133 (PROM1; Abnova, St. Taipei, Taiwan); anti-β-catenin, anti-phospho-Akt, and anti-E-cadherin (Cell Signaling, Danvers, MA). Immunohistochemistry was performed using ImmPRESS^{TM} reagents (Vector Laboratory, Burlingame, CA) according to manufacturer's recommendations. Five high power fields per section were viewed and gankyrin and CD133 immunostaining were evaluated on tissue sections of colorectal adenocarcinoma.

Cell Culture

Caco-2 and T84 cells were seeded in DMEM medium and KatoIII cells were in RPMI1640 medium (Gibco Invitrogen, Carlsbad, CA), cultured as previously described [17] and transfected with gankyrin siRNA, VEGF siRNA or non-targeting siRNA as a negative control (Santa Cruz Biotechnology, Santa Cruz, CA), using Lipofectamine RNAiMAX Reagent (Gibco Invitrogen). Twenty-four hours after transfection, cell lysates were extracted.

Statistical Analysis

Data are presented as mean ± SD. Differences were analyzed using the Student's t test, and P values <0.05 were considered significant.

Results

Correlation Between Gankyrin and CD133 Expression in Human CRC

Thirty patients with CRC were recruited in this study, including 16 men and 14 women, with ages ranging from

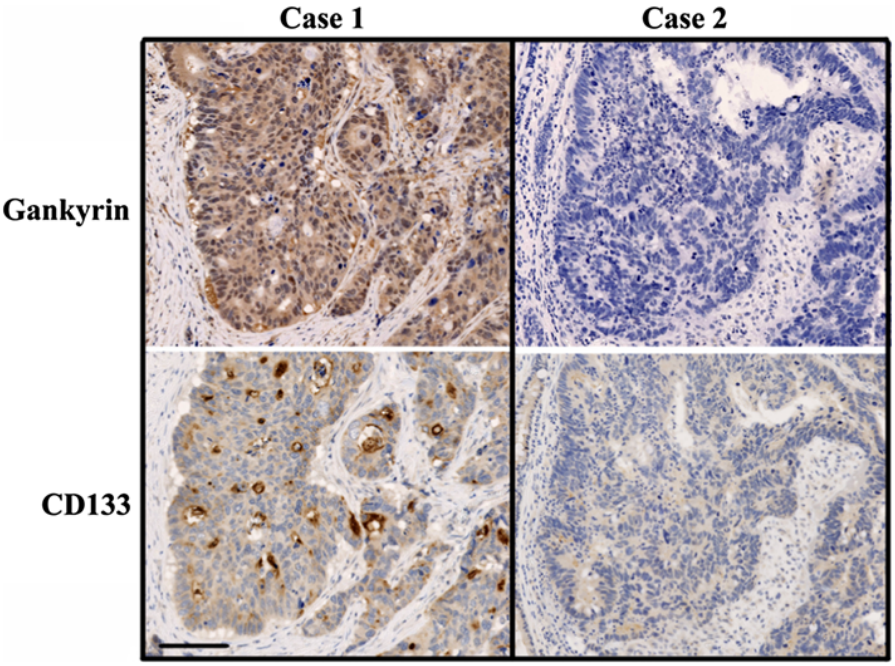

Fig. 1 Association between gankyrin and CD133 expression in colorectal cancer. Representative immunostaining images of colorectal cancer tissues with high and low gankyrin expression using antibodies against the indicated proteins. *Scale bar* = 100 μm

27 to 79 (median 69) years old. Clinicopathological profiles of the patients and their CRCs are shown in Supplementary Table 1. According to TNM staging, 53.3 % were stage I to II and 46.7 % were stage III to IV. Lymph node and hepatic metastasis were found in 43 and 17 %, respectively. Next we examined the expression of gankyrin and CD133 protein in CRC tissues by immunohistochemistry. The gankyrin signal was observed mainly in the cytoplasm and occasionally in the nucleus of CRC cells (Fig. 1). As shown in Table 1, we analyzed an association between gankyrin protein expression and clinicopathological findings. Gankyrin expression was significantly associated with differentiation of the tumor cells ($P = 0.046$). No significant association between gankyrin expression and sex, age, TNM classification or tumor metastasis was observed. CD133 signals were observed in the cytoplasm of CRC cells (Fig. 1). Importantly, the levels of gankyrin and CD133 expression covaried in CRCs (Table 2).

Down-Regulation of VEGF and Stemness Factor Expression on Gankyrin Knockdown

The role of gankyrin in the regulation of VEGF and stemness factors was evaluated using colon cancer Caco-2, KatoIII and T84 cells transfected with gankyrin siRNA (Fig. 2a and data not shown). Gankyrin knockdown resulted in a decrease in VEGF expression level (Fig. 2b). In addition, gankyrin or VEGF knock-down significantly decreased the expression of stemness factors such as Nanog, Oct4 and Cdx2 in KatoIII and Caco-2 cells (Fig. 2c, d).

Table 1 Gankyrin expression and clinicopathological characteristics

Characteristic	Gankyrin expression			*P* value
	Low	Moderate	High	
Age				
<60	2	2	0	0.099
≥60	4	8	14	
Sex distribution				
Male	3	6	7	0.89
Female	3	4	7	
Differentiation				
Well + moderate	3	9	13	0.048
Poor + mucinous	3	1	1	
TNM classification				
I +II	4	5	7	0.77
III + IV	2	5	7	
Metastasis				
With	1	1	3	0.76
Without	5	9	11	

The immunostaining levels of gankyrin were expressed as negative or weakly positive (low), moderately positive (medium), and strongly positive (high)

Since gankyrin expression was significantly higher in well or moderately differentiated adenocarcinoma than in poorly differentiated or mucinous adenocarcinoma (Table 1), we examined whether gankyrin is related to dedifferentiation of colorectal cancer cells. EMT is involved in dedifferentiation of cancer cells [18]. Gankyrin knock-down significantly decreased the expression of Snail

Table 2 Correlation of expression levels of gankyrin and CD133

CD133 expression	Gankyrin expression			*P* value
	Low	Moderate	High	
−	3	2	1	0.0086
+	2	7	2	
++	0	1	7	
+++	1	0	4	

CD133 immunoreactivity was coded as follows: no positive cells (−), 1–15 % positive cells (+), 16–30 % positive cells (++), and >31 % positive cells (+++)

and Twist, critical EMT regulators (Fig. 2e). In contrast, no significant changes were observed in E-cadherin levels, a marker for epithelial cells (Fig. 2f), implying that gankyrin is not critical for EMT in colon cancer Caco-2 cells. Similar results were obtained using T84 colorectal cancer cells (data not shown).

Increased Expression of Gankyrin, VEGF, and Stemness Factors in Large Colorectal Adenomas

According to the concept of adenoma-carcinoma sequence, adenomas continue to increase in size and finally develop into adenocarcinomas. To assess the role of gankyrin during the initiation of colorectal carcinogenesis, we examined the association between gankyrin and VEGF or stemness factors in small (<10 mm) and large adenomas (>10 mm). We analyzed four types of colorectal adenomas: small polypoid, small flat, large polypoid and large flat adenomas (Fig. 3a–d). Among 30 large adenomas, 25 flat adenomas are referred to as LSTs (Fig. 3d). The clinicopathological features of the

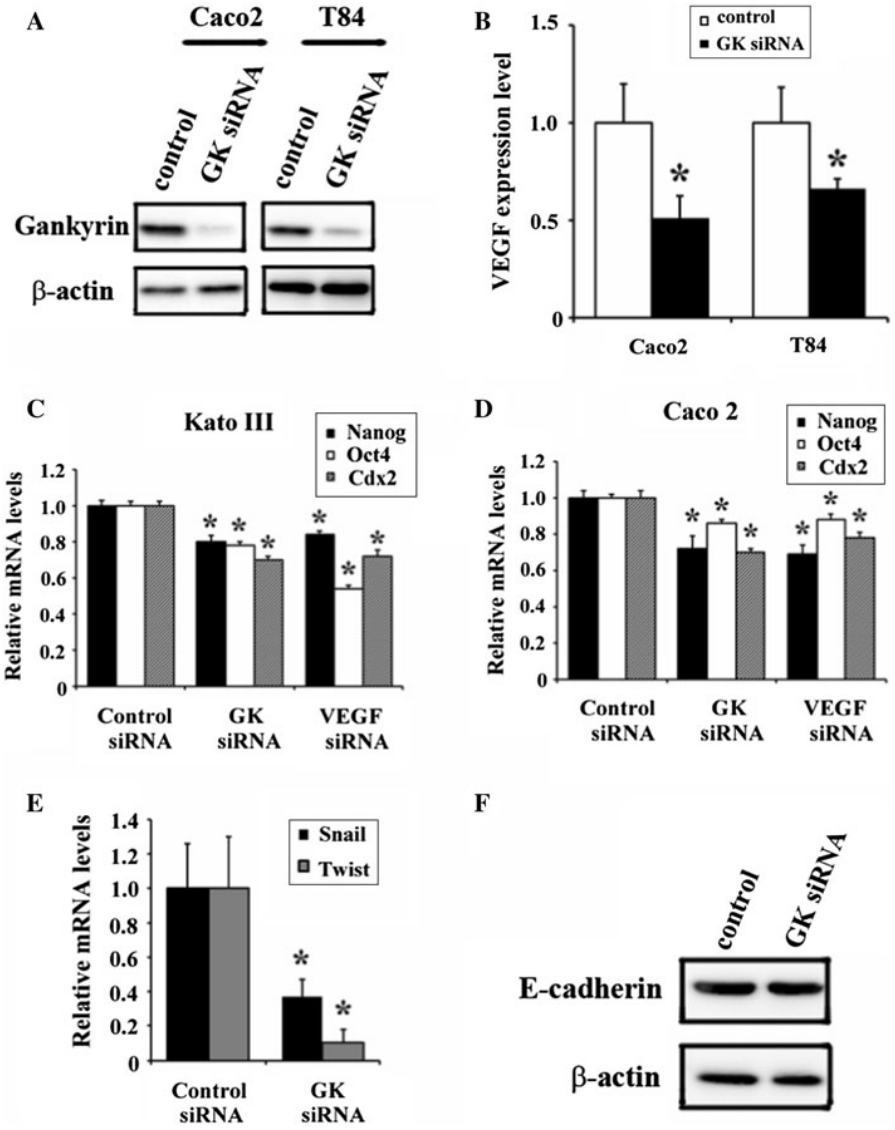

Fig. 2 Down-regulation of VEGF and Nanog expression by gankyrin knock-down. **a** Caco-2 and T84 cells were transfected with gankyrin siRNA or non-targeting siRNA. Cell lysates were immunoblotted with the indicated antibodies. **b** Caco-2 and T84 cells were transfected with gankyrin siRNA or non-targeting siRNA. mRNA levels of VEGF were quantified using real time-qPCR. Results are mean ± SD. $*P < 0.05$ vs control. **c**, **d** KatoIII and Caco-2 cells were transfected with gankyrin siRNA, VEGF siRNA or non-targeting siRNA. mRNA levels of indicated genes were quantified using real time-qPCR. The mean values of mRNA levels in cells transfected with non-targeting siRNA were given an arbitrary value of 1. Results are mean ± SD. $*P < 0.05$ vs control. **e** Caco-2 cells were transfected with gankyrin siRNA or non-targeting siRNA. mRNA levels of Snail and Twist were quantified using real time-qPCR. Results are mean ± SD. $*P < 0.05$ vs control. **f** Caco-2 cells were transfected with gankyrin siRNA or non-targeting siRNA. Cell lysates were immunoblotted with the indicated antibodies

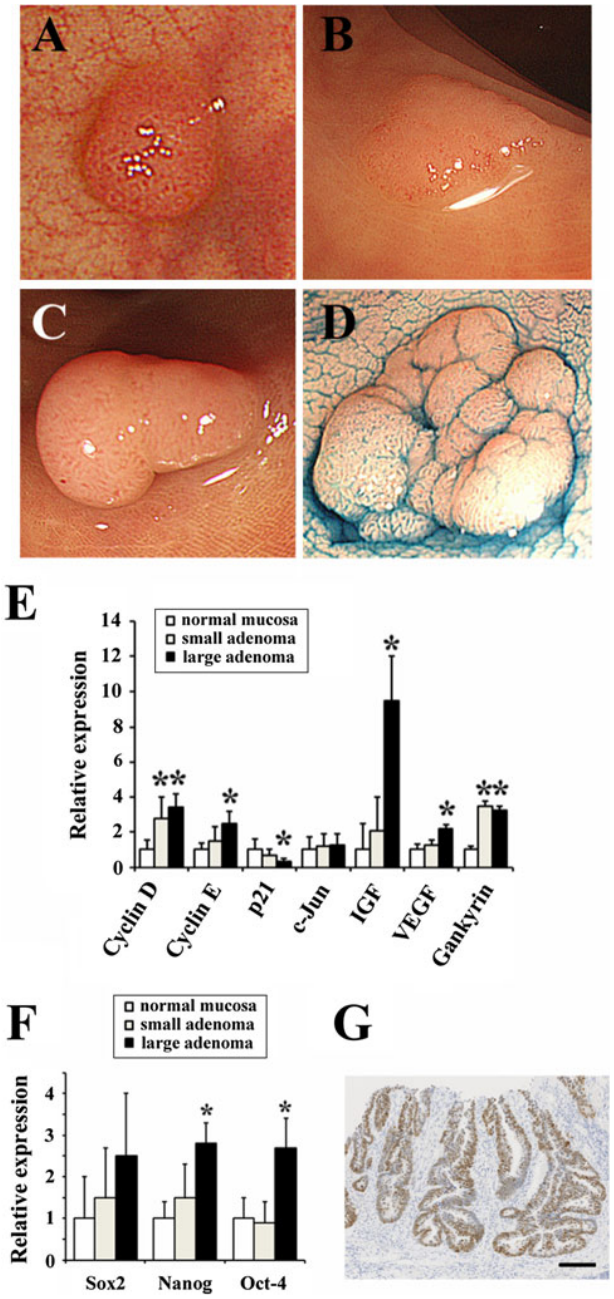

Fig. 3 Increased expression of gankyrin, VEGF and stemness factors in colorectal adenoma. Representative endoscopic views of four types of adenomas: small polypoid (**a**), small flat (**b**), large polypoid (**c**) and large flat adenomas (laterally spreading tumor [LST], **d**). **e**, **f** Using real time-qPCR, mRNA levels of the indicated genes were quantified in small (<10 mm) and large adenoma (>10 mm). The mean values of mRNA levels in surrounding normal mucosa were given an arbitrary value of 1. Results are mean ± SD. *$P < 0.05$ vs normal mucosa. *IGF* insulin-like growth factor. **g** Expression of p53 in large adenoma. Representative immunostaining image is shown. *Scale bar* = 200 μm

adenomas examined here are summarized in Table 3. Expression levels of gankyrin and cyclin D were significantly higher in both small and large adenomas compared to normal colorectal mucosa (Fig. 3e). Expression levels of cyclin E, insulin-like growth factor (IGF), and VEGF were also significantly higher in large adenomas, but not in small adenomas, than in the surrounding normal mucosa (Fig. 3e). Similarly, expression of stemness factors such as Oct-4 and Nanog was upregulated in large adenomas but not in small adenomas (Fig. 3f). In contrast, the expression level of the cyclin dependent inhibitor p21 was significantly lower in large adenomas than in the surrounding normal mucosa (Fig. 3e). In addition, nuclear accumulation of p53 protein was found in 70 % of large adenomas (21/30) (Fig. 3g), consistent with a previous report [19].

Table 3 Characteristics of patients with small and large adenomas

Variables	Small adenoma (<10 mm) $N = 20$	Large adenoma (≥10 mm) $N = 30$
Age (year)		
Mean ± SD (range)	61 ± 8 (54–78)	66 ± 10 (44–90)
Sex (*n*)		
Male	9	16
Female	11	14
Tumor size (mm)		
Mean ± SD (range)	6.4 ± 1.8 (4–9)	25 ± 14 (10–60)
Location		
Proxymal	7	7
Distal	10	12
Rectum	3	11
Macroscopic appearance		
Polypoid	16	5
Flat	4	25

A large flat adenoma is referred to as laterally spreading tumor (LST)

Correlation of Gankyrin Expression with VEGF and Nanog Expression in Large Adenomas

Correlation between gankyrin and VEGF was analyzed in large adenoma where gankyrin and VEGF were both upregulated. VEGF and cyclin D expression was significantly higher in adenomas with high gankyrin expression than in those with low gankyrin expression. A significant correlation was also observed between gankyrin and Nanog expression (Fig. 4a). Gankyrin was present in higher levels in adenomas with high VEGF expression (Fig. 4b). VEGF stimulates cancer stemness and renewal as well as neovascularization [20]. Suppression of VEGF expression downregulated expression of stemness factors in colorectal cancer cells (Fig. 2c, d). Consistently, expression of Nanog and Oct-4 was significantly higher in colorectal adenomas with high VEGF expression than in those with low VEGF expression (Fig. 4b).

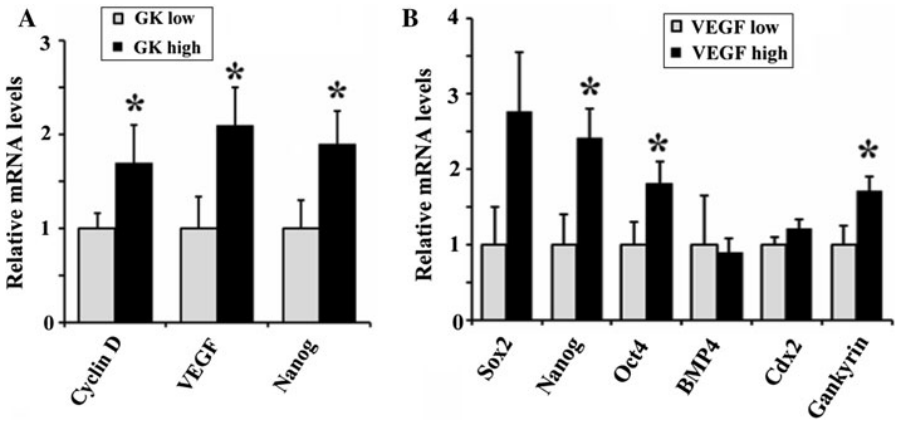

Fig. 4 Association of gankyrin and VEGF expression with stemness factor expression in large colorectal adenoma. Using real time-qPCR, mRNA levels of the indicated genes were quantified in large adenoma (≥10 mm) between high and low gankyrin expression groups (**a**) and between high and low VEGF expression groups (**b**). The median level of mRNA, as determined by real-time qPCR, was used to distinguish low- and high-expression groups. Results are mean ± SD. $^*P < 0.05$. *GK* Gankyrin

Gankyrin Expression Does Not Correlate with β-Catenin, Phospho-Akt, Snail, or Twist Expression in Large Adenoma

Although several reports have suggested an association between β-catenin, phospho-Akt, and gankyrin [21, 22], no significant correlation between β-catenin, phospho-Akt, and gankyrin expression was found in the present study on the basis of adenoma cell immunostaining (Supplementary Fig. 1). Invasive HCCs overexpressing gankyrin were featured by active EMT, whilst silencing gankyrin expression attenuated EMT in HCC cells [16]. However, no significant increase in expression of EMT regulators such as Twist and Snail was observed (Supplementary Fig. 2) and no significant relationship between gankyrin and these molecules was found in colorectal adenoma (data not shown).

Discussion

It is widely accepted that the adenoma-carcinoma sequence represents the process by which most, if not all, colorectal cancers arise. This sequence begins with adenomas, which are putative pre-neoplastic lesions. Then, adenomas continue to increase in size and finally develop into adenocarcinomas. The adenoma-carcinoma sequence model has generally been accepted for polypoid tumors as it is common to find both adenomatous and carcinomatous tissues within such tumors. In contrast, an increasing number of flat colorectal adenomas including LSTs have been reported [5, 6]. No difference in expression of gankyrin, VEGF and Nanog was found between flat and polypoid adenomas (data not shown). In addition, similar incidence of *K-ras* and *p53* gene mutations were reported in LSTs and polyploid adenomas [19]. Thus, flat adenomas as well as polypoid adenomas have been recognized as an important precursor of colorectal cancer [23], and LSTs would also follow the adenoma-carcinoma sequence.

Stem cell function is central for the maintenance of normal tissue homeostasis and is suggested to promote tumorigenesis via processes that resemble reprogramming [24, 25]. Several signaling pathways regulate stem cell self-renewal and differentiation. Nanog, Oct-4, Sox2 and Lin28 are stemness factor that have been used to produce induced pluripotent stem cells [26, 27]. These factors form a core regulatory network of self-renewal and differentiation in embryonic stem cells [28]. For example, Nanog positive cells exhibit enhanced self-renewal ability, clonogenicity, and initiation of tumors, which are consistent with the hallmarks of cancer stem cells. In addition, overexpression of Nanog predicts tumor progression and poor prognosis in colorectal cancer [12]. When tumors invade space through cancer cell proliferation and tumor mass expansion, tumor growth is maintained over time using the cancer stem cell pool, which is regulated by stemness factors. However, it remains unclear whether the stemness factors are involved in the initiation step of carcinogenesis. In this study, we showed that the expression of Nanog and Oct-4 was upregulated in large adenomas, but not in small adenomas. Our data support the hypothesis that stemness factors are involved in the transition from adenoma to cancer. Further work using knock-out mice will be necessary to answer these questions and to determine whether stemness factors play a critical role in colorectal carcinogenesis in vivo.

As the distance of initiated tumor cells to blood vessels increases during tumor growth, these cells are depleted of oxygen and nutrients and therefore depend on the recruitment of new vessels to the tumor site through angiogenesis [29]. It is well-known that VEGF, a major mediator of

tumor angiogenesis [30], is expressed by most types of cancer cells after the activation of hypoxia-inducible transcription factors 1α and 2α in response to hypoxia and metabolic stress [31]. Recently, Beck et al. [20] have identified a dual role for VEGF in promoting cancer stemness: (1) VEGF creates a perivascular niche for cancer stem cells by stimulating angiogenesis, and (2) VEGF stimulates cancer stemness and renewal by directly affecting cancer stem cells through Nrp1. Here, we have shown that VEGF expression is correlated with the expression of Nanog and Oct-4 in large colorectal adenomas, a precancerous lesion. In colorectal adenoma, VEGF signaling might increase the risk for colorectal cancer via upregulation of stemness factors.

The oncoprotein gankyrin is frequently overexpressed in human cancers such as HCCs [13] and colorectal cancers [14] and has been implicated in tumorigenesis. Gankyrin knockdown has been reported to reduce the proportion of cancer stem cells in hepatoma cells. The gankyrin-mediated dedifferentiation of hepatocytes is, at least partially, via an HNF4α-dependent mechanism [32]. Gankyrin was also reported to prevent degradation of Oct4 and promote expansion of cancer stem cells in hepatocarcinogenesis [33]. The findings presented here indicate a significant relationship between the expression of gankyrin and CD133 in human CRC tissues. In addition, a significant correlation between the expression of gankyrin and VEGF or Nanog was found in colorectal adenomas. Gankyrin knockdown downregulated the expression of both VEGF and stemness factors including Nanog. These data suggest that gankyrin would stimulate cancer stemness by upregulating VEGF and stemness factors in the development of CRC.

Invasive tumors overexpressing gankyrin were featured in active EMT through the upregulation of the EMT regulator Twist in HCCs [16]. In colon cancer cells, like in HCC cells, gankyrin regulated the expression of Snail and Twist. However, gankyrin did not seem to affect EMT in colorectal cancer cells. Gankyrin might regulate EMT induction in a cell-type specific manner. Gankyrin was found to be related with the malignant phenotypes and poor prognosis in HCC [16]. Immunohistological analysis of CRC specimens indicated a positive association of gankyrin expression with TNM grade and tumor metastasis [14]. By contrast, Umemura et al. [34] reported that immunostaining for gankyrin was significantly associated with low TNM stage, no intrahepatic metastasis and high cumulative survival rate in patients with HCC. In this study, gankyrin expression was correlated with CD133 expression, but not with TNM grade or tumor metastasis. The discrepancy might be explained by the difference in antibody used for the detection of gankyrin.

In summary, gankyrin was correlated with stem cell behavior in CRC tissues. Association of gankyrin and its downstream target genes, VEGF and Nanog, in adenomas as well as colorectal cancer cells shown here provide insight into the function of these molecules in an early step of colorectal carcinogenesis. This is consistent with a previous report suggesting that gankyrin plays an oncogenic role mainly at the early stages of hepatocarcinogenesis [34]. These findings indicate that targeting gankyrin might be a promising strategy for CRC prevention and treatment.

Acknowledgments We thank Dr. Yoshie O and Munakata H (Kinki University) for technical assistance and helpful suggestions. This research was supported by grants from the Yasuda Medical Foundation, Novartis Foundation and Grant-in-Aid for Scientific Research from the Ministry of Education, Science and Culture of Japan.

Conflict of interest None.

References

1. Ferlay J, Shin HR, Bray F et al. Cancer incidence and mortality worldwide. GLOBOCAN 2008 v1.2. IARC CancerBase No. 10; 2008.
2. Kudo S. Endoscopic mucosal resection of flat and depressed types of early colorectal cancer. *Endoscopy*. 1993;25:455–461.
3. Teixeira CR, Tanaka S, Haruma K, et al. Flat-elevated colorectal neoplasms exhibit a high malignant potential. *Oncology*. 1996;53:89–93.
4. Saitoh Y, Waxman I, West AB, et al. Prevalence and distinctive biologic features of flat colorectal adenomas in a North American population. *Gastroenterology*. 2001;120:1657–1665.
5. Hurlstone DP, Korulla C, Lobo AJ. Colorectal laterally spreading tumors: clinical evaluation and endoscopic strategies updated. *J Gastroenterol Hepatol*. 2002;17:1344–1345.
6. Kudo S, Kashida H, Nakajima T, et al. Endoscopic diagnosis and treatment of early colorectal cancer. *World J Surg*. 1997;21: 694–701.
7. Reya T, Morrison SJ, Clarke MF, Weissman IL. Stem cells, cancer, and cancer stem cells. *Nature*. 2001;414:105–111.
8. Clarke MF, Dick JE, Dirks PB, et al. Cancer stem cells–perspectives on current status and future directions: AACR workshop on cancer stem cells. *Cancer Res*. 2006;66:9339–9344.
9. O'Brien CA, Pollett A, Gallinger S, et al. A human colon cancer cell capable of initiating tumour growth in immunodeficient mice. *Nature*. 2007;445:106–110.
10. Hoei-Hansen CE. Application of stem cell markers in search for neoplastic germ cells in dysgenetic gonads, extragonadal tumours, and in semen of infertile men. *Cancer Treat Rev*. 2008;3:348–367.
11. Shan J, Shen J, Liu L, et al. Nanog regulates self-renewal of cancer stem cell through IGF pathway in human hepatocellular carcinoma. *Hepatology*. 2012;56:1004–1014.
12. Meng HM, Zheng P, Wang XY, et al. Overexpression of nanog predicts tumor progression and poor prognosis in colorectal cancer. *Cancer Biol Ther*. 2010;9:295–302.
13. Higashitsuji H, Itoh K, Nagao T, et al. Reduced stability of retinoblastoma protein by gankyrin, an oncogenic ankyrin-repeat protein overexpressed in hepatomas. *Nat Med*. 2000;6:96–99.

14. Tang S, Yang G, Meng Y, et al. Overexpression of a novel gene gankyrin correlates with the malignant phenotype of colorectal cancer. *Cancer Biol Ther*. 2010;9:88–95.
15. Higashitsuji H, Higashitsuji H, Itoh K, et al. The oncoprotein gankyrin binds to MDM2/HDM2, enhancing ubiquitylation and degradation of p53. *Cancer Cell*. 2005;8:75–87.
16. Fu J, Chen Y, Cao J, et al. p28GANK overexpression accelerates hepatocellular carcinoma invasiveness and metastasis via phosphoinositol 3-kinase/AKT/hypoxia-inducible factor-1α pathways. *Hepatology*. 2011;53:181–192.
17. Sakurai T, He G, Matsuzawa A, et al. Hepatocyte necrosis induced by oxidative stress and IL-1 alpha release mediate carcinogen-induced compensatory proliferation and liver tumorigenesis. *Cancer Cell*. 2008;14:156–165.
18. Savagner P. The epithelial-mesenchymal transition (EMT) phenomenon. *Ann Oncol*. 2010;21:vii89–vii92.
19. Noro A, Sugai T, Hababo W, et al. Analysis of K-ras and p53 gene mutations in laterally spreading tumors of the colorectum. *Pathol Int*. 2003;53:828–836.
20. Beck B, Driessens G, Goossens S, et al. A vascular niche and a VEGF-Nrp1 loop regulate the initiation and stemness of skin tumours. *Nature*. 2011;478:399–403.
21. Dong LW, Yang GZ, Pan YF, et al. The oncoprotein p28GANK establishes a positive feedback loop in β-catenin signaling. *Cell Res*. 2011;21:1248–1261.
22. Man JH, Liang B, Gu YX, et al. Gankyrin plays an essential role in Ras-induced tumorigenesis through regulation of the RhoA/ROCK pathway in mammalian cells. *J Clin Invest.* 2010;120:2829–2841.
23. Rotondano G, Bianco MA, Buffoli F, et al. The cooperative Italian FLIN study group: prevalence and clinico-pathological features of colorectal laterally spreading tumors. *Endoscopy*. 2011;43:856–861.
24. Park IH, Zhao R, West JA, et al. Reprogramming of human somatic cells to pluripotency with defined factors. *Nature*. 2008;45:141–146.
25. Chan EM, Ratanasirintrawoot S, Park IH, et al. Live cell imaging distinguishes bona fide human iPS cells from partially reprogrammed cells. *Nat Biotechnol*. 2009;27:1033–1037.
26. Takahashi K, Yamanaka S. Induction of pluripotent stem cells from mouse embryonic and adult fibroblast cultures by defined factors. *Cell*. 2006;126:663–676.
27. Yu J, Vodyanik MA, Smuga-Otto K, et al. Induced pluripotent stem cell lines derived from human somatic cells. *Science*. 2007;318:1917–1920.
28. Müller FJ, Laurent LC, Kostka D, et al. Regulatory networks define phenotypic classes of human stem cell lines. *Nature*. 2008;455:401–405.
29. Ferrara N. VEGF-A: a critical regulator of blood vessel growth. *Eur Cytokine Netw*. 2009;20:158–163.
30. Sakurai T, Kudo M. Signaling pathways governing tumor angiogenesis. *Oncology*. 2011;81:24–29.
31. Semenza GL. Targeting HIF-1 for cancer therapy. *Nat Rev Cancer*. 2003;3:721–732.
32. Sun W, Ding J, Wu K, et al. Gankyrin-mediated dedifferentiation facilitates the tumorigenicity of rat hepatocytes and hepatoma cells. *Hepatology*. 2011;54:1259–1272.
33. Qian YW, Chen Y, Yang W, et al. p28(GANK) prevents degradation of Oct4 and promotes expansion of tumor-initiating cells in hepatocarcinogenesis. *Gastroenterology*. 2012;142:1547–1558.
34. Umemura A, Itoh Y, Itoh K, et al. Association of gankyrin protein expression with early clinical stages and insulin-like growth factor-binding protein 5 expression in human hepatocellular carcinoma. *Hepatology*. 2008;47:493–502.

European Journal of Cancer (2013) **49**, 2832–2840

Available at www.sciencedirect.com

SciVerse ScienceDirect

journal homepage: www.ejcancer.com

A randomised phase II study of TSU-68 in patients with hepatocellular carcinoma treated by transarterial chemoembolisation

Yoshitaka Inaba [a,*], Fumihiko Kanai [b], Takeshi Aramaki [c], Takanobu Yamamoto [d], Toshihiro Tanaka [e], Koichiro Yamakado [f], Shuichi Kaneko [g], Masatoshi Kudo [h], Kazuho Imanaka [i], Shinichi Kora [j], Norifumi Nishida [k], Nobuyuki Kawai [l], Hiroshi Seki [m], Osamu Matsui [n], Hitoshi Arioka [o], Yasuaki Arai [p]

[a] *Department of Diagnostic and Interventional Radiology, Aichi Cancer Center Hospital, Japan*
[b] *Department of Gastroenterology, Chiba University Hospital, Japan*
[c] *Department of Diagnostic Radiology, Shizuoka Cancer Center Hospital, Japan*
[d] *Department of Diagnostic Imaging, Tochigi Cancer Center, Japan*
[e] *Department of Radiology, Nara Medical University Hospital, Japan*
[f] *Department of Radiology, Mie University Hospital, Japan*
[g] *Department of Gastroenterology, Kanazawa University Hospital, Japan*
[h] *Department of Gastroenterology and Hepatology, Kinki University Hospital, Japan*
[i] *Department of Hepatobiliary and Pancreatic Oncology, Osaka Medical Center for Cancer and Cardiovascular Diseases, Japan*
[j] *Department of Radiology, Fukuoka University Hospital, Japan*
[k] *Department of Radiology, Osaka City University Hospital, Japan*
[l] *Department of Radiology, Wakayama Medical University Hospital, Japan*
[m] *Department of Diagnostic Radiology, Niigata Cancer Center Hospital, Japan*
[n] *Department of Radiology, Kanazawa University Hospital, Japan*
[o] *Department of Medical Oncology, Yokohama Rosai Hospital, Japan*
[p] *Department of Diagnostic Radiology, National Cancer Center Hospital, Japan*

Available online 10 June 2013

KEYWORDS
Hepatocellular carcinoma
Transarterial chemoembolisation
Platelet-derived growth factor
TSU-68

Abstract ***Background:*** TSU-68 is an antitumour drug that acts by inhibiting angiogenesis. We evaluated the efficacy and safety of TSU-68 in combination with transarterial chemoembolisation (TACE) in patients with intermediate-stage hepatocellular carcinoma (HCC).
Patients and Methods: In this multicenter, open-label phase II study, we randomised patients with HCC who had been treated with a single session of TACE to receive either 200 mg TSU-68 twice daily or no medication. The primary end-point was progression-free survival (PFS).

* *Corresponding author:* Address: Department of Diagnostic and Interventional Radiology, Aichi Cancer Center Hospital, 1-1 Kanokoden, Chikusa-ku, Nagoya-shi, Aichi 464-8681, Japan. Tel.: +81 52 762 6111; fax: +81 52 764 2966.
E-mail address: 105824@aichi-cc.jp (Y. Inaba).

0959-8049/$ - see front matter
http://dx.doi.org/10.1016/j.ejca.2013.05.011

Results: A total of 103 patients were enrolled. Median PFS was 157.0 days (95% confidence interval [CI], 124.0–230.0 days) in the TSU-68 group and 122.0 days (95% CI, 73.0–170.0 days) in the control group. The hazard ratio was 0.699 (95% CI, 0.450–1.088). Fatigue, elevated aspartate aminotransferase (AST), elevated alkaline phosphatase, oedema and anorexia were more frequent in the TSU-68 group than in the control group. The most frequent grade 3/4 adverse events were AST elevation (46% of patients in the TSU-68 group and 12% of controls) and alanine aminotransferase elevation (26% of patients in the TSU-68 group and 8% of controls). Two deaths, grade 5 hepatic failure and melena were noted in the TSU-68 group.

Conclusion: This exploratory study shows a trend towards prolonged PFS with TSU-68 treatment after a single session of TACE, but this observation was not statistically significant. The two deaths were related to the study treatment. These results suggest that further examination of the study design is necessary to determine whether TSU-68 has any clinical benefits when combined with TACE.

1. Introduction

Hepatocellular carcinoma (HCC) is the fifth-most common cancer, and its incidence is still increasing worldwide.[1] It is reported to be the third leading cause of cancer death, with about 560,000 cases diagnosed per year, more than 80% of which occur in developing countries. Infection with hepatitis B virus (HBV) accounts for 55% of global HCC and 80% of cases in the Asia Pacific and sub-Saharan African regions.[2] Infection with Hepatitis C virus (HCV) is the chief cause of HCC in industrialised countries.[3,4]

Current treatments for HCC include hepatic resection, liver transplantation, radio frequency ablation (RFA), transarterial chemoembolisation (TACE) and chemotherapy. Other than sorafenib, there are no standard chemotherapy treatments for advanced-stage HCC;[5,6] accordingly, there is an urgent need to improve treatments and prevent recurrence or progression.

TACE is the most widely used standard treatment for unresectable HCC.[7–9] However, the curative effect of TACE is limited, and most patients suffer intrahepatic recurrence. Numerous reports have indicated that angiogenesis is closely associated with tumour growth after TACE; therefore treatments that combine antiangiogenic agents with TACE are anticipated to contribute to improved treatment of HCC.

TSU-68 is a receptor tyrosine kinase inhibitor that targets vascular endothelial growth factor receptor-2 (VEGFR-2) and platelet-derived growth factor receptor-β (PDGFR-β).[10–14] In phase I/II study, TSU-68 showed favourable efficacy and a high safety profile in HCC patients who had been heavily pretreated,[15] including those with Child–Pugh B cirrhosis.

We conducted a randomised phase II trial to assess the efficacy and safety of TSU-68 after TACE.

2. Patients and methods

2.1. Eligibility criteria

Eligible patients were (1) diagnosed with HCC by histology/cytology or by radiography; (2) showed no indications for, or no response to, resection or locoregional therapies such as RFA; (3) were $\geqslant$20 years of age; (4) had Eastern Cooperative Oncology Group performance status (ECOG PS) of $\leqslant$2; (5) had HCC $\leqslant$80 mm; (6) had target lesions that were all of the hypervascular and nodular type with a minimum size of 10 mm; (7) did not have any vascular invasion; (8) had no extrahepatic spread; (9) had Child–Pugh A or B liver function; (10) had a life expectancy of $\geqslant$3 months; and (11) had undergone successful TACE within the previous 2 weeks.

Patients were excluded if they showed clinical evidence of extrahepatic metastases, severe cardiovascular disorders, hepatic encephalopathy, uncontrollable pleural effusion or ascites.

All patients provided written informed consent before enrolment in the study. The study was carried out in accordance with Good Clinical Practice (GCP) and the Declaration of Helsinki guidelines. Documented approval from appropriate ethics committees and institutional review boards was obtained for all participating centres before the start of the study.

2.2. Study design and treatment

This multicenter, randomised, open-label study was conducted at 14 centres in Japan. The TACE procedure consisted of the injection of epirubicin with lipiodol into the hepatic artery followed by the administration of gelatin sponge. After assessing the disappearance of all target tumour stains using digital subtraction angiography, the TACE procedure was completed. Additional TACE procedures were not performed during treatment as per the protocol. As shown in Fig. 1A, within 2 weeks of TACE, eligible patients were randomised in a 1:1 ratio to receive either oral treatment with 200 mg of TSU-68 twice daily (the TSU-68 group) or no treatment (the control group). Because standardisation of the TACE procedure between sites is difficult, patients were stratified by site. TSU-68 was provided by Taiho Pharmaceutical Co., Ltd. (Tokyo, Japan)

Protocol treatment was discontinued when we observed radiological progression or the occurrence of unacceptable adverse events.

2.3. Objectives and assessments

The primary objective was to assess any differences between progression-free survival (PFS) after TACE in the TSU-68 group and the control group. Radiological progression was assessed according to modified Response Evaluation Criteria in Solid Tumours (mRECIST 1.0).[16,17] Contrast-enhanced computed tomography was performed at baseline, on day 28, on day 56 and every 8 weeks thereafter. Target lesions were evaluated by measurement of the longest diameter of viable lesions. Responses were assessed by an independent review committee.

Secondary objectives included an assessment of overall survival (OS), biomarkers and a safety profile evaluated according to Common Terminology Criteria for Adverse Events (CTCAE) version 3.0.

Blood samples for measuring endothelial cell markers were collected at baseline and every 4 weeks after enrolment. The concentrations of platelet-derived growth factor (PDGF)-AA, PDGF-BB, soluble vascular cell adhesion molecule-1 (sVCAM-1), soluble endothelial-leucocyte adhesion molecule-1 (sELAM-1), interleukin-8 (IL-8), tissue plasminogen activator (t-PA), plasminogen activator inhibitor-1 (PAI-1) and Willebrand factor (factor VIII) were evaluated using enzyme-linked immunosorbent assays (ELISA).

2.4. Statistical analysis

The primary end-point was PFS, defined as the time between the date of TACE and the date of disease progression or death from any cause. The median PFS in patients treated with TACE was assumed to be 6 months. To demonstrate an improvement in PFS from 6 to 12 months with a one-sided alpha of 2.5%, a statistical significance of 80% and 12 months of follow-up after 12 months of recruitment, 50 patients were needed in each group.

PFS was assessed using the Kaplan–Meier method and a log-rank test. Hazard ratios and 95% confidence intervals were estimated by employing Cox's proportional-hazards model.

Comparisons between groups were made on an intention-to-treat basis. All significance tests were two-sided and $p < 0.05$ was regarded as statistically significant, except for the one-sided log-rank test of PFS, for which $p < 0.025$ was considered to be statistically significant.

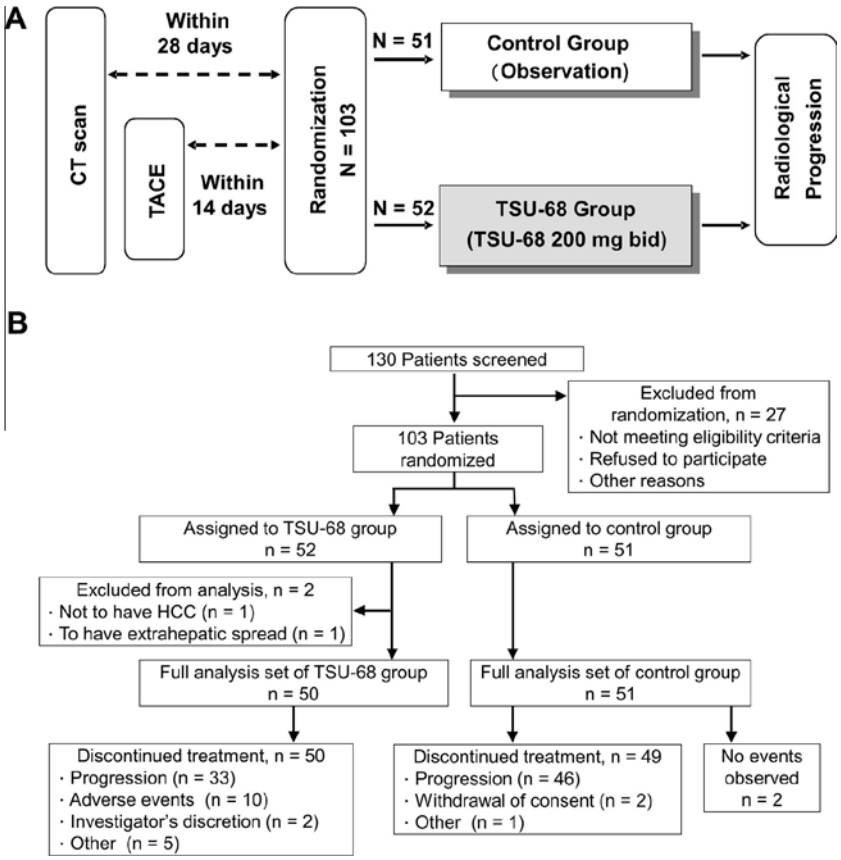

Fig. 1. Study design (A) and CONSORT diagram (B). (A) Transarterial chemoembolisation (TACE) was performed within the 2 weeks prior to randomisation. (B) Two patients in the TSU-68 group were excluded from the full analysis set by an independent data monitoring committee.

We used a full analysis set (FAS), defined as all patients who met the eligibility criteria, for primary analysis of TSU-68 efficacy.

3. Results

3.1. Patient characteristics

A total of 103 patients were enroled from 15th September 2006 to 14th November 2007. As shown in Fig. 1A and B, 52 patients were randomised into the TSU-68 group and 51 patients were randomised into the control group. The 52 patients in the TSU-68 group received treatment with the investigational drug and 50 were classified as FAS. Two patients in this group were excluded because they did not meet the eligibility criteria. The 51 patients in the control group were all eligible and were classified as FAS.

As shown in Table 1, the baseline characteristics of the 101 eligible patients were well balanced between two groups. Included in the study were 82 male patients, 20 patients who were more than 66 years of age, 48 patients with stage III disease under the Japanese classification system for HCC[18] and 51 patients in Barcelona Clinic Liver Cancer (BCLC) stage B of HCC.[19] BCLC A patients had no indications for or no response to resection or locoregional therapies because of their tumour location, such as areas adjacent to major blood vessels. BCLC C patients had an ECOG PS of one and were considered to be suitable for TACE according to their liver function and tumour status. HCV infection was the predominant cause of liver disease. Eighty-five percent of patients had Child–Pugh A liver function.

Table 1
Patient characteristics.

Characteristic	TSU-68 ($N = 50$) *n* (%)	Control ($N = 51$) *n* (%)	*P*-Value
Age			
65 >	11 (22.0)	9 (17.6)	F: 0.625
65 ⩽	39 (78.0)	42 (82.4)	
Sex			
Female	11 (22.0)	8 (15.7)	F: 0.455
Male	39 (78.0)	43 (84.3)	
Eastern Cooperative Oncology Group performance status (ECOG PS)			
0	45 (90.0)	49 (96.1)	F: 0.269
1	5 (10.0)	2 (3.9)	
Stage (Japanese classification)			
I	5 (10.0)	8 (15.7)	W: 0.720
II	21 (42.0)	19 (37.3)	
III	24 (48.0)	24 (47.1)	
Stage (Barcelona Clinic Liver Cancer (BCLC) classification)			
0	3 (6.0)	9 (17.6)	W: 0.378
A	18 (36.0)	13 (25.5)	
B	24 (48.0)	27 (52.9)	
C	5 (10.0)	2 (3.9)	
Number of target lesions			
1	20 (40.0)	23 (45.1)	W: 0.458
2	13 (26.0)	15 (29.4)	
3	10 (20.0)	7 (13.7)	
4	3 (6.0)	3 (5.9)	
⩾5	4 (8.0)	3 (5.9)	
Hepatitis B virus antigen			
+	2 (4.0)	4 (7.8)	F: 0.678
−	48 (96.0)	47 (92.2)	
Hepatitis C virus antibody			
+	40 (80.0)	36 (70.6)	F: 0.357
−	10 (20.0)	15 (29.4)	
Child–Pugh classification			
A	40 (80.0)	45 (88.2)	W: 0.361
B	9 (18.0)	6 (11.8)	
Unknown	1 (2.0)	0 (0.0)	

F, Fisher's exact test.
W, Wilcoxon's rank sum test.

3.2. Drug delivery

A CONSORT diagram is shown in Fig. 1B. The 52 patients in the TSU-68 group were treated with 200 mg of TSU-68 twice daily, starting within 2 weeks of TACE, and the median time between TACE and the first TSU-68 administration was 9 days. Ten patients (20%) discontinued the TSU-68 treatment due to adverse events. Seven of these patients discontinued for reasons related to TSU-68 (elevated aspartate aminotransferase (AST) and alanine aminotransferase (ALT), diarrhoea, ascites, HBV reactivation, achillodynia, melena or oedema in conjunction with ascites and pleural effusion). The median duration of TSU-68 treatment was 122.0 days (range, 9–363 days) and the median daily dose was 377.8 mg (range, 88.6–400.0 mg).

3.3. Efficacy

As shown in Fig. 2A, the median PFS of the TSU-68 and control groups was 157.0 days (95% confidence interval [CI], 124.0–230.0 days) and 122.0 days (95% CI, 73.0–170.0 days), respectively. There was no statistically significant difference in the median PFS between the two groups. However, TSU-68 tended to improve PFS ($p = 0.054$, one-sided log-rank test). The hazard ratio was 0.699 (95% CI, 0.450–1.088). As shown in Fig. 2B, the median overall survival in the TSU-68 group was 780.0 days (95% CI, 760.0 days–date not yet reached), but the median for the control group cannot yet be determined.

According to the 2008 National Cancer Institute consensus conference, the outcomes of HCC trials should be reported in terms of time to progression (TTP) and OS, not PFS.[20] This study was conducted before this conference, and thus, PFS was selected as the primary endpoint. In this study, no patients died before tumour progression. Therefore, all TTP values would be identical to the PFS values.

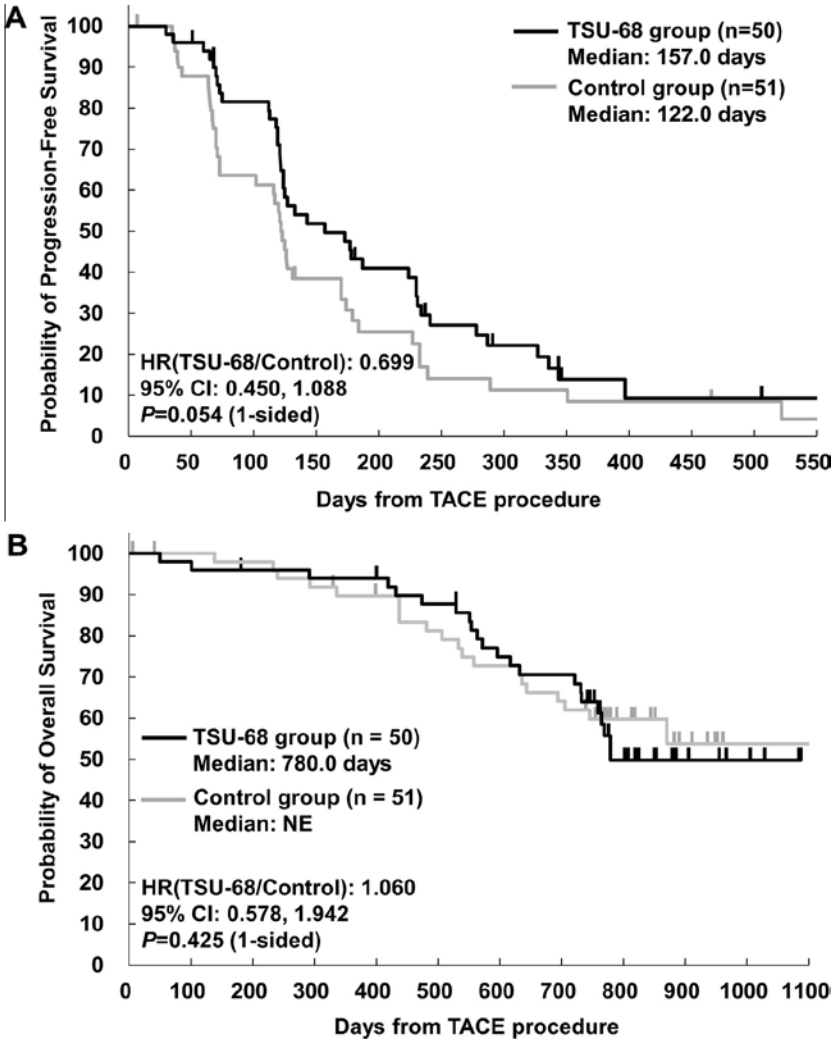

Fig. 2. Kaplan–Meier analysis. Progression-free survival (PFS) (A) and overall survival (OS) (B) among 101 patients. There were 50 patients in the TSU-68 group and 51 in the control group.

3.4. Safety

The major adverse events are shown in Table 2. The following adverse events occurred more frequently in the TSU-68 group than in the control group: fatigue (74%), elevated AST (72%), elevated alkaline phosphatase (ALP, 70%), oedema (58%), anorexia (52%), fever (48%), elevated ALT (44%), diarrhoea (40%) and ascites (24%). The most frequent grade 3/4 adverse events were elevated AST (42%) and elevated ALT (22%); however, most of these events were reversible and only one patient discontinued the study treatment due to AST/ALT elevation.

Two patients in the TSU-68 group died as a result of adverse events (4.0%, 2/50). One of these patients died of an oesophageal varix rupture that was followed by liver failure. Two weeks before liver failure, tumour progression, a Child–Pugh score of nine and uncontrollable ascites were observed. The second patient experienced a bloody bowel discharge and died at another hospital 2 months after randomisation; a Child–Pugh score of seven was observed at the final visit. The patient's family refused to grant permission for a postmortem examination. Therefore, we could not determine whether this patient's death was related to the TSU-68 treatment.

In the control group, 49 patients (93.9%) discontinued participation due to disease progression. In the TSU-68 group, 10 patients (20%) discontinued participation due to adverse events, and 33 patients (66%) discontinued due to disease progression.

3.5. Exploratory analysis

An exploratory analysis was performed using six baseline characteristics: sex, age, disease stage, ECOG PS, Child–Pugh status and type of hepatitis (Fig. 3). The analysis results suggested that TSU-68 treatment may extend PFS for patients with Child–Pugh class A

Table 2
Incidence of adverse events.

Adverse event	TSU-68 ($N = 50$) Grade (%)				Control ($N = 51$) Grade (%)			
	Any	3	4	5	Any	3	4	5
Fatigue	74	6	0	0	20	0	0	0
Elevated aspartate aminotransferase (AST)	72	42	4	0	47	12	0	0
Elevated alkaline phosphatase (ALP)	70	8	0	0	33	0	0	0
Oedema	58	4	0	0	8	0	0	0
Anorexia	52	2	0	0	20	0	0	0
Fever	48	0	0	0	10	0	0	0
Elevated alanine aminotransferase (ALT)	44	22	4	0	31	8	0	0
Hypoalbuminemia	42	0	0	0	10	0	0	0
Elevated T-Bil	42	6	0	0	24	0	0	0
Thrombocytopenia	42	12	0	0	37	2	0	0
Diarrhoea	40	2	0	0	2	0	0	0
Anaemia	36	0	0	0	8	0	0	0
Ascites	24	4	0	0	2	0	0	0
Abdominal pains	18	0	0	0	4	0	0	0
Hypertension	16	2	0	0	14	2	0	0
Melena	2	0	0	2	0	0	0	0
Hepatic failure	2	0	0	2	0	0	0	0

Listed are adverse events, as defined by National Cancer Institute Common Terminology Criteria (version 3.0), that occurred in at least 15% of patients in the TSU-68 group or that were classified as grade 5.

liver function, those of 65 years age or more and those with hepatitis C. However, there was no clear evidence that TSU-68 affects PFS within other subgroups.

To explore the predictive potential of biomarkers, we analysed the relationship between PFS and the baseline levels of several proteins in Child–Pugh A patients (Table 3). Among patients with baseline t-PA concentration below the median value, the PFS of the TSU-68 group was longer than that of the control group. TSU-68 treatment may also improve PFS among patients with VCAM-1, ELAM-1, IL-8 or PDGF-BB levels above the median.

4. Discussion

TACE is the standard treatment for unresectable HCC and is performed repeatedly for local recurrence and new intrahepatic lesions. However, there have been few studies that have reported the antitumour effects of TACE based on mRECIST or the improvement of TACE treatment by chemotherapeutic or molecular target agents.[21]

TSU-68 was initially thought to have a typical and high tolerability profile. During treatment, grade 3 or higher adverse events rarely occurred, with the exception of temporarily elevated AST/ALT. Only one patient discontinued the study treatment due to AST/ALT elevation. Unlike with sorafenib and sunitinib,[5,22] no hand-foot skin reactions and little hypertension were observed in the TSU-68 group. The differences between the safety profiles of sorafenib/sunitinib and TSU-68 are thought to result from the inhibition spectrum of the target signal transduction molecules. TSU-68 strongly inhibits PDGFR, whereas other antiangiogenic compounds predominantly inhibit VEGFR; however, the mechanisms of these drugs remain unclear. There were two deaths that occurred in the TSU-68 group. Oesophageal varix rupture, as seen in one case, is a frequent phenomenon in cirrhotic patients, but liver failure is very rare in Child–Pugh class A or B patients following such event. In the second case, we could not obtain details about the episodes of melena. Therefore, we must consider the possibility of a relationship between these deaths and TSU-68 treatment.

In a phase III study of sorafenib in patients with unresectable HCC after TACE in Japan and South Korea, there was no statistically significant difference in time to progression between the sorafenib arm and the placebo arm.[23] Subgroup analysis in this study indicated that early administration of sorafenib after TACE may increase effectiveness. VEGF levels significantly increase 3–30 days after TACE.[24–27] Therefore, angiogenic inhibitors should be administered soon after the TACE procedure. The efficacy of TSU-68 would be better if it was administered immediately after TACE. However, for reasons of safety, TSU-68 treatment was started after complications of TACE resolved.

In this study, we explored the association between the baseline levels of 14 soluble proteins and the clinical efficacy of TSU-68. These proteins are regarded as important factors in signal transduction during angiogenesis[28,29] and are therefore potential predictive factors for TSU-68 efficacy. While other antiangiogenic compounds predominantly inhibit VEGFR,[22,30] TSU-68 strongly inhibits PDGFR.[10] In phase I/II study of TSU-68 in patients with advanced HCC, patients with high levels of VCAM-1 and PDGF-BB received greater clinical benefit from TSU-68 than those with low levels of these proteins.[15] In this phase II study, patients in

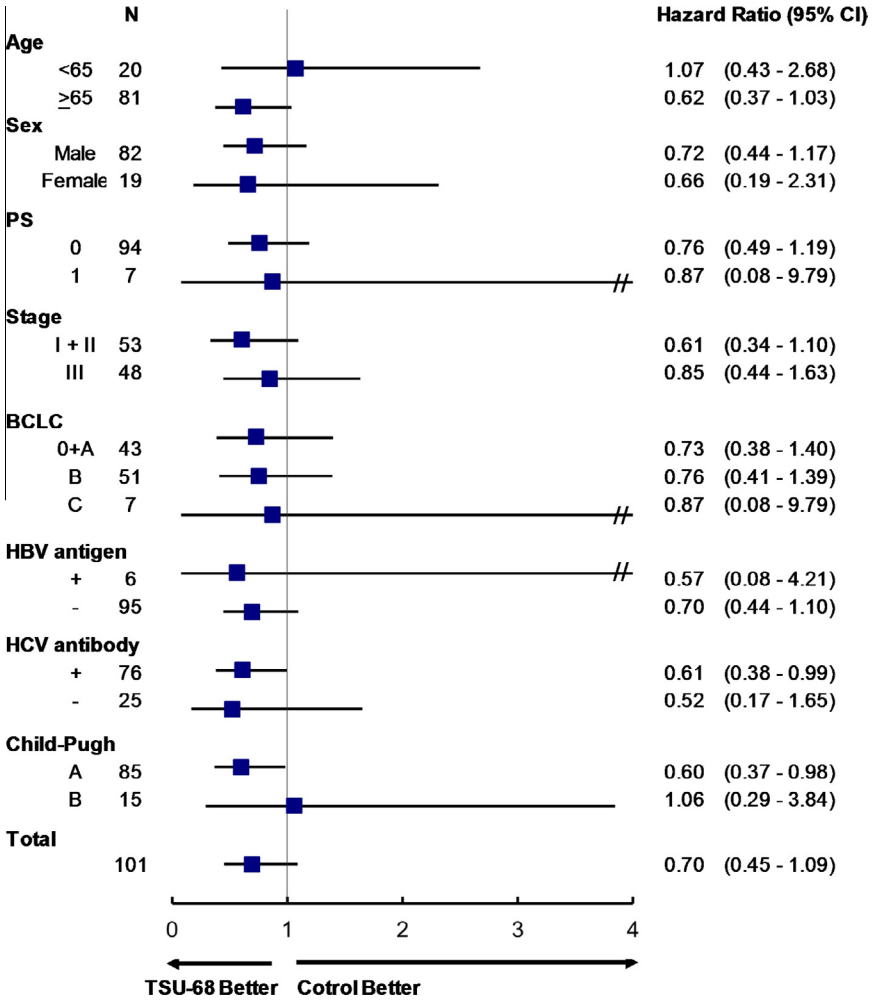

Fig. 3. Progression-free survival of selected subgroups according to background. Forest plot depicting the hazard ratio for progression-free survival (PFS) (TSU-68 group over control group) for each subgroup. The Child–Pugh classification was unknown for one patient. ECOG, Eastern Cooperative Oncology Group.

the TSU-68 group with VCAM-1, ELAM-1, IL-8 or PDGF-BB levels above the median had significantly longer PFS than those with levels below the median. The relatively long PFS we observed for those patients with high PDGF and VCAM-1 was similar to that observed in the phase I/II study.

Several reports state that PDGF-BB levels in the blood and tissue of HCC patients are higher than in healthy controls. PDGF-BB-PDGFR signals play an important role in HCC tumour growth.[31] VCAM-1 is an endothelial cell-specific marker. The concentration of this marker is reported to be associated with angiogenesis and the prognosis of several types of cancers, including HCC.[26,32,33]

A pattern similar to that shown in the previous phase I/II trial was observed for PDGF and VCAM-1. This suggests that PDGF-BB and VCAM-1 have potential for use as predictive markers. Further examination of PDGF-BB is needed, as the PDGF/PDGFR axis is an important target for the antiangiogenic activities of TSU-68.[34] It is not known how PDGF-BB contributes to the efficacy of TSU-68. Therefore, further research is required to verify the significance of these factors as novel predictive markers for the efficacy of TSU-68.

TSU-68 was found to have a safety profile that is compatible with good compliance, although the study included two protocol-related deaths, and it is anticipated to be efficacious for intermediate-stage HCC patients who have undergone TACE. A phase III study was initiated in 2010 to evaluate the survival benefit of TSU-68 in combination with repeated TACE (NCT01465464).

Clinical trials

This study is registered with JAPIC Clinical Trial Information, number JapicCTI-101087.

Table 3
Association between progression-free survival and baseline levels of angiogenic factors in patients with Child–Pugh A liver function.

Angiogenic factors	Cut off	Median progression-free survival (PFS) (days)		Hazard ratio	95% confidence interval (CI)	Log-rank test
		TSU-68	Control			*P*-Value
Tissue plasminogen activator (t-PA)	<Median	230	116	0.48	0.234–0.980	0.039[a]
	⩾Median	127	127	0.80	0.401–1.599	0.523
Vascular cell adhesion molecule-1 (VCAM-1)	<Median	224	170	0.63	0.287–1.380	0.241
	⩾Median	157	102	0.50	0.259–0.970	0.035[a]
Plasminogen activator inhibitor-1 (PAI-1)	<Median	224	123	0.50	0.236–1.050	0.061
	⩾Median	127	102	0.59	0.295–1.194	0.136
Endothelial-leucocyte adhesion molecule-1 (ELAM-1)	<Median	178	184	0.90	0.420–1.928	0.785
	⩾Median	173	73	0.49	0.245–0.968	0.035[a]
Interleukin-8 (IL-8)	<Median	125	125	0.89	0.435–1.808	0.741
	⩾Median	230	121	0.43	0.209–0.873	0.016[a]
Factor VIII	<Median	177	122	0.58	0.278–1.190	0.131
	⩾Median	167.5	127	0.65	0.329–1.290	0.214
Platelet-derived growth factor (PDGF)-AA	<Median	203.5	122	0.56	0.277–1.133	0.099
	⩾Median	127	170	0.69	0.338–1.414	0.306
PDGF-BB	<Median	124	122	0.57	0.275–1.163	0.111
	⩾Median	234	125	0.46	0.207–1.011	0.047[a]

[a] Statistically significant.

Funding

This study was supported by Taiho Pharmaceutical Co., Ltd. (Study No. 10032080).

Conflict of interest statement

None declared.

Acknowledgements

We are grateful to Drs. Yutaka Ariyoshi, Tomohide Tamura and Yuh Sakata for their extramural review. This trial was supported by Taiho Pharmaceutical Co., Ltd.

References

1. Parkin DM, Bray F, Ferlay J, Pisani P. Global cancer statistics, 2002. *CA Cancer J Clin* 2005;**55**:74–108.
2. Kew MC. Prevention of hepatocellular carcinoma. *Ann Hepatol* 2010;**9**:120–32.
3. Fassio E, Hepatitis C. And hepatocellular carcinoma. *Ann Hepatol* 2010;**9**(Suppl.):119–22.
4. Levrero M. Viral hepatitis and liver cancer: the case of hepatitis C. *Oncogene* 2006;**25**:3834–47.
5. Llovet JM, Ricci S, Mazzaferro V, et al. Sorafenib in advanced hepatocellular carcinoma. *N Engl J Med* 2008;**359**:378–90.
6. Cheng AL, Kang YK, Chen Z, et al. Efficacy and safety of sorafenib in patients in the Asia-Pacific region with advanced hepatocellular carcinoma: a phase III randomised, double-blind, placebo-controlled trial. *Lancet Oncol* 2009;**10**:25–34.
7. Llovet JM, Real MI, Montana X, et al. Arterial embolisation or chemoembolisation versus symptomatic treatment in patients with unresectable hepatocellular carcinoma: a randomised controlled trial. *Lancet* 2002;**359**:1734–9.
8. Lo CM, Ngan H, Tso WK, et al. Randomized controlled trial of transarterial lipiodol chemoembolization for unresectable hepatocellular carcinoma. *Hepatology* 2002;**35**:1164–71.
9. Bruix J, Sherman M. Management of hepatocellular carcinoma. *Hepatology* 2005;**42**:1208–36.
10. Laird AD, Vajkoczy P, Shawver LK, et al. SU6668 is a potent antiangiogenic and antitumor agent that induces regression of established tumors. *Cancer Res* 2000;**60**:4152–60.
11. Solorzano CC, Jung YD, Bucana CD, et al. In vivo intracellular signaling as a marker of antiangiogenic activity. *Cancer Res* 2001;**61**:7048–51.
12. Kuenen BC, Giaccone G, Ruijter R, et al. Dose-finding study of the multitargeted tyrosine kinase inhibitor SU6668 in patients with advanced malignancies. *Clin Cancer Res* 2005;**11**:6240–6.
13. Yorozuya K, Kubota T, Watanabe M, et al. TSU-68 (SU6668) inhibits local tumor growth and liver metastasis of human colon cancer xenografts via anti-angiogenesis. *Oncol Rep* 2005;**14**:677–82.
14. Naumova E, Ubezio P, Garofalo A, et al. The vascular targeting property of paclitaxel is enhanced by SU6668, a receptor tyrosine kinase inhibitor, causing apoptosis of endothelial cells and inhibition of angiogenesis. *Clin Cancer Res* 2006;**12**:1839–49.
15. Kanai F, Yoshida H, Tateishi R, et al. A phase I/II trial of the oral antiangiogenic agent TSU-68 in patients with advanced hepatocellular carcinoma. *Cancer Chemother Pharmacol* 2011;**67**:315–24.
16. Lenchioni R, Llovet JM. Modified RECIST (mRECIST) assessment for hepatocellular carcinoma. *Semin Liver Dis* 2010;**30**:52–60.
17. Gillmore R, Stuart S, Kirkwood A, et al. EASL and mRECIST responses are independent prognostic factors for survival in hepatocellular cancer patients treated with transarterial embolization. *J Hepatol* 2011;**55**:1309–16.

18. Ueno S, Tanabe G, Nuruki K, et al. Prognostic performance of the new classification of primary liver cancer of Japan (4th edition) for patients with hepatocellular carcinoma: a validation analysis. *Hepatol Res* 2002;**24**:395–403.
19. Llovet JM, Bru C, Bruix J. Prognosis of hepatocellular carcinoma: the BCLC staging classification. *Semin Liver Dis* 1999;**19**:329–38.
20. Thomas MB, Jaffe D, Choti MM, et al. Hepatocellular carcinoma: consensus recommendations of the National Cancer Institute Clinical Trials Planning Meeting. *J Clin Oncol* 2010;**28**:3994–4005.
21. Meza-Junco J, Montano-Loza AJ, Liu DM, et al. Locoregional radiological treatment for hepatocellular carcinoma; which, when and how? *Cancer Treat Rev* 2012;**38**:54–62.
22. Faivre S, Raymond E, Boucher E, et al. Safety and efficacy of sunitinib in patients with advanced hepatocellular carcinoma: an open-label, multicentre, phase II study. *Lancet Oncol* 2009;**10**:794–800.
23. Kudo M, Imanaka K, Chida N, et al. Phase III study of sorafenib after transarterial chemoembolisation in Japanese and Korean patients with unresectable hepatocellular carcinoma. *Eur J Cancer* 2011;**47**:2117–27.
24. Sergio A, Cristofori C, Cardin R, et al. Transcatheter arterial chemoembolization (TACE) in hepatocellular carcinoma (HCC): the role of angiogenesis and invasiveness. *Am J Gastroenterol* 2008;**103**:914–21.
25. Suzuki H, Mori M, Kawaguchi C, Adachi M, Miura S, Ishii H. Serum vascular endothelial growth factor in the course of transcatheter arterial embolization of hepatocellular carcinoma. *Int J Oncol* 1999;**14**:1087–90.
26. Li X, Feng GS, Zheng CS, Zhuo CK, Liu X. Expression of plasma vascular endothelial growth factor in patients with hepatocellular carcinoma and effect of transcatheter arterial chemoembolization therapy on plasma vascular endothelial growth factor level. *World J Gastroenterol* 2004;**10**:2878–82.
27. Poon RT, Lau C, Yu WC, Fan ST, Wong J. High serum levels of vascular endothelial growth factor predict poor response to transarterial chemoembolization in hepatocellular carcinoma: a prospective study. *Oncol Rep* 2004;**11**:1077–84.
28. Fuksiewicz M, Kowalska M, Kotowicz B, et al. Serum soluble tumour necrosis factor receptor type I concentrations independently predict prognosis in patients with breast cancer. *Clin Chem Lab Med* 2010;**48**:1481–6.
29. Okugawa Y, Miki C, Toiyama Y, Koike Y, Inoue Y, Kusunoki M. Serum level of soluble vascular cell adhesion molecule 1 is a valuable prognostic marker in colorectal carcinoma. *Dis Colon Rectum* 2009;**52**:1330–6.
30. Roodhart JM, Langenberg MH, Witteveen E, Voest EE. The molecular basis of class side effects due to treatment with inhibitors of the VEGF/VEGFR pathway. *Curr Clin Pharmacol* 2008;**3**:132–43.
31. Zhang T, Sun HC, Xu Y, et al. Overexpression of platelet-derived growth factor receptor alpha in endothelial cells of hepatocellular carcinoma associated with high metastatic potential. *Clin Cancer Res* 2005;**11**:8557–63.
32. O'Hanlon DM, Fitzsimons H, Lynch J, Tormey S, Malone C, Given HF. Soluble adhesion molecules (E-selectin, ICAM-1 and VCAM-1) in breast carcinoma. *Eur J Cancer* 2002;**38**:2252–7.
33. Alexiou D, Karayiannakis AJ, Syrigos KN, et al. Clinical significance of serum levels of E-selectin, intercellular adhesion molecule-1, and vascular cell adhesion molecule-1 in gastric cancer patients. *Am J Gastroenterol* 2003;**98**:478–85.
34. Raica M, Cinpean AM. Platelet-derived growth factor (PDGF)/PDGF receptors (PDGFR) axis as target for antitumor and antiangiogenic therapy. *Pharmaceuticals* 2010;**3**:572–99.

World Journal of Gastroenterology

Online Submissions: http://www.wjgnet.com/esps/
wjg@wjgnet.com
doi:10.3748/wjg.v19.i34.5706

World J Gastroenterol 2013 September 14; 19(34): 5706-5712
ISSN 1007-9327 (print) ISSN 2219-2840 (online)

BRIEF ARTICLE

Efficacy of treatment with rebamipide for endoscopic submucosal dissection-induced ulcers

Masaki Takayama, Shigenaga Matsui, Masanori Kawasaki, Yutaka Asakuma, Toshiharu Sakurai, Hiroshi Kashida, Masatoshi Kudo

Masaki Takayama, Shigenaga Matsui, Masanori Kawasaki, Yutaka Asakuma, Toshiharu Sakurai, Hiroshi Kashida, Masatoshi Kudo, Department of Gastroenterology and Hepatology, Kinki University, Osaka 589-8511, Japan
Author contributions: Takayama M and Matsui S contributed equally to this work; Takayama M, Matsui S, Kawasaki M, Asakuma Y, Sakurai T, Kashida H and Kudo M designed the research; Takayama M and Matsui S performed the research; Takayama M and Matsui S analyzed the data; Takayama M wrote the paper.
Correspondence to: Masaki Takayama, MD, Department of Gastroenterology and Hepatology, Kinki University, 377-2 Ohno-Higashi, Osaka-Sayama, Osaka 589-8511, Japan. masaki0742@yahoo.co.jp
Telephone: +81-72-3660221 Fax: +81-72-3672880
Received: June 9, 2013 Revised: July 25, 2013
Accepted: August 8, 2013
Published online: September 14, 2013

Abstract

AIM: To prospectively compare the healing rates of endoscopic submucosal dissection (ESD)-induced ulcers treated with either a proton-pump inhibitor (PPI) or rebamipide.

METHODS: We examined 90 patients with early gastric cancer who had undergone ESD. All patients were administered an intravenous infusion of the PPI lansoprazole (20 mg) every 12 h for 2 d, followed by oral administration of lansoprazole (30 mg/d, 5 d). After 7-d treatment, the patients were randomly assigned to 2 groups and received either lansoprazole (30 mg/d orally, *n* = 45; PPI group) or rebamipide (300 mg orally, three times a day; *n* = 45; rebamipide group). At 4 and 8 wk after ESD, the ulcer outcomes in the 2 groups were compared.

RESULTS: No significant differences were noted in patient age, underlying disease, tumor location, *Helicobacter pylori* infection rate, or ESD-induced ulcer size between the 2 groups. At both 4 and 8 wk, the healing rates of ESD-induced ulcers were similar in the PPI-treated and the rebamipide-treated patients (4 wk: PPI, 27.2%; rebamipide, 33.3%; *P* = 0.5341; 8 wk: PPI, 90.9%; rebamipide, 93.3%; *P* = 0.6710). At 8 wk, the rates of granulation lesions following ulcer healing were significantly higher in the PPI-treated group (13.6%) than in the rebamipide-treated group (0.0%; *P* = 0.0103). Ulcer-related symptoms were similar in the 2 treatment groups at 8 wk. The medication cost of 8-wk treatment with the PPI was 10945 yen *vs* 4889 yen for rebamipide. No ulcer bleeding or complications due to the drugs were observed in either treatment group.

CONCLUSION: The healing rate of ESD-induced ulcers was similar with rebamipide or PPI treatment; however, rebamipide treatment is more cost-effective and prevents granulation lesions following ulcer healing.

Key words: Early gastric cancer; Rebamipide; Endoscopic submucosal dissection; Gastric ulcer; Proton-pump inhibitor

Core tip: In this prospective randomized, parallel-controlled study, we demonstrated that rebamipide monotherapy was as effective as proton-pump inhibitor (PPI) in the healing of endoscopic submucosal dissection-induced ulcers, regardless of the location of the resected cancer, the degree of atrophic gastritis, or the presence of *Helicobacter pylori* infection. In addition, rebamipide treatment is more cost-effective and results in a better quality of ulcer healing compared with the PPI lansoprazole.

Takayama M, Matsui S, Kawasaki M, Asakuma Y, Sakurai T, Kashida H, Kudo M. Efficacy of treatment with rebamipide for endoscopic submucosal dissection-induced ulcers. *World J Gastroenterol* 2013; 19(34): 5706-5712 Available from: URL:

http://www.wjgnet.com/1007-9327/full/v19/i34/5706.htm DOI: http://dx.doi.org/10.3748/wjg.v19.i34.5706

INTRODUCTION

Endoscopic mucosal resection (EMR) is a well-established curative treatment for gastric neoplasms, such as early gastric cancer confined to the mucosa. However, EMR, performed using conventional techniques such as strip biopsy or cap EMR, does not always achieve *en bloc* resection. Thus, endoscopic submucosal dissection (ESD) has become the preferred treatment method. Compared with EMR, ESD facilitates the collection of larger specimens, regardless of lesion size or location, resulting in a higher rate of *en bloc* and histologically complete resection. Moreover, the rate of local recurrence of tumors after ESD may be lower than that after conventional EMR[1]. However, the iatrogenic ulcer that develops as a result of ESD is large, and requires a considerably longer healing time compared to that resulting from conventional EMR.

Proton-pump inhibitors (PPIs) are the most effective medications for the treatment of ESD-induced ulcers. However, studies have shown that PPI monotherapy does not heal the ESD-induced ulcers sufficiently within 4 wk[2-6]. Increased understanding of the mucosal defense system has prompted the development of mucoprotective agents for clinical use in Japan. The efficacy of combination treatment involving PPIs and the mucoprotective agent rebamipide in the early treatment of ESD-induced ulcers and in the prevention of relapse of such disorders has been clearly indicated[2-5].

Rebamipide [2-(4-chlorobenzoylamino)-3-[2-(1H)-quinolinon-4-yl]-propionic acid), a novel mucosal-protective and ulcer-healing drug, is widely prescribed in East Asia. Previous studies have indicated that rebamipide is effective in the treatment of gastric ulcers as well as decreasing the recurrence rate, without affecting the *Helicobacter pylori* infection status of the patients[7-12]. In addition, previous randomized-controlled studies have also found that rebamipide can prevent the formation of peptic ulcers induced by the administration of nonsteroidal anti-inflammatory drugs (NSAIDs) and can suppress the mucosal inflammation associated with chronic erosive gastritis[13,14]. However, to our knowledge, no reports on the use of rebamipide for the treatment of ESD-induced ulcers have been published.

In the present study, we have prospectively evaluated the efficacy of rebamipide monotherapy in comparison to PPI monotherapy for the treatment of iatrogenic ulcers resulting from ESD for early gastric cancers.

MATERIALS AND METHODS

Patients

We examined 90 consecutive patients with early gastric cancer who had been treated with ESD at Kinki University Hospital between February 2011 and January 2013. The study protocol was approved by the Kinki University Ethics Committee, and all participants provided written informed consent before undergoing ESD. In addition, the study was registered at the University Hospital Medical Information Network 000005134. All patients with early gastric cancer, including well-differentiated or moderately differentiated adenocarcinoma, were included in the study. The exclusion criteria were as follows: (1) current use of other anti-ulcer drugs, aspirin, NSAIDs, or prednisolone; (2) treatment with anti-coagulative agents; or (3) previous endoscopic treatment or surgery.

ESD procedure

ESD was performed with an insulation-tipped knife (KD-610L; Olympus Medical Systems, Tokyo, Japan) and a flush knife (BTDK2618JB; Fujifilm Medical System, Tokyo, Japan). The electrosurgical unit used was A VIO-300D (ERBE). The injection solutions contained glycerin with 1% indigo carmine dye and, depending on the tumor location, hyaluronic acid sodium (0.4%) was also added. The ulcers that developed after ESD were carefully examined endoscopically, and any visible vessels were heat-coagulated by using hot biopsy forceps (KD-410LR; Olympus Medical Systems). Thereafter, the resected specimens were stretched, pinned flat on a rubber plate, and measured.

Study design

The design of this single-center, open-label, prospective, randomized, parallel-controlled study is illustrated in Figure 1.

After ESD, all patients were administered an intravenous infusion of lansoprazole (20 mg; Takepron; Takeda Pharmaceutical, Osaka, Japan) every 12 h for 2 d, and received oral lansoprazole (30 mg/d) for 5 d. On postoperative day 7, the patients were randomly assigned to 2 groups and received either lansoprazole at a dose of 30 mg/d orally (PPI group; $n = 45$), or rebamipide (Mucosta; Otsuka Pharmaceutical Co., Tokyo, Japan) at a dose of 300 mg orally, 3 times a day ($n = 45$) for 8 wk. The primary endpoint was endoscopically documented ulcer healing; complete healing was defined as regression to the S-stage on the Sakita and Miwa scale[23]. Moreover, we evaluated the healing rates of atrophic gastritis based on the Kimura and Takemoto classification[24], in the presence or absence of *Helicobacter pylori* (*H. pylori*) infection. We also compared the response of ulcers in relation to their locations in the stomach (lower, middle, or upper).

The secondary endpoint was the ulcer reduction ratio, which was compared according to the ulcer location. For calculation of the ratio, we determined the maximum diameters of the ulcers and the diameters perpendicular to the maximum diameters, which were measured using a bendable endoscopic measuring device (M2-3; Olympus Corp., Tokyo, Japan). Moreover, we determined the ulcer size (maximal diameter × diameter perpendicular to the maximal diameter). At 4 and 8 wk after ESD, the healing and reduction rates for the ulcers were compared between the 2 groups. In addition, at 8 wk after ESD, we

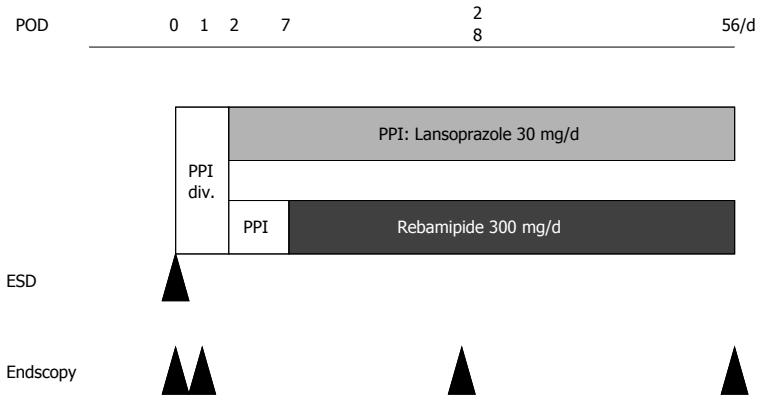

Figure 1 Study design. After ESD, all patients were administered an intravenous infusion of lansoprazole (20 mg; Takepron; Takeda Pharmaceutical, Osaka, Japan) every 12 h for 2 d, and received oral lansoprazole (30 mg/d) for 5 d. On postoperative day 7, the patients were randomly assigned to 2 groups and received either lansoprazole at a dose of 30 mg/d orally (PPI group; n = 45), or rebamipide (Mucosta; Otsuka Pharmaceutical Co., Tokyo, Japan) at a dose of 300 mg orally, 3 times a day (n = 45) for 8 wk. ESD: Endoscopic submucosal dissection; PPIs: Proton-pump inhibitors; div.: Drip intravenous infusion; POD: Postoperative days.

Table 1 Patient characteristics

	Lansoprazole group (n = 45)	Rebamipide group (n = 45)	P-value
Age (yr) (mean ± SD, median)	70 ± 7.8, 72	67 ± 8.0, 67	0.0930
Gender (M/F)	36/9	31/14	0.2269
H. pylori-infection	86.7%	84.4%	0.7643
Smoker	31.1%	33.3%	0.8215
Drinking alcohol	46.7%	42.2%	0.6714
History of disease	46.7%	31.1%	0.1301
Complicated disease	71.1%	71.1%	1.0000
Location of tumors			0.1620
Low	23	16	
Middle	17	26	
Upper	5	3	
Tumor size			0.4986
> 20 (mm)	13	16	
≤ 20 (mm)	32	29	
Histologic classification			0.6939
Tub1	41	42	
Tub2	4	3	
Dissected size (mean ± SD, mm)	30.5 ± 7.8	30.6 ± 6.4	0.9413
Dissected area (mean ± SD, mm^2)	687.9 ± 393.1.7	712.3 ± 298.6	0.7417
Glandular atrophy			0.3167
C-1	0	0	
C-2	3	2	
C-3	11	14	
O-1	19	13	
O-2	12	13	
O-3	0	3	
CandO			0.6547
C	14	16	
O	31	29	
Intestinal metaplasia	71.1%	68.9%	0.8181

H. pylori: *Helicobacter pylori*; M/F: Male/female.

evaluated the scar status of the ESD-induced ulcers according to the Quality of Ulcer Healing (QOUH).

Statistical analysis

Patient baseline characteristics and ulcer reduction ratios were compared using Pearson's χ^2 test or Student's t-test. Pearson's χ^2 test was also used to compare the healing rates of the ESD-induced ulcers and for the evaluation of the scar status of the ESD-induced ulcers according to the QOUH. Statistical significance was defined as $P < 0.05$.

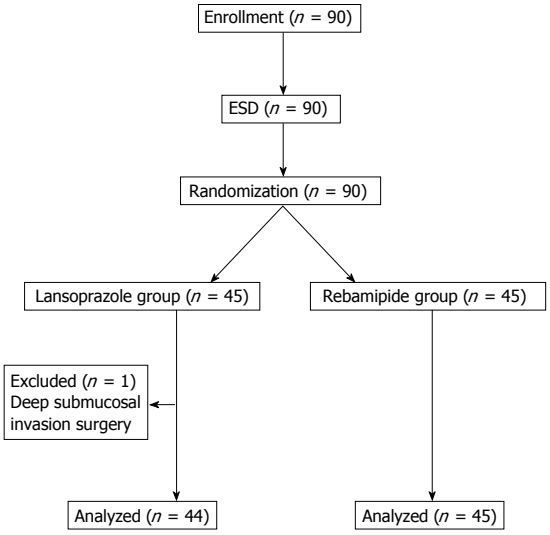

Figure 2 Flow chart of study participants. ESD: Endoscopic submucosal dissection.

RESULTS

Table 1 shows the patient characteristics of the 2 treatment groups. No significant differences were noted between the groups with regard to age; gender; tumor location; tumor size; histologic classification; ESD-induced ulcer size; glandular atrophy; history of disease; and the rates of *H. pylori* infection, smoking, drinking alcohol, or the presence of complicated disease or intestinal metaplasia. One patient was excluded from the PPI group because histologic examination of the resected specimen

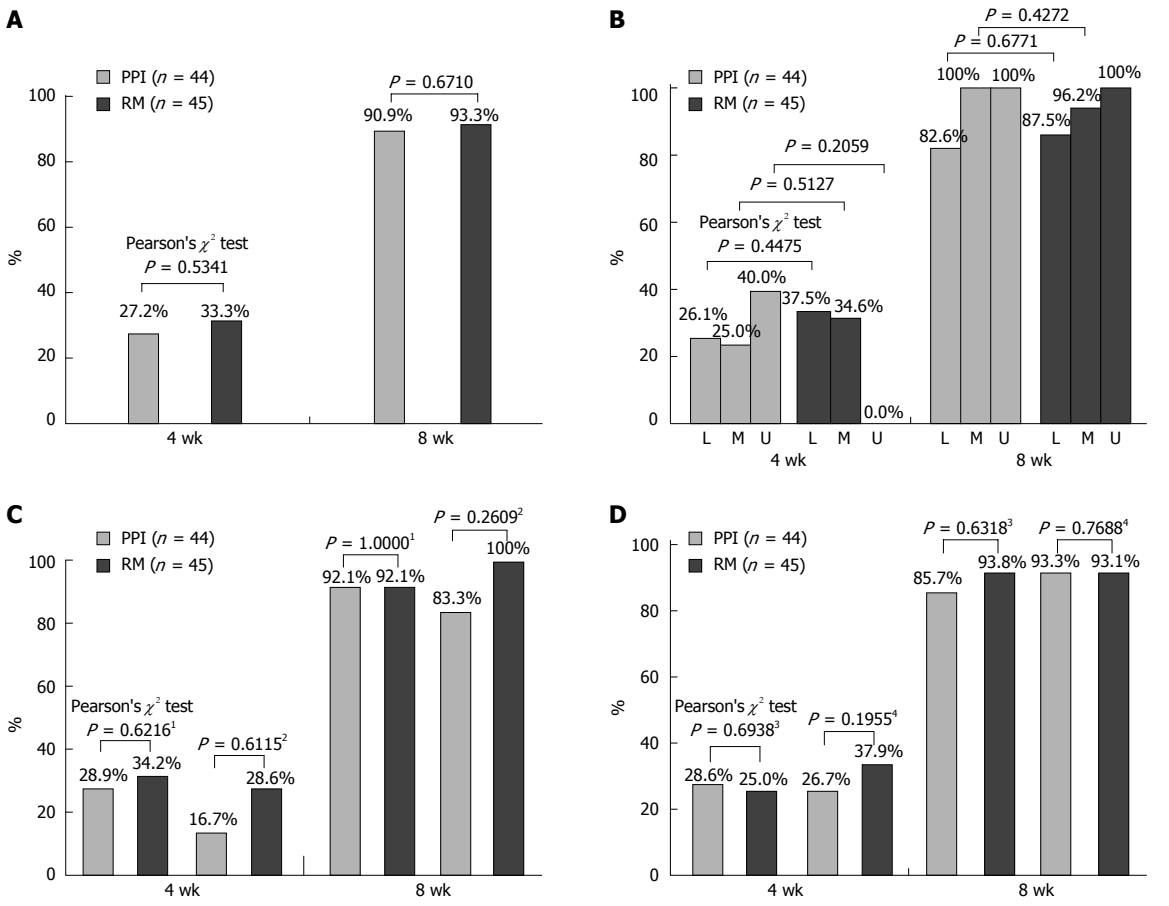

Figure 3 Rates of healing in both groups. A: The rates of healing to S stage in both groups; B: The rates of healing to S stage in both groups according to resected location. L: Low stomach, M: Middle stomach; U: Upper stomach. C: The rates of healing to S stage in both groups. [1]*Helicobacter pylori* (*H. pylori*) positive [2]*H. pylori* negative. D: The rates of healing to S stage in both groups in atrophic gastritis. [3]Closed type; [4]Open type. RM: Rebamipide.

indicated deep submucosal invasion (depth ≥ 500 μm; SM2 invasion). Hence, 44 patients in the PPI group and 45 in the rebamipide group constituted the final study cohort (Figure 2).

Ulcer responses

The rates of ulcer healing (regression to S-stage) were not significantly different between the PPI group (27.2%) and the rebamipide group (33.3%) at 4 wk ($P = 0.5341$) or at 8 wk (90.9% for the PPI group and 93.3% for the rebamipide group; $P = 0.6710$) (Figure 3A). Moreover, at 4 and 8 wk, the healing rates were not significantly different between the treatment groups with regard to ulcer location (low, middle, or upper stomach; Figure 3B) or with regard to the presence of absence of *H. pylori* infection (Figure 3C). In addition, at 4 and 8 wk, the healing rates of atrophic gastritis (closed or open type) were similar in the 2 treatment groups (Figure 3D).

Reduction ratios of ESD-induced ulcers

The reduction ratios of ESD-induced ulcers were similar at 4 and 8 wk in the rebamipide group (98.0% and 99.9%, respectively) and in the PPI group (97.2% and 99.9%, respectively) (Figure 4). These ratios were not influenced by the locations of the ulcers in the stomach (low, middle, and upper).

Quality of ulcer healing and adverse events

Six patients in the PPI group developed unusual gastric lesions, which comprised an overgrowth of granulation tissue at the ulcer site. At 8 wk, the proportion of patients who developed a flat scar in the rebamipide group (100%) was found to be significantly higher than that in the PPI group (86.3%; $P = 0.0103$) (Figure 5). No ulcer bleeding or complications related to the drugs used after ESD were observed in any of the study subjects.

DISCUSSION

Some authors have reported that the combination therapy involving PPI and rebamipide is superior to PPI monotherapy in the healing of ESD-induced ulcers[2-5]; however, to our knowledge, no reports on the efficacy of rebamipide for the treatment of ESD-induced ulcers

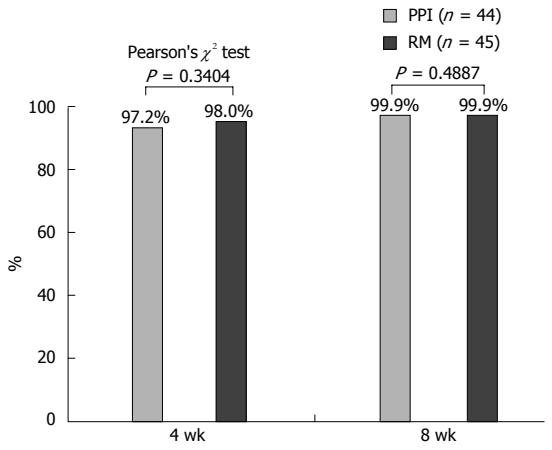

Figure 4 Reduction ratio of the endoscopic submucosal dissection-induced ulcers in both groups. PPI: Proton-pump inhibitor; RM: Rebamipide.

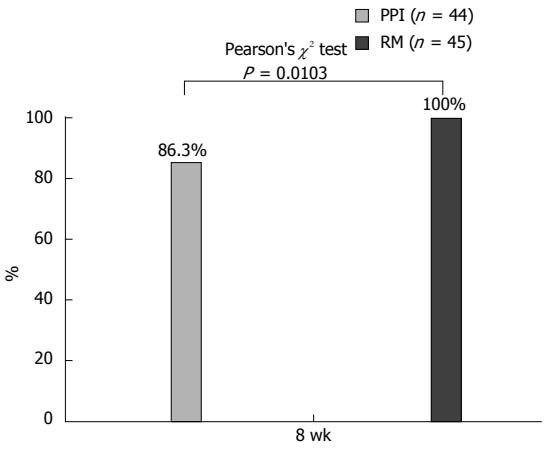

Figure 5 Proportion of patients who developed a flat scar after ulcer healing in both groups. PPI: Proton-pump inhibitor; RM: Rebamipide.

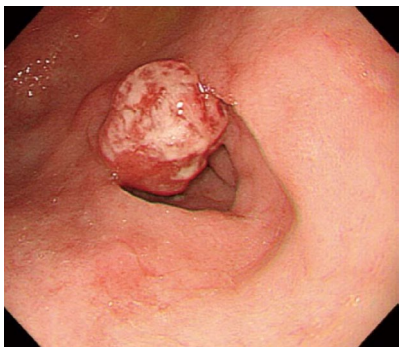

Figure 6 At 8 wk, granulation lesions following ulcer healing in the proton-pump inhibitors treated group.

have been published. In this prospective randomized, parallel-controlled study, we demonstrated that rebamipide monotherapy was as effective as PPI in the healing of ESD-induced ulcers, regardless of the location of the resected cancer, the degree of atrophic gastritis, or the presence of *H. pylori* infection.

Although the response of post-ESD ulcers to PPIs and rebamipide may be similar, the mechanisms of action of these drugs are different. PPIs decrease gastric acid production, whereas rebamipide stimulates the production of prostaglandins[19], epidermal growth factor[12,20], and nitric oxide[21], and decreases the level of oxygen-free radicals[22]. These mucosal protective actions of rebamipide appear to promote ulcer healing. Fujiwara *et al*[3] showed that 8 wk of PPI and rebamipide treatment was particularly effective for patients with severe atrophic gastritis, classified as O-3. Severe atrophic gastritis may result in the formation of a low-acid environment in the stomach; therefore, acid-suppressive agents such as PPI alone may have a limited effect. However, rebamipide can be effective in this environment because of its different mechanism of action. We believe that this is a contributing factor to the similar efficacies observed between PPIs and rebamipide regardless of the degree of atrophic gastritis.

Previous studies have reported that various mechanisms are involved in the effects of rebamipide on *H. pylori*-positive atrophic gastritis; these include prevention of adhesion of the bacteria to gastric epithelial cells, and inhibition of *H. pylori*-induced secretion of prostaglandin E2 from neutrophils and interleukin-8 expression in gastric epithelial cells[25-28]. Terano *et al*[15] indicated that the treatment of gastric ulcers with rebamipide promotes ulcer healing regardless of the success or failure of *H. pylori* eradication therapy, and Higuchi et al showed that rebamipide prevents the recurrence of gastric ulcers without affecting the *H. pylori* infection status[10]. In the present study, PPI and rebamipide appeared to aid in ulcer healing without affecting the *H. pylori* infection status.

Moreover, we noted that the proportion of patients who developed a flat scar at the ulcer site was significantly higher in the rebamipide group than in the PPI group. Thus, rebamipide appears to be more effective than PPIs in improving the QOUH. In animal studies, rebamipide was found to improve the QOUH by increasing the level of prostaglandin E_2 and decreasing the levels of malondialdehyde and interleukin-8 in the gastric mucosa[16]. In the present study, the unusual elevated gastric lesions that were observed following ulcer healing could not be easily characterized as benign granulation tissue or a malignant recurrence without performing a biopsy (Figure 6). Therefore, we believe that improvement in QOUH is essential for preventing the occurrence of mucosal protrusion due to the growth of granulation tissue.

The most frequent complication that occurs after endoscopic therapy is bleeding, and the rate of intraoperative bleeding is significantly higher with ESD than with EMR. Jeong *et al*[17] reported that PPIs may be more effective than histamine H_2 inhibitors in preventing bleeding after ESD by promoting a more rapid healing of these large iatrogenic ulcers[17]. Moreover, Uedo *et al*[18] indicated that therapy with PPI was more effective than treatment

with histamine H_2 inhibitors in preventing delayed bleeding from ulcers induced by ESD. However, in the present study, no post-ESD bleeding or complications related to the drugs used were noted in the patients receiving rebamipide or PPI treatment; moreover, the ratio of ulcer reduction was at least 90% in both groups at 8 wk after initiation of therapy. Thus, our findings indicated that the rate of intraoperative bleeding was not significantly different between both the groups.

In addition, in the present study, we found that treatment with rebamipide was more cost-effective than treatment with the PPI lansoprazole. The cost of the 56-d treatment course was 4889 yen for rebamipide and 10945 yen for lansoprazole, which is a difference of 44.7%. This high difference in cost may be a factor in determining which medication to prescribe in the treatment of ESD-induced ulcers.

In conclusion, rebamipide monotherapy was equivalent to treatment with a PPI (lansoprazole) in the healing of ulcers induced by ESD for early gastric cancer. The similarity in the treatment efficacy was observed irrespective of the presence of *H. pylori* infection, the severity of atrophic gastritis, or the locations of the ulcers in the stomach. However, rebamipide therapy also resulted in a more favorable QOUH compared with that obtained by PPI treatment. Moreover, the treatment involving rebamipide was more cost-effective compared to the treatment with the PPI lansoprazole for the treatment of ESD-induced ulcers.

ACKNOWLEDGMENTS

The authors wish to thank Otsuka Pharmaceutical Co., Ltd. for providing the drugs for the study.

COMMENTS

Background

Endoscopic submucosal dissection (ESD) is useful for treating early gastric cancer. The artificial ulcer that is generated after ESD is large, and needs a considerably longer healing time compared with conventional endoscopic mucosal resection (EMR). Rebamipide is one of the mucoprotective antiulcer drug, and is widely employed treatment of gastric ulcer in Japan.

Research frontiers

Previous studies have shown that the combination therapy involving proton pump inhibitor (PPI) and rebamipide is superior to PPI monotherapy in the healing of ESD-induced ulcers; however, to people knowledge, no reports on the efficacy of rebamipide for the treatment of ESD-induced ulcers have been published. Therefore, the authors prospectively investigated differences in healing of ESD-induced ulcers according to treatment with PPI or rebamipide only.

Innovations and breakthroughs

In this prospective randomized, parallel-controlled study, the authors demonstrated that rebamipide monotherapy was as effective as PPI in the healing of endoscopic submucosal dissection-induced ulcers. In addition, rebamipide treatment was more cost-effective and resulted in a better quality of ulcer healing compared to the PPI lansoprazole treatment.

Applications

This article suggests that the healing rate of ESD-induced ulcers was similar with rebamipide or PPI treatment; however, rebamipide treatment is more cost-effective and prevents granulation lesions following ulcer healing. However, it is a small study, therefore, a prospective multicenter study with a large sample size should be performed to assess the efficacy of treatment with rebamipide for endoscopic submucosal dissection-induced ulcers.

Terminology

ESD is a well-established curative treatment for early gastric cancer. ESD facilitates the collection of larger specimens, regardless of lesion size or location, resulting in a higher rate of en bloc and histologically complete resection. However, the iatrogenic ulcer that develops as a result of ESD is large, and requires a considerably longer healing time compared to that resulting from conventional EMR. Rebamipide is a novel mucosal-protective and ulcer-healing drug that has been widely prescribed in East Asia. Rebamipide stimulates the production of prostaglandins, epidermal growth factor, and nitric oxide, and decreases the level of oxygen-free radicals. These mucosal protective actions of rebamipide appear to promote ulcer healing.

Peer review

This paper is well written. The clinical results are appropriately described. The authors present the Efficacy of treatment with rebamipide for endoscopic submucosal dissection-induced ulcers. The data indicate the healing rate of ESD-induced ulcers was similar with rebamipide or PPI treatment; however, rebamipide treatment is more cost-effective and prevents granulation lesions following ulcer healing.

REFERENCES

1 **Oka S**, Tanaka S, Kaneko I, Mouri R, Hirata M, Kawamura T, Yoshihara M, Chayama K. Advantage of endoscopic submucosal dissection compared with EMR for early gastric cancer. *Gastrointest Endosc* 2006; **64**: 877-883 [PMID: 17140890 DOI: 10.1016/j.gie.2006.03.932]

2 **Kato T**, Araki H, Onogi F, Ibuka T, Sugiyama A, Tomita E, Nagaki M, Moriwaki H. Clinical trial: rebamipide promotes gastric ulcer healing by proton pump inhibitor after endoscopic submucosal dissection--a randomized controlled study. *J Gastroenterol* 2010; **45**: 285-290 [PMID: 19957195 DOI: 10.1007/s00535-009-0157-0]

3 **Fujiwara S**, Morita Y, Toyonaga T, Kawakami F, Itoh T, Yoshida M, Kutsumi H, Azuma T. A randomized controlled trial of rebamipide plus rabeprazole for the healing of artificial ulcers after endoscopic submucosal dissection. *J Gastroenterol* 2011; **46**: 595-602 [PMID: 21359522 DOI: 10.1007/s00535-011-0372-3]

4 **Kobayashi M**, Takeuchi M, Hashimoto S, Mizuno K, Sato Y, Narisawa R, Aoyagi Y. Contributing factors to gastric ulcer healing after endoscopic submucosal dissection including the promoting effect of rebamipide. *Dig Dis Sci* 2012; **57**: 119-126 [PMID: 21842241 DOI: 10.1007/s10620-011-1850-4]

5 **Shin WG**, Kim SJ, Choi MH, Kim KO, Jang HJ, Park CH, Baek IH, Kim KH, Baik GH, Kae SH, Kim JH, Kim HY. Can rebamipide and proton pump inhibitor combination therapy promote the healing of endoscopic submucosal dissection-induced ulcers? A randomized, prospective, multicenter study. *Gastrointest Endosc* 2012; **75**: 739-747 [PMID: 22281110 DOI: 10.1016/j.gie.2011.11.004]

6 **Asakuma Y**, Kudo M, Matsui S, Okada M, Kawasaki M, Umehara Y, Ichikawa T, Kitai S. Comparison of an ecabet sodium and proton pump inhibitor (PPI) combination therapy with PPI alone in the treatment of endoscopic submucosal dissection (ESD)--induced ulcers in early gastric cancer: prospective randomized study. *Hepatogastroenterology* 2009; **56**: 1270-1273 [PMID: 19950775]

7 **Yamasaki K**, Kanbe T, Chijiwa T, Ishiyama H, Morita S. Gastric mucosal protection by OPC-12759, a novel antiulcer compound, in the rat. *Eur J Pharmacol* 1987; **142**: 23-29 [PMID: 3480223]

8 **Ogino K**, Hobara T, Ishiyama H, Yamasaki K, Kobayashi H, Izumi Y, Oka S. Antiulcer mechanism of action of rebamipide, a novel antiulcer compound, on diethyldithiocarbamate-induced antral gastric ulcers in rats. *Eur J Pharmacol* 1992; **212**: 9-13 [PMID: 1313372]

9 **Arakawa T**, Watanabe T, Fukuda T, Yamasaki K, Kobayashi K. Rebamipide, novel prostaglandin-inducer accelerates

healing and reduces relapse of acetic acid-induced rat gastric ulcer. Comparison with cimetidine. *Dig Dis Sci* 1995; **40**: 2469-2472 [PMID: 7587834]
10 **Higuchi K**, Arakawa T, Nebiki H, Uchida T, Fujiwara Y, Ando K, Yamasaki K, Takaishi O, Fukuda T, Kobayashi K, Kuroki T. Rebamipide prevents recurrence of gastric ulcers without affecting Helicobacter pylori status. *Dig Dis Sci* 1998; **43**: 99S-106S [PMID: 9753234]
11 **Arakawa T**, Kobayashi K, Yoshikawa T, Tarnawski A. Rebamipide: overview of its mechanisms of action and efficacy in mucosal protection and ulcer healing. *Dig Dis Sci* 1998; **43**: 5S-13S [PMID: 9753220]
12 **Tarnawski A**, Arakawa T, Kobayashi K. Rebamipide treatment activates epidermal growth factor and its receptor expression in normal and ulcerated gastric mucosa in rats: one mechanism for its ulcer healing action? *Dig Dis Sci* 1998; **43**: 90S-98S [PMID: 9753233]
13 **Park SH**, Cho CS, Lee OY, Jun JB, Lin SR, Zhou LY, Yuan YZ, Li ZS, Hou XH, Zhao HC, Kachintorn U, Kositchaiwat C, Lertkupinit C. Comparison of Prevention of NSAID-Induced Gastrointestinal Complications by Rebamipide and Misoprostol: A Randomized, Multicenter, Controlled Trial-STORM STUDY. *J Clin Biochem Nutr* 2007; **40**: 148-155 [PMID: 18188417 DOI: 10.3164/jcbn.40.148]
14 **Du Y**, Li Z, Zhan X, Chen J, Gao J, Gong Y, Ren J, He L, Zhang Z, Guo X, Wu J, Tian Z, Shi R, Jiang B, Fang D, Li Y. Anti-inflammatory effects of rebamipide according to Helicobacter pylori status in patients with chronic erosive gastritis: a randomized sucralfate-controlled multicenter trial in China-STARS study. *Dig Dis Sci* 2008; **53**: 2886-2895 [PMID: 18288617 DOI: 10.1007/s10620-007-0180-z]
15 **Terano A**, Arakawa T, Sugiyama T, Suzuki H, Joh T, Yoshikawa T, Higuchi K, Haruma K, Murakami K, Kobayashi K. Rebamipide, a gastro-protective and anti-inflammatory drug, promotes gastric ulcer healing following eradication therapy for Helicobacter pylori in a Japanese population: a randomized, double-blind, placebo-controlled trial. *J Gastroenterol* 2007; **42**: 690-693 [PMID: 17701133 DOI: 10.1007/s00535-007-2076-2]
16 **Qi Z**, Jie L, Haixia C, Xiaoying Z. Effect of rebamipide on quality of peptic ulcer healing in rat. *Dig Dis Sci* 2009; **54**: 1876-1883 [PMID: 19082723 DOI: 10.1007/s10620-008-0577-3]
17 **Jeong HK**, Park CH, Jun CH, Lee GH, Kim HI, Kim HS, Choi SK, Rew JS. A prospective randomized trial of either famotidine or pantoprazole for the prevention of bleeding after endoscopic submucosal dissection. *J Korean Med Sci* 2007; **22**: 1055-1059 [PMID: 18162722 DOI: 10.3346/jkms.2007.22.6.1055]
18 **Uedo N**, Takeuchi Y, Yamada T, Ishihara R, Ogiyama H, Yamamoto S, Kato M, Tatsumi K, Masuda E, Tamai C, Yamamoto S, Higashino K, Iishi H, Tatsuta M. Effect of a proton pump inhibitor or an H2-receptor antagonist on prevention of bleeding from ulcer after endoscopic submucosal dissection of early gastric cancer: a prospective randomized controlled trial. *Am J Gastroenterol* 2007; **102**: 1610-1616 [PMID: 17403076 DOI: 10.1111/j.1572-0241.2007.01197.x]
19 **Kleine A**, Kluge S, Peskar BM. Stimulation of prostaglandin biosynthesis mediates gastroprotective effect of rebamipide in rats. *Dig Dis Sci* 1993; **38**: 1441-1449 [PMID: 8393757]
20 **Tarnawski AS**, Chai J, Pai R, Chiou SK. Rebamipide activates genes encoding angiogenic growth factors and Cox2 and stimulates angiogenesis: a key to its ulcer healing action? *Dig Dis Sci* 2004; **49**: 202-209 [PMID: 15104358]
21 **Takaishi O**, Arakawa T, Yamasaki K, Fujiwara Y, Uchida T, Tominaga K, Watanabe T, Higuchi K, Fukuda T, Kobayashi K, Kuroki T. Protective effect of rebamipide against ammonia-induced gastric mucosal lesions. *Dig Dis Sci* 1998; **43**: 78S-82S [PMID: 9753231]
22 **Naito Y**, Yoshikawa T, Tanigawa T, Sakurai K, Yamasaki K, Uchida M, Kondo M. Hydroxyl radical scavenging by rebamipide and related compounds: electron paramagnetic resonance study. *Free Radic Biol Med* 1995; **18**: 117-123 [PMID: 7896165]
23 **Sakita T**, Fukushima H. Endoscopic diagnosis. In: Yoshitoshi Y, editor. Ulcer of the stomach and duodenum. Tokyo: Nankodo, 1971: 198-208
24 **Kimura K**, Takemoto T. An endoscopic recognition of the atrophic border and its significance in chronic gastritis. *Endoscopy* 1969; **3**: 87-97
25 **Hayashi S**, Sugiyama T, Amano K, Isogai H, Isogai E, Aihara M, Kikuchi M, Asaka M, Yokota K, Oguma K, Fujii N, Hirai Y. Effect of rebamipide, a novel antiulcer agent, on Helicobacter pylori adhesion to gastric epithelial cells. *Antimicrob Agents Chemother* 1998; **42**: 1895-1899 [PMID: 9687380]
26 **Azuma T**, Yamazaki S, Yamakawa A, Ito Y, Ohtani M, Dojo M, Yamazaki Y, Higashi H, Hatakeyama M. The effects of cure of Helicobacter pylori infection on the signal transduction of gastric epithelial cells. *Aliment Pharmacol Ther* 2003; **18** Suppl 1: 39-44 [PMID: 12925139 DOI: 10.1046/j.1365-2036.18.s1.2.x]
27 **Yoshida N**, Ishikawa T, Ichiishi E, Yoshida Y, Hanashiro K, Kuchide M, Uchiyama K, Kokura S, Ichikawa H, Naito Y, Yamamura Y, Okanoue T, Yoshikawa T. The effect of rebamipide on Helicobacter pylori extract-mediated changes of gene expression in gastric epithelial cells. *Aliment Pharmacol Ther* 2003; **18** Suppl 1: 63-75 [PMID: 12925142 DOI: 10.1046/j.1365-2036.18.s1.7.x]
28 **Kim JS**, Kim JM, Jung HC, Song IS. The effect of rebamipide on the expression of proinflammatory mediators and apoptosis in human neutrophils by Helicobacter pylori water-soluble surface proteins. *Aliment Pharmacol Ther* 2003; **18** Suppl 1: 45-54 [PMID: 12925140 DOI: 10.1046/j.1365-2036.18.s1.1.x]

P- Reviewers Mizukami K, Naito Y **S- Editor** Zhai HH
L- Editor Cant MR **E- Editor** Zhang DN

百世登
Baishideng®

Published by **Baishideng Publishing Group Co., Limited**
Flat C, 23/F., Lucky Plaza,
315-321 Lockhart Road, Wan Chai, Hong Kong, China
Fax: +852-65557188
Telephone: +852-31779906
E-mail: bpgoffice@wjgnet.com
http://www.wjgnet.com

ISSN 1007-9327

9 771007 932045 34>

Preface

Digestive Diseases

Dig Dis 2013;31:405–407
DOI: 10.1159/000355379

Chronic Liver Diseases and Hepatocellular Carcinoma: An Update for 2013

Masatoshi Kudo

Department of Gastroenterology and Hepatology, Kinki University School of Medicine, Osakasayama, Japan

The 10th Korea-Japan Liver Symposium was held on July 7–8, 2013, in Busan, Korea, in conjunction with the 4th Asia Pacific Primary Liver Cancer Expert Meeting on July 5–7, 2013.

Nishida et al. [1] reported 4 cases of Budd-Chiari syndrome with complete or incomplete obstruction of the inferior vena cava and hepatic vein. Within 1 month of performing balloon angioplasty, improved liver function was evident. They therefore concluded that it is crucial to manage this rare disease before it progresses to liver cirrhosis.

Yada et al. [2] reviewed the characteristic features of IgG4-related disease and discussed its association with autoimmune hepatitis. They concluded that some patients with autoimmune hepatitis present symptoms of IgG4-related disease and respond effectively to steroid treatment.

Sugimoto et al. [3] reported that the interferon (IFN) and ribavirin (RBV) resistance-determining region with 6 or more mutations correlated with IFN-λ1 and was the only significant predictor of a sustained virological response (SVR) in patients with a high viral load of hepatitis C genotype 1b. High serum levels of IFN-λ1 may therefore be conducive to pegylated IFN and RBV combination therapy via effects on the immunomodulatory system.

Kim et al. [4] investigated the predictive factor of response to pegylated IFN plus RBV combination therapy for chronic hepatitis C genotype 2a and 2b with high viral load. They investigated the impact of host genetics represented by the single nucleotide polymorphism (SNP) of the IL28B gene and viral genetic variations within the NS5A on the outcome of pegylated IFN and RBV treatment. They concluded that the NS5A sequence heterogeneity and IL28B SNP are useful factors to predict the sensitivity to pegylated IFN plus RBV therapy in HCV-2a and HCV-2b infections.

Sugimoto et al. [5] reported that double-filtration plasmapheresis plus IFN treatment in nonresponders to pegylated IFN plus RBV combination therapy in patients with a high viral load of hepatitis C genotype 1b achieved SVR in 15% (10/40) of patients, which represents a relatively good result. The significant factors associated with SVR were interleukin-28B major type and a rapid virological response at week 4.

Sakurai et al. [6] reported that hypothermia has a direct protective effect on hepatocytes in a mouse model of fulminant hepatitis that is realized through reducing the production of reactive oxygen species. This finding may lead to the development of novel therapeutic methods for fulminant hepatitis in humans.

Nishida and Kudo [7] described the role of oxidative stress and epigenetic instability in hepatocarcinogenesis. They induced epigenetic instability via two types of DNA alterations: hypermethylation of the promoter of tumor suppressor genes (TSGs) and hypomethylation of nonpromoter CpG sites, such as repetitive elements and satellite DNA. The former causes transcriptional inactivation of TSGs, while the latter induces chromosomal instability and abnormal activation of oncogenes as well as mobile

KARGER

E-Mail karger@karger.com
www.karger.com/ddi

0257–2753/13/0316–0405$38.00/0

Masatoshi Kudo, MD
Department of Gastroenterology and Hepatology, Kinki University School of Medicine
337-2 Ohno-Higashi
Osakasayama, Osaka 589-8511 (Japan)
E-Mail m-kudo@med.kindai.ac.jp

genetic elements. These mechanisms act in concert and induce epigenetic instability, leading to hepatocellular carcinoma (HCC).

Kim et al. [8] reported that activation-induced cytidine deaminase is a nucleotide-editing enzyme and that its aberrant expression induced by the inflammatory response contributes to hepatocarcinogenesis via the accumulation of genetic alterations in various tumor-related genes.

Nishida et al. [9] reported that oxidative stress alters chromatin status, which leads to abnormal methylation of TSGs and contributes to hepatocarcinogenesis in chronic hepatitis C patients.

Tsuji et al. [10] reported that CD34 expression in the capillaries and sinusoids of noncancerous hepatic tissue is a risk factor for multicentric recurrence of HCC after surgical resection. They concluded that histologic assessment of hepatic tissue with CD34 immunohistochemistry might be useful for the prognostic evaluation of HCC patients after surgery.

Inoue et al. [11] reported previous treatment for HCC and hyperintensity on T2-weighted magnetic resonance (MR) images as risk factors for the hypervascular transformation of hypovascular nodules that show hypointensity in the hepatobiliary phase image of Gd-EOB-DTPA-enhanced MR imaging. Accordingly, these nodules require careful and extensive follow-up, even though they are hypovascular.

Minami et al. [12] examined whether ablation of the needle tract can prevent bleeding after percutaneous radiofrequency ablation (RFA) for malignant tumors. They found that ablation of the needle tract seems to have no effect on preventing iatrogenic hemorrhage after RFA.

Makino et al. [13] reported the development of a novel variation of the extracted-overlay function in computed tomography (CT)/MR-ultrasonography (US) fusion imaging for RFA, in which only the tumor extracted from CT/MR images with a virtual ablative margin of arbitrary thickness is overlaid on US images. They found this function extremely useful for treatment planning and guidance for RFA as it allows the extracted tumor with an ablative safety margin to be visualized on US images, even during and after ablation.

Kudo et al. [14] performed a multicenter retrospective study to clarify the survival benefits of nontransplant treatments for patients with HCC with associated Child-Pugh C cirrhosis. They found that nontransplant treatments such as transarterial chemoembolization [15], hepatic arterial infusion chemotherapy [16], percutaneous ethanol injection therapy [17] and RFA [18] are independent prognostic factors in these HCC patients. They recommended that medical treatment be considered for these patients, especially those with low Child-Pugh scores. They state that this fact confirms the validity of the recommendation by consensus-based treatment algorithm proposed by the Japan Society of Hepatology [19].

The symposium was highly successful and I firmly believe the findings presented will benefit the entire readership of *Digestive Diseases*, especially readers who are interested in chronic liver diseases and HCC.

References

1 Nishida N, Imamura S, Ida H, Hagiwara S, Kagioka Y, Minami Y, Maetani Y, Itoh K, Kudo M: Clinical and histological features of different types of Budd-Chiari syndrome: a comparison of 4 cases. Dig Dis 2013;31:408–414.

2 Yada N, Kudo M, Chung H, Watanabe T: Autoimmune hepatitis and immunoglobulin G4-associated autoimmune hepatitis. Dig Dis 2013;31:415–420.

3 Sugimoto K, Kim SR, El-Shamy A, Imoto S, Ando K, Kim KI, Tanaka Y, Yano Y, Kim SK, Hasegawa Y, et al: Factors of response to pegylated interferon/ribavirin combination therapy and mechanism of viral clearance. Dig Dis 2013;31:421–425.

4 Kim SR, El-Shamy A, Imoto S, Kim KI, Sugimoto K, Kim SK, Tanaka Y, Hatae T, Hasegawa Y, Fujinami A, et al: Prediction of response to pegylated interferon/ribavirin combination therapy for chronic hepatitis C genotypes 2a and 2b and high viral load. Dig Dis 2013;31:426–433.

5 Sugimoto K, Kim SR, El-Shamy A, Imoto S, Fujioka H, Kim KI, Tanaka Y, Yano Y, Kim SK, Hasegawa Y, et al: Outcome of double-filtration plasmapheresis plus interferon treatment in nonresponders to pegylated interferon plus ribavirin combination therapy. Dig Dis 2013;31:434–439.

6 Sakurai T, Kudo M, Watanabe T, Itoh K, Higashitsuji H, Arizumi T, Inoue T, Hagiwara S, Ueshima K, Nishida N, Fukumoto M, Fujita J: Hypothermia protects against fulminant hepatitis in mice by reducing reactive oxygen species production. Dig Dis 2013;31:440–446.

7 Nishida N, Kudo M: Oxidative stress and epigenetic instability in human hepatocarcinogenesis. Dig Dis 2013;31:447–453.

8 Kim SK, Marusawa H, Eso Y, Chiba T, Kudo M: Novel mouse models of hepatocarcinogenesis with stepwise accumulation of genetic alterations. Dig Dis 2013;31:454–458.

9 Nishida N, Arizumi T, Takita M, Kitai S, Yada N, Hagiwara S, Inoue T, Minami Y, Ueshima K, Sakurai T, Kudo M: Reactive oxygen species induce epigenetic instability through the formation of 8-hydroxydeoxyguanosine in human hepatocarcinogenesis. Dig Dis 2013;31:459–466.

10 Tsuji N, Ishiguro S, Sasaki Y, Kudo M: CD34 expression in noncancerous liver tissue predicts multicentric recurrence of hepatocellular carcinoma. Dig Dis 2013;31:467–471.

11 Inoue T, Hyodo T, Murakami T, Takayama Y, Nishie A, Higaki A, Korenaga K, Sakamoto A, Osaki Y, Aikata H, et al: Hypovascular hepatic nodules showing hypointense on the hepatobiliary-phase image of Gd-EOB-DTPA-enhanced MRI to develop a hypervascular hepatocellular carcinoma: a nationwide retrospective study on their natural course and risk factors. Dig Dis 2013;31:472–479.
12 Minami Y, Hayaishi S, Kudo M: Radiofrequency ablation for hepatic malignancies: is needle tract cauterization necessary for preventing iatrogenic bleeding? Dig Dis 2013; 31:480–484.
13 Makino Y, Imai Y, Igura T, Kogita S, Sawai Y, Fukuda K, Hori M, Kudo M, Murakami T: Usefulness of the extracted-overlay function in CT/MR-ultrasonography fusion imaging for radiofrequency ablation of hepatocellular carcinoma. Dig Dis 2013;31:485–489.
14 Kudo M, Osaki Y, Matsunaga T, Kasugai H, Oka H, Seki T; for the Osaka Liver Cancer Study Group: Hepatocellular carcinoma in Child-Pugh C cirrhosis: prognostic factors and survival benefit of nontransplant treatment. Dig Dis 2013;31:490–498.
15 Lencioni R: Chemoembolization in patients with hepatocellular carcinoma. Liver Cancer 2012;1:41–50.
16 Kudo M: Treatment of advanced hepatocellular carcinoma with emphasis on hepatic arterial infusion chemotherapy and molecular targeted therapy. Liver Cancer 2012;1:62–70.
17 Lin S, Hoffmann K, Schemmer P: Treatment of hepatocellular carcinoma: a systematic review. Liver Cancer 2012;1:144–158.
18 Lin SM: Local ablation for hepatocellular carcinoma in Taiwan. Liver Cancer 2013;2:73–83.
19 Kudo M, Izumi N, Kokudo N, Matsui O, Sakamoto M, Nakashima O, Kojiro M, Makuuchi M: Management of hepatocellular carcinoma in Japan: consensus-based clinical practice guidelines proposed by the Japan Society of Hepatology (JSH) 2010 updated version. Dig Dis 2011;29:339–364.

Digestive Diseases

Dig Dis 2013;31:408–414
DOI: 10.1159/000355237

Clinical and Histological Features of Different Types of Budd-Chiari Syndrome: A Comparison of 4 Cases

Naoshi Nishida[a, b] Shinichi Iwamura[d] Hiroshi Ida[b] Satoshi Hagiwara[a]
Yoshinori Kagioka[a] Yasunori Minami[a] Yoji Maetani[c] Kyo Itoh[c, e]
Masatoshi Kudo[a]

[a]Department of Gastroenterology and Hepatology, Kinki University School of Medicine, Osakasayama, and Departments of [b]Gastroenterology and Hepatology and [c]Radiology, Kyoto University Graduate School of Medicine, Kyoto, [d]Department of Gastroenterology and Hepatology, Kochi Red Cross Hospital, Kochi, and [e]Department of Radiology, Kobe City Medical Center General Hospital, Kobe, Japan

Key Words
Budd-Chiari syndrome · Liver cirrhosis · Liver congestion · Regenerative nodule · Collateral vessels

Abstract
Budd-Chiari syndrome (BCS) is a rare condition characterized by hepatic venous outflow obstruction. In this report, we present 4 cases of BCS with complete and incomplete obstruction of the inferior vena cava (IVC) and hepatic vein (HV). Each case showed different and unique features of liver damage, which were attributed to the site and degree of obstruction. Interestingly, improved liver functions such as increased serum albumin levels, decreased hyaluronic acid levels and a normal indocyanine green clearance test were evident within 1 month of the balloon angioplasty. Pericellular fibrosis and hypervascular regenerative nodules were also reversible after obstruction removal. Therefore, it is very important to manage this rare disease before it progresses to liver cirrhosis.

Introduction

Budd-Chiari syndrome (BCS) is characterized by the incomplete or complete obstruction of hepatic venous outflow, leading to liver damage caused by congestion and portal hypertension [1, 2]. BCS includes several conditions that lead to hepatic outflow obstruction from a hepatic vein (HV) branch to the junction of the inferior vena cava (IVC) and right atrium [3]. Thus far, several reports have described the clinical cause, imaging and pathological findings of BCS [4]. IVC obstruction with or without HV involvement is predominant in Asia; on the contrary, pure HV obstruction is reported more often in Western countries [1]. It is possible that the clinical manifestation differs between patients with HV branch obstruction and those with IVC obstruction. The degree of obstruction, such as a complete or partial obstruction of the HV outflow tract, may also affect the symptoms and clinical course of BCS [5]. We encountered 4 cases of BCS: 2 patients had HV obstruction and 2 patients had

KARGER

E-Mail karger@karger.com
www.karger.com/ddi

0257–2753/13/0316–0408$38.00/0

Naoshi Nishida, MD, PhD
Department of Gastroenterology and Hepatology
Kinki University School of Medicine
337-2 Ohno-higashi, Osakasayama, Osaka 589-8511 (Japan)
E-Mail naoshi@med.kindai.ac.jp

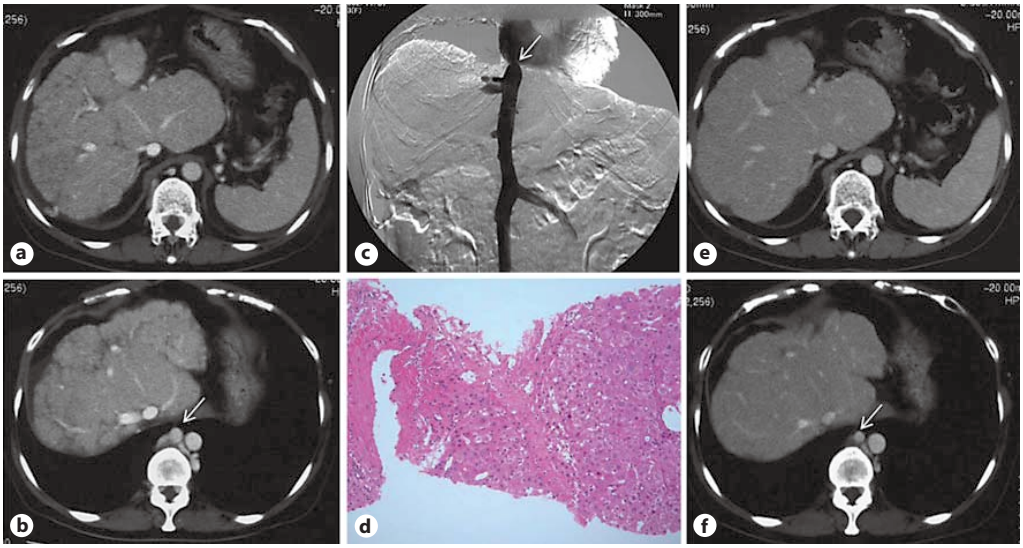

Fig. 1. Radiological and histological findings of BCS with incomplete IVC obstruction (case 1). **a** CE-CT (delayed phase) before the balloon angioplasty; caudate lobe enlargement was observed (arrow). **b** The white arrow indicates the dilation of the azygos vein. **c** The catheter venography of the IVC showed incomplete membranous obstruction of the IVC at the diaphragm level (white arrow). **d** HE staining of the liver needle biopsy; stasis of the hepatic sinusoid surrounding the central vein and bridging fibrosis were observed. **e**, **f** CE-CT (delayed phase) 4 months after the balloon angioplasty; the patchy enhancement of the liver parenchyma and azygos vein dilation were improved (white arrow).

IVC obstruction. Interestingly, their clinical presentations varied from an asymptomatic condition to acute liver failure. In this report, we summarize the clinical courses and manifestations of these 4 cases of BCS and compare the unique radiological and histological findings, which were attributed to the degree and site of obstruction.

Our institution did not require institution approval or informed consent for review of patient records and images in the case report. We explained the research content and gave patients the right to refuse inclusion in our study.

Case 1: Partial IVC Obstruction

A 53-year-old woman had a 1-year history of leg edema, body weight gain and dyspnea. She was diagnosed with liver cirrhosis by liver biopsy at the first hospital she visited, and was prescribed diuretics after she gained 4 kg of body weight. The initial laboratory findings at our hospital were as follows: white blood cell count (WBC) 5,400/μl (3,500–9,800/μl); hemoglobin (Hb) 16.1 g/dl (11.3–15.5 g/dl for women); platelet count (PLT) 146,000/μl (155,000–365,000/μl); albumin 3.3 g/dl (3.9–4.9 g/dl); total bilirubin 0.8 mg/dl (0.3–1.3 mg/dl); alkaline phosphatase (ALP) 182 IU/l (115–359 IU/l); aspartate aminotransferase (AST) 30 IU/l (10–40 IU/l); alanine aminotransferase (ALT) 25 IU/l (≤35 IU/l); prothrombin time (PT; activity percentage) 80% (≥82%); activated partial thromboplastin time (aPTT) 30.8 s (25.5–36.1 s); hepatitis B surface antigen (HBsAg) negative; hepatitis C antibody (HCVAb) negative; antinuclear antibody (ANA) negative; antimitochondrial antibody (AMA) negative; anti-liver kidney microsomal antibodies negative; hyaluronic acid 69 ng/ml (≤50.0 ng/ml); type III procollagen-N-peptide 0.7 U/ml (≤1.0 U/ml); type IV collagen 7S domain 7.7 ng/ml (≤5.0 ng/ml); indocyanine green clearance test (retention at 15 min; ICG R15) 13.9% (≤10%). Serum protein C and protein S levels were normal, and lupus anticoagulant and anticardiolipin antibodies (ACA) were negative. Contrast-enhanced computed tomography (CE-CT) performed at our hospital revealed atrophy of the right lobe of the liver with enlargement of the caudate lobe (fig. 1a). Collaterals and dilation of the vertebral venous plexus and azygos vein were observed (fig. 1b). Catheter venography revealed incomplete IVC obstruction at the diaphragm level (fig. 1c). Needle liver

Dig Dis 2013;31:408–414
DOI: 10.1159/000355237

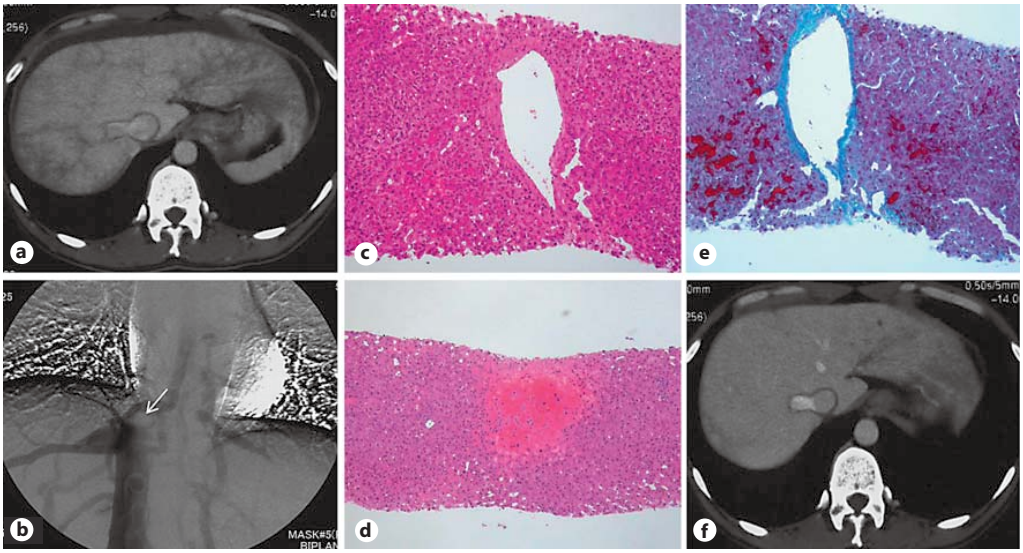

Fig. 2. Radiological and histological findings of BCS with complete IVC obstruction (case 2). **a** CE-CT (delayed phase) before the balloon angioplasty. **b** The catheter venography of the IVC showed complete membranous obstruction of the IVC (white arrow) with dilation of collateral vessels. **c** HE staining of the liver needle biopsy; dilation of the sinusoid and congestion around the central vein were detected. **d** Extravasation of red blood cells and necrosis. **e** Azan staining of the liver biopsy sample; fibrosis of the liver was mild. **f** CE-CT (delayed phase) 1 month after the balloon angioplasty.

biopsy was performed and histology showed dilation and stasis of the hepatic sinusoid with bridging fibrosis (fig. 1d). Four months after occlusion removal by balloon angioplasty the liver function test was improved with improvement of the patchy enhancement of the liver parenchyma (fig. 1e) and regression of collaterals (fig. 1f). Serum hyaluronic acid levels had dropped to 27 ng/ml 1 month after the balloon angioplasty. However, liver atrophy was still observed (fig. 1e) and ICG R15 was still increased (20%).

Case 2: Complete IVC Obstruction

A 48-year-old woman visited a private clinic because of lower leg myalgia. She had a 3-year history of leg edema and abdominal fullness. When she visited the hospital, liver damage was confirmed with biochemical blood examination. Ascites and esophageal varices were also detected and diuretics were prescribed. Leg edema and ascites improved after the administration of diuretics. Laboratory findings were as follows: WBC 5,600/μl; Hb 14.2 g/dl; PLT 169,000/μl; albumin 3.6 g/dl; total bilirubin 2.9 mg/dl; ALP 698 IU/l; AST 40 IU/l; ALT 41 IU/l; PT activity percentage 77%; aPTT 32.6 s; HBsAg negative; HCVAb negative; ANA negative; AMA negative; hyaluronic acid 37 ng/ml; type IV collagen 7S domain 11.4 ng/ml; ICG R15 25.0%. Protein C and protein S levels were normal. Lupus anticoagulant and ACA were negative. The initial CE-CT revealed patchy enhancement of the liver (fig. 2a). However, the liver surface was smooth compared to that of case 1, suggesting that the morphological change caused by liver fibrosis was not severe (fig. 2a). Catheter venography showed complete IVC obstruction caused by a membranous web at the diaphragm level accompanied by collateral vessels such as dilated azygos and hemiazygos veins and vertebral venous plexus (fig. 2b). Liver biopsy revealed dilation and congestion of the sinusoid around the central vein (fig. 2c). Extravasation of red blood cells into the liver cell plate and necrosis with congestion of the liver parenchyma were observed (fig. 2d). On the other hand, hepatic fibrosis was mild without badging fibrosis (fig. 2e). One month after balloon angioplasty, the patchy enhancement of the liver was improved (fig. 2f). Hyaluronic acid and ICG R15 serum concentrations were improved 1 month after the angioplasty (16 ng/ml and 14%, respectively).

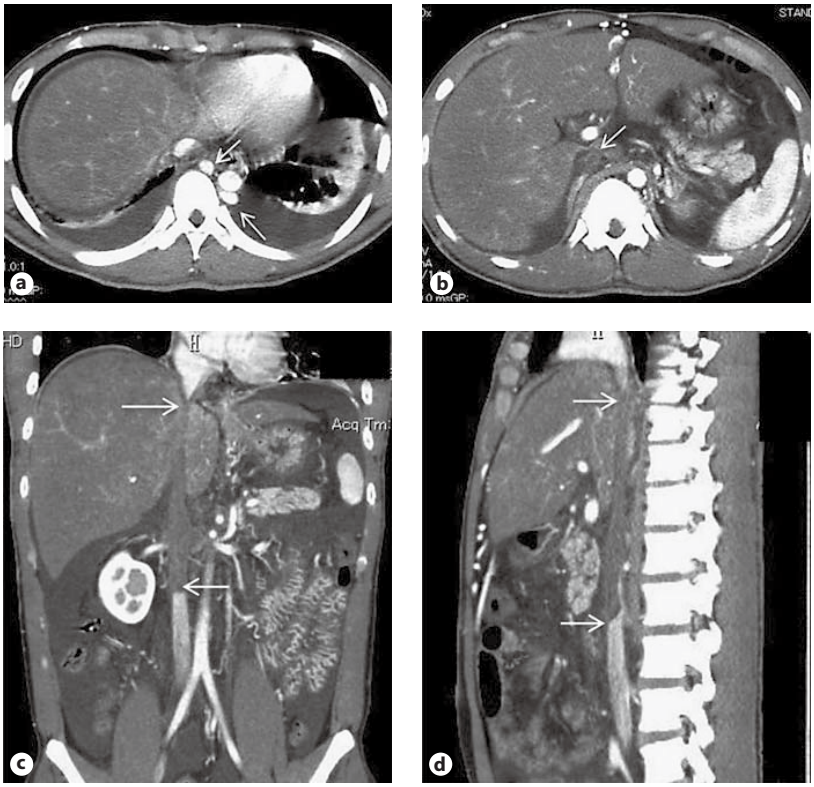

Fig. 3. Radiological findings of BCS with complete IVC and HV obstruction (case 3). **a** CE-CT (portal phase) before the balloon angioplasty; the white arrows indicate dilation of the azygos and hemiazygos veins. IVC obstruction caused by thrombus was detected on axial (**b**), coronal (**c**) and sagittal views (**d**). The white arrows indicate thrombi in the IVC.

Case 3: Complete IVC and HV Obstruction

A 22-year-old man presented to the hospital with a 2-week history of fever and dry cough. No abnormal finding was detected on chest radiographs and he was prescribed an antipyretic. The cough worsened and he also experienced nausea and abdominal discomfort. Mild proteinuria was detected by urine tests. Blood chemical tests at the time of admission showed liver damage as follows: WBC 5,300/μl; Hb 13.0 g/dl; PLT 163,000/μl; albumin 2.7 g/dl; total bilirubin 3.5 mg/dl; ALP 578 IU/l; AST 58 IU/l; ALT 83 IU/l; PT activity percentage 40.6%; hepaplastin test 41.1%; HBsAg negative; HCVAb negative; ANA negative; AMA negative; ICG R15 95.0%. IgM antibody against mycoplasma was positive. Protein C and protein S levels did not decrease. Lupus anticoagulant, ACA and anti-neutrophil cytoplasmic antibodies were negative. The patient's fever improved after hospital admission. However, abdominal discomfort, pain and fullness worsened with persistent nausea. CE-CT revealed ascites and dilation of the azygos and hemiazygos veins (fig. 3a). A massive thrombus was present in the IVC extending from the level of the diaphragm to above the right renal vein, and involved the HV branches (fig. 3b), which reached the second lumbar level (fig. 3c, d). The IVC was completely occluded without any HV enhancement, suggesting the complete obstruction of all HV branches (fig. 3b–d). There was no radiological evidence of mass lesions or thromboemboli in the chest, abdomen or pelvis. Gastroduodenal endoscopy showed formation of esophageal varices, suggesting that partial obstruction of the IVC might be present before the onset of the symptom. During the clinical course, ascites and pleural effusion increased and liver function deteriorated. The patient was diagnosed with subacute BCS caused by thrombus. He was transferred to the specialized institution for liver transplantation.

Case 4: Partial HV Obstruction

A 53-year-old man presented to the hospital with a 3-year history of persistent leg edema and abdominal fullness with thrombocytopenia and hemorrhoids. Ascites

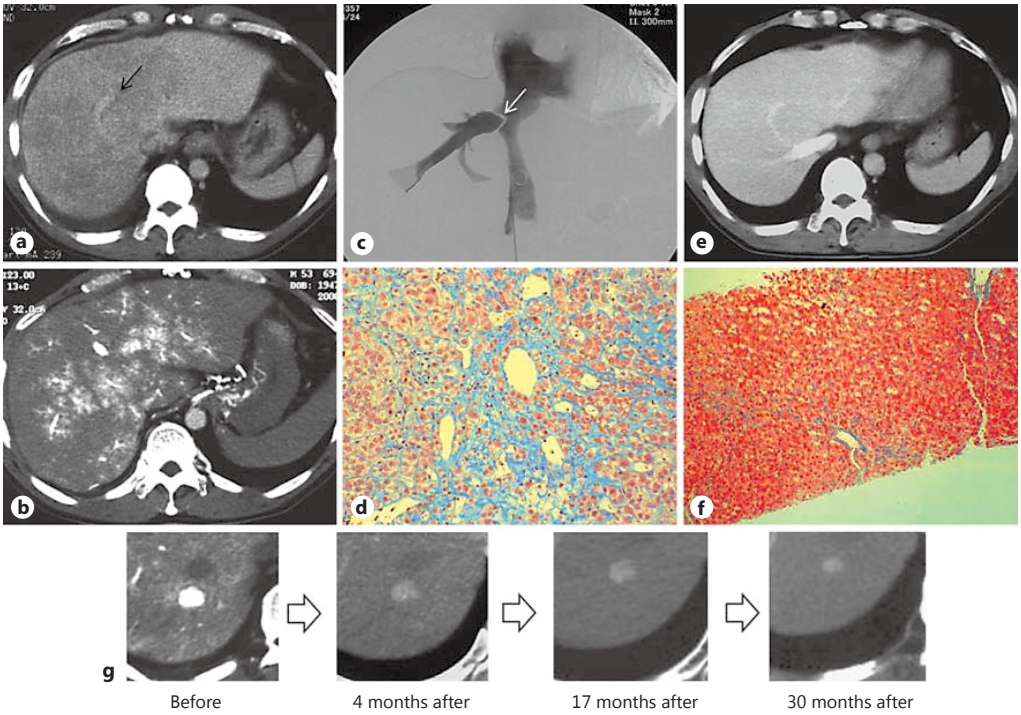

Fig. 4. Radiological findings of BCS with incomplete HV obstruction (case 4). **a** CE-CT (portal phase) before the balloon angioplasty; the arrow indicates intrahepatic venovenous collaterals from the middle to right HV. **b** CT angiography showed heterogeneous enhancement of the liver. **c** The composition of the right hepatic venography and the catheter venography of IVC; the white arrow shows the membranous web of the right HV. **d** Masson's trichrome staining of the liver biopsy sample before the angioplasty; sinusoid dilation and marked pericellular fibrosis were observed around the central vein. **e** CE-CT (delayed phase) 1 month after the balloon angioplasty; liver enhancement was homogeneous compared to the CT findings before the angioplasty (**a**). **f** Azan staining of the liver biopsy 1 month after the angioplasty; sinusoid dilation and pericellular fibrosis were markedly improved. **g** Decreased enhancement of the hypervascular regenerative nodule was shown 4, 17 and 30 months after the angioplasty.

was detected and diuretics were prescribed. He was referred to our hospital. Laboratory findings were as follows: WBC 6,600/μl; Hb 16.2 g/dl; PLT 149,000/μl; albumin 3.1 g/dl; total bilirubin 1.1 mg/dl; ALP 436 IUL; AST 44 IU/l; ALT 15 IU/l; PT activity percentage 116%; aPTT 27.8 s; HBsAg negative; HCVAb negative; ANA was positive at 1:80 dilution; AMA negative; hyaluronic acid 127 ng/ml; type IV collagen 7S domain 6.3 ng/ml; ICG R15 38.0%. Protein C and protein S levels were normal, and lupus anticoagulant and ACA were negative. CE-CT findings indicated heterogeneous enhancement of the liver parenchyma with intrahepatic venovenous collaterals from the middle to right HV (fig. 4a). CT angiography also revealed heterogeneous enhancement (fig. 4b), indicating the presence of reversed portal venous blood flow that should result from the increased postsinusoidal pressure produced by HV obstruction. Color Doppler sonography revealed complete obstruction of the left and middle HV. Incomplete obstruction of the right HV caused by a web was also detected by the sonography, portography and right hepatic venography (fig. 4c). The liver biopsy showed sinusoid dilation and marked pericellular fibrosis around the central vein (fig. 4d). After the balloon angioplasty and stent placement in the right HV, heterogeneous enhancement with the hypoattenuating portion of the liver parenchyma improved to homogeneous enhancement (fig. 4e). Histological findings of sinusoid dilation and pericellular fibrosis were also markedly improved (fig. 4f). The size and enhancement of the hypervascular regenerative nodule detected in the posterior segment by the initial CT gradually decreased during the 30 months after the angioplasty (fig. 4g). The detailed findings of this hyper-

Table 1. Comparisons of the clinical features of the 4 cases

	Case 1 IVC incomplete	Case 2 IVC complete	Case 3 IVC and HV complete	Case 4 HV incomplete
Initial symptom	Leg edema, body weight gain, dyspnea	Leg edema, body weight gain	Nausea, abdominal discomfort and fullness	Leg edema, abdominal fullness
Site of obstruction and radiological findings of the liver	Congestion and atrophy of the liver with enlargement of the caudate lobe, obstruction of the IVC by a web	Patchy enhancement of the liver, obstruction of the IVC by a web	Swelling of the intestinal wall, thrombus in the IVC and HV	Heterogeneous enhancement, obstruction of the HV by a web, hypervascular nodule
Collateral vessels	Dilation of the azygos and hemiazygos veins	Dilation of the vertebral venous plexus, azygos and hemiazygos veins	Dilation of the azygos and hemiazygos veins	Intrahepatic venovenous shunt
Histological findings	Congestion of the sinusoid and bridging fibrosis	Congestion of the sinusoid and necrosis with extravasation of red blood cells, mild fibrosis	N/A	Congestion and dilation of the sinusoid, pericellular fibrosis in the central portion
Therapy	Balloon angioplasty	Balloon angioplasty	Liver transplantation	Balloon angioplasty and stent placement
Outcome	Improvement of congestion, presence of morphological change of the liver	Improvement of congestion without major morphological change	N/A	Improvement of congestion and pericellular fibrosis, regression of the hypervascular nodule

N/A = Not available.

vascular nodule before treatment were previously reported [6]. Hyaluronic acid and ICG R15 serum concentrations were markedly improved 1 month after the angioplasty (36 ng/ml and 22.0%, respectively) with increased serum albumin concentration (3.9 g/dl).

Discussion

The clinical symptoms and radiological and histological findings of the 4 cases are summarized in table 1. Case 1 represented an IVC obstruction. Venography showed incomplete obstruction along with azygos vein dilation. Therefore, it is possible that gradual but mild progression of liver congestion caused a chronic type of BCS, which led to altered morphology with liver cirrhosis [3]. In this case, liver cirrhosis did not improve after obstruction removal by balloon angioplasty, although the extrahepatic collateral vessel showed regression. On the other hand, the patient in case 2 showed complete IVC obstruction by web formation and elevated bilirubin concentration. The histology of case 2 showed milder fibrosis but more severe sinusoid stasis and necrosis with hemorrhage in the liver parenchyma. Therefore, complete IVC obstruction induced an earlier onset of symptomatic BCS without the finding of liver cirrhosis compared to case 1. The CE-CT finding of liver congestion disappeared and hyaluronic acid and ICG R15 serum concentrations improved after the angioplasty. Case 3 was regarded as an acute to subacute type of BCS because of the wide range of thrombosis in the IVC and HV [7]. Although progression of collateral veins such as dilated azygos and hemiazygos veins and the subcutaneous vein of the abdominal wall was observed, the large thrombus in the IVC and HV should have led to rapid progression of clinical symptoms with liver failure, which was a characteristic feature of this case, although we could not perform liver biopsy because of the deteriorated liver function. The patient in case 4 showed HV branch obstruction. Unique findings of CE-CT in this case were an intrahepatic venovenous shunt

through the collaterals, which bypassed the obstructed branch, and characteristic patchy enhancement of the liver parenchyma in the obstructed segment [4]. However, progression of extrahepatic collaterals was minimal compared to that in the IVC obstruction type. Interestingly, pericellular fibrosis in the central lesion of the lobules (zone 3) could be reversed accompanied by improved hyaluronic acid and ICG R15 serum concentrations at 1 month after obstruction removal. As hyaluronic acid degradation mainly takes place in the sinusoidal endothelial cells [8], it could be reasonable to speculate that the rapid decrease in serum hyaluronic acid levels reflected the functional recovery of the endothelial cells that were damaged by liver congestion.

We presented 4 cases of BCS in this report, each of which showed a unique clinical course with unique radiological and histological findings. Although incomplete and partial obstruction of the IVC and HV branch might be asymptomatic and easily overlooked [2], obstruction removal before the establishment of liver cirrhosis is important to reverse liver function and liver fibrosis progression [9].

Acknowledgements

This work was supported in part by a Grant-in-Aid for Scientific Research (KAKENHI: 24590997) from the Japanese Society for the Promotion of Science (N. Nishida) and a grant from the Smoking Research Foundation (N. Nishida).

Disclosure Statement

The authors have no conflicts of interest to declare.

References

1 Valla DC: The diagnosis and management of the Budd-Chiari syndrome: consensus and controversies. Hepatology 2003;38:793–803.

2 Menon KV, Shah V, Kamath PS: The Budd-Chiari syndrome. N Engl J Med 2004;350:578–585.

3 Ferral H, Behrens G, Lopera J: Budd-Chiari syndrome. AJR Am J Roentgenol 2012;199:737–745.

4 Patil P, Deshmukh H, Popat B, Rathod K: Spectrum of imaging in Budd Chiari syndrome. J Med Imaging Radiat Oncol 2012;56:75–83.

5 Cazals-Hatem D, Vilgrain V, Genin P, Denninger MH, Durand F, Belghiti J, Valla D, Degott C: Arterial and portal circulation and parenchymal changes in Budd-Chiari syndrome: a study in 17 explanted livers. Hepatology 2003;37:510–519.

6 Maetani Y, Itoh K, Egawa H, Haga H, Sakurai T, Nishida N, Ametani F, Shibata T, Kubo T, Tanaka K, Konishi J: Benign hepatic nodules in Budd-Chiari syndrome: radiologic-pathologic correlation with emphasis on the central scar. AJR Am J Roentgenol 2002;178:869–875.

7 Clark PJ, Slaughter RE, Radford DJ: Systemic thrombolysis for acute, severe Budd-Chiari syndrome. J Thromb Thrombolysis 2012;34:410–415.

8 Deaciuc IV, Bagby GJ, Lang CH, Spitzer JJ: Hyaluronic acid uptake by the isolated, perfused rat liver: an index of hepatic sinusoidal endothelial cell function. Hepatology 1993;17:266–272.

9 Langlet P, Escolano S, Valla D, Coste-Zeitoun D, Denie C, Mallet A, Levy VG, Franco D, Vinel JP, Belghiti J, Lebrec D, Hay JM, Zeitoun G: Clinicopathological forms and prognostic index in Budd-Chiari syndrome. J Hepatol 2003;39:496–501.

Digestive Diseases

Dig Dis 2013;31:415–420
DOI: 10.1159/000355238

Autoimmune Hepatitis and Immunoglobulin G4-Associated Autoimmune Hepatitis

Norihisa Yada[a] Masatoshi Kudo[a] Hobyung Chung[b] Tomohiro Watanabe[c]

[a]Department of Gastroenterology and Hepatology, Kinki University School of Medicine, Osakasayama,
[b]Department of Gastroenterology and Hepatology, Kobe City Medical Center General Hospital, Kobe, and
[c]Department of Gastroenterology and Hepatology, Kyoto University Graduate School of Medicine, Kyoto, Japan

Key Words
Autoimmune hepatitis · Autoimmune pancreatitis · Immunoglobulin G4

Abstract
Autoimmune hepatitis (AIH) is a disease that is characterized by the presence of autoantibodies and elevated levels of serum immunoglobulin G (IgG) and hepatic enzymes. Its characteristic findings in the liver include interface hepatitis, infiltration of lymphocytes and plasma cells, and rosette formation, and is treated with immunosuppressive drugs. Autoimmune pancreatitis, a pancreatic disease caused by an autoimmune mechanism, is associated with elevated levels of serum IgG4 and the infiltration of IgG4-positive cells into the pancreatic parenchyma, and it is occasionally accompanied by systemic features. This systemic inflammatory disease characterized by the infiltration of IgG4-positive plasma cells and elevated serum IgG4 levels was recently classified as an IgG4-related disease. A few studies have reported AIH cases with infiltrated IgG4-positive plasma cells in the liver, suggesting the involvement of IgG4 in the pathogenesis of AIH. This feature was called IgG4-associated AIH and only two studies have been published. However, the diagnostic criteria of IgG4-associated AIH has not been defined and the epidemiology and clinical features remain uncertain. The degree of IgG4-positive plasma cell infiltration in the liver was different in each article. The serum IgG4 level was not elevated in one study, whereas it was severely elevated in the other. Corticosteroid therapy normalized liver enzymes in both studies. Further studies are needed to define the epidemiological features or diagnostic criteria.

Introduction

The serological features of autoimmune hepatitis (AIH) are the presence of antinuclear antibody (ANA), anti-smooth muscle antibody (SMA) and anti-type 1 liver-kidney microsomal antibody (anti-LKM-1), and elevated levels of serum immunoglobulin G (IgG) and hepatic enzymes. Characteristic findings in the liver include interface hepatitis, infiltration of lymphocytes and plasma cells, and rosette formation. AIH is treated with steroids and immunosuppressive drugs.

Autoimmune pancreatitis (AIP), a pancreatic disease caused by an autoimmune mechanism, is associated with elevated levels of serum IgG4 and the infiltration of IgG4-positive cells into the pancreatic parenchyma, and it is occasionally accompanied by nonpancreatic features. AIP is known to be accompanied by multiple organ failure, and

KARGER

E-Mail karger@karger.com
www.karger.com/ddi

0257–2753/13/0316–0415$38.00/0

Masatoshi Kudo
Department of Gastroenterology and Hepatology
Kinki University School of Medicine
377-2 Ohno-higashi, Osakasayama, Osaka 589-8511 (Japan)
E-Mail m-kudo@med.kindai.ac.jp

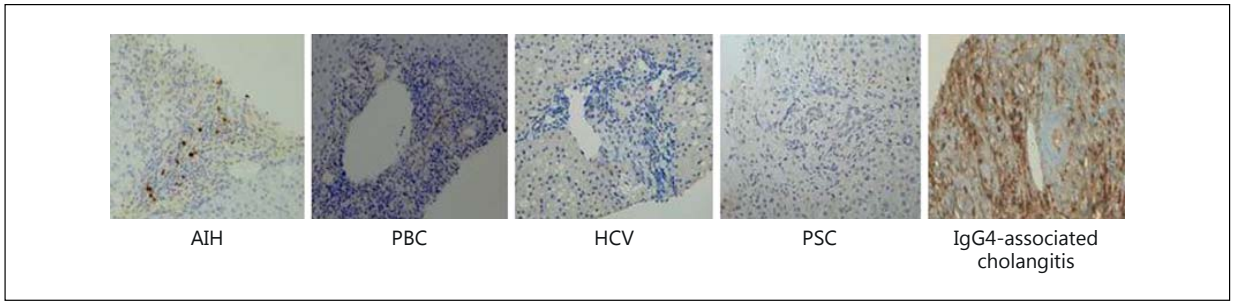

Fig. 1. Immunohistochemical staining of IgG4. From left to right: IgG4-associated AIH, primary biliary cirrhosis, chronic hepatitis C, primary sclerosing cholangitis and IgG4-related sclerosing cholangitis. From Chung et al. [9].

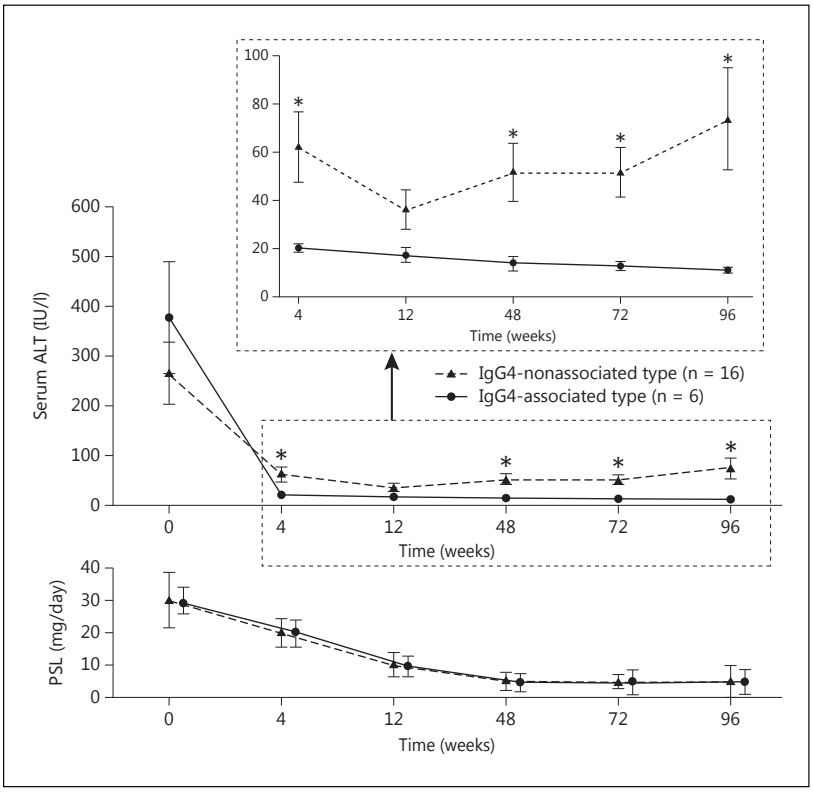

Fig. 2. Comparison of PSL-induced changes in the serum ALT levels between IgG4-associated AIH and IgG4-nonassociated AIH. Serum levels of ALT were monitored in 6 patients with IgG4-associated AIH and in 16 patients with IgG4-nonassociated AIH. These patients were treated with PSL. The doses of PSL at each time point are shown in the bottom panel. The results are shown as mean ± standard error (* $p < 0.05$). From Chung et al. [9].

systemic inflammatory diseases characterized by the infiltration of IgG4-positive plasma cells and elevated serum IgG4 levels were recently classified as IgG4-related diseases.

Recent studies have reported AIH cases with infiltrated IgG4-positive plasma cells in the liver, suggesting the involvement of IgG4 in the pathogenesis of AIH. Here, we review the characteristic features of IgG4-related disease and its association with AIH.

Autoimmune Hepatitis

Clinical Features

The term 'autoimmune hepatitis' was introduced in 1965 [1]. Upon the discovery of hepatitis C virus in 1989, chronic hepatitis C infection was separated from non-A, non-B hepatitis. Subsequently, AIH was classified as an independent disease category, and AIH diagnostic crite-

Table 1. Japanese diagnostic criteria for AIH in 1996

Concept	AIH is a disease that develops frequently in women past middle age and progresses to chronic hepatitis, and the pathogenesis of hepatocellular damage suggests the involvement of autoimmune mechanisms[1]. For effective diagnosis, viral hepatitis, alcohol- and drug-induced hepatitis, and liver damage due to other autoimmune diseases should be eliminated. For treatment, immunosuppressants, particularly corticosteroids, are highly effective[2]
Major findings	1 Positive autoantibodies in the serum (particularly ANA and SMA) 2 Elevated serum γ-globulin or immunoglobulin G levels (≥2 g/dl) 3 Continuous or repetitive increases in serum transaminase levels 4 Negative for viral hepatitis, in principle[3] 5 Histological chronic hepatitis or cirrhosis accompanied by hepatocellular necrosis and piecemeal necrosis, often with marked plasma cell infiltration and sometimes with acute hepatitis
Diagnosis	If AIH is suspected based on the major findings 1–4 above, histological analysis is needed to make a diagnosis in accordance with the diagnostic criteria for AIH recommended by the IAIHG (see table 2)
Treatment guidelines	1 In principle, immunosuppressive therapy (e.g. PSL) is recommended for cases with a definitive diagnosis of AIH 2 A sufficient dose of PSL (≥30 mg daily) is administered as the initial treatment, and efficacy is evaluated based on the improvement of serum transaminase levels. Maintenance doses are determined after the normalization of serum transaminase activity 3 For treating AIH with hepatitis C viremia: a Corticosteroid therapy is recommended for cases that score high on the international diagnostic scoring system b Interferon therapy may be used in cases with a low score calculated in accordance with the international criteria. However, the indication for interferon therapy should be carefully determined based on a virological search before administration. Upon the initiation of interferon therapy, it is necessary to examine viral titers and liver function. If no improvement is observed, administration should be promptly terminated and the administration of immunosuppressive drugs should be considered

Modified from [4]. [1] Human leukocyte antigen-DR4-positive cases are more common in Japan. [2] Interferon therapy may be effective in some AIH cases with obvious hepatitis C infection. [3] Some AIH cases are accompanied by hepatitis C viremia in Japan.

ria were established at the meeting of the International Autoimmune Hepatitis Group (IAIHG) in 1993 [2].

There is often a history of other autoimmune disorders in the patient or first-degree relatives. The disease predominates among women, the archetypal patient being a young female with endocrine abnormalities, but it also affects males and it can present at almost any age. Distribution of age at onset was thought to be bimodal, with peaks around puberty and between the fourth and sixth decades of life, but it has been suggested that this impression probably relates to patterns of patient referral to specialist centers [3].

In Japan, AIH predominantly affects women, occurring 6 times more frequently than in men, although the prevalence in men has been gradually increasing in recent years. AIH presentation is characterized by a monomodal peak after the age of 60 years, and AIH is frequently accompanied by other autoimmune diseases, including chronic thyroiditis, Sjögren's syndrome and rheumatoid arthritis. In Japan, the most frequently observed initial symptom is general malaise (60%), followed by jaundice (35%) and appetite loss (27%). Other primary symptoms include joint pain and fever (15% each), both of which are rare in chronic viral hepatitis.

Diagnostic Criteria

Serological findings are the predominant elevation of liver enzymes over biliary enzymes, elevated serum IgG levels, and the presence of antibodies such as ANA, SMA and anti-LKM-1. Characteristic findings in the liver include interface hepatitis, infiltration of lymphocytes and plasma cells, and rosette formation. AIH is treated with steroids and immunosuppressive agents.

In Japan, AIH diagnostic criteria were established in 1996 by the Intractable Liver Disease Research Project Team of the Ministry of Health, Labor and Welfare (table 1) [4], which recommended the use of the IAIHG diagnostic criteria. The IAIHG diagnostic criteria were first established in 1993, revised in 1999, and are currently used as the international criteria (table 2) [3]. Characteristic AIH findings, including sex, clinical and serological features, liver histology and treatment response, are as-

Dig Dis 2013;31:415–420
DOI: 10.1159/000355238

Table 2. IAHG scoring system for the diagnosis of AIH

Parameters/features	Score
Female	2
ALP:AST (or ALT) ratio	
<1.5	2
1.5–3.0	0
>3.0	–2
Serum globulins or IgG above normal	
>2.0	3
1.5–2.0	2
1.0–1.5	1
<1.0	0
ANA, SMA or anti-LKM-1	
>1:80	3
1:80	2
1:40	1
<1:40	0
AMA positive	–4
Hepatitis viral markers	
Positive	–3
Negative	3
Drug history	
Positive	–4
Negative	1
Average alcohol intake	
<25 g/day	2
>60 g/day	–2
Liver histology	
Interface hepatitis	3
Predominantly lymphoplasmacytic infiltrate	1
Rosetting of liver cells	1
None of the above	–5
Biliary changes	–3
Other changes	–3
Other autoimmune disease(s)	2
Optimal additional parameters	
Seropositivity for other defined autoantibodies	2
HLA-DR3 or DR4	1
Response to therapy	
Complete	2
Relapse	3
Interpretation of aggregate scores	
Pretreatment	
Definite AIH	>15
Probable AIH	10–15
Post-treatment	
Definite AIH	>17
Probable AIH	12–17

Modified from Alvarez et al. [3]. AMA = Antimitochondrial antibody; ALP = alkaline phosphatase; AST = aspartate aminotransferase; HLA = human leukocyte antigen.

Table 3. Simplified diagnostic criteria for AIH

Variable	Cutoff	Points
ANA or SMA	≥1:40	1
ANA or SMA	≥1:80	2[a]
Or anti-LKM-1	≥1:40	2[a]
Or SLA	Positive	2[a]
IgG	Above normal	1
	≥1.1 times upper normal limit	2
Liver histology (evidence or hepatitis is a necessary condition)	Compatible with	1
Absence of viral hepatitis	Typical AIH	2
	Yes	2
Total	Probable AIH	≥6
	Definite AIH	≥7

Modified from Hennes et al. [5]. SLA = Anti-soluble liver antigen. [a] Addition of points achieved for all autoantibodies (maximum 2 points).

sessed using the scoring system, and definitive and probable diagnoses are compared before and after treatment. The criteria are complex and purely meant for scientific purposes. In 2008, the IAIHG introduced the simplified version of the AIH diagnostic criteria (table 3) [5] for routine clinical practice. This has made diagnosis easier and early therapeutic intervention possible. However, the diagnosis of AIH can be difficult because of its various clinical presentations, the presence of atypical and acute cases, and the involvement of other autoimmune diseases.

Treatment

Steroids and immunosuppressive drugs such as azathioprine are effective treatments for AIH, and ursodeoxycholic acid has shown good efficacy in many studies.

IgG4-Related Diseases

AIP is known to be accompanied by multiple organ failure, including sclerosing cholangitis, liver failure, inflammation of the lacrimal and salivary glands, thyroiditis, interstitial pneumonia and interstitial nephritis. Systemic inflammatory diseases characterized by the infiltration of IgG4-positive plasma cells and elevated serum IgG4 levels were recently classified as IgG4-related disease. In 2011, the Ministry of Health, Labor and Welfare established the 2011 comprehensive diagnostic criteria for IgG4-related disease (table 4) [6].

Table 4. Comprehensive diagnostic criteria for IgG4-related disease, 2011

Concept	IgG-related disease is a disease with an unknown cause and is characterized by synchronous or asynchronous swelling, nodule formation and hypertrophic lesions in multiple organs due to tissue fibrosis and the marked infiltration of lymphocytes and IgG4-positive plasma cells. The pancreas, biliary duct, lacrimal and salivary glands, central nervous system, thyroid gland, lungs, liver, gastrointestinal tract, kidneys, prostate gland, retroperitoneum, arteries, lymph nodes, skin and mammary gland are known to be affected. In general, the disease produces systemic manifestations, with some cases of single organ involvement. Clinically, individual organs present different symptoms, with occasional severe complications such as enlarged organs, obstruction caused by hypertrophic lesions, compression, infiltration and organ dysfunction due to fibrosis. Corticosteroids are generally effective.
Clinical diagnostic criteria	1 Clinical findings of characteristic diffuse or focal swelling, nodule formation and hypertrophic lesions in single or multiple organs. 2 Hematological findings of elevated IgG4 levels (≥135 mg/dl). 3 Histopathological findings of the following: a Histologically marked infiltration of lymphocytes and plasma cells and tissue fibrosis. b Infiltration of IgG4-positive plasma cells: ≥40% IgG4/IgG-positive cells and >10 IgG4-positive plasma cells/HPF. 1+2+3 Definite IgG4-related disease. 1+3 Probable IgG4-related disease. 1+2 Possible IgG4-related disease. However, by adding a histopathological diagnosis as possible, differential diagnosis of IgG4-related disease from similar diseases (Sjögren's syndrome, primary sclerosing cholangitis, Castleman's disease, secondary retroperitoneal fibrosis, Wegener similar disease) or malignant tumors (cancer, and malignant lymphoma) is important. Even if no definite diagnosis is made using the present criteria, diagnosis may be possible if the diagnostic criteria for each organ are used.

Modified from [6].

Liver injury is observed in 60–70% of AIP cases; however, with the exception of obstructive jaundice, the cause of liver injury in AIH is not always clear. Umemura et al. [7] showed that AIP is accompanied by hepatocellular damage, such as the infiltration of IgG4-positive plasma cells near the portal vein, patterns of portal inflammation, large biliary duct damage, portal sclerosis, lobular hepatitis and cholestasis, and improvement in histological findings after steroid therapy. They called the disease IgG4 hepatopathy.

AIH and IgG4-Associated AIH

Recently, some AIH cases fulfilling the criteria of IgG4-related disease have been designated as IgG4-associated AIH [8, 9]. Chung et al. [9] reported that a group of AIH patients with infiltration of IgG4-positive plasma cells were successfully treated with prednisolone (PSL) therapy. Based on the IgG4 immunoreactivity of liver biopsy samples (≥5 IgG4-positive plasma cells/high-power field, HPF), they divided 26 patients with a definitive diagnosis of AIH into IgG4-positive (9 patients, 35%) and IgG4-negative (17 patients, 65%) groups (table 1). No pancreaticobiliary lesions were observed in the AIH patients. No IgG4-positive plasma cells were observed in 10 cases of primary biliary cirrhosis or 20 cases of chronic hepatitis C. The IgG4-positive group had a significantly higher level of serum IgG than the IgG4-negative group ($p < 0.01$), but no significant differences in IgG4 levels were observed between these two groups. In addition, there were no significant differences in alanine aminotransferase (ALT), alkaline phosphatase, γ-glutamyl transpeptidase or ANA. On the other hand, the severity of plasma cell infiltration and lobular hepatitis were significantly high in the IgG4-positive group. Although portal inflammation and interface hepatitis were similar in both groups, the severity of portal inflammation was significantly higher in the IgG4-positive group. The infiltration of B cells, T cells and plasma cells was also significantly higher in the IgG4-positive group than in the IgG4-negative group ($p < 0.05$). Furthermore, ALT levels at 4, 48, 72 and 96 weeks after the initiation of PSL therapy were significantly lower in the IgG4-positive group than in the IgG4-negative group (table 2). During the administration of PSL, hepatitis relapse was observed in 6 IgG4-negative patients (35%) but not in any IgG4-positive patients. Even with the definition of IgG4 positive as the

infiltration of ≥10 IgG4-positive plasma cells/HPF, the response to PSL therapy and the serum levels of IgG were significantly different between the groups.

Umemura et al. [8] also reported the pathology of IgG4-related AIH. In a study of 60 AIH patients, they defined IgG4-related AIH as the infiltration of IgG4-positive plasma cells (≥10 cells/HPF), IgG4-positive serum (≥135 mg/dl) and the ratio of IgG4 to IgG as 0.073. However, because only 2 cases fulfilled this definition, they concluded that the prevalence of IgG4-positive AIH is extremely low (2/60 cases, 3.3%).

The main difference between the studies by Chung et al. [9] and Umemura et al. [8] is that, in the latter study, the definition included the ratio of IgG4 to IgG in addition to high serum IgG4 concentration (≥135 mg/dl) and the infiltration of IgG4-positive plasma cells in liver tissue. Furthermore, while Chung et al. [9] examined cases that matched the definite diagnosis of AIH, the 60 AIH cases investigated by Umemura et al. [8] included 12 which were probable AIH. Moreover, the infiltration of IgG4-positive cells in the gallbladder and common bile duct was observed in 1 of the IgG4-associated AIH cases, indicating a case of IgG4-related sclerosing cholangitis rather than IgG4-associated AIH. Regardless of the differences, the two studies revealed that IgG4-related pathologies are associated with at least some AIH cases and that steroid treatment is effective in such IgG4-associated AIH, as in other IgG4-related diseases.

Conclusion

Some patients with AIH present symptoms of IgG4-related disease and respond effectively to steroid treatment. Although no unified diagnostic criteria are currently available, it is important to keep this disease in mind for definitive diagnosis and appropriate treatment. Further studies are needed to define the epidemiological features or diagnostic criteria.

Disclosure Statement

The authors have no conflicts of interest to declare.

References

1 Mackay IR, Weiden S, Hasker J: Autoimmune hepatitis. Ann NY Acad Sci 1965;124:767–780.

2 Johnson PJ, McFarlane IG: Meeting report: International Autoimmune Hepatitis Group. Hepatology 1993;18:998–1005.

3 Alvarez F, Berg PA, Bianchi FB, et al: International Autoimmune Hepatitis Group Report: review of criteria for diagnosis of autoimmune hepatitis. J Hepatol 1999;31:929–938.

4 Research Program of Intractable Disease provided by the Ministry of Health Labor, and Welfare of Japan: Guidelines for the diagnosis of autoimmune hepatitis, 1996 (in Japanese). Kanzo 1996;37:298–300.

5 Hennes EM, Zeniya M, Czaja AJ, et al: Simplified criteria for the diagnosis of autoimmune hepatitis. Hepatology 2008;48:169–176.

6 Research Program of Intractable Disease provided by the Ministry of Health Labor, and Welfare of Japan: Comprehensive diagnostic criteria for IgG4-related disease (IgG4-RD), 2011 (in Japanese). Nihon Naika Gakkai Zasshi 2012;101:795–804.

7 Umemura T, Zen Y, Hamano H, et al: Immunoglobin G4-hepatopathy: association of immunoglobin G4-bearing plasma cells in liver with autoimmune pancreatitis. Hepatology 2007;46:463–471.

8 Umemura T, Zen Y, Hamano H, et al: Clinical significance of immunoglobulin G4-associated autoimmune hepatitis. J Gastroenterol 2011;46(suppl 1):48–55.

9 Chung H, Watanabe T, Kudo M, et al: Identification and characterization of IgG4-associated autoimmune hepatitis. Liver Int 2010;30:222–231.

Digestive Diseases

Dig Dis 2013;31:421–425
DOI: 10.1159/000355239

Factors of Response to Pegylated Interferon/ Ribavirin Combination Therapy and Mechanism of Viral Clearance

Kayo Sugimoto[a] Soo Ryang Kim[b] Ahmed El-Shamy[c] Susumu Imoto[b] Kenji Ando[b] Ke Ih Kim[a] Yasuhito Tanaka[g] Yoshihiko Yano[d] Soo Ki Kim[h] Yutaka Hasegawa[e] Aya Fujinami[f] Mitsuhiro Ohta[f] Hatae Takashi[e] Hak Hotta[c] Yoshitake Hayashi[d] Masatoshi Kudo[i]

Departments of [a]Pharmacy and [b]Gastroenterology, Kobe Asahi Hospital, [c]Department of Microbiology and [d]Division for infectious Disease Pathology, Center for Infectious Diseases, Kobe University Graduate School of Medicine, and [e]Educational Center for Clinical Pharmacy and [f]Medical Biochemistry, Kobe Pharmaceutical University, Kobe, [g]Department of Virology and Liver Unit, Nagoya City University Graduate School of Medical Sciences, Nagoya, [h]Department of Gastroenterology, Kyoto University, Kyoto, and [i]Department of Gastroenterology and Hepatology, Kinki University School of Medicine, Osakasayama, Japan

Key Words
Viral clearance · Interferon λ1 · Pegylated interferon · Ribavirin · Interleukin 28B · Interferon and ribavirin resistance-determining region · Interferon sensitivity-determining region

Abstract
Objectives: This study explores viral factors of the interferon (IFN) and ribavirin (RBV) resistance-determining region (IRRDR), the IFN sensitivity-determining region (ISDR) and the core protein, and host factor interleukin 28B associated with response to pegylated IFN (PEG-IFN) and RBV combination therapy, and the correlation of viral and host factors with IFN-λ1. ***Methods:*** A total of 58 patients underwent PEG-IFN/RBV combination therapy for 48 weeks. The pretreatment factors associated with rapid virological response (RVR) and sustained virological response (SVR) were analyzed. Pretreatment IFN-λ1 serum levels were compared with the viral and host factors. ***Results:*** Univariate analysis showed that IRRDR ≥6 and ISDR ≥2 were significant pretreatment predictors of RVR, and multivariate analysis identified IRRDR ≥6 and hemoglobin as significant predictors of SVR. Pretreatment IFN-λ1 was significantly higher in the SVR group than in the non-SVR group and also in the IRRDR ≥6 group than in the IRRDR ≤5 group. ***Conclusions:*** IRRDR ≥6 was the only significant predictor of SVR and was correlated with IFN-λ1. High serum levels of IFN-λ1 may be conducive to effective PEG-IFN/RBV combination therapy because of the immunomodulatory system.

Introduction

Although the triple therapy of combined pegylated interferon (PEG-IFN), ribavirin (RBV) and protease inhibitors has already been initiated, PEG-IFN and RBV combination therapy for chronic hepatitis C virus (HCV) infection with a high viral load of genotype 1b, the standard

KARGER

E-Mail karger@karger.com
www.karger.com/ddi

0257–2753/13/0316–0421$38.00/0

Soo Ryang Kim, MD
Department of Gastroenterology
Kobe Asahi Hospital, 3-5-25 Bououji-cho, Nagata-ku
Kobe 653-0801 (Japan)
E-Mail asahi-hp@arion.ocn.ne.jp

treatment in Japan since 2004, provides sustained virological response (SVR) in only approximately 50% of such patients [1]. Single-nucleotide polymorphisms in proximity to the interleukin 28B (IL-28B) gene (rs8099917, rs12979860) on chromosome 19 is reported to be a host-related factor of virological response to PEG-IFN and RBV combination therapy [2–4]. In recent years, viral factors such as the core protein, nonstructural protein 5A (NS5A), the IFN sensitivity-determining region (ISDR) and the IFN/RBV resistance-determining region (IRRDR) [4–8] have been associated with virological response. Nonetheless, the mechanism of how these host and viral factors affect viral clearance has not been precisely elucidated to date.

IFN-λ1 is considered to be associated with the inhibition of the replication of HCV by an immunological mechanism [9, 10]. Few studies, however, have demonstrated the correlation among IFN-λ1 serum levels, the clinical outcome of PEG-IFN and RBV combination therapy, and viral and host factors. We investigated the viral and host factors associated with response to PEG-IFN and RBV combination therapy and the correlation of viral and host factors with IFN-λ1.

Table 1. Patient baseline characteristics

Age (years)	57.3±10.4
Sex (male/female)	34/24
BMI	22.6±3.8
HCV-RNA (log IU/ml)	6.0±0.6
ALT (U/l)	54.8±64.0
γ-GTP (U/l)	57.0±64.7
Hemoglobin (g/dl)	13.7±1.98
Platelets ($\times 10^4/mm^3$)	16.0±5.0
Total cholesterol (mg/dl)	174.0±34.0
IL-28B (major/minor)	43/15
IFN-λ1 (pg/ml)	31.0±24.2
ISDR (≥2/≤1)	14/44
IRRDR (≥6/≤5)	22/36
Core aa 70 (arginine/glutamine)	39/19
Core aa 91 (leucine/methionine)	39/19

Data are shown as number (n) or mean ± SD.

Patients and Methods

Patients

A total of 58 patients (32 men, 26 women; age 57.3 ± 10.4 years) seen at Kobe Asahi Hospital and diagnosed with chronic HCV and high viral loads of genotype 1b were enrolled in the study. Patients demonstrating hemoglobin levels ≥11 g/dl (women) or ≥12 g/dl (men), platelet count $\geq 9 \times 10^4/mm^3$, HCV RNA ≥5.0 log IU/ml, neutrophil count $\geq 1{,}500/mm^3$ and thyroid-stimulating hormone levels within normal limits were included in the study; those demonstrating human immunodeficiency virus or hepatitis B coinfection, creatinine clearance <50 ml/min, liver disease other than chronic hepatitis C, evidence of advanced liver disease, preexisting psychiatric conditions, or a history of severe psychiatric disorder were excluded.

Treatment comprised PEG-IFN-α2b (1.5 μg per kilogram body weight, once a week) plus RBV (600–1,000 mg daily, based on body weight) for a total of 48 weeks, according to the standard treatment protocol for Japanese patients. Informed written consent was obtained from each patient and the study protocol conformed to the ethical guidelines approved by the Ethics Committee of Kobe Asahi Hospital.

Laboratory Tests

HCV RNA was extracted from 140 μl of serum with the use of a commercially available kit (QIAmp viral RNA kit; Qiagen, Tokyo, Japan). Amplification of full-length NS5A and the core regions of the HCV genome was carried out as described [5]. The sequences of the amplified fragments of NS5A and the core regions were determined by direct sequencing without subcloning. The amino acid (aa) sequences were deduced and aligned with the use of GENETYX Win software version 7.0 (GENETYX Corp., Tokyo, Japan). Genetic polymorphism rs8099917 around the IL-28B gene was determined by real-time PCR using the TaqMan assay. We defined the IL-28B major allele as homozygous (TT) for the major sequence and the minor allele as homozygous (GG) or heterozygous (TG) for the minor sequence. IFN-λ1 was assayed before initiation of therapy and at 4, 12 and 48 weeks after therapy by ELISA Ready-SET-Go (unit, pg/ml; NatuTec, Frankfurt, Germany).

Statistical Analysis

Rapid virological response (RVR) and SVR were defined as undetectable HCV RNA at weeks 4 and 24, respectively, after treatment. The potential pretreatment factors associated with virological response and comprising age, sex, BMI, HCV RNA load, alanine aminotransferase (ALT), γ-glutamyl transpeptidase (γ-GTP), hemoglobin, platelets, IFN-λ1, single-nucleotide polymorphisms in the IL-28B gene region, mutations in NS5A – especially those in ISDR (ISDR ≥2 and ISDR ≤1) and IRRDR (IRRDR ≥6 and IRRDR ≤5) – and mutated core protein amino acid substitutions at aa 70 of arginine (Arg70), or glutamine (Gln70), and at aa 91 of leucine (Leu91), or methionine (Met91), were examined. Factors associated with virological response were assessed by univariate analysis using Student's t test, Fisher's exact test or χ^2 test, and by multivariate analysis using logistic regression analysis. The factors in multivariate logistic regression analysis were included in descending order according to correlativity. The most appropriate model was chosen by AIC (Akaike Information Crietion). We compared pretreatment IFN-λ1 in the IRRDR ≥6 and IRRDR ≤5 groups, in the ISDR ≥2 and ISDR ≤1 groups, in the IL-28B TT genotype for the major sequence and in the IL-28B GG genotype and TG genotype for the minor sequence, and in the core protein (aa 70 and aa 91) wild and mutant. Variables with a p value <0.05 were considered statistically significant. All statistical analyses were carried out with the use of Excel Statistics 2011 by SSRI.

Table 2. Correlation of baseline characteristics with clinical outcome of RVR and non-RVR

	RVR	Non-RVR	p value
Age (years)	48.6±6.2	58.2±10.7	0.054
Sex (male/female)	4/1	27/23	0.373
BMI	21.8±1.5	22.9±4.0	0.536
HCV-RNA (log IU/ml)	5.8±0.8	6.0±0.56	0.303
ALT (U/l)	141.4±178.9	47.2±36.2	0.304
γ-GTP (U/l)	99.6±67.9	49.7±61.0	0.090
Hemoglobin (g/dl)	14.0±1.7	13.7±1.8	0.707
Platelets ($\times 10^4/mm^3$)	16.0±5.8	16.0±4.8	0.982
Total cholesterol (mg/dl)	158±30.2	174.6±34.1	0.354
IL-28B (major/minor)	5/0	35/15	0.308
IFN-λ1 (pg/ml)	24.9±10.4	31.3±25.3	0.582
ISDR (≥2/≤1)	4/1	10/40	**0.012**
IRRDR (≥6/≤5)	5/0	15/35	**0.004**
Core aa 70			
arginine/glutamine	3/2	32/16	1
Core aa 91			
leucine/methionine	4/1	33/17	1

Data are shown as number (n) or mean ± SD. Bold p values are significant.

Table 3. Correlation of baseline characteristics with clinical outcome of SVR and non-SVR

	SVR	Non-SVR	p value
Age (years)	53.7±10.1	60.3±9.9	**0.015**
Sex (male/female)	20/6	14/18	**0.016**
BMI	23.0±3.7	22.3±3.9	0.484
HCV-RNA (log IU/ml)	5.9±0.7	6.1±0.5	0.300
ALT (U/l)	54.0±38.8	55.6±79.5	0.926
γ-GTP (U/l)	72.2±87.6	44.6±33.8	0.14
Hemoglobin (g/dl)	14.6±1.5	13.0±1.6	**<0.01**
Platelets ($\times 10^4/mm^3$)	17.1±4.8	15.2±5.0	0.135
Total cholesterol (mg/dl)	173.5±33.2	174.3±35.0	0.941
IL-28B (major/minor)	24/2	19/3	**0.006**
IFN-λ1 (pg/ml)	38.8±29.3	24.7±17.2	**0.037**
ISDR (≥2/≤1)	8/18	6/26	0.36
IRRDR (≥6/≤5)	18/8	4/28	**<0.01**
Core aa 70			
arginine/glutamine	20/5	17/14	0.087
Core aa 91			
leucine/methionine	19/7	20/12	0.412

Data are shown as number (n) or mean ± SD. Bold p values are significant.

Results

Patient baseline characteristics are listed in table 1. RVR was observed in 8.6% (5/58) and SVR in 44.8% (26/58) of the patients. ISDR ≥2 and IRRDR ≥6 were significantly associated with RVR as assessed by univariate analysis (p = 0.012, p = 0.004; table 2). IRRDR ≥6 was most significantly correlated with RVR, which was from biased data of distribution (table 2). As a result, we were not able to conduct multivariate analysis for RVR. By univariate analysis, the significant factors associated with SVR were age, sex, hemoglobin, IL-28B major, IRRDR ≥6 (p = 0.015, p = 0.016, p < 0.001, p = 0.006, p < 0.001, p = 0.037; table 3). The pretreatment IFN-λ1 serum level in SVR was significantly higher than in non-SVR (38.8 vs. 24.7 pg/ml, p = 0.037; table 3). By multivariate analysis, hemoglobin and IRRDR ≥6 were significantly associated with SVR (p = 0.02, p = 0.005; table 4). Pretreatment IFN-λ1 was significantly higher in the IRRDR ≥6 group than in the IRRDR ≤5 group (40.5 vs. 25.2 pg/ml, p = 0.041; fig. 1), but demonstrated no significant difference between the ISDR ≥2 group and the ISDR ≤1 group (37.2 vs. 29.1 pg/ml, p = 0.45; fig. 1), among the IL-28B TT genotype group, the TG genotype group and the GG genotype group (TT vs. TG, 33.4 vs. 24.6 pg/ml, p = 0.26; TT vs. GG, 33.4 vs. 20.8 pg/ml, p = 0.48; TG vs. GG, 24.6 vs. 20.8 pg/ml, p = 0.82; fig. 1), and between core protein wild and mutant of aa 70 and aa 91 (aa 70 wild vs. mutant, 30.8 vs. 30.0 pg/ml, p = 0.91; aa 91 wild vs. mutant, 34.6 vs. 23.7 pg/ml, p = 0.05; fig. 1).

Table 4. Factors associated with SVR by multivariate analysis

	Odds ratio	95% CI	p value
Age (years)	0.9247	0.85–1.01	0.0678
Sex	5.4742	0.44–68.64	0.1876
Hemoglobin	2.4704	1.12–5.43	**0.0244**
IL-28B (major/minor)	5.1960	0.60–45.10	0.1350
IFN-λ1 (pg/ml)	1.0230	0.98–1.07	0.2758
IRRDR (≥6/≤5)	16.9320	2.39–119.77	**0.0046**

Bold p values are significant.

Discussion

Pretreatment factors significantly and independently predictive of the outcome of treatment of patients infected with high viral loads of HCV-1b are IL-28B major genotype (TT) as a host factor [11], and substitutions of aa 70

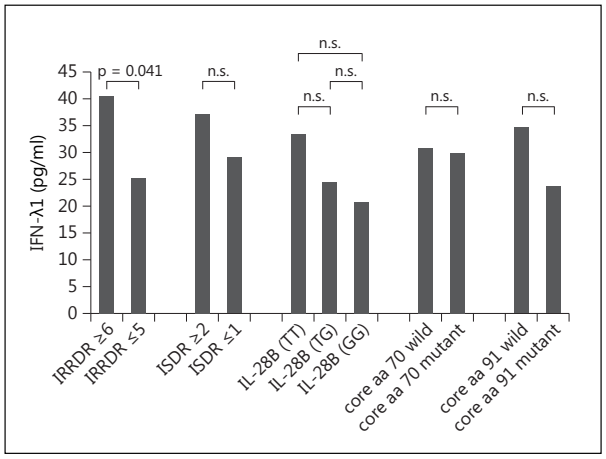

Fig. 1. Comparison of IFN-λ1 in the IRRDR ≥6 and IRRDR ≤5, ISDR ≥2 and ISDR ≤1, IL-28B, core aa 70 and core aa 91. Pretreatment IFN-λ1 was significantly higher in the IRRDR ≥6 group than in the IRRDR ≤5, but demonstrated no significant difference between the ISDR ≥2 group and the ISDR ≤1 group, among the IL-28B TT genotype group, the GG genotype group and the TG genotype group, between core protein wild and mutant of aa 70 and aa 91.

and aa 91 in the HCV core region, and high sequence variations in IRRDR (≥6) and in ISDR (≥2) as viral factors [4, 5, 7, 8, 11]. By univariate analysis, our study showed that ISDR and IRRDR were significant pretreatment predictors of RVR, and by multivariate analysis that IRRDR and hemoglobin were significant predictors of SVR. Because of the small number of RVR patients in our data, we were not able to carry out multivariate analysis for identifying RVR predictors. Our results support a previous study [12], and by univariate analysis we demonstrated a significant correlation between high pretreatment IFN-λ1 serum levels and SVR, but were unable to do so by multivariate analysis. On the other hand, although we were unable to demonstrate IL-28B as a predictor of SVR, some studies have demonstrated it as a positive predictive factor [2, 13, 14].

The level of IFN-λ1 has been reported to be significantly higher in carriers of the IL-28B major genotype than in those of the IL-28B homozygous minor sequence [9]. In the present study, the level of serum IFN-λ1 was higher in carriers of the IL-28B major genotype (TT) than in those of the IL-28B homozygous (GG) and the heterozygous (TG) minor sequence, but not significantly different ($p = 0.48$, $p = 0.26$). Because the number of carriers of the IL-28B homozygous allele (GG) was small (n = 2), we compared the level of serum IFN-λ1 in the IL-28B major homozygous allele (TT) and in the IL-28B minor homozygous (GG) as well as in the heterozygous (TG) allele. Nonetheless, for unclear reasons, no significant association was observed between a high level of serum IFN-λ1 and IL-28B major (major 33.4 pg/ml, minor 24.1 pg/ml; $p = 0.20$; data not shown). Further study is needed to clarify the relation between IL-28B and IFN-λ1.

It is well known that the antiviral mechanism of IFN comprises two phases [15, 16]. The first is direct inhibition of viral replication mediated by a number of proteins induced through the activation of the JAK-STAT pathway, including double-stranded RNA-activated protein kinase, myxovirus resistance gene A and 2′,5′-oligoadenylate synthetase, which block translation, block replication and degrade viral RNA, respectively [17–21]. The second is an indirect antiviral mechanism mediated by the stimulation of the host cell-mediated immune function including the cytotoxic T cell. The fact that IFN-λ1 significantly downregulates the secretion of IL-13 but elevates IFN-γ suggests that IFN-λ1 is related to an elevation of the Th1 response accompanied with a decrease of the Th2 response [10]. High levels of IFN-λ1 predispose to spontaneous resolution of HCV infection because of an elevation of the Th1 response [9]. Also, IFN-λ1 upregulates the chemokines MIG (Monokine induced by IFN-γ), IP-10 (IFN-γ-inducible protein 10) and I-TAC (IFN-inducible T cell α-chemoattractants), which are antimicrobial chemoattractants in peripheral blood mononuclear cells [22]. Taken together, these data suggest that IFN-λ1 stimulates the immunomodulatory effect [23].

The epitope located at position 2416, at a distance of 37 aa from IRRDR has been identified as an HLA-A26 CD8+ T cell epitope [24], which was targeted in all patients examined with acute resolving HCV infection. Therefore, IRRDR is regarded as the area (NS5A) related to immune function [5]. Our data demonstrated that IRRDR was significantly associated with IFN-λ1. From the above results, we infer that the achievement of SVR in patients with high IFN-λ1 levels is associated with the immunomodulatory system. Because of the small number of patients in our study, analysis in a large-scale multicenter study is needed.

Acknowledgment

We are indebted to Ms. Yoshiko Kawamura of Kobe Asahi Hospital for assistance in the preparation of the manuscript.

Disclosure Statement

The authors have no conflicts of interest to declare.

References

1 Kurosaki M: How to control HCV-related HCC: a personalized strategy. Liver Cancer 2013,2:167.

2 Ge D, Fellay J, Thompson AJ, Simon JS, Shianna KV, Urban TJ, Heinzen EL, Qiu P, Bertelsen AH, Muir AJ, Sulkowski M, McHutchison JG, Goldstein DB: Genetic variation in IL28B predicts hepatitis C treatment-induced viral clearance. Nature 2009;461:399–401.

3 Thompson AJ, Muir AJ, Sulkowski MS, Ge D, Fellay J, Shianna KV, Urban T, Afdhal NH, Jacobson IM, Esteban R, Poordad F, Lawitz EJ, McCone J, Shiffman ML, Galler GW, Lee WM, Reindollar R, King JW, Kwo PY, Ghalib RH, Freilich B, Nyberg LM, Zeuzem S, Poynard T, Vock DM, Pieper KS, Patel K, Tillmann HL, Noviello S, Koury K, Pedicone LD, Brass CA, Albrecht JK, Goldstein DB, McHutchison JG: Interleukin-28B polymorphism improves viral kinetics and is the strongest pretreatment predictor of sustained virologic response in genotype 1 hepatitis C virus. Gastroenterology 2010;139:120–129.

4 Enomoto N, Sakuma I, Asahina Y, Kurosaki M, Murakami T, Yamamoto C, Ogura Y, Izumi N, Marumo F, Sato C: Mutations in the nonstructural protein 5A gene and response to interferon in patients with chronic hepatitis C virus 1b infection. N Engl J Med 1996; 334:77–81.

5 El-Shammy A, Nagano-Fujii M, Sasase N, Imoto S, Kim SR, Hotta H: Sequence variation in hepatitis C virus nonstructural protein 5A predicts clinical outcome of pegylated interferon/ribavirin combination therapy. Hepatology 2008;48:38–47.

6 Fukuhara T, Taketomi A, Okano S, Ikegami T, Soejima Y, Shirabe K, Maehara Y: Mutations in hepatitis C virus genotype 1b and the sensitivity of interferon-ribavirin therapy after liver transplantation. J Hepatol 2010;42: 672–680.

7 Akuta N, Suzuki F, Kawamura Y, Yatsuji H, Sezaki H, Suzuki Y, Hosaka T, Kobayashi M, Kobayashi M, Arase Y, Ikeda K, Kumada H: Predictors of viral kinetics to peginterferon plus ribavirin combination therapy in Japanese infected with hepatitis C virus genotype 1b. J Med Virol 2007;79:1686–1695.

8 Akuta N, Suzuki F, Kawamura Y, Yatsuji H, Sezaki H, Suzuki Y, Hosaka T, Kobayashi M, Kobayashi M, Arase Y, Ikeda K, Kumada H: Predictive factors of early and sustained responses to peginterferon plus ribavirin combination therapy in Japanese patients infected with hepatitis C virus genotype 1b: amino acid substitutions in the core region and low-density lipoprotein cholesterol levels. J Hepatol 2007;46:403–410.

9 Langhans B, Kupfer B, Braunschweiger I, Arndt S, Schulte W, Nischalke HD, Nattermann J, Oldenburg J, Sauerbruch T, Spengler U: Interferon-lambda serum levels in hepatitis C. J Hepatol 2011;54:859–865.

10 Srinvas S, Dai J, Gallagher GE, Megjugorac NJ, Gallagher G: Interferon-λ1 (interloukin-29) preferentially down-regulates interleukin-13 over other T helper type 2 cytokine responses in vitro. Immunology 2008; 125:492–502.

11 Kurosaki M, Tanaka Y, Nishida N, Sakamoto N, Enomoto N, Honda M, Sugiyama M, Matsuura K, Sugauchi F, Asahina Y, Nakagawa M, Watanabe M, Sakamoto M, Maekawa S, Sakai A, Kaneko S, Ito K, Masaki N, Tokunaga K, Izumi N, Mizokami M: Pre-treatment prediction of response to pegylated interferon plus ribavirin for chronic hepatitis C using genetic polymorphism in IL28B and viral factors. J Hepatol 2011;54:439–448.

12 Kim SR, El-Sharmy A, Imoto S, Kim KI, Ide YH, Deng L, Shoji I, Tanaka Y, Hasegawa Y, Ota M, Hotta H: Prediction of response to pegylated interferon/ribavirin combination therapy for chronic hepatitis C genotype 1b and high viral load. J Gastroenterol 2012;24: 1143–1151.

13 Tanaka Y, Nishida N, Sugiyama M, Kurosaki M, Matsuura K, Sakamoto N, Nakagawa M, Korenaga M, Hino K, Hige S, Ito Y, Mita E, Tanaka E, Mochida S, Murawaki Y, Honda M, Sakai A, Hiasa Y, Nishiguchi S, Koike A, Sakaida I, Imamura M, Ito K, Yano K, Masaki N, Sugauchi F, Izumi N, Tokunaga K, Mizokami M: Genome-wide association of IL28B with response to pegylated interferon-alpha and ribavirin therapy for chronic hepatitis C. Nat Genet 2009;41:1105–1109.

14 Suppiah V, Moldovan M, Ahlenstiel G, Berg T, Weltman M, Abate ML, Bassendine M, Spengler U, Dore GJ, Powell E, Riordan S, Sheridan D, Smedile A, Fragomeli V, Müller T, Bahlo M, Stewart GJ, Booth DR, George J: IL28B is associated with response to chronic hepatitis C interferon-alpha and ribavirin therapy. Nat Genet 2009;41:1100–1104.

15 Neumann AU, Lam NP, Dahari H, Gretch DR, Wiley TE, Layden TJ, Perelson AS: Hepatitis C viral dynamics in vivo and the antiviral efficacy of interferon-alpha therapy. Science 1998;282:103–107.

16 Yasui K, Okanoue T, Murakami M, Itoh Y, Minami M, Sakamoto S, Sakamoto M, Nishioji K: Dynamics of hepatitis C viremia following interferon-alpha administration. J Infect Dis 1998;177:1475–1479.

17 Schmidt A, Zilberstein A, Shulman L, Federman P, Berissi H, Revel M: Interferon action: isolation of nuclease F, a translation inhibitor activated by interferon-induced (2′–5′) oligoisoadenylate. FEBS Lett 1978;95:257–264.

18 Nilsen TW, McCandless S, Baglioni C: 2′,5′-oligo(A)-activated endonuclease in NIH 3T3 mouse cells chronically infected with Moloney murine leukemia virus. Virology 1982;122:498–502.

19 Haller O, Frese M, Kochs G: Mx proteins mediators of innate resistance to RNA viruses. Rev Sci Tech 1998;17:220–230.

20 Itsui Y, Sakamoto N, Kurosaki M, Kanazawa N, Tanabe Y, Koyama T, Takeda Y, Nakagawa M, Kakinuma S, Sekine Y, Maekawa S, Enomoto N, Watanabe M: Expressional screening of interferon-stimulated genes for antiviral activity against hepatitis C virus replication. J Viral Hepat 2006;13:690–700.

21 Clemens MJ, Elia A: The double-stranded RNA-dependent protein kinase PKR: structure and function. J Interferon Cytokine Res 1997;17:503–524.

22 Pekarek V, Srinivas S, Eskdale J, Gallagher G: IFN lambda-1 (IFN-λ1/IL-29) induces ELR$^-$ CXC chemokine mRNA in human peripheral blood mononuclear cells, in an IFN-γ-independent manner. Genes Immun 2007;8: 177–180.

23 Ank N, Iversen MB, Bartholdy C, Staeheli P, Hartmann R, Jensen UB, Dagnaes-Hansen F, Thomsen AR, Chen Z, Haugen H, Klucher K, Paludan SR: An important role for type III interferon (IFN-λ/IL-28) in TLR-induced antiviral activity. J Immunol 2008;180:2474–2585.

24 Neumann-Haefelin C, Killinger T, Timm J, Southwood S, Mckinney D, Blum HE, Thimme R: Absence of viral escape within a frequently recognized HLA-A26-restricted CD8+ T cell epitope targeting the functionally constrained hepatitis C virus NS5A/5B cleavage site. J Gen Virol 2007;88:1986–1991.

Digestive Diseases

Dig Dis 2013;31:426–433
DOI: 10.1159/000355381

Prediction of Response to Pegylated Interferon/Ribavirin Combination Therapy for Chronic Hepatitis C Genotypes 2a and 2b and High Viral Load

Soo Ryang Kim[a] Ahmed El-Shamy[b, h] Susumu Imoto[a] Ke Ih Kim[a] Kayo Sugimoto[a] Soo Ki Kim[e] Yasuhito Tanaka[f] Takashi Hatae[c] Yutaka Hasegawa[c] Aya Fujinami[d] Mitsuhiro Ohta[d] Hak Hotta[b] Masatoshi Kudo[g]

[a]Department of Gastroenterology, Kobe Asahi Hospital, [b]Division of Microbiology, Center for Infectious Diseases, Kobe University Graduate School of Medicine, [c]Educational Center for Clinical Pharmacy and [d]Department of Medical Biochemistry, Kobe Pharmaceutical University, Kobe, [e]Department of Gastroenterology, Kyoto University, Kyoto, [f]Department of Virology and Liver Unit, Nagoya City University Graduate School of Medical Sciences, Nagoya, and [g]Department of Gastroenterology and Hepatology, Kinki University School of Medicine, Osakasayama, Japan; [h]Department of Virology, Faculty of Veterinary Medicine, Suez Canal University, Ismalia, Egypt

Key Words
Hepatitis C virus · Genotype 2a · Genotype 2b · IFN/RBV resistance-determining region · IL28B · Sustained virological response · Pegylated IFN/RBV

Abstract
Objective: We investigated the impact of host genetics represented by the single nucleotide polymorphism (SNP) of the IL28B gene and viral genetic variations within the nonstructural protein 5A (NS5A) [including the interferon (IFN)/ribavirin (RBV) resistance-determining region (IRRDR) and the IFN sensitivity-determining region (ISDR)] on the outcome of pegylated IFN and RBV (PEG-IFN/RBV) treatment. ***Methods:*** Sixty-six patients infected with hepatitis C virus (HCV)-2a or HCV-2b who received PEG-IFN/RBV for 24 weeks were examined. ***Results:*** In HCV-2a, the major genotype of IL28B SNP showed a tendency toward association with sustained virological response (SVR) and rapid virological response (RVR), and four or more mutations in IRRDR (IRRDR[2a] ≥4) and one or more mutations in ISDR plus its carboxyl-flanking region (ISDR/+C[2a] ≥1) were significantly associated with SVR and RVR. In HCV-2b, one or more mutations in the N-terminal part of IRRDR (IRRDR/N[2b] ≥1) were significantly associated with RVR. Multivariate analysis identified the major genotype of IL28B SNP and IRRDR[2a] ≥4 as independent predictive factors of SVR in HCV-2a, with IRRDR[2a] ≥4 being more powerful than the IL28B SNP. Also, IRRDR[2a] ≥4 in HCV-2a and IRRDR/N[2b] ≥1 in HCV-2b were significant determiners of RVR. ***Conclusion:*** The NS5A sequence heterogeneity and IL28B SNP are useful factors to predict the sensitivity to PEG-IFN/RBV therapy in HCV-2a and HCV-2b infections.

Introduction

In Japan, patients infected with hepatitis C virus (HCV) genotype 1b constitute about 70% of total HCV infection; the rest are infected with HCV-2a (25%) or HCV-2b (5%) [1]. The protease inhibitor, *telaprevir*, ap-

KARGER

E-Mail karger@karger.com
www.karger.com/ddi

0257–2753/13/0316–0426$38.00/0

Soo Ryang Kim, MD
Department of Gastroenterology, Kobe Asahi Hospital
3-5-25 Bouoji-cho, Nagata-ku
Kobe 653-0801 (Japan)
E-Mail asahi-hp@arion.ocn.ne.jp

proved in November 2011 by the Ministry of Health, Labor and Welfare, Japan, has shown sustained virological response (SVR) of more than 70% in HCV patients with high viral loads of genotype 1b [2].

Currently, combination therapy with pegylated interferon and ribavirin (PEG-IFN/RBV) is the standard treatment for chronic hepatitis C (CHC) patients infected with HCV-2a and HCV-2b. Patients infected with HCV genotypes 2 and 3 and treated with PEG-IFN/RBV show higher rates of SVR than those infected with HCV genotype 1 [3–5].

Sequence variations within a region in the nonstructural protein 5A (NS5A) of HCV-1b, defined as the IFN sensitivity-determining region (ISDR) [6] and the IFN/RBV resistance-determining region (IRRDR) [7], show correlation with IFN responsiveness.

In addition to the NS5A sequence variation, HCV core protein polymorphism has been proposed as a pretreatment predictor of poor virological response in HCV-1b-infected patients treated with PEG-IFN/RBV [8]. Host genetic factors associated with response to PEG-IFN/RBV therapy for HCV-1b and a high viral load are single nucleotide polymorphisms (SNPs) located in interleukin (IL)28B (rs8105790, rs11881222, rs8103142, rs28416813, rs4803219, rs8099917, rs7248668 and rs12979860) on chromosome 19 [9–12]. Moreover, on-treatment factors are mainly related to viral kinetics within the first few weeks of treatment [13].

At this stage, however, it is not clear whether NS5A sequence variation, including ISDR and IRRDR, core protein polymorphism, IL28B SNP and viral kinetics, are predictive of treatment outcome in HCV-2a and HCV-2b infections. In this context, we have recently reported that sequence heterogeneity within IRRDR of HCV-2a isolates (IRRDR[2a]) or within its N-terminus of HCV-2b isolates (IRRDR/N[2b]) is closely correlated with treatment responses, and that sequence heterogeneity within the ISDR plus its carboxyl-flanking region (ISDR/+C[2a]) is significantly associated with SVR in HCV-2a infection [14]. To further expand these observations in the present study, we investigated the effect of host genetics represented by IL28B SNP, the viral kinetics and the viral genetic heterogeneity in NS5A, and the core protein on the outcome of PEG-IFN/RBV treatment in HCV-2a and HCV-2b infections.

Materials and Methods

Patients

A total of 66 patients chronically infected with HCV-2a (n = 35) and HCV-2b (n = 31) seen at Kobe Asahi Hospital and Kobe University Hospital, Kobe, Japan, were enrolled in the study. The HCV subtype was determined according to the method of Okamoto et al. [15]. Inclusion and exclusion criteria were as follows, patients demonstrating hemoglobin levels ≥11 g/dl (women) or ≥12 g/dl (men), platelet counts $\geq 9 \times 10^4/mm^3$, HCV RNA ≥5.0 log IU/ml, neutrophil count $\geq 1{,}500/mm^3$ and thyroid-stimulating hormone levels within normal limits were included in the study; those demonstrating human immunodeficiency virus or hepatitis B virus coinfection, creatinine clearance <50 ml/min, cause of liver disease other than CHC, evidence of advanced liver disease, preexisting psychiatric conditions or a history of severe psychiatric disorder were excluded. All of the patients were treated with PEG-IFN α-2b (Pegintron®; Schering-Plough, Kenilworth, N.J., USA; 1.5 mg per kg body weight, once a week, subcutaneously) and RBV (Rebetol®; Schering-Plough; 600–800 mg daily, per os), for 24 weeks according to the standard treatment protocol for Japanese patients established by the hepatitis study group of the Ministry of Health, Labour and Welfare, Japan. The patients received >80% of the scheduled dosage of PEG-IFN and RBV. Serum samples were collected at intervals of 4 weeks before, during and after the treatment and tested for HCV RNA and core antigen titers as described [16].

Table 1. Proportion of various virological responses of HCV-2a- and HCV-2b-infected patients to PEG-IFN/RBV treatment

Response	Proportion		
	All (n = 66)	HCV-2a (n = 35)	HCV-2b (n = 31)
RVR	44 (67)	23 (66)	21 (68)
Non-RVR	22 (33)	12 (34)	10 (32)
EVR	62 (94)	34 (97)	28 (90)
ETR	63 (95)	34 (97)	29 (94)
SVR	48 (73)	28 (80)	20 (65)
Non-SVR	18 (27)	7 (20)	11 (35)

Figures in parentheses are percentages.

Genetic Variation near the IL28B Gene

Genetic polymorphism rs8099917 around the IL28B gene was determined by real-time polymerase chain reaction (PCR) with the TaqMan assay (Roche Diagnostics, Tokyo, Japan) [9]. We defined the IL28B major allele as homozygous for the major sequence (TT) and the IL28B minor allele as homozygous (GG) or heterozygous (TG) for the minor sequence.

Viral Kinetics

The amount of HCV RNA was examined by the COBAS TaqMan HCV test. The patients who cleared HCV viremia (less than 17 IU/ml) by week 4 were defined as achieving rapid virological response (RVR). The amount of HCV core antigen was assessed by the IRM assay (Ortho Clinical Diagnostics, Tokyo, Japan) that provides a good correlation between the amount of HCV core antigen and the amount of HCV RNA, as described [17]. The HCV core antigen was measured on days 0 and 7 (week 1) according to the detection limit of 20 fmol/l established by the manufacturer. Early viral drop was defined as an HCV core antigen level of less than 20 fmol/l.

Table 2. Demographic characteristics of HCV-2a- and HCV-2b-infected patients with SVR and non-SVR

Factor	All	HCV-2a			HCV-2b		
		SVR	non-SVR	p value (SVR vs. non-SVR)	SVR	non-SVR	p value (SVR vs. non-SVR)
n	66	28	7	–	20	11	–
Age, years	52.0±13.4	50.6±14.6	57.3±10.1	0.2006	50.6±13.6	54.6±10.2	0.5910
Sex (male/female)	39/27	15/13	4/3	1.0000	11/9	9/2	0.2409
Body weight, kg	60.4±8.9	58.6±8.7	60.0±10.4	0.7100	59.6±9.2	66.9±2.5	**0.0056**
Platelets, $\times 10^4/mm^3$	18.0±5.9	19.0±5.3	15.2±5.6	0.1170	18.1±5.9	17.1±7.2	0.7412
Hemoglobin, g/dl	13.9±1.8	13.7±1.8	14.5±1.8	0.3641	13.8±1.7	14.4±1.8	0.5351
γ-GTP, U/l	47.4±47.6	35.0±29.9	45.3±29.5	0.2829	34.2±29.4	104.7±74.5	**0.0004**
ALT, U/l	56.8±64.0	47.6±38.3	55.4±41.3	0.5223	43.8±37.4	105.0±124.7	**0.0369**
HCV RNA, log IU/ml	6.1±0.8	5.9±0.6	5.7±1.0	0.8147	6.3±0.8	6.5±0.4	0.8042
HCV core antigen, fmol/l	7,659.0±6,852.9	6,638.8±6,489.3	5,901.5±5,963.0	0.8469	7,751.2±6,394.2	10,175.5±8,464.5	0.4776
Response (RVR/non-RVR)	44/22	21/7	2/5	**0.0331**	16/4	5/6	0.1055
IL28B genotype (major/minor)	60/6	26/2	5/2	0.1710	19/1	10/1	1.0000

Bold p values are significant.

Sequence Analysis of the NS5A and the Core Regions

Sequence analysis of the NS5A and the core regions of HCV was carried out as described [14, 16, 18]. In brief, RNA extracted from serum was reverse transcribed and amplified for NS5A and the core regions of the HCV genome; the resultant RT-PCR products were then subjected to a second round of PCR. The sequences of the amplified fragments were determined by direct sequencing without subcloning. The amino acid (aa) sequences were deduced and aligned. The aa residues of HCV-2a and HCV-2b isolates were numbered according to the polyprotein of HCV-J6 [19] and HCV-J8 [20], respectively.

Statistical Analysis

Statistical differences in treatment response according to patient baseline parameters of age, body weight, platelets, hemoglobin, γ-glutamyl transpeptidase (γ-GTP), alanine aminotransferase (ALT), HCV RNA load and HCV core antigen were determined by the Mann-Whitney U test for numerical variables and Fisher's exact probability test for categorical variables. Similarly, statistical differences in treatment response according to NS5A and genetic variation near the IL28B gene (genotype TT) were determined by Fisher's exact probability test. Multicolinearity was tested using Spearman's correlation. Spearman's rank correlation analysis was used to test for multicolinearity among candidate variables in the multivariable analysis. When correlation was >0.5, only one of the correlated variables was used in the logistic regression model.

Results

Patient Response to PEG-IFN/RBV Combination Therapy for HCV-2a and HCV-2b Infections

Among the 35 patients infected with HCV-2a, RVR at week 4 was achieved by 66% (23/35), early virological response (EVR) at week 12 by 97% (34/35) and end-of-treatment response (ETR) by 97% (34/35). Similarly, among the 31 infected with HCV-2b, RVR was achieved by 68% (21/31), EVR by 90% (28/31) and ETR by 94% (29/31). SVR was achieved by 28 (80%) HCV-2a patients and by 20 (65%) HCV-2b patients. Only 7 (20%) HCV-2a and 11 (35%) HCV-2b patients were non-SVR. No null-response (continuous viremia throughout the treatment and follow-up periods) was observed since all the non-SVR patients achieved HCV-RNA negativity at a certain point in time followed by a rebound in viremia either before or after the treatment course (relapse; table 1).

Patient baseline demographic characteristics and clinical and treatment response are shown in table 2. Among HCV-2a patients, no significant difference was observed between SVR and non-SVR. Among HCV-2b patients, on the other hand, lighter body weight, and lower γ-GTP and ALT levels showed a significant difference between SVR and non-SVR patients.

Correlation between IL28B and SVR or RVR

The frequency of allele rs8099917 among HCV-2a patients was 89% for the IL28B major genotype (TT; 31/35) and 11% for the minor genotype (non-TT; 4/35); among HCV-2b patients it was 94% (29/31) for TT and 6% (2/31) for non-TT. Among HCV-2a patients with the IL28B major genotype, SVR was achieved by 84% (26/31; p = 0.1710) and RVR by 71% (22/31; p = 0.1061; table 3). Among HCV-2b patients, on the other hand, SVR was achieved by 66% (19/29; p = 1.0000) and RVR by 69% (20/29; p = 1.0000; table 3). Thus, there was a tendency toward SVR and RVR in HCV-2a patients with the IL28B

Table 3. Correlation between IL28B genotype and SVR or RVR in HCV-2a and HCV-2b infections

		SVR	Non-SVR	p value	RVR	Non-RVR	p value
HCV-2a	IL28B (major; n = 31)	26 (84)	5 (16)	0.1710	22 (71)	9 (29)	0.1061
	IL28B (nonmajor; n = 4)	2 (50)	2 (50)		1 (25)	3 (75)	
HCV-2b	IL28B (major; n = 29)	19 (66)	10 (34)	1.0000	20 (69)	9 (31)	1.0000
	IL28B (nonmajor; n = 2)	1 (50)	1 (50)		1 (50)	1 (50)	

Figures in parentheses are percentages.

Table 4. Correlation between IL28B genotype and SVR or RVR according to IRRDR[2a] ≥4 or IRRDR[2a] ≤3 in HCV-2a infection

		SVR	Non-SVR	p value	RVR	Non-RVR	p value
IRRDR ≥4	IL28B (major; n = 21)	20 (95)	1 (5)	0.1700	19 (90)	2 (9)	0.2490
	IL28B (nonmajor; n = 2)	1 (50)	1 (50)		1 (50)	1 (50)	
IRRDR ≤3	IL28B (major; n = 10)	6 (60)	4 (40)	1.0000	3 (30)	7 (70)	1.0000
	IL28B (nonmajor; n = 2)	1 (50)	1 (50)		0	2 (100)	

Figures in parentheses are percentages.

major genotype, although the difference was not statistically significant, probably due to the small number of the patients examined. Moreover, among HCV-2a patients with the IL28B major genotype, SVR was achieved by 95% (20/21; p = 0.1700) and RVR by 90% (19/21; p = 0.2490) when involving IRRDR with 4 or more mutations (IRRDR[2a] ≥4) while SVR was achieved by 60.0% (6/10; p = 1.0000) and RVR by 30.0% (3/10; p = 1.0000) when involving of IRRDR with 3 or less mutations (IRRDR[2a] ≤3; table 4). Thus, there was a tendency toward SVR and RVR in HCV-2a patients with the IL28B major genotype when involving of IRRDR[2a] ≥4, but not IRRDR[2a] ≤3.

Correlation between Viral Kinetics Including Early Viral Drop and SVR

SVR was achieved by 91% (21/23) of HCV-2a-infected patients who achieved RVR, but by only 9% (2/23) of those who did not achieve RVR (table 5). Thus, RVR was significantly associated with SVR in HCV-2a infection (p = 0.0331). On the other hand, RVR was not significantly associated with SVR in HCV-2b infection (p = 0.1055; table 5).

HCV core antigen titers were measured one week after the initiation of treatment in 91% (32/35) and 97% (30/31) of patients infected with HCV-2a and HCV-2b, respectively. Patients with the HCV core antigen titer of <20 fmol/l after 1 week were considered as achieving early viral drop.

Table 5. Correlation between RVR and SVR in HCV-2a and HCV-2b infections

		SVR	Non-SVR	p value
HCV-2a	RVR (n = 23)	21 (91)	2 (9)	**0.0331**
	Non-RVR (n = 12)	7 (58)	5 (42)	
HCV-2b	RVR (n = 21)	16 (76)	5 (24)	0.1055
	Non-RVR (n = 10)	4 (40)	6 (60)	

Figures in parentheses are percentages.
Bold p values are significant.

As shown in table 6, RVR was achieved by 93% (13/14) of HCV-2a-infected patients who achieved early viral drop, and by only 44% (8/18) of those who did not. Thus, the early viral drop was significantly associated with RVR (p = 0.0075) but not with SVR (p = 0.1959) in HCV-2a infection. On the other hand, early viral drop was not associated with either RVR (p = 0.1405) or SVR (p = 0.6328) in HCV-2b infection.

Sequence Analysis of NS5A of HCV-2a and HCV-2b

Alignment of all the NS5A sequences of the HCV-2a genome obtained from pretreatment sera against the consensus sequences previously reported [14] revealed that

Table 6. Correlation between early viral drop and SVR or RVR in HCV-2a and HCV-2b infections

		SVR	Non-SVR	p value	RVR	Non-RVR	p value
HCV-2a	HCV core antigen <20 fmol/l after 1 week (n = 14)	13 (93)	1 (7)	0.1959	13 (93)	1 (7)	**0.0075**
	HCV core antigen ≥20 fmol/l after 1 week (n = 18)	13 (72)	5 (28)		8 (44)	10 (56)	
HCV-2b	HCV core antigen <20 fmol/l after 1 week (n = 6)	5 (83)	1 (17)	0.6328	6 (100)	0	0.1405
	HCV core antigen ≥20 fmol/l after 1 week (n = 24)	15 (63)	9 (37)		15 (63)	9 (37)	

Figures in parentheses are percentages. Bold p values are significant.

Table 7. Average number of aa mutations within IRRDR[2a], ISDR/+C[2a] and IRRDR/N[2b] of HCV NS5A obtained from pretreatment sera of HCV-2a- and HCV-2b-infected patients with SVR, non-SVR, RVR and non-RVR

NS5A region	Mutations, n					
	SVR	non-SVR	p value	RVR	non-RVR	p value
IRRDR[2a] (aa 2332–2387)	6.0±3.9	3.0±1.2	**0.0361**	6.9±3.7	2.7±1.3	**0.0003**
ISDR/+C[2a] (aa 2232–2262)	1.8±2.4	0±0	**0.0015**	2.0±2.5	0.4±0.6	**0.0107**
IRRDR/N[2b] (aa 2332–2357)	2.2±1.6	1.4±1.5	0.1578	2.6±1.4	0.4±0.5	**0.0002**

Bold p values are significant.

Table 8. Correlation between NS5A sequence heterogeneity and SVR or RVR in HCV-2a and HCV-2b infections

Factor	SVR	Non-SVR	p value	RVR	Non-RVR	p value
IRRDR[2a] ≥4 (n = 23)	21 (91)	2 (9)	**0.0331**	20 (87)	3 (13)	**0.0005**
IRRDR[2a] ≤3 (n = 12)	7 (58)	5 (42)		3 (25)	9 (75)	
ISDR/+C[2a] ≥1 (n = 21)	21 (100)	0	**0.0005**	17 (81)	4 (19)	**0.0313**
ISDR/+C[2a] = 0 (n = 14)	7 (50)	7(50)		6 (43)	8 (57)	
IRRDR/N[2b] ≥1 (n = 23)	17 (74)	6 (26)	0.0947	19 (83)	4 (17)	**0.0059**
IRRDR/N[2b] = 0 (n = 8)	3 (37)	5 (63)		2 (25)	6 (75)	

Figures in parentheses are percentages. Bold p values are significant.

the average number of aa mutations in IRRDR[2a] (RVR = 6.9 ± 3.7 vs. non-RVR = 2.7 ± 1.3; p = 0.0003) and ISDR/+C[2a] (2.0 ± 2.5 vs. 0.4 ± 0.6; p = 0.0107) was significantly larger in the isolates from RVR than in those from non-RVR patients. More importantly, the average number of aa mutations in IRRDR[2a] (SVR = 6.0 ± 3.9 vs. non-SVR = 3.0 ± 1.2; p = 0.0361) and ISDR/+C[2a] (1.8 ± 2.4 vs. 0 ± 0; p = 0.0015) was significantly larger in SVR than in non-SVR.

Similarly, alignment of all the NS5A sequences of the HCV-2b genome against the consensus sequences [14] revealed that the average number of aa mutations in IRRDR/N[2b] was significantly larger in RVR than in non-RVR (2.6 ± 1.4 vs. 0.4 ± 0.5; p = 0.0002); however, no significant difference was observed between SVR and non-SVR (table 7).

Correlation between NS5A Sequence Heterogeneity and SVR or RVR in HCV-2a and HCV-2b Infections

Ninety-one percent (21/23) of HCV-2a-infected patients with IRRDR[2a] ≥4 achieved SVR compared to only 58% (7/12) of those with IRRDR[2a] ≤3 (table 8). This result suggests that IRRDR[2a] ≥4 was significantly associated with SVR (p = 0.0331). Similarly, 87% (20/23) of IRRDR[2a] ≥4, but only 25% (3/12) of IRRDR[2a] ≤3, achieved RVR, with the result suggest-

ing that IRRDR[2a] ≥4 was also significantly associated with RVR (p = 0.0005; table 8).

Likewise, all of the 21 patients infected with HCV-2a having one or more mutations in ISDR/+C (ISDR/+C[2a] ≥1), but only 50% (7/14) of those with ISDR/+C[2a] = 0, achieved SVR, with the result suggesting that ISDR/+C[2a] ≥1 was significantly associated with SVR (p = 0.0005). The ISDR/+C[2a] heterogeneity was also significantly associated with RVR (p = 0.0313).

In HCV-2b infection, 83% (19/23) of patients with IRRDR/N[2b] ≥1 achieved RVR whereas 25% (2/8) of those with IRRDR/N[2b] = 0 achieved RVR (p = 0.0059). Thus, IRRDR/N[2b] ≥1 was significantly associated with RVR, but not with SVR (table 8).

Correlation between HCV Core Protein Sequence Heterogeneity and RVR or SVR

A close correlation between HCV core protein sequence patterns and treatment outcome has been proposed in HCV-1b infection [17, 21]; however, this information is still unclear in HCV-2a and HCV-2b infections. Therefore, in the current study, core regions were obtained from the pretreated sera and the aa sequences deduced and aligned with prototype sequences (HCV-J6 [19] and HCV-J8 [20]). Contrary to reports on HCV-1b infection [8], the residues at positions 70 and 91 are well conserved among HCV-2a and HCV-2b isolates, suggesting no correlation between treatment outcome and these observed residues [14].

Identification of Independent Factors Predictive of SVR in HCV-2a and HCV-2b Infections

To identify significant independent predictors of SVR in HCV-2a and HCV-2b infections, univariate and multivariate logistic regression analyses were carried out using all available data on patient baseline parameters and viral genetic polymorphic factors. In HCV-2a infection, univariate analysis identified two factors, the heterogeneity of IRRDR[2a] (≥4 vs. ≤3) and RVR, that were significantly associated with SVR. Subsequently, multivariate regression analysis including these factors revealed that IRRDR[2a] heterogeneity (p = 0.0264) platelets (p = 0.0369) and IL28B major genotype (p = 0.0424) were independent factors predictive of SVR (table 9).

In HCV-2b infection, univariate analysis identified two factors, body weight and γ-GTP levels, that were significantly associated with SVR. In the subsequent multivariate analysis, only the γ-GTP level (p = 0.0287) was identified as an independent factor predictive of SVR in

Table 9. Univariate and multivariate analyses of factors associated with SVR

	HCV-2a				HCV-2b			
	univariate		multivariate		univariate		multivariate	
	odds ratio (95% CI)	p value	odds ratio (95% CI)	p value	odds ratio (95% CI)	p value	odds ratio (95% CI)	p value
Age (years)	0.9643 (0.9017–1.0293)	0.2692			0.9722 (0.9127–1.0355)	0.3807		
Sex (male/female)	0.8654 (0.1627–4.6019)	0.8653			0.2716 (0.0464–1.5904)	0.1483		
Body weight (kg)	0.9830 (0.8960–1.0783)	0.7161			0.8610 (0.7492–0.9896)	**0.0350**		
Platelets ($\times 10^4$/mm^3)	1.1375 (0.9692–1.3350)	0.1147	1.3364 (1.0178–1.7548)	**0.0369**	1.0281 (0.9112–1.1599)	0.6531		
Hemoglobin (g/dl)	0.7761 (0.4921–1.2240)	0.2755			0.7964 (0.5051–1.2557)	0.3271		
γ-GTP (U/l)	0.9900 (0.9658–1.0148)	0.4264			0.9643 (0.9353–0.9942)	**0.0198**	0.8962 (0.8124–0.9887)	**0.0287**
ALT (U/l)	0.9953 (0.9759–1.0150)	0.6361			0.9836 (0.9645–1.0031)	0.0985		
HCV RNA (log IU/ml)	1.4501 (0.4960–4.2393)	0.4972			0.6931 (0.2145–2.2393)	0.5401		
HCV core antigen (fmol/l)	1.0000 (0.9999–1.0002)	0.7996			1.0000 (0.9998–1.0001)	0.3710		
IL28B major genotype	5.2000 (0.5871–46.0546)	0.1385	31.2194 (1.1256–865.8969)	**0.0424**	1.900 (0.1071–33.6995)	0.6618		
IRRDR[2a] mutations ≥4	7.5000 (1.1798–47.6758)	**0.0327**	15.3487 (1.3773–171.0478)	**0.0264**	–	–		
IRRDR/N[2b] mutations ≥1	–	–			4.7222 (0.8564–26.0395)	0.0748	36.2264 (0.9676–1,356.2272)	0.0521
Response (RVR/non-RVR)	7.5000 (1.1798–47.6758)	**0.0327**			4.8000 (0.9544–24.1396)	0.0570		

Bold p values are significant.

HCV-2b infection. The heterogeneity of IRRDR/N[2b], a viral factor, was identified as significantly associated with RVR (p = 0.0064; data not shown) but not with SVR (p = 0.0521; table 9).

Discussion

Host factors (such as age, sex, ethnicity, platelets, liver fibrosis and obesity) have been associated with the outcome of PEG-IFN/RBV therapy [22] for HCV genotype 1. Also, the clinical outcome of this therapy for HCV infection is influenced by a number of host factors such as IL28B [9–12] and viral factors including ISDR [17, 23] and core mutations at position 70 in genotype 1 [8].

We have previously compared the impact of IRRDR, ISDR and core mutations as viral genetic polymorphisms, and the IL28B genotype as a host genetic factor, in the clinical outcome of PEG-IFN/RBV therapy – SVR, relapse and nonvirological response (NVR) – for HCV-1b with a high viral load in Japanese patients. IRRDR ≥6 was identified as a viral genetic polymorphism that independently predicts SVR to PEG-IFN/RBV treatment [7, 16, 17, 24]. The IL28B minor genotype was identified as a host genetic factor that most effectively predicts NVR [24]. On the other hand, ISDR was identified as a factor showing significant correlation with RVR in our previous study, although it has been considered a viral determiner of SVR [22, 23].

To date, except for ours [24], few factors, including host and viral factors, and viral kinetics, have been shown to predict the outcome of PEG-IFN RBV therapy for HCV-2a and HCV-2b [25]. In the present study, multivariate analysis identified platelets (OR 1.3364; p = 0.0369), IL28B major genotype (OR 31.2194; p = 0.0424) and IRRDR[2a] ≥4 (OR 15.3487; p = 0.0264), on the one hand, and γ-GTP (OR 0.8962, p = 0.0287) on the other, as factors predictive of SVR in patients infected with HCV-2a and HCV-2b, respectively. Similarly, IRRDR[2a] ≥4 (OR 23.8493; p = 0.0014) and IRRDR/N[2b] ≥1 (OR 44.7766; p = 0.064) were identified as predictive of RVR in patients infected with HCV-2a and HCV-2b, respectively. Moreover, univariate analysis showed that ISDR/+C[2a] ≥1 was significantly associated with RVR.

Consistent with previous observations of HCV-1b, we have here demonstrated that in Japanese patients sequence heterogeneity within IRRDR is closely correlated with the treatment response of HCV-2a and HCV-2b infections, and that the IL28B major genotype is significantly associated with SVR in HCV-2a infection. Nonetheless, the effect of IL28B SNP appeared to be weaker in HCV-2a and HCV-2b infections than that seen in HCV-1b infections. In HCV-2a, ISDR/+C[2a] was considered a factor related to at least early viral dynamics as shown in HCV-1b. A mutation at position 70 of the core protein of HCV-1b has been correlated with PEG-IFN/RBV treatment outcome [8]. In the present study, however, we found no significant correlation between core protein polymorphism and treatment outcome in HCV-2a or HCV-2b infection. The sequence conservation observed at position 70 might be the reason for the lack of significant correlation between core protein polymorphism and treatment outcome in HCV-2a and HCV-2b infections.

For the correlation between viral kinetics and treatment outcome, we demonstrated that RVR was related to SVR (p = 0.0327) in HCV-2a infection; however, we were not able to relate RVR to SVR by multivariate analysis. Furthermore, early viral drop was related to only RVR (p = 0.0075) in HCV-2a infection.

In conclusion, the present results suggest the clinical usefulness of the sequence heterogeneity of NS5A in HCV-2a (IRRDR[2a] ≥4) and IL28B SNP for determining viral sensitivity to PEG-IFN/RBV therapy given to HCV-2a patients. A large-scale multicenter study is needed to clarify our conclusions.

Acknowledgement

We are indebted to Mss. Yoshiko Kawamura and Miyuki Taniguchi of Kobe Asahi Hospital for assistance in the preparation of the manuscript.

Disclosure Statement

The authors have no disclosures to make.

References

1 Enomoto N, Takada A, Nakao T, Date T: There are two major types of hepatitis C virus in Japan. Biochem Biophys Res Commun 1990;170:1021–1025.

2 Kumada H, Toyota J, Okanoue T, Chayama K, Tsubouchi H, Hayashi N: Telaprevir with peginterferon and ribavirin for treatment-naive patients chronically infected with HCV of genotype 1 in Japan. J Hepatol 2012;56:78–84.

3 Kurosaki M: How to control HCV-related HCC: a personalized strategy. Liver Cancer 2013;2:167.

4 Fried MW, Shiffman ML, Reddy KR, Smith C, Marinos G, Gonçales FL Jr, Häussinger D, Diago M, Carosi G, Dhumeaux D, Craxi A, Lin A, Hoffman J, Yu J: Peginterferon alfa-2a plus ribavirin for chronic hepatitis C virus infection. N Engl J Med 2002;347:975–982.

5 Sarasin-Filipowicz M: Interferon therapy of hepatitis C: molecular insights into success and failure. Swiss Med Wkly 2009;140:3–11.

6 Enomoto N, Sakuma I, Asahina Y, Kurosaki M, Murakami T, Yamamoto C, Ogura Y, Izumi N, Marumo F, Sato C: Mutations in the nonstructural protein 5A gene and response to interferon in patients with chronic hepatitis C virus 1b infection. N Engl J Med 1996; 334:77–81.

7 El-Shamy A, Nagano-Fujii M, Sasase N, Imoto S, Kim SR, Hotta H: Sequence variation in hepatitis C virus nonstructural protein 5A predicts clinical outcome of pegylated interferon/ribavirin combination therapy. Hepatology 2008;;48:38–47.

8 Akuta N, Suzuki F, Kawamura Y, Yatsuji H, Sezaki H, Suzuki Y, Hosaka T, Kobayashi M, Kobayashi M, Arase Y, Ikeda K, Kumada H: Predictive factors of early and sustained responses to peginterferon plus ribavirin combination therapy in Japanese patients infected with hepatitis C virus genotype 1b: amino acid substitutions in the core region and low-density lipoprotein cholesterol levels. J Hepatol 2007;46:403–410.

9 Tanaka Y, Nishida N, Sugiyama M, Kurosaki M, Matsuura K, Sakamoto N, Nakagawa M, Korenaga M, Hino K, Hige S, Ito Y, Mita E, Tanaka E, Mochida S, Murawaki Y, Honda M, Sakai A, Hiasa Y, Nishiguchi S, Koike A, Sakaida I, Imamura M, Ito K, Yano K, Masaki N, Sugauchi F, Izumi N, Tokunaga K, Mizokami M: Genome-wide association of *IL28B* with response to pegylated interferon-α and ribavirin therapy for chronic hepatitis C. Nat Genet 2009;41:1105–1109.

10 Ge D, Fellay J, Thompson AJ, Simon JS, Shianna KV, Urban TJ, Heinzen EL, Qiu P, Bertelsen AH, Muir AJ, Sulkowski M, McHutchison JG, Goldstein DB: Genetic variation in *IL28B* predicts hepatitis C treatment-induced viral clearance. Nature 2009;461:399–401.

11 Suppiah V, Moldovan M, Ahlenstiel G, Ber T, Weltman M, Abate ML, Bassendine M, Spengler U, Dore GJ, Powell E, Riordan S, Sheridan D, Smedile A, Fragomeli V, Müller T, Bahlo M, Stewart GJ, Booth DR, George J: *IL28B* is associated with response to chronic hepatitis C interferon-α and ribavirin therapy. Nat Genet 2009;41:1100–1104.

12 Rauch A, Kutalik Z, Descombes P, Cai T, Di Iulio J, Mueller T, Bochud M, Battegay M, Bernasconi E, Borovicka J, Colombo S, Cerny A, Dufour JF, Furrer H, Günthard HF, Heim M, Hirschel B, Malinverni R, Moradpour D, Müllhaupt B, Witteck A, Beckmann JS, Berg T, Bergmann S, Negro F, Telenti A, Bochud PY: Genetic variation in *IL28B* is associated with chronic hepatitis C and treatment failure – a genome-wide association study. Gastroenterology 2010;138:1338–1345.

13 Ferenci P: Predictors of response to therapy for chronic hepatitis C. Semin Liver Dis 2004; 24:525–531.

14 El-Shamy A, Shoji I, Kim SR, Ide Y, Imoto S, Deng L, Yoon S, Fujisawa T, Tani S, Yano Y, Seo Y, Azuma T, Hotta H: Sequence heterogeneity in NS5A of hepatitis C virus genotypes 2a and 2b and clinical outcome of pegylated-interferon/ribavirin therapy. PLoS ONE 2012;7:e30513.

15 Okamoto H, Sugiyama Y, Okada S, Kurai K, Akahane Y, Sugai Y, Tanaka T, Sato K, Tsuda F, Miyakawa Y: Typing hepatitis C virus by polymerase chain reaction with type-specific primers: application to clinical surveys and tracing infectious sources. J Gen Virol 1992; 73:673–679.

16 El-Shamy A, Sasayama M, Nagano-Fujii M, Sasase N, Imoto S, Kim SR, Hotta H: Prediction of efficient virological response to pegylated interferon/ribavirin combination therapy by NS5A sequences of hepatitis C virus and anti-NS5A antibodies in pre-treatment sera. Microbiol Immunol 2007;51:471–482.

17 El-Shamy A, Kim SR, Ide YH, Sasase N, Imoto S, Deng L, Shoji I, Hotta H: Polymorphisms of hepatitis C virus non-structural protein 5A and core proteins and clinical outcome of pegylated-interferon/ribavirin combination therapy. Intervirology 2012;55:1–11.

18 Lusida MI, Nagano-Fujii M, Nidom CA, Soetjipto, Handajani R, Fujita T, Oka K, Hotta H: Correlation between mutations in the interferon sensitivity-determining region of NS5A protein and viral load of hepatitis C virus subtypes 1b, 1c, and 2a. J Clin Microbiol 2001;39:3858–3864.

19 Okamoto H, Okada S, Sugiyama Y, Kurai K, Iizuka H, Machida A, Miyakawa Y, Mayumi M: Nucleotide sequence of the genomic RNA of hepatitis C virus isolated from a human carrier: comparison with reported isolates for conserved and divergent regions. J Gen Virol 1991;72:2697–2704.

20 Okamoto H, Kurai K, Okada S, Yamamoto K, Lizuka H, Tanaka T, Fukuda S, Tsuda F, Mishiro S: Full-length sequence of a hepatitis C virus genome having poor homology to reported isolates: comparative study of four distinct genotypes. Virology 1992;188:331–341.

21 Akuta N, Suzuki F, Hirakawa M, Kawamura Y, Yatsuji H, Sezaki H, Suzuki Y, Hosaka T, Kobayashi M, Kobayashi M, Saitoh S, Arase Y, Ikeda K, Kumada H: Association of amino acid substitution pattern in core protein of hepatitis C virus genotype 2a high viral load and virological response to interferon-ribavirin combination therapy. Intervirology 2009; 52:301–309.

22 Kurosaki M, Sakamoto N, Iwasaki M, Sakamoto M, Suzuki Y, Hiramatsu N, Sugauchi F, Yatsuhashi H, Izumi N: Pretreatment prediction of response to peginterferon plus ribavirin therapy in genotype 1 chronic hepatitis C using data mining analysis. J Gastroenterol 2011;46:401–409.

23 Fukuhara T, Taketomi A, Okano S, Ikegami T, Soejima Y, Shirabe K, Maehara Y: Mutations in hepatitis C virus genotype 1b and the sensitivity of interferon-ribavirin therapy after liver transplantation. J Hepatol 2010;52: 672–680.

24 Kim SR, El-Shamy A, Imoto S, Kim KI, Ide YH, Deng L, Shoji I, Tanaka Y, Hasegawa Y, Ota M, Hotta H: Prediction of response to pegylated interferon/ribavirin combination therapy for chronic hepatitis C genotype 1b and high viral load. J Gastroenterol 2012;47: 1143–1151.

25 Kawaoka T, Hayes CN, Ohishi W, Ochi H, Maekawa T, Abe H, Tsuge M, Mitsui F, Hiraga N, Imamura M, Takahashi S, Kubo M, Tsunoda T, Nakamura Y, Kumada H, Chayama K: Predictive value of the *IL28B* polymorphism on the effect of interferon therapy in chronic hepatitis C patients with genotypes 2a and 2b. J Hepatol 2011;54:408–414.

Digestive Diseases

Dig Dis 2013;31:434–439
DOI: 10.1159/000355241

Outcome of Double-Filtration Plasmapheresis plus Interferon Treatment in Nonresponders to Pegylated Interferon plus Ribavirin Combination Therapy

Kayo Sugimoto[a] Soo Ryang Kim[b] Ahmed El-Shamy[c] Susumu Imoto[b] Haruma Fujioka[b] Ke Ih Kim[a] Yasuhito Tanaka[g] Yoshihiko Yano[d] Soo Ki Kim[h] Yutaka Hasegawa[e] Aya Fujinami[f] Mitsuhiro Ohta[f] Takashi Hatae[e] Hak Hotta[c] Yoshitake Hayashi[d] Masatoshi Kudo[i]

Departments of [a]Pharmacy and [b]Gastroenterology, Kobe Asahi Hospital, [c]Department of Microbiology and [d]Division for infectious Disease Pathology, Center for Infectious Diseases, Kobe University Graduate School of Medicine, and [e]Educational Center for Clinical Pharmacy and [f]Medical Biochemistry, Kobe Pharmaceutical University, Kobe, [g]Department of Virology and Liver Unit, Nagoya City University Graduate School of Medical Sciences, Nagoya, [h]Department of Gastroenterology, Kyoto University, Kyoto, and [i]Department of Gastroenterology and Hepatology, Kinki University School of Medicine, Osakasayama, Japan

Key Words
Double-filtration plasmapheresis · Interferon-β · Peginterferon · Ribavirin · Sustained virological response · Relapse · Null virological response

Abstract
Objectives: We assessed the outcome of double-filtration plasmapheresis (DFPP) combined with pegylated interferon (PEG-IFN) and ribavirin (RBV) therapy in patients infected with hepatitis C virus (HCV)-1b whose HCV had not disappeared during PEG-IFN/RBV combination therapy, or who had relapsed after the end of the therapy. Additionally, we investigated factors predictive of sustained virological response (SVR), including host and viral genetic factors, to DFPP plus IFN/RBV therapy. ***Methods:*** A total of 40 patients infected with HCV-1b whose HCV virus had not been eradicated by previous PEG-IFN/RBV therapy were enrolled for treatment by DFPP plus IFN/RBV. Rapid virological response (RVR) and SVR were assessed, and pretreatment factors associated with SVR – the interleukin (IL)28B gene, the IFN/RBV resistance-determining region (IRRDR) and the IFN sensitivity-determining region (ISDR) – were analyzed. ***Results:*** Of the 40 patients, 9 (23%) achieved RVR and 10 (25%) achieved SVR. The significant factors associated with SVR were IL28B major and RVR, as assessed by multivariate analysis ($p = 0.0182$, $p = 0.0005$). ***Conclusion:*** Patients whose HCV is not eradicated by previous PEG-IFN/RBV would be good candidates for combined DFPP and IFN/RBV retreatment provided they demonstrate IL28B major and have achieved RVR.

Introduction

The most effective treatment for patients infected with genotype hepatitis C virus (HCV)-1b has been based on pegylated interferon plus ribavirin (PEG-IFN/RBV)

KARGER

E-Mail karger@karger.com
www.karger.com/ddi

0257–2753/13/0316–0434$38.00/0

Soo Ryang Kim, MD
Department of Gastroenterology, Kobe Asahi Hospital
3-5-25 Bououji-cho, Nagata-ku
Kobe 653-0801 (Japan)
E-Mail asahi-hp@arion.ocn.ne.jp

combination therapy since 2004 in Japan. Nonetheless, sustained virological response (SVR) rates for those infected with genotype HCV-1a and HCV-1b, the most common and the most difficult to treat, still hover around 50% [1, 2]. Moreover, retreatment with PEG-IFN/RBV of patients who resist initial PEG-IFN/RBV is frequently unsuccessful, with SVR rates of only 7–9% [3]. To enhance the SVR rate more effectively for these resistant cases, several approaches have been undertaken. One such therapy is double-filtration plasmapheresis (DFPP; approved in Japan in 2008 for the treatment of chronic hepatitis C (CHC) patients with genotype HCV-1b and high viral loads) in combination with IFN administration, which has produced a substantial reduction in the viral load during the early stages of treatment and has demonstrated a high SVR rate [4, 5].

Recent reports have revealed factors associated with response to PEG-IFN/RBV therapy in HCV-1b patients: single nucleotide polymorphisms, as host genetic factors, located in interleukin (IL)28B (rs8105790, rs11881222, rs8103142, rs28416813, rs4803219, rs8099917, rs7248668 and rs12979860) on chromosome 19 [6–9]; amino acid (aa) substitutions in nonstructural protein 5A (NS5A), especially those in the IFN/RBV resistance-determining region (IRRDR) [10], and the IFN sensitivity-determining region (ISDR) [11], as viral genetic polymorphisms.

In this study, we assessed the outcome of the use of DFPP combined with IFN therapy aimed at enhancing the efficacy of the treatment of CHC patients whose HCV had not disappeared by PEG-IFN/RBV combination therapy, or who had relapsed after the end of the therapy. Additionally, we investigated factors predictive of SVR, including host and viral genetic factors associated with response to DFPP plus IFN/RBV therapy.

Patients and Methods

Patients

A total of 40 patients whose HCV virus had not been eradicated by PEG-IFNα-2b plus RBV combination therapy received DFPP plus IFN treatment. The patients comprised 2 groups according to response to previous PEG-IFN/RBV treatment: continuous viremia throughout the observation period, referred to as the null virological response (NVR) group, and transient disappearance of serum HCV RNA at a certain point in time with a subsequent rebound in viremia either before or after the end of the treatment, referred to as the relapse group. All patients were confirmed positive for HCV RNA, had high levels of transaminase persisting for 6 months or longer, demonstrated genotype HCV-1b at levels exceeding 10^5 log IU/ml in blood (as determined before the start of therapy by real-time PCR), and were negative for hepatitis B surface antigen. Patients with platelet counts $\leq 10 \times 10^4$/μl, leukocyte counts ≤3,000/μl or hemoglobin levels ≤12 g/dl were excluded from the study. Informed written consent was obtained from each patient and the study protocol conformed to the ethical guidelines approved by the Ethics Committee of Kobe Asahi Hospital.

DFPP and Blood Collection

Blood collected from the peripheral vein for DFPP by a Plasmaflo™ OP-18W filter (Asahi Kasei Medical, Tokyo, Japan) was separated into plasma and cell components. The virus was then removed from the plasma by a second filter (Cascadeflo™ EC-50W; Asahi Kasei Medical) of an average pore of 30 nm. For each session, the final volume of treated plasma was 50 ml/kg, the number of sessions was 5 over 2 weeks, and the intervals of administration of DFPP, based on the reduced plasma fibrinogen levels during DFPP, was decided by the physicians and as required by the patients.

Regimen of IFN with DFPP

During DFPP, the patients received different kinds of IFN: PEG-IFNα-2b plus RBV for 4 weeks; IFN-β 3 MU twice daily for 2 weeks and PEG-IFNα-2a plus RBV for 2 weeks; IFN-β 3 MU twice daily for 2 weeks and IFN-β 6 MU daily for 2 weeks; IFN-β 3 MU twice daily for 10 days, IFN-β 6 MU daily for 18 days and IFN-β 3 MU daily for 4 weeks; IFN-β 3 MU twice daily plus RBV for 4 weeks. The PEG-IFN dose was 1.5 μg of α-2b/kg and 180 μg of α-2a per week. After DFPP plus IFN treatment for 4 weeks, all the patients were scheduled to receive PEG-IFN/RBV combination therapy for 48 weeks. The RBV dose was 800 mg of α-2b/day and 600–800 mg of α-2a/day.

Laboratory Tests

HCV RNA was extracted from 140 μl of serum with the use of a commercially available kit (QIAmp viral RNA kit; Qiagen, Tokyo, Japan). The quantity of HCV RNA was converted to a log value at the beginning of the treatment (A) and at 4 weeks after the start of treatment (B). Δlog was then calculated as follows: $\Delta\log = \log A - \log B = \log (A/B)$. Amplification of full-length NS5A and the core regions of the HCV genome was carried out as described [10]. Before the start of treatment, HCV aa substitutions were measured in NS5A, in IRRDR and in ISDR. Genetic polymorphism rs8099917 around the IL28B gene was determined by real-time PCR with the TaqMan assay. We defined the IL28B major allele as homozygous (TT) for the major sequence and the IL28B minor allele as homozygous (GG) or heterozygous (TG) for the minor sequence.

Statistical Analysis

Rapid virological response (RVR) was defined as undetectable serum HCV RNA at week 4. SVR was defined as undetectable serum HCV RNA by week 24 after treatment. RVR and a reduction in the HCV RNA viral load ≥log 2 at week 4 after the start of treatment was assessed as being associated with SVR. The potential pretreatment factors associated with virological response including age, sex, body weight, the HCV RNA load, alanine aminotransferase (ALT), γ-glutamyl transpeptidase (γ-GTP), hemoglobin, platelets, total cholesterol, blood glucose level, single nucleotide polymorphisms in the IL-28B gene region, the mutation in NS5A, especially that in ISDR and IRRDR, were examined.

Table 1. Patient baseline characteristics

Age (years)	60.95±8.51
Sex (male/female)	13/27
Body weight (kg)	54.46±13.51
HCV RNA (KIU/ml)	6.06±0.90
Hemoglobin (g/dl)	12.18±2.94
ALT (IU/l)	37.15±30.73
γ-GTP (IU/l)	41.70±44.40
Platelets ($\times 10^4/mm^3$)	14.35±5.79
Blood glucose level	92.30±19.30
Total cholesterol (mg/dl)	151.03±32.54
IL-28 (major/minor)	18/40
ISDR	0.60±0.49
IRRDR	4.08±1.77

Data are shown as means ± SD.

Table 2. Rates of virological responses

Virological response	All	Previous relapse patients	Previous NVR patients	p value
RVR	9/40 (23)	8/18 (44)	1/22 (5)	**0.0036**
SVR	10/40 (25)	7/18 (39)	3/22 (14)	0.1401

Values in parentheses are percentages. Bold p values are significant.

Table 3. Association of baseline characteristics and clinical SVR and non-SVR

Factor	SVR (n = 10)	Non-SVR (n = 30)	p value
Age (years)	60.60±9.47	61.07±8.16	0.9626
Sex (male/female)	5/5	8/22	0.2464
Body weight (kg)	47.90±16.93	56.50±11.63	0.2717
Platelets ($\times 10^4/mm^3$)	17.76±6.26	13.21±5.14	0.0588
Hemoglobin (g/dl)	12.92±2.08	11.93±2.04	0.2540
γ-GTP (IU/l)	31.10±24.15	45.23±48.83	0.3814
ALT (IU/l)	45.60±41.18	34.33±25.73	0.4251
HCV RNA (KIU/ml)	5.97±1.00	6.09±0.87	0.4880
Blood glucose level	103.33±32.79	88.75±9.75	0.2216
T-Cho	155.20±29.69	149.63±33.32	0.5843
IL28B (major/minor)	8/2	10/20	**0.0246**
IRRDR mutations	3.60±0.92	4.23±1.94	0.4944
ISDR mutations	0.43±0.49	0.67±0.47	0.2850
Previous treatment response			
(Relapse/NVR)	7/3	11/19	0.1401
RVR/non-RVR	7/3	2/28	**0.0002**

Data are shown as means ± SD. Bold p values are significant.

Additionally, the significant factors associated with SVR were compared with those of NVR and relapse patients. Factors associated with the virological response were assessed by univariate analysis using the Mann-Whitney U test, Fisher's exact test or χ^2 test, and by multivariate analysis using logistic regression analysis. Variables with a p value <0.05 were considered statistically significant. All statistical analyses were carried out with EXCEL multivariate statistical analysis software version 6.0 (ESUMI Inc., Toyo, Japan).

Results

Treatment Responses and Viral Dynamics

The baseline characteristics of the patients and the laboratory data are shown in table 1. Of the 40 patients, 9 (23%) achieved RVR and 10 (25%) achieved SVR.

RVR was achieved in 44% (8/18) of previously relapsed patients and in 5% (1/22) of previously NVR patients, with a significant difference between the two groups (p = 0.0036; table 2). SVR was achieved in 39% (7/18) of relapsed patients and in 14% (3/22) of NVR patients, with no significant difference between the two groups (p = 0.1401; table 2). A reduction of ≥2 log in the viral load was observed in 61.5% (24/39). The number of patients who achieved ≥2 log reduction was larger in SVR than in non-SVR patients, with a significant difference between the two (p = 0.034).

Analysis of Factors Associated with SVR

By univariate analysis, the significant factors associated with SVR were IL28B major and RVR (p = 0.0246, p = 0.0002; table 3). By multivariate analysis, both factors were also significantly associated with SVR (p = 0.0182, p = 0.0005; table 4).

Analysis of the correlation between SVR and RVR in both groups revealed that of 18 previously relapsed patients, RVR was achieved in 100% (7/7) of the SVR patients, but in only 9% (1/11) of the non-SVR patients, with a significant difference between the two (p = 0.0011; table 5). Of 22 previously NVR patients, RVR was achieved in 0% (0/3) of the SVR patients and in 5% (1/19) of the non-SVR patients, with no significant difference between the two (p = 0.8636; table 6).

In previously relapsed patients, IL28B major was demonstrated in 86% (6/7) of the SVR patients and in 64% (7/11) of the non-SVR patients (p = 0.3235; table 5). In previously NVR patients, IL28B major was demonstrated in 67% (2/3) of the SVR patients, but in 16% (3/19) of the non-SVR patients; it was not associated with SVR in either relapsed or NVR patients (p = 0.1169; table 6).

Table 4. Factors associated with SVR by multivariate analysis

Factor	Odds ratio	95% CI	p value
Age (years)	0.994	0.914–1.080	0.8806
Sex (male/female)	2.75	0.626–12.085	0.1805
Body weight (kg)	0.953	0.896–1.014	0.1305
Platelets ($\times 10^4$/mm^3)	1.162	1.002–1.346	0.0464
Hemoglobin (g/dl)	1.264	0.880–1.814	0.2046
γ-GTP (IU/l)	0.99	0.967–1.014	0.4058
ALT (IU/l)	1.011	0.989–1.033	0.3330
HCVRNA (KIU/ml)	0.864	0.399–1.870	0.7110
Blood glucose level	1.041	0.987–1.098	0.1405
T-Cho	1.01	0.983–1.028	0.6404
IL28B (major/minor)	8	1.425–44.920	**0.0182**
IRRDR mutations	0.803	0.514–1.253	0.3328
ISDR mutations	0.375	0.063–2.244	0.2826
Previous treatment response			
(Relapse/NVR)	2.591	0.598–11.234	0.2034
RVR/non-RVR	32.667	4.548–234.616	**0.0005**

Bold p values are significant.

Table 5. Correlation between SVR and IL28B, RVR of previously relapsed patients

	SVR (n = 7)	Non-SVR (n = 11)	p value
RVR/non-RVR	7/0	1/10	**0.0011**
IL28B (major/minor)	6/1	7/4	0.3235

Bold p values are significant.

Table 6. Correlation between SVR and IL28B, RVR of previously NVR patients

	SVR (n = 3)	Non-SVR (n = 19)	p value
RVR/non-RVR	0/3	1/18	0.8636
IL28B (major/minor)	2/1	3/16	0.1169

Discussion

SVR by PEG-IFN/RBV treatment of patients previously nonresponsive to PEG-IFN/RBV therapy is difficult to achieve. To enhance the SVR rate, several trials have been undertaken: among patients with relapse after previous treatment, those who attain SVR on retreatment require a longer period of therapy than that of the previous treatment [12]; retreatment of nonresponders with PEG-IFN-α2b plus RBV therapy for 72 weeks increases SVR rates significantly compared with retreatment for 48 weeks [13].

An alternative therapeutic method is treatment with the use of DFPP, which was approved in Japan in 2008. Granulocyte apheresis, plasma exchange and hemofiltration are modalities that have shown a reduction of HCV RNA in blood during the treatment of HCV-infected patients for cryoglobulinemia and vasculitis [14, 15]. The mechanisms of plasmapheresis have been described as related to the enhancement of the effects of IFN therapy by synergistically removing HCV from the blood [16]. Hemodialysis, hemofiltration and peritoneal dialysis given to chronic dialysis patients infected with HCV significantly lower HCV RNA levels in the blood [17]. The change in serum HCV RNA levels after starting therapy is an important predictor of treatment outcome [18–20]. Especially, a 2-log reduction in the HCV RNA viral load by week 4 is a prerequisite to achieving SVR with PEG-IFN/RBV combination therapy [21]. Thus, the potential for effective IFN therapy combined with early physical removal of the virus is of particular interest.

Combined DFPP and IFN/RBV therapy contributes to early virological response and achieves high SVR [4, 22]. In the current study, although a 2-log reduction in the HCV RNA viral load by week 4 was observed in 61.5% of patients, RVR and SVR was observed in 23 and 25%, respectively. A previous study has concluded that relapsed patients would be better candidates for DFPP therapy than NVR patients in view of a significant difference in viral reduction at 24 and 48 h, and by weeks 1, 2, 4, 8 and 12, between NVR and relapsed patients [23]. In the current study, although a significant difference was observed in RVR between NVR and relapsed patients, no significant difference in SVR was apparent between them.

Factors predictive of virological response to PEG-IFN/RBV combination therapy have been reported in patients infected with high viral loads of genotype HCV-1b. IL28B major genotype (TT) as a host factor, a high degree (≥6) of sequence variation in IRRDR and a high degree (≥2) of sequence variation ISDR as viral factors have independently been demonstrated as significant pretreatment predictors of host- or viral-related factors [8–10, 14–16, 24, 25]. Multivariate analysis in our study showed that IL28B was the only significant pretreatment predictor of SVR in DFPP therapy, whereas IRRDR and ISDR were not significantly associated with SVR; RVR was, however,

Dig Dis 2013;31:434–439
DOI: 10.1159/000355241

significantly associated with SVR. RVR was also significantly related to SVR in the previously relapsed group. Patients achieving RVR have a high likelihood of achieving SVR by PEG-IFN/RBV combination therapy [26, 27]. Our study also suggested that achievement of RVR is essential for achieving SVR.

The recently accepted triple combination therapy comprising PEG-IFN, RBV and protease inhibitors such as telaprevir has shown that SVR is attained in 88% of relapse and 34% of NVR patients [28]. In the current study, SVR was achieved in 39% of relapse and 14% of NVR patients. Thus, combination therapy of DFPP with IFN and RBV is considered inferior to triple therapy for difficult-to-treat CHC patients. Nonetheless, triple therapy entails frequent discontinuation attributed to adverse events such as anemia and skin eruption [29]. Therefore, DFPP with IFN and RBV could become an alternative treatment for CHC patients intolerant of the triple combination therapy. Because of the small number of patients in our study, analysis in a large-scale multicenter study is needed to clarify this issue. In conclusion, we believe that patients with high viral loads of genotype HCV-1b whose HCV had not been eradicated by PEG-IFN/RBV are good candidates for treatment by DFPP combined with IFN/RBV provided they demonstrate IL28B major and have achieved RVR.

Acknowledgment

We are indebted to Ms. Yoshiko Kawamura of Kobe Asahi Hospital for assistance in the preparation of the manuscript.

Disclosure Statement

The authors have no conflicts of interest to declare.

References

1 Manns MP, McHutchison JG, Gordon SC, Rustgi VK, Shiffman M, Reindollar R, Goodman ZD, Koury K, Ling M, Albrecht JK: Peginterferon alfa-2b plus ribavirin compared with interferon alfa-2b plus ribavirin for initial treatment of chronic hepatitis C: a randomised trial. Lancet 2001;358:958–965.

2 Kurosaki M: How to control HCV-related HCC: a personalized strategy. Liver Cancer 2013;2:167.

3 Bacon BR, Shiffman ML, Mendes F, Ghalib R, Hassanein T, Morelli G, Joshi S, Rothstein K, Kwo P, Gitlin N: Retreating chronic hepatitis C with daily interferon alfacon-1/ribavirin after nonresponse to pegylated interferon/ribavirin: DIRECT results. Hepatology 2009;49:1838–1846.

4 Fujiwara K, Kaneko S, Kakumu S, Sata M, Hige S, Tomita E, Mochida S: Double filtration plasmapheresis and interferon combination therapy for chronic hepatitis C patients with genotype 1 and high viral load. Hepatol Res 2007;37:701–710.

5 Kaneko S, Sata M, Ide T, Yamashita T, Hige S, Tomita E, Mochida S, Yamashita Y, Inui Y, Kim SR, Komada N, Mikami T, Satoh S, Morita S, Takaguchi K, Hirashima N, Nishio Y, Watanabe D, Kioka K, Fujiwara K: Efficacy and safety of double filtration plasmapheresis in combination with interferon therapy for chronic hepatitis C. Hepatol Res 2010;40:1072–1081.

6 Tanaka Y, Nishida N, Sugiyama M, Kurosaki M, Matsuura K, Sakamoto N, Nakagawa M, Korenaga M, Hino K, Hige S, Ito Y, Mita E, Tanaka E, Mochida S, Murawaki Y, Honda M, Sakai A, Hiasa Y, Nishiguchi S, Koike A, Sakaida I, Imamura M, Ito K, Yano K, Masaki N, Sugauchi F, Izumi N, Tokunaga K, Mizokami, M: Genome-wide association of *IL28B* with response to pegylated interferon-α and ribavirin therapy for chronic hepatitis C. Nat Genet 2009;41:1105–1109.

7 Ge D, Fellay J, Thompson AJ, Simon JS, Shianna KV, Urban TJ, Heinzen EL, Qiu P, Bertelsen AH, Muir AJ, Sulkowski M, McHutchison, JG, Goldstein DB: Genetic variation in *IL28B* predicts hepatitis C treatment-induced viral clearance. Nature 2009;461:399–401.

8 Suppiah V, Moldovan M, Ahlenstiel G, Berg T, Weltman M, Abate ML, Bassendine M, Spengler U, Dore GJ, Powell E Riordan S, Sheridan D, Smedile A, Fragomeli V, Muller T, Bahlo M, Stewart GJ, Booth DR: George: *IL28B* is associated with response to chronic hepatitis C interferon-α and ribavirin therapy. Nat Genet 2009:41:1100–1104.

9 Rauch A, Kutalik Z, Descombes P, Cai T, Di Iulio J, Mueller T, Bochud M, Battegay M, Bernasconi E, Borovicka J, Colombo S, Cerny A, Dufour JF, Furrer H, Gunthard HF, Heim M, Hirschel B, Malinverni R, Moradpour D, Mullhaupt B, Witteck A, Beckmann JS, Berg T, Bergmann S, Negro F, Telenti A, Bochud PY: Genetic variation in *IL28B* is associated with chronic hepatitis C and treatment failure: a genome-wide association study. Gastroenterology 2010;138:1338–1345.

10 El-Shamy A, Nagano-Fujii M, Sasase N, Imoto S, Kim SR, Hotta H: Sequence variation in hepatitis C virus nonstructural protein 5A predicts clinical outcome of pegylated interferon/ribavirin combination therapy. Hepatology 2008;48:38–47.

11 Enomoto N, Sakuma I, Asahina Y, Kurosaki M, Murakami T, Yamamoto C, Ogura Y, Izumi N, Marumo F, Sato C: Mutations in the nonstructural protein 5A gene and response to interferon in patients with chronic hepatitis C virus 1b infection. N Engl J Med 1996;334:77–81.

12 Oze T, Hiramatsu N, Yakushijin T, Mochizuki K, Oshita M, Hagiwara H, Mita E, Ito T, Inui Y, Fukui H, Hijioka T, Katayama K, Tamura S, Yoshihara H, Inoue A, Imai Y, Hayashi E, Kato M, Hosui A, Miyagi T, Ishida H, Yoshida Y, Tatsumi T, Kiso S, Kanto T, Kasahara A, Takehara T, Hayashi N: Efficacy of re-treatment with pegylated interferon plus ribavirin combination therapy for patients with chronic hepatitis C in Japan. J Gastroenterol 2011;46:1031–1037.

13 Jensen DM, Marcellin P, Freilich B, Andreone P, Di Bisceglie A, Brandao-Mello CE, Reddy KR, Craxi A, Martin AO, Teuber G, Messinger D, Thommes JA, Tietz A: Re-treatment of patients with chronic hepatitis C who do not respond to peginterferon-α2b: a randomized trial. Ann Intern Med 2009;150:528–540.

14 Fabrizi F, Martin P, Dixit V, Brezina M, Cole MJ, Vinson S, Mousa M, Gitnick G: Biological dynamics of viral load in hemodialysis patients with hepatitis C virus. Am J Kidney Dis 2000;35:122–129.

15 Manzin A, Candela M, Solforosi L, Gabrielli A, Clementi M: Dynamics of hepatitis C viremia after plasma exchange. J Hepatol 1999;31:389–393.

16 Sakai A, Kaneko S, Matsushita E, Kobayashi K: Floating density of hepatitis C virus particles and response to interferon treatment. J Med Virol 1998;55:12–17.
17 Ishida H, Tanabe K, Tokumoto T, Shimizu T, Shimmura H, Yoshioka T, Toma H: Hepatitis C virus decreases in patients with maintenance hemofiltration therapy. Artif Organs 2004;28:316–318.
18 Zeuzem S, Herrmann E, Lee JH, Fricke J, Neumann AU, Modi M, Colucci G, Roth WK: Viral kinetics in patients with chronic hepatitis C treated with standard or peginterferon α2a. Gastroenterology 2001;120:1438–1447.
19 Buti M, Sanchez-Avila F, Lurie Y, Stalgis C, Valdes A, Martell M, Esteban R: Viral kinetics in genotype 1 chronic hepatitis C patients during therapy with 2 different doses of peginterferon alfa-2b plus ribavirin. Hepatology 2002;35:930–936.
20 Berg T, Sarrazin C, Herrmann E, Hinrichsen H, Gerlach T, Zachoval R, Wiedenmann B, Hopf U, Zeuzem S: Prediction of treatment outcome in patients with chronic hepatitis C: significance of baseline parameters and viral dynamics during therapy. Hepatology 2003; 37:600–609.
21 Nomura H, Miyagi Y, Tanimoto H, Higashi M, Ishibashi H: Effective prediction of outcome of combination therapy with pegylated interferon alpha 2b plus ribavirin in Japanese patients with genotype-1 chronic hepatitis C using early viral kinetics and new indices. J Gastroenterol 2009;44:338–345.
22 Yamashita T, Arai K, Sakai A, Mizukoshi E, Sakai Y, Kagaya T, Nakamoto Y, Honda M, Wada T, Yokoyama H, Kaneko S: Virological effects and safety of combined double filtration plasmapheresis (DFPP) and interferon therapy in patients with chronic hepatitis C: a preliminary study. Hepatol Res 2006;36:167–175.
23 Kim SR, Saito J, Imoto S, Komaki T, Nagata Y, Kim KI, Sasase N, Kimura N, Sasatani K, Konishi E, Hasegawa Y, Fujinami A, Ohta M, El-Shamy A, Tanaka Y, Sugano M, Sakashita M, Nakamura A, Tsuchida S, Makino T, Kawada T, Nakajima T, Morikawa T, Muramatsu A, Kasugai H, Hotta H, Kudo M: Double-filtration plasmapheresis plus interferon-β for HCV-1b patients with non-sustained virological response to previous combination therapy. Digestion 2011;84(suppl 1):10–16.
24 Kim SR, El-Shamy A, Imoto S, Kim KI, Ide YH, Deng L, Shoji I, Tanaka Y, Hasegawa Y, Ota M, Hotta H: Prediction of response to pegylated interferon/ribavirin combination therapy for chronic hepatitis C genotype 1b and high viral load. J Gastroenterol 2012;47: 1143–1151.
25 Kurosaki M, Tanaka Y, Nishida N, Sakamoto N, Enomoto N, Honda M, Sugiyama M, Matsuura K, Sugauchi F, Asahina Y, Nakagawa M, Watanabe M, Sakamoto M, Maekawa S, Sakai A, Kaneko S, Ito K, Masaki N, Tokunaga K, Izumi N, Mizokami M: Pre-treatment prediction of response to pegylated-interferon plus ribavirin for chronic hepatitis C using genetic polymorphism in *IL28B* and viral factors. J Hepatol 2011;54:439–448.
26 Martinot-Peignoux M, Maylin S, Moucari R, Ripault MP, Boyer N, Cardoso AC, Giuily N, Castelnau C, Pouteau M, Stern C, Auperin A, Bedossa P, Asselah T, Marcellin P: Virological response at 4 weeks to predict outcome of hepatitis C treatment with pegylated interferon and ribavirin. Antivir Ther 2009;14:501–511.
27 Toyoda H, Kumada T, Kiriyama S, Tanikawa M, Hisanaga Y, Kanamori A, Tada T, Arakawa T, Fujimori M, Niinomi T, Ando N, Yasuda S, Sakai K, Kimura J: High ability to predict the treatment outcome of peginterferon and ribavirin combination therapy based on the reduction in HCV RNA levels at 4 weeks after starting therapy and amino acid substitutions in the hepatitis C virus in patients infected with HCV genotype 1b. J Gastroenterol 2011; 46:501–509.
28 Hayashi N, Okanoue T, Tsubouchi H, Toyota J, Chayama K, Kumada H: Efficacy and safety of telaprevir, a new protease inhibitor, for difficult-to-treat patients with genotype 1 chronic hepatitis C. J Viral Hepat 2012;19:134–142.
29 McHutchison JG, Everson GT, Gordon SC, Jacobson IM, Sulkowski M, Kauffman R, McNair L, Alam J, Muir AJ: Telaprevir with peginterferon and ribavirin for chronic HCV genotype 1 infection. N Engl J Med 2009;360: 1827–1838.

Digestive Diseases

Dig Dis 2013;31:440–446
DOI: 10.1159/000355242

Hypothermia Protects against Fulminant Hepatitis in Mice by Reducing Reactive Oxygen Species Production

Toshiharu Sakurai[a] Masatoshi Kudo[a] Tomohiro Watanabe[b] Katsuhiko Itoh[c] Hiroaki Higashitsuji[c] Tadaaki Arizumi[a] Tatsuo Inoue[a] Satoru Hagiwara[a] Kazuomi Ueshima[a] Naoshi Nishida[a] Manabu Fukumoto[d] Jun Fujita[c]

[a]Department of Gastroenterology and Hepatology, Kinki University School of Medicine, Osakasayama, [b]Center for Innovation in Immunoregulative Technology and Therapeutics and [c]Department of Clinical Molecular Biology, Graduate School of Medicine, Kyoto University, Kyoto, and [d]Department of Pathology, Institute of Development, Aging and Cancer, Tohoku University, Sendai, Japan

Key Words
Reactive oxygen species · Fulminant hepatitis · Hypothermia · Cold-inducible RNA-binding protein · Cold shock

Abstract
Objective: Mild hypothermia (32–33°C) shows protective effects in patients with brain damage and cardiac arrest. Although cold-inducible RNA-binding protein (CIRP) contributes to the protective effects of hypothermia through extracellular signal-regulated kinase activation in fibroblasts, the effects of hypothermia in the liver remain unclear. ***Methods:*** We analysed the effects of cold temperature on fulminant hepatitis, a potentially fatal disease, using the D-galactosamine (GalN)/lipopolysaccharide (LPS) and concanavalin (con) A-induced hepatitis models in mice. After GalN/LPS administration and anaesthesia, mice in the hypothermia group were kept at 25°C and those in control group were kept at 35°C. After concanavalin A (con A) administration, the mice in the hypothermia group were placed in a chamber with an ambient temperature of 6°C for 1.5 h. ***Results:*** Hypothermia attenuated liver injury and prolonged survival. Activation of c-Jun N-terminal kinase and Akt, which are involved in reactive oxygen species (ROS) accumulation, was suppressed by low temperature. Hypothermia significantly decreased oxidized protein levels, and treatment with N-acetyl-L-cysteine, an antioxidant, attenuated GalN/LPS-induced liver injury. In con A-induced hepatitis, CIRP expression was upregulated and Bid expression was downregulated, resulting in decreased apoptosis of hepatocytes in the hypothermia group. ***Conclusions:*** These data suggest that hypothermia directly protects hepatocytes from cell death via reduction of ROS production in fulminant hepatitis.

Introduction

Mild hypothermia has been reported to protect central neurons from ischemic damage [1–3]. Although clinical application of mild hypothermia (32–35°C) for patients with brain injury and cardiac arrest has been conducted

KARGER

E-Mail karger@karger.com
www.karger.com/ddi

0257–2753/13/0316–0440$38.00/0

Dr. Toshiharu Sakurai
Department of Gastroenterology and Hepatology, Faculty of Medicine, Kinki University
377-2 Ohno-Higashi
Osakasayama, Osaka 589-8511 (Japan)
E-Mail sakurai@med.kindai.ac.jp

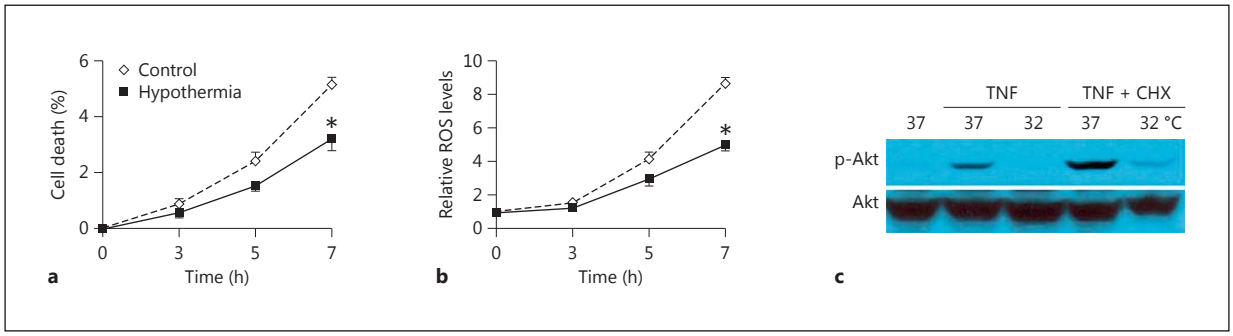

Fig. 1. Low temperature (32°C) reduced ROS production and cell death in TNF-α-treated cells. HeLa cells were cultured at 37 (control) or 32°C (hypothermia) in media containing TNF-α (50 ng/ml) and/or CHX (10 μg/ml). **a**, **b** The cell survival rates and relative ROS levels were examined at the indicated times after initiation of TNF-α treatment. The number of viable cells was estimated by the Trypan blue assay. ROS accumulation was assessed using 5-[and-6]-chloromethyl-2′,7′-dichlorodihydrofluorescein diacetate (CM-H_2DCFDA). The values are shown relative to non-treated cells; results are the mean ± SEM. * $p < 0.05$ versus culture at 37°C (control). **c** After treatment with TNF-α or TNF-α plus CHX, cell lysates were prepared and analysed by Western blotting using the indicated antibodies.

with promising results [4], the molecular mechanisms underlying the protective effects of hypothermia are unknown. In endothelial cells kept under hypothermic conditions, significant upregulation of the anti-apoptotic protein Bcl-2 has been reported. Hypothermia decreased the levels of inflammatory chemokines such as IL-8, MCP-1 and COX-2, which could lead to reduced leukocyte recruitment [5]. Low temperature protects mammalian cells from apoptosis initiated by various stimuli in vitro [6]. Cold-inducible RNA-binding protein (CIRP), a protein induced by mild hypothermia, protects against tumour necrosis factor (TNF)-α-induced apoptosis via activation of extracellular signal-regulated kinase (ERK) [7].

Fulminant hepatitis, resulting from the acute hepatitis caused by viral infection, alcohol or drugs, is associated with high mortality, and development of a new therapy is necessary. This pathophysiological disturbance is caused by excessive hepatocyte death, in which TNF-α plays an important role [8]. Reactive oxygen species (ROS) are another major mediator of inflammation and reduction of ROS levels leads to attenuation of hepatic injury [9]. Akt activation increases intracellular ROS levels [10]. ROS accumulation inhibits mitogen-activated protein kinase (MAPK) phosphatases, resulting in prolonged c-Jun N-terminal kinase (JNK) activation, which contributes to ROS accumulation and hepatocyte death [11]. Here, we analysed the effects of hypothermia on fulminant hepatitis using murine hepatitis models.

Materials and Methods

Cell Culture

Human HeLa cells were maintained in Dulbecco's modified Eagle medium supplemented with 10% foetal bovine serum at 32 or 37°C in a humidified atmosphere of 5% CO_2 in air. For induction of cell death, confluent cultures of cells were incubated with TNF-α (50 ng/ml) in the presence of cycloheximide (CHX; 10 μg/ml). The number of viable cells was estimated by Trypan blue assay. To assess intracellular ROS levels, TNF-α-treated cells were resuspended in PBS containing 10 μM 5-[and-6]-chloromethyl-2′,7′-dichlorodihydrofluorescein diacetate (CM-H_2DCFDA; Invitrogen, Carlsbad, Calif., USA), maintained at 37°C in the dark for 30 min, and analysed by flow cytometry.

Western Blot Analysis

Western blot analysis was performed as previously described [12]. The antibodies used were as follows: anti-phospho Akt, anti-Akt, anti-phospho-JNK, anti-JNK, anti-phospho-ERK, anti-ERK (Cell Signaling Technology, Danvers, Mass., USA), anti-Bcl-2, anti-Bad, anti-Bid (BD Transduction Laboratory, Lexington, Ky., USA), anti-β-actin (Sigma, St. Louis, Mo., USA), anti-Bcl-xL and anti-HNF-3γ (Santa Cruz Biotechnology, Santa Cruz, Calif., USA). Rabbit polyclonal antibody recognizing C terminus of mouse CIRP was prepared as described [13]. To quantify ROS accumulation, an OxyBLOT™ Protein Oxidation Detection Kit (Millipore, Billerica, Mass., USA) was used.

Fulminant Hepatitis Model

C57BL/6 mice, 4–12 weeks old, were purchased from Japan SLC (Shizuoka, Japan) and were kept at 25°C and 55% relative humidity in a 12-hour day/night cycle with free access to food and water. To induce hepatitis, D-galactosamine (GalN; 1,000 mg/kg, Sigma) and lipopolysaccharide (LPS; 0.1 or 35 μg/kg, Sigma) were injected i.p. Thereafter, mice were anesthetized with urethane or

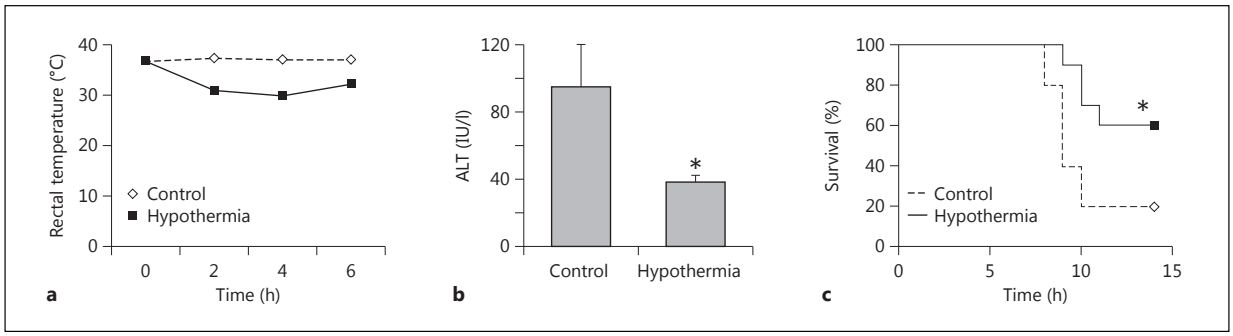

Fig. 2. Hypothermia ameliorates GalN/LPS-induced hepatitis. **a** Rectal temperatures of mice in the control (n = 10) and hypothermia (n = 10) groups were monitored after injection of GalN (1,000 mg/kg) and LPS (0.1 μg/kg); results are the mean. **b** Mice were injected with GalN (1,000 mg/kg) and LPS (0.1 μg/kg), and 8 h after the injection serum ALT levels were examined; results are the mean ± SEM. * $p < 0.05$ versus the control. **c** After injection with GalN (1,000 mg/kg) and LPS (35 μg/kg), the survival rates of mice in the control group (n = 10) and those in the hypothermia group (n = 10) were examined. The difference in the survival rate was analysed by the Kaplan-Meier method and log-rank test. * $p < 0.05$ versus the control.

pentobarbital and divided into 2 groups: mice placed in a chamber with an ambient temperature of 25°C (hypothermia group) and those placed on a plate of 35°C (control group). To investigate the protective effects of N-acetyl-L-cysteine (NAC; Sigma), which is an antioxidant, mice were administered with NAC (150 mg/kg, i.p.) 30 min before GalN/LPS administration (1,000 mg/0.1 μg/kg, i.p.). NAC dissolved in PBS was neutralized before injection. The volume of insensible perspiration was 15 ml/kg/day and increased by 15% per 1°C upshift of body temperature [14]. The volume of PBS as calculated was injected i.p. into mice in the control group to reduce the effect of dehydration.

Concanavalin A (con A; Sigma) was dissolved in sterile saline and injected into the tail vein at a final volume of 200 μl. To examine the effect of hypothermia on their survival, the mice were treated with con A at a lethal dose of 35 mg/kg body weight and divided into 2 groups. One hour after con A injection, the mice in the hypothermia group were placed in a chamber with an ambient temperature of 6°C for 1.5 h. Then, all mice were observed at 22°C. For histological and gene expression analyses, mice were treated with 25 mg/kg of con A, divided into 2 groups, and euthanised at 24 h after con A injection.

This work was conducted under the Japanese Law Concerning the Care and Control of Animals and was approved by the Animal Research Committee of the Faculty of Medicine of Kinki and Kyoto University.

Histopathological Examination

The liver was removed and fixed in 10% formalin, embedded in paraffin and sliced into 5-μm sections for light microscopy. Immunohistochemistry was performed using ImmPRESS™ reagents (Vector Laboratory, Burlingame, Calif., USA) according to the manufacturer's recommendations. The number of proliferating cells was estimated by staining the sections with a mouse monoclonal anti-proliferating cell nuclear antigen (PCNA) antibody (Cell Signaling Technology). TUNEL staining was performed using tissue sections with an in situ Apoptosis Detection Kit (Takara, Tokyo, Japan).

Statistical Analysis

Data are presented as the mean ± SEM. Statistical differences between sample means were calculated by analysis of variance, followed by unpaired Student's t test. To compare the survival rates between groups of mice, the log-rank test was used. $p < 0.05$ was considered significant.

Results

Low Temperature (32°C) Reduced ROS Production and Cell Death in TNF-α-Treated Cells

Treatment with TNF-α and CHX induced death of HeLa cells cultured at 37°C within 6 h (fig. 1a). The number of surviving cells was significantly higher when cells were cultured at 32°C (hypothermia) than when they were cultured at 37°C (control). Similar results were obtained with the human hepatoma cell line HuH-7 [7]. Decreased H_2O_2 accumulation in cells cultured at 32°C was detected using the ROS indicator 5-[and-6]-chloromethyl-2′,7′-dichlorodihydrofluorescein diacetate (CM-H_2DCFDA; fig. 1b). Akt activation promotes ROS production [10]. At 60 min after treatment with TNF-α, the protein level of phospho-Akt was lower in HeLa cells cultured at 32°C than in cells cultured at 37°C (fig. 1c).

Hypothermia Ameliorates GalN/LPS-Induced Hepatitis

The mean rectal temperature was kept at approximately 30°C in the hypothermia group and at 37°C in the control group (fig. 2a). As shown in fig. 2b and c, hypothermic treatment significantly reduced hepatic injury and improved the survival rate in GalN/LPS-induced hepatitis.

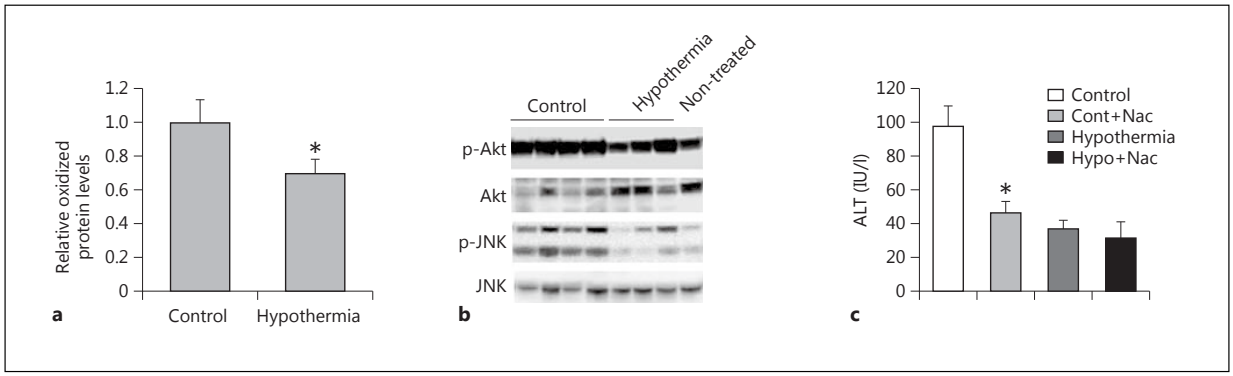

Fig. 3. Hypothermia reduces ROS accumulation in GalN/LPS-treated livers. Mice in the control (n = 8) and hypothermia (n = 8) groups were injected with GalN (1,000 mg/kg) and LPS (0.1 μg/kg), and 24 h after the GalN/LPS injection, tissue lysates were extracted. **a** ROS accumulation was assessed using the OxyBLOT™ Protein Oxidation Detection Kit; the results are the mean ± SEM. * $p < 0.05$ versus the control. **b** Tissue lysates were analysed by Western blotting using the indicated antibodies. **c** Mice in the control group (n = 8) and hypothermia group (n = 8) were injected with GalN (1,000 mg/kg) and LPS (0.1 μg/kg). Mice received NAC (150 mg/kg, i.p.) in the control group (Cont+Nac; n = 8) and the hypothermia group (Hypo+Nac; n = 8) 30 min before GalN/LPS administration (1,000 mg/0.1 μg/kg, i.p.). Eight hours after the GalN/LPS injection, the mice were euthanised and serum ALT levels were examined; results are the mean ± SEM. * $p < 0.05$ versus the control.

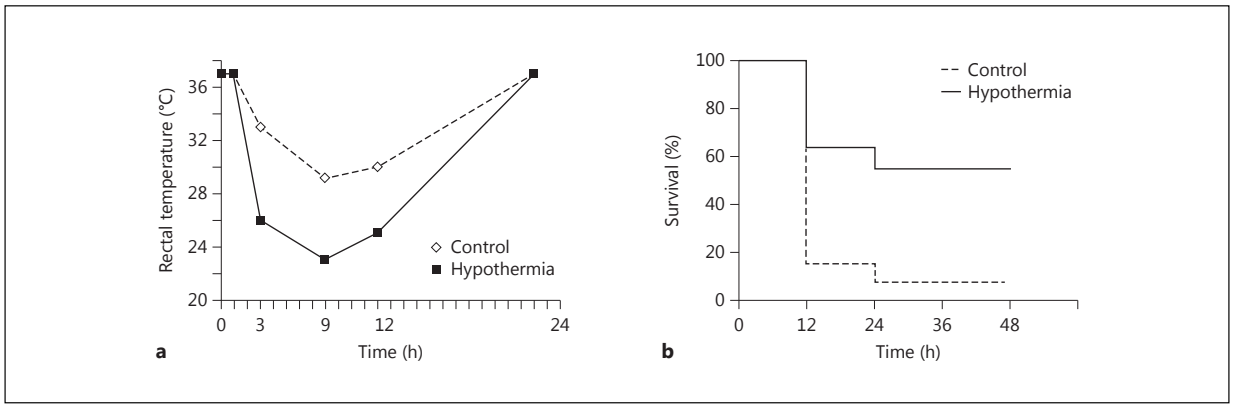

Fig. 4. Hypothermia improves the survival rate in con A-induced hepatitis. **a** Rectal temperatures of mice in the control (n = 14) and hypothermia (n = 11) groups were monitored after injection of con A (35 mg/kg); results are the mean. **b** After injection with con A (35 mg/kg), the survival rates of mice in the control group (n = 14) and those in the hypothermia group (n = 11) were examined. The difference in the survival rate was analysed by the Kaplan-Meier method and log-rank test.

Hypothermia Reduces ROS Accumulation in GalN/LPS-Treated Livers

Mice in the hypothermia group were found to have lower levels of oxidized protein than those in the control group (fig 3a). ROS accumulation inhibits MAPK phosphatases, resulting in prolonged JNK activation, which contributes to hepatocyte death [11]. Accordingly, Akt and JNK activity were decreased in hypothermia-treated livers (fig. 3b). To evaluate the contribution of oxidative stress to GalN/LPS-induced liver damage, we injected the antioxidant NAC. NAC-treated mice showed a significant reduction in GalN/LPS-induced liver injury (fig. 3c). Thus, hypothermia reduces GalN/LPS-induced hepatocyte death through mechanisms that may depend on attenuated ROS accumulation.

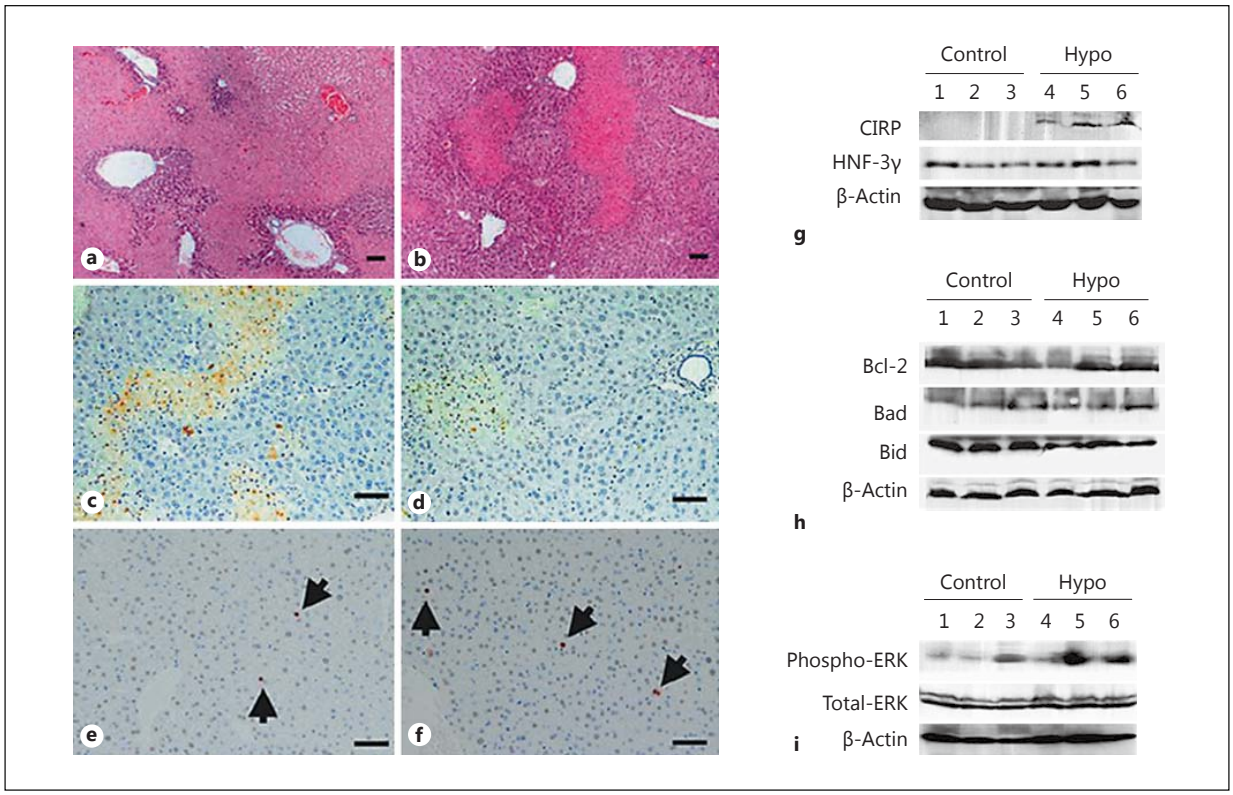

Fig. 5. Hypothermia upregulates CIRP in con A-induced hepatitis. **a–f** Liver histology. Mice were injected with 25 mg/kg body weight of con A. One hour later, the ambient temperature was changed to 25°C (**a**, **c**, **e**) or 6°C (**b**, **d**, **f**) for 1.5 h, and then returned to room temperature. Twenty-four hours after the injection, the mice were euthanised and liver sections were obtained after fixation. Haematoxylin and eosin staining (**a**, **b**); TUNEL staining (**c**, **d**); immunohistochemical staining with mouse anti-PCNA antibody and horseradish peroxidase-conjugated anti-mouse antibody (**e**, **f**). Arrows indicate PCNA-positive cells. Scale bar = 50 μm. **g–i** Gene expression. Groups of mice were treated as above, and the expression of CIRP and HNF-3γ (**g**), Bcl-2 family members (**h**) and ERK (**i**) in the livers of control mice and hypothermic mice (Hypo) was analysed by Western blotting using the indicated antibodies. Results with representative samples are shown.

Hypothermia Upregulates CIRP Expression and Improves the Survival Rate in con A-Induced Hepatitis

TNF-α has been suggested to be a crucial factor in fulminant hepatitis [8]. In con A-induced hepatitis, a mouse model of fulminant hepatitis, the intrahepatic levels of cytokines, including TNF-α, maximally increase 1 h after con A administration [15]. As shown in figure 4, hypothermic treatment improved the survival rate, but the improvement was not significant ($p = 0.096$).

Histological examinations revealed that con A induced severe morphological changes in the liver (fig. 5a). Dilatation of veins and bile ducts was prominent. Massive degenerative lesions consisting of dead parenchymal cells were observed in the midlobular area. The liver of mice in the hypothermia group showed smaller areas of the lesion than the liver of the mice in the control group (fig. 5b). Cells positive for TUNEL staining were localized in the parenchymal cells in the midlobular area and adjacent to the degenerative lesions, and the areas with TUNEL-positive cells were smaller in the hypothermia group (fig. 5c, d). Cold exposure slightly reduced the number of PCNA-positive cells in mice without con A challenge (4.5 ± 1.2 vs. 3.4 ± 0.8 per 1,000 cells). As shown in figure 5e and f, PCNA immunoreactivity was decreased after con A administration in the control and hypothermia groups

to equivalent levels (1.4 ± 0.5 vs. 1.8 ± 0.6 per 1,000 cells). These results suggest that in con A-induced hepatitis, hypothermia improves the survival of mice not by enhancing hepatocyte regeneration but rather by suppressing apoptosis.

The stress response protein CIRP protects cells by activating the ERK pathway [7]. HNF-3γ shows a hepatoprotective effect in acute liver injury [16]. Hypothermia induced the expression of CIRP, but not HNF-3γ, in the livers of con A-treated mice (fig. 5g). As shown in figure 5h, Bid was downregulated in livers in the hypothermia group. There was no difference in the protein levels of XIAP/ILP and other Bcl-2 family members, including Bcl-2, Bcl-xL, Bad and Mcl-1 (fig. 5h and data not shown). The level of phosphorylated ERK was increased in 2 out of 3 examined mice in the hypothermia group (fig. 5i).

Discussion

Fulminant hepatitis is a devastating liver disease with a progressive course and a high mortality rate [17]. Although several studies have shown that mild hypothermia has a protective effect against the encephalopathy resulting from severe liver injury [18], the direct effect of hypothermia on the liver has not been determined. In the present study, we found that hypothermia inhibited apoptosis in the liver and increased the survival rate in mice with con A-induced hepatitis and GalN/LPS-induced hepatitis, which are considered to be relevant to human fulminant hepatitis [19]. Apoptosis is essential for the homeostasis of organs such as the liver [20]. In both human fulminant hepatitis and its animal models, apoptosis of hepatocytes is mediated by death receptors such as Fas (CD95) and the TNF-α receptor [20, 21]. In the death receptor pathway, the pro-apoptotic protein Bid is processed, and its translocation to the mitochondria activates the mitochondrial apoptotic pathway [22]. Bid is required, at least in some cells, for death receptor activation to initiate the apoptosis cascade. Here, we showed that in the livers of mice treated with con A, the Bid protein level was lower in the hypothermia group than in the control group (fig. 5). These results suggest that the protective effect of hypothermia in mice is mediated, at least partly, by the decrease in the Bid protein level in the liver. CIRP blunts TNF-α-mediated apoptosis via ERK activation [7] and inhibits H_2O_2-induced apoptosis through upregulation of thioredoxin expression [23]. CIRP, which was upregulated by hypothermia in this study, may contribute to the anti-apoptotic effects of hypothermia by regulating ERK activity and ROS accumulation in the liver.

Several mechanisms have been proposed to explain the increased resistance of humans and animals to tissue damage as body temperature is reduced. Hypothermia suppresses the production of superoxide anions, nitric oxide and TNF-α in ischemic cells [24]. The hepatic inflammatory response after ischemia is suppressed by hypothermia through selective inhibition of JNK and activator protein-1 [25]. ROS promote TNF-α-induced death and sustained JNK activation by inhibiting MAP kinase phosphatases [11, 26]. Akt activation increases intracellular ROS levels through increased oxygen consumption and by inhibition of the expression of ROS scavengers downstream of FoxO, particularly *sestrin 3* [10]. In the present study, we demonstrated that hypothermia suppressed liver injury and the Akt and JNK pathways in the livers of GalN/LPS-treated mice (fig. 3). Furthermore, mice treated with an antioxidant showed a significant reduction in the severity of liver injury. These data suggest that the attenuation of ROS accumulation is involved in the cyto-protective effect of hypothermia. Further elucidation of the underlying mechanisms of these protective effects will lead to the future development of novel therapeutic modalities.

Acknowledgements

We thank A.M. Park and H. Munakata for technical assistance and discussions. This work was partly supported by Grants-in-Aid from the Ministry of Education, Culture, Sports, Science and Technology of Japan, the Japan Society for the Promotion of Science, Takeda Science Foundation and the Smoking Research Foundation of Japan.

Disclosure Statement

The authors have no conflicts of interest to disclose.

References

1 Curfman GD: Hypothermia to protect the brain. N Engl J Med 2002;346:546.
2 Darby JM: Therapeutic hypothermia after cardiac arrest. N Engl J Med 2002;347:63–65.
3 Wu TC, Grotta JC: Hypothermia for acute ischaemic stroke. Lancet Neurol 2013;12:275–284.
4 Hong MF, Dorian P: Update on advanced life support and resuscitation techniques. Curr Opin Cardiol 2005;20:1–6.

5 Diestel A, Roessler J, Berger F, Schmitt KR: Hypothermia downregulates inflammation but enhances IL-6 secretion by stimulated endothelial cells. Cryobiology 2008;57:216–222.
6 Sakurai T, Itoh K, Liu Y, Higashitsuji H, Sumitomo Y, Sakamaki K, Fujita J: Low temperature protects mammalian cells from apoptosis initiated by various stimuli in vitro. Exp Cell Res 2005;309:264–272.
7 Sakurai T, Itoh K, Higashitsuji H, Nonoguchi K, Liu Y, Watanabe H, Nakano T, Fukumoto M, Chiba T, Fujita J: Cirp protects against tumor necrosis factor-α-induced apoptosis via activation of extracellular signal-regulated kinase. Biochim Biophys Acta 2006;1763:290–295.
8 Bradham CA, Plumpe J, Manns MP, Brenner DA, Trautwein C: Mechanisms of hepatic toxicity. I. TNF-induced liver injury. Am J Physiol 1998;275:G387–G392.
9 Sakurai T, Kudo M, Umemura A, He G, Elsharkawy AM, Seki E, Karin M: p38α inhibits liver fibrogenesis and consequent hepatocarcinogenesis by curtailing accumulation of reactive oxygen species. Cancer Res 2013;73:215–224.
10 Nogueira V, Park Y, Chen CC, Xu PZ, Chen ML, Tonic I, Unterman T, Hay N: Akt determines replicative senescence and oxidative or oncogenic premature senescence and sensitizes cells to oxidative apoptosis. Cancer Cell 2008;14:458–470.
11 Sakurai T, He G, Matsuzawa A, Yu GY, Maeda S, Hardiman G, Karin M: Hepatocyte necrosis induced by oxidative stress and IL-1α release mediate carcinogen-induced compensatory proliferation and liver tumorigenesis. Cancer Cell 2008;14:156–165.
12 Mine H, Sakurai T, Kashida H, Matsui S, Nishida N, Nagai T, Hagiwara S, Watanabe T, Kudo M: Association of Gankyrin and stemness factor expression in human colorectal cancer. Dig Dis Sci 2013;58:2337–2344.
13 Masuda T, Itoh K, Higashitsuji H, Higashitsuji H, Nakazawa N, Sakurai T, Liu Y, Tokuchi H, Fujita T, Zhao Y, Nishiyama H, Tanaka T, Fukumoto M, Ikawa M, Okabe M, Fujita J: Cold-inducible RNA-binding protein (Cirp) interacts with Dyrk1b/Mirk and promotes proliferation of immature male germ cells in mice. Proc Natl Acad Sci USA 2012;109:10885–10890.
14 Guyton AC: Textbook of Medica Physiology, ed 7. Philadelphia, Saunders, 1986.
15 Sass G, Heinlein S, Agli A, Bang R, Schumann J, Tiegs G: Cytokine expression in three mouse models of experimental hepatitis. Cytokine 2002;19:115–120.
16 Nakamura T, Akiyoshi H, Shiota G, Isono M, Nakamura K, Moriyama M, Sato K: Hepatoprotective action of adenovirus-transferred HNF-3γ gene in acute liver injury caused by CCl_4. FEBS Lett 1999;459:1–4.
17 Galun E, Axelrod JH: The role of cytokines in liver failure and regeneration: potential new molecular therapies. Biochim Biophys Acta 2002;1592:345–358.
18 Jalan R: Intracranial hypertension in acute liver failure: pathophysiological basis of rational management. Semin Liver Dis 2003;23:271–282.
19 Tiegs G, Hentschel J, Wendel A: A T cell-dependent experimental liver injury in mice inducible by concanavalin A. J Clin Invest 1992;90:196–203.
20 Galle PR, Hofmann WJ, Walczak H, Schaller H, Otto G, Stremmel W, Krammer PH, Runkel L: Involvement of the CD95 (APO-1/Fas) receptor and ligand in liver damage. J Exp Med 1995;182:1223–1230.
21 Hengartner MO: The biochemistry of apoptosis. Nature 2000;407:770–776.
22 Luo X, Budihardjo I, Zou H, Slaughter C, Wang X: Bid, a Bcl2 interacting protein, mediates cytochrome c release from mitochondria in response to activation of cell surface death receptors. Cell 1998;94:481–490.
23 Li S, Zhang Z, Xue J, Liu A, Zhang H: Cold-inducible RNA binding protein inhibits H_2O_2-induced apoptosis in rat cortical neurons. Brain Res 2012;1441:47–52.
24 Kataoka K, Yanase H: Mild hypothermia – a revived countermeasure against ischemic neuronal damages. Neurosci Res 1998;32:103–117.
25 Kato A, Singh S, Mcleish KR, Edwards MJ, Lentsch AB: Mechanisms of hypothermic protection against ischemic liver injury in mice. Am J Physiol Gastrointest Liver Physiol 2002;282:G608–G616.
26 Kamata H, Honda S, Maeda S, Chang L, Hirata H, Karin M: Reactive oxygen species promote TNFα-induced death and sustained JNK activation by inhibiting MAP kinase phosphatases. Cell 2005;120:649–661.

Digestive Diseases

Dig Dis 2013;31:447–453
DOI: 10.1159/000355243

Oxidative Stress and Epigenetic Instability in Human Hepatocarcinogenesis

Naoshi Nishida Masatoshi Kudo

Department of Gastroenterology and Hepatology, Kinki University School of Medicine, Osakasayama, Japan

Key Words
DNA methylation · Oxidative stress · Reactive oxygen species · Tumor suppressor gene · Oncogene · Histone · Epigenetic instability · Hepatocellular carcinoma

Abstract
Hepatocellular carcinoma (HCC) is a major cause of cancer death, and its development is influenced by the status of inflammation and oxidative stress in the liver. Although oxidative stress might induce genetic changes and play a role in HCC development, many epigenetic alterations have also been reported in this type of tumor, suggesting the importance of epigenetic instability in hepatocarcinogenesis. Epigenetic instability results in 2 types of DNA alterations: hypermethylation of the promoter of tumor suppressor genes (TSGs), and hypomethylation of nonpromoter CpG, such as repetitive elements and satellite DNA. The former causes transcriptional inactivation of TSGs, while the latter reportedly induces chromosomal instability and an abnormal activation of oncogenes as well as mobile genetic elements. Oxidative stress could induce epigenetic instability and inactivate TSGs through the recruitment of the polycomb repressive complex to the promoter sequence carrying DNA damage induced by oxidation. Inflammatory cytokines from immune cells also reportedly induce expression of several histone and DNA modulators. On the other hand, DNA oxidation could lead to activation of DNA repair pathways and affect the binding of methyl cytosine-binding protein to DNA, which could cause DNA hypomethylation. The decrease of the level of methyl group donors also contributes to the alteration in the methylation status. These mechanisms should act in concert and induce epigenetic instability, leading to HCC.

Introduction

The accumulation of several genetic and epigenetic alterations is observed in hepatocellular carcinoma (HCC) cells, and these are considered to play a critical role in the alteration of cancer-related genes for the emergence of HCC [1]. The development of this tumor is closely associated with chronic inflammation as well as induction of oxidative stress [2]. For example, chronic infection with the hepatitis virus, the deposition of iron and copper, and steatosis of the liver are risk factors that can contribute to HCC emergence [3]; all of these factors also reportedly induce oxidative stress in hepatocytes. There is strong support to indicate that oxidative stress, possibly an important risk factor for HCC, can induce genetic as well as epigenetic alterations in cancer-related genes. This review focuses on the role of oxidative stress in the induction of epigenetic instability during the development of HCC.

KARGER

E-Mail karger@karger.com
www.karger.com/ddi

0257–2753/13/0316–0447$38.00/0

Naoshi Nishida, MD, PhD
Department of Gastroenterology and Hepatology, Kinki University School of Medicine
337-2 Ohno-higashi
Osakasayama, Osaka 589-8511 (Japan)
E-Mail naoshi@med.kindai.ac.jp

Oxidative Stress and Human Hepatocarcinogenesis

Several environmental factors, which are reportedly the risk of developing HCC, trigger the induction of oxidant-generating enzymes and increase the concentration of free radicals, leading to the activation of immune responses [4, 5]. Free radicals include reactive oxygen species (ROS) such as alkoxy radicals and nitrogen species; among these, ROS could be produced endogenously and exogenously.

8-Oxo-7,8-dihydroguanine (8-oxodG) has been regarded as the most reliable marker of DNA damage induced by ROS [4]. Compared to healthy individuals, a high level of 8-oxodG was reported in several types of cancer [4], suggesting a close link between oxidative stress and the emergence of cancer. Furthermore, patients with chronic hepatitis showed an increase of 8-oxodG levels in hepatocytes, with an increased risk of HCC [6]. Nonalcoholic steatohepatitis, which is usually accompanied by diabetes mellitus and obesity, is another important example of chronic liver injury and the development of HCC though the increased production of endogenous ROS and 8-oxodG in hepatocytes [7, 8]. These findings indicate that oxidative stress and induction of ROS production plays an important role in human hepatocarcinogenesis.

The carcinogenic potential of oxidative stress can be attributable to the genotoxic effects of ROS, which are capable of causing base modifications and genetic instability. The formation of 8-oxodG is known to induce DNA base mutations such as G>T/C>A transversions. Under normal conditions, the enzymes involved in the base excision repair mechanism, including DNA glycosylase, 8-oxoguanine glycosylase and MutY glycosylase homologue, excise 8-oxodG that is paired with cytosine and adenine [4, 9]. However, an increase in oxidative stress could impair the repair mechanism, which could lead to the increase of mutations in oncogenes and tumor suppressor genes (TSGs) [9]. On the other hand, although G>T/C>A transversions are common base substitutions reported in HCC, a recently published whole genome analysis suggests that the mutational spectrum of this type of tumor is heterogeneous [10]. This suggests that another mechanism of modification of cancer-related genes, such as the inactivation of TSGs through epigenetic pathways, could be induced by 8-oxodG.

Induction of Oxidative Stress and Hepatitis Virus Infection

As mentioned above, an exposure to several environmental factors, including hepatitis B virus and hepatitis C virus (HCV) infection, alcohol, deposition of iron (hemochromatosis) and copper (Wilson's disease), obesity and type 2 diabetes (nonalcoholic fatty liver disease), is associated with chronic liver damage; these factors could induce oxidative stress in hepatocytes and cause the emergence of HCC. Here, we mainly focus on the oxidative stress induced by chronic viral hepatitis.

There is an established connection between chronic infection with the hepatitis virus and oxidative stress. Infection with hepatitis B virus has been reported to trigger several cellular pathways that lead to the generation of oxygen/nitrogen-reactive species. It could cause an increase of ROS and 8-oxodG production, and significant changes in intracellular levels of antioxidant enzymes and glutathione (GSH), with an impairment of the GSH redox cycle [11–13]. In a case of chronic hepatitis C, increased ROS production and the reduced expression and activity of the repair enzyme NEIL1 glycosylase was reported [14]. In patients with chronic hepatitis C and HCC, an increased level of 8-oxodG was positively associated with the degree of inflammation. Additionally, the cumulative disease-free survival after curative resection of HCC was shorter in HCC patients with a high percentage of 8-oxodG-positive hepatocytes [15]. Chronic HCV infection is also associated with the induction of endoplasmic reticulum (ER) stress [16–18]. The HCV-derived protein NS5A reportedly induces ER stress with the subsequent release of Ca^{2+} from the ER, which leads to a mitochondrial Ca^{2+} uptake and the generation of ROS in mitochondria [19]. An examination of HCV core transgenic mice revealed an accumulation of ROS that was associated with the emergence of HCC [20]. Another report found that the interaction of the HCV core protein with mitochondria, accompanied by ROS production and reduced GSH activity, was observed in HCV transgenic mice [21]. A transient expression of NS5A resulted in an alteration of intracellular Ca^{2+} levels, leading to oxidative stress and activation of the STAT3 and NF-κB signaling pathways [22].

Iron deposition also induces oxidative stress through the Fenton reaction [23]. Excess amounts of iron deposits are frequently observed in the liver of individuals with a chronic hepatitis C infection, and an iron overload induces mitochondrial injury and increases the risk of developing HCC [24]. The removal of excess iron by phle-

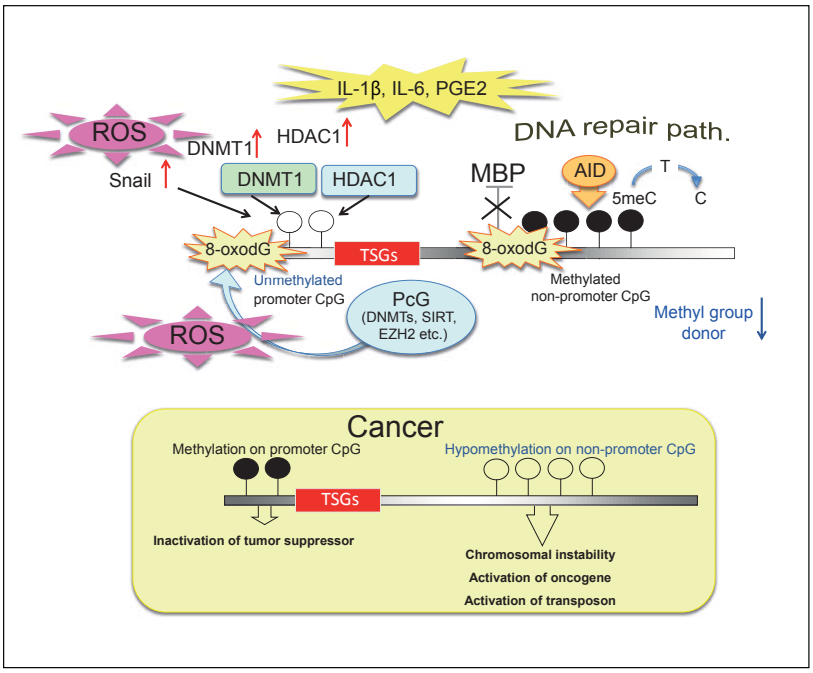

Fig. 1. A schematic representation of the mechanism of alteration of the methylation status under conditions of oxidative stress and inflammation (upper panel), and the alteration of the methylation status in cancer cells (lower panel). ROS induce the expression of the transcription factor Snail, which leads to the expression and recruitment of DNMTs and HDACs to the TSG promoters. The induction of ROS production also leads to the recruitment of the polycomb complex to the damaged chromatin. Inflammatory cytokines induce the transcription of DNMTs and HDACs. These events contribute to the emergence of an abnormal methylation of the TSG promoters. On the other hand, DNA repair pathways and AID activities affect 5-methyl cytosine and yield thymine. The thymine is replaced by an unmethylated cytosine through the base excision repair processes. 8-OxodG weakens the binding of MBP to DNA, leading to a global hypomethylation. The closed and open circles represent methylated and unmethylated CpGs, respectively.

botomy attenuates hepatocyte injury in patients with HCV infection [25], and reduces the rate of HCC emergence [26]. Alcohol intake and steatosis also contribute to the development of oxidative stress in hepatocytes and increase the risk of HCC, especially in patients with chronic hepatitis C. Acetaldehyde, the main metabolite of ethanol, elicits overproduction of ROS through acetaldehyde metabolism in mitochondria, which induces the apoptosis of hepatocytes and increases ROS formation in hepatic stellate cells [27]. In hepatic steatosis, the increase in β-oxidation in hepatocytes enhances electron delivery to the electron acceptors in the respiratory chain in mitochondria, which results in the generation of ROS due to the imbalance between a high input and a restricted outflow of electrons [18].

Induction of Epigenetic Instability by Oxidative Stress

DNA methylation usually takes place at the cytosine residues of the CpG dinucleotide. In normal cells, CpG islands in the promoters of transcriptionally active genes, such as TSGs, remain unmethylated, whereas CpG islands in nonpromoter regions (such as repetitive sequences) show dense methylation. Strikingly, global DNA hypomethylation and regional hypermethylation in TSG promoters are hallmarks of certain common cancer types, including HCC. It is also known that specific histone modifications, acetylation of histone H3 and H4, and trimethylation of lysine 4 of histone H3, are characteristics of active gene transcription. In contrast, dimethylation and trimethylation of H3 lysine 9 and trimethylation of H3 lysine 27 are associated with gene repression. Dimethylation of H3 lysine 9 is reportedly associated with DNA methylation in gene promoters [28]. Oxidative stress could induce an alteration in the methylation status of DNA, mainly by affecting the function and activity of the enzymes responsible for maintaining the epigenetic status, such as DNA methyltransferases (DNMTs), histone methylase and histone deacetylase (HDAC).

Oxidative Stress and Regional Hypermethylation in the Promoters of TSGs

Several reports suggest that oxidative stress affects the epigenetic machinery (fig. 1). It was reported that the induction of oxidative stress in the HCC cell line by hydrogen peroxide (H_2O_2) resulted in hypermethylation of the promoter of the *E-Cadherin* gene by increasing Snail expression [29]. Snail was shown to induce DNA methyla-

tion by recruiting HDAC1 and DNMT1. A correlation between ROS induction, E-Cadherin downregulation, Snail upregulation and *E-Cadherin* promoter methylation was also observed in human HCC samples [29]. Another study indicated that treatment of the human colorectal cancer cell line with H_2O_2 led to the upregulation of DNMT1 and HDCA, and increased the binding of DNMT1 to HDAC and DNMT1 binding to the promoter of a TSG such as the *Runt domain transcription factor 3 (RUNX3)*. This effect was abolished by treatment with the ROS scavenger N-acetylcysteine, suggesting that ROS silenced *RUNX3* expression by an epigenetic mechanism and may be associated with the progression of colorectal cancer [30]. Furthermore, O'Hagan et al. [31] reported that oxidative stress results in the recruitment of the polycomb repressive complex to damaged chromatin. They showed that a colon cancer cell line treated with H_2O_2 showed the delocalization of the polycomb complex, which includes DNMT1, histone deacetylase (sirtuin-1), and histone methyltransferase (an enhancer of zeste homolog 2) from a non-CpG-rich region to CpG island-containing promoters carrying 8-oxodG [31]. These findings suggested that the oxidative stress induced by H_2O_2 could recruit histone modulators to the promoter sequence of active genes carrying DNA oxidation, and lead to the inactivation of TSGs through an epigenetic mechanism.

Additionally, several reports have suggested that inflammatory cytokines could play a role in the alteration of the epigenetic status. The expression level of inflammation-related molecules correlated with increased levels of DNA methylation in the gastric mucosa in cases of *H. pylori*-related gastric cancer [32]. Similar changes were also observed in the colonic mucosa in a model of dextran sulfate sodium-induced colon cancer [33]. These findings strongly support the idea that inflammation could induce aberrant DNA hypermethylation [34]. Several studies have been conducted to clarify the inflammatory signal that leads to DNA methylation. Interleukin (IL)-1β treatment of the insulinoma cell line increased the activity of DNMTs and resulted in the methylation of endogenous genes [35]. IL-6 also enhanced the promoter activity of DNMTs and increased transcription of this gene. It also decreased the levels of the microRNA that targets DNMT1 [36, 37]. Treatment of cancer cell lines with prostaglandin E2 reportedly increased DNMT1 and DNMT3B expression and induced DNA methylation [38]. An in vitro model of IL-6-mediated chronic inflammation showed that IL-6 induced CpG methylation in the promoters of several TSGs and also induced a hypomethylation in interspersed nuclear element-1 (LINE-1) sequences in an oral squamous cell carcinoma line [39]. IL-6 has been reported to control DNA methylation through the IL-6-mediated janus kinase (JAK)/transducers and activator of transcription (STAT) 3 pathway [40, 41]. Therefore, inflammation could induce the epigenetic silencing and abnormal methylation in the promoters of TSGs through inflammation-mediated signaling pathways, which might play a role in carcinogenesis.

Oxidative Stress and Global DNA Hypomethylation

Global DNA hypomethylation has been identified as a common feature of various cancers, including HCC. Decrease of DNA methylation level in cancer cells generally takes place in repetitive DNA elements and is also observed in the gene body after the first exon. The demethylation of DNA in these regions may contribute to carcinogenesis through the following mechanisms. Firstly, demethylation of repetitive elements or satellite DNA might cause chromosomal instability [42, 43]. Secondly, hypomethylation at retroviral mobile repetitive elements could induce the transcriptional activation of transposition [44]. Thirdly, demethylation could activate oncogenes, which might play a role in carcinogenesis [45, 46].

Recently, activation-induced cytidine deaminase (AID) was shown to be involved in the active DNA demethylation that occurs during fetal development [47]. AID deaminates 5-methyl cytosine to yield thymine, and this thymine is subsequently removed and replaced by an unmethylated cytosine through the base excision repair processes, resulting in DNA demethylation. Moreover, AID reportedly targets the chromatin marked by the trimethylation of lysine 4 of histone 3 [48]. Another report also suggested that the activation of the DNA repair pathway also induces DNA demethylation, which might lead to a global DNA hypomethylation [49].

On the other hand, cancer is usually characterized by a hypoxic state because of the lack of blood supply caused by the rapid progression of tumor growth and the resulting structural changes [50, 51]. It was found that hypoxia induced oxidative stress, with an increased production of ROS. Hypoxia-inducible factor-1α (HIF-1α) was frequently induced in cancer cells and the generation of ROS was positively correlated with the upregulation of HIF-1α, VEGF and DNA oxidation [52]. Furthermore, HIF-1α has recently been shown to regulate epigenetic modulators such as lysine demethylases. HIF-1α functionally associates with HDACs to regulate gene expression in response to hypoxia [53–55].

Oxidative stress has been shown to inhibit the binding of methyl-CpG binding protein (MBP) 2, a critical epigenetic regulator that recruits DNMTs and histone HDAC to DNA [56, 57]. The formation of 8-oxodG was reportedly associated with the hypomethylation of the CpG site. In normal conditions, the N7 position of guanine acts as a hydrogen bond acceptor during the formation of the MBP-DNA complex. The oxidation converts guanine to 8-oxodG, which transforms the guanine at the N7 position from a hydrogen bond acceptor to a hydrogen donor. The replacement of guanine by 8-oxodG diminishes MBP binding when 8-oxodG is adjacent to the 5-methyl-cytosine [56, 58, 59]. Furthermore, the oxidation product of 5-methyl-cytosine, hydroxymethyl cytosine, also decreases the binding affinity of MBPs, resulting in DNA hypomethylation [60]. Mice containing mutations in the superoxide dismutase 1 gene showed an increase in 8-oxodG levels in the liver, with the progression of global DNA hypomethylation [61]. The presence of 8-oxodG in CpG strongly inhibits the methylation of the adjacent cytosine. Therefore, it could be possible that the DNA adduct-mediated inhibition of DNA methylation results in a progressive global demethylation.

The increased demand for methyl groups, a decrease in the availability of methyl group donors such as S-adenosylmethionine (SAM), and an increase in the levels of the methylation inhibitor S-adenosylhomocysteine (SAH) could also contribute to the global hypomethylation that is implicated in HCC development. An increase in inflammation in the liver tissue with reduced SAH hydrolase (SAHH) activity, and increased liver SAH, which could also cause global DNA hypomethylation [62], was observed in a mouse model of Wilson's disease. In this model, the methylation level was increased by copper chelation or by treatment with a methyl group donor. This suggested that Wilson's disease is a condition associated with an increased demand for methyl groups due to an increase in the levels of the methylation inhibitor SAH, which is attributable to an inhibitory effect of copper on SAHH [62]. The association between oxidative stress and hypomethylation of LINE-1 sequences was reported in bladder cancer patients [63]. Under the oxidative stress, the resynthesis of GSH was increased in response to GSH depletion. As SAM is required in the production of homocysteine that is used in the synthesis of GSH, increased production of GSH leads to the decrease of SAM necessary for maintaining the DNA methylation and the emergence of global DNA hypomethylation [64].

Conclusions

In this review, we have summarized the links between oxidative stress and epigenetic alterations in human hepatocarcinogenesis. Although the precise underpinnings of these processes are still unclear, it is very likely that oxidative stress is an underlying cause of the epigenetic instability that contributes to the initiation and progression of HCC. Understanding these molecular events is attractive from a therapeutic standpoint because several agents that could modulate the epigenetic status are going to be available in the coming years. Therefore, knowledge of these events will help in the prevention and management of HCC.

Acknowledgements

This work was supported in part by Grant-in-Aid for Scientific Research (KAKENHI: 24590997) from the Japanese Society for the Promotion of Science (N. Nishida) and a grant from the Smoking Research Foundation (N. Nishida).

Disclosure Statement

The authors have no conflicts of interest to declare.

References

1 Nishida N, Goel A: Genetic and epigenetic signatures in human hepatocellular carcinoma: a systematic review. Curr Genomics 2011; 12:130–137.

2 Stauffer JK, Scarzello AJ, Jiang Q, Wiltrout RH: Chronic inflammation, immune escape, and oncogenesis in the liver: a unique neighborhood for novel intersections. Hepatology 2012;56:1567–1574.

3 Kim DY, Han K: Epidemiology and surveillance of hepatocellular carcinoma. Liver Cancer 2012;1:2–14.

4 Ziech D, Franco R, Pappa A, Panayiotidis MI: Reactive oxygen species (ROS)-induced genetic and epigenetic alterations in human carcinogenesis. Mutat Res 2011;711:167–173.

5 Murata M, Thanan R, Ma N, Kawanishi S: Role of nitrative and oxidative DNA damage in inflammation-related carcinogenesis. J Biomed Biotechnol 2012;2012:623019.

6 Kitada T, Seki S, Iwai S, Yamada T, Sakaguchi H, Wakasa K: In situ detection of oxidative DNA damage, 8-hydroxydeoxyguanosine, in chronic human liver disease. J Hepatol 2001; 35:613–618.

7 Seki S, Kitada T, Yamada T, Sakaguchi H, Nakatani K, Wakasa K: In situ detection of lipid peroxidation and oxidative DNA damage in non-alcoholic fatty liver diseases. J Hepatol 2002;37:56–62.

8 Tanaka S, Miyanishi K, Kobune M, Kawano Y, Hoki T, Kubo T, Hayashi T, Sato T, Sato Y, Takimoto R, Kato J: Increased hepatic oxidative DNA damage in patients with nonalcoholic steatohepatitis who develop hepatocellular carcinoma. J Gastroenterol 2013, E-pub ahead of print.

9 Beard WA, Batra VK, Wilson SH: DNA polymerase structure-based insight on the mutagenic properties of 8-oxoguanine. Mutat Res 2010;703:18–23.

10 Totoki Y, Tatsuno K, Yamamoto S, Arai Y, Hosoda F, Ishikawa S, Tsutsumi S, Sonoda K, Totsuka H, Shirakihara T, Sakamoto H, Wang L, Ojima H, Shimada K, Kosuge T, Okusaka T, Kato K, Kusuda J, Yoshida T, Aburatani H, Shibata T: High-resolution characterization of a hepatocellular carcinoma genome. Nat Genet 2011;43:464–469.

11 Hagen TM, Huang S, Curnutte J, Fowler P, Martinez V, Wehr CM, Ames BN, Chisari FV: Extensive oxidative DNA damage in hepatocytes of transgenic mice with chronic active hepatitis destined to develop hepatocellular carcinoma. Proc Natl Acad Sci USA 1994;91:12808–12812.

12 Wang JH, Yun C, Kim S, Lee JH, Yoon G, Lee MO, Cho H: Reactive oxygen species modulates the intracellular level of HBx viral oncoprotein. Biochem Biophys Res Commun 2003;310:32–39.

13 Georgakilas AG, Mosley WG, Georgakila S, Ziech D, Panayiotidis MI: Viral-induced human carcinogenesis: an oxidative stress perspective. Mol Biosyst 2010;6:1162–1172.

14 Pal S, Polyak SJ, Bano N, Qiu WC, Carithers RL, Shuhart M, Gretch DR, Das A: Hepatitis C virus induces oxidative stress, DNA damage and modulates the DNA repair enzyme NEIL1. J Gastroenterol Hepatol 2010;25:627–634.

15 Maki A, Kono H, Gupta M, Asakawa M, Suzuki T, Matsuda M, Fujii H, Rusyn I: Predictive power of biomarkers of oxidative stress and inflammation in patients with hepatitis C virus-associated hepatocellular carcinoma. Ann Surg Oncol 2007;14:1182–1190.

16 Pavio N, Romano PR, Graczyk TM, Feinstone SM, Taylor DR: Protein synthesis and endoplasmic reticulum stress can be modulated by the hepatitis C virus envelope protein E2 through the eukaryotic initiation factor 2α kinase perk. J Virol 2003;77:3578–3585.

17 Tardif KD, Waris G, Siddiqui A: Hepatitis C virus, ER stress, and oxidative stress. Trends Microbiol 2005;13:159–163.

18 Sasaki Y: Does oxidative stress participate in the development of hepatocellular carcinoma? J Gastroenterol 2006;41:1135–1148.

19 Ma Y, Hendershot LM: The mammalian endoplasmic reticulum as a sensor for cellular stress. Cell Stress Chaperones 2002;7:222–229.

20 Moriya K, Fujie H, Shintani Y, Yotsuyanagi H, Tsutsumi T, Ishibashi K, Matsuura Y, Kimura S, Miyamura T, Koike K: The core protein of hepatitis C virus induces hepatocellular carcinoma in transgenic mice. Nat Med 1998;4:1065–1067.

21 Korenaga M, Wang T, Li Y, Showalter LA, Chan T, Sun J, Weinman SA: Hepatitis C virus core protein inhibits mitochondrial electron transport and increases reactive oxygen species (ROS) production. J Biol Chem 2005;280:37481–37488.

22 Gong G, Waris G, Tanveer R, Siddiqui A: Human hepatitis C virus NS5A protein alters intracellular calcium levels, induces oxidative stress, and activates STAT-3 and NF-κB. Proc Natl Acad Sci USA 2001;98:9599–9604.

23 Lloyd DR, Phillips DH: Oxidative DNA damage mediated by copper(II), iron(II) and nickel(II) fenton reactions: evidence for site-specific mechanisms in the formation of double-strand breaks, 8-hydroxydeoxyguanosine and putative intrastrand cross-links. Mutat Res 1999;424:23–36.

24 Furutani T, Hino K, Okuda M, Gondo T, Nishina S, Kitase A, Korenaga M, Xiao SY, Weinman SA, Lemon SM, Sakaida I, Okita K: Hepatic iron overload induces hepatocellular carcinoma in transgenic mice expressing the hepatitis C virus polyprotein. Gastroenterology 2006;130:2087–2098.

25 Yano M, Hayashi H, Yoshioka K, Kohgo Y, Saito H, Niitsu Y, Kato J, Iino S, Yotsuyanagi H, Kobayashi Y, Kawamura K, Kakumu S, Kaito M, Ikoma J, Wakusawa S, Okanoue T, Sumida Y, Kimura F, Kajiwara E, Sata M, Ogata K: A significant reduction in serum alanine aminotransferase levels after 3-month iron reduction therapy for chronic hepatitis C: a multicenter, prospective, randomized, controlled trial in Japan. J Gastroenterol 2004;39:570–574.

26 Kato J, Kobune M, Nakamura T, Kuroiwa G, Takada K, Takimoto R, Sato Y, Fujikawa K, Takahashi M, Takayama T, Ikeda T, Niitsu Y: Normalization of elevated hepatic 8-hydroxy-2′-deoxyguanosine levels in chronic hepatitis C patients by phlebotomy and low iron diet. Cancer Res 2001;61:8697–8702.

27 Novitskiy G, Traore K, Wang L, Trush MA, Mezey E: Effects of ethanol and acetaldehyde on reactive oxygen species production in rat hepatic stellate cells. Alcohol Clin Exp Res 2006;30:1429–1435.

28 You JS, Jones PA: Cancer genetics and epigenetics: two sides of the same coin? Cancer Cell 2012;22:9–20.

29 Lim SO, Gu JM, Kim MS, Kim HS, Park YN, Park CK, Cho JW, Park YM, Jung G: Epigenetic changes induced by reactive oxygen species in hepatocellular carcinoma: methylation of the E-cadherin promoter. Gastroenterology 2008;135:2128–2140.

30 Kang KA, Zhang R, Kim GY, Bae SC, Hyun JW: Epigenetic changes induced by oxidative stress in colorectal cancer cells: methylation of tumor suppressor RUNX3. Tumour Biol 2012;33:403–412.

31 O'Hagan HM, Wang W, Sen S, Destefano Shields C, Lee SS, Zhang YW, Clements EG, Cai Y, Van Neste L, Easwaran H, Casero RA, Sears CL, Baylin SB: Oxidative damage targets complexes containing DNA methyltransferases, SIRT1, and polycomb members to promoter CpG islands. Cancer Cell 2011;20:606–619.

32 Maekita T, Nakazawa K, Mihara M, Nakajima T, Yanaoka K, Iguchi M, Arii K, Kaneda A, Tsukamoto T, Tatematsu M, Tamura G, Saito D, Sugimura T, Ichinose M, Ushijima T: High levels of aberrant DNA methylation in *Helicobacter pylori*-infected gastric mucosae and its possible association with gastric cancer risk. Clin Cancer Res 2006;12:989–995.

33 Rosenberg DW, Giardina C, Tanaka T: Mouse models for the study of colon carcinogenesis. Carcinogenesis 2009;30:183–196.

34 Chiba T, Marusawa H, Ushijima T: Inflammation-associated cancer development in digestive organs: mechanisms and roles for genetic and epigenetic modulation. Gastroenterology 2012;143:550–563.

35 Hmadcha A, Bedoya FJ, Sobrino F, Pintado E: Methylation-dependent gene silencing induced by interleukin 1β via nitric oxide production. J Exp Med 1999;190:1595–1604.

36 Hodge DR, Xiao W, Clausen PA, Heidecker G, Szyf M, Farrar WL: Interleukin-6 regulation of the human DNA methyltransferase (HDNMT) gene in human erythroleukemia cells. J Biol Chem 2001;276:39508–39511.

37 Braconi C, Huang N, Patel T: Microrna-dependent regulation of DNA methyltransferase-1 and tumor suppressor gene expression by interleukin-6 in human malignant cholangiocytes. Hepatology 2010;51:881–890.

38 Xia D, Wang D, Kim SH, Katoh H, DuBois RN: Prostaglandin E2 promotes intestinal tumor growth via DNA methylation. Nature Med 2012;18:224–226.

39 Gasche JA, Hoffmann J, Boland CR, Goel A: Interleukin-6 promotes tumorigenesis by altering DNA methylation in oral cancer cells. Int J Cancer 2011;129:1053–1063.

40 To KF, Chan MW, Leung WK, Ng EK, Yu J, Bai AH, Lo AW, Chu SH, Tong JH, Lo KW, Sung JJ, Chan FK: Constitutional activation of IL-6-mediated JAK/STAT pathway through hypermethylation of SOCS-1 in human gastric cancer cell line. Br J Cancer 2004;91:1335–1341.

41 Isomoto H, Mott JL, Kobayashi S, Werneburg NW, Bronk SF, Haan S, Gores GJ: Sustained IL-6/STAT-3 signaling in cholangiocarcinoma cells due to SOCS-3 epigenetic silencing. Gastroenterology 2007;132:384–396.

42 Wong NC, Wong LH, Quach JM, Canham P, Craig JM, Song JZ, Clark SJ, Choo KH: Permissive transcriptional activity at the centromere through pockets of DNA hypomethylation. PLoS Genet 2006;2:e17.

43 Vera E, Canela A, Fraga MF, Esteller M, Blasco MA: Epigenetic regulation of telomeres in human cancer. Oncogene 2008;27:6817–6833.
44 Howard G, Eiges R, Gaudet F, Jaenisch R, Eden A: Activation and transposition of endogenous retroviral elements in hypomethylation induced tumors in mice. Oncogene 2008;27:404–408.
45 Wainfan E, Poirier LA: Methyl groups in carcinogenesis: effects on DNA methylation and gene expression. Cancer Res 1992;52:2071s–2077s.
46 Stefanska B, Huang J, Bhattacharyya B, Suderman M, Hallett M, Han ZG, Szyf M: Definition of the landscape of promoter DNA hypomethylation in liver cancer. Cancer Res 2011;71:5891–5903.
47 Cortellino S, Xu J, Sannai M, Moore R, Caretti E, Cigliano A, Le Coz M, Devarajan K, Wessels A, Soprano D, Abramowitz LK, Bartolomei MS, Rambow F, Bassi MR, Bruno T, Fanciulli M, Renner C, Klein-Szanto AJ, Matsumoto Y, Kobi D, Davidson I, Alberti C, Larue L, Bellacosa A: Thymine DNA glycosylase is essential for active DNA demethylation by linked deamination-base excision repair. Cell 2011;146:67–79.
48 Kato L, Begum NA, Burroughs AM, Doi T, Kawai J, Daub CO, Kawaguchi T, Matsuda F, Hayashizaki Y, Honjo T: Nonimmunoglobulin target loci of activation-induced cytidine deaminase (AID) share unique features with immunoglobulin genes. Proc Natl Acad Sci USA 2012;109:2479–2484.
49 Ma DK, Guo JU, Ming GL, Song H: DNA excision repair proteins and Gadd45 as molecular players for active DNA demethylation. Cell Cycle 2009;8:1526–1531.
50 Goudar RK, Vlahovic G: Hypoxia, angiogenesis, and lung cancer. Curr Oncol Rep 2008;10:277–282.
51 Lawless MW, O'Byrne KJ, Gray SG: Oxidative stress induced lung cancer and COPD: opportunities for epigenetic therapy. J Cell Mol Med 2009;13:2800–2821.
52 Pialoux V, Mounier R, Brown AD, Steinback CD, Rawling JM, Poulin MJ: Relationship between oxidative stress and HIF-1α mRNA during sustained hypoxia in humans. Free Radic Biol Med 2009;46:321–326.
53 Carrero P, Okamoto K, Coumailleau P, O'Brien S, Tanaka H, Poellinger L: Redox-regulated recruitment of the transcriptional coactivators CREB-binding protein and SRC-1 to hypoxia-inducible factor 1α. Mol Cell Biol 2000;20:402–415.
54 Ruas JL, Poellinger L, Pereira T: Functional analysis of hypoxia-inducible factor-1α-mediated transactivation: identification of amino acid residues critical for transcriptional activation and/or interaction with CREB-binding protein. J Biol Chem 2002;277:38723–38730.
55 Xenaki G, Ontikatze T, Rajendran R, Stratford IJ, Dive C, Krstic-Demonacos M, Demonacos C: PCAF is an HIF-1α cofactor that regulates p53 transcriptional activity in hypoxia. Oncogene 2008;27:5785–5796.
56 Valinluck V, Tsai HH, Rogstad DK, Burdzy A, Bird A, Sowers LC: Oxidative damage to methyl-CpG sequences inhibits the binding of the methyl-CpG binding domain (MBD) of methyl-CpG binding protein 2 (MeCP2). Nucleic Acids Res 2004;32:4100–4108.
57 Cortessis VK, Thomas DC, Levine AJ, Breton CV, Mack TM, Siegmund KD, Haile RW, Laird PW: Environmental epigenetics: prospects for studying epigenetic mediation of exposure-response relationships. Human Genet 2012;131:1565–1589.
58 Weitzman SA, Turk PW, Milkowski DH, Kozlowski K: Free radical adducts induce alterations in DNA cytosine methylation. Proc Natl Acad Sci USA 1994;91:1261–1264.
59 Turk PW, Laayoun A, Smith SS, Weitzman SA: DNA adduct 8-hydroxyl-2′-deoxyguanosine (8-hydroxyguanine) affects function of human DNA methyltransferase. Carcinogenesis 1995;16:1253–1255.
60 Donkena KV, Young CY, Tindall DJ: Oxidative stress and DNA methylation in prostate cancer. Obstet Gynecol Int 2010;2010:302051.
61 Bhusari SS, Dobosy JR, Fu V, Almassi N, Oberley T, Jarrard DF: Superoxide dismutase 1 knockdown induces oxidative stress and DNA methylation loss in the prostate. Epigenetics 2010;5:402–409.
62 Medici V, Shibata NM, Kharbanda KK, LaSalle JM, Woods R, Liu S, Engelberg JA, Devaraj S, Torok NJ, Jiang JX, Havel PJ, Lonnerdal B, Kim K, Halsted CH: Wilson's disease: changes in methionine metabolism and inflammation affect global DNA methylation in early liver disease. Hepatology 2013;57:555–565.
63 Patchsung M, Boonla C, Amnattrakul P, Dissayabutra T, Mutirangura A, Tosukhowong P: Long interspersed nuclear element-1 hypomethylation and oxidative stress: correlation and bladder cancer diagnostic potential. PLoS One 2012;7:e37009.
64 Hitchler MJ, Domann FE: An epigenetic perspective on the free radical theory of development. Free Radic Biol Med 2007;43:1023–1036.

Digestive Diseases

Dig Dis 2013;31:454–458
DOI: 10.1159/000355244

Novel Mouse Models of Hepatocarcinogenesis with Stepwise Accumulation of Genetic Alterations

Soo Ki Kim[a] Hiroyuki Marusawa[a] Yuji Eso[a] Tsutomu Chiba[a]
Masatoshi Kudo[b]

[a]Department of Gastroenterology and Hepatology, Graduate School of Medicine, Kyoto University, Kyoto, and
[b]Department of Gastroenterology and Hepatology, Kinki University School of Medicine, Osakasayama, Japan

Key Words
Hepatocellular carcinoma · Activation-induced cytidine deaminase · Chronic inflammation · Hepatocarcinogenesis

Abstract
Hepatocellular carcinoma (HCC) is one of the most common cancers worldwide. Various risk factors are involved in hepatocarcinogenesis. Among them, chronic inflammation, including chronic hepatitis and cirrhosis mainly caused by hepatitis B virus and/or hepatitis C virus infection, plays an important role in HCC development. On the other hand, comprehensive genetic analyses of HCC using whole genome and exome sequencing revealed that cancer cells possess a large number of somatic mutations, suggesting that a wide variety of genetic alterations and the resultant dysregulated molecular pathways contribute to the development of HCC. Activation-induced cytidine deaminase (AID) is a nucleotide-editing enzyme, and aberrant expression of AID induced by inflammatory responses contributes to hepatocarcinogenesis via the accumulation of genetic alterations in various tumor-related genes. Constitutive expression of AID in hepatocyte-lineage cells provides novel mouse models that recapitulate the tumorigenesis of human HCC through stepwise accumulation of genetic alterations.

Introduction

Hepatocellular carcinoma (HCC) is the fifth most common cancer in men, the seventh most common cancer in women and the third most common cause of cancer-related death worldwide [1]. The risk factors for HCC vary by region and race, but hepatitis B virus (HBV) infection, hepatitis C virus (HCV) infection, alcoholic liver disease and nonalcoholic fatty liver disease/nonalcoholic steatohepatitis are considered to be major causes worldwide [2, 3]. Most of these risk factors are closely related with inflammation-associated chronic liver damage and thus the majority of HCCs develop under the background of chronic hepatitis or cirrhosis. Here we review the mechanisms underlying the contribution of chronic inflammation to the development of HCC.

Chronic Inflammation and HCC

HCV infection is a major risk factor for human HCC. The prevalence of HCV infection is 80–90% in patients with HCC in Japan, 30–50% in the USA and 44–66% in Italy [4]. The estimated risk for HCC is 15–20 times higher in HCV-infected patients compared with those who are negative for HCV infection. Epidemiologic

KARGER

E-Mail karger@karger.com
www.karger.com/ddi

0257–2753/13/0316–0454$38.00/0

Hiroyuki Marusawa, MD, PhD
Department of Gastroenterology and Hepatology
Graduate School of Medicine, Kyoto University
54 Kawaharacho, Shogoin, Sakyo-ku, Kyoto 606-8507 (Japan)
E-Mail maru@kuhp.kyoto-u.ac.jp

studies have clearly revealed that most human HCCs arise in the setting of chronic hepatic inflammation associated with liver cirrhosis or chronic hepatitis caused by HCV infection [5, 6], and the estimated annual rate of HCC development in those with chronic hepatitis and liver cirrhosis is 0.5–1.0% and 5–8%, respectively. We previously revealed that HCC developed in 237 out of 846 patients (28.0%) with chronic HCV infection with a mean follow-up of 4.66 years [7]. The cumulative incidence rate of HCC among those patients was 18.1% at 5 years and 45.6% at 10 years. Based on the classification of chronic liver disease at study entry, 94 out of 576 patients with hepatitis (16.3%) and 143 out of 270 patients with cirrhosis (53.0%) developed HCC over a 10-year period. In addition, the incidence rate of HCC in interferon-treated patients with chronic HCV infection was 15.6% (35/224) over 10 years, much lower than that of HCV-infected patients without interferon therapy. These findings indicate that chronic inflammation in the liver is closely related with HCC development, and suppression of HCV-related chronic inflammation by interferon therapy successfully contributes to reduce the incidence of HCC.

The number of people with HBV-chronic hepatitis is approximately 300 million worldwide and HBV is the most frequent cause of HCC worldwide, accounting for more than 50% of HCC cases and 70–80% of HCC cases in highly HBV endemic regions [1, 4]. Although HBV infection sometimes causes HCC in the liver in the absence of hepatic inflammation, most HBV-related HCCs are found in patients with chronic hepatitis and cirrhosis. Previous meta-analyses revealed that HBsAg-positive individuals have an approximately 15- to 20-fold greater risk for HCC than HBsAg-negative individuals, similar to those with chronic HCV infection. Furthermore, patients with chronic HBV infection under the condition of cirrhosis have a greater risk of developing HCC. Indeed, the annual incidence rate of HCC in HBV-infected patients with and without cirrhosis is 2.0–6.6% and 0–4%, respectively [8]. In addition, another study reported that the incidence rate of HCC development in individuals with HBV-related cirrhosis was 820–2,247 (per 100,000 person years), whereas in those without cirrhosis the incidence rate was much lower, at 280–474 [9].

Taken together, these findings indicate that chronic inflammation caused by HCV or HBV infection plays an important role in the development of HCC. How chronic inflammation contributes to HCC development, however, has not been fully elucidated.

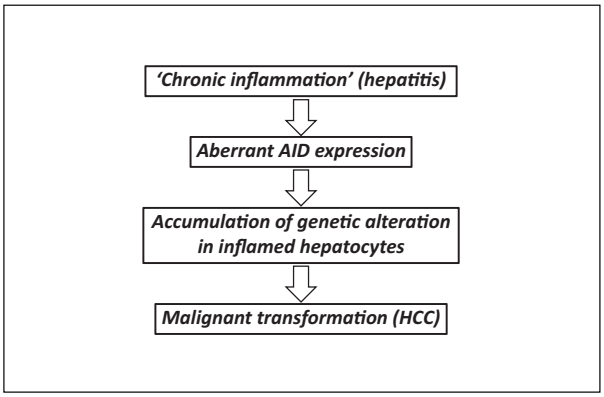

Fig. 1. Linkage between chronic inflammation and hepatocarcinogenesis.

Mechanism of Chronic Inflammation-Induced Genetic Aberrations in Hepatocytes

Cancer cells possess various genetic alterations, including somatic mutations, chromosomal rearrangements, copy number alterations and epigenetic changes [10, 11]. Recent dramatic advancements in genome-wide analysis methods and progress in technology have allowed for whole genome and exome sequencing of various types of cancers, which has unveiled the overall genetic landscape of human cancers, including HCC [12]. Several comprehensive genetic analyses of HCC with various etiologies, including HBV-HCC, HCV-HCC and alcohol-related HCC, have been performed [13–15]. Approximately tens of thousands of somatic mutations on average are detected by whole-genome sequencing in each HCC tissue, and generally ~100 mutations are detected throughout the whole exons per tumor. These findings indicate that normal liver cells acquire a large number of genetic alterations during the process of tumorigenesis and a wide variety of genetic alterations and resultant dysregulated molecular pathways might contribute to the development of HCC. When and how the accumulation of so many somatic mutations are generated under the background of inflamed liver tissues, however, remains unclear.

We recently found that a nucleotide-editing enzyme, activation-induced cytidine deaminase (AID), plays a critical role in chronic inflammation-associated hepatocarcinogenesis by inducing genetic alterations [6, 11]. AID possesses a nucleotide-editing capacity that induces DNA mutations in the human genome by deaminating

Dig Dis 2013;31:454–458
DOI: 10.1159/000355244

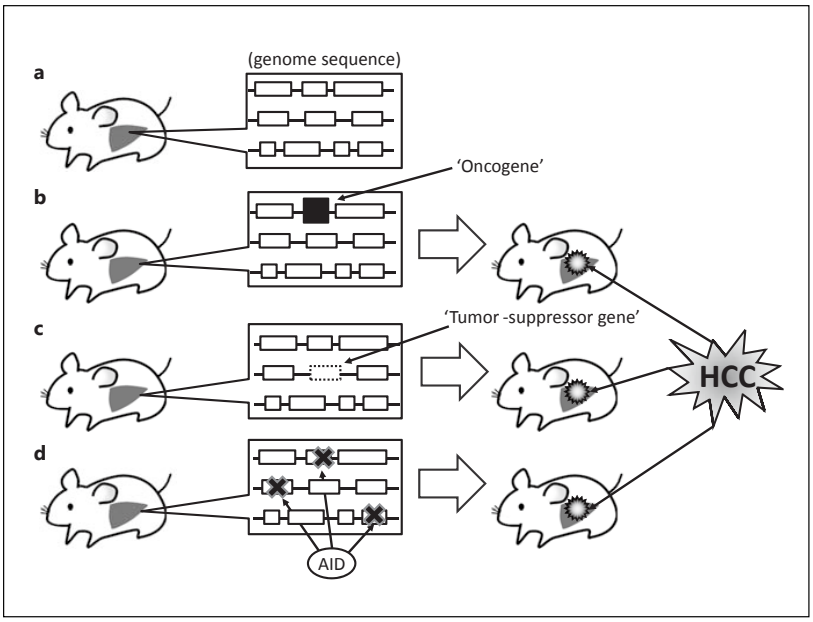

Fig. 2. Schema of genetically engineered HCC mice models. **a** Wild-type mouse. **b** Transgenic mouse model with overexpression of a specific oncogene. **c** Knockout mouse model with disruption of a specific tumor-suppressor gene. **d** AID-expression mouse model: stepwise accumulation of genetic alterations in oncogenes and/or tumor-suppressor genes are induced by mutagenic activity of AID, which leads to tumorigenesis.

cytidine. AID is expressed only in activated B cells under physiologic conditions and is essential for two important molecular mechanisms' immune diversity, somatic hypermutation and class switch recombination [16]. Aberrant AID expression is induced by the stimulation of proinflammatory cytokines such as tumor necrosis factor-α (TNF-α) or interleukin-1β in various epithelial cells through the nuclear factor-κB (NF-κB) pathway [17–19]. TNF-α is upregulated in the liver of patients with chronic viral hepatitis or cirrhosis due to HCV infection. We demonstrated that AID expression is induced in response to TNF-α stimulation. In addition, AID expression is also upregulated in cultured human hepatocytes expressing HCV core protein via activation of the NF-κB pathway [17]. Enhanced AID protein expression is widely detectable in both human HCC and the surrounding inflamed hepatocytes, whereas no AID expression is detected in normal liver tissues lacking an inflammatory response [20]. Importantly, aberrant expression of AID in hepatocytes leads to the accumulation of genetic alterations in tumor-related genes, such as TP53. These findings suggest that in adult hepatocytes, both the response to HCV infection itself and the resultant chronic inflammation trigger aberrant AID upregulation, and due to the mutagenic activity of AID, nucleotide alterations gradually accumulate in tumor-related genes in chronically inflamed liver tissues (fig. 1).

Novel Mouse Models with Stepwise Accumulation of Genetic Alterations Leading to Hepatocarcinogenesis

To gain a better understanding of human hepatocarcinogenesis, various animal models mimicking the process of human HCC development have been established [21]. Mouse models of HCC are divided into two types: chemical induced and genetically engineered. Chemical-induced models of HCC include mice exposed to diethylnitrosamine [22], aflatoxin B1 [23] and thioacetamide [24], but these models mainly reflect chemical-induced carcinogenesis, although chronic inflammation might be related to cancer development to some extent. Genetically engineered mouse models of HCC include c-myc/TGF-α transgenic mice [25], Trp53 knockout mice [26] and others. Certainly, HCC develops in these models via overexpression of the specific oncogene or disruption of the specific tumor-suppressor gene. These models, however, do not necessarily mimic the process of chronic inflammation-associated human hepatocarcinogenesis (fig. 2), because hepatocarcinogenesis might not result from an abnormality of only one or two specific tumor-related genes or pathways, but rather from stepwise accumulation of genetic alterations.

Several novel mouse models have been established by taking advantage of AID-mediated stepwise genotoxicity

(fig. 2). Okazaki et al. [27] and Morisawa et al. [28] generated AID transgenic (Tg) mice with constitutive and ubiquitous AID expression and found that AID Tg mice developed malignant T cell lymphomas as well as various epithelial tumors, including liver, lung and gastric cancers, indicating that normal epithelial cells with constitutive AID expression could transform into tumor cells via the accumulation of genetic alterations. Unfortunately, however, AID Tg mice tend to die young because of lethal malignant lymphomas, and thus detailed analyses of epithelial tumors, including HCC, in AID Tg mice are difficult. Therefore, to examine the effect of constitutive AID expression in mainly hepatic-lineage cells, we established two mouse models: (i) tissue nonspecific alkaline phosphatase (TNAP)-AID mice and (ii) a transplantation model of hepatic progenitor cells derived from AID Tg mice.

AID conditional Tg mice were established by insertion of the gene encoding GFP flanked by two loxP sites into the CAG promoter-driven AID transgene, which allows for AID expression only after Cre-mediated deletion of the GFP cDNA from the transgene [29]. On the other hand, TNAP is a member of the alkaline phosphatase family and is also a marker of embryonic stem cells and immature stem cells, especially in murine hepatocytes. TNAP-Cre mice were generated by inserting the coding sequence of Cre recombinase into the locus of the TNAP gene. To obtain double-transgenic mice in which AID is expressed only in cells that produce TNAP (TNAP-AID mice), we crossed AID conditional Tg mice with TNAP-Cre mice [30]. HCC developed spontaneously in 4 out of 15 (27%) TNAP-AID mice at approximately 90 weeks of age, whereas no tumors were detected in the littermate control mice [30]. Furthermore, a high accumulation of *Trp53* gene mutations was observed in both HCC tissues and noncancerous liver tissues in TNAP-AID mice. These findings suggest that the TNAP-AID mouse is a useful model of HCC that shares genetic and phenotypic features with human HCC.

Next, to investigate whether liver cancer originates from fetal hepatic progenitor cells with constitutive AID expression, we constructed a transplantation model of hepatic progenitor cells derived from AID Tg mice. We enriched hepatic progenitor cells from the E13.5 fetal liver of AID Tg mice and transplanted those cells, which have enhanced liver regeneration activity, into recipient mice. HCC developed in 7 out of 11 (63.6%) recipient mice receiving enriched hepatic progenitor cells from AID Tg mice, whereas no tumorigenesis was observed in recipient mice transplanted with hepatic progenitor cells from wild-type mice (control) [31]. Furthermore, whole exome sequencing of tumor cells allowed us to determine the landscape of the accumulated genetic alterations during tumorigenesis and clarified that several dozen genes acquired single nucleotide variants in tumor tissues originating from the transplanted hepatic progenitor cells of AID Tg mice. Pathway analysis using a KEGG database revealed that the acquired genetic aberrations affected several important signaling pathways, thereby disturbing normal homeostasis [31]. These results indicate that accumulation of genetic alterations in fetal hepatic progenitor cells could lead to HCC development.

Conclusion

Human hepatocarcinogenesis is closely related with chronic inflammation, and aberrant AID expression in the inflamed liver could play an important role in inflammation-associated HCC development by inducing accumulation of genetic alterations in various genes. Taking advantage of the mutagenic activity of AID, we established novel mouse models of hepatocarcinogenesis.

Many mechanisms underlying chronic inflammation-associated hepatocarcinogenesis, such as the contribution of epigenetic modulations to HCC formation, however, remain unsolved. In addition, the detailed relevance of chronic inflammation for the development of NASH-related HCC is unknown. Further genetic and molecular investigations are required to understand the actual state of chronic inflammation-related HCC.

Disclosure Statement

The authors have no conflicts of interest to declare.

References

1 El-Serag HB: Hepatocellular carcinoma. N Engl J Med 2011;365:1118–1127.
2 Kim SK, Marusawa H, Eso Y, Nishikawa H, Ueda Y, Kita R, Kimura T, Chiba T, Osaki Y, Kudo M: Clinical characteristics of non-B non-C hepatocellular carcinoma: a single-center retrospective study. Digestion 2011; 84(suppl 1):43–49.
3 Kim DY, Han KH: Epidemiology and surveillance of hepatocellular carcinoma. Liver Cancer 2012;1:2–14.
4 El-Serag HB: Epidemiology of viral hepatitis and hepatocellular carcinoma. Gastroenterology 2012;142:1264–1273.

5 Kiyosawa K, Umemura T, Ichijo T, Matsumoto A, Yoshizawa K, Gad A, Tanaka E: Hepatocellular carcinoma: recent trends in Japan. Gastroenterology 2004;127:S17–S26.

6 Shimizu T, Marusawa H, Endo Y, Chiba T: Inflammation-mediated genomic instability: roles of activation-induced cytidine deaminase in carcinogenesis. Cancer science 2012; 103:1201–1206.

7 Ikeda K, Marusawa H, Osaki Y, Nakamura T, Kitajima N, Yamashita Y, Kudo M, Sato T, Chiba T: Antibody to hepatitis B core antigen and risk for hepatitis C-related hepatocellular carcinoma: a prospective study. Ann Intern Med 2007;146:649–656.

8 Llovet JM, Burroughs A, Bruix J: Hepatocellular carcinoma. Lancet 2003;362:1907–1917.

9 Nguyen VT, Law MG, Dore GJ: Hepatitis B-related hepatocellular carcinoma: epidemiological characteristics and disease burden. J Viral Hepat 2009;16:453–463.

10 Vogelstein B, Kinzler KW: Cancer genes and the pathways they control. Nat Med 2004;10: 789–799.

11 Chiba T, Marusawa H, Ushijima T: Inflammation-associated cancer development in digestive organs: mechanisms and roles for genetic and epigenetic modulation. Gastroenterology 2012;143:550–563.

12 Meyerson M, Gabriel S, Getz G: Advances in understanding cancer genomes through second-generation sequencing. Nat Rev Genet 2010;11:685–696.

13 Fujimoto A, Totoki Y, Abe T, Boroevich KA, Hosoda F, Nguyen HH, Aoki M, Hosono N, Kubo M, Miya F, et al: Whole-genome sequencing of liver cancers identifies etiological influences on mutation patterns and recurrent mutations in chromatin regulators. Nat Genet 2012;44:760–764.

14 Guichard C, Amaddeo G, Imbeaud S, Ladeiro Y, Pelletier L, Maad IB, Calderaro J, Bioulac-Sage P, Letexier M, Degos F, et al: Integrated analysis of somatic mutations and focal copy-number changes identifies key genes and pathways in hepatocellular carcinoma. Nat Genet 2012;44:694–698.

15 Huang J, Deng Q, Wang Q, Li KY, Dai JH, Li N, Zhu ZD, Zhou B, Liu XY, Liu RF, et al: Exome sequencing of hepatitis B virus-associated hepatocellular carcinoma. Nat Genet 2012;44:1117–1121.

16 Muramatsu M, Kinoshita K, Fagarasan S, Yamada S, Shinkai Y, Honjo T: Class switch recombination and hypermutation require activation-induced cytidine deaminase (AID), a potential RNA editing enzyme. Cell 2000;102: 553–563.

17 Endo Y, Marusawa H, Kinoshita K, Morisawa T, Sakurai T, Okazaki IM, Watashi K, Shimotohno K, Honjo T, Chiba T: Expression of activation-induced cytidine deaminase in human hepatocytes via NF-κB signaling. Oncogene 2007;26:5587–5595.

18 Matsumoto Y, Marusawa H, Kinoshita K, Endo Y, Kou T, Morisawa T, Azuma T, Okazaki IM, Honjo T, Chiba T: *Helicobacter pylori* infection triggers aberrant expression of activation-induced cytidine deaminase in gastric epithelium. Nat Med 2007;13:470–476.

19 Nagata N, Akiyama J, Marusawa H, Shimbo T, Liu Y, Igari T, Nakashima R, Watanabe H, Uemura N, Chiba T: Enhanced expression of activation-induced cytidine deaminase in human gastric mucosa infected by *Helicobacter pylori* and its decrease following eradication. J Gastroenterol 2013, E-pub ahead of print.

20 Kou T, Marusawa H, Kinoshita K, Endo Y, Okazaki IM, Ueda Y, Kodama Y, Haga H, Ikai I, Chiba T: Expression of activation-induced cytidine deaminase in human hepatocytes during hepatocarcinogenesis. Int J Cancer 2007;120:469–476.

21 Aravalli RN, Steer CJ, Sahin MB, Cressman EN: Stem cell origins and animal models of hepatocellular carcinoma. Dig Dis Sci 2010; 55:1241–1250.

22 Vesselinovitch SD, Mihailovich N, Rao KV: Morphology and metastatic nature of induced hepatic nodular lesions in C57BL × C3H F1 mice. Cancer Res 1978;38:2003–2010.

23 McGlynn KA, Hunter K, LeVoyer T, Roush J, Wise P, Michielli RA, Shen FM, Evans AA, London WT, Buetow KH: Susceptibility to aflatoxin B1-related primary hepatocellular carcinoma in mice and humans. Cancer Res 2003;63:4594–4601.

24 Salguero Palacios R, Roderfeld M, Hemmann S, Rath T, Atanasova S, Tschuschner A, Gressner OA, Weiskirchen R, Graf J, Roeb E: Activation of hepatic stellate cells is associated with cytokine expression in thioacetamide-induced hepatic fibrosis in mice. Lab Invest 2008;88:1192–1203.

25 Calvisi DF, Thorgeirsson SS: Molecular mechanisms of hepatocarcinogenesis in transgenic mouse models of liver cancer. Toxicol Pathol 2005;33:181–184.

26 Katz SF, Lechel A, Obenauf AC, Begus-Nahrmann Y, Kraus JM, Hoffmann EM, Duda J, Eshraghi P, Hartmann D, Liss B, et al: Disruption of Trp53 in livers of mice induces formation of carcinomas with bilineal differentiation. Gastroenterology 2012;142:1229–1239.

27 Okazaki IM, Hiai H, Kakazu N, Yamada S, Muramatsu M, Kinoshita K, Honjo T: Constitutive expression of AID leads to tumorigenesis. J Exp Med 2003;197:1173–1181.

28 Morisawa T, Marusawa H, Ueda Y, Iwai A, Okazaki IM, Honjo T, Chiba T: Organ-specific profiles of genetic changes in cancers caused by activation-induced cytidine deaminase expression. Int J Cancer 2008;123:2735–2740.

29 Muto T, Okazaki IM, Yamada S, Tanaka Y, Kinoshita K, Muramatsu M, Nagaoka H, Honjo T: Negative regulation of activation-induced cytidine deaminase in B cells. Proc Natl Acad Sci USA 2006;103:2752–2757.

30 Takai A, Toyoshima T, Uemura M, Kitawaki Y, Marusawa H, Hiai H, Yamada S, Okazaki IM, Honjo T, Chiba T, et al: A novel mouse model of hepatocarcinogenesis triggered by AID causing deleterious p53 mutations. Oncogene 2009;28:469–478.

31 Kim SK, Nasu A, Komori J, Shimizu T, Matsumoto Y, Minaki Y, Kohno K, Shimizu K, Uemoto S, Chiba T, Marusawa H: A model of liver carcinogenesis originating from hepatic progenitor cells with accumulation of genetic alterations. Int J Cancer 2013, E-pub ahead of print.

Digestive Diseases

Dig Dis 2013;31:459–466
DOI: 10.1159/000355245

Reactive Oxygen Species Induce Epigenetic Instability through the Formation of 8-Hydroxydeoxyguanosine in Human Hepatocarcinogenesis

Naoshi Nishida[a, b] Tadaaki Arizumi[a] Masahiro Takita[a] Satoshi Kitai[a] Norihisa Yada[a] Satoru Hagiwara[a] Tatsuo Inoue[a] Yasunori Minami[a] Kazuomi Ueshima[a] Toshiharu Sakurai[a] Masatoshi Kudo[a]

[a]Department of Gastroenterology and Hepatology, Kinki University School of Medicine, Osakasayama, and
[b]Department of Gastroenterology and Hepatology, Kyoto University Graduate School of Medicine, Kyoto, Japan

Key Words
Chronic hepatitis C · Hepatocellular carcinoma · Tumor suppressor genes · Chromatin immunoprecipitation

Abstract
Chronic hepatitis C (CHC) triggers oxidative stress and contributes to the emergence of hepatocellular carcinoma (HCC). We previously reported that tumor suppressor gene (TSG) methylation is a critical factor during the early stages of hepatocarcinogenesis. In this study, we clarify the association between oxidative stress and epigenetic alterations during hepatocarcinogenesis. We examined DNA oxidation and methylation profiles in 128 liver biopsy samples from CHC patients. The DNA oxidation and methylated TSG numbers were quantified using immunohistochemical analysis of 8-hydroxydeoxyguanosine (8-OHdG) and quantitative PCR for 11 TSGs, respectively. The quantitative chromatin immunoprecipitation-PCR (ChIP-qPCR) assay in HepG2 and fetal liver Hc cells treated with H_2O_2 was used to quantify trimethyl-H3K4, acetylated-H4K16 (an active chromatin marker), trimethyl-H3K27 (a repressive chromatin marker) and 8-OHdG. We analyzed 30 promoters of 25 different TSGs by qPCR. The high levels of 8-OHdG was the only variable that was significantly associated with the increased number of methylated TSGs in CHC ($p < 0.0001$). The ChIP-qPCR revealed that after H_2O_2 treatment of the cell lines, the 8-OHdG-bound promoters showed a modification from an active chromatin (trimethyl-H3K4 and acetylated-H4K16 dominant) to a repressive chromatin (trimethyl-H3K27 dominant) status. We conclude that oxidative stress alters the chromatin status, which leads to abnormal methylation of TSGs, and contributes to hepatocarcinogenesis in CHC patients.

Introduction

It has been reported that chronic inflammation is a critical factor in the development of cancers such as hepatocellular carcinoma (HCC). Additionally, oxidative stress due to increased production of reactive oxygen species (ROS) plays a pivotal role in carcinogenesis by inducing DNA damage [1, 2]. These DNA alterations, which activate oncogenes and inactivate tumor suppressor

KARGER

E-Mail karger@karger.com
www.karger.com/ddi

0257–2753/13/0316–0459$38.00/0

Naoshi Nishida, MD, PhD
Department of Gastroenterology and Hepatology
Kinki University School of Medicine, 337-2 Ohno-higashi
Osakasayama, Osaka 589-8511 (Japan)
E-Mail naoshi@med.kindai.ac.jp

genes (TSGs), could contribute to the development of cancer in the oxidative stress-affected organs [3, 4].

A well-known marker of oxidative DNA damage induced by ROS is 8-hydroxydeoxyguanosine (8-OHdG). A high level of 8-OHdG could be considered as a risk factor in several types of cancer. For example, a higher accumulation of 8-OHdG has been reported in breast, renal and gastric tumor tissues, when compared to adjacent or normal tissues [5–7]. In addition, the cumulative incidence rate of HCC in patients with high 8-OHdG levels in the liver was significantly greater than that in patients with low 8-OHdG levels [8]. Generally, the genotoxic effect of ROS could increase the carcinogenic potential through the induction of base modifications. The formation of 8-OHdG is known to induce G>T/C>A transversions; unrepaired 8-OHdG causes transversion mutations due to its ability to pair with adenine as well as cytosine bases [9]. However, the recently published whole genome analysis suggests that the mutational spectrum of this type of tumor is heterogeneous [10]. Therefore, it is conceivable that an alternative mechanism for the modulation of cancer-related genes, such as the inactivation of TSGs through epigenetic pathways, might be induced by an increase in 8-OHdG levels.

Previously, we have reported that a number of TSGs, which were abnormally hypermethylated in chronic hepatitis C (CHC) liver tissues, were strongly and independently associated with an early onset of HCC in patients without any history of HCCs [11]. However, the mechanism responsible for the induction of abnormal methylation of the TSG promoters is still ambiguous. In this study, we addressed this important issue by focusing on the association between the degree of oxidative stress and hypermethylation of TSGs, which is a critical factor in the early stages of human hepatocarcinogenesis. Here, we clearly demonstrate that the generation of ROS and 8-OHdG could play a critical role in the abnormal methylation of TSGs, which in turn should play an important role in the early stages of HCV-related human hepatocarcinogenesis.

Materials and Methods

Subjects

For analyzing the relationship between the accumulation of 8-OHdG and hypermethylation of TSGs in CHC, we used the biopsy specimens from 126 CHC subjects, who had no prior history of HCC. The detailed information describing the patient cohort has been described previously [11]. The median age of the patients (25–75%) was 57 (46–64), and the cohort included 85 male and 43 female subjects. The liver fibrosis stage (F-stage) of each biopsy specimen was determined by the METAVIR scoring system. Among the subjects, 6 cases were scored as F0, 40 were F1, 37 were F2, 23 were F3 and 22 were F4. Informed consent was obtained from each patient and the study was approved by the institutional review boards of the involved institutions.

Immunohistochemical Analyses of 8-OHdG

We used an archive of liver biopsy specimens, which were fixed in buffered formalin and embedded in paraffin. Sections were stained with hematoxylin and eosin and Masson's trichrome for assessment of morphological changes and the stage of fibrosis. Immunohistochemistry (IHC) staining of 8-OHdG was performed using the avidin-biotin complex method. A mouse monoclonal antibody against 8-OHdG (Japan Institute of the Control of Aging, NIKKEN SEIL Co. Ltd., Tokyo, Japan) was used as described previously [12]. A semiquantitative estimation of the degree of 8-OHdG formation was done by counting the number of stained hepatocyte nuclei. The 8-OHdG levels were classified as strong (50% or more of total hepatocytes; fig. 1a), moderate (10–49%; fig. 1b) and weak (9% or less; fig. 1c). Perls' Prussian blue staining was performed to evaluate the levels of iron deposits. The histologic quantification of hepatic iron was based on the number of hepatocytes showing positive Perls' Prussian blue staining: strong (25% or more of total hepatocytes; fig. 1d), moderate (5–24%; fig. 1e), and weak (4% or less; fig. 1f). For both IHC and Perls' Prussian blue staining, ten visual fields from different areas of the liver were used for the evaluation, and 100 nuclei of hepatocytes were counted for each visual field.

Analyses of Abnormal TSG Methylation in Hepatitis Tissue

The methylation status of the promoters of the 11 TSGs was analyzed in the CHC biopsy specimens. Methylation events of 11 TSGs, *HIC-1*, *GSTP1*, *SOCS1*, *RASSF1*, *CDKN2A*, *APC*, *RUNX3*, *PRDM2*, *CASP8*, *CACNA1G* and *PTGS2* genes were determined. These TSGs were selected because of a unique profile of abnormal methylation in early HCC [11]. For determination of abnormal methylation, we performed quantitative MethyLight assays using the StepOne™ real-time detection system (Applied Biosystems, Foster City, Calif., USA). The methylation status of 8 TSGs *(HIC1*, *GSTP1*, *SOCS1*, *RASSF1*, *CDKN2A*, *APC*, *RUNX3* and *PRDM2)* in CHC specimens were reported previously [11]; PCR primers and probes for these TSGs have already been described. We further examined 3 additional TSGs, *CASP8*, *CACNA1G* and *PTGS2* in this study. The sequences of PCR primers and TaqMan probes of these 3 TSGs are as follows: the CASP8-forward primer, 5′-AAGTATGTTTAGCGTTCGGGTTTT-3′, CASP8-reverse primer, 5′-ATACCCAATTTCCAACCATTCAA-3′, and CASP8-probe, FAM-TTGTACGTTTATGAATTGT-MGB; the CACNA1G-forward primer, 5′-TTTTTTCGTTTCGCGTTTAGGT-3′, CACNA1G-reverse primer, 5′-CTCGAAACGACTTCGCCG-3′, and CACNA1G-probe, FAM-AAATAACGCCGAATCCGACAACCGA-MGB; the PTGS2-forward primer, 5′-CGGAAGCGTTCGGGTAAAG-3′, PTGS2-reverse primer, 5′-AATTCCACCGCCCCAAAC-3′, and PTGS2-probe, FAM-TTTCCGCCAAATATCTTTTCTTCTTCGCA-MGB. The PCR was performed following the manufacturer's protocol using TaqMan® Fast universal PCR Master Mix (Applied Biosystems), as reported previously [11].

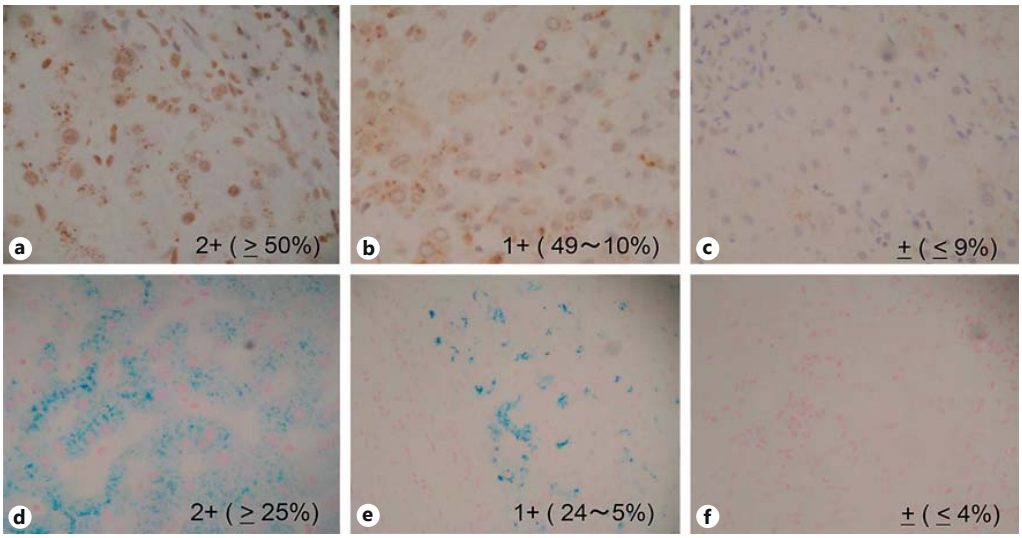

Fig. 1. Immunohistochemical staining of 8-OHdG (**a–c**) and iron staining using Perls' Prussian blue (**d–f**). Among 128 biopsy specimens, 34 showed positive staining of 50% or more of the total hepatocyte nuclei and were classified as strong (2+) staining (**a**); similarly, 30 were classified as moderate (1+) staining (10–49% of total nuclei; **b**) and 61 were weak (±) staining (less than 10%; **c**). The classification of the specimens based on the hepatic iron deposits were as follows: 10 were classified as strong (2+) deposits (25% or more of total hepatocyte; **d**), 40 were moderate (1+) deposits (5–24%; **e**) and 75 were shown as weak (±) deposits (less than 5%; **f**).

Reagents and Cell Lines for Chromatin Immunoprecipitation

The human HCC cell line, HepG2, was obtained from American Type Culture Collection (Rockville, Md., USA) and human fetal liver Hc cells was purchased from Applied Cell Biology Research Institute (Kirkland, Wash., USA). HepG2 and Hc cells were maintained in Dulbecco's modified Eagle's medium with 10% fetal bovine serum in a humidified atmosphere with 5% CO_2 at 37°C. Antibodies for chromatin immunoprecipitation (ChIP) were as follows: 8-OHdG (Japan Institute of the Control of Aging, NIKKEN SEIL Co. Ltd.), acetylated-H4K16 (AcK16H4; Millipore, Billerica, Mass., USA), trimethyl-H3K4 (3MeK4H3), trimethyl-H3K27 (3MeK27H3), panhistone H3 (H3; Wako Pure Chemical Industries Ltd., Osaka, Japan), and rabbit IgG (Genetein Co. Ltd., Tokyo, Japan).

Treatment of HCC Cell Lines with Hydrogen Peroxide, and ChIP before and after Treatment with Hydrogen Peroxide

HepG2 and Hc cells were treated with hydrogen peroxide (H_2O_2), and ChIP was performed before and after treatment using antibodies against Ack16H4 and 3MeK4H3 (an active histone marker), 3MeK27H3 (a repressive histone marker), 8-OHdG (a DNA damage marker), H3 (ChIP-positive control) and rabbit IgG (ChIP-negative control). In 10-cm culture dishes, 3×10^6 of the cells were seeded 24 h prior to the experiments. HepG2 cells were treated with 250 μM H_2O_2 for 1 h and Hc cells were treated with 50 μM of H_2O_2 for 1 h, respectively. The cells were harvested with trypsin, washed twice and suspended in 0.5 ml of PBS. For the cross-linking of histone and DNA, 13.5 μl of 36.6% (w/v) of formaldehyde was added, and cells were incubated for 8 min at room temperature. In order to stop the crosslink reaction, 57 μl of 1.25 M glycine was subsequently added to the cells; cells were incubated for 5 min at room temperature and washed with cold PBS. For the ChIP reaction for histone, we used Auto ChIP kit and the SX-8G IP-Star Automated System (Diagenode Inc., Denville, N.J., USA). Chromatin was sheared to a length of 400–800 bp using sonication instruments (Bioruptor®). For the 8-OHdG ChIP reaction, we used the Auto MeDIP kit (Diagenode Inc.). The chromatin was incubated with antibodies for 10 h, antibody precipitated and eluted from the magnetic beads following the manufacturer's protocol (Diagenode Inc.).

Quantitative ChIP-PCR Analyses of the Promoters of TSGs

Quantitative ChIP-PCR (ChIP-qPCR) of 30 gene promoters of 25 different TSGs was studied to indicate the methylation status in human cancer. qPCR was performed using the EpiScope® Promoter qPCR Array with SYBR Green-based detection (TaKaRa Bio Inc., Otsu, Japan) and the StepOne™ real-time detection system (Applied Biosystems) according to the manufacturer's protocol. The specificity of targeted PCR product was confirmed by melt-curve analysis, which is essential in an efficient and specific quantitative PCR assay. Alterations in the chromatin associated with damaged DNA (i.e. 8-OHdG-bound DNA elements) before and after the H_2O_2 treatment were also assessed. Samples were run in triplicate and data were normalized to amplifications of 5% input samples. The fold changes in the measures of histone modification and the 8-OHdG level in treated and untreated cells were calculated.

Statistical Analysis

To determine the significant variables that contribute to an increase in the number of methylated TSGs, the χ^2 test was used. Multiple comparisons between the fold changes of AcK16H4, 3MeK4H3, 3MeK27H3, 8-OHdG and that of H3 were done using

Steel's method. The correlation between each fold change (for AcK16H4, 3MeK4H3, 3MeK27H3 and H3) and the 8-OHdG level was evaluated by Spearman's rank correlation test. All p values were calculated employing a two-tailed analysis and $p < 0.05$ was considered statistically significant. All statistical analyses were performed by using JMP version 9.0 software (SAS Institute Inc., Cary, N.C., USA).

Results

Association between ROS-Mediated DNA Damage and TSG Methylation Events in the Liver during CHC Infection

In order to evaluate the ROS-mediated DNA damage, we performed IHC staining of 8-OHdG in 125 out of 128 liver biopsy specimens of CHC tissues. The CHC cases were categorized into 3 subgroups as described in Materials and Methods. Among the 125 specimens, 34 were classified as having a strong staining (2+) of 8-OHdG, 30 as moderate (1+) and 61 as weak (±). Similarly, 10 specimens showed strong deposits (2+) of iron, 40 moderate (1+) and 75 weak (±). We also assessed TSG promoter methylation in all the 128 CHC biopsy specimens. Of these, 27 CHC specimens showed methylation in 3 or more TSGs, and 101 specimens showed fewer than 3 methylated TSGs.

The association between each clinicopathological factor and the number of methylated TSGs in the liver tissues is summarized in table 1. Although an increase in the number of methylated TSGs (≥3) was more prevalent in CHC of older-aged males (≥55 years) with advanced F-stage fibrosis (F2–F4) and strong deposits of iron, the 8-OHdG level in the liver tissues was the only factor that significantly correlated with the increased TSG methylation in CHC ($p < 0.0001$).

Table 1. Association between the number of methylated TSGs and clinicopathological factors in patients with CHC

Variables	Cases, n	Methylated TSGs[1], n		p value[2]
		<3	≥3	
Age				
<55 years	54	46	8	
≥55 years	74	55	19	0.1311
Gender				
Female	43	38	5	
Male	85	63	22	0.0522
F-stage				
F0 or F1	46	39	7	
F2–F4	82	62	20	0.2135
Staining of 8-OHdG				
±	61	58	3	
1+	30	22	8	
2+	34	20	14	<0.0001
Iron deposit				
±	75	63	12	
1+	40	31	9	
2+	10	6	4	0.2191

[1] The number of methylated TSGs was determined using MethyLight. Eleven TSGs *(HIC-1*, *GSTP1*, *SOCS1*, *RASSF1*, *CDKN2A*, *APC*, *RUNX3*, *PRDM2*, *CASP8*, *CACNA1G* and *PTGS2)* were analyzed. [2] p values were calculated using the χ^2 test.

Alteration of Histone Modification Induced by H_2O_2 Treatment

The strong relationship between the 8-OHdG level and TSG methylation suggested that the formation of 8-OHdG might induce methylation-associated gene silencing through the formation of repressive histone markers. To test this hypothesis, we used ChIP to measure the fold changes of repressive and active histone markers at the CpG-containing TSG promoters with 8-OHdG before and after H_2O_2 treatment. For this purpose, we performed ChIP-qPCR on the promoters of 30 transcripts in the 25 genes using antibodies against AcK16H4 and 3MeK4H3 (the active histone markers), 3MeK27H3 (the repressive histone marker) and 8-OHdG (to detect damaged DNA elements in the HepG2 cells).

Among the promoters of the 30 transcripts, we successfully amplified the promoter regions of 29 transcripts using the post-ChIP DNA for the measurement of AcK16H4. Similarly, 25, 27 and 26 promoters could be amplified after the ChIP for 3MeK4H3, 3MeK27H3 and 8-OHdG, respectively. All but one promoter (the *LOX* gene) were amplified after the ChIP for H3. Moreover, 23 promoters were amplified by all 4 ChIP-qPCRs, and the fold changes of the ChIP-qPCR values were determined for these loci using H_2O_2-treated and untreated cells (fig. 2a). In the rabbit IgG-negative control ChIP assay, 10 of the 30 gene promoters were slightly amplified; however, the fold changes for the negative control could not be calculated because of its low levels. The median values (25–75%) of fold changes were 0.70 (0.55–0.90) for AcK16H4, 0.80 (0.60–1.10) for 3MeK4H3, 1.60 (1.30–1.80) for 3MeK27H3, 1.45 (1.00–1.93) for 8-OHdG and 1.10 (0.90–1.40) for H3. For 17 promoters, the 8-OHdG fold changes were more than 1.0, suggesting the increase of 8-OHdG at CpG island-containing TSG promoters after H_2O_2 treatment. Simi-

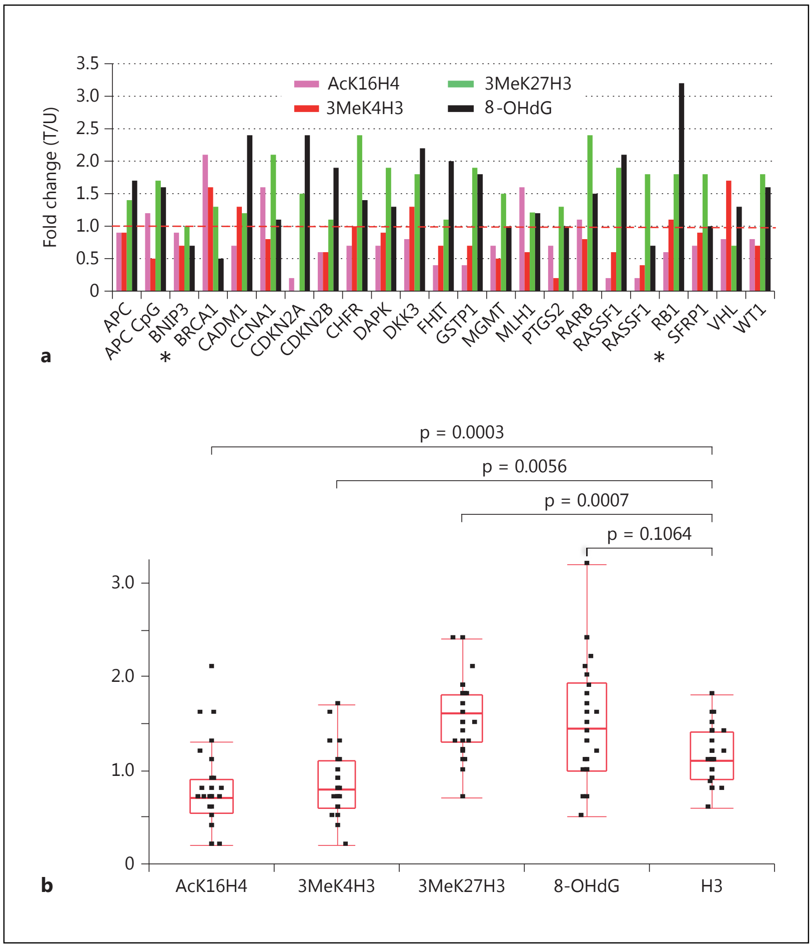

Fig. 2. Alteration of histone modification and its association with 8-OHdG levels after H_2O_2 treatment at the CpG island-containing promoters of TSGs. **a** HepG2 cells were either treated with or without 250 μM of H_2O_2 for 1 h, followed by ChIP for AcK16H4, 3MeK4H3 as an active histone marker, 3MeK27H3 as a repressive histone marker, 8-OHdG, positive control of H3 or negative control of rabbit IgG. The y-axis indicates the fold changes of ChIP-qPCR values over H3 values between the treated and untreated samples. T/U = Ratio of PCR values of treated/untreated cells. * Indicates the splice variants of the corresponding gene. **b** Comparisons of the fold changes indicated by ChIP-qPCR between the IP of each histone modification or 8-OHdG and that of H3. p values were calculated using Steel's method for nonparametric multiple comparison.

larly, the fold changes of the recessive histone marker 3MeK27H3 were greater than 1.0 for 21 TSG promoters. On the other hand, there was a reduction of the active histone markers Ack16H4 and 3MeK4H3 for 17 and 15 promoters, respectively, after treatment with H_2O_2 (fig. 2a). The correlation between the fold changes of AcK16H4, 3MeK4H3, 3MeK27H3, H3 and that of 8-OHdG were also analyzed (fig. 2b). Although it was not statistically significant, the 8-OHdG fold change comparatively increased to that of H3 ($p = 0.1064$ by Steel's method for nonparametric multiple comparison; fig. 2b). The AcK16H4 and 3MeK4H3 fold change values were significantly lower, and the fold change values for 3MeK27H3 were significantly higher than that of H3 ($p = 0.0003$, 0.0056 and 0.0007 for AcK16H4, 3MeK4H3 and 3MeK27H3, respectively, by Steel's multiple comparison test).

We further examined the relationship between the fold changes of 8-OHdG and active and recessive histone markers using H_2O_2-treated and untreated fetal liver Hc cells. Although the correlation was not prominent for AcK16H4 ($r = -0.2789$, $p = 0.1507$; fig. 3a), there was a moderate inverse correlation between the fold changes of 8-OHdG and those of active histone markers ($r = -0.5273$, $p = 0.0039$ for 3MeK4H3; fig. 3b). Interestingly, a strong correlation was detected between the fold changes of 8-OHdG and those of recessive histone markers of 3MeK27H3 ($r = 0.7605$, $p < 0.0001$; fig. 3c). As expected, no correlation was observed between the fold changes of 8-OHdG and those of H3

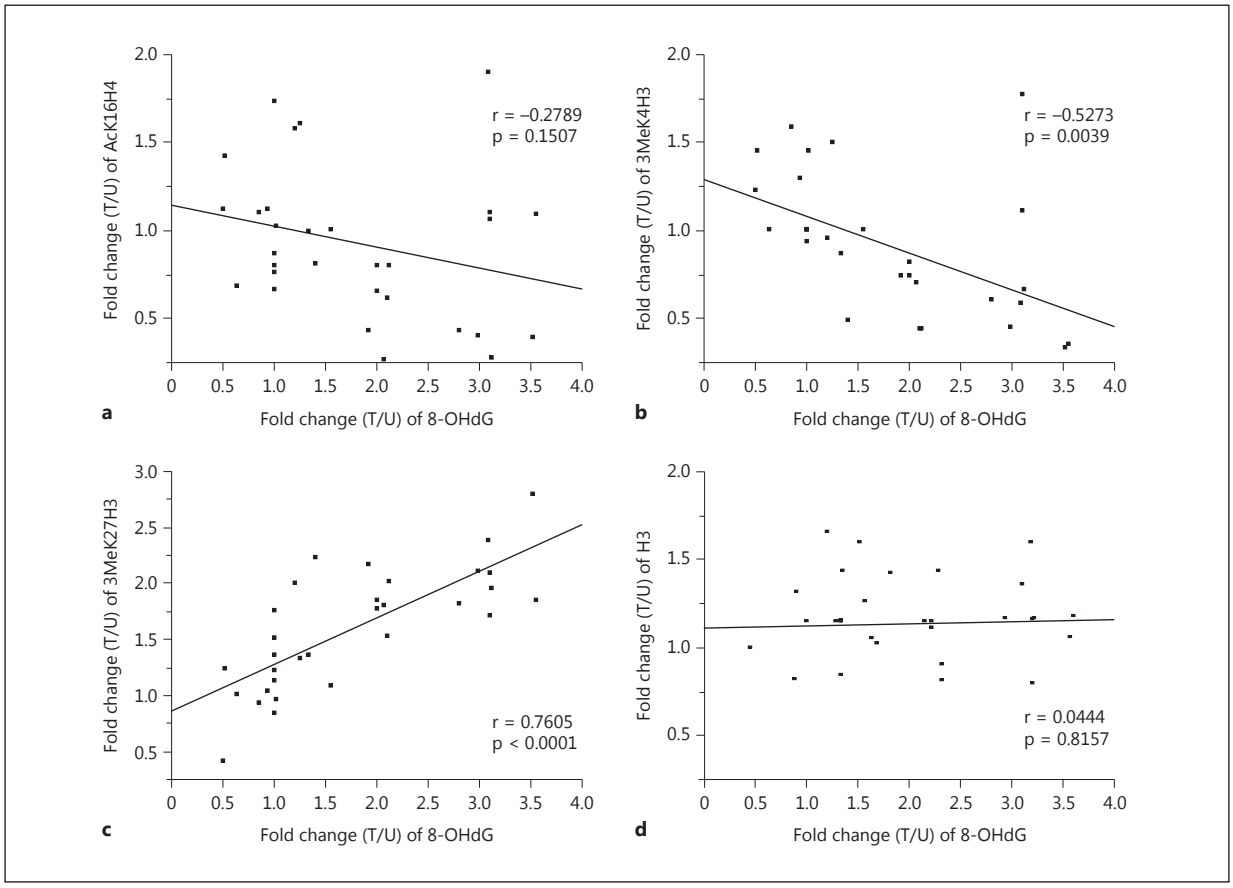

Fig. 3. Correlations between the fold changes of ChIP-qPCR values for histone and 8-OHdG. Correlations between the fold changes of AcK16H4 and 8-OHdG (**a**), 3MeK4H3 and 8-OHdG (**b**), 3MeK27H3 and 8-OHdG (**c**), and H3 and 8-OHdG (**d**). Correlations between each fold change and that of 8-OHdG were evaluated by Spearman's rank correlation test.

(fig. 3d). These findings also indicated that the decrease in active chromatin and the increase in repressive chromatin take place on the 8-OHdG-enriched CpG island-containing TSG promoters, after H_2O_2 treatment.

Discussion

A number of reports suggested that the activation of oncogenes and inactivation of TSGs was a characteristic feature of human cancers, including HCC [3, 4]. We previously reported that the inactivation of TSGs through promoter methylation was more prevalent in HCV-related HCCs than in HCV-negative tumors [13]. On the other hand, it was also reported that oxidative stress could play a central role in the pathogenesis of CHC, and could increase the risk of HCC development [13, 14]. In this study, we examined whether persistent stimulation by ROS and subsequent DNA damage, indicated by the formation of 8-OHdG, could increase the risk for HCC development through the induction of epigenetic instability in hepatocytes. Here, we demonstrated that the 8-OHdG level was the only factor associated with an increased number of methylated TSGs in the liver of CHC, and that TSGs carrying higher levels of 8-OHdG facilitated the modification of the active chromatin to a repressive form after stimulation by ROS.

So far, several reports have suggested that increased ROS production is observed in CHC and the amount of ROS is associated with the onset of HCC [8, 14, 15]. Ac-

tivation of oxidative stress pathways in noncancerous human liver tissue reportedly predicted the recurrence of HCC in patients who underwent a hepatectomy [16]. ROS could also induce genetic alterations such as point mutations because oxidative DNA damage, indicated by 8-OHdG, could induce DNA base mutations such as G>T/C>A transversions [9]. However, although this type of base mutation is commonly found in HCC, whole genome and exome analyses revealed that the mutational spectrum of HCC is heterogeneous [10]. In addition, so far, the frequencies of common mutations in specific TSGs in HCC were not high; the frequencies of the mutations were around 30 and 15% for *p53* and *β-catenin*, respectively [17–21]. On the other hand, a considerable number of cancer-related genes, such as the *CDKN2A*, *RASSF1A*, *GSTP1* and *APC*, showed an alteration in the methylation status in HCC [13, 21]. Regional hypermethylation of the gene promoters leads to transcriptional inactivation of the corresponding TSGs and hypomethylation could cause increased expression of oncogene and transposable DNA elements, both of which could contribute to carcinogenesis.

Previously, we selected the TSGs that showed a high level of methylation in early HCC, and reported that methylation of these TSGs was a unique marker for early-stage HCV-related HCC [11]. In addition, we found that a number of these methylated TSGs in the liver were significantly associated with the onset of HCC in patients with CHC without a prior history of HCC [11]. In this study, we further clarified that the level of 8-OHdG in the liver was the only factor that showed significant association with the methylated TSG number in the same CHC cohort. Previous reports suggested that the treatment of the HCC cell line by H_2O_2 induced an increase in Snail expression and hypermethylation of the *E-Cadherin* promoter. Snail was also shown to recruit HDAC1 and DNMT1 to the *E-Cadherin* gene [22]. Another report showed that oxidative stress induced by H_2O_2 recruits DNA methyltransferase 1 (DNMT1) to damaged chromatin in colon cancer cell lines [23]. It resulted in relocalization of the polycomb repressive protein complex from non-GC-rich to GC-rich areas [23]. Thus, it was reasonable to speculate that oxidative damage led to the formation and relocalization of a polycomb repressive complex, which may explain cancer-specific aberrant DNA methylation and transcriptional silencing of TSGs. To explore this possibility, we treated HCC-derived cell lines and fetal liver cells with H_2O_2, and determined the effect of ROS on the modulation of histone. As expected, treatment with H_2O_2 induced the formation of 8-OHdG on the CpG island-containing TSGs. Interestingly, after treatment the measurement of the repressive histone marker, 3MeK27H3, increased, and that of the active histone markers, AcK16H4 and 3MeK4H4, decreased. It was well known that the polycomb complex could induce repressive histone markers such as 3MeK27H3. The repressive histone marker was associated with the induction of DNA methylation in the corresponding region. On the other hand, our results also indicated that the 8-OHdG fold change using H_2O_2-treated and untreated cells was clearly correlated to that of 3MeK27K3, and inversely correlated to that of AcK16H4 and 3MeK4H4. These facts support the idea that ROS induced an alteration of histone modification to the repressive form at the CpG island-containing TSG promoters and induced hypermethylation through the formation of 8-OHdG, which could lead to inactivation of TSGs by epigenetic mechanisms.

In this study, we clearly demonstrated that the ROS-induced DNA damage could cause the induction of repressive histone markers on TSG promoters. Therefore, it is reasonable to believe that the increased TSG methylation seen in HCC could be reflective of the alteration of chromatin status induced by ROS. As the accumulation of methylated TSGs in CHC tissues has been shown to be a strong risk factor for the early onset of HCC, ROS probably plays a critical role in human hepatocarcinogenesis through the induction of epigenetic instability and regional hypermethylation in CHC.

Acknowledgements

This work was supported in part by Grant-in-Aid for Scientific Research (KAKENHI: 24590997) from the Japanese Society for the Promotion of Science (N. Nishida) and a grant from the Smoking Research Foundation (N. Nishida).

Disclosure Statement

The authors have no conflicts of interest to disclose.

References

1 Stauffer JK, Scarzello AJ, Jiang Q, Wiltrout RH: Chronic inflammation, immune escape, and oncogenesis in the liver: a unique neighborhood for novel intersections. Hepatology 2012;56:1567–1574.

2 Kim DY, Han K: Epidemiology and surveillance of hepatocellular carcinoma. Liver Cancer 2012;1:2–14.

3 Nishida N: Impact of hepatitis virus and aging on DNA methylation in human hepatocarcinogenesis. Histol Histopathol 2010;25:647–654.
4 Nishida N, Goel A: Genetic and epigenetic signatures in human hepatocellular carcinoma: a systematic review. Curr Genomics 2011;12:130–137.
5 Okamoto K, Toyokuni S, Uchida K, Ogawa O, Takenewa J, Kakehi Y, Kinoshita H, Hattori-Nakakuki Y, Hiai H, Yoshida O: Formation of 8-hydroxy-2′-deoxyguanosine and 4-hydroxy-2-nonenal-modified proteins in human renal-cell carcinoma. Int J Cancer 1994;58:825–829.
6 Musarrat J, Arezina-Wilson J, Wani AA: Prognostic and aetiological relevance of 8-hydroxyguanosine in human breast carcinogenesis. Eur J Cancer 1996;32A:1209–1214.
7 Lee BM, Jang JJ, Kim HS: Benzo[*a*]pyrene diol-epoxide-i-DNA and oxidative DNA adducts associated with gastric adenocarcinoma. Cancer Lett 1998;125:61–68.
8 Chuma M, Hige S, Nakanishi M, Ogawa K, Natsuizaka M, Yamamoto Y, Asaka M: 8-hydroxy-2′-deoxy-guanosine is a risk factor for development of hepatocellular carcinoma in patients with chronic hepatitis C virus infection. J Gastroenterol Hepatol 2008;23:1431–1436.
9 Unfried K, Schurkes C, Abel J: Distinct spectrum of mutations induced by crocidolite asbestos: clue for 8-hydroxydeoxyguanosine-dependent mutagenesis in vivo. Cancer Res 2002;62:99–104.
10 Nishida N, Kudo M: Recent advancements in comprehensive genetic analyses for human hepatocellular carcinoma. Oncology 2013;84(suppl 1):93–97.
11 Nishida N, Kudo M, Nagasaka T, Ikai I, Goel A: Characteristic patterns of altered DNA methylation predict emergence of human hepatocellular carcinoma. Hepatology 2012;56:994–1003.
12 Toyokuni S, Tanaka T, Hattori Y, Nishiyama Y, Yoshida A, Uchida K, Hiai H, Ochi H, Osawa T: Quantitative immunohistochemical determination of 8-hydroxy-2′-deoxyguanosine by a monoclonal antibody n45.1: its application to ferric nitrilotriacetate-induced renal carcinogenesis model. Lab Invest 1997;76:365–374.
13 Nishida N, Nagasaka T, Nishimura T, Ikai I, Boland CR, Goel A: Aberrant methylation of multiple tumor suppressor genes in aging liver, chronic hepatitis, and hepatocellular carcinoma. Hepatology 2008;47:908–918.
14 Tanaka S, Miyanishi K, Kobune M, Kawano Y, Hoki T, Kubo T, Hayashi T, Sato T, Sato Y, Takimoto R, Kato J: Increased hepatic oxidative DNA damage in patients with nonalcoholic steatohepatitis who develop hepatocellular carcinoma. J Gastroenterol 2013, E-pub ahead of print.
15 Maki A, Kono H, Gupta M, Asakawa M, Suzuki T, Matsuda M, Fujii H, Rusyn I: Predictive power of biomarkers of oxidative stress and inflammation in patients with hepatitis C virus-associated hepatocellular carcinoma. Ann Surg Oncol 2007;14:1182–1190.
16 Tanaka S, Mogushi K, Yasen M, Ban D, Noguchi N, Irie T, Kudo A, Nakamura N, Tanaka H, Yamamoto M, Kokudo N, Takayama T, Kawasaki S, Sakamoto M, Arii S: Oxidative stress pathways in noncancerous human liver tissue to predict hepatocellular carcinoma recurrence: a prospective, multicenter study. Hepatology 2011;54:1273–1281.
17 Nishida N, Fukuda Y, Kokuryu H, Sadamoto T, Isowa G, Honda K, Yamaoka Y, Ikenaga M, Imura H, Ishizaki K: Accumulation of allelic loss on arms of chromosomes 13q, 16q and 17p in the advanced stages of human hepatocellular carcinoma. Int J Cancer 1992;51:862–868.
18 Nishida N, Fukuda Y, Kokuryu H, Toguchida J, Yandell DW, Ikenega M, Imura H, Ishizaki K: Role and mutational heterogeneity of the p53 gene in hepatocellular carcinoma. Cancer Res 1993;53:368–372.
19 Nishida N, Fukuda Y, Komeda T, Kita R, Sando T, Furukawa M, Amenomori M, Shibagaki I, Nakao K, Ikenaga M, et al: Amplification and overexpression of the cyclin D1 gene in aggressive human hepatocellular carcinoma. Cancer Res 1994;54:3107–3110.
20 Nishida N, Fukuda Y, Ishizaki K, Nakao K: Alteration of cell cycle-related genes in hepatocarcinogenesis. Histol Histopathol 1997;12:1019–1025.
21 Nishida N, Nishimura T, Nagasaka T, Ikai I, Goel A, Boland CR: Extensive methylation is associated with *β-catenin* mutations in hepatocellular carcinoma: evidence for two distinct pathways of human hepatocarcinogenesis. Cancer Res 2007;67:4586–4594.
22 Lim SO, Gu JM, Kim MS, Kim HS, Park YN, Park CK, Cho JW, Park YM, Jung G: Epigenetic changes induced by reactive oxygen species in hepatocellular carcinoma: Methylation of the E-cadherin promoter. Gastroenterology 2008;135:2128–2140.
23 O'Hagan HM, Wang W, Sen S, Destefano Shields C, Lee SS, Zhang YW, Clements EG, Cai Y, Van Neste L, Easwaran H, Casero RA, Sears CL, Baylin SB: Oxidative damage targets complexes containing DNA methyltransferases, SIRT1, and polycomb members to promoter CpG islands. Cancer Cell 2011;20:606–619.

Digestive Diseases

Dig Dis 2013;31:467–471
DOI: 10.1159/000355246

CD34 Expression in Noncancerous Liver Tissue Predicts Multicentric Recurrence of Hepatocellular Carcinoma

Naoko Tsuji[a] Shingo Ishiguro[b] Yo Sasaki[c] Masatoshi Kudo[d]

[a]Department of Gastroenterology, Sakai Hospital, Kinki University Faculty of Medicine, Sakai, Departments of [b]Pathology and [c]Surgery, Osaka Medical Center for Cancer and Cardiovascular Diseases, Osaka, and [d]Department of Gastroenterology and Hepatology, Kinki University School of Medicine, Osakasayama, Japan

Key Words
Hepatocellular carcinoma · CD34 expression · Labeling index

Abstract
Background: Metachronous multicentric recurrence of hepatocellular carcinoma (HCC) is a common cause of morbidity and mortality following curative surgical resection. Clinical and laboratory predictors of these processes can markedly aid in managing these patients. Capillarization of hepatic sinusoids is also a well-known phenomenon in many liver diseases, especially in neoplastic liver diseases. Here, we investigated the clinical features, fibrosis scores and distribution of CD34 in noncancerous hepatic tissues of postresection patients with and without multicentric recurrence. ***Methods:*** Eighteen patients with multicentric recurrence of HCC diagnosed by histological examination of repeated hepatectomy specimens and 72 HCC patients with more than 5-year disease-free survival postresection participated in the study. We compared the clinicopathological features of these two groups. We examined noncancerous hepatic tissues for iron deposition by Prussian blue staining and computed the CD34-labeling index (LI) through immunohistochemistry using anti-CD34 antibody. ***Results:*** CD34-LI was significantly higher in the multicentric recurrence group ($p < 0.001$) and staging scores of fibrosis were also significantly higher in the recurrence group ($p = 0.035$). A high histological activity grade ($p = 0.057$) and a high alanine aminotransferase level ($p = 0.060$) were also associated with recurrence. There were no significant differences between the two groups in age, sex, hepatitis B virus surface antigen and anti-hepatitis C virus antibody levels, or grade of iron deposition. On multivariate analysis, high CD34-LI was the only independent risk factor ($p = 0.001$) for metachronous multicentric recurrence. ***Conclusion:*** CD34 expression in the capillaries and sinusoids of noncancerous hepatic tissue is a risk factor for multicentric recurrence of HCC. Histologic assessment of hepatic tissue with CD34 immunohistochemistry might be useful for the prognostic evaluation of HCC patients after surgery.

Introduction

The incidence of intrahepatic recurrence after curative resection of hepatocellular carcinoma (HCC) is very high [1], and many HCC recurrences develop in a multicentric fashion. Effective predictors of multicentric recurrence must be clarified to manage patients after curative hepatectomy. There have been many investigations of cancerous tissues of HCC to predict intrahepatic recurrence, especially intrahepatic metastasis [2, 3]. To predict multicentric recurrence, we have to investigate noncancerous

KARGER

E-Mail karger@karger.com
www.karger.com/ddi

0257–2753/13/0316–0467$38.00/0

Masatoshi Kudo, MD
Department of Gastroenterology and Hepatology, Kinki University School of Medicine
337-2 Ohno-Higashi
Osakasayama, Osaka 589-8511 (Japan)
E-Mail m-kudo@med.kindai.ac.jp

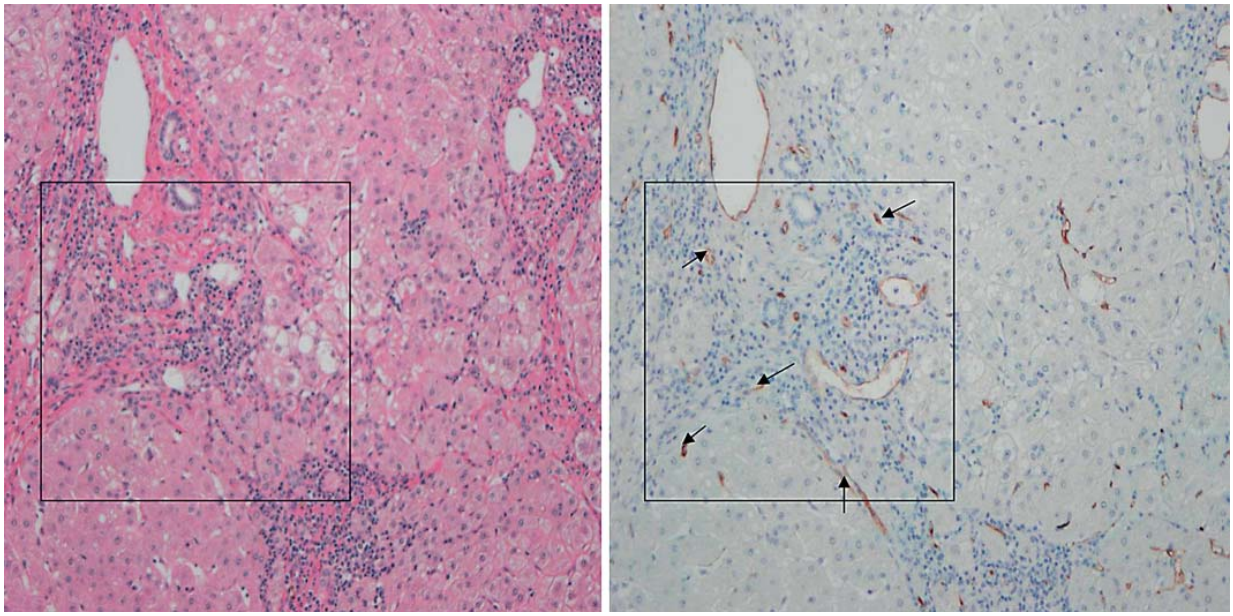

Fig. 1. CD34 immunostaining of noncancerous hepatic tissue. CD34-LI is the average number of CD34-positive capillaries and sinusoids in 10 portal areas. Original magnification ×200.

liver tissue. Multicentric recurrence of HCC is thought to be associated with underlying liver diseases. Angiogenesis and sinusoidal remodeling are closely related to liver inflammation and fibrosis. Normal sinusoidal endothelial cells do not express CD34; however, they show an altered phenotype in chronic liver inflammation to express CD34. In this study, we investigated the noncancerous liver tissue of multicentric recurrence patients and nonrecurrence patients with CD34 immunostaining to clarify the difference in background livers of those patients.

Material and Methods

Between 1990 and 1999, 469 HCC patients underwent curative hepatic resection at Osaka Medical Center for Cancer and Cardiovascular Diseases. Metachronous multicentric recurrence of HCC was diagnosed by histological examination of repeated hepatectomy specimens. For the accurate evaluation of a noncancerous background liver, cases in which resected liver specimens were very small or showed degenerative change due to transarterial chemoembolization before surgery were excluded. The definition of metachronous multicentric recurrence was according to the histological criteria of the Liver Cancer Study Group of Japan on the multicentric occurrence of HCC, i.e. recurrent tumors are early HCCs maintaining the existing liver structure, or well-differentiated HCCs found at the edge of moderately or poorly differentiated cancer tissues [4].

Suspected multicentric recurrence patients diagnosed based on clinical images, i.e. CT scan, ultrasonography or needle biopsies of a new nodule after surgery, were also excluded. Eighteen patients met the strict criteria and 72 patients with a more than 5-year disease-free survival were included in our study.

Clinicopathological comparison was made between the 18 patients in the metachronous multicentric recurrence group and the 72 in the nonrecurrence group regarding age, sex, hepatitis B virus surface antigen, anti-hepatitis C virus (HCV) antibodies and background liver tissue. Paraffin-embedded, noncancerous liver tissue sections were stained with hematoxylin and eosin, and Perls' Prussian blue. The grade of necro-inflammatory activity and stage of fibrosis were classified according to the New Inuyama scoring system for chronic hepatitis [5]. The necro-inflammatory activity and the fibrosis stage were as follows: A0, no necro-inflammatory reaction; A1, mild; A2, moderate, and A3, severe; F0, no fibrosis; F1, fibrous portal expansion; F2, bridging fibrosis; F3, bridging fibrosis with lobular distortion, and F4, cirrhosis. The iron contents in the noncancerous liver tissue were graded according to Seale et al. [6], i.e.: grade 0, absent – iron granules absent/barely discernible at ×400; grade 1, scarce – barely discernible at ×250 but easily discernible at ×400; grade 2, mild – discrete granules resolved at ×100; grade 3, moderate – discrete granules resolved at ×25, and grade 4, severe – massive iron granules visible at ×10 or with the naked eye.

For immunohistochemistry, anti-CD34 monoclonal mouse antibody (diluted 1:50; QBEnd 10, Dako, Glostrup, Denmark) was used. The avidin-biotin-peroxidase complex immunohistochemistry method (Vectastatin Elite ABC Kit, Vector Laboratories Inc., Burlingame, Calif., USA) was used. CD34-positive capillaries and

sinusoids of noncancerous liver tissue in 10 portal areas under a high-power field (200× magnifications) were counted, and the average number was defined as the CD34 labeling index (LI; fig. 1).

Statistical Analysis

Frequencies of various characteristics were compared between the groups with and without multicentric recurrence. Statistical analysis was performed using the χ^2 test for categorical data and Mann-Whitney U test for continuous data. A multivariate analysis of risk factors for multicentric recurrence was performed using a logistic regression method. IBM SPSS 17.0 software was used and significance was accepted at $p < 0.05$.

Results

CD34 immunoreactivity was observed in peribiliary capillaries and periportal and perilobular sinusoids, but no reactivity was shown in parenchymal cells (fig. 1).

Univariate Analysis of Risk Factors Predicting Multicentric Recurrence

Clinicopathological characteristics with and without metachronous multicentric recurrences are shown in table 1. There were no significant differences in age, sex, hepatitis B virus surface antigen and anti-HCV antibodies between the two groups. The serum alanine aminotransferase (ALT) level ($p = 0.060$) and a high histological activity grade ($p = 0.057$) showed tendencies to associate with recurrence. Staging scores of fibrosis were significantly higher in the recurrence group ($p = 0.035$) and CD34-LI was also significantly higher in the multicentric recurrence group ($p < 0.001$). A high deposition of iron was negatively related to recurrence ($p = 0.086$).

Multivariate Analysis of Risk Factors Predicting Multicentric Recurrence

Selected factors that were significant on univariate analysis, including the histological stage of fibrosis and CD34-LI, and other relevant factors, including the serum ALT level, histological grade of activity and grade of iron deposition, were included in the model. CD34-LI and the serum ALT level were converted into categorical data. High CD34-LI (OR, 34.06; 95% CI, 6.39–181.47; $p < 0.001$) was independently associated with metachronous multicentric recurrence based on multivariate analysis, and a high stage of fibrosis showed a tendency to associate with recurrence (OR, 5.62; 95% CI, 0.98–31.95; $p = 0.05$; table 2).

Table 1. Results of univariate analysis between patients with and without metachronous multicentric recurrence

	Recurrence (+) (n = 18)	Recurrence (–) (n = 72)	p value
Age, years	59.6±9.0	59.0±9.0	0.806
Male sex	14 (78)	58 (79)	0.913
ALT level, IU/l	97.6±57.8	75.4±58.0	0.060
HBsAg positive	4 (22)	13 (17)	0.686
HCV-Ab positive	14 (78)	45 (59)	0.345
Grade of activity: A2/3	17 (94)	56 (74)	0.057
Stage of fibrosis: F3/4	15 (83)	40 (57)	0.035
Iron deposition: grade 3/4	1 (6)	17 (24)	0.086
CD34-LI	45.2±23.1	14.3±7.9	<0.001

Values are either mean ± SD or number with percentage in parentheses. Statistical analysis was performed using the χ^2 test for categorical and Mann-Whitney U test for continuous data.

Table 2. Results of multivariate analysis of the risk factors for metachronous multicentric recurrence

	p value	OR	95% CI
ALT >100 IU/l	0.18	2.89	0.61–13.71
Grade of activity: A2/3	0.39	3.25	0.21–50.07
Stage of fibrosis: F3/4	0.05	5.62	0.98–31.95
Iron deposition: grades 3/4	0.27	0.23	0.17–3.16
CD34-LI >25	<0.01	34.06	6.39–181.47

Discussion

The intrahepatic recurrence rate of HCC after curative surgical resection remained very high. Long-term follow-up data after surgery showed that the recurrence rate of HCV-positive HCC patients was 80%, and that of HBV-positive HCC patients was 59% [7]. There are two different types of recurrence: intrahepatic metastasis and multicentric recurrence. In Japan, 45–60% of recurrence after surgical resection was reported to be multicentric. Kumada et al. [8] reported that 50.9% of recurrence after ethanol infection therapy was multicentric. However in China, Li et al. [9] reported that the rate of multicentric recurrence after surgical resection was 30%. We adopted histopathological criteria to strictly differentiate whether the recurrent HCC was intrahepatic metastasis or multicentric recurrence, and several clonal analyses of both primary HCC and recurrent HCC were reported for a more accu-

rate diagnosis [10–12]. However, according to a nationwide survey, repeat hepatectomy has been performed in 1.6% of all patients [13]. Therefore, in many clinical situations, the mode of recurrence was diagnosed based on clinical data such as vascular invasion of primary HCC, the period of recurrence, size and site of the recurrent tumor, and hemodynamics of the recurrent tumor assessed by dynamic CT or contrast-enhanced ultrasonography. The risk factors for synchronous and metachronous multicentric occurrence of HCC were reported to be: male gender, HCV positive, aged, low platelet count, high grading and staging scores, high ALT activity, and high concentration of type 4 collagen [14–16]. Tarao et al. [17] reported the increased DNA synthesis activity of hepatocytes in the residual liver of multicentric recurrence patients using an in vitro BrdU assay of biopsied specimens, and, recently, a few studies have investigated gene expression in noncancerous liver tissue to predict risk factors of multicentric recurrence [18, 19]. In our study, the multicentric recurrence group also showed a significantly higher stage of fibrosis and tendency toward a higher ALT activity and grade of activity on univariate analysis; however, regarding the HCV status, there were no significant differences between the two groups. Many HCV positive patients in our study showed recurrence after curative hepatectomy, and many of them had suspected multicentric recurrence according to the clinical findings, but did not undergo repeat hepatectomy because of the functional reserve of the liver or selection of another therapy.

In our study, CD34 expression in noncancerous liver tissue was a significant risk factor of multicentric recurrence on uni- and multivariate analyses. CD34 antigen is expressed in hematopoietic stem cells and endothelial cells. In normal liver tissue, CD34 expression is restricted to portal vascular structures. It is also detected in oval cells in rat liver [20], but we identified no immunoreactivity in hepatocytes or oval cell-like cells in this study. The hepatic sinusoidal endothelial cells have numerous holes (fenestrae) and lack a basement membrane. They do not contain molecules characteristically found in the vascular endothelium, such as CD34 and GMP-140. However, in chronic liver disease, intrahepatic angiogenesis and sinusoidal remodeling occurs, characterized by the deposition of a basement membrane, loss of sinusoidal endothelial fenestrae, and by the expression of CD34, which is commonly referred to as the 'capillarization' of sinusoids [21, 22]. Angiogenesis of chronic liver disease evaluated by CD34 positivity is correlated with the degree of fibrosis [23], and strong staining was reported in HCC and hepatocellular adenoma [24–27]. Ohmori et al. [28, 29] reported that high expression of CD34-positive sinusoidal endothelial cells was a risk factor for developing HCC in HCV and HBV chronic hepatitis patients using liver biopsy specimens. Angiogenesis occurs under conditions associated with tissue damage, wound healing and remodeling. Angiogenesis also occurs in tumors. High CD34-LI in noncancerous liver tissue seems to be the result of severe tissue damage and inflammation. To prevent multicentric recurrence, anti-inflammatory therapy is essential, as long-term interferon therapy reduced the carcinogenesis rate of HCV patients [30]. Are angiogenesis and sinusoidal remodeling new targets for preventing carcinogenesis? Sorafenib is a multikinase inhibitor compound approved for liver cancer and it inhibits tumor angiogenesis. In animal models, sorafenib also inhibits both matrix restructuring and vascular remodeling that accompanies chronic liver disease [31]. It may be a candidate for a new therapy to treat liver fibrosis and prevent carcinogenesis, but further investigation is needed before clinical application to humans.

Liver iron overload was reported as a risk factor for HCC. Liver iron accumulation causes oxidative stress and leads to liver cell DNA mutations, and the development of HCC. Several studies reported that liver iron overload contributed to the development of HCC in patients with viral C hepatitis [32, 33]. In our study, iron deposition in noncancerous liver tissue had a negative impact on multicentric recurrence. Nahon et al. [34] reported that liver iron overload is associated with a higher risk of HCC in patients with alcoholic but not HCV-related cirrhosis, and Sorrentino et al. [35] reported that iron deposition was associated with NASH-related cirrhosis. In our study, the nonrecurrence group included patients whose etiologies of hepatitis were nonviral.

This study has some limitations. We selected patients with multicentric recurrence diagnosed by repeat hepatectomy; therefore, the number of studied patients was small, and the histological types of second primary HCC were limited to the early HCC type or well-differentiated type. Therefore, our multicentric recurrence group had some biases.

In conclusion, CD34 expression in the capillaries and sinusoids of noncancerous hepatic tissue is a risk factor for the multicentric recurrence of HCC. Histologic assessment of hepatic tissue with CD34 immunohistochemistry is a simple and straightforward method, and might be useful for the prognostic evaluation of HCC patients after surgery.

Disclosure Statement

The authors have no conflicts of interest to declare.

References

1 Kubo S, Takemura S, Sakata C, Urata Y, Ueni-shi T: Adjuvant therapy after curative resection for hepatocellular carcinoma associated with hepatitis virus. Liver Cancer 2013;2:40–46.
2 Kim YK: Prediction of HCC recurrence by CT and MRI. Liver Cancer 2013;2:181.
3 Burak KW: Prediction of hepatocellular carcinoma recurrence by molecular biomarkers. Liver Cancer 2013;2:185.
4 Japan Liver Cancer Study Group: General Rules for the Clinical and Patholoical Study of Primary Liver Cancer, English ed 3. Tokyo, Kanehara 2010, p 54.
5 Ichida F, Tsuji T, Omata M, Ichida T, Inoue K, Kamimura T, Yamada G: New Inuyama classification; new criteria for histological assessment of chronic hepatitis. Int Hepatol Commun 1996;6:112–119.
6 Seale J, Leggett BA, Crawford DHG, Powell LW: Iron storage disease; in MacSween RNM, Burt AD, Portmann BC, Ishak KG, Scheuer PJ, Anthony PP (eds): Pathology of the Liver, ed 4. Edinburgh, Churchill Livingstone, 2002, p 260.
7 Sasaki Y, Yamada T, Tanaka H, Ohigashi H, Eguchi H, Yano M, Ishikawa O, Imaoka S: Risk of recurrence in a long-term follow-up after surgery in 417 patients with hepatitis B- or hepatitis C-related hepatocellular carcinoma. Ann Surg 2006;244:771–780.
8 Kumada T, Nakano S, Takeda I, Sugiyama K, Osada T, Kiriyama S, Sone Y, Toyoda H, Shimada S, Takahashi M, et al: Patterns of recurrence after initial treatment in patients with small hepatocellular carcinoma. Hepatology 1997;25:87–92.
9 Li Q, Wang J, Juzi JT, Sun Y, Zheng H, Cui Y, Li H, Hao X: Clonality analysis for multicentric origin and intrahepatic metastasis in recurrent and primary hepatocellular carcinoma. J Gastrointest Surg 2008;12:1540–1547.
10 Morimoto O, Nagano H, Sakon M, Fujiwara Y, Yamada T, Nakagawa H, Miyamoto A, Kondo M, Arai I, Yamamoto T, et al: Diagnosis of intrahepatic metastasis and multicentric carcinogenesis by microsatellite loss of heterozygosity in patients with multiple and recurrent hepatocellular carcinomas. J Hepatol 2003;39:215–221.
11 Tsuda H, Oda T, Sakamoto M, Hirohashi S: Different pattern of chromosomal allele loss in multiple hepatocellular carcinomas as evidence of their multifocal origin. Cancer Res 1992;52:1504–1509.
12 Nakashima O, Kojiro M: Recurrence of hepatocellular carcinoma: multicentric occurrence or intrahepatic metastasis? A viewpoint in terms of pathology. J Hepatobiliary Pancreat Surg 2001;8:404–409.
13 Arii S, Teramoto K, Kawamura T, Okamoto H, Kaido T, Mori A, Imamura M: Characteristics of recurrent hepatocellular carcinoma in Japan and our surgical experience. J Hepatobiliary Pancreat Surg 2001;8:397–403.
14 Kubo S, Yamamoto T, Ikebe T, Shuto T, Hirohashi K, Tanaka H, Tsukamoto T, Wakasa K, Kinoshita H: Relationship between multicentric occurrence of hepatocellular carcinoma and histology of noncancerous hepatic tissue in patients with chronic hepatitis C. Jpn J Cancer Res 1999;90:1076–1080.
15 Ikeda K, Arase Y, Kobayashi M, Saitoh S, Someya T, Hosaka T, Suzuki Y, Suzuki F, Tsubota A, Akuta N, et al: Significance of multicentric cancer recurrence after potentially curative ablation of hepatocellular carcinoma: a longterm cohort study of 892 patients with viral cirrhosis. J Gastroenterol 2003;38:865–876.
16 Tomimaru Y, Sasaki Y, Yamada T, Eguchi H, Ohigashi H, Ishikawa O, Imaoka S: Fibrosis in non-cancerous tissue is the unique prognostic factor for primary hepatocellular carcinoma without hepatitis B or C viral infection. World J Surg 2006;30:1729–1735.
17 Tarao K, Hoshino H, Shimizu A, Ohkawa S, Nakamura Y, Harada M, Ito Y, Tamai S, Akaike M, Sugimasa Y, et al: Role of increased DNA synthesis activity of hepatocytes in multicentric hepatocarcinogenesis in residual liver of hepatectomized cirrhotic patients with hepatocellular carcinoma. Jpn J Cancer Res 1994;85:1040–1044.
18 Okamoto M, Utsunomiya T, Wakiyama S, Hashimoto M, Fukuzawa K, Ezaki T, Hanai T, Inoue H, Mori M: Specific gene-expression profiles of noncancerous liver tissue predict the risk for multicentric occurrence of hepatocellular carcinoma in hepatitis C virus-positive patients. Ann Surg Oncol 2006;13:947–954.
19 Hoshida Y, Villanueva A, Kobayashi M, Peix J, Chiang DY, Camargo A, Gupta S, Moore J, Wrobel MJ, Lerner J, et al: Gene expression in fixed tissues and outcome in hepatocellular carcinoma. New Engl J Med 2008;359:1995–2004.
20 Omori N, Omori M, Evarts RP, Teramoto T, Miller MJ, Hoang TN, Thorgeirsson SS: Partial cloning of rat CD34 cDNA and expression during stem cell-dependent liver regeneration in the adult rat. Hepatology 1997;26:720–727.
21 Schaffner F, Poper H: Capillarization of hepatic sinusoids in man. Gastroenterology 1963;44:239–242.
22 Couvelard A, Scoazec JY, Feldmann G: Expression of cell-cell and cell-matrix adhesion proteins by sinusoidal endothelial cells in the normal and cirrhotic human liver. Am J Pathol 1993;143:738–752.
23 Amarapurkar AD, Amarapurkar DN, Vibhav S, Patel ND: Angiogenesis in chronic liver disease. Ann Hepatol 2007;6:170–173.
24 Ruck P, Xiao JC, Kaiserling E: Immunoreactivity of sinusoids in hepatocellular carcinoma: an immunohistochemical study using lectin UEA-1 and antibodies against endothelial markers, including CD34. Arch Pathol Lab Med 1995;119:173–178.
25 Kimura H, Nakajima T, Kagawa K, Deguchi T, Kakusui M, Katagishi T, Okanoue T, Kashima K, Ashihara T: Angiogenesis in hepatocellular carcinoma as evaluated by CD34 immunohistochemistry. Liver 1998;18:14–19.
26 Maeda T, Adachi E, Kajiyama K, Takenaka K, Honda H, Sugimachi K, Tsuneyoshi M: CD34 expression in endothelial cells of small hepatocellular carcinoma: its correlation with tumour progression and angiographic findings. J Gastroenterol Hepatol 1995;10:650–654.
27 Cui S, Hano H, Sakata A, Harada T, Liu T, Takai S, Ushigome S: Enhanced CD34 expression of sinusoid-like vascular endothelial cells in hepatocellular carcinoma. Pathol Int 1996;46:751–756.
28 Ohmori S, Shiraki K, Sugimoto K, Sakai T, Fujikawa K, Wagayama H, Takase K, Nakano T: High expression of CD34-positive sinusoidal endothelial cells is a risk factor for hepatocellular carcinoma in patients with HCV-associated chronic liver diseases. Hum Pathol 2001;32:1363–1370.
29 Ohmori S, Shiraki K, Sugimoto K, Yamanaka Y, Yamaguchi Y, Saitou Y, Fujikawa K, Murata K, Nakano T: Expression of CD34-positive sinusoidal endothelial cells in patients with HBV-associated chronic liver diseases. Int J Mol Med 2004;14:179–184.
30 Ikeda K, Saitoh S, Kobayashi M, Suzuki Y, Suzuki F, Tsubota A, Arase Y, Murashima N, Chayama K, Kumada H: Long-term interferon therapy for 1 year or longer reduces the hepatocellular carcinogenesis rate in patients with liver cirrhosis caused by hepatitis C virus: a pilot study. J Gastroenterol Hepatol 2001;16:406–415.
31 Thabut D, Routray C, Lomberk G, Shergill U, Glaser K, Huebert R, Patel L, Masyuk T, Blechacz B, Vercnocke A, et al: Complementary vascular and matrix regulatory pathways underlie the beneficial mechanism of action of sorafenib in liver fibrosis. Hepatology 2011;54:573–585.
32 Tanaka H, Fujita N, Sugimoto R, Urawa N, Horiike S, Kobayashi Y, Iwasa M, Ma N, Kawanishi S, Watanabe S, et al: Hepatic oxidative DNA damage is associated with increased risk for hepatocellular carcinoma in chronic hepatitis C. Br J Cancer 2008;98:580–586.
33 Chapoutot C, Esslimani M, Joomaye Z, Ramos J, Perney P, Laurent C, Fabbro-Peray P, Larrey D, Domergue J, Blanc F: Liver iron excess in patients with hepatocellular carcinoma developed on viral C cirrhosis. Gut 2000;46:711–714.
34 Nahon P, Sutton A, Rufat P, Ziol M, Thabut G, Schischmanoff PO, Vidaud D, Charnaux N, Couvert P, Ganne-Carrie N, et al: Liver iron, HFE gene mutations, and hepatocellular carcinoma occurrence in patients with cirrhosis. Gastroenterology 2008;134:102–110.
35 Sorrentino P, D'Angelo S, Ferbo U, Micheli P, Bracigliano A, Vecchione R: Liver iron excess in patients with hepatocellular carcinoma developed on non-alcoholic steato-hepatitis. J Hepatol 2009;50:351–357.

Digestive Diseases

Dig Dis 2013;31:472–479
DOI: 10.1159/000355248

Hypovascular Hepatic Nodules Showing Hypointense on the Hepatobiliary-Phase Image of Gd-EOB-DTPA-Enhanced MRI to Develop a Hypervascular Hepatocellular Carcinoma: A Nationwide Retrospective Study on Their Natural Course and Risk Factors

Tatsuo Inoue[a] Tomoko Hyodo[b] Takamichi Murakami[b] Yukihisa Takayama[c] Akihiro Nishie[c] Atsushi Higaki[d] Keiko Korenaga[d, e] Azusa Sakamoto[f] Yukio Osaki[f] Hiroshi Aikata[g] Kazuaki Chayama[g] Takeshi Suda[h] Toru Takano[i] Kennichi Miyoshi[j] Masahiko Koda[j] Kazushi Numata[k] Hironori Tanaka[l, m] Hiroko Iijima[l] Hironori Ochi[n] Masashi Hirooka[n] Yasuharu Imai[o] Masatoshi Kudo[a]

Departments of [a]Gastroenterology and Hepatology and [b]Diagnostic Radiology, Kinki University, Osakasayama, [c]Department of Clinical Radiology, Graduate School of Medical Sciences, Kyushu University, Fukuoka City, [d]Department of Hepatology and Pancreatology, Kawasaki Medical School, Kurashiki, [e]Department of Gastroenterology and Hepatology, Kohnodai Hospital, National Center for Global Health and Medicine, Ichikawa, [f]Department of Gastroenterology and Hepatology, Osaka Red Cross Hospital, Osaka, [g]Department of Gastroenterology and Metabolism, Hiroshima University Hospital, Hiroshima, Divisions of [h]Gastroenterology and Hepatology and [i]Radiation Oncology, Graduate School of Medical and Dental Sciences, Niigata University, Niigata, [j]Division of Medicine and Clinical Science, Department of Multidisciplinary Internal Medicine, Tottori University, Yonago, [k]Gastroenterological Center, Yokohama City University Medical Center, Yokohama, [l]Ultrasound Imaging Center and [m]Division of Hepatobiliary and Pancreatic Disease, Department of Internal Medicine, Hyogo College of Medicine, Nishinomiya, [n]Department of Gastroenterology and Metabology, Ehime University Graduate School of Medicine, Toon, and [o]Department of Gastroenterology, Ikeda Municipal Hospital, Ikeda, Japan

Key Words
Gadolinium ethoxybenzyl diethylenetriamine pentaacetic acid · Enhanced MRI · Hepatocellular carcinoma · Hypervascular transformation

Abstract
Objective: We aimed to investigate the natural outcome of nonhypervascular lesions detected in the hepatobiliary phase of gadolinium ethoxybenzyl diethylenetriamine pentaacetic acid (Gd-EOB-DTPA)-enhanced MRI by performing a longitudinal study retrospectively enrolled in a nationwide manner. ***Methods:*** Between February 2008 and March 2011, 224 patients with 504 nodules that were diagnosed as nonhypervascular by imaging were recruited from institutions that participated in the present study. We examined the natural outcome of nonhypervascular lesions and evaluated the risk factors. ***Results:*** Of the 504 nodules, 173 (34.3%) showed hypervascular transformation. The overall cumulative incidence of hypervascular transformation was 14.9% at 12

KARGER

E-Mail karger@karger.com
www.karger.com/ddi

0257–2753/13/0316–0472$38.00/0

Masatoshi Kudo, MD, PhD
Division of Gastroenterology and Hepatology
Department of Internal Medicine, Kinki University Faculty of Medicine
377-2 Ohno-Higashi, Osakasayama, Osaka 589-8511 (Japan)
E-Mail m-kudo@med.kindai.ac.jp

months and 45.8% at 24 months. Multivariate analysis using the Cox regression model revealed previous treatment history for hepatocellular carcinoma (HCC; relative risk = 1.498; p = 0.036, 95% CI 1.03–2.19) and hyperintensity on T2-weighted images (relative risk = 1.724; p = 0.015, 95% CI 1.11–2.67) were identified as independent factors for hypervascular transformation. ***Conclusions:*** Patients who have a previous treatment history for HCC and with hypointense nodules showing hyperintensity on T2-weighted images need careful follow-up because of the high incidence of hypervascular transformation.

Table 1. Baseline characteristics of the patients

Sex (male/female)	134/90
Median age, years (range)	70 (49–88)
Child-Pugh classification (A/B/C)	187/37/0
Etiology and histology of underlying liver disease	
HCV-related chronic hepatitis	26
HCV-related cirrhosis	118
HBV-related chronic hepatitis	14
HBV-related cirrhosis	40
Others	26
Past history of HCC (yes/no)	180/44
Coexistence of hypervascular HCCs (yes/no)	85/139

Introduction

Hepatocellular carcinoma (HCC) is one of the most common cancers worldwide and is a major cause of death in patients with cirrhosis; therefore, it is important to detect and treat HCC at an early stage. The development of screening programs for high-risk HCC patients, involving periodic ultrasonography (US) and computed tomography (CT), has enabled small HCCs less than 2 cm in diameter to be easily detected and safely resected. As a result, we have encountered more early-stage HCCs [1], low-grade dysplastic nodules and high-grade dysplastic nodules. Histological features of these nodules are sequential and they often display heterogeneous internal histological features, the precise differential diagnosis between borderline lesions and early-stage, highly well-differentiated HCC (early HCC) is often difficult even by histological examination [2, 3]. Consequently, the imaging findings of these two are similar and overlapping, typically showing nonhypervascularity on dynamic CT, dynamic MRI and contrast-enhanced US; and internal portal blood supply on CT during arterial portography (CTAP) [4]. A previous study reported the existence of a significant correlation between the intranodular blood supply, as evaluated by CTAP and CT during hepatic arteriography (CTHA), and the prognosis of hepatocellular nodules associated with liver cirrhosis [5]. CTAP and CTHA are recognized as the most sensitive modalities for detecting HCC and borderline lesions [6–12]; however, a less invasive and more accurate diagnostic procedure is preferable. A hepatocyte-specific contrast agent, gadolinium ethoxybenzyl diethylenetriamine pentaacetic acid (Gd-EOB-DTPA; Primovist®), was approved in Japan in January 2008. This contrast agent is hepatocyte specific and enhances the blood pool – it is taken up by hepatocytes and excreted into the biliary tract. The liver parenchyma is strongly stained white in the hepatocyte phase on T1-weighted images, 20 min after the intravenous injection of Gd-EOB-DTPA. This liver-specific MRI phase has been reported to increase the detection of focal liver lesions, including HCC [13–17], and is expected to detect early pathological change in hepatocarcinogenesis [18–20]. Hypointense lesions in the hepatobiliary phase of Gd-EOB-DTPA-enhanced MRI that show nonhypervascularity on dynamic imaging are commonly encountered, and it is recommended that these lesions be monitored closely due to their potential for malignancy and transitioning to HCC through a multistep progression of hepatocarcinogenesis [21–23]. Several studies have reported the outcome of patients with these hypointense lesions [22–29]; however, only a small number of such cases have been reported and all were from a single center. The present investigation was a longitudinal retrospective nationwide study that examined the natural outcome of nonhypervascular lesions in the hepatobiliary phase of Gd-EOB-DTPA-enhanced MRI.

Materials and Methods

Our retrospective analysis of data was approved by the institutional review board of Kinki University Faculty of Medicine. The requirement to obtain informed consent was waived.

Patients

Between February 2008 and March 2011, 224 patients with 504 nodules that were diagnosed as nonhypervascular by imaging modalities including Gd-EOB-DTPA-enhanced MRI were recruited from institutions that participated in the present study. Baseline characteristics of the patients are shown in table 1.

Image Analysis: Evaluation of Tumor Vascularity

Evaluation of tumor vascularity was performed using at least 2 imaging modalities including Gd-EOB-DTPA-enhanced MRI at each institution according to the local standard of care. All im-

Table 2. Characteristics of vascularized and nonvascularized nodules

Variables	Hypervascularization		p value
	yes (n = 173)	no (n = 331)	
Tumor size, mm	9.74±4.04	9.11±4.04	0.059
Past history of HCC treatment (yes/no)	139/34	232/99	0.014
Precontrast MRI T1WI (hyper-iso/low)	24/149	27/304	0.061
Fat containing nodule on in- and opposed-phase images (yes/no)	36/137	64/267	0.72
Precontrast MRI T2WI (hyper/iso-low)	25/148	28/303	0.037
Dynamic image[1] arterial phase (iso/low)	108/65	235/96	0.0501
Dynamic image[1] portal phase (iso/low)	124/49	245/86	0.59
Observation period, days	379	566	0.00

Continuous variables are expressed as median with range. T1WI = T1-weighted imaging; T2WI = T2-weighted imaging; hyper = hyperintensity; iso = iso intensity; low = low intensity on MRI.

[1] Dynamic image means any of the available modalities were used (Gd-EOB-DTPA-enhanced MRI, dynamic CT, contrast-enhanced US, CTHA and CTAP). When CTHA and CTAP were performed, we adopted those image findings.

ages were interpreted independently by an experienced board-certified radiologist or gastroenterologist who knew that the patients were at risk for HCC but had no other clinical information. A nonhypervascular nodule was defined as a nodule in which all parts showed nonhypervascularity relative to the surrounding liver parenchyma during the arterial phase of dynamic imaging when any of the available modalities were used (Gd-EOB-DTPA-enhanced MRI, dynamic CT, CTHA and contrast-enhanced US). The exclusion criteria for hypointense lesions in the hepatobiliary-phase image of Gd-EOB-DTPA-enhanced MRI were as follows: (a) hypervascularity on initial dynamic MRI (i.e. exclusion of classical HCC and other hypervascular tumors); (b) delayed enhancement on initial dynamic MRI (i.e. exclusion of slow-filling hemangiomas); (c) strong high intensity on T2-weigthed images (i.e. excluding cysts), and (d) lesion size of <2 mm (since the slice thickness for the hepatobiliary phase of Gd-EOB-DTPA-enhanced MRI was 3 mm).

Statistical Analysis

Continuous variables were presented as the median and range. Continuous variables such as tumor size and observation period were compared by Mann-Whitney U test, and other categorical variables were compared by Fisher's exact test or χ^2 test. Based on the analysis of lesions, the cumulative risk of a nonhypervascular tumor turning into classical HCC was calculated according to the Kaplan-Meier method. We calculated relative risk using Cox proportional hazard regression analysis. Based on the analysis of tumors, hypervascularization curves were constructed according to the Kaplan-Meier method, and the log-rank test was used for statistical comparisons. A p value <0.05 was considered to denote a statistically significant difference. All analyses were performed with SPSS statistics software (version 11, SPSS, Chicago, Ill., USA) for Microsoft Windows.

Table 3. Univariate analysis

Variables	p value
Tumor diameter >11 mm	**0.018**
Previous treatment history for HCC	**0.023**
Coexistence of hypervascular HCC	0.32
MRI finding	
T1-weighted imaging	**0.00**
T2-weighted imaging	**0.004**
Fat-containing nodule on in- and opposed-phase images	0.84
Image findings of dynamic study[1]	
Arterial phase	0.06
Portal phase	0.30

Bold p values are statistically significant.

[1] Dynamic study means any of the available modalities were used (Gd-EOB-DTPA-enhanced MRI, dynamic CT, contrast-enhanced US, CTHA and CTAP). When CTHA and CTAP were performed, we adopted those image findings.

Results

Nodule Characteristics

Table 2 shows the characteristics of the nodules that were vascularized and those that were not. Of the 504 nodules, 173 (34.3%) showed hypervascular transformation in the arterial phase of dynamic imaging during the follow-up period. The results of data analysis using Fish-

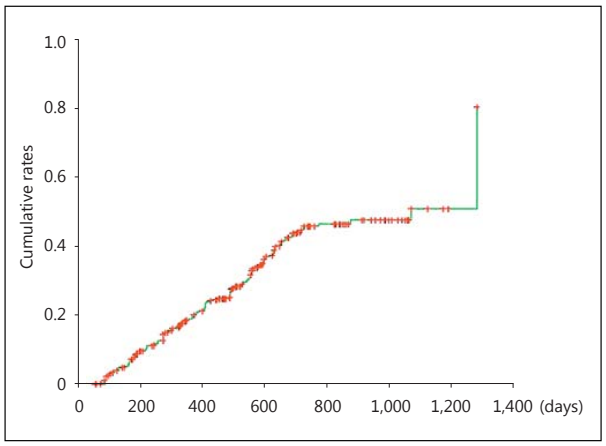

Fig. 1. Cumulative rates for hypointense lesions to hypervascularization. The cumulative rates for hypointense lesions that became classical HCC were 14.9% at 1 year and 45.8% at 2 years.

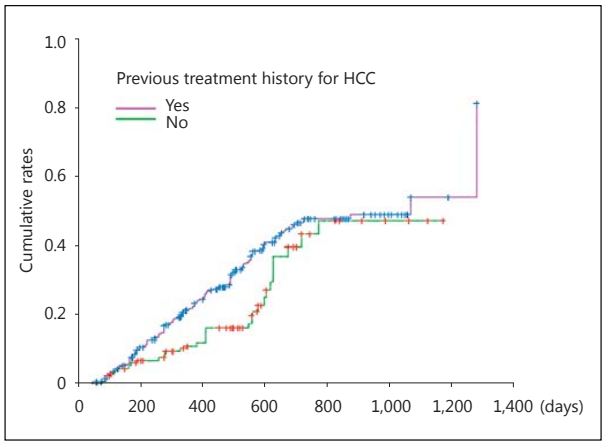

Fig. 2. Differences in the incidence of hypervascular transformation in relation to previous treatment history for HCC. The log-rank test p value was 0.023, indicating that the incidence of hypervascular transformation was significantly higher among patients who had a previous history of treatment for HCC.

er's exact test showed that, at the start of follow-up, nodules with and without vascularization showed significant differences in the proportion of patients who had a past history of HCC (p = 0.014) and the incidence of tumors displaying hyperintensity on T2-weighted images (p = 0.037). There were no differences between nodules with and without vascularization with respect to average tumor diameter, T1-weighted images, being fat containing on in- and opposed-phase images, and arterial and portal-phase images of dynamic study.

Table 4. Multivariate analysis

Variables	Relative risk	95% CI	p value
Previous treatment history for HCC (yes)	1.498	1.026–2.187	**0.036**
Tumor diameter >11 mm	1.344	0.971–1.860	0.075
T1-weighted imaging (low)	0.979	0.675–1.420	0.910
T2-weighted imaging (hyper)	1.724	1.111–2.673	**0.015**

Bold p values are statistically significant.

Cumulative Incidence of Hypervascular Transformation

The overall cumulative incidence of hypervascular transformation was 14.9% at 12 months and 45.8% at 24 months (fig. 1). Univariate analysis using the log-rank test revealed that a past history of HCC, tumor diameter >11 mm, and T1- and T2-weighted images were correlated with hypervascular transformation (table 3). Next, the four significant factors identified by univariate analysis were analyzed by multivariate analysis using the Cox regression model (table 4). Previous treatment history for HCC (relative risk = 1.498; p = 0.036, 95% CI 1.03–2.19) and hyperintensity on T2-weighted images (relative risk = 1.724; p = 0.015, 95% CI 1.11–2.67) were identified as independent factors for hypervascular transformation. Subsequently, we compared the incidence of hypervascular transformation of tumors with these risk factors based on the Kaplan-Meier curve. The incidence of hypervascularization was significantly higher in the groups with these prognostic factors (fig. 2–4).

Discussion

Since the introduction of Gd-EOB-DTPA-enhanced MRI in clinical practice, there have been several reports describing the effectiveness of the hepatobiliary phase of Gd-EOB-DTPA-enhanced MRI for the detection of HCC, including early HCC, because these lesions tend to show hypointensity on hepatobiliary-phase images [17, 30]. Although these hypointense lesions have been reported to exhibit a high rate of hypervascular transformation [22–29], the natural histories of such nodules had not

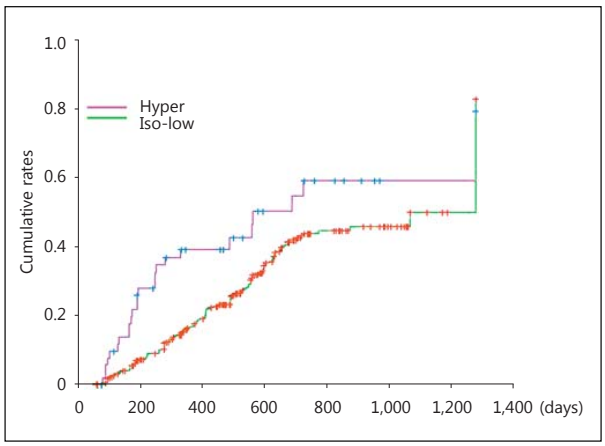

Fig. 3. Differences in the incidence of hypervascular transformation in relation to the T2-weighted images. The log-rank test p value was 0.004, indicating that the incidence of hypervascular transformation was significantly higher for hyperintense tumors.

been investigated in a nationwide study involving a large number of cases. Therefore, we aimed to identify tumor imaging findings associated with subsequent hypervascular transformation in nonhypervascular tumors that show hypointensity in the hepatobiliary phase of Gd-EOB-DTPA-enhanced MRI in patients with chronic liver diseases. Among the initial imaging findings analyzed in the present study, previous treatment history for HCC and hyperintensity on T2-weighted images were significantly correlated with hypervascular transformation, indicating that these parameters may be useful predictive marker factors for hypervascular transformation of nonhypervascular tumors. Even though we performed curative therapy by resection or radiofrequency ablation to prevent HCC recurrence, the recurrence rate was nonetheless extremely high [31–33]. A longer duration of infection with hepatitis B or C virus is usually associated with progression of liver fibrosis. In that condition, oxidative stress in the liver is considered to be higher, and genetic and epigenetic mechanisms activate oncogenes and inactivate tumor suppressor genes. Activation of these pathological processes results in hepatocarcinogenesis [34–36]. Patients who have a previous history of treatment for HCC are likely to have suffered from the condition for a long time, resulting in a high prevalence of hepatocarcinogenesis. Considering this status, it is speculated that nonhypervascular tumors of patients who have past history of HCC have been suffering such an oxidative stress for a long time, leading to hypervascular transformation as the next step at an earlier period. Another variable associated with an increased risk of hypervascular transformation was hyperintensity on T2-weighted images. Hyodo et al. [27] reported that the most important variable associated with an increased risk of hypervascular transformation was hyperintensity on T2-weighted images. They discussed that T2-weighted images might reflect peliotic changes in the intratumoral sinusoids of HCC, and that nodular regeneration, fibrosis and scarring that occur in the course of cirrhosis occasionally appear as hyperintense round lesions on T2-weighted images. For that reason, it is speculated that nonhypervascular tumors, for example dysplastic nodules with fibrosis and scarring, can be hyperintense on T2-weighted images [37, 38]. The findings from our present study suggest that the combination of T2-weighted images and hepatobiliary-phase images of Gd-EOB-DTPA-enhanced MRI could be useful in the prediction of hypervascular transformation of previously nonhypervascular nodules.

Based on patient background in the present study, the enrolled patients are considered to represent the daily practice of patients who are suffering from chronic liver diseases. Therefore, when we detected nonhypervascular tumors on hepatobiliary-phase image, it was important to recheck the findings of the T2 image of the precontrast MRI and to confirm the presence or absence of treatment history for HCC. Although we conducted a cooperative study and collected many nonhypervascular tumors and investigated the natural outcome of hypointense lesions in a nationwide manner, this study did have some limitations. The principal limitation was the variety of imaging equipment used. This limitation may have been inevitable because this was a multicenter study. Second, this was a retrospective study and, therefore, on imaging analysis our study was potentially limited by consensus review, although well-trained radiologists and physicians reviewed the images. Third, the interval between follow-up examinations was not consistent; a fixed follow-up interval would have enabled us to calculate more accurately. Fourth was the lack of a pathological diagnosis of the nodules examined. However, we consider that our image-based findings have clinical implications even though the pathological findings were unknown. Also, the purpose of the present study was to evaluate the incidence and predictive factors for hypervascular transformation in nonhypervascular tumors detected on the hepatobiliary phase of Gd-EOB-DTPA-enhanced MRI, not to distinguish between dysplastic nodules, early HCCs and well-differentiated HCCs that show to be nonhypervascular on dynamic study.

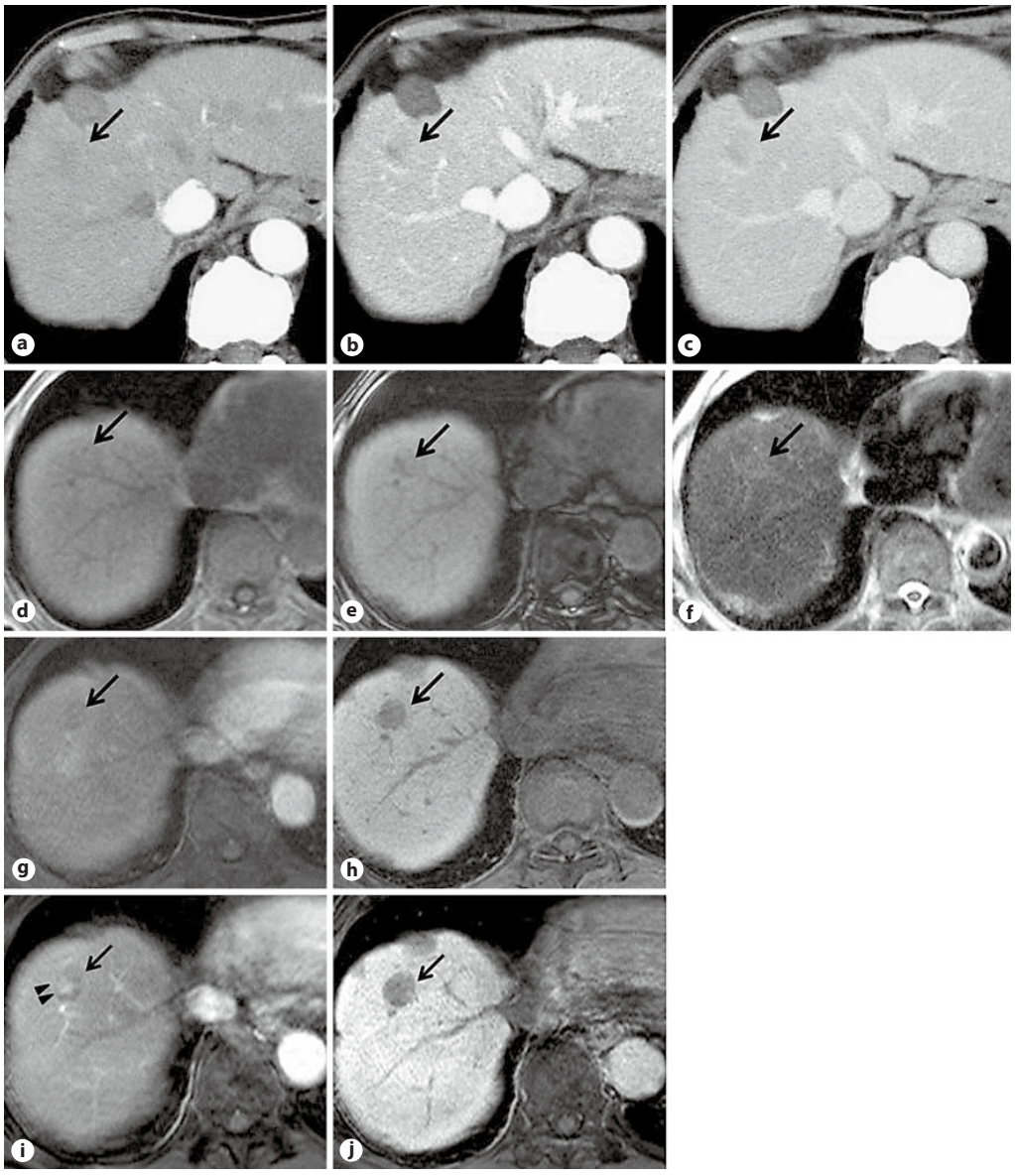

Fig. 4. A 79-year-old man with hepatitis C-related cirrhosis. **a–c** Initial dynamic CT. The hepatic nodule in segment 8 of the liver showed no contrast enhancement (arrow). **d–e** Initial Gd-EOB-DTPA-enhanced MRI. The nodule showed fat deposition on chemical-shift imaging (arrow, in-phase, **d**; out-of phase, **e**). On T2-weighted imaging, the nodule showed slight hyperintensity (arrow, **f**). Images for the arterial phase (arrow, **g**) and hepatobiliary phase (arrow, **h**) of Gd-EOB-DTPA-enhanced MRI at the start of follow-up showed a hypointense nodule. **i** The arterial-phase image from Gd-EOB-DTPA-enhanced MRI 16 months after the start of follow-up showed a hypervascular spot in the nodule: tumor (arrow), hypervascular spot (arrowheads). **j** A hepatobiliary-phase image of Gd-EOB-DTPA-enhanced MRI 16 months after the start of follow-up showed a markedly hypointense nodule (arrow).

In conclusion, patients who have a previous treatment history for HCC and with hypointense nodules showing hyperintensity on T2-weighted images need careful follow-up because of the high incidence of hypervascular transformation.

Disclosure Statement

The authors have no conflicts of interest to declare.

References

1 Kudo M: Early hepatocellular carcinoma: definition and diagnosis. Liver Cancer 2013;2:69–72.
2 Lee JM, Yoon JH, Joo I, Woo HS: Rencet advances in CT and MR imaging for evaluation of hepatocellular carcinoma. Liver Cancer 2012;1:22–40.
3 Joo I, Choi BI: New paradigm for management of hepatocellular carcinoma by imaging. Liver Cancer 2012;1:94–109.
4 Shinmura R, Matsui O, Kadoya M, Kobayashi S, Terayama N, Sanada J, Demachi H, Gabata T: Detection of hypervascular malignant foci in borderline lesions of hepatocellular carcinoma: comparison of dynamic multi-detector row CT, dynamic MR imaging and superparamagnetic iron oxide-enhanced MR imaging. Eur Radiol 2008;18:1918–1924.
5 Hayashi M, Matsui O, Ueda K, Kawamori Y, Gabata T, Kadoya M: Progression to hypervascular hepatocellular carcinoma: correlation with intranodular blood supply evaluated with CT during intraarterial injection of contrast material. Radiology 2002;225:143–149.
6 Matsui O, Kadoya M, Suzuki M, Inoue K, Itoh H, Ida M, Takashima T: Work in progress: dynamic sequential computed tomography during arterial portography in the detection of hepatic neoplasms. Radiology 1983;146:721–727.
7 Matsui O, Kadoya M, Kameyama T, Yoshikawa J, Takashima T, Nakanuma Y, Unoura M, Kobayashi K, Izumi R, Ida M, et al: Benign and malignant nodules in cirrhotic livers: distinction based on blood supply. Radiology 1991;178:493–497.
8 Ueda K, Matsui O, Kawamori Y, Nakanuma Y, Kadoya M, Yoshikawa J, Gabata T, Nonomura A, Takashima T: Hypervascular hepatocellular carcinoma: evaluation of hemodynamics with dynamic CT during hepatic arteriography. Radiology 1998;206:161–166.
9 Hayashi M, Matsui O, Ueda K, Kawamori Y, Kadoya M, Yoshikawa J, Gabata T, Takashima T, Nonomura A, Nakanuma Y: Correlation between the blood supply and grade of malignancy of hepatocellular nodules associated with liver cirrhosis: evaluation by CT during intraarterial injection of contrast medium. AJR Am J Roentgenol 1999;172:969–976.
10 Inoue E, Fujita M, Hosomi N, Sawai Y, Hashimoto T, Kuroda C, Nakano H, Sasaki Y, Ishiguro S: Double phase CT arteriography of the whole liver in the evaluation of hepatic tumors. J Comput Assist Tomogr 1998;22:64–68.
11 Murakami T, Takamura M, Kim T, Hori M, Federle MP, Onishi H, Tomoda K, Nakamura H: Double phase CT during hepatic arteriography for diagnosis of hepatocellular carcinoma. Eur J Radiol 2005;54:246–252.
12 Bruix J, Sherman M, Llovet JM, Beaugrand M, Lencioni R, Burroughs AK, Christensen E, Pagliaro L, Colombo M, Rodes J: Clinical management of hepatocellular carcinoma: conclusions of the Barcelona-2000 EASL conference – European Association for the Study of the Liver. J Hepatol 2001;35:421–430.
13 Huppertz A, Balzer T, Blakeborough A, Breuer J, Giovagnoni A, Heinz-Peer G, Laniado M, Manfredi RM, Mathieu DG, Mueller D, et al: Improved detection of focal liver lesions at MR imaging: multicenter comparison of gadoxetic acid-enhanced MR images with intraoperative findings. Radiology 2004;230:266–275.
14 Halavaara J, Breuer J, Ayuso C, Balzer T, Bellin MF, Blomqvist L, Carter R, Grazioli L, Hammerstingl R, Huppertz A, et al: Liver tumor characterization: comparison between liver-specific gadoxetic acid disodium-enhanced MRI and biphasic CT – a multicenter trial. J Comput Assist Tomogr 2006;30:345–354.
15 Kim YK, Kim CS, Han YM, Kwak HS, Jin GY, Hwang SB, Chung GH, Lee SY, Yu HC: Detection of hepatocellular carcinoma: gadoxetic acid-enhanced 3-dimensional magnetic resonance imaging versus multi-detector row computed tomography. J Comput Assist Tomogr 2009;33:844–850.
16 Kim SH, Lee J, Kim MJ, Jeon YH, Park Y, Choi D, Lee WJ, Lim HK: Gadoxetic acid-enhanced MRI versus triple-phase MDCT for the preoperative detection of hepatocellular carcinoma. AJR Am J Roentgenol 2009;192:1675–1681.
17 Inoue T, Kudo M, Komuta M, Hayaishi S, Ueda T, Takita M, Kitai S, Hatanaka K, Yada N, Hagiwara S, et al: Assessment of Gd-EOB-DTPA-enhanced MRI for HCC and dysplastic nodules and comparison of detection sensitivity versus MDCT. J Gastroenterol 2012;47:1036–1047.
18 Tanimoto A, Lee JM, Murakami T, Huppertz A, Kudo M, Grazioli L: Consensus report of the 2nd International Forum for Liver MRI. Eur Radiol 2009;19(suppl 5):S975–S989.
19 Kogita S, Imai Y, Okada M, Kim T, Onishi H, Takamura M, Fukuda K, Igura T, Sawai Y, Morimoto O, et al: Gd-EOB-DTPA-enhanced magnetic resonance images of hepatocellular carcinoma: correlation with histological grading and portal blood flow. Eur Radiol 2010;20:2405–2413.
20 Kitao A, Zen Y, Matsui O, Gabata T, Kobayashi S, Koda W, Kozaka K, Yoneda N, Yamashita T, Kaneko S, et al: Hepatocellular carcinoma: signal intensity at gadoxetic acid-enhanced MR imaging – correlation with molecular transporters and histopathologic features. Radiology 2010;256:817–826.
21 Takayama T, Makuuchi M, Hirohashi S, Sakamoto M, Okazaki N, Takayasu K, Kosuge T, Motoo Y, Yamazaki S, Hasegawa H: Malignant transformation of adenomatous hyperplasia to hepatocellular carcinoma. Lancet 1990;336:1150–1153.
22 Kumada T, Toyoda H, Tada T, Sone Y, Fujimori M, Ogawa S, Ishikawa T: Evolution of hypointense hepatocellular nodules observed only in the hepatobiliary phase of gadoxetate disodium-enhanced MRI. AJR Am J Roentgenol 2011;197:58–63.
23 Akai H, Matsuda I, Kiryu S, Tajima T, Takao H, Watanabe Y, Imamura H, Kokudo N, Akahane M, Ohtomo K: Fate of hypointense lesions on Gd-EOB-DTPA-enhanced magnetic resonance imaging. Eur J Radiol 2012;81:2973–2977.
24 Motosugi U, Ichikawa T, Sano K, Sou H, Onohara K, Muhi A, Amemiya F, Enomoto N, Matsuda M, Fujii H, et al: Outcome of hypovascular hepatic nodules revealing no gadoxetic acid uptake in patients with chronic liver disease. J Magn Reson Imaging 2011;34:88–94.
25 Takayama Y, Nishie A, Nakayama T, Asayama Y, Ishigami K, Kakihara D, Ushijima Y, Fujita N, Hirakawa M, Honda H: Hypovascular hepatic nodule showing hypointensity in the hepatobiliary phase of gadoxetic acid-enhanced MRI in patients with chronic liver disease: prediction of malignant transformation. Eur J Radiol 2012;81:3072–3078.

26 Kobayashi S, Matsui O, Gabata T, Koda W, Minami T, Ryu Y, Kozaka K, Kitao A: Relationship between signal intensity on hepatobiliary phase of gadolinium ethoxybenzyl diethylenetriaminepentaacetic acid (Gd-EOB-DTPA)-enhanced MR imaging and prognosis of borderline lesions of hepatocellular carcinoma. Eur J Radiol 2012;81:3002–3009.

27 Hyodo T, Murakami T, Imai Y, Okada M, Hori M, Kagawa Y, Kogita S, Kumano S, Kudo M, Mochizuki T: Hypovascular nodules in patients with chronic liver disease: risk factors for development of hypervascular hepatocellular carcinoma. Radiology 2013;266:480–490.

28 Higaki A, Ito K, Tamada T, Teruki S, Yamamoto A, Higashi H, Kanki A, Sato T, Noda Y: High-risk nodules detected in the hepatobiliary phase of Gd-EOB-DTPA-enhanced MR imaging in cirrhosis or chronic hepatitis: incidence and predictive factors for hypervascular transformation, preliminary results. J Magn Reson Imaging 2013;37:1377–1383.

29 Takechi M, Tsuda T, Yoshioka S, Murata S, Tanaka H, Hirooka M, Mochizuki T: Risk of hypervascularization in small hypovascular hepatic nodules showing hypointense in the hepatobiliary phase of gadoxetic acid-enhanced MRI in patients with chronic liver disease. Jpn J Radiol 2012;30:743–751.

30 Sano K, Ichikawa T, Motosugi U, Sou H, Muhi AM, Matsuda M, Nakano M, Sakamoto M, Nakazawa T, Asakawa M, et al: Imaging study of early hepatocellular carcinoma: usefulness of gadoxetic acid-enhanced MR imaging. Radiology 2011;261:834–844.

31 Shiina S, Tateishi R, Arano T, Uchino K, Enooku K, Nakagawa H, Asaoka Y, Sato T, Masuzaki R, Kondo Y, et al: Radiofrequency ablation for hepatocellular carcinoma: 10-year outcome and prognostic factors. Am J Gastroenterol 2012;107:569—577, quiz 578.

32 Wood TF, Rose DM, Chung M, Allegra DP, Foshag LJ, Bilchik AJ: Radiofrequency ablation of 231 unresectable hepatic tumors: indications, limitations, and complications. Ann Surg Oncol 2000;7:593–600.

33 Cho YK, Rhim H, Noh S: Radiofrequency ablation versus surgical resection as primary treatment of hepatocellular carcinoma meeting the Milan criteria: a systematic review. J Gastroenterol Hepatol 2011;26:1354–1360.

34 Nishida N, Goel A: Genetic and epigenetic signatures in human hepatocellular carcinoma: a systematic review. Curr Genomics 2011;12:130–137.

35 Nishida N, Kudo M, Nagasaka T, Ikai I, Goel A: Characteristic patterns of altered DNA methylation predict emergence of human hepatocellular carcinoma. Hepatology 2012;56:994–1003.

36 Nishida N, Kudo M: Recent advancements in comprehensive genetic analyses for human hepatocellular carcinoma. Oncology 2013;84(suppl 1):93–97.

37 Ohtomo K, Baron RL, Dodd GD 3rd, Federle MP, Ohtomo Y, Confer SR: Confluent hepatic fibrosis in advanced cirrhosis: evaluation with MR imaging. Radiology 1993;189:871–874.

38 Kim T, Baron RL, Nalesnik MA: Infarcted regenerative nodules in cirrhosis: CT and MR imaging findings with pathologic correlation. AJR Am J Roentgenol 2000;175:1121–1125.

Digestive Diseases

Dig Dis 2013;31:480–484
DOI: 10.1159/000355254

Radiofrequency Ablation for Hepatic Malignancies: Is Needle Tract Cauterization Necessary for Preventing Iatrogenic Bleeding?

Yasunori Minami Sosuke Hayaishi Masatoshi Kudo

Department of Gastroenterology and Hepatology, Kinki University School of Medicine, Osakasayama, Japan

Key Words
Bleeding · Complications · Hepatic malignancy · Needle tract cauterization · Radiofrequency ablation

Abstract
Objective: To evaluate whether iatrogenic hemorrhage can be prevented by intrahepatic tract ablation following radiofrequency ablation (RFA) therapy for hepatic malignancies. ***Methods:*** A retrospective cohort study analyzing a prospective database in a single institution was conducted. The incidence of postprocedural complications was compared in two groups: one with cauterization of the needle tracts after RFA and the other without. ***Results:*** The complication rates of intraperitoneal hemorrhage were 1.05% (4/380) and 0.92% (6/652) in the nonablation group and the ablation group, respectively (p = 0.90). All of these 10 patients with iatrogenic bleeding were classified as Child-Pugh grade A. Among the 15 hemodialysis patients in this study, hemorrhage was seen in 2 (13.3%), compared with 8 (0.79%) of the nonhemodialysis patients (p = 0.0002). There were no statistically significant differences in the incidence of other complications including pleural effusion, serous ascites, pneumothorax, hemothorax, hepatic infarction, bile duct injury and pericardial effusion between the two groups. Gastrointestinal perforation, peritonitis or tumor seeding were not observed. ***Conclusion:*** Our study found a high incidence of bleeding after RFA among hemodialysis patients. Irrespective of tract ablation being after RFA, iatrogenic hemorrhage appeared to be equivalent in this population.

Introduction

Percutaneous radiofrequency ablation (RFA) has been accepted as a safe and effective technique for the treatment of unresectable hepatic primary and metastatic malignancies [1–8]. Although the advantages of the use of RFA include low mortality and morbidity [9], early detection and treatment of complications is essential for a favorable RFA outcome.

General complications of RFA may be related to imaging-guided electrode placement (e.g. bleeding, arterial-portal shunt, tumor seeding, pneumothorax), thermal therapy (e.g. nontarget thermal damage, grounding pad burns) or others (e.g. infection, infarction) [10–13]. Intraperitoneal bleeding is a serious complication that can result in mortality if not appropriately managed. This bleeding can develop from direct mechanical injury to the vascular structure by the radiofrequency (RF) needle electrode rather than from RF thermal injury to the vessel. Thus, the potential for bleeding depends on placement of the RF needle electrode without traversing major

KARGER

E-Mail karger@karger.com
www.karger.com/ddi

0257–2753/13/0316–0480$38.00/0

Masatoshi Kudo, MD, PhD
Department of Gastroenterology and Hepatology
Kinki University Faculty of Medicine
377-2 Ohno-Higashi, Osakasayama, Osaka 589-8511 (Japan)
E-Mail m-kudo@med.kindai.ac.jp

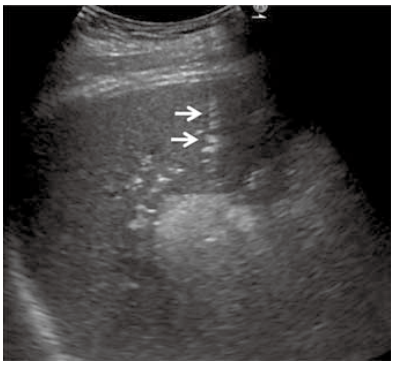

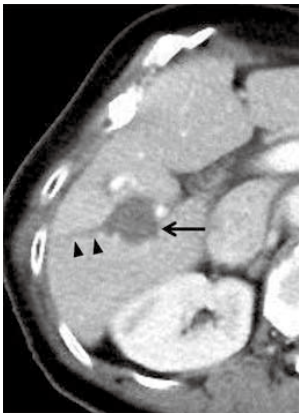

Fig. 1. Linear hyperechogenicity following RFA was seen along the RF needle tract on B-mode US (arrows).
Fig. 2. An 80-year-old woman with an HCC. Contrast-enhanced CT showed that the ablated tumor (arrow) was not enhanced in segment VI of the liver. The ablated needle tract is depicted as a low-density line (arrowheads).

vessels and minimizing the amount of needle repositioning. In addition, cauterization of the needle tracts is thought to prevent bleeding after percutaneous RFA. However, to our knowledge, no previous studies have evaluated whether needle tract ablation actually contributes to reducing postprocedural bleeding. The purpose of this study was to assess whether intraperitoneal hemorrhage is prevented by intrahepatic tract ablation following RFA for hepatic malignancies.

Materials and Methods

Patients

Written informed consent to perform percutaneous RFA was obtained from all patients before treatment. This cohort study was conducted as a retrospective analysis of a prospective database in a single institution in which RFAs are routinely performed. After the introduction of RFA, our hospital has conducted procedures with or without intrahepatic tract ablation based on the preferences of two senior doctors. The records of consecutive patients who did or did not receive intrahepatic tract ablation following RFA or not between January 2007 and June 2011 at Kinki University Hospital were reviewed.

Hepatocellular carcinoma (HCC) was diagnosed based on three-phase contrast-enhanced CT findings such as positive enhancement in the arterial phase and washout in the equilibrium phase in patients with chronic liver disease. Liver metastases were diagnosed by ring enhancement on contrast-enhanced CT in patients with past cancer illness. Intrahepatic cholangiocarcinoma has been described as an irregular mass with markedly low attenuation, and minimal peripheral enhancement noted with ancillary findings in dilatation of the peripheral intrahepatic ducts. All patients met the following criteria for treatment with RFA: percutaneous accessibility of the tumors, absence of portal tumor thrombus and extrahepatic metastasis, prothrombin time ratio greater than 50%, total bilirubin less than 4.0 mg/dl and platelet count greater than 30,000/μl.

Equipment and Technique

B-mode ultrasound (US) scans were obtained using a LOGIQ 7 (GE Medical Systems, Milwaukee, Wisc., USA) or an EUB 8500 unit (HITACHI Medico, Tokyo, Japan). A multidetector CT (LightSpeed VCT, GE Medical Systems, Milwaukee, Wisc., USA) was used for diagnosis. Triple-phase contrast-enhanced CT scans were performed with a 5.0-mm slice thickness at 30, 60 and 180 s after initiating the injection of contrast media to obtain hepatic arterial-, portal venous- and equilibrium-phase images, respectively. A total of 100 ml of nonionic contrast material containing 300 mg of iodine per milliliter (Iomeprol, Eisai Co., Tokyo, Japan) was injected intravenously at a rate of 3 ml/s using an automatic power injector.

Patients were treated by RFA (Cooled-tip RF ablation system; Radionics, Burlington, Mass., USA). Twenty-centimeter-long, 17-gauge, monopolar internally cooled electrodes with 3- or 2-cm-long exposed metallic tips (Radionics) were used to deliver RF energy. A 200-Watt, 480-kHz monopolar RF generator regulated by impedance (CC-1; Radionics) was used as the energy source.

RFA is mainly performed percutaneously under B-mode US guidance. If necessary, it can also be used under the guidance of contrast-enhanced US or virtual CT/MRI US. After RF energy was delivered, the hyperechoic zone appeared and gradually increased at the ablated site with monitoring to assess the ablation. The ablation was stopped when the entire target (including the safety margin) was completely covered by the zone of hyperechogenicity. In patients with tract ablation, RF energy was delivered again before removing the RF needle. Thereafter, the RF needle was slowly withdrawn so that the linear hyperechogenicity passed along the RF needle tract (fig. 1).

Complications

We assessed the laboratory data obtained before and after RFA, including serum hemoglobin level, prothrombin time and platelet count. Furthermore, we obtained a CT scan of the liver from 1–5 days (median 3 days) after RFA for the assessment of treatment response (fig. 2). The maximum thickness of perihepatic ascites was also recorded using CT scans obtained before RFA and after RFA (fig. 3). We considered hemoperitoneum to be present if the attenuation of ascites had increased around the perihepatic spaces in patients with serum hemoglobin levels reduced by more than 1.0 g/dl in 1 day after RFA.

Dig Dis 2013;31:480–484
DOI: 10.1159/000355254

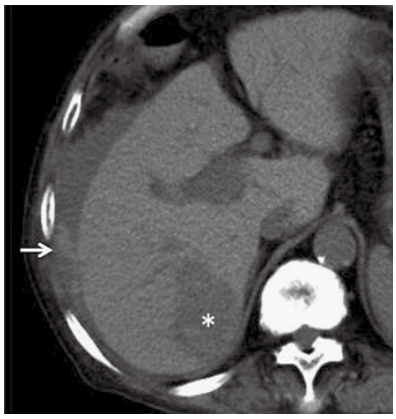

Fig. 3. A 65-year-old male hemodialysis patient with an HCC 2.5 cm in diameter. Plain CT detected the ablated area by RFA as low density (*). Ascitic fluid appeared and intraperitoneal hemorrhage was depicted as high attenuation in ascites (arrow).

Endpoint and Statistical Analysis

The primary endpoint was the incidence of intraperitoneal hemorrhage after percutaneous RFA. The secondary endpoint was the occurrence of other postprocedural complications during an observation period of at least 1 month after RFA, including pleural effusion, ascites, pneumothorax, hemothorax, hepatic infarction, bile duct injury, pericardial effusion, gastrointestinal perforation and peritonitis, etc.

All values were expressed as mean ± standard deviation (SD). Comparisons between the two groups were analyzed using Fisher's test. A χ^2 test was used to compare differences in the use of RFA modifications among the four groups. $p < 0.05$ was considered statistically significant. Statistical analyses were performed using SPSS software (version 12.0; SPSS, Chicago, Ill., USA).

Results

Baseline Characteristics of Patients

In total, 1,072 patients with 1,730 hepatic malignancies were enrolled. The patient population included 685 men and 347 women. The maximal diameter of tumors ranged from 0.5 to 11 cm on dynamic CT. Of all 1,072 patients who underwent percutaneous RFA for the treatment, 922 (86.0%) had HCC, 10 (0.9%) had intrahepatic cholangiocarcinoma and the other 99 (9.2%) had liver metastases, mostly from colorectal cancer.

Table 1 shows the characteristics of both groups. The distributions of sex and age were not different between the two groups. In the nonablation group, 316 (83.2%), 62 (16.3%) and 2 (0.5%) patients were classified with Child-Pugh A, B and C liver function, respectively, whereas 567 (87.0%), 80 (12.3%) and 5 (0.8%) patients in the ablation group were classified into Child-Pugh A, B and C, respectively. The proportions of patients with Child-Pugh classification did not differ significantly.

Table 1. Baseline clinical characteristics of patients

Characteristics	Nonablation group (380 patients/ 660 nodules)	Ablation group (652 patients/ 1,070 nodules)	p value
Sex, n			0.56
Male	248	437	
Female	132	215	
Age, years	67.9±9.5	69.0±9.8	0.57
Range	33–88	32–90	
Child-Pugh class, n			0.23
A	316	567	
B	62	80	
C	2	5	
Malignancies, n			0.18
HCC	331	591	
Intrahepatic cholangiocarcinoma	5	5	
Liver metastases	45	54	
Tumor size, cm	1.9±1.1	1.7±1.1	0.47
Range	0.5–11	0.5–8	
Tumor location in liver subsegments, n			0.19
Left lateral	101	161	
Left medial	92	116	
Right medial	243	448	
Right lateral	220	335	
Segment 1	4	10	

Data are presented as mean ± SD unless otherwise indicated.

Of 380 patients in the nonablation group, 596 patients underwent RFA for treatment of their primary liver tumor, including HCC (87.1%; 331/380) and intrahepatic cholangiocarcinoma (1.3%; 5/380). The other 45 (11.8%) had liver metastases including colorectal cancer (n = 30), gastric cancer (n = 6), ovarian cancer (n = 1), pancreatic cancer (n = 1), renal cell carcinoma (n = 1) and others (n = 6). In contrast, in the ablation group, 591 (90.6%), 5 (0.8%) and 54 (8.3%) patients had HCC, intrahepatic cholangiocarcinoma and metastatic liver tumors, respectively. Secondary hepatic malignancies included colorectal cancer (n = 35), gastric cancer (n = 4), ovarian cancer (n = 2), pancreatic cancer (n = 2), renal cell carcinoma (n = 3) and others (n = 8).

The tumor size was not significantly different between the two groups. The mean tumor diameter was 1.9 ± 1.1 cm (range 0.5–11 cm) in the nonablation group, and 1.7 ± 1.1 cm (range 0.5–8 cm) in the ablation group.

Table 2. Complications between groups

Complications	Nonablation group (n = 380)	Ablation group (n = 652)	p value
Intraperitoneal hemorrhage	6 (0.9)	4 (1.1)	0.90
Pleural effusion	27 (7.1)	31 (4.8)	0.11
Serous ascites	8 (2.1)	8 (1.2)	0.40
Pneumothorax	3 (0.8)	6 (0.9)	0.90
Hemothorax	3 (0.8)	4 (0.6)	0.95
Hepatic infarction	2 (0.5)	4 (0.6)	0.81
Bile duct injury	0	4 (0.6)	–
Pericardial effusion	0	1 (0.2)	–

Values in parentheses are percentages.

Intraperitoneal Hemorrhage

Table 2 shows the complications in both groups in this study. No death was considered RFA related.

Procedural hemorrhage occurred in 10 (0.93%) patients (HCC, n = 8; liver metastases, n = 2). In the nonablation group and the ablation group, the complication rates of hemorrhage were, respectively, 1.05% (4/380) and 0.92% (6/652). No significant difference was observed in the incidence of iatrogenic bleeding (p = 0.90). Fortunately, these patients did not need transcatheter arterial embolization for the treatment of iatrogenic bleeding after RFA, and improved with conservative therapy including blood transfusion. Of these 10 patients with bleeding, the platelet counts before ablation ranged from 48,000 to 325,000/μl (mean ± SD 12,600 ± 8,100). The prothrombin time before ablation was 67–103% (mean ± SD 85.0 ± 10.1), and all patients were classified as Child-Pugh grade A (5 points, n = 7; 6 points, n = 3). The mean tumor diameter was 2.1 ± 0.9 cm (range 0.9–11 cm).

Among the 15 hemodialysis patients in this study, hemorrhage was seen in 2 (13.3%), whereas 8 (0.79%) patients with bleeding were nonhemodialysis (p = 0.0002).

Other Complications

The complications of RFA excluding hemorrhage were pleural effusion, serous ascites, pneumothorax, hemothorax, hepatic infarction, bile duct injury and pericardial effusion (table 2). Gastrointestinal perforation, peritonitis and tumor seeding by RFA was not observed in this study. No significant differences were observed in the incidences of these complications between the two groups. Three patients with pneumothorax (nonablation group, n = 1; ablation group, n = 2) were treated with chest tube drainage, and the fluid was drained in a patient with pericardial effusion. The other patients with complications subsided after conservative treatments.

Discussion

The overall rate of intraperitoneal hemorrhage for 1,730 ablated lesions was 0.93% in our study, a value that coincides with other experiences. The rates of iatrogenic bleeding treated with percutaneous RFA have been reported to be 0.32–1.6% [14–21]. Arterial bleeding causes robust hemorrhage that could contribute to mortality, and transcatheter arterial embolization would be needed for interventional hemostasis.

When an RF electric current meets tissue resistance, the electrical energy is converted into thermal energy via molecular agitation or ohmic heating (direct heating). This heat could cause denaturation of vessels and blood coagulation. Thus, cauterization of the needle tracts is considered to prevent intraperitoneal bleeding through the injured vessels. Laeseke et al. [22] reported that biopsy sites after ablation had significantly less blood loss than did control biopsy sites using porcine liver or kidney. However, the volume of blood loss was very low, at less than 3 g, in the ablation group and control group from their data. Therefore, it could be expected that a RFA needle laparotomy technique could decrease nonarterial bleeding from the liver after a needle biopsy. Regardless of the procedure of hemostasis, nonarterial bleeding will stop in time without clinical problems.

In this study, no significant differences were observed in the incidence of iatrogenic bleeding between the nonablation group and the ablation group. Without needle tract cauterization, hemostasis can be achieved in several ways: (1) closure of the electrode puncture wound, (2) vascular spasm and (3) blood clotting or coagulation. Perihepatic bleeding might occur with disorders of these steps even in patients with tract ablation. It is considered from our results that needle tract cauterization does not contribute directly to hemostasis. Thus, intraperitoneal hemorrhage appeared to be equivalent regardless of nontract ablation following RFA.

The 10 patients with peritoneal hemorrhage were classified as Child-Pugh grade A, while many Child-Pugh B/C patients were included in this study. Intraperitoneal hemorrhage is usually related to mechanical injuries caused by the RF electrode traversing a vessel or thermal injuries sustained during ablation [15, 16]. The incidence of bleeding was thus not necessarily related to liver dys-

function, low levels of the platelets or the prothrombin time. However, our results showed a high incidence of bleeding among hemodialysis patients. Bleeding is common for patients with chronic renal failure, and is caused by the following: (1) increased capillary fragility, (2) disturbance of blood coagulation and (3) administration of heparin during dialysis. Therefore, we have to perform RFA carefully in hemodialysis patients. However, further studies are needed to clarify whether the iatrogenic hemorrhage could be prevented by needle tract cauterization following RFA in hemodialysis patients.

Our study was limited by its retrospective and nonrandomized design, leading to possible inaccurate or incomplete data collection, which may result in an underestimation of complications. The nonrandomized retrospective design is also known to be associated with possible selection case bias.

In conclusion, iatrogenic bleeding after RFA could contribute to several complicated situations including elevated blood pressure, the condition of injured arteries (branching vessel level, depth from the liver surface, capillary fragility), or past history of disease (chronic renal failure, chronic liver disease). Irrespective of needle tract cauterization following RFA, iatrogenic hemorrhage appeared to be equivalent in this population.

Disclosure Statement

The authors have no conflicts of interest to declare.

References

1 Rossi S, Di Stasi M, Buscarini E, Cavanna L, Quaretti P, Squassante E, Garbagnati F, Buscarini L: Percutaneous radiofrequency interstitial thermal ablation in the treatment of small hepatocellular carcinoma. Cancer J Sci Am 1995;1:73–81.

2 Kudo M: Local ablation therapy for hepatocellular carcinoma: current status and future perspective. J Gastroenterol 2004;39:205–214.

3 Shiina S, Teratani T, Obi S, Sato S, Tateishi R, Fujishima T, Ishikawa T, Koike Y, Yoshida H, Kawabe T, Omata M: A randomized controlled trial of radiofrequency ablation with ethanol injection for small hepatocellular carcinoma. Gastroenterology 2005;129:122–130.

4 Llovet JM, Bruix J: Novel advancements in the management of hepatocellular carcinoma in 2008. J Hepatol 2008;48(suppl 1):S20–S37.

5 Lencioni R, Crocetti L: Local-regional treatment of hepatocellular carcinoma. Radiology 2012;262:43–58.

6 Mahnken AH, Pereira PL, de Baère T: Interventional oncologic approaches to liver metastases. Radiology 2013;266:407–430.

7 Minami Y, Kudo M: Radiofrequency ablation of liver metastases from colorectal cancer: a literature review. Gut Liver 2013;7:1–6.

8 Lin S, Hoffmann K, Schemmer P: Treatment of hepatocellular carcinoma: a systematic review. Liver Cancer 2012;1:144–158.

9 Lin SM: Local ablation for hepatocellular carcinoma in Taiwan. Liver Cancer 2013;2:73–83.

10 Tateishi R, Shiina S, Teratani T, Obi S, Sato S, Koike Y, Fujishima T, Yoshida H, Kawabe T, Omata M: Percutaneous radiofrequency ablation for hepatocellular carcinoma: an analysis of 1,000 cases. Cancer 2005;103:1201–1209.

11 Livraghi T, Meloni F, Di Stasi M, Rolle E, Solbiati L, Tinelli C, Rossi S: Sustained complete response and complications rates after radiofrequency ablation of very early hepatocellular carcinoma in cirrhosis: is resection still the treatment of choice? Hepatology 2008;47:82–89.

12 Sato M, Tateishi R, Yasunaga H, Horiguchi H, Yoshida H, Matsuda S, Koike K: Mortality and morbidity of hepatectomy, radiofrequency ablation, and embolization for hepatocellular carcinoma: a national survey of 54,145 patients. J Gastroenterol 2012;47:1125–1133.

13 Hasegawa K, Kokudo N, Makuuchi M, Izumi N, Ichida T, Kudo M, Ku Y, Sakamoto M, Nakashima O, Matsui O, Matsuyama Y: Comparison of resection and ablation for hepatocellular carcinoma: a cohort study based on a Japanese nationwide survey. J Hepatol 2013;58:724–729.

14 Livraghi T, Solbiati L, Meloni MF, Gazelle GS, Halpern EF, Goldberg SN: Treatment of focal liver tumors with percutaneous radio-frequency ablation: complication encountered in a multicenter study. Radiology 2003;226:441–451.

15 Rhim H, Dodd GD 3rd, Chintapalli KN, Wood BJ, Dupuy DE, Hvizda JL, Sewell PE, Goldberg SN: Radiofrequency thermal ablation of abdominal tumors: lessons learned from complications. Radiographics 2004;24:41–52.

16 Chen MH, Yang W, Yan K, Gao W, Dai Y, Wang YB, Zhang XP, Yin SS: Treatment efficacy of radiofrequency ablation of 338 patients with hepatic malignant tumor and the relevant complications. World J Gastroenterol 2005;11:6395–6401.

17 Carrafiello G, Laganà D, Ianniello A, Craparo G, Recaldini C, Lumia D, Dionigi G, Cuffari S, Fugazzola C: Bleeding after percutaneous radiofrequency ablation: successful treatment with transcatheter embolization. Eur J Radiol 2007;61:351–355.

18 Kasugai H, Osaki Y, Oka H, Kudo M, Seki T, Osaka Liver Cancer Study Group: Severe complications of radiofrequency ablation therapy for hepatocellular carcinoma: an analysis of 3,891 ablations in 2,614 patients. Oncology 2007;721:72–75.

19 Poggi G, Riccardi A, Quaretti P, Teragni C, Delmonte A, Amatu A, Saini G, Mazzucco M, Bernardo A, Palumbo R, Canto A, Bernieri S, Bernardo G: Complications of percutaneous radiofrequency thermal ablation of primary and secondary lesions of the liver. Anticancer Res 2007;27:2911–2916.

20 Takaki H, Yamakado K, Nakatsuka A, Yamada T, Shiraki K, Takei Y, Takeda K: Frequency of and risk factors for complications after liver radiofrequency ablation under CT fluoroscopic guidance in 1,500 sessions: single-center experience. AJR Am J Roentgenol 2013;200:658–664.

21 Koda M, Murawaki Y, Hirooka Y, Kitamoto M, Ono M, Sakaeda H, Joko K, Sato S, Tamaki K, Yamasaki T, Shibata H, Shimoe T, Matsuda T, Toshikuni N, Fujioka S, Ohmoto K, Nakamura S, Kariyama K, Aikata H, Kobayashi Y, Tsutsui A: Complications of radiofrequency ablation for hepatocellular carcinoma in a multicenter study: an analysis of 16,346 treated nodules in 13,283 patients. Hepatol Res 2012;42:1058–1064.

22 Laeseke PF, Winter TC 3rd, Davis CL, Stevens KR, Johnson CD, Fronczak FJ, Webster JG, Lee FT Jr: Postbiopsy bleeding in a porcine model: reduction with radio-frequency ablation – preliminary results. Radiology 2003;227:493–499.

Digestive Diseases

Dig Dis 2013;31:485–489
DOI: 10.1159/000355257

Usefulness of the Extracted-Overlay Function in CT/MR-Ultrasonography Fusion Imaging for Radiofrequency Ablation of Hepatocellular Carcinoma

Yuki Makino[a] Yasuharu Imai[a] Takumi Igura[a] Sachiyo Kogita[a] Yoshiyuki Sawai[a]
Kazuto Fukuda[a] Masatoshi Hori[b] Masatoshi Kudo[c] Takamichi Murakami[d]

[a]Department of Gastroenterology, Ikeda Municipal Hospital, Ikeda, [b]Department of Radiology, Osaka University Graduate School of Medicine, Suita, and Departments of [c]Gastroenterology and Hepatology and [d]Radiology, Kinki University School of Medicine, Osakasayama, Japan

Key Words
Extracted-overlay function · Hepatocellular carcinoma · Radiofrequency ablation · Volume Navigation · Fusion imaging

Abstract
Objectives: We developed a novel technique of the extracted-overlay function in CT/MR-ultrasonography (US) fusion imaging for radiofrequency ablation (RFA), in which only a tumor extracted from CT/MR images with a virtual ablative margin of arbitrary thickness is overlaid on US. The usefulness of this function is investigated in this preliminary report. ***Methods:*** The volume data of the extracted tumor with a virtual ablative margin were created on an image-processing workstation, and transported into a US unit equipped with a CT/MR-US fusion imaging system. After the positional registration of US and transported images, the extracted tumor with an ablative margin could be overlaid on US. In RFA, using this function, an electrode was inserted targeting the overlaid tumor with an ablative safety margin of 5 mm on US, and the treatment effect was evaluated by dynamic CT. Treatment results of 23 consecutive hepatocellular carcinomas (HCCs) that underwent RFA using this function were retrospectively analyzed. ***Results:*** Complete tumor ablation was achieved in 22 (95.7%) and 1 (4.3%) HCCs in 1 and 2 treatment sessions, respectively. ***Conclusions:*** Due to the visualization of an extracted tumor with an ablative safety margin on a US image, even during and after ablation, this function is useful for treatment planning and guidance of RFA.

Introduction

The CT/MR-ultrasonography (US) fusion imaging system has recently been reported to be useful for radiofrequency ablation (RFA) of hepatocellular carcinoma (HCC) [1–5]. In this system, any cross-sectional multiplanar reconstruction images of CT or MR are synchronously displayed as reference images, side-by-side with US. This system has enabled RFA of HCCs with poor conspicuity on US and made it easy to evaluate the treatment effect at the bedside [1–4]. The CT/MR-US fusion imaging system is also capable of the overlay display of reference images on US, which directly indicates the location of the target tumor. However, it is difficult to perform RFA on the overlaid images, since background US usually becomes quite obscured [2, 3]. To solve this problem, we developed a novel technique which we call the extracted-overlay function, in which only the target tumor is ex-

KARGER

E-Mail karger@karger.com
www.karger.com/ddi

0257–2753/13/0316–0485$38.00/0

Yasuharu Imai, MD, PhD
Department of Gastroenterology, Ikeda Municipal Hospital
3-1-18 Johnan
Ikeda, Osaka 563-8510 (Japan)
E-Mail yasuimai@hosp.ikeda.osaka.jp

tracted from reference images and overlaid on US, together with a virtual safety ablative margin of arbitrary thickness around the tumor. This preliminary study aimed to investigate the feasibility and efficacy of this function for RFA.

Materials and Methods

Patients and Tumors

Our institutional review board approved this retrospective study and informed consent was waived. From November 2012 to January 2013, we conducted RFA with the extracted-overlay function for 18 consecutive patients with 23 HCCs diagnosed based on the typical imaging features or biopsy [6]. In this period, this function was used for all cases that underwent RFA.

CT and MRI Acquisition

Dynamic CT and CT angiography was conducted with the 64-channel multidetector row helical CT, MDCT (Discovery CT 750HD, GE Healthcare, Milwaukee, Wisc., USA) with slice thicknesses of 1.25 and 0.675 mm, respectively. For dynamic CT, patients were intravenously administered 2.0 ml/kg of nonionic contrast material with a concentration of 300 mg iodine (mgI)/ml, which was injected with a fixed duration of 30 s using an automatic injector. The arterial-, portal- and equilibrium-phase images were obtained at approximately 35–45, 65–80 and 190–205 s, respectively, after the initiation of the contrast material injection [7].

For CT angiography, two catheters were selectively placed, one in the superior mesenteric artery for CT during arterioportography (CTAP) and the other in the common hepatic artery for CT during hepatic arteriography (CTHA). CTAP images were obtained 30–33 s after injection of 66–80 ml of 150–160 mgI/ml nonionic contrast medium, at a rate of 2.0 ml/s. CTHA images were obtained 5–8 s after administration of 20–33 ml of 150–160 mgI/ml nonionic contrast material, at a rate of 1.0 ml/s [8].

Gadolinium ethoxybenzyl diethylenetriamine pentaacetic acid (Gd-EOB-DTPA)-enhanced MR images were acquired with a 1.5-tesla MR system (Signa Excite HD 1.5T, GE Healthcare). At first, an unenhanced MR imaging was obtained using a T1-weighted gradient-echo sequence (dual echoes; in-phase and out-of-phase). Then, unenhanced-, arterial-, portal-, late- and hepatobiliary-phase images were acquired just before, 25, 70, 180 s and 20 min, respectively, after bolus injection of 25 μmol/kg body weight (0.1 ml/kg) of Gd-EOB-DTPA at a rate of 2.0 ml/s, using a T1-weighted high-resolution sequence in a single breath hold (18–20 s) [6, 7]. Dynamic- and hepatobiliary-phase images were acquired with three-dimensional gradient-echo sequences (Liver Acquisition with Volume Acceleration, LAVA, GE Healthcare). The slice thickness of dynamic- and hepatobiliary-phase images were 5 and 3 or 5 mm, respectively.

The Extracted-Overlay Function

For the extracted-overlay function, the imaging modality in which a tumor was most clearly depicted was used as a reference (fig. 1a). CT or MR imaging data for a reference were imported into an image processing workstation (Advantage Workstation Volumeshare 4, GE Healthcare). At first, the contour of the tumor was traced on each slice by an operator of RFA and the tumor was extracted from the original images. Then, by tracing around the extracted tumor circumferentially using a virtual brush, we added a virtual safety margin to the extracted tumor. Since the thickness of the virtual brush can be freely modified, we can add a virtual ablative margin of arbitrary thickness. In this study, the thickness was set at 5 mm, which has been reported to be related with a low local tumor progression rate [9–11] (fig. 1b). The volume data of the extracted tumor and the tumor with a virtual ablative safety margin were saved in the digital imaging and communication in medicine, DICOM, format. Subsequently, these volume data were transported into a US unit (LOGIQ E9, GE Healthcare) equipped with a CT/MR-US fusion imaging system (Volume Navigation, GE Healthcare), together with the original CT or MR imaging data, and used as reference images. After the positional registration of US and the original images [1], these three data sets could be displayed together or separately as references, simultaneously with US. The color of each reference could be modified for clear discrimination.

Subsequently, by means of the overlay display, these three data sets were overlaid on US, together or individually. In this way, since only an extracted tumor, with or without a virtual ablative safety margin, could be overlaid, the background US images did not get obscured (fig. 1d).

RFA Procedure

RFA was performed by 1 of 3 operators with more than 10 years of experience, using a cool-tip single electrode with a 2- or 3-cm exposed tip (Cool-tip RF Ablation System, Covidien, Boulder, Colo., USA). We used artificial ascites when necessary.

Using the extracted-overlay function, an extracted tumor with a virtual ablative safety margin was overlaid on US. Targeting the overlaid tumor, an electrode was inserted and ablation was conducted. To achieve complete ablation of the tumor, together with a virtual ablative safety margin when possible, ablation was repeated.

After the ablation, we evaluated whether the overlaid tumor was completely encompassed with the spreading hyperechoic bubbling area [12, 13]. If an overlaid tumor was protruding from the bubbling area, additional ablation was performed until it was completely within the bubbling area.

Treatment Evaluation of RFA

The treatment effect was evaluated by the consensus of 2 radiologists with more than 10 years of experience, who were blind to the clinical information. We defined complete ablation as meeting all of the following conditions on dynamic CT performed within 7 days after RFA: (i) no sign of tumor stain was present around the coagulated area on the arterial phase and (ii) the coagulated area circumferentially extended beyond a tumor boundary in the portal and equilibrium phases. When residual tumor was suspected, additional ablation was conducted until these conditions were satisfied.

Results

All 18 patients with 23 HCCs were treated without major complications. The profiles of these patients are listed in table 1. The time required for the preparation of the extracted-overlay function was less than 30 min in all cases.

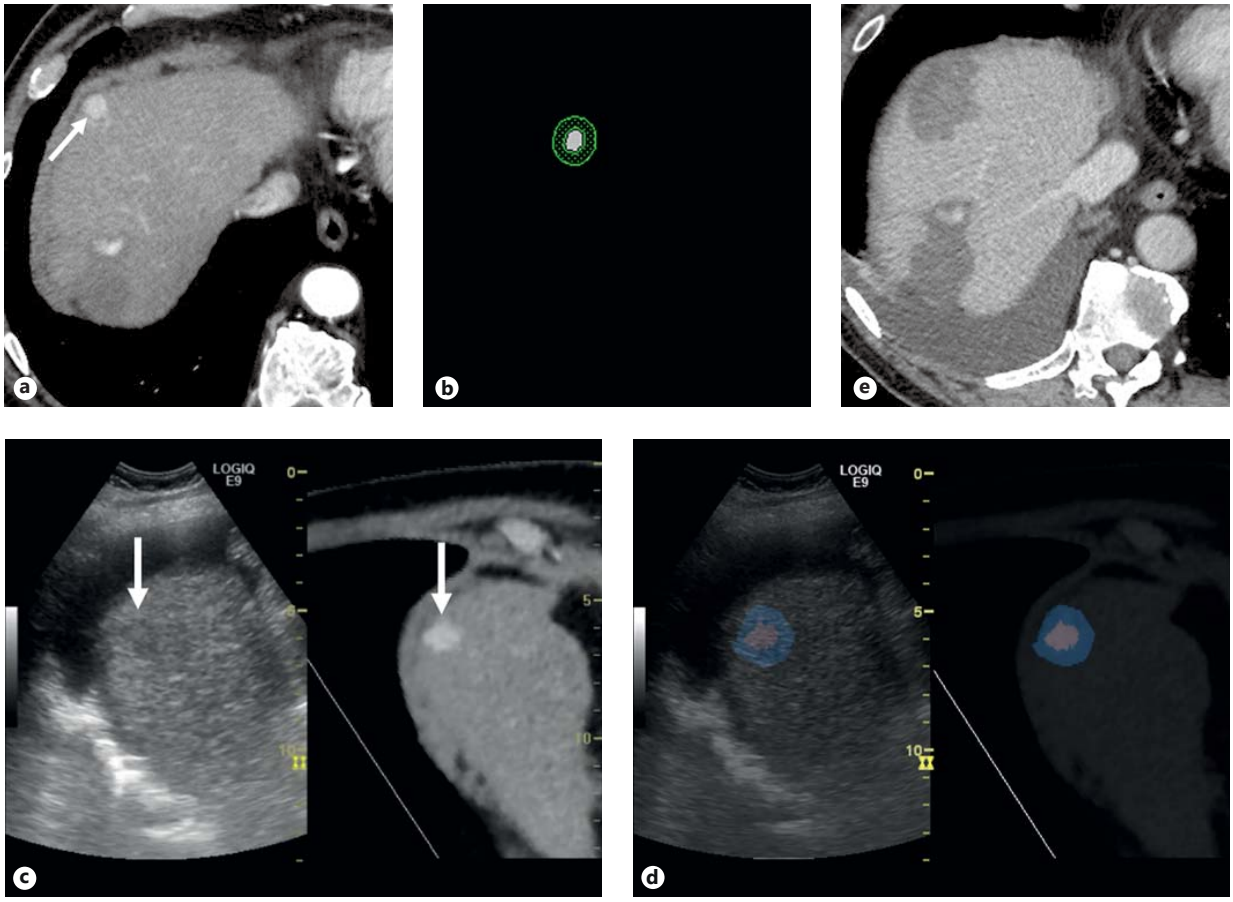

Fig. 1. A 68-year-old man with hepatitis C-related cirrhosis and HCC underwent RFA with the extracted-overlay function using artificial ascites. **a** The arterial phase of dynamic CT showed hypervascular HCC (arrow), 15 mm in diameter, in segment VIII, which was used as a reference for CT/MR-US fusion imaging (Volume Navigation, GE Healthcare). **b** On an image-processing workstation (Advantage Workstation Volumeshare 4, GE Healthcare), the tumor was extracted from original data of the arterial phase of dynamic CT (white portion), and an ablative safety margin of 5 mm was added to the extracted tumor by tracing around it circumferentially with a virtual brush of 5 mm thickness (green portion). When a portion of the added margin protruded beyond the edge of the liver, it was trimmed. After the volume data of the extracted tumor and the tumor with a virtual ablative safety margin were imported into a US unit (LOGIQ E9, GE Healthcare), they were used as a reference for Volume Navigation, together with the original CT data. **c** Side-by-side display of real-time grayscale US and original CT images, in which the target tumor (arrow) was depicted as a hypoechoic nodule on grayscale US. **d** The extracted-overlay function, in which the tumor (pink portion) and a virtual ablative safety margin (blue portion) were overlaid on US. Since only the tumor with a virtual ablative safety margin was overlaid, the background US images did not become obscured. Aiming at the overlaid tumor with a virtual ablative safety margin, a cool-tip electrode was inserted and ablation was carried out. **e** The portal-phase image of dynamic CT 3 days after RFA showed complete ablation of the tumor.

All 23 HCCs were judged to be completely encompassed with the surrounding hyperechoic bubbling area just after the first treatment session, and 22 (95.7%) HCCs were revealed to be completely ablated on dynamic CT. The 1 remaining HCC was located in segment VIII beneath the diaphragm, which was considered to be a difficult location to conduct RFA [14]. However, complete ablation was also achieved after the second treatment session, using the extracted-overlay function. The procedure of the extracted-overlay function in RFA is demonstrated through the presentation of 2 cases in figures 1 and 2.

Table 1. Characteristics of 18 patients with 23 HCCs

Characteristics	Value
Age, years	75 (60–83)
Gender (male/female)	9/9
Etiology (HBV/HCV/other)	1/15/2
Tumor diameter, mm	14.8 (7.0–31.4)
Segmental location of tumor (2/3/4/5/6/7/8)	1/2/5/3/3/1/8
Tumor vascularity (hypervascular/hypovascular)	20/3
Imaging modalities used for the extracted-overlay function (arterial phase of dynamic CT/portal phase of dynamic CT/CTHA/CTAP/hepatobiliary phase of Gd-EOB-DTPA-enhanced MR imaging)	4/2/5/1/11
Size of exposed tip of cool-tip needle (2/3 cm)	22/1
Treatment sessions per tumor before complete ablation (1/2), n	22/1
Ablations per tumor, n	2 (1–4)

Data are presented as median (range) or number. HBV = Hepatitis B virus; HCV = hepatitis C virus.

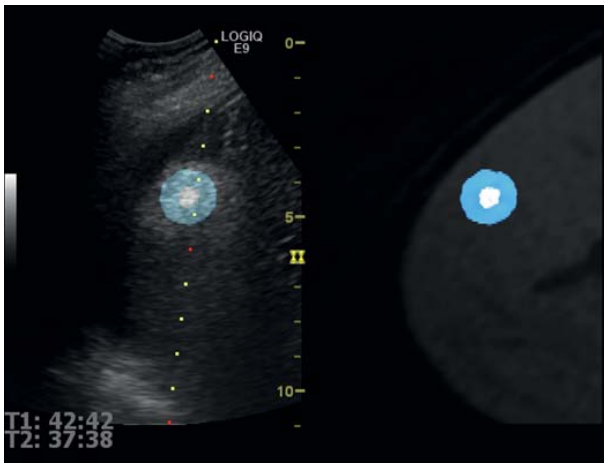

Fig. 2. The extracted-overlay function during RFA of HCC in a 65-year-old man with hepatitis C-related cirrhosis. The hepatobiliary phase of Gd-EOB-DTPA-enhanced MR imaging was used as a reference and the tumor (yellow portion) with a virtual ablative safety margin (blue portion) was overlaid on US. Although the tumor usually becomes invisible due to spreading hyperechoic bubbles during ablation, it remains visible using the extracted-overlay function. Therefore, the depth of the inserted electrode can be adjusted so that the extracted tumor, together with a virtual ablative safety margin when possible, becomes completely encompassed by the spreading hyperechoic bubbling area.

Discussion

Although the CT/MR-US fusion imaging system is considered to be useful for RFA [1–4], misregistration is inevitable in the conventional side-by-side display of US and reference images. Although registration accuracy should be originally confirmed by the overlay display, background US images often become too obscure for practical use, because of the simple overlaying of different imaging modalities. Although we can use the global positioning system (GPS) tool of Volume Navigation for indicating the tumor location of CT/MR reference images on US images, the GPS marker cannot indicate the tumor three-dimensionally [1, 3, 15]. On the other hand, the extracted-overlay function could overlay an entire tumor extracted from CT/MR images on US, and background US images did not become indistinct, leading to good treatment results of RFA in this study.

The extracted-overlay function has two other significant advantages. First, the visualization of an extracted tumor from reference images, with a virtual ablative safety margin, on real-time US enables effective treatment planning since the site, angle, depth and number of times of electrode insertion can be efficiently planned before RFA puncture. This advantage is considered to be especially apparent in HCCs which are not conspicuous on US [1, 2, 4, 15]. Second, the tumor remains visible, despite spreading hyperechoic bubbles, during and after ablation. During ablation, by comparing an overlaid tumor with the bubbles, the depth of an electrode can be adjusted so that the overlaid tumor becomes completely encompassed by the bubbles (fig. 2). In addition, the treatment effect can

Dig Dis 2013;31:485–489
DOI: 10.1159/000355257

be evaluated three-dimensionally, simply by comparing an overlaid tumor with spreading hyperechoic bubbles, or more accurately, by using contrast-enhanced US [1, 3, 12, 13]. Besides, by adding a virtual margin to the extracted tumor, an ablative margin can be evaluated quantitatively. Even if a tumor is protruding from the ablation zone, the target point of additional ablation is clear, since the tumor remains visible even after ablation.

One of the limitations of the extracted-overlay function lies in the registration accuracy of CT/MR-US fusion imaging. In addition to respiratory movement and nonrigid characteristics of the liver [2, 3, 10], the lack of intrahepatic landmarks makes registration difficult. This might be one of the causes of the only case of incomplete ablation after the first treatment session, since the tumor was located just beneath the diaphragm where there were few intrahepatic landmarks suitable for registration, such as branches of large blood vessels. Another limitation remains in terms of the accuracy of the manual process of extracting the tumor and adding a virtual ablative safety margin. Also, the outline of cranial and caudal portions of the tumor may be somewhat inaccurate when an imaging modality with a thick slice is used as a reference.

In conclusion, the extracted-overlay function in the CT/MR-US fusion imaging system is useful for treatment planning and guidance of RFA. This is due to the visualization of a tumor extracted from CT/MR reference images with an ablative safety margin on US images.

Disclosure Statement

The authors declare that no financial or other conflict of interest exists in relation to the content of the article.

References

1 Makino Y, Imai Y, Igura T, Ohama H, Kogita S, Sawai Y, Fukuda K, Ohashi H, Murakami T: Usefulness of the multimodality fusion imaging for the diagnosis and treatment of hepatocellular carcinoma. Dig Dis 2012;30:580–587.

2 Kunishi Y, Numata K, Morimoto M, Okada M, Kaneko T, Maeda S, Tanaka K: Efficacy of fusion imaging combining sonography and hepatobiliary phase MR imaging with Gd-EOB-DTPA to detect small hepatocellular carcinoma. AJR Am J Roentgenol 2012;198:106–114.

3 Numata K, Fukuda H, Morimoto M, Kondo M, Nozaki A, Oshima T, Okada M, Takebayashi S, Maeda S, Tanaka K: Use of fusion imaging combining contrast-enhanced ultrasonography with a perflubutane-based contrast agent and contrast-enhanced computed tomography for the evaluation of percutaneous radiofrequency ablation of hypervascular hepatocellular carcinoma. Eur J Radiol 2012;81:2746–2753.

4 Lee MW, Rhim H, Cha DI, Kim YJ, Choi D, Kim YS, Lim HK: Percutaneous radiofrequency ablation of hepatocellular carcinoma: fusion imaging guidance for management of lesions with poor conspicuity at conventional sonography. AJR Am J Roentgenol 2012;198:1438–1444.

5 Joo I, Choi BI: New paradigm for management of hepatocellular carcinoma by imaging. Liver Cancer 2012;1:94–109.

6 Kogita S, Imai Y, Okada M, Kim T, Onishi H, Takamura M, Fukuda K, Igura T, Sawai Y, Morimoto O, Hori M, Nagano H, Wakasa K, Hayashi N, Murakami T: Gd-EOB-DTPA-enhanced magnetic resonance images of hepatocellular carcinoma: correlation with histological grading and portal blood flow. Eur Radiol 2010;20:2405–2413.

7 Onishi H, Kim T, Imai Y, Hori M, Nagano H, Nakaya Y, Tsuboyama T, Nakamoto A, Tatsumi M, Kumano S, Okada M, Takamura M, Wakasa K, Tomiyama N, Murakami T: Hypervascular hepatocellular carcinomas: detection with gadoxetate disodium-enhanced MR imaging and multiphasic multidetector CT. Eur Radiol 2012;22:845–854.

8 Imai Y, Murakami T, Yoshida S, Nishikawa M, Ohsawa M, Tokunaga K, Murata M, Shibata K, Zushi S, Kurokawa M, Yonezawa T, Kawata S, Takamura M, Nagano H, Sakon M, Monden M, Wakasa K, Nakamura H: Superparamagnetic iron oxide-enhanced magnetic resonance images of hepatocellular carcinoma: correlation with histological grading. Hepatology 2000;32:205–212.

9 Nishikawa H, Inuzuka T, Takeda H, Nakajima J, Sakamoto A, Henmi S, Matsuda F, Eso Y, Ishikawa T, Saito S, Kita R, Kimura T, Osaki Y: Percutaneous radiofrequency ablation therapy for hepatocellular carcinoma: a proposed new grading system for the ablative margin and prediction of local tumor progression and its validation. J Gastroenterol 2011;46:1418–1426.

10 Makino Y, Imai Y, Igura T, Hori M, Fukuda K, Sawai Y, Kogita S, Ohama H, Matsumoto Y, Nakahara M, Zushi S, Kurokawa M, Isotani K, Takamura M, Fujita N, Murakami T: Utility of computed tomography fusion imaging for the evaluation of the ablative margin of radiofrequency ablation for hepatocellular carcinoma and the correlation to local tumor progression. Hepatol Res 2012, E-pub ahead of print.

11 Nakazawa T, Kokubu S, Shibuya A, Ono K, Watanabe M, Hidaka H, Tsuchihashi T, Saigenji K: Radiofrequency ablation of hepatocellular carcinoma: correlation between local tumor progression after ablation and ablative margin. AJR Am J Roentgenol 2007;188:480–488.

12 Nouso K, Shiraga K, Uematsu S, Okamoto R, Harada R, Takayama S, Kawai W, Kimura S, Ueki T, Okano N, Nakagawa M, Mizuno M, Araki Y, Shiratori Y: Prediction of the ablated area by the spread of microbubbles during radiofrequency ablation of hepatocellular carcinoma. Liver Int 2005;25:967–972.

13 Koda M, Mandai M, Matono T, Sugihara T, Nagahara T, Ueki M, Ohyama K, Hosho K, Murawaki Y: Assessment of the ablated area after radiofrequency ablation by the spread of bubbles: comparison with virtual sonography with magnetic navigation. Hepatogastroenterology 2011;58:1638–1642.

14 Tang Z, Fang H, Kang M, Zhang B, Dong X, Chen X, Xu J, Chen J, Wu Y: Percutaneous radiofrequency ablation for liver tumors: is it safer and more effective in low-risk areas than in high-risk areas? Hepatol Res 2011;41:635–640.

15 Makino Y, Imai Y, Ohama H, Igura T, Kogita S, Sawai Y, Fukuda K, Takamura M, Ohashi H, Murakami T: Ultrasonography fusion imaging system increased the chance of radiofrequency ablation for hepatocellular carcinoma with poor conspicuity on conventional ultrasonography. Oncology 2013;84(suppl 1):44–50.

Digestive Diseases

Dig Dis 2013;31:490–498
DOI: 10.1159/000355259

Hepatocellular Carcinoma in Child-Pugh C Cirrhosis: Prognostic Factors and Survival Benefit of Nontransplant Treatments

Masatoshi Kudo[a] Yukio Osaki[b] Takashi Matsunaga[c] Hiroshi Kasugai[d]
Hiroko Oka[e] Toshihito Seki[f] for the Osaka Liver Cancer Study Group

[a]Department of Gastroenterology and Hepatology, Kinki University School of Medicine, Osakasayama, [b]Department of Gastroenterology and Hepatology, Osaka Red Cross Hospital, Departments of [c]Medical Informatics and [d]Gastrointestinal Oncology, Osaka Medical Center for Cancer and Cardiovascular Diseases, [e]Department of Gastroenterology, Osaka City General Hospital, and [f]Department of Gastroenterology and Hepatology, Kansai Medical University Takii Hospital, Osaka, Japan

Key Words
Hepatocellular carcinoma · Child-Pugh C cirrhosis · Nontransplant treatment

Abstract
A retrospective multicenter study was conducted to clarify the survival benefit of nontransplant treatments for patients with hepatocellular carcinoma (HCC) associated with Child-Pugh C cirrhosis. Data on 436 patients, including 203 treated patients with HCC, were collected from 20 institutions in Japan. Cox's proportional hazards model corrected for bias by propensity score analysis clearly showed the following as significant independent prognostic factors, including all four nontransplant treatments examined: transarterial chemoembolization, hepatic arterial infusion chemotherapy, percutaneous ethanol injection therapy, radiofrequency ablation, hepatitis B virus, number of tumors, log α-fetoprotein, encephalopathy, ascites and prothrombin time. The cumulative survival rate was significantly higher in the treated group than in the untreated group. The present findings suggest that prognosis can be improved by nontransplant treatments in patients with low Child-Pugh scores. Since this study was retrospective, the possibility of selection bias cannot be ruled out. Therefore, verification by a prospective controlled study is warranted.

Introduction

The strong association of underlying chronic liver disease in patients with hepatocellular carcinoma (HCC) means that prognosis is largely determined not only by tumor stage, but also by liver function. Although both diseases are closely related, each is a major independent prognostic factor [1, 2]. In patients with Child-Pugh C liver function, prognosis is extremely poor [3]. Therefore, most of the HCC practice guidelines, including the American Association for the Study of Liver Diseases, AASLD [4], the European Association for the Study of the Liver and the European Organisation for Research and Treatment of Cancer, EASL-EORTC [5], the Asian Pacific Association for the Study of the Liver [6], and the Japan Society of Hepatology, JSH (evidence based) [7], recommend liver transplantation for patients meeting the Milan criteria [8] and best supportive care for patients exceeding the criteria. Only the consensus-based treatment algorithm proposed by the JSH recommends transarterial chemoembolization (TACE) or ablation for HCC patients with Child-Pugh C liver function [9]. This retrospective multicenter study was conducted to clarify

Masatoshi Kudo and Yukio Osaki contributed equally to this study.

KARGER

E-Mail karger@karger.com
www.karger.com/ddi

0257–2753/13/0316–0490$38.00/0

Masatoshi Kudo, MD
Department of Gastroenterology and Hepatology
Kinki University School of Medicine, 337-2 Ohno-Higashi
Osakasayama, Osaka 589-8511 (Japan)
E-Mail m-kudo@med.kindai.ac.jp

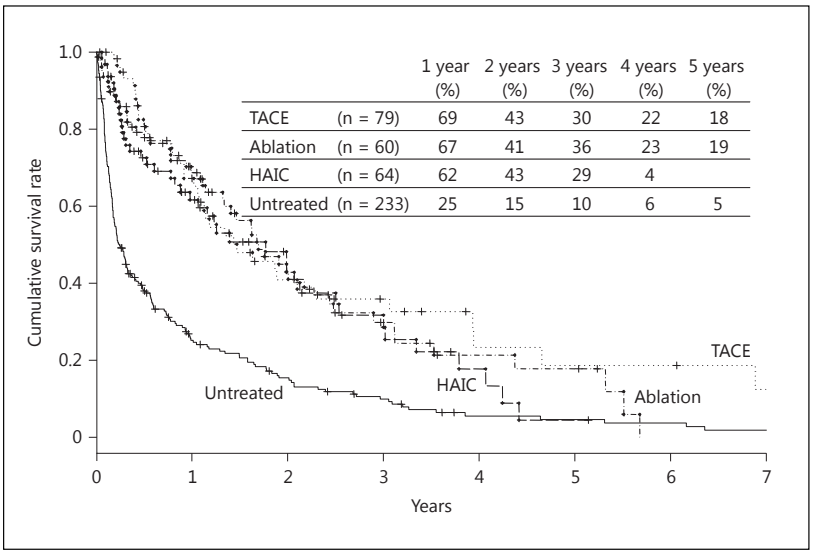

		1 year (%)	2 years (%)	3 years (%)	4 years (%)	5 years (%)
TACE	(n = 79)	69	43	30	22	18
Ablation	(n = 60)	67	41	36	23	19
HAIC	(n = 64)	62	43	29	4	
Untreated	(n = 233)	25	15	10	6	5

Fig. 1. Cumulative survival rate by treatment.

the prognostic factors and survival benefit of nontransplant treatment for HCC patients with Child-Pugh C cirrhosis.

Patients and Methods

Patients with underlying Child-Pugh C cirrhosis who were histologically or clinically diagnosed with HCC by diagnostic imaging and tumor markers during the 10-year period from 1994 to 2003 were assessed. A total of 454 patients were collected from 20 institutions in Japan. After excluding 18 patients who underwent liver transplantation or whose date of death or last day of follow-up was missing, 436 patients were left for analysis.

To clarify the prognostic factors, multivariate analysis was performed using Cox's proportional hazards model corrected for bias by propensity score weighting. The cumulative survival rate was calculated based on the time of diagnosis to the time of death and compared between patients who received nontransplant treatments (treated group) and those who did not (untreated group) according to Child-Pugh score, tumor size, number of tumors, tumor stage, and meeting or exceeding the Milan criteria. Observation was started at the time of HCC diagnosis and was continued until March 31, 2005. Cumulative survival rates were compared by Kaplan-Meier analysis and the log-rank test. Statistical significance was set at $p < 0.05$.

Results

Prognostic Factors

Multivariate analysis was performed for 17 of the 23 factors investigated, excluding those irrelevant to prognosis, and the following significant independent factors were extracted: all medical treatments including TACE, hepatic arterial infusion chemotherapy (HAIC), percutaneous ethanol infection therapy (PEIT), percutaneous radiofrequency ablation (RFA), negative hepatitis B virus, small number of tumors, low log α-fetoprotein values, no encephalopathy, no ascites and high prothrombin time values (table 1).

Table 1. Predictive factors of HCC associated with Child-Pugh C liver cirrhosis

	Coef.	Exp(coef.)	SE(coef.)	z	p
TACE	–0.539	0.583	0.199	–2.71	0.007
HAIC	–1.049	0.350	0.235	–4.47	<0.001
PEIT	–0.536	0.585	0.219	–2.45	0.014
RFA	–0.626	0.535	0.293	–2.14	0.032
HBV	0.392	1.481	0.178	2.20	0.028
Tumors (n)	0.073	1.076	0.034	2.17	0.030
log AFP	0.247	1.280	0.059	4.17	<0.001
Encephalopathy	–0.507	0.603	0.101	–5.02	<0.001
Ascites	–0.469	0.626	0.118	–3.98	<0.001
PT	0.018	1.018	0.005	3.49	<0.001
Fit[1]	–2.449	0.086	0.391	–6.27	<0.001

Results of Cox's proportional hazards model corrected for bias by propensity score weighting. HBV = Hepatitis B virus; AFP = α-fetoprotein; PT = prothrombin time.

[1] Propensity score.

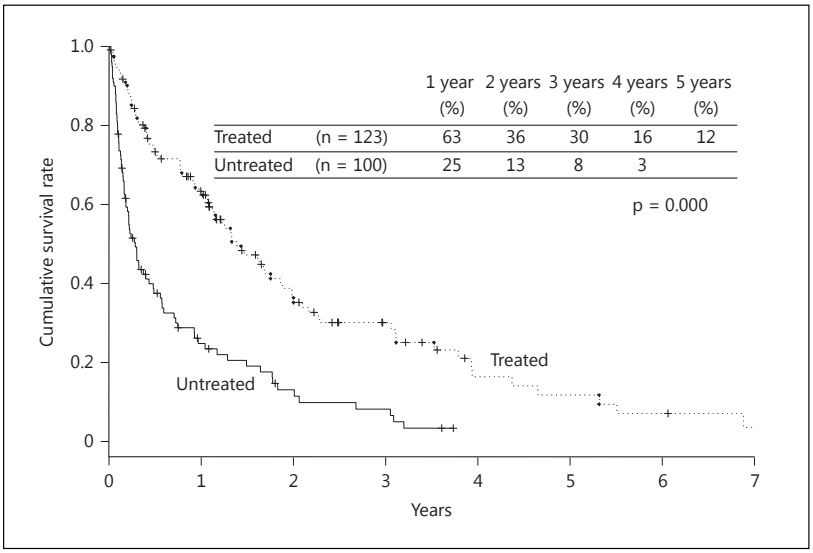

Fig. 2. Cumulative survival rate by Child-Pugh score of 10 or 11 points.

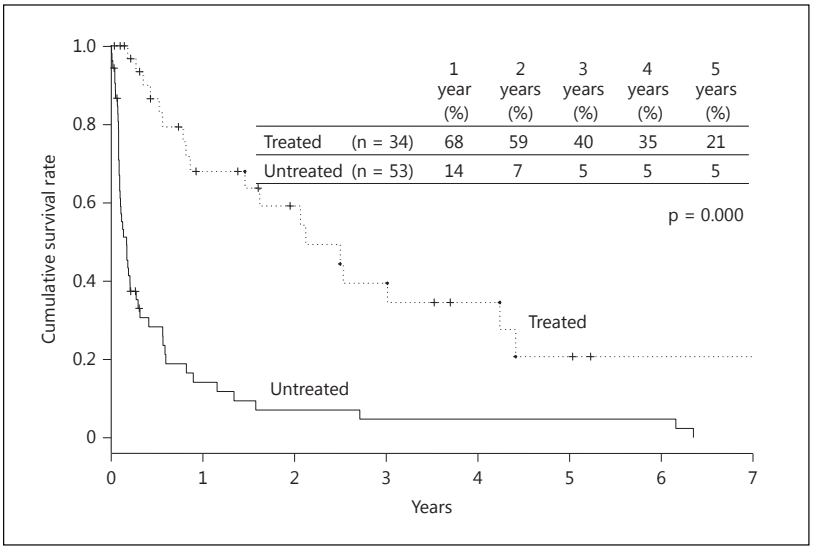

Fig. 3. Cumulative survival rate by Child-Pugh score of 12 or 13 points.

Cumulative Survival Rate Classified by Treatment Modalities

The cumulative survival rate in treated patients was 69% (1 year), 30% (3 years) and 18% (5 years) in the TACE group (n = 79), 62, 29 and 4%, respectively, in the HAIC group (n = 64), and 67, 36 and 19%, respectively, in the local ablation group. The survival rate was significantly higher in all three of these treated groups than in the untreated group [n = 233; 25% (1 year), 10% (3 years) and 5% (5 years); fig. 1].

Prognosis Classified by Child-Pugh Score

Patients were divided into the following 3 groups based on their Child-Pugh score: 10–11 points, 12–13 points and 14–15 points. The cumulative survival rate in all three of these treated groups was significantly

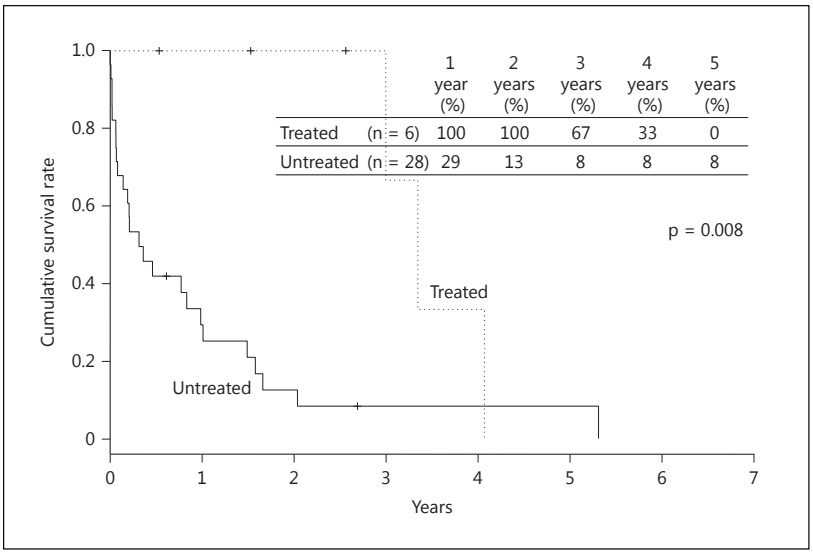

Fig. 4. Cumulative survival rate by Child-Pugh score of 14 or 15 points.

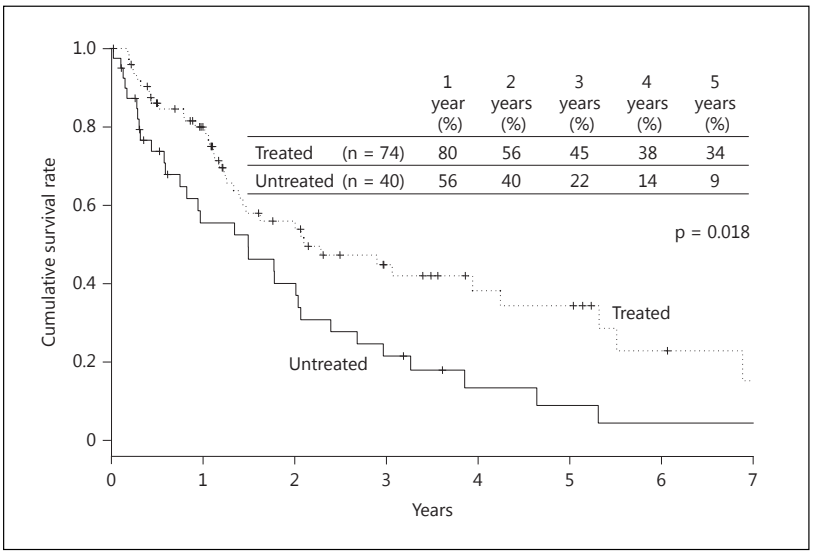

Fig. 5. Cumulative survival rate by tumor size ≤2 cm.

higher than in the untreated group (fig. 2–4). However, only 6 patients in the 14- to 15-point group received treatment.

Prognosis Classified by Tumor Size and Number of Tumors

The cumulative survival rate was significantly higher in the treated group than in the untreated group for patients with tumors ≤2 cm in diameter (fig. 5), those with tumors >2 to ≤5 cm in diameter (fig. 6), and those with tumors >5 cm in diameter (fig. 7).

Similarly, the cumulative survival rate in the treated group was significantly higher in patients with a solitary tumor [76% (1 year), 40% (3 years) and 26% (5 years)] than in the untreated group (37, 11 and 0%, respectively), in patients with 2 or 3 tumors (68, 29 and 12%, respectively) than

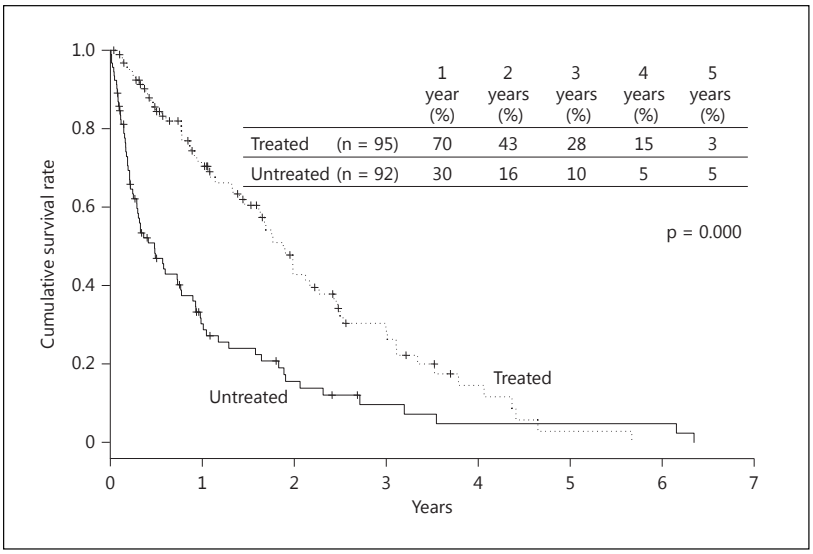

Fig. 6. Cumulative survival rate by tumor size >2 and ≤5 cm.

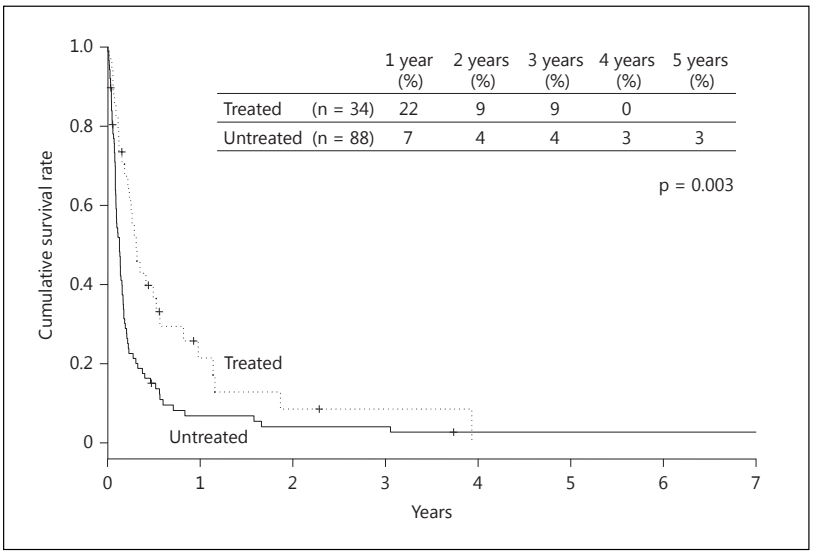

Fig. 7. Cumulative survival rate by tumor size >5 cm.

in the untreated group (29, 11 and 7%, respectively), and in patients with >3 tumors (48, 22 and 4%, respectively) than in the untreated group (15, 8 and 6%, respectively).

Prognosis Classified by TNM Stage by the Liver Cancer Study Group of Japan

All patients were classified into stage I–IV according to their TNM stage by the Liver Cancer Study Group of Japan [1, 2]. The cumulative survival rate was significantly higher in the treated group than in the untreated group for stage I patients [85% (1 year), 51% (3 years) and 38% (5 years); fig. 8], stage II patients (fig. 9), and stage III or stage IV patients (fig. 10, 11).

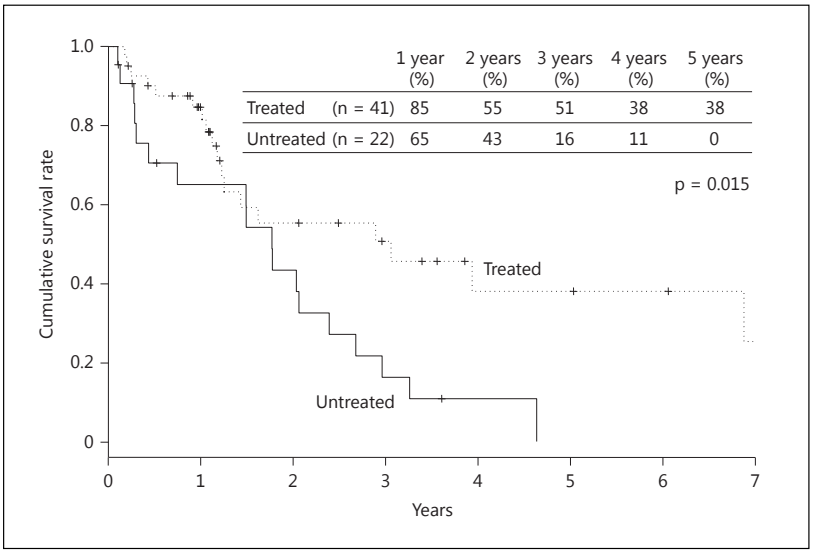

Fig. 8. Cumulative survival rate by TNM stage I.

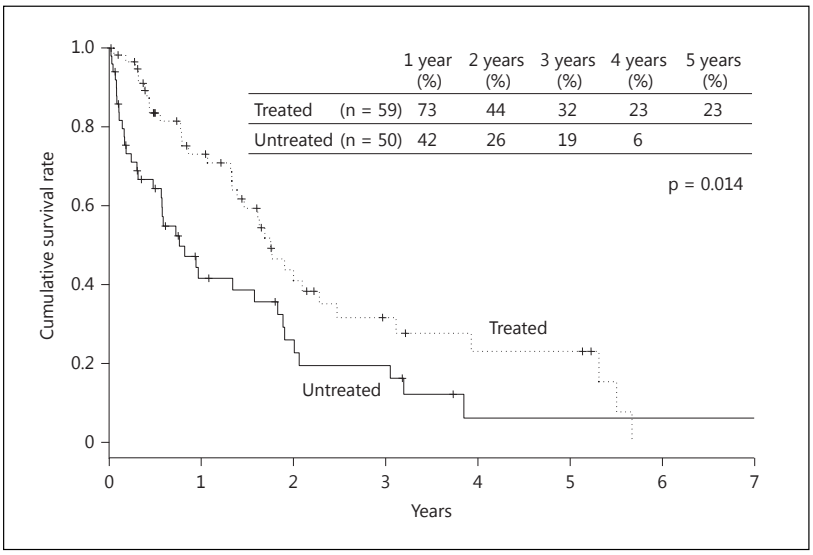

Fig. 9. Cumulative survival rate by TNM stage II.

Prognosis Classified by ≤3 Tumors ≤3 cm in Diameter and Tumors Meeting or Exceeding the Milan Criteria

The cumulative survival rate in the treated group was significantly higher in patients with ≤3 tumors ≤3 cm in diameter [79% (1 year), 40% (3 years) and 30% (5 years)] than in the untreated group (54, 17 and 6%, respectively). Similarly, the cumulative survival rate in the treated group was significantly higher in patients with ≥3 tumors or with tumors ≥3 cm in diameter than in the untreated group.

The cumulative survival rate was significantly higher in the treated group than in the untreated group for patients meeting the Milan criteria [8] (≤3 tumors ≤3 cm in diameter or a solitary tumor ≤5 cm in diameter; fig. 12) and was also higher for patients exceeding the criteria (fig. 13).

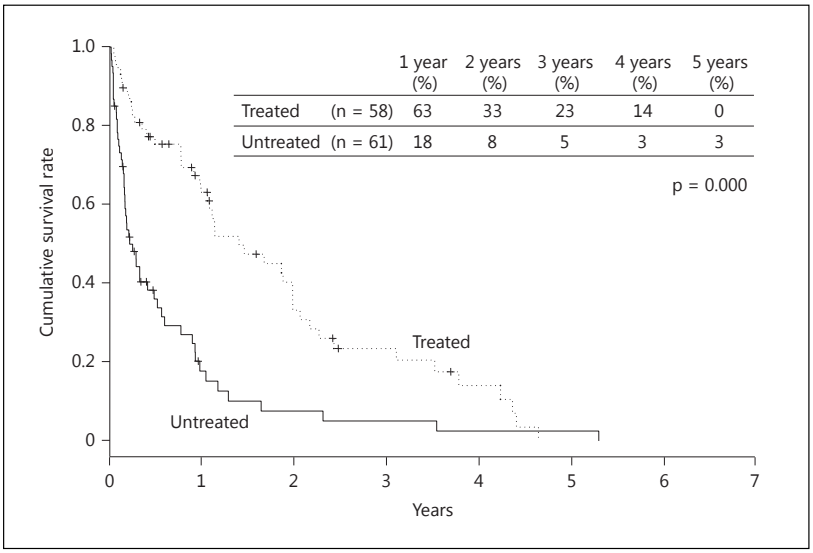

		1 year (%)	2 years (%)	3 years (%)	4 years (%)	5 years (%)
Treated	(n = 58)	63	33	23	14	0
Untreated	(n = 61)	18	8	5	3	3

Fig. 10. Cumulative survival rate by TNM stage III.

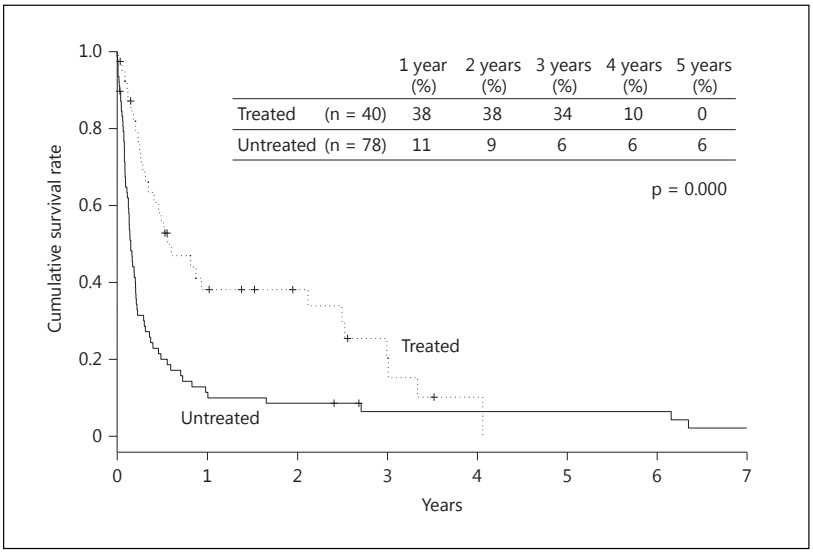

		1 year (%)	2 years (%)	3 years (%)	4 years (%)	5 years (%)
Treated	(n = 40)	38	38	34	10	0
Untreated	(n = 78)	11	9	6	6	6

Fig. 11. Cumulative survival rate by TNM stage IV.

Discussion

The most important goal of cancer treatment is to improve patient prognosis. The prognosis of HCC is often determined by the stage of liver cirrhosis or the deterioration of liver function associated with cancer treatment, irrespective of tumor presence or stage. Therefore, to determine the treatment indications and select appropriate treatment, comprehensive judgments should be made considering both factors carefully.

Patients with Child-Pugh C disease are generally not treated, regardless of tumor stage, because of their poor prognosis. As mentioned earlier, according to the treatment algorithm recommended by the AASLD and EASL-EORTC, patients with Child-Pugh C liver function should be regarded as having end-stage (terminal) disease and giv-

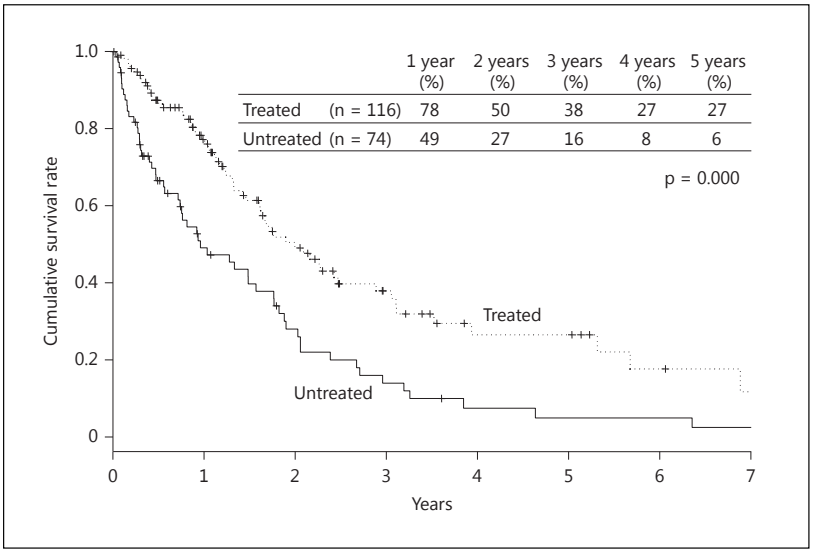

Fig. 12. Cumulative survival rate by meeting the Milan criteria.

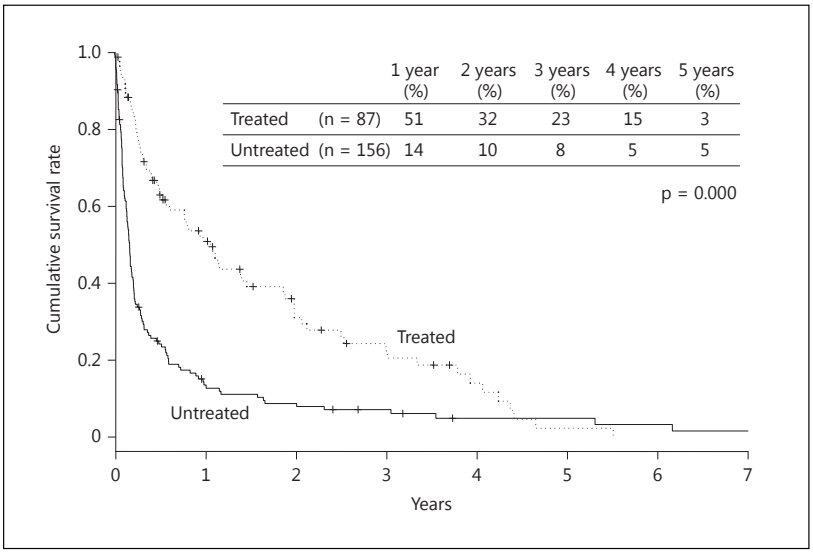

Fig. 13. Cumulative survival rate by exceeding the Milan criteria.

en only symptomatic treatment. With respect to HCC associated with Child-Pugh C disease, the evidence-based guidelines for the treatment of liver cancer published by the JSH [7] recommend liver transplantation [10] for patients meeting the Milan criteria, and palliative therapy for all other patients. However, even in patients with HCC meeting the Milan criteria, liver transplantation is not a standard in Japan because of the shortage of brain-death donors.

This study revealed several interesting findings. One such finding is that only around half (53%) of the patients included in the analysis received some kind of medical treatment. The most notable findings, however, are that all nontransplant treatments (TACE [11], PEIT [12, 13], RFA and HAIC [14]) were independent prognostic factors and that survival was better in patients who received medical treatment than in those who did not. In view of

the current state of clinical practice, it can be presumed that some kind of treatment is being administered to patients with HCC associated with Child-Pugh C cirrhosis and that the treatment might be contributing to an improved prognosis in a limited number of treated patients. An unexpected finding was that so many patients received treatment, with significantly better outcome in treated patients than in untreated patients. However, since the present study is retrospective, it is possible that only patients with relatively good liver function were treated as they were expected to respond to treatment; as a result, those who were not considered able to tolerate treatment were likely placed in the untreated group. Therefore, a strong selection bias may have been present in this study. Nevertheless, it is clearly evident that a considerable number of patients with HCC associated with Child-Pugh C cirrhosis received and responded to cancer treatment. Therefore, treatment may improve prognosis.

Assessment of prognosis in the three groups with different Child-Pugh scores revealed that survival was better in the treated than in the untreated patients. However, the 14- to 15-point group had only a small number of treated patients (n = 6), so this finding does not necessarily indicate the superiority of the treatment in this group. Patients in the treated group who met the Milan criteria or the general criteria for local ablation (≤3 tumors ≤3 cm in diameter) showed a higher survival rate throughout the study period. Interestingly, patients with HCCs exceeding the Milan criteria in the treatment group also showed a better survival than untreated patients. This may be attributed to the frequent use of superselective TACE even in multinodular HCC patients in Japan, which does not cause deterioration of liver function. A previous report also described that superselective TACE was identified as having survival benefit in HCC patients with Child-Pugh C [15].

These results suggest that prognosis may be improved by treating eligible patients with early-stage tumors for radical cure. Despite the poor prognosis of Child-Pugh C disease, the present results show that treatment might improve prognosis in patients with low Child-Pugh scores, which is in agreement with the results reported by Nouso et al. [15].

In conclusion, this retrospective multicenter study of 436 HCC patients with Child-Pugh C cirrhosis showed that nontransplant medical treatments (i.e. TACE, RFA, PEIT and HAIC) confer survival benefit. In addition, medical treatment should be considered for HCC patients, especially for patients with low Child-Pugh scores. Finally, this result confirmed the validity of recommendation by the consensus-based JSH treatment algorithm [9].

Disclosure Statement

The authors have no conflicts of interest to declare.

References

1 Kudo M, Chung H, Osaki Y: Prognostic staging system for hepatocellular carcinoma (CLIP score): its value and limitations, and a proposal for a new staging system, the Japan Integrated Staging Score (JIS score). J Gastroenterol 2003;38:207–215.

2 Kudo M, Chung H, Haji S, Osaki Y, Oka H, Seki T, Kasugai H, Sasaki Y, Matsunaga T: Validation of a new prognostic staging system for hepatocellular carcinoma: the JIS score compared with the CLIP score. Hepatology 2004;40:1396–1405.

3 Pugh RN, Murray-Lyon IM, Dawson JL, Pietroni MC, Williams R: Transection of the oesophagus for bleeding oesophageal varices. Br J Surg 1973;60:646–649.

4 Bruix J, Sherman M: Management of hepatocellular carcinoma: an update. Hepatology 2011;53:1020–1022.

5 Llovet JM, Ducreux M: EASL-EORTC clinical practice guidelines: management of hepatocellular carcinoma. J Hepatol 2012;56:908–943.

6 Omata M, Lesmana LA, Tateishi R, Chen PJ, Lin SM, Yoshida H, Kudo M, Lee JM, Choi BI, Poon RT, et al: Asian Pacific Association for the Study of the Liver consensus recommendations on hepatocellular carcinoma. Hepatol Int 2010;4:439–474.

7 Makuuchi M, Kokudo N, Arii S, Futagawa S, Kaneko S, Kawasaki S, Matsuyama Y, Okazaki M, Okita K, Omata M, et al: Development of evidence-based clinical guidelines for the diagnosis and treatment of hepatocellular carcinoma in Japan. Hepatol Res 2008;38:37–51.

8 Mazzaferro V, Regalia E, Doci R, Andreola S, Pulvirenti A, Bozzetti F, Montalto F, Ammatuna M, Morabito A, Gennari L: Liver transplantation for the treatment of small hepatocellular carcinomas in patients with cirrhosis. N Engl J Med 1996;334:693–699.

9 Kudo M, Izumi N, Kokudo N, Matsui O, Sakamoto M, Nakashima O, Kojiro M, Makuuchi M: Management of hepatocellular carcinoma in Japan: consensus-based clinical practice guidelines proposed by the Japan Society of Hepatology (JSH) 2010 updated version. Dig Dis 2011;29:339–364.

10 Belghiti J, Fuks D: Liver resection and transplantation in hepatocellular carcinoma. Liver Cancer 2012;1:71–82.

11 Lencioni R: Chemoembolization in patients with hepatocellular carcinoma. Liver Cancer 2012;1:41–50.

12 Lin S, Hoffmann K, Schemmer P: Treatment of hepatocellular carcinoma: a systematic review. Liver Cancer 2012;1:144–158.

13 Lin SM: Local ablation for hepatocellular carcinoma in Taiwan. Liver Cancer 2013;2:73–83.

14 Kudo M: Treatment of advanced hepatocellular carcinoma with emphasis on hepatic arterial infusion chemotherapy and molecular targeted therapy. Liver Cancer 2012;1:62–70.

15 Nouso K, Ito Y, Kuwaki K, Kobayashi Y, Nakamura S, Ohashi Y, Yamamoto K: Prognostic factors and treatment effects for hepatocellular carcinoma in Child C cirrhosis. Br J Cancer 2008;98:1161–1165.

Liver Cancer

Liver Cancer 2013;2:151–152
DOI: 10.1159/000343847
Published online: August 26, 2013

2235-1795/13/0024-0151$38.00/0
www.karger.com/lic

Editorial

Alpha-fetoprotein-L3: Useful or Useless for Hepatocellular Carcinoma?

Prof. M. Kudo

Editor *Liver Cancer*

Japan is the only country where alpha-fetoprotein (AFP)-L3 can be measured in the routine clinical setting. Since AFP-L3 examination has been covered by health insurance in Japan for over 10 years, it is now routinely measured during general medical checkups for patients with chronic liver disease. To increase the specificity of AFP, the AFP-L3 glycoform can be used as a measure of cancerous changes in the AFP composite carbohydrate moiety. The most frequently used cut-off value is 10% [1], which gives a positive rate of 0/71 (0.0%), 1/90 (1.1%), 0/13 (0.0%), 0/14 (0.0%), and 18/82 (22.0%) for chronic hepatitis, hepatic cirrhosis, dysplastic nodules, early hepatocellular carcinoma, and advanced hepatocellular carcinoma, respectively. This yields a sensitivity of 18.8% and a specificity of 99.4%. Therefore, although AFP-L3 has high specificity, due to its low sensitivity, it is considered to be of limited use in screening. It is possible, however, to diagnose a marginally higher number of patients with advanced hepatocellular carcinoma [2]. Furthermore, as AFP-L3 may be elevated during hepatic failure, interpretation should be made with caution.

AFP-L3 dynamics are largely related to the degree of biological malignancy of hepatocellular carcinoma [2, 3]. Results of pathological investigations conducted on patients who have undergone hepatic resection showed that those with infiltrative growth, capsular invasion, septum formation, portal vein infiltration, and hepatic vein infiltration were significantly more likely to have AFP-L3-positive (>10%) cancer [4].

To investigate cases of hepatocellular carcinoma for which therapeutic intervention was given and in which tumor markers were measured chronologically, an investigation was conducted prior to therapeutic intervention with a group of 196 AFP-L3-positive (>10%) patients and a group of 645 AFP-L3-negative patients. When the overall survival rate was compared between the AFP-L3-positive and negative groups, the latter group showed more favorable survival than the former group ($p < 0.001$). When the AFP-L3 dynamics before and at six months after treatment were compared, 599 cases remained negative, 113 remained positive, 83 underwent conversion from positive to negative (negative conversion), and 46 underwent conversion from negative to positive (positive conversion). When survival rates were investigated, the constantly negative and negative conversion groups had more favorable survival rates than the constantly positive and positive conversion group. In other words, even though there are AFP-L3-positive cancers with poor prognosis and a

Liver Cancer 2013;2:151–152
DOI: 10.1159/000343847
Published online: August 26, 2013

high degree of biological malignancy, when negative conversion is induced from therapeutic intervention, a survival rate equivalent to that of AFP-L3-negative cancer can be obtained.

Recently, highly sensitive AFP-L3 measurements have become available, and the usefulness of these has increased rapidly [5, 6]. Using conventional methods, AFP-L3 measurement was only possible at AFP levels >10 ng/ml, whereas using the highly sensitive method enables measurement at AFP levels >2 ng/ml. The highly sensitive AFP-L3 measurements are particularly effective in patients with low AFP values. In an investigation of 270 hepatocellular carcinoma patients with an AFP value >20 ng/ml and a Child-Pugh score of A or B [5], when the cut-off value was set at 5%, the conventional AFP-L3 measurement method yielded a sensitivity of 7% and a specificity of 98.5%. Conversely, the highly sensitive method yielded a sensitivity of 41.5% and a specificity of 85.1%, indicating that the sensitivity of the highly sensitive method was significantly higher than that of the conventional method ($p < 0.05$).

Furthermore, the sensitivity for Stage I (n = 89) and Stage II (n = 127) was 4.5% and 2.4%, respectively when the cut-off value using the conventional method was set at 10%, while the sensitivity for the same stages was more favorable at 34.8% and 42.5%, respectively when the cut-off value using the highly sensitive method was set at 5%. In terms of prognostic assessment, when using the conventional method with the cut-off value set at 10%, no significant difference was observed between those with values >10% or <10%. However, reports indicate that when using the highly sensitive method with a cut-off value of 5%, patients with values < 5% have a significantly more favorable prognosis than those with values >5% ($p < 0.01$). In addition, even in patients with an AFP <10 ng/ml, when the cut-off value is set at 5% using the highly sensitive method, patients with values below 5% have a significantly more favorable prognosis than those with values 5% or above ($p = 0.035$). With regard to prognosis and the use of AFP-L3, multivariate analysis using the Cox proportional hazard model showed the following. For values of 5% and above the hazard ratio was 1.697 and 95% confidence interval was 1.066 – 3.440, $p = 0.026$. For treatment consisting of non-hepatic resection the hazard ratio was 3.627 and 95% confidence interval was 2.066 – 6.708, $p < 0.001$. These findings enabled factors contributing to prognosis to be selected [5].

In conclusion, AFP-L3, in particular its high sensitivity measurement, is extremely useful as an index of prognostication and for the degree of biological malignancy of hepatocellular carcinoma. Consequently, it is highly expected that AFP-L3 will become more popular worldwide, and not just in Japan.

References

1 Shimizu K, Katoh H, Yamashita F, Tanaka M, Tanikawa K, Taketa K, et al: Comparison of carbohydrate structures of serum alpha-fetoprotein by sequential glycosidase digestion and lectin affinity electrophoresis. Clin Chim Acta 1996;254:23–40.
2 Kumada T, Nakano S, Takeda I, Kiriyama S, Sone Y, Hayashi K, et al: Clinical utility of Lens culinaris agglutinin-reactive alpha-fetoprotein in small hepatocellular carcinoma: special reference to imaging diagnosis. J Hepatol 1999;30:125–130.
3 Tamura Y, Igarashi M, Suda T, Wakai T, Shirai Y, Umemura T, et al: Fucosylated fraction of alpha-fetoprotein as a predictor of prognosis in patients with hepatocellular carcinoma after curative treatment. Dig Dis Sci 2010;55:2095–2101.
4 Tada T, Kumada T, Toyoda H, Kiriyama S, Sone Y, Tanikawa M, et al: Relationship between Lens culinaris agglutinin-reactive alpha-fetoprotein and pathologic features of hepatocellular carcinoma. Liver Int 2005;25:848–853.
5 Toyoda H, Kumada T, Tada T, Kaneoka Y, Maeda A, Kanke F, et al: Clinical utility of highly sensitive Lens culinaris agglutinin-reactive alpha-fetoprotein in hepatocellular carcinoma patients with alpha-fetoprotein <20 ng/ml. Cancer Sci 2011;102:1025–1031.
6 Tamura Y, Igarashi M, Kawai H, Suda T, Satomura S, Aoyagi Y: Clinical advantage of highly sensitive on-chip immunoassay for fucosylated fraction of alpha-fetoprotein in patients with hepatocellular carcinoma. Dig Dis Sci 2010;55:3576–3583.

Liver Cancer

Liver Cancer 2013;2:365–366
DOI: 10.1159/000343851
Published online: August 26, 2013

2235-1795/13/0024-0365$38.00/0
www.karger.com/lic

Editorial

Molecular Link between Liver Fibrosis and Hepatocellular Carcinoma

Toshiharu Sakurai Masatoshi Kudo

Department of Gastroenterology and Hepatology, Kinki University, Osaka, Japan

Hepatocellular carcinoma (HCC) is the most common form of liver cancer, which is usually associated with a very poor prognosis [1], and is the third leading cause of cancer deaths worldwide. Most HCCs develop in the context of severe liver fibrosis and cirrhosis caused by chronic liver inflammation. Chronic infections with hepatitis B virus (HBV) or hepatitis C virus (HCV) as well as hepatosteatosis, are the major risk factors for both liver cirrhosis and HCCs. In the case of HCV, HCC develops after one or more decades of chronic infection, and an elevated risk of HCC progression is restricted largely to patients with cirrhosis or advanced fibrosis. Thus, the risk of hepatocarcinogenesis depends on background liver factors, of which fibrosis is a major determinant. Development and progression of liver fibrosis are associated with hepatocyte death and a subsequent inflammatory response [2], both of which involve reactive oxygen species (ROS) accumulation in injured hepatocytes. Given that the risk of human HCC recurrence after hepatectomy is positively correlated with protein oxidation in the liver, augmented oxidative stress of liver parenchymal cells may explain the close relationship between liver fibrosis and hepatocarcinogenesis [3].

In this issue, Ramakrishna et al. review possible molecular links between liver fibrosis and HCC [4]. Critical regulators of liver cancer development are inflammation in the context of the NF-κB/STAT3/JNK axis and inflammasome, and also cellular senescence. Like IKKβ, the catalytic subunit of the IκB kinase complex required for NF-κB activation, p38α prevents ROS accumulation and excessive JNK activation, thereby maintaining hepatocyte survival and suppressing liver injury [3, 5]. Hepatocyte IKKβ and p38α inhibit hepatocarcinogenesis by suppressing accumulation of ROS and inflammation, whereas JNK activation promotes ROS accumulation, hepatitis, and carcinogenesis [5, 6]. p38 is essential for ras-induced senescence, an important tumor-suppressing defense mechanism [7], while JNK suppresses p53-dependent senescence [8]. p38 and JNK antagonistically control senescence and cytoplasmic $p16^{INK4A}$ expression in doxorubicin-treated endothelial progenitor cells [9]. A better understanding of cross-talk between inflammation and cellular senescence is of great importance.

Identification of the cellular origin of HCC will help in targeted therapeutics directed towards the most dreadful consequence of chronic inflammation, HCC development. The concept that tumors are maintained by dedicated stem cells, the so-called cancer stem cell hypothesis, has attracted much interest. According to this hypothesis, cancer cannot be viewed as simple monoclonal expansions of functionally equal tumor cells. Instead, only a small minority of tumor cells, the cancer stem cells or tumor-initiating cells, have the ability to maintain the malignant population [10]. Deletion of IKKβ enhances proliferation of tumor-initiated cells and accelerates HCC development. These effects of IKKβ are correlated

Liver Cancer

Liver Cancer 2013;2:365–366
DOI: 10.1159/000343851
Published online: August 26, 2013

with increased accumulation of ROS that leads to JNK and STAT3 activation [11]. The positive cross-talk between JNK and stem cell expansion is evident in human HCC studies [12]. Deletion of p38α, which leads to JNK activation, upregulates expression of SOX2 and Gankyrin, which may be involved in cancer stem cell maintenance [3]. The NF-κB/STAT3/JNK signaling pathway in cancer stem cells may be a promising therapeutic target.

The molecular etiology of HCC has been extensively studied using transgenic or chemically induced mouse models [13, 14]. The chemical procarcinogen diethylnitrosamine (DEN)-induced HCC depends on production of the NF-κB-regulated cytokine IL-6 by resident Kupffer cells [15]. In this case, Kupffer cells are activated by IL-1α released by apoptosing hepatocytes [5]. Interestingly, male mice produce more IL-6 upon DEN administration than females, which accounts for the marked male bias in HCC induction studies. Mice administered thioacetamide for 10 months develop HCCs subsequent to appearance of severe liver fibrosis, thus providing a model that closely mimics the natural history of human HCV-related liver disease [3]. These animal models are critical for finding answers to key questions raised by the authors.

Unlike most solid tumors, the incidence and mortality of HCC have increased in the United States and Europe in the past decade. The findings implicating a pivotal signaling pathway in HCC development suggest the potential use for blocking agents and/or modulators for HCC treatment. Therefore, it is important to improve our understanding of the molecular pathogenesis of HCC.

References

1 Thorgeirsson SS, Grisham JW: Molecular pathogenesis of human hepatocellular carcinoma. Nat Genet 2002;31:339–346. [Medline]
2 Ghany MG, Kleiner DE, Alter H, Doo E, Khokar F, Promrat K, Herion D, Park Y, Liang TJ, Hoofnagle JH: Progression of fibrosis in chronic hepatitis C. Gastroenterology 2003;124:97–104. [Medline]
3 Sakurai T, Kudo M, Umemura A, He G, Elsharkawy AM, Seki E, Karin M: p38α Inhibits Liver Fibrogenesis and Consequent Hepatocarcinogenesis by Curtailing Accumulation of Reactive Oxygen Species. Cancer Res 2013;73:215–224. [Medline]
4 Ramakrishna G, Rastogi A, Trehanpati N, Sen B, Khosla R, Sarin SK: Cirrhosis to hepatocellular carcinoma: Newer molecular insights on inflammation and cellular senescence. Liver Cancer 2013 (in press).
5 Sakurai T, He G, Matsuzawa A, Yu GY, Maeda S, Hardiman G, Karin M: Hepatocyte necrosis induced by oxidative stress and IL-1α release mediate carcinogen-induced compensatory proliferation and liver tumorigenesis. Cancer Cell 2008;14:156–165. [Medline]
6 Sakurai T, Maeda S, Chang L, Karin M: Loss of hepatic NF-kappa B activity enhances chemical hepatocarcinogenesis through sustained c-Jun N-terminal kinase 1 activation. Proc Natl Acad Sci USA 2006;103:10544–10551. [Medline]
7 Zheng H, Seit-Nebi A, Han X, Aslanian A, Tat J, Liao R, Yates JR 3rd, Sun P: A Posttranslational Modification Cascade Involving p38, Tip60, and PRAK Mediates Oncogene-Induced Senescence. Mol Cell 2013;50:699–710.
8 Das M, Jiang F, Sluss HK, Zhang C, Shokat KM, Flavell RA, Davis RJ: Suppression of p53-dependent senescence by the JNK signal transduction pathway. Proc Natl Acad Sci USA 2007;104:15759–15764. [Medline]
9 Spallarossa P, Altieri P, Barisione C, Passalacqua M, Aloi C, Fugazza G, Frassoni F, Podestà M, Canepa M, Ghigliotti G, Brunelli C: p38 MAPK and JNK Antagonistically Control Senescence and Cytoplasmic p16INK4A Expression in Doxorubicin-Treated Endothelial Progenitor Cells. PLoS ONE 2010;5:e15583.
10 Reya T, Morrison SJ, Clarke MF, Weissman IL: Stem cells, cancer, and cancer stem cells. Nature 2001;414:105–111. [Medline]
11 He G, Yu GY, Temkin V, Ogata H, Kuntzen C, Sakurai T, Sieghart W, Peck-Radosavljevic M, Leffert HL, Karin M: Hepatocyte IKKbeta/NF-kappaB inhibits tumor promotion and progression by preventing oxidative stress-driven STAT3 activation. Cancer Cell 2010;17:286–297. [Medline]
12 Hagiwara S, Kudo M, Nagai T, Inoue T, Ueshima K, Nishida N, Watanabe T, Sakurai T: Activation of JNK and High Expression Level of CD133 Predict a Poor Response to Sorafenib in Hepatocellular Carcinoma. Br J Cancer 2012;106:1997–2003. [Medline]
13 Calvisi DF, Thorgeirsson SS: Molecular mechanisms of hepatocarcinogenesis in transgenic mouse models of liver cancer. Toxicol Pathol 2005;33:181–184. [Medline]
14 Fausto N: Mouse liver tumorigenesis: models, mechanisms, and relevance to human disease. Semin Liver Dis 1999;19:243–252. [Medline]
15 Naugler WE, Sakurai T, Kim S, Maeda S, Kim K, Elsharkawy AM, Karin M: Gender disparity in liver cancer due to sex differences in MyD88-dependent IL-6 production. Science 2007;317:121–124. [Medline]

J Med Ultrasonics (2013) 40:211–218
DOI 10.1007/s10396-012-0412-5

ORIGINAL ARTICLE

Diagnostic value of endoscopic ultrasound-guided directional eFLOW in solid pancreatic lesions

Kunal Das · Masatoshi Kudo · Masayuki Kitano · Hiroki Sakamoto · Takamitsu Komaki · Tadayuki Takagi · Kenji Yamao

Received: 15 December 2011 / Accepted: 15 October 2012 / Published online: 23 January 2013

Abstract
Aim Ultrasound using microbubble-based contrast agents is useful for vascular imaging. Directional eFLOW (D-eFLOW) is a novel technology for vascular assessment that provides high spatial and temporal resolution. The purpose of this study was to investigate the utility of endoscopic ultrasound (EUS)-guided D-eFlow before and after administration of an ultrasound contrast agent (USCA) for assessing the vascularity of solid pancreatic lesions.
Materials and methods D-eFlow was compared to power Doppler EUS (PD-EUS) or color Doppler EUS (CD-EUS) before and after USCA injection. We also evaluated the Visual Vascular Assessment (ViVA) scale for the estimation of vascularity and investigated its reliability using the interclass correlation coefficient (ICC). From January 2007 to March 2007, 35 patients (mean age, 64.5 years old; age range, 28–81 years) underwent EUS followed by D-eFLOW EUS, PD-EUS, and CD-EUS before and after administration of USCA. The pancreatic parenchymal ViVA score, pancreatic vascular pattern, and ICC were evaluated for all lesions.
Results Concerning the sensitivity for detection of the hypovascular pattern in pancreatic adenocarcinoma, D-eFLOW (before and after USCA) had similar sensitivity to PD-EUS (before and after USCA) and CD-EUS (before and after USCA). D-eFLOW after contrast showed the highest accuracy (82.3 %) and negative predictive value (53.8 %) among all the modalities investigated. There was a good correlation among the ViVA scores for D-eFLOW before contrast, those for D-eFLOW EUS, and those for PD-EUS and CD-EUS. The reliability of the ViVA scale was excellent with an ICC of 0.81. In conclusion, D-eFLOW EUS is a sensitive, reliable, and highly accurate method of assessment of pancreatic vascularity. D-eFLOW EUS with contrast was more sensitive than PD-EUS and CD-EUS for assessment of pancreatic vascularity.

Keywords Pancreatic cancer · Sonazoid^{TM} · Ultrasound contrast agents · Directional eFLOW · Power Doppler

K. Das and M. Kudo contributed equally to this work.

K. Das · M. Kudo (✉) · M. Kitano · H. Sakamoto · T. Komaki
Department of Gastroenterology and Hepatology,
Kinki University School of Medicine,
Osaka-Sayama, Osaka, Japan
e-mail: m-kudo@med.kindai.ac.jp

K. Das
Department of Gastroenterology, Max Balaji Hospital,
Patparganj, New Delhi, India

T. Takagi · K. Yamao
Department of Gastroenterology, Aichi Cancer Center,
Nagoya, Japan

Introduction

Ultrasound imaging is inexpensive, portable, and widely available. With the introduction of the second-generation perfluorobutane-based microbubble ultrasound contrast agent Sonazoid^{TM} (Daiichi Sankyo, Tokyo, Japan), ultrasound has become a method for assessment of vascularity, is useful for measuring blood volume and flow [1], and has shown good correlation with CT and MRI data [2, 3]. PD-EUS or CD-EUS with or without a sonographic contrast agent has been used for the diagnosis of pancreatic tumors. PD-EUS and CD-EUS were found to be better than conventional EUS for the evaluation of vascularity, and they were also useful for the differential diagnosis of pancreatic carcinomas from chronic pancreatitis [4]. EUS is well

known as a highly sensitive modality for evaluation of pancreatic carcinomas (especially for lesions <2 cm) [5]. D-eFLOW (Aloka Co., Ltd., Tokyo, Japan) is a new modality for blood flow imaging that detects blood flow in small vessels in detail and with high sensitivity. In the present study, we investigated the utility of the combined use of these two important advanced techniques, EUS-guided D-eFLOW before and after administration of USCA (Sonazoid^{TM}), for assessing the vascular perfusion of solid pancreatic lesions compared to power Doppler or color Doppler before and after administration of USCA. We also developed and evaluated a new objective protocol for a Visual Vascular Assessment (ViVA) scale for estimation of vascular perfusion of solid pancreatic lesions and assessed its reliability using the interclass correlation coefficient.

Materials and methods

This study was performed with the approval of the ethics committee of Kinki University School of Medicine. All the patients were informed of the purpose of the study, and written informed consent was obtained from all patients according to the ethics guidelines of the Declaration of Helsinki. Between January 2007 and March 2007, 75 patients were prospectively evaluated using EUS for pancreatic lesions, which included cystic lesions ($n = 32$), space-occupying lesions (SOL) of the pancreas ($n = 35$), and chronic pancreatitis ($n = 8$). The maximum diameter of the lesions was 29 ± 9 mm.

Inclusion criteria

Inclusion criteria were: (1) age >18 years; (2) a pancreatic solid mass on radiology (transabdominal ultrasonography, CT scan, MRI, or EUS); (3) histological diagnosis by EUS-FNA and surgical histopathology.

Exclusion criteria

Exclusion criteria included: (1) cystic mass of the pancreas; (2) severe co-morbid conditions; (3) incomplete study ($n = 2$); (4) non-availability of histological diagnosis ($n = 3$).

All patients underwent B-mode EUS followed by D-eFLOW EUS, PD-EUS, and CD-EUS before and after USCA administration.

Directional eFLOW imaging

D-eFLOW (Aloka Co., Ltd., Tokyo, Japan), a new high-definition modality for blood flow imaging, can detect blood flow in minute vessels in more detail than conventional power or color Doppler. D-eFLOW is a type of directional power Doppler method, but with improved spatial and temporal resolution. In order to increase spatial resolution, D-eFLOW uses broadband transmission and an optimized transmitting waveform. D-eFLOW uses a transmitting waveform that is designed not only for broadband but also has less overlap computed by frequency domain simulation. Also, D-eFLOW increases packet size to calculate Doppler shift in order to increase transmitting power. Further, at the receiving end, a moving target indicator (MTI) filter is optimized, and the cutoff frequency of the MTI filter is changed dynamically by the estimated clutter signal. In order to increase the temporal resolution, a parallel processing block is enhanced. This enhancement can increase the parallel processing number at one processing block of a partial scan operation, so it can increase the real pulse repeating frequency (PRF) without increasing the PRF for the calculation of Doppler shift. Thus, D-eFLOW imaging provides improved spatial and temporal resolution of the finer parenchymal blood vessels.

Endoscopic ultrasound imaging protocol

One EUS procedure (B-mode EUS, PD-EUS, and CD-EUS) was performed by one endosonographer (M.K. or H.S.), qualified by the Japan Gastroenterological Endoscopy Society, using the Olympus GF-UCT260 convex array echoendoscope (Olympus Corp., Tokyo, Japan) and the ALOKA ProSound-α10 (Aloka Co., Ltd., Tokyo, Japan) ultrasound console for image analysis. EUS was first performed with gray-scale imaging using fundamental B-mode EUS. When B-mode EUS detected a lesion, the mode was changed sequentially from the D-eFLOW mode to power Doppler and color Doppler modes. At first, signals from the vessels in the tissue lesion and the surrounding tissues were observed by the D-eFLOW mode followed by power Doppler and color Doppler modes before using USCA. The differences in flow imaging between the nodule and surrounding tissue were analyzed. When the tumor lesions were large, we compared the vascularity of the tumor lesions with that of the surrounding pancreatic parenchyma by rotating, advancing, or retracting the scope. The Doppler frequency was 5 MHz for power and color Doppler and 6 MHz for D-eFLOW, and the gain examination was set to just below the level that produced random power noise. Secondly, 0.7 ml of the echo-enhancing agent Sonazoid^{TM} was injected. When given as a bolus, enhancement persisted for approximately 10 min. After the signal enhancement reached the maximum level, the differences in flow imaging between the nodule and the surrounding tissues were analyzed. When the tumor lesions were large, we compared the vascularity of the tumor lesions with that of the surrounding pancreatic parenchyma by rotating, advancing, or retracting

the scope. Maximum enhancement was obtained in around 30 s, and all measurements by the D-eFLOW, power Doppler, and color Doppler modes were taken sequentially within 90–150 s after USCA administration. The sequence and the protocol after USCA were the same for all patients. All interventional procedures such as EUS-FNA were done after contrast vascular assessment by D-eFLOW/power Doppler/color Doppler protocols.

To prevent interoperator variability, all procedures (B-mode EUS, D-eFLOW EUS, PD-EUS, and CD-EUS) were performed by the same operators using the same examination protocols. All data were continuously recorded using digital video recorders as DVDs, while still pictures of each lesion were documented on both HDD and compact disks. All the EUS (EUS, PD-EUS, and CE-EUS) data were then independently peer reviewed (for assessment of ICC) by two reviewers (K.D. and M.K.), and the final scoring and ranking were decided by consensus.

EUS-guided fine-needle aspiration (EUS-FNA)

We performed EUS-guided fine-needle aspiration (EUS-FNA) using disposable 22-gauge aspiration needles (NA-200H-8022, Olympus, Tokyo, Japan, and Echotip, Wilson Cook Medical Inc., Winston-Salem, NC, USA). The EUS-FNA technique is well established [6]. Briefly, the needle was advanced into the lesion under EUS visualization. The central stylet was removed, a 10-ml syringe with extension tubing was attached to the hub of the needle, and suction was applied as the needle was moved backward and forward within the lesion. This back and forward motion of the needle was repeated more than ten times within the lesion during one puncture session. After ceasing suction, the needle was then retracted into the sheath, and the entire assembly was removed. We followed all patients, and adverse events related to EUS-FNA were assessed immediately, after 24 h, and after 30 days.

Methodology for definitive diagnosis

All lesions were ultimately diagnosed by histological and/or cytological examination of tissues obtained surgically, EUS-FNA, biopsy of liver metastases, or autopsy. When EUS-FNA was the only source for histological analysis, a negative biopsy was not sufficient to rule out the possibility of carcinoma. Patients with negative biopsies on EUS-FNA were followed for a minimum of 6 months. Six months after the evaluation, patients with no signs of disease progression or patients with disease regression were considered to have pancreatic inflammation at the time of EUS-FNA. Some of the patients (e.g., chronic pancreatitis with SOL) included in this study had been followed up at different times before their inclusion in the study. Further, the author evaluating the EUS images (K.D.) was blinded to the clinical history/final diagnosis of the study.

Visual Vascular Assessment scale

The following criteria (Fig. 1a–g) were used to quantify the vascularity of the solid pancreatic lesions. Independently gained conclusions of the two reviewers were compared to determine the intraobserver ICC.

Scoring was: (0) no vessels, (1) discrete spotty (1–2) vessels less than 1 cm in length, (2) discrete multiple scattered vessels (>2) less than 1 cm in length but no longitudinal vessel formation, (3) discrete thin longitudinal vessels (1–2) more than 1 cm in length, (4) discrete multiple longitudinal vessels (>2) more than 1 cm in length, (5) non-discrete diffuse signals in <50 % of the visualized area, and (6) non-discrete diffuse signals in >50 % of the visualized area.

Vascular ranks were assigned to all lesions after assessment of ViVA scores by D-eFLOW/power Doppler/color Doppler. Hypovascular lesions, where the ViVA score of the lesion was less than the ViVA score of the surrounding pancreatic parenchyma, were assigned vascular rank 1; similarly, isovascular and hypervascular lesions, where the ViVA score of the lesion was equal to or greater than the ViVA score of the surrounding pancreatic parenchyma, were assigned vascular ranks 2 and 3, respectively.

Statistical analysis

Sensitivities for detecting pancreatic nodules were calculated for EUS. The McNemar test was performed to compare the detection values between the two examinations. The diagnostic ability (sensitivity, specificity, and accuracy) of differentiating pancreatic carcinomas from other tumors by evaluating vascularity was calculated and compared between PD-EUS and CD-EUS by the McNemar test. A p value less than 0.05 was considered significant. For interobserver effects, the ICC was calculated using the single-measure intraclass correlation coefficient-two-way mixed effect model (absolute agreement definition). Spearman's rank test (2-tailed) was used for correlation of the vascular ranks and the rho correlation coefficient, and the p values were calculated using SPSS. All statistical analyses were done using the SPSS statistical software package, version 10.0 (SPSS Inc., USA).

Results

Patients

Thirty-five patients were included in this study. The characteristics of the patients, their age and sex distribution,

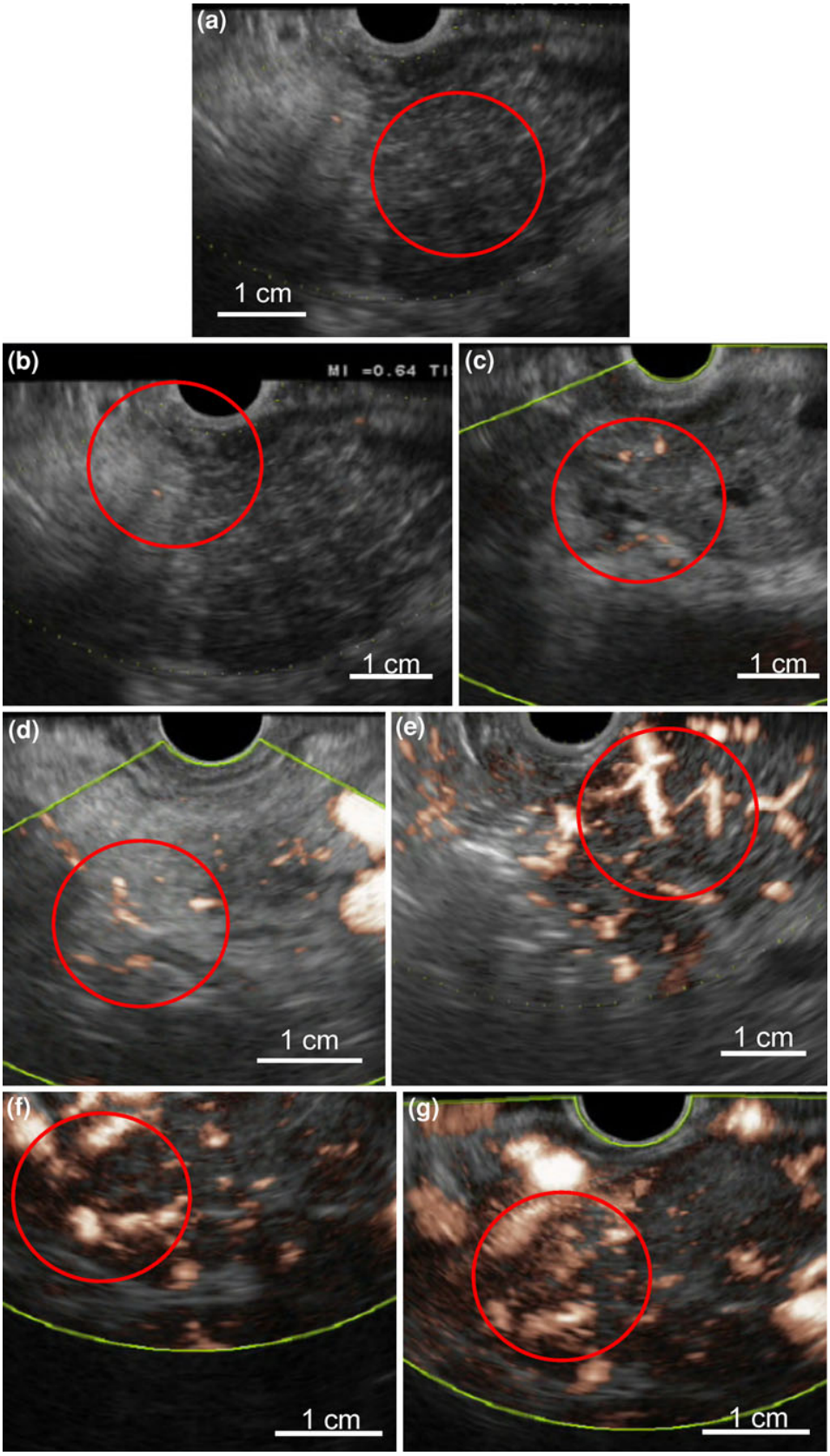

Fig. 1 Visual Vascular Assessment (ViVA) scale for directional eFLOW (or power Doppler or color Doppler) (*red circle* represents the lesion). No vessels: **a** score 0. Spotty vessel: **b** score 1 (1–2 vessels), **c** score 2 (>2 vessels). Longitudinal vessel: **d** score 3 (1 vessel), **e** score 4 (≥2 vessels). Oversaturating vessel: **f** score 5 (<50 % of visualized area), **g** score 6 (>50 % of visualized area)

and histology are shown in Table 1. The mean age of the patients was 64.5 ± 10.8 years, and the male-to-female ratio was 20:15.

Visual Vascular Assessment scale

Figure 1a–g shows the sample ViVA scores for D-eFLOW (and the same for power Doppler and color Doppler) standardized for all cases. Figure 2a–f shows the comparative D-eFLOW, power Doppler, and color Doppler images and rankings before and after USCA. Table 2 shows the correlation of the ViVA vascularity assessment by D-eFLOW, power Doppler, and color Doppler assigned to the cases in accordance to the ViVA scores. The vascular assessment by D-eFLOW before USCA administration correlated significantly well with power Doppler (before USCA) and color Doppler ($p < 0.05$). Further, D-eFLOW after USCA administration also correlated significantly with power Doppler after USCA ($p = 0.013$). Expectedly, power Doppler and color Doppler vascular ranks strongly correlated both before and after contrast. There were no significant adverse effects in the immediate post-procedure follow-up period.

Sensitivity, specificity, PPV, NPV, and diagnostic accuracy

For calculating sensitivity and specificity values, we assumed that the hypovascular pattern of the lesion on D-eFLOW/PD-EUS/CD-EUS was diagnostic of pancreatic adenocarcinoma. D-eFLOW after USCA administration had the highest sensitivity at 84.6 % (Table 3). D-eFLOW before USCA was less sensitive for assessing the vascularity of pancreatic lesions. D-eFLOW vascularity patterns both before and after USCA administration were more sensitive and accurate than corresponding power Doppler and color Doppler patterns. While NPV was comparable and low in all the groups, D-eFLOW after USCA resulted in the highest PPV values comparable to CE-MDCT and the highest diagnostic accuracy rates among all the groups. However, these differences were not significant.

Interobserver interclass correlation coefficient

The interobserver ICC values were calculated for both the ViVA scores and the derived vascular ranks (Table 4). The overall ICC value was 0.81 (95 % CI = 0.75–0.86), while the D-eFLOW pattern had the highest ICC value at 0.87 (95 % CI = 0.75–0.93).

Discussion

The results of vascularity assessment by the new imaging modality D-eFLOW correlated well with those by PD-EUS and CD-EUS. This shows that D-eFLOW is comparable to power Doppler and color Doppler for vascularity assessment of solid pancreatic lesions. Further, the new objective ViVA scale is useful for assessing pancreatic tissue vascularity. D-eFLOW before USCA administration correlated with the assessment by PD-EUS and CD-EUS, thus confirming that D-eFLOW is reliable for evaluation of imaging vascularity in solid pancreatic lesions.

In this study, the sensitivity of D-eFLOW was comparable to that of EUS-FNA for the diagnosis of pancreatic adenocarcinomas. This was because D-eFLOW after USCA administration detected two additional (of 26) hypovascular patterns compared to D-eFLOW before USCA. To the best of our knowledge, there have been no previous studies on EUS-guided D-eFLOW with Sonazoid™ in pancreatic adenocarcinomas. D-eFLOW patterns both before and after USCA administration showed a higher sensitivity than both PD-EUS and CD-EUS. The higher sensitivity obtained by D-eFLOW for the assessment of pancreatic parenchymal vascularity may result from the fact that D-eFLOW shows less blood flow outside of the vessels than the color Doppler and power Doppler methods, because the tissues, blood flow, and B-mode

Table 1 Patient characteristics for 35 solid pancreatic lesions

	Pancreatic cancer ($n = 26$)	Inflammatory mass ($n = 5$)	Endocrine tumor ($n = 4$)
Mean age ± SD (years)	66.0 ± 10.4	64.9 ± 10.7	65.8 ± 10.5
M:F ratio	15:11	3:2	2:2
Maximum diameter of the tumor lesion (mm)	30 ± 10	28 ± 10	25 ± 5
Duration of disease (days)[a]	17	242	17.25
Histology	Pancreatic adenocarcinoma ($n = 26$)	Autoimmune pancreatitis ($n = 2$) Chronic pancreatitis ($n = 3$)	Insulinoma ($n = 2$) Endocrine tumor ($n = 2$)

[a] Duration of disease = time of onset of symptoms to inclusion in the study

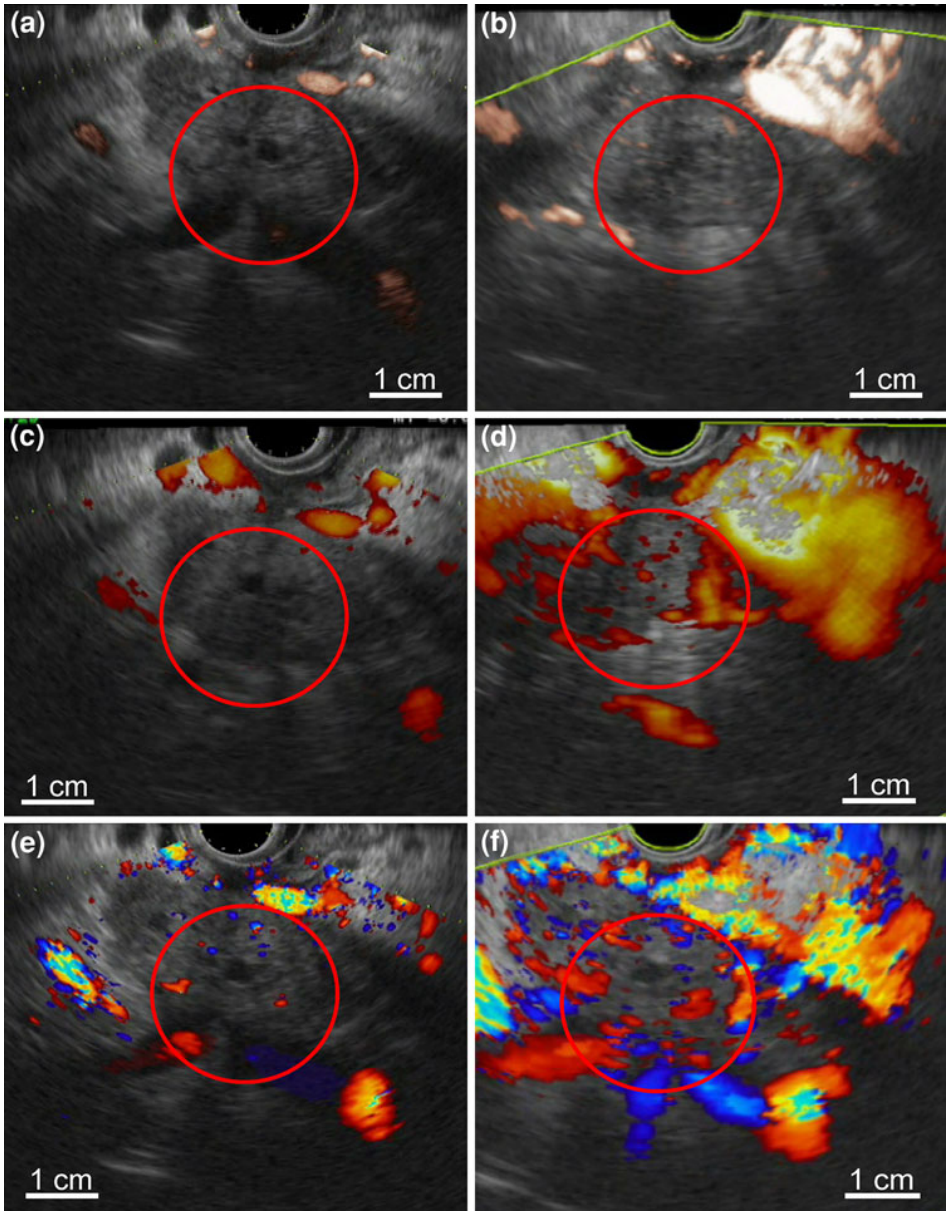

Fig. 2 Parenchymal vascularity before and after contrast administration using the ViVA scale. Hypovascular lesion (*red circle* represents the lesion). **a** Directional eFLOW before contrast administration [ViVa score = 1/10 (S/T)], **b** directional eFLOW after contrast administration [ViVa score = 5/3 (S/T)], **c** power Doppler before contrast administration [ViVa score = 3/2 (S/T)], **d** power Doppler after contrast administration [ViVa score = 6/4 (S/T)], **e** color Doppler before contrast administration [ViVa score = 4/2 (S/T)], and **f** color Doppler after contrast administration [ViVa score = 6/4 (S/T)]

Table 2 Correlation among histological diagnosis, MDCT, D-eFLOW, power Doppler, and color Doppler ViVA scale

		Diagnosis	Directional e-FLOW		Power Doppler		Color Doppler	
			BC	AC	BC	AC	BC	AC
Diagnosis		×	$p = 0.034$	NS	NS	NS	NS	NS
Directional e-FLOW	BC	$p = 0.034$	×	NS	$p < 0.026$	NS	$p = 0.044$	NS
	AC	NS	NS	×	$p = 0.018$	$p = 0.002$	$p = 0.003$	$p = 0.001$
Power Doppler	BC	NS	$p < 0.026$	$p = 0.018$	×	$p = 0.047$	$p < 0.001$	$p = 0.044$
	AC	NS	NS	$p = 0.002$	$p = 0.047$	×	NS	$p < 0.001$
Color Doppler	BC	NS	$p = 0.044$	$p = 0.003$	$p < 0.001$	NS	×	NS
	AC	NS	NS	$p = 0.001$	$p = 0.044$	$p < 0.001$	NS	×

rho correlation coefficient, *BC* before administration of ultrasound contrast agent, *AC* after administration of ultrasound contrast agent, *NS* not significant

Table 3 Sensitivity, specificity, accuracy, PPV, and NPV of the different imaging modalities among the patients

Pancreatic cancer ($n = 26$), inflammatory mass ($n = 5$), and endocrine tumor ($n = 4$)

	Sensitivity	Specificity	Accuracy	PPV	NPV
D-eFLOW before contrast (%)	69.2	77.8	71.4	90	46.7
D-eFLOW after contrast (%)	84.6	77.8	82.3	91.7	53.8
Power Doppler before contrast (%)	65.4	77.8	68.8	89.5	43.8
Power Doppler after contrast (%)	61.5	66.7	62.9	84.2	37.5
Color Doppler before contrast (%)	61.5	88.9	68.6	94.1	44.4
Color Doppler after contrast (%)	61.5	77.8	65.7	88.9	41.2

Table 4 Interobserver interclass correlation coefficient (ICC) scores of solid pancreatic lesions

	ICC coefficient	95 % confidence intervals	Standardized item alpha
Overall	0.81	0.75–0.86	0.91
Directional-eFLOW	0.87	0.79–0.93	0.93
Power Doppler	0.77	0.62–0.86	0.89
Color Doppler	0.85	0.74–0.91	0.92
Directional-eFLOW vascularity rank	0.72	0.55–0.83	0.83
Power Doppler vascularity rank	0.58	0.36–0.74	0.74
Color Doppler vascularity rank	0.80	0.68–0.88	0.89

ultrasound are imaged simultaneously. Moreover, because there are no angle-dependent problems like those encountered with the Doppler method, more accurate blood flow delineation is possible. Furthermore, to optimize color Doppler sonography, it is common to increase the color gain setting as much as possible until noise develops and then to lower the gain slightly to eliminate noise [7]. However, this method tends to exaggerate the spatial location of the real flow signal, leading to "oversaturation" and resulting in flow signals that are not confined to the patent lumen [8, 9]. Due to oversaturation, the spatial distribution of the color signals can substantially exceed the true dimensions of vessels, especially when evaluating the tissue parenchyma, whereas the high spatial resolution of D-eFLOW imaging enables excellent display. This phenomenon of "oversaturation" is accentuated after the administration of microbubble contrast agents and leads to blooming of the visualized field. This makes the evaluation of vascularity very difficult and is the main reason why both power and color Doppler after contrast agent administration have poor sensitivities compared to D-eFLOW. D-eFLOW imaging rarely "oversaturates" results, and the displays are excellent even after the administration of microbubble contrast agents. It gives more confidence in assessing tissue vascularity. For the same reasons, D-eFLOW had a better specificity than power Doppler. We observed that the specificity of power Doppler and color Doppler decreased after administration of contrast, but in the case of D-eFLOW, there was no such decrease. This further demonstrates that D-eFLOW is perhaps a better technology for vascular imaging compared to power Doppler or color Doppler. D-eFLOW after contrast had higher PPV, NPV, and accuracy than other modalities and hence was the most valuable.

Many other studies on CE-EUS or CE-US have used subjective criteria for the assessment of tissue vascularity and graded tissues as hypovascular, isovascular, and hypervascular after comparing the enhancement patterns of the SOL and the surrounding tissues. Subjective methods may have intraoperator and interoperator reliability issues, making it difficult to compare studies between different centers and different contrast agents [2, 4, 9, 10, 11]. For this study, we developed an easy, objective assessment method for the tissue vascularity of solid pancreatic lesions. We divided the vascular patterns into three broad categories: spotty, linear, and oversaturation. Each vascular pattern was additionally subdivided into two other patterns based on few (1–2) or multiple (>2) signals, thus leading to a total of seven scores from a minimum score of 0 to a maximum score of 6. The positive correlation obtained between the vascular values from power Doppler and color Doppler confirmed the possible use of the scores obtained in this work to study tissue vascularity. This objective assessment does not preclude the classification of the lesions into hypovascular, isovascular, and hypervascular, and in fact makes it easier, objective, and reliable.

We also evaluated the interobserver ICC values for D-eFLOW/power Doppler/color Doppler ViVA scores, as well as the D-eFLOW/power Doppler/color Doppler vascular ranks. We found a very good overall ICC value of 0.81 (95 % CI = 0.75–0.86). This demonstrated that our objective ViVA scoring method was easy to understand,

reliable, and highly standardizable. Furthermore, we observed that the D-eFLOW ICC values were the best compared to those obtained from power Doppler and color Doppler. Thus, the D-eFLOW patterns are the easiest to standardize and may be useful for tasks such as vascular follow-up assessment of individual lesions after chemotherapy or radiotherapy.

We conclude that D-eFLOW is a simple, sensitive, reliable, and highly accurate method for the assessment of tissue vascularity in solid pancreatic lesions. D-eFLOW with a contrast agent is more sensitive than power Doppler and color Doppler for the vascular assessment of pancreatic adenocarcinomas. However, the limitations of this study include a limited number of patients ($n = 35$) and a relatively skewed patient distribution (pancreatic cancer, 26 with inflammatory masses and 4 with endocrine tumors). Another limitation is that the same examiner sequentially used eFLOW, power Doppler, and color Doppler. Therefore, this protocol itself may lead to a significant examiner bias. Larger studies of D-eFLOW with Sonazoid^{TM} contrast and a further rigorous evaluation of the vascular scores are needed before this method can be universally accepted.

Acknowledgments The present study was supported by grants from the Japan Society for Promotion of Science and the Japan Research Foundation for Clinical Pharmacology.

Conflict of interest None.

References

1. Umemura S. Debut of a new contrast agent (Ed). J Med Ultrasound. 2007;34:81.
2. Kitano M, Kudo M, Maekawa K, Suetomi Y, Sakamoto H, Fukuta N, et al. Dynamic imaging of pancreatic diseases by contrast enhanced coded phase inversion harmonic ultrasonography. Gut. 2004;53(6):854–9.
3. Kiessling F, Krix M, Heilmann M, Vosseler S, Lichy M, Fink C, et al. Comparing dynamic parameters of tumor vascularization in nude mice revealed by magnetic resonance imaging and contrast-enhanced intermittent power Doppler sonography. Invest Radiol. 2003;38(8):516–24.
4. Hocke M, Schulze E, Gottschalk P, Topalidis T, Dietrich CF. Contrast-enhanced endoscopic ultrasound in discrimination between focal pancreatitis and pancreatic cancer. World J Gastroenterol. 2006;12(2):246–50.
5. Boujaoude J. Role of endoscopic ultrasound in diagnosis and therapy of pancreatic adenocarcinoma. World J Gastroenterol. 2007;13(27):3662–6.
6. Bhutani MS, Hawes RH, Baron PL, Sanders-Cliette A, van Velse A, Osborne JF, et al. Endoscopic ultrasound guided fine needle aspiration of malignant pancreatic lesions. Endoscopy. 1997;29(9):854–8.
7. Kruskal JB, Newman PA, Sammons LG, Kane RA. Optimizing Doppler and color flow US: application to hepatic sonography. Radiographics. 2004;24(3):657–75.
8. Machi J, Sigel B, Roberts AB, Kahn MB. Oversaturation of color may obscure small intraluminal partial occlusions in color Doppler imaging. J Ultrasound Med. 1994; 13(10):735–41; quiz 821–732.
9. Sakamoto H, Kitano M, Suetomi Y, Maekawa K, Takeyama Y, Kudo M. Utility of contrast-enhanced endoscopic ultrasonography for diagnosis of small pancreatic carcinomas. Ultrasound Med Biol. 2008;34(4):525–32.
10. Numata K, Ozawa Y, Kobayashi N, Kubota T, Shimada H, Nozawa A, et al. Contrast-enhanced sonography of pancreatic carcinoma: correlations with pathological findings. J Gastroenterol. 2005;40(6):631–40.
11. Okamoto Y, Kawamoto H, Takaki A, Ishida E, Ogawa T, Kuwaki K, et al. Contrast-enhanced ultrasonography depicts small tumor vessels for the evaluation of pancreatic tumors. Eur J Radiol. 2007;61:163–9.

J Med Ultrasonics (2013) 40:325–357
DOI 10.1007/s10396-013-0460-5

REVIEW ARTICLE

JSUM ultrasound elastography practice guidelines: liver

Masatoshi Kudo · Tsuyoshi Shiina · Fuminori Moriyasu · Hiroko Iijima · Ryosuke Tateishi · Norihisa Yada · Kenji Fujimoto · Hiroyasu Morikawa · Masashi Hirooka · Yasukiyo Sumino · Takashi Kumada

Received: 21 April 2013 / Accepted: 26 April 2013 / Published online: 16 August 2013

Abstract In diffuse liver disease, it is extremely important to make an accurate diagnosis of liver fibrosis prior to determining indications for therapy or predicting treatment outcome and malignant potential. Although liver biopsy has long been the gold standard in the diagnosis of liver fibrosis, it is still an invasive method. In addition, the sampling error is an intrinsic problem of liver biopsy. Non-invasive serological methods for the diagnosis of liver fibrosis can be affected by factors unrelated to the liver. Recently, after the introduction of FibroScan, it became possible to measure liver fibrosis directly and non-invasively by elastography, which has attracted attention as a non-invasive imaging diagnostic tool for liver fibrosis. In addition, real-time tissue elastography is currently being used to conduct clinical trials at many institutions. Moreover, virtual touch quantification enables the observation of liver stiffness at any location by simply observing B-mode images. Furthermore, the recently developed ShearWave elastography visualizes liver stiffness on a color map. Elastography is thought to be useful for all types of diffuse liver diseases. Because of its association with portal hypertension and liver carcinogenesis, elastography is expected to function as a novel prognostic tool for liver disease. Although various elastographic devices have been developed by multiple companies, each device has its own measurement principle, method, and outcome, creating

M. Kudo (✉) · N. Yada
Department of Gastroenterology and Hepatology, Kinki University School of Medicine, 377-2 Ohno-Higashi, Osakasayama, Osaka 589-8511, Japan
e-mail: m-kudo@med.kindai.ac.jp

T. Shiina
Human Health Sciences, Graduate School of Medicine, Kyoto University, Kyoto, Japan

F. Moriyasu
Department of Gastroenterology and Hepatology, Tokyo Medical University, Tokyo, Japan

H. Iijima
Department of Internal Medicine, Hyogo College of Medicine, Nishinomiya, Hyogo, Japan

R. Tateishi
Department of Gastroenterology, Graduate School of Medicine, The University of Tokyo, Tokyo, Japan

K. Fujimoto
Department of Internal Medicine, Nagayama Hospital, Kumatori, Osaka, Japan

K. Fujimoto
Division of Clinical Research, ONH Minamiwakayama Medical Center, Tanabe, Wakayama, Japan

H. Morikawa
Department of Hepatology, Graduate School of Medicine, Osaka City University, Osaka, Japan

M. Hirooka
Department of Gastroenterology and Metabology, Ehime University Graduate School of Medicine, Toon, Ehime, Japan

Y. Sumino
Division of Gastroenterology and Hepatology, Toho University Ohmori Medical Center, Tokyo, Japan

T. Kumada
Department of Gastroenterology and Hepatology, Ogaki Municipal Hospital, Ogaki, Gifu, Japan

confusion in clinical settings. Therefore, it is extremely important to understand the characteristics of each device in advance. The objective of this guideline, which describes the characteristics of each device based on the latest knowledge, is for all users to be able to make the correct diagnosis of hepatic fibrosis by ultrasound elastography.

Keywords Elastography · Elasticity · Shear wave · Stiffness · Strain · Liver fibrosis

Preamble

In diffuse liver disease, it is extremely important to make an accurate diagnosis of liver fibrosis prior to determining indications for antiviral therapy or predicting treatment outcome and malignant potential. Although liver biopsy has long been the gold standard in the diagnosis of liver fibrosis, it is still an invasive method with potential bleeding and severe pain. In addition, sampling error is an intrinsic problem of liver biopsy because of the small sampling size, and diagnostic consistency may be influenced by inter-observer variability. There are many reports of non-invasive serological methods for the diagnosis of liver fibrosis, including the use of serum markers for liver fibrosis (e.g., platelet, hyaluronic acid, type IV collagen 7S domain), and algorithm-based serum models (e.g., aminotransferase/platelet ratio index (APRI), FibroIndex, FIB-4, FibroTest). However, these methods can be affected by factors unrelated to the liver.

Elastography, developed as a non-invasive tool to measure tissue elasticity, has advanced particularly in the field of breast cancer. Recently, it became possible to measure liver fibrosis directly and non-invasively by elastography, which has attracted attention as a non-invasive imaging diagnostic tool for liver fibrosis. Especially after the introduction of FibroScan, a device to measure the stiffness of liver, the application of elastography for the measurement of liver stiffness has been investigated. In addition, real-time tissue elastography, that is, the world's first practical ultrasound (US) elastographic technology developed in Japan, is currently being used to conduct clinical trials at many institutions. Moreover, virtual touch quantification (VTQ), in which constant pressure exerted by focused US generates a shear wave, enables the observation of liver stiffness at any location by simply observing B-mode images. With this technology, it is possible to examine cases with ascites retention for which FibroScan is not useful. Furthermore, a recently developed ShearWave elastography visualizes liver stiffness on a color map. Although elastography has been used mostly to examine viral liver disease, non-alcoholic fatty liver disease (NAFLD), autoimmune hepatitis, drug-induced liver injury, and alcoholic liver disease, the technology is thought to be useful for all types of diffuse liver diseases, such as primary biliary cirrhosis, Budd–Chiari syndrome, and idiopathic portal hypertension. Because of its association with portal hypertension and liver carcinogenesis, elastography is expected to function as a novel prognostic tool for liver disease. Although various elastographic devices have been developed by multiple companies, each device has its own measurement principle, method, and outcome, creating confusion in clinical settings. Therefore, it is extremely important to understand the characteristics of each device in advance.

In this guideline, we provide the latest knowledge and understanding of elastographic devices, particularly those widely used for the diagnosis of liver fibrosis.

Characteristics of each device

US elastography is categorized into four groups based on the excitation method and measurement quantity, as described in Basics and Terminology. We will discuss the devices that are currently used to diagnose liver fibrosis.

1. Strain elastography: Hitachi, Siemens, GE, and Toshiba
2. Acoustic radiation force impulse (ARFI) imaging: Siemens
3. Shear wave elastography: Siemens, Philips, and SuperSonic Imagine
4. Transient elastography: FibroScan

Strain imaging

Strain elastography

Real-time tissue elastography (Hitachi)

(A) Introduction

Commercialized by Japanese companies using technology developed in Japan, Real-time Tissue Elastography® (RTE) is the world's first practical imaging modality for the diagnosis of tissue elasticity. RTE belongs to the category of strain elastography and uses the combined autocorrelation method to measure tissue strain caused by manual compression or heartbeat. With RTE, relative tissue strain is displayed on conventional B-mode images in real time. Areas with lower strain (relatively hard tissue) and those with higher strain (relatively soft tissue) in the region of interest (ROI) are displayed in blue and red, respectively, with a 256-color gradation (Figs. 1, 2) [1–3].

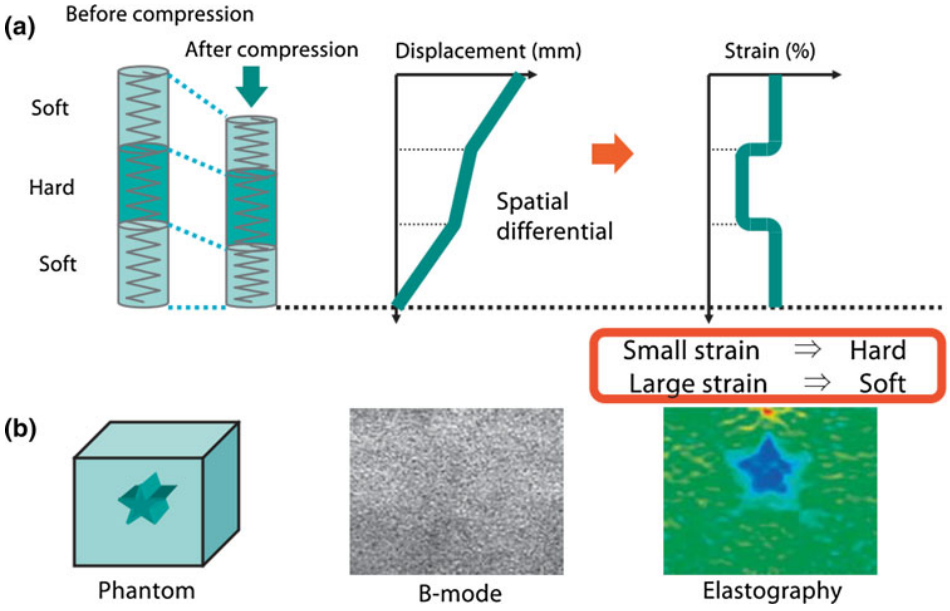

Fig. 1 Principle of RTE

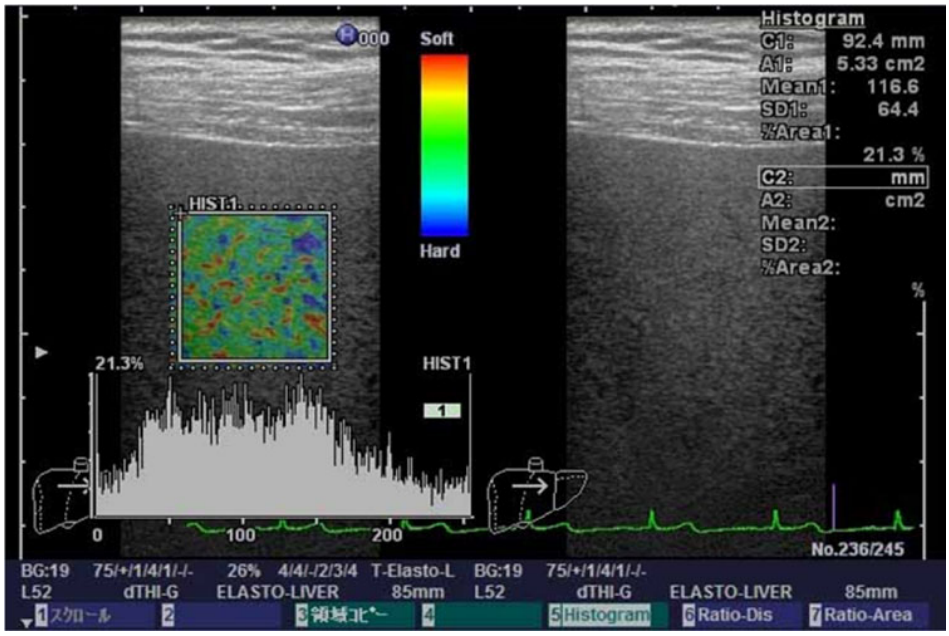

Fig. 2 RTE imaging. *Left* superimposition of RTE and B-mode images, *right* B-mode image. The measurement tool calculates feature values and strain ratio

(B) Indication

RTE is indicated for various diffuse liver diseases, including virus liver disease [2–9], NAFLD [10], autoimmune hepatitis, primary biliary liver disease, alcoholic liver disease, and drug-induced liver injury. RTE is also reportedly useful for the diagnosis of portal hypertension [11]. In addition, the usefulness of RTE in the prognosis of liver cancer is currently being investigated in a multicenter study.

(C) Procedures (including tips and tricks)

RTE application software can be loaded by different US imaging devices from Hitachi Aloka Medical (Tokyo, Japan), including but not limited to HI VISION Ascendus, HI VISION Preirus, HI VISION Avius, Noblus, HI VISION 900, EUB-8500, and EUB-7500. Imaging is performed with a 7–3 MHz linear probe (EUP-L52).

(1) Scanning method [2–4, 7–9]

Successful RTE imaging depends on the clarity of B-mode images—the fundamental US images—and therefore B-mode images need to be void of artifacts.

1. Visualize the right hepatic lobe from the right intercostal space of a patient in the supine position with the right arm elevated to make the intercostal space wider.
2. Place a probe lightly against the skin without vibration.

3. Select an extraction point at which B-mode images are void of artifacts.
4. Try to obtain images displaying vertical, not horizontal, strain by placing the probe to generate an echo beam in the direction of the heart.
5. While the patient is lightly holding breath, make sure that RTE images are displayed periodically by cardiac motion.

(2) ROI setup

The ROI can be established in two ways: place the ROI only inside the liver [2–4, 7–9, 12] or place it over the liver and the surrounding tissue, such as subcutaneous and/or muscle layer [13, 14]. In the latter case, however, color distribution on RTE images changes depending on the ratio between the liver and the surrounding tissue in the ROI because RTE displays relative tissue strain. Accordingly, any inappropriate area or object should be excluded from the ROI to avoid introducing artifacts. Placing ROI inside the liver is the key to generating uniform images of the entire liver [3, 7, 9, 15]. Although selecting a large ROI area with presumably no or few artifacts can result in successful imaging, it is difficult to avoid large blood vessels if ROI is too large. For this reason, a 2.5 × 2.5 cm square ROI is often used [8, 9].

1. Avoid large blood vessels (to eliminate artifacts from the anechoic area) (Fig. 3a).
2. Avoid the area near the ribs because the acoustic shadow will be displayed in blue on US images (Fig. 3b).
3. Avoid the surface of the liver because it is often displayed in blue due to multiple reflection echo (Fig. 3c).
4. Avoid areas deep inside the liver because they often appear blue due to poor ultrasound penetration (Fig. 3d).

(3) When having trouble with observation

1. Try another intercostal space.
2. Select an intercostal space which is softer and has a thinner subcutaneous layer.
3. Avoid including body organs under the subcutaneous layer, such as ribs and lungs, in imaging.

(4) Selection of frames for analysis

1. Select frames with strain generated in the direction of depth.
2. Select frames with no artifacts.
3. Good images may be obtained in the end of left ventricular diastole in electrocardiographic gating or at the largest downward wave on a strain graph (Fig. 4).

(D) Results (what do the values mean?)

In chronic hepatitis, the liver tissue hardens unevenly as fibrosis advances. Accordingly, if the ROI is placed only over the liver, it will enhance the color variation of RTE images, increasing areas with relatively low strain (blue area). This results in the generation of images with a mottled appearance (Fig. 5) [2, 4, 9]. Using a mechanical model of fibrosis progression in basic research, Shiina et al. [16] showed that areas with low strain increase as fibrosis progresses, and strain distribution becomes complex, as shown in clinical cases.

(1) Subjective evaluation method

Because liver elasticity score, obtained by visual assessment of low strain areas (blue area) on RTE images

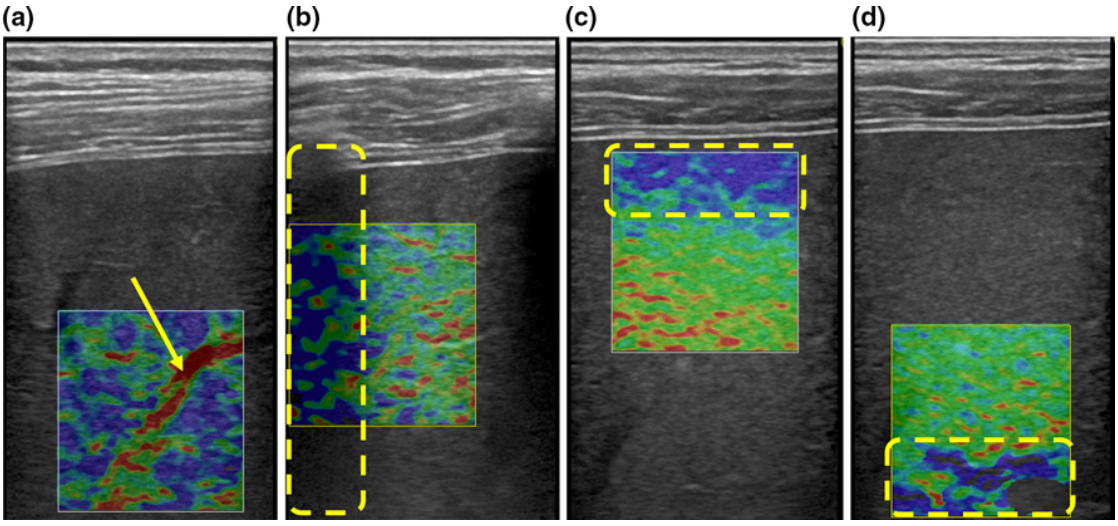

Fig. 3 RTE image artifacts. Large blood vessel (**a**), acoustic shadow (**b**), multiple reflection echo (**c**), and poor ultrasound penetration (**d**) are major artifacts of RTE. For RTE, these artifacts should be avoided [12]

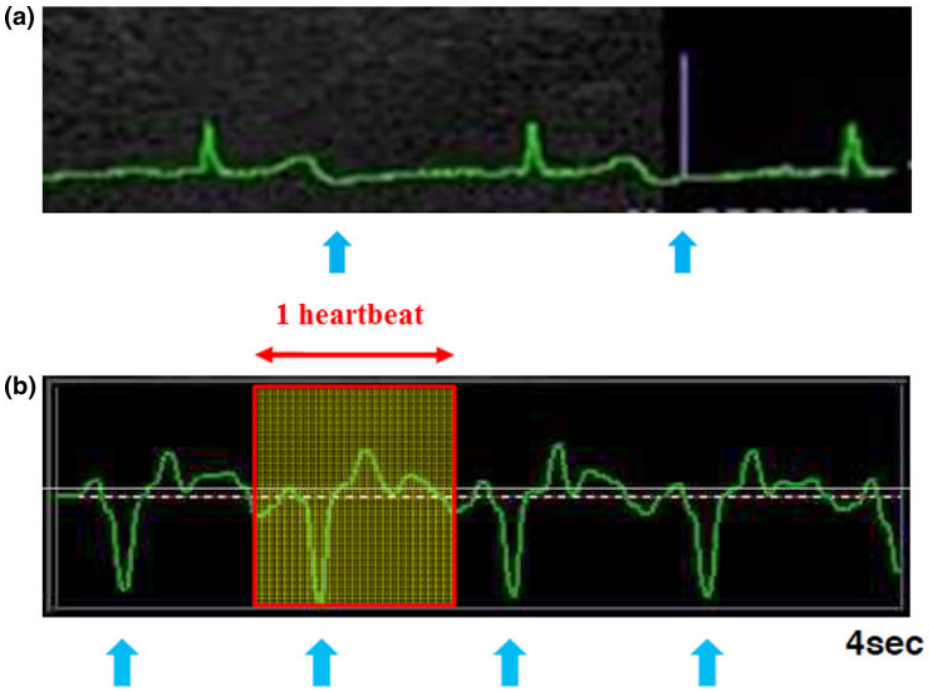

Fig. 4 Electrocardiogram and strain graph in liver RTE. Good RTE images may be obtained in the end of left ventricular diastole in electrocardiographic gating (*arrows*; **a**) or at the largest downward wave on a strain graph (*arrows*; **b**). *Double-headed red arrow* corresponds to one heartbeat

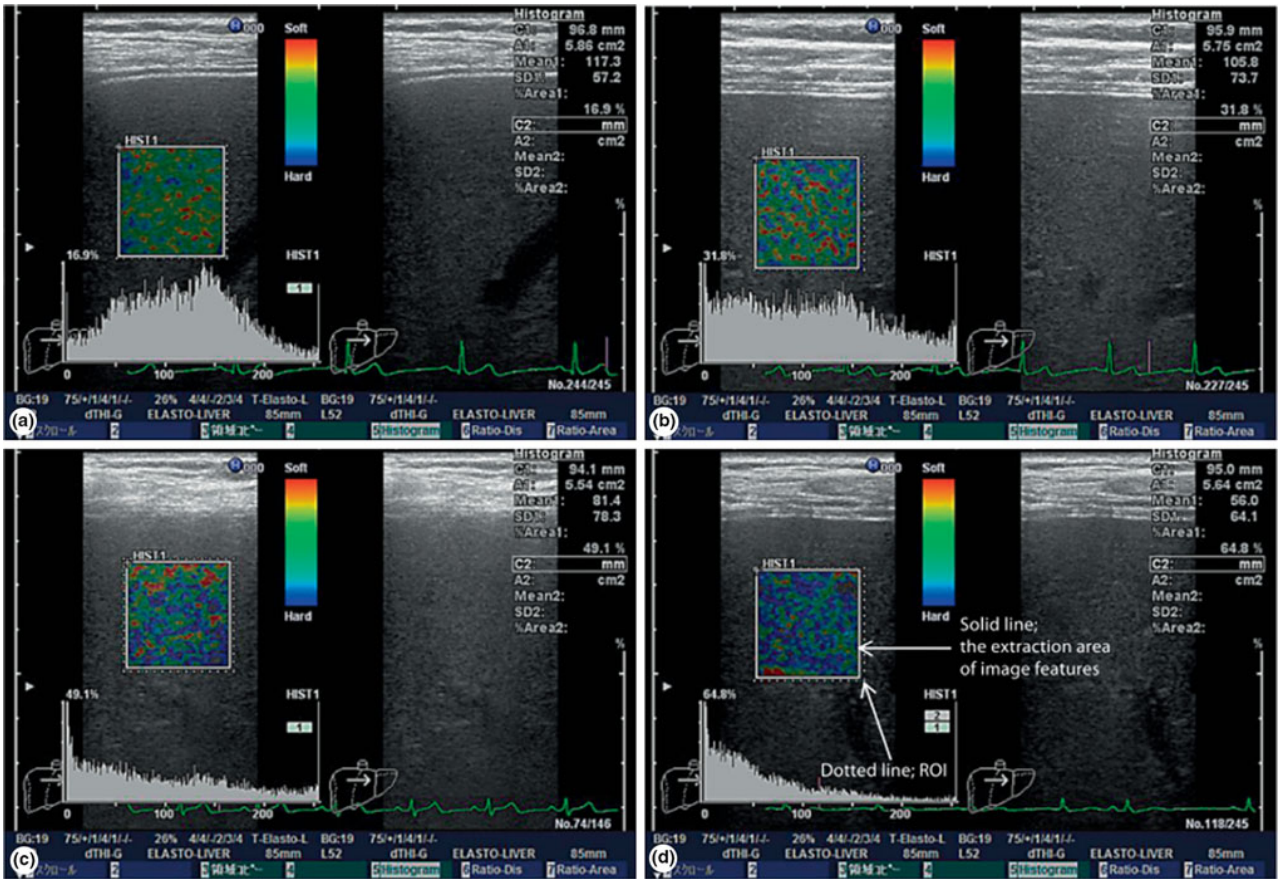

Fig. 5 RTE images reflecting different stages of liver fibrosis in chronic viral hepatitis C patients. With fibrosis associated to progress, strain elastogram increases color variation between relatively low strain regions and generates a patched image pattern. F1 stage (**a**), F2 stage (**b**), F3 stage (**c**), F4 stage (**d**) [9]

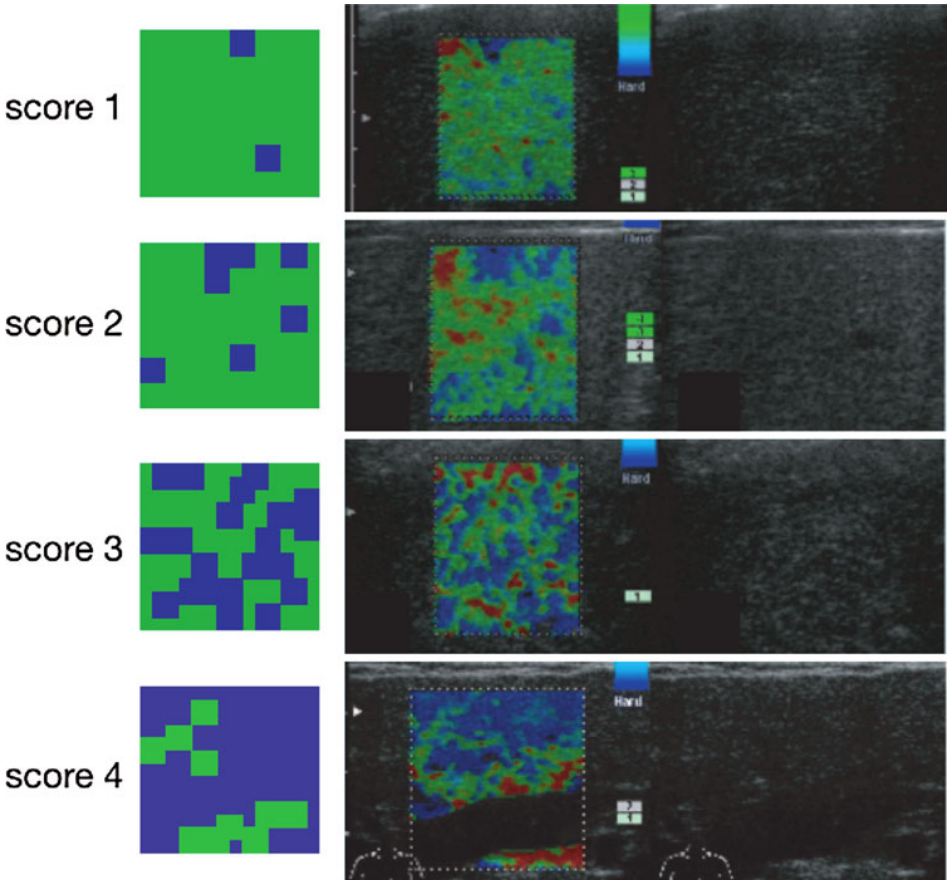

Fig. 6 Liver elasticity score. Liver elasticity scores is obtained by visual assessment of low strain areas (*blue*) on RTE images. *Score 1* The entire colored area of the ROI is distorted (the entire colored area is shown as relatively uniform *light green*). *Score 2* Partially mottled *blue* regions are shown in the *light green* colored area. *Score 3 Light green* and *blue* are mixed in the colored area (almost a 50 : 50 mix). *Score 4* Most of the colored area is shown as *blue* [4]

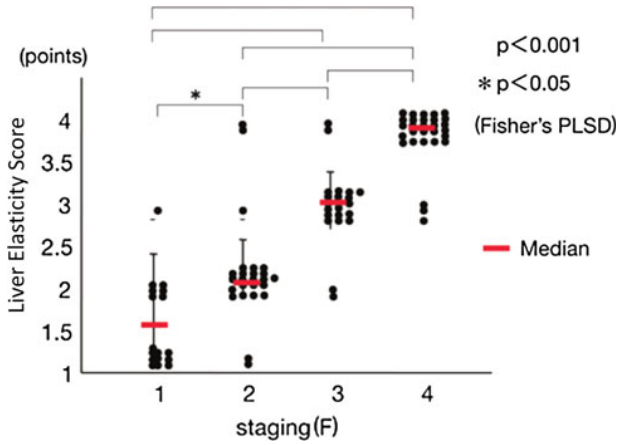

Fig. 7 Relationship between liver elasticity score and liver fibrosis stage. Statistical analysis for comparison of fibrosis stages of patients with chronic hepatitis C revealed that liver elasticity score was significantly higher with progression of fibrosis stage [4]

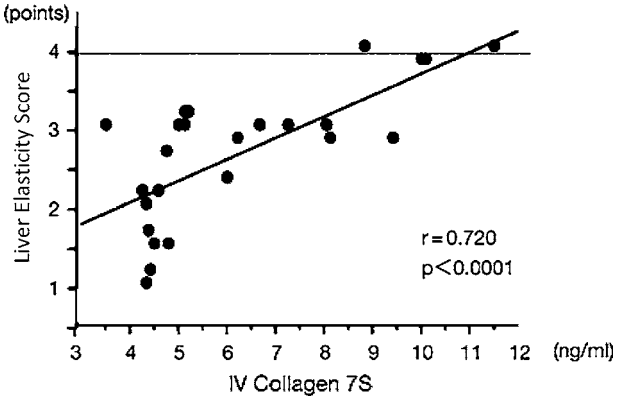

Fig. 8 Correlation between liver elasticity score and type IV collagen 7S. In patients with chronic hepatitis C, type IV Collagen 7S showed a significant correlation with liver elasticity score [4]

(Fig. 6), are positively correlated with fibrosis progression and the level of type 4 collagen 7S (Figs. 7, 8) [4], these scores are useful for the diagnosis of liver fibrosis.

However, because examiner subjectivity influences liver elasticity score, more objective evaluation methods are needed.

(2) Objective evaluation methods

Examiner subjectivity and past experiences influence the outcome of visual assessment. To overcome this problem, various quantitative methods have been developed to objectively assess tissue elasticity. Here, we discuss image pattern recognition and strain ratio calculation.

- Image pattern recognition

Parameters obtained by adjusting grayscale, histogram, and binarization are called feature values, and these values are used in pattern recognition. In RTE imaging, feature values obtained by the US device itself or by separate imaging software can be used to calculate a correlation with liver fibrosis. The degrees of strain are converted to feature values using 256 color gradations, with blue being 0 and red being 255.

Tatsumi et al. [2] and Morikawa et al. [7] reported that mean relative strain values (MEAN) inversely correlated with liver stiffness and fibrosis in patients with chronic hepatitis C (Figs. 9, 10). The standard deviation of relative strain values (SD), the percentage of low strain area (percentage of blue color area, %AREA), and the complexity of the low strain (blue) area (calculated as perimeter^2/area, COMP) positively correlated with liver stiffness and fibrosis (Figs. 9, 10, 11) [2, 7].

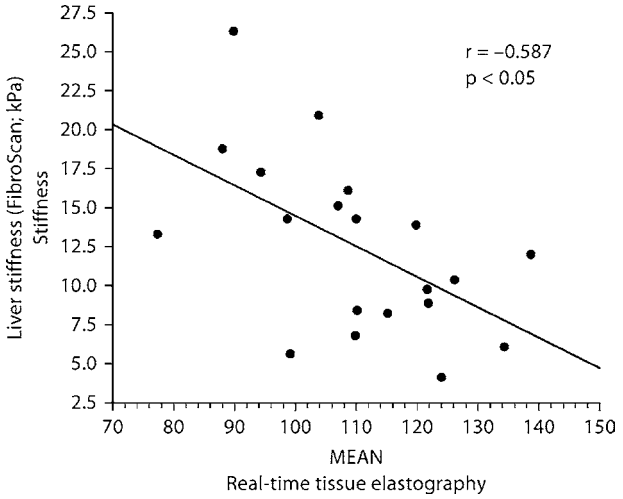

Fig. 9 Inverse correlation between MEAN values of RTE and liver stiffness measured by FibroScan. There was a negative correlation between liver stiffness and MEAN values of RTE ($r = -0.587$, $p < 0.05$) [2]

– Calculation of function values

Some methods use feature values as an independent variable to perform multiple regression and principal component analysis to calculate the function values.

a. Liver fibrosis index

Fujimoto et al. [8] performed RTE imaging of 295 patients with chronic hepatitis C and cirrhosis and 15 healthy individuals (310 cases in total) and extracted nine feature values: MEAN, SD, %AREA, COMP, skewness (SKEW) and kurtosis (KURT) of the histogram, and the homogeneity (entropy, or ENT), complexity (inverse differential moment, or IDM), and uniformity (angular second moment, or ASM) of texture. The authors used these nine

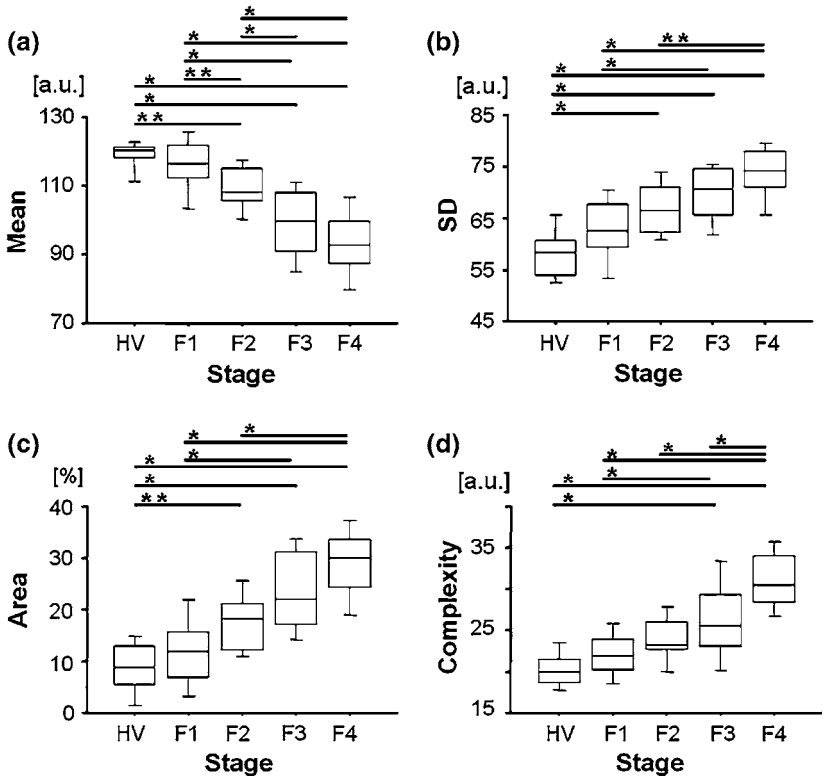

Fig. 10 Relationships between the stages of liver fibrosis and four RTE feature values (MEAN, SD, %AREA, COMP). Box plots of each feature value corresponding to fibrosis stages F1–4 and the healthy volunteer group (HV). **a** MEAN, **b** SD, **c** 5AREA, **d** COMP. HV, $n = 10$. F1–4, $n = 95$. $^*p < 0.01$, and $^{**}p < 0.05$ [7]

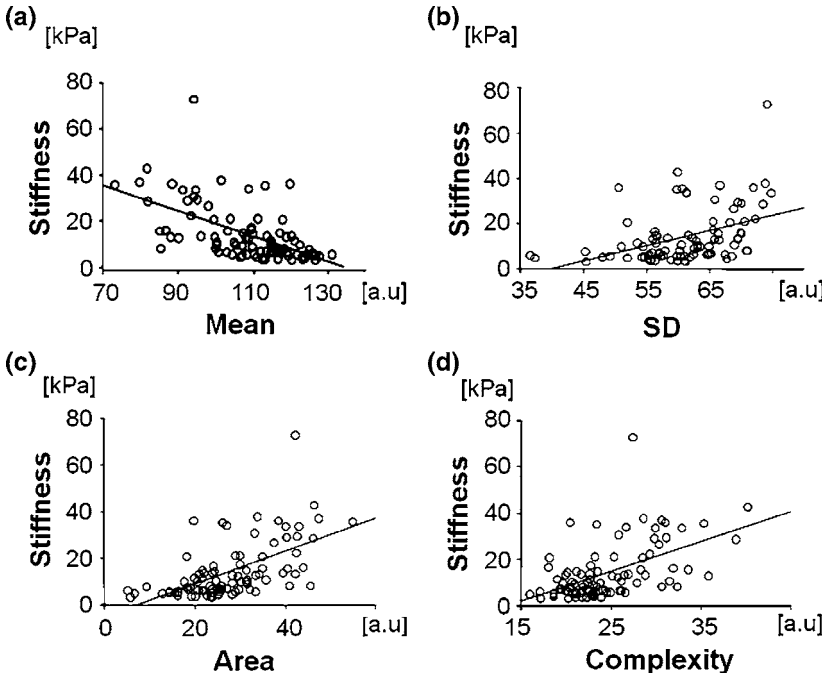

Fig. 11 Relationships between liver stiffness and four RTE feature values (MEAN, SD, %AREA, COMP). **a** MEAN was negatively correlated with liver stiffness (kPa; $p < 0.01$). Correlation coefficient was −0.585. **b** SD was significantly correlated with liver stiffness (kPa; $p < 0.01$). Correlation coefficient was 0.425. **c** %AREA was significantly correlated with liver stiffness (kPa; $p < 0.01$). Correlation coefficient was 0.590. **d** COMP was significantly correlated with liver stiffness (kPa; $p < 0.01$). Correlation coefficient was 0.532 ($n = 96$). *a.u.* Arbitrary units [7]

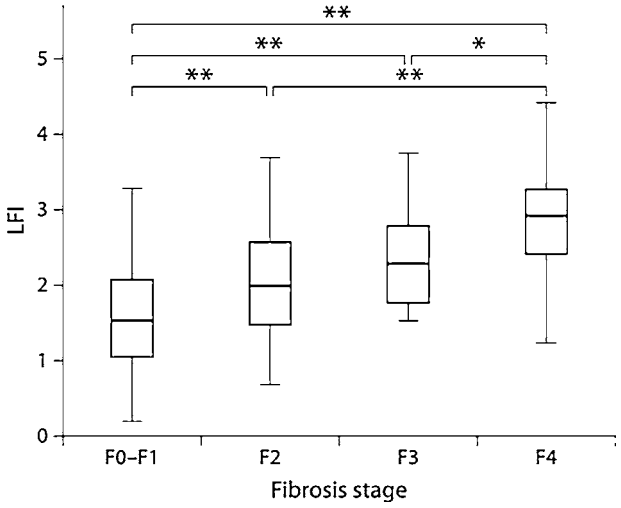

Fig. 12 Relationship between the stages of liver fibrosis and LF index. FibroIndex for each fibrosis stage; many outliers were present. *$p < 0.05$, **$p < 0.001$, comparing between each fibrosis stage. *LFI* liver fibrosis index [9]

feature values as independent variables and the histological fibrosis (F) stage as dependent variables in multiple regression analysis to calculate a liver fibrosis index (LF index) [5, 8].

In a validation study of the LF index using 245 patients with cirrhosis and chronic hepatitis B and C, Yada et al. [9] observed significant differences between F0–F1 and F4, F2 and F4, and F3 and F4 (Fig. 12). The sensitivity, specificity, and accuracy of diagnosis were as high as 73.5, 79.7, and 78.3 % for F4; 78.4, 80.2, and 79.6 % for F3 or higher; and 70.0, 76.4, and 73.0 % for F2 or higher. The area under the receiver operating characteristic (AUROC) was also high, with corresponding values of 0.946, 0.865, and 0.800 (Fig. 13) [9].

b. Elasticity index

Wang et al. [44] examined 55 chronic hepatitis B patients and 10 healthy individuals and used the feature values as independent variables to perform principal component analysis. Four types of principal components extracted from the analysis were used as integrative functions to calculate an elasticity index. They found a significant correlation between elasticity index and liver fibrosis ($p < 0.001$; Fig. 14), and AUROC was 0.93 for F1 or above ($p < 0.001$), 0.92 for F2 or above ($p < 0.001$), 0.84 for F3 or above ($p < 0.05$), and 0.66 for F4 ($p > 0.05$) [17].

- Strain ratios

There are two types of evaluation methods that use the strain ratio in analysis. The mainstream method places the ROI only in liver parenchyma for analysis and calculates the ratio between the parenchyma and blood vessels. In another method, the ROI includes liver parenchyma and the surrounding tissue, and the strain ratio between the two tissues is used in the analysis.

Koizumi et al. [6] performed imaging of 70 chronic hepatitis C patients with the ROI placed only in liver parenchyma, and they used the strain ratio (elastic ratio, Fig. 15) between the liver parenchyma and the peripheral hepatic vein for evaluation. Elastic ratios increased with the progression of liver fibrosis, from a ratio of 2.21 in F1

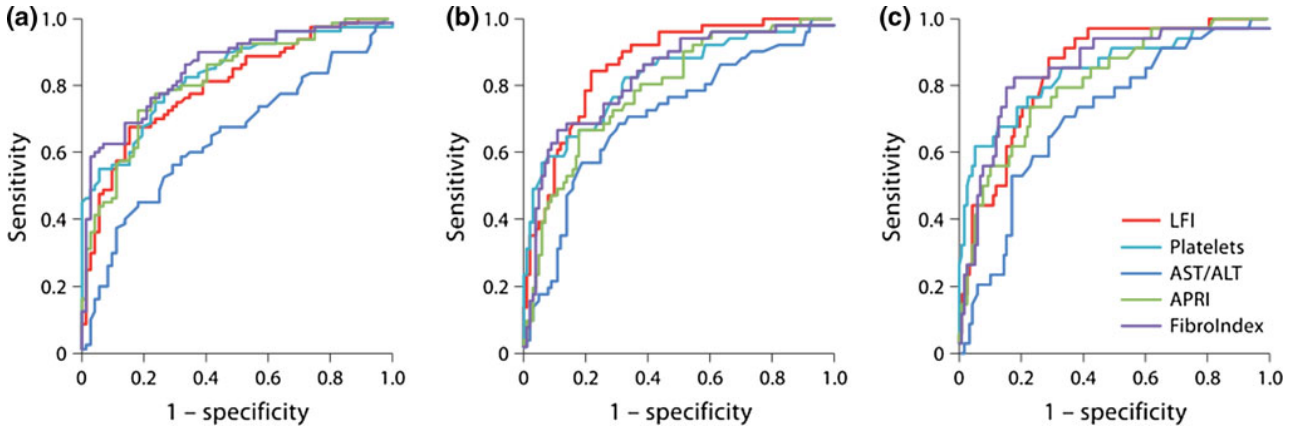

Fig. 13 Receiver operating characteristic (ROC) curve of LFI, platelet count, AST/ALT ratio, APRI, and FibroIndex. **a** ROC of predicting F2 stage or higher fibrosis (F0–F1 vs F2–F4). **b** ROC of predicting F3 stage or higher fibrosis. **c** ROC of predicting stage F4 fibrosis [9]

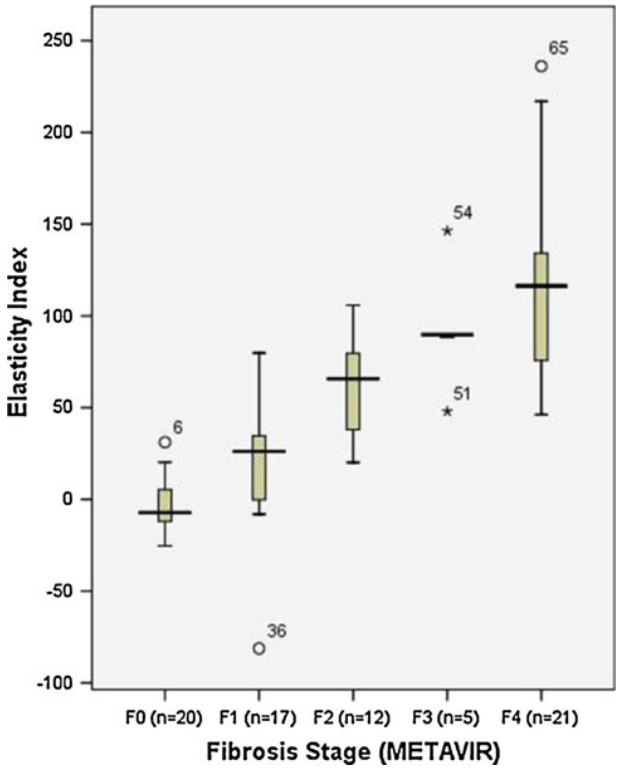

Fig. 14 Relationship between liver fibrosis and the elasticity index in patients with chronic hepatitis B. *Small circles* represent outliers. There was a significant correlation between the elasticity index and liver fibrosis ($p < 0.001$) [17]

(95 % confidence interval 1.94–2.70), 2.69 in F2 (2.29–2.97), 3.42 in F3 (3.07–3.65), to 4.66 in F4 (4.40–4.93), with a significant positive correlation between the ratios and hepatic fibrosis ($r^2 = 0.82$, $p < 0.001$). In addition, there was a significant difference between F2 and F3 ($r^2 = 0.36$, $p = 0.02$) as well as F3 and F4 ($r^2 = 0.41$, $p = 0.001$); but no significant difference was observed between F1 and F2 (Fig. 16). In addition, the elastic ratio was not correlated with inflammation ($p = 0.36$). The measurement results of two examiners showed a strong correlation ($r^2 = 0.869$, $p < 0.0001$), demonstrating that inter observer variability was extremely low (Fig. 17) [6].

In a study using patients with NAFLD, Ochi et al. [10] observed a significant correlation between elastic ratio and liver fibrosis. In addition, there was a significant difference in elastic ratios between patients with NAFLD activity score (NAS) $\leq$4 and those with score $\geq$5 (Fig. 18) [10].

- Other methods

Using hepatitis B and C patients, Friedrich-Rust et al. [18] calculated tissue elasticity from every pixel in the RTE image and perform multivariate analysis to obtain a unique formula. Elasticity scores calculated using the formula showed a significant correlation with liver fibrosis, as with other analysis. The authors also improved the diagnostic capability of the system for liver fibrosis by incorporating platelet counts and γ-glutamyl transpeptidase (GGT) (Fig. 19) [18].

- Influences other than liver fibrosis

In a study of hepatitis C patients by Fujimoto et al. [8], none of the feature values were correlated with inflammatory grade (Fig. 20). Moreover, in a validation study using chronic hepatitis B and C patients, Yada et al. [9] observed no correlation between inflammatory grade and LF index. In addition to liver fibrosis, inflammation, jaundice, and liver congestion are known to affect shear wave imaging, such as FibroScan and VTQ [19]. In contrast, RTE can evaluate liver fibrosis without being affected by these factors.

(E) Limitations

While FibroScan cannot be used in patients with ascites retention, RTE is able to perform measurements in such cases (Fig. 21) [23].

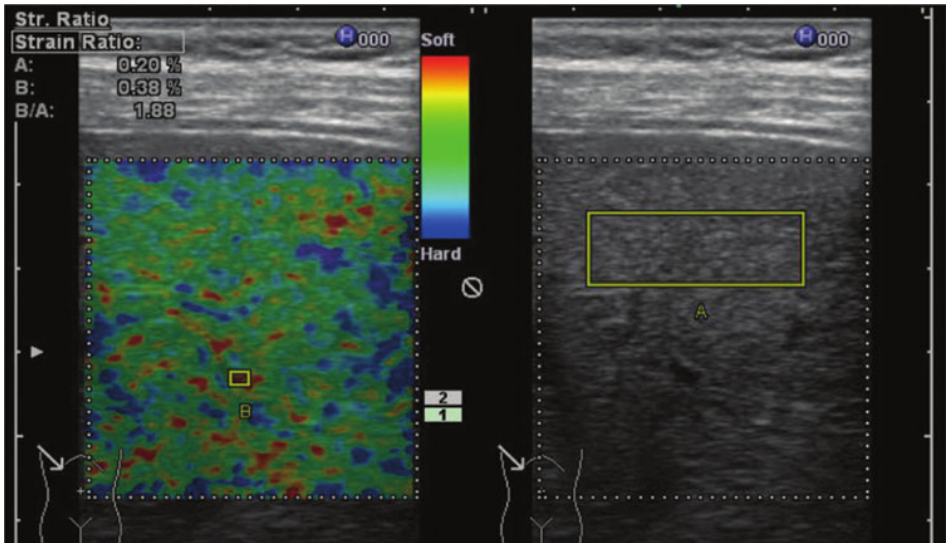

Fig. 15 Measurement of elastic ratio. The elasticity of the hepatic vein was used as the reference because the elasticity of the veins does not change over time, since they do not undergo transformations with disease, such as arteriosclerosis, and it also does not increase or decrease even when liver parenchyma becomes stiffer. Thus, small vessels with a diameter of 3 mm in the liver were used as the standard for computing the elasticity ratio, and the ROI was set as large as possible (usually 0.3 × 0.5 cm). The ROI in the liver parenchyma was placed 1 cm from the liver surface and was 2 × 1 cm in size [6]

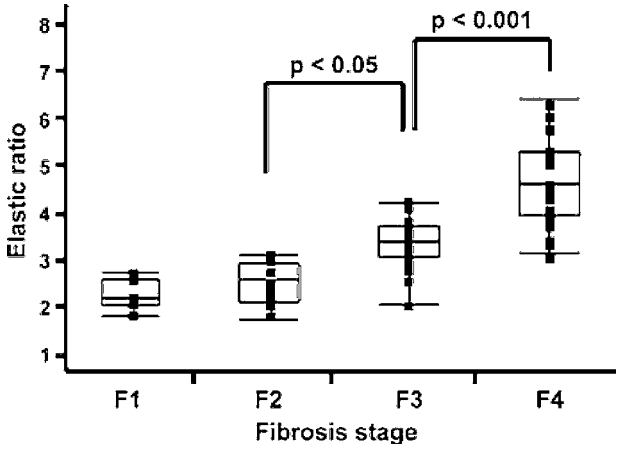

Fig. 16 Relationship between elastic ratio and liver fibrosis in patients with chronic hepatitis C [6]

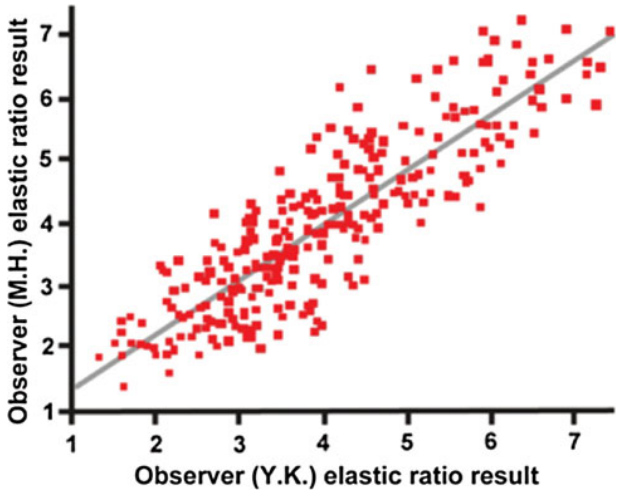

Fig. 17 Correlation of elastic ratios calculated by two examiners [6]

Various RTE imaging and analysis methods are currently available, and they all show a clear correlation with liver fibrosis. However, a comparative study is needed to reveal superiority among these methods. Although the technique that uses heartbeat is most popular today, weak pulsation can adversely affect the quality of RTE images. Moreover, even though RTE can be applied to most cases owing to its ability to assess patients with ascites retention and narrow intercostal spaces, it is difficult to generate clear RTE images of severely obese patients due to ultrasound attenuation. It is also necessary to learn tips and tricks to, for example, prevent artifacts. The experience and skills of examiners can influence the accuracy of ultrasonography; however, in liver RTE, variability among examiners with proper training is reportedly low [6]. To spread liver RTE and further improve accuracy, it is necessary to standardize the imaging and analysis methods and establish an effective RTE training system.

(F) Recommendations

RTE is a tissue elasticity imaging method that has been put into practical use for the first time in the world.

In diffuse liver diseases, the hardness of hepatic tissue becomes irregular as liver fibrosis progresses. This can be seen as uneven, patchy color distribution on RTE images, with an increase in areas with relatively low strain (blue area). Such change can be easily observed visually; however, objective assessment can be made only by the use of LF index and elastic ratio, or strain ratio.

RTE accurately measures liver fibrosis without adverse effects of ascites accumulation, inflammation, jaundice, and liver congestion.

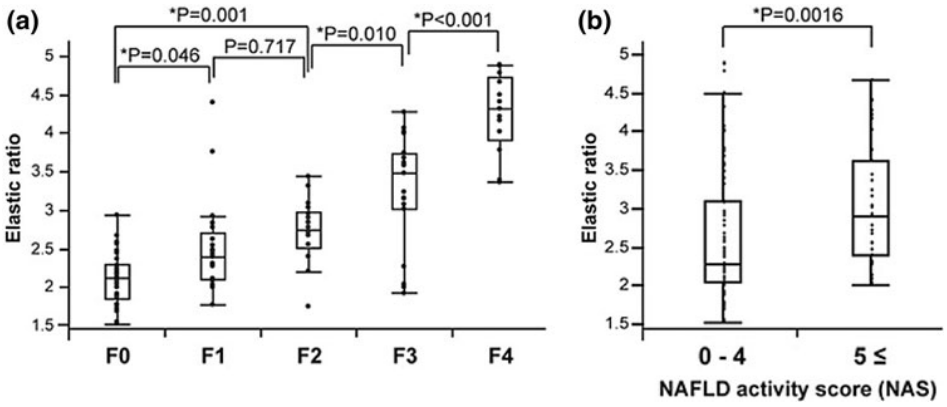

Fig. 18 Relationship between elastic ratios and liver fibrosis or NAS in patients with NAFLD. **a** Hepatic elastic ratio for each NAFLD fibrosis stage. F1 versus F2 was not significantly different ($p = 0.717$), whereas all other combinations were significantly different. **b** Hepatic elastic ratio for each NAS. The median elastic ratios with NAS >5 were significantly high ($p = 0.0016$) [10]

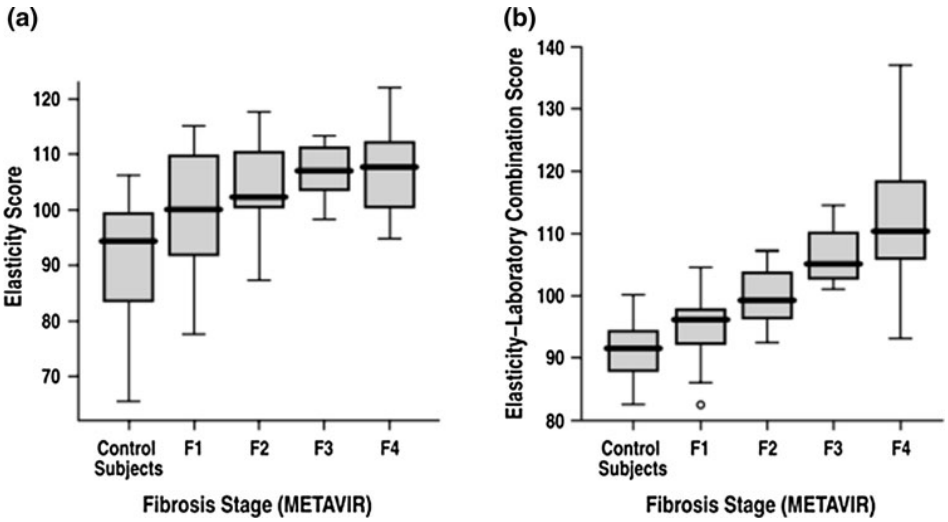

Fig. 19 Elasticity score and elasticity–laboratory combination score (with the addition of platelet counts and GGT) [18]

Multicenter studies are currently being performed to compare RTE imaging results with histological findings in specimens obtained by resection and biopsy and also to use RTE as a non-invasive prognostic tool in, for example, esophageal varix and liver cancer incidence. We looked forward to the results of these studies.

eSie touch Elasticity Imaging (Siemens)

(A) Introduction

This is a strain elastography-based technology that uses the spatial correlation method to measure tissue strain caused by minute body movements such as breathing or heartbeat. An acquired image is superimposed onto a B-mode image and can be displayed side by side with the original B-mode image.

(B) Indication

The efficacy of eSie Touch Elasticity Imaging for the diagnosis of fibrosis in diffuse liver disease has not been fully elucidated.

(C) Procedures (including tips and tricks)

This technology has been used for the diagnosis of hepatic tumors, especially for the differential diagnosis between benign and malignant tumors.

Switch to elasticity imaging mode and visualize the lesion while watching the B-mode image.

When evaluating tumors, both tumor and normal parenchyma should be displayed in the ROI.

Regardless of the size of the ROI, the system always uses an entire B-mode image to perform arithmetic processing for strain imaging. Therefore, the size and location of ROI can be altered, with the former as large as the size of the B-mode image, after obtaining a still image.

The ROI image is displayed in grayscale or color, and colors representing soft and hard tissues can be reversed. However, measurement of strain ratios is possible only when a grayscale image is displayed.

(D) Results (what does the value mean?)

eSie Touch Elasticity Imaging has not been used extensively in the diagnosis of fibrosis in diffuse liver diseases.

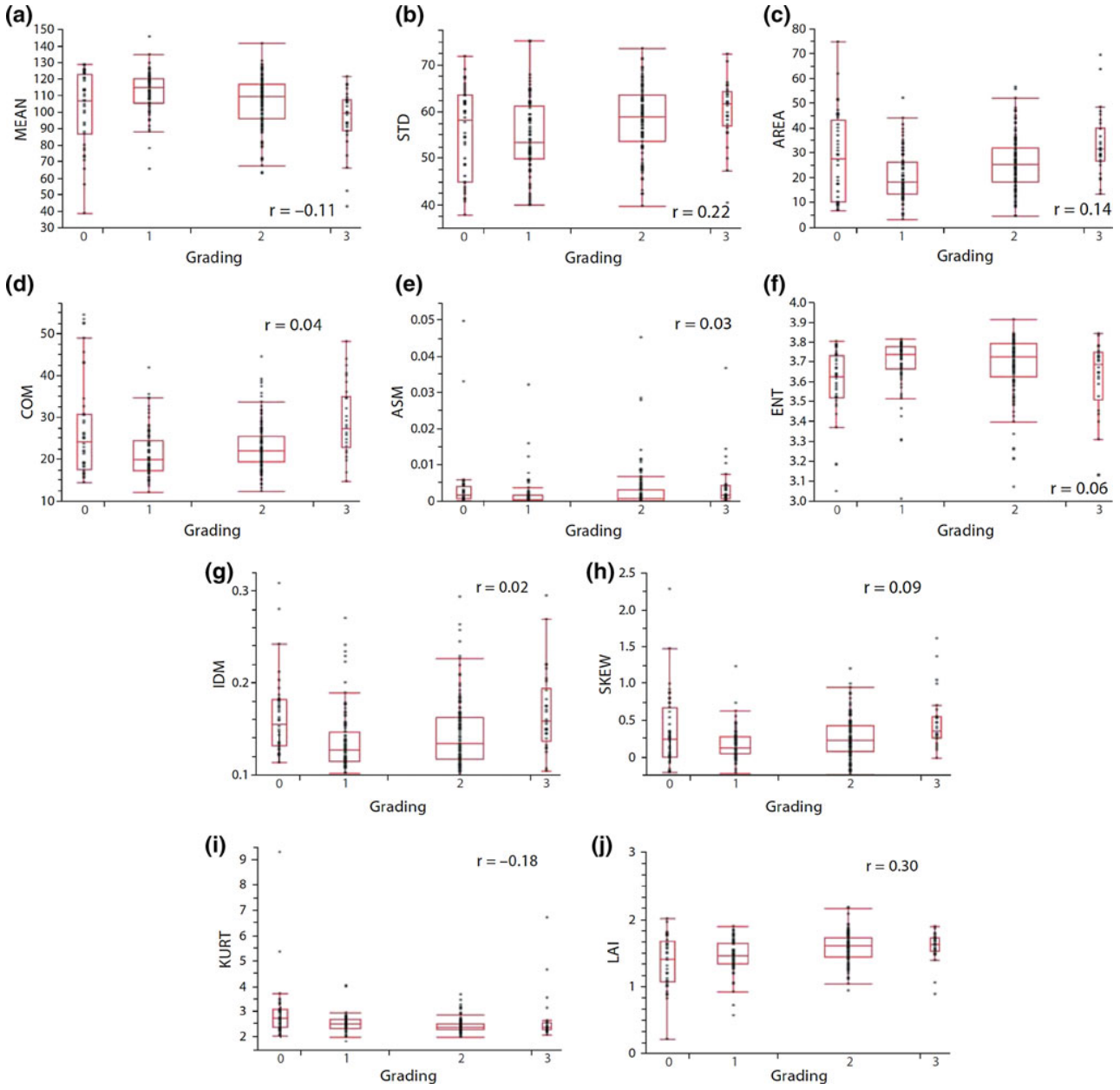

Fig. 20 Relationship between histological grading of liver fibrosis in biopsy and RTE feature values. These graphs shows the comparison between grades and the nine image features for evaluating the effect of inflammation on the RTE image. None of the nine image features has a correlation with grades; and liver activity index (LAI), which was calculated by multiple regression analysis similar to LFI, also did not correlate with grades ($r = 0.30$) [8]

The technology captures tumor homogeneity/heterogeneity as well as differences in elasticity between the tumor and the surrounding tissue as differences in relative strains (Fig. 22). Grayscale images are used to measure strain ratios to display the relative stiffness in the two regions numerically (Fig. 23).

(E) Limitations

The efficacy of this technology for the diagnosis of fibrosis in diffuse liver disease has not been fully elucidated.

Although tissue at a depth of 16 cm can be visualized, images generated at such depth may not be reliable.

Imaging may not be successful in patients with difficulty in holding breath or in severely obese patients.

(F) Recommendations

eSie Touch Elasticity Imaging is one of the Strain elastography methods using the spatial correlation method to measure tissue strain.

Neoplastic lesions can be evaluated as a relative tissue strain.

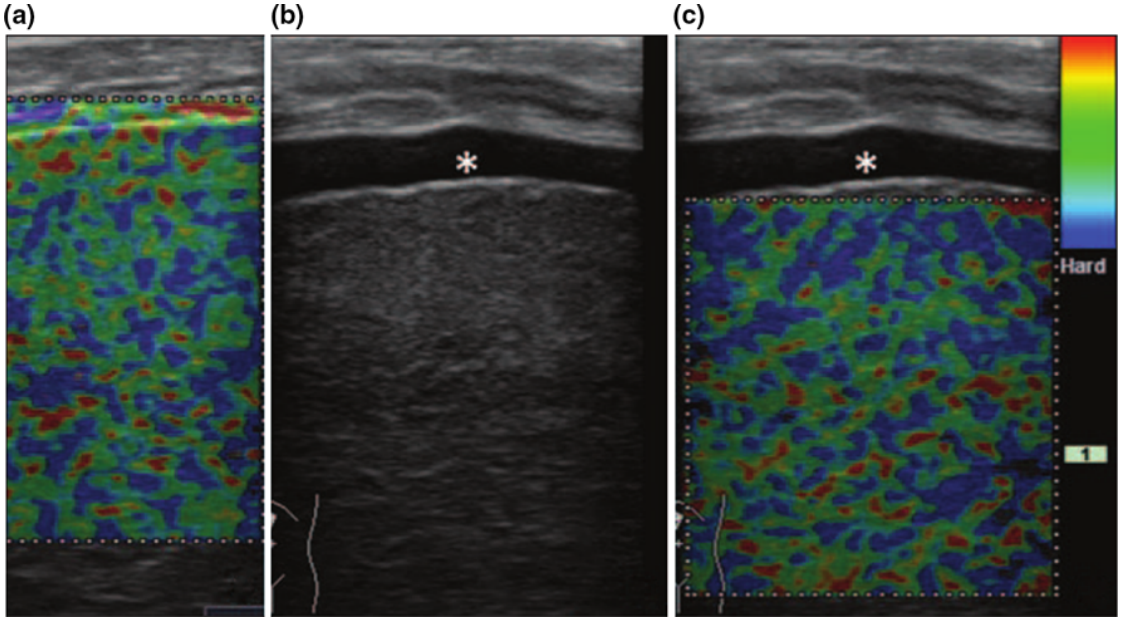

Fig. 21 RTE image before and after the injection of artificial ascites. **a** Tissue elastographic image before injection for artificial ascites shows elastic ratio of 2.79. **b** B-mode ultrasound image shows layer of artificial ascites (*asterisk*). **c** Tissue elastographic image shows elastic ratio of 2.80 in the presence of ascites (*asterisk*) [23]

The number of studies using this technology is not sufficient for making a definitive conclusion. We look forward to further study results in the near future.

Elastography (direct strain elastography; GE)

(A) Introduction

Direct strain elastography belongs to the category of strain elastography and uses the revised direct strain method to measure tissue dislocation. The system assigns warm colors to a group of pixels representing strains higher than the mean value on the strain distribution graph and cool colors to a group of pixels representing lower strains, followed by the superimposition of this color map on a conventional B-mode image in real time (Fig. 24). The machine also provides a color mapping function of absolute strain values (S-Map) (Fig. 25).

(B) Indication

Diffuse liver diseases, hepatic tumors

(C) Procedures (including tips and tricks)

Visualize the target area using B-mode.

Push the "Elasto" button to start elastography mode.

Set the ROI large enough to cover the target area.

Apply gentle and steady pressure to the probe to maintain the quality bar or the quality graph at a high level.

Elastography is also obtained by heartbeat. In this case, place a probe lightly against the skin without vibration.

Save the still image and/or video clip.

To prevent calculation errors, artifacts should be avoided.

Measure the index after switching on the measuring function.

(D) Results (what do the values mean?)

It is possible to evaluate the liver elasticity by using Elasticity Index and Strain Index during the usage of S-Map (Fig. 26). Both indices reflect the value of color indices calculated from strain distribution, therefore, they do not directly indicate the liver stiffness or strain modulus (kPa).

(E) Limitations

The efficacy of this technology for the diagnosis of fibrosis in diffuse liver disease has not been fully elucidated.

The system is not applicable to tumors located deep inside the liver where compression hardly reaches.

Imaging may not be successful in patients with difficulty in holding breath or in severely obese patients.

(F) Recommendations

The number of studies on this technology is not sufficient for making a definitive conclusion. We look forward to further study results in the near future.

Elastography (Toshiba)

(A) Introduction

This technology belongs to the category of strain elastography and measure tissue displacement using tissue Doppler, with excellent real-time performance and relatively good signal to noise ratios. However, because of its

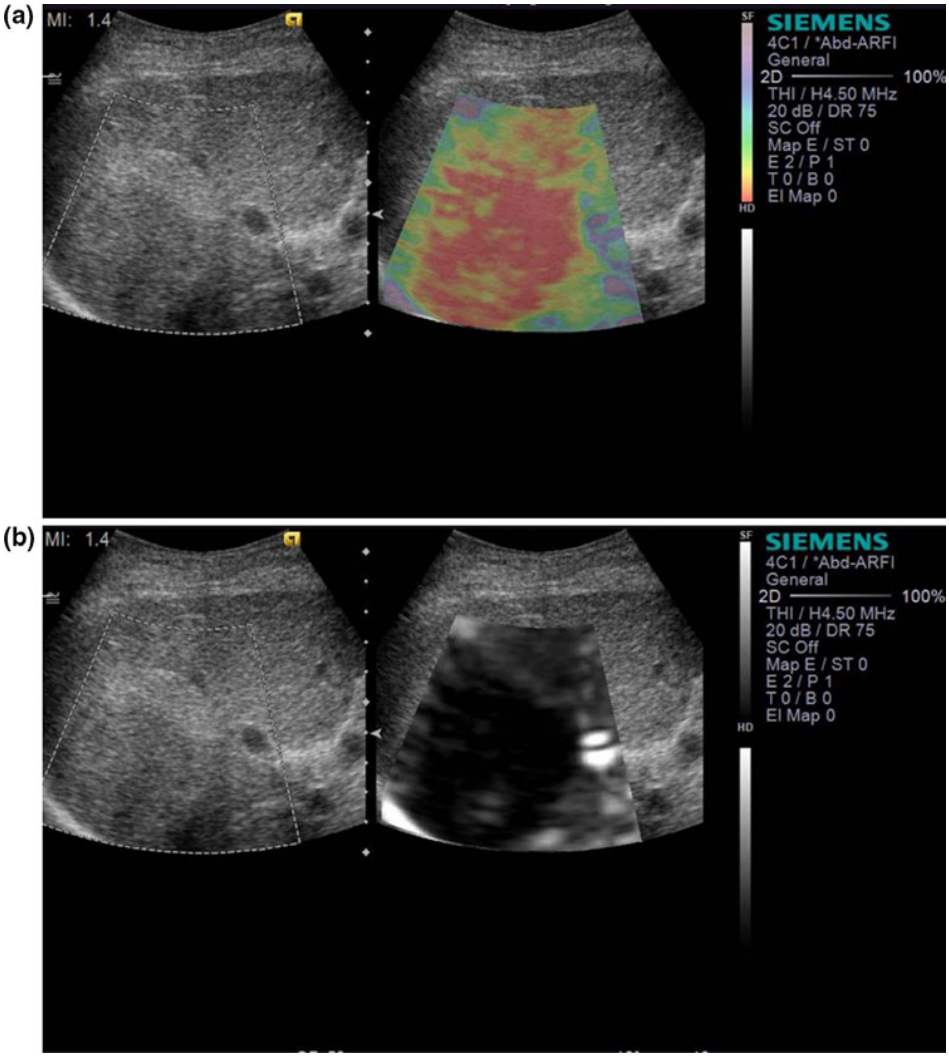

Fig. 22 eSie Touch Elasticity Imaging of metastatic liver cancer. Color-mapping (**a**) and grayscale display (**b**). *Left* B-mode imaging, *right* eSie Touch Elasticity Imaging superimposed on the B-mode image. Tumor appears relatively stiff compared with the surrounding non-tumor area. *SF* Soft, *HD* hard

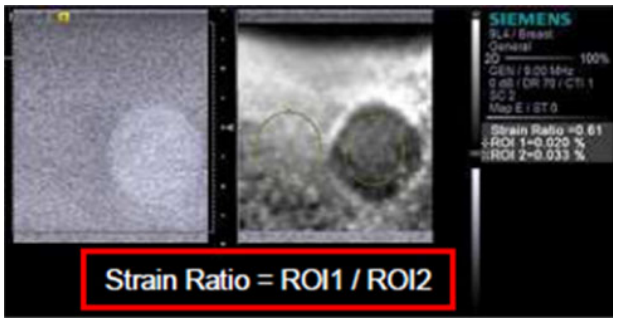

Fig. 23 Strain ratio. *Left* B-mode imaging, *right* eSie Touch Elasticity Imaging superimposed on the B-mode image. The strain ratio is the ratio of elasticity indexes between ROI1 and ROI2, calculated as ROI1/ROI2

angle-dependent nature, the system measures tissue displacement in a one-dimensional plane in the direction of the beams. In addition, the measurement of displacement which is larger than half the wavelength of the beam causes errors due to aliasing.

(B) Indication

Diffuse liver diseases, hepatic tumors

(C) Procedures (including tips and tricks)

A B-mode image is used to confirm that the target area is sufficiently compressed by manual compression.

When measuring liver stiffness using a compression technique, press the corresponding area iteratively by hand to make sure that tissue strain is observable on the screen. At this point, strain can be quantitated by comparing it with another organ with relatively uniform stiffness, such as a kidney, or by calculating strain values while manually applying constant pressure (Fig. 27). There is also a method of measuring strain pattern or strain caused by heartbeat.

To quantitatively measure liver stiffness in diffuse liver disease, constant pressure should be applied to the probe. The key to the compression method is to perform measurement at the maximum or minimum compression point. The velocity vector of compression is a near-sinusoidal

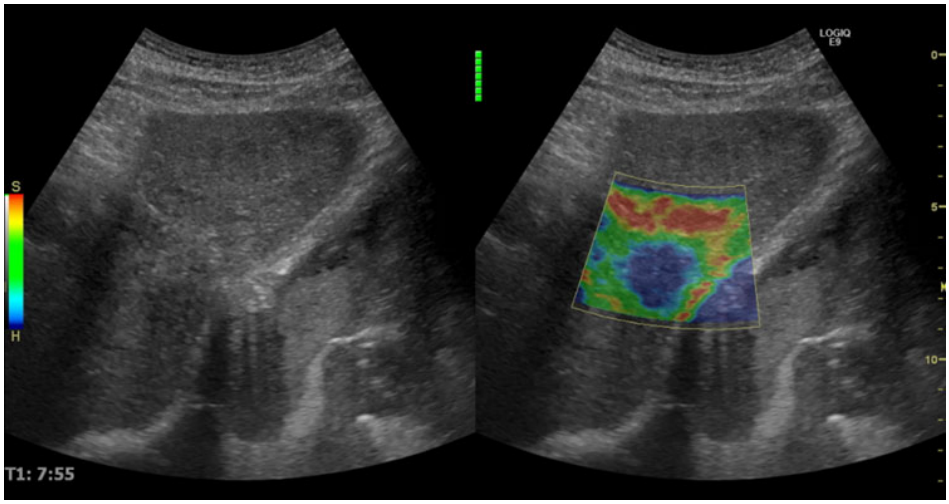

Fig. 24 Elastography (GE) of the tumor

wave. In addition, the area of interest needs to be compressed evenly for successful quantitation. The uniformity of measurement at multiple sites having uniform stiffness should be confirmed.

(D) Results (what does the value mean?)

The use of a strain distribution map (unevenness on the strain image) may be able to diagnose the progression of liver fibrosis (has not been published; Fig. 28).

When evaluating tumor stiffness, tissue stiffness of a tumor is calculated by comparing it with normal parenchyma. In general, metastatic liver cancers have a high strain ratio.

(E) Limitations

The efficacy of this technology for the diagnosis of fibrosis in diffuse liver disease has not been fully elucidated.

Aliasing may occur because the system uses the Doppler method.

(F) Recommendations

This is one of the strain elastography methods using the tissue Doppler method, and therefore, attention must be paid to aliasing.

At present, the number of studies using this technology is not sufficient for making a definitive conclusion. We look forward to further study results in the near future.

Acoustic radiation force impulse imaging

Virtual touch imaging (Siemens)

(A) Introduction

Virtual Touch^{TM} imaging (VTI) uses ARFI to compress tissue and thus cause tissue dislocation, which is measured to display relative tissue strains. The spatial correlation method is used to measure dislocation. The system is minimally operator-dependent because there is no requirement for manual compression.

VTI images are displayed in grayscale or color mapping, next to the original B-mode image (Fig. 29). In grayscale, areas with lower strain appear in black and those with higher strain in white.

(B) Indication

The efficacy of VTI for the diagnosis of fibrosis in diffuse liver disease has not been fully elucidated.

A previous study has also reported the efficacy of VTI in differential diagnosis between benign and malignant liver cancers [24].

(C) Procedures (including tips and tricks)

Switch to VTI mode.

Adjust the size and location of ROI. Because of focus dependency, the size of ROI should not be excessively larger than the size of the tumor unless absolutely necessary, and place the focus near the bottom of the tumor.

Start imaging and keep the liver in place while acquiring the image.

(D) Results (what does the value mean?)

The efficacy of this technology for the diagnosis of fibrosis in diffuse liver disease has not been fully elucidated.

VTI captures tumor homogeneity/heterogeneity as well as differences in elasticity between the tumor and normal parenchyma as differences in relative strains.

(E) Limitations

The technology is applicable regardless of ascites retention.

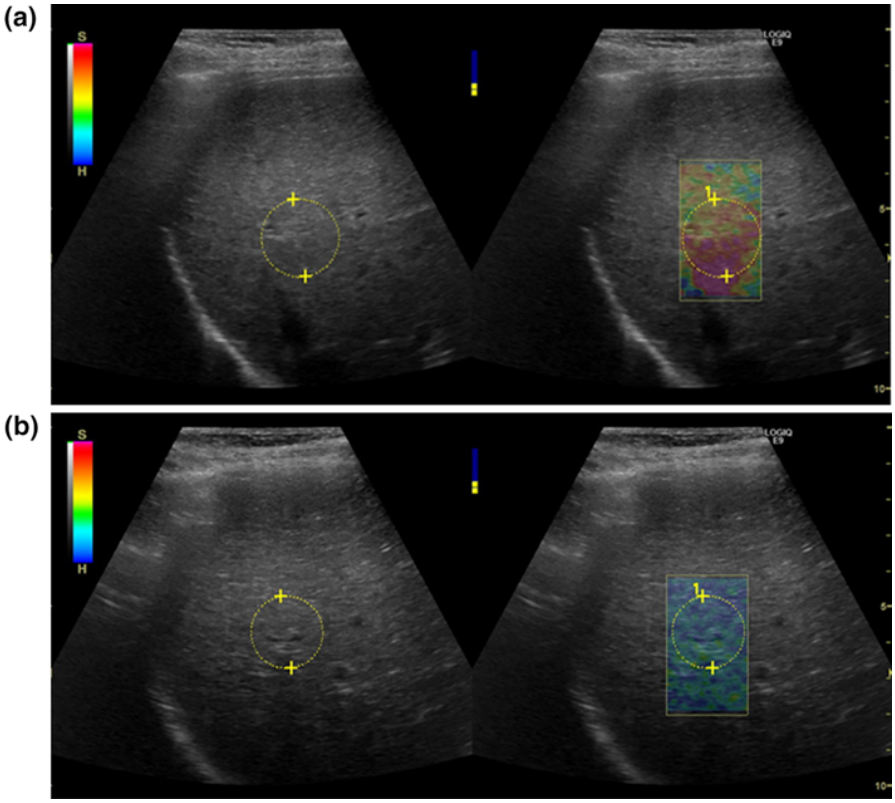

Fig. 25 S-Map in normal volunteer (**a**) and that in a patient with hepatitis C related cirrhosis (**b**). Almost same slice, which showed the largest displacement due to heartbeat, are compared between both cases at the same strain scale. Absolute strain value in a patient with hepatitis C related cirrhosis was smaller than that in a normal volunteer

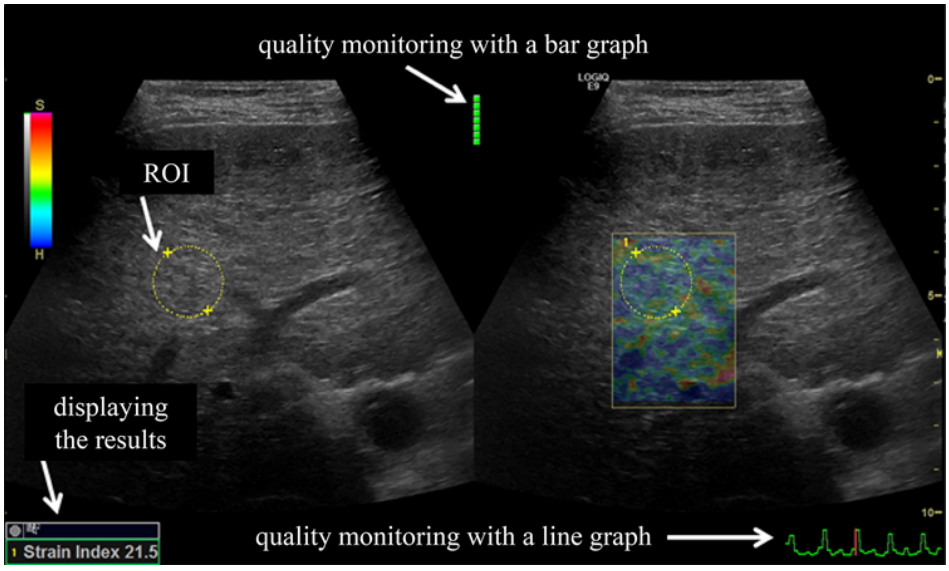

Fig. 26 Example of S-Map in a patient with hepatitis C related cirrhosis. Quality monitoring with a *bar* graph and a *line* graph, and the measuring results are shown

Unlike strain elastography, the screen freezes every time an image is acquired.

Imaging reliability is not displayed.

(F) Recommendations

Because ARFI is used to compress tissue, VTI is operator-independent.

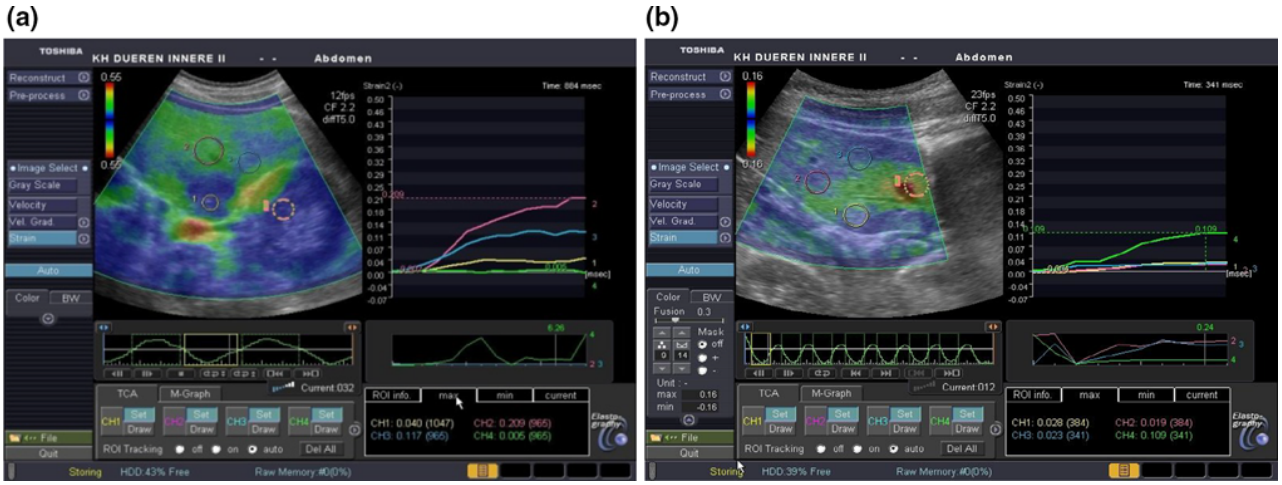

Fig. 27 Diagnostic imaging of diffuse liver disease with elastography (Toshiba). Strain can be quantitated by two methods: comparison with kidney (**a**), and strain distribution in the liver (**b**)

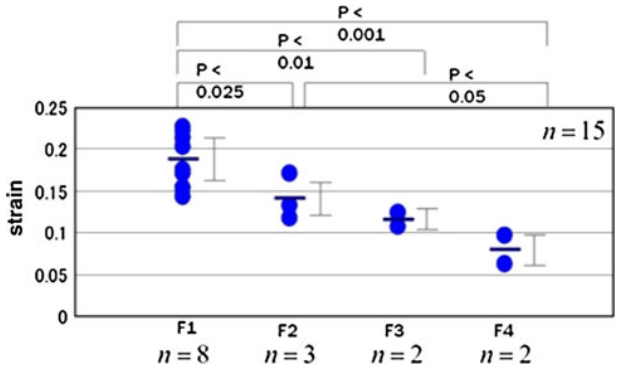

Fig. 28 Correlation between liver fibrosis and strain. There was a significant correlation between liver fibrosis and strain distribution map (provided by Dr. Koji Yamamoto, Saiseikai Matsusaka General Hospital)

At present, only a small number of studies have reported the use of VTI for the diagnosis of liver fibrosis in diffuse liver disease. We look forward to further reports in the future.

Shear wave imaging

Shear wave elastography

Virtual touch quantification (Siemens)

(A) Introduction

Virtual Touch™ quantification (VTQ) was the first commercially available ARFI-based elastography technique and is currently one of the most widely used elastography methods in Japan.

The shear wave propagation velocity in an object (elastic body) is positively correlated with the elastic modulus of the object. In other words, the faster the shear wave speed traveling through the object, the harder the object. VTQ uses pulsed focused US (acoustic push pulse) to generate transverse elastic wave (shear wave) and uses tracking US pulses to measure the shear wave speed and thus tissue stiffness. Convex or linear probes for diagnostic ultrasonography are used in VTQ. Shear waves are generated by irradiating biological tissue with push pulses with a duration of 200–300 μs, and shear wave speed is calculated by measuring tissue dislocation through the transmission and reception of US pulses for B-mode imaging. A B-mode image for positioning and measurement results is displayed on the same screen (Fig. 30).

In VTQ, tissue stiffness is expressed by shear wave speed, V_s (m/s):

$$V_s = \sqrt{\frac{E}{2(1+\gamma)\rho}}$$

where E is the Young's modulus, γ the Poisson's ratio, and ρ is the density.

FibroScan measures shear wave speed like VTQ, but calculates the Young's modulus E (kPa) using the equation $E = 3\rho V_s^2$ [tissue density, $\rho = 1$ g/cm^3; shear wave speed, V_s (m/s)]. However, the system assumes that the deformation of an object does not cause any change in the volume (Poisson's ratio, $\gamma = 0.5$), and the density of liver is the same as the density of water (tissue density, $\rho = 1$ g/cm^3). This may be reasonable for a liver with advanced fibrosis; however, the validity of this assumption in relation to other organs has not been fully elucidated, and Siemens has been using shear wave speed, V_s (m/s), to characterize the properties, including stiffness.

(B) Indication

VTQ is indicated for patients with chronic liver disease, particularly viral hepatitis [25–28], requiring the diagnosis

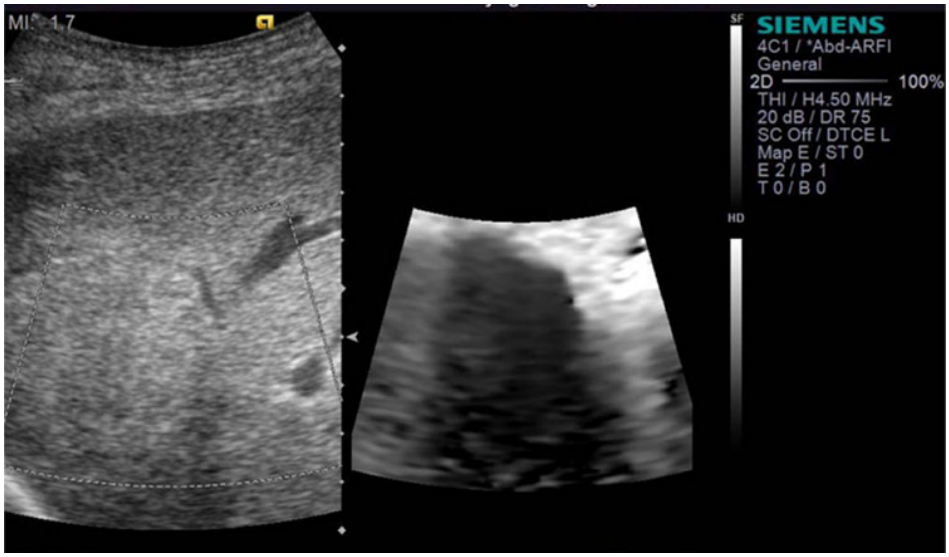

Fig. 29 Assessment of stiffness of metastatic liver tumor with VTI. *Left* B-mode image, *right* VTI. Compared with the non-tumor area, the strain of a metastatic liver tumor is relatively hard (*black*). *SF* Soft, *HD* hard

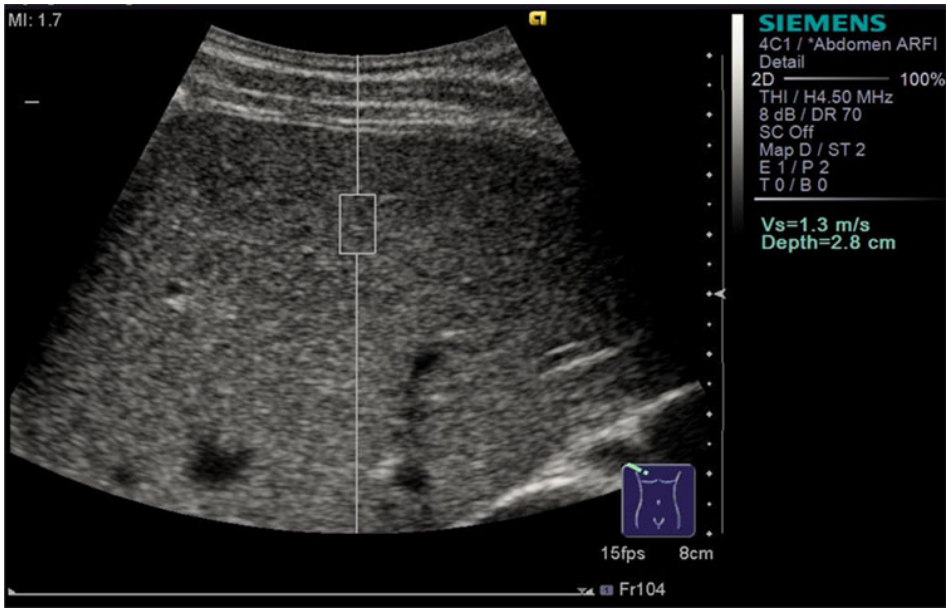

Fig. 30 VTQ display panel. V_s is 1.3 m/s, depth of ROI is 2.8 cm

of liver fibrosis. Aggressive treatment is needed for patients with viral hepatitis, and VTQ is useful for patients contraindicated for liver biopsy.

VTQ is expected to be useful in the assessment of non-viral hepatitis such as non-alcoholic steatohepatitis [29–32], portal hypertension [33, 34], esophageal varices [16], and cancer prognosis.

(C) Procedures (including tips and tricks)

Device: ACUSON S2000

Probe: Convex probe for abdominal imaging or linear probe for superficial imaging

In general, imaging is performed from the right intercostal space of a patient in the supine position holding a normal breath. Prolonged breath holding should be avoided because it will increase central venous pressure, causing the values of V_s to increase. The probe is held lightly against the body, and while observing the B-mode image, a 0.6 × 1.0 cm ROI devoid of large blood vessels is placed 1–2 cm below the liver surface. Measurement is started by pushing the button and is repeated several times to obtain the mean or median V_s values. Imaging of the right hepatic lobe is recommended to be undertaken as possible, because imaging of the left hepatic lobe is often influenced by the movement of body organs, such as the heart, lungs, diaphragm, and stomach (Fig. 31) [35].

Tips and tricks for generating stable focused US

1. Place the ROI 1–2 cm below the liver surface.
2. Press the probe parallel to the liver surface.

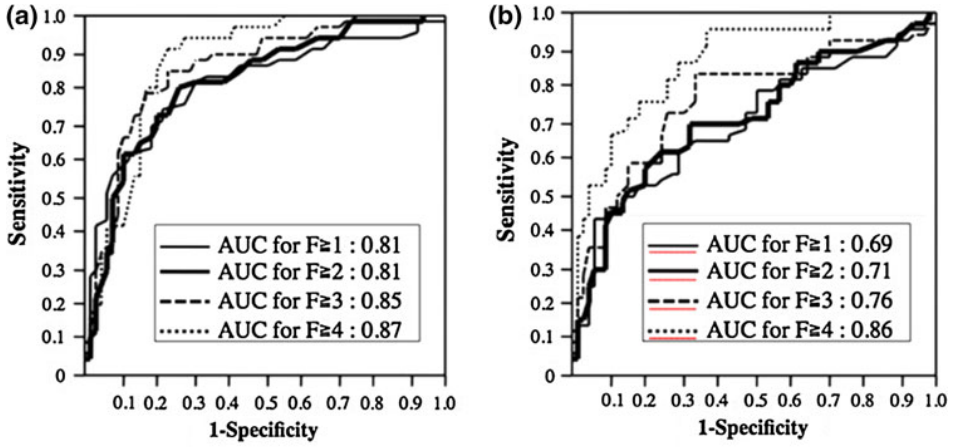

Fig. 31 Diagnostic value of VTQ for liver fibrosis at the right hepatic lobe and left hepatic lobe. **a** ROC with VTQ at right hepatic lobe for diagnosing liver fibrosis grade F ≥1 (*thin black line*, ROC = 0.81), F ≥2 (*bold black line*, 0.81), F ≥3 (*dashed line*, 0.85), and F = 4(*dotted line*, 0.87) are shown. **b** ROC with VTQ at left hepatic lobe for diagnosing liver fibrosis grade F ≥1(*thin black line*, 0.69), F ≥2(*bold black line*, 0.71), F ≥3(*dashed line*, 0.76), and F = 4(*dotted line*, 0.86) are shown. Diagnostic values of liver fibrosis with VTQ at the right hepatic lobe are higher than at the left hepatic lobe [35]

Table 1 Diagnostic value of VTQ for liver fibrosis [28]

Fibrosis	Cut-off (m/s)	AUROC	Se (%)	Sp (%)	Positive predictive value-PPV (%)	Negative predictive value-NPV (%)	Accuracy (%)
F ≥1	>1.19	0.779	69.9	80	95.4	16	70.4
F ≥2	>1.33	0.792	69.1	79.8	87.3	56.1	72.6
F ≥3	>1.43	0.829	74.8	81.5	76.3	79.8	78.2
F = 4	>1.55	0.842	84.3	76.3	53.1	93.7	77.9

A p value <0.05 was regarded as significant

3. Make sure that no large vessels or other objects, such as a space occupying lesion, are present between the ROI and probe.

(D) Results (what does the value mean?)

*Measurement results are expressed as X.XX kPa if the reliability is low.

V_s values reportedly increase with the progression of liver fibrosis. The diagnostic sensitivity of VTQ is reportedly similar to the sensitivity of FibroScan [25, 28, 36].

In a previous study investigating the diagnostic capability of VTQ in chronic hepatitis C and B patients, Friedrich-Rust et al. [25] used the cut-off value of 1.75 m/s and obtained a sensitivity of 81.8 %, specificity of 91.5 %, positive predictive value of 78.3 %, and negative predictive value of 93.1 %. The AUC for fibrosis of F2 or above was 0.82 (95 % confidence interval 0.73–0.91) in VTQ, 0.84 (0.75–0.93) in FibroScan, 0.82 (0.75–0.93) in FibroTest, and 0.75 (0.64–0.86) in APRI, showing similar values between them. However, the AUC for F4 cirrhosis was 0.91 (0.84–0.98) in VTQ, 0.91 (0.84–0.97) in FibroScan, 0.82 (0.73–0.92) in FibroTest, and 0.76 (0.64–0.87) in APRI, indicating that VTQ and FibroScan were superior to serum markers (Fig. 32) [25].

In a multicenter study of chronic hepatitis C patients in five countries, Sporea et al. [28] defined that measurement was reliable if the result was not "X.XX" in VTQ imaging and if the result was >60 % valid and the interquartile range (IQR) was <1/3 of the measurement value in FibroScan [10]. They found a reliability of 98.8 % for VTQ and 93.7 % for FibroScan ($p = 0.003$). V_s values were 1.09 ± 0.42 m/s in F0 fibrosis, 1.22 ± 0.41 m/s in F1, 1.37 ± 0.48 m/s in F2, 1.70 ± 0.59 m/s in F3, and 2.23 ± 0.71 m/s in F4, with a significant difference between adjacent stages (Fig. 33). In addition, the positive predictive value for patients with F1 or more advanced fibrosis and the negative predictive value for patients with F4 cirrhosis were as high as 95.4 and 93.7 %, respectively (Table 1). Although the diagnostic capability of FibroScan was superior to VTQ for F1 or above (AUROC, FibroScan 0.857 vs VTQ 0.772, $p = 0.01$) and F4 (0.932 vs 0.885, $p = 0.01$), FibroScan and VTQ had similar diagnostic capabilities for F2 or above (0.818 vs 0.813, $p = 0.77$) and F3 or above (0.866 vs 0.862, $p = 0.81$). Moreover, the levels of alanine aminotransferase (ALT) affected VTQ measurements as the cut-off values increased with increasing ALT values (Table 2) [28].

Table 2 Comparison of mean liver fibrosis values assessed by ARFI (m/s) for the same stage of liver fibrosis, according to the ALT level

Fibrosis	ALT ≤ ULN* ($n = 394$)	ALT = 1.1–3.0 × ULN# ($n = 376$)	ALT > 3 × ULN¤ ($n = 94$)	p
F0–1	1.10 ± 0.35 ($n = 156$)	1.23 ± 0.26 ($n = 101$)	1.42 ± 0.49 ($n = 16$)	**0.003**$^{*,\#}$ **0.01**$^{*,¤}$ 0.18$^{\#,¤}$
F2–3	1.40 ± 0.49 ($n = 160$)	1.63 ± 0.63 ($n = 175$)	1.61 ± 0.47 ($n = 43$)	**0.002**$^{*,\#}$ **0.002**$^{*,¤}$ 0.36$^{\#,¤}$
F4	2.07 ± 0.76 ($n = 78$)	2.31 ± 0.64 ($n = 100$)	2.45 ± 0.63 ($n = 35$)	**0.02**$^{*,\#}$ **0.006**$^{*,¤}$ 0.13$^{\#,¤}$

Significantly high V_s values in patients with high ALT levels [28]

A p value <0.05 was regarded as significant

* Patients with ALT < ULN

Patients with ALT = 1.1–3.0 × ULN

¤ Patients with ALT > 3.0 × ULN

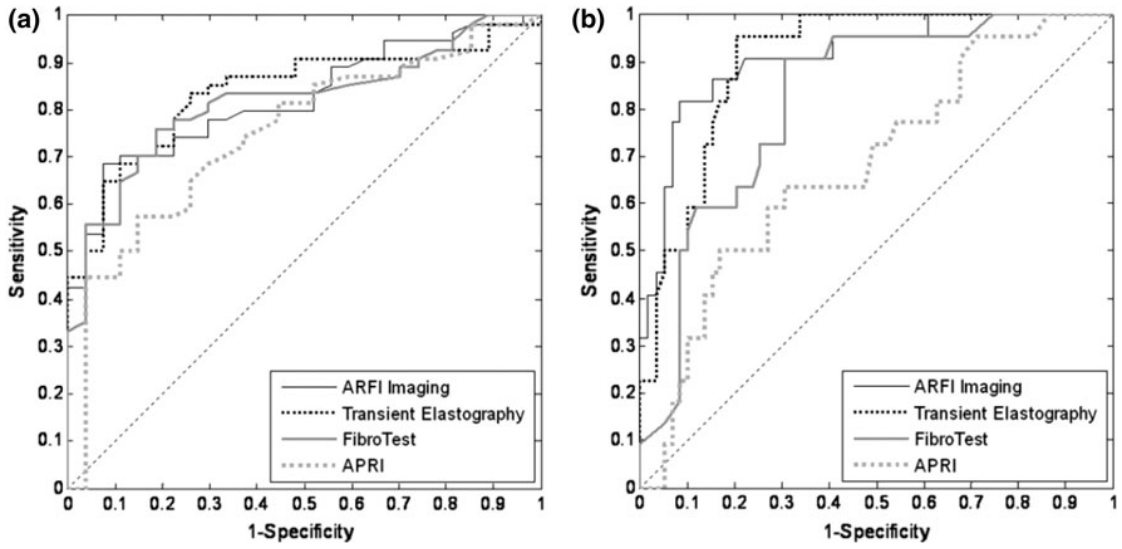

Fig. 32 ROC curves for F2 fibrosis or above (**a**) and F4 cirrhosis (**b**) in VTQ (ARFI imaging), FibroScan (transient elastography) [25]

(E) Limitations

Measurement may not be successful in extremely obese patients. It should be noted that liver stiffness and V_s values increase in acute liver failure and obstructive jaundice, as in FibroScan, for this phenomenon is common to all shear wave imaging (Fig. 34) [37, 38].

It is essential to perform imaging at a sufficient depth to generate stable shear waves. However, the depth of ROI should be <8 cm, and while this would not cause any problem in the measurement of liver stiffness because the ROI is generally placed at 1–2 cm from the surface of the liver, this depth may be problematic in the assessment of liver tumors.

Although FibroScan cannot be applied to cases with ascites retention, VTQ is applicable in such cases because focused US can propagate in ascites.

VTQ fulfills the certification criteria established by both the Ministry of Health, Labour and Welfare in Japan and the Food and Drug Administration (FDA) in the United States. However, because the transmitted US wave form and the wave length are different from those of the conventional US wave, the influence of VTQ on the human body is not yet clear, and further investigation is needed for cases where safety is the highest priority. In addition, if a contrast agent is used, VTQ should be used with caution only after enough time has passed for micro bubbles and the derivatives to be excreted from the body (the Ultrasound Equipment and Safety Committee of the Japan Society of Ultrasonics in Medicine; http://www.jsum.or.jp/committee/m_and_s/acoustic_radiation.html).

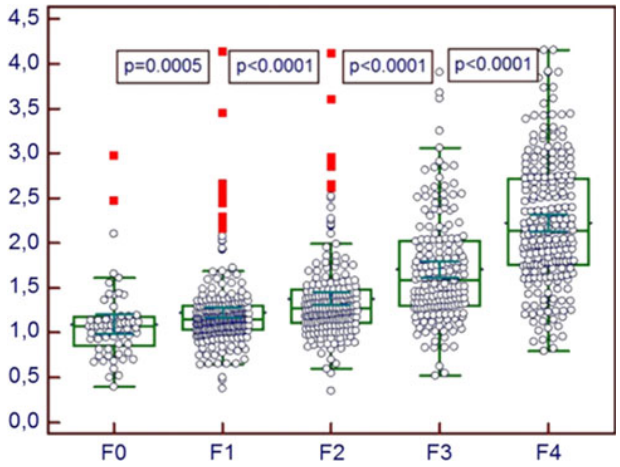

Fig. 33 Relationship between fibrosis stages based on METAVIR score and liver stiffness based on VTQ results [28]

The earlier version VTQ had issues such as no elasticity mapping function or the selection of only one site per measurement. These issues have been improved in the S3000 version, which is currently on the market under the name virtual touch IQ (VTIQ) and is used only for superficial imaging with a linear probe. Therefore, further improvement of the system is desired.

(F) Recommendations

In VTQ, it is possible to quantify shear wave propagation velocity with the B-mode image. Unlike FibroScan developed earlier, VTQ uses B-mode to effectively capture a diseased area and generates stable measurement results. VTQ also measures liver stiffness in patients with ascites retention because focused US propagates through ascites. Furthermore, because the probes can be used for B-mode imaging, the diagnosis of liver stiffness can be started immediately after routine clinical examination.

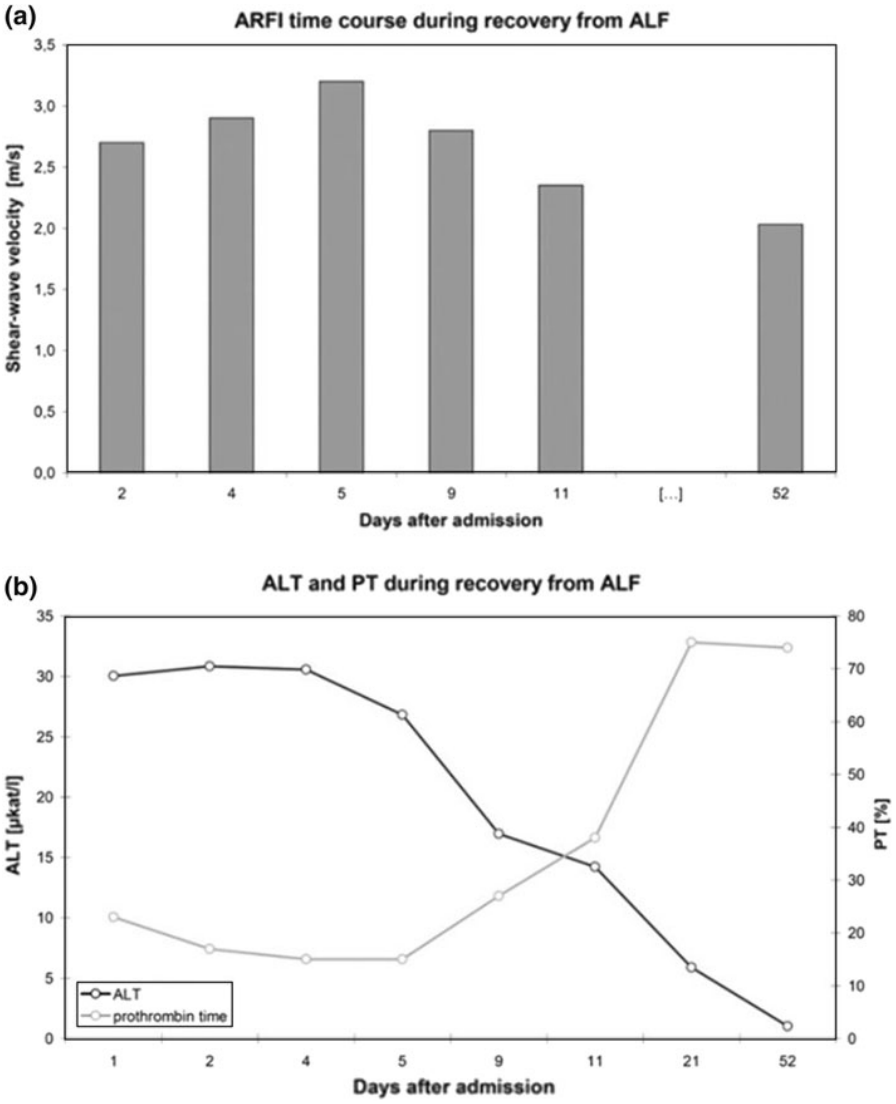

Fig. 34 Decrease in VTQ measurement values along with recovery from acute liver failure [37]

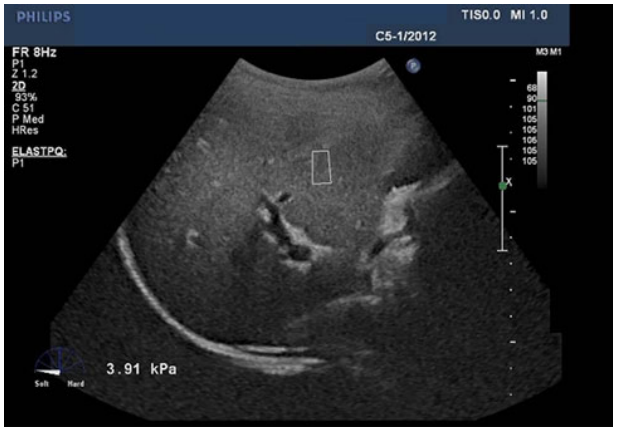

Fig. 35 Quantification of liver stiffness with ElastPQ. The speed of shear wave is 1.14 m/s, and the velocity is converted into elasticity (3.91 kPa) using the equation described in the text

ElastPQ (Philips)

(A) Introduction

Name: ElastPQ (PQ: point quantification)

Equipment: The iU22 xMATRIX ultrasound system (iU: intelligent ultrasound)

ElastPQ is a non-invasive diagnostic tool to measure tissue stiffness using an ARFI-based technology.

Immediately after image acquisition, the screen displays the image and measurement results, including the mean and median values and the deviations in kPa or m/s (Fig. 35).

*If measurement reliability is low, 0.00 kPa will be displayed as the result.

Elastic value E (kPa) is calculated using the equation $E = 3\rho V_s^2$ where V_s (m/s) is defined as the shear wave propagation velocity and ρ as tissue density (whose approximated value in the human body is 1).

An ROI can be placed anywhere but at a depth of <8 cm.

(B) Indication

1. Quantitative assessment of liver fibrosis in diffuse liver diseases
2. Neoplastic lesions of the liver

(C) Procedures (including tips and tricks)

1. Perform right intercostal scanning to visualize the liver.
2. Steadily place the probe with minimum compression.
3. Set the ROI with a depth of <8 cm.
4. Ask the patient to breath hold (if not possible, ask the patient to breathe as shallowly as possible).
5. Push the "Update" button for quantification.
6. The use of a mean value from more than 10 measurements is recommended.

Approach the right hepatic lobe from the right intercostal space. Avoid the left hepatic lobe because the measurement is affected by cardiac movement.

Hold breath without exerting abdominal pressure.

The most appropriate ROI is the center of the image, namely, immediately below the probe and 3–5 cm from the probe surface.

Avoid blood vessels, any necrotic areas, the boundary between organs, and areas influenced by cardiac movement (e.g., left hepatic lobe).

Three frequencies (R1/RP/P1) are available. The measurement sensitivity of areas deep inside the body can be improved by using a lower frequency.

(D) Results (what does the value mean?)

Healthy liver: 4 kPa (2.5–4.7 kPa, 1–1.5 m/s)

Mild fibrosis: 7 kPa (4.7–12.0 kPa, 1.5–2.0 m/s)

Moderate–severe fibrosis: 12 kPa (12.0–21.0 kPa, 2.0–2.5 m/s)

Severe fibrosis: >21 kPa (>2.5 m/s)

(E) Limitations

There is a limit to measurable depth.

ElastPQ is affected by respiratory and body movement.

Cardiac movement also affects the system.

Accuracy of measurement depends on the skills of the examiner.

Measurement accuracy is generally low at the sides of an image.

Ribs may cast lateral acoustic shadows.

(F) Recommendations

At present, the number of studies using ElastPQ is not large enough to reach a definitive conclusion. We look forward to having more study results in the near future.

ShearWave^{TM} elastography (SWE) [SuperSonic Imagine (SSI)]

(A) Introduction

When tissue is dislocated posteriorly by focused US beams from the probe, the restorative force of the tissue propagates laterally, generating shear waves. A conical shear wave front is formed when US beams are transmitted continuously to tissue at different depths. All the transducers are used to transmit and receive US simultaneously, and by repeating this process at high speed, which is known as Ultrafast^{TM} imaging, the propagation velocity of the shear wave is measured and video mapping is performed. A two-dimensional map is created when the speed of the passing shear wave is calculated based on the speed of the Doppler phase shift on a scan line. In ShearWave^{TM} elastography (SWE), UltraFast^{TM} imaging of the liver is performed at 3000 frames/s.

The relationship between tissue elasticity (E) and propagation velocity of the shear wave (c) is expressed by $E = 3\rho c^2$ (ρ, tissue density). Shear waves propagate fast

through hard tissue and slow through soft tissue. Tissue elasticity is calculated and based on the velocity. The measured value is expressed in elasticity (kPa) or speed (m/s). The elastic values or velocities are color-coded, and the color map is superimposed onto a B-mode image in real time (Fig. 36).

(B) Indication

SWE has been used for the diagnosis of liver fibrosis [39–42] and the prognosis of liver transplant rejection and recurrent hepatitis [43].

Potential application of SWE to the diagnosis and localized treatment of neoplastic hepatic lesions is currently being investigated.

(C) Procedures (including tips and tricks)

1. Use the SC6-1 convex probe and select the abdominal application.
2. Display the area of interest at the center of the screen.
3. Turn on the "SWE" switch.
4. Adjust the size and location of the ROI.
5. Push the "Freeze" button after the SWE color map stabilizes.
6. Before activating the "Q-Box" quantification tool, select and save the most appropriate frame on the system's hard drive. The saved raw data can be used to adjust the range of a color map or to perform Q-Box quantification.
7. Adjust the range of color mapping as needed.
8. Use the Q-Box tool to quantify shear wave speed and elasticity at any location in the ROI.

Size and depth of ROI

The ROI size for color mapping is adjustable up to 3 × 3 cm. The depth is also adjustable and can be set at any location on the frame.

Measurement results are often unreliable at a depth of >8 cm or when the ROI is placed near the edge of an image.

Imaging tips and tricks

Successful SWE images can be obtained by right intercostal scanning of the right hepatic lobe. Compared with the right hepatic lobe, measurement of the left hepatic lobe is difficult because of cardiac movement. Intercostal scanning is recommended to avoid excessive compression of the liver by the probe.

Before starting the SWE mode, clear B-mode images with no or few artifacts should be displayed.

In SWE mode, the movement of the probe should be kept to a minimum, and the patient needs to hold breath for a few seconds.

The use of lower B-mode frequencies may be necessary if deep attenuation occurs.

(D) Results (what does the value mean?)

SWE measures the propagation velocity of the shear wave and converts it to a Young's modulus (E) for display. The relationship between Young's modulus (E) and shear wave speed (c) is expressed by the equation $E = 3\rho c^2$ (ρ, tissue density). Strictly speaking, the actual density of the body organ or tissue where the elasticity is being measured should be entered as ρ. However, SWE uses the density of water (i.e., 1000 kg/m^3) to calculate the Young's modulus, with the assumption that the density of tissue is close to that of water. In other words, when using the SWE quantification tool, it should be remembered that Young's modulus is calculated based on the assumption that tissue densities are uniform. The United States FDA has approved only the use of m/s as a velocity indicator; however, both kPa and m/s are displayed in other regions (Fig. 37). The maximum measurement value is 300 kPa (10 m/s).

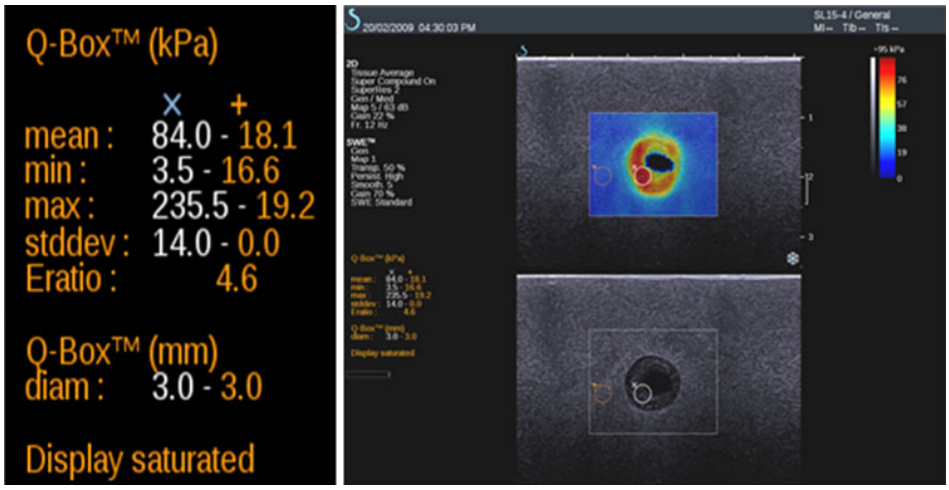

Fig. 36 SWE in phantom. It is possible to measure and display the propagation velocity of the shear waves and tissue elasticity within an arbitrary ROI (Q-Box). Other information such as the minimum, maximum, and standard deviations of elastic values as well as the size of the Q-Box are displayed on the same screen

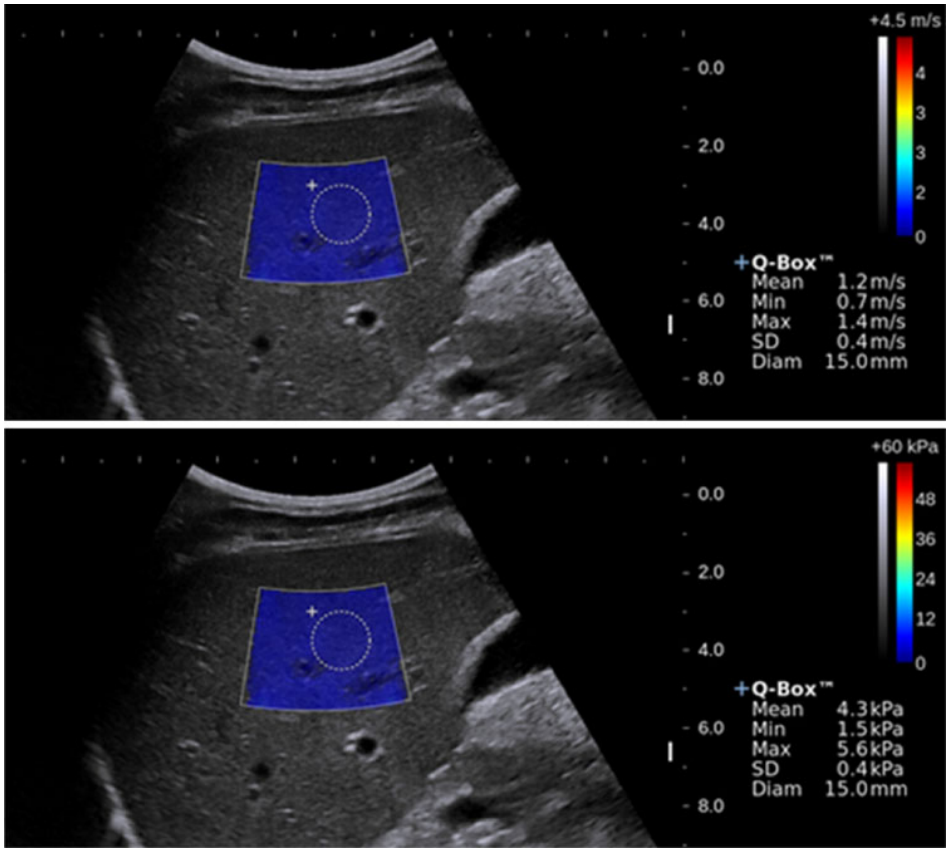

Fig. 37 SWE in healthy liver. The system measures the propagation velocity of the shear wave per pixel to display a color map (*upper panel*), and the velocity is converted into elasticity (*lower panel*) using the equation described in the text. Shown here, the mean shear wave speed is 1.2 m/s, and the elasticity after conversion is 4.3 kPa

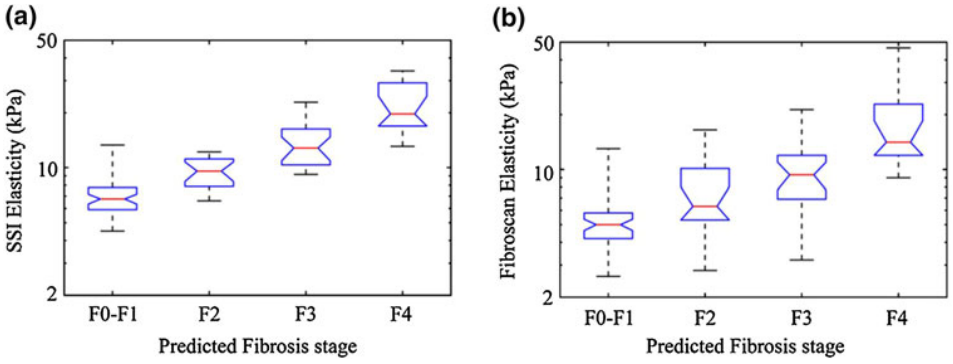

Fig. 38 Box and whisker plots of **a** SWE [supersonic shear imaging (SSI)] and **b** FibroScan values in biopsy staging of liver fibrosis [39]

(1) Diagnosis of liver fibrosis

Bavu et al. [39] reported that biopsy staging of liver fibrosis correlated with the calculated values of Young's modulus (Fig. 38). The AUROC for F2 or above, F3 or above, and F4 were 0.846, 0.857, and 0.940, respectively, using FibroScan, whereas SWE had overall higher values of 0.948, 0.962, and 0.968, respectively (Fig. 39) [39]. Ferraioli et al. [40] also reported high AUROC values of 0.92 for F2 or above, 0.98 for F3 or above, and 0.98 for F4 in fibrosis staging (Fig. 40).

In addition, Bavu et al. [39] reported that, despite the different measurement values between FibroScan and SWE, the SSI values (c) became very similar to those of FibroScan (d) when shear wave spectroscopy was used to recalculate supersonic shear imaging (SSI) data, under the assumption that the original measurement had been performed at 50 Hz, the shear wave frequency used in FibroScan (Fig. 41). When heterogeneity was defined as $\tau = \frac{\sigma}{E}$, it tended to increase with the progression of fibrosis from 14.24 % at F0–1 to 16.63 % at F2, 17.62 % at F3, and 19.29 % at F4 (Fig. 42) [39].

(2) Space occupying lesion

It is possible to comparatively assess differences between a tumor and non-tumor area or between homogenous and heterogeneous parts of the tumor, and by using the Q-Box tool, tissue elasticity and shear wave speed at

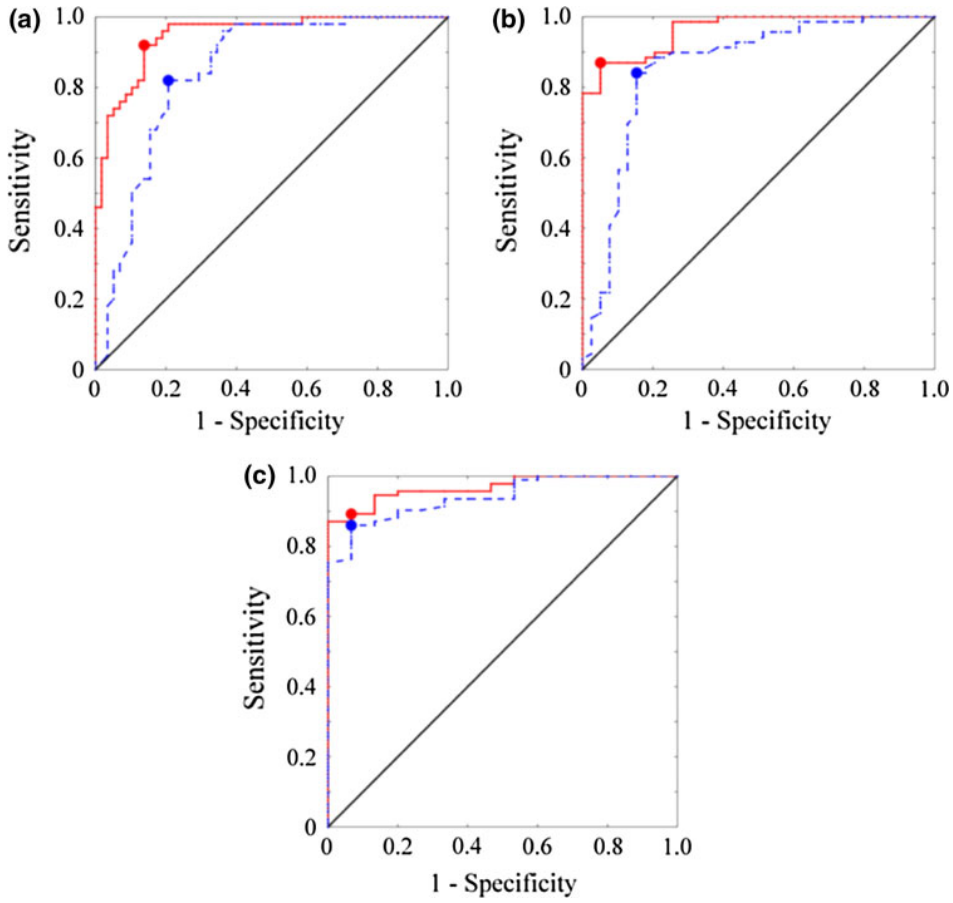

Fig. 39 ROC curves for SWE (*solid line*) and FibroScan (FS) (*dashed line*) for different fibrosis thresholds: **a** F0–F1 versus F2–F4 ($p = 0.005$), **b** F0–F2 versus F3–F4 ($p = 0.001$), **c** F0–F3 versus F4 ($p = 0.154$) [39]

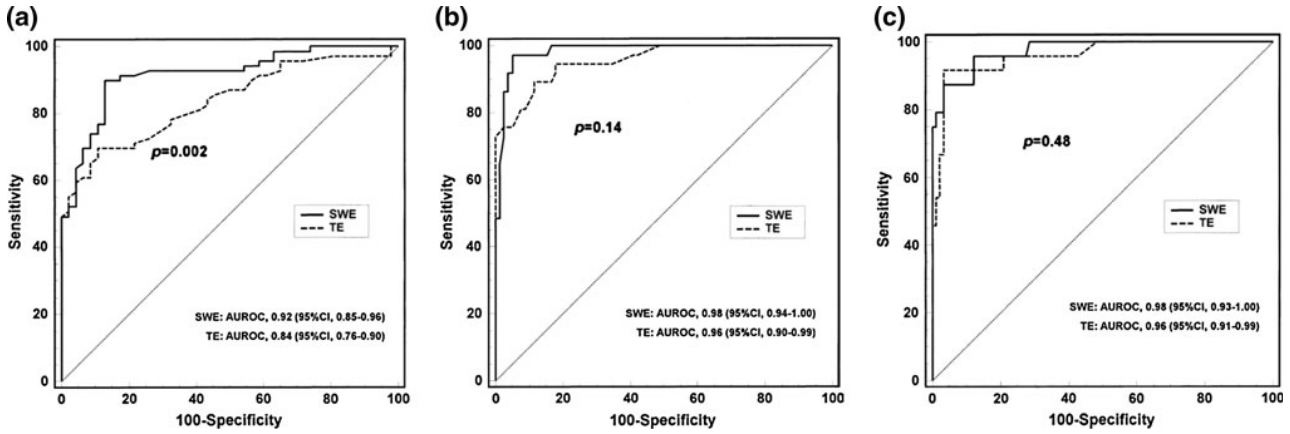

Fig. 40 Comparison between SWE and FibroScan (TE) of ROC curves for the diagnosis of fibrosis in chronic hepatitis C patients. **a** F0–F1 versus F2–F4 (≥F2), **b** F0–F2 versus F3–F4 (≥F3), and **c** F0–F3 versus F4 (F = 4). In *parentheses*, 95 % confidence intervals are shown. *p* values of differences between AUROCs are given [40]

any location in the ROI can be expressed in absolute numbers (Figs. 43, 44).

(E) Limitations

Accurate subcostal scanning of the left hepatic lobe may be difficult due to cardiac movement.

Because there is a limit to the measurable depth because of its dependency on the acoustic output, measurement may not be successful for tumors located deep inside or on the surface of the liver.

Because the maximum ROI size is 3 × 3 cm, one scan may not be sufficient for some lesions.

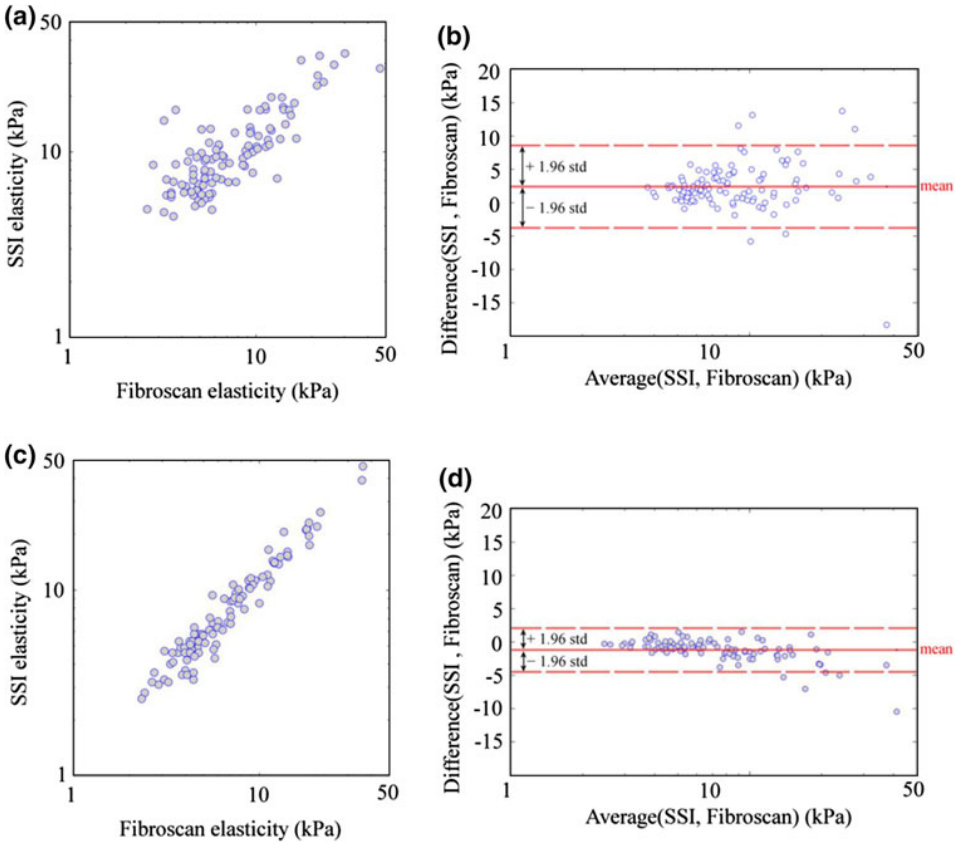

Fig. 41 Correlation between SSI and FibroScan. **a** Scatter plot between liver stiffness distributions (normalized by log transformation) assessed by FS and SWE (SSI) technique. **b** Bland–Altman plot between the SWE (SSI) measurement and the FS measurement. **c** Scatter plot between liver stiffness distributions (normalized by log transformation) assessed by FS and SWE (SSI) technique extracted from fit at 50 Hz. **d** Bland–Altman plot between the SWE (SSI) measurements fitted at 50 Hz and the FS measurement [39]

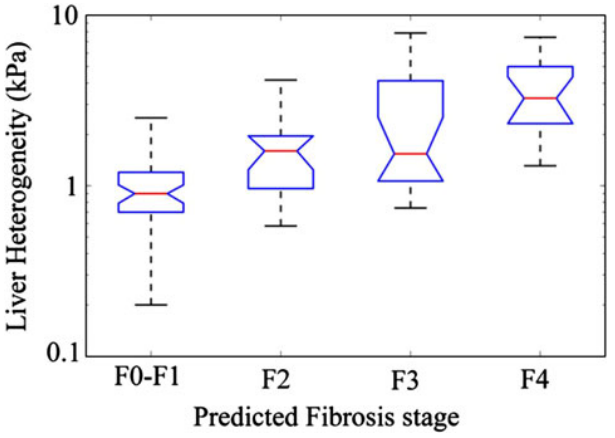

Fig. 42 Comparison between liver heterogeneity and fibrosis [39]

Because of its relatively short time on the market, the number of evidence-based studies using this new technology is insufficient to establish diagnostic criteria.

SWE is reportedly influenced by blood stasis, or congestion [44]. In principle, SWE is also affected by inflammation and jaundice.

(F) Recommendations

SWE quantifies the shear wave propagation velocity and displays it on a two-dimensional map. Owing to the mapping

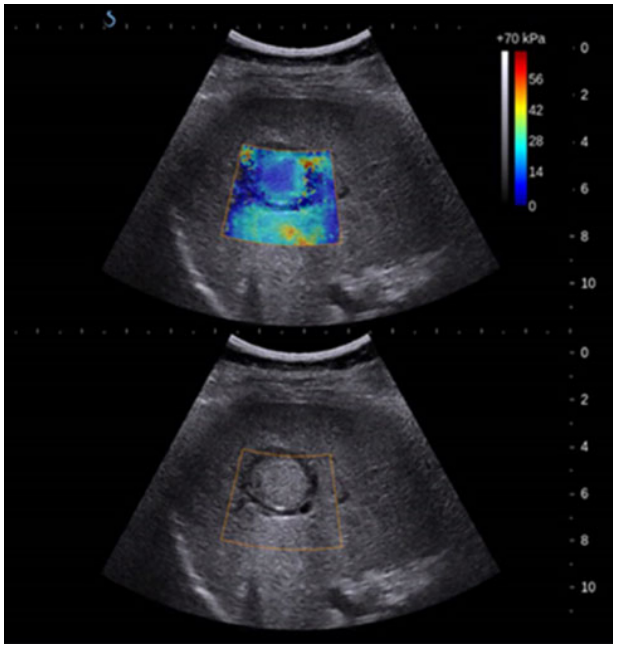

Fig. 43 SWE image of liver cancer. The image shows stiffness distribution in the tumor and surrounding tissue. The tumor has a low elasticity of 12 kPa at the center and much lower elasticity at the margin, compared to 30 kPa in the non-tumor area which is equivalent to the stiffness of cirrhosis

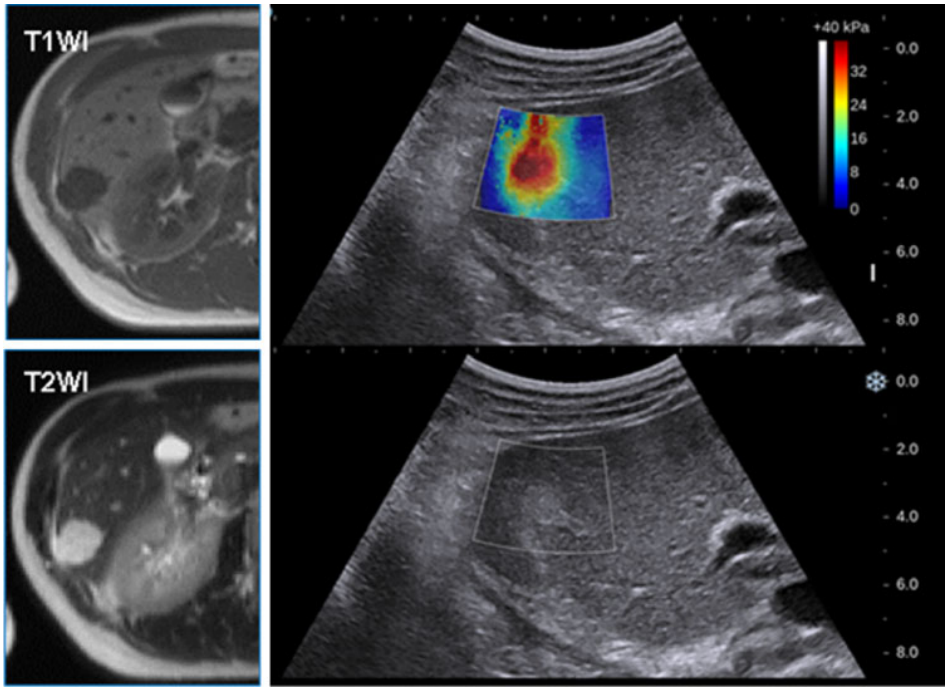

Fig. 44 Typical SWE image of cavernous hemangioma. The tumor has high elasticity of 42 kPa at the center and it appears the hard mass is surrounded by soft liver tissue of 5.5 kPa. It is clear that the hemangioma has increased viscoelasticity

capability, velocity heterogeneity in diffuse liver disease is displayed on the map. This is particularly useful for the assessment of liver with inconsistent elasticity, as found in patients with focal fatty infiltration or Budd–Chiari syndrome.

In space occupying lesions, SWE visualizes the changes in the elasticity of the tumor and surrounding tissue, and studies are currently underway to elucidate the efficacy of SWE in the differential diagnosis of space occupying lesions of the liver and in the determination of ablation range in localized treatment, such as radiofrequency ablation therapy.

Transient elastography

FibroScan® (Echosens)

(A) Introduction

There is a positive correlation between liver stiffness and fibrosis. To quantify liver elasticity, FibroScan® measures the propagation velocity of a single-cycle shear wave generated by a probe unique to FibroScan [45, 46]. A low-frequency elastic wave is generated by vibration at the probe tip and is transmitted from the body surface to the liver through the skin and adipose tissue. The system uses US to track the vibration and measures the velocity. To quantify liver stiffness, the elastic value E (kPa) is calculated using the following equation, where V_s (m/s) is the shear wave propagation velocity and ρ is tissue density (the approximate density of the human body is 1):

$$E = 3\rho V_s^2$$

Measurement sites should be somewhere between 25 and 65 mm from the body surface, and numerical conversion takes place upon the imaging of at least 20 mm (Fig. 45).

(B) Indication

FibroScan is indicated for patients who have or who are suspected to have chronic liver disease and require an assessment of liver fibrosis. For example, because aggressive therapy is recommended for patients with advanced fibrosis, the severity of liver fibrosis in chronic hepatitis C patients needs to be diagnosed before deciding an indication for treatment with potential side effects [46–50]. In addition, the rate of fibrosis progression can be estimated by performing measurement on a regular basis [51–54], and the elastic values of liver tissue are an important indicator for the screening of esophageal varices [55–57]. FibroScan is also useful in the assessment of hepatitis B [58, 59], alcoholic hepatitis, non-alcoholic steatohepatitis [60, 61], autoimmune liver disease such as primary biliary cirrhosis and primary sclerosing cholangitis [62, 63], and HCV–HIV co-infection cases [64]. FibroScan has also been used to evaluate the severity of portal hypertension after a liver transplant [65, 66]. Because it is extremely minimally invasive and can be completed quickly, FibroScan will be useful for the screening of chronic liver disease in outpatients with diabetes [67, 68].

(C) Procedures (including tips and tricks)

In principle, imaging should be performed while fasting because liver stiffness reportedly increases after a meal [69]. With appropriate force, press the FibroScan® probe vertically against the skin, with the patient lying down with the right arm elevated to make the intercostal spaces wider.

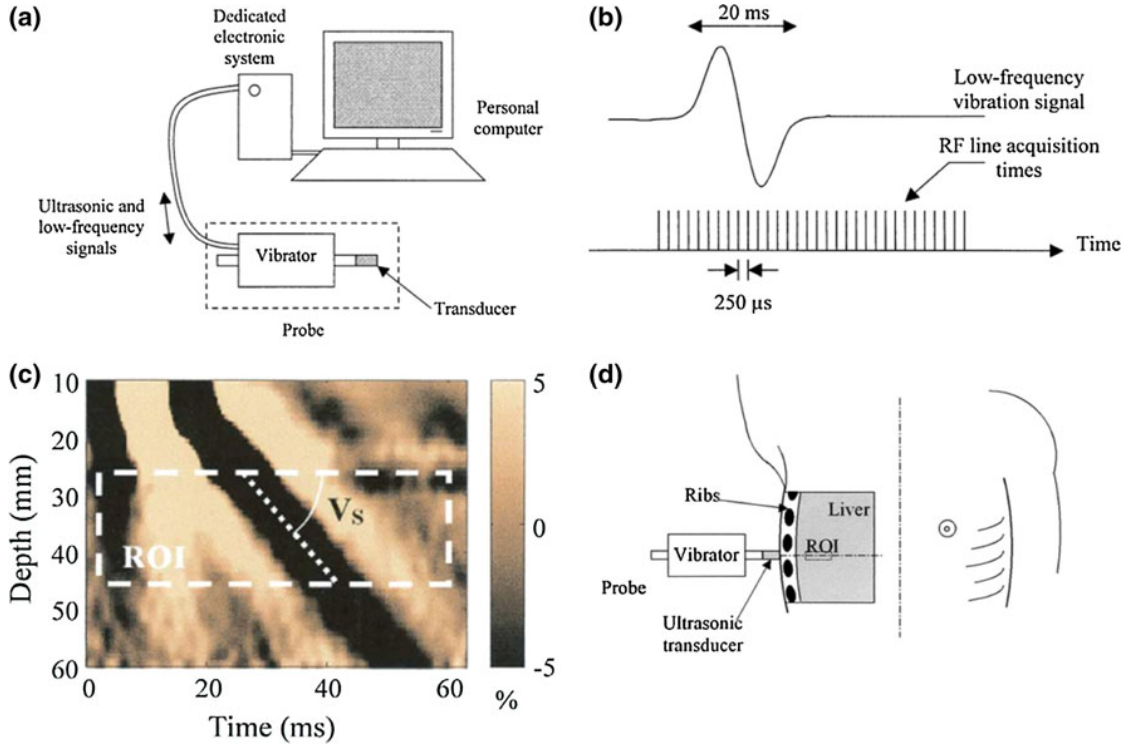

Fig. 45 The principle of FibroScan®. **a** An ultrasonic probe and a shear wave generator. **b** The propagation velocity of a 20-ms shear wave is measured using 4000-Hz US. **c** The shear wave propagation velocity is equivalent to V_s. **d** Scanning is performed from the right lateral intercostal space [45]

While watching the pressure indicator on the screen, adjust the compression to the chest and push the button to generate a low frequency wave. This light impacts on the liver, and the system uses US pulses to measure the velocity of the low frequency wave and calculates tissue elasticity for display (Fig. 45).

It may be necessary to confirm the location of the liver in advance using B-mode US beams because the location varies greatly among individuals. In addition, select a wide intercostal space to capture a large portion of the liver. With practice, it will be easier to determine which intercostal space is more appropriate for B-mode imaging. To avoid the adverse effects of the ribs, the probe should be pressed vertically against the thoracic wall on the axillary line and between the ribs. Errors can be minimized if imaging is performed while holding breath [70]. An error indication appears after unsuccessful measurement. Measurement should be repeated at least 10 times to obtain a median value and IQR. When the rate of successful measurements out of all measurements is <60 % or when the value of IQR/median is >0.3, measurement values are of low quality and should not be used in clinical decision making.

(D) Results (what does the value mean?)

Measurement values are expressed in elasticity (kPa). The higher the value, the more difficult it is to deform the liver, indicating that fibrosis is more advanced. Although there is certain variability between studies and diseases, elasticity of ≥7.0 and ≥12.5–15.0 kPa is considered to indicate significant fibrosis and cirrhosis, respectively (Fig. 46) [45]. A meta-analysis of previous studies using transient elastography, or FibroScan, have shown that the sensitivity and specificity for the diagnosis of cirrhosis were 0.87 (95 % confidence interval 0.84–0.90) and 0.91

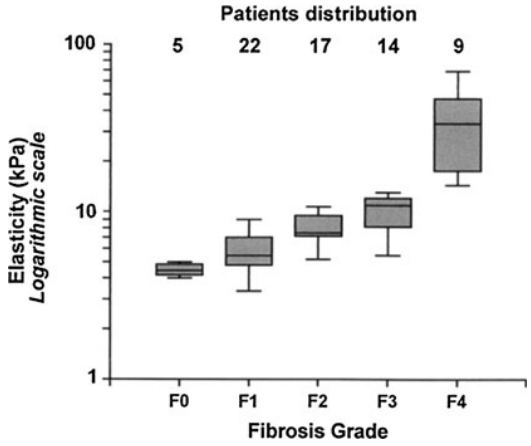

Fig. 46 Relationship between histologic liver fibrosis staging in biopsy and liver elasticity [45]

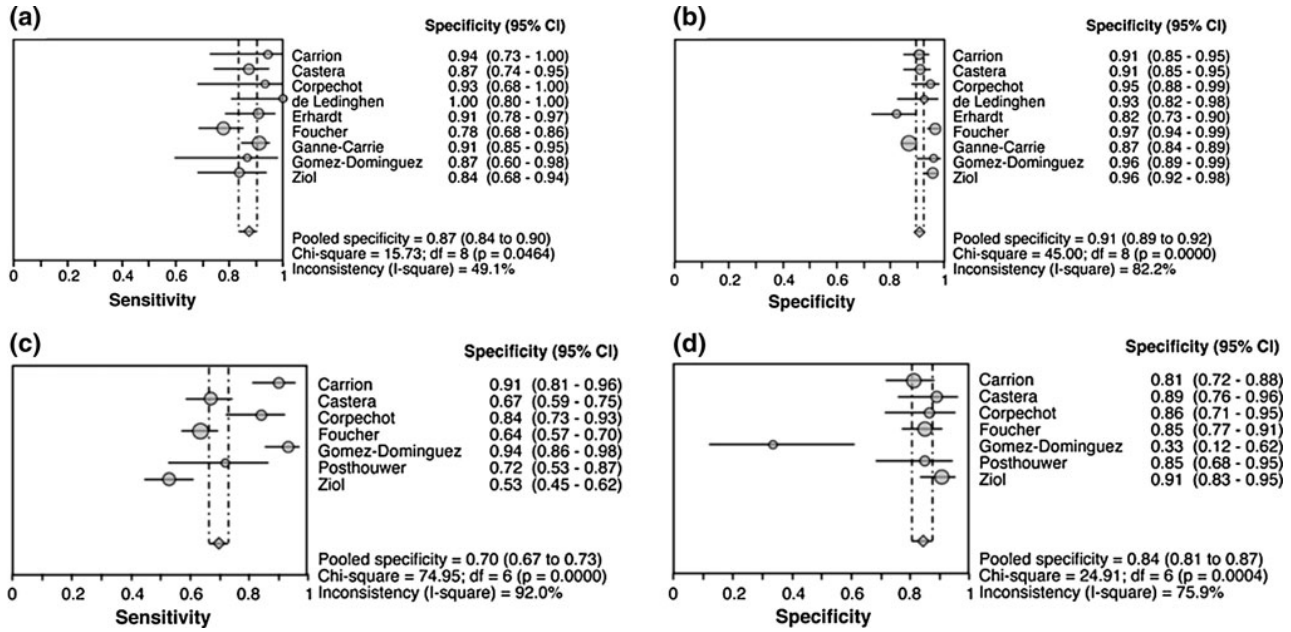

Fig. 47 Meta-analysis of nine studies on the diagnosis of liver fibrosis. The sensitivity (**a**) and specificity (**b**) for the diagnosis of cirrhosis, and sensitivity (**c**) and specificity (**d**) for the diagnosis of F2–F4 fibrosis [71]

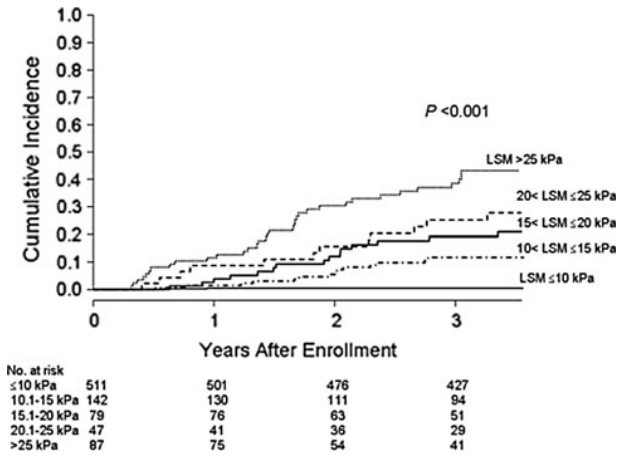

Fig. 48 Cumulative incidence of HCC development stratified based on LSM ($n = 866$). *LSM* Liver stiffness measurement [72]

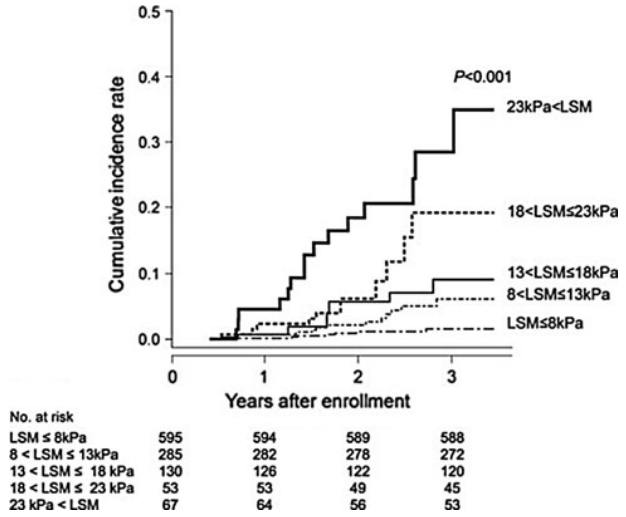

Fig. 49 Cumulative incidence rates of HCC based on stratified LSM (Kaplan–Meier plot). The cumulative incidence rates increased significantly in association with higher LSM (log-rank test, $p < 0.001$) [73]

(0.89–0.92), respectively, and those for fibrosis staging of F2–4 were 0.91 (0.81–0.96) and 0.85 (0.81–0.87), respectively (Fig. 47) [71]. The upper limit of measurement is 75 kPa, and although liver cirrhosis based on biopsy is generally categorized as F4, several studies have shown that there is a positive correlation between liver stiffness (elasticity) and cancer risks even if the elasticity is >15 kPa (Figs. 48, 49) [72, 73]. It should be noted that measurement values are also high when liver elasticity is increased by factors other than fibrosis, such as acute hepatitis, jaundice, and congestive liver (Figs. 50, 51, 52, 53) [19–22, 74, 75].

(E) Limitations

Approximately 5 % of all FibroScan imaging has some problem in quantification [76–78]. Imaging is not possible

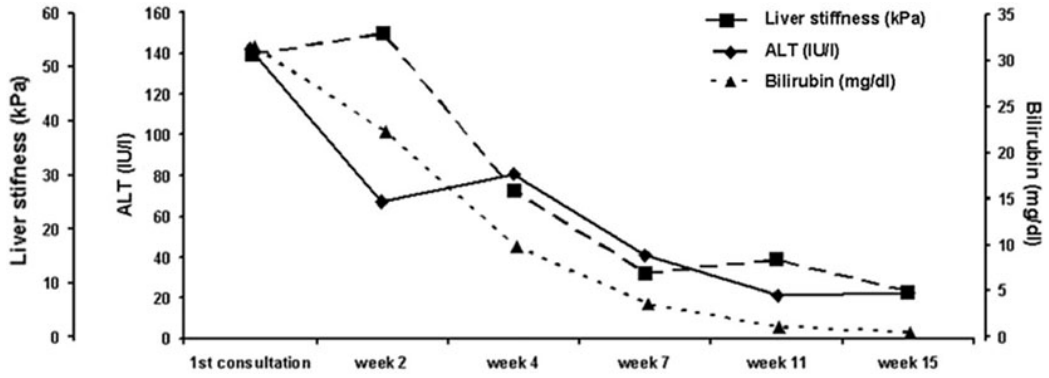

Fig. 50 Transition in the levels of alanine aminotransferase (ALT), bilirubin, and liver stiffness in patients with drug-induced liver injury caused by nitrofurantoin [20]

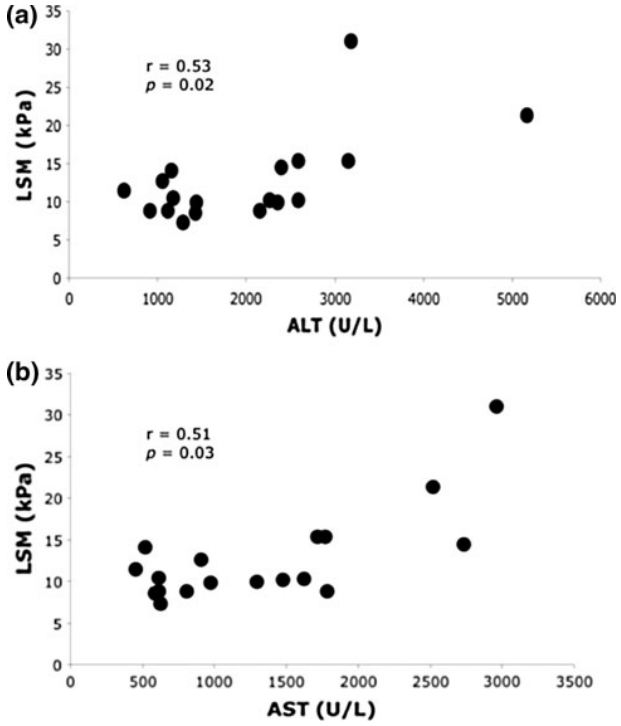

Fig. 51 Relationship between liver stiffness and the level of transaminase in patients with acute viral hepatitis [19]

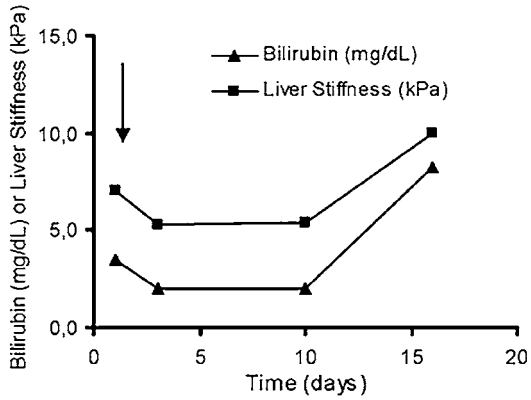

Fig. 52 Transition in the levels of bilirubin and liver stiffness in patients with obstructive jaundice [21]

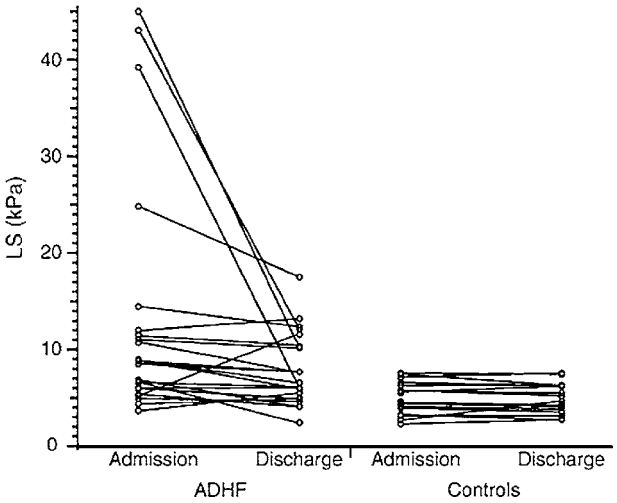

Fig. 53 Comparison of liver stiffness between patients with acute decompensated heart failure (ADHF) and controls. Liver stiffness can be improved in ADHF patients. *LS* Liver stiffness [22]

in cases in which ascites retention is near the surface of the liver being examined. In addition, measurement reproducibility decreases in fatty liver and obese cases [79]. The relationship between liver elasticity and the progression of liver fibrosis reportedly varies depending on the underlying liver disease [80]. Inflammation, jaundice, and congestion frequently exacerbate liver stiffness, making accurate assessment of fibrosis difficult [21, 22, 75]. The severity of fibrosis may be underestimated in a cirrhotic liver with large regenerative nodules [81]. In addition, measurements are difficult in severely obese individuals because of the relatively long distance between body surface and liver. Overseas, a probe has been developed for use with severely obese individuals and is used in clinical practice [82, 83].

(F) Recommendations

FibroScan is the most popular and highly trusted liver elastography technique because of the large amount of validation data accumulated to date.

The system is recommended for the screening of chronic liver diseases and follow-up observations.

Depending on the existing disease conditions, measurement values may not accurately reflect the actual severity of liver fibrosis, and the system should therefore be used with the limitations described above in mind.

References

1. Matsumura T, Shiina T, Oosaka T, et al. Development of real-time tissue elastography. MEDIX. 2004;41:30–5.
2. Tatsumi C, Kudo M, Ueshima K, et al. Noninvasive evaluation of hepatic fibrosis using serum fibrotic markers, transient elastography (FibroScan) and real-time tissue elastography. Intervirology. 2008;51:27–33.
3. Tatsumi C, Kudo M, Ueshima K, et al. Non-invasive evaluation of hepatic fibrosis for type C chronic hepatitis. Intervirology. 2010;53:76–81.
4. Fujimoto K, Wada S, Oshita M, et al. Non-invasive evaluation of hepatic fibrosis in patients with chronic hepatitis C using elastography. MEDIX. 2007;Suppl.:24–7.
5. Fujimoto K, Kato M, Tonomura A, et al. Non-invasive evaluation method of the liver fibrosis using real-time tissue elastography - usefulness of judgment liver fibrosis stage by liver fibrosis index (LF index). Kanzo. 2010;59:539–41.
6. Koizumi Y, Hirooka M, Kisaka Y, et al. Liver fibrosis in patients with chronic hepatitis C: noninvasive diagnosis by means of real-time tissue elastography—establishment of the method for measurement. Radiology. 2011;258:610–7.
7. Morikawa H, Fukuda K, Kobayashi S, et al. Real-time tissue elastography as a tool for the noninvasive assessment of liver stiffness in patients with chronic hepatitis C. J Gastroenterol. 2011;46:350–8.
8. Fujimoto K, Kato M, Kudo M, et al. Novel image analysis method using ultrasound elastography for non-invasive evaluation of hepatic fibrosis in patients with chronic hepatitis C. Oncology. 2013;84:3–12.
9. Yada N, Kudo M, Morikawa H, et al. Assessment of liver fibrosis with real-time tissue elastography in chronic viral hepatitis. Oncology. 2013;84:13–20.
10. Ochi H, Hirooka M, Koizumi Y, et al. Real-time tissue elastography for evaluation of hepatic fibrosis and portal hypertension in nonalcoholic fatty liver diseases. Hepatology. 2012;56:1271–8.
11. Hirooka M, Ochi H, Koizumi Y, et al. Splenic elasticity measured with real-time tissue elastography is a marker of portal hypertension. Radiology. 2011;261:960–8.
12. Tonomura A, Waki K, Imura T, et al. Development of strain histogram measurement function and clinical applications in hepatic region. MEDIX. 2011;54:37–41.
13. Saftoiu A, Gheonea DI, Ciurea T. Hue histogram analysis of real-time elastography images for noninvasive assessment of liver fibrosis. AJR Am J Roentgenol. 2007;189:W232–3.
14. Kanamoto M, Shimada M, Ikegami T, et al. Real time elastography for noninvasive diagnosis of liver fibrosis. J Hepatobiliary Pancreat Surg. 2009;16:463–7.
15. Ferraioli G, Lissandrin R, Filice C. Real-time tissue elastography in the assessment of liver stiffness. Hepatology. 2012. doi:10.1002/hep.26215.
16. Shiina T, Maki T, Yamakawa M, et al. Mechanical model analysis for quantitative evaluation of liver fibrosis based on ultrasound tissue elasticity imaging. Jpn J Appl Phys. 2012;51:07GF11.1–8.
17. Wang J, Guo L, Shi X, et al. Real-time elastography with a novel quantitative technology for assessment of liver fibrosis in chronic hepatitis B. Eur J Radiol. 2012;81:e31–6.
18. Friedrich-Rust M, Ong MF, Herrmann E, et al. Real-time elastography for noninvasive assessment of liver fibrosis in chronic viral hepatitis. AJR Am J Roentgenol. 2007;188:758–64.
19. Arena U, Vizzutti F, Corti G, et al. Acute viral hepatitis increases liver stiffness values measured by transient elastography. Hepatology. 2008;47:380–4.
20. Sagir A, Erhardt A, Schmitt M, et al. Transient elastography is unreliable for detection of cirrhosis in patients with acute liver damage. Hepatology. 2008;47:592–5.
21. Millonig G, Reimann FM, Friedrich S, et al. Extrahepatic cholestasis increases liver stiffness (FibroScan) irrespective of fibrosis. Hepatology. 2008;48:1718–23.
22. Colli A, Pozzoni P, Berzuini A, et al. Decompensated chronic heart failure: increased liver stiffness measured by means of transient elastography. Radiology. 2010;257:872–8.
23. Hirooka M, Koizumi Y, Hiasa Y, et al. Hepatic elasticity in patients with ascites: evaluation with real-time tissue elastography. AJR Am J Roentgenol. 2011;196:W766–71.
24. Shuang-Ming T, Ping Z, Ying Q, et al. Usefulness of acoustic radiation force impulse imaging in the differential diagnosis of benign and malignant liver lesions. Acad Radiol. 2011;18:810–5.
25. Friedrich-Rust M, Wunder K, Kriener S, et al. Liver fibrosis in viral hepatitis: noninvasive assessment with acoustic radiation force impulse imaging versus transient elastography. Radiology. 2009;252:595–604.
26. Boursier J, Isselin G, Fouchard-Hubert I, et al. Acoustic radiation force impulse: a new ultrasonographic technology for the widespread noninvasive diagnosis of liver fibrosis. Eur J Gastroenterol Hepatol. 2010;22:1074–84.
27. Takahashi H, Ono N, Eguchi Y, et al. Evaluation of acoustic radiation force impulse elastography for fibrosis staging of chronic liver disease: a pilot study. Liver Int. 2010;30:538–45.
28. Sporea I, Bota S, Peck-Radosavljevic M, et al. Acoustic radiation force impulse elastography for fibrosis evaluation in patients with chronic hepatitis C: an international multicenter study. Eur J Radiol. 2012;81:4112–8.
29. Yoneda M, Suzuki K, Kato S, et al. Nonalcoholic fatty liver disease: US-based acoustic radiation force impulse elastography. Radiology. 2010;256:640–7.
30. Palmeri ML, Wang MH, Rouze NC, et al. Noninvasive evaluation of hepatic fibrosis using acoustic radiation force-based shear stiffness in patients with nonalcoholic fatty liver disease. J Hepatol. 2011;55:666–72.
31. Friedrich-Rust M, Romen D, Vermehren J, et al. Acoustic radiation force impulse-imaging and transient elastography for noninvasive assessment of liver fibrosis and steatosis in NAFLD. Eur J Radiol. 2012;81:e325–31.
32. Guzman-Aroca F, Frutos-Bernal MD, Bas A, et al. Detection of non-alcoholic steatohepatitis in patients with morbid obesity before bariatric surgery: preliminary evaluation with acoustic radiation force impulse imaging. Eur Radiol. 2012;22:2525–32.
33. Furuichi Y, Moriyasu F, Taira J, et al. Noninvasive diagnostic method for idiopathic portal hypertension based on measurements of liver and spleen stiffness by ARFI elastography. J Gastroenterol. 2012.

34. Ye XP, Ran HT, Cheng J, et al. Liver and spleen stiffness measured by acoustic radiation force impulse elastography for noninvasive assessment of liver fibrosis and esophageal varices in patients with chronic hepatitis B. J Ultrasound Med. 2012;31:1245–53.
35. Toshima T, Shirabe K, Takeishi K, et al. New method for assessing liver fibrosis based on acoustic radiation force impulse: a special reference to the difference between right and left liver. J Gastroenterol. 2011;46:705–11.
36. Ebinuma H, Saito H, Komuta M, et al. Evaluation of liver fibrosis by transient elastography using acoustic radiation force impulse: comparison with Fibroscan®. J Gastroenterol. 2011;46:1238–48.
37. Karlas TF, Pfrepper C, Rosendahl J, et al. Acoustic radiation force impulse (ARFI) elastography in acute liver failure: necrosis mimics cirrhosis. Z Gastroenterol. 2011;49:443–8.
38. Bota S, Sporea I, Sirli R, et al. Factors that influence the correlation of acoustic radiation force impulse (ARFI), elastography with liver fibrosis. Med Ultrason. 2011;13:135–40.
39. Bavu E, Gennisson JL, Couade M, et al. Noninvasive in vivo liver fibrosis evaluation using supersonic shear imaging: a clinical study on 113 hepatitis C virus patients. Ultrasound Med Biol. 2011;37:1361–73.
40. Ferraioli G, Tinelli C, Dal Bello B, et al. Accuracy of real-time shear wave elastography for assessing liver fibrosis in chronic hepatitis C: a pilot study. Hepatology. 2012;56:2125–33.
41. Ling W, Lu Q, Quan J, et al. Assessment of impact factors on shear wave based liver stiffness measurement. Eur J Radiol. 2013;82:335–41.
42. Poynard T, Munteanu M, Luckina E, et al. Liver fibrosis evaluation using real-time shear wave elastography: applicability and diagnostic performance using methods without a gold standard. J Hepatol. 2013;58:928–35.
43. Yoon JH, Lee JY, Woo HS, et al. Shear wave elastography in the evaluation of rejection or recurrent hepatitis after liver transplantation. Eur Radiol. 2013.
44. Wang HK, Lai YC, Tseng HS, et al. Hepatic venous congestion after living donor liver transplantation: quantitative assessment of liver stiffness using shear wave elastography—a case report. Transplant Proc. 2012;44:814–6.
45. Sandrin L, Fourquet B, Hasquenoph JM, et al. Transient elastography: a new noninvasive method for assessment of hepatic fibrosis. Ultrasound Med Biol. 2003;29:1705–13.
46. Castera L, Vergniol J, Foucher J, et al. Prospective comparison of transient elastography, Fibrotest, APRI, and liver biopsy for the assessment of fibrosis in chronic hepatitis C. Gastroenterology. 2005;128:343–50.
47. Colletta C, Smirne C, Fabris C, et al. Value of two noninvasive methods to detect progression of fibrosis among HCV carriers with normal aminotransferases. Hepatology. 2005;42:838–45.
48. Ziol M, Handra-Luca A, Kettaneh A, et al. Noninvasive assessment of liver fibrosis by measurement of stiffness in patients with chronic hepatitis C. Hepatology. 2005;41:48–54.
49. Sebastiani G, Vario A, Guido M, et al. Stepwise combination algorithms of non-invasive markers to diagnose significant fibrosis in chronic hepatitis C. J Hepatol. 2006;44:686–93.
50. Shaheen AA, Wan AF, Myers RP. FibroTest and FibroScan for the prediction of hepatitis C-related fibrosis: a systematic review of diagnostic test accuracy. Am J Gastroenterol. 2007;102:2589–600.
51. Castera L, Forns X, Alberti A. Non-invasive evaluation of liver fibrosis using transient elastography. J Hepatol. 2008;48:835–47.
52. Ogawa E, Furusyo N, Toyoda K, et al. The longitudinal quantitative assessment by transient elastography of chronic hepatitis C patients treated with pegylated interferon alpha-2b and ribavirin. Antivir Res. 2009;83:127–34.
53. Ogawa E, Furusyo N, Murata M, et al. Longitudinal assessment of liver stiffness by transient elastography for chronic hepatitis B patients treated with nucleoside analog. Hepatol Res. 2011;41:1178–88.
54. Martinez SM, Foucher J, Combis JM, et al. Longitudinal liver stiffness assessment in patients with chronic hepatitis C undergoing antiviral therapy. PLoS ONE. 2012;7:e47715.
55. Kazemi F, Kettaneh A, N'Kontchou G, et al. Liver stiffness measurement selects patients with cirrhosis at risk of bearing large oesophageal varices. J Hepatol. 2006;45:230–5.
56. Vizzutti F, Arena U, Romanelli RG, et al. Liver stiffness measurement predicts severe portal hypertension in patients with HCV-related cirrhosis. Hepatology. 2007;45:1290–7.
57. Castera L, Pinzani M, Bosch J. Non invasive evaluation of portal hypertension using transient elastography. J Hepatol. 2012;56:696–703.
58. Fung J, Lai CL, But D, et al. Prevalence of fibrosis and cirrhosis in chronic hepatitis B: implications for treatment and management. Am J Gastroenterol. 2008;103:1421–6.
59. Wong GL, Wong VW, Choi PC, et al. Evaluation of alanine transaminase and hepatitis B virus DNA to predict liver cirrhosis in hepatitis B e antigen-negative chronic hepatitis B using transient elastography. Am J Gastroenterol. 2008;103:3071–81.
60. Foucher J, Chanteloup E, Vergniol J, et al. Diagnosis of cirrhosis by transient elastography (FibroScan): a prospective study. Gut. 2006;55:403–8.
61. Nahon P, Kettaneh A, Tengher-Barna I, et al. Assessment of liver fibrosis using transient elastography in patients with alcoholic liver disease. J Hepatol. 2008;49:1062–8.
62. Corpechot C, El Naggar A, Poujol-Robert A, et al. Assessment of biliary fibrosis by transient elastography in patients with PBC and PSC. Hepatology. 2006;43:1118–24.
63. Gomez-Dominguez E, Mendoza J, Garcia-Buey L, et al. Transient elastography to assess hepatic fibrosis in primary biliary cirrhosis. Aliment Pharmacol Ther. 2008;27:441–7.
64. de Ledinghen V, Douvin C, Kettaneh A, et al. Diagnosis of hepatic fibrosis and cirrhosis by transient elastography in HIV/hepatitis C virus-coinfected patients. J Acquir Immune Defic Syndr. 2006;41:175–9.
65. Carrion JA, Navasa M, Bosch J, et al. Transient elastography for diagnosis of advanced fibrosis and portal hypertension in patients with hepatitis C recurrence after liver transplantation. Liver Transplant. 2006;12:1791–8.
66. Carrion JA, Torres F, Crespo G, et al. Liver stiffness identifies two different patterns of fibrosis progression in patients with hepatitis C virus recurrence after liver transplantation. Hepatology. 2010;51:23–34.
67. Roulot D, Czernichow S, Le Clesiau H, et al. Liver stiffness values in apparently healthy subjects: influence of gender and metabolic syndrome. J Hepatol. 2008;48:606–13.
68. Casey SP, Kemp WW, McLean CA, et al. A prospective evaluation of the role of transient elastography for the detection of hepatic fibrosis in type 2 diabetes without overt liver disease. Scand J Gastroenterol. 2012;47:836–41.
69. Mederacke I, Wursthorn K, Kirschner J, et al. Food intake increases liver stiffness in patients with chronic or resolved hepatitis C virus infection. Liver Int. 2009;29:1500–6.
70. Boursier J, Konate A, Gorea G, et al. Reproducibility of liver stiffness measurement by ultrasonographic elastometry. Clin Gastroenterol Hepatol. 2008;6:1263–9.
71. Talwalkar JA, Kurtz DM, Schoenleber SJ, et al. Ultrasound-based transient elastography for the detection of hepatic fibrosis: systematic review and meta-analysis. Clin Gastroenterol Hepatol. 2007;5:1214–20.
72. Masuzaki R, Tateishi R, Yoshida H, et al. Prospective risk assessment for hepatocellular carcinoma development in patients

with chronic hepatitis C by transient elastography. Hepatology. 2009;49:1954–61.
73. Jung KS, Kim SU, Ahn SH, et al. Risk assessment of hepatitis B virus-related hepatocellular carcinoma development using liver stiffness measurement (FibroScan). Hepatology. 2011;53:885–94.
74. Coco B, Oliveri F, Maina AM, et al. Transient elastography: a new surrogate marker of liver fibrosis influenced by major changes of transaminases. J Viral Hepat. 2007;14:360–9.
75. Millonig G, Friedrich S, Adolf S, et al. Liver stiffness is directly influenced by central venous pressure. J Hepatol. 2010;52: 206–10.
76. Foucher J, Castera L, Bernard PH, et al. Prevalence and factors associated with failure of liver stiffness measurement using FibroScan in a prospective study of 2114 examinations. Eur J Gastroenterol Hepatol. 2006;18:411–2.
77. Kettaneh A, Marcellin P, Douvin C, et al. Features associated with success rate and performance of FibroScan measurements for the diagnosis of cirrhosis in HCV patients: a prospective study of 935 patients. J Hepatol. 2007;46:628–34.
78. Castera L, Foucher J, Bernard PH, et al. Pitfalls of liver stiffness measurement: a 5-year prospective study of 13,369 examinations. Hepatology. 2010;51:828–35.
79. Fraquelli M, Rigamonti C, Casazza G, et al. Reproducibility of transient elastography in the evaluation of liver fibrosis in patients with chronic liver disease. Gut. 2007;56:968–73.
80. Friedrich-Rust M, Ong MF, Martens S, et al. Performance of transient elastography for the staging of liver fibrosis: a meta-analysis. Gastroenterology. 2008;134:960–74.
81. Ganne-Carrie N, Ziol M, de Ledinghen V, et al. Accuracy of liver stiffness measurement for the diagnosis of cirrhosis in patients with chronic liver diseases. Hepatology. 2006;44:1511–7.
82. Myers RP, Pomier-Layrargues G, Kirsch R, et al. Discordance in fibrosis staging between liver biopsy and transient elastography using the FibroScan XL probe. J Hepatol. 2012;56:564–70.
83. Wong VW, Vergniol J, Wong GL, et al. Liver stiffness measurement using XL probe in patients with nonalcoholic fatty liver disease. Am J Gastroenterol. 2012;107:1862–71.

Optimal scan timing of hepatic arterial-phase imaging of hypervascular hepatocellular carcinoma determined by multiphasic fast CT imaging technique

Yuki Kagawa, Masahiro Okada, Yukinobu Yagyu, Seishi Kumano, Masayuki Kanematsu, Masayuki Kudo and Takamichi Murakami

Acta Radiol 2013 54: 843 originally published online 9 May 2013
DOI: 10.1177/0284185113485571

Original article

Optimal scan timing of hepatic arterial-phase imaging of hypervascular hepatocellular carcinoma determined by multiphasic fast CT imaging technique

Yuki Kagawa[1], Masahiro Okada[1], Yukinobu Yagyu[1], Seishi Kumano[1], Masayuki Kanematsu[2], Masayuki Kudo[3] and Takamichi Murakami[1]

[1]Department of Radiology, Kinki University Faculty of Medicine, Osaka; [2]Department of Radiology, Gifu University, School of Medicine, Gifu; [3]CT Research Japan, GE Healthcare Japan Corporation, Tokyo, Japan
Correspondence to: Takamichi Murakami. Email: murakami@med.kindai.ac.jp

Abstract

Background: A new multiphasic fast imaging technique, known as volume helical shuttle technique, is a breakthrough for liver imaging that offers new clinical opportunities in dynamic blood flow studies. This technique enables virtually real-time hemodynamics assessment by shuttling the patient cradle back and forth during serial scanning.

Purpose: To determine optimal scan timing of hepatic arterial-phase imaging for detecting hypervascular hepatocellular carcinoma (HCC) with maximum tumor-to-liver contrast by volume helical shuttle technique.

Material and Methods: One hundred and one hypervascular HCCs in 50 patients were prospectively studied by 64-channel multidetector-row computed tomography (MDCT) with multiphasic fast imaging technique. Contrast medium containing 600 mg iodine per kg body weight was intravenously injected for 30 s. Six seconds after the contrast arrival in the abdominal aorta detected with bolus tracking, serial 12-phase imaging of the whole liver was performed during 24-s breath-holding with multiphasic fast imaging technique during arterial phase. By placing regions of interest in the abdominal aorta, portal vein, liver parenchyma, and hypervascular HCCs on the multiphase images, time-density curves of anatomical regions and HCCs were composed. Timing of maximum tumor-to-liver contrast after the contrast arrival in the abdominal aorta was determined.

Results: For the detection of hypervascular HCC at arterial phase, mean time and value of maximum tumor-to-liver contrast after the contrast arrival were 21 s and 38.0 HU, respectively.

Conclusion: Optimal delay time for the hepatic arterial-phase imaging maximizing the contrast enhancement of hypervascular HCCs was 21 s after arrival of contrast medium in the abdominal aorta.

Keywords: Abdomen/GI, CT, liver, hemodynamics/flow dynamics

Submitted July 1, 2012; accepted for publication March 17, 2013

Multiphase dynamic computed tomography (CT) imaging with intravenous injection of contrast medium is essential for the diagnosis of hepatocellular carcinoma (HCC). HCC usually shows hypervascularity (1–3). Hepatic arterial-phase images are the most important to detect hypervascular HCCs, because tumor-to-liver contrast (TLC) becomes maximum in this phase. Recently, as multidetector-row CT (MDCT) enabling fast imaging technique is widely employed for liver imaging, previous researchers tried to determine the optimal scan timing of the hepatic arterial-phase imaging with two- or three-phase MDCT imaging (4–7), but more time-resolved assessment is yet to be conducted.

We have developed a new multiphasic fast imaging technique, known as volume helical shuttle technique (VHS) (GE Healthcare, Hino, Japan) (8). The VHS is a breakthrough technique for liver imaging that offers new clinical opportunities particularly in dynamic blood flow studies. The VHS enables virtual real-time hemodynamics assessment by shuttling the patient cradle back and forth (reciprocating

Table 1 Data of patient population in our study

Parameters	
Sex	Male (33 patients), female (17 patients)
Age (years)	Mean, 71 (range, 31–86)
Weight (kg)	Mean, 58 (range, 45–85)
Treatment history	TACE ($n = 20$), RFA ($n = 6$), TACE and RFA ($n = 7$), hepatic intra-arterial chemotherapy ($n = 1$), hepatic resection ($n = 3$), no treatment history ($n = 13$)
Hepatitis	B ($n = 7$), C ($n = 31$), neither B nor C ($n = 12$)
Child-Pugh classification	A ($n = 24$), B ($n = 21$), C ($n = 4$)
Elevation of tumor marker	AFP ($n = 39$), PIVKA-II ($n = 41$), AFP or PIVKA-II ($n = 49$)
Histology of HCC	Poor ($n = 1$), moderate ($n = 32$), well ($n = 7$)
HCC size (mm)	Mean, 21.4 (range, 7.6–86.2)
HCC location	S1 ($n = 4$), S2 ($n = 9$), S3 ($n = 13$), S4 ($n = 14$), S5 ($n = 7$), S6 ($n = 11$), S7 ($n = 19$), S8 ($n = 24$)

AFP, alpha-fetoprotein; HCC, hepatocellular carcinoma; moderate, moderately-differentiated HCC; PIVKA-II, protein induced by Vitamin K absence or antagonists-II; poor, poorly-differentiated HCC; RFA, radiofrequency ablation; S1-S8, Couinaud's liver segment classification; TACE, transarterial chemo-embolization; well, well-differentiated HCC

movement) during serial scanning, and also allows wider coverage for the whole liver. The whole liver can be seamlessly scanned 12 times (six round trips) during a single 24-s breath-hold (i.e. each scan takes no more than 2 s).

The thrust of our study was to determine the optimal scan timing of the hepatic arterial-phase imaging that maximized the contrast enhancement of hypervascular HCCs, by using the VHS technique that enabled serial 12-phase imaging during the hepatic arterial phase.

Material and Methods

Patients

This study was a prospective study following the principles of the Declaration of Helsinki (9). The ethics committee of our institution approved all study protocols, and informed consent was obtained from all patients who underwent dynamic MDCT examination.

Fifty consecutive patients (33 men, 17 women; age range, 31–86 years; mean age, 71 years) with a total of 101 untreated hypervascular HCCs, who underwent contrast-enhanced dynamic MDCT with VHS technique, were included in this study. All HCCs were diagnosed according to American Association for the Study of Liver Diseases (AASLD) guideline (10). Size of HCCs ranged from 7.6 to 86.2 mm (mean $\pm$ 1 SD, 21.4 $\pm$ 11.7 mm)

Twenty patients had a history of transcatheter arterial chemoembolization (TACE), six of radiofrequency ablation (RFA), seven of both of TACE and RFA, one of intrahepatic arterial infusion chemotherapy, three of partial hepatectomy, and 13 of none (Table 1). Patients had chronic hepatitis or cirrhosis due to hepatitis B virus ($n = 7$), hepatitis C virus ($n = 31$), non-B and non-C hepatitis virus ($n = 3$), and alcohol abuse ($n = 3$). Based on Child-Pugh classification, 24 patients were classified into grade A, 21 into grade B, and five into grade C. Body weight of the 50 patients ranged from 38 to 85 kg (mean, 58 kg).

Definition of hypervascular HCC

CT images with VHS technique were reviewed by two radiologists with >10 years of experience in liver CT imaging. Any discrepancies encountered in interpretation sessions were resolved by establishing a consensus with the participation of a third radiologist (with 20 years of experience in liver CT imaging). The reviewers knew that the patients had chronic hepatitis or cirrhosis, and their treatment histories were available. Each hepatic arterial-phase image set was evaluated for the presence of early-enhancing hypervascular HCCs. Hypervascularity was defined as a focal area of higher density compared with the surrounding liver parenchyma during the hepatic arterial phase. Wash-out in the equilibrium phase 5 min after contrast injection was defined as a focal area of lower density compared with the surrounding liver parenchyma. The reviewers diagnosed the area as a hypervascular HCC when both hypervascularity and wash-out were seen in the area.

Reference standard of lesions

One hundred and one lesions were determined as hypervascular HCCs by referring to any of confirmatory studies including CT hepatic arteriography, CT during arterial portography, CT following arterial infusion of iodized oil, or a combination. We also took into amount growth on follow-up imaging and response to TACE. On multiphase contrast-enhanced CT images, all of 53 HCCs <2 cm in diameter and 33 of 48 HCCs $\geq$2 cm in diameter or larger showed homogeneous enhancement during the hepatic arterial phase, and the remaining 15 HCCs ($\geq$2 cm) showed heterogeneous enhancement.

Dynamic MDCT with volume helical shuttle (VHS) technique

Dynamic MDCT examination with VHS technique (8) was performed with a 64-channel MDCT (VCT-Vision; GE Healthcare, Milwaukee, WI, USA). The VHS is a fast imaging technique of serial 40-mm X-ray beam cine scan while rapidly, seamlessly moving the patient cradle back and forth. It also provides virtually real-time hemodynamics information of the whole liver thanks to its wide coverage in the axial direction. The VHS technique minimizes radiation exposure by enabling continuous CT data acquisition even during the deceleration and acceleration of patient cradle (8).

A bolus-tracking cursor was placed in the abdominal aorta at the level of porta hepatis, and the contrast arrival was defined as a moment when CT value of the aorta reached 150 HU. A total of 600 mgI/kg of contrast medium was injected intravenously with a constant injection duration of 30 s. Six seconds after the arrival of contrast medium in the aorta, (liver hilar level) determined by bolus tracking technique, the VHS scan was started. The whole liver was serially and seamlessly scanned in 12 phases (six round trips) during 24-s breath-hold (i.e. 2-s acquisition per phase).

CT parameters with VHS were as follows: slice thickness of 5 mm, helical pitch of 1.375mm, longitudinal (z axis)

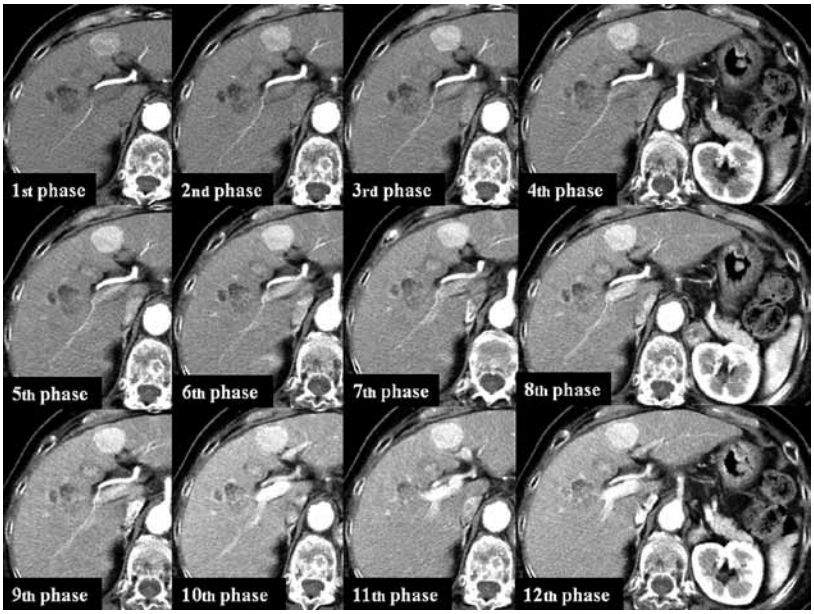

Fig. 1 Volume helical shuttle (VHS) image in a 74-year-old man. Hepatocellular carcinoma (HCC) in the segment 4 showed hyper-enhancement relative to the liver parenchyma from the first phase, and the degree of enhancement increases linearly up to the 12th phase. However, as the enhancement of the liver parenchyma also increases up to the 12th phase, tumor to liver contrast starts to decrease after the eighth phase

coverage of 18 cm, rotation time of 0.4 s, noise index of 17, tube current by auto mA program (100–700 mA), and tube voltage of 120 kV. Adaptive statistical iterative reconstruction (ASiR) (GE Healthcare, Milwaukee, WI, USA) (8, 11, 12) was employed with the VHS technique. The ASiR enables a reduction in radiation dose compared with the usual filtered back projection algorithm; alternatively, when employed at the same dose as that for the filtered back-projection algorithm, ASiR provides better image quality. We used setting with 40% of ASIR to achieve dose reduction.

Patient radiation dose

Dose-length product (DLP) was calculated by using the equation: DLP = CT dose index volume (CTDI vol) × scanning length. Effective dose was calculated by a following formula (13). Effective dose = DLP × 0.015.

Analysis by time-density curve (TDC)

The arterial enhancement profile of HCCs was evaluated using time-density curve (TDC) analysis. The 12-phase CT image sets were sent to a clinical workstation (Advantage Windows, GE-Healthcare, Milwaukee, WI, USA). Using a multi-window frame setting on this system, a region of interest (ROI) was placed in the abdominal aorta (ROI size, 300 mm^2) at the level of celiac artery, portal vein (ROI size, 30–50 mm^2), liver parenchyma (ROI size, 150 mm^2), and each hypervascular HCC (ROI was placed within homogeneous enhancement or within the highest density area of heterogeneous enhancement) by two observers. The density of liver parenchyma was measured with three ROIs at the slice level where HCC existed, and that of the portal vein at the porta hepatis. The TDC was created using commercially available Excel software (Microsoft Excel 2007; Microsoft, Tokyo, Japan). Thus, hemodynamics change of HCCs through the 12 arterial phases were quantitatively analyzed.

We calculated the following parameters: (i) CT values and times of peak enhancement of the abdominal aorta, portal vein, liver parenchyma, and HCCs after arrival of contrast medium in the abdominal aorta; and (ii) value and time of peak TLC after arrival of contrast medium in the abdominal aorta.

The intra-observer variance was calculated by free statistical software 'R' (R, version 2.6.1; The R Project for Statistical Computing; http://www.r-project.org/). Simple regression analysis and Bland-Altman analysis were performed to assess the agreement between the two observers' CT measurements for aorta, portal vein, liver parenchyma, and HCC. Measurements of CT values by two observers were finally averaged.

To evaluate the effect of previous TACE therapy to enhancement timing of HCCs, enhancement profile of hypervascular HCCs in patients with TACE was compared with those without TACE by using the Mann-Whitney U test.

Results

In the 50 patients, serial 12-phase scanning with the VHS technique was successfully completed (Fig. 1). CT values of the abdominal aorta increased from the first to the seventh phase, and then decreased. Time of peak aortic enhancement after arrival of contrast medium in the

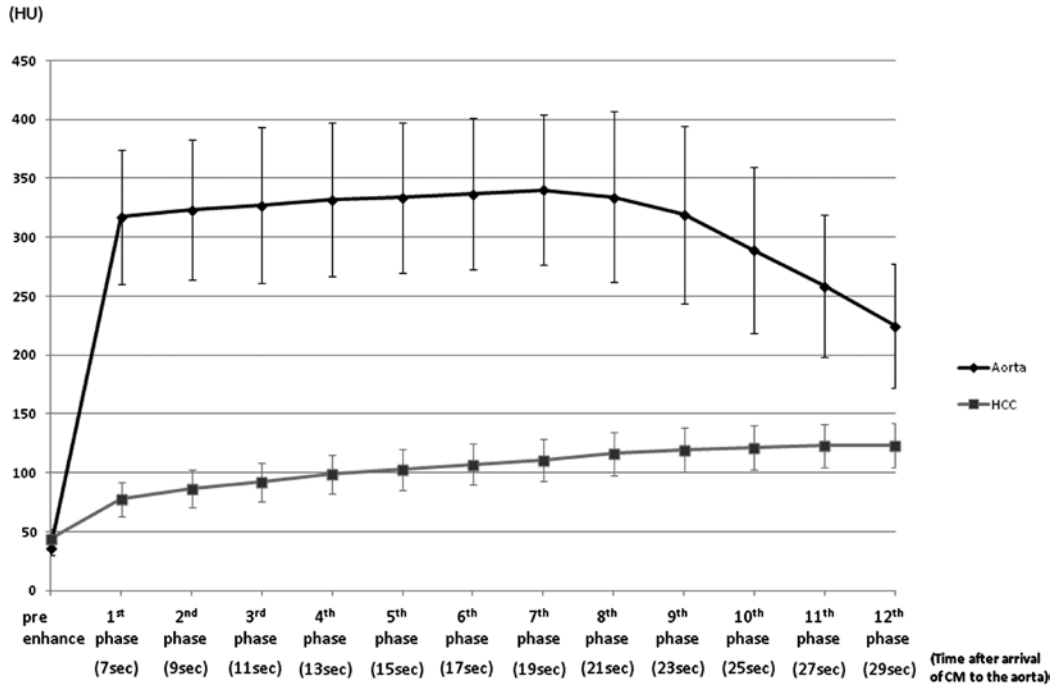

Fig. 2 Time-density curves of aorta and hypervascular HCC. Aortic enhancement showed plateau from first to eighth phase of the arterial phase, and gradually decreased from ninth to 12th phase. Whereas, the enhancement of hypervascular HCC increased linearly from the first to 12th phase

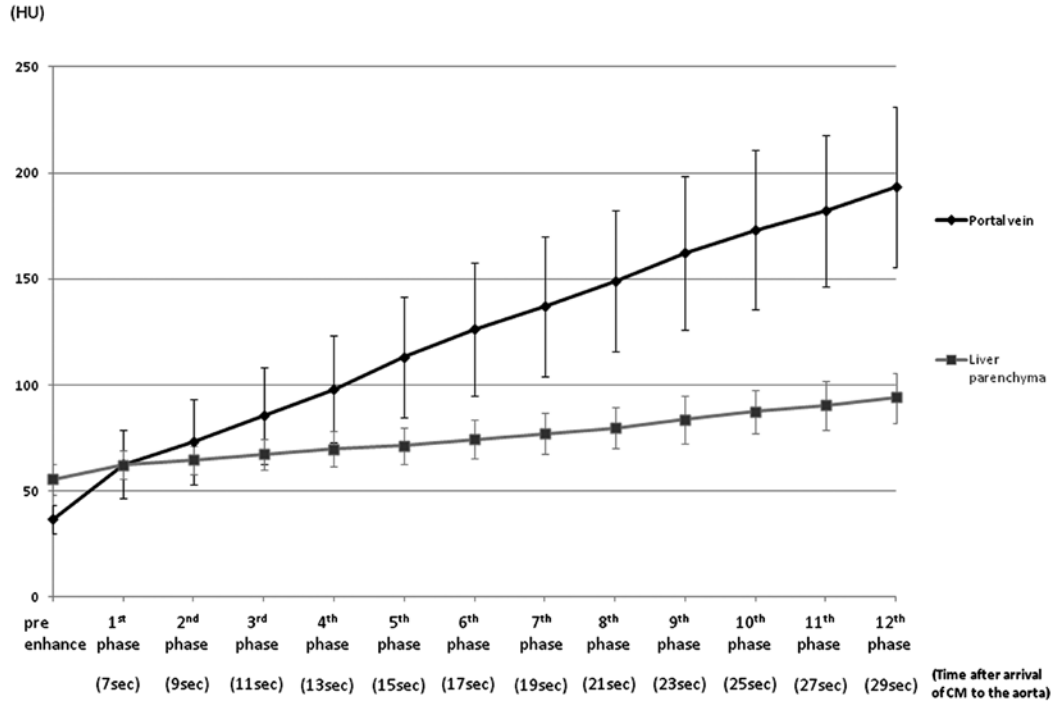

Fig. 3 Time-density curves of portal vein and liver. The density of portal vein was lower than that of liver parenchyma at pre-enhancement, and increased to almost same level as that of liver at first phase. Moreover the contrast between portal vein and liver increased gradually from first to 12th phase

abdominal aorta was 19 s, and the peak enhancement value of the aorta was 340.3 ± 63.7 HU (Fig. 2).

The portal vein started to enhance from the first phase mainly due to inflow of contrast medium from the splenic

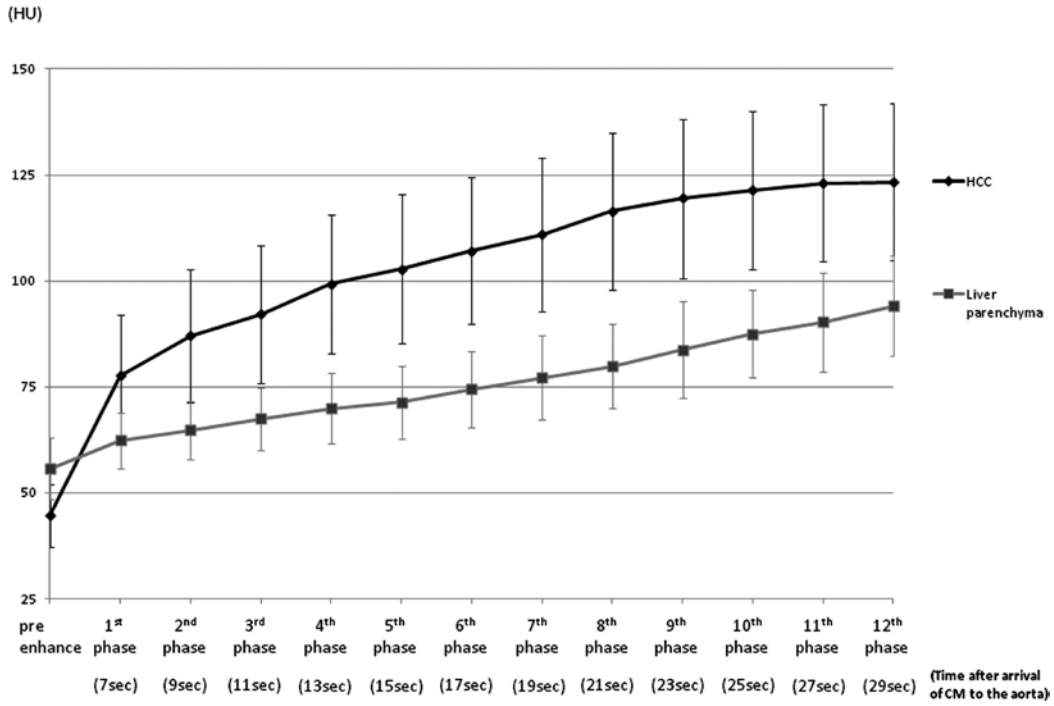

Fig. 4 Time-density curves of hypervascular HCC and liver. The density of HCC showed lower than that of liver parenchyma at pre-enhancement, and showed higher than that of liver from first phase in the arterial phase. The highest contrast between hypervascular HCC and liver showed at eighth phase in the arterial phase

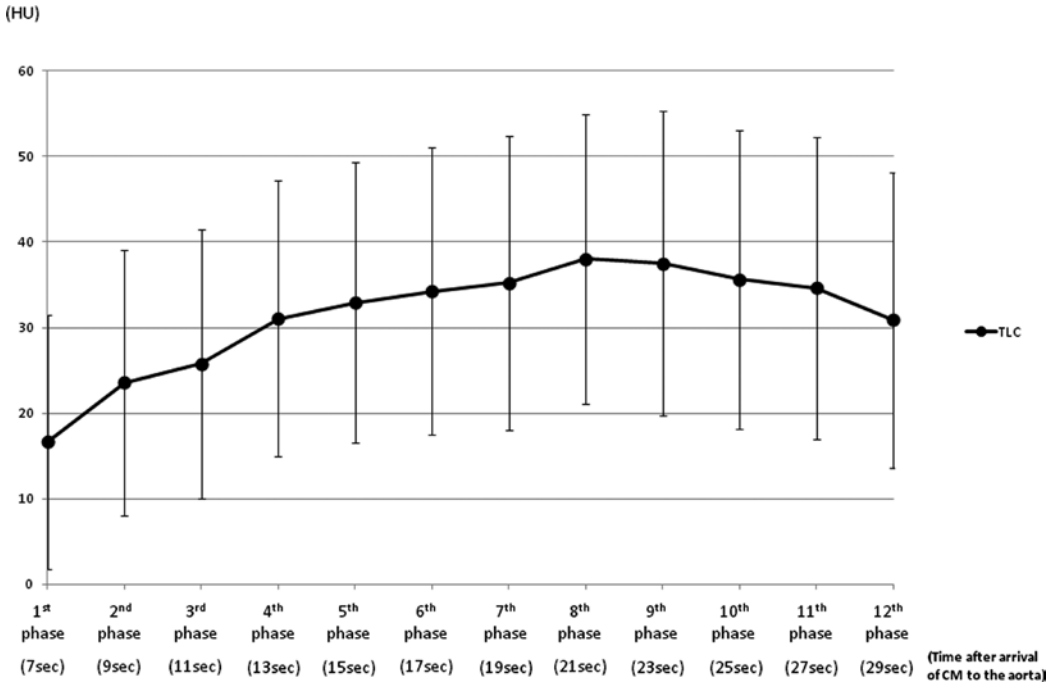

Fig. 5 Tumor liver contrast (TLC) between hypervascular HCC and liver. The tumor liver contrast (TLC) peak is eighth phase. TLC between fourth phase and 12th phases shows >30 HU

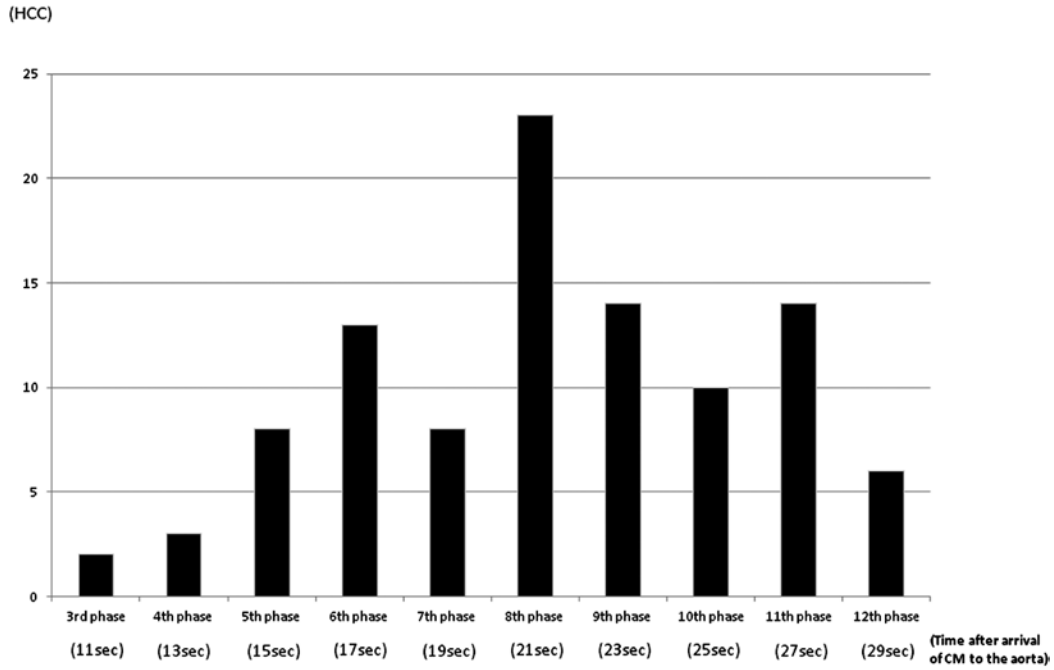

Fig. 6 Relation between peak tumor liver contrast (TLC) and the phase of volume helical shuttle (VHS). Twenty-three HCCs showed peak tumor liver contrast (TLC) at eighth phase. Seventy-eight HCCs showed peaks of a wide range between third to 12th phase. There was no peak of TLC at first and second phase

Table 2 Patients with or without TACE analyzed by time-intensity curves after injection

Parameters	Patient with TACE	Patient without TACE	*P* value
Time of peak aortic enhancement (s)	18.5 ± 4.4	17.5 ± 4.2	NS
Time of peak HCC enhancement (s)	25.6 ± 3.4	26.7 ± 2.6	NS
Time of peak TLC	21.2 ± 4.7	21.8 ± 4.2	NS

HCC, hepatocellular carcinoma; NS, not significant; TACE, transarterial chemo-embolization; TLC, tumor liver contrast

vein, and the enhancement reached maximum in the 12th phase. Only in 11 of the 50 patients was inflow of contrast medium from the mesenteric vein also seen. According to the TDC of the portal vein, enhancement of the portal vein increased linearly at a rate of 5.9 HU/s (Fig. 3). The liver parenchyma also started to enhance from the first phase, and the enhancement gradually and linearly increased at a rate of 1.4 HU/s (Fig. 3).

Eighty-nine of the 101 HCCs were markedly enhanced relative to the liver parenchyma from the first phase. The remaining 12 HCCs started to enhance at the second phase ($n = 8$), third phase ($n = 2$), fourth phase ($n = 2$). From the second phase, enhancement of HCCs increased almost linearly at a rate of 2.1 HU/s (Fig. 4). Five of the 101 HCC showed peak enhancement at the seventh phase, six at eighth, 18 at ninth, 18 at 10th, 24 at 11th, and 30 at 12th.

Twenty-three HCCs showed peak TLC at the eighth phase, namely, 21 s after arrival of contrast medium in the abdominal aorta (Fig. 5), although peak of TLC was found in wide range (third to 12th phase) for the remaining HCCs (Fig. 6), whereas, six HCCs showed peak TLC value at the 12th phase. Maximum peak value of TLC was 38.0 HU. The TLC reached 30 HU or greater from the fourth to12th phase.

There was no significant difference in time of peak enhancement of hypervascular HCCs ($P = 0.14$), time of peak aortic enhancement of aorta ($P = 0.25$), and time of peak TLC ($P = 0.70$) between patients with TACE and those without TACE (Table 2). Effective dose in this study was 17.9 ± 6.2 mSv.

Agreement between the two observers' CT measurements

Simple regression analysis and Bland-Altman analysis of agreement between the two measurements for pre-enhancement and enhanced 12 phases of the aorta, portal vein, liver parenchyma, and HCC were displayed in Fig 7. Simple regression analysis showed a high correlation between two observers' CT measurements on volume helical shuttle (VHS) images. And Bland-Altman analysis showed narrow limits of agreement between two observers' CT measurements of aorta, portal vein, liver, and HCC.

Discussion

Dynamic MDCT is an essential examination for the detection of hypervascular HCCs. Hypervascular HCCs may be imaged best during a phase of maximal tumor enhancement and minimal hepatic parenchymal enhancement, contrast

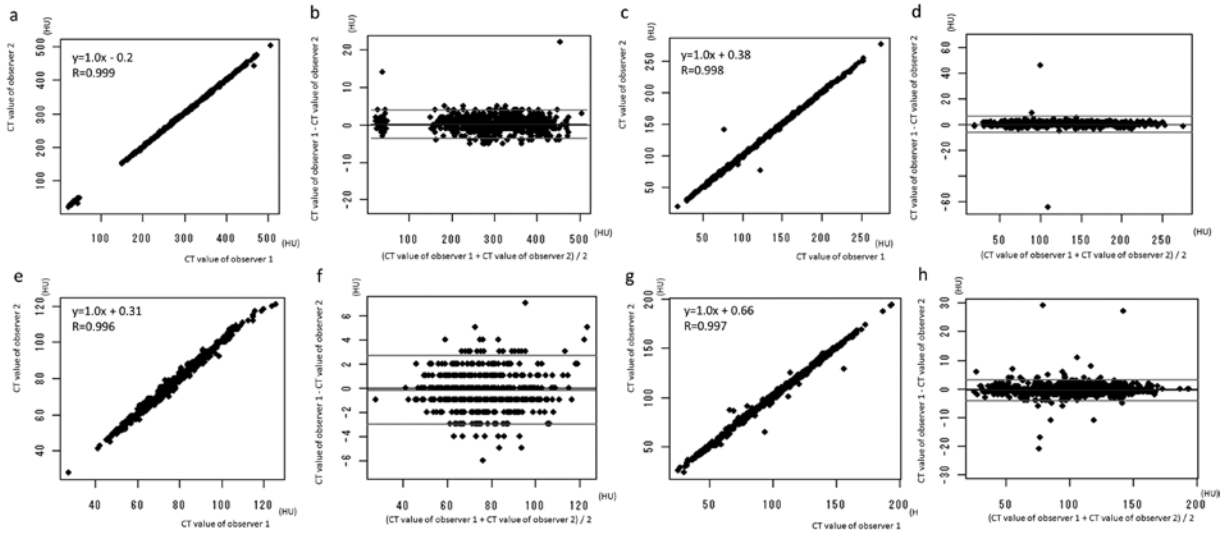

Fig. 7 Agreement between the two observers' CT measurements. Simple regression analyses (a; aorta, c; portal vein, e; liver, g; HCC) and Bland-Altman analyses of agreement (b; aorta, d; portal vein, f; liver, h; HCC) between the two measurements for pre-enhancement and enhanced 12 phases were displayed. Simple regression analysis showed a high correlation between the means of the observers' manual measurements of the CT values on volume helical shuttle (VHS) images. Bland-Altman analysis yielded narrow limits of agreement of −3.7 to 4.1 HU for aorta, of −6.5 to 6.2 HU for portal vein, of −3.0 to 2.7 HU for liver, of −4.0 to 3.4 HU for HCC. Note: Black line (center) = mean of differences. Gray lines (top and bottom) = upper and lower limits of agreement (mean difference, +/− 2 SD). HU, Hounsfield unit

enhancement phase referred to as the hepatic arterial-dominant phase. The exact definition and optimal timing of the arterial phase remains somewhat uncertain and controversial. Recently, a test bolus imaging (14) or automatic bolus tracking technique (15) is employed to determine the optimal scan delay for the hepatic arterial phase. However, although these techniques can determine the time of contrast arrival in the abdominal aorta, scan delay from bolus detection to scan start has been still uncertain. Our data revealed that optimal scan delay to start scan for best detecting hypervascular HCC was 21 s after the contrast arrival in the abdominal aorta.

Our results also showed that greater enhancement of HCCs was seen in the late phases of the 12 phases (Fig. 4). In this study, most HCCs showed peak enhancement in the 12th phase, however, the peak of TLC was seen at the eighth phase, and TLC as great as 31.0–38.0 HU was observed between the fourth and 12th phases (Fig. 5). This wide duration of high TLC was partially due to the variation in magnitude and timing of the hepatic parenchymal enhancement. We found that optimal imaging window for detecting hypervascular HCCs was as long as 18 s (nine phases in our study).

We did not evaluate portal venous-phase images, because our main aim of this study was to determine the optimal default delay time of the hepatic arterial phase imaging. It is well known that portal venous-phase images should be obtained routinely in any CT evaluation for known or suspected primary or metastatic tumor (6, 7, 14, 15) and are necessary for additional characterization of liver tumors or demonstration of vascular anatomy and pathology.

One criticism of our study could be the lack of histological proof for all HCCs. However, the examinations we used for determining the reference standard had high accuracy for the diagnosis of hypervascular HCCs. Moreover, we carefully confirmed the growth over time or response to TACE. We believe that we could prepare efficient standard-of-reference lesions to assess enhancement profile of hypervascular HCCs. Repeated whole-liver imaging with the VHS technique increased the radiation dose. So, we employed ASiR which reduced radiation dose while keeping imaging quality (8, 11, 12). In this study, we could reduce effective radiation dose to 17.9 ± 6.2 mSv as low as usual contrast-enhanced CT of the liver.

In conclusion, hepatic arterial-phase imaging aimed at detection of hypervascular HCCs should be performed at 21 s after the arrival of contrast medium in the abdominal aorta, although there was a wide window of time for efficiently detecting hypervascular HCCs during the hepatic arterial phase.

Conflict of interest: None.

REFERENCES

1 Ohishi H, Uchida H, Yoshimura H, *et al.* Hepatocellular carcinoma detected by iodized oil. Use of anticancer agents. *Radiology* 1985;**154**:25–9
2 Merine D, Takayasu K, Wakao F. Detection of hepatocellular carcinoma: comparison of CT during arterial portography with CT after intraarterial injection of iodized oil. *Radiology* 1990;**175**:707–10
3 Yoshimatsu S, Inoue Y, Ibukuro K, *et al.* Hypovascular hepatocellular carcinoma undetected at angiography and CT with iodized oil. *Radiology* 1989;**171**:343–7
4 Murakami T, Kim T, Kawata S, *et al.* Evaluation of optimal timing of arterial phase imaging for the detection of hypervascular hepatocellular carcinoma by using triple arterial phase imaging with multidetector-row helical computed tomography. *Invest Radiol* 2003;**38**:497–503
5 Murakami T, Onishi H, Mikami K, *et al.* Determining the optimal timing for early arterial phase hepatic CT imaging by measuring abdominal

aortic enhancement in variable contrast injection protocols. *J Comput Assist Tomogr* 2006;**30**:206–11
6 Kanematsu M, Goshima S, Kondo H, *et al.* Optimizing scan delays of fixed duration contrast injection in contrast-enhanced biphasic multidetector-row CT for the liver and the detection of hypervascular hepatocellular carcinoma. *J Comput Assist Tomogr* 2005;**29**:195–201
7 Goshima S, Kanematsu M, Kondo H, *et al.* MDCT of the liver and hypervascular hepatocellular carcinomas: optimizing scan delays for bolus-tracking techniques of hepatic arterial and portal venous phases. *Am J Roentgenol* 2006;**187**:W25–32
8 Okada M, Kim T, Murakami T. Hepatocellular nodules in liver cirrhosis: state of the art CT evaluation (perfusion CT/volume helical shuttle scan/dual-energy CT, etc.). *Abdom Imaging* 2011;**36**:273–81
9 World Medical Association Declaration of Helsinki. Ethical principles for medical research involving human subjects. *Bull World Health Organ* 2001;**79**:373–4
10 Bruix J, Sherman M. Management of hepatocellular carcinoma: An update. *Hepatology* 2011;**53**:1020–2
11 Marin D, Nelson RC, Schindera ST, *et al.* Low-tube-voltage, high-tube-current multidetector abdominal CT: improved image quality and decreased radiation dose with adaptive statistical iterative reconstruction algorithm–initial clinical experience. *Radiology* 2010;**254**:145–53
12 Yanagawa M, Tomiyama N, Honda O, *et al.* Multidetector CT of the lung: image quality with garnet-based detectors. *Radiology* 2010;**255**:944–54
13 The 2007 Recommendations of the International Commission on Radiological Protection. ICRP publication 103. *Ann ICRP* 2007;**37**:1–332
14 Murakami T, Kim T, Takamura M, *et al.* Hypervascular hepatocellular carcinoma: detection with double arterial phase multi-detector row helical CT. *Radiology* 2001;**218**:763–7
15 Kim T, Murakami T, Hori M, *et al.* Small hypervascular hepatocellular carcinoma revealed by double arterial phase CT performed with single breath-hold scanning and automatic bolus tracking. *Am J Roentgenol* 2002;**178**:899–904

SHORT COMMUNICATION

BJC

British Journal of Cancer (2013) 109, 1904–1907 | doi: 10.1038/bjc.2013.542

Keywords: chemotherapy; 5-fluorouracil; cisplatin; liver neoplasm; hepatocellular carcinoma; propensity score

Effect of hepatic arterial infusion chemotherapy of 5-fluorouracil and cisplatin for advanced hepatocellular carcinoma in the Nationwide Survey of Primary Liver Cancer in Japan

K Nouso*[,1], K Miyahara[2], D Uchida[2], K Kuwaki[2], N Izumi[3,14], M Omata[4], T Ichida[5,14], M Kudo[6,14], Y Ku[7,14], N Kokudo[8,14], M Sakamoto[9,14], O Nakashima[10,14], T Takayama[11,14], O Matsui[12,14], Y Matsuyama[13,14], K Yamamoto[2] and the Liver Cancer Study Group of Japan

*[1]Department of Molecular Hepatology, Okayama University Graduate School of Medicine, Dentistry, and Pharmaceutical Sciences, 2-5-1 Shikata-cho, Kita-ku, Okayama-city, Okayama, 700-8558, Japan; [2]Department of Gastroenterology and Hepatology, Okayama University Graduate School of Medicine, Dentistry, and Pharmaceutical Sciences, 2-5-1 Shikata-cho, Kita-ku, Okayama-city, Okayama, 700-8558, Japan; [3]Department of Gastroenterology, Musashino Red Cross Hospital, Musashino-city, Tokyo, 180-8610, Japan; [4]Yamanashi Prefectural Hospital Organization, Kofu-city, Yamanashi, 400-8506, Japan; [5]Department of Gastroenterology, Juntendo University Shizuoka Hospital, Izunokuni-city, Shizuoka, 410-2295, Japan; [6]Department of Gastroenterology and Hepatology, Kinki University School of Medicine, Sayama-city, Osaka, 589-8511, Japan; [7]Division of Hepato-Biliary-Pancreatic Surgery, Kobe University Graduate School of Medicine, Kobe-city, Hyogo, 650-0017, Japan; [8]Department of Hepato-Biliary-Pancreatic Surgery Division, Department of Surgery, Graduate School of Medicine, University of Tokyo, Bunkyo-ku, Tokyo, 113-0033, Japan; [9]Department of Pathology, Keio University School of Medicine, Shinjuku-ku, Tokyo, 160-8582, Japan; [10]Department of Pathology, Kurume University School of Medicine, Kurume-city, Fukuoka, 830-0011, Japan; [11]Department of Digestive Surgery, Nihon University School of Medicine, Itabashi-ku, Tokyo, 173-8610, Japan; [12]Department of Radiology, Kanazawa University Graduate School of Medical Science, Kanazawa-city, Ishikawa, 920-8641, Japan and [13]Department of Biostatistics, School of Public Health, University of Tokyo, Bunkyo-ku, Tokyo, 113-0033, Japan

Background: The efficacy of hepatic arterial infusion chemotherapy for the treatment of advanced hepatocellular carcinoma (HCC) remains unclear.

Methods: The outcome of 476 patients with HCC who underwent hepatic arterial infusion chemotherapy with 5-fluorouracil and cisplatin (HAIC) were compared with 1466 patients who did not receive active therapy.

Results: A survival benefit of the therapy after adjusting for known risk factors was observed (hazard ratio, 0.48; 95% CI, 0.41–0.56; $P<0.0001$). In propensity score-matched analysis ($n=682$), median survival time was longer for patients who underwent chemotherapy (14.0 months) than for patients who did not receive active treatment (5.2 months, $P<0.0001$).

Conclusion: For advanced HCC, HAIC is considered to be an effective treatment.

*Correspondence: Dr K Nouso; E-mail: nouso@cc.okayama-u.ac.jp
[14]These authors are part of the Liver Cancer Study Group of Japan.

Received 26 April 2013; revised 2 August 2013; accepted 14 August 2013; published online 5 September 2013

Hepatocellular carcinoma (HCC) is one of the most common malignancies worldwide (Jemal *et al*, 2011). Screening patients with chronic liver diseases increases the chance that HCC can be diagnosed in the early stage (Kudo *et al*, 2011; European Association for Study of Liver; European Organisation for Research and Treatment of Cancer, 2012; Sherman *et al*, 2012). However, many HCCs are detected at an advanced stage.

According to the treatment algorithm of HCC, patients with advanced disease are candidates for chemotherapy (Kudo *et al*, 2011; European Organisation for Research and Treatment of Cancer, 2012; Sherman *et al*, 2012). Currently, sorafenib is the only chemotherapy proven to be effective for advanced HCC (Llovet *et al*, 2008; Cheng *et al*, 2009). Several other therapies have been evaluated, including hepatic arterial infusion of 5-fluorouracil (5-FU) and cisplatin, which was the most common regimen in Japan (Ueshima *et al*, 2010; Kim do *et al*, 2011; Yamashita *et al*, 2011). However, most of these studies were retrospective and nonrandomised; therefore, its efficacy remains unclear.

The Liver Cancer Study Group of Japan uses questionnaires to collect data from patients with HCC every 2 years, with several minor modifications of the contents since 1965 (Ikai *et al*, 2005, 2007). We used the three most recent sets of data to determine the efficacy of arterial infusion therapy with 5-FU and cisplatin for advanced HCC.

MATERIALS AND METHODS

Data sources. From January 2000 to December 2005, a total of 62 315 patients with primary liver cancer were newly registered by the Liver Cancer Study Group of Japan (Ikai *et al*, 2005, 2007). The cohort was followed up biannually and their clinical outcome was examined. Of these 62 315 patients, 57 445 (92.2%) received a diagnosis of HCC, and 31 743 patients with complete data were selected for this study. Among the patients, 1150 patients initially underwent chemotherapy and 1466 patients received no active therapy (no therapy group). In patients who underwent chemotherapy, 476 (41.4%) underwent arterial infusion chemotherapy with 5-FU and cisplatin using a subcutaneous infusion port (HAIC group). All patients in the HAIC group and in the no therapy group were enrolled in this study (Supplementary Figure 1).

Hepatocellular carcinoma was diagnosed primarily by imaging modalities such as computed tomography (1579, 81.3%), magnetic resonance imaging (257, 13.2%), ultrasonography (1167, 60.1%), and/or angiography (360, 18.5%) with the findings of hyperattenuation at the arterial phase and hypoattenuation at the portal phase and/or tumour staining. A histological diagnosis was made in 4.5% ($n=87$) of the patients. Treatment effect was evaluated by a criteria, 'Treatment effect of the target nodule', outlined by the Liver Cancer Study Group of Japan (Liver Cancer Study Group of Japan, 2003).

All data were provided anonymously. This study was approved by the review board of the Liver Cancer Study Group of Japan.

Statistical analysis. Continuous variables were compared by *t*-test, and categorical variables were compared by χ^2 test. Survival was estimated by the Kaplan–Meier method and compared by the log-rank test.

Univariate and multivariate analyses of the primary cohort ($n=1942$) were carried out using the Cox proportional hazard model. Adjusted hazard ratios for HAIC according to subgroups (prognostic tumour factors in multivariate analysis) were also analysed and presented as a forest plot.

To determine the efficacy of HAIC, propensity score-matching analysis was performed (HAIC, $n=476$; no therapy, $n=1466$). A propensity score for use of HAIC was estimated using a logistic regression model fit with 15 variables: sex, age, hepatitis B surface antigen (HBsAg) positivity, hepatitis C virus (HCV) antibody positivity, alcohol intake, presence of encephalopathy, presence of ascites, total bilirubin, albumin, prothrombin time, maximum tumour size, tumour number, portal vein invasion, extrahepatic metastasis, and α-fetoprotein level. To create a propensity-matched cohort of patients who underwent HAIC or no therapy (1 : 1 match), a nearest-neighbour-matching algorithm with a 'greedy' heuristic was used (Austin and Mamdani, 2006).

The same matching procedure was carried out in patients with Child–Pugh A/B disease and portal vein invasion or more than three tumours, and survival rates for each matched cohort were compared.

RESULTS

Patient characteristics. The HAIC group was significantly younger and had more males than the no therapy group (Supplementary Table 1). Patients in the HAIC group had better liver function but more cases of hepatitis B infection and more advanced tumours than the no therapy group. These differences except follow-up period disappeared after propensity score matching.

Treatment effect of HAIC. In the HAIC group, the response rates were as follows: complete response (CR, $n=19$, 4.0%), partial response (PR, $n=173$, 36.5%), stable disease (SD, $n=112$, 23.6%), progressive disease (PD, $n=129$, 27.2%), and undefined ($n=41$, 8.7%). The 1- and 3-year survival rates according to response were CR/PR (77.7% and 34.6%), SD (44.2% and 13.3%), and PD (23.7% and 10.3%), respectively ($P<0.0001$, Figure 1). All factors including HAIC treatment correlated with prognosis in the univariate analysis (Table 1). Multivariate analysis revealed that HBsAg, more than three tumours, large tumours (>3 cm), distant metastasis, portal vein invasion (VP3 and VP4), and high α-fetoprotein levels (>400 ng ml^{-1}) were associated with poor survival. The VP3 and VP4 indicated tumour invasion to the first-order branches of the portal vein and the invasion to the main trunk of the portal vein, respectively (Liver Cancer Study Group of Japan, 2003). Conversely, Child–Pugh A/B disease (hazard ratio,

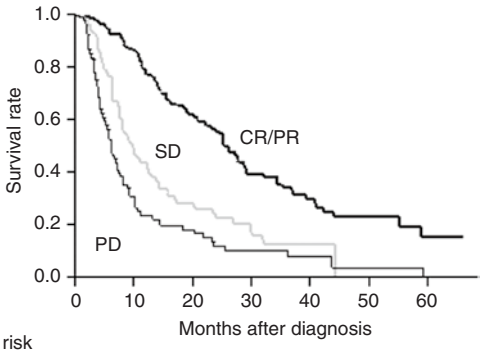

Patients at risk

CR/PR	192	136	72	37	20	9	5
SD	112	34	16	9	2	0	0
PD	129	29	12	6	4	2	0

Figure 1. Survival of patients who underwent hepatic arterial infusion of 5-fluorouracil and cisplatin using a subcutaneous infusion port. The 1- and 3-year survival rates and median survival times according to response were as follows: CR/PR (77.7%, 34.6%, 25.8 months), SD (44.2%, 13.3%, 9.5 months), and PD (23.7%, 10.3%, 6.0 months) ($P<0.0001$). Abbreviations: CR = complete response; PD = progressive disease; PR = partial response; SD = stable disease.

Table 1. Risk factors for survival

	Univariate			Multivariate		
Characteristics	**HR**	**95% CI**	***P*-value**	**HR**	**95% CI**	***P*-value**
Age >70 years	0.87	0.77–0.98	0.025	1.02	0.89–1.16	0.708
Male sex	1.19	1.04–1.37	0.007	1.04	0.90–1.21	0.541
HBsAg positive	1.47	1.27–1.69	<0.001	1.20	1.01–1.44	0.037
HCV Ab positive	0.78	0.69–0.88	<0.001	0.93	0.81–1.08	0.379
Alcohol intake >90 g day^{-1}	1.18	1.05–1.34	0.006	1.08	0.94–1.23	0.259
Child–Pugh grade A/B	0.51	0.45–0.58	<0.001	0.51	0.45–0.59	<0.001
Total bilirubin >2 mg dl^{-1}	1.99	1.76–2.24	<0.001			
Albumin >3 g dl^{-1}	0.65	0.57–0.73	<0.001			
Prothrombin time >80%	0.71	0.63–0.80	<0.001			
Ascites	2.54	2.26–2.86	<0.001			
Encephalopathy	1.28	1.09–1.50	0.002			
More than three tumours	1.84	1.64–2.07	<0.001	1.47	1.29–1.67	<0.001
Tumour >3 cm	2.26	1.98–2.58	<0.001	1.76	1.51–2.04	<0.001
Distant metastasis	2.11	1.81–2.45	<0.001	1.43	1.22–1.67	<0.001
Portal vein invasion, VP3 and VP4	3.08	2.72–3.47	<0.001	2.28	1.99–2.62	<0.001
AFP >400 ng ml^{-1}	2.35	2.09–2.65	<0.001	1.46	1.28–1.67	<0.001
HAIC/no therapy	0.71	0.62–0.81	<0.001	0.48	0.41–0.56	<0.001

Abbreviations: AFP = α-fetoprotein; CI = confidence interval; HAIC = hepatic arterial infusion chemotherapy with 5-fluorouracil and cisplatin; HBsAg = hepatitis B virus surface antigen; HCV Ab = hepatitis C virus antibody; HR = hazard ratio; VP3 = tumour invasion to the first-order branches of the portal vein; VP4 = tumour invasion to the main trunk of the portal vein.

0.51; 95% confidence interval (CI), 0.45–0.59; $P<0.0001$) and HAIC (hazard ratio, 0.48; 95% CI, 0.41–0.56; $P<0.0001$) were associated with better survival.

An exploratory subgroup analysis of patients who underwent HAIC therapy evaluated six prognostic variables: presence of HBsAg, tumour number, tumour size, presence of extrahepatic metastasis and vascular invasion, and α-fetoprotein levels. Compared with no therapy, HAIC improved survival, regardless of the values of these six prognostic factors (Supplementary Figure 2).

Survival rates of propensity score-matched cohorts. In the propensity score-matched cohort ($n=682$), 198 patients in the HAIC group and 199 patients in the no therapy group died during the observation period. The cause of death was liver related that included death by liver cancer as well as by liver failure in 184 patients (92.9%) in the HAIC group and 180 patients (90.4%) in the no therapy group ($P=0.47$). Median survival times were 14.0 months (HAIC group) and 5.2 months (no therapy group), and survival was significantly higher in the HAIC group ($P<0.0001$) (Figure 2). Hazard ratio of HAIC in this propensity score-matched cohort was 0.60 (95% CI, 0.49–0.73; $P<0.0001$). The same relationship was observed even when the event was limited to liver-related death ($P<0.0001$). Median survival times were 15.4 months (HAIC group) and 7.3 months (no therapy group).

Because most treatment guidelines for HCC recommend chemotherapy for patients with Child–Pugh A/B disease who have portal vein invasion and/or more than three tumours, we analysed the effect of HAIC in patients who met these criteria in the propensity score-matched cohort. In cases of Child–Pugh A/B disease with more than three tumours (370 propensity score-matched patients), median survival times were 13.9 months (HAIC) and 3.7 months (no therapy), and a survival benefit of HAIC treatment was observed ($P<0.0001$; Supplementary Figure 3). The same relationship was also observed in cases of Child–Pugh A/B disease with portal vein tumour thrombus (378 propensity score-matched patients, $P<0.0001$; Supplementary Figure 4). Median survival times were 7.9 months (HAIC) and 3.1 months (no therapy).

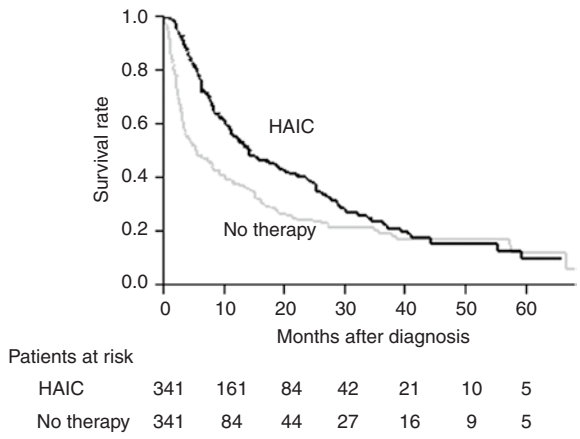

Figure 2. Survival of propensity score-matched patients who underwent hepatic arterial infusion of 5-fluorouracil and cisplatin (HAIC) or no active therapy (no therapy). Median survival times were 14.0 months (HAIC) and 5.2 months (no therapy) ($P<0.0001$).

DISCUSSION

Hepatic arterial infusion of cisplatin and 5-FU using a subcutaneous infusion port has been widely used in Japan to treat advanced

HCC because of its relatively high response rate (27.8–57.1%) (Ando *et al*, 2002; Eun *et al*, 2009; Ueshima *et al*, 2010; Kim do *et al*, 2011; Kim *et al*, 2011); however, no randomized control trial has been conducted to demonstrate its effectiveness and survival benefit. Most reports of HAIC were retrospective studies with small numbers of patients. In this study we used data from a large-scale nationwide survey and found that the response rate to HAIC was high (40.5%), survival was prolonged, and response to therapy could be used as a surrogate marker for overall survival. The survival benefit was also observed when only liver-related deaths were treated as 'events'.

Cisplatin interacts with DNA, preferentially binding nucleophilic N7 sites on purine bases (Galluzzi *et al*, 2012). As a consequence, protein–DNA complexes and DNA–DNA inter- and intra-strand adducts are generated, inducing cytotoxicity. Cisplatin also increases the folate concentration in cancer cells, reinforcing the effect of 5-FU through the formation of an inactive ternary complex (Scanlon *et al*, 1986; Kim *et al*, 2002). This synergistic effect of cisplatin and 5-FU is the basis of HAIC therapy.

Our study has some limitations. The information of dose reduction or termination due to drug toxicity is missing. Propensity scores were used to adjust for patient characteristics; however, it is not possible to adjust for all possible confounding factors related to survival, and the exact reasons of no therapy in control group were not known. Another weak point in this study is that performance status was not included as a covariate because two-thirds of the patients enrolled in this study lacked these data. However, the survival benefit of HAIC was observed even when the event was limited to liver-related death and when analysing the most recent database, which included performance status (median observation period 3 months, data not shown). Finally, we did not know the precise regimen used in this study population; however, many studies of HAIC report the administration of low-dose cisplatin (5–20 mg) several times a week, and continuous infusion of 5-FU for a few weeks.

As sorafenib has become the standard treatment for advanced HCC, several randomized controlled trials have been planned to evaluate new drugs using sorafenib as a control (Kudo, 2012). Some of these trials will evaluate HAIC, which will clarify some of the uncertainties of the present study.

In this large-scale retrospective study, we demonstrated the effectiveness of HAIC, although it was difficult to achieve long-term survival because HCCs re-grew even after response to the drugs. Our findings indicate that HAIC could be an alternative therapy for advanced HCC. Further examination of the factors that can predict the therapeutic effect is important for achieving long survival in future.

ACKNOWLEDGEMENTS

This work was supported in part by a Grant-in-Aid for Scientific Research from the Japan Society for the Promotion of Science.

CONFLICT OF INTEREST

The authors declare no conflict of interest.

REFERENCES

Ando E, Tanaka M, Yamashita F, Kuromatsu R, Yutani S, Fukumori K, Sumie S, Yano Y, Okuda K, Sata M (2002) Hepatic arterial infusion chemotherapy for advanced hepatocellular carcinoma with portal vein tumor thrombosis: analysis of 48 cases. *Cancer* **95**(3): 588–595.

Austin PC, Mamdani MM (2006) A comparison of propensity score methods: a case-study estimating the effectiveness of post-AMI statin use. *Stat Med* **25**(12): 2084–2106.

Cheng AL, Kang YK, Chen Z, Tsao CJ, Qin S, Kim JS, Luo R, Feng J, Ye S, Yang TS, Xu J, Sun Y, Liang H, Liu J, Wang J, Tak WY, Pan H, Burock K, Zou J, Voliotis D, Guan Z (2009) Efficacy and safety of sorafenib in patients in the Asia-Pacific region with advanced hepatocellular carcinoma: a phase III randomised, double-blind, placebo-controlled trial. *Lancet Oncol* **10**(1): 25–34.

Eun JR, Lee HJ, Moon HJ, Kim TN, Kim JW, Chang JC (2009) Hepatic arterial infusion chemotherapy using high-dose 5-fluorouracil and cisplatin with or without interferon-alpha for the treatment of advanced hepatocellular carcinoma with portal vein tumor thrombosis. *Scand J Gastroenterol* **44**(12): 1477–1486.

European Organisation for Research and Treatment of Cancer (2012) EASL-EORTC clinical practice guidelines: management of hepatocellular carcinoma. *Eur J Cancer* **48**(5): 599–641.

Galluzzi L, Senovilla L, Vitale I, Michels J, Martins I, Kepp O, Castedo M, Kroemer G (2012) Molecular mechanisms of cisplatin resistance. *Oncogene* **31**(15): 1869–1883.

Ikai I, Arii S, Ichida T, Okita K, Omata M, Kojiro M, Takayasu K, Nakanuma Y, Makuuchi M, Matsuyama Y, Yamaoka Y (2005) Report of the 16th follow-up survey of primary liver cancer. *Hepatol Res* **32**(3): 163–172.

Ikai I, Arii S, Okazaki M, Okita K, Omata M, Kojiro M, Takayasu K, Nakanuma Y, Makuuchi M, Matsuyama Y, Monden M, Kudo M (2007) Report of the 17th Nationwide Follow-up Survey of Primary Liver Cancer in Japan. *Hepatology Res* **37**(9): 676–691.

Jemal A, Bray F, Center MM, Ferlay J, Ward E, Forman D (2011) Global cancer statistics. *CA Cancer J Clin* **61**(2): 69–90.

Kim BK, Park JY, Choi HJ, Kim do Y, Ahn SH, Kim JK, Lee do Y, Lee KH, Han KH (2011) Long-term clinical outcomes of hepatic arterial infusion chemotherapy with cisplatin with or without 5-fluorouracil in locally advanced hepatocellular carcinoma. *J Cancer Res Clin Oncol* **137**(4): 659–667.

Kim do Y, Ahn SH, Kim SU, Choi SB, Lee KH, Park MS, Park JY, Lee do Y, Han KH, Kim KS (2011) Adjuvant hepatic arterial infusional chemotherapy with 5-fluorouracil and cisplatin after curative resection of hepatocellular carcinoma. *Oncology* **81**(3-4): 184–191.

Kim R, Tanabe K, Inoue H, Toge T (2002) Mechanism(s) of antitumor action in protracted infusion of low dose 5-fluorouracil and cisplatin in gastric carcinoma. *Int J Oncol* **20**(3): 549–555.

Kudo M (2012) Targeted therapy for liver cancer: updated review in 2012. *Curr Cancer Drug Targets* **12**(9): 1062–1072.

Kudo M, Izumi N, Kokudo N, Matsui O, Sakamoto M, Nakashima O, Kojiro M, Makuuchi M. HCC Expert Panel of Japan Society of Hepatology (2011) Management of hepatocellular carcinoma in Japan: Consensus-Based Clinical Practice Guidelines proposed by the Japan Society of Hepatology (JSH) 2010 updated version. *Dig Dis* **29**(3): 339–364.

Liver Cancer Study Group of Japan (2003) *General Rules for the Clinical and Pathological Study of Primary Liver Cancer*. Second English edition. Kanehara & Co. Ltd: Tokyo.

Llovet JM, Ricci S, Mazzaferro V, Hilgard P, Gane E, Blanc JF, de Oliveira AC, Santoro A, Raoul JL, Forner A, Schwartz M, Porta C, Zeuzem S, Bolondi L, Greten TF, Galle PR, Seitz JF, Borbath I, Haussinger D, Giannaris T, Shan M, Moscovici M, Voliotis D, Bruix J, SIS Group (2008) Sorafenib in advanced hepatocellular carcinoma. *N Engl J Med* **359**(4): 378–390.

Scanlon KJ, Newman EM, Lu Y, Priest DG (1986) Biochemical basis for cisplatin and 5-fluorouracil synergism in human ovarian carcinoma cells. *Proc Natl Acad Sci USA* **83**(23): 8923–8925.

Sherman M, Bruix J, Porayko M, Tran T, Committee APG (2012) Screening for hepatocellular carcinoma: the rationale for the American Association for the Study of Liver Diseases recommendations. *Hepatology* **56**(3): 793–796.

Ueshima K, Kudo M, Takita M, Nagai T, Tatsumi C, Ueda T, Kitai S, Ishikawa E, Yada N, Inoue T, Hagiwara S, Minami Y, Chung H (2010) Hepatic arterial infusion chemotherapy using low-dose 5-fluorouracil and cisplatin for advanced hepatocellular carcinoma. *Oncology* **78**(Suppl 1): 148–153.

Yamashita T, Arai K, Sunagozaka H, Ueda T, Terashima T, Yamashita T, Mizukoshi E, Sakai A, Nakamoto Y, Honda M, Kaneko S (2011) Randomized, phase II study comparing interferon combined with hepatic arterial infusion of fluorouracil plus cisplatin and fluorouracil alone in patients with advanced hepatocellular carcinoma. *Oncology* **81**(5-6): 281–290.

Supplementary Information accompanies this paper on British Journal of Cancer website (http://www.nature.com/bjc)

VOLUME 31 · NUMBER 32 · NOVEMBER 10 2013

JOURNAL OF CLINICAL ONCOLOGY

ORIGINAL REPORT

Sunitinib Versus Sorafenib in Advanced Hepatocellular Cancer: Results of a Randomized Phase III Trial

Ann-Lii Cheng, Yoon-Koo Kang, Deng-Yn Lin, Joong-Won Park, Masatoshi Kudo, Shukui Qin, Hyun-Cheol Chung, Xiangqun Song, Jianming Xu, Guido Poggi, Masao Omata, Susan Pitman Lowenthal, Silvana Lanzalone, Liqiang Yang, Maria Jose Lechuga, and Eric Raymond

Ann-Lii Cheng, National Taiwan University Hospital, Taipei; Deng-Yn Lin, Chang Gung Memorial Hospital, Chang Gung University, Guishan Township, Taiwan, Republic of China; Yoon-Koo Kang, Asan Medical Center, University of Ulsan College of Medicine; Hyun-Cheol Chung, Yonsei Cancer Center, Yonsei University College of Medicine, Seoul; Joong-Won Park, National Cancer Center, Goyang, Republic of Korea; Masatoshi Kudo, Kinki University Hospital, Osaka; Masao Omata, Yamanashi Prefecture Central Hospital, Kofu, Yamanashi, Japan; Shukui Qin, Nanjing Bayi Hospital, Nanjing; Xiangqun Song, Tumor Hospital of Guangxi Zhuang Autonomous Region, Nanning; Jianming Xu, Beijing 307 Hospital Cancer Centre, Beijing, People's Republic of China; Guido Poggi, Istituto di Ricovero e Cura a Carattere Scientifico Fondazione Maugeri, Pavia; Silvana Lanzalone, Maria Jose Lechuga, Pfizer Italia Srl, Milan, Italy; Susan Pitman Lowenthal, Pfizer Oncology, New York, NY; Liqiang Yang, Pfizer Oncology, La Jolla, CA; Eric Raymond, Service Inter Hospitalier de Cancerologie Bichat-Beaujon, Clichy, France.

Published online ahead of print at www.jco.org on September 30, 2013.

Written on behalf of the SUN1170 HCC Study Group.

Supported by Pfizer.

Presented at the 47th Annual Meeting of the American Society of Clinical Oncology, Chicago, IL, June 3-7, 2011.

Authors' disclosures of potential conflicts of interest and author contributions are found at the end of this article.

Clinical trial information: NCT00699374.

Corresponding author: Ann-Lii Cheng, MD, Department of Oncology, National Taiwan University Hospital, 7 Chung-Shan South Rd, Taipei, Taiwan; e-mail: alcheng@ntu.edu.tw.

0732-183X/13/3132w-4067w/$20.00

DOI: 10.1200/JCO.2012.45.8372

ABSTRACT

Purpose
Open-label, phase III trial evaluating whether sunitinib was superior or equivalent to sorafenib in hepatocellular cancer.

Patients and Methods
Patients were stratified and randomly assigned to receive sunitinib 37.5 mg once per day or sorafenib 400 mg twice per day. Primary end point was overall survival (OS).

Results
Early trial termination occurred for futility and safety reasons. A total of 1,074 patients were randomly assigned to the study (sunitinib arm, n = 530; sorafenib arm, n = 544). For sunitinib and sorafenib, respectively, median OS was 7.9 versus 10.2 months (hazard ratio [HR], 1.30; one-sided P = .9990; two-sided P = .0014); median progression-free survival (PFS; 3.6 *v* 3.0 months; HR, 1.13; one-sided P = .8785; two-sided P = .2286) and time to progression (TTP; 4.1 *v* 3.8 months; HR, 1.13; one-sided P = .8312; two-sided P = .3082) were comparable. Median OS was similar among Asian (7.7 *v* 8.8 months; HR, 1.21; one-sided P = .9829) and hepatitis B–infected patients (7.6 *v* 8.0 months; HR, 1.10; one-sided P = .8286), but was shorter with sunitinib in hepatitis C–infected patients (9.2 *v* 17.6 months; HR, 1.52; one-sided P = .9835). Sunitinib was associated with more frequent and severe adverse events (AEs) than sorafenib. Common grade 3/4 AEs were thrombocytopenia (29.7%) and neutropenia (25.7%) for sunitinib; hand-foot syndrome (21.2%) for sorafenib. Discontinuations owing to AEs were similar (sunitinib, 13.3%; sorafenib, 12.7%).

Conclusion
OS with sunitinib was not superior or equivalent but was significantly inferior to sorafenib. OS was comparable in Asian and hepatitis B–infected patients. OS was superior in hepatitis C–infected patients who received sorafenib. Sunitinib-treated patients reported more frequent and severe toxicity.

J Clin Oncol 31:4067-4075. © 2013 by American Society of Clinical Oncology

INTRODUCTION

Hepatocellular carcinoma (HCC) is a leading cause of death in Eastern countries, where hepatitis B (HBV) and C (HCV) viruses are prevalent, and emerges in Western countries primarily as a result of alcoholic and nonalcoholic steatohepatitis and HCV infection.[1-4] Proangiogenic signaling pathways are rational therapeutic targets for this disease. HCC is characterized by vascular recruitment as well as invasion, and high microvessel density predicts early recurrence after potentially curative surgery.[5] The vascular endothelial growth factor signaling pathway in particular is involved in HCC angiogenesis and lymphangiogenesis and seems to play a crucial role in disease pathogenesis.[6-8]

The current standard of care for unresectable HCC is sorafenib (Bayer, Wayne, NJ). As no other systemic therapies with proven efficacy are available for advanced HCC, additional treatments are needed.

Sunitinib (Pfizer, New York, NY) is an oral, multitargeted tyrosine kinase inhibitor of vascular endothelial growth factor receptors and other receptor tyrosine kinases.[9-15] Sunitinib has shown antitumor activity in three phase II studies of patients with advanced HCC.[16-18] Each study evaluated a different dosing regimen: 37.5 mg/d on a 4-week-on-2-week-off schedule (Schedule 4/2), 50 mg/d on Schedule 4/2, and 37.5 mg via continuous daily dosing (CDD). The 50 mg/d Schedule 4/2 regimen was associated with pronounced toxicities,[16,17] and the 37.5 mg CDD schedule was selected for further

study. In this article, we report findings from an open-label, phase III study comparing sunitinib versus sorafenib in advanced HCC.

PATIENTS AND METHODS

Patients

Patients at least 18 years old had histologically confirmed, locally advanced or metastatic HCC and were candidates for systemic anticancer treatment. Additional inclusion criteria are listed in the Appendix (online only). The presence of esophageal varices was documented by endoscopy before enrollment. Barcelona Clinic Liver Cancer (BCLC) staging[19] was assigned retrospectively. Cirrhosis was defined using pathology information provided by investigators.

The study was conducted in accordance with Good Clinical Practice guidelines, the declaration of Helsinki, and applicable local regulatory requirements and laws. Approval from the relevant institutional review board or independent ethics committee was required for each participating investigator/center, and written informed consent was obtained from all patients. An independent data monitoring committee consisting of a medical oncologist, a hepatologist, and a statistician reviewed safety and efficacy data periodically from April 2009.

Study Design and Treatment

Patients were enrolled by clinical-site staff and were randomly assigned 1:1 to sunitinib or sorafenib using a centralized interactive voice-response system. Randomization was stratified by geographic region (Asia *v* other regions), prior transarterial chemoembolization (≤ three or > three courses), and tumor invasion (presence *v* absence of vascular invasion and/or extrahepatic spread).

Treatment was given in 4-week cycles. Patients self-administered sunitinib orally at a starting dosage of 37.5 mg once daily in the morning; 12.5 mg incremental dose reductions were permitted to manage toxicities. Sorafenib 400 mg twice per day was self-administered orally, with dose reductions permitted as per the package insert. Treatment breaks were allowed to manage dose-limiting toxicities. Treatment continued for as long as patients derived clinical benefit or until disease progression, unacceptable toxicity, or patient withdrawal occurred. Concomitant antiviral treatment was recommended for HBV-positive patients. Patients received follow-up until death or study termination.

Study Assessments

Screenings included medical history, physical examination, assessment of Eastern Cooperative Oncology Group performance status, biochemistry and hematology, 12-lead ECGs, left ventricular function testing, brain and bone scans (if indicated), and assessment of ongoing symptoms and adverse events (AEs); they were performed within 21 days preceding study treatment. Laboratory testing was repeated every 2 weeks during cycle 1 and at 4-week intervals thereafter; ECGs were repeated on day 28 of cycle 1 and at the end of treatment or on withdrawal. AEs were graded according to National Cancer Institute Common Terminology Criteria for Adverse Events version 3.0 and were evaluated for causality. Tumor assessments were done by computed tomography or magnetic resonance imaging and were performed at screening, every 6 weeks for the first 24 weeks, and every 8 weeks thereafter. Disease response was evaluated by investigators using RECIST.[20]

Statistical Analysis

The primary end point of the study was overall survival (OS). Secondary end points included progression-free survival (PFS), time to progression (TTP), and safety.

The study was designed to detect a hazard ratio (HR) of 0.8045 for OS in favor of sunitinib and assumed 30 months of enrollment plus a median survival of 10.7 months for sorafenib[21] and 13.3 months for sunitinib, requiring 929 patient deaths for a one-sided stratified log-rank superiority test with a significance level of 0.025 and 90% power, and a noninferiority test with a one-sided significance level of 0.025 and approximately 80% power. The noninferiority test decision was based on the one-sided confidence limit of the HR, after adjusting the type 1 error rate for the prior interim analyses. The superiority/noninferiority hybrid design was considered in the sample size calculation. A total of 1,200 patients were required. The sample size calculation was based on a nonstratified log-rank test. However, the stratified log-rank test was performed for OS as planned.

A group-sequential design was used with two interim analyses (after approximately 232 and 557 patient deaths) and one final analysis. The O'Brien-Fleming and Lan-DeMets methods were used to determine efficacy and futility boundaries.[22,23] The futility stopping boundaries (sunitinib/sorafenib) were HRs of 1.207 or worse and 0.940 or worse for the first and

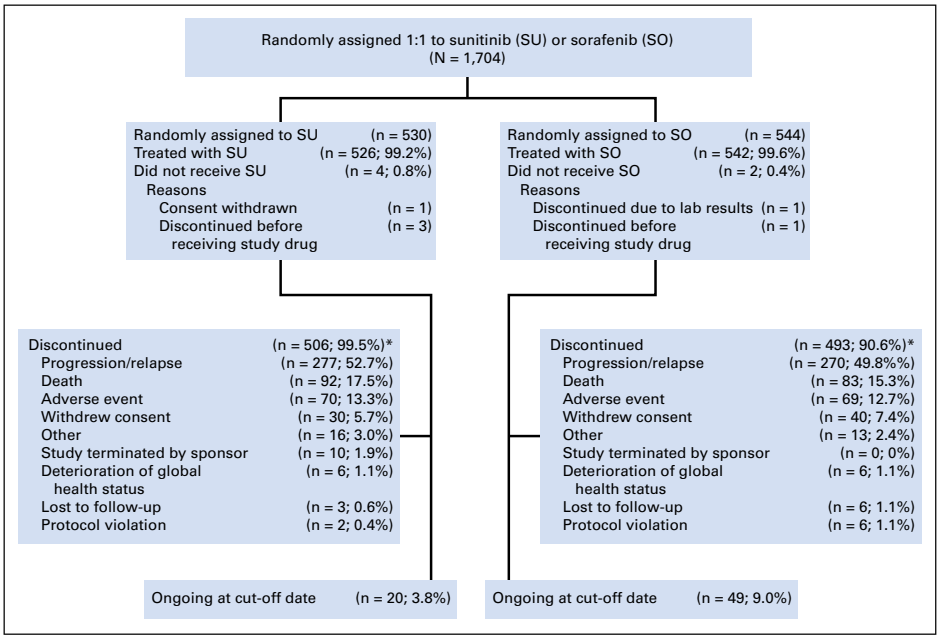

Fig 1. CONSORT diagram. (*) The percentage of patients who discontinued treatment for any reason is based on the total number of randomly assigned patients; however, the percentages for each primary reason are based on the number of patients who actually received treatment.

Table 1. Baseline Patient Characteristics

Characteristic	Sunitinib						Sorafenib					
	Total (n = 530)		Asia[a] (n = 402)		Non-Asia[b] (n = 128)		Total (n = 544)		Asia[a] (n = 410)		Non-Asia[b] (n = 134)	
	No. of Patients	%	No. of Patients	%	No. of Patients	%	No. of Patients	%	No. of Patients	%	No. of Patients	%
Age, years												
Median	59.0		57.0		66.0		59.0		56.0		66.0	
Range	18-85		18-85		18-85		18-84		18-84		23-83	
Male sex	436	82.3	334	83.1	102	79.7	459	84.4	346	84.4	21	15.7
Race												
White	111	20.9	0		111	86.7	112	20.6	0		112	83.6
Black	6	1.1	0		6	4.7	10	1.8	0		10	7.5
Asian	411	77.5	402	100	9	7.0	418	76.8	410	100	8	6.0
Other	2	0.4	0		2	1.6	4	0.7	0		4	3.0
Time since diagnosis, weeks												
Median	7.1		5.1		11.2		6.3		5.1		9.0	
Range	0.1-520.0		0.1-520.0		0.4-289.7		0.1-761.3		0.1-501.1		0.1-761.3	
ECOG PS												
0	278	52.5	207	51.5	71	55.5	288	52.9	203	49.5	85	63.4
1	248	46.8[c]	194	48.3	54	42.2[c]	254	46.7	206	50.2	48	35.8
Missing	4	0.8	1	0.2	3	2.3	2	0.4	1	0.2	1	0.7
Vascular invasion and/or extrahepatic spread	418	78.9	335	83.3	83	64.8	415	76.3	335	81.7	80	59.7
CLIP score												
0	50	9.4	41	10.2	9	7.0	70	12.9	51	12.4	19	14.2
1/2	308	58.1	228	56.7	80	62.5	309	56.8	224	54.6	85	63.4
≥ 3	155	29.2	127	31.6	28	21.9	153	28.1	131	32.0	22	16.4
Missing	17	3.2	6	1.5	11	8.6	12	2.2	4	1.0	8	6.0
Child-Pugh score												
5-6	529	99.8[d]	401	99.8[d]	128	100	541	99.4[e]	410	100	131	97.8[e]
> 6	0		0		0		1	0.1	0		1	0.7
BCLC stage[f]												
B	67	12.6[d]	40	10.0	27	21.1[d]	89	16.4[d]	48	11.7	41	30.6[d]
C	462	87.2[d]	362	90.0	100	78.1[d]	454	83.5[d]	362	88.3	92	68.7[d]
Sum of longest diameter target lesions, mm												
Median	115.0		119.0		111.5		107.0		107.5		106.0	
Range	10-961[e]		10-961[d]		11-494[g]		10-860		10-828		11-860	
Involved disease sites per patient												
1	209	39.4	143	35.6	66	51.6	226	41.5	150	36.6	76	56.7
2	185	34.9	145	36.1	40	31.3	205	37.7	170	41.5	35	26.1
≥ 3	133	25.1	113	28.1	20	15.6	113	20.8	90	22.0	23	17.2
Involved disease sites												
Liver	470	88.7	351	87.3	119	93.0	497	91.4	371	90.5	126	94.0
Lung	192	36.2	165	41.0	27	21.1	209	38.4	183	44.6	26	19.4
Lymph nodes	142	26.8	121	30.1	21	16.4	128	23.5	101	24.6	27	20.1
Other[h]	185	34.9	151	37.6	34	26.6	147	27.0	112	27.3	69	51.5
Medical history relevant to primary diagnosis												
Esophageal varices	147	27.7	103	25.6	44	34.4	156	28.7	107	26.1	49	36.6
Hepatitis B infection	290	54.7	269	66.9	21	16.4	288	52.9	263	64.1	25	18.7
Hepatitis C infection	113	21.3	65	16.2	48	37.5	119	21.9	80	19.5	39	29.1
History of alcohol abuse	91	17.2	47	11.7	44	34.4	82	15.1	45	11.0	37	27.6
Underlying cirrhosis	265	50.0	195	48.5	70	54.7	247	45.4	177	43.2	70	52.2
Nonalcoholic steatohepatitis	18	3.4	10	2.5	8	6.3	16	2.9	6	1.5	10	7.5
Partial or complete portal vein thrombosis	179	33.8	136	33.8	43	33.6	166	30.5	169	41.2	24	17.9
Prior treatment												
≤ 3 courses TACE	447	84.3	332	82.6	115	89.8	453	83.3	331	80.7	122	91.0
> 3 courses TACE	82	15.5	70	17.4	12	9.4	91	16.7	79	19.3	12	9.0

(continued on following page)

Table 1. Baseline Patient Characteristics (continued)

Characteristic	Sunitinib						Sorafenib					
	Total (n = 530)		Asia[a] (n = 402)		Non-Asia[b] (n = 128)		Total (n = 544)		Asia[a] (n = 410)		Non-Asia[b] (n = 134)	
	No. of Patients	%	No. of Patients	%	No. of Patients	%	No. of Patients	%	No. of Patients	%	No. of Patients	%
≥ 1 course of radiotherapy	40	7.6	35	8.7	5	3.9	35	6.4	31	7.6	4	3.0
≥ 1 surgical procedure for primary diagnosis	516	97.4	390	97.0	126	98.4	519	95.4	393	95.9	126	94.0

Abbreviations: BCLC, Barcelona Clinic Liver Cancer; CLIP, Cancer of the Liver Italian Program; ECOG PS, Eastern Cooperative Oncology Group performance status; TACE, transarterial chemoembolization.
[a]The Asian countries are the Republic of Korea, the Philippines, Taiwan, Malaysia, China, Japan, Hong Kong, Thailand, and Singapore.
[b]The non-Asian countries are Australia, Italy, Canada, France, United Kingdom, Spain, Germany, Belgium, the Russian Federation, Poland, Turkey, Sweden, South Africa, and United States.
[c]Includes one patient with ECOG PS of 2.
[d]Data missing for one patient.
[e]Data missing for three patients.
[f]BCLC staging was assigned retrospectively.
[g]Data missing for two patients.
[h]Includes adrenal, peritoneum, and additional sites.

second interim analyses, respectively. Efficacy analyses were based on the intent-to-treat population that included all randomized patients. Safety was analyzed in the per-protocol population, comprising all patients who received at least one dose of the study drug. OS, PFS, and TTP were summarized using Kaplan-Meier estimates and were compared by stratified log-rank testing ($\alpha = .025$). As defined in the protocol, one-sided *P* values were calculated for OS, PFS, and TTP comparisons. Additional two-sided *P* values were derived as required by *JCO* guidelines.

Cox regression was used to analyze the influence of stratification factors. If OS with sunitinib was not superior to that of sorafenib based on a one-sided stratified log-rank test, then a noninferiority test was performed using a superiority/noninferiority hybrid design.[24]

RESULTS

Patient Characteristics

From July 2008 to May 2010, 1,074 patients were randomly assigned to receive sunitinib (n = 530) or sorafenib (n = 544) at 136 sites. Overall, 1,068 patients received treatment (Fig 1), including 812 patients (75.6%) from nine Asian countries and 262 non-Asian patients (24.4%; 14 countries). Baseline demographics of the treatment arms were generally similar (Table 1). In the sunitinib and sorafenib arms, respectively, 78.9% and 76.3% of patients had vascular invasion and/or extrahepatic spread. BCLC staging was assigned retrospectively. Of 916 patients with stage C disease at baseline, 833 (90.9%) had extrahepatic disease and/or vascular invasion. The remaining 83 patients (9.1%) were classified as stage C based on an Eastern Cooperative Oncology Group performance status of 1.

In each study arm, Asian-region patients had more advanced disease than non-Asian patients, based on Cancer of the Liver Italian Program score[25] and BCLC stage (Table 1). Cancer of the Liver Italian Program scores of ≥ 3 were reported for 31.6% and 32.0% of Asian-region patients, as well as 21.9% and 16.4% of non-Asian patients in the sunitinib and sorafenib arms, respectively. BCLC staging revealed a slight imbalance between treatment arms (Table 1). This was particularly marked in non-Asian patients, with stage C (advanced) disease in 68.7% of sorafenib-treated patients (n = 134) compared with 78.1% of sunitinib-treated patients (n = 128).

At baseline, approximately 50% of patients in either group had cirrhosis and/or HBV infection, and approximately 20% were infected with HCV (Table 1). As expected, approximately two thirds of Asian-region patients had HBV infection, compared with less than 20% in non-Asian countries. In contrast, HCV infection was present in about one-third of non-Asian patients versus less than 20% in Asia; except in Japan where HCV infection was more prevalent than in other Asian countries (total, 54.1%; sunitinib, 51.6%; sorafenib, 56.3%). Within the overall HBV and HCV subpopulations, 48.8% and 66.5% of patients had cirrhosis, respectively.

Study Treatment

The median number of treatment cycles was four in each group, and median relative dose intensity (mRDI) was comparable (sunitinib, 66.6% *v* sorafenib, 71.3%). For Asian and non-Asian patients, respectively, mRDIs were 65.5% and 69.9% for sunitinib and 71.4% and 69.3% for sorafenib. Among HBV-infected patients, mRDIs were 69.5% for sunitinib and 67.4% for sorafenib, whereas in HCV-infected patients, mRDIs were 46.0% and 59.3%, respectively.

Treatment management was different between arms: more patients had at least one dose reduction with sorafenib (69.0%) versus sunitinib (47.7%), and more patients had at least one dosing interruption with sunitinib (69.0%) than sorafenib (55.7%). Twenty-six patients in the sunitinib arm received at least 1 year of treatment, compared with 55 sorafenib-treated patients.

In total, 506 sunitinib-arm patients (95.5%) and 493 sorafenib-arm patients (90.6%) discontinued treatment, primarily owing to relapse/progression, death, or AEs (Fig 1). At data cutoff, treatment was ongoing in 69 patients (sunitinib, n = 20; sorafenib, n = 49). After progressive disease, 5.7% of sorafenib- and 0.6% of sunitinib-treated patients remained on assigned therapy; 1.9% crossed over from sorafenib to sunitinib, and 14.5% crossed over from sunitinib to sorafenib.

Efficacy

As a result of a planned safety review by the independent data monitoring committee carried out after the first interim analysis, the

trial was terminated and enrollment was stopped for futility and safety reasons, after the HR for OS crossed the futility boundary. Median follow-up was 7.4 months for sunitinib and 7.8 months for sorafenib, and 372 and 314 patients, respectively, had died. Median OS was 7.9 months for sunitinib and 10.2 months for sorafenib (HR, 1.30; one-sided $P = .9990$; two-sided $P = .0014$; Fig 2; Table 2). The OS difference was in the opposite direction to what was expected. PFS was 3.6 versus 3.0 months (HR, 1.13; one-sided $P = .8785$; two-sided $P = .2286$) and TTP was 4.1 versus 3.8 months (HR, 1.13; one-sided $P = .8312$; two-sided $P = .3082$; Fig 2; Table 2). The 6-month PFS rate was 21.5% and 26.0%, for sunitinib and sorafenib, respectively.

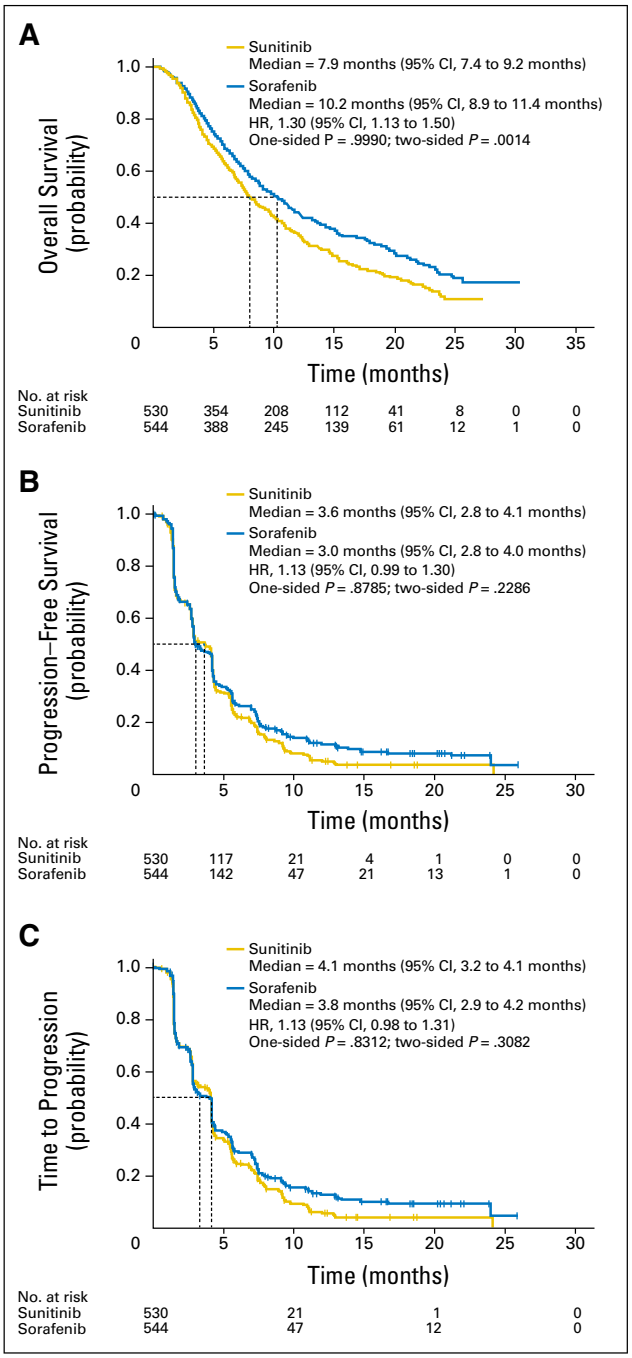

Fig 2. Kaplan-Meier curves of (A) overall survival, (B) progression-free survival, and (C) time to tumor progression for the intent-to-treat population. HR, hazard ratio.

Median OS for sorafenib versus sunitinib was similar among Asian patients but markedly different in non-Asian patients (Table 2). PFS and TTP were longer in both treatment arms for non-Asian patients, compared with Asian-region patients (Table 2). Cox proportional hazards analysis found that the OS treatment effect favoring sorafenib occurred regardless of selected prognostic factors, including Asian versus non-Asian region and ≤ 3 versus more than 3 prior transarterial chemoembolization courses (data not shown). No significant differences between treatments were observed in clinical-benefit rates (Table 2).

An exploratory analysis in HBV-positive patients showed no significant difference in OS between treatments, regardless of geographic region (Table 2). Among HCV-positive patients, median OS was longer with sorafenib (17.6 *v* 9.2 months; HR, 1.52; one-sided $P = .9835$; Table 2), although the differences were not statistically significant. Similar findings were observed in Asian and non-Asian subpopulations with HCV infection (Table 2).

In patients with portal vein thrombosis at baseline, an exploratory analysis found that median OS was longer with sorafenib than sunitinib (6.4 *v* 5.9 months; HR, 1.31; one-sided $P = .9791$; Table 2). Median PFS was 2.8 months in both treatment arms (HR, 1.11; one-sided $P = .5774$).

Safety

The most frequent treatment-emergent AEs reported were thrombocytopenia and diarrhea with sunitinib and hand-foot syndrome and diarrhea with sorafenib (Table 3). Most AEs were grade 1/2 in severity. Grade 3/4 events occurred in 432 sunitinib patients (82.1%) and 402 sorafenib patients (74.2%); the most common were thrombocytopenia (29.7%) and neutropenia (25.7%) for sunitinib and hand-foot syndrome (21.2%) for sorafenib (Table 3). Grade 5 events of any cause occurred in 18.8% of sunitinib and 16.8% of sorafenib patients and consisted primarily of disease progression (12.0% and 11.6%, respectively; Appendix Table A1). Discontinuations as a result of AEs were observed in 13.3% and 12.7% of sunitinib- and sorafenib-treated patients, respectively.

Bleeding events were generally of mild-to-moderate severity and were reported in 195 patients receiving sunitinib (37.1%) and 109 patients receiving sorafenib (20.1%). Grade 3 to 5 events of this type occurred in 11.4% and 4.8% of patients, respectively. Bleeding events (all grades) affected the gastrointestinal system in 18.3% and 12.0% of sunitinib- and sorafenib-treated patients, respectively, and accounted for the majority of such events reported. Grade ≥ 3 gastrointestinal bleeding was reported in 42 patients receiving sunitinib (8.0%) and 21 receiving sorafenib (3.9%).

AEs led to more dose reductions with sorafenib than sunitinib (35.1% *v* 30.0%), whereas temporary treatment discontinuation because of AEs was more frequent with sunitinib (76.6% *v* 58.7%). Sunitinib dose reductions were predominantly as a result of thrombocytopenia (6.7%), hand-foot syndrome (6.5%), and neutropenia (4.0%); sorafenib dose reductions primarily resulted from hand-foot syndrome (16.2%), diarrhea (4.2%), and rash (2.2%). Most sunitinib

Table 2. Efficacy Results

Variable	Sunitinib	Sorafenib	Hazard Ratio	95% CI of Hazard Ratio	*P*[a]
Median overall survival, months					
Intent-to-treat population[b]	7.9	10.2	1.30	1.13 to 1.50	.9990[c]
Asian regions[d]	7.7	8.8	1.21	1.03 to 1.42	.9829
Non-Asian regions[e]	9.3	15.1	1.64	1.20 to 2.26	.9964
Patients with hepatitis B[f]	7.6	8.0	1.10	0.92 to 1.33	.8286
Asian regions[g]	7.6	7.9	1.10	0.91 to 1.33	.8156
Non-Asian regions[h]	7.9	15.3	1.08	0.49 to 2.36	.6251
Patients with hepatitis C[i]	9.2	17.6	1.52	1.09 to 2.13	.9835
Asian regions[j]	9.7	12.6	1.40	0.92 to 2.14	.9279
Non-Asian regions[k]	8.6	18.3	1.76	0.99 to 3.10	.9456
Patients with portal vein thrombosis[l]	5.9	6.4	1.31	1.03 to 1.67	.9791
Median progression-free survival, months					
Intent-to-treat population[b]	3.6	3.0	1.13	0.99 to 1.30	.8785[m]
Asian regions[d]	2.9	2.8	1.03	0.88 to 1.20	.6070
Non-Asian regions[e]	4.2	5.6	1.46	1.07 to 2.00	.9818
Patients with hepatitis B[f]	2.9	2.8	1.01	0.84 to 1.20	.4496
Patients with hepatitis C[i]	4.2	2.9	0.89	0.65 to 1.22	.1043
Patients with portal vein thrombosis[l]	2.8	2.8	1.11	0.87 to 1.42	.5774
Time to progression, months					
Intent-to-treat population[b]	4.1	3.8	1.13	0.98 to 1.31	.8312[n]
Asian regions[d]	4.0	2.8	1.03	0.88 to 1.21	.6150
Non-Asian regions[e]	5.0	6.0	1.41	1.00 to 1.99	.9505
Patients with portal vein thrombosis[l]	2.9	2.8	1.14	0.87 to 1.48	.6301
Tumor response[b]					
Complete					
No.	2	1			
%	< 1.0	< 1.0			
Partial					
No.	33	32			
%	6.2	5.9			
Stable disease ≥ 12 months					
No.	232	247			
%	43.8	45.4			
Clinical benefit rate[o]			1.03[p]	0.81 to 1.31	.816
No.	267	280			
%	50.8	51.5			

NOTE. Patient numbers for each outcome are listed in the table footnotes.

[a]One-sided, stratified log-rank test. *P* values calculated for the data presented by Cheng et al[26] were based on a one-sided stratified log-rank test with the alternative hypothesis in favor of sorafenib. The *P* values in this article are based on the same statistical test but with the alternative hypothesis in favor of sunitinib. Because the different *P* values are from exactly the same stratified log-rank test (but with different directions of the alternative hypothesis), the testing results and the conclusions are exactly the same.

[b]Intent-to-treat population: sunitinib, n = 530; sorafenib, n = 544.

[c]Two-sided, stratified log-rank test *P* = .0014.

[d]Patients in Asian countries (the Republic of Korea, the Philippines, Taiwan, Malaysia, China, Japan, Hong Kong, Thailand, and Singapore): sunitinib, n = 402; sorafenib, n = 410.

[e]Patients in other countries (Australia, Italy, Canada, France, United Kingdom, Spain, Germany, Belgium, the Russian Federation, Poland, Turkey, Sweden, South Africa, and the United States): sunitinib, n = 128; sorafenib, n = 134.

[f]Patients with hepatitis B, exploratory analysis: sunitinib, n = 290; sorafenib, n = 288.

[g]Patients with hepatitis B in Asian countries, exploratory analysis: sunitinib, n = 269; sorafenib, n = 263.

[h]Patients with hepatitis B in non-Asian regions, exploratory analysis: sunitinib = 21; sorafenib = 25.

[i]Patients with hepatitis C, exploratory analysis: sunitinib = 113; sorafenib = 119.

[j]Patients with hepatitis C in Asian countries, exploratory analysis: sunitinib, n = 65; sorafenib, n = 80.

[k]Patients with hepatitis C in non-Asian regions, exploratory analysis: sunitinib, n = 48; sorafenib, n = 39.

[l]Patients with partial or complete portal vein thrombosis, exploratory analysis: sunitinib, n = 174; sorafenib, n = 162.

[m]Two-sided, stratified log-rank test: *P* = .2286.

[n]Two-sided, stratified log-rank test: *P* = .3082.

[o]Clinical benefit rate = percentage of complete responses + partial responses + stable disease ≥ 12 weeks.

[p]Odds ratio for clinical benefit rate.

dosing delays were as a result of thrombocytopenia (18.1%), hand-foot syndrome (13.9%), and neutropenia (12.4%). Sorafenib dosing delays were mainly caused by hand-foot syndrome (21.0%), diarrhea (9.6%), and increased AST (4.6%).

During the study period, 92 and 83 fatal AEs occurred in the sunitinib and sorafenib groups, respectively; 70 and 71 patient deaths were disease-related, 17 and two were attributed to toxicity, and six and 11 were as a result of unknown or other reasons (Table 4).

Table 3. Most Common All-Causality Treatment-Emergent Adverse Events (≥ 15% of patients in either group)

Adverse Event	Sunitinib (n = 526)						Sorafenib (n = 542)					
	Any Grade		Grade 3		Grade 4		Any Grade		Grade 3		Grade 4	
	No. of Patients	%	No. of Patients	%	No. of Patients	%	No. of Patients	%	No. of Patients	%	No. of Patients	%
Thrombocytopenia	267	50.8	124	23.6	32	6.1	94	17.3	22	4.1	3	0.6
Diarrhea	247	47.0	37	7.0	1	0.2	256	47.2	49	9.0	0	0
Decreased appetite	233	44.3	30	5.7	0	0	184	33.9	20	3.7	0	0
Hand-foot syndrome	233	44.3	70	13.3	0	0	330	60.9	114	21.1	1	0.2
Neutropenia	192	36.5	123	23.4	12	2.3	25	4.6	10	1.8	2	0.4
Anemia	189	35.9	33	6.3	16	3.0	61	11.3	18	3.3	4	0.7
Fatigue	172	32.7	32	6.1	1	0.2	114	21.0	20	3.7	1	0.2
Leukopenia	167	31.7	65	12.4	4	0.8	43	7.9	5	0.2	0	0
Nausea	130	24.7	6	1.1	0	0	94	17.3	5	0.9	0	0
Abdominal pain	122	23.2	18	3.4	2*	0.4	108	19.9	14	2.6	0	0
Pyrexia	117	22.2	3	0.6	0	0	107	19.7	3	0.6	0	0
Hypertension	110	20.9	20	3.8	0	0	95	17.5	15	2.8	0	0
Rash	108	20.5	4	0.8	0	0	146	26.9	16	3.0	2	0.4
Vomiting	106	20.2	14	2.7	0	0	62	11.4	7	1.3	0	0
Abdominal distention	90	17.1	11	2.1	1	0.2	56	10.3	7	1.3	0	0
Constipation	87	16.5	2	0.4	0	0	80	14.8	1	0.2	0	0
Stomatitis	87	16.5	8	1.5	0	0	53	9.8	2	0.4	0	0
Ascites	81	15.4	24	4.6	3	0.6	66	12.2	18	3.3	0	0
Increased aspartate aminotransferase	80	15.2	44	8.4	2	0.4	92	17.0	47	8.7	2	0.4
Asthenia	80	15.2	33	6.3	1	0.2	62	11.4	24	4.4	0	0
Weight decreased	43	8.2	5	1.0	0	0	112	20.7	8	1.5	0	0
Alopecia	19	3.6	0	0	0	0	154	28.4	1	0.2	0	0

NOTE. In both study arms, the most common serious adverse events for sunitinib and sorafenib were disease progression (9.7%; 10.9%), GI, esophageal varices, or tumor hemorrhage (8.0%; 3.0%), and pyrexia (3.0%; 1.7%), respectively.
*Includes one grade 5 event.

DISCUSSION

Sunitinib did not achieve its primary end point of equivalent or superior OS versus sorafenib in advanced HCC. Despite apparent similarities in PFS and TTP, the lack of OS benefit emphasizes the limitations of surrogate end points in HCC. The OS difference in favor of sorafenib was consistent across all stratification groups and was maintained after adjustment for baseline factors.

Table 4. Deaths During the Study or Within 28 Days After the Last Dose of Study Medication

Event	Sunitinib (n = 526)		Sorafenib (n = 542)	
	No. of Patients	%	No. of Patients	%
Deaths, all causes*	92	17.5	83	15.3
Cause†				
Disease progression	70	76.1	71	85.5
Toxicity	17	18.5	2	2.4
Dehydration with or without organ failure	3	3.3	0	
CNS hemorrhage	3	3.3	0	
Esophageal varices/GI hemorrhage‡	3	3.3	1	1.2
Other/unknown cause	6	6.5	11	13.3
Pneumonia	2	2.2	1	1.2
Septic shock/sepsis	1	1.1	2	2.4
Unknown reason	0		2	2.4

*Patients may have more than one cause of death.
†Cause shown as number and percentage of total deaths: sunitinib, n = 92; sorafenib, n = 83.
‡Includes deaths attributed to tumor hemorrhage.

Median OS with sorafenib (10.2 months) in this mixed Asian and non-Asian trial was similar to that reported in the non-Asian trial Sorafenib HCC Assessment Randomized Protocol (SHARP; 10.7 months),[21] and higher than in the Asia-Pacific study (6.5 months).[27] However, Asian and non-Asian subpopulations in our study showed longer OS than expected with sorafenib, based on the Asia-Pacific and SHARP trials, respectively.[21,27] The median survival of 7.9 months observed with sunitinib was less than 9.3 months seen in a phase II trial of CDD of sunitinib 37.5 mg in advanced HCC,[18] but was similar to the lower range of 8.0 to 9.8 months reported in other phase II studies in advanced HCC with different doses and/or treatment schedules.[16,17]

BCLC staging showed an imbalance between study arms in non-Asian patients (BCLC stage C [advanced] disease: sunitinib, 78.7%; *v* sorafenib, 68.7%). In addition, a trend toward less advanced disease at baseline was pronounced in the sorafenib arm of our study in patients from non-Asian regions (BCLC stage C, 68.7%), compared with sorafenib-treated patients in the SHARP study (BCLC stage C, 81.6%). Non-Asian patients receiving sorafenib achieved a median OS of 15.1 months in our study, considerably higher than the 10.7 months in the SHARP trial.[21] Our trial and others comparing sorafenib with novel agents[28] were designed using OS reported in previous sorafenib studies. The study design for future superiority and noninferiority trials should take into account the most recent results of large phase III studies.

The OS difference between sunitinib and sorafenib was particularly marked in patients from non-Asian regions (Table 2). The non-Asian population included one-quarter of patients, many of whom were HCV-positive. Median OS was similar between treatment groups in HBV-infected patients at baseline (Table 2). This finding suggests that HBV-related and HCV-related HCC may respond differently to targeted therapies, although geographic disparities in HBV-related and HCV-related HCC disease management cannot be excluded as contributing, in part, to the differential survival observed. Recently, an exploratory subgroup analysis from the SHARP study reported that median OS with sorafenib was numerically longer in patients with HCV-related disease than in those with alcohol- or HBV-related HCC (17.6, 10.0, and 8.0 months, respectively).[29]

Among patients with HCV infection in our study, median OS was markedly longer with sorafenib versus sunitinib (Table 2). This may be related to sorafenib-mediated inhibition of Raf-1, as HCC development and progression is associated with Raf-1/MAP kinase pathway activation.[30,31] In response to mitogenic stimuli, HCV proteins activate the Raf-1/MEK/ERK pathway.[32-34] Raf-1 kinase activity is crucial for HCV (but not HBV) replication,[34] and direct comparison of HBV- and HCV-infected tissues suggests higher expression of ERK in HCV-related disease.[35] Sorafenib inhibits Raf-1and blocks HCV replication at clinically relevant concentrations.[36] This does not occur with sunitinib treatment. However, sorafenib-mediated inhibition of Raf-1 is not consistently associated with downstream MAP kinase (Ras/Raf/ERK) inhibition.[37] Therefore, the activity of sorafenib in HCC may be partly as a result of Raf/MAP kinase-independent mechanisms.[38-40]

Results from our trial emphasize the limitations of PFS and TTP as end points for evaluating HCC anticancer agents.[41,42] Also, these findings stress that PFS in nonrandomized, single-arm, phase II trials of HCC[21,27] may not be a reliable end point for the design of phase III studies evaluating OS. Another pitfall may be the overoptimistic expectation that sunitinib could extend median OS to at least 13 months, based on phase II data in which median OS did not exceed 10 months.[16,17] However, when the study was designed, it was expected that OS with sunitinib may be superior or equivalent to that of sorafenib.[21,27]

Sunitinib was associated with more frequent toxicity than sorafenib, and this may in part be related to differences in clinical experience and management of study treatments. Rates of dose reductions and interruptions differed in this unblinded study, with more dosing interruptions occurring with sunitinib than sorafenib (69.0% *v* 55.7% of patients) and more dose reductions occurring with sorafenib (69.0% *v* 47.7%).

Overall, the frequency and severity of AEs were comparable to those seen in a phase II study of sunitinib administered on a CDD schedule.[18] Bleeding events of any grade were generally more frequent with sunitinib. This may be due to sunitinib-mediated effects on endothelial cells.[43] Although thrombocytopenia was one of the most common grade 3/4 AEs in the sunitinib arm, it was not associated with bleeding events. Though the sunitinib schedule used in this study (37.5 mg/d) was well tolerated in other tumor types,[44-46] we observed poor tolerability in advanced HCC.

In conclusion, OS with sunitinib was neither superior nor equivalent but significantly inferior to that with sorafenib. OS was comparable in Asian and HBV-infected patients. In HCV-infected patients, superior OS was seen with sorafenib. Sunitinib was associated with more frequent and severe toxicities than sorafenib.

AUTHORS' DISCLOSURES OF POTENTIAL CONFLICTS OF INTEREST

Although all authors completed the disclosure declaration, the following author(s) and/or an author's immediate family member(s) indicated a financial or other interest that is relevant to the subject matter under consideration in this article. Certain relationships marked with a "U" are those for which no compensation was received; those relationships marked with a "C" were compensated. For a detailed description of the disclosure categories, or for more information about ASCO's conflict of interest policy, please refer to the Author Disclosure Declaration and the Disclosures of Potential Conflicts of Interest section in Information for Contributors.

Employment or Leadership Position: Susan Pitman Lowenthal, Pfizer (C); Silvana Lanzalone, Pfizer (C); Liqiang Yang, Pfizer (C); Maria Jose Lechuga, Pfizer (C) **Consultant or Advisory Role:** Ann-Lii Cheng, Bayer Schering Pharma (C), Pfizer (C), Merck Serono (C); Yoon-Koo Kang, Bayer (C), Pfizer (C); Joong-Won Park, Bristol-Myers Squibb (U), Taiho Pharmaceutical (U); Masatoshi Kudo, Bayer (C), Taiho Pharmaceutical (C); Masao Omata, Boehringer Ingelheim (C), Bristol-Myers Squibb (C), Otsuka (C); Eric Raymond, Pfizer (C), Bayer (C) **Stock Ownership:** Susan Pitman Lowenthal, Pfizer; Silvana Lanzalone, Pfizer; Liqiang Yang, Pfizer; Maria Jose Lechuga, Pfizer. **Honoraria:** Ann-Lii Cheng, Bayer Schering Pharma, Pfizer, Merck Serono; Yoon-Koo Kang, Bayer, Pfizer; Joong-Won Park, Bayer, Bristol-Myers Squibb; Masatoshi Kudo, Bayer; Masao Omata, Bayer, Bristol-Myers Squibb, Roche; Eric Raymond, Pfizer, Bayer **Research Funding:** Yoon-Koo Kang, Bayer; Eric Raymond, Pfizer, Bayer **Expert Testimony:** None **Patents:** None **Other Remuneration:** None

AUTHOR CONTRIBUTIONS

Conception and design: Ann-Lii Cheng, Yoon-Koo Kang, Susan Pitman Lowenthal, Silvana Lanzalone, Liqiang Yang, Maria Jose Lechuga, Eric Raymond

Provision of study materials or patients: Yoon-Koo Kang, Eric Raymond

Collection and assembly of data: Deng-Yn Lin, Joong-Won Park, Masatoshi Kudo, Shukui Qin, Hyun-Cheol Chung, Xiangqun Song, Jianming Xu, Guido Poggi, Silvana Lanzalone, Liqiang Yang, Eric Raymond

Data analysis and interpretation: Yoon-Koo Kang, Joong-Won Park, Masao Omata, Susan Pitman Lowenthal, Silvana Lanzalone, Liqiang Yang, Eric Raymond

Manuscript writing: All authors

Final approval of manuscript: All authors

REFERENCES

1. Ferlay J, Shin HR, Bray F, et al: Estimates of worldwide burden of cancer in 2008: GLOBOCAN 2008. Int J Cancer 127:2893-2917, 2010
2. Jemal A, Bray F, Center MM, et al: Global cancer statistics. CA Cancer J Clin 61: 69-90, 2011
3. Perz JF, Armstrong GL, Farrington LA, et al: The contributions of hepatitis B virus and hepatitis C virus infections to cirrhosis and primary liver cancer worldwide. J Hepatol 45:529-538, 2006
4. Smedile A, Bugianesi E: Steatosis and hepatocellular carcinoma risk. Eur Rev Med Pharmacol Sci 9:291-293, 2005
5. Poon RT, Ng IO, Lau C, et al: Tumor microvessel density as a predictor of recurrence after resection of hepatocellular carcinoma: A prospective study. J Clin Oncol 20:1775-1785, 2002
6. Yao DF, Wu XH, Zhu Y, et al: Quantitative analysis of vascular endothelial growth factor, microvascular density and their clinicopathologic features in human hepatocellular carcinoma. Hepatobiliary

Pancreat Dis Int 4:220-226, 2005

7. Zhang ZL, Liu ZS, Sun Q: Expression of angiopoietins, Tie2 and vascular endothelial growth factor in angiogenesis and progression of hepatocellular carcinoma. World J Gastroenterol 12:4241-4245, 2006

8. Mäkinen T, Veikkola T, Mustjoki S, et al: Isolated lymphatic endothelial cells transduce growth, survival and migratory signals via the VEGF-C/D receptor VEGFR-3. EMBO J 20:4762-4773, 2001

9. Mendel DB, Laird AD, Xin X, et al: In vivo antitumor activity of SU11248, a novel tyrosine kinase inhibitor targeting vascular endothelial growth factor and platelet-derived growth factor receptors: Determination of a pharmacokinetic/pharmacodynamic relationship. Clin Cancer Res 9:327-337, 2003

10. Murray LJ, Abrams TJ, Long KR, et al: SU11248 inhibits tumor growth and CSF-1R-dependent osteolysis in an experimental breast cancer bone metastasis model. Clin Exp Metastasis 20:757-766, 2003

11. O'Farrell AM, Abrams TJ, Yuen HA, et al: SU11248 is a novel FLT3 tyrosine kinase inhibitor with potent activity in vitro and in vivo. Blood 101: 3597-3605, 2003

12. Abrams TJ, Lee LB, Murray LJ, et al: SU11248 inhibits KIT and platelet-derived growth factor receptor beta in preclinical models of human small cell lung cancer. Mol Cancer Ther 2:471-478, 2003

13. Kim DW, Jo YS, Jung HS, et al: An orally administered multitarget tyrosine kinase inhibitor, SU11248, is a novel potent inhibitor of thyroid oncogenic RET/papillary thyroid cancer kinases. J Clin Endocrinol Metab 91:4070-4076, 2006

14. Kodera Y, Katanasaka Y, Kitamura Y, et al: Sunitinib inhibits lymphatic endothelial cell functions and lymph node metastasis in a breast cancer model through inhibition of vascular endothelial growth factor receptor 3. Breast Cancer Res 13:R66, 2011

15. Faivre S, Demetri G, Sargent W, et al: Molecular basis for sunitinib efficacy and future clinical development. Nat Rev Drug Discov 6:734-745, 2007

16. Faivre S, Raymond E, Boucher E, et al: Safety and efficacy of sunitinib in patients with advanced hepatocellular carcinoma: An open-label, multicentre, phase II study. Lancet Oncol 10:794-800, 2009

17. Zhu AX, Sahani DV, Duda DG, et al: Efficacy, safety, and potential biomarkers of sunitinib monotherapy in advanced hepatocellular carcinoma: A phase II study. J Clin Oncol 27:3027-3035, 2009

18. Koeberle D, Montemurro M, Samaras P, et al: Continuous sunitinib treatment in patients with advanced hepatocellular carcinoma: A Swiss Group for Clinical Cancer Res (SAKK) and Swiss Association for the Study of the Liver (SASL) multicenter phase II trial (SAKK 77/06). Oncologist 15:285-292, 2010

19. Llovet JM, Brú C, Bruix J: Prognosis of hepatocellular carcinoma: The BCLC staging classification. Semin Liver Dis 19:329-338, 1999

20. Therasse P, Arbuck SG, Eisenhauer EA, et al: New guidelines to evaluate the response to treatment in solid tumors: European Organisation for Research and Treatment of Cancer, National Cancer Institute of the United States, National Cancer Institute of Canada. J Natl Cancer Inst 92:205-216, 2000

21. Llovet JM, Ricci S, Mazzaferro V, et al: Sorafenib in advanced hepatocellular carcinoma. N Engl J Med 359:359-378, 2008

22. O'Brien PC, Fleming TR: A multiple testing procedure for clinical trials. Biometrics 35:549-556, 1979

23. Lan KKG, DeMets DL: Discrete sequential boundaries for clinical trials. Biometrika 70:659-663, 1983

24. Freidlin B, Korn EL, George SL, et al: Randomized clinical trial design for assessing noninferiority when superiority is expected. J Clin Oncol 25:5019-5023, 2007

25. Cancer of the Liver Italian Program Investigators: Prospective validation of the CLIP score: A new prognostic system for patients with cirrhosis and hepatocellular carcinoma—The Cancer of the Liver Italian Program (CLIP) Investigators. Hepatology 31: 840-845, 2000

26. Cheng A, Kang Y, Lin D, et al: Phase 3 trial of sunitinib (Su) versus sorafenib (So) in advanced hepatocellular carcinoma (HCC). J Clin Oncol 29: 256s, 2011 (suppl; abstr 4000)

27. Cheng AL, Kang YK, Chen Z, et al: Efficacy and safety of sorafenib in patients in the Asia-Pacific region with advanced hepatocellular carcinoma: A phase III randomised, double-blind, placebo-controlled trial. Lancet Oncol 10:25-34, 2009

28. Hoffman K, Glimm H, Radeleff B, et al: Prospective, randomized, double-blind, multi-center, phase III clinical study on transarterial chemoembolization (TACE) combined with sorafenib versus TACE plus placebo in patients with hepatocellular cancer before liver transplantation: HeiLivCa [ISRCTN24081794]. BMC Cancer 8:349, 2008

29. Bruix J, Raoul JL, Sherman M, et al: Efficacy and safety of sorafenib in patients with advanced hepatocellular carcinoma: Subanalyses of a phase III trial. J Hepatol 57:821-829, 2012

30. Ito Y, Sasaki Y, Horimoto M, et al: Activation of mitogen-activated protein kinases/extracellular signal-regulated kinases in human hepatocellular carcinoma. Hepatology 27:951-958, 1998

31. Schmidt CM, McKillop IH, Cahill PA, et al: Increased MAPK expression and activity in primary human hepatocellular carcinoma. Biochem Biophys Res Commun 236:54-58, 1997

32. Aoki H, Hayashi J, Moriyama M, et al: Hepatitis C virus core protein interacts with 14-3-3 protein and activates the kinase Raf-1. J Virol 74:1736-1741, 2000

33. Giambartolomei S, Covone F, Levrero M, et al: Sustained activation of the Raf/MEK/Erk pathway in response to EGF in stable cell lines expressing the Hepatitis C Virus (HCV) core protein. Oncogene 20:2606-2610, 2001

34. Bürckstümmer T, Kriegs M, Lupberger J, et al: Raf-1 kinase associates with Hepatitis C virus NS5A and regulates viral replication. FEBS Lett 580:575-580, 2006

35. Schmitz KJ, Wohlschlaeger J, Lang H, et al: Activation of the ERK and AKT signalling pathway predicts poor prognosis in hepatocellular carcinoma and ERK activation in cancer tissue is associated with hepatitis C virus infection. J Hepatol 48:83-90, 2008

36. Himmelsbach K, Sauter D, Baumert TF, et al: New aspects of an anti-tumour drug: Sorafenib efficiently inhibits HCV replication. Gut 58:1644-1653, 2009

37. Wilhelm SM, Carter C, Tang L, et al: BAY 43-9006 exhibits broad spectrum oral antitumor activity and targets the RAF/MEK/ERK pathway and receptor tyrosine kinases involved in tumor progression and angiogenesis. Clin Cancer Res 64:7099-7109, 2004

38. Chen KF, Tai WT, Huang JW, et al: Sorafenib derivatives induce apoptosis through inhibition of STAT3 independent of Raf. Eur J Med Chem 46: 2845-2851, 2011

39. Tai WT, Cheng AL, Shiau CW, et al: Signal transducer and activator of transcription 3 is a major kinase-independent target of sorafenib in hepatocellular carcinoma. J Hepatol 55:1041-1048, 2011

40. Ou DL, Shen YC, Yu SL, et al: Induction of DNA damage-inducible gene GADD45beta contributes to sorafenib-induced apoptosis in hepatocellular carcinoma cells. Cancer Res 70:9309-9318, 2010

41. Llovet JM, Di Bisceglie AM, Bruix J, et al: Design and endpoints of clinical trials in hepatocellular carcinoma. J Natl Cancer Inst 100:698-711, 2008

42. Lencioni R, Llovet JM: Modified RECIST (mRECIST) assessment for hepatocellular carcinoma. Semin Liver Dis 30:52-60, 2010

43. Je Y, Schutz FA, Choueiri TK: Risk of bleeding with vascular endothelial growth factor receptor tyrosine-kinase inhibitors sunitinib and sorafenib: A systematic review and meta-analysis of clinical trials. Lancet Oncol 10:967-974, 2009

44. Raymond E, Dahan L, Raoul JL, et al: Sunitinib malate for the treatment of pancreatic neuroendocrine tumors. N Engl J Med 364:501-513, 2011

45. Escudier B, Roigas J, Gillessen S, et al: Phase II study of sunitinib administered in a continuous once-daily dosing regimen in patients with cytokine-refractory metastatic renal cell carcinoma. J Clin Oncol 27:4068-4075, 2009

46. George S, Blay JY, Casali PG, et al: Clinical evaluation of continuous daily dosing of sunitinib malate in patients with advanced gastrointestinal stromal tumour after imatinib failure. Eur J Cancer 45:1959-1968, 2009

Acknowledgment

We thank all the participating patients and their families, as well as the global network of investigators, research nurses, study coordinators, and operations staff. In addition, we are grateful to Olga Valota (study clinician, Pfizer) for critically reviewing the manuscript. Medical writing support was provided by Molly Heitz at ACUMED (Tytherington, United Kingdom) and was funded by Pfizer.

Appendix

Supplementary patients and methods. Other inclusion criteria comprised: cirrhotic status Child-Pugh A; Eastern Cooperative Oncology Group performance status 0 or 1; measurable disease according to Response Evaluation Criteria in Solid Tumors[20]; and adequate hepatic, renal, and hematologic function (neutrophils $\geq$ 1,500/μL; platelets $\geq$ 75,000/μL; serum AST and ALT $\leq 5\times$ the upper limit of normal; and total bilirubin $<$ 2 mg/dL or $\leq$ 3 mg/dL with albumin $>$ 3.5 g/dL). Key exclusion criteria were: prior local therapy within 4 weeks of study entry or any prior systemic therapy or previous liver transplantation; clinically relevant ascites; National Cancer Institute Common Terminology Criteria for Adverse Events version 3.0 grade $\geq$ 3 hemorrhage within 4 weeks of starting study treatment or documented variceal hemorrhage (any grade) within 12 months of study entry; esophageal varices at risk of bleeding or serious or nonhealing wound or ulcer, or history of abdominal fistula, gastrointestinal perforation, or intra-abdominal abscess within 28 days of study entry; or uncontrolled hypertension ($>$ 150/100 mmHg) despite optimal treatment.

Table A1. Grade 5 Adverse Events of All Causes Reported in at Least Two Patients per Arm

	Sunitinib (n = 526)		Sorafenib (n = 542)	
Grade 5 Event	No. of Patients	%	No. of Patients	%
Disease progression	63	12.0	63	11.6
Esophageal varices/GI hemorrhage*	6	1.2	2	0.4
Cerebral hemorrhage	2	0.4	0	
Hepatic encephalopathy	2	0.4	1	0.1
Liver carcinoma rupture	2	0.4	0	
Renal failure	2	0.4	1	0.1
Hepatic failure	1	0.2	3	0.6
Sepsis	0		3	0.6

*Includes tumor hemorrhage.

VOLUME 31 · NUMBER 28 · OCTOBER 1 2013

JOURNAL OF CLINICAL ONCOLOGY

ORIGINAL REPORT

Brivanib Versus Sorafenib As First-Line Therapy in Patients With Unresectable, Advanced Hepatocellular Carcinoma: Results From the Randomized Phase III BRISK-FL Study

Philip J. Johnson, Shukui Qin, Joong-Won Park, Ronnie T.P. Poon, Jean-Luc Raoul, Philip A. Philip, Chih-Hung Hsu, Tsung-Hui Hu, Jeong Heo, Jianming Xu, Ligong Lu, Yee Chao, Eveline Boucher, Kwang-Hyub Han, Seung-Woon Paik, Jorge Robles-Aviña, Masatoshi Kudo, Lunan Yan, Abhasnee Sobhonslidsuk, Dmitry Komov, Thomas Decaens, Won-Young Tak, Long-Bin Jeng, David Liu, Rana Ezzeddine, Ian Walters, and Ann-Lii Cheng

See accompanying editorial on page 3483 and articles on pages 3501 and 3509

Author affiliations appear at the end of this article.

Published online ahead of print at www.jco.org on August 26, 2013.

Supported by Bristol-Myers Squibb.

Presented at the 63rd Annual Meeting of the American Association for the Study of Liver Diseases, Boston, MA, November 9-13, 2012.

Authors' disclosures of potential conflicts of interest and author contributions are found at the end of this article.

Clinical trial information: NCT00858871.

Corresponding author: Philip J. Johnson, MD, Institute of Translational Medicine, University of Liverpool, Liverpool L69 3BX, United Kingdom; e-mail: Philip.Johnson@liverpool.ac.uk.

0732-183X/13/3128w-3517w/$20.00

DOI: 10.1200/JCO.2012.48.4410

ABSTRACT

Purpose
Brivanib is a dual inhibitor of vascular-endothelial growth factor and fibroblast growth factor receptors that are implicated in the pathogenesis of hepatocellular carcinoma (HCC). Our multinational, randomized, double-blind, phase III trial compared brivanib with sorafenib as first-line treatment for HCC.

Patients and Methods
Advanced HCC patients who had no prior systemic therapy were randomly assigned (ratio, 1:1) to receive sorafenib 400 mg twice daily orally (n = 578) or brivanib 800 mg once daily orally (n = 577). Primary end point was overall survival (OS). Secondary end points included time to progression (TTP), objective response rate (ORR), disease control rate (DCR) based on modified Response Evaluation Criteria in Solid Tumors (mRECIST), and safety.

Results
The primary end point of OS noninferiority for brivanib versus sorafenib in the per-protocol population (n = 1,150) was not met (hazard ratio [HR], 1.06; 95.8% CI, 0.93 to 1.22), based on the prespecified margin (upper CI limit for HR ≤ 1.08). Median OS was 9.9 months for sorafenib and 9.5 months for brivanib. TTP, ORR, and DCR were similar between the study arms. Most frequent grade 3/4 adverse events for sorafenib and brivanib were hyponatremia (9% and 23%, respectively), AST elevation (17% and 14%), fatigue (7% and 15%), hand-foot-skin reaction (15% and 2%), and hypertension (5% and 13%). Discontinuation as a result of adverse events was 33% for sorafenib and 43% for brivanib; rates for dose reduction were 50% and 49%, respectively.

Conclusion
Our study did not meet its primary end point of OS noninferiority for brivanib versus sorafenib. However, both agents had similar antitumor activity, based on secondary efficacy end points. Brivanib had an acceptable safety profile, but was less well-tolerated than sorafenib.

J Clin Oncol 31:3517-3524. © 2013 by American Society of Clinical Oncology

INTRODUCTION

Hepatocellular carcinoma (HCC) is the third leading cause of cancer-related death worldwide.[1] Patients often present with unresectable, recurrent, or metastatic HCC, for which chemotherapy has been shown to be ineffective.[2,3] As HCC is a vascularized tumor, one approach to treatment is to target angiogenic factors, such as vascular endothelial growth factor (VEGF). Sorafenib, a multikinase inhibitor that targets multiple signaling pathways including VEGF signaling, is the only systemic agent to demonstrate overall survival (OS) benefit as first-line therapy in advanced HCC.[4,5] However, disease control with sorafenib is short-lived, some patients are intolerant of sorafenib, and the median survival rate is still less than 1 year. Thus, more effective first-line treatments for advanced HCC are needed.[3]

Like VEGF, fibroblast growth factor (FGF) is a key driver of angiogenesis in HCC.[6] FGF may have direct and indirect effects on tumors.[7-12] Upregulation of alternate angiogenic signals, such as FGF,

may play a role in evasive resistance to VEGF-targeted therapy.[13-16] Notably, the combined administration of anti-FGF and anti-VEGF antibodies in a mouse HCC model has shown additive antitumor activity.[17] Thus, targeting both VEGF and FGF may offer therapeutic advantages over a blockade of VEGF alone.

Brivanib, a tyrosine kinase inhibitor, is an orally active, selective, dual inhibitor of FGF and VEGF signaling.[18] Brivanib had antiangiogenic and antiproliferative effects on tumor cells from multiple tumor types, including liver.[18-20] Brivanib demonstrated antitumor activity in xenograft HCC models expressing FGF receptors and in those resistant to sorafenib.[20-22] In a phase II study, brivanib showed evidence of antitumor activity in patients with previously untreated advanced HCC as well as in those who had experienced prior antiangiogenic therapy failure.[23,24] In the phase III BRISK-PS study of HCC patients who experienced sorafenib treatment failure, brivanib did not significantly improve OS as compared with placebo but did demonstrate improved time to progression (TTP), objective response rate (ORR), and disease control rate (DCR) according to modified Response Evaluation Criteria in Solid Tumors (mRECIST).[25] Herein, we present the results from a phase III study comparing brivanib with sorafenib as first-line therapy in patients with unresectable, advanced HCC.

PATIENTS AND METHODS

Ethics and Study Management

The study (No. NCT00858871) was approved by the institutional review board or ethics committee at each participating center and was conducted according to Good Clinical Practice guidelines, the Declaration of Helsinki, and local laws. The study was monitored for safety and disease status by an independent Data Monitoring Committee, and an interim analysis for futility was performed.

Patients

Adults with advanced HCC who had no prior systemic therapy were eligible. Advanced disease was defined as disease not eligible for surgical and/or locoregional therapies, or progressive disease after surgical and/or locoregional therapies. Other key inclusion criteria included a Child-Pugh A liver function score, an Eastern Cooperative Oncology Group performance status (ECOG-PS) score of 0 or 1, and at least one untreated measurable lesion by computed tomography or magnetic resonance imaging. See Appendix Table A1 (online-only) for eligibility criteria.

Trial Design and Treatment

This was a multinational, randomized, double-blind, phase III trial. Eligible patients were randomly assigned centrally (assignment ratio, 1:1) by Interactive Voice Response System to receive brivanib 800 mg once daily orally plus sorafenib-matched placebo or sorafenib 400 mg twice daily orally plus brivanib-matched placebo. Randomization was stratified by ECOG-PS score (0 *v* 1), extrahepatic spread and/or vascular invasion (yes *v* no), and study site. Dose reductions for toxicity were permitted (Appendix Table A2). Treatment continued until unacceptable toxicity or disease progression. Treatment could continue beyond radiographic progression if the investigator determined that the patient was benefiting from the blinded treatment.

Assessments

The primary end point of the study was OS, defined as the time from randomization until the date of death from any cause. Secondary end points were TTP, ORR, DCR based on mRECIST, and safety. TTP was defined as the time from randomization to radiographic disease progression, ORR as the percentage of randomly assigned patients with complete response or partial response, DCR as the percentage of randomly assigned patients with complete response, partial response, or stable disease. Tumor measurements were performed at screening and every 6 weeks during treatment by contrast-enhanced, dual-phase spiral computed tomography or magnetic resonance imaging. A complete or partial response was confirmed by a second tumor measurement at least 4 weeks after the first assessment. Scans were assessed by the investigators using mRECIST for HCC.[3,26,27] The mRECIST for HCC takes into account the induction of intratumoral necrotic areas (using contrast-enhanced radiologic imaging) in estimating the decrease in viable tumor load rather than just a reduction in overall tumor size (modified WHO criteria or standard RECIST).

Safety was assessed in patients who received at least one dose of study therapy. Adverse events (AEs) were graded using National Cancer Institute Common Terminology Criteria for Adverse Events (version 3.0). Quality of life was assessed by several instruments including the European Organisation for Research and Treatment of Cancer Quality of Life Questionnaire C30 (EORTC QLQ-C30). Physical and role function scores of the EORTC QLQ-C30 questionnaire are presented, as these scores are representative of the patients' overall health status. The QLQ-C30 was self-administered by patients at baseline, at every 6-week clinic visit, and at the end-of-treatment visit.

Statistical Methods

The primary end point of OS was first tested for noninferiority for brivanib compared with sorafenib in the per-protocol population. Superiority was to be tested if noninferiority was concluded. A prespecified noninferiority margin of 1.08 (the upper limit of the 95% CI for hazard ratio [HR]) corresponding to a 2.8-week decrease in median OS on brivanib versus sorafenib was considered clinically acceptable. Assuming an exponential survival distribution and a median OS of 37.3 weeks (the average of the median OS in the SHARP [46.3 weeks][4] and the Asia-Pacific [28.3 weeks][5] trials), and taking into account one formal interim analysis for futility, it was estimated that 777 deaths were required in the per-protocol population (817 deaths in the intention-to-treat population, assuming a 5% protocol deviation) to have a 90% power to claim noninferiority, given a true HR of 0.85. A minimum observed HR of 0.94 was needed to claim noninferiority. Based on these assumptions, a maximum of 1,182 patients were to be randomly assigned.

The HR of brivanib to sorafenib for OS and its associated two-sided 95.8% CI (based on the interim analysis for futility) were computed using a Cox proportional hazards model stratified by ECOG PS (0 *v* 1), extrahepatic spread and/or vascular invasion (yes *v* no), and region (Asia *v* rest of the world). Median OS and associated 95% CI were estimated using the Kaplan-Meier method. OS was compared between arms using a stratified log-rank test at a two-sided alpha of .042. A Cox proportional-hazards model stratified by the above factors ($\alpha = .05$) was used to evaluate the association of prespecified baseline factors (age, risk factors [hepatitis B or C virus, alcohol], α-fetoprotein, tumor morphologic features, size of the largest tumor nodule, previous locoregional treatment and/or surgery, Child-Pugh score, and major portal vein invasion) with OS and to adjust the treatment effect for these factors. Analyses conducted to determine the *P* value, median, HR, and 95% CIs for TTP were as described for OS. Exact 95% CIs for ORR and DCR were calculated using the Clopper-Pearson method.[28] ORR and DCR in the two arms were compared using a Cochran-Mantel-Haenszel test with associated odds ratio estimates and 95% CIs stratified by the factors used for OS. Changes from baseline of symptom assessment score in physical and role functions at weeks 6 and 12 were compared between the two treatment groups using a Wilcoxon rank-sum test.

RESULTS

Patients

A total of 1,155 patients (intention-to-treat population) with advanced HCC were randomly assigned from May 2009 until August 2011 across Asia (62%), Europe (23%), the Americas (13%), Australia (0.8%), and Africa (0.6%); 1,150 patients were treated (Fig 1). At the time of the final analysis, 62 patients (11%) in the sorafenib arm and 35 patients (6%) in the brivanib arm remained on study. The most common reasons for study discontinuation were disease progression (sorafenib, 53%; brivanib, 46%) and study-drug toxicity (sorafenib,

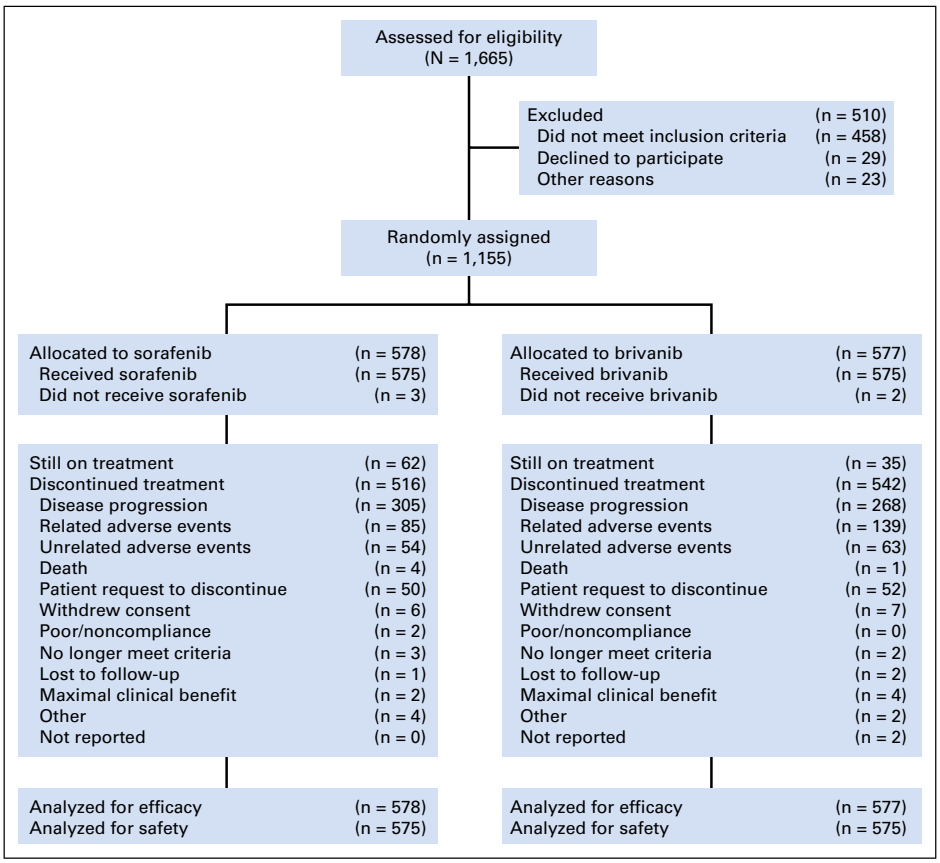

Fig 1. CONSORT diagram of patients with advanced hepatocellular carcinoma who had no prior systemic therapy in the BRISK-FL study, a multicenter, randomized, double-blind, placebo-controlled, phase III trial.

15%; brivanib, 24%). Baseline characteristics of the study population were balanced between the arms (Table 1). Patients had advanced HCC (Barcelona Clinical Liver Cancer stage C, 77%) with good liver function (Child-Pugh A, 92%) and good performance status (ECOG PS 0, 62%). The predominant risk factor was hepatitis B virus infection (44%), followed by hepatitis C virus infection (20%) and alcohol use (16%).

Treatment Exposure

The Kaplan-Meier estimate of the median treatment duration was 4.1 months (95% CI, 3.4 to 4.2) for sorafenib and 3.2 months (95% CI, 2.8 to 3.8) for brivanib. The median of the mean daily dose was 661 mg/d (range, 146 to 1,156 mg/d) for sorafenib and 716 mg/d (range, 204 to 1,070 mg/d) for brivanib. The median cumulative doses were 66,000 mg and 62,400 mg, respectively.

Efficacy

The study did not meet its primary objective of OS noninferiority for brivanib compared with sorafenib. In the per-protocol population (n = 1,150), the HR for brivanib to sorafenib was 1.06 with a 95.8% CI of 0.93 to 1.22 (Table 2). The upper limit of this CI exceeded the prespecified noninferiority boundary of 1.08. The median OS was 9.9 months in the sorafenib arm and 9.5 months in the brivanib arm. OS results were similar in the intention-to-treat population (HR, 1.07; 95.8% CI, 0.94 to 1.23; Fig 2A). A prespecified analysis showed that subset results were consistent with those for the overall study population (Fig 3). A multivariate Cox proportional-hazards model identified the following baseline factors as prognostic of OS: α-fetoprotein, tumor morphologic feature, size of the largest nodule, Child-Pugh score, and major portal vein invasion. After adjusting for the baseline factors, the effect of brivanib or sorafenib on OS remained unchanged (HR, 1.09; 95% CI, 0.95 to 1.25). Proportions of patients who received poststudy systemic treatments were similar between the sorafenib and brivanib arms (21% *v* 22%), as were proportions of poststudy nonsystemic treatments (17% *v* 19%).

TTP was similar between the sorafenib and brivanib arms (Table 2, Fig 2B) as were DCR and ORR (Table 2). In patients with baseline α-fetoprotein $\geq$ 200 ng/mL and at least one on-study α-fetoprotein assessment, α-fetoprotein reduction of $\geq$ 50% relative to baseline was observed in 31% of the sorafenib and 58% of the brivanib patients (Appendix Figure A1). Similar α-fetoprotein reductions were noted when baseline α-fetoprotein cutoff used was the upper limit of the normal or 400 ng/mL.

Safety

AEs (regardless of relationship) that occurred in at least 15% of the treated patients are listed in Table 3. Diarrhea, abdominal pain, constipation, hyperbilirubinemia, elevated AST, elevated ALT, and weight loss occurred at a similar rate in the two study arms. Hand-foot-skin reaction, alopecia, rash, and pyrexia were more frequent among sorafenib patients than with brivanib, whereas decreased appetite, fatigue, hypertension, nausea, vomiting, hyponatremia,

Table 1. Baseline Demographics and Disease Characteristics

Variable	Sorafenib (n = 578) No. of Patients	%	Brivanib (n = 577) No. of Patients	%
Age, years				
Median	60		61	
Range	25-89		19-87	
Sex				
Male	484	84	483	84
Female	94	16	94	16
Region				
Asia	372	64	346	60
Europe	135	23	134	23
Americas	65	11	87	15
Others	6	1	10	2
ECOG PS				
0	352	61	361	64
1	226	39	216	36
Time from initial diagnosis of HCC to start of study therapy, days				
Median	149		138	
Range	4-9,368		2-6,134	
BCLC stage				
A	30	5	37	6
B	97	17	95	17
C	449	78	444	77
Child-Pugh class				
A	531	92	531	92
B	47	8	46	8
Macrovascular invasion				
Yes	158	27	155	27
No	420	73	422	73
Portal vein invasion and/or thrombosis				
Yes	111	19	112	19
No	47	8	43	7
Distant metastasis	291	50	283	49
Lymph node metastasis	161	28	156	27
Direct invasion of adjacent organs	45	8	60	10
Extrahepatic spread and/or macrovascular invasion				
Absent	217	38	216	37
Present	361	62	361	63
Risk factors				
Any	434	75	449	78
Alcohol	83	14	106	18
Hepatitis B	258	45	254	44
Hepatitis C	119	21	116	20
Other	37	6	39	7
Serum alpha-fetoprotein				
No. of patients	563		555	
Median, ng/mL	180		142	
Range, ng/mL	0.6-9.3 $\times$ 10^5		0.4-1.5 $\times$ 10^6	
> 200 ng/mL	278	49	261	47
Previous nonsystemic treatment	326	56	318	55
Liver resection	171	30	162	28
Transcatheter arterial embolization	37	6	32	6
Transcatheter arterial chemoembolization	208	36	204	35
Percutaneous ethanol injection	31	5	29	5
Radiofrequency ablation	98	17	74	13

Abbreviations: BCLC, Barcelona Clinic Liver Cancer Staging System; ECOG PS, Eastern Cooperative Oncology Group performance status; HCC, hepatocellular carcinoma.

Table 2. Summary of Efficacy

Variable	Sorafenib (n = 578) No. of Patients	%	Brivanib (n = 577) No. of Patients	%
Overall survival, per protocol population*				
Median, months	9.9		9.5	
95.8% CI	8.5 to 11.5		8.4 to 10.7	
Hazard ratio	1.06			
95% CI	0.93 to 1.22			
P†	.3730			
Overall survival, intention-to-treat population				
Median, months	9.9		9.5	
95% CI	8.5 to 11.5		8.3 to 10.6	
Hazard ratio	1.07			
95.8% CI	0.94 to 1.23			
P†	.3116			
Time to progression, intention-to-treat population				
Median, months	4.1		4.2	
95% CI	3.1 to 4.2		4.1 to 4.3	
Hazard ratio	1.01			
95% CI	0.88 to 1.16			
P†	.8532			
Best response, intention-to-treat population‡				
Complete response	5	1	2	< 1
Partial response	46	8	67	12
Stable disease	323	56	309	54
Progressive disease	138	24	94	16
Unable to assess	66	11	105	18
Objective response rate				
%	9			12
95% CI	7 to 11		9 to 15	
Odds ratio	1.45			
95% CI	0.99 to 2.13			
P§	.0569			
Disease control rate	65			66
95% CI	61 to 69		61 to 69	
Odds ratio	1.02			
95% CI	0.80 to 1.30			
P§	.8739			

Abbreviation: HCC, hepatocellular carcinoma.
*575 patients in each study arm.
†Stratified log-rank test.
‡Based on investigator assessments using modified RECIST for HCC.
§Cochran-Mantel-Haenszel test.

headache, dysphonia, and dizziness were more frequent among brivanib patients. The most frequent grade 3 AEs were hand-foot-skin reactions in the sorafenib arm and hyponatremia, fatigue, and hypertension in the brivanib arm. Grade 4 events were infrequent.

The rate of treatment discontinuation as a result of AEs was 33% with sorafenib patients and 43% with brivanib. The most frequent AEs leading to treatment discontinuation were hyperbilirubinaemia (3%) and AST elevations (2%) in the sorafenib arm; fatigue (5%), hyponatremia (2%), decreased appetite (2%), hyperbilirubinemia (2%), and AST elevations (2%) in the brivanib arm.

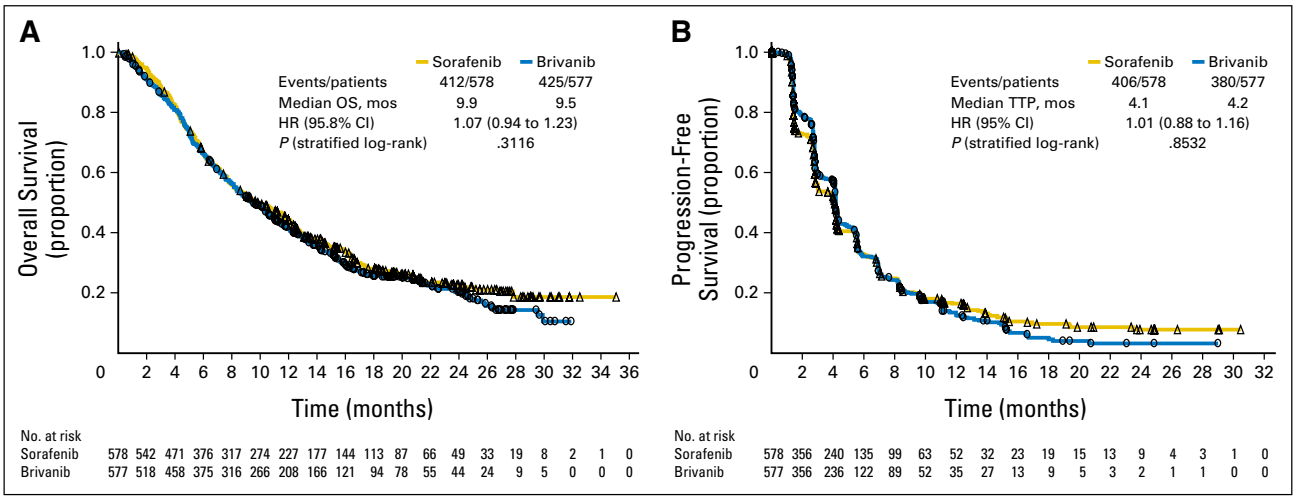

Fig 2. Kaplan-Meier estimates of overall survival (OS) and time to progression (TTP). (A) OS was computed based on the intention-to-treat (ITT) population. Patients who had not died or who were lost to follow-up were censored on the last date on which they were known to have been alive. (B) TTP was computed based on the ITT population. Patients whose disease had not progressed were censored on the date of last tumor assessment. Patients who had no on-study tumor assessments or who had no independent radiologic review were also censored on the date of random assignment. HR, hazard ratio.

The rate of dose reduction was similar between sorafenib and brivanib patients (50% *v* 49%). The rate of dose interruption was 58% in both treatment arms. In the sorafenib arm, dermatologic events were the dominant reason for both dose reduction (20% *v* 2% for brivanib) and dose interruption (21% *v* 3% for brivanib). No single AE caused dose reduction or interruption in more than 7% of brivanib-treated patients.

The overall incidence of serious AEs was 48% for sorafenib patients and 56% for brivanib patients. The most frequent serious AEs (grades 1 to 5) in the sorafenib arm were malignant neoplasm

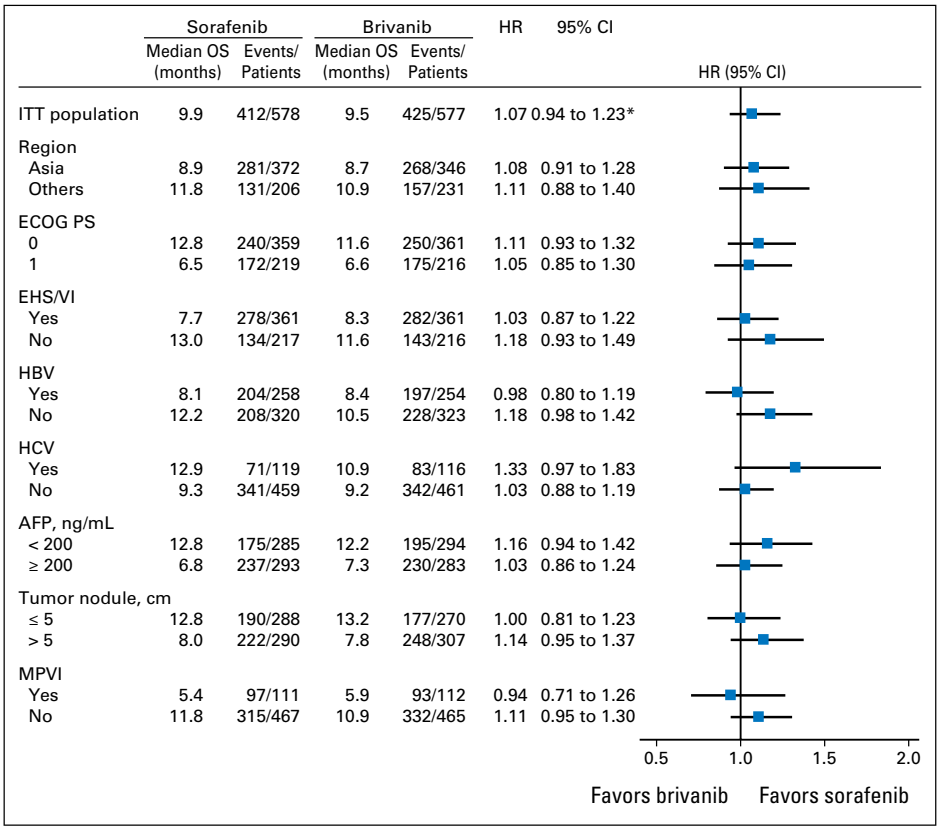

Fig 3. Overall survival (OS) in selected subsets. AFP, α-fetoprotein; ECOG PS, Eastern Cooperative Oncology Group performance status; EHS/VI, extrahepatic spread and/or vascular invasion; HBV, hepatitis B virus; HCV, hepatitis C virus; HR, hazard ratio; ITT, intention-to-treat; MPVI, major portal vein invasion. (*) 95.8% CI.

Table 3. Incidence of Adverse Events by Percentage of Patients

Adverse Event	Sorafenib (n = 575)			Brivanib (n = 575)		
	Any Grade	Grade 3	Grade 4	Any Grade	Grade 3	Grade 4
Overall incidence	99	55	10	98	52	15
Decreased appetite	35	3	0	52	8	0.3
Fatigue	35	7	0	52	14	0.5
Hand-foot-skin reaction	52	15	0	18	2	0
Diarrhea	50	7	0	49	6	0.3
Hypertension	27	5	0.3	41	13	0.3
Nausea	19	0.3	0	38	2	0
Abdominal pain	32	5	0.3	32	6	1
Vomiting	16	0.5	0	27	3	0
AST increased	26	15	2	25	13	2
Hyponatremia	11	9	0.2	26	20	3
Alopecia	22	NA	NA	2	NA	NA
Pyrexia	21	0.3	0	15	0.5	0
Rash	21	2	0	10	1	0
Weight decreased	21	2	0	21	4	0
ALT increased	18	7	1	19	7	0.3
Headache	11	0.3	0	19	1	0
Hyperbilirubinemia	18	7	2	19	10	2
Constipation	16	0.2	0	18	0.3	0
Dysphonia	10	0	0	18	0	0
Dizziness	7	0.3	0	17	1	0

NOTE. Listed are adverse events (any grade, any cause) that occurred in at least 15% of the patients in either group.
Abbreviation: NA, not applicable.

Table 4. Quality of Life by EORTC QLQ-C30 Questionnaire

Variable	Sorafenib	Brivanib	*P**
Physical function			
Baseline point score			.3181
No. of patients	557	551	
Mean	83	83	
SD	17	17	
Median	87	87	
Range	0-100	0-100	
Change in point score at week 12 from baseline			.0002
No. of patients	423	396	
Mean	−18	−24	
SD	28	29	
Median	−7	−13	
Range	−100-87	−100-53	
Role function			
Baseline point score			.6061
No. of patients	557	551	
Mean	84	85	
SD	25	23	
Median	100	100	
Range	0-100	0-100	
Change in point score at week 12 from baseline			.0002
No. of patients	421	396	
Mean	−20	−28	
SD	33	34	
Median	−17	−33	
Range	−100-83	−100-67	

Abbreviations: EORTC QLC-C30, European Organisation for Research and Treatment of Cancer Quality of Life Questionnaire C30; SD, standard deviation.
*Based on comparison of brivanib to sorafenib using the Wilcoxon rank-sum test.

progression (14%), fatigue (2%), and hyponatremia (1%); the corresponding rates for brivanib patients were 13%, 5%, and 5%, respectively. Hepatic encephalopathy was reported as serious in 2% of sorafenib and 3% of brivanib patients. Serious AEs are listed in Appendix Table A3.

Overall patient deaths (sorafenib, 71%; brivanib, 74%), and deaths within 30 days of the last dose (sorafenib, 17%; brivanib, 16%) were similar between the two arms. The primary reason for death within 30 days of the last dose was disease progression (sorafenib, 13%; brivanib, 11%). Six patient deaths (sorafenib, one patient; brivanib, five patients) attributed by the investigators to study drug toxicity occurred within 30 days of the last dose. There were five additional treatment-related deaths (sorafenib, one patient; brivanib, four patients) that occurred after the 30 days after the last dose. Two treatment-related deaths in the sorafenib arm were as a result of esophageal variceal hemorrhage and myocardial ischemia. Nine treatment-related deaths in the brivanib arm were ascribed to hepatic failure, upper gastrointestinal hemorrhage, cardiorespiratory arrest/abdominal pain, depressed level of consciousness/cerebral infarction/cerebral hemorrhage, diarrhea/vomiting, cerebrovascular accident, asthenia/nausea, gastrointestinal hemorrhage, and hematemesis.

Quality of Life

At baseline, mean and median scores in physical function and role function, as assessed by the EORTC QLQ-C30 questionnaire, were similar in the two treatment arms (Table 4). After 12 weeks of treatment, mean and median scores in physical function and role function declined in both arms. The decline was more pronounced among brivanib patients than sorafenib patients.

DISCUSSION

Despite the success of sorafenib in the first-line treatment of advanced HCC, a need for safer and more effective treatments remains. This phase III study compared brivanib with sorafenib as first-line therapy in this patient population. The study did not meet its primary objective of OS noninferiority for brivanib versus sorafenib, because the upper limit of the CI for the HR exceeded the prespecified margin of 1.08. The difference in median OS for sorafenib and brivanib was 2.0 weeks in favor of sorafenib. The median OS for sorafenib (9.9 months) in this well-controlled study involving a large patient population is closer to that in the SHARP trial (10.7 months) than to that in the Asia-Pacific study (6.5 months), even though the majority of the patients in our study (64%) were from the Asia-Pacific region.[4,5] Although the underlying reason for the discrepancy in median OS is unclear, differences in baseline factors prognostic for OS between these studies, such as ECOG-PS, may have contributed to this.

The median OS of 9.5 months for brivanib is consistent with results from previously reported phase II and III trials of brivanib

in advanced HCC.[23-25] The phase II study showed a median OS of 10 months in previously untreated patients and 9.8 months in patients who had prior antiangiogenic therapies, whereas a median OS of 9.4 months was reported in the phase III trial of patients who were intolerant to or experienced sorafenib failure.[23-25] Data for secondary efficacy end points showed that both brivanib and sorafenib had similar antitumor activity in our study. TTP, DCR, and ORR were all comparable between the drugs. The rate of α-fetoprotein reduction was higher with brivanib. These data are consistent with those in the phase III BRISK-PS study of post-sorafenib HCC patients, in which brivanib improved TTP, ORR, and DCR and reduced α-fetoprotein compared with placebo.[25] It should be noted that ORR in our study was higher than historical data for sorafenib.[4,5] This higher rate is likely a reflection of the use of mRECIST for HCC that is believed to better capture tumor response to targeted therapies in HCC patients by differentiating viable tumors from necrotic tissues.[3,26,27]

Overall, brivanib had an acceptable safety profile. There were no new or unexpected safety findings with either agent. Certain AEs typical of VEGF inhibition were more frequent with brivanib than with sorafenib, consistent with brivanib being a more potent VEGF inhibitor. Skin toxicities including hand-foot-skin reaction were more common with sorafenib than with brivanib, whereas hyponatremia was reported more frequently with brivanib, suggesting that these AEs are compound-specific. Similar results for skin toxicities and hyponatremia were reported in previous studies evaluating brivanib in various cancer types including HCC, sarcoma, ovarian, and colorectal cancers.[23-25,29-32] Causes for 11 patient deaths (sorafenib, two patients; brivanib, nine patients) considered by investigators to be treatment-related were not unusual for this patient population.

Brivanib appeared to be less well-tolerated than sorafenib, based on overall safety profile and treatment discontinuation. Although treatment discontinuation owing to AEs was more frequent with brivanib than with sorafenib, the rate of dose reduction/interruption was similar for both agents. Given the clinical relevance of skin toxicities for sorafenib therapy, it is noteworthy that skin toxicities caused dose reduction/interruption in 20% to 21% of the sorafenib-treated patients versus 2% to 3% of the brivanib-treated ones. In our study, declines in physical and role functions were more pronounced in the brivanib arm than in the sorafenib arm. The differences between arms were represented by six points for physical function and eight points for role function. However, though the decrease in both domains was statistically greater for brivanib compared with sorafenib, the clinical impact of these differences remains unclear.[33]

The present data underscore the difficulty in developing drugs for HCC, a disease with complex molecular abnormalities. A large phase III study evaluating sunitinib against sorafenib in the first-line treatment of advanced HCC was halted at the interim analysis, because of an unfavorable risk-benefit profile for sunitinib versus sorafenib.[34] Interestingly, in the sunitinib study, patients with prior Hepatitis C infection had a longer OS rate with sorafenib than with sunitinib. In our study, sorafenib seemed to have longer OS than brivanib in patients with prior Hepatitis C, but no conclusion can be drawn because of the exploratory nature associated with subset analyses. Though both sorafenib and sunitinib inhibit VEGF and platelet-derived growth factor signaling, sorafenib is also a potent inhibitor of raf kinase, raising the intriguing possibility that raf kinase inhibition may contribute to the therapeutic effects of sorafenib.[35] Further understanding of the disease at the molecular level should help select patient subtypes most likely to benefit from a specific treatment.

In conclusion, this study did not meet its primary OS objective in the first-line treatment of advanced HCC, based on a noninferiority statistical design, but it did show similar antitumor activity for brivanib and sorafenib, based on TTP, ORR, and DCR data. Brivanib had an acceptable safety profile; however, it was less well-tolerated than sorafenib.

AUTHORS' DISCLOSURES OF POTENTIAL CONFLICTS OF INTEREST

Although all authors completed the disclosure declaration, the following author(s) and/or an author's immediate family member(s) indicated a financial or other interest that is relevant to the subject matter under consideration in this article. Certain relationships marked with a "U" are those for which no compensation was received; those relationships marked with a "C" were compensated. For a detailed description of the disclosure categories, or for more information about ASCO's conflict of interest policy, please refer to the Author Disclosure Declaration and the Disclosures of Potential Conflicts of Interest section in Information for Contributors.
Employment or Leadership Position: David Liu, Bristol-Myers Squibb (C); Rana Ezzeddine, Bristol-Myers Squibb (C); Ian Walters, Bristol-Myers Squibb (C) **Consultant or Advisory Role:** Philip J. Johnson, Bristol-Myers Squibb (C); Joong-Won Park, Taiho Pharmaceutical (C); Ronnie T.P. Poon, Bristol-Myers Squibb (C); Jean-Luc Raoul, Bristol-Myers Squibb (C), Bayer Schering Pharma (C); Philip A. Philip, Bristol-Myers Squibb (C), Roche (C), Bayer (C); Ann-Lii Cheng, Eisai (C), Bayer HealthCare (C) **Stock Ownership:** David Liu, Bristol-Myers Squibb; Rana Ezzeddine, Bristol-Myers Squibb; Ian Walters, Bristol-Myers Squibb **Honoraria:** Philip J. Johnson, Bayer Healthcare; Joong-Won Park, Bayer Healthcare; Jean-Luc Raoul, Bayer Schering Pharma; Philip A. Philip, Bristol-Myers Squibb, Sanofi-Aventis, Bayer; Ann-Lii Cheng, Eisai, Bayer HealthCare **Research Funding:** Philip A. Philip, Bristol-Myers Squibb, Lilly, Bayer; Chih-Hung Hsu, Bristol-Myers Squibb; Seung-Woon Paik, Bristol-Myers Squibb, Bayer **Expert Testimony:** None **Patents:** None **Other Remuneration:** Philip J. Johnson, Bristol-Myers Squibb

AUTHOR CONTRIBUTIONS

Conception and design: Philip J. Johnson, Joong-Won Park, Ronnie T.P. Poon, Philip A. Philip, Ian Walters, Ann-Lii Cheng
Provision of study materials or patients: Shukui Qin, Jean-Luc Raoul, Philip A. Philip, Chih-Hung Hsu, Jeong Heo, Ligong Lu, Eveline Boucher, Jorge Robles-Aviña, Masatoshi Kudo, Lunan Yan, Thomas Decaens
Collection and assembly of data: Philip J. Johnson, Shukui Qin, Joong-Won Park, Ronnie T.P. Poon, Chih-Hung Hsu, Tsung-Hui Hu, Jeong Heo, Jianming Xu, Ligong Lu, Yee Chao, Eveline Boucher, Kwang-Hyub Han, Jorge Robles-Aviña, Masatoshi Kudo, Lunan Yan, Abhasnee Sobhonslidsuk, Thomas Decaens, Won-Young Tak, Long-Bin Jeng, David Liu, Rana Ezzeddine, Ian Walters
Data analysis and interpretation: Philip J. Johnson, Shukui Qin, Jean-Luc Raoul, Tsung-Hui Hu, Seung-Woon Paik, Dmitry Komov, David Liu, Rana Ezzeddine, Ian Walters
Manuscript writing: All authors
Final approval of manuscript: All authors

REFERENCES

1. Jemal A, Bray F, Center MM, et al: Global cancer statistics. CA Cancer J Clin 61:69-90, 2011
2. Cao H, Phan H, Yang LX: Improved chemotherapy for hepatocellular carcinoma. Anticancer Res 32:1379-1386, 2012
3. European Association for the Study of the Liver–European Organisation for Research and Treatment of Cancer: EASL-EORTC clinical practice guidelines: Management of hepatocellular carcinoma. J Hepatol 56:908-943, 2012
4. Llovet JM, Ricci S, Mazzaferro V, et al: Sorafenib in advanced hepatocellular carcinoma. N Engl J Med 359:378-390, 2008
5. Cheng AL, Kang YK, Chen Z, et al: Efficacy and safety of sorafenib in patients in the Asia-Pacific region with advanced hepatocellular carcinoma: A phase III randomised, double-blind, placebo-controlled trial. Lancet Oncol 10:25-34, 2009
6. Presta M, Dell'Era P, Mitola S, et al: Fibroblast growth factor/fibroblast growth factor receptor system in angiogenesis. Cytokine Growth Factor Rev 16:159-178, 2005
7. Grose R, Dickson C: Fibroblast growth factor signaling in tumorigenesis. Cytokine Growth Factor Rev 16:179-186, 2005
8. Mise M, Arii S, Higashituji H, et al: Clinical significance of vascular endothelial growth factor and basic fibroblast growth factor gene expression in liver tumor. Hepatology 23:455-464, 1996
9. Ogasawara S, Yano H, Iemura A, et al: Expressions of basic fibroblast growth factor and its receptors and their relationship to proliferation of human hepatocellular carcinoma cell lines. Hepatology 24: 198-205, 1996
10. El-Assal ON, Yamanoi A, Ono T, et al: The clinicopathological significance of heparanase and basic fibroblast growth factor expressions in hepatocellular carcinoma. Clin Cancer Res 7:1299-1305, 2001
11. Uematsu S, Higashi T, Nouso K, et al: Altered expression of vascular endothelial growth factor, fibroblast growth factor-2 and endostatin in patients with hepatocellular carcinoma. J Gastroenterol Hepatol 20:583-588, 2005
12. Poon RT, Ng IO, Lau C, et al: Correlation of serum basic fibroblast growth factor levels with clinicopathologic features and postoperative recurrence in hepatocellular carcinoma. Am J Surg 182:298-304, 2001
13. Casanovas O, Hicklin DJ, Bergers G, et al: Drug resistance by evasion of antiangiogenic targeting of VEGF signaling in late-stage pancreatic islet tumors. Cancer Cell 8:299-309, 2005
14. Bergers G, Hanahan D: Modes of resistance to anti-angiogenic therapy. Nat Rev Cancer 8:592-603, 2008
15. Pàez-Ribes M, Allen E, Hudock J, et al: Antiangiogenic therapy elicits malignant progression of tumors to increased local invasion and distant metastasis. Cancer Cell 15:220-231, 2009
16. Ebos JM, Lee CR, Cruz-Munoz W, et al: Accelerated metastasis after short-term treatment with a potent inhibitor of tumor angiogenesis. Cancer Cell 15:232-239, 2009
17. Wang L, Park H, Chhim S, et al: A novel monoclonal antibody to fibroblast growth factor 2 effectively inhibits growth of hepatocellular carcinoma xenografts. Mol Cancer Ther 11:864-872, 2012
18. Cai ZW, Zhang Y, Borzilleri RM, et al: Discovery of brivanib alaninate ((S)-((R)-1-(4-(4-fluoro-2-methyl-1H-indol-5-yloxy)-5-methylpyrrolo[2,1-f][1,2,4] triazin-6-yloxy)propan-2-yl)2-aminopropanoate), a novel prodrug of dual vascular endothelial growth factor receptor-2 and fibroblast growth factor receptor-1 kinase inhibitor (BMS-540215). J Med Chem 51:1976-1980, 2008
19. Huynh H, Ngo VC, Fargnoli J, et al: Brivanib alaninate, a dual inhibitor of vascular endothelial growth factor receptor and fibroblast growth factor receptor tyrosine kinases, induces growth inhibition in mouse models of human hepatocellular carcinoma. Clin Cancer Res 14:6146-6153, 2008
20. Bhide RS, Lombardo LJ, Hunt JT, et al: The antiangiogenic activity in xenograft models of brivanib, a dual inhibitor of vascular endothelial growth factor receptor-2 and fibroblast growth factor receptor-1 kinases. Mol Cancer Ther 9:369-378, 2010
21. Allen E, Walters IB, Hanahan D: Brivanib, a dual FGF/VEGF inhibitor, is active both first and second line against mouse pancreatic neuroendocrine tumors developing adaptive/evasive resistance to VEGF inhibition. Clin Cancer Res 17:5299-5310, 2011
22. Tovar V, Cornella, Villanueva A: FGF signaling is involved in acquired resistance to sorafenib in an in vivo model of hepatocellular carcinoma. Presented at the International Liver Cancer Association Conference, Hong Kong, China, September 2-4, 2011 (abstr 0-006)
23. Park JW, Finn RS, Kim JS, et al: Phase II, open-label study of brivanib as first-line therapy in patients with advanced hepatocellular carcinoma. Clin Cancer Res 17:1973-1983, 2011
24. Finn RS, Kang YK, Mulcahy M, et al: Phase II, open-label study of brivanib as second-line therapy in patients with advanced hepatocellular carcinoma. Clin Cancer Res 18:2090-2098, 2012
25. Llovet JM, Decaens T, Raoul J-L, et al: Brivanib in patients with advanced hepatocellular carcinoma who were intolerant to sorafenib or for whom sorafenib failed: Results from the randomized phase III BRISK-PS study. J Clin Oncol 31:3509-3516, 2013
26. Edeline J, Boucher E, Rolland Y, et al: Comparison of tumor response by Response Evaluation Criteria in Solid Tumors (RECIST) and modified RECIST in patients treated with sorafenib for hepatocellular carcinoma. Cancer 118:147-156, 2012
27. Lencioni R, Llovet JM: Modified RECIST (mRECIST) assessment for hepatocellular carcinoma. Semin Liver Dis 30:52-60, 2010
28. Clopper CJ, Pearson ES: The use of confidence or fiducial limits illustrated in the case of the binomial. Biometrika 26:404-413, 1934
29. Garrett CR, Siu LL, El-Khoueiry A, et al: Phase I dose-escalation study to determine the safety, pharmacokinetics and pharmacodynamics of brivanib alaninate in combination with full-dose cetuximab in patients with advanced gastrointestinal malignancies who have failed prior therapy. Br J Cancer 105:44-52, 2011
30. Kaye SB, Siu LL, Jassem J, et al: Brivanib (B) in advanced ovarian cancer (OC): Subset results of a phase 2 randomized discontinuation trial (RDT). Ann Oncol 23:ix319, 2012 (suppl 9; abstr 9660)
31. Ratain MJ, Schwartz GK, Oza AM, et al: Brivanib (BMS-582664) in advanced solid tumors (AST): Results of a phase II randomized discontinuation trial (RDT). J Clin Oncol 29:213s, 2011(suppl; abstr 3079)
32. Schwartz GK, Maki RG, Ratain MJ, et al: Brivanib (BMS-582664) in advanced soft-tissue sarcoma (STS): Biomarker and subset results of a phase II randomized discontinuation trial. J Clin Oncol 29:605s, 2011 (suppl; abstr 10000)
33. Osoba D, Rodrigues G, Myles J, et al: Interpreting the significance of changes in health-related quality-of-life scores. J Clin Oncol 16:139-144, 1998
34. Cheng A, Kang Y, Lin D, et al: Phase III trial of sunitinib (Su) versus sorafenib (So) in advanced hepatocellular carcinoma (HCC). J Clin Oncol 29: 256s, 2011 (suppl; abstr 4000)
35. MaverickNY: Pharma Strategy Blog: Why does sorafenib work in HCC but sunitinib does not? http://pharmastrategyblog.com/2011/01/why-does-sorafenib-work-in-hcc-but-sunitinib-does-not.html/. (weblog) Accessed on November 29, 2012

Affiliations

Philip J. Johnson, University of Birmingham, Birmingham, United Kingdom; Shukui Qin, Nanjing Bayi Hospital, Nanjing; Jianming Xu, 307 Hospital of PLA, Beijing; Ligong Lu, Guangdong Provincial People's Hospital, Guangdong; Lunan Yan, West China Hospital of Sichuan University, Chengdu; Ronnie T.P. Poon, University of Hong Kong, Hong Kong, Special Administrative Region, People's Republic of China; Joong Won Park, Center for Liver Cancer, National Cancer Center, Goyang; Jeong Heo, Pusan National University School of Medicine, Pusan; Kwang Hyub Han, Yonsei University College of Medicine; Seung Woon Paik, Samsung Medical Center, Sungkyunkwan University School of Medicine, Seoul; Won Young Tak, Kyungpook National University Hospital, Daegu, Republic of Korea; Jean-Luc Raoul, Institut Paoli Calmettes, Marseille; Eveline Boucher, Central Eugene Marquis, Rennes Cedex, Rennes; Thomas Decaens, Hôpital Henri Mondor, University of Paris-Est, and INSERM, Creteil Cedex, Creteil, France; Philip A. Philip, Karmanos Cancer Center, Detroit, MI; David Liu, Rana Ezzeddine, Ian Walters, Bristol-Myers Squibb, Princeton, NJ; Chih-Hung Hsu, Ann-Lii Cheng, National Taiwan University Hospital; Yee Chao, Cancer Center, Taipei Veterans General Hospital, Taipei; Tsung-Hui Hu, Kaohsiung Chang Gung Memorial Hospital and Chang Gung University College of Medicine, Kaohsiung; Long-Bin Jeng, China Medical University Hospital, Taichung, Taiwan, Republic of China; Jorge Robles-Aviña, High Specialty Central South Hospital, Mexico City, Mexico; Masatoshi Kudo, Kinki University School of Medicine, Osaka, Japan; Abhasnee Sobhonslidsuk, Ramathibodi Hospital, Bangkok, Thailand; Dmitriy Komov, N.N. Blokhin Cancer Research Center, Moscow, Russia.

Acknowledgment

We thank our patients and their families around the globe. We also thank the investigators for their enthusiastic participation in the study, Bristol-Myers Squibb Company for sponsoring the trial, and Motasim Billah of Bristol-Myers Squibb Company for providing writing assistance.

Appendix

Table A1. Patient Eligibility Criteria

Inclusion criteria
• Men and women ages 18 years or older
• Histologically or cytologically confirmed, advanced HCC
• Advanced disease was defined as disease not eligible for or progressive after surgical or locoregional therapy
• No prior systemic therapy for HCC
• Locoregional therapy must have been completed at least 3 weeks before the baseline scan
• At least one untreated measurable lesion by MRI or spiral CT
• Cirrhotic status of Child-Pugh Class A
• ECOG performance status 0 or 1
• Life expectancy of at least 12 weeks
• Adequate hematologic function with absolute neutrophil counts $\geq$ 1,500/μL, platelet count $\geq 60 \times 10^9$/L, and hemoglobin $\geq$ 8.5 g/dL
• Adequate hepatic function with serum total bilirubin $\leq$ 3 mg/dL, serum albumin $\geq$ 2.8 g/dL, and ALT and AST $\leq 5 \times$ the institutional ULN
• Amylase and lipase $< 1.5 \times$ ULN
• Adequate renal function with serum creatinine $\leq$ 2.0 mg/dL
• INR $\leq$ 2.3 or PT $\leq$ 6 seconds above control
Exclusion criteria
• Brain metastasis or evidence of leptomeningeal disease
• Known fibrolamellar HCC or mixed cholangiocarcinoma and HCC
• Any encephalopathy
• Any ascites
• Bleeding esophageal or gastric varices within 2 months before inclusion
• Previous or concurrent cancer except cervical carcinoma-in-situ, treated basal cell carcinoma, superficial bladder tumors (Ta, Ti, and T1). Any cancer curatively treated $>$ 5 years before entry is permitted
• History of active cardiac disease including uncontrolled hypertension congestive heart failure, active coronary artery disease, unstable or newly diagnosed angina or myocardial infarction less than 12 months before study, cardiac arrhythmias requiring antiarrhythmic therapy other than beta blockers or digoxin, and valvular heart disease $\geq$ CTCAE grade 2
• QTc (Fridericia) $>$ 450 msec on two consecutive ECGs
• Thrombotic or embolic events within the past 6 months and pulmonary embolism
• Any other hemorrhage/bleeding event $\geq$ CTCAE grade 3 within 8 weeks except for esophageal or gastric varices
• Infection
• History of HIV infection
• Active, untreated hepatitis B virus infection
• Active bacterial infection, fewer than 7 days after completing systemic antibiotic therapy
• History of nonhealing wounds or ulcers, or bone fractures within 3 months of fracture
• Pre-existing thyroid abnormality with thyroid function that cannot be maintained in the normal range with medication
• Hyponatremia with sodium $<$ 130 mmol/L
• Baseline serum potassium $<$ 3.5 mmol/L
• Prior use of any systemic anticancer chemotherapy, immunotherapy, or targeted agents for HCC except for sorafenib
• Radiotherapy within 4 weeks before start of study drug (palliative radiotherapy for symptomatic control was acceptable)

Abbreviations: CT, computed tomography; CTCAE, Common Terminology Criteria for Adverse Events; ECOG, Eastern Cooperative Oncology Group; HCC, hepatocellular carcinoma; INR, international normalized ratio; MRI, magnetic resonance imaging; PT, prothrombin time; ULN, upper limits of normal.

Table A2. Dose Modification Schedule for Toxicity

AE	Occurrence	Dose Modification
Baseline ALT/AST < 2.5 × ULN increase to > 5 × ULN or baseline ALT/AST 2.5-5 × ULN increase to > 10 × ULN	First	• Hold study drugs until ALT/AST ≤ 5 × ULN. • When resuming study drugs, decrease by one dose level from the previous dose level.
	Second	• Hold study drugs until ALT/AST ≤ 5 × ULN. • When resuming study drugs, decrease by one dose level from the previous dose level.
	Third	• Stop study drugs or discuss with medical monitor.
Total bilirubin ≥ 3 × ULN	First	• Hold study drugs until bilirubin < 3 × ULN. • When resuming study drugs, decrease by one dose level from the previous dose level.
	Second	• Hold study drugs until bilirubin < 3 × ULN. • When resuming study drugs, decrease by one dose level from the previous dose level.
	Third	• Stop study drugs or discuss with medical monitor.
Grade 3 hyponatremia <130-120 mmol/L	First	• Continue study drugs and start medical intervention until sodium ≥ 130 mmol/L.
	Persistent for ≥ 7 days or second	• Hold study drugs and start medical intervention. • Resume study drugs when sodium ≥ 130 mmol/L; decrease by one dose level from the previous dose level.
	Third	• Hold study drugs and start medical intervention. • Resume study drugs when sodium ≥ 130 mmol/L; decrease by one dose level from the previous dose level.
	Fourth	• Stop study drugs or discuss with medical monitor.
Grade 4 hyponatremia < 120 mmol/L	First	• Hold study drugs and start medical intervention. • Resume study drugs when sodium ≥ 130 mmol/L; decrease by one dose level from the previous dose level.
	Second	• Stop study drugs or discuss with medical monitor.
Grade 1 skin AEs	Any	• Continue study drugs and consider topical therapy for symptomatic relief.
Grade 2 skin AEs	First	• Continue study drugs and consider topical therapy for symptomatic relief. • If no improvement within 7 days, see next section.
	No improvement within 7 days or second or third occurrence	• Interrupt study drugs until toxicity resolves to grade 0-1. • When resuming treatment, decrease dose by one dose level.
	Fourth	• Stop study drugs.
Grade 3 skin AEs	First or second	• Interrupt study drugs until toxicity resolves to grade 0-1. • When resuming treatment, decrease dose by one dose level.
	Third	• Stop study drugs.
Any other drug-related grade 3 nonhematologic or hematologic toxicity	First	• Hold study drugs. • Resume study drugs when toxicity decreases to ≤ grade 1; decrease by one dose level from the previous dose level.
	Second	• Hold study drugs. • Resume study drugs when toxicity decreases to ≤ grade 1; decrease by one dose level from the previous dose level.
	Third	• Stop study drugs or discuss with medical monitor.
Any other drug-related grade 4 nonhematologic or hematologic toxicity	First	• Stop study drugs or discuss with medical monitor.

NOTE. Two dose reductions were allowed for brivanib with the first at 600 mg once daily and second at 400 mg every other day. Two dose reductions were allowed for sorafenib with the first at 400 mg once daily and second at 400 mg every other day.
Abbreviations: AE, adverse event; ULN, upper limit of normal.

Table A3. Percentage of Patients Experiencing Serious Adverse Events Resulting From Any Cause (> 1% of patients)

Event	Sorafenib (n = 575)				Brivanib (n = 575)			
	Grade 1-5	Grade 3	Grade 4	Grade 5	Grade 1-5	Grade 3	Grade 4	Grade 5
Any	47.8	20.2	5.4	15.3	56.3	25.7	8.9	15.0
Neoplasm malignant*	14.3	2.8	0.5	8.7	12.5	2.8	0.7	7.7
Hyponatremia	1.0	1.0	0	0	5.2	4.3	0.9	0
Fatigue	2.3	1.9	0	0	4.9	3.5	0.2	0
Decreased appetite	1.0	0.9	0	0	3.5	2.8	0.2	0
Hepatic encephalopathy	1.7	0.9	0.7	0.2	3.5	2.4	0.5	0.3
Abdominal pain	2.8	1.4	0.3	0	3.3	2.3	0.3	0.2
Diarrhea	2.3	1.9	0	0	3.1	1.7	0.3	0
Ascites	2.8	1.9	0.2	0	2.4	1.9	0	0
Dehydration	0.5	0	0	0	2.4	1.9	0	0
Hypertension	0.7	0.2	0.3	0	2.4	1.2	0.2	0
Hepatic failure	2.1	0.3	0.2	1.2	2.3	0.5	0.9	0.7
Hyperbilirubinemia	2.1	1.2	0.9	0	2.3	1.9	0.3	0
Vomiting	0.3	0.2	0	0	2.1	1.4	0	0
Esophageal varices hemorrhage	1.6	0.9	0.5	0	1.7	1.0	0.2	0.2
Nausea	0.3	0	0	0	1.6	0.9	0	0.2
Hyperkalemia	0.2	0.2	0	0	1.6	0.9	0.2	0
Abdominal pain upper	1.0	0.7	0	0	1.4	0.9	0	0
Encephalopathy	0.5	0.3	0	0	1.4	0.9	0.3	0
Pyrexia	2.8	0	0	0	1.4	0.2	0	0
Upper GI hemorrhage	1.4	0.7	0.2	0.5	0.7	0.2	0	0.3
AST increased	0.7	0.5	0.2	0	1.2	0.9	0.3	0
Asthenia	1.0	0.7	0	0	1.2	1.0	0	0
Gastrointestinal hemorrhage	1.2	0.3	0.2	0	1.0	0.3	0.2	0.2
General physical health deterioration	0.5	0	0.2	0.2	1.2	1.0	0	0
Hepatic neoplasm malignant	1.2	0.2	0	1.0	1.2	0	0	1.0
Pneumonia	0.7	0.3	0	0	1.2	0.7	0	0.5
Urinary tract infection	0.2	0.2	0	0	1.2	0.9	0	0

*Grade was unknown for 32 patients (5.6%) in the sorafenib group and 20 patients (3.5%) in the brivanib group.

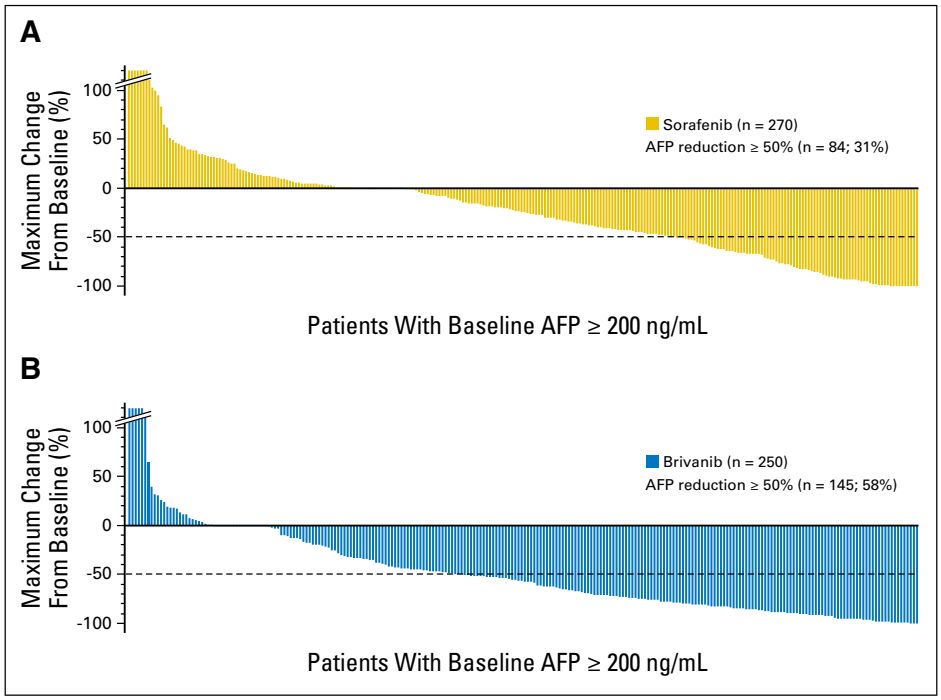

Fig A1. Waterfall plots for changes in serum α-fetoprotein (AFP) relative to baseline in patients with advanced hepatocellular carcinoma treated with (A) sorafenib or (B) brivanib. Plotted were the patients who had baseline assessments and at least one on study assessment.

VOLUME 31 · NUMBER 28 · OCTOBER 1 2013

JOURNAL OF CLINICAL ONCOLOGY

ORIGINAL REPORT

Brivanib in Patients With Advanced Hepatocellular Carcinoma Who Were Intolerant to Sorafenib or for Whom Sorafenib Failed: Results From the Randomized Phase III BRISK-PS Study

Josep M. Llovet, Thomas Decaens, Jean-Luc Raoul, Eveline Boucher, Masatoshi Kudo, Charissa Chang, Yoon-Koo Kang, Eric Assenat, Ho-Yeong Lim, Valerie Boige, Philippe Mathurin, Laetitia Fartoux, Deng-Yn Lin, Jordi Bruix, Ronnie T. Poon, Morris Sherman, Jean-Frédéric Blanc, Richard S. Finn, Won-Young Tak, Yee Chao, Rana Ezzeddine, David Liu, Ian Walters, and Joong-Won Park

See accompanying editorial on page 3483 and articles on pages 3501 and 3517

Author affiliations appear at the end of this article.

Published online ahead of print at www.jco.org on August 26, 2013.

Presented at the 47th Annual Meeting of the European Association of the Study of Liver, Barcelona, Spain, April 18-22, 2012.

Authors' disclosures of potential conflicts of interest and author contributions are found at the end of this article.

Clinical trial information: NCT00825955.

Corresponding author: Josep M. Llovet, MD, Division of Liver Diseases, Icahn School of Medicine at Mount Sinai, 1425 Madison Ave, Room 11F-70, Box 1123, New York, NY 10029; e-mail: josep.llovet@mssm.edu.

0732-183X/13/3128w-3509w/$20.00

DOI: 10.1200/JCO.2012.47.3009

ABSTRACT

Purpose
Brivanib is a selective dual inhibitor of vascular endothelial growth factor and fibroblast growth factor receptors implicated in tumorigenesis and angiogenesis in hepatocellular carcinoma (HCC). An unmet medical need persists for patients with HCC whose tumors do not respond to sorafenib or who cannot tolerate it. This multicenter, double-blind, randomized, placebo-controlled trial assessed brivanib in patients with HCC who had been treated with sorafenib.

Patients and Methods
In all, 395 patients with advanced HCC who progressed on/after or were intolerant to sorafenib were randomly assigned (2:1) to receive brivanib 800 mg orally once per day plus best supportive care (BSC) or placebo plus BSC. The primary end point was overall survival (OS). Secondary end points included time to progression (TTP), objective response rate (ORR), and disease control rate based on modified Response Evaluation Criteria in Solid Tumors (mRECIST) and safety.

Results
Median OS was 9.4 months for brivanib and 8.2 months for placebo (hazard ratio [HR], 0.89; 95.8% CI, 0.69 to 1.15; $P = .3307$). Adjusting treatment effect for baseline prognostic factors yielded an OS HR of 0.81 (95% CI, 0.63 to 1.04; $P = .1044$). Exploratory analyses showed a median time to progression of 4.2 months for brivanib and 2.7 months for placebo (HR, 0.56; 95% CI, 0.42 to 0.76; $P < .001$), and an mRECIST ORR of 10% for brivanib and 2% for placebo (odds ratio, 5.72). Study discontinuation due to treatment-related adverse events (AEs) occurred in 61 brivanib patients (23%) and nine placebo patients (7%). The most frequent treatment-related grade 3 to 4 AEs for brivanib included hypertension (17%), fatigue (13%), hyponatremia (11%), and decreased appetite (10%).

Conclusion
In patients with HCC who had been treated with sorafenib, brivanib did not significantly improve OS. The observed benefit in the secondary outcomes of TTP and ORR warrants further investigation.

J Clin Oncol 31:3509-3516. © 2013 by American Society of Clinical Oncology

INTRODUCTION

Hepatocellular carcinoma (HCC) is often diagnosed at an unresectable, advanced stage that requires systemic treatment.[1-4] The only systemic treatment resulting in significant improvement in survival in patients with advanced HCC is sorafenib, a multikinase inhibitor that targets multiple signaling pathways, including vascular endothelial growth factor (VEGF) signaling.[5,6] Effective treatments for patients with advanced HCC who progress on/after or are intolerant to sorafenib remain an unmet medical need.[2-4]

Fibroblast growth factor (FGF) proteins are involved in tumor growth and angiogenesis in various cancers, including HCC.[7-12] Increased serum FGF levels are predictive of invasive HCC and recurrence after surgical resection.[13] Upregulation of alternate angiogenic signaling pathways such as FGF signaling may contribute to the evasion of blockade of VEGF

signaling by sorafenib, leading to relapse.[14-16] Thus, targeting both VEGF and FGF signaling pathways may benefit patients with HCC who progress on anti-VEGF therapies such as sorafenib.

Brivanib is a selective dual inhibitor of VEGF and FGF receptor tyrosine kinases.[17] It has potent antiangiogenic and antiproliferative effects on tumor cells from various tumor types, including liver.[18,19] In addition, brivanib has demonstrated antitumor activity in xenograft HCC models resistant to sorafenib.[20,21] In a phase II study in patients with advanced HCC who had progressed after prior antiangiogenic therapy (primarily sorafenib), brivanib had an objective response rate (ORR) of 11%, disease control rate (DCR) of 72% based on post hoc analysis using modified Response Evaluation Criteria in Solid Tumors (mRECIST) for HCC, and a median overall survival (OS) of 9.8 months; similar results have been reported in patients with advanced HCC who had no prior systemic treatment.[22-25] This phase III BRISK-PS (Comparison of Brivanib and Best Supportive Care to Placebo + Best Supportive Care in Subjects With Advanced Hepatocellular Cancer Who Have Failed or Are Intolerant to Sorafenib Treatment) trial evaluated the efficacy and safety of brivanib in patients with advanced HCC whose tumor had progressed on/after or who were intolerant to sorafenib.

PATIENTS AND METHODS

Patients

Patients with histologically or cytologically confirmed advanced HCC who had documented radiographic or symptomatic progression on/after or were intolerant to sorafenib were eligible. Patients were required to have one or more measurable lesions. Other inclusion criteria included liver function of Child-Pugh Class A or B (a total score ≤ 7) without ascites or encephalopathy, an Eastern Cooperative Oncology Group performance status (ECOG PS) ≤ 2, and adequate hematologic, hepatic, and renal functions. Details of eligibility criteria can be found in Appendix Table A1 (online only).

All patients provided written informed consent before enrollment. The study was approved by the institutional review board or ethics committee at each center and complied with provisions of the Good Clinical Practice guidelines and the Declaration of Helsinki and local laws.

Trial Design and Treatment

In this multinational, double-blind, randomized, placebo-controlled phase III trial, eligible patients were randomly assigned (2:1) to receive brivanib 800 mg once per day plus best supportive care or matching placebo plus best supportive care. Randomization was done centrally by the Sponsor (Bristol-Myers Squibb) -managed Interactive Voice Response System and was conducted with stratification by reason for sorafenib discontinuation (progression *v* intolerance), ECOG-PS score (0 *v* 1 or 2), extrahepatic spread and/or vascular invasion (yes *v* no), and study site.[26]

The dose modification schedule is described in Appendix Table A2 (online only). Treatment continued until unacceptable toxicity or progression. Since there were no approved treatments available for these patients, study therapies were allowed beyond radiographic progression if investigators determined that patients were still benefiting from blinded treatments.

Assessments

The primary end point of OS was defined as the time from random assignment until the date of death as a result of any cause. Secondary end points were time to progression (TTP), ORR, DCR as assessed by mRECIST, and safety. TTP was defined as the time from random assignment to radiologic disease progression, ORR as the percentage of patients with complete response or partial response, and DCR as the percentage of patients with complete response, partial response, or stable disease.

Tumor measurements were performed every 6 weeks during treatment by contrast-enhanced, dual-phase computed tomography or magnetic resonance imaging. Confirmatory assessments were performed ≥ 28 days after the initial demonstration of the response. Assessment was initially performed locally by investigators using modified WHO (mWHO) criteria and subsequently using mRECIST for HCC per protocol amendment. Treatment decisions were based on this local radiologic review. Scans were collected, archived, and reviewed centrally by a blinded independent radiologic review committee according to mRECIST for HCC.[22,23] Results for TTP, ORR, and DCR were based on this central review. The mRECIST for HCC is a set of criteria that has been proposed to more accurately reflect antitumor activity and changes in viable tumor burden than does standard RECIST. Because RECIST cannot account for the component of intratumoral necrotic areas, which may be seen on contrast-enhanced imaging, mRECIST was used in the central review reported here. Safety assessments in patients who received at least one dose of study therapy included adverse events (AEs) and clinical laboratory tests (National Cancer Institute Common Terminology Criteria for Adverse Events, version 3.0). AEs and serious AEs were monitored for up to 14 and 30 days, respectively, after the last dose.

Statistical Analysis

Sample size was calculated assuming an exponential survival distribution in each treatment group and taking into account one interim analysis for superiority. The study required at least 282 deaths to ensure that the two-sided $\alpha = .05$ level log-rank test had 90% power to show a statistically significant difference in OS between the treatment arms when the hazard ratio (HR) is 0.67. A minimum observed HR of 0.78 was needed for the trial to be positive. A maximum of 414 patients were to be randomly assigned.

The final analysis of OS compared brivanib with placebo by using a log-rank test at a two-sided α of .042 (adjusting for the preplanned interim analysis), stratified by reason for sorafenib discontinuation, ECOG-PS score, extrahepatic spread, and/or vascular invasion. Median OS and associated 95% CI were estimated by using Kaplan-Meier methods. The HRs and their associated CIs for OS were computed by using unadjusted and adjusted Cox proportional hazards models. Subsets prespecified for OS analysis were the aforementioned stratification factors (reason for sorafenib discontinuation, ECOG PS score, extrahepatic spread, and/or vascular invasion), region, age, race, sex, risk factors (hepatitis B or C virus, alcohol-induced liver disease), tumor morphology, tumor size, and α-fetoprotein at baseline. A prespecified multivariate Cox proportional hazards model stratified by the aforementioned stratification factors was used to evaluate whether prespecified baseline factors (age, hepatitis B or C virus infection, alcohol-induced liver disease, α-fetoprotein, and major portal vein invasion) were prognostic of OS and to adjust the treatment effect for all these prespecified factors. The variables were assessed by using a Wald test at a two-sided α of .05. A stepwise Cox regression approach was used for model building on a post hoc basis. A prespecified stratified log-rank test compared TTP between the two arms. The same methodology as described above for OS in this section was used to compute median TTP, HR, and CI and to adjust for the aforementioned prespecified baseline factors in this section. Exact 95% CIs for ORR and DCR were calculated by using the Clopper-Pearson method. ORR and DCR in the two groups were compared by using a Cochran-Mantel-Haenszel test stratified by the aforementioned factors (reason for sorafenib discontinuation, ECOG PS, extrahepatic spread and/or vascular invasion); associated odds ratios (ORs) and 95% CIs were estimated. Secondary efficacy end points were to be tested hierarchically in the following order: TTP, ORR, and DCR. The *P* values presented were nominal and were not adjusted for multiplicity.

RESULTS

Patients

Of 565 patients screened, 395 were randomly assigned between February 2009 and June 2011 to receive brivanib (n = 263) or placebo (n = 132) in 107 centers across 18 countries (Fig 1). The data cutoff date for this analysis was November 16, 2011. Forty-two percent of the randomly assigned patients were from Europe, 41% from Asia, and 17% from the Americas. Among the randomly assigned patients, 261 received

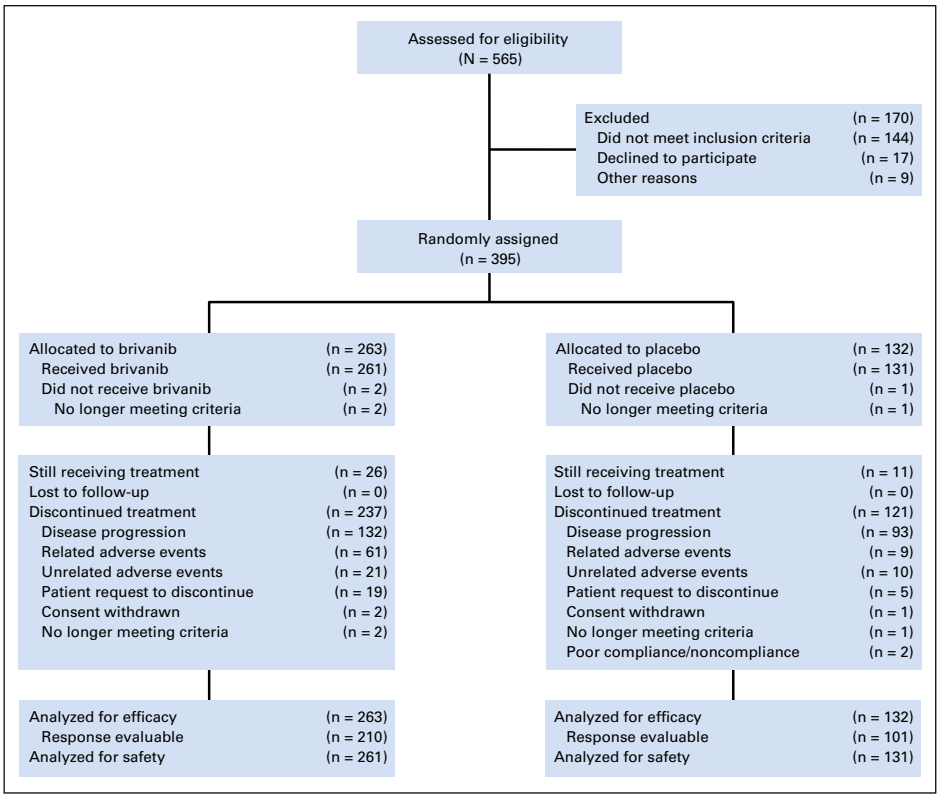

Fig 1. CONSORT diagram of sorafenib-pretreated patients with advanced hepatocellular carcinoma in the BRISK-PS study. Of the enrolled patients, 144 did not meet inclusion criteria and thus were excluded from random assignment. There were no dominant reasons for these exclusions.

one or more doses of brivanib and 131 received one or more doses of placebo.

Demographics and disease characteristics were generally balanced between the arms, except for macrovascular invasion (brivanib, 31%; placebo, 25%; Table 1), portal vein invasion and/or thrombosis (brivanib, 18%; placebo, 12%), and α-fetoprotein level (median: brivanib, 204 ng/mL; placebo, 100 ng/mL). Most patients had progression on prior sorafenib (87%) and one or more known risk factors for HCC (84%), with hepatitis B (37%), hepatitis C (27%), and alcoholic liver disease (25%) being the most common. Patients had advanced-stage HCC (Barcelona Clinic Liver Cancer [BCLC] stage C, 86%) with preserved liver function (Child-Pugh Class A, 92%) and good performance status (ECOG PS of 0, 59%).

Patient Disposition and Treatment Exposure

Ninety percent of the patients receiving brivanib and 92% receiving placebo discontinued treatment (Fig 1). The most common reasons for discontinuation were disease progression (brivanib, 50%; placebo, 70%) and study drug toxicity (brivanib, 23%; placebo, 7%). As estimated by Kaplan-Meier analysis, median treatment duration was 3.1 months (95% CI, 2.6 to 4.0 months) for brivanib and 2.5 months (95% CI, 1.6 to 2.8 months) for placebo. Median mean daily dose was 661 mg per day (range, 201 to 802 mg per day) for brivanib and 800 mg per day (range, 324 to 819 mg per day) for placebo.

Efficacy

Based on the intention-to-treat analysis with 284 deaths, the primary end point of a statistically significant improvement in OS with brivanib versus placebo (HR, 0.89; 95.8% CI, 0.69 to 1.15; $P = .3307$) was not met (Fig 2A); median OS was 9.4 and 8.2 months for brivanib and placebo groups, respectively. A prespecified analysis showed that OS results across subgroups were generally consistent with the primary OS analysis. Figure 3 shows the results for selected subgroups.

A multivariate Cox analysis of the prespecified baseline factors (see Patients and Methods) identified α-fetoprotein (< 200 ng/mL $v \geq 200$ ng/mL: $P < .001$) and portal vein invasion (no v yes; $P < .001$) to be significant prognostic factors for OS. Adjusting the treatment effect for all the prespecified factors yielded an HR for OS of 0.81 (95% CI, 0.63 to 1.04; $P = .1044$).

Some patients received cancer therapy subsequent to discontinuation of study treatments, including systemic (brivanib, 27%; placebo, 35%) and nonsystemic (brivanib, 18%; placebo, 20%) regimens. Post hoc analyses using poststudy treatments as a time-dependent covariate did not show a differential impact of poststudy treatment on OS (data not shown).

In total, 108 placebo patients (82%) and 226 brivanib patients (86%) were evaluable for response (ie, baseline and at least one on-study scans) by an independent radiologic review committee. Fifty-two patients (placebo, n = 24 [26%]; brivanib, n = 28 [21%]) had an assessment of radiographic progression based on local review but did not have documented radiographic progression by central review and were censored for the analyses of TTP, ORR, and DCR. TTP was longer for brivanib than for placebo (median, 4.2 v 2.7 months), with an HR of 0.56 (95% CI, 0.42 to 0.76) and $P < .001$ (Fig 2B). Adjusting for prespecified baseline prognostic factors (see Patients and

Table 1. Baseline Demographics and Disease Characteristics

Demographic or Characteristic	Brivanib (n = 263) No.	%	Placebo (n = 132) No.	%
Age, years				
Median	64		62	
Range	19-89		19-87	
Sex				
Male	216	82	113	86
Female	47	18	19	14
Race				
White	122	46	66	50
Asian	125	48	59	45
Black/African American	10	4	6	5
Other	6	2	1	1
Reason for sorafenib discontinuation				
Progression	227	86	116	88
Intolerance	35	13	16	12
Prior nonsystemic treatment	211	80	97	73
TACE	149	57	65	49
Liver resection	103	39	47	36
Radio-frequency ablation	49	19	28	21
ECOG PS				
0	151	57	81	61
1	102	39	46	35
2	10	4	5	4
BCLC stage				
A	9	3	1	1
B	23	9	19	14
C	229	87	112	85
D	2	1	0	
Child-Pugh Class				
A	242	92	120	91
B	19	7	12	9
C	2	1	0	
Distant metastasis	171	65	84	64
Regional lymph node metastasis	92	35	47	36
Vascular invasion	81	31	24	18
Portal vein invasion and/or thrombosis	65	25	16	12
Risk factors				
Any	218	83	112	85
Alcoholic liver disease	61	23	36	27
Hepatitis B	102	39	45	34
Hepatitis C	73	28	35	27
Other	18	7	12	9
α-fetoprotein				
Patients with baseline α-fetoprotein assessment	256		129	
Median, ng/mL	204		100	
Range	1.2-13.6 $\times$ 10^5		1.0-5.1 $\times$ 10^5	
> 200 ng/mL	129	50	57	44

Abbreviations: BCLC, Barcelona Clinic Liver Cancer; ECOG PS, Eastern Cooperative Oncology Group performance status; TACE, trans-catheter arterial chemo-embolization.

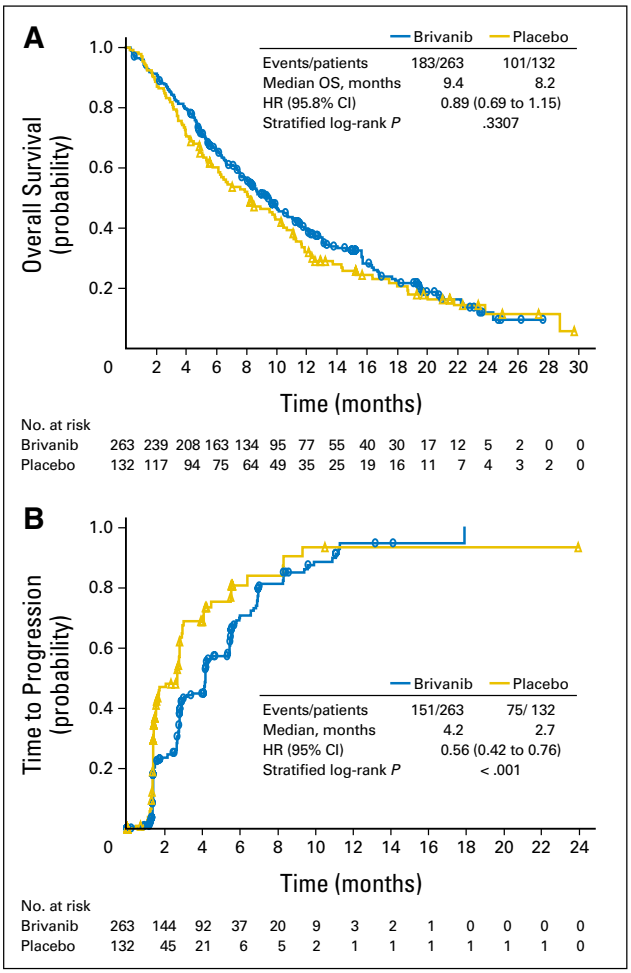

Fig 2. Kaplan-Meier estimates of overall survival (OS) and time to progression. (A) OS was computed on all randomly assigned patients. Patients who had not died or who were lost to follow-up were censored on the last date on which they were known to have been alive. CI for the hazard ratio (HR) was adjusted for the results of the preplanned interim analysis and was based on an adjusted two-sided α of .042. (B) Time to progression was computed on all randomly assigned patients. Patients who had not progressed were censored on the date of last tumor assessment. Patients who had no on-study tumor assessments or who had no independent radiologic review were also censored on the date of random assignment.

Methods) in a preplanned Cox model yielded similar results (HR, 0.56; 95% CI, 0.42 to 0.76).

There were no complete responses. Based on the intention-to-treat analysis, ORR was higher with brivanib than with placebo (10% *v* 2%; OR, 5.75; $P = .0030$; Table 2) as was DCR (61% *v* 40%; OR, 2.38; $P < .001$). Similar results were noted in those patients assessed by an independent radiologic review committee (brivanib: n = 226; ORR, 12%; DCR, 71% *v* placebo: n = 108; ORR, 2%; DCR, 49%). Figure 4A depicts the percent maximum changes from baseline in target tumor lesions in patients with both baseline and on-treatment tumor assessments by mRECIST for HCC. In patients with baseline α-fetoprotein concentration greater than the upper limit of normal (74% of randomly assigned patients) and one or more on-study α-fetoprotein assessments (brivanib, n = 179; placebo, n = 89), 54% of brivanib and 7% of placebo recipients had an α-fetoprotein reduction of $\geq$ 50% relative to baseline (Fig 4B).

Safety

The overall frequency of treatment-related AEs was 92% with brivanib and 62% with placebo (Table 3). Treatment-related grade 3

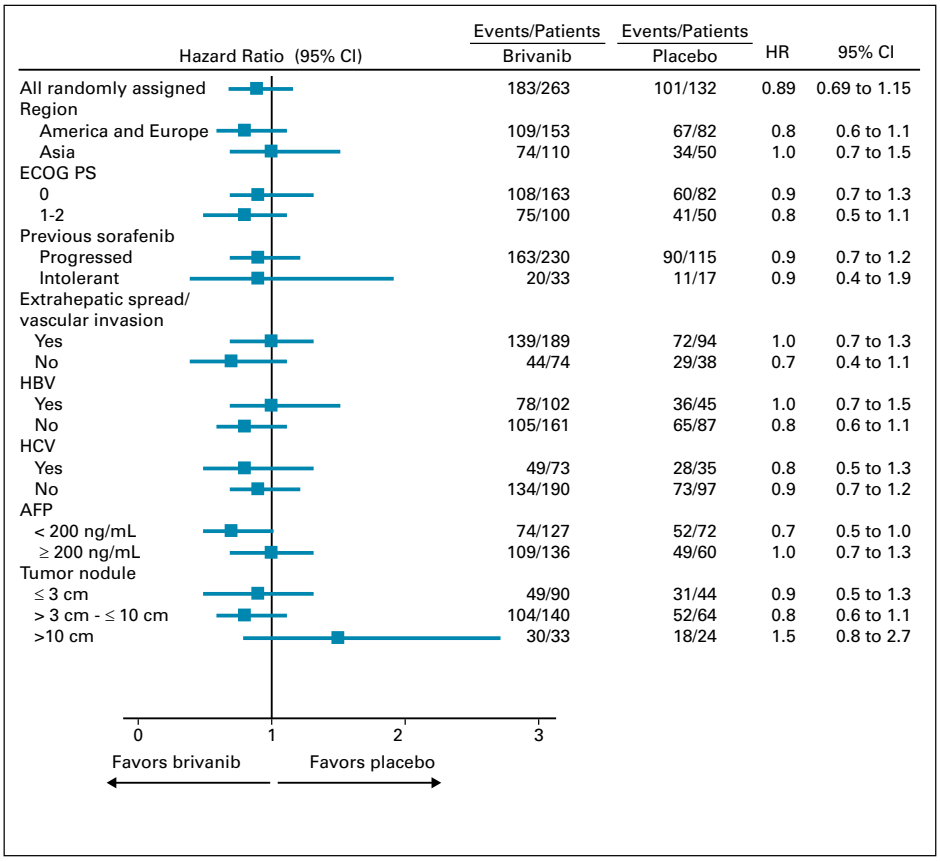

Fig 3. Overall survival in selected subsets. AFP, α-fetoprotein; ECOG PS, Eastern Cooperative Oncology Group performance status; HBV, hepatitis B virus; HCV, hepatitis C virus; HR, hazard ratio.

AEs that occurred at a frequency of ≥ 5% with brivanib included hypertension, fatigue, hyponatremia, decreased appetite, asthenia, diarrhea, increased AST, and increased ALT; these AEs occurred at a frequency of ≤ 4% with placebo (Table 3). Grade 4 AEs were infrequent. The most frequent (> 5%) grade 3 to 4 laboratory abnormalities listed in Table 3 were more common with brivanib than with placebo.

Other AEs (not listed in Table 3) of potential relevance to antiangiogenic therapies (predefined: any grade, any relationship)

Table 2. Tumor Response

	Brivanib (n = 263)		Placebo (n = 132)		Brivanib Versus Placebo		
Response	No.	%	No.	%	OR	95% CI	$P^{\dagger}$
Best response							
Complete response	0		0				
Partial response	26	10	2	2			
Stable disease	135	51	51	39			
Progressive disease	49	19	48	36			
Not evaluable*	53	20	31	23			
Objective response rate					5.72	1.41 to 23.25	.0030†
%	10		2				
95% CI	6.6 to 14.2		0.2 to 5.4				
Disease control rate					2.38	1.54 to 3.68	< .001
%	61		40				
95% CI	55.0 to 67.1		31.7 to 49.0				

NOTE. Data are based on blinded independent radiologic review using modified Response Evaluation Criteria in Solid Tumors (RECIST) for hepatocellular carcinoma,[22,23] and analysis based on the intention-to-treat population.
Abbreviation: OR, odds ratio.
*Included patients without independent radiologic review.
†Cochran-Mantel-Haenszel test.

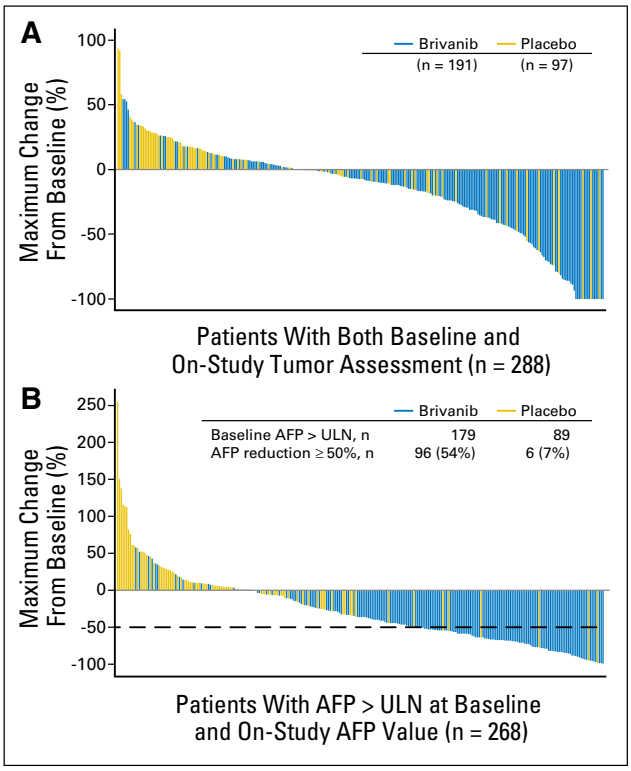

Fig 4. Waterfall plots for changes in tumor (A) and serum α-fetoprotein (AFP) (B) relative to baseline. Patients who had baseline assessments as well as one or more on-study assessments were plotted. ULN, upper limit of normal.

Table 3. Percent of Treatment-Related AEs and Laboratory Abnormalities

Variable	Brivanib (n = 261)			Placebo (n = 131)		
	Grades 1 to 4	Grade 3	Grade 4	Grades 1 to 4	Grade 3	Grade 4
AE*						
Overall incidence	94	61	7	62	22	2
Decreased appetite	50	10	0	15	2	0
Fatigue	41	13	0	14	1	0
Hypertension	41	16	< 1	5	2	0
Diarrhea	39	7	0	12	2	0
Nausea	28	2	0	15	1	0
Vomiting	24	2	0	5	1	0
Asthenia	21	8	1	12	4	0
Dysphonia	17	< 1	0	0	0	0
Headache	17	1	0	2	0	0
Hand-foot-skin reaction	15	2	0	6	0	0
Hyponatremia	15	11	< 1	2	2	0
Decreased weight	15	< 1	0	2	1	0
Increased AST	14	7	1	6	4	0
Hypothyroidism	14	< 1	0	2	0	0
Dizziness	13	< 1	0	3	0	0
Abdominal pain	11	2	0	5	1	0
Increased ALT	11	7	< 1	3	2	0
Dyspepsia	10	< 1	0	2	0	0
Proteinuria	10	4	0	1	1	0
Laboratory abnormalities†						
Increased AST	95	24	3	91	22	2
Increased ALT	83	16	1	78	6	1
Increased AP	82	12	< 1	80	6	1
Hyponatremia	75	25	2	45	12	2
Hyperbilirubinemia	69	17	4	54	13	5
Thrombocytopenia	67	7	< 1	58	3	0

Abbreviations: AE, adverse event; AP, alkaline phosphatase.
*Treatment-related AEs that occurred in at least 10% of the patients in either group between day 1 and at least 14 days after the last dose.
†Laboratory abnormalities (grade 3 or 4) that occurred in at least 5% of the patients in either group between day 1 and at least 14 days after the last dose.

reported for brivanib and placebo were hemorrhage of any origin (17% and 16%, respectively), ascites (14% and 14%), encephalopathy (4% and 2%), hepatic encephalopathy (5% and 2%), hepatic failure (3% and 2%), acute hepatic failure (< 1% and 2%), venous thromboembolism (3% and 4%), arterial thromboembolism (2% and 1%), esophageal variceal bleeding (2% and 2%), and gastric variceal bleeding (0% and 1%). Two patients (1%) receiving brivanib (none who received placebo) had reversible posterior leukoencephalopathy syndrome.

Discontinuation due to treatment-related AEs was reported in 61 patients (23%) receiving brivanib and nine patients (7%) receiving placebo. The most frequent treatment-related AEs leading to discontinuation of brivanib were fatigue, asthenia, decreased appetite, hypertension, and vomiting (8, 6, 6, 5, and 4 patients, respectively). Both dose interruptions (brivanib, 61%; placebo, 26%) and dose reductions (brivanib, 54%; placebo, 11%) were more frequent with brivanib.

The incidence of serious AEs was 63% for brivanib and 57% for placebo. No individual serious AEs were reported in more than 5% of brivanib recipients except for malignant neoplasm progression (brivanib, 17%; placebo, 21%). All AEs are listed in Appendix Table A3 (online only), and serious AEs from any cause are listed in Appendix Table A4 (online only).

Forty patients (15%) receiving brivanib and 24 (18%) receiving placebo died within 30 days of the last dose; the most common reason for death was disease progression (brivanib, 12%; placebo, 17%). Six deaths on the study were considered by investigators possibly related to treatment, all of which were in the brivanib arm and occurred within 30 days of the final dose. Two of these deaths were a result of encephalopathy, and one each due to liver failure, acidosis, sudden death, and coma/cerebral edema.

DISCUSSION

The lack of effective treatments for patients with advanced HCC who are intolerant to sorafenib or for whom sorafenib has failed represents an unmet medical need.[2-4] In this phase III study evaluating brivanib as second-line treatment in this patient population, no difference was detected between groups for the primary end point of OS. Survival in patients with HCC is influenced by many factors related not only to tumor burden but also to underlying liver condition and minor imbalances in prognostic factors can have a meaningful impact on OS. Despite multiple stratification factors, numerical imbalances in some baseline factors were observed in this study, most notably in α-fetoprotein level and the presence of vascular invasion, favoring

placebo. Although extrahepatic spread and/or vascular invasion was a stratification factor, the high prevalence of extrahepatic spread (74%) relative to vascular invasion (brivanib, 31%; placebo, 18%) masked the imbalance in vascular invasion. Adjusting for all the prespecified baseline factors resulted in an HR for OS of 0.81. Although the adjusted HR did not reach statistical significance, this prespecified analysis and consistent results from exploratory analyses, including baseline stratification factors and other prognostic factors (HR, 0.79 to 0.82), suggested that there may have been an underestimate of the HR due to potential imbalances in some prognostic factors such as α-fetoprotein and vascular invasion. Another possible explanation for the failure to detect a difference in OS is because of insufficient power as patients with a better prognosis than in previous trials were enrolled. For example, the observed median OS of 8.2 months for placebo recipients is similar to or even longer than those reported for placebo patients in the first-line study of sorafenib in HCC[5,6] and the recent phase II data in patients with HCC who failed sorafenib who had a median survival of less than 7 months for patients receiving placebo.[27] Finally, the antitumor activity of brivanib may not be strong enough to extend survival. This explanation is consistent with the results of a recently completed phase III study, which compared brivanib with sorafenib head-to-head as first-line therapy, suggesting antitumor activity of brivanib without meeting the primary end point of OS noninferiority.[28]

In our trial, we observed improvements in secondary outcomes such as TTP, ORR, and DCR based on mRECIST. This suggests a potential antitumor activity of brivanib. However, it should be emphasized that the data for TTP, ORR, and DCR in our trial and other trials were based on the so far unvalidated mRECIST for HCC.[22,23] The mRECIST for HCC incorporates the extent of tumor necrosis into its scoring system for response assessment and has a more conservative assignment for progression compared with RECIST. Further research is needed to determine whether mRECIST for HCC is a valid marker of antitumor activity in patients with HCC.[22,23] In addition, because the primary end point was not met, the data for TTP, ORR, and DCR should be considered exploratory based on the planned hierarchical testing paradigm.

Consistent with previously published data for tyrosine kinase inhibitors such as sorafenib and sunitinib,[5,6,29-32] hypertension, hypothyroidism, proteinuria, and hand-foot skin reaction were observed with brivanib. Of note, hand-foot skin reaction, a hallmark of the sorafenib safety profile, appeared to be less frequent and severe in this study than reported previously in first-line studies of sorafenib in HCC. Hyponatremia, a frequently reported AE in this study as well as in previous early trials of brivanib in various tumor types, including colorectal cancer and sarcoma,[25,33-35] has not been reported for other targeted agents,[5,6] suggesting that this AE may be relatively specific to brivanib. Notably, the safety profile was similar between sorafenib-intolerant patients and those who progressed on/after sorafenib (Appendix Table A5, online only), suggesting a lack of cross tolerance between brivanib and sorafenib for toxicity. It is unclear whether the reduced dose intensity resulting from dose reductions, dose interruptions, and treatment discontinuations due to AEs had an impact on efficacy. Causes of six deaths (brivanib arm) considered by investigators to be treatment-related were not unusual for this patient population. Of note, however, is that almost one quarter of brivanib patients withdrew from the trial prematurely because of drug toxicity.

In conclusion, this first phase III study of brivanib in patients with HCC who have already been treated with sorafenib did not meet its primary end point of OS improvement. The results of our trial may inform the design of future studies in this patient population.

AUTHORS' DISCLOSURES OF POTENTIAL CONFLICTS OF INTEREST

Although all authors completed the disclosure declaration, the following author(s) and/or an author's immediate family member(s) indicated a financial or other interest that is relevant to the subject matter under consideration in this article. Certain relationships marked with a "U" are those for which no compensation was received; those relationships marked with a "C" were compensated. For a detailed description of the disclosure categories, or for more information about ASCO's conflict of interest policy, please refer to the Author Disclosure Declaration and the Disclosures of Potential Conflicts of Interest section in Information for Contributors.
Employment or Leadership Position: Rana Ezzeddine, Bristol-Myers Squibb (C); David Liu, Bristol-Myers Squibb (C); Ian Walters, Bristol-Myers Squibb (C) **Consultant or Advisory Role:** Josep M. Llovet, Bristol-Myers Squibb (C), Bayer Pharmaceuticals (C), Lilly Imclone (C), Novartis (C), Onyx Pharmaceuticals (C), Blueprint (C); Jean-Luc Raoul, Bayer Pharmaceuticals (C), Bristol-Myers Squibb (C); Charissa Chang, Onyx Pharmaceuticals (C); Yoon-Koo Kang, Bayer Pharmaceuticals (C); Eric Assenat, Bristol-Myers Squibb (C), Novartis (C); Valerie Boige, sanofi-aventis (C), Bayer Pharmaceuticals (C); Philippe Mathurin, Bristol-Myers Squibb (C), Bayer HealthCare (C); Jordi Bruix, Bayer Pharmaceuticals (C), ArQule (C), Bristol-Myers Squibb (C), Novartis (C), Roche (C); Ronnie T. Poon, Bristol-Myers Squibb (C); Morris Sherman, Bristol-Myers Squibb (C), Bayer Pharmaceuticals (C); Richard S. Finn, Bristol-Myers Squibb (C); Won-Young Tak, Bayer HealthCare (C), Gilead Sciences Korea (C); Joong-Won Park, Taiho Pharmaceutical (C), Bristol-Myers Squibb (C) **Stock Ownership:** Rana Ezzeddine, Bristol-Myers Squibb; David Liu, Bristol-Myers Squibb; Ian Walters, Bristol-Myers Squibb **Honoraria:** Josep M. Llovet, Bayer Pharmaceuticals, Bristol-Myers Squibb; Jean-Luc Raoul, Bayer Pharmaceuticals; Eric Assenat, Roche, Bayer Pharmaceuticals; Valerie Boige, Bayer Pharmaceuticals, Ipsen, Merck Serono; Philippe Mathurin, Bristol-Myers Squibb, Bayer HealthCare; Laetitia Fartoux, Bristol-Myers Squibb, Bayer Pharmaceuticals; Jordi Bruix, Bayer Pharmaceuticals; Ronnie T. Poon, Bristol-Myers Squibb; Morris Sherman, Bristol-Myers Squibb, Bayer Pharmaceuticals, Imclone Systems, Arqule; Won-Young Tak, Bayer HealthCare; Joong-Won Park, Bayer HealthCare **Research Funding:** Josep M. Llovet, Bristol-Myers Squibb; Yoon-Koo Kang, Bayer Pharmaceuticals; Valerie Boige, Merck Serono; Jordi Bruix, Bayer Pharmaceuticals; Won-Young Tak, Samil Pharmaceutical **Expert Testimony:** Morris Sherman, Bristol-Myers Squibb (C) **Patents:** None **Other Remuneration:** None

AUTHOR CONTRIBUTIONS

Conception and design: Josep M. Llovet, Ronnie T. Poon, Richard S. Finn, Rana Ezzeddine, Ian Walters, Joong-Won Park
Provision of study materials or patients: Thomas Decaens, Yoon-Koo Kang, Eric Assenat, Valerie Boige, Philippe Mathurin, Morris Sherman, Richard S. Finn, Joong-Won Park
Collection and assembly of data: Thomas Decaens, Eveline Boucher, Masatoshi Kudo, Charissa Chang, Yoon-Koo Kang, Eric Assenat, Valerie Boige, Deng-Yn Lin, Ronnie T. Poon, Jean-Frédéric Blanc, Richard S. Finn, Won-Young Tak, Yee Chao, Rana Ezzeddine, David Liu, Ian Walters
Data analysis and interpretation: Josep M. Llovet, Thomas Decaens, Jean-Luc Raoul, Ho-Yeong Lim, Philippe Mathurin, Laetitia Fartoux, Deng-Yn Lin, Jordi Bruix, Morris Sherman, Rana Ezzeddine, David Liu, Ian Walters, Joong-Won Park
Manuscript writing: All authors
Final approval of manuscript: All authors

REFERENCES

1. Jemal A, Bray F, Center MM, et al: Global cancer statistics. CA Cancer J Clin 61:69-90, 2011
2. European Association for the Study of the Liver, European Organisation for Research and Treatment of Cancer: EASL-EORTC clinical practice guidelines: Management of hepatocellular carcinoma. J Hepatol 56:908-943, 2012
3. Forner A, Llovet JM, Bruix J: Hepatocellular carcinoma. Lancet 379:1245-1255, 2012
4. Llovet JM, Di Bisceglie AM, Bruix J, et al: Design and endpoints of clinical trials in hepatocellular carcinoma. J Natl Cancer Inst 100:698-711, 2008
5. Llovet JM, Ricci S, Mazzaferro V, et al: Sorafenib in advanced hepatocellular carcinoma. N Engl J Med 359:378-390, 2008
6. Cheng AL, Kang YK, Chen Z, et al: Efficacy and safety of sorafenib in patients in the Asia-Pacific region with advanced hepatocellular carcinoma: A phase III randomised, double-blind, placebo-controlled trial. Lancet Oncol 10:25-34, 2009
7. Presta M, Dell'Era P, Mitola S, et al: Fibroblast growth factor/fibroblast growth factor receptor system in angiogenesis. Cytokine Growth Factor Rev 16:159-178, 2005
8. Grose R, Dickson C: Fibroblast growth factor signaling in tumorigenesis. Cytokine Growth Factor Rev 16:179-186, 2005
9. Mise M, Arii S, Higashituji H, et al: Clinical significance of vascular endothelial growth factor and basic fibroblast growth factor gene expression in liver tumor. Hepatology 23:455-464, 1996
10. Ogasawara S, Yano H, Iemura A, et al: Expressions of basic fibroblast growth factor and its receptors and their relationship to proliferation of human hepatocellular carcinoma cell lines. Hepatology 24: 198-205, 1996
11. El-Assal ON, Yamanoi A, Ono T, et al: The clinicopathological significance of heparanase and basic fibroblast growth factor expressions in hepatocellular carcinoma. Clin Cancer Res 7:1299-1305, 2001
12. Uematsu S, Higashi T, Nouso K, et al: Altered expression of vascular endothelial growth factor, fibroblast growth factor-2 and endostatin in patients with hepatocellular carcinoma. J Gastroenterol Hepatol 20:583-588, 2005
13. Poon RT, Ng IO, Lau C, et al: Correlation of serum basic fibroblast growth factor levels with clinicopathologic features and postoperative recurrence in hepatocellular carcinoma. Am J Surg 182: 298-304, 2001
14. Bergers G, Hanahan D: Modes of resistance to anti-angiogenic therapy. Nat Rev Cancer 8:592-603, 2008
15. Casanovas O, Hicklin DJ, Bergers G, et al: Drug resistance by evasion of antiangiogenic targeting of VEGF signaling in late-stage pancreatic islet tumors. Cancer Cell 8:299-309, 2005
16. Villanueva A, Llovet JM: Second-line therapies in hepatocellular carcinoma: Emergence of resistance to sorafenib. Clin Cancer Res 18:1824-1826, 2012
17. Cai ZW, Zhang Y, Borzilleri RM, et al: Discovery of brivanib alaninate ((S)-((R)-1-(4-(4-fluoro-2-methyl-1H-indol-5-yloxy)-5-methylpyrrolo[2,1-f][1,2,4] triazin-6-yloxy)propan-2-yl)2-aminopropanoate), a novel prodrug of dual vascular endothelial growth factor receptor-2 and fibroblast growth factor receptor-1 kinase inhibitor (BMS-540215). J Med Chem 51:1976-1980, 2008
18. Bhide RS, Lombardo LJ, Hunt JT, et al: The antiangiogenic activity in xenograft models of brivanib, a dual inhibitor of vascular endothelial growth factor receptor-2 and fibroblast growth factor receptor-1 kinases. Mol Cancer Ther 9:369-378, 2010
19. Huynh H, Ngo VC, Fargnoli J, et al: Brivanib alaninate, a dual inhibitor of vascular endothelial growth factor receptor and fibroblast growth factor receptor tyrosine kinases, induces growth inhibition in mouse models of human hepatocellular carcinoma. Clin Cancer Res 14:6146-6153, 2008
20. Allen E, Walters IB, Hanahan D: Brivanib, a dual FGF/VEGF inhibitor, is active both first and second line against mouse pancreatic neuroendocrine tumors developing adaptive/evasive resistance to VEGF inhibition. Clin Cancer Res 17:5299-5310, 2011
21. Tovar V, Cornella, Villanueva A: FGF signaling is involved in acquired resistance to sorafenib in an in vivo model of hepatocellular carcinoma. International Liver Cancer Association, 2011 (abstr 0-006)
22. Lencioni R, Llovet JM: Modified RECIST (mRECIST) assessment for hepatocellular carcinoma. Semin Liver Dis 30:52-60, 2010
23. Edeline J, Boucher E, Rolland Y, et al: Comparison of tumor response by Response Evaluation Criteria in Solid Tumors (RECIST) and modified RECIST in patients treated with sorafenib for hepatocellular carcinoma. Cancer 118:147-156, 2012
24. Park JW, Finn RS, Kim JS, et al: Phase II, open-label study of brivanib as first-line therapy in patients with advanced hepatocellular carcinoma. Clin Cancer Res 17:1973-1983, 2011
25. Finn RS, Kang YK, Mulcahy M, et al: Phase II, open-label study of brivanib as second-line therapy in patients with advanced hepatocellular carcinoma. Clin Cancer Res 18:2090-2098, 2012
26. Pocock SJ, Simon R: Sequential treatment assignment with balancing for prognostic factors in the controlled clinical trial. Biometrics 31:103-115, 1975
27. Santoro A, Rimassa L, Borbath I, et al: Tivantinib for second-line treatment of advanced hepatocellular carcinoma: A randomised, placebo-controlled phase 2 study. Lancet Oncol 14:55-63, 2013
28. Johnson PJ, Qin S, Park J-W, et al: Brivanib versus sorafenib as first-line therapy in patients with unresectable, advanced hepatocellular carcinoma: Results from the randomized phase III BRISK-FL study. J Clin Oncol 31:3517-3524, 2013
29. Izzedine H, Ederhy S, Goldwasser F, et al: Management of hypertension in angiogenesis inhibitor-treated patients. Ann Oncol 20:807-815, 2009
30. Izzedine H, Massard C, Spano JP, et al: VEGF signalling inhibition-induced proteinuria: Mechanisms, significance and management. Eur J Cancer 46:439-448, 2010
31. Launay-Vacher V, Deray G: Hypertension and proteinuria: A class-effect of antiangiogenic therapies. Anticancer Drugs 20:81-82, 2009
32. Feldt S, Schüssel K, Quinzler R, et al: Incidence of thyroid hormone therapy in patients treated with sunitinib or sorafenib: A cohort study. Eur J Cancer 48:974-981, 2012
33. Schwartz GK, Maki RG, Ratain MJ, et al: Brivanib (BMS-582664) in advanced soft-tissue sarcoma (STS): Biomarker and subset results of a phase II randomized discontinuation trial (RDT). J Clin Oncol 29:605s, 2011 (suppl; abstr 10000)
34. Ratain MJ, Schwartz GK, Oza AM, et al: Brivanib (BMS-582664) in advanced solid tumors (AST): Results of a phase II randomized discontinuation trial (RDT). J Clin Oncol 29:213s, 2011 (suppl; abstr 3079)
35. Garrett CR, Siu LL, El-Khoueiry A, et al: Phase I dose-escalation study to determine the safety, pharmacokinetics and pharmacodynamics of brivanib alaninate in combination with full-dose cetuximab in patients with advanced gastrointestinal malignancies who have failed prior therapy. Br J Cancer 105:44-52, 2011

Affiliations

Josep M. Llovet and Charissa Chang, Icahn School of Medicine at Mount Sinai, New York, NY; Josep M. Llovet and Jordi Bruix, Institut d'investigacions Biomèdiques August Pi i Sunyer (IDIBAPS) –Hospital Clinic, University of Barcelona, Barcelona, Spain; Thomas Decaens, University of Paris-Est, and Institut National de la Santé et de la Recherche Médicale, Creteil; Jean-Luc Raoul, Institut Paoli Calmette, Marseille; Eveline Boucher, Service d'Oncologie Médicale, Central Eugene Marquis, Rennes; Eric Assenat, Hôpital Saint Eloi, Montpellier; Valerie Boige, Institut Gustave Roussy, Villejuif; Philippe Mathurin, Hôpital Claude Huriez, Lille; Laetitia Fartoux, Hôpital Saint Antoine, Paris; Jean-Frederic Blanc, Saint-Andre Hospital, Bordeaux, France; Masatoshi Kudo, Kinki University School of Medicine, Osaka, Japan; Yoon-Koo Kang, Asan Medical Center; Ho-Yeong Lim, Samsung Medical Center, Seoul; Won-Young Tak, Kyungpook National University Hospital, Daegu; Joong-Won Park, National Cancer Center, Goyang, Republic of Korea; Deng-Yn Lin, Chang Gung Memorial Hospital and Chang Gung University; Yee Chao, Taipei Veterans General Hospital, Taipei, Taiwan, Republic of China; Ronnie T. Poon, University of Hong Kong, Hong Kong Special Administrative Region, People's Republic of China; Morris Sherman, Toronto General Hospital, Toronto, Ontario, Canada; Richard S. Finn, University of California at Los Angeles, Los Angeles, CA; and Rana Ezzeddine, David Liu, and Ian Walters, Bristol-Myers Squibb, Wallingford, CT.

Acknowledgment

We express our heartfelt thanks and gratitude to patients and their families around the globe. We also thank the investigators for their enthusiastic participation in the study, Bristol-Myers Squibb for sponsoring the trial, and Motasim Billah of Bristol-Myers Squibb for providing writing assistance.

Appendix

Table A1. Patient Eligibility Criteria

Inclusion criteria
Men and women age 18 years or older
Histologically or cytologically confirmed advanced HCC
Advanced disease was defined as disease not eligible for or progressive after surgical or locoregional therapy
Prior sorafenib therapy for at least 14 days (not necessarily consecutive) before discontinuing the therapy due to radiographic or symptomatic progression or intolerance
Sorafenib discontinuation at or prior to study entry and off sorafenib therapy for at least 8 days prior to the first dose of study treatment
Progression on sorafenib was defined as radiographic progression according to mWHO criteria or RECIST, or symptomatic progression defined as a decrease of ECOG performance status from 0 to 2 and/or development of symptomatic disease from asymptomatic disease
Intolerance was defined as persistence of sorafenib-related AEs of at least grade 2, despite supportive therapy, and/or persistence/recurrence of AEs after dose interruption and reduction of sorafenib
Locoregional therapy must have been completed at least 3 weeks prior to the baseline scan
At least one untreated measurable lesion by MRI or spiral CT
Cirrhotic status of Child-Pugh Class A or B with a score of ≤ 7
ECOG performance status 0, 1, or 2
Life expectancy of at least 8 weeks
Adequate hematologic function with absolute neutrophil counts $\geq$ 1,500/μL, platelet count $\geq 60 \times 10^9$/L, and hemoglobin $\geq$ 8.5 g/dL
Adequate hepatic function with serum total bilirubin $\leq$ 3 mg/dL, serum albumin $\geq$ 2.8 g/dL, and ALT and AST $\leq 5\times$ institutional ULN
Amylase and lipase $< 1.5\times$ ULN
Adequate renal function with serum creatinine $\leq$ 2.0 mg/dL
INR $\leq$ 2.3 or PT $\leq$ 6 seconds above control
Exclusion criteria
Brain metastasis or evidence of leptomeningeal disease
Known fibrolamellar HCC or mixed cholangiocarcinoma and HCC
Any encephalopathy
Any ascites
Bleeding esophageal or gastric varices within 2 months prior to inclusion
Previous or concurrent cancer except cervical carcinoma in situ, treated basal cell carcinoma, superficial bladder tumors (Ta, Tis, and T1). Any cancer curatively treated $>$ 5 years prior to entry is permitted
History of active cardiac disease including uncontrolled hypertension, congestive heart failure, active coronary artery disease, unstable or newly diagnosed angina, or myocardial infarction less than 12 months prior to study, cardiac arrhythmias requiring anti-arrhythmic therapy other than beta blockers or digoxin, and valvular heart disease $\geq$ CTCAE grade 2
QTc (Fridericia) $>$ 450 msec on two consecutive ECGs
Thrombotic or embolic events within the past 6 months and pulmonary embolism
Any other hemorrhage/bleeding event
Grade 2 within the past 2 months
Grade 3 within the past 6 months
Grade 4 except for esophageal and gastric varices (see above)
Infection
History of HIV infection
Active, untreated hepatitis B virus infection
Active bacterial infection less than 7 days after completing systemic antibiotic therapy
History of nonhealing wounds or ulcers, or bone fractures within 3 months of fracture
Pre-existing thyroid abnormality with thyroid function that cannot be maintained in the normal range with medication
Hyponatremia with sodium $<$ 130 mmol/L
Baseline serum potassium $<$ 3.5 mmol/L
Prior use of any systemic anticancer chemotherapy, immunotherapy, or targeted agents for HCC except for sorafenib

NOTE. Radiotherapy within 4 weeks prior to start of study drug (palliative radiotherapy for symptomatic control) was acceptable.
Abbreviations: AE, adverse event; CT, computed tomography; CTCAE, Common Terminology Criteria for Adverse Events; ECOG, Eastern Cooperative Oncology Group; HCC, hepatocellular carcinoma; INR, international normalized ratio; MRI, magnetic resonance imaging; mWHO, modified WHO; PT, prothrombin time; RECIST, Response Evaluation Criteria in Solid Tumors; ULN, upper limit of normal.

Table A2. Dose Modification Schedule for Toxicity

AE Occurrence	Occurrence	Dose Modification
Baseline ALT/AST < 2.5× ULN increase to > 5× ULN or baseline ALT/AST 2.5 to 5× ULN increase to > 10× ULN	First	Hold study drugs until ALT/AST ≤ 5× ULN. When study drugs are resumed, decrease by one dose level from the previous dose level.
	Second	Hold study drugs until ALT/AST ≤ 5× ULN. When study drugs are resumed, decrease by one dose level from the previous dose level.
	Third	Stop study drugs or discuss with medical monitor.
Total bilirubin ≥ 3× ULN	First	Hold study drugs until bilirubin < 3× ULN. When study drugs are resumed, decrease by one dose level from the previous dose level.
	Second	Hold study drugs until bilirubin < 3× ULN. When study drugs are resumed, decrease by one dose level from the previous dose level.
	Third	Stop study drugs or discuss with medical monitor.
Grade 3 hyponatremia < 130 to 120 mmol/L	First	Continue study drugs and start medical intervention until sodium ≥ 130 mmol/L.
	Second or persistent for ≥ 7 days	Hold study drugs and start medical intervention. Resume study drugs when sodium ≥ 130 mmol/L; decrease by one dose level from the previous dose level.
	Third	Hold study drugs and start medical intervention. Resume study drugs when sodium ≥ 130 mmol/L; decrease by one dose level from the previous dose level.
	Fourth	Stop study drugs or discuss with medical monitor.
Grade 4 hyponatremia < 120 mmol/L	First	Hold study drugs and start medical intervention. Resume study drugs when sodium ≥ 130 mmol/L; decrease by one dose level from the previous dose level.
	Second	Stop study drugs or discuss with medical monitor.
Any other drug-related grade 3 nonhematologic or hematologic toxicity	First	Hold study drugs. Resume study drugs when toxicity decreases to grade ≤ 1; decrease by one dose level from the previous dose level.
	Second	Hold study drugs. Resume study drugs when toxicity decreases to grade ≤ 1; decrease by one dose level from the previous dose level.
	Third	Stop study drugs or discuss with medical monitor.
Any other drug-related grade 4 nonhematologic or hematologic toxicity	First	Stop study drugs or discuss with medical monitor.

NOTE. Two dose reductions were allowed with the first at 600 mg and the second at 400 mg.
Abbreviations: AE, adverse event; ULN, upper limit of normal.

Table A3. Percent of AEs Resulting From Any Cause

AE	Brivanib (n = 261)			Placebo (n = 131)		
	Grades 1 to 4	Grade 3	Grade 4	Grades 1 to 4	Grade 3	Grade 4
Overall incidence	86	56	16	76	33	11
Decreased appetite	61	12	0	24	2	0
Fatigue	48	15	< 1	24	2	1
Hypertension	48	18	< 1	14	2	1
Diarrhea	47	9	0	15	2	0
Nausea	36	2	0	21	1	0
Vomiting	32	2	0	9	1	0
Abdominal pain	28	5	< 1	21	5	0
Decreased weight	23	< 1	0	8	1	0
Asthenia	22	8	1	19	5	0
Increased AST	21	10	2	15	8	2
Dysphonia	21	< 1	0	2	0	0
Headache	21	1	0	8	1	0
Constipation	19	0	0	15	2	0
Upper abdominal pain	17	2	0	11	2	1
Hypothyroidism	16	< 1	0	2	0	0
Peripheral edema	16	1	0	18	1	0
Increased ALT	15	8	< 1	7	3	1
Cough	15	1	0	12	0	0
Dizziness	15	1	0	6	0	0
Dyspnea	15	3	0	11	0	0
Hand-foot syndrome	15	2	0	7	0	0
Ascites	14	3	0	14	5	0
Pyrexia	14	< 1	0	9	0	0
Dyspepsia	13	< 1	0	3	0	0
Back pain	11	1	0	8	1	1
Abdominal distension	10	2	0	10	2	0
Mucosal inflammation	10	< 1	0	3	0	0
Insomnia	10	0	0	8	1	0
Proteinuria	10	4	0	2	1	0
Pruritus	10	0	0	10	0	0

NOTE. Adverse events (AEs; grades 1 to 4) that occurred in at least 10% of the patients in either group between day 1 and at least 14 days after the last dose.

Table A4. Percent of Serious AEs Resulting From Any Cause in at Least 1% of Patients

Serious AE	Brivanib (n = 261)				Placebo (n = 131)			
	Grades 1 to 5	Grade 3	Grade 4	Grade 5	Grades 1 to 5	Grade 3	Grade 4	Grade 5
Overall incidence	63.2	29.9	11.5	13.4	56.5	22.9	6.1	16.0
Malignant neoplasm	17.2	2.7	1.1	6.9	20.6	2.3	0.8	11.5
Hepatic encephalopathy	4.6	2.3	0.8	1.1	1.5	0.8	0	0.8
Decreased appetite	3.8	3.4	0	0	0	0	0	0
Abdominal pain	3.4	2.3	0.4	0	6.9	3.8	0	0
Hepatic failure	3.1	0	1.1	1.9	1.5	0	0.8	0.8
Ascites	2.7	1.1	0	0	3.8	3.1	0	0
Fatigue	2.7	2.7	0	0	1.5	0.8	0	0
Health deterioration	2.7	0.8	0.4	0.4	0.8	0.8	0	0
Dehydration	2.3	1.9	0	0	0.8	0	0	0
Pyrexia	2.3	0	0	0	0.8	0	0	0
Diarrhea	1.9	1.1	0	0	0	0	0	0
Abnormal hepatic function	1.9	0.8	0.4	0.4	0.8	0	0	0
Acute renal failure	1.5	1.5	0	0	1.5	0.8	0.8	0
Hyperbilirubinemia	1.5	1.1	0.4	0	0.8	0	0.8	0
Hyponatremia	1.5	0.8	0.4	0	0.8	0.8	0	0
Muscular weakness	1.5	1.1	0	0	0	0	0	0
Esophageal varices hemorrhage	1.5	1.1	0	0.4	1.5	0.8	0	0.8
Vomiting	1.5	0.8	0	0	1.5	0.8	0	0

NOTE. Grade was not reported for 10 patients (3.8%) in the brivanib group and seven patients (5.3%) in the placebo group.
Abbreviation: AE, adverse event.

Table A5. Percent of AEs Resulting From Any Cause in Patients Who Progressed or Were Intolerant to Sorafenib

	Brivanib		Placebo	
AE	Progressed	Intolerant	Progressed	Intolerant
Overall incidence	99	100	94	94
Decreased appetite	59	69	23	29
Hypertension	47	50	14	12
Diarrhea	46	53	13	24
Fatigue	45	66	24	29
Nausea	35	47	20	29
Abdominal pain	29	22	19	29
Vomiting	29	50	8	18
Decreased weight	23	22	7	12
Asthenia	21	31	17	35
Dysphonia	21	28	2	0
Hyponatremia	21	19	9	0
Headache	20	28	10	0
Constipation	19	19	16	6
Upper abdominal pain	17	19	11	12
Peripheral edema	17	9	18	12
Hypothyroidism	16	13	2	6
Increased ALT	15	16	7	6
Dyspnea	15	9	11	18
Hand-foot syndrome	15	13	7	6
Cough	14	16	13	6
Dizziness	14	22	7	0
Pyrexia	14	13	9	12
Ascites	13	22	14	12
Dyspepsia	13	16	3	6
Back pain	11	16	9	6
Abdominal distension	10	6	11	6
Mucosal inflammation	10	9	3	6
Insomnia	10	9	9	6
Proteinuria	10	9	2	6
Rash	10	6	8	0
Stomatitis	10	3	1	0

NOTE. Adverse events (AEs; all grades) that occurred in at least 10% of the progressed patients in the brivanib arm between day 1 and at least 14 days after the last dose.

OPEN ACCESS Freely available online

PLOS ONE

Unique Association between Global DNA Hypomethylation and Chromosomal Alterations in Human Hepatocellular Carcinoma

Naoshi Nishida[1,2]*, Masatoshi Kudo[1], Takafumi Nishimura[3], Tadaaki Arizumi[1], Masahiro Takita[1], Satoshi Kitai[1], Norihisa Yada[1], Satoru Hagiwara[1], Tatsuo Inoue[1], Yasunori Minami[1], Kazuomi Ueshima[1], Toshiharu Sakurai[1], Naosuke Yokomichi[4], Takeshi Nagasaka[4], Ajay Goel[5]

1 Department of Gastroenterology and Hepatology, Kinki University Faculty of Medicine, Osaka-sayama, Japan, **2** Department of Gastroenterology and Hepatology, Kyoto University Graduate School of Medicine, Kyoto, Japan, **3** Outpatient Oncology Unit, Kyoto University Hospital, Kyoto, Japan, **4** Department of Gastroenterological Surgery and Surgical Oncology, Okayama University Graduate School of Medicine, Dentistry, and Pharmaceutical Sciences, Okayama, Japan, **5** Division of Gastroenterology, Department of Internal Medicine and Charles A. Sammons Cancer Center and Baylor Research Institute, Baylor University Medical Centre, Dallas, Texas, United States of America

Abstract

Global DNA hypomethylation is a characteristic feature of cancer cells that closely associates with chromosomal instability (CIN). However, the association between these characteristics during hepatocarcinogenesis remains unclear. Herein, we determined the relationship between hypomethylation and CIN in human hepatocellular carcinoma (HCC) by analyzing 179 HCCs, 178 matched non-tumor livers and 23 normal liver tissues. Hypomethylation at three different repetitive DNA (rDNA) sequences and hypermethylation of 12 CpG loci, including 11 tumor suppressor gene (TSG) promoters, were quantified using MethyLight or combined bisulfite restriction analysis. Fractional allelic loss (FAL) was used as a marker for CIN, calculated by analyzing 400 microsatellite markers. Gains and losses at each chromosome were also determined using semi-quantitative microsatellite analysis. The associations between rDNA hypomethylation and FAL, as well as between TSG hypermethylation and FAL were investigated. Significantly more hypomethylation was observed in HCC tissues than in normal liver samples. Progression of hypomethylation during carcinogenesis was more prominent in hepatitis C virus (HCV)-negative cases, which was in contrast to our previous reports of significantly increased TSG methylation levels in HCV-positive tumors. Absence of liver cirrhosis and higher FAL scores were identified as independent contributors to significant hypomethylation of rDNA in HCC. Among the chromosomal alterations frequently observed in HCC, loss of 8p, which was unique in the earliest stages of hepatocarcinogenesis, was significantly associated with hypomethylation of rDNA by multivariable analysis ($p = 0.0153$). rDNA hypomethylation was also associated with a high FAL score regardless of tumor differentiation ($p = 0.0011$, well-differentiated; $p = 0.0089$, moderately/poorly-differentiated HCCs). We conclude that DNA hypomethylation is an important cause of CIN in the earliest step of HCC, especially in a background of non-cirrhotic liver.

Citation: Nishida N, Kudo M, Nishimura T, Arizumi T, Takita M, et al. (2013) Unique Association between Global DNA Hypomethylation and Chromosomal Alterations in Human Hepatocellular Carcinoma. PLoS ONE 8(9): e72312. doi:10.1371/journal.pone.0072312

Editor: Chun-Ming Wong, University of Hong Kong, Hong Kong

Received May 8, 2013; **Accepted** July 9, 2013; **Published** September 2, 2013

Funding: This work was supported in part by Grant-in-Aid for Scientific Research (KAKENHI: 24590997; http://www.jsps.go.jp/j-grantsinaid/) from the Japanese Society for the Promotion of Science (N. Nishida) and a grant from the Smoking Research Foundation (http://www.srf.or.jp) (N. Nishida). The funders had no role in study design, data collection and analysis, decision to publish, or preparation of the manuscript.

Competing Interests: The authors declare that co-author Dr. Ajay Goel is a PLOS ONE Editorial Board member. This does not alter the authors' adherence to all the PLOS ONE policies on sharing data and materials.

* E-mail: naoshi@med.kindai.ac.jp

Introduction

Several reports suggest that promoter hypermethylation accounts for inactivation of the corresponding tumor suppressor genes (TSGs) [1]. In contrast, global DNA hypomethylation commonly found in cancer is thought to induce activation of potential oncogenes as well as chromosomal alterations, thereby contributing to carcinogenesis [2,3]. A significant link between global DNA hypomethylation and chromosomal aberrations has been reported in several cancers, implying that global hypomethylation may play an important role in inducing chromosomal instability (CIN) [4–6]. Furthermore, high levels of CpG island methylation are inversely correlated with CIN in CRC, again indicating an important role for these processes in carcinogenesis [7].

In human hepatocellular carcinoma (HCC), multiple genomic alterations are thought to be involved in carcinogenesis, suggesting the heterogeneity in the molecular pathogenesis of HCC [8]. Previously, we reported that inactivation of TSGs by regional hypermethylation in their promoters is a major mechanism driving human hepatocarcinogenesis, especially in hepatitis C virus (HCV)-related cases [9]. Nonetheless, the role of increased DNA hypomethylation within different types of repetitive elements in HCC is unclear. Our goal was to determine whether DNA hypomethylation is linked to CIN and influenced by background

Table 1. Profile of patients with well-differentiated and moderately or poorly differentiated HCC.

Clinical background	HCC cases		*p* value
	Well differentiated	Moderately/poorly differentiated	
	(*n* = 66)	(*n* = 113)	
Age (y.o.)			
Median (25^{th}–75^{th} percentiles)	61 (56–68)	60 (54–66)	0.3817*
Gender			
male/female/missing data	44/22/0	75/35/3	0.8353†
Hepatitis virus			
B/BC/C/NBNC‡	12/0/51/3	27/3/64/19	0.0166†
Adjacent non-cancerous liver			
non-LC/LC/missing data§	23/42/1	32/74/7	0.4801†
Child-Pugh classification			
Grade A/Grade B/missing	57/5/4	54/5/54	0.9347
Tumor size (cm)			
Median (25^{th}–75^{th} percentiles)	2.5 (1.4–4.0)	3.2 (2.5–6.0)	0.0021*
Serum AFP levels (ng/ml)			
Median (25^{th}–75^{th} percentiles)	16.9 (5.6–55.4)	119 (14.7–1615.8)	0.0009*

CI, confidence interval; HCC, hepatocellular carcinoma;
*p value by Wilcoxon rank-sum test;
†p value by the chi-square test. Missing cases of gender, missing adjacent non-cancerous liver samples, or hepatitis virus-positive cases carrying both HBs Ag and HCV Ab were excluded from statistical analysis using the chi-square test.
‡"B" denotes the cases with HBsAg-positive, "BC" denotes both HBsAg and HCV Ab-positive, "C" denotes HCV Ab-positive, and "NBNC" denotes the cases with both negative, respectively. All non-cancerous liver of HBV or HCV-positive cases was revealed as chronic hepatitis or liver cirrhosis according to the histological examination.
§"non-LC" denotes background liver without cirrhosis and "LC" denotes liver cirrhosis.?The presence of LC was determined by histological examination [12]. Child-Pugh classification represented the background liver function.
doi:10.1371/journal.pone.0072312.t001

disease and hepatitis virus infections, and if so, whether this association changes at various steps of human HCC.

In this study, we quantified DNA methylation levels at three repetitive DNA (rDNA) sequences, in the promoters of several TSGs and also determined the degree of CIN in a large number of HCC and liver tissues at various stages of tumorigenesis. Potential relationships between the degree of CIN and methylation status at rDNA and TSGs were extensively examined. We also analyzed characteristics of HCC with significant levels of DNA hypomethylation particularly in the context of degree of CIN. Our results demonstrated that global DNA hypomethylation took place at early stage of hepatocarcinogenesis especially in cases without HCV. Hypomethylation was also associated with degree of CIN and non-cirrhotic background liver. This study allowed us to provide a novel insight into the importance of epigenetic events, which may potentially drive CIN, leading to a more aggressive HCC phenotype.

Materials and Methods

Ethics

This study was approved by the institutional review boards of the involved institutions (reference number G365 by Kyoto University Graduate School and Faculty of Medicine, Ethnic Committee on July 13, 2010, reference number 24-001 at Kinki University Faculty of Medicine, Ethnic Committee on Apr. 20, 2012). Written informed consent was obtained from all patients.

Samples

DNA from 179 HCCs was used for quantification of methylation levels on rDNA sequences. Among them, 66 were well-differentiated and 113 were moderately- or poorly-differentiated HCCs. Adjacent non-cancerous liver and 23 normal liver tissue samples were included [10]. Patient characteristics and distributions of tumor stages are summarized in **Table 1**. The 149 tumors and their surrounding non-cancerous liver were fresh frozen tissues. The tumors and their surrounding non-cancerous liver were frozen immediately after surgical removal and stored at -80°C until DNA isolation [11]. The remaining 30 pairs of HCC and non-cancerous liver tissues and 23 normal liver tissues were obtained as formalin-fixed paraffin-embedded samples [11]. Differentiation of HCC was determined by histological examination. Similarly, presence of liver cirrhosis (LC) was examined histologically using Ishak fibrosis score [12]. All the samples were obtained during the surgery and samples with the availability of adequate DNA quantity were selected for further analyses. Among 23 normal liver tissues, 19 specimens came from patients who had colon cancer with hepatic metastasis. The remaining normal liver tissues were from focal nodular hyperplasia, hepatic hemangioma, and hepatic adenoma [9]. Histology of normal livers showed no evidence of fibrosis or inflammation. In addition, all cases of normal liver were confirmed to be free of serum Hepatitis B virus (HBV) surface antigen and HCV antibody and to have normal serum alanine aminotransferase levels and normal blood platelet counts.

Quantification of Methylation Levels in Repetitive DNA Sequences and TSG Promoters

DNA extraction and bisulfite modification treatment were described previously [13]. For extraction of tumorous DNA, we carefully selected tumorous tissue without containing non-tumor-

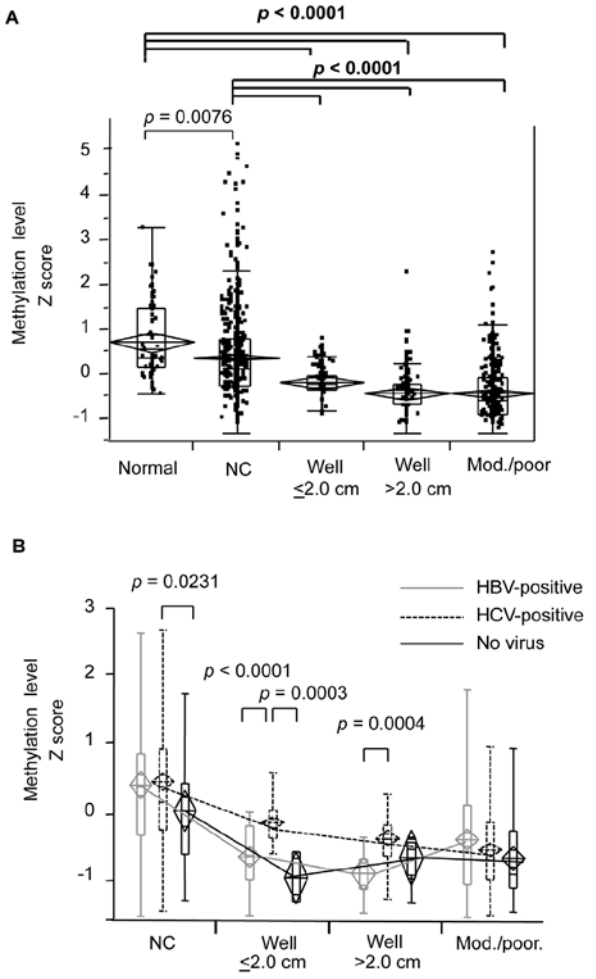

Figure 1. Distribution of the percentage methylation levels of repetitive DNA sequences in liver tissues. (A) Distribution of the percentage methylation levels (shown as *Z* scores) in all tumors. Box and whisker plots denote 75% and 95% distributions; lines within boxes show median values; mean methylation levels and 95% CI are shown as diamonds and lines within the diamonds, respectively. 'Normal' denotes normal liver ($n = 69$); 'NC' denotes matched, non-cancerous liver samples ($n = 520$); 'Well' denotes well-differentiated HCCs ($n = 87$ for ≤ 2.0 cm; $n = 111$ for > 2.0 cm); Mod./poor denotes moderately or poorly differentiated HCCs ($n = 339$). *P* values were calculated by post-hoc Tukey-Kramer HSD multiple comparison. Significant differences ($p < 0.0001$) are shown in bolt lines. The F and *p* values for the ANOVA test are as follows: F (4, 1125) = 69.64; $p < 0.0001$. (B) Significant hypomethylation of repetitive DNA sequences in tumors from HBV-positive (gray solid line), HCV-positive (black dashed line), and virus-negative (black solid line) patients. Methylation levels of three sequences (Alu, LINE-1, and SAT2) in each type of liver tissue were normalized to CpG methylase-treated DNA levels and expressed as a *Z* score. The box and whisker plots denote 75% and 95% distributions; lines within boxes show median values; mean methylation levels and 95% CI are shown as diamonds and lines within the diamonds, respectively. The three samples carrying both HBV and HCV were excluded from this analysis. The greatest difference in HCC hypomethylation was between virus-negative and HCV-infected tumors. *P* values were calculated using Tukey-Kramer HSD multiple comparison. The *p* values for each ANOVA test are as follows: F (2, 485) = 3.50, $p = 0.0311$ for NC; F (2, 78) = 22.21, $p < 0.0001$ for well-differentiated HCCs≤ 2.0 cm; F (2, 105) = 8.32, $p = 0.0004$ for well-differentiated HCCs > 2.0 cm.

doi:10.1371/journal.pone.0072312.g001

ous surrounding liver. rDNA methylation levels were quantified at two types of interspersed nucleotide repeats, long interspersed nuclear element-1 (LINE-1) and Alu, and one juxtacentromeric heterochromatin region, juxtacentromeric satellite 2 (SAT2), using the MethyLight methodology. The analysis of Alu sequences was performed using the consensus Alu sequence, and details of all PCR primers and probes used in this assay have been described previously [14]. Real-time quantitative PCR was performed using a StepOne real-time detection system (Applied Biosystems, Foster City, CA). PCR was performed according to the manufacturer's protocol using TaqMan Fast universal PCR Master Mix (Applied Biosystems). A standard curve for each assay was generated from serial dilutions of the reference sample, bisulfite-treated CpGenome Universal Methylated DNA (CHEMICON International Inc., Temecula, CA). The methylation-independent consensus Alu sequence was used as an endogenous control, as described previously [14]. Methylation levels at each rDNA sequence were normalized to those of CpG methylase-treated DNA.

Quantification of methylation levels in 11 TSG promoters and 1 MINT locus (*APC*, *CACNA1G*, *CASP8*, *CDKN2A*, *GSTP1*, *HIC1*, *PRDM2*, *PTGS2*, *RASSF1*, *RUNX3*, *SOCS1*, and MINT31) was performed using combined bisulfite restriction analysis, as previously described [9]. Based on our previous study, we selected 12 CpG loci for evaluation of status of regional hyermethylation because methylation levels of these CpG loci were markedly higher in well-differentiated HCC compared to non-cancerous liver, suggesting their potential role in early steps of human hepatocarcinogenesis [10].

Classification of HCC According to the Methylation Levels in Repetitive DNA Sequences and TSG Promoters

We applied hierarchical clustering analysis using methylation levels of 3 rDNA sequences as well as those of 11 TSG promoters and 1 MINT locus to discriminate tumors according to degree of hypomethylation and hypermethylation, respectively, because hierarchical clustering analysis is the most appropriate method to statistically discriminate HCC according to methylation levels of multiple loci. We compared the methylation levels of each cluster and classified HCCs as having either significant hypomethylation or slight hypomethylation in rDNA sequences and with either extensive hypermethylation or limited hypermethylation at the 12 CpG loci of the TSG promoters/MINT locus [9].

Quantification of Chromosomal Alterations by Fractional Allelic Loss

In order to determine the amount of chromosomal alterations in HCC samples, we analyzed allelic imbalance (AI) in 110 out of 179 liver tumor samples using 400 microsatellite markers equally distributed throughout all 23 chromosomes (ABI PRISM Linkage Mapping Set MD-10, Applied Biosystems). We could not obtain enough DNA from the remaining 69 samples for this analysis. Details of PCR conditions and assessment of AI were published previously [15]. Fractional allelic loss (FAL) scores, which broadly represent an index of CIN, were calculated as the number of microsatellite loci with AI divided by number of total informative loci and expressed as a percentage. We also evaluated allelic dose with multiples PCR using a retained allele and determined whether AI was the results of chromosomal gain or loss as described previously [15].

Statistical Analysis

We use Pearson's chi-square test or Fisher's exact test for comparison of categorical variables and Wilcoxon rank-sum test

Table 2. Mean methylation levels in different liver tissues.

Locus	Mean methylation level (%; 95% CI)					
	Normal liver	Non-cancerous liver	Well-differentiated HCC		Moderately or poorly-differentiated HCC	*p* value according to ANOVA*
			≤2.0 cm	>2.0 cm		
	(*n* = 23)	(*n* = 178)	(*n* = 29)	(*n* = 37)	(*n* = 113)	
Alu	0.70 (0.62–0.78)	**0.58 (0.55–0.61)**	**0.46 (0.41–0.50)**	**0.39 (0.35–0.42)**	**0.41 (0.37–0.45)**	**<0.0001**
LINE-1	0.72 (0.63–0.82)	0.69 (0.65–0.74)	**0.49 (0.42–0.56)**	**0.35 (0.29–0.41)**	**0.35 (0.31–0.38)**	**<0.0001**
SAT2	1.33 (1.14–1.53)	**1.02 (0.93–1.12)**	**0.54 (0.48–0.60)**	**0.50 (0.40–0.60)**	**0.45 (0.38–0.52)**	**<0.0001**

CI, confidence interval; HCC, hepatocellular carcinoma. Mean percent methylation (95% CI) at individual CpG loci in each type of liver sample is shown. Values in bold denote significant differences in methylation levels compared to normal liver tissue.
*F values are as follows: F (4, 374) = 21.87 for Alu; F (4, 375) = 50.78 for LINE1; F (4, 374) = 37.00 for SAT2.
doi:10.1371/journal.pone.0072312.t002

and Student's *t*-test for continuous variables. In order to compare the amount of methylation in all rDNA sequences (used to indicate global DNA hypomethylation) among different stages of liver tissues, analysis of variance (ANOVA) with post-hoc Tukey-Kramer honestly significant difference (HSD) multiple comparison was applied. For normalization of methylation levels on multiple loci, the Z score was applied which was defined as difference between individual and mean methylation level divided by standard deviation [9]. The mean and median value of FAL was 20%. Therefore, to discriminate HCCs according to the degree of CIN, we also classified tumors into two groups: those with an FAL score >20% and those with an FAL score ≤20%. To identify independent predictors of significant hypomethylation, we used multiple logistic regression analysis. All p values were two-sided, and $p<0.05$ was considered to indicate statistical significance. All statistical analyses were conducted using the JMP version 9.0 software (SAS Institute Inc., Cary, NC).

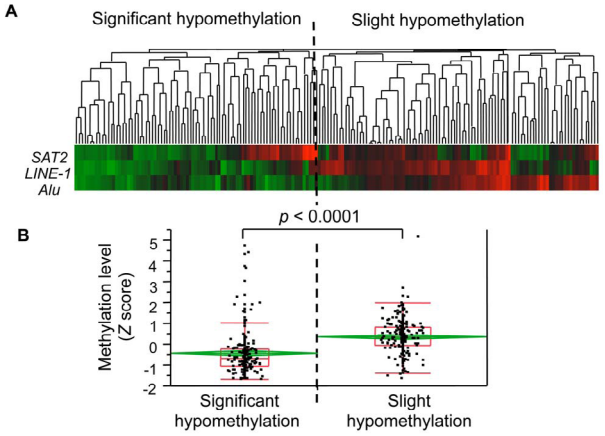

Figure 2. Categorization of tumors with significant hypomethylation of repetitive DNA sequences. All tumors were classified as either having "significant" or "slight" hypomethylation based on the methylation signatures at three different repetitive DNA elements (Alu, LINE-1 and SAT2). (A) The color map represents: green, low methylation level; red, high methylation level. (B) Distribution of methylation levels for each tumor subgroup classified in (A). Box and whisker plots (red line) denote 75% and 95% distribution; lines in the boxes denote median values; diamonds and lines within diamonds (green line) indicate the mean and 95% CI values, respectively. Methylation levels are expressed as Z scores. Mean and median Z values were −0.45949 and −0.66030 for HCCs with significant hypomethylation; and 0.34908 and 0.32342 for tumors with slight hypomethylation. P values were determined using the Student's t-test and the Wilcoxon rank-sum test. Both tests yielded the same p value.
doi:10.1371/journal.pone.0072312.g002

Results

Hypomethylation Status of rDNA Elements at Different Steps of Hepatocarcinogenesis

We compared the methylation levels of three different rDNA sequences in normal liver, non-tumor liver from HCC patients, and well-differentiated or moderately/poorly-differentiated HCC tissues [16]. Profiles of patients with tumors of each differentiation are shown in **Table 1**. HCV-positive status was more frequent in HCC samples classified as well-differentiated ($p = 0.0116$; chi-square test). Similarly, patients with well-differentiated HCC had smaller tumors and lower serum alpha-fetoprotein (AFP) levels ($p = 0.0021$ and $p = 0.0009$, respectively; Wilcoxon rank-sum test). For analysis of progression of hypomethylation during early step of hepatocarcinogenesis, we also compared rDNA methylation levels in well-differentiated HCCs of two different size categories: ≤2.0 cm and >2.0 cm.

Of the CpG loci analyzed, methylation at the Alu and SAT2 sequences in non-cancerous liver tissues was slightly lower than that in normal liver ($p = 0.0494$ for Alu and $p = 0.0334$ for SAT2: **Fig. S1**). HCC tumors at all stages of development had less rDNA methylation compared to normal liver and non-cancerous liver tissue at all three sequences, suggesting that hypomethylation is specific to carcinogenesis (**Table 2** and **Fig. S1**). **Fig. 1A** shows the decrease in global methylation levels at different HCC stages expressed as a Z score of methylation levels at all three rDNA elements. Overall, rDNA methylation decreased with progression of the liver disease ($p<0.0001$, ANOVA: **Fig. 1A**). Less methylation was observed in non-cancerous liver tissues compared to normal liver tissues ($p = 0.0076$, post-hoc Turkey-Kramer HSD multiple comparison), and methylation levels in HCC tissues were significantly decreased compared to normal liver samples even at the earliest stages of tumor development ($p<0.0001$: **Fig. 1A**).

Hypomethylation Reduces during HCC Development with Differing Viral Status

Next, we wanted to determine whether viral status affected alterations in rDNA methylation during tumor progression. We compared methylation levels in rDNA sequences from HBV, HCV, and virus-negative human HCC tumor samples. Hypo-

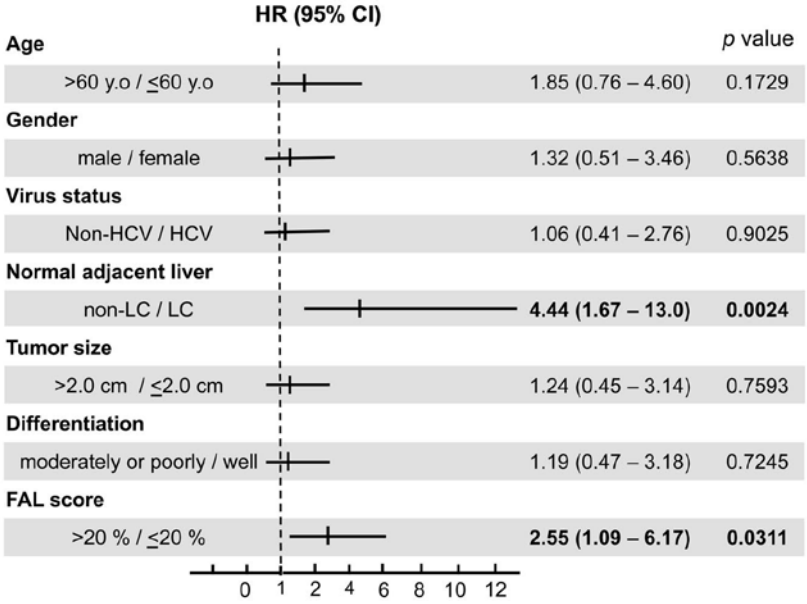

Figure 3. Multivariate analysis for contribution of each variable to significant hypomethylation in HCC. The *p* values were calculated using multiple logistic regression analysis. The total number of patients and the number of cases with significant hypomethylation in each group and the associated *p* values of univariate analyses calculated using the chi-square test are shown in **Table S2**. *P* values <0.05 are shown in bold.
doi:10.1371/journal.pone.0072312.g003

methylation of rDNA sequences was more prominent in HCV-negative tumors than in HCV-infected tumors in well-differentiated HCCs, especially in tumors <2.0 cm (well-differentiated HCCs≤2.0 cm in size: $p<0.0001$ for HBV-infected vs. HCV-infected tumors, $p=0.0003$ for virus-negative vs. HCV-infected tumors; well-differentiated HCC≥2.0 cm: $p=0.0004$ for HBV-infected vs. HCV-infected tumors; post-hoc Tukey-Kramer HSD multiple comparison; **Fig. 1B**). However, there were no significant

Table 3. Association between significant hypomethylation on repetitive DNA and alteration of specific chromosomal arms.

chromosome	Number of cases with significant hypomethylation/ total cases (%)	*P* value	chromosome	Number of cases with significant hypomethylation/ total cases (%)	*P* value
Loss of 1p			Loss of 9p		
with	20/54 (37%)		with	15/30 (50%)	
without	30/59 (51%)	0.1398	without	35/83 (42%)	0.4592
Gain of 1q			**Loss of 13q**		
with	34/82 (41%)		**with**	**21/35 (60%)**	
without	16/31 (52%)	0.3324	**without**	**29/78 (37%)**	**0.0239**
Loss of 4q			Loss of 16p		
with	23/46 (50%)		with	16/33 (48%)	
without	27/67 (40%)	0.3077	without	34/80 (43%)	0.5603
Loss of 6q			Loss of 16q		
with	**18/28 (64%)**		with	21/46 (46%)	
without	**32/85 (38%)**	**0.0138**	without	29/67 (43%)	0.8033
Loss of 8p			**Loss of 17p**		
with	**33/55 (60%)**		**with**	**28/51 (55%)**	
Without	**17/58 (29%)**	**0.0010**	**without**	**22/62 (35%)**	**0.0386**
Gain of 8q					
with	23/46 (50%)				
without	27/67 (40%)	0.3077			

Among 11 chromosomal arms frequently altered in HCC, significant association between alteration of chromosomal arms and global hypomethylation (determined by methylation status of repetitive DNA) were observed for loss of 6q, 8p, 13q, and 17p (shown in bold). Each *p* value was determined by chi-square test.
doi:10.1371/journal.pone.0072312.t003

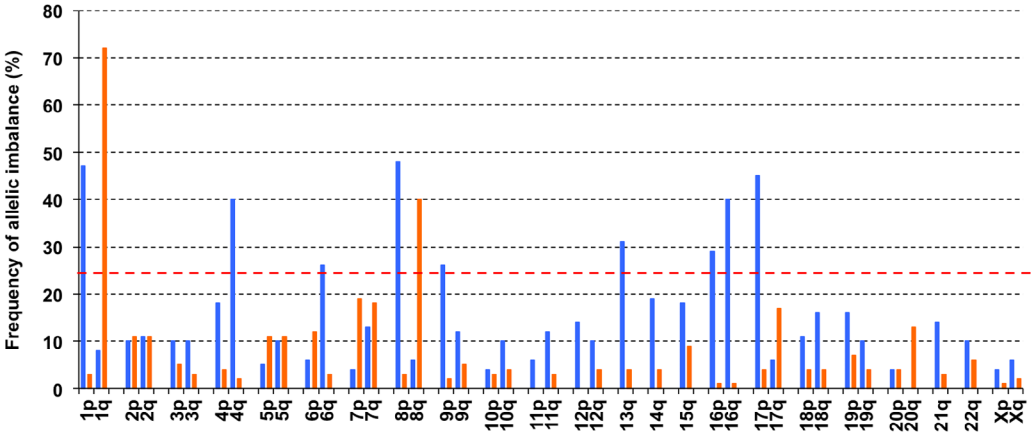

Figure 4. Frequencies of allelic imbalance in HCC on each chromosomal arm. The vertical bars show frequencies of allelic loss (shown in blue) and allelic gain (red); the allelic doses were determined by multiples PCR using a retained allele as a internal control [14]. The red horizontal dotted bar indicates the frequencies of 25%.
doi:10.1371/journal.pone.0072312.g004

differences associated with viral status among moderately or poorly differentiated HCCs. Thus, these data indicate that an increase in rDNA demethylation occurs more profoundly during early-stage tumor development in HCV-negative than in HCV-positive hepatocarcinogenesis.

Characterization of HCCs with Significant DNA Hypomethylation

We classified HCCs with significant global DNA hypomethylation according to methylation levels at Alu, LINE-1, and SAT2 sequences by using hierarchical clustering analysis, which objectively identifies statistical differences in DNA demethylation profiles (**Fig. 2A**). Following this analysis, all 179 HCCs were classified into two subclasses: in 83 liver tumors with significant levels of hypomethylation, rDNA methylation was much lower than that in HCCs with slight hypomethylation (mean and median Z scores were −0.45949 and −0.66030 for samples with significant hypomethylation versus 0.34908 and 0.32342 for those with slight hypomethylation, $p<0.0001$; Student's t-test and Wilcoxon rank-sum test; **Fig. 2B**). These results indicate that significant differences in global DNA hypomethylation levels in HCC tumors classified as having significant hypomethylation compared with those with slight hypomethylation. We also compared each methylation levels of Alu, LINE-1 and SAT2 between tumors classified as significant hypomethylation and slight hypomethylation. Methylation levels of tumors with significant hypomethylation were markedly lower than those of slight hypomethylation for all 3 CpG loci. These results also conformed that the classification by hierarchal clustering analysis is appropriate to discriminate the tumors based on global hypomethylation ($p<0.0001$ for Alu, $p<0.0001$ for LINE-1, and $p=0.0094$ for SAT2 by Wilcoxon rank-sum test; **Table S1**).

Variables such as age (>60 y.o., $p=0.0292$), gender (male, $p=0.0440$), viral status (non-HCV, $p=0.0337$), status of normal adjacent liver (non-LC, $p=0.0001$), tumor size (>2.0 cm, $p<0.0001$), tumor differentiation (moderately or poorly differentiated, $p=0.0075$), and FAL score (>20%, $p=0.0079$) were all associated with significant hypomethylation (**Table S2**). When we compared FAL scores as continuous variables in tumors with significant versus slight hypomethylation, tumors with significant hypomethylation had higher FAL scores (mean and median FAL scores of 27.1% vs. 18.5% and 23.1% vs. 17.0%, respectively, for HCCs with significant hypomethylation vs. slight hypomethylation; $p=0.0012$, Student's t-test, and $p=0.0023$, Wilcoxon rank-sum test: **Table S2**).

To further analyze the contribution of each variable to hypomethylation levels in HCC, we applied multiple logistic regression analysis. Among the variables which showed significant relation to hypomethylation, non-LC and higher FAL score were identified as independent contributors to significant global hypomethylation ($p=0.0024$, odds ratio = 4.44, 95% CI = 1.67–13.0 for non-LC; $p=0.0311$, odds ratio = 2.55, 95% CI = 1.09–6.17 for FAL score >20%; **Fig. 3**).

Association between Alterations on Specific Chromosomal Arms and rDNA Hypomethylation

According to semi-quantitative microsatellite analyses, the following chromosomal arms showed frequent alterations at more than 25% of tumors, which is a unique observation in human HCC: loss of 1p (45%), 4q (42%), 6q (28%), 8p (54%), 9p (28%), 13q (34%), 16p (30%), 16q (41%), and 17p (48%); gain of 1q (71%) and 8q (42%) (**Fig. 4**). Among these, we tried to clarify chromosomal alterations specifically affected by global hypomethylation. For this purpose, we compared frequencies of losses and gains of these chromosomal arms between tumors with significant and slight hypomethylation (**Table 3**). Of these, loss of 6q, 8p, 13q, and 17p were significantly associated with significant global hypomethylation. Notably, non-LC and loss of 8p was also identified as independent factors for accompanying significant global hypomethylation by multivariable analysis using age, gender, virus status, tumor size, tumor differentiation and loss of 6q, 8p, 13q, and 17p as co-variables ($p=0.0018$, odds ratio = 5.19, 95% CI = 1.81–16.2 for non-LC; $p=0.0153$, odds ratio = 3.14, 95% CI = 1.24–8.28 for loss of 8p: **Table 4**).

rDNA Hypomethylation is Associated with Chromosomal Instability in HCC

Multivariate analysis revealed that a high FAL score is an independent factor related to significant hypomethylation. To confirm that the association between significant hypomethylation and FAL score is tumor stage-independent, FAL scores were analyzed by hypomethylation status using hierarchical clustering

Table 4. Multivariate analysis for the contribution of specific chromosomal alterations to significant hypomethylation in HCC.

	Univariate analysis	Multivariate analysis	
Variables	***p* value***	***p* value†**	**Odds ratio (95% CI)**
Age (y.o)			
≤60	–	–	1
>60	**0.0292**	0.3329	1.61 (0.61–4.26)
Gender			
Female	–	–	1
Male	**0.0440**	0.4441	1.48 (0.55–4.12)
Virus status			
HCV	–	–	1
Non-HCV	**0.0337**	0.2106	1.93 (0.69–5.70)
Normal adjacent liver			
LC	–	–	1
Non-LC	**0.0001**	**0.0018**	**5.16 (1.81–16.2)**
Tumor size			
≤2.0 cm	–	–	1
>2.0 cm	**<0.0001**	0.9303	1.06 (0.27–4.61)
Differentiation			
Well	–	–	1
Moderately/Poorly	**0.0075**	0.9000	1.08 (0.34–3.53)
Loss of 6q			
Absent	–	–	1
Present	**0.0428**	0.1592	5.27 (0.55–128)
Loss of 8p			
Absent	–	–	1
Present	**0.0010**	**0.0153**	**3.14 (1.24–8.28)**
Loss of 13q			
Absent	–	–	1
Present	**0.0239**	0.4176	1.54 (0.54–4.47)
Loss of 17p			
Absent	–	–	1
Present	**0.0386**	0.0850	2.42 (0.89–6.95)

HCC, hepatocellular carcinoma;
*p value from the chi-square test or Fisher's exact test for comparison of two categorical variables;
†p value from multiple logistic regression analysis; p values <0.05 are shown in bold. Numbers of each case were shown in **Table S2** and **Table 3**.
doi:10.1371/journal.pone.0072312.t004

analyses (significant vs. slight) within each tumor grade (well-differentiated and moderately/poorly differentiated). We performed a similar analysis on tumor grade categorized according to extensive or limited TSG hypermethylation by using hierarchical clustering analysis of methylation levels at the 12 selected TSGs/MINT loci. The classification of significant or slight global hypomethylation, and extensive or limited TSG hypermethylation within each tumor grade based upon hierarchical clustering analyses is shown in **Figure S2**.

As shown in **Fig. 5**, higher FAL scores were exclusively associated with significant hypomethylation in well-differentiated tumors ($p = 0.0011$, Student's t-test; $p = 0.0015$, Wilcoxon rank-sum test; **Fig. 5A)**, but showed no association with extensive TSG methylation ($p = 0.2670$, Student's t-test; $p = 0.1601$, Wilcoxon rank-sum test; **Fig. 5B**). An association between global hypomethylation and CIN phenotype was also observed in moderately or poorly differentiated HCCs; HCCs with significant hypomethylation carried higher FAL scores than those with slight hypomethylation ($p = 0.0089$, Student's t-test; $p = 0.0270$, Wilcoxon rank-sum test; **Fig. 5C).** Again, no association was observed between TSG methylation levels and FAL scores ($p = 0.4527$, Student's t-test; $p = 0.6663$, Wilcoxon rank-sum test; **Fig. 5D**). Since we used matched pairs of tissue samples of HCC and non-cancerous liver, we also calculated the differences in the methylation levels between non-cancerous liver and HCC, and examined the relationship between the difference of methylation levels and FAL scores. The median difference of Z scores was 0.3; therefore we arbitrarily classified cases as with progressive hypomethylation if a difference in Z score was 0.3 or more. The cases with progressive hypomethylation carried HCC with higher FAL scores compared to those without progressive hypomethylation ($p = 0.0040$ by student-t test and $p = 0.0056$ by Wilcoxon rank-sum test: **Table S3**).

Discussion

In this study, we quantitatively and comprehensively analyzed DNA hypomethylation and CIN in HCCs using a structured approach that involved analysis of liver tissues during several stages of HCC development. Our findings indicated that rDNA hypomethylation increases with progression of liver disease. However, according to the analyses of rDNA hypomethylation and chromosomal alterations, hypomethylation is clearly associated with the amount of chromosomal alterations, regardless of tumor differentiation status. In addition, significant global hypomethylation is more often observed in non-cirrhotic livers; well-differentiated HCCs that are HCV-negative show greater hypomethylation than HCV-positive HCCs.

Repetitive DNA elements comprise approximately 45% of the human genome and consist of interspersed repeats and tandem repeats of simple (satellite DNA) or complex sequences. The Alu repeat and the LINEs are abundant nucleotide elements; their methylation status is reported to be associated with global methylation levels [14]. In contrast, satellite DNA is largely confined to centromeres or juxtacentromeric chromatin, and SAT2 is predominantly found in the juxtacentromeric heterochromatin of specific human chromosomes, such as chromosomes 1 and 16, where chromosomal alterations are frequently reported in HCC [17]. Therefore, we consider that methylation levels at these three types of rDNA sequences are representative of the global DNA methylation status [14,18]. Secondly, we investigated changes in hypomethylation at defined stages of HCC development. Several reports suggested that increases in global DNA hypomethylation are related to advanced tumor stages with poor tumor differentiation and argued that this phenomenon might be a consequence of carcinogenesis [6,19]. However, our analysis showed that significant demethylation could be detected in HCC regardless of tumor differentiation, compared to normal liver and adjacent non-cancerous tissue from HCC patients, suggesting an important role of global hypomethylation on emergence of HCC. However, despite the histological and serological determination of normal liver in this analysis, samples as normal controls were obtained from patients with metastatic colon cancer, which might affect the global methylation status of the liver. As we could not rule out the use of chemotherapy before liver resection, this might affect the methylation status in normal liver samples. In addition,

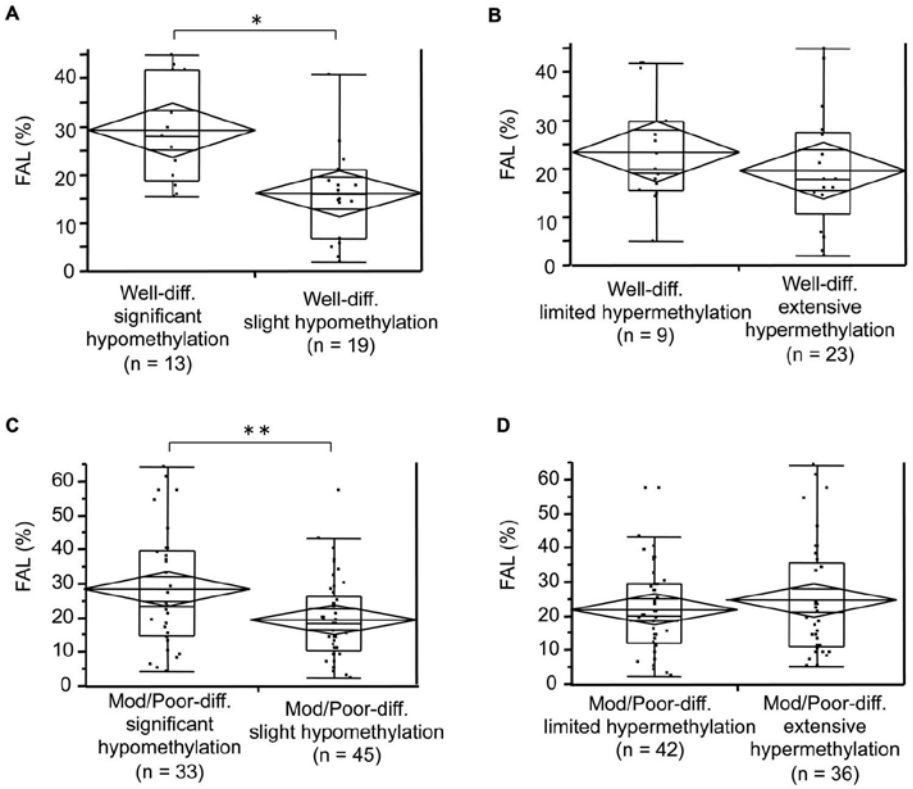

Figure 5. Association of FAL score and methylation status of repetitive DNA and TSG promoter in HCCs. Comparisons of FAL score (%) between HCCs with significant or slight hypomethylation at repetitive DNA (A, C), and between tumors with extensive or limited hypermethylation at TSG promoter (B, D) in well-differentiated and moderately/poorly differentiated HCCs. 'Well-diff.' denotes well-differentiated tumors and 'Mod/Poor diff.' denotes moderately/poorly differentiated tumors. Tumors were classified as having significant or slight hypomethylation following hierarchical clustering analysis of methylation levels at three repetitive DNA sequences (Alu, LINE-1 and SAT2: **Figure S2A, S2C**). Similarly, tumors were classified as having extensive or limited TSG hypermethylation following hierarchical clustering analysis of methylation levels at 12 TSGs/MINT loci that are frequently involved in HCC (**Figure S2B, S2D**). n = number of FAL scores in each group. Box and whisker plots denote 75% and 95% distribution; lines in the boxes denote median values; diamonds and lines within the diamonds indicate the mean and 95% CIs, respectively. *, $p = 0.0011$ by Student's *t*-test and $p = 0.0015$ by Wilcoxon rank-sum test; **, $p = 0.0089$ by Student's *t*-test and $p = 0.0270$ by Wilcoxon rank-sum test.
doi:10.1371/journal.pone.0072312.g005

selection of the patients may be affected by the liver function, as only patients with good liver function would get surgical resection, which may possibly be a potential limitation of this study.

Our previous study suggested that TSG inactivation via abnormal promoter methylation is a common occurrence, especially in HCV-related HCCs [9]. In contrast, in the present study, rDNA methylation levels at the early steps of tumor development were significantly lower in HCV-negative HCCs than in HCV-positive tumors. This suggests that increased DNA hypomethylation could be a unique characteristic at early step of hepatocarcinogenesis in HCV-negative livers. To confirm these traits in HCCs carrying significant hypomethylation, we applied hierarchical clustering analysis and categorized HCCs by increasing hypomethylation based on Alu, LINE-1, and SAT2 methylation. In addition to the absence of HCV, older age (>60 y.o.), male gender, absence of cirrhosis, large tumor size, tumor dedifferentiation, and high FAL scores were also associated with significant tumor hypomethylation. Some report suggested the association between DNA hypomethylation and gender as well as aging [20,21]. Global DNA methylation level in the mouse liver is reportedly affected by methyl-deficient diet more profoundly in male mice [20]. Aging might also affect a global DNA methylation level although it should be confirmed by a large-scale study [21]. So far, it might be attractive to speculate that DNA hypomethylation in the background liver might accelerate an emergence of HCC with significant hypomethylation, although no significant differences in the degree of hypomethylation was detected between non-LC and LC in background liver in this study ($p = 0.8397$ and 0.1081 by Student's t-test and Wilcoxon rank-sum test, respectively; data not shown). On the other hand, multivariate analysis revealed that the absence of cirrhosis and high FAL scores were independent risk factors for significant hypomethylation, supporting the idea that HCC with significant global hypomethylation tend to carry high FAL and emerge from background liver without cirrhosis.

In this study, we also found a significant correlation between global DNA hypomethylation and specific chromosomal alterations: losses of 6q, 8p, 13q, and 17p. Loss of 8p was identified as an independent factor for accompanying significant hypomethylation. Interestingly, recurrent losses of 8p and 17p were reportedly observed even in well-differentiated HCC and loss of 8p was unique in the earliest stages of hepatocarcinogenesis [15]. Therefore, to confirm an association between global hypomethylation and CIN at early steps of hepatocarcinogenesis, we classified both well-differentiated and moderately/poorly differentiated tumors as having "significant" or "slight" hypomethylation using

hierarchical clustering analysis and compared FAL scores between them. Interestingly, even in well-differentiated HCCs, tumors with significant levels of hypomethylation were clearly associated with high FAL scores, while no association was detected between extensive TSG hypermethylation and high FAL scores. Similar results were observed in moderately or poorly differentiated tumors. In addition, progression of hypomethylation from surrounding background liver to HCC tissues was also associated with higher FAL of HCC tissues. These results indicate that the relationship between DNA hypomethylation and high FAL scores is stage-independent and support the idea that global DNA hypomethylation is not simply a consequence of tumor progression but induces chromosome fragility, which could in turn lead to CIN in HCC, even at early steps of tumorigenesis.

Although mouse models revealed a clear association between DNA hypomethylation and the induction of CIN, the mechanism is still not clear. Activation of retrotransposition can lead to chromosomal arrangements [2,22]. Recently, Stefanska *et al.* reported that promoter DNA hypomethylation induces the expression of several genes involved in cell growth, signal transduction, and invasion, and thus contributes to hepatocarcinogenesis [23]. Therefore, genes that are activated through promoter DNA hypomethylation may also cause CIN if such hypomethylation is associated with rDNA hypomethylation within these genes [24]. Further study is required to clarify how DNA hypomethylation could be responsible for induction of CIN during hepatocarcinogenesis.

Our analysis revealed that HCC with significant hypomethylation is characterized by both a lack of cirrhosis and high FAL scores. Liver cirrhosis is a well-recognized premalignant condition, especially in HCV-positive patients. However, HCC can develop in the absence of cirrhosis, especially in HCV-negative cases [25]. Interestingly, TSG hypermethylation is reported to be more prevalent in HCC arising in a background of liver cirrhosis [26]. Another report suggested that environmental factors such as alcohol intake and HBV infection could contribute to HCC through global hypomethylation [18,27]. Recent analysis of whole genome sequence of HCC also revealed that a high degree of copy number alteration was more frequently observed in HBV-related tumor and tumors developed in non-cirrhotic liver [28]. Therefore, patients without HCV or cirrhosis may be more likely to develop HCC via DNA hypomethylation and CIN-related pathways, in contrast to HCV-related carcinogenesis, where HCV infection may reportedly introduce methylation-related TSG inactivation [9].

In this study, we characterized HCC cases carrying significant global DNA hypomethylation. rDNA hypomethylation occurred at an earlier step of hepatocarcinogenesis in the absence of HCV, and significant hypomethylation was associated with CIN and the absence of liver cirrhosis. This suggests that more than one pathway is involved in hepatocarcinogenesis; in the absence of HCV, increased global DNA hypomethylation is accompanied by CIN, which differs from the "CpG island methylator (CIMP) pathway" involved in HCV-related hepatocarcinogenesis [9]. Recently, DNA methyltransferase inhibitor and histone deacethylase inhibitor are applied for epithelial malignancy including HCC [29,30]. However, as both "CIMP" and "global hypomethylation and CIN" type pathways were suspected to exist, analysis of methylation profile should be critical for management of HCC.

Supporting Information

Figure S1 Alterations in methylation levels of repetitive DNA sequences.
(DOC)

Figure S2 Hierarchical clustering analysis for categorization of methylation status of global hypomethylation and hypermethylation of TSGs in well-differentiated HCCs and moderately or poorly differentiated HCCs.
(DOC)

Table S1 Difference of methylation levels of Alu, LINE-1, and SAT2 between tumor with significant hypomethylation and with slight hypomethylation.
(DOC)

Table S2 Univariate analysis of the contribution of each variable to significant hypomethylation at repetitive DNA sequences in HCC.
(DOC)

Table S3 Association between progression of hypomethylation and FAL score of HCC.
(DOC)

Author Contributions

Conceived and designed the experiments: NN AG. Performed the experiments: NN T. Nishimura. Analyzed the data: NN T. Nishimura MK. Contributed reagents/materials/analysis tools: NN T. Nishimura N. Yokomichi T. Nagasaka TA MT SK N. Yada SH TI YM KU TS. Wrote the paper: NN AG. Acquisition of data: NN T. Nishimura N. Yokomichi T. Nagasaka TA MT SK N. Yada SH TI YM KU TS. Obtain and support materials: NN N. Yokomichi T. Nishimura.

References

1. Baylin SB, Ohm JE (2006) Epigenetic gene silencing in cancer–a mechanism for early oncogenic pathway addiction? Nat Rev Cancer 6: 107–116.
2. Gaudet F, Hodgson JG, Eden A, Jackson-Grusby L, Dausman J, et al. (2003) Induction of tumors in mice by genomic hypomethylation. Science 300: 489–492.
3. Hansen KD, Timp W, Bravo HC, Sabunciyan S, Langmead B, et al. (2011) Increased methylation variation in epigenetic domains across cancer types. Nat Genet 43: 768–775.
4. Ogino S, Kawasaki T, Nosho K, Ohnishi M, Suemoto Y, et al. (2008) LINE-1 hypomethylation is inversely associated with microsatellite instability and CpG island methylator phenotype in colorectal cancer. Int J Cancer 122: 2767–2773.
5. Martínez JG, Pérez-Escuredo J, Castro-Santos P, Marcos CA, Pendas JL, et al. (2012) Hypomethylation of LINE-1, and not centromeric SAT-α, is associated with centromeric instability in head and neck squamous cell carcinoma. Cell Oncol 35: 259–267.
6. Igarashi S, Suzuki H, Niinuma T, Shimizu H, Nojima M, et al. (2010) A novel correlation between LINE-1 hypomethylation and the malignancy of gastrointestinal stromal tumors. Clin Cancer Res 16: 5114–5123.
7. Goel A, Nagasaka T, Arnold CN, Inoue T, Hamilton C, et al. (2007) The CpG island methylator phenotype and chromosomal instability are inversely correlated in sporadic colorectal cancer. Gastroenterology 132: 127–138.
8. Nishida N, Goel A (2011) Genetic and epigenetic signatures in human hepatocellular carcinoma: a systematic review. Curr Genomics 12: 130–137.
9. Nishida N, Nagasaka T, Nishimura T, Ikai I, Boland CR, et al. (2008) Aberrant methylation of multiple tumor suppressor genes in aging liver, chronic hepatitis, and hepatocellular carcinoma. Hepatology 47: 908–918.
10. Nishida N, Kudo M, Nagasaka T, Ikai I, Goel A (2012) Characteristic pattern of DNA methylation alterations predict emergence of human hepatocellular carcinoma. Hepatology 56: 994–1003.
11. Moore HM, Kelly AB, Jewell SD, McShane LM, Clark DP, et al. (2011) Biospecimen reporting for improved study quality (BRISQ). Cancer Cytopathol 119: 92–101.
12. Ishak K, Baptista A, Bianchi L, Callea F, De Groote J, et al. (1995) Histological grading and staging of chronic hepatitis. J Hepatol 22: 696–699.
13. Nishida N, Nishimura T, Nagasaka T, Ikai I, Goel A, et al. (2007) Extensive methylation is associated with beta-catenin mutations in hepatocellular

carcinoma: evidence for two distinct pathways of human hepatocarcinogenesis. Cancer Res 67: 4586–4594.
14. Weisenberger DJ, Campan M, Long TI, Kim M, Woods C, et al. (2005) Analysis of repetitive element DNA methylation by MethyLight. Nucleic Acids Res 33: 6823–6836.
15. Nishimura T, Nishida N, Itoh T, Kuno M, Minata M, et al. (2002) Comprehensive allelotyping of well-differentiated human hepatocellular carcinoma with semiquantitative determination of chromosomal gain or loss. Genes Chromosomes Cancer 35: 329–339.
16. International consensus group for hepatocellular neoplasia (2009) Pathologic diagnosis of early hepatocellular carcinoma: a report of the international consensus group for hepatocellular neoplasia. Hepatology 49: 658–664.
17. Saito Y, Kanai Y, Sakamoto M, Saito H, Ishii H, et al. (2002) Overexpression of a splice variant of DNA methyltransferase 3b, DNMT3b4, associated with DNA hypomethylation on pericentromeric satellite regions during human hepatocarcinogenesis. Proc Natl Acad Sci U S A 99: 10060–10065.
18. Wu HC, Wang Q, Yang HI, Tsai WY, Chen CJ, et al. (2012) Global DNA methylation levels in white blood cells as a biomarker for hepatocellular carcinoma risk: a nested case-control study. Carcinogenesis 33: 1340–1345.
19. Calvisi DF, Ladu S, Gorden A, Farina M, Lee JS, et al. (2007) Mechanistic and prognostic significance of aberrant methylation in the molecular pathogenesis of human hepatocellular carcinoma. J Clin Invest 117: 2713–2722.
20. Nohara K, Baba T, Murai H, Kobayashi Y, Suzuki T, et al. (2011) Global DNA methylation in the mouse liver is affected by methyl deficiency and arsenic in a sex-dependent manner. Arch Toxicol 85: 653–661.
21. Bollati V, Schwartz J, Wright R, Litonjua A, Tarantini L, et al. (2009) Decline in genomic DNA methylation through aging in a cohort of elderly subjects. Mech Ageing Dev 130: 234–239.
22. Kazazian HH Jr, Goodier JL (2002) LINE drive. retrotransposition and genome instability. Cell 110: 277–280.
23. Stefanska B, Huang J, Bhattacharyya B, Suderman M, Hallett M, et al. (2011) Definition of the landscape of promoter DNA hypomethylation in liver cancer. Cancer Res 71: 5891–5903.
24. Gordon DJ, Resio B, Pellman D (2012) Causes and consequences of aneuploidy in cancer. Nat Rev Genet 13: 189–203.
25. Kawada N, Imanaka K, Kawaguchi T, Tamai C, Ishihara R, et al. (2009) Hepatocellular carcinoma arising from non-cirrhotic nonalcoholic steatohepatitis. J Gastroenterol 44: 1190–1194.
26. Shen L, Ahuja N, Shen Y, Habib NA, Toyota M, et al. (2002) DNA methylation and environmental exposures in human hepatocellular carcinoma. J Natl Cancer Inst 94: 755–761.
27. Kim MJ, White-Cross JA, Shen L, Issa JP, Rashid A (2009) Hypomethylation of long interspersed nuclear element-1 in hepatocellular carcinomas. Mod Pathol 22: 442–449.
28. Guichard C, Amaddeo G, Imbeaud S, Ladeiro Y, Pelletier L, et al. (2012) Integrated analysis of somatic mutations and focal copy-number changes identifies key genes and pathways in hepatocellular carcinoma. Nat Genet. 44: 694–698.
29. Lin KT, Wang YW, Chen CT, Ho CM, Su WH, et al. (2012) HDAC inhibitors augmented cell migration and metastasis through induction of PKCs leading to identification of low toxicity modalities for combination cancer therapy. Clin Cancer Res 18: 4691–4701.
30. Lachenmayer A, Toffanin S, Cabellos L, Alsinet C, Hoshida Y, et al. (2012) Combination therapy for hepatocellular carcinoma: additive preclinical efficacy of the HDAC inhibitor panobinostat with sorafenib. J Hepatol 56: 1343–1350.

Covered Self-Expandable Metal Stents With an Anti-Migration System Improve Patency Duration Without Increased Complications Compared With Uncovered Stents for Distal Biliary Obstruction Caused by Pancreatic Carcinoma: A Randomized Multicenter Trial

Masayuki Kitano, MD, PhD[1], Yukitaka Yamashita, MD, PhD[2], Kiyohito Tanaka, MD, PhD[3], Hideyuki Konishi, MD, PhD[4], Shujiro Yazumi, MD, PhD[5], Yoshitaka Nakai, MD[6], Osamu Nishiyama, MD, PhD[7], Hiroyuki Uehara, MD, PhD[8], Akira Mitoro, MD, PhD[9], Tsuyoshi Sanuki, MD, PhD[10], Makoto Takaoka, MD, PhD[11], Tatsuya Koshitani, MD, PhD[12], Yoshifumi Arisaka, MD, PhD[13], Masatsugu Shiba, MD, PhD[14], Noriyuki Hoki, MD[15], Hideki Sato, MD, PhD[16], Yuichi Sasaki, MD[17], Masako Sato, MD[18], Kazunori Hasegawa, MD, PhD[19], Hideaki Kawabata, MD[20], Yoshihiro Okabe, MD[21] and Hidekazu Mukai, MD, PhD[22]

OBJECTIVES: **The requirements of biliary stents used in the palliation of malignant biliary obstruction are a long duration of patency and minimal adverse effects. Covered self-expandable metal stents (SEMSs) have been shown to prevent tumor ingrowth, which is the most frequent complication of uncovered SEMSs. However, because they are prone to migration, the superiority of covered SEMS has yet to be convincingly demonstrated. The aim of this study was to evaluate the superiority of covered over uncovered SEMSs in the palliation of distal biliary obstruction due to unresectable pancreatic carcinoma, using both stent types with relatively low axial force and uncovered flared ends to prevent their migration.**

METHODS: **From April 2009 to December 2010, 120 patients who were admitted to 22 tertiary-care centers because of distal biliary obstruction from unresectable pancreatic carcinomas were enrolled in this prospective randomized multicenter study. Patients were randomly assigned to receive a covered or uncovered SEMS deployed at the site of the biliary stricture during endoscopic retrograde cholangiopancreatography. Stent patency time, patient survival time, patient survival time without stent dysfunction (time to stent dysfunction or patient death), cause of stent dysfunction (ingrowth, overgrowth, migration, or sludge formation), and serious adverse events were compared between covered and uncovered SEMS groups.**

RESULTS: **Patient survival time in the two groups did not significantly differ (median: 285 and 223 days, respectively; *P*=0.68). Patient survival time without stent dysfunction was significantly longer in the covered than in the uncovered SEMS group (median: 187 vs. 132 days; *P*=0.043).**

[1]Department of Gastroenterology and Hepatology, Kinki University, Osaka-sayama, Japan; [2]Department of Gastroenterology, Japanese Red Cross Wakayama Medical Center, Wakayama, Japan; [3]Department of Gastroenterology, Kyoto Second Red Cross Hospital, Kyoto, Japan; [4]Molecular Gastroenterology and Hepatology, Kyoto Prefectural University of Medicine Postgraduate School of Medical Science, Kyoto, Japan; [5]Digestive Disease Center, The Tazuke Kofukai Medical Research Institute Kitano Hospital, Osaka, Japan; [6]Center for Hepatogastroenterology, Kyoto-Katsura Hospital, Kyoto, Japan; [7]Department of Gastroenterology, Osaka Medical Center, Osaka, Japan; [8]Department of Hepatobiliary and Pancreatic Oncology, Osaka Medical Center for Cancer and Cardiovascular Diseases, Osaka, Japan; [9]Third Department of Internal Medicine, Nara Medical University, Nara, Japan; [10]Department of Gastroenterology, Kobe University Graduate School of Medicine, Kobe, Japan; [11]Division of Gastroenterology and Hepatology, Department of Internal Medicine, Kansai Medical University, Hirakata, Japan; [12]Department of Gastroenterology, Kyoto City Hospital, Kyoto, Japan; [13]The Second Department of Internal Medicine, Osaka Medical College, Takatsuki, Japan; [14]Department of Gastroenterology, Osaka City University Graduate School of Medicine, Osaka, Japan; [15]Department of Gastroenterology, Bell Land General Hospital, Sakai, Japan; [16]Division of Gastroenterology, Japanese Red Cross Kyoto Daiichi Hospital, Kyoto, Japan; [17]Department of Gastroenterology, Hokusetsu General Hospital, Takatsuki, Japan; [18]Department of Gastroenterology, Osaka Rosai Hospital, Sakai, Japan; [19]Department of Gastroenterology and Hepatology, Otsu Red Cross Hospital, Otsu, Japan; [20]Gastroenterology, Otsu Municipal Hospital, Otsu, Japan; [21]Department of Gastroenterology and Hepatology, Osaka Red Cross Hospital, Osaka, Japan; [22]Department of Gastroenterology, Yodogawa Christian Hospital, Osaka, Japan. **Correspondence:** Kiyohito Tanaka, MD, PhD, Department of Gastroenterology, Kyoto Second Red Cross Hospital, 355-5 Haruobi-cho Kamigyo-ku, Kyoto city, Kyoto, Japan. E-mail: seijin7705@gmail.com

Received 18 February 2013; accepted 6 August 2013

Stent patency was also significantly longer in the covered than in the uncovered SEMS group (mean±s.d.: 219.3±159.1 vs. 166.9±124.9 days; $P=0.047$). Reintervention for stent dysfunction was performed in 14 of 60 patients with covered SEMSs (23%) and in 22 of 60 patients with uncovered SEMSs (37%; $P=0.08$). Stent dysfunction was caused by tumor ingrowth, tumor overgrowth, and sludge formation in 0 (0%), 3 (5%), and 11 (18%) patients in the covered SEMSs group, and in 15 (25%), 2 (3%), and 6 (10%) patients in the uncovered SEMSs group, respectively. Stent migration was not observed in either group. Rates of tumor overgrowth and sludge formation did not significantly differ between the two groups, whereas the rate of tumor ingrowth was significantly lower in the covered than in the uncovered SEMS group ($P<0.01$). Acute pancreatitis occurred in only one patient in the covered SEMS group. Acute cholecystitis occurred in one patient in the covered SEMS group and in two patients in the uncovered SEMS group. There was no significant difference between the two groups in the incidence of serious adverse events.

CONCLUSIONS: **By preventing tumor ingrowth and migration, covered SEMSs with an anti-migration system had a longer duration of patency than uncovered SEMSs, which recommends their use in the palliative treatment of patients with biliary obstruction due to pancreatic carcinomas.**

Am J Gastroenterol 2013; 108:1713–1722; doi:10.1038/ajg.2013.305; published online 17 September 2013

INTRODUCTION

Distal malignant biliary obstruction is a common problem in patients with pancreatic carcinoma. In unresectable pancreatic carcinomas, endoscopic stent placement has been pivotal in providing relief from obstructive jaundice, improving the quality of life, and allowing the maintenance of chemotherapy regimens (1–22). Compared with plastic stents, which are prone to occlusion by microbiofilm formation, several studies have reported high patency rates for self-expandable metal stents (SEMSs) (9–14). However, SEMSs are plagued by several as yet unresolved obstacles; in uncovered SEMS, stent occlusion due to epithelial hyperplasia and tumor ingrowth through the metal mesh is a frequent problem (9), whereas covered SEMSs are prone to migration (17,21,22,24). Moreover, the higher risk of cholecystitis associated with stent use has limited the adoption of either covered or uncovered SEMSs (17,24). In the light of these considerations, the advantages to be gained by using these stents for palliation in patients with distal malignant biliary obstruction have been controversially discussed. However, recent technological innovations have improved stent flexibility, in part by altering their axial force, which is the recovery force that straightens the SEMS after being bent (25). Previous reports showed covered SEMSs with low axial force to be less prone to migration (26,27). The aim of this randomized multicenter study was to assess the advantages of covered vs. uncovered SEMSs in terms of stent patency and safety. The tested SEMSs were composed of platinum-cored nitinol and were designed with relatively low axial force and flared ends, both of which contribute to preventing stent migration (27).

METHODS

Patients

This study was a prospective multicenter, open-labeled, randomized trial conducted at 22 tertiary-care centers. The study was approved by the Institutional Review Boards of each of the participating centers and performed according to the guidelines described in the Helsinki Declaration for biomedical research involving human subjects (Clinical trial registration number: UMIN000009778). Between April 2009 and December 2010, 427 patients who were admitted to 22 centers because of obstructive jaundice with lower biliary stricture were assessed for eligibility as described below. Of the 427 patients, 120 fulfilled the eligibility criteria and were enrolled in the study after providing written informed consent (**Figure 1**).

Eligibility criteria

Patients with an initial diagnosis of pancreatic carcinoma and malignant biliary obstruction were assessed using the following eligibility criteria. The inclusion criteria of the study were: (i) malignant distal biliary obstruction, (ii) pathologically diagnosed unresectable pancreatic carcinoma, and (iii) clinical stage > IIb (TNM classification of the UICC). The exclusion criteria were: (i) inability to obtain informed consent, (ii) Eastern Cooperative Oncology Group performance status of 4, (iii) severe dysfunction in other organs (American Society of Anesthesiologist physical status classification grade III or IV) (28), (iv) life expectancy of 3 months or less, (v) hilar biliary obstruction due to lymph node metastases, (vi) prior biliary surgery, (viii) intraductal papillary mucinous carcinomas, and (viii) failure of a previous drainage by nasobiliary tube or plastic stent. The diagnoses were based on the pathology results obtained by endoscopic retrograde cholangiopancreatography (ERCP) and/or endoscopic ultrasound-guided fine needle aspiration. Resectability was determined by the radiologic findings.

Randomization and blinding

Written consent was obtained from patients with known unresectable pancreatic carcinomas who were suffering from obstructive jaundice and fulfilled the eligibility criteria. They were then registered online. Otherwise, patients who were

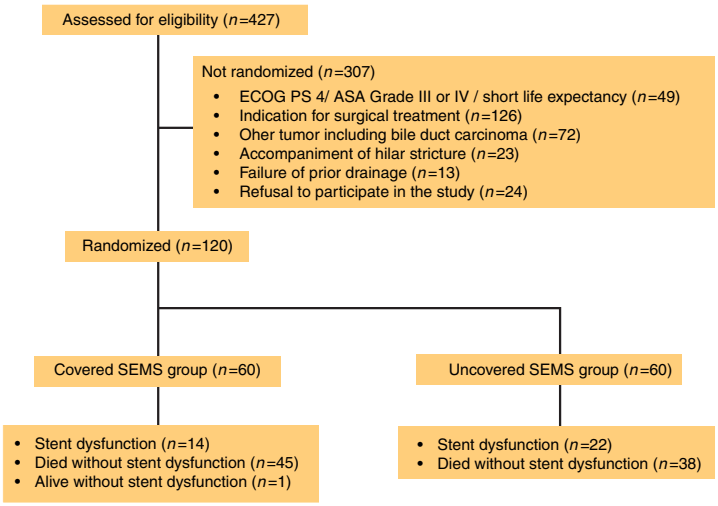

Figure 1. Flowchart showing results of inclusion, randomization, and follow-up of patients. ASA, American Society of Anesthesiologist; ECOG, Eastern Cooperative Oncology Group; SEMS, self-expandable metal stent.

urgently admitted to the hospitals because of obstructive jaundice first underwent biliary drainage with a nasobiliary tube or plastic stent (19). The diagnosis of pancreatic carcinoma was made by cytology or biopsy during ERCP or endoscopic ultrasound-guided fine needle aspiration. Thereafter, imaging studies were performed to diagnose the tumor stage. If the eligibility criteria were met following these pathological and radiological examinations, patients were registered on the Web. Immediately after Web registration, they were randomly assigned in a 1:1 ratio to either the covered or the uncovered SEMS group without stratification using a random number generator. The results of randomization were open labeled.

Procedures

A covered or uncovered SEMS (Wallflex biliary RX stent, Boston Scientific, Natick, MA) was deployed at the biliary stricture after sphincterotomy during ERCP. Both SEMSs are braided by a wire composed of platinum-cored nitinol with 5-mm uncovered flared portions at both ends (27). Their axial force at a 20-mm distance from the bending point (0.65 N) is relatively low compared with the other SEMSs such as Wallstent (Boston Scientific) (27). Covered SEMSs are covered by a silicone membrane. The diameter of the stent was 10 mm in all patients whereas its length (40, 60, or 80 mm) was determined according to the location and length of the biliary stricture; the stent extended at least 1 cm above the top of the stricture and approximately 5 mm into the duodenum.

Study design

Patients underwent periodic follow-up at the hospital where the stent was deployed and at the branch hospital until the patients' death. Improvement of jaundice was confirmed with serum total bilirubin at 2 and 4 weeks after the deployment of the SEMS. Stent dysfunction and adverse events were also monitored at 4-week intervals after the stent deployment. Stent dysfunction was diagnosed when patients presented with jaundice or cholangitis according to the protocol in a previously published study (19). Whenever apparent jaundice with high-grade fever occurred, patients urgently visited the hospitals and underwent reintervention as inpatients. Otherwise, physical examinations, complete blood cell counts, and biochemistry tests including liver function were performed at 4-week intervals on an outpatient basis in both groups. If any changes of liver function tests or findings related to inflammation were observed, imaging examinations such as ultrasonography, computed tomography, and magnetic resonance imaging were studied. If bile duct dilation was observed by any of these examinations, reintervention was immediately performed. If bile duct dilation was not observed, reintervention was not performed until bile duct dilation was confirmed, until there was an increase of serum total bilirubin, or until there was acute cholangitis refractory to antibiotics. Data on chemotherapy or radiotherapy after stent insertion were collected for later analyses. Clinical data were recorded until the patient's death or until 31 March 2012 (the date of last follow-up). The primary end point was the duration of stent patency, defined as the time of stent deployment until biliary reintervention due to stent dysfunction. The rates and causes of stent dysfunction were determined throughout the follow-up period. Secondary end points were overall patient survival and adverse events. Serious adverse events were defined as adverse events requiring an invasive procedure or hospitalization, or resulting in death. The rates of total adverse events, cholecystitis, pancreatitis, and migration were calculated for each group and the results were compared.

Statistical analysis

The primary analysis was a superiority comparison between covered and uncovered SEMSs for the primary end point of stent patency time using an intention-to-treat analysis. The required sample size to achieve statistical relevance was determined based on a previous study of covered and uncovered SEMSs, in which the stent patency rates for covered and uncovered SEMSs were 86% and 62%, respectively (16). To demonstrate a 24% difference (86% vs. 62%) in the stent patency rate, using a statistical power of 80% and with the assumption of a two-sided error rate of 0.05, the protocol required at least 112 randomly assigned patients. Therefore, by taking loss to follow-up into consideration, we determined that a sample size of 120 patients was adequate.

In each assigned group, the duration of stent patency was estimated using the Kaplan–Meier method. Patients who had not experienced recurrent biliary obstruction were censored at the date of last follow-up (31 March 2012) or date of death. The Kaplan–Meier method was used to evaluate overall patient survival, with living patients censored at the date of last follow-up (31 March 2012). The Kaplan–Meier method was also used to evaluate overall patient survival without stent dysfunction (the time to stent dysfunction or patient death), with living patients without stent dysfunction censored at the date of last follow-up (31 March 2012) (22). The time to stent dysfunction, time to patient's death, and time to stent dysfunction or patient's death between the two groups were compared using the log-rank test. In patients without stent dysfunction, the time to stent dysfunction was substituted for the time to patient death or the date of last follow-up to measure stent patency and mean values of stent patency were calculated for both groups (19). Fisher's exact test for categorical data and the unpaired *t*-test for continuous data were used to compare the two groups, with respect to their baseline characteristics, serum total bilirubin level before stent deployment and at 2 and 4 weeks after stent deployment, mean values of stent patency, stent dysfunction rates, the rates of the various causes of stent dysfunction, and the number of adverse events. The hazard ratios of prognostic factors for stent dysfunction were estimated using a Cox proportional hazards model, which included age, sex, clinical stage, serum total bilirubin level, chemotherapy, prior drainage, and stent length. All statistical analyses were conducted using SPSS statistical software version 11.0 (SPSS Institute, Tokyo, Japan).

RESULTS

Patient characteristics

Of the 427 patients assessed for eligibility, 307 were excluded for the following reasons: poor performance status, poor condition of other organs, and short life expectancy ($n=49$); indication for surgical intervention ($n=126$); other tumors including bile duct carcinomas and peripancreatic lymph node metastases ($n=72$); an accompanying hilar stricture ($n=23$); failure of prior drainage ($n=13$); and patient's refusal to participate in the study ($n=24$). The remaining 120 patients fulfilled the eligibility criteria and were enrolled in the study after providing written informed consent (**Figure 1**). The mean age of the 54 male and 66 female patients was 69.6 years (range, 46–90 years). Pancreatic carcinoma of clinical stage IIb, III, and IV was diagnosed in 21, 6, and 93 patients, respectively. No patients were excluded after enrollment. The characteristics of the patients who participated in the study are shown in **Table 1**. The two groups showed no significant difference in patient age, gender distribution, tumor stage, the number of patients receiving prior drainage, serum total bilirubin level before stent deployment and 2 and 4 weeks after stent deployment, and the number of patients treated with chemotherapy. Stents of 8 cm in length were used more often in the uncovered SEMS group. All patients, except one patient with a covered SEMS, experienced stent dysfunction or died during the follow-up period (**Figure 1**). No patients were lost to follow-up in either group (**Figure 1**).

Table 1. Patient characteristics in covered and uncovered SEMS groups

	Covered SEMS (n=60)	Uncovered SEMS (n=60)	P value
Mean age (years)	70.6±10.7	68.7±8.9	0.56
Gender (male:female)	25:35	29:31	0.30
Clinical stage (%)			
II	7 (11.7)	14 (23.3)	0.08
III	5 (8.3)	1 (1.7)	
IV	48 (80.0)	45 (75.0)	
Prior drainage	51 (85.0)	50 (83.3)	1.00
Total bilirubin (mg/dl)			
Before stent deployment	5.07±4.84	5.29±6.02	0.23
2 Weeks after stent deployment	1.62±1.37	1.84±3.02	0.61
4 Weeks after stent deployment	1.22±0.98	1.37±2.67	0.69
Stent length (cm)			
4	3 (5.0)	3 (5.0)	0.02
6	55 (91.7)	45 (75.0)	
8	2 (3.3)	12 (20.0)	
Chemotherapy (%)	47 (78.3)	47 (78.3)	0.53

SEMS, self-expandable metal stent.
Values expressed as mean±s.d. The variables were compared using the Fisher's exact test or the unpaired *t*-test.

Patient survival

The median follow-up period was 233 days (range, 17–996 days). At the time of final evaluation (30 March 2012), 112 patients (93.3%) had died, 56 (93.3%) in each group. The Kaplan–Meier curves for overall patient survival time are shown in **Figure 2**. The median survival time was 285 days in the covered SEMS group and 222 days in the uncovered SEMS group, a difference that was not statistically significant ($P=0.68$, log-rank test).

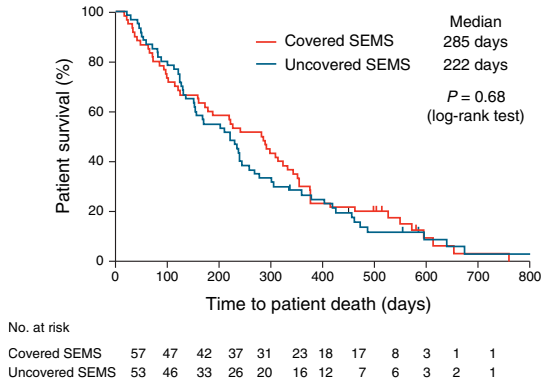

Figure 2. Kaplan–Meier curve showing cumulative patient survival (intention-to-treat analysis). There was no significant difference in patient survival between the covered and uncovered self-expandable metal stent (SEMS) groups (P=0.68, log-rank test).

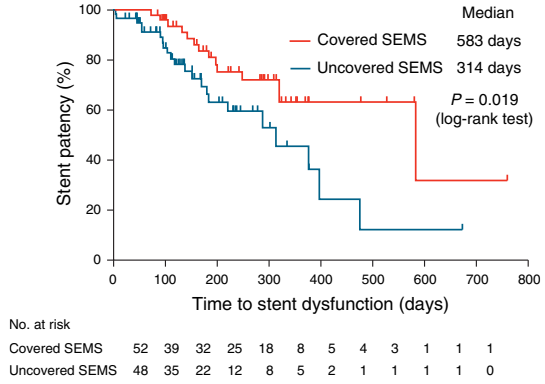

Figure 3. Kaplan–Meier curve showing cumulative stent patency (intention-to-treat analysis). Cumulative stent patency was significantly higher in covered than in uncovered self-expandable metal stents (SEMSs; P=0.019, log-rank test).

Stent patency

The Kaplan–Meier curves for the overall duration of stent patency time are shown in **Figure 3**. Referring to **Figure 3**, 84 of the 120 patients were censored because of death without stent dysfunction (n=83) or for being alive without stent dysfunction at the study conclusion (n=1); however, none of these patients were lost to follow-up. The cumulative duration of stent patency was significantly higher (P=0.019, log-rank test) in the covered than in the uncovered group (median: 583 vs. 314 days, respectively). The Kaplan–Meier curves for overall patient survival without stent dysfunction (duration of time to stent dysfunction or death) are shown in **Figure 4**, in which patients who died without stent dysfunction were considered as having stent dysfunction. The time to stent dysfunction or death was significantly longer in the covered (median: 187 days) than in the uncovered (median: 132 days) SEMS group (P=0.043, log-rank test). When time to death, or the date of last follow-up, was substituted for stent patency in patients without stent dysfunction in order to measure stent patency, the stent patency (mean±s.d.) was also significantly higher in the covered SEMS group (219.3±159.1 days) than in the uncovered SEMS group (166.9±124.9 days; P=0.047, unpaired t-test; **Table 2**).

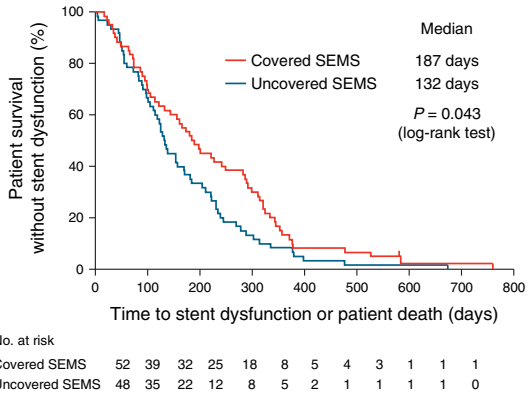

Figure 4. Kaplan–Meier curve showing cumulative patient survival without stent dysfunction (intention-to-treat analysis). The cumulative time to stent dysfunction or patient death was significantly higher in covered than in uncovered self-expandable metal stents (SEMSs; P=0.043, log-rank test).

Causes of stent dysfunction

Stent dysfunction was observed in 14 (23.3%) and 22 (36.7%) patients for covered and uncovered SEMS groups, respectively (P=0.08; **Table 2**). The rates of tumor ingrowth, tumor overgrowth, sludge formation, and stent migration, as causes of stent dysfunction for the covered and uncovered SEMSs, are summarized in **Table 2**. Tumor ingrowth did not occur in any of the covered SEMSs, in contrast to 25% of the uncovered type (P<0.01). Both tumor ingrowth and overgrowth were observed in one patient with an uncovered SEMS. There were no significant differences between the two groups in the incidence of tumor overgrowth and sludge formation, although the latter was approximately twice as high in the covered SEMS group (18.3% vs. 10.0% in the uncovered SEMS group).

Risk factors for stent dysfunction

The univariate and multivariate analyses of the risk factors for stent dysfunction are shown in **Table 3**. Univariate analysis revealed that covered SEMSs were at less risk of stent dysfunction (hazard ratio=0.45, P=0.02). Stent length and stent type were included in the multivariate analyses, because their associated P values were <0.25 in univariate analysis. Only stent type was an independent predictor of stent dysfunction, with a relative

Table 2. Stent patency duration, dysfunction and causes in covered and uncovered SEMSs

	Covered SEMS	Uncovered SEMS	*P* value
Stent patency: days (mean±s.d.)	219.3±159.1	166.9±124.9	0.047
Stent dysfunction: *n* (%)	14 (23.3)	22 (36.7)	0.081
Causes			
Tumor ingrowth: *n* (%)	0 (0)	15 (25.0)	<0.01
Tumor overgrowth: *n* (%)	3 (5.0)	2 (3.3)	0.65
Sludge formation: *n* (%)	11 (18.3)	6 (10.0)	0.19
Stent migration: *n* (%)	0 (0)	0 (0)	NA

NA, not applicable; SEMS, self-expandable metal stent.
Both tumor ingrowth and over growth were observed in one patient with an uncovered SEMS. $P<0.05$ was considered significant. Stent patency was defined as time to stent dysfunction, patient death, or the date of last follow-up.

risk of 0.44 for covered SEMS in comparison with uncovered SEMSs ($P=0.02$).

Adverse events

Acute pancreatitis occurred in only one patient, who had received a covered SEMS. The patient recovered after 7 days of conservative therapy. Acute cholecystitis occurred in one patient in the covered SEMS group, who was managed conservatively, and in two patients in the uncovered SEMS group, both of whom underwent percutaneous transhepatic gallbladder aspiration. There was no significant difference in the incidence of serious adverse events between the two groups.

DISCUSSION

A long duration of patency and minimal adverse effects are desired properties of biliary stents used in the palliation of malignant biliary obstruction. Recently published meta-analyses of multicenter randomized trials based on five full articles alone (17,21,22,29,30) (781 patients) and plus four studies published only in abstract form (31–34) (1061 patients) failed to prove the superiority of covered over uncovered SEMSs in terms of stent dysfunction rates at 3, 6, or 12 months or at study conclusion (35,36). This may be because patients with covered SEMSs tend to show a lower rate of tumor ingrowth and a higher rate of stent migration and tumor overgrowth (35,36). In addition, it is unclear whether covered SEMSs have a longer duration of stent patency than uncovered SEMSs (35,36), as this was the case in only three randomized multicenter studies of patients with distal malignant biliary obstruction (16,29,30). The discrepancies in the conclusions of these previous studies may have been due to heterogeneity in patient selection as well as differences in stent materials and stent configuration (35,36).

We implanted covered and uncovered SEMSs specifically designed to prevent migration. Both SEMSs were equipped with 5-mm uncovered flared portions at both ends. The stent covering was the only difference in design between the two types. The total serum bilirubin levels of two groups did not differ before stent deployment or at 2 and 4 weeks after stent deployment, suggesting that both groups were equivalent in terms of the improvement of biliary obstruction within 1 month of stent deployment. The stent dysfunction rate with covered SEMSs (23%) was lower than with uncovered SEMSs (37%), although they did not differ significantly ($P=0.08$). The cumulative patency duration of the covered SEMS group was significantly longer than that of the uncovered SEMS group ($P=0.019$). These results suggest that the anti-migration system of the covered SEMSs prevents stent dysfunction and prolongs stent patency, a distinct advantage over the use of uncovered SEMS.

At the date of last follow-up, 119 of 120 patients had died or undergone reintervention due to stent dysfunction, suggesting that the follow-up period was adequate to assess stent patency duration. However, considering the Kaplan–Meier analysis of stent patency, 84 of the 120 patients were censored because of death without stent dysfunction ($n=83$) or for being alive without stent dysfunction at the study conclusion ($n=1$), although no patients were lost to follow-up in either group. Also, the Kaplan–Meier curves showed that the median stent patency time was longer than the median patient survival time in both groups. Thus, we analyzed patient survival without stent dysfunction (times to stent dysfunction or patient death) in both groups, as per the method of Telford *et al.* (22). Patient survival without stent dysfunction was significantly longer in the covered SEMS group than in the uncovered SEMS group. Moreover, as per Isayama *et al.* (16), we measured mean values of stent patency in both groups. When time to death or the date of last follow-up was substituted for stent patency in patients without stent dysfunction (16), the mean stent patency was also significantly higher in the covered SEMS group than in the uncovered SEMS group. Therefore, because the patient survival times of covered and uncovered SEMS groups did not differ significantly, these facts indirectly suggest that covered SEMSs have an advantage over uncovered SEMSs in preventing stent dysfunction.

Percutaneous transhepatic biliary drainage was used in two of the three studies that showed superiority of covered SEMSs over uncovered SEMSs in terms of patency duration (29,30). Together with the first randomized controlled study (16), this only demonstrated the longer patency of covered SEMSs deployed during ERCP. However, compared with the first randomized controlled study comparing covered and uncovered SEMSs, which showed a 24% difference in stent dysfunction rates (14% vs. 38%) between both types (16), this study demonstrated a smaller difference (14%) in the stent dysfunction rates. In particular, the stent dysfunction rate for the covered SEMSs was higher in our study (23%) than in the previous study (14%), which may be caused by difference in the stent material, patient selection and follow-up duration. Regarding the follow-up duration, we followed up 119 of 120 patients until stent dysfunction or patient death. The longer follow-up

Table 3. Univariate and multivariate analyses of risk factors for stent dysfunction

	Patients (*n*)	Stent dysfunction (*n*)	%	Crude—HR (95% CI)	*P* value	Multiple-adjusted HR (95% CI)	*P* value
Age (years)	120	36	30.0	0.99 (0.96–1.02)	0.49		
Gender							
Female	66	23	34.8	1.00	0.30		
Male	54	13	24.1	0.70 (0.35–1.38)			
Clinical stage							
II	21	5	23.8	1.00			
III	6	2	33.3	0.63 (0.24–1.63)	0.34		
IV	93	29	31.2	0.95 (0.22–4.00)	0.94		
Total bilirubin (mg/dl)	120	36	30.0	0.99 (0.93–1.05)	0.73		
Prior drainage							
Absent	19	7	36.8	1.00	0.37		
Present	101	29	28.7	0.68 (0.29–1.57)			
Chemotherapy							
No	30	5	16.7	1.00	0.71		
Yes	90	31	34.4	1.20 (0.46–3.14)			
	14	6	42.9	3.67 (0.44–30.62)			
Stent length							
4 cm	6	1	16.7	1.00		1.00	
6 cm	100	29	24.2	3.08 (0.4–23.33)	0.23	2.87 (0.38–21.57)	0.31
8 cm	14	6	42.9	3.67 (0.4–30.62)	0.29	2.28 (0.27–19.65)	0.45
Stent type							
Uncovered	60	22	36.7	1.00	0.02	1.00	0.02
Covered	60	14	23.3	0.45 (0.23–0.88)		0.44 (0.21–0.9)	

CI, confidence interval; HR, hazards ratio.
Cox's proportional hazards model was used.

duration in our study may possibly be related to the higher dysfunction rate of the covered SEMSs.

Among the findings of this study, of particular interest is the absence of stent migration even with the covered SEMSs, as several studies have reported a higher rate of migration, and thus reduced duration of patency, with covered rather than uncovered SEMSs (17,18,21,22,35,36). Indeed, in three of the five randomized controlled studies where covered SEMSs exhibited longer patency than uncovered SEMSs, stent migration was not observed in all cases (16,30,31), whereas, in the other two studies where stent patency of both types did not differ, stent migration was observed in 6% and 12% of the covered SEMS group (21,22). These results suggest that stent migration mostly affects the patency of covered SEMSs. The risk of stent migration is related to the conformability of the stent in the bile duct, which is influenced by the axial force exerted by the stent. SEMSs with high axial force do not fit well in the curved bile duct, thus increasing the risk of stent-related complications including migration and bile duct kinking (16,17,18,22). By contrast, covered SEMSs with low axial force have been shown to have a lower stent migration rate than those with high axial force (26). The lower axial force and reduced incidence of stent migration of the covered Wallflex stent used in this study were recently demonstrated (27). It is therefore reasonable to assume that the migration of the covered stent used in our patients was prevented by its relatively low axial force.

Other factors accounting for the low incidence of migration of covered SEMS in our study may be the stent configuration and the deployment method. The covered Wallflex stent has 5-mm uncovered flared portions at both ends. We deployed the stent such that it extended at least 1 cm above the top of the stricture. Thus, the uncovered flared portion at this end may have anchored the stent to this segment of the bile duct; alternatively, it may have integrated into the duct wall at this site. In a recent study, fully covered SEMSs (Wallflex) with flared

ends were implanted in patients with biliary obstruction from pancreatic carcinomas (37). Despite the high stent patency rate (97% at 12 months), stent migration was still observed in 5% of cases (37). This finding supports the argument that anchoring or integration of the uncovered portion of SEMSs may prevent stent migration.

Tumor ingrowth occurs more frequently in uncovered SEMSs (35,36). In two earlier studies reporting no significant difference in stent patency between covered and uncovered SEMSs, tumor ingrowth occurred in 9–19% of covered SEMSs (21,22). By contrast, in four studies, including this study, that reported a statistically significant difference in duration of stent patency between covered and uncovered SEMSs, tumor ingrowth occurred in none of the covered SEMSs and in 25–29% of the uncovered SEMSs (16,29,30). These results suggest that the efficacy of covered SEMSs partly depends on the durability of the membrane covering and that SEMSs with a high durability membrane are warranted.

However, this covering also promotes sludge formation subsequent to bacterial biofilm, which is unavoidable in some cases. Indeed, in this study, the rate of sludge formation was approximately twice as high in the covered (18%) than in the uncovered SEMS group (10%). In all five aforementioned randomized controlled studies, the rates of sludge formation were higher in covered SEMS groups (4–7%) than in the uncovered SEMS groups (0–3%) (16,21,22,29,30,35,36). These results highlight the difficulty of avoiding sludge formation when using covered SEMSs. The rates of sludge formation for both groups in our study were higher than those in the five aforementioned studies, which may be caused by the long duration of our follow-up. Our results suggest that, following development of this anti-migration system, the development of a new cover material that minimizes sludge formation is required for longer patency.

Pancreatic carcinoma accounts for 59–82% of malignant biliary strictures (15–22,27) and differs from bile duct carcinoma by its rapid progression and the very poor prognosis of affected patients. We enrolled only patients with pancreatic carcinoma so that the properties of covered and uncovered SEMSs could be compared strictly in the same clinical setting. In a randomized controlled study comparing covered and uncovered SEMSs implanted via a percutaneous transhepatic approach in patients with pancreatic carcinoma, significant differences in the stent dysfunction rates of covered (10%) vs. uncovered (30%) SEMSs were reported (29). Isayama *et al.* (16) also noted a significantly higher cumulative patency of covered SEMSs in patients with pancreatic carcinoma, based on a subgroup analysis. Conversely, the two articles where both SEMS types did not differ in stent patency included tumors with other etiologies (18% and 23%) than pancreatic carcinoma (21,22). Thus, the detection of significant differences in duration of stent patency between the two types may depend on strict patient selection. To the best of our knowledge, this is the first report to show distinct advantages of covered over uncovered SEMSs for persistent biliary drainage in patients with pancreatic carcinoma. A further study comparing the two types of SEMSs in other tumors, such as ampullary, bile duct, and gallbladder carcinomas, may further support our hypothesis.

Chemotherapy prolongs the overall patient survival of patients with pancreatic carcinoma and, by inhibiting tumor ingrowth and overgrowth, it is reasonable to assume that it also prolongs stent patency. However, the univariate analyses performed in this study found no effect of chemotherapy on stent patency; rather, stent type was the only risk factor for stent dysfunction, suggesting that the effectiveness of SEMSs is independent of tumor progression.

The deployment of covered SEMSs in some patients is accompanied by the development of adverse events such as cholecystitis and pancreatitis. Covered SEMSs may be prone to causing occlusion of the pancreatic and the cystic duct orifices (17,37–39). However, all five aforementioned randomized controlled studies and meta-analyses did not find differences in the rates of cholecystitis and pancreatitis between patients with covered and uncovered SEMSs (16,21,22,29,30,35,36). Isayama *et al.* (40) similarly did not find a significant difference in the incidence of cholecystitis in patients with covered (5.8%) and uncovered (4.0%) SEMSs. They proposed that occlusion of the cystic duct was not associated with the stent membrane but with tumor involvement to the orifice of the cystic duct. In this study, pancreatitis occurred in only one patient with a covered SEMS, whereas cholecystitis developed in two patients with uncovered SEMSs and in one with a covered SEMS. There was no significant difference in the incidence of serious adverse events between the two groups, which is consistent with previous reports (16,21,22,29,30,35,36).

This study has several limitations. First, although the two groups did not significantly differ in terms of patient age, gender distribution, tumor stage, serum total bilirubin level before and after stent deployment, and the number of patients treated with chemotherapy, there was a difference in the length of the stents implanted in the two groups of patients. In the uncovered SEMS group, 8-cm stents were more frequently used. Regardless of stent length, however, care was taken during all deployments to procure adequate safety margins at both the proximal and distal ends of the narrowed bile duct to prevent tumor overgrowth because, when fully expanded, the Wallflex stents shorten by one-third. In this study, the rates of tumor overgrowth did not differ significantly between the two groups and stent length was not identified as a risk factor for stent dysfunction in the univariate and multivariate analyses, suggesting that the deployed stents were long enough to prevent tumor overgrowth. However, meta-analyses have shown a higher rate of tumor overgrowth with covered SEMSs (35,36). The reasons underlying the lower incidence rates of tumor overgrowth and stent migration in the covered SEMS group of this study, compared with similar groups in previous studies or in the meta-analyses have not been clearly elucidated (16,21,22,29–36).

A second limitation relates to the potential bias for patient selection, and the time and criteria for deciding when reintervention should be performed. We excluded patients with poor performance status, poor condition of other organs, and short life expectancy. If patient survival times were shorter because

of poorer medical conditions among patients, it would be likely that more patients would been censored before stent dysfunction occurred. Nevertheless, exclusion of patients in poor medical condition might affect the duration of stent patency in both groups. Although periodic liver function tests were performed, the intervals between follow-up imaging studies were not uniform. Also, it was difficult to define the absolute values of liver function tests for deciding reintervention because the conditions in each patient and each hospital differed. These facts might also lead to the long stent patency time in both groups.

A third limitation is that prior drainage confounded an assessment of the efficacy of SEMSs alone in improving clinical symptoms, although both groups did not differ significantly in serum total bilirubin level within a month of stent deployment and the number of patients receiving post-treatment chemotherapy. In this study, prior drainage was performed in 101 of 120 patients. Indeed, in the previous three randomized controlled studies comparing both types of SEMS with endoscopic treatment, 15%, 64%, and 100% of the enrolled patients received prior biliary drainage, which made it difficult to assess directly the efficacy of SEMSs alone in improving clinical symptoms (19,20,21). The use of removable fully covered SEMSs may allow a more accurate assessment of their ability to improve obstructive jaundice because they can be used for malignant distal biliary stricture, irrespective of the patient's surgical resectability status (37). A fourth potential limitation is that patient survival greatly affected the outcomes of the stent patency, because 83 patients (69%) died (censored) without stent dysfunction, which resulted in the small sample sizes for the subgroup comparisons. Therefore, increased variation occurred in the later portions of the Kaplan–Meier curves.

In conclusion, stent migration did not occur in patients with either covered or uncovered SEMSs, an advantage most likely due to the use of stents with relatively low axial force and uncovered flared ends. Conversely, the rate of tumor ingrowth was significantly lower in the group of patients with covered SEMSs. Importantly, covered SEMSs with an anti-migration system had a longer duration of stent patency than uncovered SEMSs. We therefore strongly recommend the use of these covered SEMSs for the palliative treatment of patients with distal biliary obstruction due to unresectable pancreatic carcinoma.

ACKNOWLEDGMENTS

We thank all the patients, their families, and our medical staff for their participation in the study.

CONFLICT OF INTEREST

Guarantor of the article: Masayuki Kitano, MD, PhD.

Specific author contributions: Masayuki Kitano: wrote the manuscript; Yukitaka Yamashita, Hideyuki Konishi, Yoshitaka Nakai, Osamu Nishiyama, Hiroyuki Uehara, Akira Mitoro, Tsuyoshi Sanuki, Makoto Takaoka, Tatsuya Koshitani, Noriyuki Hoki, Hideki Sato, Yuichi Sasaki, Masako Sato, Kazunori Hasegawa, Hideaki Kawabata, and Yoshihiro Okabe: substantive revision of the manuscript; Kiyohito Tanaka, Shujiro Yazumi, and Yoshifumi Arisaka: drafted conception and design, and substantive revision of the manuscript; Masatsugu Shiba: statistical analysis and substantive revision of the manuscript; Hidekazu Mukai: proposed the randomized multicenter study as well as its conception and design, and substantive revision of the manuscript.

Financial support: None.

Potential competing interests: None.

LIVER

Study Highlights

WHAT IS CURRENT KNOWLEDGE

- ✓ In unresectable pancreatic carcinomas, endoscopic stent placement has been pivotal in providing relief from obstructive jaundice.
- ✓ The advantages of using covered vs. uncovered self-expandable metal stents (SEMSs) in the palliation of distal malignant biliary obstruction are controversial.
- ✓ Uncovered SEMSs are prone to tumor ingrowth through the metal mesh, whereas covered SEMSs are prone to stent migration.

WHAT IS NEW HERE

- ✓ Covered SEMSs with an anti-migration system (relatively low axial force and uncovered flared ends) had a longer duration of patency than uncovered SEMSs for the palliative treatment of patients with distal biliary obstruction due to pancreatic carcinoma.
- ✓ The membrane covering lowered the rate of tumor ingrowth, whereas the anti-migration system prevented migration of the covered SEMSs.

REFERENCES

1. Soehendra N, Reynders-Frederix V. Palliative bile duct drainage: a new endoscopic method of introducing a transpapillary drain. Endoscopy 1980;12:8–11.
2. Huibregtse K, Tytgat GN. Palliative treatment of obstructive jaundice by transpapillary introduction of large bore bile duct endoprosthesis. Gut 1982;23:371–5.
3. Walta DC, Fausel CS, Brant B. Endoscopic biliary stents and obstructive jaundice. Am J Surg 1987;153:444–7.
4. Speer AG, Cotton PB, Russell RC *et al.* Randomised trial of endoscopic versus percutaneous stent insertion in malignant obstructive jaundice. Lancet 1987;2 (8550): 57–62.
5. Dowsett JF, Cairns SR, Vaira D *et al.* Endoscopic endoprosthesis insertion following failure of cholecystojejunostomy in pancreatic carcinoma. Br J Surg 1989;76:454–6.
6. Huibregtse K, Cheng J, Coene PP *et al.* Endoscopic placement of expandable metal stents for biliary strictures--a preliminary report on experience with 33 patients. Endoscopy 1989;21:280–2.
7. Irving JD, Adam AD, Dick R *et al.* Gianturco expandable metallic biliary stents: results of a European clinical trial. Radiology 1989;172:321–6.
8. Lammer J, Klein GE, Kleinert R *et al.* Obstructive jaundice: use of expandable metal endoprosthesis for biliary drainage. Radiology 1990;177: 789–92.
9. Davids PHP, Groen AK, Rauws EAJ *et al.* Randomized trial of self-expanding metal stents versus polyethylene stents for distal malignant biliary obstruction. Lancet 1992;340:1488–92.
10. Knyrim K, Wagner HJ, Pausch J *et al.* A prospective, randomized, controlled trial of metal stents for malignant obstruction of the common bile duct. Endoscopy 1993;25:207–12.
11. Hoepffner N, Foerster EC, Högemann B *et al.* Long-term experience in Wallstent therapy for malignant choledochal stenosis. Endoscopy 1994;26:597–602.

12. Smith AG, Dowset JF, Rassell RCG *et al.* Randomized trial of endoscopic stenting versus surgical bypass in malignant low bileduct obstruction. Lancet 1994;344:1655–60.
13. Lammer J, Hausegger KA, Flükiger F *et al.* Common bile duct obstruction due to malignancy: treatment with plastic versus metal stents. Radiology 1996;201:167–72.
14. Prat F, Chapat O, Ducot B *et al.* A randomized trial of endoscopic drainage methods for inoperable malignant strictures of the common bile duct. Gastrointest Endosc 1998;47:1–7.
15. Dumonceau JM, Cremer M, Auroux J *et al.* A comparison of Ultraflex diamond stents and Wallstents for palliation of distal malignant biliary strictures. Am J Gastroenterol 2000;95:670–6.
16. Isayama H, Komatsu Y, Tsujino T *et al.* A prospective randomised study of "covered" versus "uncovered" diamond stents for the management of distal malignant biliary obstruction. Gut 2004;53:729–34.
17. Park DH, Kim MH, Choi JS *et al.* Covered versus uncovered Wallstent for malignant extrahepatic biliary obstruction: a cohort comparative analysis. Clin Gastroenterol Hepatol 2006;4:790–6.
18. Yoon WJ, Lee JK, Lee KK *et al.* A comparison of covered and uncovered Wallstents for the management of distal malignant biliary obstruction. Gastrointest Endosc 2006;63:996–1000.
19. Loew BJ, Howell DA, Sanders MK *et al.* Comparative performance of uncoated, self-expanding metal biliary stents of different designs in 2 diameters: final results of an international multicenter, randomized, controlled trial. Gastrointest Endosc 2009;70:445–53.
20. Weston BR, Ross WA, Liu J *et al.* Clinical outcomes of nitinol and stainless steel uncovered metal stents for malignant biliary strictures: is there a difference? Gastrointest Endosc 2010;72:1195–200.
21. Kullman E, Frozanpor F, Söderlund C *et al.* Covered versus uncovered self-expandable nitinol stents in the palliative treatment of malignant distal biliary obstruction: results from a randomized, multicenter study. Gastrointest Endosc 2010;72:915–23.
22. Telford JJ, Carr-Locke DL, Baron TH *et al.* A randomized trial comparing uncovered and partially covered selfexpandable metal stents in the palliation of distal malignant biliary obstruction. Gastrointest Endosc 2010;72:907–14.
23. Song TJ, Lee SS, M *et al.* Paclitaxel-eluting covered metal stents versus covered metal stents for distal malignant biliary obstruction: a prospective comparative pilot study. Gastrointest Endosc 2011;73:727–33.
24. Ho H, Mahajan A, Gosain S *et al.* Management of complications associated with partially covered biliary metal stents. Dig Dis Sci 2010;55:516–22.
25. Isayama H, Nakai Y, Toyokawa Y *et al.* Measurement of radial and axial forces of biliary self-expandable metallic stents. Gastrointest Endosc 2009;70:37–44.
26. Isayama H, Kawabe T, Nakai Y *et al.* Management of distal malignant biliary obstruction with the ComVi stent, a new covered metallic stent. Surg Endosc 2010;24:131–7.
27. Isayama H, Mukai T, Itoi T *et al.* Comparison of partially covered nitinol stents with partially covered stainless stents as a historical control in a multicenter study of distal malignant biliary obstruction: the WATCH study. Gastrointest Endosc 2012;76:84–92.
28. Dripps RD, Lamont A, Eckenhoff JE. The role of anesthesia in surgical mortality. JAMA 1961;178:261–6.
29. Krokidis M, Fanelli F, Orgera G *et al.* Percutaneous palliation of pancreatic head cancer: randomized comparison of ePTFE/FEP–covered versus uncovered nitinol biliary stents. Cardiovasc Intervent Radiol 2011;34:352–61.
30. Krokidis M, Fanelli F, Orgera G *et al.* Percutaneous treatment of malignant jaundice due to extrahepatic cholangiocarcinoma: covered viabil stent versus uncovered Wallstents. Cardiovasc Intervent Radiol 2010;33:97–106.
31. Cho YD, Cheon YK, Yoo K *et al.* Uncovered versus covered self-expanding metallic stents for inoperable malignant distal biliary obstruction: a prospective randomized multicenter study. Gastrointest Endosc 2009;69:AB137.
32. Gonzalez-Huix F, Huertas C, Figa M *et al.* A randomized controlled trial comparing the covered (CSEMS) versus uncovered self-expandable metal stents (USEMS) for the palliation of malignant distal biliary obstruction (MDBO): interim analysis. Gastrointest Endosc 2008;67:AB166.
33. Lee SH, Cha SW, Cheon YK *et al.* A randomized controlled comparative study of covered versus uncovered self-expandable metal stent for malignant biliary obstruction. Gastrointest Endosc 2004;59:P188.
34. Smits ME, Rauws EAJ, Groen AK *et al.* Preliminary results of a prospective randomized study of partially covered Wallstents vs noncovered Wallstents. Gastrointest Endosc 1995;41:416.
35. Saleem A, Leggett CL, Murad MH *et al.* Meta-analysis of randomized trials comparing the patency of covered and uncovered self-expandable metal stents for palliation of distal malignant bile duct obstruction. Gastrointest Endosc 2011;74:321–7.
36. Almadi MA, Barkun AN, Martel M. No benefit of covered vs uncovered self-expandable metal stents in patients with malignant distal biliary obstruction: a meta-analysis. Clin Gastroenterol Hepatol 2013;11:27–37.
37. Siddiqui AA, Mehendiratta V, Loren D *et al.* Fully covered self-expandable metal stents are effective and safe to treat distal malignant biliary strictures, irrespective of surgical resectability status. J Clin Gastroenterol 2011;45:824–7.
38. Willingham FF. All wrapped up: metal biliary stents and the effect of stent coverings. Gastrointest Endosc 2010;72:924–6.
39. Kubota Y, Mukai H, Nakaizumi A *et al.* The covered Wallstent for palliation of malignant common bile duct stricture: a prospective multicenter evaluation. Digest Endosc 2005;17:218–23.
40. Isayama H, Kawabe T, Nakai Y *et al.* Cholecystitis after metallic stent placement in patients with malignant distal biliary obstruction. Clinical Gastroenterol Hepatol 2006;4:1148–53.

Japanese multicenter experience of endoscopic necrosectomy for infected walled-off pancreatic necrosis: The JENIPaN study

Authors I. Yasuda[1], M. Nakashima[1], T. Iwai[2], H. Isayama[3], T. Itoi[4], H. Hisai[5], H. Inoue[6], H. Kato[7], A. Kanno[8], K. Kubota[9], A. Irisawa[10], H. Igarashi[11], Y. Okabe[12], M. Kitano[13], H. Kawakami[14], T. Hayashi[15], T. Mukai[16], N. Sata[17], M. Kida[2], T. Shimosegawa[8]

Institutions Institutions are listed at the end of article.

submitted
18. November 2012
accepted after revision
26. March 2013

Bibliography
DOI http://dx.doi.org/10.1055/s-0033-1344027
Published online: 27.6.2013
Endoscopy 2013; 45: 627–634

ISSN 0013-726X

Corresponding author
I. Yasuda, MD, PhD
First Department of Internal Medicine
Gifu University Hospital
1-1 Yanagido
Gifu 501-1194
Japan
Fax: +81-58-2306310
YASUDAIC@aol.com

Background and study aims: Only a few large cohort studies have evaluated the efficacy and safety of endoscopic necrosectomy for infected walled-off pancreatic necrosis (WOPN). Therefore, a multicenter, large cohort study was conducted to evaluate the efficacy and safety of endoscopic necrosectomy and to examine the procedural details and follow-up after successful endoscopic necrosectomy.

Patients and methods: A retrospective review was conducted in 16 leading Japanese institutions for patients who underwent endoscopic necrosectomy for infected WOPN between August 2005 and July 2011.The follow-up data were also reviewed to determine the long-term outcomes of the procedures.

Results: Of 57 patients, 43 (75 %) experienced successful resolution after a median of 5 sessions of endoscopic necrosectomy and 21 days of treatment. Complications occurred in 19 patients (33 %) during the treatment period. Six patients died (11 %): two due to multiple organ failure and one patient each from air embolism, splenic aneurysm, hemorrhage from a Mallory–Weiss tear, and an unknown cause. Of 43 patients with successful endoscopic necrosectomy, recurrent cavity formation was observed in three patients during a median follow-up period of 27 months.

Conclusions: Endoscopic necrosectomy can be an effective technique for infected WOPN and requires a relatively short treatment period. However, serious complications can arise, including death. Therefore, patients should be carefully selected, and knowledgeable, skilled, and experienced operators should perform the procedure. Further research into safer technologies is required in order to reduce the associated morbidity and mortality.

Introduction

Acute post-necrotic pancreatic/peripancreatic fluid collection occurs because of liquefaction of necrotic tissue. Over 4 weeks, a thick wall without an epithelial lining can form over the fluid collection, developing into walled-off pancreatic necrosis (WOPN) with variable fluid and solid components [1]. Infected pancreatic necrosis, which is a major risk factor for sepsis-related multiple organ failure, is the main life-threatening complication in the late phase of acute pancreatitis. The associated mortality is at least 20 %, and up to 80 % of deaths result from septic complications [2]. Therefore, patients with infected WOPN require timely and effective interventions. Open necrosectomy with drainage has been the standard of treatment for infected WOPN, but carries significant morbidity (13 %–53 %) and high mortality (6 %–34 %) [3,4]. In addition, patients experience a prolonged recovery. These limitations have led to investigations of alternative techniques.

In 1996, Baron et al. [5] were the first to report successful endoscopic drainage of WOPN, wherein several transgastric or transduodenal drainage catheters and a nasopancreatic irrigation tube were placed into the retroperitoneum and lavage was continued until the collection successfully resolved. In 2000, Seifert et al. [6] performed a more aggressive technique of inserting the endoscope directly into the necrotic cavity and removing the necrotic tissue. Several subsequent reports have described initial experiences with direct endoscopic necrosectomy for WOPN [3,7–12]. More recently, two large multicenter studies demonstrated the efficacy and safety of endoscopic necrosectomy for WOPN [13,14]. However, indications and techniques vary between studies. Therefore, a multicenter, large cohort study was conducted to evaluate the efficacy and safety of endoscopic necrosectomy in a carefully selected

population of patients with infected WOPN and to examine the procedural details and follow-up after successful endoscopic necrosectomy.

Patients and methods

Patients

A total of 16 leading Japanese institutions participated in this study. The participating institutions were: Gifu University Hospital (Gifu); Kitasato University East Hospital (Sagamihara); The University of Tokyo (Tokyo); Tokyo Medical University (Tokyo); Date Red Cross General Hospital (Date); Mie University Hospital (Tsu); Okayama University Graduate School of Medicine, Dentistry, and Pharmaceutical Sciences (Okayama); Tohoku University Graduate School of Medicine (Sendai); Yokohama City University School of Medicine (Yokohama); Fukushima Medical University (Fukushima); Kyushu University (Fukuoka); Kurume University School of Medicine (Fukuoka-Kurume); Kinki University School of Medicine (Sayama); Hokkaido University Graduate School of Medicine (Sapporo); Sapporo Medical University School of Medicine (Sapporo); and Gifu Municipal Hospital (Gifu). Institutional review board approval was obtained at each institution for participation in the study.

A standardized data collection form was sent to each institution. Each institution retrospectively reviewed their database and data for patients who underwent endoscopic necrosectomy for infected WOPN between August 2005 and July 2011 were included in the study. Follow-up data for patients who underwent successful endoscopic necrosectomy treatment were obtained by interviews at the outpatient clinic. However, if patients had not been followed periodically, each institutional attending physician contacted the patients or their family by telephone. The data were completely updated in January 2013.

Procedures

The standard technique for endoscopic necrosectomy involves the following steps. First, a curvilinear array endoscopic ultrasound (EUS) is used to visualize the extent of the necrosis and determine the optimal puncture site. Before puncture, color Doppler is used to confirm that there are no interposed vessels on the puncture line. The cavity is then punctured with a 19-gauge EUS needle. After withdrawing the inner stylet, a guide wire is inserted through the needle into the necrotic cavity under fluoroscopic guidance. The puncture site is then dilated using a dilator and/or a balloon catheter. Then, one or more double pigtail stent(s) and/or a nasocystic drainage catheter are inserted. In a few select cases, endoscopic necrosectomy is performed on the same day.

In most cases, the tract is dilated using a large balloon (12–20 mm) several days after stent placement or insertion of the drainage catheter (**Fig. 1**). A conventional forward-viewing endoscope is subsequently advanced into the cavity and endoscopic accessories are used to remove necrotic tissue with forceful irrigation of normal saline (**Fig. 2**). Endoscopic necrosectomy is performed 1–4 times per week, until all necrotic tissue has been removed. In anticipation of a subsequent endoscopic necrosectomy, the route to the necrotic cavity is maintained by placing stents and/or a nasocystic drainage catheter. Daily irrigation using 500–1000 mL of normal saline through a nasocystic drainage catheter is performed between endoscopic necrosectomy sessions at some institutions. Endoscopic necrosectomy is continued until the majority of necrotic tissue is removed and pink granulation tissue lining the wall is observed. At the final endoscopic necrosectomy session, stents may be placed depending on each institution's protocol.

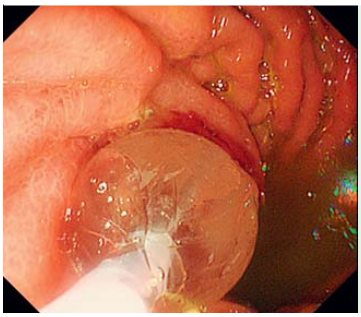

Fig. 1 Dilation of the transgastric entry tract into the necrotic cavity using a large balloon.

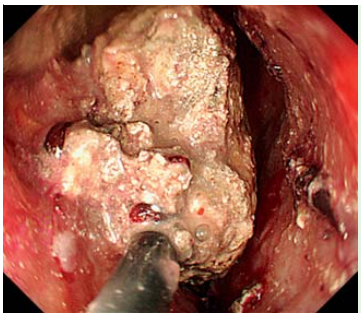

Fig. 2 Endoscopic removal of necrotic material using pentapod forceps.

Outcomes

The primary outcomes were successful resolution of pancreatic necrosis by endoscopic necrosectomy and the mortality and complication rates associated with endoscopic necrosectomy. Successful resolution was defined as remission of clinical symptoms and the disappearance of the necrotic cavity on endoscopic necrosectomy imaging. Incomplete resolution was defined as the need for surgery or additional non-surgical treatments to cure the infected WOPN. The secondary outcome was prognosis after endoscopic necrosectomy.

Statistical analysis

Statistical comparisons were performed to determine the factors associated with successful resolution of the necrotic cavity. Continuous variables with Gaussian distribution were tested using the Student's *t*-test and those with non-Gaussian distributions were analyzed using the non-parametric Wilcoxon rank-sum test. Categorical and binary variables were tested using the chi-squared test with Yates' correction or Fisher's exact test for small-expected frequencies. All statistical tests were two tailed at the probability level of 0.05. Statistical analyses were performed using JMP software, version 8.0 (SAS Institute, Inc., Cary, North Carolina, USA).

Table 1 Patient demographics.

Female/male	11/46
Age, median (range), years	58 (19 – 81)
BMI, median (range), kg/m^2	21.3 (16.2 – 38.9)
Etiological factors, n (%)	
Idiopathic	20 (35)
Alcohol	18 (32)
Gallstone	8 (14)
Post-ERCP	7 (12)
Others*	4 (7)
ASA classification, n	
Grade 2	18
Grade 3	29
Grade 4	8
Grade 5	2
CT findings	
Main location, n	
Head and body	2
Body and tail	30
Entire pancreas	25
Lower extremity of the necrotic cavity, n	
Peripancreatic region	29
Beyond the lower extremity of the left kidney	22
Pelvic cavity	6
Form, n	
Simple	38
Multiple	19
Size, median (range), cm	
Long axis	14.0 (4.0 – 30.5)
Short axis	7.0 (2.0 – 22.0)

ASA, American Society of Anesthesiologists physical status classification; BMI, body mass index; ERCP, endoscopic retrograde cholangiopancreatography.
* Other etiological factors included pancreas divisum, anomalous connection of pancreatobiliary ducts, hypertriglyceridemia, and ampullary tumors.

Results

Patients

From August 2005 to July 2011, 57 patients underwent endoscopic necrosectomy for infected WOPN at the 16 institutions. Patient demographics are shown in **Table 1**.

Of the 57 patients, 10 were in very poor health (grade 4 or 5 in the American Society of Anesthesiologists (ASA) physical status classification) [15]. In six patients, the necrotic cavity extended to the pelvis.

Initial outcomes of endoscopic necrosectomy

Initial drainage was performed after a median duration of 50 days (range 13 – 436 days) from the onset of pancreatitis. The initial puncture was performed using a conventional 19-gauge EUS needle, and in most cases the tract was then dilated using a dilator and balloon catheter. Subsequently, a single nasocystic catheter and one or two indwelling stents were placed in the necrotic cavity (**Table 2**).

Endoscopic necrosectomy was performed on the same day as the initial drainage in 11 patients (19 %), and the remaining 46 patients (81 %) underwent initial endoscopic necrosectomy some days after the initial drainage. A gastroscope with water-jet function was used in 37 patients (65 %), and carbon dioxide (CO_2) gas was used instead of room air for insufflation in 39 patients (68 %) during endoscopic necrosectomy. Various endoscopic devices were used to remove the necrotic tissue, with the majority being pentapod forceps, rat-tooth forceps, and polypectomy snares.

Table 2 Initial drainage.

Time from onset of pancreatitis to initial drainage, median (range), days	50 (13 – 436)
Puncture needle, n	
Electrocautery needle	2
Non-electrocautery 19-G needle	55
Dilator, n	
NA	7
6 or 7 Fr	39
10 Fr	11
Diameter of dilation balloon, n	
NA	7
≤ 10 mm	41
≥ 15 mm	9
Placed drain, n	
Single nasocystic catheter	4
Single nasocystic catheter with a single stent	25
Single nasocystic catheter with 2 stents	18
Single nasocystic catheter with 3 or 4 stents	4
Two stents	4
Three stents	2

NA, not applicable.

Table 3 Endoscopic necrosectomy.

Timing of the first endoscopic necrosectomy, n	
At the initial drainage	11
After the initial drainage	46
1 – 7 days	20
8 – 14 days	20
≥ 15 days	6
Diameter of dilation balloon, n	
12 – 15 mm	16
18 mm	16
20 mm	25
Type of endoscope, n	
Conventional gastroscope	20
With water-jet function	37
Devices for necrosectomy, n*	
Pentapod forceps	30
Tripod forceps	3
Rat-tooth forceps	28
Biopsy forceps	7
Polypectomy snare	15
Basket catheter	5
Net catheter	3
Insufflation during the procedure, n	
Room air	18
CO_2 gas	39
Daily saline irrigation between sessions, n	
Done	25
Not done	25
NA	7

NA, not applicable.
* Multiple devices used per patient.

Daily irrigation with normal saline solution from a nasocystic drainage catheter was performed between endoscopic necrosectomy sessions in 25 patients (44 %) (**Table 3**).

Successful resolution was achieved in 43 patients (75 %) following a median of 5 (range 1 – 20) endoscopic necrosectomy sessions. Endoscopic necrosectomy was typically performed twice a week. The median duration of one endoscopic necrosectomy ses-

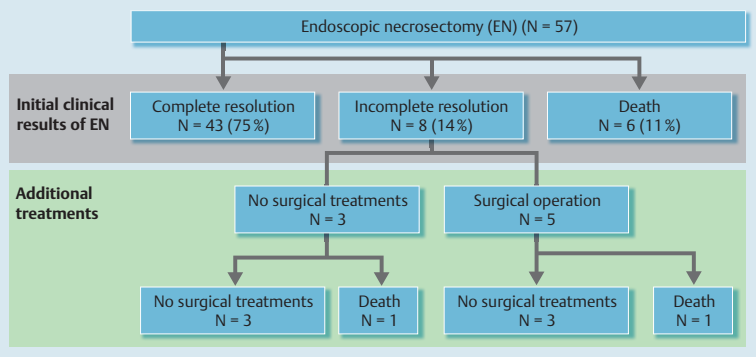

Fig. 3 Initial clinical results of endoscopic necrosectomy.

Table 4 Factors associated with failed cavity resolution by endoscopic necrosectomy.

Factor	Successful endoscopic necrosectomy (n = 43)	Failed endoscopic necrosectomy (n = 14)	*P* value
Female, n (%)	6 (14)	5 (36)	0.1155
Age, median (range), years	59 (19 – 81)	53 (22 – 74)	0.1445
BMI, median (range), kg/m²	21.0 (16.2 – 38.9)	22.9 (17.4 – 26.3)	0.5920
Etiology (gallstone), n (%)	5 (12)	3 (21)	0.3912
ASA classification ≥ 3, n (%)	26 (60)	13 (93)	0.0437
Lower extremity of the cavity extended beyond the lower extremity of the left kidney, n (%)	20 (47)	8 (57)	0.5497
Size of necrosis, long axis, median (range), cm	14.0 (4.0 – 30.5)	14.5 (7.0 – 24.0)	0.6626
Multilocular form, n (%)	12 (28)	7 (50)	0.1916
Time from onset of pancreatitis to initial drainage < 6 weeks, n (%)	17 (40)	8 (57)	0.5441
Number of sessions, median (range)	5 (1 – 17)	4.5 (1 – 20)	0.9330
Maximum number of stents placed, median (range)	2 (1 – 7)	1.5 (1 – 4)	0.1223
Enteral feeding, n (%)	8 (19)	4 (29)	0.4631

ASA, American Society of Anesthesiologists physical status classification; BMI, body mass index.

sion was 63 minutes (range 27 – 173 minutes). The median duration of the treatment period was 21 days (range 10 – 101 days). The patients initially received parenteral nutrition. However, 12 patients recommenced normal food intake within 7 days. Another 12 patients received enteral feeding of an elemental diet. Only six patients underwent endoscopic retrograde cholangiopancreatography (ERCP) after the completion of endoscopic necrosectomy, and four patients received pancreatic stenting for pancreatic duct leakage.

Of the 14 patients for whom treatment was unsuccessful, six (11%) died during the treatment period before resolution and eight (14%) were converted to other treatments because of persistent sepsis after a median endoscopic necrosectomy treatment period of 29 days (range 2 – 56 days) and required surgery (n = 5) or additional percutaneous drainage (n = 3). Of these eight patients, six eventually experienced successful resolution, but two died after further treatment (**Fig. 3**).

Baseline characteristics were compared between the successful and failed endoscopic necrosectomy groups (**Table 4**). Patients in poor medical health (ASA classification ≥ 3) were significantly more likely to experience an unsuccessful endoscopic necrosectomy (*P* = 0.0437). The success rate was not significantly different between the group of institutions with more than two treatment cases and the group of institutions with only one or two treatment cases; the mean success rates (range) were 70.0% (0% – 100%) and 78.6% (0% – 100%), respectively (*P* = 0.1726).

Complications arose in 19 patients (33%) during the treatment period. They occurred during endoscopic necrosectomy in 12 patients and between sessions in 7 (**Table 5**). Bleeding from the fistula occurred during endoscopic necrosectomy in five patients following large balloon dilation. Hemostasis was achieved using endoscopic procedures in four patients (clipping in two patients and balloon compression by re-inflation of the balloon in the other two patients), while the remaining patient required coil embolization of a branch of the inferior pancreaticoduodenal artery under interventional radiologic guidance. Another three patients bled from the cavity wall during removal of the necrotic tissue. Conservative management and blood transfusion were sufficient for one patient. Compression by the tip of the endoscope was successful in another patient, and the remaining patient required coil embolization under interventional radiologic guidance. Perforation occurred in another three patients. In two patients, abdominal free air was found following dilation of the large balloon and in the remaining one patient, the cavity wall was perforated during removal of the necrotic tissue. In all three patients, the procedure was immediately terminated and a nasocystic tube and stents were placed. All patients recovered with conservative management and without any sequelae. One patient developed an air embolism. Following insertion of the endoscope into the necrotic cavity, the patient manifested the clinical picture of shock and was diagnosed with air embolism on computed tomography (CT). Brain death occurred and the patient died after 32 days.

Of the seven patients who experienced complications between endoscopic necrosectomy sessions, four experienced massive hematemesis. Rupture of a splenic pseudoaneurysm occurred in two patients, and coil embolization under interventional radiologic guidance was attempted for both. Although one patient was successfully treated, the other died. In the third case of bleeding, the patient was successfully treated with a local epinephrine injection. In the remaining case, the patient vomited frequently following the 4th endoscopic necrosectomy and massive hematemesis occurred several hours later. The patient's hemodynamic status rapidly deteriorated and she died before any interventions could be attempted. An autopsy showed the presence of a Mallory–Weiss tear, but the cause of vomiting remained unclear. Other complications arising between endoscopic necrosectomy sessions included aspiration pneumonia and ileus. Both patients were successfully treated by conservative treatments such as antibiotic therapy and bowel rest. Another patient experienced sudden cardiorespiratory arrest in the ward at 32 hours after completion of the 8th endoscopic necrosectomy. Despite resuscitation, the patient developed brain death and died after 40 weeks. The cause of the sudden cardiorespiratory arrest was not known.

Six patients (11 %) died during the treatment period of endoscopic necrosectomy. Multiple organ failure secondary to sepsis resulted in two deaths, and one patient each died because of air embolism, rupture of a splenic aneurysm, a Mallory–Weiss tear, and an unknown cause.

Table 5 Complications during the treatment period of endoscopic necrosectomy.

During the procedure, n	12 (21 %)
Bleeding from the fistula	5
Bleeding from the cavity wall	3
Perforation	3
Air embolism	1[1]
Between sessions, n	7 (12 %)
Rupture of splenic aneurysm	2[2]
Mallory – Weiss tear	1[1]
Bleeding from the fistula	1
Aspiration pneumonia	1
Ileus	1
Sudden cardiorespiratory arrest (unknown cause)	1[1]
Total	19 (33 %)

[1] Fatal cases.
[2] One patient died.

Table 6 Follow-up of 43 patients following successful endoscopic necrosectomy.

Follow-up period after completion of endoscopic necrosectomy, median (range), months	27 (5 – 59)
Removal of stents, n	
Removed at final session	7
Removed later	23
Spontaneously dislodged	9
Still in situ	4
Recurrent cavity	3 (7 %)
Without infection	1
With infection	2
Died	2 (4 %)*

* Two patients died due to unrelated causes: 1 from the bile duct cancer after 6 months and another from pneumonia after 14 months.

Follow-up results

Complete follow-up data were obtained for all 43 patients who were successfully treated with endoscopic necrosectomy. A total of 32 patients were regularly followed every 3 – 6 months, with blood tests performed as appropriate at each institution. Follow-up abdominal CT (every 3 – 6 months) was obtained until 1 year after the endoscopic necrosectomy in 37 patients, 2 years in 20 patients, and more than 3 years in 10 patients. The median follow-up period for these 43 patients was 27 months (range 5 – 59 months). Stents were removed at the final endoscopic necrosectomy session in 7 patients, whereas 23 patients had their stents removed after a median duration of 13 weeks (range 3 weeks – 17 months). Another nine patients experienced spontaneous dislodgement of the stents after a median duration of 15 weeks (range 8 weeks – 9 months). In the remaining four patients, the stents were still in situ at the time of the last follow-up (median 22 months; range 11 – 30 months) (**Table 6**).

Two patients died due to causes unrelated to the endoscopic necrosectomy procedure or pancreatitis. One died from bile duct cancer after 6 months and another from pneumonia after 14 months. Cavity recurrence was observed in three patients after 2 – 8 months: in one patient, the cavity was sterile but the cavity was infected in the other two patients (**Table 6**). These patients were successfully treated by endoscopic or percutaneous drainage.

Discussion

In a multicenter randomized controlled trial, the Dutch Pancreatitis Study Group compared standard open necrosectomy with a step-up approach that involved percutaneous drainage followed by minimally invasive retroperitoneal necrosectomy if necessary [16]. Major complications occurred less frequently in the step-up approach compared with open necrosectomy (40 % vs. 69 %; P = 0.006), and 35 % of patients in the step-up group were successfully treated with percutaneous drainage alone. In a subsequent study, the same group prospectively examined 639 consecutive patients with necrotizing pancreatitis and found that patients whose first intervention was catheter drainage had fewer complications than those undergoing primary necrosectomy (42 % vs. 64 %; P = 0.003) [17]. Furthermore, in a retrospective study, Gardner et al. [18] compared direct endoscopic necrosectomy with conventional transmural endoscopic drainage for WOPN and found that the former procedure achieved higher rates of successful resolution (88 % vs. 45 %; P < 0.01), with complications limited to mild periprocedural bleeding, which occurred at equivalent rates between the two groups (32 % vs. 20 %; P = 0.502). More recently, Bakker et al. [19] compared the proinflammatory response, as measured by serum interleukin-6 (IL-6) levels, and clinical outcomes of endoscopic transgastric and surgical necrosectomy in a randomized controlled trial. There was a decreased proinflammatory response following endoscopic necrosectomy, as evidenced by post-procedural IL-6 levels, compared with the response to surgical necrosectomy. In addition, major complications or death occurred less frequently after endoscopic necrosectomy than surgical necrosectomy (20 % vs. 80 %; P = 0.03). Thus, in light of the improved outcomes, minimally invasive interventions to treat WOPN are becoming increasingly popular.

After the initial introduction of endoscopic necrosectomy by Seifert et al. [6], subsequent reports have described successful endoscopic necrosectomy for treating infected pancreatic necrosis, as

Table 7 Previous reports on endoscopic necrosectomy for infected pancreatic necrosis.

First author (year) [Ref]	Study design	n	Successful treatment, %	Morbidity, %	Mortality, %
Seifert (2000) [6]	Retrospective	3	100	0	0
Seewald (2005) [3]	Retrospective	13	69	31	0
Charnley (2006) [8]	Retrospective	13	92[1] (69)	0	15[2]
Papachristou (2007) [10]	Retrospective	53[3]	53	21	0
Voermans (2007) [7]	Retrospective	25	93	7	0
Kang (2008) [11]	Retrospective	1[4]	100	0	0
Mathew (2008) [20]	Retrospective	6	100	0	0
Escourrou (2008) [9]	Retrospective	13	100[5] (85)	46	0
Schrover (2008) [12]	Retrospective	8	75	25	13
Gardner (2009) [18]	Retrospective	25	88	32	0
Seifert (2009) [13]	Retrospective	93	80	26	7.5
Gardner (2011) [14]	Retrospective	104	91	14	5.8
Seewald (2012) [21]	Retrospective	80[6]	83.8	26	0
Bakker (2012) [19]	Prospective[7]	10	80	20	10
Present study	Retrospective	57	75	33	11

[1] After excluding 2 patients with additional percutaneous drainage and a patient with laparoscopic drainage, the success rate decreased to 69%.
[2] Non-related death.
[3] Drainage alone was studied, with endoscopic necrosectomy performed in 22 cases.
[4] Transduodenal approach.
[5] After excluding 2 patients with additional percutaneous drainage, the success rate decreased to 85%.
[6] Drainage alone was studied, with endoscopic necrosectomy performed in 49 cases.
[7] Prospective randomized controlled trial comparing endoscopic necrosectomy with surgical necrosectomy.

shown in **Table 7** [3, 7–14, 18–21]. The rate of complete resolution of pancreatic necrosis after endoscopic necrosectomy ranged from 53% to 100%. Procedure-related morbidity and mortality was 0%–46% and 0%–13%, respectively. However, most reports were small case series. Recently, multicenter studies enrolling a relatively large number of patients have been reported from Germany [13] and the United States [14]. In the German study, Seifert et al. [13] showed that initial clinical success was obtained in 80% of 93 patients, with a mean hospital stay of 46 days (range 8–170 days), complication rate of 26%, and associated mortality rate of 7.5%. The American study performed by Gardner et al. [14] reported successful resolution in 91% of 104 patients with a mean hospital stay of 12 days (range 9–15 days) after the initial drainage, a morbidity rate of 14%, and a mortality rate of 5.8%. In comparison, in the present study, the successful resolution rate was 75%, with a median hospital stay of 21 days (range 10–101 days) for endoscopic necrosectomy; the morbidity and mortality rates were 33% and 11%, respectively.

The rate of successful resolution in the present study was slightly lower, and the morbidity and mortality may be higher. It was initially hypothesized that these differences might be attributed to the relatively small sample size at each institution, given that the median number of patients enrolled at each institution was 3 (range 1–8) and experience with endoscopic techniques might be insufficient at many institutions. However, the analysis showed that the success rates were not significantly different between the group of institutions with more than two treatment cases and the group of institutions with only one or two treatment cases. Another possible reason is that the study population included several patients with extremely poor medical health. In the 10 patients with extremely poor medical health (ASA grades 4 and 5), the successful resolution rate was 50% and the complication rate was 50%. A subanalysis of factors associated with failed endoscopic necrosectomy also showed that the ratio of patients with poor medical health (ASA grades 3 and more) was significantly higher in the failed endoscopic necrosectomy group than in the successful group (**Table 4**). These results suggest that endoscopic necrosectomy is less favorable for patients in poor medical health. However, it is also true that such patients are also likely to respond poorly to surgical intervention. Indeed, in the present study, 34 of 39 patients with ASA≥3 were initially refused surgical interventions by surgeons. A previous randomized controlled trial also showed that major complications or death occurred more frequently after surgical necrosectomy than after endoscopic necrosectomy (80% vs. 20%; $P=0.03$) [19]. Therefore, we believe that endoscopic necrosectomy, as a less invasive option, is preferable to surgery, especially for patients in poor medical health.

The most common complication associated with endoscopic necrosectomy is bleeding, which may occur during balloon dilation of the transluminal tract or during the removal of necrotic material [22]. In the present study, bleeding arose during balloon dilation in five patients and during the necrosectomy in three. Another four patients developed massive hematemesis between endoscopic necrosectomy sessions. To reduce the risk of bleeding during the necrosectomy, the procedure should be performed under a clear endoscopic view. In this respect, forceful saline lavage was useful and an endoscope with water jet function (GIF-Q260J, Olympus, Tokyo, Japan) was used for many patients (**Table 3**). Although various devices were used to remove the necrotic material, no differences were observed among the devices with respect to bleeding rates. Interestingly, all fatal bleeding episodes occurred between endoscopic necrosectomy sessions. The most common cause was rupture of a pseudoaneurysm, which often forms in response to inflammation, and the subsequent, massive bleeding was difficult to contain using conservative and/or endoscopic treatments. Embolization under interventional radiologic guidance or surgery should be performed in the early stage of this potentially life-threatening complication.

Although air embolism is uncommon, it is one of the most concerning complications. Fatal cases have been reported in both aforementioned multicenter studies [13, 14]; the authors recommended using CO_2 gas rather than room air for insufflation. A fatal case of air embolism was also experienced in the current

study; although CO_2 gas was not used in this case, it was used for 68 % of the patients. The use of CO_2 gas is mandatory for preventing air emboli. Moreover, insufflation during the procedure should be reduced to the minimum possible extent, and the procedure should also not be unnecessarily prolonged.

As a comparison, the contemporary number of surgical necrosectomies at the participating institutions was 21, and treatment was successful in 71.4 %, with associated morbidity and mortality rates of 52.3 % and 28.6 %, respectively. The median hospital stay was 140 days (range 30 – 304 days). While endoscopic necrosectomy is clearly much less invasive than surgical necrosectomy, serious complications can nevertheless occur during endoscopic necrosectomy and the procedure can be ineffective. To optimize outcomes and minimize complications, a multidisciplinary approach involving skilled interventional endoscopists, radiologists, and surgeons is necessary to manage the WOPN successfully. Therefore, patients with WOPN should be referred to tertiary care centers where this multidisciplinary approach is available.

In the present study, the timing of stent removal varied according to each case and institution. Stents were removed at the final endoscopic necrosectomy session in 7 patients and electively removed after a median duration of 13 weeks (range 3 weeks – 17 months) in 23 patients. Before stent removal, resolution of the cavity was confirmed on CT imaging in all patients. In nine patients, stents spontaneously dislodged after a median duration of 15 weeks (8 weeks – 9 months), and in 4 patients, the stents were still in situ at the time of the last follow-up (median 22 months; range 11 – 30 months). The timing of stent removal remains controversial, although the stents were typically removed 1 – 3 months after documented resolution of the cavity in previous studies [7, 12 – 14, 18]. Further research is required to examine the optimal time for stent removal.

There are several limitations to the current study. First, due to the retrospective nature, case selection bias cannot be avoided. There are various indications for endoscopic necrosectomy, depending on the institution. In addition, data collection may be imperfect. Inclusion criteria might have been inappropriately applied, and some minor complications might have been missed. Second, each institution only enrolled a small number of patients, which likely affected the treatment outcomes and contributed to increased complication rates.

In conclusion, endoscopic necrosectomy can be an effective treatment for infected WOPN and requires a relatively short treatment period. However, serious complications, including death, can occur. Therefore, patients should be carefully selected, and knowledgeable, skilled, and experienced operators should perform this procedure. Further research into safer technologies is required to reduce the associated morbidity and mortality.

Competing interests: None

Institutions
[1] First Department of Internal Medicine, Gifu University Hospital, Gifu
[2] Department of Gastroenterology, Kitasato University East Hospital, Sagamihara
[3] Department of Gastroenterology, Graduate School of Medicine, The University of Tokyo, Tokyo
[4] Department of Gastroenterology and Hepatology, Tokyo Medical University, Tokyo
[5] Department of Gastroenterology, Japan Red Cross Date General Hospital, Date
[6] Department of Gastroenterology, Mie University Hospital, Tsu
[7] Department of Gastroenterology and Hepatology, Okayama University Graduate School of Medicine, Dentistry, and Pharmaceutical Sciences, Okayama
[8] Division of Gastroenterology, Tohoku University Graduate School of Medicine, Sendai
[9] Division of Gastroenterology, Yokohama City University School of Medicine, Yokohama
[10] Department of Gastroenterology, Fukushima Medical University Aizu Medical Center, Aizu
[11] Department of Medicine and Bioregulatory Science, Graduate School of Medical Science, Kyushu University, Fukuoka
[12] Division of Gastroenterology, Department of Medicine, Kurume University School of Medicine, Kurume
[13] Department of Gastroenterology and Hepatology, Kinki University School of Medicine, Osaka-Sayama
[14] Department of Gastroenterology and Hepatology, Hokkaido University Graduate School of Medicine, Sapporo
[15] Fourth Department of Internal Medicine, Sapporo Medical University School of Medicine, Sapporo
[16] Department of Gastroenterology, Gifu Municipal Hospital, Gifu
[17] Department of Surgery, Jichi Medical University, Tochigi, Japan

Acknowledgments

This work was supported in part by the Research Committee of Intractable Pancreatic Diseases (principal investigator: Tooru Shimosegawa), Ministry of Health, Labor, and Welfare of Japan.

The authors wish to thank the following colleagues for their helpful advice and encouragement: Shinpei Doi, MD (First Department of Internal Medicine, Gifu University Hospital); Keisuke Yamamoto, MD, PhD, Hirofumi Kogure, MD, PhD, Natsuyo Yamamoto, MD, PhD, and Naoki Sasahira, MD, PhD (Department of Gastroenterology, Graduate School of Medicine, The University of Tokyo).

References

1 *Sheu Y, Furlan A, Almusa O* et al. The revised Atlanta classification for acute pancreatitis: a CT imaging guide for radiologists. Emerg Radiol 2012; 19: 237 – 243
2 *Werner J, Feuerbach S, Uhl W* et al. Management of acute pancreatitis: from surgery to interventional intensive care. Gut 2005; 54: 426 – 436
3 *Seewald S, Groth S, Omar S* et al. Aggressive endoscopic therapy for pancreatic necrosis and pancreatic abscess: a new safe and effective treatment algorithm (videos). Gastrointest Endosc 2005; 62: 92 – 100
4 *Horvath K, Freeny P, Escallon J* et al. Safety and efficacy of video-assisted retroperitoneal debridement for infected pancreatic collections: a multicenter, prospective, single-arm phase 2 study. Arch Surg 2010; 145: 817 – 825
5 *Baron TH, Thaggard WG, Morgan DE* et al. Endoscopic therapy for organized pancreatic necrosis. Gastroenterology 1996; 111: 755 – 764
6 *Seifert H, Wehrmann T, Schmitt T* et al. Retroperitoneal endoscopic debridement for infected peripancreatic necrosis. Lancet 2000; 356: 653 – 655
7 *Voermans RP, Veldkamp MC, Rauws EA* et al. Endoscopic transmural debridement of symptomatic organized pancreatic necrosis (with videos). Gastrointest Endosc 2007; 66: 909 – 916
8 *Charnley RM, Lochan R, Gray H* et al. Endoscopic necrosectomy as primary therapy in the management of infected pancreatic necrosis. Endoscopy 2006; 38: 925 – 928
9 *Escourrou J, Shehab H, Buscail L* et al. Peroral transgastric/transduodenal necrosectomy: success in the treatment of infected pancreatic necrosis. Ann Surg 2008; 248: 1074 – 1080
10 *Papachristou GI, Takahashi N, Chahal P* et al. Peroral endoscopic drainage/debridement of walled-off pancreatic necrosis. Ann Surg 2007; 245: 943 – 951
11 *Kang SG, Park doH, Kwon TH* et al. Transduodenal endoscopic necrosectomy via pancreaticoduodenal fistula for infected peripancreatic necrosis with left pararenal space extension (with videos). Gastrointest Endosc 2008; 67: 380 – 383
12 *Schrover IM, Weusten BL, Besselink MG* et al. EUS-guided endoscopic transgastric necrosectomy in patients with infected necrosis in acute pancreatitis. Pancreatology 2008; 8: 271 – 276
13 *Seifert H, Biermer M, Schmitt W* et al. Transluminal endoscopic necrosectomy after acute pancreatitis: a multicentre study with long-term follow-up (the GEPARD Study). Gut 2009; 58: 1260 – 1266

14 *Gardner TB, Coelho-Prabhu N, Gordon SR* et al. Direct endoscopic necrosectomy for the treatment of walled-off pancreatic necrosis: results from a multicenter U.S. series. Gastrointest Endosc 2011; 73: 718 – 726
15 American Society of Anesthesiologists. ASA physical status classification system. Available from: http://www.asahq.org/Home/For-Members/Clinical-Information/ASA-Physical-Status-Classification-System
16 *van Santvoort HC, Besselink MG, Bakker OJ* et al. A step-up approach or open necrosectomy for necrotizing pancreatitis. N Engl J Med 2010; 362: 1491 – 1502
17 *van Santvoort HC, Bakker OJ, Bollen TL* et al. A conservative and minimally invasive approach to necrotizing pancreatitis improves outcome. Gastroenterology 2011; 141: 1254 – 1263
18 *Gardner TB, Chahal P, Papachristou GI* et al. A comparison of direct endoscopic necrosectomy with transmural endoscopic drainage for the treatment of walled-off pancreatic necrosis. Gastrointest Endosc 2009; 69: 1085 – 1094
19 *Bakker OJ, van Santvoort HC, van Brunschot S* et al. Endoscopic transgastric vs surgical necrosectomy for infected necrotizing pancreatitis: a randomized trial. JAMA 2012; 307: 1053 – 1061
20 *Mathew A, Biswas A, Meitz KP.* Endoscopic necrosectomy as primary treatment for infected peripancreatic fluid collections (with video). Gastrointest Endosc 2008; 68: 776 – 782
21 *Seewald S, Ang TL, Richter H* et al. Long-term results after endoscopic drainage and necrosectomy of symptomatic pancreatic fluid collections. Dig Endosc 2012; 24: 36 – 41
22 *Haghshenasskashani A, Laurence JM, Kwan V* et al. Endoscopic necrosectomy of pancreatic necrosis: a systematic review. Surg Endosc 2011; 25: 3724 – 3730

WFUMB 2013

14th World Congress of Ultrasound in Medicine and Biology

FLAUS 2013

16th Congress of the Latin American Federation of Ultrasound

JPR'2013

43th Sao Paulo Radiological Meeting

May 2 – 5, 2013

Transamerica Expo Center – Sao Paulo – Brazil

ENGLISH

Scientific Program

Support

CBR Colégio Brasileiro de Radiologia e Diagnóstico por Imagem

BRASIL

SÃO PAULO É TUDO DE BOM

SÃO PAULO

www.wfumb2013.org

Scientific Committee WFUMB/FLAUS/JPR'2013

(World and Latin American Congresses of Ultrasound)

■ MAIN COMMITTEE

Dr. Masatoshi Kudo
President of the Congress by WFUMB

Dr. Leandro Fernández
President of the Congress by FLAUS

Dr. Giovanni Guido Cerri
President of the Congress by SPR

Dr. David Evans
President of the Scientific Committee by WFUMB

Dr. Ramon Bataglia
President of the Scientific Committee by FLAUS

Dr. M. Cristina Chammas
President of the Scientific Committee by SPR and SPR Ultrasound Coordinator

Medical Ultrasound Society, Singapore
11th Annual Seminar
in conjunction with
AFSUMB Workshop 2013

Programme Details

28th Sep 2013 Saturday

8:30 – 8:50 am	Welcome *Ong Chiou Li*
8:50 – 9:00 am	Introduction by Education Committee Chair *Kanu Bala*

Ultrasound of the Uterus

9:00 – 9:30 am	Ultrasound of endometrium: The most versatile tissue *Kanu Bala*
9:30 – 10:00 am	Amenorrhoea – what to look for on ultrasound *Teo Sze Yiun*
10:00 – 10:30 am	Is 3-D ultrasound essential in routine pelvicultrasound? *Ong Chiou Li*

10:30 – 11:00 am Morning Break

Obstetric Ultrasound Part 1

11:00 – 11:30 am	How to avoid missing fetal abnormalities *Leung Kwok Yin*
11:30 – 12:00 am	Fringes of normalcy in obstetric ultrasound *Arijit Biswas*
12:00 – 12:30 pm	Tips on performing fetal echocardiography *Leung Kwok Yin*

12:30 – 2:00 pm Lunch

Ultrasound of the Abdomen Part 1

2:00 – 2:30 pm	Ultrasound of spleen: The forgotten organ *Kanu Bala*
2:30 – 3:00 pm	Ultrasound evaluation of fatty liver *Kanu Bala*
3:00 – 3:30 pm	CEUS of Abdominal Aortic Aneurysms *Albert Low*

3:30 – 4:00 pm Tea

Obstetric Ultrasound Part 2

4:00 – 4:30 pm	1st trimester foetal anomalies *Yeo Seow Heong*
4:30 – 5:00 pm	Screening of Down's syndrome in 1st trimester *Lai Fon Min*
5:00 – 5:30 pm	Quiz

29th Sep 2013: Sunday morning

8:50 – 9:00 am	Introduction by AFSUMB president *Kim Seung Hyup*

Ultrasound of the Abdomen Part 2

9:00 – 9:30 am	Diagnosis of Diffuse Liver Diseases *Masatoshi Kudo*
9:30 – 10:00 am	Contrast-enhanced US of Hepatic Tumors with Sonazoid *Masatoshi Kudo*
10:00 – 10:30 am	Radiofrequency ablation of hepatic malignancy: Techniques for Difficult Areas *Chou Yi Hong*

10:30 – 11:00 am Morning Break

Ultrasound of the Breast

11:00 – 11:30 am	Recent Advances of Breast ultrasound *Chou Yi Hong*
11:30 – 12:00 pm	Elastography of Breast Tumours *Chou Yi Hong*

Ultrasound of the Ovaries and Prostate

12:00 – 12:30 pm	TRUS and TRUS-Biopsy of the prostate *Kim Seung Hyup*
12:30 – 1:00 pm	US of adnexal masses: Comparison with CT and MRI *Kim Seung Hyup*

XII AFSUMB Education Workshop

28th February & 1st March, 2014
Kathmandu, Nepal

Acknowledgment Certificate

Presented to

Prof. Masatoshi Kudo

In recognition of your graciousness in sharing your knowledge in the XII AFSUMB Education Workshop, we would like to acknowledge your participation in our Education Workshop as a distinguished guest speaker.

.....

Dr. Mukhtar Alam Ansari
President
Ultrasound Society of Nepal (USN)

第2回 三重先端がんフォーラム

2013年 7月19日(金) 18:00-19:50 / 7月20日(土) 9:00-11:40

会場:三重大学医学部 臨床講義棟2F 臨床第2講義室

代表世話人： 小川朋子(三重大)

世話人 ： 野阪 哲哉(三重大)・伊奈田 宏康(鈴鹿医療科学大)・中山 浩伸(鈴鹿医療科学大)

問合せ先 ： 三重大学医学部附属病院乳腺センター 小川 朋子 <TEL> 059-231-5584

鈴鹿医療科学大学薬学部・医薬品開発学研究室 中山 浩伸<TEL>

固形がんの基礎と臨床

-インフォメーションからコミュニケーションへ-

◆ 7月19日(金) 18:00～19:50

18:00-18:10 開会のあいさつ:緒方 正人(三重大・医学系研究科長)

18:10-19:00 山本 美智子(昭和薬科大学) 座長:増田 直樹 (三重県健康福祉部)

『医薬品情報基盤の構築』

-医薬品の安全性に対する取り組みと課題-

19:00-19:50 太田 智彦 (聖マリアンナ医大) 座長:小川 朋子 (三重大・医)

『BRCA1によるDNA修復機構と化学療法感受性』

20:00- 情報交換会;三重大学医学部臨床講義棟2F臨床第1講義室

◆ 7月20日(土)8:40～11:20

8:40-9:30 笹野公伸(東北大・医) 座長:白石 泰三 (三重大・医)

『乳腺脂肪細胞と乳癌』

9:30-10:20 工藤 正俊(近畿大・医) 座長:伊佐地 秀司(三重大・医)

『肝発癌の予測と分子標的治療』

10:20-11:10 佐谷 秀行 (慶應大・医) 座長:片山 直之(三重大・医)

『がん幹細胞の性状解析に基づく治療戦略の考案』

11:10-11:20 閉会のあいさつ:川西 正祐(鈴鹿医療大・薬学部長)

参加費無料

アクセスマップ

近鉄名古屋線 江戸橋駅より
徒歩15分

JR、近鉄津駅より三重交通バス
「大学病院」 バス停下車 すぐ
「大学病院前」バス停下車徒歩3分

※大学病院方面のバスは、
津駅東口 4番バス停より発車

主催: 三重大学医学部・鈴鹿医療科学大学薬学部 共催: 一般社団法人 中外Oncology学術振興会議

後援:三重県・三重県医師会・三重大学医師会・三重県薬剤師会・三重県病院薬剤師会

日本肝臓学会主催

平成25年度「肝がん撲滅運動」

日　時　平成25年12月8日(日) 13:00～16:00(開場12:30)

会　場　堺市民会館(大ホール)
〒590-0061　大阪府堺市翁橋町2-1-1　TEL 072(238)1481

参加費無料 定員500名

平成25年度大阪府責任者　近畿大学 消化器内科 教授　工藤 正俊 先生

開会の挨拶　13:00～13:05

近畿大学 消化器内科 教授　工藤 正俊 先生

第一部　肝臓の病気　13:05～14:15

Ⅰ 13:05～13:15	肝臓の病気(総論)	近畿大学医学部 消化器内科 准教授　西田 直生志 先生
Ⅱ 13:15～13:35	ウイルス性肝炎の最新治療	近畿大学医学部 消化器内科 講師　萩原 智 先生
Ⅲ 13:35～13:55	超音波で見える肝臓の硬さ －超音波エラストグラフィを用いた最新の検査－	近畿大学医学部 消化器内科 講師　矢田 典久 先生
Ⅳ 13:55～14:15	肝蔵病の薬剤管理	近畿大学医学部附属病院 薬剤部 薬剤師　伊藤 武志 先生

休　憩(10分)

第二部　肝がんの診断と治療　14:25～15:25

Ⅰ 14:25～14:45	分かりやすい肝がんの診断とラジオ波焼灼術	近畿大学医学部 消化器内科 講師　井上 達夫 先生
Ⅱ 14:45～15:05	肝動脈塞栓療法と分子標的治療･最近の話題	近畿大学医学部 消化器内科 講師　南 康範 先生
Ⅲ 15:05～15:25	外科治療	近畿大学医学部 外科 准教授　中居 卓也 先生

休　憩(10分)

第三部　質疑応答･健康相談　15:35～16:00

Q&A　あらかじめ入り口で質問用紙をお配りしますのでご記入下さい。

日　時　平成25年12月8日(日) 13:00～16:00(開場12:30)

会　場　堺市民会館(大ホール)
〒590-0061　大阪府堺市翁橋町2-1-1　TEL 072(238)1481

入場料　無料

どなたでも、ご自由に参加していただけます。

事務局:近畿大学医学部 消化器内科
〒589-8511　大阪狭山市大野東377-2
TEL:072-366-0221(内線3149)　FAX:072-367-2880
E-mail:syoukaki@med.kindai.ac.jp
Home page: http://www.med.kindai.ac.jp/shoukaki/

■主催: 日本肝臓学会　近畿大学 消化器内科 教授　工藤正俊
■後援: 大阪府医師会、大阪府看護協会、大阪狭山市、堺市、堺市医師会、大阪狭山市医師会、和泉市医師会、河内長野市医師会、富田林医師会、岸和田市医師会、羽曳野市医師会、大阪肝臓友の会

第3回
関西消化器内視鏡ライブコース
3rd Kansai Gastrointestinal Endoscopy Live Course

顧　問　工藤正俊（近畿大学）

代表世話人　樫田博史（近畿大学）

会　期　2014年02月09日（日）
※開催日程が変更となりました
10:00～16:00（予定）

場　所　近畿大学医学部附属病院　円形講堂および光学治療センター
〒589-8511　大阪府大阪狭山市大野東377-2
Tel: 072-366-0221（代）
＊駐車場は、台数に限りがございます。ご来場の際は、できるだけ公共交通機関を
ご利用いただくよう、お願いいたします。

定　員　300名（定員になり次第、締め切らせていただきます）

内　容　上下部消化管、膵胆道における内視鏡処置のポイントを、
基礎から最新技術まで、ライブデモンストレーションでお示しいたします。
■画像強調・拡大内視鏡検査
■ESD/EMR
■EIS/EVL
■EUS/EUS-FNA/Interventional EUS（消化管・胆膵）
■ERCP/EST/Stenting
■ランチョンセミナー　　その他予定

術　者　山本博徳　先生（自治医科大学　消化器センター）
中井陽介　先生（東京大学医学部附属病院　消化器内科）
樫田博史　北野雅之　松井繁長（近畿大学）

参加費　医師：事前申し込み5,000円（当日受付 7,000円）
研修医、コメディカル、その他：2,000円（当日受付 2,000円）
学生、留学生：無料
ー事前申し込みは2014年01月20日までー

お申し込み方法　お名前、御所属、連絡先住所・Fax番号・メールアドレスを明記の上、
下記連絡先にFaxまたはE-mailで参加費振込み口座をお問い合わせ下さい。
振込みを確認させていただいた後、受理番号を発行させて頂きます。
当日は受付でその番号をお申し出ください。

お問い合わせ先　近畿大学医学部　消化器内科
関西消化器内視鏡ライブコース事務局（松井繁長）
E-mail:kin-live@med.kindai.ac.jp
Fax:072-367-2880　　Tel:072-366-0221（内線3525）

同門会　名簿

名前	施設	卒業年度	出身大学
工藤　正俊	近畿大学医学部	昭和53年	京都大学
樫田　博史	近畿大学医学部	昭和58年	京都大学
汐見　幹夫	近畿大学医学部	昭和55年	近畿大学
北野　雅之	近畿大学医学部	平成　2年	鳥取大学
西田　直生志	近畿大学医学部	昭和60年	大阪医科大学
松井　繁長	近畿大学医学部	平成　3年	近畿大学
上嶋　一臣	近畿大学医学部	平成　7年	神戸大学
櫻井　俊治	近畿大学医学部	平成　7年	京都大学
南　康範	近畿大学医学部	平成　9年	近畿大学
萩原　智	近畿大学医学部	平成 10年	近畿大学
井上　達夫	近畿大学医学部	平成 11年	近畿大学
矢田　典久	近畿大学医学部	平成 11年	滋賀医科大学
坂本　洋城	近畿大学医学部	平成 12年	近畿大学
朝隈　豊	近畿大学医学部	平成 14年	近畿大学
北井　聡	近畿大学医学部	平成 14年	近畿大学
川崎　正憲	近畿大学医学部	平成 15年	近畿大学
田北　雅弘	近畿大学医学部	平成 15年	近畿大学
永井　知行	近畿大学医学部	平成 16年	近畿大学
永田　嘉昭	近畿大学医学部	平成 16年	近畿大学
今井　元	近畿大学医学部	平成 17年	近畿大学
山雄　健太郎	近畿大学医学部	平成18年	東京医科大学
山田　光成	近畿大学医学部	平成18年	近畿大学
有住　忠晃	近畿大学医学部	平成 19年	近畿大学
鎌田　研	近畿大学医学部	平成 19年	近畿大学
峯　宏昌	近畿大学医学部	平成 19年	近畿大学
宮田　剛	近畿大学医学部	平成 19年	近畿大学
高山　政樹	近畿大学医学部	平成 19年	近畿大学
足立　哲平	近畿大学医学部	平成 21年	近畿大学
大本　俊介	近畿大学医学部	平成 21年	近畿大学
門阪　薫平	近畿大学医学部	平成 21年	近畿大学
田中　梨絵	近畿大学医学部	平成 22年	近畿大学
千品　寛和	近畿大学医学部	平成 22年	近畿大学
南　知宏	近畿大学医学部	平成 23年	近畿大学
岡元　寿樹	近畿大学医学部	平成 23年	近畿大学
黒木　恵美(旧姓 石川)		平成 11年	近畿大学
岡田　無文	山本病院	平成 13年	近畿大学
柴田　千栄(旧姓 辰巳)		平成 15年	近畿大学
上田　泰輔		平成 15年	近畿大学
上硲　俊法	近畿大学医学部臨床検査学	昭和60年	近畿大学
前川　清	近畿大学医学部超音波室		
辻　直子	近畿大学医学部堺病院	昭和60年	京都府立医科大学
谷池　聡子	近畿大学医学部堺病院	平成 7年	奈良県立医科大学
奥村　直己	近畿大学医学部堺病院		近畿大学
高場　雄久	近畿大学医学部堺病院		近畿大学

川崎　俊彦	近畿大学医学部奈良病院	昭和58年	京都大学
岸谷　譲	近畿大学医学部奈良病院	昭和 62年	近畿大学
宮部　欽生	近畿大学医学部奈良病院	平成 14年	近畿大学
清水　昌子	近畿大学医学部奈良病院	平成 12年	近畿大学
茂山　朋広	近畿大学医学部奈良病院	平成 17年	近畿大学
奥田　英之	近畿大学医学部奈良病院	平成19年	
木下　大輔	近畿大学医学部奈良病院	平成20年	
秦　康倫	近畿大学医学部奈良病院	平成21年	
水野　成人	近畿大学医学部奈良病院	昭和61年	京都府立医科大学
加藤　玲明	近畿大学医学部奈良病院	平成11年	近畿大学
宮本　容子(旧姓 北口)	近畿大学医学部奈良病院	平成12年	近畿大学
林　道友	林内科クリニック		
梅原　康湖	JR大阪鉄道病院	平成 12年	近畿大学
山本　俊夫(ご逝去)		昭和26年	京都大学
山本　健二	岡本クリニック		神戸大学
亀山　千晴	しあわせクリニック	平成　7年	近畿大学
南野　達夫	なんの医院	昭和55年	近畿大学
中里　勝	上ヶ原病院		
鍋島　紀滋	三菱京都病院	昭和61年	京都大学
由谷　逸朗	高石藤井病院	昭和62年	近畿大学
遠田　弘一	慈温堂遠田医院	平成 7年	近畿大学
遠田　由紀			
川端　一史	川端内科クリニック	平成元年	近畿大学
米田　円	米田内科胃腸科	平成 元年	近畿大学
小川　力	高松赤十字病院	平成11年	近畿大学
渡邉　和彦	結核予防会大阪府支部相談診療所	平成　3年	近畿大学
森村　正嗣	森村医院	平成　3年	帝京大学
中岡　良介	山本病院	平成 8年	近畿大学
冨田　崇文	冨田病院	平成 14年	近畿大学
西尾　健	南堺病院	平成 14年	近畿大学
仲谷　達也	仲谷クリニック	平成　3年	近畿大学
福永　豊和	北野病院	平成　4年	京都大学
福田　信宏	朝日大学村上記念病院	平成 10年	近畿大学
坂口　康浩	河崎内科病院	平成 11年	近畿大学
永島　美樹	桃坂クリニック	平成 12年	近畿大学
坂本　康明	坂本クリニック	平成 15年	近畿大学
市川　勉	内海町いちかわ診療所	平成 12年	近畿大学
齊藤　佳寿(旧姓 野田)	介護老人保健施設　徳田山	平成 14年	近畿大学
高橋　俊介	市立堺病院	平成 14年	近畿大学
末冨　洋一郎	末冨放射線科医院	平成　8年	近畿大学
梅原　泰	辻腎太郎クリニック	平成 11年	近畿大学
鄭　浩柄	神戸市立医療センター中央市民病院	平成　8年	東京慈恵医科大学
小牧　孝充	富田林病院	平成　7年	近畿大学
畑中　絹世		平成 13年	川崎医科大学
早石　宗右	早石病院	平成 18年	近畿大学
工藤　可苗	近畿大学医学部	平成 12年	近畿大学
山本　典雄	医療法人山紀会	平成 19年	近畿大学

鄭　扶美	近畿大学医学部　元秘書		
木村　由佳	近畿大学医学部　元秘書		
川辺　仁美	近畿大学医学部　元秘書		
西川　由佳	近畿大学医学部　元秘書		
二見　佳央里	近畿大学医学部　元秘書		
井上　真由美	近畿大学医学部　元秘書		
坂上　浩美	近畿大学医学部　元秘書		
小田　智裕子	近畿大学医学部　元秘書		
土井　由香利	近畿大学医学部　元秘書		
田中　真紀	近畿大学医学部　教授秘書		
村橋　亜季	近畿大学医学部　教授秘書		
上田　由未子	近畿大学医学部　教授秘書		
本廣　佳香	近畿大学医学部　教授秘書		
和田　千尋	近畿大学医学部　教授秘書		
胡桃　由佳	近畿大学医学部　医局秘書		
朝隈　智	近畿大学医学部　医局秘書		
林　直子	近畿大学医学部　医局秘書		
田村　利恵	近畿大学医学部　肝癌研究会事務局		
前原　なつみ	近畿大学医学部　肝癌研究会事務局		
弓削　公子	近畿大学医学部　臨床研究補助員		
児玉　美由紀	近畿大学医学部　データマネージャー（CRC業務）		
鏡　郁子	近畿大学医学部　基礎研究補佐員（実験助手）		
垣井　麻莉	近畿大学医学部　基礎研究補佐員（実験助手）		

近畿大学消化器内科　同門会役員

会長　　工藤正俊

副会長　　北野雅之

幹事　　松井繁長

会計　　上嶋一臣

庶務　　西田直生志

同門会誌作製　秘書一同

近畿大学医学部消化器内科教室同門会会則

第一条　名称

本会は近畿大学医学部消化器内科教室同門会と称する。

第二条　目的

本会は会員相互の親睦及び教室の隆盛を図ることを目的とする。

第三条　会員

会員は消化器内科教室出身者、教室員及び同教室の発展に寄与するものをもって構成される。

第四条　役員

１．　本会の運営を円滑にするために幹事会を設ける。幹事会は代表幹事を長とし、代表幹事が指名する教室員をもって構成する。尚、幹事会は代表幹事が随時召集するものとする。その他、会計をおく。

２．　会長

①　会長は現職主任教授より選出される。

②　会長退任後は名誉会長となる。また、名誉会長は主任教授経験者からも選出できる。

３．　顧問

本会の発展に寄与したもので、幹事会が推戴する。

４．　役員の選出

①　幹事は役員より選出する。

②　代表幹事は医局長が兼任する。

５．　幹事の任期は２年とする。但し再任を妨げない。

第五条　会議

１．　総会は年１回の開催とする。

２．　幹事会において仮決議された条件の最終決定権は総会に委ねられる。

３．　決議は総会出席者の多数決により成立する。

第六条　会計

１．　本会の経費は会費をもって充てる。

２．　本会の会費は年額壱萬円とする。

３．　会計年度は４月１日から翌年３月 31 までとし、会計担当者は年１回会計報告を行う。

第七条

事務局は近畿大学医学部消化器内科教室内に置く。

第八条　会則の改正

会則の改正は幹事会の仮決議を経て総会で議決されるものとする。

附則　除名規定

本会の名誉を毀損したものや、その他本会に不適当と考えられるものは幹事会の動議により総会にて除名が議決される。

編集後記

2013 年版の annual report が完成しました。

消化器内科の秘書は、現在、胡桃さん、田中さん、朝隈さん、田村さん、前原さん、村橋さん、弓削さん、鏡さん、垣井さん、本廣さん、児玉さん、和田さん、上妻さん、東野さん、山本さん（現在教授室 4 名、医局秘書 3 名、肝癌研究会事務局 4 名、データマネージャー（CRC 業務） 1 名、臨床研究補助 1 名、実験助手 2 名）での 15 人体制となっております。

2013 年版年報も遅い発刊となってしまいましたが、2014 年版はもう少し早い機会に発刊できるよう頑張ります。

年報業務に加えまして、その他業務におきましても、今後とも何卒宜しく御願い申し上げます。

平成 26 年 9 月 26 日

秘書一同